U.S. Geological Survey
Toxic Substances Hydrology Program—

Proceedings of the Technical Meeting, Charleston, South Carolina, March 8–12, 1999

Water-Resources Investigations Report 99-4018C
Volume 3 of 3 - Subsurface Contamination From Point Sources

USGS
science for a changing world

U.S. Geological Survey
Toxic Substances Hydrology Program—
Proceedings of the Technical Meeting,
Charleston, South Carolina,
March 8-12, 1999

David W. Morganwalp and Herbert T. Buxton, Editors

U.S. GEOLOGICAL SURVEY

Water-Resources Investigations Report 99-4018C

Volume 3 of 3 - Subsurface Contamination From Point Sources

West Trenton, New Jersey

1999

USGS
science for a changing world

U.S. DEPARTMENT OF THE INTERIOR

BRUCE BABBITT, *Secretary*

U.S. GEOLOGICAL SURVEY

Charles G. Groat, *Director*

For additional information
write to:

Coordinator
Toxic Substances Hydrology Program
U.S. Geological Survey
412 National Center
Reston, Virginia 20192

Copies of this report can be
purchased from:

U.S. Geological Survey
Branch of Information Services
Box 25286
Denver, Colorado 80225-0286

PREFACE

The U.S. Geological Survey (USGS) Toxic Substances Hydrology (Toxics) Program was initiated in 1982. The goal of the Program is to provide earth science information on the behavior of toxic substances in the Nation's hydrologic environments. Contamination of surface water, ground water, soil, sediment, and the atmosphere by toxic substances is among the most significant issues facing the Nation. Contaminants such as excessive nutrients, organic chemicals, metals, and pathogens enter the environment, often inadvertently, via industrial, agricultural, mining, or other human activities. The extent of their migration and their persistence often are difficult to ascertain. Estimates of the costs and time frames for cleanup of contamination and protection of human and environmental health can best be described as astounding, despite continual efforts by governments and industries worldwide to improve environmental technologies.

Contaminant sources and environmental occurrence have a wide range of scales. Some contaminants are released from point sources, such as leaks or discharges from industrial facilities. Some are released from multiple, closely spaced releases, such as domestic septic systems. Still others are released relatively uniformly over broad areas with similar land-use practices, such as agricultural and residential land uses. Contaminants are detected at high concentrations locally in the immediate vicinity of a release, at varied concentrations where multiple releases disperse within watersheds or regional hydrologic systems, and at relatively low (but still potentially toxic) concentrations where they enter systems from broad uniform sources. Common to contamination at all these scales is the need to:

- Measure the contaminants and their transformation products in environmental samples;
- Characterize the physical processes and properties that affect their propagation in the environment;
- Define the chemical and microbial processes that transform or degrade the contaminants;
- Describe contaminant-biota interactions that control their effects on ecosystems, the food chain, and human health;
- Understand the ultimate fate of contaminants with the potential long-term implications for human and environmental health; and
- Develop simulation models that enable prediction of potential exposure and effective design of waste disposal facilities, monitoring networks, and remediation alternatives.

To meet these needs, the Toxics Program provides information and technology to Federal and State resource-management agencies and industry. The Toxics Program: (1) conducts intensive field investigations of representative cases of subsurface contamination at local releases; (2) conducts watershed- and regional-scale investigations of contamination affecting aquatic ecosystems from nonpoint and distributed point sources; and (3) develops methods and models — methods to detect, identify, and measure emerging environmental contaminants; and models to interpret the persistence and fate of contamination and to design waste-disposal and remediation strategies.

Intensive field investigations are established at sites contaminated with predominant types of environmental contamination, in commonly occurring geohydrologic and geochemical settings. Contamination types currently under investigation include chlorinated solvents, sewage effluent, toxic metals, radionuclides, and petroleum products, including fuel oxygenates. These long-term research projects are conducted by interdisciplinary research teams that comprehensively identify and characterize the physical, chemical, and biological processes that affect contaminant transport, transformation, and fate at the site. Through extensive characterization and field experimentation, the sites provide field-laboratory conditions that enhance research opportunities. Results from the sites are generalized by focused field and laboratory experiments at other sites that describe the range of field conditions for the controlling

processes. Knowledge and methods produced at these representative sites improve the effectiveness and reduce the cost of characterization and remediation at similar sites across the Nation.

A unifying theme of these investigations is characterization of the natural response of hydrologic systems to contamination. This, when combined with comprehensive assessment of the processes that affect contaminant transport and fate, make assessing the potential of natural attenuation and remediation-performance monitoring undertakings in which the Toxics Program can excel. The long-term nature of the research provides a unique opportunity to evaluate the potential and limitations of natural-attenuation remediation alternatives.

Watershed- and regional-scale investigations are developed to address contamination problems typical of specific land uses or human activities that may pose a threat to human and environmental health throughout significant parts of the Nation. Current watershed- and regional-scale investigations address contamination from agricultural chemicals in the Midwest corn belt; cotton agriculture across the southern U.S.; human activities in estuarine ecosystems; historic hard-rock mining in watersheds in mountain terrain and southwestern alluvial basins; and mercury emissions on aquatic ecosystems.

In some cases, these investigations involve characterizing contaminant sources and their mechanisms for affecting aquatic ecosystems. This is the case in ongoing investigations of watersheds that may be affected by hundreds of abandoned mine sites. In some cases, watershed- and regional-scale investigations involve widespread detection of mixtures of contaminants or contaminant transformation products at levels near or below existing water-quality standards or advisories. This is the case in investigations of agricultural land uses which have documented that mixtures of pesticides and their metabolites accumulate to significantly higher levels than the individual parent compounds. In still other cases, these investigations identify chemicals in environmental samples for which standards have not yet been developed. In these cases, the Program provides information to resource managers and regulators that is useful for developing new water-quality standards or registering use of new chemicals, such as new pesticides or industrial chemicals.

These investigations complement the National Water-Quality Assessment (NAWQA) Program, which has the goal of assessing the status and trends of the quality of the Nation's ground- and surface-water resources. The Toxics Program watershed- and regional-scale investigations focus rapidly on new issues, emerging contaminants, and understanding the processes that affect whether a chemical may be of widespread concern. This information is used for planning future NAWQA Program activities.

New scientific models and methods are developed as part of both intensive field investigations and watershed- and regional-scale investigations. Simulation models provide tools to predict environmental occurrence and estimate exposure risks, as well as design remediation and monitoring strategies. A strength of models developed by the Toxics Program is that they are developed and applied to explain the complex field conditions at Program field sites. This makes them particularly well suited for application to real problems. New and improved water-quality analytical methods enable (1) detection of new chemicals in environmental samples, such as new pesticides and fuel oxygenates; (2) detection of chemicals at lower levels, which enables our understanding of the processes that control the environmental and human health effects of chemicals, such as mercury; and (3) identification of persistent transformation products of contaminants, such as pesticide metabolites. These methods and models are transferred to public and private practitioners for widespread use across the Nation.

Most scientists involved with Toxics Program activities are from the USGS National Research Program and District (state) Offices. However, as interdisciplinary approaches to solving contamination problems have become more successful, more ecologists, geologists, chemists, hydrologists, geochemists, and digital data-collection experts from across the USGS have become involved in Program activities. In

addition, many scientists from universities, other Federal agencies, and industry are taking advantage of research opportunities afforded by the Program and its field sites, and are active members of the research teams.

Each project is steered by a core group of scientists from the research team. This core group, led by the project coordinator(s), guides the development of a research plan that integrates the multi-disciplinary activities at the site. They facilitate opportunities that become available for a wide range of related research. Although not an emphasis of the Toxics Program, many innovative, engineered-remediation technologies have been tested at the Program field sites because their extensive characterization provides a basis for effective evaluation of technology design and performance. Long-term data sets from the sites have been used by other Federal agencies to test decision-support software for site characterization or to test new hydrologic simulation models. Research plans for each project undergo periodic review by a panel of USGS and non-USGS scientists to improve the research approach and identify opportunities to enhance the research team. Field support for research projects is provided by experienced specialists located in the local USGS District Office.

The Toxics Program is coordinated with the U.S. Environmental Protection Agency, the U.S. Department of Agriculture, the Department of Defense, the Department of Energy, the Nuclear Regulatory Commission, and other U.S. Department of the Interior agencies to ensure that current and future research priorities are being addressed.

The long-term cooperation and assistance offered by the Federal, State, and local agencies, and by private entities that administer or own the Program's research sites has been essential to the success of the Toxics Program. Their continued support is greatly appreciated.

Herb Buxton
Coordinator, Toxic Substances
Hydrology Program

CONTENTS

CONTENTS--Continued

Page

CONTENTS--Continued

CONTENTS--Continued

Page

CONTENTS--Continued

Page

CONTENTS OF VOLUME 1 - CONTAMINATION FROM HARD-ROCK MINING

SECTION C—Research on Hard-Rock Mining in Arid Southwest Alluvial Basins

SECTION D—Additional Research on Contamination from Mining-Related Activities

CONTENTS OF VOLUME 2 - CONTAMINATION OF HYDROLOGIC SYSTEMS AND RELATED ECOSYSTEMS

SECTION B—Mercury Contamination of Aquatic Ecosystems

SECTION C—Occurrence, Distribution, and Fate of Agricultural Chemicals in the Mississippi River Basin

INTRODUCTION

This report contains papers presented at the seventh Technical Meeting of the U.S. Geological Survey (USGS), Toxic Substances Hydrology (Toxics) Program. The meeting was held March 8-12, 1999, in Charleston, South Carolina. Toxics Program Technical Meetings are held periodically to provide a forum for presentation and discussion of results of recent research activities.

The objectives of these meetings are to:

- Present recent research results to essential stakeholders,
- Encourage synthesis and integrated interpretations among scientists with different expertise who are working on a contamination issue, and
- Promote exchange of ideas among scientists working on different projects and issues within the Toxics Program.

The Proceedings is published in three volumes. Volume 1 contains papers that report on results of research on contamination from hard-rock mining. Results include research on contamination from hard rock mining in arid southwest alluvial basins, research on hard rock mining in mountainous terrain, and progress from the USGS Abandoned Mine Lands Initiative. This Initiative is designed to develop a watershed-based approach to characterize and remediate contamination from abandoned mine lands and transfer technologies to Federal land management agencies and stakeholders.

Volume 2 contains papers on contamination of hydrologic systems and related ecosystems. The papers discuss research on the response of estuarine ecosystems to contamination from human activities. They include research on San Francisco Bay; mercury contamination of aquatic ecosystems; and investigation of the occurrence, distribution, and fate of agricultural chemicals in the Mississippi River Basin. This volume also contains results on development and reconnaissance testing of new methods to detect emerging contaminants in environmental samples.

Volume 3 contains papers on subsurface contamination from point sources. The papers discuss research on: hydrocarbons and fuel oxygenates at gasoline release sites; ground-water contamination by crude oil; complex contaminant mixtures from treated wastewater discharges; waste disposal and subsurface transport of contaminants in arid environments; ground water and surface water affected by municipal landfill leachate; natural attenuation of chlorinated solvents; and characterizing flow and transport in fractured rock aquifers.

In all, the more than 175 papers contained in this proceedings reflect the contributions of more than 350 scientists who are co-authors. These scientists are from across the USGS, as well as from universities, other Federal and State agencies, and industry.

More information on the Toxic Substances Hydrology Program, including a searchable bibliography of publications and selected on-line publications, is available on the World Wide Web at: **http://toxics.usgs.gov/toxics/**

ACKNOWLEDGMENTS

The editors acknowledge with great appreciation the assistance provided by Kim Crutchfield, Judy Salvo, Nana Snow, Judy Griffin, Patti Greene, and Ray Douglas. Their efforts in the planning, organization, and arrangements made for this seventh Technical Meeting of the Toxics Program made it both successful and enjoyable. Sincere thanks to Bill Ellis for assisting authors with preparation of papers for publication and for preparation and layout of this manuscript. Chet Zenone, Larry Slack, Anthony Buono, and John Flager assisted through review and improvement of the papers in this proceedings. Thanks are extended to the South Carolina District for their warm hospitality. Thanks also to the many scientists whose contributions and accomplishments are reflected in this proceedings; their continued efforts ensure continued success for the USGS Toxic Substances Hydrology Program.

Scale Considerations of Chlorinated Solvent Source Zones And Contaminant Fluxes: Insights From Detailed Field Studies

By Beth L. Parker and John A. Cherry, Department of Earth Sciences
University of Waterloo, Waterloo, Ontario. N2L 3G1

Chlorinated solvents are the most common contaminants of industrial origin found in groundwater in industrialized countries. They pose exceptional challenges for monitoring and remediation because they commonly penetrate deeper than other contaminants and they are persistent and mobile. The increasing dependence on risk assessment and natural attenuation for site management decisions and mass removal or in situ mass destruction for groundwater remediation has created an urgent need for improved information on the subsurface distribution of solvent mass and the contaminant mass flux in groundwater. Since 1981 the University of Waterloo has used the Borden research site situated 50 km northwest of Toronto, Ontario, for many experiments involving the release of chlorinated solvents, including experiments in which free-phase solvents (DNAPLs) are released directly into the shallow sandy aquifer. Visual examination of solvent DNAPL distributions (TCE and PCE) in excavations at Borden and in aquifer cores indicates strong influence of small-scale or subtle variations in sediment texture and at greater depth, the influence of fractures and thin discrete sandy beds in the clayey aquitard. These observations in DNAPL zones demonstrated the need for data acquisition at much smaller spatial scales than was necessary when Borden experiments involved only aqueous-phase releases for attenuation studies. The Borden site however offers only a narrow set of geological conditions, and a short time frame of contamination relative to actual contaminated sites.

In a new phase of research initiated three years ago, with continued focus on the distribution and fate of chlorinated solvents in groundwater, we have expanded the field studies to include twelve contaminated industrial sites in Canada and the United States. Also, a second site for solvent release experiments has been established on fractured clay (the Laidlaw site in southern Ontario), while use of the Borden site for sand aquifer experiments continues. Three of the industrial sites are on fractured clay, three on fractured sedimentary rock (sandstone, shale and dolomite) and the rest on surficial sand aquifers of various origins underlain by clayey aquitards. Therefore a portfolio of sites are available to us and our team of graduate students, research associates and technicians; each site offers sufficient hydrogeologic simplicity and monitoring feasibility for studies to answer specific questions in practical time frames. Except for the fractured rock sites, all of the solvent contamination occurs at depths less than 30 m in deposits easily penetrated by direct-push equipment for continuous coring and groundwater sampling. To expand the usefulness of the sites and to accommodate the variety of site conditions, existing sampling equipment is modified and new types of equipment are developed. In site selection priority is given to hydrogeologic simplicity and also their simplicity of contaminant types and input histories, which greatly enhances prospects for meaningful data interpretation. However even with this relative simplicity, the number of factors influencing the contaminant distribution and behaviour is large. The potential to accommodate more complexity in site conditions is increasing with experience and equipment improvements. The sites also must have cooperative site owners, minimal litigation activity, and good terrain access. The field studies are complemented by lab measurements of parameters such as porosity, hydraulic conductivity, effective diffusion coefficients, fraction organic carbon and other sorption-related parameters. Large column experiments (0.3 – 0.5 m diameter) of relatively undisturbed sand or fractured clay are used to assess particular affects of geologic structure on DNAPL and solute behaviour.

At solvent DNAPL sites nearly all of the DNAPL normally resides below the water table, which causes a plume of dissolved-phase contamination to emanate from the source zone. However only in rare cases does a site offer good prospects for investigation of both the source zone and the plume. Therefore at some sites studies emphasize the source zone and at other sites the plume. Ultimately the smallest spatial scale relevant to the understanding of the behaviour and fate of solvents is the diffusion scale. This scale becomes most important for the time scales relevant to most contaminated industrial sites where DNAPL entered the subsurface decades ago. The field studies have in common the collection of thousands of samples of water and sediment or rock for chemical analyses. The samples are obtained from vertical holes to provide detailed profiles of concentration versus depth. The vertical space between samples for volatile contaminant analysis (VOC) is tailored to sediment type and age of the contamination, or in some cases sampling is done at scales as small as is feasible, which for groundwater sampling can be 0.2 – 0.4 m vertical spacing in sediment and several meters in fractured rock. Smaller vertical spacing of groundwater samples is generally not appropriate because of limitations imposed by disturbance of in situ conditions caused by purging prior to sampling. Data acquisition is accelerated by rapid on-site VOC analyses. Subsamples from sediment or rock cores are commonly taken at even smaller intervals, as close as a few millimeters in some cases. The sediment and rock core VOC analyses provide total concentrations that are connected to dissolved concentrations in pore water and concentrations sorbed on solids. In some situations the sample spacing is extremely small because the scale of diffusion effects is uncertain a priori and therefore sampling feasibility rather than prediction of contaminant distributions is the overriding factor. Networks of conventional monitoring wells exist at most of the sites and therefore comparisons are made between three sampling scales: wells, discrete-sample groundwater profiles and core subsampling.

Some preliminary conclusions can be drawn. Regardless of the depositional origin of the sandy aquifer, DNAPL accumulation zones (source zones) in sandy aquifers are comprised of many thin layers of DNAPL rather than substantial free-product pools. In some cases the DNAPL layers are associated with silt or clay layers and in other cases the control by geologic layering is much more subtle or not discernable. At locations where the DNAPL rests on top of a thick clayey layer, diffusion-scale profiles from the DNAPL into the clay are used to define the bottom of contamination and to identify advection effects and also to estimate the time of arrival of DNAPL at the location. Diffusion zones in clayey layers situated within the aquifer can comprise a large percentage of the total aqueous and sorbed mass within plumes. In sandy aquifers vertical diffusion from suspended DNAPL layers combined with lateral advection produces mixing that smooths the vertical concentration distributions within plumes short distances downgradient from the source zones. The tops and in some cases the bottoms of plumes are abrupt over vertical distances of less than a meter, which suggests diffusion control with advective influence on apparent vertical transverse dispersion.

Vertical profiles in sandy aquifers along sections (transects) across plumes at locations a short distance downgradient of the source zones show extreme variability of solvent concentrations. They show that much of the total contaminant plume mass flux occurs in small zones. Estimates of total annual contaminant mass discharge through these transects provides insight into the evolution of the source zones during previous decades and their future longevity. At sites where a network of conventional monitoring wells were used prior to our investigations, plume characteristics from these networks were generally indistinct or misleading when compared to our delineation at the finer sampling scale.

In clayey aquitards, diffusion zones (haloes) along fractures and along thin horizontal sandy layers indicate the pathways of DNAPL flow. Natural fractures in clayey deposits are commonly so small (10-50 μm apertures) that solvent DNAPL entering the fractures disappears quickly from most fractures due to diffusion. The diffusion-driven chemical mass transfer that puts the solvent mass, as aqueous and sorbed phases, into the matrix blocks between fractures. The matrix blocks, which have porosity in the 35-50% range, offer large solvent mass storage capacity relative to the fracture network. Small-scale

mapping of diffusion haloes along fractures provides information on channeling of DNAPL flow and indicates variable DNAPL arrival times along fractures within the same local zone.

In fractured sedimentary rock such as sandstone the porosity of the matrix blocks (5-15%) is much smaller than the matrix porosity of the clayey deposits. However over decades this rock porosity is large enough for measurable diffusion haloes to form along the fractures where DNAPL flow or solute transport has occurred. The haloes and therefore the pathways are determined from analysis of subsamples of rock core. This approach for pathway identification has proven to be more precise and more reliable than the conventional approaches of well sampling or open borehole packer sampling that lump concentrations from various fractures, or that are influenced by borehole cross-contamination that is usually unavoidable due to natural hydraulic gradients. The rate of expansion of plumes in fractured sandstone and other sedimentary rocks can be severely restricted by the diffusion-driven chemical mass transfer from fractures where active flow occurs to the matrix blocks where the pore water is relatively immobile. Site-specific proof of this retardation of plume expansion lies in determination of the chemical mass distribution in the rock matrix.

In most of the hydrogeological environments being studied, diffusion has caused much solvent mass to enter low-permeability zones, such as clayey layers within or below sandy aquifers, or matrix blocks between fractures in clay or rock. This mass distribution causes futility of groundwater restoration efforts involving advection-based approaches such as pump-and-treat and chemical flushing. Remediation possibilities are enhanced when the technologies are capable of seeking out the solvent mass in the diffusion-controlled zones.

Selecting Remediation Goals by Assessing the Natural Attenuation Capacity of Ground-Water Systems

By Francis H. Chapelle and Paul M. Bradley

ABSTRACT

Remediation goals for the source areas of a chlorinated ethene-contaminated ground-water plume in Kings Bay, GA were identified by assessing the natural attenuation capacity of the aquifer system. The redox chemistry of the site indicates that sulfate-reducing (H_2 ~ 2 nanomoles per liter, (nM)) conditions near the contaminant source grades to Fe(III)-reducing conditions (H_2 ~ 0.5 nM) downgradient of the source. Sulfate-reducing conditions facilitate the initial reduction of perchloroethene (PCE) to trichloroethene (TCE), cis-dichloroethene (cis-DCE), and vinyl chloride (VC). Subsequently, the Fe(III)-reducing conditions drive the oxidation of cis-DCE and VC to carbon dioxide and chloride. This sequence of redox conditions gives the aquifer a substantial capacity for biodegrading chlorinated ethenes. Natural attenuation capacity, defined as the slope of the steady-state contaminant concentration profile along a ground-water flowpath, is a function of biodegradation rates, aquifer dispersive characteristics, and ground-water flow velocity.

Natural attenuation capacity at the Kings Bay site was assessed by estimating ground-water flow rates (~0.23 ± 0.12 m/d) and aquifer dispersivity (~1 m) from hydrologic and scale considerations. Apparent biodegradation rate constants (PCE and TCE ~ 0.01d^{-1}; cis-DCE and VC ~ 0.025 d^{-1}) were estimated from observed contaminant concentration changes along aquifer flowpaths. Given estimates for these parameters, a boundary-value problem approach was used to estimate levels to which contaminant concentrations in the source-areas must be lowered (by engineered removal), or ground-water flow velocities lowered (by pumping) in order for the natural attenuation capacity to achieve maximum concentration limits (MCLs) prior to reaching a predetermined regulatory point of compliance.

INTRODUCTION

Chlorinated ethenes are subject to natural attenuation processes such as dilution, adsorption, and biodegradation in all ground-water systems (Wiedemeier et al., 1997). However, the efficiency of biodegradation, the process that causes the actual destruction of contaminants, varies widely. In many ground-water systems, biodegradation and other natural attenuation processes are not sufficient to protect downgradient receptors from contamination. For this reason, U.S. Environmental Protection Agency (EPA) guidance has stressed that natural attenuation is most often appropriate when used in conjunction with engineered reduction of contaminant sources:

> "In the majority of cases where monitored natural attenuation is proposed as a remedy, its use may be appropriate as one component of the total remedy, that is, either in conjunction with active remediation or as a follow-up measure" (U.S. EPA, 1997, p.1).

The manner in which natural attenuation and active remediation measures (such as source removal, pump-and-treat, chemical oxidation, or enhanced bioremediation) are combined depends on the natural attenuation capacity of a system. If the natural attenuation capacity is small, for example, then active remediation measures will need to remove or immobilize a high proportion of the contaminant source in order to protect

downgradient receptors from contamination. Conversely, if the natural attenuation capacity is large, then less source removal may be required in order to protect downgradient receptors. In either case, it is necessary to quantify the natural attenuation capacity of a system in order to effectively combine contaminant source-removal methods with natural attenuation. The purpose of this paper is to assess the natural attenuation capacity of a chlorinated ethene-contaminated aquifer in Kings Bay, GA, and to use this assessment for selecting engineered source-reduction goals at the site.

Natural Attenuation Capacity

The concept of "assimilative capacity" is well-known in soil science (Charbeneau and Daniel, 1993, p. 15.1) and surface water hydrology (Chapra, 1996, p. 11) and refers to the capacity of a system to absorb and/or transform pollutants. By analogy, a "natural attenuation capacity" can be defined for ground-water systems as being the ability to lower contaminant concentrations along aquifer flowpaths.

In surface-water systems, assimilative capacity depends upon hydrologic (stream flow, mixing, and hydrodynamic dispersion), and biological (biological oxygen demand) factors and is assessed using analytical or digital water-quality models. Similarly , the natural attenuation capacity of ground-water systems depends upon hydrologic (dispersion and advection) and biological (biodegradation rates) factors that can also be assessed using quantitative models. The sum of dispersive, advective, sorptive, and biodegradative processes acting on a solute in a one-dimensional flow system is given by the solute-transport equation:

$$\frac{\partial C}{\partial t} = D\frac{\partial^2 C}{\partial x^2} - v\frac{\partial C}{\partial x} - \frac{\rho_b K_d}{n}\frac{\partial C}{\partial x} - kC \qquad (1)$$

where D is the coefficient of hydrodynamic dispersion (m^2/d), v is the velocity of ground-water flow (M/d), ρ_b is bulk density, K_d is a linear sorption distribution coefficient, n is porosity, and k is a first-order biodegradation rate constant (d^{-1}) (Freeze and Cherry, 1979, p. 402 and p. 552). The coefficient of hydrodynamic dispersion, in turn, is proportional to ground-water velocity and scale-dependent aquifer dispersivity D* (m):

$$D = v\,D^* \qquad (2)$$

Appropriate procedures for solving equation (1) depend on the ground-water system in question, and the specific problems being addressed. When a contaminant plume has reached approximate steady-state conditions (that is, the plume is not expanding or contracting with time and $\partial C/\partial t=0$), the sorption term becomes small relative to the other three terms, and the solute-transport equation simplifies to the ordinary differential equation:

$$D\frac{d^2C}{dx^2} - v\frac{dC}{dx} - kC = 0 \qquad (3)$$

For boundary conditions of $C = C_0$ at $x=0$, and $C=0$ as $x \to \infty$, equation 3 has the particular solution:

$$C(x) = C_o \exp^{-\left[\frac{-v+\sqrt{v^2+4Dk}}{2D}\right]x} \qquad (4)$$

Equation (4) indicates that the steady-state solute concentration decrease away from a constant source is dependent on hydrodynamic dispersion (D), the biodegradation rate constant (k), and ground-water velocity (v). With this usage, a positive value of k indicates contaminant loss. The slope of the solute concentration profile along a flowpath is proportional to the value of:

$$\left[\frac{-v+\sqrt{v^2+4Dk}}{2D}\right] \qquad (5)$$

The term *natural attenuation capacity* (NAC), as used in this paper refers to the quantity given in

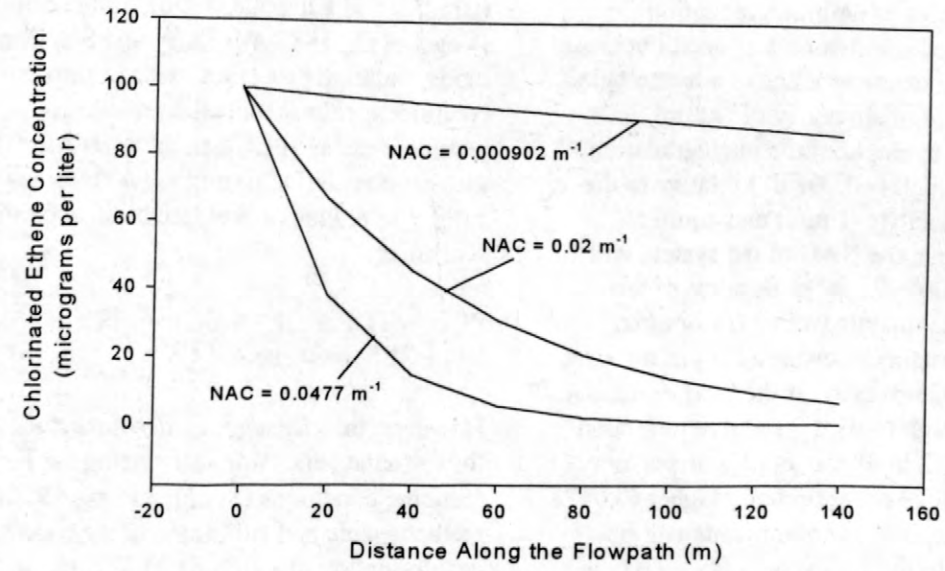

(A)

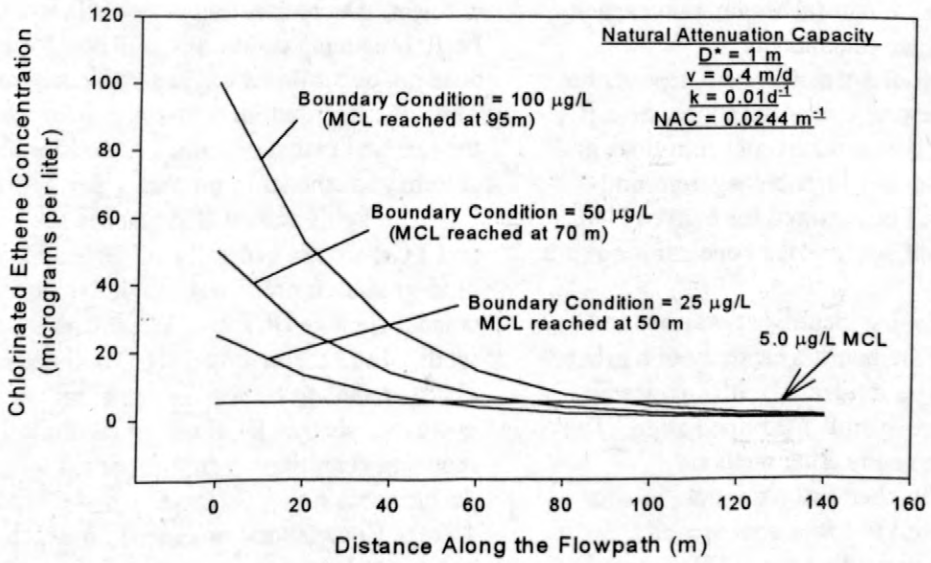

(B)

Figure 1.--Schematic diagram showing (A) the affect of natural attenuation capacity and (B) the affect of source-area concentrations on the distance required to decrease contaminant concentrations below MCLs.

equation 5, which has units of m^{-1}. Conceptually, it may be thought of as the contaminant-lowering capacity of an aquifer per meter of flowpath.

The concept of natural attenuation capacity as defined in equation 5 is useful because it illustrates those characteristics of a hydrologic system that affect the efficiency of natural attenuation. For example, if the biodegradation rate constant is small (~0.001 d^{-1}) relative to the ground-water velocity (~1 m/d) and aquifer dispersivity (10 m), the NAC of the system will also be small (0.009902 m^{-1}). Because of this small NAC, contaminants will be transported relatively long distances downgradient of a source area (Fig. 1A). Conversely, if the biodegradation rate constant is high (0.01 d^{-1}) relative to ground-water velocity (0.2 m/d) and aquifer dispersivity (1 m), the NAC will be proportionally higher (0.0477 m^{-1}) and the transport of contaminants will be restricted closer to the source area (Fig. 1A).

In addition to natural attenuation capacity, the distance that contaminants are transported in a ground-water system depends on contaminant concentrations at the source area (C_o in equation 4). If contaminant concentrations at the source are relatively high, a longer ground-water flowpath will be required for a given NAC to reach MCLs than if source-area concentrations are lower (Fig. 1B).

This reasoning identifies two ways in which the natural attenuation capacity of a ground-water system can be integrated with engineered methods to achieve overall site remediation. The first way is to use engineering methods (excavation, in-situ chemical oxidation, in-situ bioremediaiton, etc.) to lower source area concentrations to levels that the NAC present in the aquifer can lower contaminant concentrations to MCLs at a given point of compliance. The second way is to decrease the velocity of ground-water flow away from a contaminant source area, which in turn increases NAC (Fig. 1A). This can be accomplished using conventional pump-and-treat technology.

Biodegradation of Chlorinated Ethenes

The biodegradation of chlorinated ethenes is complex because these compounds are subject to reductive (Vogel et al., 1987; McCarty and Semprini, 1994; Bouwer, 1994), oxidative (Bradley and Chapelle, 1996), and cometabolic (Vogel et al., 1987; McCarty and Semprini, 1994) biodegradation processes. Under anoxic conditions, chlorinated ethenes such as perchloroethene (PCE), trichloroethene (TCE), dichloroethene (DCE) and vinyl chloride (VC) are subject to reductive dechlorination according to the sequence:

$$PCE \Rightarrow TCE + Cl^- \Rightarrow DCE + 2Cl^- \Rightarrow VC + 3Cl^- \Rightarrow ethene + 4\ Cl^- \quad (6)$$

However, the efficiency of dechlorination differs for methanogenic, sulfate-reducing, or Fe(III)-reducing conditions (Smatlak et al., 1996). Under methanogenic and sulfate-reducing conditions, dechlorination of PCE and TCE is rapid and efficient. Dechlorination is less efficient under Fe(III)-reducing conditions, and dechlorination does not occur under oxygen-reducing conditions. Thus, the distribution of redox conditions affects the rate and extent of reductive dechlorination of chlorinated ethenes in ground-water systems.

Highly chlorinated ethenes such as PCE and TCE are not generally subject to oxidative biodegradation precesses. Lightly chlorinated ethenes such as DCE and VC, however, can be oxidized to carbon dioxide (CO_2) under oxic or Fe(III)-reducing conditions. It is not yet clear, however, whether DCE oxidation under Fe(III) reducing conditions is first preceded by reductive dechlorination to VC (Bradley and Chapelle, 1996). Cometabolic processes, in which chlorinated ethenes are gratuitously degraded by enzymatic processes designed to metabolize organic compounds other than chlorinated ethenes, have been widely documented (Vogel et al., 1987; McCarty and Semprini, 1994) and can be an important component of natural attenuation in some systems.

It is observed that sequential reduction of PCE and TCE followed by oxidation of DCE and VC is the most efficient combination of mechanisms for completely degrading chlorinated ethenes (Cox and others, 1995). Thus, the efficiency of natural attenuation, and thus the

natural attenuation capacity of ground-water systems, is directly related to the distribution of ambient redox processes (Chapelle, 1996).

Estimating Natural Attenuation Capacity

The natural attenuation capacity at individual field sites can be estimated by obtaining estimates of k, v, and D (equation 5). Values of v can be estimated using standard field hydrologic methods, and D can be estimated from v (equation 2) and the scale of the plume (Gelhar and others, 1992) . Similarly, the kinetics of biodegradation can be estimated using field methods (Buscheck and Alcantar, 1995; Chapelle and others, 1996; Weaver and others, 1996). If v and D can be reliably estimated, and if concentration changes of contaminants can be documented with field data, k can be estimated by curve-fitting solutions of equation 4 to field data. This can be done by coding equation 4 as a transform in a spreadsheet, or can be done using an established computer code such as Bioscreen (Newell and others, 1996). Site-specific D, v, and k values, in turn, can be used to quantitatively describe the natural attenuation capacity (equation 5) of particular ground-water systems.

Sources of Uncertainty

Estimating biodegradation rate constants using field data is subject to numerous sources of uncertainty which need to be explicitly considered in any application. These uncertainties include (1) variation of ground-water flow rates, (2) uncertainty in adequately sampling contaminant concentrations within the plume, and (3) deviations from steady-state conditions within the plume. Variation of ground-water flow rates in time and space due to heterogeneity of hydraulic conductivity and hydraulic gradient changes due to recharge events occurs in all shallow aquifers. This is an important source of uncertainty in estimating biodegradation rate constants because an n-fold error in groundwater flow velocity (v) results in an n-fold error in calculated biodegradation rate constant (k) (equation 3). Because of this inherent error, which can vary in time, it is appropriate to use ranges of v in estimating k, and reporting k values as ± the range of variation. This is the procedure used in this paper. If variations in ground-water flow with time are large, then the steady-state assumption inherent in equation 3 is not appropriate and time-dependent solutions of equation 1 must be used (Rifai and others, 1995). Furthermore, if transverse dispersion is significant in a system, than a 2-D or 3-D treatment of the problem is more appropriate (Weaver and others, 1996).

Adequate sampling of contaminant concentrations in a plume can be a significant source of uncertainty in evaluating the behavior of chlorinated ethene concentrations (Cherry, 1996). Contaminant concentrations are observed to vary significantly between the "core" and "fringes" of plumes. These variations can significantly effect natural attenuation capacity estimates and calculated biodegradation rates.

Field methods for estimating biodegradation rate constants were first applied to petroleum hydrocarbon contaminants (Buscheck and Alcantar, 1995; Chapelle and others, 1996) in ground water. For chlorinated ethenes, this procedure is complicated by the fact that TCE, DCE, and VC are produced as daughter products from PCE as well as being degraded. TCE, DCE, and VC concentration changes along a flowpath segment reflect the difference between production and degradation. Thus, for TCE, cis-DCE, and VC, this procedure yields overall degradation rate constants which *underestimate* actual degradation rate constants.

Clearly there are numerous sources of uncertainty inherent in quantifying biodegradation rate constants using field data. Furthermore, many of these uncertainties are difficult or impossible to quantify. While uncertainty can be reduced by extensive data collection, they cannot be eliminated entirely. For these reasons, biodegradation rate constants, and estimates of natural attenuation capacity, obtained using these methods should be regarded as estimates.

RESULTS AND DISCUSSION

Geology, Hydrology, and Site History

The site used for this study is an

abandoned landfill known as the Old Camden Road Landfill located at the Naval Submarine Base (NSB) Kings Bay, Georgia. A map of the landfill and the orientation of the contaminant plume, as determined by monitoring wells and direct-push data is shown in Figure 2. This site is underlain by sediments of back-barrier island and barrier island origin. The most permeable sands underlying the site are present between depths of 10 and 11 m below land surface, and record the sedimentation of a prograding barrier island. This permeable zone is referred to informally as the "11 meter" aquifer in this report. This permeable zone is underlain and overlain by finer-grained sands

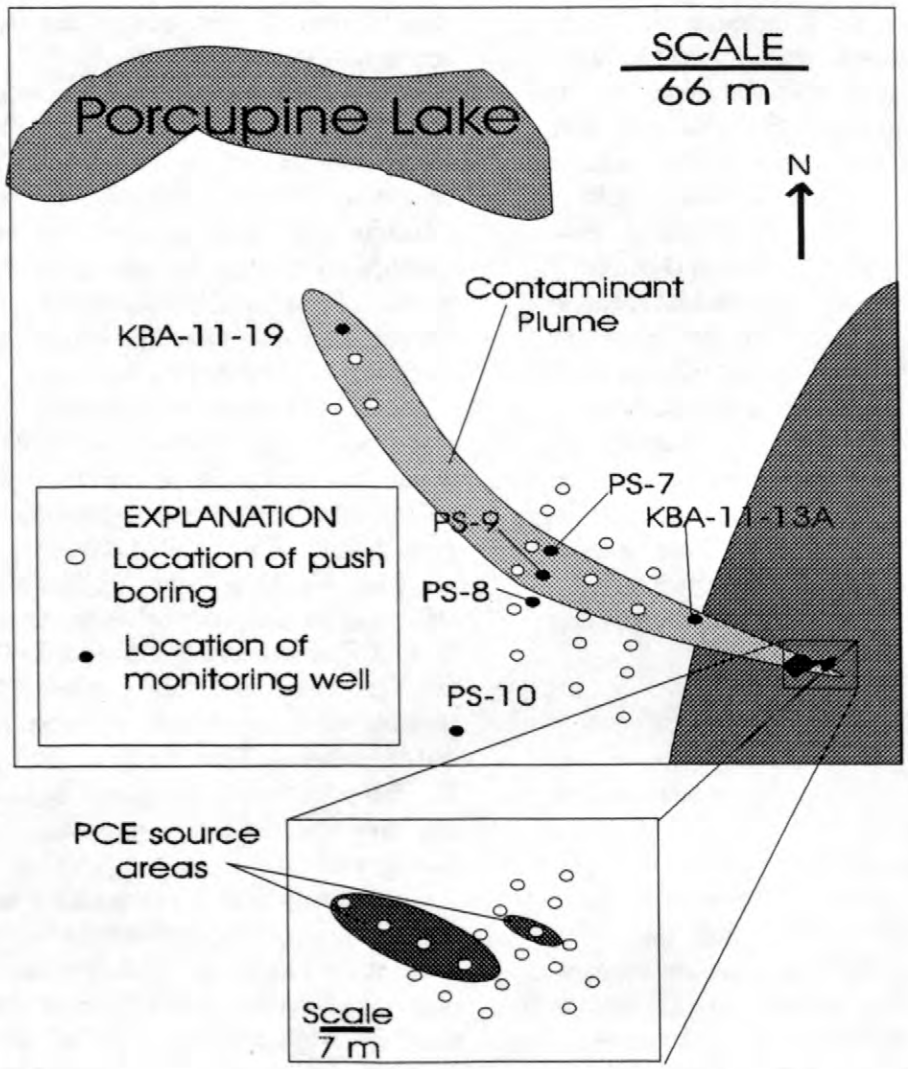

Figure 2.--Location of PCE source areas and orientation of chlorinated ethene contaminant plume.

exhibiting lower hydraulic conductivity. Aquifer tests and slug tests at this site indicate that hydraulic conductivities of the sands range from 0.6 to 3 m/d. The lithology of the these sands suggest that the 11-meter aquifer is characterized by higher hydraulic conductivities (K~10 m/d) relative to overlying and underlying sands. Because of its relative permeability, the 11-meter aquifer is a preferential pathway for horizontal ground-water flow and contaminant transport in this system.

Overlying the 11-meter aquifer at depths of approximately 3-5 meters below land surface is a layer of organic-rich sands. This organic-rich layer has the important effect of removing dissolved oxygen from recharging water and producing uniformly anoxic conditions in the 11-meter aquifer. In addition, organic matter that was disposed of in the landfill contributes to highly reducing conditions. Ground-water flow in the 11-meter aquifer is predominantly to the west, and can be easily traced by methane-bearing water originating from the landfill.

The Old Camden Road landfill was used to dispose of municipal waste between 1974 and 1981. Trenches were excavated to a

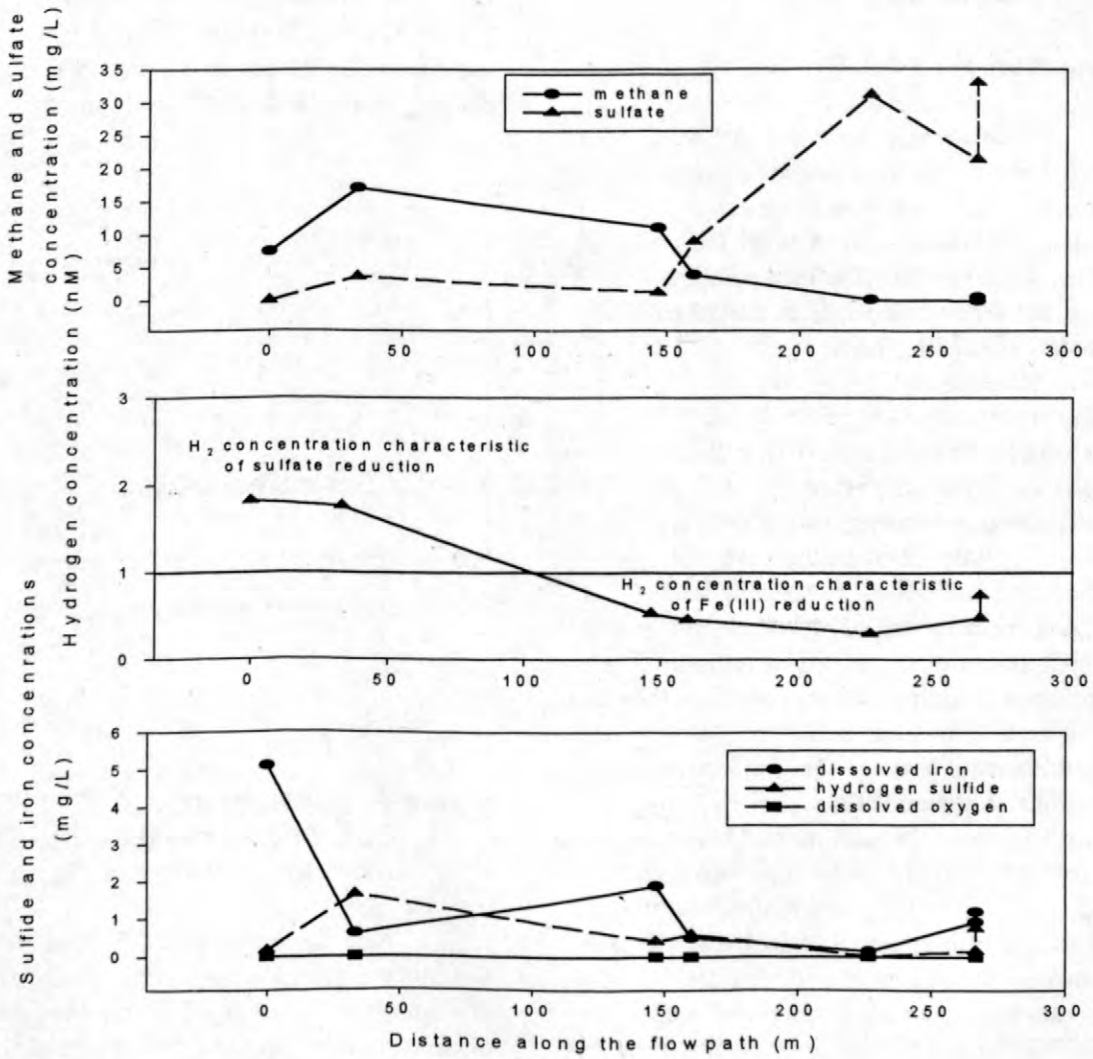

Figure 3.--Redox chemistry of ground water in the contaminant plume.

depth of between 2 and 4 meters, filled with waste, and covered with fill. At some time during waste-disposal operations, PCE was released at the landfill. Two discrete PCE sources were identified by direct-push sampling of ground water and aquifer sediments (Fig. 2) as part of this study. These sources are highly localized suggesting that the contamination events occurred at two discrete times. Emanating from these sources is a discrete plume of chlorinated ethene-contaminated ground water that flows toward Porcupine Lake located adjacent to the landfill (Fig. 2). The geometry and extent of the contaminant plume was previously delineated by direct push methods (ABB Environmental Services, Inc., 1997).

Delineation of Redox Processes

Ground-water chemistry data were used to delineate the distribution of redox processes in the ground-water system underlying and downgradient of the Old Camden Road landfill. The methodology used in this delineation has been described previously (Chapelle, 1996). Concentrations of redox-sensitive parameters dissolved oxygen, methane, sulfate, molecular hydrogen (H_2), sulfide and dissolved iron are plotted versus distance along the flowpath are shown in Figure 3. Sulfate concentrations are relatively low underlying the landfill, while methane concentrations are relatively high. The high methane concentrations indicate the presence of active methanogenesis in the landfill itself. However, measured concentrations of hydrogen (H_2) indicate that sulfate reduction is the predominant redox process in the 11- meter aquifer underlying the landfill, and grades into uniformly Fe(III)-reducing conditions downgradient of the landfill. Concentrations of dissolved sulfide and ferrous iron are consistent with this interpretation, with relatively high concentrations of sulfide underlying the landfill that decrease downgradient. Downgradient of the landfill, concentrations of ferrous iron (1-2 mg/L) are consistent with ongoing Fe(III) reduction. These sequential reducing (sulfate reducing) to more oxidizing (Fe(III) reduction) conditions are favorable for degrading chlorinated ethenes, and would be expected to confer a substantial natural attenuation capacity to the system.

Concentration Changes of Chlorinated Ethenes

Ground-water chemistry data collected by direct push methods in this study (Fig. 2) indicate that PCE is the principal contaminant in the source area, and that PCE is sequentially dechlorinated along the ground-water flowpath. Additional direct-push data (ABB Environmental Services, Inc., 1997) documents contaminant behavior in the plume. Concentrations of PCE, TCE, cis-DCE, and VC within the plume are plotted versus distance along the flowpath in Figure 4.

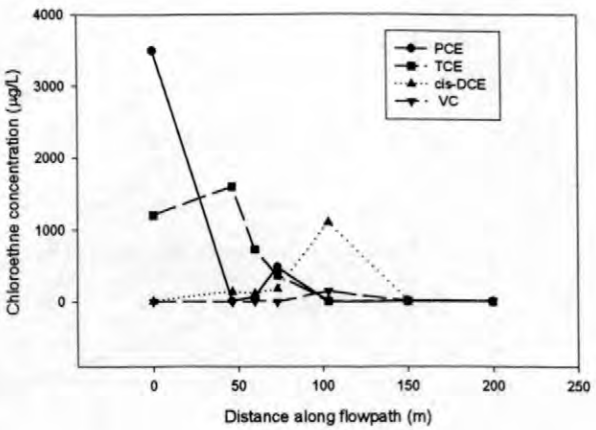

Figure 4. Concentrations of PCE, TCE, cis-DCE, and VC along the flowpath within the contaminant plume.

Near the source areas, PCE and TCE are the only measureable contaminants. By 50 meters downgradient, however, PCE concentrations have decreased to near the detection limit and the principal contaminant is TCE. TCE concentrations decrease along the flowpath and by 100 meters along the flowpath, cis-DCE is the principal contaminant and VC concentrations

increase. By 150 meters along the flowpath, VC is the principal contaminant remaining. These data show that daughter products of reductive dechlorination are actively produced in this system, and are direct evidence of reductive dechlorination in this ground-water system. Furthermore, the decrease of cis-DCE and VC along the flowpath suggests continued reductive biodegradation, the initiation of oxidative biodegradation, or both.

Kinetics of Chlorinated Ethene Biodegradation

The data of Figure 4 can be used to estimate degradation rate constants for individual chlorinated ethenes. Observed decreases in individual chlorinated ethene concentrations with fixed values of v and D* are shown fitted to the

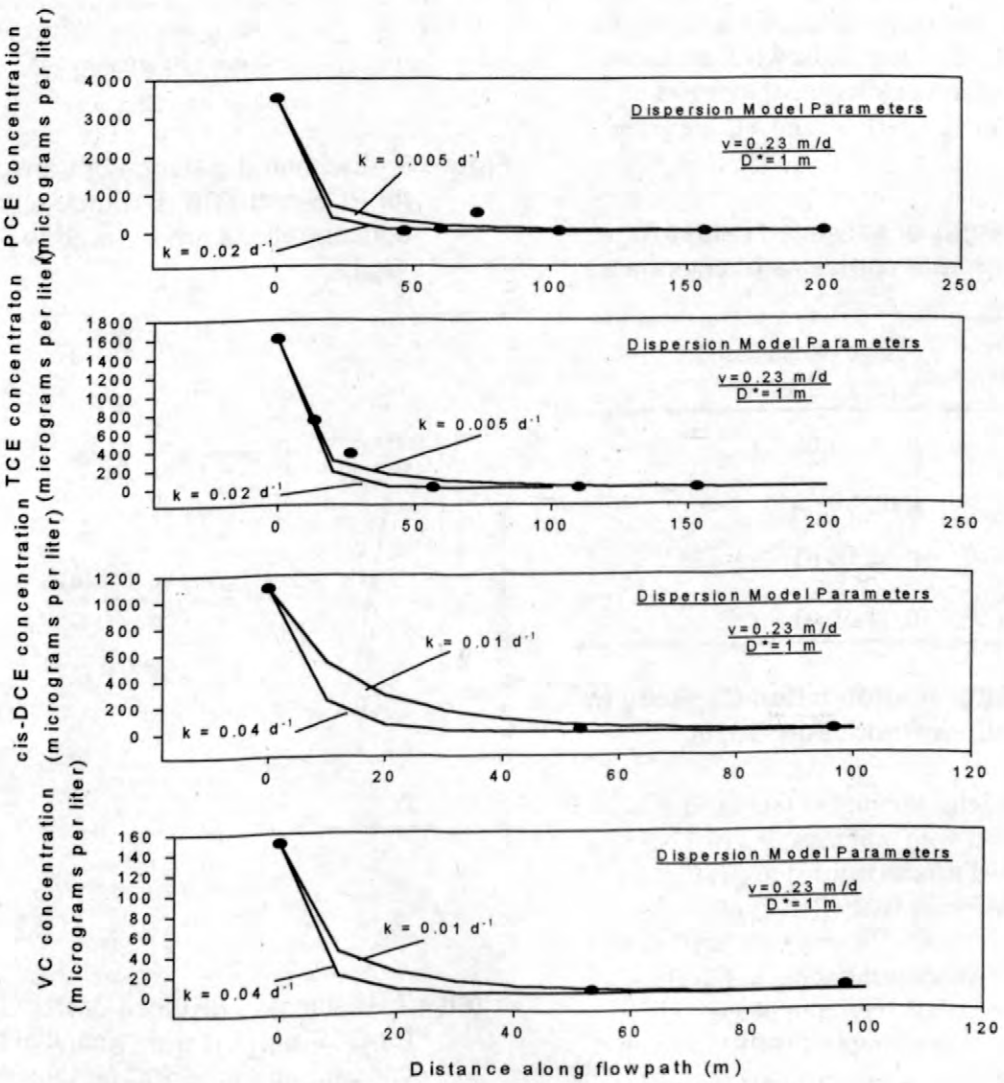

Figure 5.--Estimated values for PCE degradation rate constant and apparent degradation rate constants for TCE, cis-DCE, and VC.

dispersion equation in Figure 5. These individual rate constant estimates were made by curve-fitting only those portions of the concentration profiles where concentrations were declining (Fig. 4). Thus, the PCE curve began at zero distance downgradient, TCE at 50 meters downgradient, and cis-DCE and VC at 100 meters downgradient (Fig. 4). As pointed out previously, this procedure probably underestimates true degradation rate constants. Because ground-water flow velocity estimates have a factor of 2 range (0.23±0.12 m/d), the estimated degradation rate constants also have a range of ± a factor of 2, in addition to the upper and lower k estimates. Values for estimates of k for the chlorinated ethenes PCE, TCE, cis-DCE, and VC are given in Table 1.

Table 1.--Ranges of estimated values for biodegradation rate constants of chlorinated ethenes.

Chlorinated Ethene	Range of estimated k (d^{-1}) values
PCE	0.02 - 0.005
TCE	0.02 - 0.005
cis-DCE	0.04 - 0.01
VC	0.04 - 0.01

Using the Natural Attenuation Capacity to Estimate Source-Reduction Goals

The kinetic parameters estimated in Table 1, together with estimates of v (0.11-.35 m/d) and D* (~1 m) can be used to quantify the natural attenuation capacity (NAC) of this ground-water system. The observed NAC can then be used to estimate distances of travel for each chlorinated ethene given an initial concentrations. For example, if PCE concentrations in the source area are lowered to 100 µg/L by engineered removal, then contaminant concentrations are predicted to be below the 5 µg/L cleanup standard approximately 70 meters along the flowpath (Figure 6). However, because of the uncertainty associated with the parameter

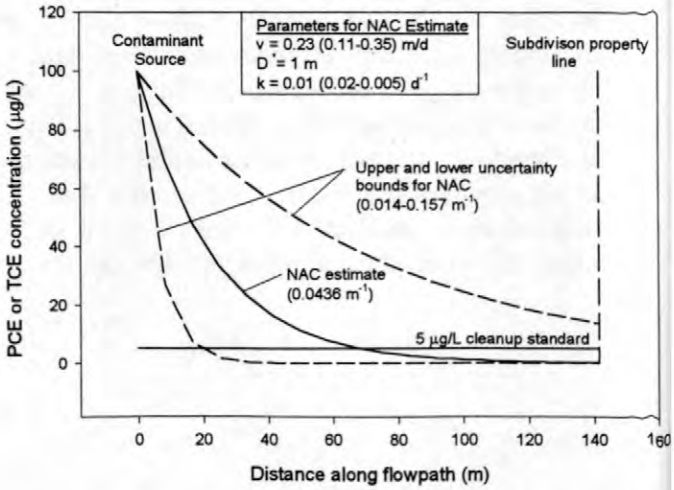

Figure 6.--Estimated distance of transport for PCE and TCE is source area concentrations are lowered to 100 µg/L.

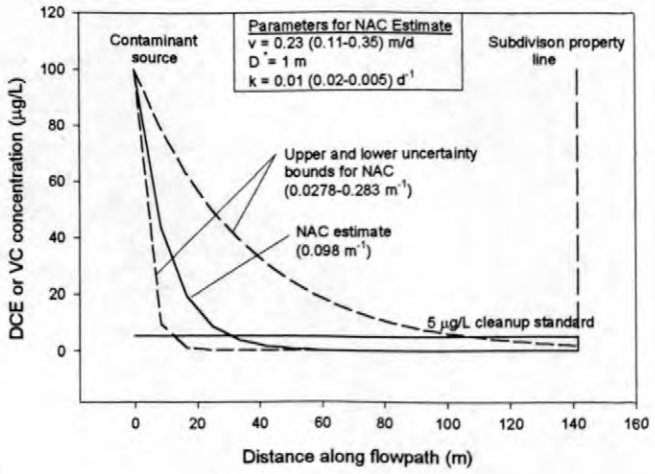

Figure 7.--Estimated distance of transport for DCE and VC from an initial source concentrations of 100 µg/L.

estimates, the cleanup standard may be reached in as little as 20 meters, or as much as 160 meters. Similar estimates can be made for TCE (Fig. 6), or DCE and VC (Fig. 7). For DCE and VC, an initial concentration of 100 µg/L would is

estimated to be lowered below the 5 µg/L cleanup standard in 30 meters. Because of the uncertainty, however, this distance may be as little as 10 meters or as much as 110 meters.

Estimating Ground-water Velocity Decrease Goals

Source reduction is not the only engineering option that can be evaluated by considering the natural attenuation capacity. Pump and treat technology is widely used to contain contaminants from offsite migration (NRC, 1997). One effect of pump and treat is to change the rate that contaminated ground water migrates away from a site. This, in turn, can be used to increase the NAC of a site. Given a fixed biodegradation rate constant (0.01 d^{-1}) and a fixed value of D^* (1 m), decreasing the average velocity of ground water leaving a source area by a factor of two increases the NAC by about the same amount (Fig. 8). Because of this increase in NAC, the 5 µg/L cleanup standard for these individual compounds can be achieved in proportionally less flowpath distance than with unmodified ground-water velocity. Because pump-and-treat is an established technology, increasingthe NAC by lowering ground-water velocity may be an appropriate strategy at some sites.

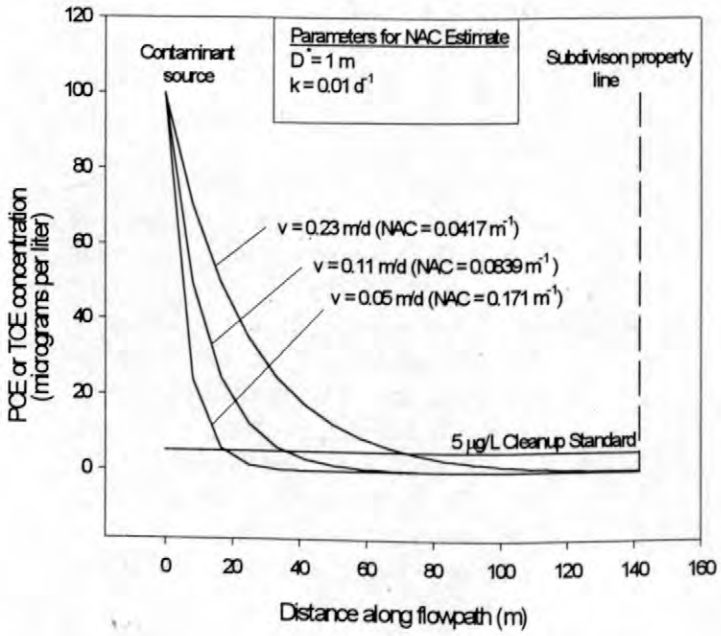

Figure 8.--Estimated distance of transport for PCE and TCE if ground-water velocity away from a source area are decreased from 0.23 to 0.05 m/d.

CONCLUSIONS

The ground-water system underlying the Kings Bay site grades from relatively reducing (sulfate-reducing) to more oxidizing (Fe(III)-reducing) conditions. In the zone of sulfate reduction, PCE and TCE are rapidly dechlorinated to cis-DCE and VC. In the Fe(III)-reducing zone, cis-DCE and VC are oxidized to carbon dioxide and chloride. This sequence of redox conditions results in efficient contaminant biodegradation and gives the ground-water system a substantial natural attenuation capacity for chlorinated ethenes. Despite this natural attenuation capacity, ground water containing concentrations of chlorinated ethenes higher than regulatory limits leaves the site and migrates to a nearby point of compliance. This, in turn, necessitates engineered remediation in order to achieve the required site remediation. A kinetic assessment of the natural attenuation capacity indicates that concentrations of PCE and TCE must be lowered below 100 µg/L at least 70 meters from the point of compliance, and that concentrations of DCE and VC must be lowered below 100 µg/L at least 30 meters from the point of compliance. Because the natural attenuation capacity of a system can be increased by decreasing rates of ground-water flow away from a source area, remediation goals can also be accomplished using conventional pump-and-treat technology.

ACKNOWLEDGMENTS

This research was funded jointly by Southern Division, Naval Facilities Engineering Command and the Toxic Substances Hydrology Program. The authors would like to thank Stephen P. Garabedian for a thorough technical review.

REFERENCES

ABB Environmental Services, 1997. Summary of 1997 focused groundwater investigations, Site 11, Old Camden County Landfill, 32 pp. Prepared for Southern Division, Naval Facilities Engineering Command, North Charleston, SC.

Bouwer, E. J., 1994., Bioremediation of Chlorinated Solvents using Alternate Electron Acceptors. In: Handbook of Bioremediation, p. 149-175. Boca Raton, FL: Lewis Publishers.

Bradley, P.M. and Chapelle, F.H., 1996. Anaerobic Mineralization of Vinyl Chloride in Fe(III)-reducing Aquifer Sediments. Environmental Science and Technology 30: 2084-2086.

Buscheck. T.E., and Alcantar, C.M., 1995, Regression Techniques and Analytical Solutions to Demonstrate Intrinsic Bioremediation. In: Proceedings of the 1995 Battelle International Conference on In-situ and On Site Bioreclaimation, p. 109-116. (Hinchee, R.E., Wilson, J.T., and Downey, D.C., Eds.) Columbus, OH: Battelle Press.

Chapelle, F.H., 1996, Identifying Redox Conditions that Favor the Natural Attenuation of Chlorinated Ethenes in Contaminated Ground-Water Systems. Symposium on Natural Attenuation of Chlorinated Organics in Ground Water, p. 17-20. EPA/540/R-96/509.

Chapelle, F.H., Bradley, P.M, Lovley, D.R., and Vroblesky, D.A., 1996, Measuring Rates of Biodegradtion in a Contaminated Aquifer using Field and Laboratory Methods. Ground Water 34: 691-698.

Chapra, S.C. 1996. Surface Water-Quality Monitoring, 844 pp. New York, NY: McGraw Hill.

Charbeneau, R.J. and Daniel, D.E., 1993. Contaminant Transport in Unsaturated Flow, In: Handbook of Hydrology, p 15.1 (Maidment, D.R. Ed.). New York, NY: McGraw-Hill.

Cherry, J.A. 1996. Conceptual Models for Chlorinated Solvent Plumes and Their Relevance to Intrinsic Remediation. Symposium on Natural Attenuation of Chlorinated Organics in Ground Water, p. 29-30. EPA/540/R-96/509.

Cox, E., Edwards, E., Lehmicke, L., and Major, D., 1995, Intrinsic Biodegradation of Trichloroethene and Trichloroethane in a Sequential Anaerobic-Aerobic Aquifer, In: Proceedings of the 1995 Battelle International Conference on In-situ and On Site Bioreclaimation, p. 223-231. (Hinchee, R.E., Wilson, J.T., and Downey, D.C., Eds.) Columbus, OH: Battelle Press.

Freeze, R.A. and Cherry, J.A. 1979. Groundwater, p. 554. Englewood Cliffs, New Jersey, Prentice-Hall, Inc.

Gelhar, L.W., Welty, C., and Rehfeldt, K.R. 1992. A Critical Review of Data on Field-Scale Dispersion in Aquifers. Water Resources Research 28: 955-1974.

McCarty, P.L. and Semprini, L., 1994 Ground-Water Treatment for Chlorinated Solvents, In: Handbook of Bioremediation, Boca Raton, FL: Lewis Publishers.

Newell, C.J., McLeod, R.K., and Gonzales, J.R., 1996, The BIOSCREEN Computer Tool. Symposium on Natural Attenuation of Chlorinated Organics in Ground Water, p. 60-63. EPA/540/R-96-509.

Rifai, H.S., Borden, R.C., Wilson, J.T., and Ward, C.H. 1995, Intrinsic Bioattenuation for Subsurface Restoration. In: Proceedings of the 1995 Battelle International Conference on In-situ and On Site Bioreclaimation, p. 1-31. (Hinchee, R.E., Wilson, J.T., and Downey, D.C., Eds.) Columbus, OH: Battelle Press.

Smatlak, C. R. Gossett, J. M. Zinder, S. H., 1996. Comparative Kinetics of Hydrogen Utilization for Reductive Dechlorination of Tetrachloroethene and Methanogenesis in an Anaerobic Enrichment Culture. Environmental Science and Technology 30: 2850-2858.

U.S. EPA Office of Solid Waste and Emergency Response Directive 9200.4-17, 1997. Use of Monitored Natural Attenuation at Superfund, RCRA Corrective Action, and Underground Storage Tanks, 42 pp.

Vogel, T.M.,Criddle, C.S., and McCarty, P.L., 1987. Transformation of Halogenated Aliphatic Compounds. Applied Environmental Microbiolology 21:722-737.

Weaver, J.W., Wilson, J.T., and Kampbell, D.H. 1996. Extraction of Degradation Rate Constants from the St. Joseph, Michigan, Trichloroethene Site. Symposium on Natural Attenuation of Chlorinated Organics in Ground Water, p. 69-73. EPA/540/R-96-509.

Wiedemeier, T.H., Swanson, M.A., Moutoux, D.E., Gordon, E.K., Wilson, J.T., Wilson, B.H.,Kampbell, D.H., Hansen, J.E., Haas, P. and Chapelle, F.H. 1997. Technical Protocol for Evaluating Natural Attenuation of Chlorinated Solvents in Ground Water. p 1-5. Air Force Center for Environmental Excellence, Brooks Air Force Base, San Antonio, TX.

Sampling Throughout The Hydrologic Cycle To Characterize Sources Of Volatile Organic Compounds In Ground Water

By Arthur L. Baehr, Leon J. Kauffman, Emmanuel G. Charles, Ronald J. Baker, Paul E. Stackelberg, Mark A. Ayers, and Otto S. Zapecza U.S. Geological Survey, West Trenton, New Jersey

ABSTRACT

Results of three studies in New Jersey demonstrate that analysis of samples collected throughout the hydrologic cycle can improve understanding of the sources of volatile organic compounds (VOCs) in ambient ground water. Results of the first study indicate that atmospheric concentrations of methyl-tert butyl ether (MTBE) are sufficiently high to cause detection in ground water, whereas atmospheric concentrations of the chlorinated VOCs trichloromethane (chloroform), 1,1,1-trichloroethane (TCA), and tetrachloroethene (PCE) are not. Results of analysis of unsaturated-zone gas and ground-water samples indicate that point sources of MTBE, such as spills or infiltration of urban runoff, are also prevalent and that these are the only possible sources of the chlorinated compounds. In the second study, VOC concentrations in three ground-water monitoring networks in a surficial aquifer were compared. Although it was anticipated that deeper ground water from the public supply wells would be associated with less frequent detections and lower concentrations of VOCs than water from the shallower observation wells, the opposite was found for many chlorinated VOCs. The integration of chlorinated VOCs from multiple point sources within the larger contributing areas of the public supply wells may explain this result. Chloroform, however, is detected frequently throughout the ground-water- monitoring network, indicating that its sources are widespread. MTBE is detected less frequently in observation wells that tap 10- to 15-year-old ground water than in shallow observation wells that tap recently recharged ground water and public supply wells. This result is not contradictory because some of the ground water in a given sample from a public supply well would have been recharged during the past 10 years, a period of increased MTBE use due to oxygenated-fuel programs. In the third study, the occurrence of MTBE in a lake, caused by the use of gasoline-powered watercraft, may explain the frequent occurrence of MTBE in samples from lakeside wells in the fractured-rock aquifer. The probable lake/well interaction complicates investigations of ground-water contamination with MTBE due to fuel spillage because of the difficulty of determining point-source plume dimensions with a nonpoint-source signature superimposed on the ground water.

INTRODUCTION

Research conducted as part of the U.S. Geological Survey (USGS) Toxic Substances Hydrology Program on the physical, chemical, and microbial processes that define the movement and attenuation of volatile organic compounds (VOCs) in ground water has improved understanding of the evolution of plumes originating from known sources. Even with advanced capability to predict the migration of plumes, however, it is impossible to assess the effects of all VOC releases on regional ground-water quality because of the existence of undiscovered point and nonpoint sources.

Results of work conducted as part of the USGS National Water Quality Assessment Program (NAWQA) indicate that VOCs such as trichloromethane (chloroform), methyl-tert butyl ether (MTBE), 1,1,1-trichloroethane (TCA), and tetrachloroethene (PCE) are detected frequently in shallow ground water in urban areas across the

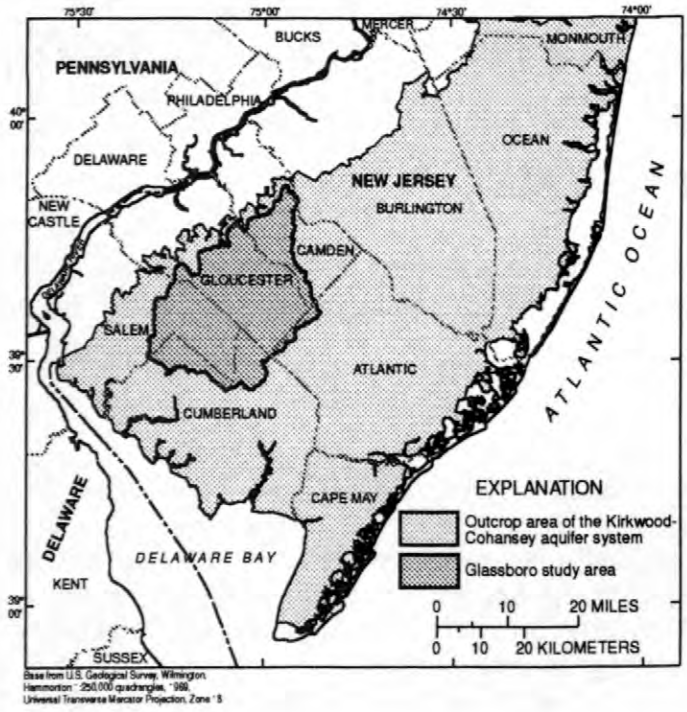

Figure 1. Location of the Glassboro study area in southern New Jersey.

Nation (Squillace and others, 1996). These findings raise many questions: What are the sources of thesecompounds, and will their concentrations increase? What is the relevance of these VOC detections to the quality of the ground-water supply? What is the ultimate fate of the contaminants? In order to begin to answer these questions, comprehensive regional-scale characterization of the distribution, movement, and attenuation of contaminants in relevant components of the hydrologic cycle is needed. This paper presents three examples of results of studies in New Jersey that demonstrate that analysis of samples collected throughout the hydrologic cycle can improve understanding of the sources and distribution of VOCs in ground water at spatial scales relevant to water supplies.

VOLATILE ORGANIC COMPOUNDS IN SHALLOW GROUND WATER, THE ATMOSPHERE, AND THE UNSATURATED ZONE

A network of 78 shallow monitoring wells was installed over a 380-square-mile study area (fig. 1), referred to as the Glassboro study area, as part of the NAWQA study of the Long Island-New Jersey Coastal Plain. This network is referred to as the land-use survey (LUS) wells because the objective of sampling these wells is to determine the quality of recently recharged ground water as a function of land use. Each well was screened over a 2-ft (foot) interval about 10 ft below the water table in the surficial Kirkwood-Cohansey aquifer system. Wells were located in agricultural, new-urban (residential and commercial development less than 25 years old), old-urban (urban development more than 25 years old), and undeveloped areas. Well locations in each land-use setting were selected randomly in an attempt to minimize bias and to ensure that data collected from the network would be representative of conditions across the study area. The locations of the LUS wells and other monitoring sites discussed in this paper are shown in figure 2.

Seventy-two of the wells were sampled from September 1 to December 31, 1996; the remaining 6 wells were sampled in November 1997. Samples from each well were analyzed for nutrients, pesticides, and VOCs (Stackelberg and others, 1997). The most frequently detected VOCs were chloroform, MTBE, TCA, and PCE. Carbon disulfide (not a VOC) also was frequently detected.

Atmospheric samples are collected at three sites in the Glassboro study area. The sites represent conditions of heavy, intermediate, and light vehicular traffic. Atmospheric samples are collected once every 12 days at each site and have been analyzed for VOCs at the Oregon Graduate Institute (OGI) since April 1997. Samples are collected approximately 6 ft above land surface by drawing air intermittently through a sorbent cartridge with a programmable pump over a 24-hour period. The cartridges are shipped to OGI, where VOC concentrations are determined by using a method of thermal desorption and gas chromatography/mass spectroscopy (GC/MS) detection. This method (Pankow and others, 1998) was developed by OGI for the USGS to provide atmospheric and unsatur-

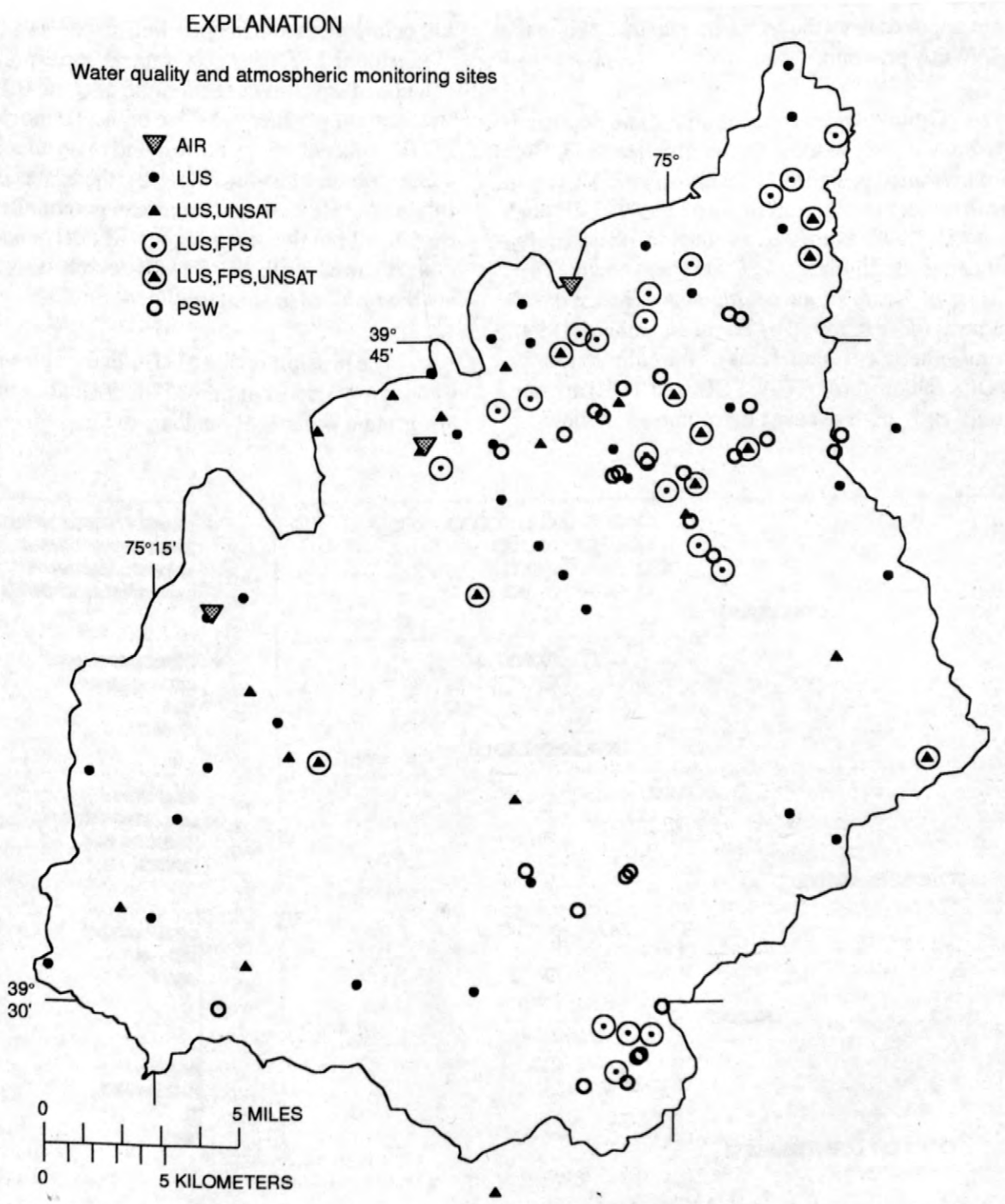

Figure 2. Location of atmospheric monitoring sites (AIR), land-use survey (LUS) and flow-path study (FPS) monitoring wells, unsaturated-zone-gas and shallow-ground-water monitoring sites (UNSAT), and public supply wells (PSW) in the Glassboro study area, New Jersey.

ated-zone-gas concentration data for a list of VOCs that approximates the VOC analyte list used in the NAWQA program.

Ground-water concentrations and detection frequencies of the most frequently detected VOCs are presented in figure 3 . Atmospheric VOC concentrations measured from April 29, 1997, through June 25, 1998, expressed as aqueous-phase equivalent concentrations at 15 °C also are shown. The values of Henry's Law coefficients used are the same as those reported by Baehr and others (1999). Atmospheric concentrations of the chlorinated VOCs (chloroform, TCA, PCE, and TCE) are not sufficiently high to cause detections in shallow ground water, as their aqueous-phase equivalents are below method detection limits. Median-level atmospheric MTBE concentrations correspond to a calculated aqueous concentration of about 0.1 µg/L (microgram per liter), and the highest atmospheric MTBE concentrations correspond to an aqueous concentration of about 1.0 µg/L; therefore, atmospheric MTBE concentrations can potentially explain all but the seven highest MTBE concentrations reported for the LUS wells, which most likely are the result of gasoline spills.

The possibility that MTBE in the atmosphere is the cause of most of the MTBE detections in shallow ground water is of fundamental importance. If

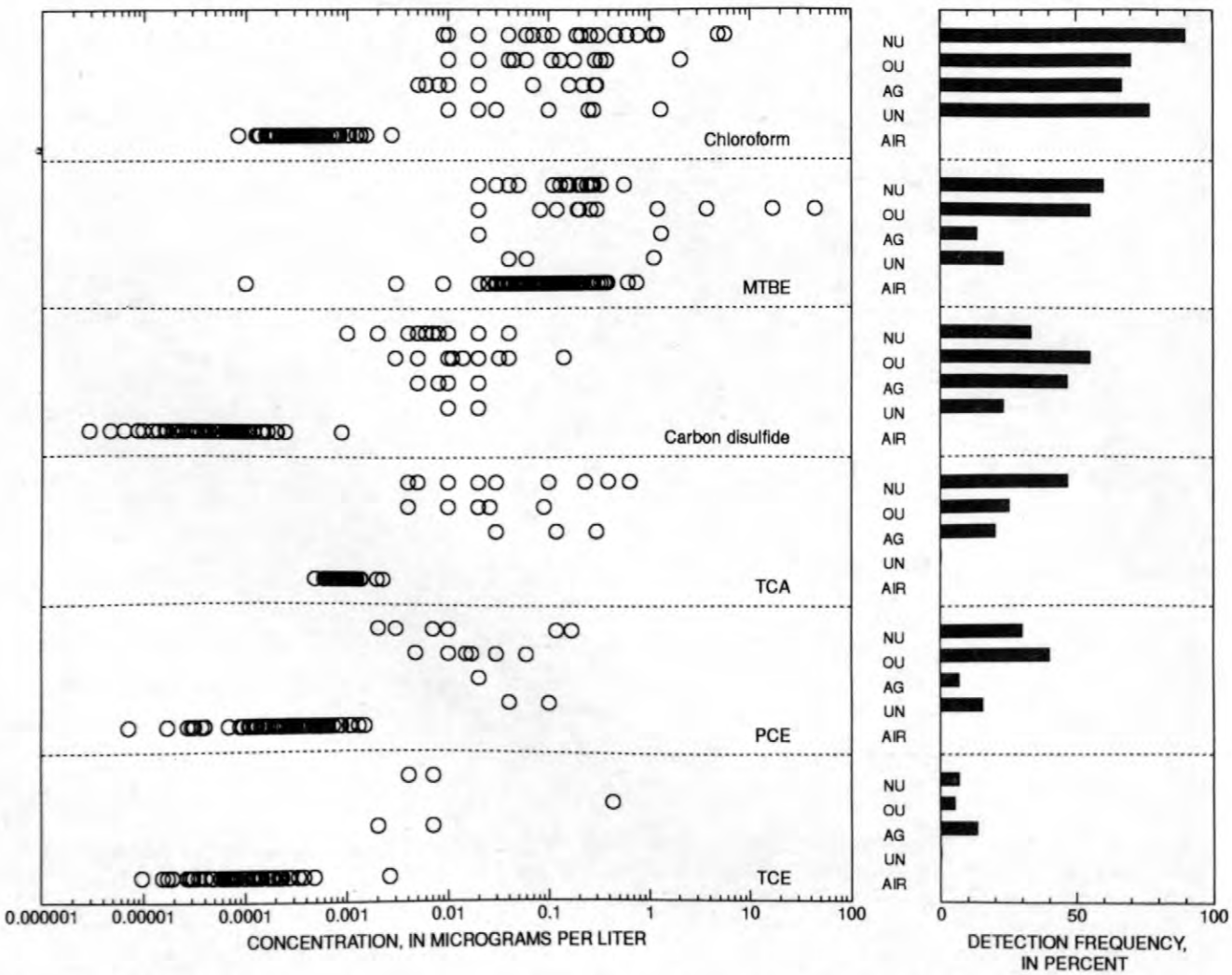

Figure 3. Volatile-organic-compound concentrations and detection frequencies in samples collected from land-use survey wells and atmospheric aqueous-phase equivalent concentrations, Glassboro study area, New Jersey. (NU, new urban; OU, old urban; AG, agricultural; UN, undeveloped; AIR, atmosphere)

low concentrations are the result of evolving plumes emanating from point sources, then MTBE concentrations theoretically could increase with time because the source concentrations from spills of oxygenated gasoline could be on the order of grams per liter. If the source is the atmosphere, however, then changes in MTBE concentrations in ground water over time would be constrained, and concentrations would remain low and proportional to atmospheric concentrations (Baehr and others, 1999).

Concentrations of VOCs in unsaturated-zone gas in the Glassboro study area provide additional information to help understand the sources and movement of these compounds. When installed, nearly all of the 78 LUS wells were instrumented with an unsaturated-zone-gas sampling probe and a shallow-ground-water sampling probe in addition to the standard 2-inch well (fig. 4). The unsaturated-zone gas probes typically are situated about 3 ft above the water table. The shallow-ground-water sampling probes typically are situated about 3 ft below the water table. Twenty-five sites were selected for simultaneous sampling of unsaturated-zone gas and shallow ground water. Some sites in each of the three land-use areas were included to ensure that the samples collected would be representative of conditions across the Glassboro study area. The minimum, median, and maximum depths to the water table at these 25 sites were 6, 12, and 23 ft, respectively. The 25 unsaturated-zone probes and corresponding shallow-ground-water probes were sampled from August to December 1997. Unsaturated-zone gas was sampled before shallow ground water so that the established unsaturated-zone gas profile would not be disturbed. Unsaturated-zone gas samples were obtained by connecting a sorbent cartridge to the vapor probe and drawing unsaturated-zone gas through the cartridge with a peristaltic pump. Cartridges were analyzed at OGI as previously described, with minor modifications for eliminating moisture accumulated in the cartridge as a result of the high relative humidity of unsaturated-zone gas. The shallow-ground-water sample was collected within 1 day of the unsaturated-zone-gas sample by filling 40-mL (milliliter) vials by using a peristaltic pump. These samples were analyzed at the USGS National Water Quality Laboratory (NWQL) in Arvada, Colo., by purge-and-trap GC/MS methods (Connor and others, 1998). This method of water analysis was the same as that used for samples from the 78 LUS wells.

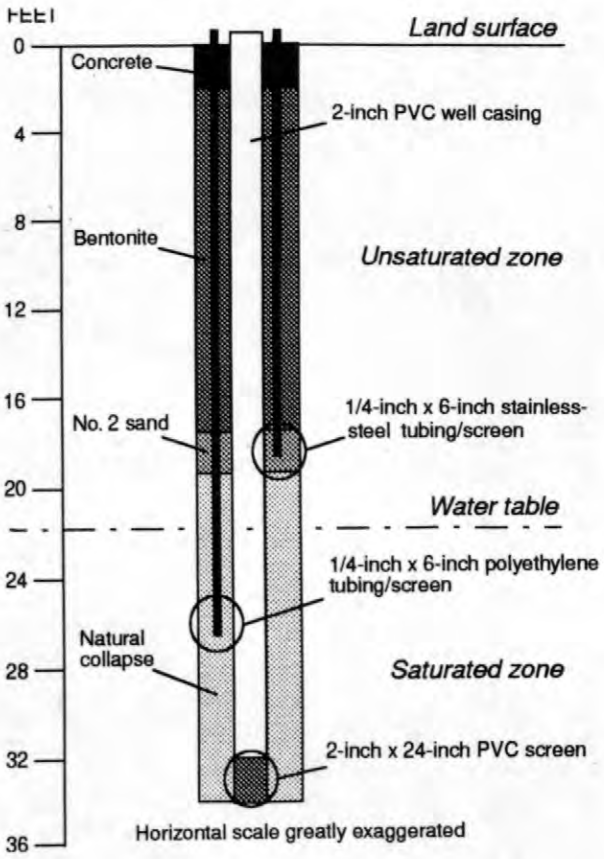

Figure 4. Typical installation of a shallow-ground-water observation well with attached probes for sampling very shallow ground water and unsaturated-zone gas.

Equivalent pore-water concentrations calculated from results of analysis of unsaturated- zone-gas samples for MTBE, PCE, chloroform, and TCA and the corresponding concentrations in shallow ground water at the 25 sites are shown in figure 5. Boxplots of atmospheric concentrations of these compounds expressed as equivalent aqueous-phase concentrations also are provided for comparison.

MTBE was detected in samples of shallow ground water from 7 of the 25 sites (28 percent). At the three sites where MTBE concentrations were highest, the concentration was greater than both the calculated unsaturated-zone concentration and the atmospheric concentration range. On the basis of the concentration gradient, the net movement of MTBE at these sites is upward across the water

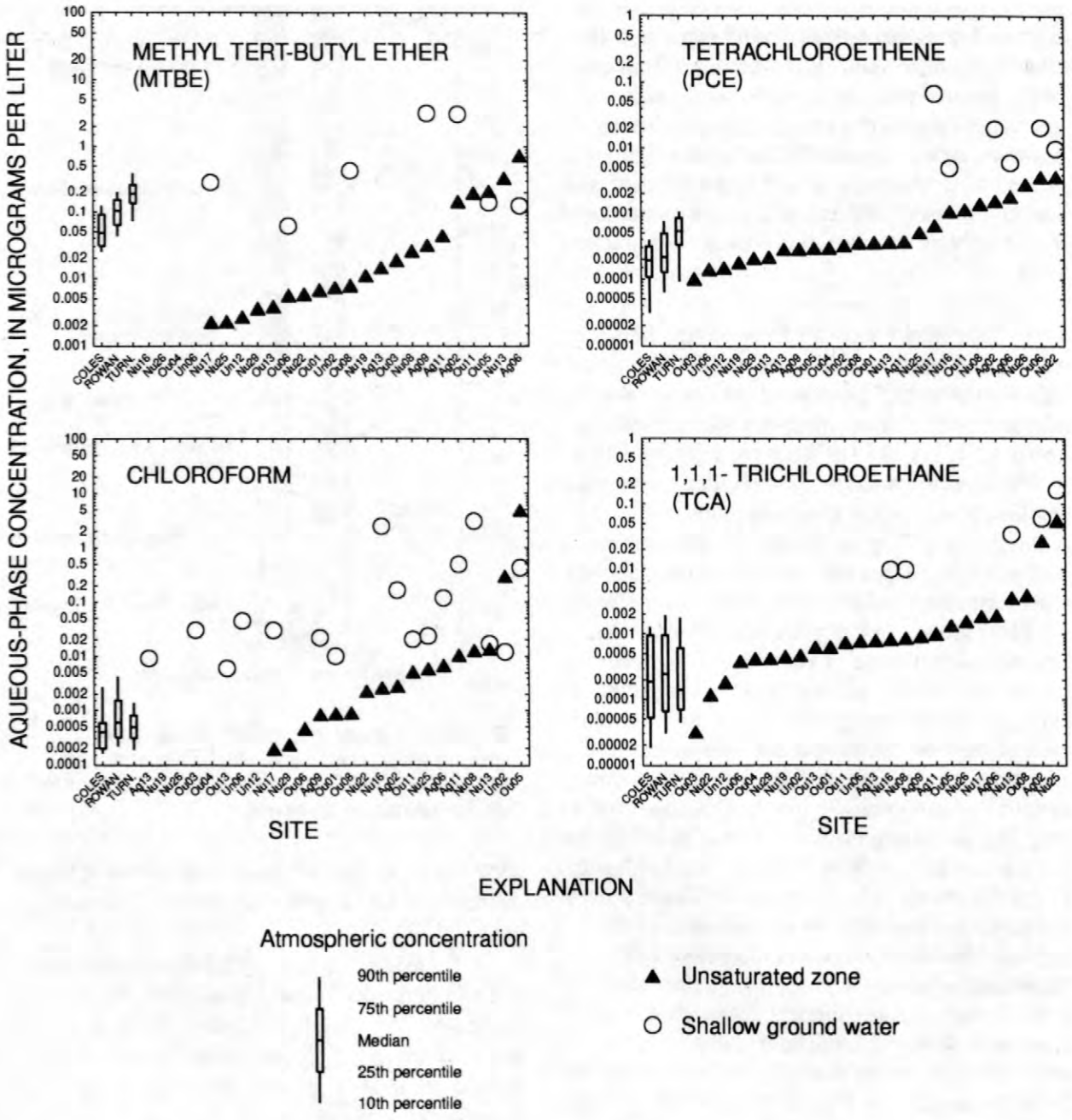

Figure 5. Distribution of MTBE, PCE, chloroform, and TCA in the atmosphere, unsaturated zone, and shallow ground water, Glassboro study area, New Jersey.

table, indicating that MTBE is outgassing or volatilizing from ground water to the unsaturated zone. The source of MTBE at these three sites is likely a gasoline spill and MTBE migrated to the site as a solute in ground water. At two sites, concentrations in ground water were lower than the calculated unsaturated-zone aqueous concentration, but within the atmospheric concentration range. The net movement of MTBE at these sites, therefore, is downward across the water table, with the atmosphere the likely source. At the remaining two sites where MTBE was detected in shallow ground water, the ground-water concentration was greater than the calculated unsaturated-zone aqueous concentration. This situation also indicates outgassing from ground water. The MTBE source could be a

distant gasoline spill or runoff from paved surfaces that eventually infiltrated to ground water; however, the atmospheric source cannot be ruled out because recharge could occur upgradient.

In contrast, the distributions of PCE and TCA indicate a consistent and simpler explanation for movement across the water table. At all six sites (24 percent) where PCE was detected and all five sites (20 percent) where TCA was detected in ground water, the concentrations in ground water were greater than those that could be attributed to the atmosphere. PCE and TCA outgassing therefore is indicative of an upgradient source and migration of each of these compounds to the site as a solute in ground water.

The frequent detection of chloroform in ground water at 17 of the sites (68 percent) is attributed to a more widespread source (discussed below). At 14 of the 17 sites where chloroform was detected in ground water, the concentration gradient across the water table indicates outgassing and, therefore, the source was upgradient and chloroform migrated to the site as a solute in ground water. At three sites the direction of chloroform movement was downward, indicating that the source most likely was nearby at land surface or within the unsaturated zone.

COMPARISON OF VOLATILE ORGANIC COMPOUNDS IN THREE GROUND-WATER MONITORING NETWORKS

The outcrop of the surficial Kirkwood-Cohansey aquifer system forms the western boundary of the study area. The aquifer thickens toward the southeast to a maximum thickness of about 200 ft within the study area. The base of the surficial Kirkwood-Cohansey aquifer system is formed by a thick confining unit. Because the sediments that comprise the aquifer are highly permeable, it is vulnerable to contamination from the land surface in developed parts of the study area, which are expanding rapidly as a result of population growth.

In addition to the LUS network, designed to assess the quality of the youngest ground water, 30 monitoring wells were installed at intermediate depths in the surficial aquifer as part of the NAWQA study of water quality in the Kirkwood-Cohansey aquifer system in the Glassboro study area. These wells have 2-ft screened intervals, typically 30 to 40 ft below the water table. The well depth at each location was selected to sample ground water predicted with a regional ground-water-flow model to be 10 to 15 years old. These wells, referred to as flow-path study (FPS) wells, were colocated with a new-urban or old-urban LUS well. The FPS wells were sampled in November 1997.

The ground-water monitoring network also includes 30 public supply wells (PSWs) in the Glassboro study area that are screened in the surficial Kirkwood-Cohansey aquifer system. Most of the PSWs are in new-urban or old-urban land use areas. The minimum, median, and maximum depths from land surface to the top of the screened interval for the 30 PSWs sampled are 50, 100, and 151 ft, respectively, and the screened interval typically is about 30 ft. From February to March 1998, untreated (raw) water was collected from 20 of these PSWs; the remaining 10 PSWs were sampled in December 1998.

VOC concentrations and detection frequencies in samples collected from the three classes of wells are summarized in figure 6. Only data from 50 of the 78 LUS wells that are located in new-urban or old-urban land-use areas are plotted because these land uses predominate in the vicinity of the 30 PSW and 30 FPS wells. Before sampling, it was anticipated that the PSWs would be associated with less frequent VOC detections and lower concentrations because of older water, longer flow paths, and natural attenuation of contaminants. The frequency of detection of many chlorinated VOCs (including TCA, PCE, and TCE), however, was significantly higher in the PSWs than in both LUS and FPS wells. Some chlorinated VOCs (including carbon tetrachloride, cis-1,2-dichloroethene, 1,2-dibromomethane, and trans-1,2- dichloroethene) were detected frequently in PSWs but rarely in LUS and FPS wells. This may indicate that the larger contributing area (the area at the land surface that contributes water to a well) of a PSW integrated a sufficient number of sources of these less frequently used VOCs to cause detection. Chemical transformation of parent VOCs along extended flow paths

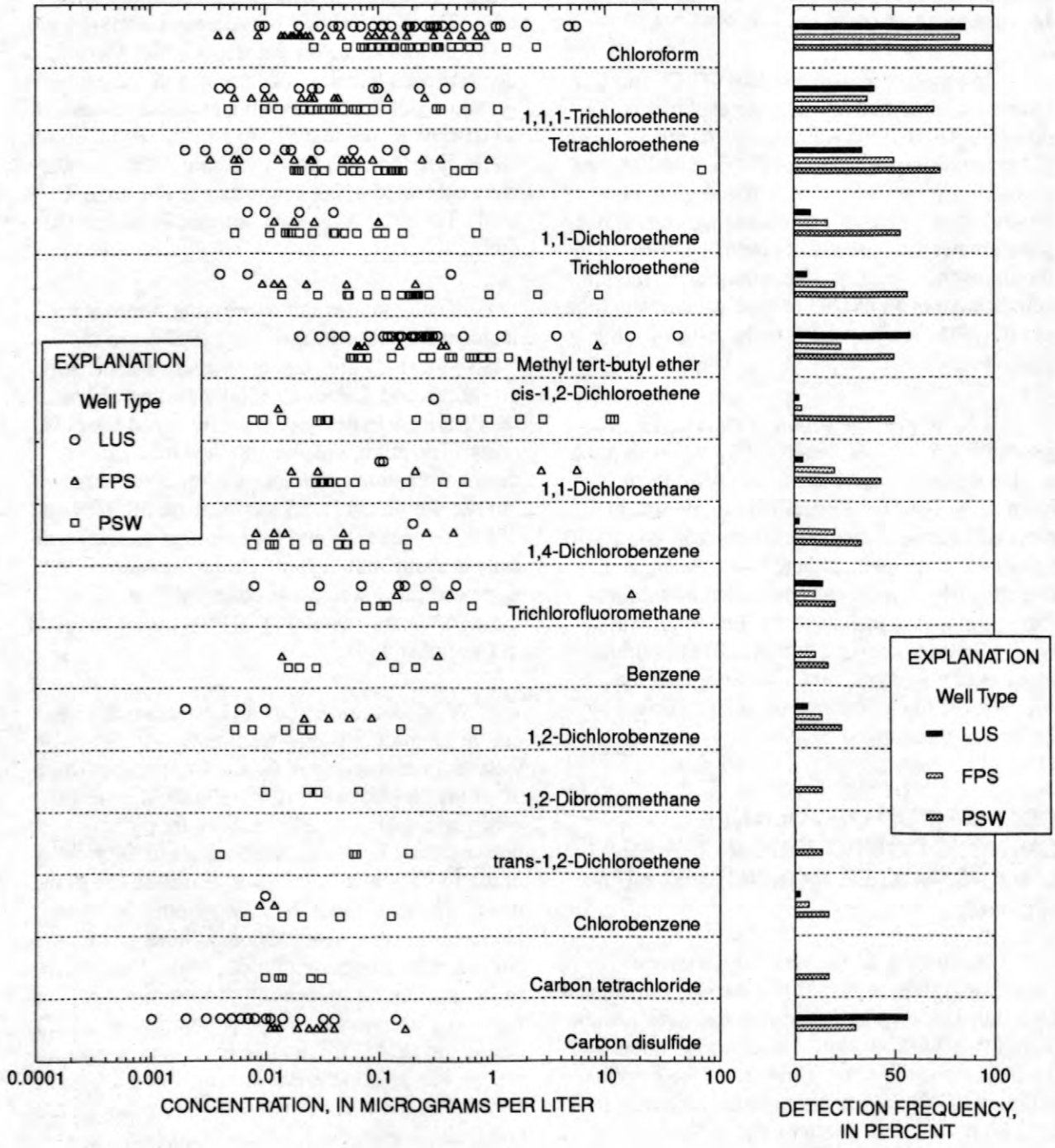

Figure 6. Distribution of volatile-organic-compound concentrations and detection frequencies in samples from land-use survey (LUS), flow-path study (FPS), and public supply wells (PSW), Glassboro study area, New Jersey.

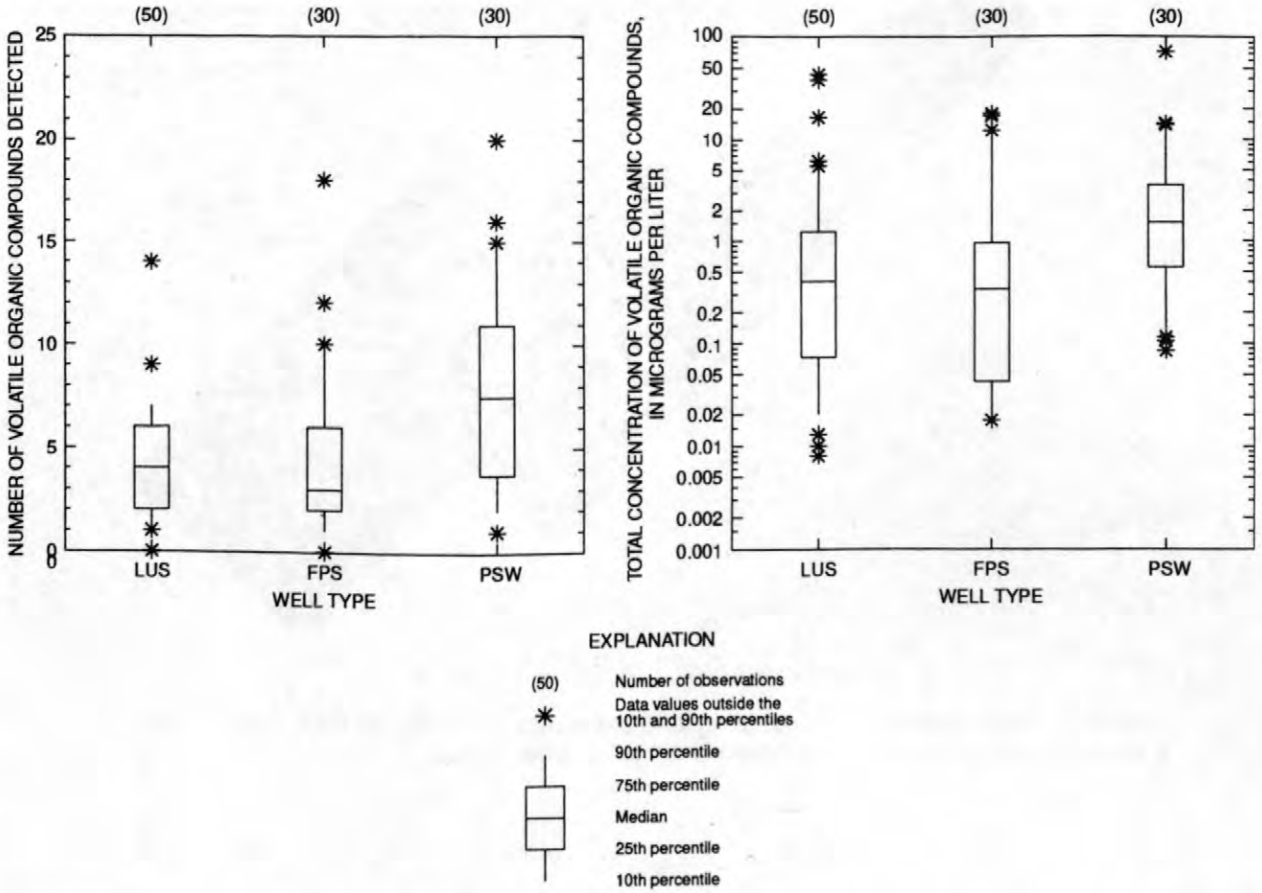

Figure 7a. Distribution of the number of volatile organic compounds detected per sample in the land-use survey (LUS), flow-path study (FPS), and public supply wells (PSW), Glassboro study area, New Jersey.

Figure 7b. Distribution of total volatile-organic-compound concentration per sample in the land-use survey (LUS), flow-path study (FPS), and public supply wells (PSW), Glassboro study area, New Jersey.

also may explain, in part, the occurrence of these VOCs in PSWs. When all VOCs are considered in aggregate, the number of VOCs per sample (fig. 7a) and the total VOC concentration per sample (fig. 7b) are significantly higher in PSWs than in LUS and FPS observation wells. (As in figure 6, only data from 50 of the 78 LUS wells are plotted in figures 7a and 7b.)

The PSW contributing areas are proportional in size to water use and vary widely among the 30 PSWs sampled. A typical contributing area, given a regional recharge rate of 17 inches per year, is about 200 acres for a well producing 100 million gallons per year (17 inches per year multiplied by 200 acres equals approximately 100 million gallons per year). An aerial photograph illustrating land uses within the contributing area of a typical PSW is shown in figure 8a. The contributing area was estimated with a ground-water flow model by applying particle tracking. The model also was used to demonstrate that water entering the well is a blend of very young water from the part of the contributing area nearest the well and older water from the outer extent of the contributing area. The ground-water flow model's particle-tracking application was used to predict the time required for ground water to travel from the point of recharge to the well throughout the contributing area (fig. 8b). The median age of ground water in this typical con-

Figure 8a. Aerial photograph illustrating land-use variability within the contributing area of a typical public supply well, Glassboro study area, New Jersey.

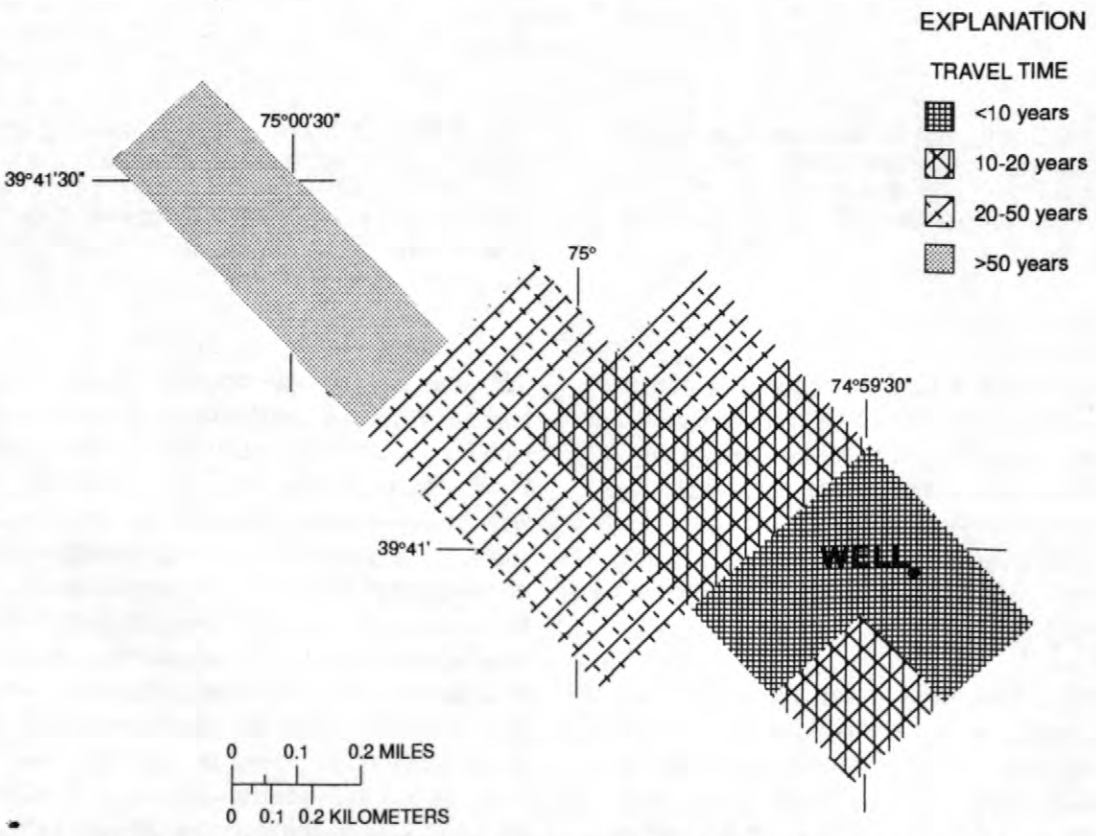

Figure 8b Map of time of travel from point of recharge to well within the contributing area of a typical public supply well , Glassboro study area, New Jersey.

tributing area is estimated to be 20 years, with 25 percent of the ground water entering the well being less than 10 years old, 25 percent between 10 and 20 years old, 30 percent between 20 and 50 years old, and 20 percent more than 50 years old. In contrast to PSWs, observation wells such as the LUS and FPS wells have very small contributing areas and, therefore, yield water that was recharged over a small area and that is essentially of a discrete age rather than a blend of water of different ages. Sampling domestic wells in the study area would provide data from another class of observation wells with contributing areas that are smaller than those of PSWs but larger than those of LUS and FPS wells.

Concentrations and detection frequencies of the two most frequently detected VOCs in the ground-water monitoring network, chloroform and MTBE, require different explanations (fig. 6). Chloroform was detected frequently throughout the monitoring network. The sources of chloroform, therefore, are thought to be widespread. For example, chloroform could be formed during the treatment of drinking water and then subsequently could enter ground water through recharge from septic tanks and irrigation of crops and lawns. Chloroform also can be produced naturally in the subsurface (Hoekstra and others, 1998), although it is uncertain whether this source can account for the detection frequencies and concentrations observed. Chloroform, like other chlorinated VOCs, is used in industry. Because of its frequent detection in water samples, a study was conducted as part of the NAWQA program to assess whether frequent chloroform detection is caused by sample preservation with hydrochloric acid (Squillace and others, in press). Results showed that such chloroform production is minor and, therefore, chloroform detections can be attributed largely to the environment.

MTBE was detected less frequently in the FPS wells than in the LUS wells and PSWs. Use of MTBE as a gasoline oxygenate did not increase until after 1992 in response to changes in the Clean Air Act and, consequently, MTBE would be expected to occur less frequently in 10- to 15-year-old ground water (FPS) than in recently recharged ground water (LUS). The higher detection frequency of MTBE in the PSW network is not contradictory, however, because a significant percentage of ground water in a given sample from a PSW would be less than 10 years old and may have intercepted both point sources and areas of high traffic density that could contribute to MTBE loading from the atmosphere. Regardless of the mechanisms, however, these results emphasize the vulnerability of the surficial aquifer to contamination, as the water pumped from PSWs includes the youngest water in the aquifer, which is in contact with developing VOC sources.

MTBE IN LAKES AND POSSIBLE EFFECTS ON GROUND-WATER SUPPLY

In the summer of 1998, MTBE concentrations in samples collected from Cranberry Lake and Lake Lackawanna in Sussex County, N.J., were as high as 29 and 14 µg/L , respectively. Although other VOCs were detected as well, concentrations of MTBE were by far the highest. These concentrations are among the highest observed in ground- and surface-water surveys conducted by USGS and are of concern, as the U.S. Environmental Protection Agency has classified MTBE as a possible human carcinogen and has issued a drinking-water advisory based on the aesthetic concerns of taste and odor of 20 to 40 µg/L (U.S. Environmental Protection Agency, 1997). The occurrence of MTBE in these lakes is attributed to the use of gasoline- powered watercraft (Baehr and Zapecza, 1998). Ground water from domestic wells and wells of small water companies is the major source of water supply for the residents of the communities of Cranberry Lake and Lake Lackawanna. These lakes have been enlarged and water levels are maintained with dams. The combination of maintained water levels in the lake and clustered well withdrawals in the densely populated lakeside communities makes lake/well interaction likely.

During November and December 1998, 14 randomly selected wells surrounding Cranberry Lake were sampled to begin assessing ground-water quality. MTBE was detected in 13 of these wells (93 percent), in concentrations ranging from 0.12 to 19.8 µg/L and a median concentration of 0.44 µg/L. Although the sample size is small, the frequency of detection of MTBE in this lakeside fractured-crystalline-rock setting appears to be sig-

nificantly greater than that in random domestic-well sampling in other parts of New Jersey. Results obtained as part of the Long Island-New Jersey NAWQA study indicate a 48-percent detection frequency of MTBE above a detection limit of 0.1 µg/L in 23 samples collected from domestic wells in crystalline-rock aquifers of the New Jersey Highlands (J.A. Hopple, U.S. Geological Survey, written commun., 1999). A 7-percent detection frequency of MTBE above the 0.1- µg/L detection limit was recorded for 30 samples collected from domestic wells screened in the Kirkwood-Cohansey aquifer system across southern New Jersey (P.E. Stackelberg, U.S. Geological Survey, written commun., 1999). Concentrations and detection frequencies of MTBE in these three domestic-well surveys are shown in figure 9 (Zapecza and Baehr, these proceedings). The concentration of MTBE was equal to or greater than 0.2 µg/L in water from 13 of 34 (38-percent detection frequency) unconfined public supply wells across New Jersey sampled in 1998 as part of the USGS Drinking Water Initiative (E.F. Vowinkel, U.S. Geological Survey, written commun., 1999).

It is possible that Cranberry Lake is a source of MTBE to the community water supply and therefore may be the cause of the very high detection frequency. If such lake/well interaction occurs, then MTBE concentrations in ground water may increase during summer months when MTBE concentrations in the lake are highest (Zapecza and Baehr, these proceedings). Furthermore, lake/well interaction would greatly complicate investigations of MTBE ground-water contamination due to fuel spillage because determination of point-source plume dimensions would be difficult with a non-point-source signature superimposed on the ground water. The very high MTBE detection frequency could also result from the frequent handling of gasoline by residents because of the high rate of boat ownership. Small spills of gasoline probably are more prevalent in these communities than in the population at large and, therefore, the very high MTBE detection frequency in these in wells could be a result of the unique land use. These explanations could also work in concert.

Many lakes throughout the Highlands and the Valley and Ridge provinces of northern New Jersey are surrounded by communities similar to Cranberry Lake that depend on lakeside wells for water supplies. A regional assessment of lakes and the surrounding wells would help to determine the effect of the use of oxygenated gasoline on water quality in lakeside environments and to discern the role of lake/well interaction and land use in ground-water quality.

SUMMARY

Even with advanced capability to predict the migration of contaminant plumes it is impossible to assess the effects of all VOC releases on ground-water quality because of the existence of undiscovered sources. Results of studies in New Jersey demonstrate that analysis of samples collected throughout the hydrologic cycle can improve understanding of the sources and distribution of VOCs in ground water at spatial scales relevant to water supplies.

Atmospheric concentrations of the fuel oxygenate MTBE in southern New Jersey are sufficiently high to explain the frequent detection of this compound in ground water at concentrations below 1 µg/L. For other frequently detected VOCs (chloroform, TCA, and PCE), the atmospheric-source hypothesis is infeasible because atmospheric concentrations are low. Point sources of MTBE, such as upgradient gasoline spills, can also explain the detections even if the atmosphere can account for the ground-water concentrations, because outgassing of MTBE across the water table has been observed at some sites. Outgassing is always observed for TCA and PCE, indicating upgradient point sources of these compounds.

Less frequent VOC detection and lower VOC concentrations were anticipated in samples from public supply wells in the Kirkwood-Cohansey aquifer system than in samples from shallow- and intermediate-depth observation wells as a result of longer flow paths and natural attenuation. The frequency of detection of many chlorinated VOCs (including TCA and PCE), however, was significantly higher in the public supply wells, as was the median total VOC concentration. This result is attributed to the fact that the public supply wells have large contributing areas that can integrate

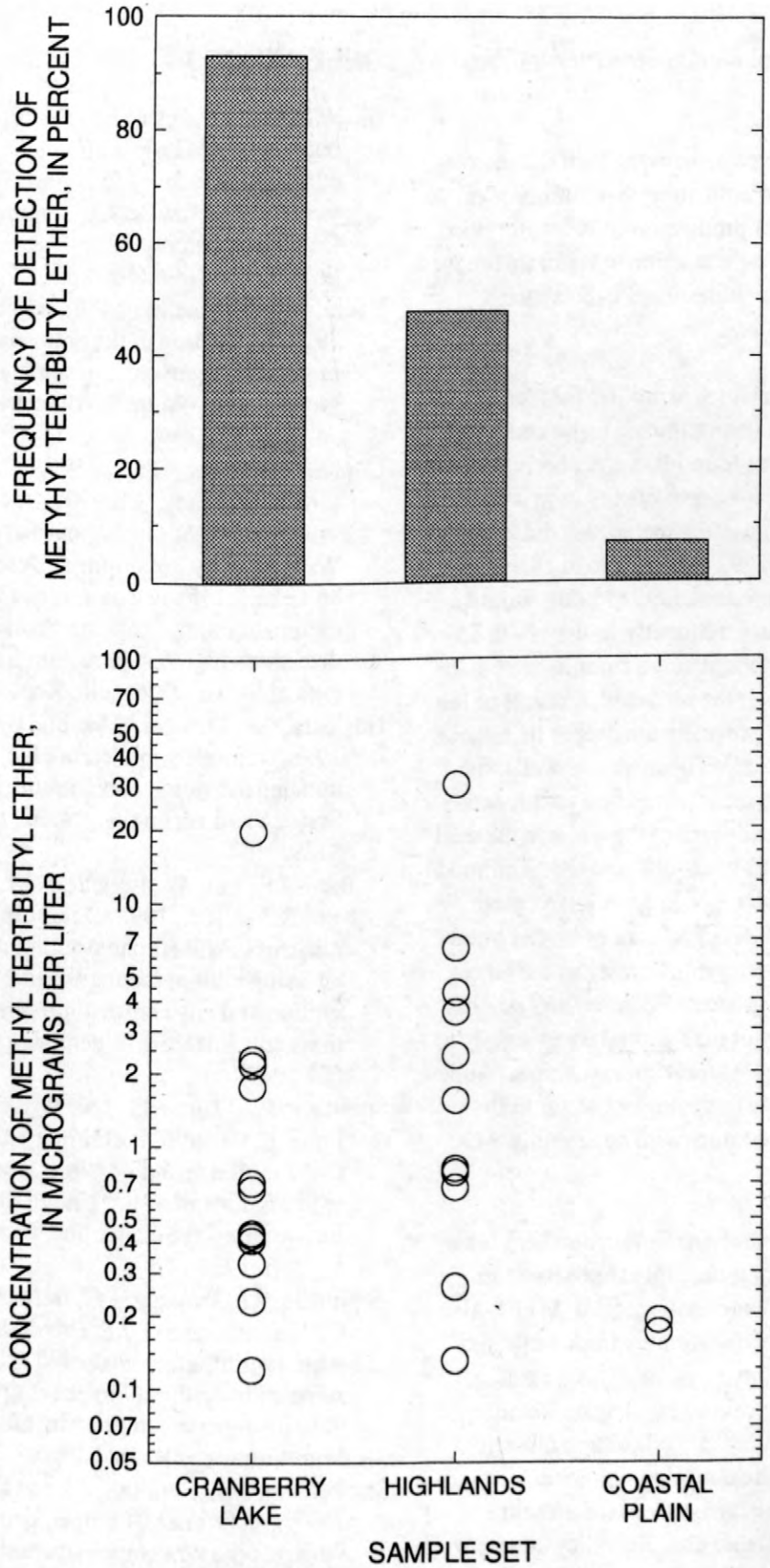

Figure 9. Distribution of concentrations and detection frequencies of MTBE in samples collected during three surveys of domestic wells, New Jersey. (from Zapecza and Baehr, these proceedings)

point sources located throughout their contributing areas.

Chloroform was detected at high frequencies in all types of wells, indicating that its source is widespread. Natural production of chloroform in the subsurface and its production in water treatment may contribute to its widespread occurrence throughout the aquifer.

MTBE was detected at similar frequencies in samples from shallow monitoring wells and public supply wells, but was found less frequently in samples from intermediate-depth observation wells. Use of MTBE as a gasoline oxygenate did not increase until after 1992 in response to changes in the Clean Air Act; consequently, MTBE would be expected to occur less frequently in the 10- to 15-year old ground water collected from intermediate-depth wells. Although the screened intervals of the public supply wells generally are deeper than those of the intermediate-depth observation wells, the MTBE detection frequency in public supply wells may be higher because some of the water in the well would be less than 10 years old, and the likelihood that some of this water would have intercepted point sources of MTBE or an area of higher atmospheric loading due to traffic density in the larger contributing area is greater. These results emphasize the vulnerability of the regional water supply to contamination, as the water withdrawn from public supply wells includes the youngest water in the aquifer, which is in contact with developing VOC sources.

MTBE concentrations in two northern New Jersey lakes are among the highest observed in ground and surface water nationwide. MTBE also was detected in 13 of 14 samples from wells surrounding one of the lakes, possibly as a result of lake/well interaction caused by the combination of maintained water levels in the lake and clustered well withdrawal in the densely populated lakeside community. Because many lakes are present throughout the Highlands and the Valley and Ridge provinces of northern New Jersey and in adjacent states, such lake/well interaction may define a regional phenomenon.

REFERENCES

Baehr, A.L., and Zapecza, O.S., 1998, Methyl tert-butyl ether (MTBE) and other volatile organic compounds in lakes in Byram Township, Sussex County, New Jersey, summer 1998: U.S. Geological Survey Water-Resources Investigations Report 98-4264, 8 p.

Baehr, A.L., Stackelberg, P.E., and Baker, R.J., 1999, Evaluation of the atmosphere as a source of volatile organic compounds in shallow ground water: Water Resources Research, v. 35, no. 1, p. 127-136.

Connor, B.F., Rose, D.L., Noriega, M.C., Murtagh, L.K., and Abney, S.R., 1998, Methods of analysis by the U.S. Geological Survey National Water Quality Laboratory--Determination of 86 volatile organic compounds in water by gas chromatography/mass spectrometry, including detections less than reporting limits: U.S. Geological Survey Open-File Report 97-829, 78 p.

Hoekstra, E.J., De Leer, E.W., and Brinkman, U. A., 1998, Natural formation of chloroform and brominated trihalomethanes in soil: Environmental Science and Technology, v. 32, no. 23, p. 3724-3729.

Pankow, J.F., Luo, W., Isabelle, L.M., Bender, D.A., and Baker, R.J., 1998, Determination of a wide range of volatile organic compounds in ambient air using multisorbent adsorption/thermal desorption and gas chromatography/mass spectrometry: Analytical Chemistry, v. 70, no. 24, p. 5213-5221.

Squillace, P.J., Zogorski, J.S., Wilber, W.G., and Price, C.V., 1996, Preliminary assessment of the occurrence and possible sources of MTBE in ground water of the United States, 1993-94: Environmental Science and Technology, v. 30, no. 5, p. 1721-1730.

Squillace, P.J., Pankow, J.F., Barbash, J.E., Price, C.V., and Zogorski, J.S. (in press), Possible formation of trihalomethanes in ground-water samples by hydrochloric acid preservation for volatile organic compounds: Ground Water Monitoring and Remediation.

Stackelberg, P.E., Hopple, J.A., and Kauffman, L.J., 1997, Occurrence of nitrate, pesticides, and volatile organic compounds in the Kirkwood-Cohansey aquifer system, southern New Jersey: U.S. Geological Survey Water-Resources Investigations Report 97-4241, 8 p.

U.S. Environmental Protection Agency, 1997, Drinking-water advisory: Consumer acceptability advice and health effects analysis on methyl tertiary-butyl ether (MTBE): U.S. Environmental Protection Agency, Office of Water, EPA-822-F-97-008.

Zapecza, O.S., and Baehr, A.L., in press, Methyl tert-butyl ether (MTBE) in lakes in Byram Township, Sussex County, New Jersey, 1998, and vulnerability of ground water in lakeside communities, in Morganwalp, D.W., and Buxton, H.T., eds., U.S. Geological Survey Toxic Substances Hydrology Program--Proceedings of the Technical Meeting, Charleston, South Carolina, March 8-12, 1999--Volume 3--Subsurface Contamination from Point Sources: U.S. Geological Survey Water-Resources Investigations Report 99-4018C, this volume.

AUTHOR INFORMATION

Arthur L. Baehr, Leon J. Kauffman, Emmanuel G. Charles, Ronald J. Baker, Paul E. Stackelberg, Mark A Ayers, and Otto S. Zapecza , U.S. Geological Survey, West Trenton, New Jersey.

Capabilities and Challenges of Natural Attenuation in the Subsurface: Lessons from the U.S. Geological Survey Toxics Substances Hydrology Program

By Barbara A. Bekins, Arthur L. Baehr, Isabelle M. Cozzarelli, Hedeff I. Essaid, Sheridan K. Haack, Ronald W. Harvey, Allen M. Shapiro, James A. Smith, and Richard L. Smith

ABSTRACT

Natural attenuation has been used as a practical method to dispose of wastes throughout human history. However the presumption of natural attenuation as a strategy for disposal of wastes has had serious consequences for human health and the environment in the twentieth century. It is now clear that the environment has a limited ability to assimilate wastes and that this ability depends on the nature and quantity of the waste compounds and the characteristics of the subsurface. Thus, increasing our knowledge of the capabilities and limitations of natural attenuation is of high priority. To this end, the U.S. Geological Survey Toxic Substances Hydrology Program (Toxics Program) conducts studies on the fate of contaminants in the natural environment. Results from the Toxics Program research sites have documented the effectiveness of a variety of individual processes that together contribute to natural attenuation in the subsurface. The site studies also indicate that many challenges remain in our efforts to understand the effectiveness of natural attenuation. These include spatial heterogeneity and slow, rate-limiting processes that result in long time frames for cleanup. The subsurface microbial populations that catalyze biotransformation reactions also are poorly understood. However, recent results have yielded insights into controls on the spatial and temporal distribution of the various microorganisms. Quantitative models have been used successfully at several sites for estimating the relative contribution of each natural attenuation process to the overall mass loss. Future research is needed that targets gaps in our understanding of compound-specific behavior, subsurface microbial ecology, and uncertainties associated with heterogeneities and long time frames.

INTRODUCTION

Total spending on environmental remediation in the United States was estimated to be $9 billion in 1996 alone (National Research Council, 1997). Furthermore, cleanup of contaminated soil and ground water may ultimately cost $500 billion to $1 trillion (National Research Council, 1994). Because of the high cost of remediation, the National Research Council sponsored a study in 1997 to evaluate innovative technologies in ground water and soil cleanup (National Research Council, 1997). One of the emerging technologies for treatment identified in the study was remediation by natural attenuation (RNA). The EPA defines natural attenuation as

> A variety of physical, chemical, or biological processes that, under favorable conditions, act without human intervention to reduce the mass, toxicity, mobility, volume, or concentration of contaminants in soil or ground water. These in situ processes include biodegradation; dispersion; dilution; sorption; volatilization; and chemical or

biological stabilization, transformation, or destruction of contaminants. (EPA, 1997).

Each of these attenuation mechanisms represents complex interactions among physical, chemical, and in some cases, biological processes and thus many are still subjects of active research.

Although the current level of active research would classify RNA as an emerging technology, its use as a remediation option for hydrocarbon contamination has increased dramatically in recent years. By January, 1998, RNA was permitted as a sole remedy for ground water petroleum hydrocarbon cleanup in 43 states (Martinson, 1998). This rapid increase is due to three main developments. First, an analysis of a large database of empirical observations from gasoline sites suggested that most hydrocarbon plumes have not expanded beyond 250 m (Rice and others, 1995). Second, results from lab and field studies have documented many of the significant mechanisms driving natural attenuation for gasoline compounds (see Wiedemeier and others, 1995, for a summary). Third, performance evaluations of cleanup methods such as pump and treat systems indicate that cleanup to drinking water standards is unrealistic in many cases (National Research Council, 1994). However, as the use of RNA has increased, public concern about potential abuses also has increased.

Concern about RNA is reflected in a widespread attitude that this is a "do nothing" option. Specific issues include the time frame for cleanup, whether the plume extends to a receptor, and whether the contaminant is truly rendered harmless. Addressing these issues requires a thorough understanding of the processes that control contaminant transport and contribute to natural attenuation. Measurement and modeling techniques are needed to determine the effects of each specific process and to design monitoring programs that demonstrate the sustainability of these processes. For chemical and biological reactions, knowledge of the reactants, products, reaction rates, microbial populations, and hydrologic controls on transport are all important. However, it would be prohibitively expensive to conduct investigations leading to a thorough understanding of the fate of contaminants at every site. The goal of research conducted by the USGS Toxic Substances Hydrology Program (USGS Toxics Program) has been to arrive at general scientific principles to guide investigations, monitoring strategies, and regulatory decisions on ground-water cleanup. The research results from the program are especially relevant to RNA because the primary focus of the studies has been on natural processes.

The first part of this paper summarizes the capabilities of several key attenuation processes that have been described and quantified at sites studied under the USGS Toxics Program. In particular, the role of volatilization and biotransformation in the unsaturated zone and aerobic and anaerobic biodegradation in the saturated zone are well documented. However, many challenges to implementation of RNA still exist. The second section of the paper describes results from the study sites that illuminate these challenges. One challenge concerns the common occurrence in aquifers of sharp geochemical gradients and spatial and temporal variability in flow conditions. These heterogeneous conditions have a profound effect on the fate of the contaminants. Another challenge stems from rate-limiting aspects of contaminant flux including desorption, matrix diffusion, and nonaqueous-phase liquid (NAPL) dissolution. The combined effect of heterogeneity and long time frames make it difficult to predict the future sustainability of RNA processes at a site. Finally the microbial communities that perform biodegradation reactions contributing to natural attenuation are poorly understood and are the focus of research at several of the sites. In assessing the potential for RNA at a site, it is necessary to balance the capabilities against the limitations in knowledge imposed by the various challenges described above. Various types of quantitative analyses can be used to perform such an assessment. The third section of the paper describes how quantitative analyses have been successfully used at the Toxics Program sites to identify the relative contribution of individual processes to the total mass loss of a contaminant and to assess their

sustainability. On the basis of the cumulative knowledge gained under the USGS Toxics Program a set of recommendations for future research on the fate of contaminants in the subsurface is provided at the end of the paper.

CAPABILITIES OF NATURAL ATTENUATION

Natural attenuation is caused by a variety of physical, chemical, or biological processes that include dispersion, dilution, sorption, volatilization, and chemical or biological reactions. The effectiveness of each individual process in the subsurface varies depending on the level of saturation, the geochemical conditions, and the ground-water flow field. The research results summarized below provide general principles that can be used to predict the capabilities of natural attenuation under different subsurface conditions. The capabilities discussed are limited to biodegradation and volatilization because these are the primary attenuation mechanisms at the research sites described. For other sites and particularly for contaminant metals, the most important natural attenuation mechanisms may be sorption and chemical reactions. The discussion is divided according to processes that occur primarily above the water table in the unsaturated zone or below the water table, in the saturated zone.

Unsaturated Zone Processes

Two of the key processes in natural attenuation are volatilization and biodegradation. Results from USGS Toxics Program study sites in Galloway, NJ, (leaded gasoline) and Picatinny Arsenal, NJ, (solvents) show that these processes are especially rapid in the unsaturated zone. The unsaturated zone is an active area for transfer of contaminants between phases because contaminants may be present in either the vapor, dissolved, or non-aqueous phases. In addition, exchange of gases with the atmosphere can lead to conditions for efficient aerobic biodegradation and also gas-phase transport.

Results from the Galloway site show that transport and biodegradation processes occurring at the base of the unsaturated zone, near the water table, can contribute significantly to natural attenuation of subsurface spills of gasoline. At this site, leaded gasoline that leaked from an underground storage tank is present as a non-aqueous phase in the unsaturated zone and at the water table (Fischer and others, 1996). The water table is a barrier to the movement of nonaqueous contaminants downward into ground water because gasoline is less dense than water. Fluctuation in the water table elevation over time causes the nonaqueous contaminants to be spread vertically. Constituents such as benzene, toluene, ethylbenzene, and xylenes (BTEX) volatilize into the air-filled pore space of the capillary zone and migrate upward into the unsaturated zone via diffusion. This pathway combined with microbial degradation results in mass removal of compounds and thus reduces the mass available for solubilization into ground water. The source attenuation is compound-specific and therefore the composition of the remaining product changes over time by processes similar to those described by Baehr (1987).

Although volatilization is most important in the source area, compounds transported downgradient from the source area as solutes in ground water can also volatilize into the unsaturated zone from the ground-water plume. Biodegradation near the water table directly contributes to mass removal and results in sharp concentration gradients that enhance the upward diffusive transport of BTEX compounds into the unsaturated zone. At Galloway, oxygen in the unsaturated zone just above the capillary zone is below atmospheric concentrations but well above zero (about 5 percent) and hydrocarbon concentrations decrease rapidly with distance above the water table. These gradients imply a small vertical zone of active aerobic degradation above the water table. Lahvis and Baehr (1996) used the observed gradients to constrain a model estimating the overall BTEX transformation rates in this zone.

Research results from Picatinny Arsenal show that a significant quantity of trichloroethylene (TCE) volatilizes from water in the capillary fringe into the unsaturated-zone soil gas and is transported to the atmosphere. At

the Picatinny site, improper disposal of wastewater from degreasing operations between 1960 and 1983 resulted in the formation of a trichloroethylene TCE plume in an unconfined, sand-and-gravel aquifer with concentrations as high as 44 mg/L in the ground water (Smith and others, 1996a). Prior to installation of a pump-and-treat system in 1992, the plume extended about 500 m from the source area to a nearby brook. Because the brook acts as the discharge point for the water-table aquifer in the valley, no TCE has been detected in the ground water beyond it. TCE also has been detected in the unsaturated-zone water and soil gas at the site (Smith and others, 1990). Smith and others (1996a) used direct measurements of TCE vapor fluxes from the unsaturated zone to calculate a total TCE vapor flux to the atmosphere of approximately 50 kg/yr. They concluded that natural atmospheric pressure variations cause air flow in the unsaturated zone and lead to advective TCE vapor fluxes that are much greater than diffusive fluxes in the gas phase. However, the rate of volatilization is ultimately controlled by diffusion of dissolved TCE across the water table. Thus, the changing position of the water table at the site also may enhance TCE fluxes to the atmosphere.

Biodegradation in the Saturated Zone

In the saturated zone, aqueous-phase organic contaminants are biodegraded by indigenous microorganisms that have adapted to the conditions in the plume. Results from many of the USGS Toxics Program sites have documented the effectiveness of microbial transformations in reducing contaminant mass and concentrations. The nature and extent of microbial transformations are controlled, to a large degree, by the availability of electron acceptors which, in turn, determines the dominant terminal electron-accepting processes (TEAP) in any given environment. The most common TEAPs are aerobic respiration, denitrification, iron and manganese reduction, sulfate reduction and methanogenesis. Certain contaminants degrade or are transformed best under aerobic conditions, while for others, anaerobic conditions or specific TEAPs are optimal. Therefore, assessing the potential for microbial transformations requires understanding: (1) which TEAPs are dominant within a contaminated environment (see Smith, 1997); (2) hydrologic factors that affect the supply of TEAP's; (3) geochemical factors that affect TEAP processes; and (4) the fate of each contaminant when subjected to the various TEAPs. Thus, transformation rates depend on a complicated set of interactions between the microbial processes, the environment and the contaminant compounds. Each of these interactions needs to be carefully elucidated, but all are best examined both at field sites and with controlled laboratory experiments that carefully reproduce field conditions. Research results from study sites at Picatinny, Galloway, Bemidji, MN (crude-oil), and Cape Cod, MA (treated sewage effluent), illuminate various issues to consider when assessing the degree of natural attenuation caused by microbial transformation of contaminants in the saturated zone.

Research at Picatinny has demonstrated that biodegradation and volatilization exceed removal rates by pump-and-treat technology. However, even at this well-characterized site, significant uncertainties exist in rate estimations. Anaerobic biotransformation is occurring in the plume by reductive dechlorination of TCE to cis-1,2-DCE and vinyl chloride. Using soil collected from the site, several researchers have documented the biodegradation of TCE in soil-water microcosms under anaerobic conditions (Wilson and others, 1991; Ehlke and others, 1996). Both cis-1,2-dichloroethylene and vinyl chloride have been detected in the plume, even though neither of these chemicals were used at the site. Fitted first-order biotransformation rate constants for TCE range from less than 0.052 to 1.04 yr^{-1} (Wilson and others, 1991). Using these biotransformation rates and an estimate of the mass of TCE in the aqueous phase in the contaminant plume Imbrigiotta and others (1995) calculated that the rate of TCE biotransformation ranges from less than 52 kg/yr to 1,040 kg/yr. These results indicate the large degree of uncertainty present even at relatively well-understood research sites. In

1995, the rate of TCE withdrawal by the pump and treat system was 70 kg/yr. Thus, the sum of the TCE flux to the atmosphere (50 kg/yr) and the minimum biodegradation loss exceeds removal rate of the pump-and-treat system. Because pump-and-treat systems can be comparatively ineffective at mass removal, they are often used today as a containment strategy in conjuction with natural attenuation processes.

Research at the Galloway site has explored the intricate relationships between aquifer mineralogy, aqueous geochemistry and TEAPs, and has found that many significant processes occur in very narrow zones. At this site, the primary attenuation mechanism of hydrocarbons below the water table is anaerobic degradation. In the absence of oxygen, the oxidized forms of other inorganic species available in subsurface environments are utilized by bacteria to mediate the oxidation of hydrocarbons. Cozzarelli (1993) described the predominant reaction mechanisms and their spatial scale. The presence of a narrow zone at the water table where nitrate is transformed to N_2O and ammonia indicates that nitrate entering in the recharge water is rapidly utilized. Below the water table, a zone of iron-reduction is present. However, the depletion of microbially reducible solid iron-oxyhydroxides in narrow zones has allowed sulfate reduction to begin at small spatial scales. Reduced iron and sulfide are elevated in the plume and have combined to form the mineral pyrite on the aquifer solids. The presence of reaction products such as reduced iron, sulfide, and resulting minerals in concentrations that exceed background values is one line of evidence indicating that anaerobic biodegradation has contributed to mass loss at the site.

Important results from the Bemidji crude oil site are (1) the rate and extent of biotransformation reactions under different redox conditions; (2) the documented effects of organic contaminant chemistry on aquifer geochemistry; (3) the slow evolution of conditions in the plume from aerobic to iron-reducing to methanogenic conditions. These results frequently are cited in protocols that summarize our knowledge of petroleum hydrocarbon natural attenuation processes (see, for example, Wiedemeier and others, 1995). The Bemidji site became contaminated in 1979 when a pipeline broke spilling 10,000 barrels of crude oil on the land surface (Hult, 1984). After cleanup operations, about 40 percent of the oil remained and subsequently infiltrated into the sand-and-gravel glacial outwash aquifer. The oil is present in residual concentrations in the unsaturated zone and as two floating oil bodies on the water table. An aqueous plume emanating from the northern oil body has been extensively studied under the USGS Toxics Program.

Baedecker and others (1993) found that geochemical conditions in the Bemidji plume could be classified into three zones corresponding to anaerobic, transition, and aerobic conditions. In the anaerobic zone, degradation of the hydrocarbons by iron reduction initially dominated (Lovley and others, 1989). However, as ferric iron has been depleted, narrow methanogenic zones have formed in areas of high contaminant flux (Bekins and others, 1999). Reduced iron and methane concentrations are elevated in the plume along with aliphatic and aromatic organic acids. The organic acid composition and concentration shifts as the dominant TEAP evolves from iron reduction to methanogenesis (Cozzarelli and others, 1994). In the anaerobic portion of the plume, concentrations of benzene and alkylbenzenes decrease relatively slowly compared to other hydrocarbons. However, in the transition zone between anaerobic and aerobic conditions, the concentrations of hydrocarbons decrease rapidly (Eganhouse and others, 1993). Anderson and others (Anderson and others, 1998) showed that rapid degradation of benzene occurred over a narrow region at the downgradient-edge of the Fe(III) reduction zone in an area associated with elevated numbers of *Geobacter* species. The microbial degradation reactions lead to significant perturbations in the inorganic as well as the organic chemistry of the water and the aquifer material (Bennett and others, 1993). Changes in the aquifer include formation of authigenic minerals (Baedecker and others, 1992; Bennett and others, 1993; (Tuccillo, 1998) and dissolution of aquifer

mineral phases (Hiebert and Bennett, 1992; Rogers and others, 1998).

Nitrate is the most prevalent anthropogenic groundwater contaminant. In aqueous solution, it is generally a stable compound that is transported conservatively after entering the subsurface. However, when significant concentrations of organic carbon lead to anerobic conditions, denitrification reduces nitrate to nitrogen gas. This reaction has resulted in significant natural attenuation of nitrate at the Cape Cod, MA, USGS Toxics Program site. A long-term study of the site has included: a) factors that control occurrence of denitrification in an aquifer (Smith and Duff, 1988); b) measurement of in situ rates (Smith and others, 1996b); c) the effect on ground water nitrogen geochemistry (Smith and others, 1991b); d) identification and characterization of unique subsets of the denitrifying microbial population in the aquifer (Smith and others, 1994); and e) the inability of certain soils techniques to assess denitrification in the subsurface (Brooks and others, 1992). The ground water at the Cape Cod site has been contaminated with secondarily treated sewage effluent from rapid infiltration ponds located on Otis Air Force Base. The sewage-contaminated ground water has formed a plume more than 6 km long containing chlorinated hydrocarbons, detergents, metals, microbes, and nitrate.

At the Cape Cod site denitrification is electron-acceptor limited throughout the center of the contaminant plume, having completely consumed the source nitrate. However, it is electron-donor limited in a 5- to 7-m thick zone that extends for several kilometers downgradient from the contaminant source. Denitrification occurs primarily in the aquifer under suboxic conditions within the 10-30 μM region of the oxygen gradient. In high nitrate zones, nitrite and nitrous oxide are present. Concentrations of these intermediates can vary significantly on a meter scale (both vertically and laterally), though neither persists with downgradient transport on the kilometer scale. Elevated concentrations of nitrogen gas also are present within the aquifer, particularly in zones in which denitrification is electron-acceptor limited. Natural gradient tracer tests with ^{15}N-enriched nitrate have demonstrated that unequal amounts of N (and electron equivalents) pass through the individual steps of the denitrification pathway. A comprehensive picture of the interacting processes that may limit denitrification rates in an aquifer is emerging from the Cape Cod results.

CHALLENGES OF NATURAL ATTENUATION

The potential success of natural attenuation as a remedial strategy is complicated or limited by several aspects of the subsurface environment. The physical and chemical properties of subsurface rocks and sediments can be highly variable within a single site. Moreover, the subsurface flow fluctuates temporally. Ground-water flow rates are typically very slow and dissolution and desorption rates are limited by the small flux of clean ground water contacting concentrated sources of contaminants. Natural chemical fluxes into the subsurface from the surface also are limited and this affects the number and diversity of subsurface microbial populations. The sections below describe how these various aspects of the subsurface have complicated and limited the processes controlling the natural attenuation of contaminants at several of the Toxics Program sites. The discussion is divided into sections on spatial and temporal variability, slow time frames, and microbial ecology.

Spatial and Temporal Variability

Ground-water contaminant plumes are characterized by longitudinal and vertical gradients of both naturally-occurring and contaminant solutes. These heterogeneities are due to various combinations of: a) changes in contaminant source; b) differential rates of transport; c) physical and chemical heterogeneity of aquifer properties; d) geochemical and microbiological processes; and e) changes in hydrologic conditions along the flow path. As geochemical conditions change in space and time, the carbon sources, electron acceptors, and other environmental variables that limit microbial degradation in the

subsurface also change. These changes complicate attempts to monitor or predict remediation outcomes. Nevertheless, it is clear that proper evaluation of the effects of spatial and temporal changes are necessary in order to monitor, predict, or model either specific or composite processes at sites proposed for RNA. Efforts to characterize the effects of heterogeneity on natural attenuation have been an important aspect of Toxics Program research at the Cape Cod, Bemidji, and Galloway sites and at Wurtsmith Air Force Base, MI (mixed wastes). The results indicate that changes in redox conditions on small spatial scales and over short time frames are common and that these changes have profound effects on the fate of contaminants in the subsurface.

At the Cape Cod site, small vertical dispersivity limits vertical mixing and maintains sharp gradients in oxygen and other solutes even after several kilometers and several decades of transport (Smith and others, 1991a) . Studies with large-scale tracer tests have estimated the vertical dispersivity in the aquifer to be 0.15 cm, or >600 times smaller than longitudinal dispersivity (Garabedian and others, 1991). Concomitant with the large concentration gradients are large changes over a vertical distance of a few meters in bacterial abundance, growth rates, and heterotrophic activity, as well as cell morphology (Smith and others, 1991a). In the horizontal direction, the plume character changes more gradually with increasing recalcitrance in the residual DOC downgradient (Harvey and Barber, 1992) and increasing importance of autotrophic processes (such as nitrification) as oxygen-consuming mechanisms (Ceazan, 1987; Ceazan and others, 1988) over a scale of kilometers.

Dramatic spatial and temporal changes in TEAP zonation (Chapelle and others, 1996; McGuire and others, 1999), microbial community composition, and bacterial population abundance (Haack and Reynolds, 1999; Reynolds and Haack, 1999) also have been observed in Toxics Program research at the former Wurtsmith Air Force base. Fire training exercises conducted at the site from 1958 until 1986, resulted in dispersal of waste fuel, solvents, and fire-fighting compounds to a shallow water table aquifer composed of glacial deposits of gravel, sand, silt and clay (USGS, 1991; Huffman and others, 1995). The contaminant plume extends about 500 m downgradient from the central site of fire-training activities and the majority of the contaminants are located on the aquifer solids near the water table. The water table ranges from 5-8 m below land surface and water levels fluctuate 0.3-1 m annually. The average ground-water velocity is 0.1-0.3 m per day.

The research at the Wurtsmith site had three primary objectives: (1) determine spatial and temporal heterogeneity in TEAPs, microbial communities and TEAP-related microbial populations; (2) relate spatial and temporal heterogeneity in these parameters to evidence of biodegradation in the contaminant plume; and (3) evaluate the significance of spatial and temporal heterogeneity for intrinsic remediation. In October 1995, June 1996, and October 1996, the dominant TEAP was assessed at specific locations and depths in the aquifer by determining the ground-water redox chemistry and hydrogen gas concentration. Aquifer sediments were then collected from specific depths, and assigned a TEAP based on analyses from a well less than 4 m upgradient of the sediment collection site. Preliminary results indicate that TEAPs and microbial communities and populations vary over spatial scales of less than 1 m and over temporal scales of months. Changes in microbial communities and populations were related to gradients in aquifer water chemistry at the site. Current research focuses on relating these gradients to patterns of biodegradation products within the plume. It is likely that specific biodegradation reactions occur only at certain locations within the Wurtsmith plume, or only at certain times.

Data from the Bemidji site confirm that the potential for degradation of specific hydrocarbons and also reaction rates vary with redox zone (Baedecker and others, 1993; Eganhouse and others, 1993; Cozzarelli and others, 1994; Anderson and others, 1998). Moreover, the spatial extent of the reaction zones was found to be especially narrow at both the Galloway gasoline site and the Bemidji crude-oil site, where maximum hydrocarbon

contamination within the plumes corresponded to anoxic zones of only one to two meters in thickness. Within the anoxic zones, observations of submeter-scale intervals of sulfate reduction at the Galloway site (Cozzarelli, 1993) and methanogenesis at the Bemidji site (Tuccillo, 1998; Bekins and others, 1999) are associated with depletion of microbially reducible solid iron-oxyhydroxides. Interpretation of reaction processes is complicated by mixing of degradation products from different redox zones. At the Galloway site, the mixing of end products of different biogeochemical reactions was enhanced by fluctuations in the water table and the small spatial scale of the reaction zones (Cozzarelli, 1993).

In summary, results from the USGS Toxics Program sites show that understanding whether environmental conditions favor biodegradation depends on our ability to measure these processes at an appropriate scale. Ground-water samples obtained from wells with long screens have little relevance if the chemistry of the composite sample does not exist anywhere in the aquifer. Thus, sample intervals and well-screen lengths must be matched to the steepness of the subsurface gradients. Research conducted by the USGS Toxics program has made extensive use of short-interval sampling, and provides exceptional examples of the significance of scale. A variety of innovative technologies have been used to achieve this objective. At the USGS Cape Cod study site, multilevel samplers (MLSs) were constructed with short vertical intervals between ports making them particularly useful for sampling across steep gradients (LeBlanc and others, 1991; Smith and others, 1991a). Currently the Cape Cod site has ~2000 15-port MLSs in place to study the sewage-derived contaminant plume. At the Wurtsmith site, a hydropunch was used in conjunction with short well screens to study the relationship between TEAPs and microbial communities. Unprecedented spatial resolution for studying the relationship between pore water chemistry and adjacent sediments and microbial populations was possible at the Bemidji site using a freezing drive shoe designed by Murphy and Herkelrath (1996). Using the drive shoe, hundreds of cores containing both the aquifer material and pore fluids collected from the plume and the oil body have enhanced understanding of the effects of spatial variability on natural attenuation at the Bemidji site.

Time Frame

The decision to rely on natural attenuation processes at a site is simplified when it is clear that the contamination will be degraded or immobilized within the foreseeable future. Some state regulators have expressed a concern that the predicted cleanup time by natural attenuation not exceed a few decades. However, slow rates of matrix diffusion, desorption, and nonaqueous-phase liquid (NAPL) dissolution may result in natural attenuation time frames much longer than can be planned for in a regulatory process or predicted with models. Results from three very different USGS Toxics Program sites illustrate situations where the time frame of natural attenuation is very long and our ability to predict the future sustainability may be questionable. At the Mirror Lake, NH (fractured rock), site rate-limiting aspects of matrix diffusion in fractured rock aquifers have been the focus of several studies. At the Picatinny site, it is estimated that slow desorption will result in a substantial long-term mass flux of TCE from the aquifer solids into the ground water. Finally, an analysis of the dissolution rate of nonaqueous-phase oil at the Bemidji crude oil spill suggests that contamination will persist for hundreds of years. The results of these studies show that a clear understanding of the expected progress of natural attenuation over long time frames will be crucial for guiding remediation decisions about certain types of contaminant sources and aquifer conditions.

Results from the Mirror Lake site, show that matrix diffusion and (or) "effective" matrix diffusion acts as a "storage" and "release" mechanism in heterogeneous formations. Initially matrix diffusion is an uptake mechanism that reduces the concentration in the mobile phase. Later, when concentration gradients are conducive for transfer from the "immobile" to the "mobile" phase the stored

contaminants are slowly released from the formation matrix. The geology of the Mirror Lake site is characterized by fractured metamorphic and igneous rocks overlain by a thin veneer of glacial drift. Although the site is uncontaminated, research has focused on developing and testing methods for characterization of the physical properties of the fractured network that affect the advective and dispersive movement of dissolved chemicals in ground water.

Investigations at Mirror Lake have included tests on multiple scales ranging from meters to kilometers and emphasized integration of geologic, hydrologic, geophysical, and geochemical methods to characterize and simulate ground-water flow and transport. Laboratory-scale studies of fractured rocks from the Mirror Lake site show that granite and schist have an intrinsic interconnected porosity that is capable of transporting dissolved constituents (in this case ^{137}Cs) by diffusion over several centimeters in a period of 100 days (Wood and others, 1996). ^{137}Cs is highly retarded so the effect on a conservative constituent would be much greater. Field-scale investigations were conducted using an injection of a tracer (sodium-bromide) under controlled hydraulic conditions (Shapiro, 1994). In addition, regional-scale investigations of chemical migration were inferred from tritium and CFC concentrations in ground-water samples (Shapiro, 1996).

In both the field and regional-scale investigations at Mirror Lake, fitting the chemical data required including an "effective" matrix diffusion orders of magnitude larger than the value from the laboratory investigation (Shapiro, 1996). The reason for this increase is that at the laboratory scale, the flow regime (in this case only diffusion) is known explicitly, while at the field and regional scales, the intricacies of the flow regime are not known. In addition to diffusion of dissolved constituents into the rock matrix, there also are advective processes that give the appearance of "matrix diffusion" when considered over larger dimensions. For example, dissolved constituents can be advected from a higher-permeability region into a lower-permeability region and then eventually back into a high-permeability region. If this process occurs over a small distance, it gives the appearance of "diffusing" into an "immobile" flow regime and then back into a "mobile" flow regime. In these investigations, this effect could not be represented by dispersion alone. Similar processes to those observed in fractured rock at the Mirror Lake site will also arise in other geologic environments where there are contrasts in the hydraulic properties, such as clay lenses within a sand and gravel aquifer, sand stringers within till, etc.

Matrix diffusion and (or) "effective" matrix diffusion can contribute significantly to the inefficiency of pump-and-treat remediation in heterogeneous formations. While a contaminant is present in the "mobile" or high-permeability flow regime there is a large chemical gradient driving the constituent into the "immobile" or low-permeability flow regime. After pumping has started, however, the contaminant is first removed from the high permeability regions, increasing the chemical gradient driving the constituent back to the "mobile" flow regime. The chemical gradient from the “immobile” to the “mobile” flow regime, however, is small in comparison to the original gradient driving the contaminant into the low-permeability region. Thus, the time-frame for diffusive migration out of the low-permeability region will always be significantly longer than the period of untreated contamination. In other words, the diffusive exchange between “immobile” and “mobile” flow regimes will control the rate at which contaminants can be removed by pump-and-treat technology, regardless of the pumping rate employed. Contrasts in hydraulic properties similarly will affect flushing technologies (steam, co-solvents, surfactants, etc.) used in treatment of NAPL's. Contact between the NAPL and water occurs mainly in the "mobile" high permeability flow regime whereas NAPL's may have infiltrated lower-permeability regions or water flow may be limited through areas of high NAPL saturation.

Storage and release can account for a major percentage of the ground-water contamination source. This behavior has been

observed and quantified at the Picatinny Arsenal study site where desorption from the solid phase is a significant source of TCE transfer to the ground water. Imbrigiotta and others (1995) estimate that approximately 3,000 to 4,000 kg of TCE are sorbed to the aquifer sediments and that this quantity is 3-4 times greater than the estimated total mass of TCE in the ground water at the site. Recent studies have concluded that the rate of TCE desorption from the aquifer sediments is slow relative to other processes such as advection (Koller and others, 1996; Sahoo and others, 1998). Koller and others (1996) quantified TCE soil-water mass transfer coefficients for contaminated soil collected from the site using laboratory soil-column experiments with native ground water. These mass-transfer coefficients can be used to estimate the mass flux of TCE from the contaminated aquifer sediments to the ground water using a first-order mass-transfer relation. On the basis of best estimates of the mass of contaminated soil, the water and soil TCE concentrations, soil density, porosity, and coefficients for mass transfer and sorption, the estimated TCE mass flux from soil to water at the site ranges from 474 kg/yr to 2,300 kg/yr. Because the measurements of mass-transfer coefficients were made in the laboratory on disturbed soil samples from the site, it is reasonable to assume that the estimated desorption fluxes have a large degree of uncertainty relative to other fluxes at the site. Nevertheless, the minimum estimated value exceeds the sum of minimum estimates of removal rates by volatilization (50 kg/yr), anaerobic degradation (52 kg/yr), and pump and treat (70 kg/yr).

Nonaqueous-phase liquids that enter the subsurface may act as long-term sources of ground-water contamination as the organic constituents dissolve from the nonaqueous phase. The amount and rate of dissolution depends on many factors, including the flow field in the vicinity of the oil body. To examine the flow of water and resulting dissolution rate at the Bemidji, MN site, Essaid and others (1995b) simulated steady-state water flow through the oil bodies and used particle-tracking to determine the volumetric water flux through the oil body and the resulting dissolution of contaminants. Water relative hydraulic conductivities used in the model were computed from kriged oil saturation and hydraulic conductivity data. The effective solubility of a hydrocarbon was determined by multiplying the mole fraction of the component in the oil times the solubility of the component. Assuming that concentrations of benzene, toluene, ethylbenzene, and xylene (BTEX) in the water are in equilibrium with the oil, the total mass flux of a hydrocarbon component from the oil body can be estimated by multiplying the volumetric water flux through the oil times the effective solubility. Finally, the time to completely dissolve the BTEX can be estimated by dividing the total mass of each component in the oil by the mass flux of the component due to dissolution. These simulations suggested that the total dissolution time for the Bemidji oil body is on the order of 100 years for benzene, 500 years for toluene, and 1000 years for ethylbenzene and xylene (H. I. Essaid and W. N. Herkelrath, pers. comm., 1999). These calculations are approximate because they do not account for the changing composition of the oil body during dissolution. Nevertheless, they indicate that non-aqueous phase sources may persist for time frames that exceed the current regulatory framework.

Microbial Ecology of Contaminant Plumes

The potential for significant biotransformation of contaminants depends on the capabilities and numbers of indigenous microorganisms that mediate the reactions. A microbial population must be present that is capable of degrading the contaminants under the geochemical conditions in the aquifer. Moreover, as conditions in the plume change, the microbial population must also change. Despite the critical role of microorganisms in natural attenuation, knowledge of how the active degrading microorganisms become established and function in a plume is limited (Madsen, 1998). For example, total counts of bacteria do not correlate with contaminant degradation (Madsen and others, 1991).

Moreover, the specific organisms that carry out the degradation reactions are rarely known. In many cases, cooperation of several populations within a microbial community is required but the mechanisms of the community interactions are poorly understood. The results of studies of the active microbial populations at Wurtsmith Air Force Base, together with results from the Bemidji, Pensacola, FL (wood-treatment wastes), and Cape Cod USGS Toxics Program sites have contributed to an increased understanding of these issues and provide a sense of the current level of knowledge.

Research conducted by the USGS Toxics Program at the former Wurtsmith Air Force Base in Michigan used new methods in microbial ecology based on analysis of the nucleic acids DNA (deoxyribonucleic acid) and RNA (ribonucleic acid) extracted from aquifer materials to examine in situ microorganisms. Sediment samples taken from specified TEAP zones in two (field replicate) cores exhibited similar community DNA compositions, suggesting similar community structure and demonstrating the reproducibility of both procedures. Cluster analysis of community DNA patterns indicated five major community groups (Haack and Reynolds, 1999). Current work is focused on defining the environmental gradients associated with these groupings. Preliminary data based on RNA analysis suggest that populations of methanogens (or other *Archaea*) are most abundant in sediments where the TEAP indicates methanogenesis or sulfate reduction during most of the year (Reynolds and Haack, 1999). Samples from the capillary fringe exhibited the largest amount of total bacterial RNA. The capillary fringe also was found to be an area of enhanced bacterial activity by Bone and Balkwill (1988) in a study of a pristine aquifer in Lula, Oklahoma. Dramatic changes in methanogen (or other Archaea) abundance occurred over vertical intervals of less than 1 m on each tested date. RNA analysis demonstrated spatial and temporal correlations between in situ abundance of a "TEAP - active population" (methanogens) and geochemical indications of methanogenesis (H_2 and CH_4 concentration). Additional population studies by Dojka and others (1998) also documented that methanogens were important populations in samples taken from zones at Wurtsmith where methane (CH_4) was in highest concentration in October 1996. However, this research also demonstrated that TEAP zones defined as iron-reducing or sulfate-reducing by H_2 gas analysis did not harbor significant populations of currently known iron- or sulfate-reducing bacteria. In fact, this research, employing DNA-based methods, demonstrated that there exist numerically dominant and (as of yet) uncultured, and therefore unknown, populations of microbes at this site.

Results from the Bemidji site provide insight into the microbial ecology of the anaerobic portion of a crude-oil plume. Lovley and others (1989) isolated an organism from the site that can degrade a variety of aromatic organic compounds under iron-reducing conditions. Bekins and others (1999) analyzed microbial populations, pore water chemistry, sediment grain sizes, and extractable iron at 15-30 cm intervals from cores containing both sediment and pore water. The most probable number method (MPN) was used to characterize the spatial distribution of six physiologic types of microorganisms: aerobes, denitrifiers, iron reducers, heterotrophic fermenters, sulfate reducers, and methanogens. Areas in the plume that have changed from iron-reducing to methanogenic conditions are clearly indicated by lower numbers of iron-reducers and the presence of culturable methanogens, heterotrophic fermenters, and sulfate reducers. These conditions are found in areas of high contaminant flux either in the vicinity of the nonaqueous oil or in the dissolved plume where higher concentrations are associated with local increases in aquifer permeability. In the older part of the plume under the oil body, the methanogenic niche spans 50 percent of the vertical thickness of the dissolved plume. At 30 m downgradient where the change to methanogenic conditions is more recent, the methanogenic niche spans 25 percent of the vertical thickness of the plume.

At the Pensacola USGS Toxics Program site, creosote wastes from a wood treatment facility operated from 1898-1982 have migrated

from unlined impoundment ponds into a deltaic sand aquifer. Conditions in the contaminant plume are primarily methanogenic and concentrations of DOC decreased from 357 mg/L at the impoundment ponds to 50 mg/L at 100 m down gradient. The presence of methane and organic acids in the plume provide evidence that methanogenic degradation was active in the aquifer (Goerlitz and others, 1985). Godsy and others (1992) found a 100-fold increase in culturable methanogens within the plume compared to the uncontaminated background. Modeling of the degradation processes by Bekins and others (1993) indicated that observations of a steady-state plume are consistent with a steady-state microbial population. One possible explanation for lack of growth in the microbial population is the toxicity of the creosote compounds. Laboratory studies indicate that enriched cultures of acetate-utilizing methanogens from the field site are inhibited by the soluble fraction of the creosote compounds (Bekins and others, 1997).

Results from microbiological studies at the Cape Cod study site demonstrate that 60 years of discharge of treated sewage to a highly-permeable, unconfined, sandy aquifer has resulted in a diverse and dynamic microbial community within the resultant 5 km-long contaminant plume. In spite of the long-term input of organic material into the aquifer, denitrification in the contaminant plume is limited with respect to organic carbon (Smith and Duff, 1988) and the bacteria therein appear to be metabolically stressed (Metge and others, 1993). A large (up to 10^6/mL) community of unattached bacteria is being advected downgradient along with the dissolved organic contaminants that they are degrading (Harvey and Barber, 1992) and the partitioning of the bacteria to the aqueous phase increases steadily with decreasing distance from the loading beds. Abundance of unattached bacteria correlates strongly with dissolved organic carbon (DOC) within the first 3 km and with the more readily-degraded (non-alkyl benzene sulfonate) DOC in the more distal portion of the plume.

Bacterial abundance within the Cape Cod contaminant plume also appears to be strongly controlled (Kinner and others, 1997) by a diverse (Novarino and others, 1997) protistan community that includes a number of species that are hitherto undescribed (Novarino and others, 1994). Large numbers of protozoa (up to 10^5/g) have been observed in both the oxic and suboxic zones of the contaminant plume (Kinner and others, written communication, U. of New Hampshire). Results from laboratory clearance rate studies suggest that the protistan community may be completely consuming the unattached population of bacteria immediately downgradient from the loading beds every few days (Kinner and others, 1998). Furthermore, the presence of protozoa appears to be causing a marked increase in the growth rate of the unattached bacteria within the plume (Kinner and others, written communication, U. of New Hampshire), thus promoting a greater efficiency in organic contaminant degradation. The community of protozoa is dominated by 2-3 μm nanoflagellates that feed selectively on the 0.8-1.5 μm size class of unattached bacteria (Kinner and others, 1998) that constitute much of the pore water biomass within the plume (Harvey and Garabedian, 1991). Although often weakly associated with grain surfaces, in situ and laboratory studies suggest the nanoflagellates are capable of a high degree of mobility within the aquifer (Harvey and others, 1995). This appears to be due, in part, to their strong motility, optimal size for transport (Harvey and Garabedian, 1991), and low buoyant density (Harvey and others, 1997), which contributes to their observed ability to respond quickly to spatial and temporal changes in DOC within the aquifer (Kinner, written communication, U. of New Hampshire).

THE ROLE OF MASS BALANCE

One of the desirable steps in demonstrating the efficacy of natural attenuation at a site is to quantify the relative contribution of individual processes to the total mass loss. In some cases a quantitative analysis may be required by the state regulators (for example, Minnesota Pollution Control Agency, 1996). In addition, the ability to demonstrate the magnitude of specific attenuation mechanisms strengthens public confidence in an RNA

decision. Depending on the goals of the analysis and the complexity of the site, a range of quantitative approaches can be used. An effective approach used for the Picatinny site combines simple rate laws with a range of estimates of parameters or fluxes. The results give a sense of both the role of individual processes and also the uncertainty in each of the values. A more complex approach was used at the Bemidji crude-oil site. In this case, a model of two-dimensional flow and transient transport with biodegradation reactions provided an estimate of the relative mass loss from each of the important biotransformation reactions. The Bemidji example illustrates how concentrations of reaction products can be used to constrain the contribution of a specific reaction to the observed attenuation. Regardless of whether the approach used is simple or complex, it is important that the quantification be based on measured data from the sites as in both the Picatinny and Bemidji examples. Another key aspect is that each of these site analyses is based on a careful understanding of the hydrologic processes controlling transport of the contaminants.

Using simple rate laws and parameter estimates, researchers at Picatinny Arsenal estimated the mass losses from several natural remediation processes and compared their effectiveness to a pump-and-treat system. Table 1 summarizes the estimated mass flux for contaminants at Picatinny Arsenal due to vapor flux, anaerobic biotransformation, desorption, and discharge into Green Pond Brook. Discharge of TCE dissolved in ground water into nearby Green Pond Brook and subsequent volatilization into the atmosphere also was an important mass sink prior to installation of the pump-and-treat system. Using the TCE concentration in ground-water and the average, base-flow ground-water discharge rate, Imbrigiotta and others (1995) estimated that between 32 and 63 kg/yr of TCE were discharged into the brook. It is apparent from these data that the pump-and-treat system is ineffective relative to natural remediation processes. The table shows that the sum of the flux of TCE to Green Pond Brook, the TCE flux to the atmosphere, and losses from anaerobic biodegradation processes may be several times greater than the flux of TCE from the pump-and-treat system. The mass balance exercise clarifies the emerging picture that pump-and-treat systems frequently are more useful for containment than for mass removal.

It should be noted that several possibly significant TCE sources and sinks have not been estimated. Specifically, no estimate has been made for the rate of TCE dissolution from a nonaqueous phase. To date, no positive confirmation of a nonaqueous TCE phase has been made, let alone estimates of TCE dissolution rates. No estimate of TCE transport across the unconfined aquifer's lower confining unit has been made, despite the fact that TCE has been detected in the deeper, confined aquifer. Lack of adequate concentration data and information on the physicochemical properties of the confining layer prevent a meaningful calculation. Lastly, estimates of TCE desorption and biodegradation rates are based on laboratory experiments using soil and ground water from the field site. These estimates likely have more uncertainty than the direct field estimates of TCE removal by volatilization, pump-and-treat extraction, and discharge to Green Pond Brook.

Table 1. Estimates of TCE sinks and sources for ground water from the Building 24 contamination plume at Picatinny Arsenal, New Jersey.

Process	TCE source or sink	Mass TCE flux, kg/yr
Pump-and-treat system	Sink	70*
Diffusion/advection of TCE vapors through unsaturated zone	Sink	50
Anaerobic biotransformation	Sink	52 to 1040
Desorption from aquifer sediments	Source	474 to 2300
Discharge to Green Pond Brook	Sink	32 to 63

*Based on data from 1995.

In the Bemidji site model created by Essaid and others (1995a), volatile and nonvolatile organic compounds in the petroleum hydrocarbon plume are transported and undergo degradation by three microbial populations; aerobes, Mn and Fe-reducers, and methanogens. The biotransformation reactions in the model consume dissolved oxygen, and solid-phase Fe(III) and Mn(IV). In addition they produce dissolved Fe(II), Mn(II), and methane. Observations of concentrations of these reactants and products in the ground-water plume over the period 1984-1992 were used to constrain the relative contribution of each reaction to the overall mass loss of petroleum hydrocarbons. The simulations were performed with the BIOMOC model code (Essaid and Bekins, 1997). By using an inhibition formulation in the code, iron-reduction was delayed until dissolved oxygen was exhausted. Similarly, methanogenesis was inhibited if solid phase Fe(III) and Mn(IV) were still present. The model results accurately reproduce the temporal and spatial concentration changes in volatile and nonvolatile organic compounds, dissolved Fe(II), Mn(II), and methane. The simulation indicates that, over a distance of 200 m, 46 percent of the total dissolved organic carbon introduced into the aquifer is degraded. Of this, aerobic processes account for 40 percent of the degradation, while the remaining 60 percent is by anaerobic processes (5 percent by Mn reduction, 19 percent by Fe reduction, and 36 percent by methanogenesis). The Bemidji modeling illustrates how concentrations of reaction products can be used to constrain the fraction of the total contaminant mass loss that results from each biotransformation process.

SUMMARY AND FUTURE DIRECTIONS

The increased use of natural attenuation as a remediation strategy in recent years is based on careful study results that document the effectiveness of specific attenuation processes in the field. The goal of the U. S. Geological Survey Toxic Substances Hydrology Program is to better understand the fate of contaminants in the environment in support of improved strategies for contaminated site assessments, monitoring programs, and decisions regarding remedial options. Results from the program have documented the effectiveness of volatilization and biotransformation as attenuation processes in the subsurface for several types of contaminants. Additional studies of the subsurface microbial populations that transform contaminants have provided insights into the distributions of organisms and some estimates of the biotransformation rates.

Research results also show that a number of problems and research challenges remain for understanding natural attenuation. One of these challenges is the spatial and temporal variability inherent in aquifers and hydrologic systems. This variability is now well documented and several associated research challenges are clear. These include methods to predict the effect of variability on natural attenuation; methods to assess uncertainty in the fate of ground-water plumes associated with incomplete characterization, and designs for optimal monitoring strategies that can provide early warning of failure of the natural attenuation processes. Another challenge is the long time frame over which unrecoverable immobile contaminant phases will continue to act as sources of dissolved contaminants to the ground water. Although the expected longevity is now well documented (National Research Council, 1994), the regulatory community is still grappling with policies for managing this problem with risk-based assessments. An important goal of future research will be to enhance the current understanding of the sustainability of natural attenuation processes into the distant future (hundreds of years). This understanding will be necessary to assess whether a long-term source ultimately poses a threat to human health and the environment.

Research at the USGS Toxics Program study sites has focussed on several classes of compounds including petroleum hydrocarbons, the chlorinated solvent TCE, wood treatment wastes, nitrogen, and sewage wastewater. The results show that natural attenuation processes are highly specific to the individual compounds, interactions among compounds, and the natural geochemistry of the contaminated aquifer. Thus,

another set of challenges is to understand the fate of specific compounds under a variety of redox conditions, the interactions between compounds, and the fate of compounds not yet studied. For example, the recent use of ether-oxygenates such as MTBE as gasoline additives challenges the paradigm of natural attenuation remediation which has developed within a BTEX frame of reference. Compared to BTEX, MTBE is much more soluble and is believed to be less degradable than BTEX in the subsurface. These facts together with field evidence that MTBE solute migration advances ahead of BTEX at gasoline-spill sites (for example, Landmeyer and others, 1996) suggest that volatile losses of MTBE from the source area may be significant in assessing natural attenuation with respect to MTBE.

Understanding the capabilities of subsurface microorganisms that mediate biotransformation reactions represents another challenge to implementing natural attenuation. Many open questions remain with respect to these organisms. These include (1) biotransformation rates under various conditions and what controls them; (2) the extent to which multiple compounds either interfere with or enhance transformation rates; (3) whether the transformations are mediated by single species or consortia; (4) how degradative capabilities are acquired; and (5) how the microbial populations become established in the aquifer and what controls their growth. Finally, work at the USGS Toxics Program study sites has demonstrated the efficacy of quantitative mass balances in understanding the contributions of specific processes to the overall attenuation. The desire for an accounting of the fate of contaminants is emerging as a priority of regulators tasked with site decisions (for example, Minnesota Pollution Control Agency, 1996). Quantitative assessments may be based on a spectrum of approaches. However, regardless of the approach, the value is highly dependent on how well the model represents the processes at the site. Thus a need exists for strategies that increase the use and quality of quantitative mass balances. These may include wider use of parameter estimation techniques, graphical user interfaces, better training of modelers, and a more iterative approach to modeling.

Continued research work on subsurface processes at the USGS Toxics Program study sites will be directed toward some of these research challenges. Other work in the program focuses on the fate of contaminants in surface waters, acid mine drainage, the regional-scale fate of pesticides, and metals and pesticides in the San Francisco Bay Estuary. More information about the program and the results from individual research sites can be found at the web site at http://toxics.usgs.gov/toxics/.

REFERENCES

Anderson, R.T., Rooney-Varga, J.N., Gaw, C.V., and Lovley, D.R., 1998, Anaerobic benzene oxidation in the Fe(III) reduction zone of petroleum-contaminated aquifers: Environmental Science and Technology, v. 32, no. 9, p. 1222-1229.

Baedecker, M.J., Cozzarelli, I.M., Eganhouse, R.P., Siegel, D.I., and Bennett, P.C., 1993, Crude oil in a shallow sand and gravel aquifer-III. Biogeochemical reactions and mass balance modeling in anoxic groundwater: Applied Geochemistry, v. 8, p. 569-586.

Baedecker, M.J., Cozzarelli, I.M., Evans, J.R., and Hearn, P.P., 1992, Authigenic mineral formation in aquifers rich in organic material, *in* 7th International Symposium on Water-Rock Interaction: Balkema, Rotterdam, p. 257-261.

Baehr, A.L., 1987, Selective transport of hydrocarbons in the unsaturated zone due to aqueous and vapor phase partitioning: Water Resources Research, v. 23, no. 10, p. 1926-1938.

Bekins, B.A., Cozzarelli, I.M., Godsy, E.M., Warren, E., Tuccillo, M.E., Essaid, H.I., and Paganelli, V.V., 1999, Chemical and physical controls on microbial populations in the Bemidji Toxics Site crude-oil plume, *in* U.S. Geological Survey Toxic Substances Hydrology Program--Proceedings of the Technical Meeting, Charleston, South Carolina, March 8-12, 1999-- Volume 3 -- Subsurface Contamination from Point

Sources: U.S. Geological Survey Water-Resources Investigations Report 99-4018C, this volume.

Bekins, B.A., Godsy, E.M., and Goerlitz, D.F., 1993, Modeling steady-state methanogenic degradation of phenols in groundwater: Journal of Contaminant Hydrology, v. 14, no. 3-4, p. 279-294.

Bekins, B.A., Godsy, E.M., and Warren, E., 1997, Inhibition of acetoclastic methanogenesis by complex mixtures of hydrocarbons: EOS, Transactions, American Geophysical Union, v. 78, no. 46, p. F289.

Bennett, P.C., Siegel, D.E., Baedecker, M.J., and Hult, M.F., 1993, Crude oil in a shallow sand and gravel aquifer-I. Hydrogeology and inorganic geochemistry: Applied Geochemistry, v. 8, p. 529-549.

Bone, T.L. and Balkwill, D.L., 1988, Morphological and cultural comparison of microorganisms in surface and subsurface sediments at a pristine study site in Oklahoma: Microbial Ecology, v. 16, p. 49-64.

Brooks, M.H., Smith, R.L., and Macalady, D.L., 1992, Inhibition of existing denitrification activity by chloramphenicol: Applied and Environmental Microbiology, v. 58, no. 5, p. 1746-1753.

Ceazan, M., 1987, Migration and transformations of ammonium and nitrate in a sewage-contaminated aquifer at Cape Cod, Massachusetts: Colorado School of Mines, p.

Ceazan, M.L., Thurman, E.M., and Smith, R.L., 1988, Retardation of ammonium and potassium transport through a contaminated sand and gravel aquifer: The role of cation exchange: Environmental Science and Technology, v. 23, no. 11, p. 1402-1408.

Chapelle, F.H., Haack, S.K., Adriaens, P., Henry, M.A., and Bradley, P.M., 1996, Comparison of Eh and H_2 measurements for delineating redox processes in a contaminated aquifer: Environmental Science and Technology, v. 30, p. 3565-3569.

Cozzarelli, I.M., 1993, the biogeochemical fate of organic acids in a shallow aquifer contaminated with gasoline: Charlottesville, University of Virginia, 240 p.

Cozzarelli, I.M., Baedecker, M.J., Eganhouse, R.P., and Goerlitz, D.F., 1994, The geochemical evolution of low-molecular-weight organic acids derived from the degradation of petroleum contaminants in groundwater: Geochimica et Cosmochimica Acta, v. 58, p. 863-877.

Dojka, M.A., Hugenholtz, P., Haack, S.K., and Pace, N.R., 1998, Microbial diversity in a hydrocarbon- and chlorinated solvent-contaminated aquifer undergoing intrinsic bioremediation: Applied and Environmental Microbiology, v. 64, p. 3869-3877.

Eganhouse, R.P., Baedecker, M.J., Cozzarelli, I.M., Aiken, G.R., Thorn, K.A., and Dorsey, T.F., 1993, Crude oil in a shallow sand and gravel aquifer-II. Organic geochemistry: Applied Geochemistry, v. 8, p. 551-567.

Ehlke, T.E., Wilson, B.H., Wilson, J.T., and Imbrigiotta, T.E., 1996, In situ biotransformation of trichloroethylene and cis-1,2-dichloroethylene at Picatinny Arsenal, New Jersey, *in* U.S. Geological Survey Toxic Substances Hydrology Program--Proceedings of the Technical Meeting, Colorado Springs, Colorado, September 20-24, 1993: U.S. Geological Survey Water-Resources Investigations Report 94-4015, p. 329-338.

Essaid, H.I. and Bekins, B.A., 1997, BIOMOC, A multispecies transport model with biodegradation: U. S. Geological Survey Water Resources Investigation Report 97-4022, 68 p.

Essaid, H.I., Bekins, B.A., Godsy, E.M., Warren, E., Baedecker, M.J., and Cozzarelli, I.M., 1995a, Simulation of aerobic and anaerobic biodegradation processes at a crude oil spill site: Water Resources Research, v. 31, no. 12, p. 3309-3327.

Essaid, H.I., Herkelrath, W.N., and Dillard, L.A., 1995b, The influence of spatial variability of hydraulic properties on the flow of water near a subsurface oil body: EOS, Transactions, American Geophysical Union, v. 76, no. 46, p. F266.

Fischer, J.M., Smith, N.P., and Baehr, A.L., 1996, Hydrogeology, contaminant distribution, and biodegradation processes at a gasoline-spill research site in Galloway Township, New Jersey, *in* U.S. Geological Survey Toxic Substances Hydrology Program--Proceedings of the Technical Meeting, Colorado Springs, Colorado, September 20-24, 1993: U.S. Geological Survey Water-Resources Investigations Report 94-4015, p. 7-16.

Garabedian, S.P., LeBlanc, D.R., Gelhar, L.W., and Celia, M.A., 1991, Large-scale natural gradient tracer test in sand and gravel, Cape Cod, Massachusetts: 2. Analysis of spatial moments for a nonreactive tracer: Water Resources Research, v. 27, no. 5, p. 911-924.

Godsy, E.M., Goerlitz, D.F., and Grbic-Galic, D., 1992, Methanogenic biodegradation of creosote contaminants in natural and simulated ground water ecosystems: Ground Water, v. 30, no. 2, p. 232-242.

Goerlitz, D.F., Troutman, D.E., Godsy, E.M., and Franks, B.J., 1985, Migration of wood preserving chemicals in contaminated groundwater in a sand aquifer at Pensacola, Florida: Environmental Science and Technology, v. 19, p. 955-961.

Haack, S.K. and Reynolds, L.A., 1999, Using molecular approaches to describe microbial populations at contaminated sites, *in* U.S. Geological Survey Toxic Substances Hydrology Program--Proceedings of the Technical Meeting, Charleston, South Carolina, March 8-12, 1999-- Volume 3 -- Subsurface Contamination from Point Sources: U.S. Geological Survey Water-Resources Investigations Report 99-4018C, this volume.

Harvey, R.W. and Barber, L.B., 1992, Associations of free-living bacteria and dissolved organic compounds in a plume of contaminated groundwater: Journal of Contaminant Hydrology, v. 9, no. 1-2, p. 91-103.

Harvey, R.W. and Garabedian, S., 1991, Use of colloid filtration theory in modeling movement of bacteria through a contaminated sandy aquifer: Environmental Science and Technology, v. 25, p. 178-185.

Harvey, R.W., Kinner, N.E., Bunn, A., MacDonald, D., and Metge, D., 1995, Transport behavior of groundwater protozoa and protozoa-sized microspheres in sandy aquifer sediments: Applied and Environmental Microbiology, v. 61, p. 209-217.

Harvey, R.W., Metge, D.W., Kinner, N., and Mayberry, N., 1997, Physiological considerations in applying laboratory-determined buoyant densities to predictions of bacterial and protozoan transport in groundwater: Results of in-situ and laboratory tests: Environmental Science and Technology, v. 31, p. 289-295.

Hiebert, F.K. and Bennett, P.C., 1992, Microbial control of silicate weathering in organic-rich ground water: Science, v. 258, no. 9 October, p. 278-281.

Huffman, G.C., Cummings, T.R., Gillespie, J.L., and Brannen, J.R., 1995, Wurtsmith Air Force Base, Michigan. Investigation of soil and ground water contamination at selected sites. Installation Restoration Program Phase-II - Confirmation/Quantification Stage 2: U.S. Geological Survey.

Hult, M.F., 1984, Groundwater contamination by crude oil at the Bemidji, Minnesota, research site-An introduction, *in* Goundwater Contamination by Crude Oil at the Bemidji, Minnesota, Research Site: U.S. Geological Survey Water-Resources Investigations Report 84-4188, p. 1-15.

Imbrigiotta, T.E., Ehlke, T.A., Martin, M., Koller, D., and Smith, J.A., 1995, Chemical and biological processes affecting the fate and transport of trichloroethylene in the subsurface at Picatinny Arsenal: Hydrological Science and Technology, v. 11, p. 26-50.

Kinner, N.E., Harvey, R.W., Blakeslee, K., Novarino, G., and Meeker, L.D., 1998, Size-selective predation of groundwater bacteria by nanoflagellates in an organically-contaminated aquifer: Applied and Environmental Microbiology, v. 64, p. 618-625.

Kinner, N.E., Harvey, R.W., and Kazmierkiewicz-Tabaka, M., 1997, Effect of flagellates on free-living bacterial abundance in an organically-contaminated aquifer: FEMS Microbiological Reviews, v. 20, p. 249-259.

Koller, D., Imbrigiotta, T.E., Baehr, A.L., and Smith, J.A., 1996, Desorption of trichloroethylene from aquifer sediments at Picatinny Arsenal, New Jersey, *in* U.S. Geological Survey Toxic Substances Hydrology Program--Proceedings of the Technical Meeting, Colorado Springs, Colorado, September 20-24, 1993: U.S. Geological Survey Water-Resources Investigations Report 94-4015, p. 329-338.

Lahvis, M.A. and Baehr, A.L., 1996, Estimation of rates of aerobic hydrocarbon biodegradation by simulation of gas transport in the unsaturated zone: Water Resources Research, v. 32, no. 7, p. 2231-2249.

Landmeyer, J.E., Chapelle, F.H., and Bradley, P.M., 1996, Assessment of intrinsic bioremediation of gasoline contamination in the shallow aquifer, Laurel Bay Exchange, Marine Corps Air Station Beaufort,South Carolina: U.S. Geological Survey Water-Resources Investigations Report 96-4026, 50 p.

LeBlanc, D.R., Garabedian, S.P., Hess, K.M., Gelhar, L.W., Quadri, R.D., Stollenwerk, K.G., and Wood, W.W., 1991, Large-scale natural gradient tracer test in sand and gravel aquifer, Cape Cod, Massachusetts: 1. Experimental design and observed tracer movement: Water Resources Research, v. 27, no. 5, p. 895-910.

Lovley, D.R., Baedecker, M.J., Lonergan, D.J., Cozzarelli, I.M., Phillips, E.J.P., and Siegel, D.I., 1989, Oxidation of aromatic compounds coupled to microbial iron reduction: Nature, v. 339, p. 297-299.

Madsen, E.L., 1998, Epistemology of Environmental Microbiology: Environmental Science and Technology, v. 32, no. 4, p. 429-439.

Madsen, E.L., Sinclair, J.L., and Ghiorse, W.C., 1991, In situ biodegradation: Microbiological patterns in a contaminated aquifer: Science, v. 252, no. May 10, p. 830-833.

Martinson, M., 1998, 1998 national RNA survey: Underground Tank Technology Update, Madison, WI, University of Wisconsin-Madison, 12, 14-16.

McGuire, J.T., Smith, E.W., Long, D.T., Hyndman, D.W., Haack, S.K., Kolak, J.J., Klug, M.J., Velbel, M.A., and Forney, L.J., 1999, Temporal variations in biogeochemical processes that influence ground-water redox zonation, *in* U.S. Geological Survey Toxic Substances Hydrology Program--Proceedings of the Technical Meeting, Charleston, South Carolina, March 8-12, 1999-- Volume 3 -- Subsurface Contamination from Point Sources: U.S. Geological Survey Water-Resources Investigations Report 99-4018C, this volume.

Metge, D.W., Brooks, M., Smith, R., and Harvey, R.W., 1993, Effect of treated-sewage contamination upon bacterial energy charge, adenine nucleotides, and DNA in a sandy aquifer on Cape Cod: Applied and Environmental Microbiology, v. 59, p. 2304-2310.

Minnesota Pollution Control Agency, 1996, Natural Attenuation of Chlorinated Solvents in Ground Water - Draft Guidelines: Minnesota Pollution Control Agency, Site Response Section 24 p.

Murphy, F. and Herkelrath, W.N., 1996, A sample-freezing drive shoe for a wire line piston core sampler: Ground Water Monitoring and Remediation, v. 16, p. 86-90.

Novarino, G., Warren, A., Butler, H., Lambourne, G., Boxshall, A., Bateman, J., Kinner, N.E., Harvey, R.W., Mosse, R.A., and Teltsch, B., 1997, Protistan communities in aquifers: a review: FEMS Microbiological Reviews, v. 20, p. 261-275.

Novarino, G., Warren, A., Kinner, N.E., and Harvey, R.W., 1994, Protists from a sewage-contaminated aquifer on Cape Cod, Massachusetts: U.S.A. Geomicrobiology Journal, v. 12, p. 23-36.

NRC, 1994, Alternatives for Ground Water Cleanup: Washington, D. C., National Academy Press, p. 315.

NRC, 1997, Innovations in ground water and soil cleanup: From concept to commercialization: Washington, D. C., National Academy Press, p. 265.

Reynolds, L.A. and Haack, S.K., 1999, Evaluation of RNA hybridization to assess bacterial population dynamics at natural attenuation sites, *in* U.S. Geological Survey Toxic Substances Hydrology Program--Proceedings of the Technical Meeting, Charleston, South Carolina, March 8-12, 1999-- Volume 3 -- Subsurface Contamination from Point Sources: U.S. Geological Survey Water-Resources Investigations Report 99-4018C, this volume.

Rice, D.W., Grose, R.D., Michaelsen, J.C., Dooher, B.P., MacQueen, D.H., Cullen, S.J., Kastenberg, W.E., Everett, L.E., and Marino, M.A., 1995, California Leaking Underground Fuel Tank (LUFT) Historical Case Study: Lawrence Livermore National Laboratory UCRL-AR-122207, 20 p.

Sahoo, D., Smith, J.A., Imbrigiotta, T.E., and McLellan, H.M., 1998, Surfactant-enhanced remediation of a trichloroethene (TCE) contaminated aquifer: II. Transport of TCE: Environmental Science and Technology, v. 32, p. 1686-1693.

Shapiro, A.M., 1994, Estimating transport properties of crystalline rock over distances from meters to kilometers using laboratory- and field-scale tests and geochemical and isotopic data: Preliminary results from the Mirror Lake site, New Hampshire, *in* American Geophysical Union Chapman conference on Aqueous Phase and Multiphase Transport in Fractured Rock: Burlington, VT.

Shapiro, A.M., 1996, Using environmental tracers to estimate matrix diffusion in fractured rock over distances of kilometers: Results from the Mirror Lake site, New Hampshire: EOS, Transactions, American Geophysical Union, v. 77, no. 17, p. S107.

Smith, J.A., Chiou, C.T., Kammer, J.A., and Kile, D.E., 1990, Effect of soil moisture on the sorption of trichloroethene vapor to vadose-zone soil at Picatinny Arsenal: Environmental Science and Technology, v. 24, p. 676-683.

Smith, J.A., Tisdale, A.K., and Cho, H., 1996a, Quantification of natural vapor fluxes of trichloroethene in the unsaturated zone at Picatinny Arsenal, New Jersey: Environmental Science and Technology, v. 30, p. 2243-2250.

Smith, R.L., 1997, Determining the terminal electron-accepting reaction in the saturated subsurface, *in* Manual of Environmental Microbiology Washington, D.C., ASM Press, p. 577-585.

Smith, R.L., Ceazan, M.L., and Brooks, M.H., 1994, Autotrophic, hydrogen-oxidizing, denitrifying bacteria in groundwater, potential agents for bioremediation of nitrate contamination: Applied and Environmental Microbiology, v. 60, no. 6, p. 1949-1955.

Smith, R.L. and Duff, J.H., 1988, Denitrification in a sand and gravel aquifer: Applied and Environmental Microbiology, v. 54, no. 5, p. 1071-1078.

Smith, R.L., Garabedian, S.P., and Brooks, M.H., 1996b, Comparison of denitrification activity measurements in groundwater using cores and natural-gradient tracer tests: Environmental Science and Technology, v. 30, no. 12, p. 3448-3456.

Smith, R.L., Harvey, R.W., and LeBlanc, D.R., 1991a, Importance of closely spaced vertical sampling in delineating chemical and microbiological gradients in groundwater studies: Journal of Contaminant Hydrology, v. 7, p. 285-300.

Smith, R.L., Howes, B.L., and Duff, J.H., 1991b, Denitrification in nitrate-contaminated groundwater: Occurrence in steep vertical gradients: Geochimica et Cosmochimica Acta, v. 77, no. 7, p. 1815-1825.

Tuccillo, M.E., 1998, Processes and effects of iron reduction in anoxic surficial aquifers: Charlottesville, University of Virginia, Ph.D., 194 p.

USGS, 1991, Wurtsmith Air Force Base, Michigan: Investigations of groundwater

and soil contamination at selected sites. Installation restoration program Phase II - Confirmation/Quantification Stage 1. Vol. I.: U.S. Geological Survey Administrative Report.

Wiedemeier, T., Wilson, J.T., Kampbell, D.H., Miller, R.N., and Hansen, J.E., 1995, Technical protocol for implementing intrinsic remediation with long-term monitoring for natural attenuation of fuel contamination dissolved in groundwater, Volume I: Air Force Center for Environmental Excellence, Technology Transfer Division, Brooks Air Force Base.

Wilson, B.H., Ehlke, T.A., Imbrigiotta, T.E., and Wilson, J.T., 1991, Reductive dechlorination of trichloroethylene in anoxic aquifer material from Picatinny Arsenal, New Jersey, *in* U.S. Geological Survey Toxic Substances Hydrology Program--Proceedings of the Technical Meeting, Monterey, California, March 11-15, 1991: U.S. Geological Survey Water-Resources Investigations Report 91-4034, p. 329-338.

Wood, W.W., Shapiro, A.M., Hsieh, P.A., and Councell, T.B., 1996, Observational experimental and inferred evidence for solute diffusion in fracture granite aquifers: Examples from the Mirror Lake watershed, Grafton County, New Hampshire, *in* U.S. Geological Survey Toxic Substances Hydrology Program--Proceedings of the Technical Meeting, Colorado Springs, Colorado, September 20-24, 1993: U.S. Geological Survey Water-Resources Investigations Report 94-4015, p. 167-170.

AUTHOR INFORMATION

Barbara A. Bekins, Hedeff I. Essaid, U. S. Geological Survey, Menlo Park, California

Ronald W. Harvey, Richard L. Smith, U. S. Geological Survey, Boulder, Colorado

Arthur L. Baehr, U. S. Geological Survey, Trenton, New Jersey

Isabelle M. Cozzarelli, Allen M. Shapiro, U. S. Geological Survey, Reston, Virginia

Sheridan K. Haack, U. S. Geological Survey, Lansing, Michigan

James A. Smith, University of Virginia, Charlottesville, Virginia

Processes that Control the Natural Attenuation of Hydrocarbons and Fuel Oxygenates at Gasoline Release Sites

Gasoline releases are perhaps the most frequently cited cause of ground-water contamination. The most soluble constituents of conventional gasoline are the aromatic hydrocarbons - benzene, toluene, ethyl benzene, and xylenes (BTEX). Processes that control the transport and natural attenuation of BTEX in ground water have been the focus of longstanding activity in the Toxic Substances Hydrology Program through research projects conducted at Bemidji Minnesota; Galloway Township, New Jersey; and Laurel Bay, South Carolina. Results of this research are often cited by the petroleum industry as the concept of natural attenuation has gained acceptance over the past ten years. Regulators have realized that, in many cases, the use of engineered remediation to re-establish pristine conditions at a spill site is more ideological than practical. This awareness has culminated in the recent release of the U.S. Environmental Protection Agency's "Monitored Natural Attenuation Policy Directive 9200.4-17" from the EPA's Office of Solid Waste and Emergency Response.

Extensive monitoring of the geochemical signature of contaminated ground water at these sites has lead to fundamental understanding of BTEX degradation by indigenous microbes through aerobic and anaerobic reactions involving various terminal electron acceptors. In particular, this monitoring led to the development of using hydrogen (a ubiquitous intermediate of hydrocarbon degradation) concentrations to facilitate the evaluation of the efficiency of natural attenuation processes. Mathematical models of reactive transport of BTEX in the plumes have been applied to quantify reaction rates and study the dynamics of plume migration subject to natural attenuation processes.

BTEX mass loss from ground water to the unsaturated zone due to volatilization and aerobic degradation in the capillary zone also is a factor contributing to natural attenuation. Unsaturated-zone gas composition data collected at the Galloway and Laurel Bay sites and transport modeling allows for quantification of contaminant mass loss. For BTEX these two processes are coupled, that is aerobic degradation enhances the rate of volatilization. The overall process is significant near the source, where spilled product is at the water table.

Increased usage of oxygenated gasoline in recent years challenges the natural attenuation paradigm because methyl tert-butyl ether (MTBE), the most widely used fuel oxygenate, is much more soluble, less readily adsorbed, and believed to be much less reactive in many aquifer systems than BTEX. MTBE has been added to gasoline in small quantities as an octane enhancer since the late 1970s. However, MTBE use is now (1999) substantially greater; since the winter of 1992, the compound has been blended in gasoline in urban areas throughout the country to meet the gasoline oxygen-content requirements of amendments to the Federal Clean Air Act. The gasoline that contaminates shallow ground water at Laurel Bay, S.C. contains MTBE. The contaminated ground water discharges to an adjacent surface-water body. Consequently, this site has become the focus of gasoline release research in the Toxic Substances Hydrology Program.

Collaborative studies on MTBE at Laurel Bay include the following hydrologic compartments:

(1) The saturated zone - Horizontal and vertical distributions of MTBE relative to benzene and the relation of these distributions to ambient redox conditions have been monitored since 1993. Simulation of these distributions using numerical models specifically developed to directly account for redox conditions provide a method for quantifying attenuation processes and predicting the relative behavior of benzene and MTBE. Integral to these investigations is the application of new analytical techniques to detect MTBE and potential MTBE-biotransformation intermediates. Laboratory microcosms containing aquifer materials are used to assess the potential for MTBE mineralization and intermediate formation under a wide range of redox conditions.

(2) The unsaturated zone - Methods previously developed to study volatilization and aerobic degradation for BTEX have been extended to study these processes for MTBE. New analytical methods for sampling unsaturated zone gas and pore water have been developed to quantify volatile losses to the unsaturated zone downgradient from the source area. Laboratory column experiments allow for detailed study of the role of the capillary zone in limiting mass transfer. Attenuation involving the unsaturated zone is potentially more important for MTBE than for BTEX because degradation of MTBE in contaminated ground water may not be significant for MTBE, and preliminary results suggest that MTBE degradation is favored under aerobic conditions.

(3) Trees – Trees growing above the contaminated aquifer use ground water during transpiration and remove MTBE from the aquifer, suggesting the potential application of phytoremediation strategies to contain shallow plumes of MTBE-contaminated ground water.

(4) Streambed sediments - Significant mineralization of MTBE has been observed in streambed sediments that receive ground-water discharge containing MTBE. This observation indicates that sediments at such hydrologic interfaces may be a significant and previously unrecognized sink for both ground-water and atmospheric sources of MTBE.

Combined, these collaborative studies suggest that pathways for natural attenuation of MTBE do exist; however, the magnitude of each pathway needs to be examined and compared to BTEX to understand the environmental liability associated with releases of MTBE-oxygenated gasoline.

For additional information contact:

James E. Landmeyer, USGS, Columbia,
South Carolina (email: jlandmey@usgs.gov), or

Arthur L. Baehr, USGS, W. Trenton,
New Jersey (email: abaehr@usgs.gov)

Fate of MTBE Relative to Benzene in a Gasoline-Contaminated Aquifer (1993-98)

By James E. Landmeyer, Paul M. Bradley, and Francis H. Chapelle

ABSTRACT

Methyl *tert*-butyl ether (MTBE) and benzene have been measured since 1993 in a shallow, sandy aquifer contaminated by a mid-1980's release of gasoline containing fuel oxygenates. In wells downgradient of the release area, MTBE was detected before benzene, reflecting a chromatographic-like separation of these compounds in the direction of ground-water flow. Higher concentrations of MTBE and benzene were measured in the deeper sampling ports of multilevel sampling wells located near the release area, and also up to 10 feet (3 meters) below the water-table surface in nested wells located farther from the release area. This distribution of higher concentrations at depth is caused by recharge events that deflect originally horizontal ground-water flowlines. In the laboratory, microcosms containing aquifer material incubated with uniformly labeled ^{14}C-MTBE under aerobic and anaerobic, Fe(III)-reducing conditions indicated a low but measurable biodegradation potential (<3% ^{14}C-MTBE as $^{14}CO_2$) after a seven-month incubation period. *Tert*-butyl alcohol (TBA), a proposed microbial-MTBE transformation intermediate, was detected in MTBE-contaminated wells, but TBA was also measured in unsaturated release-area sediments. This suggests that TBA may have been present in the original fuel spilled and not necessarily reflect microbial degradation of MTBE. Combined, these data suggest that milligram per liter to microgram per liter decreases in MTBE concentrations relative to benzene are caused by the natural attenuation processes of dilution and dispersion with less-contaminated ground water in the direction of flow rather than biodegradation at this point-source gasoline release site.

INTRODUCTION

Fuel oxygenates are petroleum-derived compounds that contain oxygen and have been used in motor-vehicle fuels since the phase-out of tetra-ethyl lead in the late 1970's. Of the ether and alcohol compounds commonly used as fuel oxygenates, methyl *tert*-butyl ether (MTBE) is the most widely used, and was the second most-produced organic compound in the United States in 1993 (Reisch, 1994). Because of this increased and widespread use of MTBE, the frequency of MTBE detection in the environment has increased proportionately. MTBE has been detected in many parts of the hydrologic cycle, including precipitation, runoff, surface water, and ground water (Squillace and others, 1996; Zogorski and others, 1996).

In ground-water systems, the presence of MTBE can be caused by both point and non-point sources. The highest concentrations (milligram per liter (mg/L)) of MTBE in ground water, however, are related to point-source releases from underground storage tanks (UST's) that contain gasoline amended with fuel oxygenates. This situation raises concern, because UST sites are often located near heavily populated areas. In addition, because MTBE has not been measured during routine remedial investigations at many UST sites, there is a singular absence of time-series field data describing the behavior of MTBE compared to benzene, toluene, ethylbenzene, and xylenes (BTEX) (Buxton and others, 1997). This data gap presents a significant obstacle to managers and regulatory officials tasked with protecting current and future drinking-water quality from MTBE contamination.

The purpose of this paper is to present the areal and vertical distributions of MTBE relative to the most soluble BTEX compound, benzene, in a shallow, gasoline-contaminated aquifer investigated between 1993 and 1998 in South Carolina. The implications of measuring *tert*-butyl

alcohol (TBA) and *tert*-butyl formate (TBF), potential MTBE biotransformation intermediates, are also discussed. Also presented are MTBE biodegradation potentials determined using laboratory microcosms containing natural microbial communities. The authors believe this is the first paper to document the long-term spatial distribution of MTBE and benzene at a point-source gasoline-spill site containing fuel oxygenates.

BACKGROUND AND STUDY AREA

The study area is located on Port Royal Island, South Carolina (SC), in the Lower Coastal Plain of the Atlantic Coastal Plain geophysical province. Gasoline containing fuel oxygenates from a gasoline station (Figure 1) near Beaufort, SC, was detected in the shallow aquifer in September 1991, although the UST had most likely leaked since the mid-1980's. An initial remedial investigation in 1993 indicated BTEX concentrations above United States Environmental Protection Agency (EPA) maximum contaminant levels (MCLs). In October 1993, the UST and surrounding sediments were excavated. In 1994, the U.S. Geological Survey (USGS), the Southern Division, Naval Facilities Engineering Command (Southdiv), and Marine Corps Air Station Beaufort (MCAS) assessed the fate and transport of BTEX based on a numerical solute-transport model protocol (Landmeyer and others, 1996).

The shallow, unconfined water-table aquifer contaminated by the gasoline release is comprised of silty, well-sorted sand grains of Pleistocene to Holocene age to a depth around 45 feet (ft) (13.7 m), where a regional clay-rich confining unit is encountered. No clays or discontinuous clay lenses are present in the aquifer. The average depth to water from land surface near the source area is about 13 ft (3.9 m), and between 2 to 9 ft (0.6 to 2.7 m) near a concrete-lined drainage ditch located about 700 ft (215 m) from the source area. Although designed to contain surface runoff, a discharge measurement indicated that 50% of the flow in the ditch is from ground-water discharge (J.E. Landmeyer and W.B. Guimaraes, unpublished data, 1995). The uncontaminated silty sand is characterized by ferric oxyhydroxide grain coatings, which is consistent with the measured presence of considerable dissolved oxygen (about 4 mg/L) in uncontaminated wells in the aquifer. The frequency of iron oxyhydroxide coatings on sand grains inspected visually decreases as the saturated depth increases and as the petroleum compound concentrations increase.

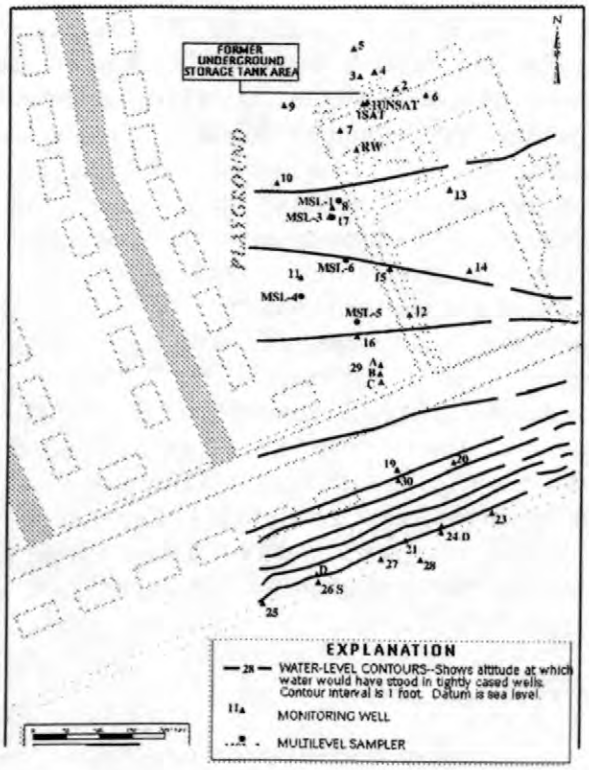

Figure 1. Locations of monitoring wells, multilevel sampling wells, source-area sediment samples, and representative water-table surface (January 27, 1998).

Ground-water flow at the site is from higher heads at the source area to the south under the influence of lower heads adjacent to the concrete-lined ditch (Figure 1). The fine-grained sand of the aquifer and absence of clay materials give an average hydraulic conductivity of 11 ft/d (3.4 m/d), resulting in an average ground-water flow rate of 70 ft/yr (21 m/yr) near the source area, and about 500 ft/yr (153 m/yr) near the concrete-lined ditch under the influence of steeper topographic gradients (Figure 1). Recharge to the aquifer is by rainwater infiltration, and is on the order of 20 to 25 in. (22 to 33 cm) per year. The direction of flow and the hydraulic gradient have

remained fairly consistent between 1993 and 1996 (Landmeyer and others, 1996) and, more recently, from 1996 to 1998. This is because any changes in water levels due to changes in precipitation amounts have been uniform across the site. These water level fluctuations are significant (2 to 3 ft [0.6 to 0.9 m]), as depicted in water levels from 1993 to 1998 from two representative wells (Figure 2).

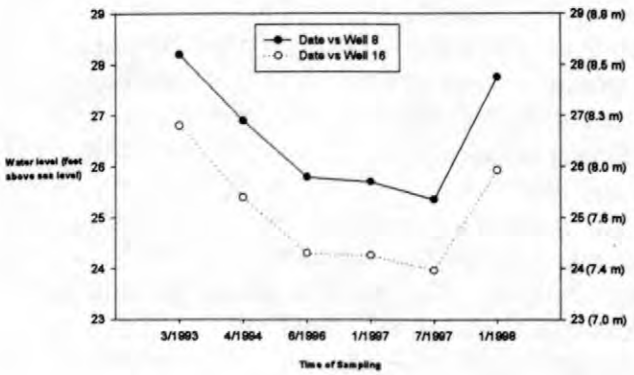

Figure 2. Representative water-level fluctuations from 1993 to 1998 in wells 8 and 16.

METHODS

Field Sampling

Ground-water samples were collected between 1993 and 1998 from monitoring wells and multilevel sampling wells (MLS) to provide areal and vertical distributions of MTBE and BTEX. Microbially active solutes, such as dissolved H_2, Fe(II), sulfide, sulfate, CH_4, and oxygen concentrations, were also measured to determine if changes in MTBE and BTEX (specifically benzene) were related to specific microbial processes. Fifteen 2-inch (4.4 cm) PVC monitoring wells screened across or below the water table with 12.5 ft (3.8 m) screens (well depths ranged from 19.5 ft (5.9 m) to 23 ft (7 m) below land surface [bls]) were analyzed for MTBE and BTEX in April 1993, and analyzed for MTBE, BTEX, and microbially reactive solutes in March 1994, June 1996, January 1997, and July 1997. As part of the 1996 and 1997 sampling events, five MLS wells constructed in cooperation with Dr. Mark A. Widdowson (Virginia Polytechnic Institute and State University) were measured for BTEX, MTBE, TBA, TBF (*tert*-butyl formate), and the microbially-reactive solutes as described. Two types of MLS wells were installed; (1) one well (MLS-1) was constructed of 25 ft (7.6 m) of 2-inch (4.4 cm) diameter PVC casing, with Tygon® tubes attached to copper ports every 2.5 ft (0.76 m) from 12.5 ft (3.8 m) to 25 ft (7.6 m) (MLS-1); and (2) four MLS wells (MLS's -3,-4,-5, and -6) consisting of individual Tygon® tubes installed using direct-push installation every 2.5 ft (0.76 m) from 12.5 ft (3.8 m) to 25 ft (7.6 m) without casing material. The MLS wells were installed along a ground-water flowpath from the former source area to downgradient areas (Figure 1) in order to more accurately delineate the vertical distributions and chromatographic separation of MTBE and benzene. To further characterize vertical concentration distributions in the areas farther downgradient from the source, twelve 1-inch (2.2 cm) PVC monitoring wells with screened intervals starting at 10 ft (3.0 m) below the water table were installed and sampled in January 1998.

Before sampling for MTBE, BTEX, or microbially reactive solutes, each monitoring or MLS well was purged until stable measurements of water temperature (in °Celsius) and pH (in standard units) were obtained. The analytical methods for BTEX, H_2, Fe(II), sulfide, SO_4^{2-}, CH_4, and dissolved oxygen concentrations used for the 1994, 1996, 1997, and 1998 sampling events have been described elsewhere (Vroblesky and Chapelle, 1994). To summarize, BTEX samples were collected in 40-mL glass vials using a bottom-discharge bailer, preserved with 3 drops of concentrated HCl, and capped using Teflon-lined septa. Dissolved hydrogen (H_2), an indicator of the predominant terminal electron-accepting process (Chapelle and others, 1995), was collected using the bubble-strip method described in Chapelle and McMahon (1991) and quantified using a gas chromatograph equipped with a reduction gas detector. Ground water was analyzed for Fe(II) (Stookey, 1970) and sulfide concentrations (Hach, 1989) using colorimetric methods. Sulfate concentrations were measured by using anion-exchange chromatography with conductivity detection. Methane was collected in sealed serum

vials using a syringe with a 0.2-μm filter. Methane concentrations were measured using a gas chromatograph equipped with a thermal conductivity detector. Dissolved oxygen was determined in the field by the Winkler titration method (Hach, 1989). Ground-water samples analyzed in June 1996, January and July 1997, and January 1998 for MTBE, TBA, and TBF concentrations were collected using the same method described above for BTEX. BTEX compounds were quantified using purge-and-trap gas chromatography. MTBE, TBA, and TBF were quantified using a direct-aqueous injection gas chromatography method developed by Church and others (1997). Samples to be analyzed for dissolved inorganic carbon (DIC), an indicator of the mineralization of petroleum compounds to CO_2, were obtained by injecting 5 mL of filtered (0.2-μm poresize) ground water into a sealed vial. Quantification of DIC concentration occurred using a gas chromatograph equipped with a thermal conductivity detector. Samples for inorganic cation and anion analyses were passed through a 0.2-μm filter and placed in polyethylene bottles. All ions were measured using ion-exchange chromatography with conductivity detection. Results for the microbially active solutes are not reported in this paper; however, they were used to delineate redox zones in the aquifer for subsequent aquifer material sampling (results are on file in the USGS Columbia, SC office).

Laboratory Experiments

MTBE biodegradation potentials were examined by quantifying the production of $^{14}CO_2$ from a known amount of uniformly labeled (UL) ^{14}C-MTBE added to microcosms containing aquifer material. The ^{14}C-[UL]-MTBE (specific activity of 10 mCi/mmol) in ethanol was acquired from New England Nuclear Chemical Company. A purity of 99.79 % was determined by HPLC. All treatments discussed below were comprised of triplicate 40-mL glass microcosms containing 5 mL of a slurry of water-table aquifer material and ground water. Dead controls for the triplicate treatments were initially made sterilize by autoclaving the control microcosms for 1 hour at 121°C, and maintained sterile for the duration of the experiment by addition of 8 millimolar (*mM*) $HgCl_2$. All incubations were done at room temperature (25°C) and in the dark.

Treatments were designed to assess differences in MTBE biodegradation potential based on differences in MTBE concentration, redox condition, and presence of alternative organic substrate. To assess the effect of MTBE concentration on biodegradation potential, approximately 73,000 (low) to 666,000 (high) dpm (decays per minute) of ^{14}C-[UL]-MTBE were added to the microcosms. To observe differences in degradation based on redox conditions, aerobic (oxygen headspace) and anaerobic (helium headspace) treatments were created with identically prepared dead controls for both low and high MTBE concentration treatments. The anaerobic treatments were naturally Fe(III) reducing. To observe the effect of alternative organic substrates, such as BTEX compounds, on MTBE biodegradation potential, the above two treatments were set up with aquifer sediment from near well 8 that had both MTBE and BTEX, and with aquifer sediments from near well 16 which had MTBE and lower BTEX concentrations (Figure 1). At specified times, all treatments triplicate vials and dead controls were sacrificed through addition of 1 mL of 45 % phosphoric acid (H_3PO_4), which converted the dissolved $^{14}CO_2$ to its gaseous form. This evolved $^{14}CO_2$ was trapped in a cup filled with 0.4 mL of 3 molar *(M)* potassium hydroxide (KOH) suspended from the serum vial stopper. The sequestered $^{14}CO_2$ was withdrawn by a syringe, placed in 15 mL of scintillation cocktail (Ultima Gold; Packard Instrument Company), and the radioactivity (in dpm) counted in a TR1600 scintillation counter (Packard Instrument Company) for 1 minute.

RESULTS AND DISCUSSION

Areal Distribution of MTBE Relative to Benzene

MTBE and benzene concentrations in ground water were measured during six sampling events between 1993 and 1998. Contour lines that represent equal MTBE and benzene concentration

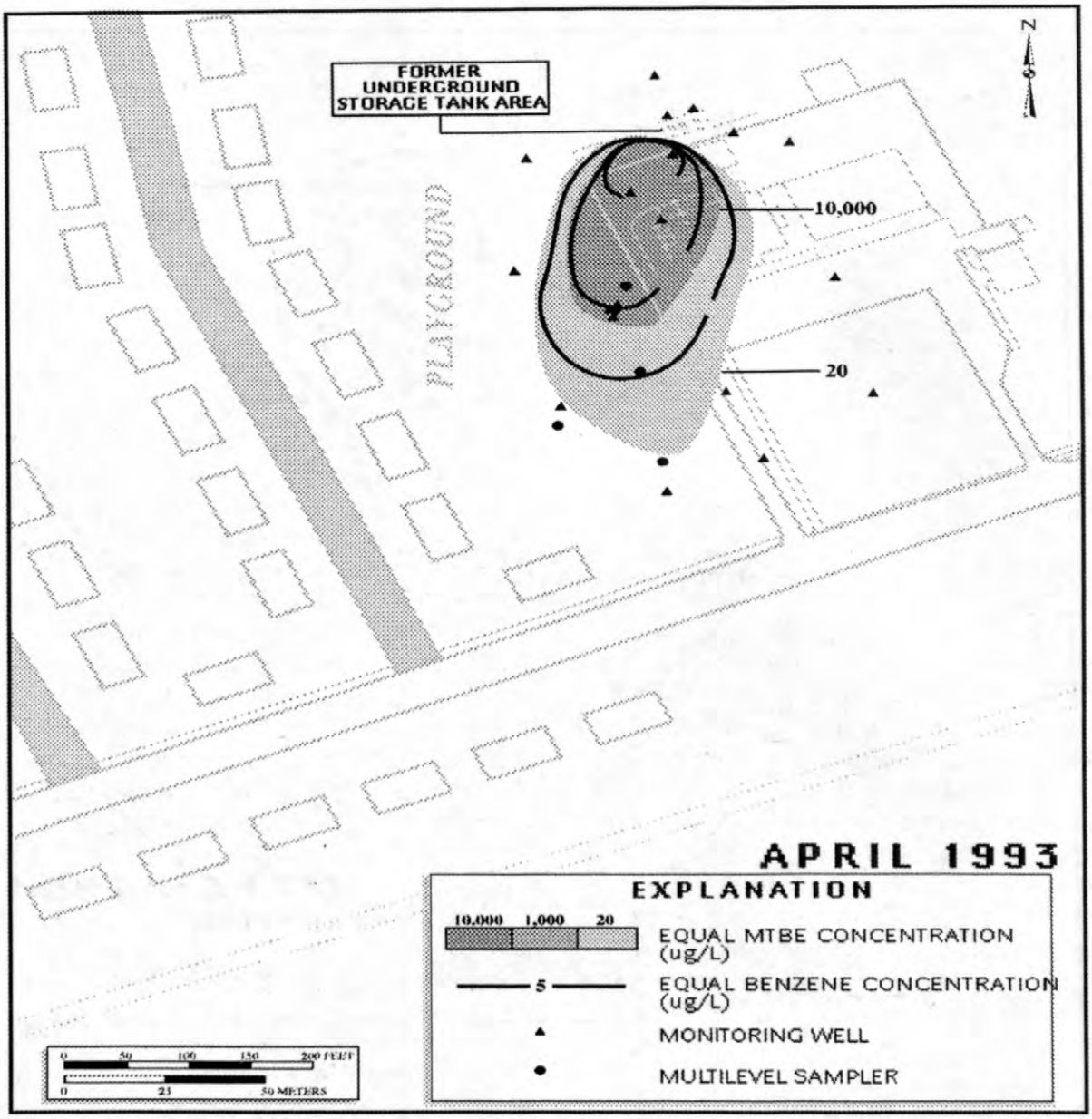

Figure 3A. MTBE and benzene concentrations in micrograms per liter, shallow ground water, April 1993.

for 1993, 1994, 1996, January and July 1997, and 1998 are shown in Figures 3A-F, respectively. The extent of MTBE ground- water contamination is defined as the area bounded by the 20 μg/L isoconcentration contour; 20 μg/L is the most conservative value in the recently issued (December 1997) MTBE drinking-water advisory of 20-40 μg/L. The extent of benzene ground-water contamination is defined as the 5 μg/L isoconcentration contour, the current (1998) EPA drinking-water MCL.

In April 1993, the 20 μg/L MTBE contour had migrated about 330 ft (100 m) in the direction of ground-water flow from the source area (Figure 3A). Because MTBE can be assumed to behave conservatively and move at the rate of ground-water advection (about 70 ft/yr [21 m/yr] in this area of flatter gradients), this transport distance of MTBE suggests that the initial release of fuel probably occurred as early as 1988. Conversely, the 5 μg/L benzene contour had only migrated about 270 ft (83 m) since the fuel was released, or roughly 80% the distance MTBE was transported. The resulting benzene retardation factor with

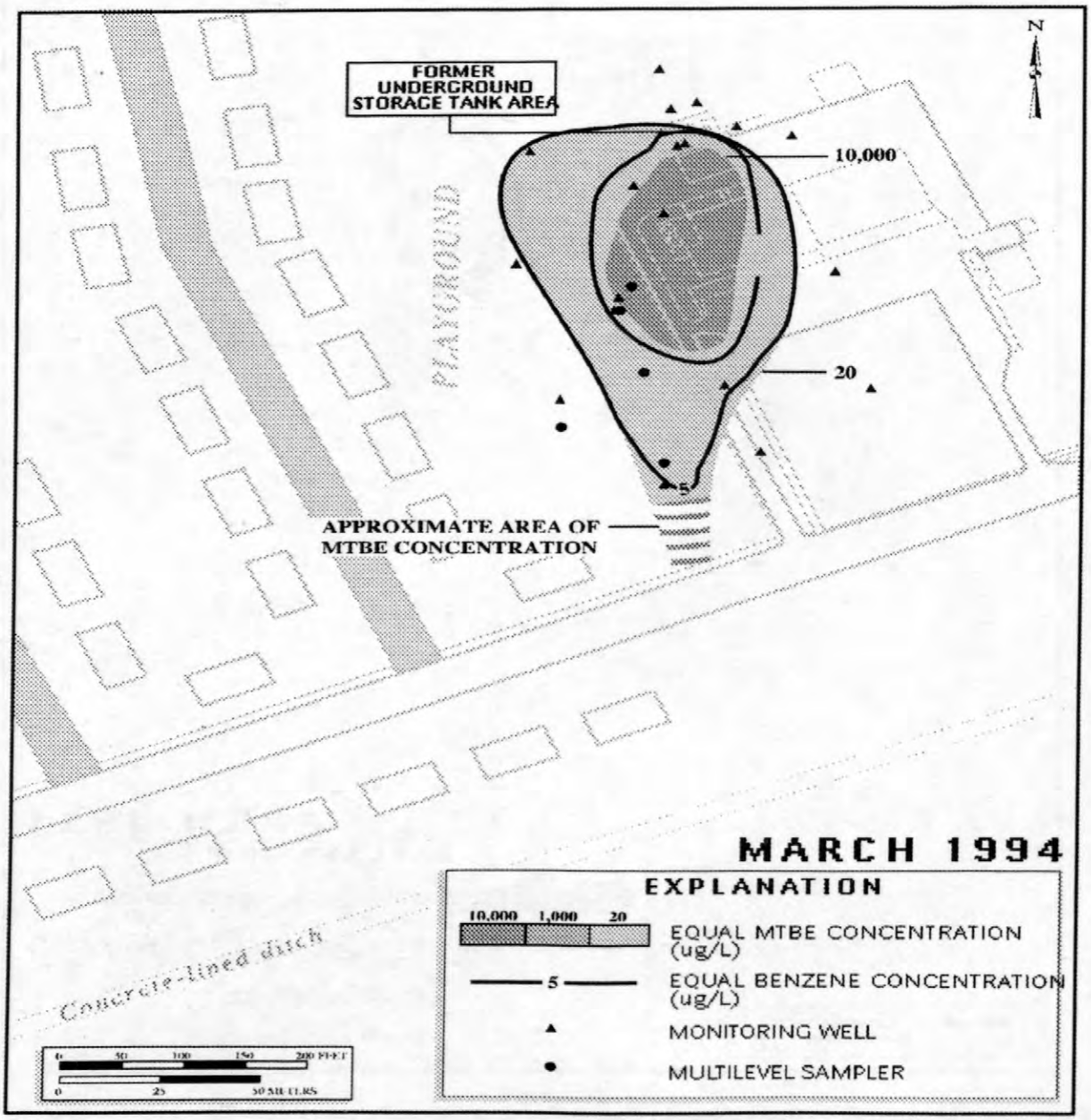

Figure 3B. MTBE and benzene concentrations in micrograms per liter, shallow ground water, March 1994.

respect to ground-water flow (near 0.8) is similar to benzene retardation factors reported elsewhere (Knox and others, 1993). This observation of benzene transport retarded with respect to ground-water advection and MTBE transport can be explained by the higher solubility, lower adsorption, and lower biodegradation potential of MTBE compared to benzene. Additionally, although MTBE has been transported farther than benzene, the spread of MTBE and benzene transverse to the direction of ground-water flow is roughly one-half the distance that both compounds have been transported downgradient from the release area. The highest MTBE concentration recorded in the source area was near 250 mg/L.

By March 1994, the location of the 20 μg/L MTBE contour had extended at least an additional 100 ft (30 m) (Figure 3B) from the April 1993 distribution. This MTBE transport distance is only an approximation, because well 16 was the most downgradient well at the time of sampling. The 5 μg/L benzene contour had also moved about 100 ft (30 m) since 1993, and concentrations of benzene decreased in the most

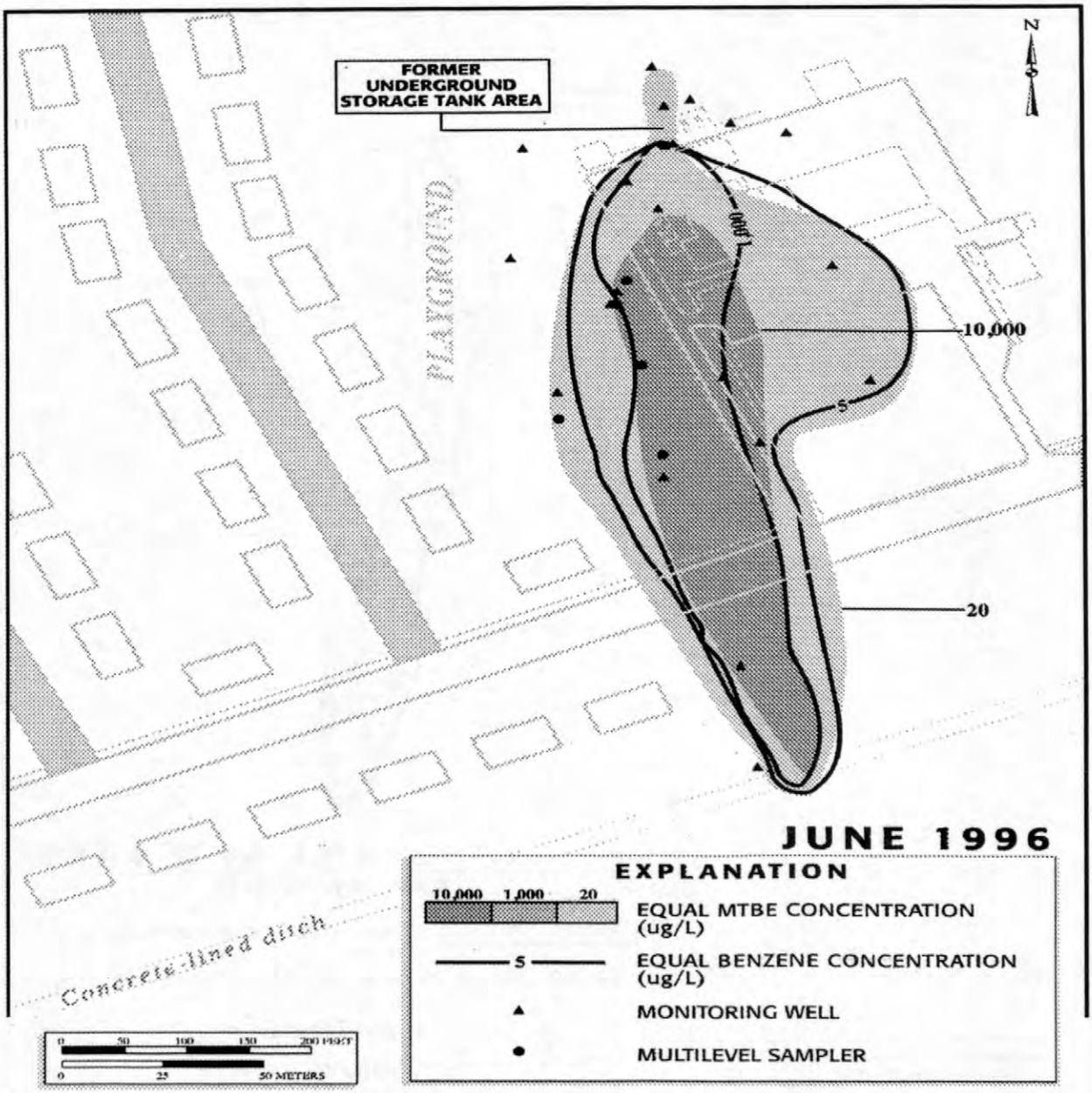

Figure 3C. MTBE and benzene concentrations in micrograms per liter, shallow ground water, June 1996.

contaminated wells (1,7, and RW) by up to 1 mg/L. The spread of MTBE and benzene transverse to the direction of flow increased, probably in response to lower recharge amounts (Figure 2) and, consequently, an increase in dispersion processes relative to advection. Because of the lack of an accurate delineation of MTBE and benzene distributions in downgradient areas, two additional wells (19 and 21) were installed in late 1995.

In June 1996, MTBE and benzene concentrations up to 18 and 1 mg/L, respectively, were measured in well 21 (Figure 3C). Such high concentrations in this most downgradient well are a result of (a) well 21 intercepts converging shallow and deep ground-water flow lines that had originated near the release area, and (b) the order of magnitude increase in ground-water flow rates between well 19 and 21. By comparison, in the region of the water-table aquifer characterized by a relatively flat topography and low ground-water flow rates (70 ft/yr [21 m/yr]) nearer the release

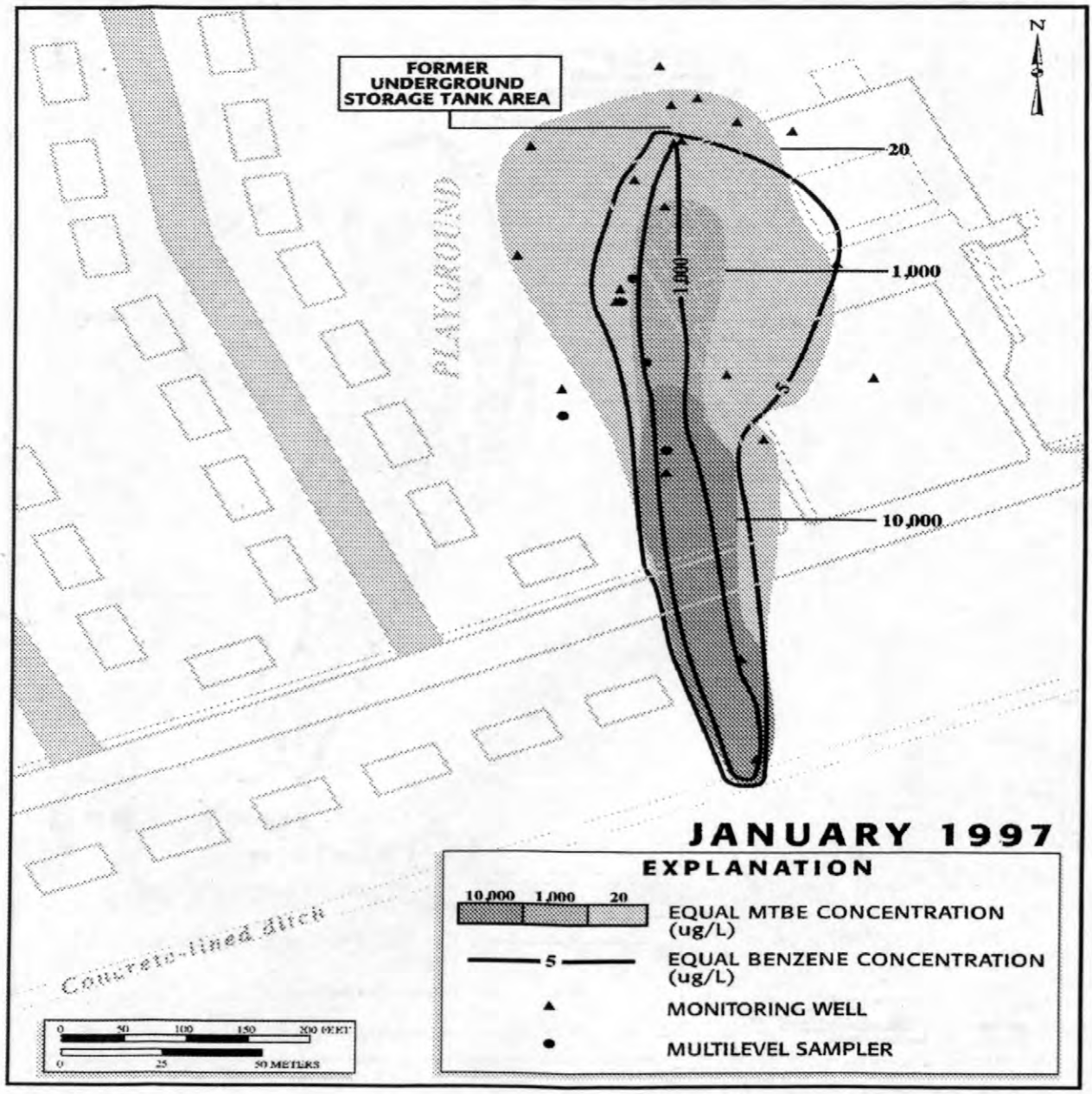

Figure 3D. MTBE and benzene concentrations in micrograms per liter, shallow ground water, January 1997.

area, the areal distribution of MTBE and benzene reflects a tendency for both lateral and transverse dispersion. MTBE and benzene had probably been transported to well 21 sometime in early 1995, because evidence of petroleum-hydrocarbon contamination was noted there during well installation. Upgradient, the 10,000 μg/L MTBE contour had migrated about 75 ft (23 m) from the source area.

In January 1997, milligram per liter concentrations of MTBE and benzene were still being detected in well 21 (Figure 3D). However, the upgradient edge of the 10,000 μg/L MTBE contour was displaced 100 ft (30 m) downgradient from the location measured in June 1996 (Figure 3C), and MTBE concentrations in the center of this plume were 2 orders of magnitude lower compared to initial values measured in 1993 (Figure 3A). Conversely, the less soluble benzene did not show a similar downgradient movement of the 1,000 μg/L contour. The overall segregation of a wider MTBE and benzene plume in the area dominated by slower ground-water flow rates and narrower distributions where flow rates are highest

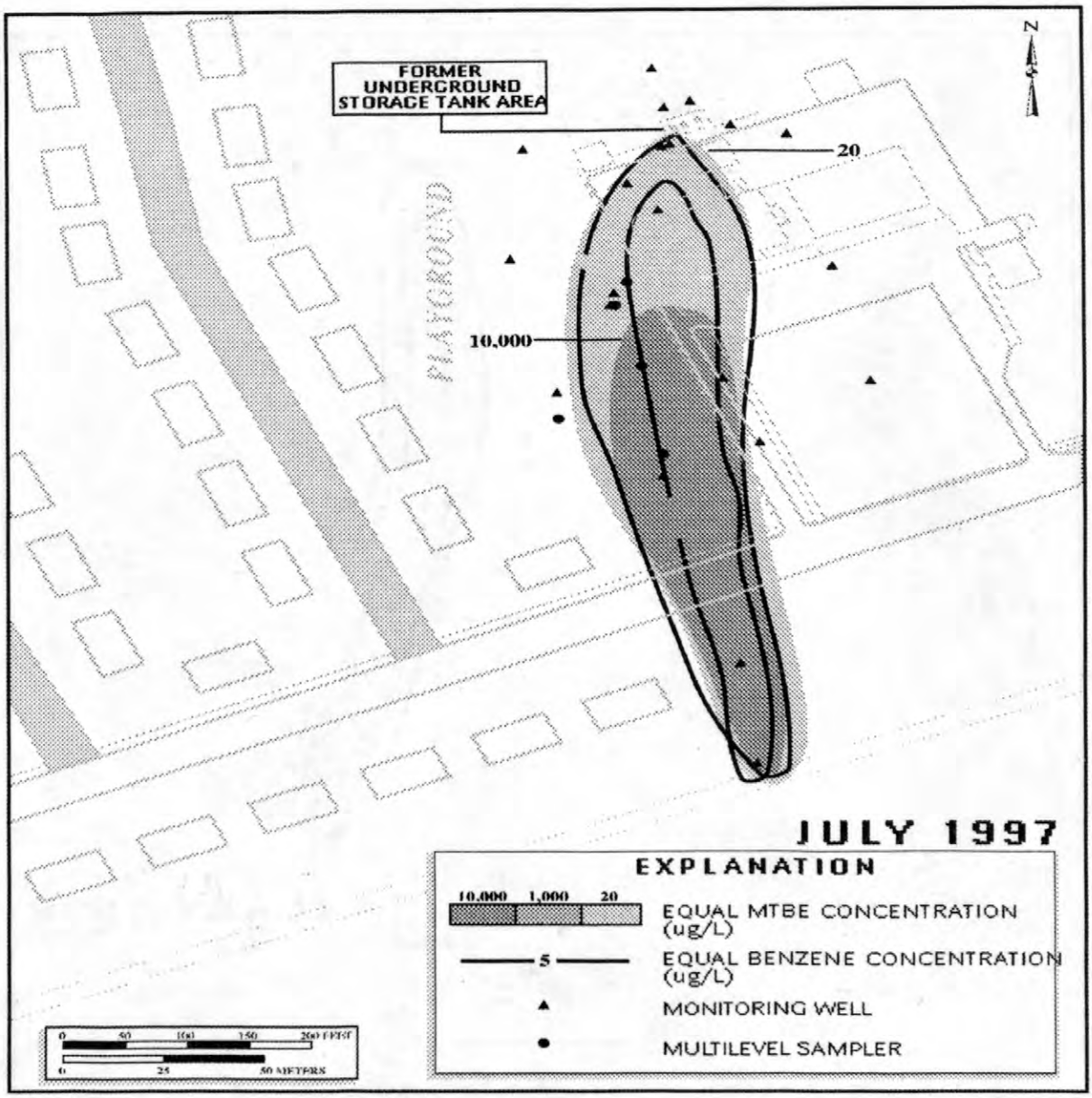

Figure 3E. MTBE and benzene concentrations in micrograms per liter, shallow ground water, July 1997.

continues to be observed.

The July 1997 sampling event shows similar MTBE and benzene concentration distributions as measured in January. This lack of additional transport may reflect the fact that the lowest water levels measured during the five-year study occurred during this sampling period (Figure 2). There is also a slight restriction in the transverse distribution of both MTBE and benzene in both low and high ground-water flow rate areas (Figure 3E).

In January 1998, (Figure 3F) distributions of MTBE and benzene at the 20 and 5 μg/L values, respectively, were similar to locations measured in July 1997 (Figure 3E). However, the 10,000 μg/L MTBE contour had been transported about 200 ft (61 m) from the July 1997 location (Figure 3E). This increase in MTBE transport rate reflects not only increases in hydraulic gradients in this vicinity, but also increases in water levels (Figure 2) as a result of above normal rainfall for the period between July 1997 and January 1998. Another artefact of this increase in recharge amount is a decrease in the width of the MTBE and benzene distributions in areas nearer the

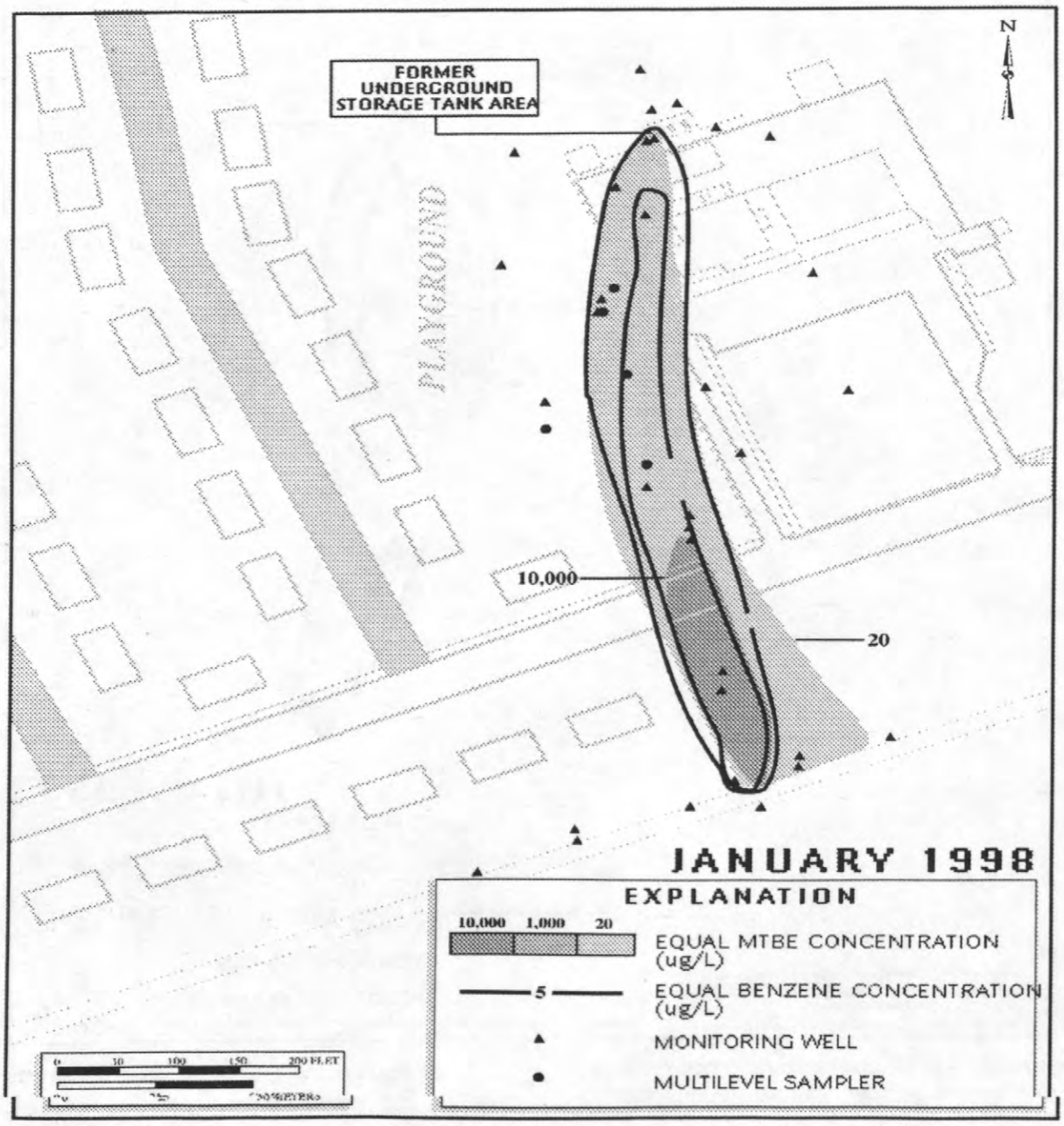

Figure 3F. MTBE and benzene concentrations in micrograms per liter, shallow ground water, January 1998.

release and an increase in the transverse distribution of the 20 μg/L MTBE contour near the discharge area. Even though it appears that the highest MTBE concentrations are moving to the discharge zone away from the source area, a large portion of the aquifer remains contaminated with MTBE concentrations above the drinking-water advisory of 20 μg/L.

Vertical Distribution of MTBE Relative to Benzene

Higher concentrations of MTBE and benzene were consistently detected in the deeper sampling ports of the MLS wells and in conventional wells screened below the water-table surface. This observation of higher concentrations of light, nonaqueous-phase liquids (LNAPLs) at depth suggests that recharge is causing the dissolved-phase MTBE and benzene to be displaced deeper into the aquifer. The most extreme water-table fluctuation observed over the study period was near 3 ft (0.9 m) (Figure 2). This maximum fluctuation represents about 0.9×10^6 gal (3.5×10^6 L) of recharge (contaminated aquifer = 420,000 ft^3 (11,894 m^3); porosity = 0.30). The affect of this fluctuation on contaminant distribution can be observed in the cross-sectional plots (Figures 4A-D).

Vertical MTBE and benzene isoconcentration contours for the June 1996 and January 1998 sampling events, respectively, are depicted in Figures 4A-D. In June 1996, MTBE concentrations greater than 1,000 $\mu g/L$ (Figure 4A) occupy a larger vertical area of the water-table aquifer than a similar concentration range for benzene (Figure 4B). The highest MTBE concentration is an order of magnitude higher than benzene, primarily due to the greater solubility of MTBE and was at least 10% (by volume) more present than benzene in the fuel spilled. It is also significant that the highest MTBE and benzene concentrations are not found near the surface of the water table, as would be expected from a LNAPL gasoline product floating on the water table, but rather nearer the center sampling ports of MLS's -4 and -6 for MTBE (Figure 4A), and MLS-3 and well 8 for benzene (Figure 4B). Again, this vertical distribution suggests that recharge by rainwater infiltration is causing a vertical component of ground-water flow, which moves both dissolved MTBE and benzene compounds deeper into the aquifer as the distance from the source area increases. This has important implications for the outcome of site remedial investigations, many of which although contain wells downgradient from source areas have screens placed near the water-table surface. Similar to the transverse dispersion shown in the areal plots, the vertical dispersion of MTBE in the aquifer nearer the source area is also about one-half the horizontal plume distribution.

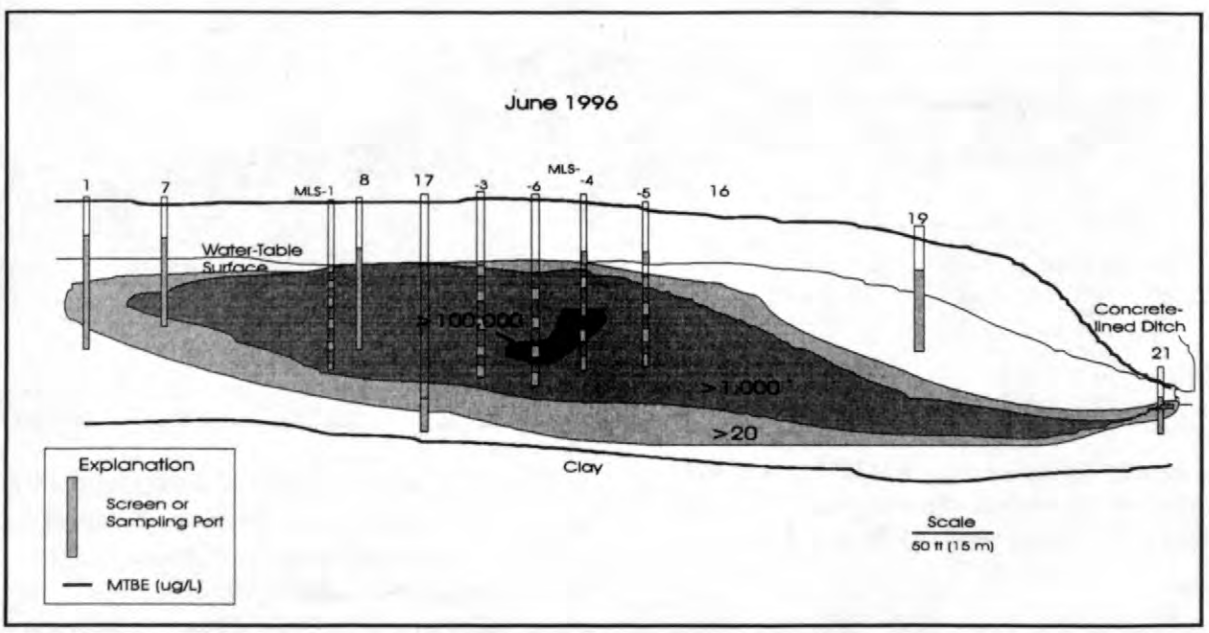

Figure 4A. Cross-section of MTBE concentration in micrograms per liter in monitoring and multilevel sampling wells in June 1996.

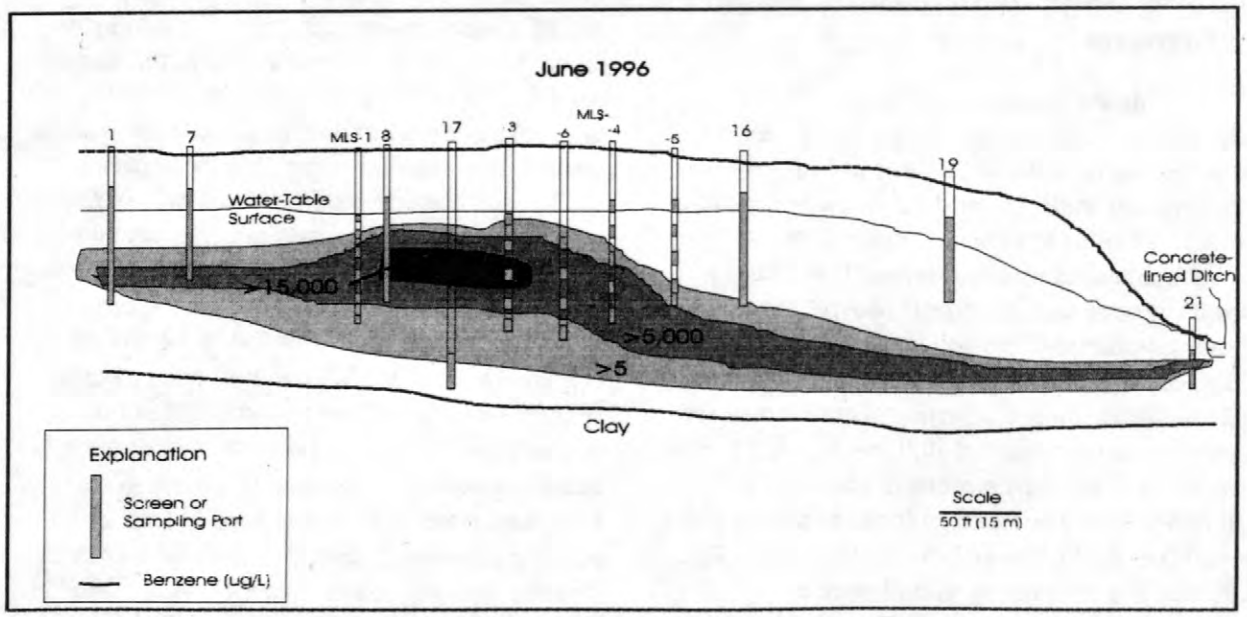

Figure 4B. Cross-section of benzene concentration in micrograms per liter in monitoring and multilevel sampling wells in June 1996.

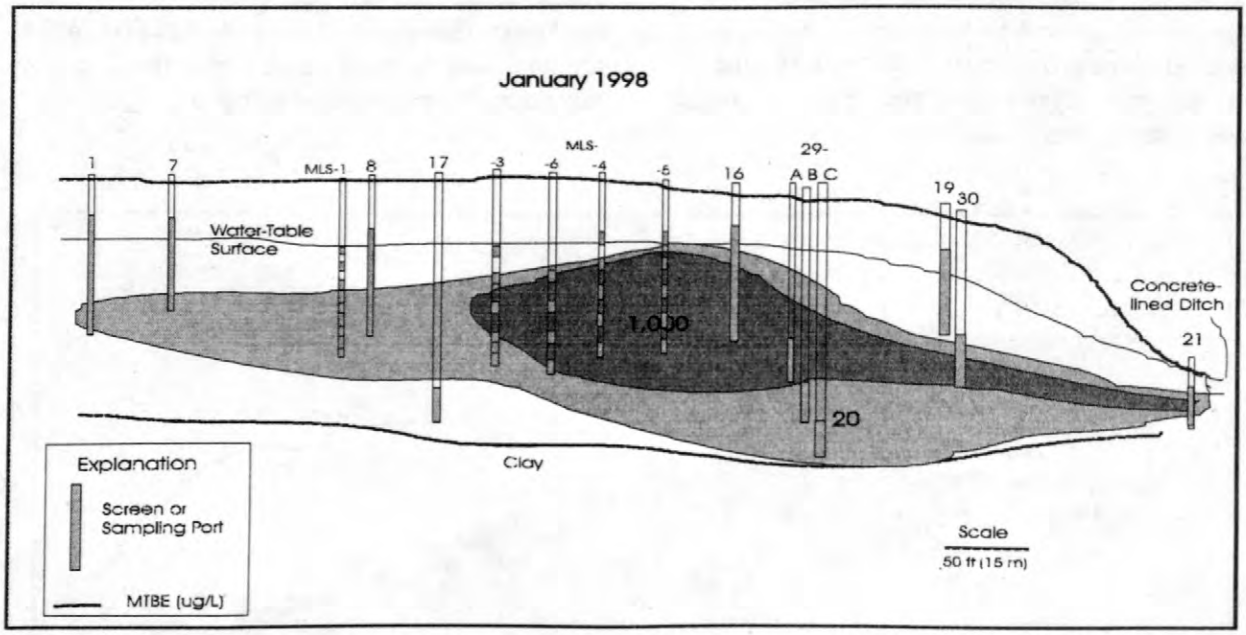

Figure 4C. Cross-section of MTBE concentration in micrograms per liter in monitoring and multilevel sampling wells in January 1998.

In January 1998, although the area of the aquifer contaminated by MTBE and benzene above 20 and 5 μg/L, respectively, has not changed measurably since June 1996, the upgradient limit of the 1,000 μg/L MTBE contour has moved some 200 ft (60 m) in the direction of flow (Figure 4C). For benzene, concentration measured in January 1998 (Figure 4D) are an order of magnitude less than that measured in June 1996 (Figure 4C). The 5 μg/L contour line has been displaced deeper in the aquifer than measured in June 1996, as evidenced by the lack of benzene detection in shallower sampling ports that were contaminated in 1996.

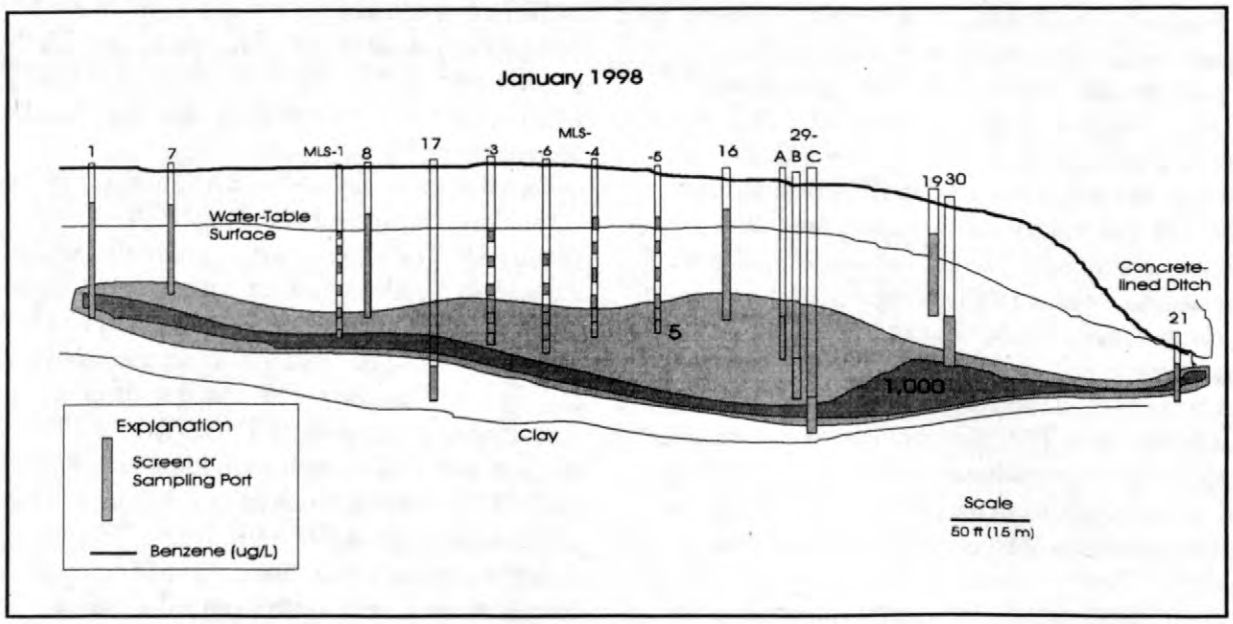

Figure 4D. Cross-section of benzene concentration in micrograms per liter in monitoring and multilevel sampling wells in January 1998.

Biodegradation Potential of ^{14}C-[UL]-MTBE

The consensus on the environmental fate of MTBE is that it is not easily biodegraded under either aerobic or anaerobic conditions (Zogorski and others, 1996). Although a laboratory-based study reported complete MTBE degradation under aerobic conditions (Mo and others, 1996), this was achieved only using acclimated enrichment cultures, a condition which tends to over predict degradation processes than can be expected of natural microbial communities at most gasoline-contaminated sites. Additional evidence from other isolates have also suggested the potential for aerobic MTBE degradation (Salanitro and others, 1994; Mo and others, 1997). Aerobic degradation of MTBE was also observed using an unidentified mixed enrichment culture, but this degradation occurred only between 15 and 35°C (Park and Cowan 1997). TBA production was observed as an intermediate breakdown product in the degradation of low concentrations of MTBE in microcosms containing gasoline-contaminated aquifer sediments; however, TBA production was not observed when MTBE concentrations were

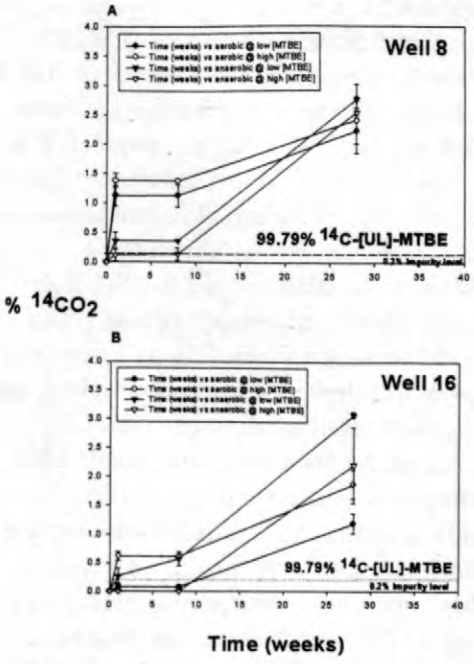

Figure 5. Production of radiolabeled carbon dioxide from radiolabeled MTBE incubated in microcosms containing aquifer sediments from near (A) well 8 and (B) well 16. Error bars represent standard deviation of triplicate microcosms.

greater than 1 mg/L (Daniel 1995; Borden and others 1997). Under anaerobic conditions, researchers have reported little evidence of MTBE biodegradation under nitrate reducing, sulfate

reducing, or methanogenic conditions (Fujiwara and others, 1984; Moller and Arvin 1990; Salanitro and others, 1994; Suflita and Mormile 1993; Yeh 1992; Yeh and Novak 1991; Yeh and Novak 1994; Yeh and Novak 1995). One laboratory-based study using fuel-contaminated aquifer sediments incubated under anaerobic conditions showed that decreases in MTBE were related to stoichiometric increases in TBA concentration, but this was only evident in a single replicate after a lengthy (152 day) acclimation period (Mormile and others, 1994). Although it appears that MTBE is recalcitrant in contaminated aquifers, recent evidence suggests that MTBE can be co-metabolized in the presence of short-chain alkanes found in gasoline (Hardison and others, 1997).

In our study, laboratory microcosms containing natural, *in-situ* microbial populations in aquifer material and were incubated under conditions that differed with respect to MTBE concentration, redox state, and presence of BTEX contamination. Treatments of aquifer sediment collected from near well 8 that contained BTEX contamination (Figure 5A) and sediment from near well 16 that contained little BTEX contamination (Figure 5B) indicated low but measurable biodegradation potentials (<3% ^{14}C-MTBE as $^{14}CO_2$) under Fe(III) reducing conditions. This was the total accumulation of CO_2 as a byproduct after a seven-month incubation period. There was no statistically significant difference in $^{14}CO_2$ production between the various treatments. It is possible that biodegradation intermediate compounds other than CO_2 were produced in the microcosms, but none were quantified as part of this study. Such low biodegradation potentials for MTBE are partly responsible for the continued presence of tens of milligrams per liter of MTBE in wells even 700 ft [215 m] from the release area.

TBA, TBF, and MTBE in Source-Area Sediments

Concentrations of TBA in MTBE-contaminated wells ranged from microgram per liter concentrations to 5 mg/L between June 1996, January and July 1997, and January 1998. Sediments samples in the release area were collected to determine (1) if the TBA detected in MTBE-contaminated wells was a result of TBA being a component of the fuel released, and (2) the concentration-distribution differences of MTBE and TBA across the water-table interface. Aquifer sediment samples were collected at the water table (1SAT) and 3 ft (0.9 m) above in the unsaturated zone (1UNSAT) (Figure 1). The samples were equilibrated with autoclaved distilled water for 1 week, and analyzed for MTBE, TBA, and *tert*-butyl formate (TBF) using the method outlined in Church and others, (1997). In summary, the saturated sediments contained no measurable MTBE, TBA, or TBF concentrations, whereas the unsaturated sediments had MTBE concentrations up to 6,272 μg/l, TBA concentrations up to 397 μg/L, but no TBF. A possible explanation for this large difference in concentration across a small vertical distance is that the contaminated unsaturated-zone sediments are only exposed to water during recharge events, whereas the deeper sediments are continually flushed with clean ground water originating from areas upgradient of the release. The lack of TBF in either saturated or unsaturated sediment can be explained by the rapid hydrolysis of TBF to TBA (Clinton D. Church, Oregon Graduate Institute, person. commun., 1998).

CONCLUSIONS

This long-term study of the fate of MTBE relative to benzene at point-source release of fuel containing oxygenates highlights the importance of routine MTBE monitoring at such sites, because 1) MTBE has the potential to be transported farther than benzene; 2) MTBE and benzene can migrate deeper than the location of many conventional water-table well screens, and therefore remain undetected when MTBE is actually present; 3) MTBE may persist in ground-water systems because of low biodegradation potentials; 4) the unknown toxicological effects of MTBE on humans; and 5) the limited number of studies that have monitored MTBE relative to benzene in ground water for more than one sampling event. Although natural attenuation of contaminant compounds is usually demonstrated by evoking biodegradation processes that removes contaminant mass from a ground-water system, this study suggests that the abiotic natural

attenuation processes of dilution and dispersion in the direction of ground-water flow also play an important role in reducing MTBE concentrations. Such processes may be more effective in reducing contaminant concentrations where sensitive receptors are not adjacent to source areas.

AUTHOR INFORMATION

James E. Landmeyer, Paul M.Bradley, and Francis H. Chapelle are with the U.S. Geological Survey in Columbia, SC.

REFERENCES

Borden, R.C., Daniels, R.A., LeBrun IV, L.E., and Davis, C.V., 1997, Intrinsic biodegradation of MTBE and BTEX in a gasoline-contaminated aquifer: *Water Resources Research,* v. 33, no. 5, p.1105-1115.

Buxton, H.T., Landmeyer, J.E., Baehr, A.L., Church, C.D., and Tratnyek, P.G., 1997, Interdisciplinary investigation of subsurface contaminant transport and fate at point-source releases of gasoline containing MTBE, in Proceedings of the Petroleum Hydrocarbons and Organic Chemicals in Ground Water: Prevention, Detection, and Remediation Conference, Houston, TX, November 11-14, 1997: p. 2-16.

Chapelle, F.H., McMahon, P.B., Dubrovsky, N.M.,Fujii, R.F., Oaksford, E.T., and Vroblesky, D.A., 1995, Deducing the distribution of terminal electron-accepting processes in hydrologically diverse ground-water systems: *Water Resources Research, v.* 31, no.2, p. 359-371.

Chapelle, F.H., and McMahon, P.B., 1991, Geochemistry of dissolved inorganic carbon in a coastal plain aquifer: Sulfate from confining beds as an oxidant in microbial CO_2 production: *Journal of Hydrology*, v.127, p. 85-108.

Church, C.D., Isabelle, L.M., Pankow, J.F., Rose, D.L., and Tratnyek, P.G.,1997, Method for determination of methyl *tert*-butyl ether and its degradation products in water: *Environmental Science & Technology,* v. 31, no. 12, p. 3723-3726.

Daniel, R.A.,1995, Intrinsic bioremediation of BTEX and MTBE: Field, laboratory and computer modeling studies: North Carolina State University M.S. thesis, 325 p.

Fujiwara, T., Kinoshita, T., Sato, H., and Kojima, L.,1984, Biodegradation and bioconcentration of alkyl ethers:*Yukaguku,* v. 33, no. 2, p.111-114.

Hach Company, 1989, Water analysis handbook: Loveland, CO, 689 p.

Hardison, L.K., Curry, S.S., Ciuffetti, L.M., and Hyman, M.R., 1997, Metabolism of diethyl ether and cometabolism of methyl *tert*-butyl ether by a filamentous fungus, a *Graphium* sp.: *Applied & Environmental Microbiology,* v. 63, no. 8, p.3059-3067.

Knox, R.C., Sabatini, D.A., and Canter, L.W., 1993, Subsurface transport and fate processes: Lewis Publishers, Boca Raton, FL, 430 p.

Landmeyer, J.E., Chapelle, F.H., and Bradley, P.M., 1996, Assessment of intrinsic bioremediation of gasoline contamination in the shallow aquifer, Laurel Bay Exchange, Marine Corps Air Station Beaufort, South Carolina: *U.S. Geological Survey Water-Resources Investigations Report 96-4026,* 50 p.

Mo, K., Lora, C.O., Javanmardian, M., Yang, X., and Kulpa, C.F., 1996, Biodegradation of gasoline oxygenate, methyl-t-butyl ether by mixed and pure cultures:*Abstracts of the 96th General Meeting of the American Society for Microbiology,* p. 437.

Mo, K., Lora, C.O., Wanken, A.E., Javanmardian, M., Yang, X., and Kulpa, C.F.,1997, Biodegradation of methyl t-butyl ether by pure bacterial cultures: *Appl. Microbiol. Biotechnol.*, v. 47, p. 69-72.

Moller, H. and Arvin, E., 1990, Solubility and degradability of the gasoline additive MTBE, methyl-tert-butyl-ether and gasoline compounds in water, in Ardent, F. M. Hinsenveld, and van den Brink, V.J., eds., *Contaminated Soils '90, p.* 445-448.

Mormile, M.R., Liu, S., and Suflita, J.M., 1994, Anaerobic biodegradation of gasoline

oxygenates: extrapolation of information to multiple sites and redox conditions: *Environ. Science & Technol.*, v.28, no. 9, p. 727-1732.

Park, K. and Cowan, R.M., 1997, Effects of oxygen and temperature on the biodegradation of MTBE: *Book of Abstracts, 213th American Chemical Society National Meeting,* San Francisco, CA, April 13-17, 1997.

Reisch, M.S., 1994, Top 50 chemicals production rose modestly last year: *Chemical & Engineering News,* v.72, no. 15, p.12-15.

Salanitro, J.P., Diaz, L.A., Williams, M.P., and Wisniewski, H.L., 1994, Isolation of a bacterial culture that degrades methyl t-butyl ether: *Applied & Environmental Microbiology,* v.60, no. 7, p.2593-2596.

Squillace, P.J., Zogorski, J.S., Wilber, W.G., and Price, C.V.,1996, Preliminary assessment of the occurrence and possible sources of MTBE in groundwater in the United States, 1993-1994: *Environ. Science & Technol.,* v.30, no. 5, p.1721-1730.

Stookey, L.L.,1970, FerroZine, a new spectrophotometric reagent for iron: *Analytical Chemistry,* v. 42, p.779-781.

Suflita, J.M., and Mormile, M.R., 1993, Anaerobic biodegradation of known and potential gasoline oxygenates in the terrestrial subsurface: *Environmental Science & Technology,* v.27, no. 5, p.976-78.

Vroblesky, D.A., and Chapelle, F.H., 1994, Temporal and spatial changes of terminal electron-accepting processes in a petroleum-hydrocarbon contaminated aquifer and the significance for contaminant biodegradation: *Water Resources Research*, v.30, no. 5, p.1561-1570.

Yeh, C.K., 1992, Degradation of gasoline oxygenates in the subsurface: Virginia Polytechnic Institute, Ph.D. thesis.

Yeh, C.K., and Novak, J.T., 1991, Anaerobic biodegradation of oxygenates in the subsurface, in *Proceedings of the 1991 petroleum hydrocarbons and organic chemicals in ground water: prevention, detection and restoration:* Ground Water Management Book 8 of the Series.

Yeh, C.K., and Novak, J.T., 1994, Anaerobic biodegradation of gasoline oxygenates in soils: *Water Environment Research*, v.66, no. 5, p. 744-752.

Yeh, C.K.,and Novak, J.T., 1995, The effect of hydrogen peroxide on the degradation of methyl and ethyl tert-butyl ether in soils: *Water Environment Research*, v. 67, no. 5, p. 828.

Zogorski, J.S., Morduchowitz, A., Baehr, A.L., Bauman, B.J., Conrad, D.L., Drew, R.T., Korte, N.E., Lapham, W.W., Pankow, J.F., and Washington, E.F.,1996, Fuel oxygenates and water quality: current understanding of sources, occurrence in natural waters, environmental behavior, fate, and significance: *Office of Science and Technology Policy,*37 p.

Mass Transport of Methyl Tert-Butyl Ether (MTBE) Across The Water Table and Significance for Natural-Attenuation Remediation at a Gasoline-Spill Site in Beaufort, South Carolina

by Matthew A. Lahvis, Ronald J. Baker, and Arthur L. Baehr

ABSTRACT

Mass transport of methyl tert-butyl ether (MTBE) across the water table coupled with diffusion through the unsaturated zone is a possible mechanism for natural attenuation of MTBE in ground water. Field and laboratory investigations were conducted to assess the significance of this pathway for natural-attenuation remediation. At a gasoline-spill site in Beaufort, S.C., estimates of the volatilization rate of MTBE downgradient from the spill ranged from 0.007 to 0.012 g m^{-2} yr^{-1} depending on the assumed rates of ground-water infiltration and MTBE biodegradation in the unsaturated zone. The volatilization rates were determined by model calibration to MTBE concentrations in the unsaturated zone. Results of solute-transport modeling indicate that volatilization has only a minor effect on migration of MTBE in ground water downgradient from the gasoline spill. Volatilization rates downgradient from a spill were compared to rates near a spill in laboratory column experiments. Results of these experiments indicate that the capillary zone is a significant barrier to MTBE volatilization. Rates of volatilization can range over several orders of magnitude depending on whether the source is above or below the capillary zone. This large difference implies that volatilization in the spill area may have a significant effect on the migration of MTBE in ground water.

INTRODUCTION

The success of natural-attenuation remediation of a petroleum product depends largely on the geochemical properties of the organic constituents that comprise the spilled product. These properties will determine the tendency of the constituent to volatilize and diffuse upward through the unsaturated zone, solubilize and migrate downward to the water table, or undergo biodegradation (fig. 1). The geochemical properties of gasoline constituents can differ significantly. For example, MTBE, a widely used gasoline oxygenate, is more soluble and more resistant to microbial degradation than other constituents such as benzene, toluene, ethylbenzene, and xylenes (BTEX). MTBE takes longer, therefore, to remediate by natural attenuation. Volatilization coupled with diffusion through the unsaturated zone has not received consideration as an natural-attenuation mechanism for MTBE at

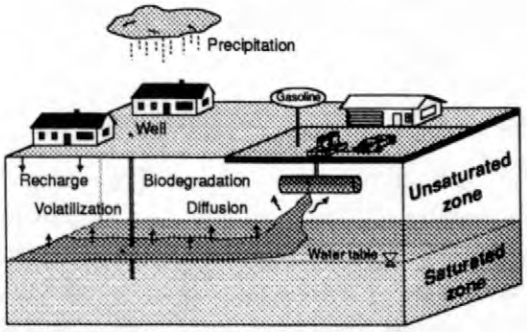

Figure 1. Conceptualization of natural-attenuation remediation at a petroleum-product spill site. (from Lahvis and Baehr, 1998)

gasoline-spill sites. In comparison to biodegradation, however, volatilization may be more relevant for MTBE than for BTEX. Although biodegradation of MTBE has been demonstrated in the laboratory (Salanitro and others, 1994; Mormile and

others, 1994; Mo and others, 1997; Park and Cowan, 1997; Steffan and others, 1997), biodegradation rates are generally considered low and evidence of MTBE biodegradation in situ (Borden and others, 1997; Landmeyer and others, 1998; and Schirmer and Barker, 1998) is extremely limited. This paper describes the results of laboratory and field investigations conducted at a field site in Beaufort, S.C., to assess the significance of the volatilization pathway for natural-attenuation remediation at gasoline-spill sites.

EVALUATION OF MTBE VOLATILIZATION AT A FIELD SITE

Site Description

The study site is in Laurel Bay Exchange, Marine Corps Air Station, Beaufort, S.C., in the Atlantic Coastal Plain physiographic province (see fig. 2). The unsaturated zone is approximately 3 to 5 m thick and is composed of uniform silts and fine-grained sands that contain little organic matter. Gasoline hydrocarbons were detected in the subsurface in September 1991. The source was a leaking underground storage tank at the service station (fig. 2), and the amount of product lost is estimated to be more than 5,000 L (1,500 gallons). The tanks and surrounding sediments were excavated and removed in October 1993.

Data Collection

A monitoring network consisting of five vapor-probe and four lysimeter nests was installed to measure the distribution of MTBE in unsaturated-zone gas, pore water, and shallow ground water. The distribution of sampling locations at the site is illustrated in figure 2. Gas samples, approximately 1 L in volume, were collected from unsaturated-zone vapor probes on sorbent cartridges by using a peristaltic pump. These samples were analyzed by gas chromatography/mass spectrometry (GC/MS) according to the method described by Pankow and others (1998). Pore-water samples from the unsaturated zone were collected from suction lysimeters in 2-mL vials by using a

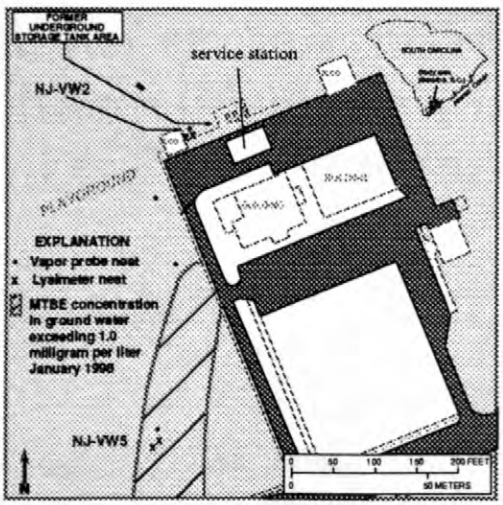

Figure 2. Site map showing location of source area and distribution of MTBE in concentrations above 1 milligram per liter in ground water at Beaufort, S.C., November 1997. (modified from Landmeyer and others, 1998)

pressure/vacuum hand pump. The use of a vacuum pump can result in lower than actual concentrations of MTBE because mass can be stripped from the aqueous phase. Lysimeters were located, therefore, near vapor probes to compare sampling techniques. Water samples collected from lysimeters were analyzed by GC/MS according to the method described by Church and others (1997). Shallow-ground-water samples were collected in 40-mL vials from probes submerged just below the water table by using a peristaltic pump. The samples were analyzed by purge-and-trap gas chromatography according to the methods described by Conner and others (1998). Unsaturated-zone sediments were collected by split spoon and analyzed for moisture content, total porosity, and bulk density. Unsaturated-zone temperatures were measured by using a thermistor lowered through a shallow-ground-water access tube.

Results of synoptic sampling performed in November 1997 indicated high concentrations of MTBE (10.4-30.5 mg L^{-1}) in ground water just below the water table at NJ-VW5, approximately 100 m (350 ft) downgradient from the spill. Concentrations of MTBE in the unsaturated zone at NJ-VW5 were several orders of magnitude less (table 1). These concentrations were measured in samples from separate nests of vapor probes and lysimeters.

Table 1. Summary of measured aqueous-phase concentrations of MTBE at NJ-VW5, Beaufort, S.C., November 1997

[All distances (z) are in centimeters below land surface and all concentrations (c) are in grams per cubic centimeter]

z	C
UNSATURATED ZONE	
[1]61	9.7E-11
[1]305	6.2E-09
[2]360	9.5E-09
[2]433	3.1E-10
SATURATED ZONE	
[3]488	1.0E-05
[3]549	3.1E-05

[1]Vapor-probe sample. Aqueous-phase concentration calculated on the basis of Henry's Law (C = G/H), where G = gaseous-phase concentration and H = 0.026 (at 25 °C-- an average temperature in the unsaturated zone at the field site).

[2]Lysimeter sample.

[3]Ground-water sample.

Their distribution in the unsaturated zone is shown in figure 3. Concentrations of MTBE measured in the suction lysimeters compared favorably to concentrations measured in the vapor probes. Henry's Law was applied to convert gaseous-phase concentrations measured in samples from vapor probes to equivalent aqueous-phase concentrations.

Mathematical Model

Calibration of a mathematical model to the unsaturated-zone concentration data provided estimates of the volatilization rate at the water table. The model is based on the governing transport equation described as:

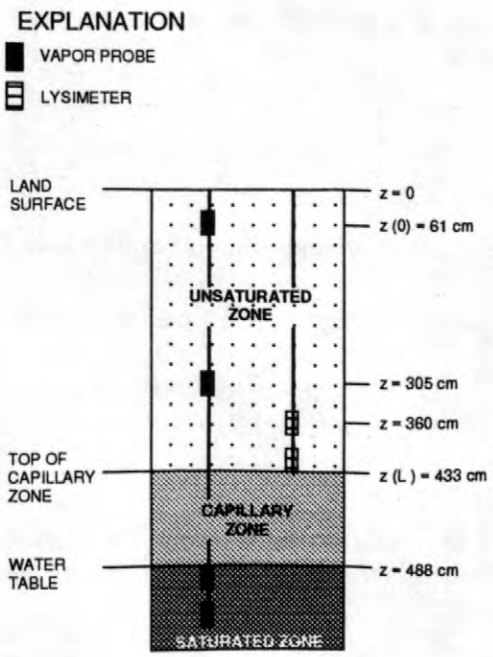

Figure 3. Diagram of model geometry and boundary conditions used to determine volatilization rates at Beaufort, S.C., November 1997.

$$\frac{\delta^2 C}{\delta x^2} - P_e \frac{\delta C}{dx} - D_m C = 0 , \qquad (1)$$

subject to boundary conditions,

$$\text{at } x = 0 \qquad C = C_o \qquad (1a)$$

$$\text{at } x = 1 \qquad C = C_L, \qquad (1b)$$

where C = aqueous-phase concentration ($g\ cm^{-3}$),

C_o = aqueous-phase concentration at upper boundary ($g\ cm^{-3}$),

C_L = aqueous-phase concentration at lower boundary ($g\ cm^{-3}$), and

x = normalized distance below land surface (dimensionless).

P_e is a dimensionless grouping of parameters referred to as the Peclet Number, defined as follows:

$$P_e = \frac{qL}{D}, \quad (2)$$

where q = ground-water infiltration rate (cm sec^{-1}),
L = length of the model domain (cm), and
D = effective diffusion coefficient (cm^2 sec^{-1}).

D_m is a dimensionless grouping of parameters referred to as the Damkohler Number, defined as follows:

$$D_m = \frac{kL^2}{D}, \quad (3)$$

where k = first-order biodegradation-rate constant (sec^{-1}).

The Peclet Number— scales advection and dispersion. The higher the value of P_e, the more dominant advective transport is relative to diffusion. The Damkohler Number scales biodegradation and dispersion. The higher the value of D_m, the more dominant biodegradation is relative to diffusion.

The solution to (1), subject to boundary conditions (1a) and (1b), is given by:

$$C(x) = \left(\frac{1}{\exp(r_2) - \exp(r_1)}\right) \left[[C_o \exp(r_2) - C_L] \exp(r_1 x) + [C_L - C_o \exp(r_1)] \exp(r_2 x) \right], \quad (4)$$

where

$$r_1 = \left(\frac{P_e}{2} + \frac{P_e^2}{4} + D_m\right)^{0.5}, \text{ and} \quad (4a)$$

$$r_2 = \left(\frac{P_e}{2} - \frac{P_e^2}{4} + D_m\right)^{0.5}. \quad (4b)$$

For non-reactive constituents, $D_m = 0$, and the solution (4) simplifies to:

$$C(x) = \left[\frac{1}{1 - \exp(P_e)}\right] \left[(C_o - C_L) \exp(P_e x) + C_L - C_o \exp(P_e) \right]. \quad (5)$$

In (1a), the concentration (C_o) at the upper model boundary (x = 0) represents the MTBE concentration measured at the uppermost sampling point (z = 61 cm). In (1b), the concentration (C_L) at the lower model boundary (x = 1) represents the MTBE concentration measured near the top of the capillary zone (z = 433 cm).

Mass flux across the lower boundary is defined as:

$$J(x) = qC - \frac{D}{L}\frac{dC}{dx}, \quad (6)$$

where J(x) = mass flux (g cm^{-2} sec^{-1}).

The first term on the right-hand side of (6) represents the mass flux due to aqueous-phase advection (ground-water infiltration) and the second term represents the mass flux due to gaseous diffusion. Diffusion is modeled according to Fick's Law; therefore, advective contributions to the mass flux caused by barometric or water-table fluctuations are assumed to be negligible.

For reactive constituents ($D_m > 0$), equation (4) implies that:

$$\frac{dC}{dx} = \left[\frac{1}{\exp(r_2) - \exp(r_1)}\right] \left[\begin{array}{l} [C_o \exp(r_2) - C_L]\, r_1 \exp(r_1 x) \\ + [C_L - C_o \exp(r_1)]\, r_2 \exp(r_2 x) \end{array}\right] . \quad (7)$$

For non-reactive constituents, equation (5) implies that:

$$\frac{dC}{dx} = \left[\frac{1}{1 - \exp(P_e)}\right] [(C_o - C_L)\, P_e \exp(P_e x)] \quad (8)$$

Equations (4), (6), and (7) allow for the calculation of the mass flux for reactive constituents. Equations (5), (6), and (8) allow for the calculation of the mass flux for non-reactive constituents. In particular, evaluation of the flux at x = 1 yields an estimate of the flux at the top of the capillary zone (J_L). If reactions of the compound are assumed to be negligible in the capillary zone, then J_L is the volatilization rate or the rate of mass transfer from ground water to the unsaturated zone.

For this analysis, both the ground-water infiltration rate (q) and effective diffusion coefficient (D) are assumed to be constant. The ground-water infiltration rate (q) is unknown and was varied from 36 cm yr^{-1} (15 in. yr^{-1}) to 65 cm yr^{-1} (25 in. yr^{-1}). The effective diffusion coefficient (D) was determined from laboratory column experiments on sediment cores from the unsaturated zone, and is defined as:

$$D = D_a H , \quad (9)$$

where D_a = effective diffusion coefficient of the gaseous phase ($cm^2\ sec^{-1}$), and
H = Henry's law coefficient.

In (9), aqueous-phase diffusion is assumed to be negligible. Model-parameter values used in the analysis are summarized in table 2.

Determination of Volatilization Rate

The results of model calibration to the MTBE concentrations in the unsaturated zone with MTBE assumed to be non-reactive are illustrated in figure 4. Model calibration was defined by a least-root-mean-squares fit of measured and simulated aqueous-phase concentration data. The best fit of the concentration data was achieved for a value of $P_e = 3.1$. This value corresponds to a volatilization rate of J_L = 4.0E-04 g $m^{-2}\ yr^{-1}$, if it is assumed that D = 1.9E-04 and q = 50 cm yr^{-1}. According to (2), a $P_e = 3.1$ with L = 372 cm implies a range of diffusion coefficients (1.3E-04 ≤ D ≤ 2.5E-04 $cm^2\ sec^{-1}$) for the corresponding range of infiltration rates (36 cm yr^{-1} ≤ q ≤ 65 cm yr^{-1}) (see fig. 5). On the basis of this relation, the estimated value of the diffusion coefficient from the laboratory experiments (D = 3.7E-04 $cm^2\ sec^{-1}$) corresponds to an infiltration rate of q = 97 cm yr^{-1}. This estimate of q exceeds plausible infiltration rates at the site, which implies either an overestimate in the value of D or that MTBE is being biodegraded.

If biodegradation of MTBE is considered, then best fits of the MTBE concentration data are achieved for a range of values of P_e from 1.1 to 2.1 and a range of values of D_m from 3.6 to 6.8, if it is assumed that D = 3.7E-04 $cm^2\ sec^{-1}$ (the laboratory-derived estimate) and L = 372 cm. According to (3), this range of D_m corresponds to a range of biodegradation rates (k) from 1.6E-03 to 2.5E-03 d^{-1}. Biodegradation in the unsaturated zone results in an increase in the concentration gradient of MTBE in the unsaturated zone and, thus, an increase in the rate of volatilization, a diffusion-driven process. Estimated volatilization rates for the range of 3.6 ≤ D_m ≤ 6.8 and 1.1 ≤ P_e ≤ 2.1 are significantly higher (6.9E-03 g $m^{-2}\ yr^{-1}$ ≤ J_L ≤ 1.2E-02 g $m^{-2}\ yr^{-1}$) than they are if MTBE is assumed to be non-reactive (J_L = 4.0E-04 g $m^{-2}\ yr^{-1}$), even though the biodegradation rates (1.6E-03 d^{-1} ≤ k ≤ 2.5E-03 d^{-1}) are low. Volatilization rates would be even higher than this range if biodegradation was assumed to occur between the lower probe (x = 1) and the water table (the capillary zone). Model-calibrated volatilization rates (J_L) are summarized in table 3.

Table 2. Summary of input values used for model application, Beaufort, S.C., November 1997

PARAMETER	VALUE	UNITS
UNSATURATED-ZONE ANALYSIS		
Length of model domain (L)	372	centimeters
Ground-water infiltration rate (q_w)	36 - 65	centimeters per year
Henry's Law constant (H)	0.026	dimensionless
Effective diffusion coefficient (D)[1]	variable	square centimeters per second
Aqueous-phase concentration (C_o)	0.097	micrograms per liter
Aqueous-phase concentration (C_L)	0.31	micrograms per liter
SATURATED-ZONE ANALYSIS		
Ground-water flow velocity	1900	centimeters per year
Longitudinal dispersivity	100	cm
Storage coefficient	0.46	dimensionless
Source concentration	5.0E-05	grams per cubic centimeter

[1]The laboratory estimate (D = 3.7E-04 cm^2 sec^{-1}) was calculated on the basis of $D = \tau_a \theta_a d_a$, where $\tau_a = 0.61$ was estimated from column experiments on intact sediment cores, $\theta_a = 0.3$, and $d_a = 0.094$.

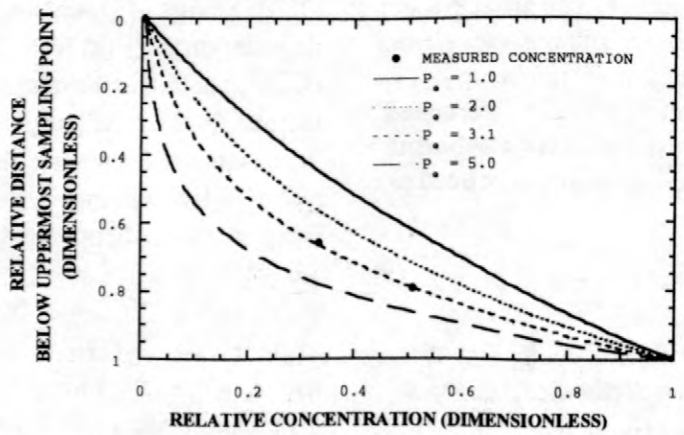

Figure 4. Plot of the results of model calibration to MTBE concentrations in the unsaturated zone at Beaufort, S.C., November 1997.

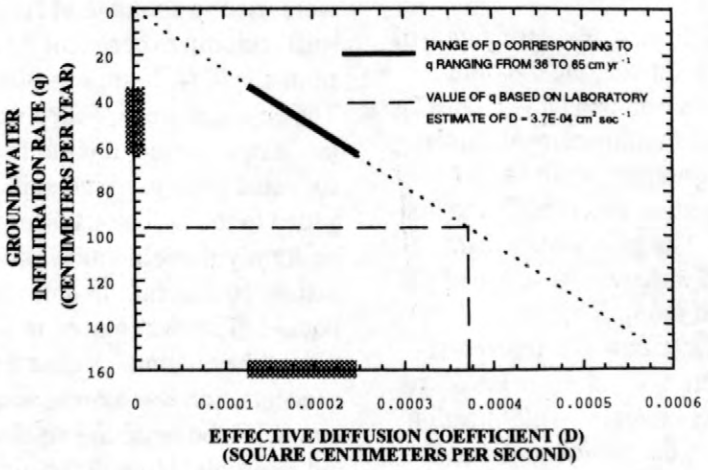

Figure 5. Plot of the relation between the ground-water infiltration rate (q) and effective diffusion coefficient (D) at Beaufort, S.C., November 1997.

Table 3. Summary of the model-calibrated mass-fluxes (J_L) as a function of Peclet (P_e) and Damkohler (D_m) Numbers, Beaufort, South Carolina, November 1997

[All mass fluxes (J_L) are in grams per square meter per year, all Peclet Numbers (P_e) are dimensionless, all ground-water infiltration rates (q) are in centimeters per year, all Damkohler Numbers (D_m) are dimensionless, all biodegradation rates (k) are in per day, and all effective diffusion coefficients (D) are in square centimeters per second]

J_L[1]	P_e	q	D_m	k	D
1.4E-02	0.0032	0.01	11	2.5E-03	3.7E-04
1.2E-02	1.1	36	6.8	1.6E-03	3.7E-04
6.9E-03	2.1	65	3.6	8.4E-04	3.7E-04
2.8E-04	3.1	36	0	0	1.4E-04
5.1E-04	3.1	65	0	0	2.5E-04
5.3E-04	3.1	97	0	0	3.7E-04

[1]Rates are computed on the basis of L = 372 cm.

Significance of Volatilization Rates

To assess the significance of volatilization of MTBE at the Beaufort, S.C., site, the maximum model-calibrated volatilization rate (J_L = 1.2E-02 g m^{-2} yr^{-1}) was input into a one-dimensional, advection-dispersion ground-water transport model. Mass loss due to volatilization was modeled as first-order decay for MTBE. The steady-state distribution of MTBE in ground water as a function of distance downgradient from the spill given representative ground-water flow and transport properties for the Beaufort, S.C., site (see table 2) is illustrated in figure 6. As indicated, volatilization has only a minor effect on the steady-state distribution of MTBE in ground water. The volatilization rate, however, is highly sensitive to biodegradation in the unsaturated zone. This sensitivity implies that significant increases in the volatilization rate could result if biodegradation of MTBE between the lower probe (x = 1) and the water table (the capillary zone) is considered. Subsequent modeling investigations are aimed at verifying this hypothesis.

LABORATORY INVESTIGATION

Column experiments were conducted to evaluate MTBE fluxes under controlled conditions. The experimental apparatus shown in figures 7a and 7b were used to simulate MTBE volatilization near a spill (column experiment A) and downgradient from a spill (column experiment B), respectively. The columns were packed uniformly with uncontaminated, sieved, fine- to medium-grained sand collected from gasoline-spill sites. Water was added to the sediments prior to filling to create a uniform volumetric moisture content of approximately 10 percent. In column experiment A, pure liquid MTBE was placed in the reservoir at the bottom of the column. A constant hydrocarbon-vapor concentration was maintained at the base of the column with the saturated head-space vapor in the liquid reservoir. Humidified air was cycled through the reservoir above the porous medium to form a sweep gas. MTBE flux was determined by multiplying the volumetric-flow rate of the sweep gas by the MTBE concentration in the sweep gas. Periodic sampling along the length of the column was used to confirm when steady-state conditions had been reached (approximately 2 weeks). Gas samples were collected in gas-tight syringes and analyzed with a gas chromatograph (Varian 3600) with a 2-mL vapor sample injection loop and a flame ionization detector (GC/FID). (Use of trade names in this paper is for identification purposes only and does not constitute endorsement by the U.S. Geological Survey.) Chromatographic separation was

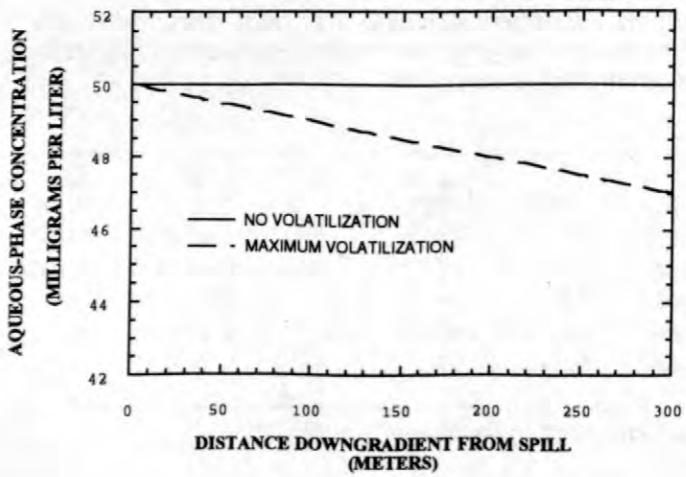

Figure 6. Plot of the concentration of MTBE in ground water as a function of distance downgradient from the spill area at Beaufort, S.C.

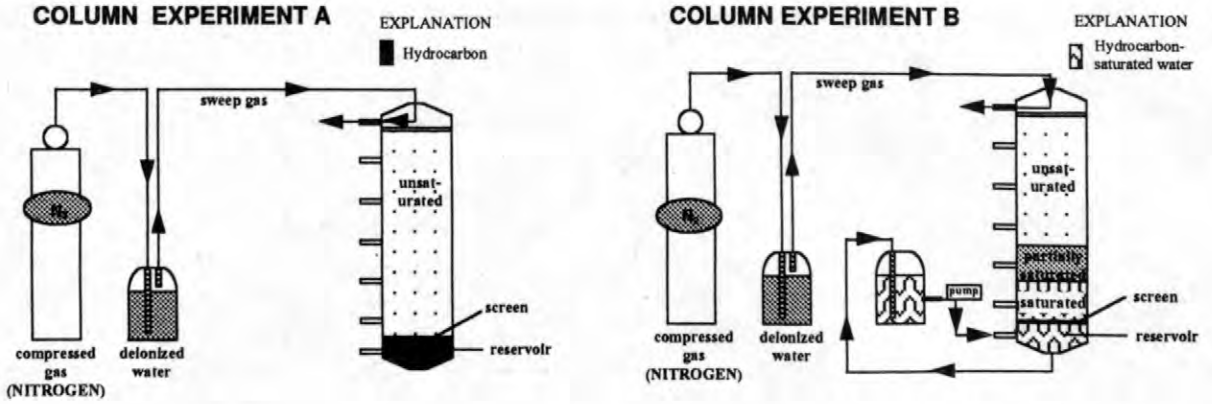

Figure 7. Diagram of the hardware configuration used for (a) column experiment A, and (b) column experiment B.

achieved with a 0.53-mm x 30-m DB-MTBE capillary column (Supelco, Inc., Bellefonte, Pa.) at isothermal conditions (50 °C). Column experiment A was designed to simulate the maximum volatilization of MTBE that can occur near a spill.

In column experiment B, dissolved MTBE at a concentration of approximately 720 mg L^{-1} was recirculated through the reservoir below the column screen. Recirculation of the water created a constant aqueous-concentration boundary at the base of the column and partially saturated conditions (emulative of capillary rise) in the overlying sediments. The lower two ports in column B were water-saturated. Fifteen-mL aqueous samples were collected from these ports with a gas-tight syringe equilibrated with 15 mL of helium gas. The helium was analyzed according to the (GC/FID) methods described above. Henry's Law was applied to convert the vapor-phase MTBE concentration to aqueous-phase concentrations in the original sample. Gas samples were collected from the remaining ports on sorbent cartridges and analyzed with a Tekmar 2000 purge-and-trap unit with a 6016 desorption autosampler connected to the Varian GC. Analysis of the MTBE concentration in the sweep gas required collection of a 4-L-volume sample in the sorbent cartridge over a 12-hour period. Column experiment B was designed to simulate volatilization of MTBE from ground water downgradient from a spill.

Results of the column experiments A and B are illustrated in figures 8a and 8b, respectively. As indicated, gas concentrations of MTBE measured in the unsaturated portions of column B were several orders of magnitude less than in column A. In addition, the mass flux (volatilization rate) measured in column B (1.6 g cm^2 yr^{-1}) was several orders of magnitude less than in column A (64,700 g cm^2 yr^{-1}). The volatilization rate measured in column B is consistent with the rates obtained at the field site (6.9E-03 g m^2 yr^{-1} $\leq J_L \leq$ 1.2E-02 g m^2 yr^{-1}) when differences in source concentration (C = 717 mg L^{-1} (lab) compared to C = 10.4 mg L^{-1} (field)) and the possibility of biodegradation in the capillary zone at the field site are considered. The results from column A imply that volatilization in a spill zone can be a significant natural-attenuation pathway for MTBE. In addition, because the volatilization rate measured in column A is several orders of magnitude greater than the rate measured in column B, volatilization in the spill area may have a significant effect on the extent of downgradient migration of MTBE in ground water.

The effective diffusion coefficient is a transport parameter required for sitewide mass-loss calculations. Quantification of the effective diffusion coefficient is extremely difficult in highly saturated sediments because of the inability to accurately quantify gas concentrations. The gas-sampling methods used in column experiment B, however, provide a means to overcome this limitation. Estimates of the effective diffusion coefficient are obtained by calibrating a steady-state transport model to the gas-concentration data. The model is described by Baehr and Baker (1995). Model-calibrated estimates of the diffusion coefficient across the capillary zone range from 1.0E-8 to 1.0E-2 cm^2

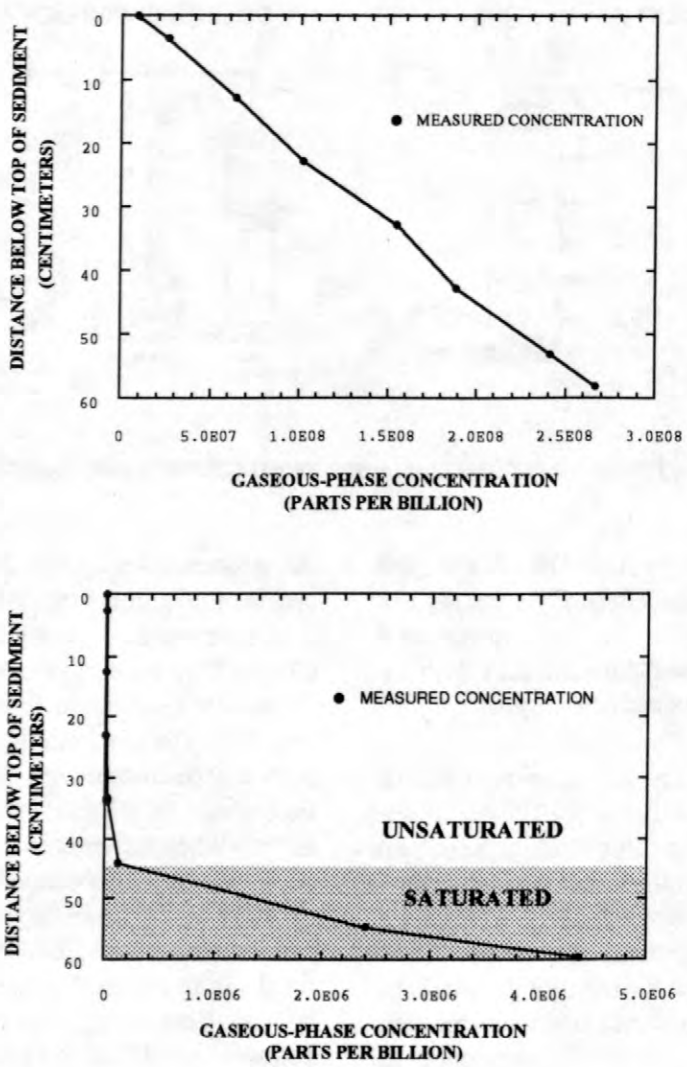

Figure 8. Plot of the steady-state distribution of MTBE determined in (a) column experiment A and (b) column experiment B

sec^{-1}. The method provides a means for evaluating mass transport across the water table and quantifying the significance of the capillary zone as a barrier to volatilization.

CONCLUSIONS

Volatilization coupled with transport through the unsaturated zone can be an important mechanism for the natural attenuation of MTBE at gasoline-spill sites. Rates of volatilization are dependent on source strength, rates of ground-water infiltration and biodegradation above the water table, and the diffusive properties of the unsaturated-zone sediments. Rates increase with a decrease in ground-water infiltration (unlike for BTEX), an increase in biodegradation above the water table, and an increase in the effective diffusion coefficient. The capillary zone is a significant barrier to MTBE volatilization. Results of solute-transport modeling indicate that volatile-mass losses of MTBE from ground water are minor. Additional investigations are needed, however, to determine whether biodegradation of MTBE in the capillary zone could significantly increase the volatilization rate. Additional data on spatial and temporal variations in concentrations of MTBE in the unsaturated zone also are needed to support calcuations of the volatilization rate downgradient from

the spill. These data would help assess the significance of equilibrium and negligible gaseous-phase-advection assumptions. By comparison, volatilization rates of MTBE from sources above the capillary zone can be several orders of magnitude higher than those from sources at the water table. This difference implies that volatilization in a spill area may have a large effect on downgradient migration of MTBE in ground water. Although the estimated rates of volatilization from ground water are small, volatilization may be an important component of natural attenuation of MTBE at gasoline-spill sites given that biodegradation at these sites has not been fully demonstrated.

REFERENCES

Baehr, A. L., and Baker, R. J., 1995, Use of a reactive gas transport model to determine rates of hydrocarbon biodegradation in unsaturated porous media: Water Resources Research, v. 31, p. 2877-2882.

Borden, R. C., Daniels, R. A., LeBrun IV, L. E., and Davis, C. W., 1997, Intrinsic biodegradation of MTBE and BTEX in a gasoline-contaminated aquifer: Water Resources Research, v. 33, p. 1105-1115.

Church, C. D., Isabelle, L. M., Pankow, J. F., Rose, D. L., and Tratnyek, P. G., 1997, Method for determination of methyl tert-butyl ether and its degradation products in water: Environmental Science and Technology, v. 31, p. 3723-3726.

Conner, B. F., Rose, D. L., Noriega, M. C., Murtagh, L. K., and Abney, S. R., 1998, Methods of analysis by the U.S. Geological Survey National Water-Quality Laboratory--Determination of 86 volatile organic compounds in water by gas chromatography/mass spectrometry, including detections less than reporting limits: U.S. Geological Survey Open-File Report 97-829, 78 p.

Lahvis, M. A., and Baehr, A. L., 1998, Simulating transport of volatile organic compounds in the unsaturated zone using the computer model R-UNSAT: U.S. Geological Survey Fact Sheet FS-019-98, 4 p.

Landmeyer, J. E., Chapelle, F. H., Bradley, P. M., Pankow, J. F., Church, C. D., and Tratnyek, P. G., 1998, Fate of MTBE relative to benzene in a gasoline-contaminated aquifer (1993-1998): Groundwater Monitoring and Remediation, v. 18, p. 93-102.

Mo, K., Lora, C. O., Wanken, A. E., Javanmardian, M., Yang, X., and Kulpa, C. F., 1997, Biodegradation of methyl t-butyl ether by pure bacterial cultures: Applied Microbiology and Biotechnology, v. 47, p. 69-72.

Mormile, M. R., Liu, S., and Suflita, J. M., 1994, Anaerobic biodegradation of gasoline oxygenates: Extrapolation of information to multiple sites and redox conditions: Environmental Science and Technology, v. 28, p. 1727-1732.

Pankow, J. F., Luo, W., Isabelle, L. M., Bender, D. A., and Baker, R. J., 1998, Determination of a wide range of volatile organic compounds in ambient air using multisorbent adsorption/thermal desorption and gas chromatography/mass spectrometry: Analytical Chemistry, v. 70, p. 5213-5221.

Park, K., and Cowan, R. M., 1997, Effects of oxygen and temperature on the biodegradation of MTBE *in* Preprints of extended abstracts from the 213th American Chemical Society National Meeting, San Francisco, California, April 13-17, 1997: American Chemical Society Division of Environmental Chemistry, Washington, D.C., v. 37, p. 421-424.

Salanitro, J. P., Diaz, M. P., Williams, M. P., and Wisniewski, H. L., 1994, Isolation of a bacterial culture that degrades MTBE: Applied and Environmental Microbiology, v. 60, p. 2593-2596.

Schirmer, M., and Barker, J. F., 1998, A study of long-term MTBE attenuation in the Borden aquifer, Ontario, Canada: Groundwater Monitoring and Remediation, v. 18, p. 113-122.

Steffan, R. J., McClay, K., Vainberg, S., Condee, C. W., and Zhang, D., 1997, Biodegradation of the gasoline òxygenates methyl tert-butyl ether, ethyl tert-butyl ether, and tert-amyl methyl ether by propane-oxidizing bacteria: Applied and Environmental Microbiology, v. 63, p. 4216-4222.

AUTHOR INFORMATION

Matthew A. Lahvis, Ronald J. Baker, and Arthur L. Baehr, U.S. Geological Survey, West Trenton, New Jersey.

Aerobic Mineralization of MTBE and *t*-Butanol by Stream-Bed-Sediment Microorganisms

Paul M. Bradley, James E. Landmeyer and Francis H. Chapelle

ABSTRACT

Microorganisms indigenous to the bed sediments of two streams receiving seepage of gasoline-contaminated ground water demonstrated significant mineralization of the fuel oxygenates, methyl-*t*-butyl ether (MTBE) and *t*-butyl alcohol (TBA). Up to 73% of [U-^{14}C] MTBE and 84% of [U-^{14}C] TBA were degraded to $^{14}CO_2$ under mixed aerobic/anaerobic conditions. No significant mineralization was observed under strictly anaerobic conditions. The results indicate that, under the mixed aerobic/anaerobic conditions characteristic of stream bed sediments, microbial processes may provide a significant environmental sink for MTBE and TBA delivered to surface-water bodies by contaminated ground-water or by atmospheric deposition.

INTRODUCTION

Methyl *t*-butyl ether (MTBE) was introduced in the 1970s as an octane replacement for tetraethyl lead. Since that time, MTBE has been employed as a fuel oxygenate to lower carbon monoxide emissions in accordance with the Clean Air Acts Amendments of 1990. Consequently, MTBE has become an important component of reformulated gasoline and is currently added to 30% of the gasoline consumed in the United States (Squillace and others, 1995; 1996). Because MTBE is highly soluble in water, is readily transported in ground- and surface-water systems, has a low taste and odor threshold (Zogorski and others, In Press), and is tentatively classified by the USEPA as a possible human carcinogen (Squillace and others, 1996; Zogorski and others, In Press), the potential contamination of drinking water supplies with MTBE has rapidly become a national concern. Contamination of drinking water with TBA merits similar consideration due to its usage as a fuel oxygenate, reported presence in gasoline spills (Landmeyer and others, 1998; Zogorski and others, In Press), demonstrated carcinogenicity in laboratory animals (Cirvello and others, 1995), and potential significance as an intermediate in microbial degradation of MTBE (Mormile and others, 1994; Salanitro and others, 1994). Although monitoring data are currently limited, the detection of MTBE in 27% of shallow wells sampled in urban areas (Squillace and others, 1996), 1% of shallow wells sampled in agricultural areas (Squillace and others, 1996), 29-35% of stream water samples collected from urban areas (O'Brien and others, 1997; Terracciano and O'Brien, 1997; Zogorski and others, In Press), and in lake water samples (Zogorski and others, In Press) suggests that concern is warranted. Growing recognition of the potential harmful health effects of these fuel additives has prompted the USEPA to establish a drinking water advisory of 20-40 μg/L for MTBE.

Because approximately 60% of the drinking water consumed in the continental United States comes from surface water systems, the potential contamination of these systems with MTBE and TBA is particularly problematic. Although contamination of surface water sources with fuel oxygenates can result from atmospheric deposition (Pankow and others, 1997; Zogorski and others, In Press), storm-water runoff (Delzer and others, 1996; Lopes and Dionne, 1998; O'Brien and others, 1997; Zogorski and others, In Press), and

releases directly to surface water systems by industrial (Delzer and others, 1996; O'Brien and others, 1997; Terracciano and O'Brien, 1997; Zogorski and others, In Press) and recreational activities (Zogorski and others, In Press), the dissolved concentrations of MTBE associated with these processes are reported to be quite low (less than 10 μg/L: Lopes and Dionne, 1998; Pankow and others, 1997; Zogorski and others, In Press). In contrast, leakage from underground gasoline storage tanks and subsequent discharge of contaminated ground-water can deliver high concentrations of fuel oxygenates to local surface water systems (Happel and others, 1998; Landmeyer and others, 1998; Zogorski and others, In Press; this study). At a gasoline spill site in Beaufort, South Carolina, for example, contaminated ground water containing 10,000 μg/L dissolved MTBE is presently discharging to a nearby stream (Landmeyer and others, 1998). However, ground water discharging to a surface water body must pass through bed sediment microbial communites which are often highly active, metabolically diverse, and capable of efficient degradation of otherwise recalcitrant compounds (Bradley and Chapelle, 1997; 1998; In Press; Bradley and others, 1998). Thus the potential exists that bed sediment microbial communities can degrade MTBE and TBA and significantly diminish the impact of these contaminants on surface water quality. The purpose of this study is to present evidence that bed sediment microorganisms can rapidly degrade MTBE and TBA. These microbial processes, in turn, may constitute a significant biological barrier to the discharge of MTBE- and TBA-contaminated ground water into surface water systems. Moreover, bed sediment microbial activity may provide an important sink for MTBE and TBA introduced into surface-water bodies from atmospheric deposition or other pathways.

METHODS

Chemicals

The potential for microbial degradation of MTBE and TBA was investigated in stream-bed-sediment microcosms using [U-^{14}C] MTBE and [U-^{14}C] TBA. Uniformly labeled ([U-^{14}C]) MTBE (10.1 mCi/mmol; 10% MTBE in ethanol) was obtained from New England Nuclear Research Products, Du Pont (Boston, Massachusetts). The radiochemical purity of the [U-^{14}C] MTBE was determined by the manufacturer and independently confirmed in our lab using radiometric detection gas chromatography (GC/GRD) to be greater than 99%. [U-^{14}C] TBA (5 mCi/mmol) was obtained from Moravek Biochemicals, Inc. (Brea, California). The radiochemical purity of the [U-^{14}C] TBA was determined by the manufacturer and independently confirmed in our lab using GC/GRD to be greater than 98%.

Study Sites

Microcosm studies were conducted using bed sediments from two underground gasoline spill sites located in Laurens, South Carolina (Laurens) and Charleston, South Carolina (Oasis). At both sites, groundwater containing soluble components of reformulated gasoline (including BTEX, MTBE, and TBA) discharges to a shallow stream located 15-30 m downgradient. At the Laurens site, maximun dissolved concentrations of total BTEX compounds, MTBE, and TBA of 105 mg/L, 64 mg/L, and 14 mg/L, respectively, were observed in ground water monitoring wells 20 m up gradient of the stream at the time of bed sediment collection. The Laurens bed sediments were characterized by poorly sorted coarse sand with angular grains, 26±1% water content (% of wet weight), and 0.8±0.2% organic content (% of dry weight). Based on major redox species (dissolved O_2, Fe(II), NO_3, SO_4, and CH_4) collected from the bed sediment and overlying water column, the bed sediment system at the Laurens site was predominantly aerobic at the time of sample collection. At the Oasis site, maximum dissolved concentrations of total BTEX compounds, MTBE, and TBA of 476 μg/L, 138

μg/L, and 2,094 μg/L, respectively, were observed in ground-water monitoring wells 7 m upgradient of the stream at the time of bed sediment collection. The Oasis bed sediments were characterized by fine grained, organic-rich silt and clay, 66±4% water content, and 17±3% organic content. Based on major redox species (dissolved O_2, Fe(II), NO_3, SO_4, and CH_4) collected from the bed sediment and overlying water column at the time of sediment collection, the bed sediment system at the Oasis site was predominantly aerobic at the surface of the sediment shifting to methanogenic with depth.

Microcosm Studies

Bed sediment microcosms were prepared as described previously (Bradley and Chapelle, 1997). In brief, 20 mL serum vials were amended with about 15 g saturated bed sediment, sealed with teflon-lined butyl rubber stoppers, and flushed with 1000 mL of zero air (aerobic) or high purity helium (anaerobic). Five replicate experimental treatments were prepared for each substrate and sediment. Triplicate killed control microcosms were prepared for each substrate and sediment and autoclaved twice for 1 h at 15 PSI and 121 C. Sediment microcosms were amended with approximately 0.1 μCi of [U-^{14}C] MTBE or 0.2 μCi [U-^{14}C] TBA to yield initial dissolved concentrations of 150 μg/L or 400 μg/L for MTBE and TBA, respectively.

Headspace concentrations of CH_4, $^{14}CH_4$, CO_2, and $^{14}CO_2$ were monitored by analyzing 0.5 ml of headspace sample using GC/GRD combined with thermal conductivity detection. The headspace sample volumes were replaced with air (aerobic treatments) or helium (anaerobic treatments). The GC/GRD output was calibrated by liquid scintillation counting using $H^{14}CO_3$. The results of the [U-^{14}C] MTBE and [U-^{14}C] TBA mineralization studies presented in Figures 1 and 2 were corrected for the loss of constituents due to headspace sample collection.

RESULTS AND DISCUSSION

Microorganisms indigenous to the bed sediments at both study sites demonstrated significant aerobic mineralization of [U-^{14}C] MTBE to $^{14}CO_2$ within 105 days. Final recoveries of 73±14% and 30±8% as $^{14}CO_2$ were observed for aerobic microcosms containing Laurens and Oasis bed sediments, respectively (Figure 1). Degradation of [U-^{14}C] MTBE to $^{14}CO_2$ was entirely attributable to biological activity, because no mineralization was observed in autoclaved control microcosms (Figure 1). Microbial mineralization of MTBE under aerobic conditions has been demonstrated previously for pure cultures, bench-top bioreactors, and sludge (Mo and others, 1997; Salanitro and others, 1994; Stefan and others, 1997). To our knowledge, however, this is the first demonstration of extensive, aerobic MTBE mineralization by naturally occurring microbial assemblages.

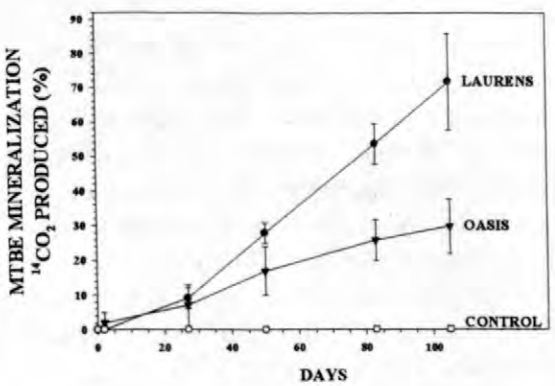

Figure 1. Aerobic mineralization of [U-^{14}C] MTBE to $^{14}CO_2$ in microcosms containing bed sediment from the Laurens and Oasis sites. Data are means±SD.

No significant mineralization of [U-^{14}C] MTBE was observed in Laurens or Oasis microcosms under strictly anaerobic conditions (data not shown). A previous study (Landmeyer and others, 1998) reported low but statistically significant (2.7±0.3%) mineralization of [U-^{14}C] MTBE by aquifer microorganisms under Fe(III)-

reducing conditions. In this study, anaerobic microcosms for both sites were highly methanogenic, producing 5-10 μmol CH_4 per liter of headspace per day (data not shown). The lack of [U-^{14}C] MTBE mineralization observed in this study under methanogenic conditions is consistent with the lack of mineralization in previous microbial studies conducted under methanogenic conditions (Mormile and others, 1994; Suflita and Mormile, 1993).

The rate of mineralization of [U-^{14}C] MTBE observed under aerobic conditions was significantly lower in the Oasis microcosms relative to the Laurens microcosms. This difference in mineralization may be due to the high organic content of the Oasis bed sediments. The Oasis sediments contained 17±3% organic material compared to less than 1% in the Laurens sediments. Competitive inhibition of MTBE biodegradation in the presence of alternative carbon substrates has been demonstrated previously (Mo and others, 1997). Moreover, the high organic content of the Oasis sediments supported significant methanogenic activity (3 μmol CH_4 per liter of headspace per day) even under an aerobic headspace. Because MTBE mineralization is inhibited under methanogenic conditions (Mormile and others, 1994; Suflita and Mormile, 1993; this study), the lower rate of mineralization observed in these sediments may reflect a restriction of MTBE mineralization activity to a thin aerobic zone at the surface of the sediment column. It is likely that a similar pattern exists in situ at the Oasis site.

The bed sediment microbial communities from both sites also rapidly mineralized [U-^{14}C] TBA to $^{14}CO_2$. The rate and magnitude of [U-^{14}C] TBA mineralization did not differ significantly between Laurens and Oasis treatments (Figure 2). Both sediments mineralized 70±6% of the added [U-^{14}C] TBA within 27 days. Mineralization subsequently tapered off with a final mean $^{14}CO_2$ recovery for both sediments of 84±8% (Figure 2). No significant mineralization of [U-^{14}C] TBA was observed in autoclaved control microcosms or in experimental microcosms incubated under anaerobic (methanogenic) conditions. The results of the current study are consistent with previous reports that TBA biodegradation in subsurface soils is rapid under aerobic conditions but proceeds slowly under anaerobic conditions (Novak and others, 1985; Hickman and others, 1989).

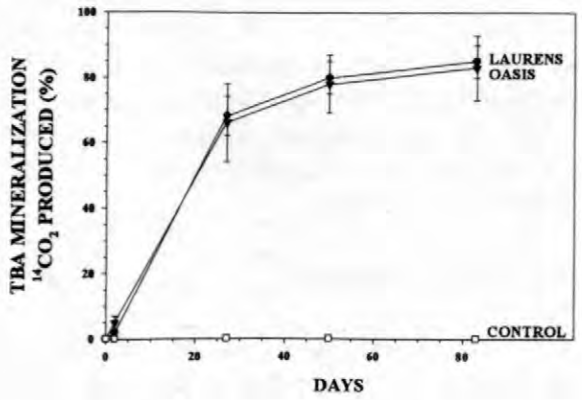

Figure 2. Aerobic mineralization of [U-^{14}C] TBA to $^{14}CO_2$ in microcosms containing bed sediment from the Laurens and Oasis sites. Data are means±SD.

The results of this study have important implications for the potential impact of MTBE and TBA on surface, drinking water supplies. Ground water contaminated with MTBE and TBA represents a particular risk to surface water systems for a number of reasons. The widespread use of these compounds as fuel oxygenates essentially guarantees that they will remain a major component of underground gasoline spills for the foreseeable future. Such spills primarily occur in the shallow subsurface and characteristically become anaerobic. Thus, because MTBE and TBA are highly soluble and recalcitrant under anaerobic conditions, there is a greater probability that these compounds will be transported to local surface water receptors at relatively high concentrations. The results of the current study indicate that the microorganisms which inhabit the bed sediments of these systems can rapidly degrade MTBE and TBA and may provide effective protection against contamination of surface drinking water supplies.

REFERENCES

Bradley, P. M. and Chapelle, F. H., 1997, Effect of contaminant concentration on aerobic microbial mineralization of DCE and VC in stream-bed sediments: Environmental Science and Technology, v. 31, p. 2692-2696.

Bradley, P. M. and Chapelle, F. H., 1998, Microbial mineralization of VC andDCE under different terminal electron accepting conditions: Anaerobe, v. 4, p. 81-87.

Bradley, P. M. and Chapelle, F. H., In Press, methane as a product of chloroethene biodegradation under methanogenic conditions: Environmental Science and Technology.

Bradley, P. M., Chapelle, F. H., and Lovley, D. R., 1998, Humic acids as electron acceptors for anaerobic microbial oxidation of vinyl chloride and dichloroethene: Applied and Environmental Microbiology, v. 64, p. 3102-3105.

Cirvello, J. D., Radovsky, A., Heath, J. E., Farnell, D. R., and Landamood, C., III., 1995, Toxicity and carcinogenicity of t-butyl alcohol in rats and mice following chronic exposure in drinking water: Toxicology and Industrial Health, v. 11, p. 151-166.

Delzer, G. C., Zogorski, J. S., Lopes, T. J., and Bosshart, R. L., 1996, Occurrence of the gasoline oxygenate MTBE and BTEX compounds in the urban stormwater in the United States, 1991-95: U. S. Geological Survey Water Resources Investigation Report, WRIR-96-4145, p. 6.

Happel, A. M., Beckenbach, E. H., and Halden, R. U., 1998, An evaluation of MTBE impacts to California groundwater resources: Univ. Calif. UCRL-AR-130897, p. 68.

Hickman, G. T., Novak, J. T., Morris, M. S., and Rebhun, M., 1989, Effects of site variations on subsurface biodegradation potential: Journal of the Water Pollution Control Federation, v. 61, p. 1564-1575.

Landmeyer, J. E., Chapelle, F. H., Bradley, P. M., Pankow, J. F., Church, C. D., and Tratnyek, P. G., 1998, Fate of MTBE relative to benzene in a gasoline-contaminated aquifer 1993-1998: Ground Water Monitoring and Remediation: Fall issue, p. 93-102.

Lopes, T. J. and Dionne, S. G., 1998, Study plan for urban stream indicator sites of the National Water-Quality Assessment Program: U. S. Geological Survey Open File Report, OFR-98-409, p. 67.

Mo, K., Lora, C. O., Wanken, A. E., Javanmardian, M., Yang, X., and Kulpa, C. F., 1997, Biodegradation of methyl t-butyl ether by pure bacterial cultures: Applied Microbiology and Biotechnology, v. 47, p. 69-72.

Mormile, M. R., Liu, S., and Suflita, J. M., 1994, Anaerobic biodegradation of gasoline oxygenates: extrapolation of information to multiple sites and redox conditions: Environmental Science and Technology, v. 28, p. 1727-1732.

Novak, J. T., Goldsmith, C. D., Benoit, R. E., and O'Brien, J. H., 1985, biodegradation of methanol and tertiary butyl alcohol in subsurface systems: Water Science and Technology, v.17, p. 71-85.

O'Brien, A. K., Reiser, R. G., and Gylling, H., 1997, Spatial variability of volatile organic compounds in streams on Long Island, New York and in New Jersey: U. S. Geological Survey Fact Sheet, FS-194-97, p. 6.

Pankow, J. F., Thomson, N. R., Johnson, R. L., Baehr, A. L., and Zogorski, J. S., 1997, The urban atmosphere as a non-point source for the transport of MTBE and other volatile organic compounds (VOCs) to shallow groundwater: Environmental Science and Technology, v. 31, p. 2821-2828.

Salanitro, J. P., Diaz, L. A., Williams, M. P., and Wisniewski, H. L., 1994, Isolation of a bacterial culture that degrades methyl t-butyl ether: Applied and Environmental Microbiology, v. 60, p. 2593-2596.

Stefan, R. J., McClay, K., Vainberg, S., Condee, C. W., and Zhang, D., 1997, biodegradation of the gasoline oxygenates methyl *tert*-butyl ether, ethyl *tert*-butyl ether, and *tert*-amyl methyl ether by propane oxidizing bacteria: Applied and Environmental Microbiology, v. 63, p. 4216-4222.

Squillace, P. J., Pope, D. A., and Price, C. V., 1995, Occurrence of the gasoline addtitive MTBE in shallow ground water in urban and agricultural areas: U. S. Geological Survey Fact Sheet, FS-114-95, p. 4.

Squillace, P. J., Zogorski, J. S., Wilber, W. G., and Price, C. V., 1996, preliminary assessment of the occurrence and possible sources of MTBE in groundwater in the United States: Environmental Science and Technology, v. 30, p. 1721-1730.

Suflita, J. M. and Mormile, M. R., 1993, anaerobic biodegradation of known and potential gasoline oxygenates in the terrestrial subsurface: Environmental Science and Technology, v. 27, p. 976-978.

Terracciano, S. A., and O'Brien, A. K., 1997, Occurrence of volatile organic compounds in streams on Long Island, New York, and New Jersey: U. S. Geological Survey Fact Sheet, FS-063-97, p. 4.

Zogorski, J. S., Delzer, G. C., Bender, D. A., Squillace, P. J., Lopes, T. J., Baehr, A. L., Stackelberg, P. E., Landmeyer, J. E., Boughton, C. J., Lico, M. S., Pankow, J. F., Johnson, R. L., and Thomson, N. R., In Press, MTBE–summary of findings and research by the U.S. Geological Survey: Proc. 1998 Ann. Conf. Am. Water Works Assoc.

AUTHOR INFORMATION

Paul M. Bradley, James E. Landmeyer, and Francis H. Chapelle, U.S. Geological Survey, Columbia, S.C.

Effects of Environmental Conditions on MTBE Degradation in Model Column Aquifers

By Clinton D. Church, Paul G. Tratnyek, James F. Pankow, James E. Landmeyer, Arthur L. Baehr, Mary Ann Thomas, and Mario Schirmer

ABSTRACT

The current concern over point-source and non-point-source contamination of ground water by methyl *tert*-butyl ether (MTBE) has increased the need for a better understanding of the processes that control its environmental fate. As part of an ongoing study to characterize the potential for natural attenuation of MTBE, we have prepared a series of model column aquifers to investigate the pathways and kinetics of MTBE biodegradation under controlled conditions. The sediments used for these columns were collected aseptically from a variety of geographically and geologically distinct sites: (i) an urban site near Detroit, Michigan; (ii) an urban site in Turnersville, New Jersey; (iii) a controlled spill test site at Base Borden, Ontario, Canada; and (iv) a leaking underground storage tank site at the Laurel Bay Exchange, South Carolina. In all cases, autoclaved site ground water spiked with approximately 100 micrograms/liter MTBE was used as the column influent, and the column effluent was analyzed for MTBE and its potential degradation products. In aerobic column microcosms prepared with core materials from three sites, conversion of MTBE to TBA was observed after a lag period of approximately 35 days, but no evidence of subsequent TBA degradation was observed. This apparent MTBE to TBA conversion subsequently declined, as did measured dissolved oxygen. However, in similar columns with anaerobic influents, or with BTEX (gasoline constituents: benzene, toluene, ethyl benzene, and o-, m-, and p-xylene) contaminated aerobic influents, we have not seen any evidence of MTBE degradation up to 120 days. These results suggest that, if *in situ* biodegradation of MTBE occurs, it is most likely under aerobic conditions, and only in the absence of significant concentrations of more readily metabolized contaminants such as BTEX compounds.

INTRODUCTION

Evidence that methyl *tert*-butyl ether (MTBE) has become a widely distributed environmental contaminant has led to increased concern over its environmental fate and effects (Tratnyek and others, 1997; National Science and Technology Council, 1997; Squillace and others, 1997a; Squillace and others, 1997b). One question that has attracted a great deal of attention is the degree to which MTBE fate is determined by *in situ* biodegradation (for example, Borden and others, 1997; Landmeyer and others, 1998; Odencrantz, 1998; Schirmer and Barker, 1998).

The environmental fate of MTBE depends, in part, on the rates and products of MTBE degradation and, in part, on the physical transfer of MTBE among the different environmental compartments (Baehr and others, 1997; Pankow and others, 1996; Shaffer and Urchin, 1997; Squillace and others, 1997). For this reason, measurements of MTBE disappearance from ground water alone are not adequate to prove whether it has biodegraded *in situ*.

In order to demonstrate that *in situ* biodegradation of MTBE is occurring, measurements of MTBE disappearance need to be accompanied by evidence that microorganisms present at a particular site have the potential to degrade MTBE under realistic environmental conditions, and that this potential is realized in the field (Madsen, 1991; National Science and Technology Council, 1993).

There is evidence that MTBE is biodegradable under favorable circumstances. Numerous investigators have reported biodegradation of MTBE in pure cultures, enrichments, and batch microcosms (Borden and others, 1997; Cowan and Park, 1996; Eweis and others, 1997; Hardison and others, 1997; Landmeyer and others, 1998; Mormile and others, 1994; Salanitro and others, 1994; Schirmer and others, 1998; Steffan and others, 1997; Yeh and Novak, 1994). However, despite evidence that MTBE biodegradation is *possible*, these results do not show that MTBE

biodegradation is a *significant* process in the field. Nor do these results provide a means to estimate likely field degradation rates, because batch microcosms generally do not simulate aquifer conditions.

More compelling evidence for *in situ* degradation of MTBE would be the appearance of characteristic metabolic intermediates or products (Madsen, 1991). Of the studies that have reported MTBE degradation products, the most commonly observed products are *tert*-butyl alcohol (TBA) and CO_2, although *tert*-butyl formate (TBF) is the initial oxidation product of some aerobic microbial degradation pathways (Cain, 1981).

Recently, it has been reported that the cometabolic degradation of MTBE by a *Graphium* sp. produces both TBF and TBA when the mycelia are incubated under air, and exclusively TBA only when incubated in liquid culture (Hardison and others, 1997). The authors of that study concluded that TBF is the primary metabolite in both media, and that rapid hydrolysis of TBF to TBA in the liquid media is responsible for the apparent difference in product distributions. Further work has shown that *Mycobacterium vaccae* and a *Xanthobacter* strain also produce TBF as the primary degradation product (Hyman and others, 1998).

Rates of abiotic TBF hydrolysis to TBA in our laboratory support the suggestion by Hardison and others (1997) that previous studies may have underestimated the role of TBF as an intermediate in the biodegradation of MTBE. We found that TBF is hydrolyzed with half-lives (at 22°C) of 5 days, 8 hours, and 8 minutes at pH 7, 3, and 11, respectively (Church and others, 1999). Thus, TBF is unlikely to accumulate to detectable levels in groundwater, and is likely to be a poor tracer for *in situ* MTBE degradation.

A few studies have shown TBA to be further degraded to isopropanol, acetone, and ultimately CO_2. However, isopropanol and acetone are more biodegradable than TBA under most conditions, and so, like TBF, are unlikely to accumulate to detectable concentrations. Furthermore, isopropanol, acetone, and CO_2 may be degradation products of many other compounds, and as such, are not likely to provide characteristic evidence of MTBE degradation. Of all the products and intermediates reported in the degradation of MTBE, TBA remains the most promising indicator of degradation because it is (i) common to most MTBE degradation pathways (Church and others, 1997), (ii) a demonstrated product of MTBE biodegradation (Salanitro and others, 1994; Yeh and Novak, 1994), and (iii) sufficiently resistant to further degradation that it may accumulate as an intermediate before being further degraded (Cowan and Park, 1996; Mormile and others, 1994; Salanitro and others, 1994).

Unfotunately, even the detection of TBA in ground water samples does not provide unequivocal proof of MTBE degradation (Landmeyer and others, 1998). The reason for this is twofold: (i) TBA itself has occasionally been used as a fuel oxygenate, and (ii) TBA is often present as a contaminant in the MTBE that is subsequently blended into gasoline. Thus, unless it can be shown that TBA has never been introduced into a site, the most convincing way to demonstrate MTBE degradation to TBA is to show a mass decrease of MTBE with a concomitant TBA mass increase. This can be a difficult and costly task because it requires extensive multi-level sampling of an entire plume at multiple points in time. To the authors' knowledge, there are not yet enough data on any field site to unequivocally demonstrate the biodegradation of MTBE from the apearance of TBA. Of course, the lack of unequivocal proof of MTBE degradation from field studies does not mean that it does not occur under certain environmental conditions.

An alternative approach to investigate degradation of MTBE is to use controlled model systems that are designed to simulate typical field conditions. To perform this investigation, six model column aquifers were constructed using aseptically collected sediments from four sites and operated under various conditions. In order to compare sites that were geographically and geologically distinct, the sediments used in the columns were obtained from three US Geological Survey (USGS) projects and from a controlled release site in Ontario, Canada. The preliminary results presented here suggest that MTBE may be degraded only under aerobic conditions and only in the absence of significant levels of BTEX (gasoline constituents: benzene, toluene, ethyl benzene, and o-, m-, and p-xylene) compounds. Further studies are under way to determine (i) the kinetics of MTBE degradation, (ii) whether the observed degradation is metabolic or cometabolic, and (iii) which environmental parameters can be manipulated to enhance the degradation of MTBE.

MATERIALS AND METHODS

Standards and Analytical Techniques

Standard solutions were made using the highest purity MTBE and TBA that were available from commercial sources (Aldrich, >97%) and Millipore water. Standards and the effluent from column experiments were analyzed by direct aqueous injection with gas chromatography and detection by mass spectrometry (DAI-GC/MS) according to a method described previously (Church and others, 1997). DAI-GC/MS was particularly useful in this study because it allowed: (i) simultaneous quantification of MTBE and TBA; (ii) detection and identification of other substances that might be intermediates or degradation products, such as *tert*-butyl formate, isopropanol, and acetone; and (iii) monitoring of reaction progress over a wide range of concentrations.

Column Sediments

The sediments for the column studies were collected from four geographically and geologically distinct sites using either a hand auger or a split-spoon core sampler. In all cases, care was taken to use aseptic sampling techniques. Sediments were packaged to exclude oxygen and shipped on ice to the Oregon Graduate Institute where they were kept in a 4°C cold-room until they were repacked in the columns. A brief description of the sediments and aquifer conditions at each site follows.

Michigan Sediments

The Michigan sediments came from an urban National Aquifer Water Quality Assessment (NAWQA) Program study site in Farmington Hills, a suburb of Detroit. The sediments consisted of fine sand mixed with some silt and gravel, with an organic-carbon content ranging from 4 to 7 g/kg. The samples were collected from a depth interval of 1.5-4.0 m (5-13 feet), which is just below the water table in an unconfined aquifer composed of glacial outwash. The dissolved-oxygen concentration in the ground water was 1.2 mg/L.

New Jersey Sediments

Sediments from New Jersey were collected at an urban NAWQA study site in Turnersville, near the western edge of the surficial Kirkwood-Cohansey aquifer system in the coastal plain. Unsaturated zone sediment in this region is sandy and layered, as typical of marine deposition processes. Sediment used in the columns was collected at 5.7 m (18.8 feet), which is at the water table, and consisted of fine silty orange sand with intermixed clay. Organic content was not measured, but these sediments are typically low in organic content (Baehr and others, 1997).

Borden Sediments

The sediments for these columns were obtained from 3.0-4.0 m (10-15 feet) below the water table at the Canadian Forces Base Borden (Ontario, Canada) in an area that had previously been exposed to the Borden MTBE plume (Schirmer and Barker, 1998). The Borden aquifer is relatively homogeneous and composed of clean, well-sorted, fine- to medium-grained sand. The Borden aquifer has a relatively low carbon content of 0.02 percent and thus a low sorption capacity for organic compounds (Mackay and others, 1986). The dissolved oxygen content in the ground water ranged from 1-2 mg/L.

Laurel Bay Sediments

Sediments were collected at the water table from the Laurel Bay Exchange study site near Beaufort, South Carolina (SC), in the Atlantic Coastal Plain. The aquifer is comprised of silty, well-sorted sand grains. The grains are coated with Fe(III) oxides in uncontaminated areas that become progressively less prevalent with increases in contaminant concentration. Natural organic carbon content in these sediments is less than 0.02 percent. The depth to water is about 3.9 m (13 feet) near the underground storage tank (UST), and from 0.6 to 2.7 m (2 to 9 feet) nearer a concrete-lined drainage ditch, some 215 m (700 feet) downgradient of the UST source area (Landmeyer and others, 1998). Sediments used for the aerobic column experiments were collected from an aerobic ($\approx$4.0 mg/L) part of the aquifer downgradient of the plume, where MTBE was detected but BTEX was absent. Sediments used for the anaerobic column experiment were collected from an anaerobic (<0.5 mg/L) part of the aquifer near the plume source that contained both MTBE and BTEX.

Column Construction and Operation

The columns were constructed using segments of 2.54 cm I.D. stainless steel pipe totaling 360 cm in length. Sediments were aseptically packed into autoclaved column segments using alcohol-flamed tools inside a linear flow hood or anaerobic glove box. The packed column segments were connected using autoclaved 1.5 mm O.D. stainless steel tubing with stainless steel fittings and incubated in a 15°C cold-room.

Column influent solutions were autoclaved site ground water which were either equilibrated with the atmosphere or purged of oxygen by sparging with N_2 prior to autoclaving. For the BTEX contaminated experiments, the ground water solutions were ammended with 100 micrograms/liter (µg/L) of each of the constituents. These feed solutions were pumped through the column in upflow mode for 14 days at 40 milliliters/day (mL/day) using a syringe pump. After this initial equilibration period, the column feed was switched to identical solutions ammended with approximately 100 µg/L (1.13 micromoles/liter) MTBE delivered at 40 mL/day. This pump rate was maintained and daily samples were taken until MTBE breakthrough was observed. After steady concentrations of MTBE were observed for five days, the flow rate was reduced to 1.5 mL/day to achieve a linear flow velocity between 0.67 and 1.0 cm/day (depending upon column porosity).

RESULTS AND DISCUSSION

Columns with MTBE Degradation

Three columns containing three different sediments from pristine sites were operated with aerobic influent that contained no detectable BTEX compounds. In each of these columns, TBA appeared in the effluent after a lag period of approximately 35 days (Figure 1, A and B and Figure 2, A). This was followed by a concomitant decrease in the concentration of MTBE.

Accompanying a decrease in conversion of MTBE to TBA was a decrease in measured dissolved oxygen in the effluent from approximately 9 mg/L to 1 mg/L. This correlation suggests that biodegradation of MTBE is favored by aerobic conditions, and will be investigated in subsequent experiments.

No evidence of TBA degradation (through product appearance) was observed in any of the columns. This suggests that, under the conditions tested, either TBA is recalcitrant or MTBE is a more favorable substrate. The mass balances, with the exception of as yet unexplained "spikes" at the onset of TBA appearance in the effluent, suggests a stoichiometric conversion of MTBE to TBA.

Columns without MTBE Degradation

One column had an anaerobic influent free of BTEX compounds. In this column, no MTBE to TBA conversion was observed up to 120 days (Figure 2, A, same sediment as in Figure 2, B). Two of the columns were fed with both aerobic and anaerobic site waters containing 100 µg/L BTEX compounds. No MTBE to TBA conversion was observed up to 120 days (Figure 3, A and B). The mass balances in these columns were equal to the MTBE concentrations, and so, were not included.

Conclusions

The preliminary results discussed above suggest that, if *in situ* biodegradation of MTBE occurs, it is most likely under aerobic conditions and in the absence of significant levels of more readily metabolized contaminants (such as BTEX). This finding is consistent with reports of batch experiments which show that biodegradation of MTBE can occur under aerobic conditions (Cowan and Park, 1996; Eweis and others, 1997; Hardison and others, 1997; Salanitro and others, 1994; Steffan and others, 1997) and that it is generally not observed or slow under anaerobic conditions (Mormile and Suflita, 1994; Yeh and Novak, 1994). Additional studies are being performed in the model column aquifers described here to determine (i) the rates of the MTBE degradation observed, (ii) whether the observed degradation is metabolic or cometabolic, and (iii) whether environmental parameters can be manipulated to enhance the degradation of MTBE.

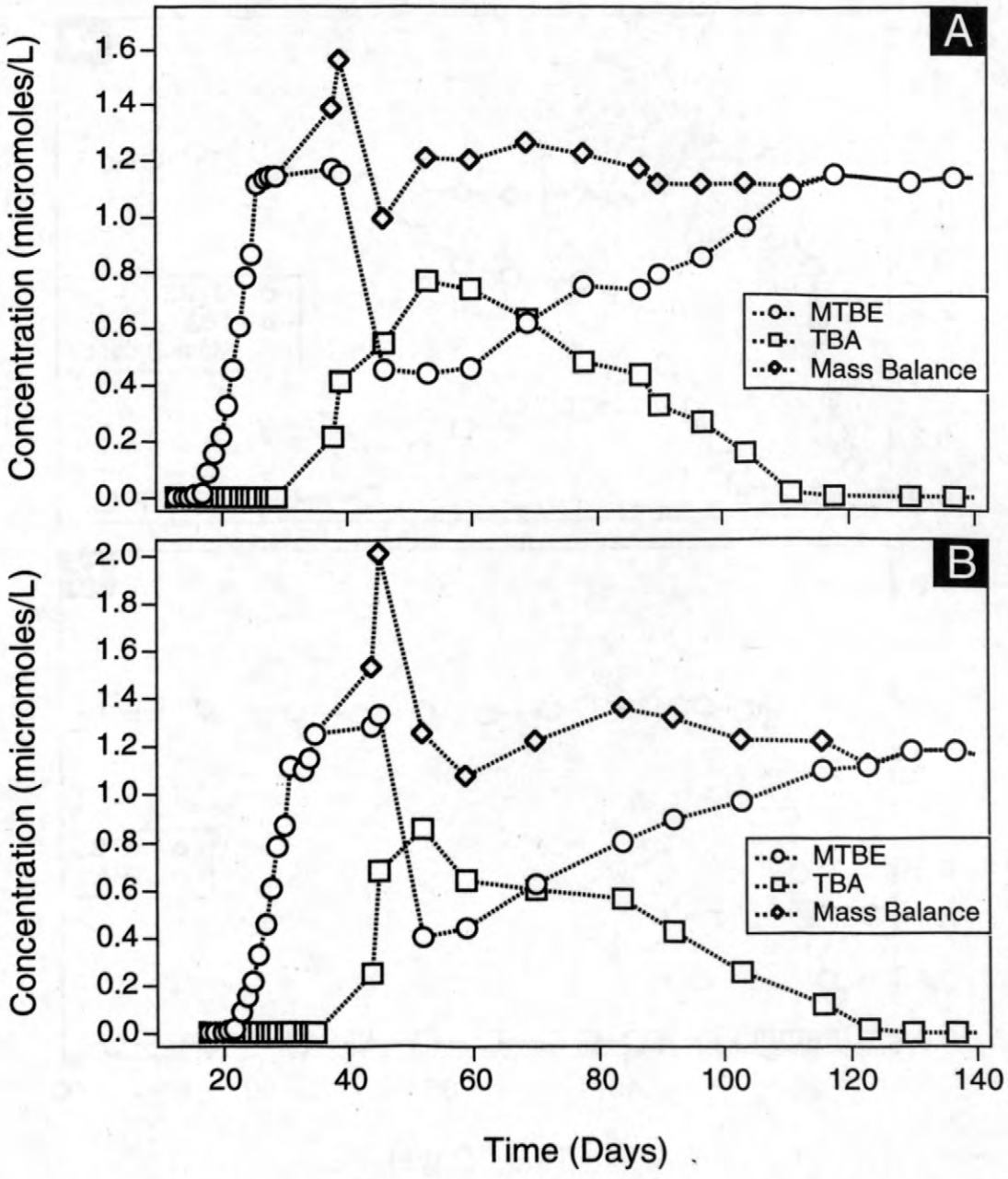

Figure 1. MTBE and TBA concentrations in effluents from two columns containing previously uncontaminated sediments. The columns were challenged with aerobic influent containing MTBE. (A) Michigan Sediments, USGS urban NAWQA Study Site, Detroit, MI. (B) New Jersey Sediments, USGS urban NAWQA Study Site, Trenton, NJ.

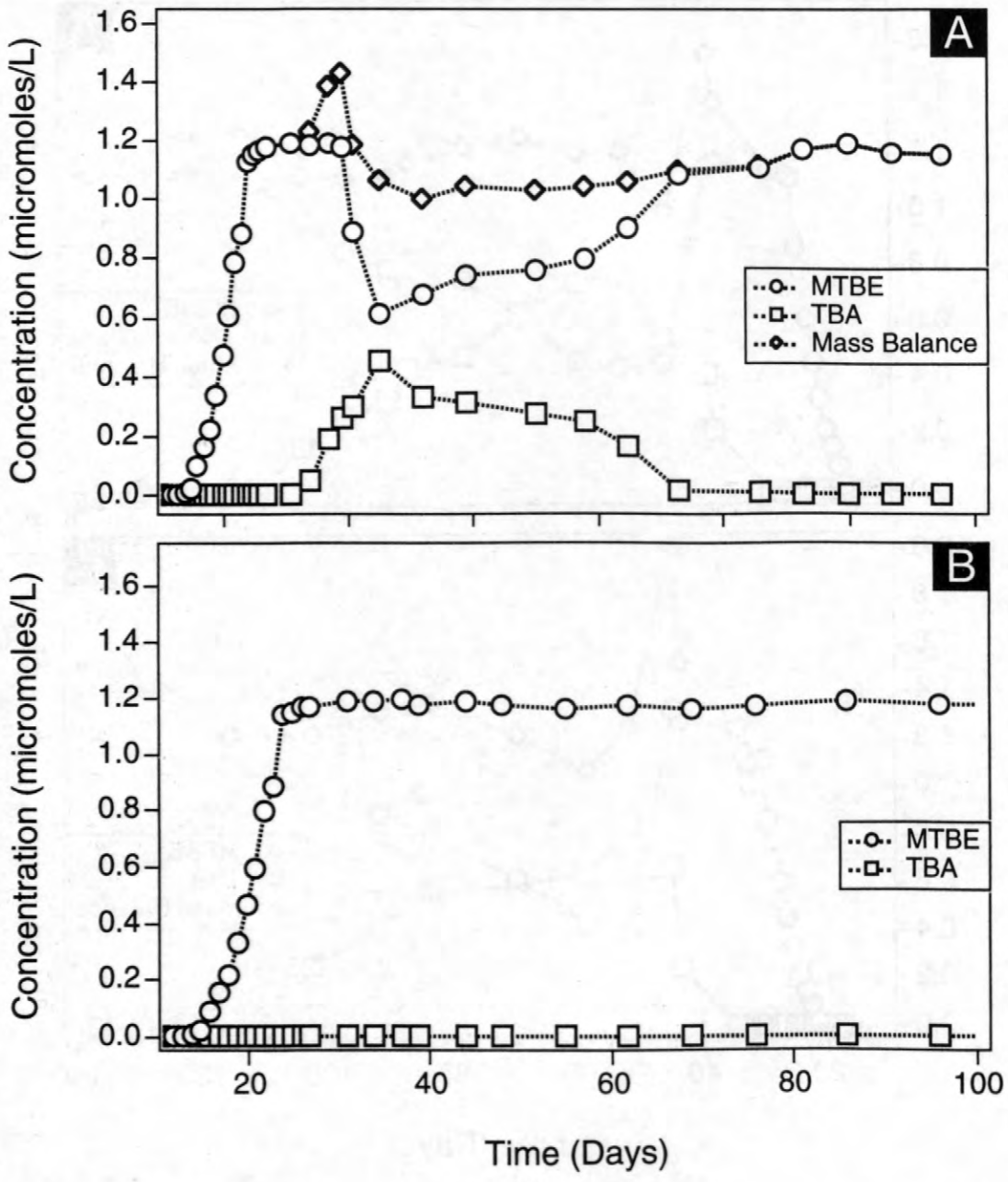

Figure 2. MTBE and TBA concentrations in column effluents from a previously contaminated sediment operated with both aerobic and anaerobic influent containing MTBE (A) Base Borden Sediments with aerobic influent, University of Waterloo Study Site, Ontario, Canada. (B) Base Borden Sediments with anaerobic influent, University of Waterloo Study Site, Ontario, Canada.

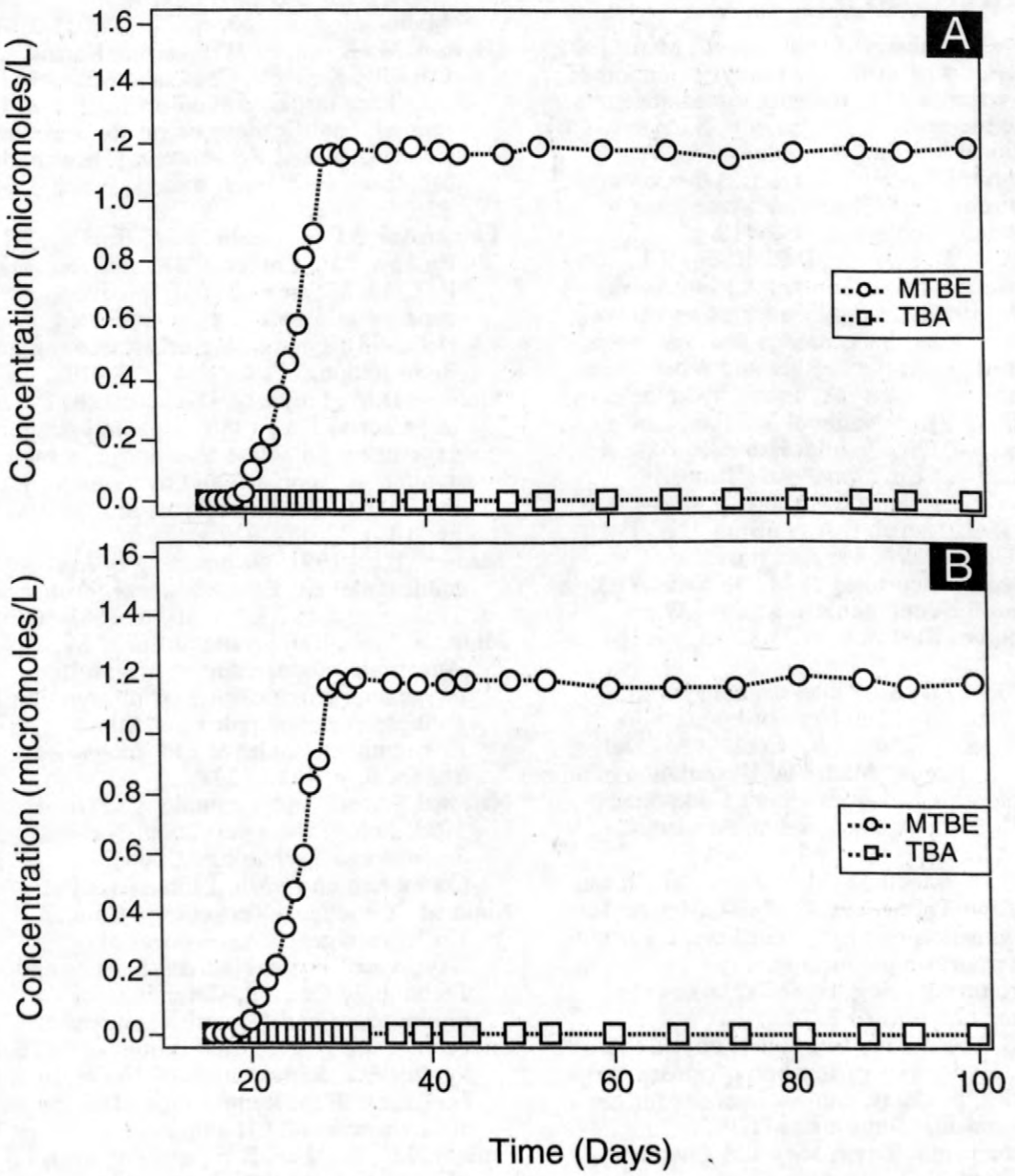

Figure 3. MTBE and TBA concentrations in column effluent from MTBE- and MTBE- plus BTEX-contaminated sediment. Influent for both columns contained both MTBE and BTEX compounds. (A) Laurel Bay MTBE -contaminated sediments, USGS Toxic Substances Study Site, Laurel Bay Exchange, Beufort, SC. (B) Laurel Bay MTBE- and BTEX-contaminated sediments, USGS Toxic Substances Study Site, Laurel Bay Exchange, Beufort, SC.

REFERENCES

Baehr, A.L., Baker, R.J., and Lahvis, M.A., 1997, Transport of methyl tert-butyl ether across the water table to the unsaturated zone at a gasoline-spill site in Beaufort, S.C., *in* 213th National Meeting, San Francisco, CA, Preprint Extended Abstracts, Division of Environmental Chemistry, American Chemical Society, p. 417-418.

Baehr, A.L., Stackelberg, P.E., Baker, R.J., Kauffman, L.J., Hopple, J.A., and Ayers, M.A., 1997, Design of a sampling network to determine theoccurence and movement of methyl tert-butyl ether and other organics through the urban hydrologic cycle. *in* 213th National Meeting, San Francisco, CA, Preprint Extended Abstracts, Division of Environmental Chemistry, American Chemical Society, p. 400-401.

Borden, R.C., Daniel, R.A., LeBrun, L.E., IV, and Davis, C.W., 1997, Intrinsic biodegradation rates of MTBE and BTEX in a gasoline-contaminated aquifer: Water Resources Research, v. 33, no. 5, p. 1105-1115.

Cain, R.B., 1981, Microbial degradation of surfactants and "builder" compounds, *in* Leisinger, T., Hütter, R., Cook, A.M., and Nüesch, J., eds., Microbial Degradation of Xenobiotics and Recalcitrant Compounds: FEMS Symposium: London, Academic, p. 325-370.

Church, C.D., Isabelle, L.M., Pankow, J.F., Rose, D.L., and Tratnyek, P.G., 1997, Method for determination of methyl tert-butyl ether and its degradation products in water: Environmental Science & Technology, v. 31, no. 12, p. 3723-3726.

Church, C.D., Pankow, J.F., and Tratnyek, P.G., 1999, Hydrolysis of tert-butyl formate: Kinetics, products, and implications for the environmental impact of MTBE. Environmental Toxicology and Chemistry, Submitted.

Cowan, R.M., and Park, K., 1996, Biodegradation of the gasoline oxygenates MTBE, ETBE, TAME, TBA, and TAA by aerobic mixed cultures, *in* 28th Mid-Atlantic Conference, Buffalo, NY, p. 523-530.

Eweis, J.B., Schroeder, E.D., Chang, D.P.Y., Scow, K.M., Morton, R., and Caballero, R., 1997, Meeting the challenge of MTBE Biodegradation, *in* 90th Annual Meeting and Exhibition, Toronto, Canada, Air and Waste Management Association.

Hardison, L.K., Curry, S.S., Ciuffetti, L.M., and Hyman, M.R., 1997, Metabolism of diethyl ether and cometabolism of methyl tert-butyl ether by a filamentous fungus, a *Graphium* sp. Applied and Environmental Microbiology, v. 63, no. 8, p. 3059-3076.

Hyman, M., Kwon, P., Williamson, K., and O'Reilly, K., 1998, Cometabolism of MTBE by alkane-utilizing microorganisms. *in* First International Conference on Remediation of Chlorinated and Recalcitrant Compounds, Monterey, California, Battelle Press, p. 321-326.

Landmeyer, J.E., Chapelle, F.H., Bradley, P.M., Pankow, J.F., Church, C.D., and Tratnyek, P.G., 1998, Fate of MTBE relative to benzene in a gasoline-contaminated aquifer (1993-98): Ground Water Monitoring and Remediation, v. 18, no. 4, p. 93-102.

Mackay, D.M., Freyberg, D.L., Roberts, P.V., and Cherry, J.A., 1986, A natural gradient experiment on solute transport in a sand aquifer, 1. Approach and overview of plume movement. Water Resources Research, v. 22, no. 13, p. 2017-2029.

Madsen, E.L., 1991, Determining *in situ* biodegradation: Environmental Science and Technology, v. 25, no. 10, p. 1663-1673.

Mormile, M.R., Liu, S., and Suflita, J.M., 1994, Anaerobic biodegradation of gasoline oxygenate: extrapolation of information to multiple sites and redox conditions. Environmental Science and Technology, v. 28, no. 9, p. 1727-1732.

National Science and Technology Council, 1993, *In Situ* Bioremediation: National Science and Technology Council, Committee on *In Situ* Bioremediation.

National Science and Technology Council, 1997, Interagency Assessment of Oxygenated Fuels: National Science and Technology Council, Committee on Environment and Natural Resources.

Odencrantz, J.E., 1998, Implications of MTBE for Intrinsic Remediation of Underground Fuel Tank Sites: Remediation: The Journal of Environmental Cleanup, v. 8, no. 3, p. 7.

Pankow, J.F., Rathbun, R.E., and Zogorski, J.S., 1996, Calculated volatilization rates of fuel oxygenate compounds and other gasoline-related compounds from rivers and streams: Chemosphere, v. 33, no. 5, p. 921-937.

Salanitro, J.P., Diaz, L.A., Williams, M.P., and Wisniewski, H.L., 1994, Isolation of a bacterial culture that degrades methyl t-butyl ether: Applied and Environmental Microbiology, v. 60, no. 7, p. 2593-2596.

Schirmer, M., and Barker, J.F., 1998, A study of long-term MTBE attenuation in the Border Aquifer, Ontario, Canada: Ground Water Monitoring and Remediation, v. 18, no. 2, p. 113-122.

Schirmer, M., Barker, J.F., Butler, B.J., Church, C.D., and Schirmer, K., 1998, Natural attenuation of MTBE at the Borden field site, *in* Wickramanayake, G.B., and Hinchee, R.E., eds., Natural Attenuation: Proceedings of the First International Conference on Remediation of Chlorinated and Recalcitrant Compounds, 18-21 May 1998, Monterey, CA: Columbus, OH, Battelle Press, p. 327-331.

Shaffer, K.L., and Urchin, C.G., 1997, Uptake of methyl tertiary butyl ether (MTBE) by groundwater solids: Bulletin of Environmental Contamination and Toxicology, v. 59, no. 5, p. 744.

Squillace, P.J., Pankow, J.F., and Zogorski, J.S., 1997a, Review of the environmental behavior and fate of methyl tert-butyl ether: Environmental Toxicology and Chemistry, v. 16, no. 9, p. 1836-1844.

Squillace, P.T., Zogorski, J.S., Wilber, W.G., and Price, C.V., 1997b, Preliminary assessment of the occurrence and possible sources of MTBE in groundwater in the United States, 1993-1994., *in* 213th National Meeting, San Francisco, CA, Preprint Extended Abstracts, Division of Environmental Chemistry, American Chemical Society, p. 372-374.

Steffan, R.J., McClay, K., Vainberg, S., Condee, C.W., and Zhang, D., 1997, Biodegradation of the gasoline oxygenates methyl *tert*-butyl ether, ethyl *tert*-butyl ether, and *tert*-amyl methyl ether by propane-oxidizing bacteria. Applied and Environmental Microbiology, v. 63, no. 11, p. 4216-4222.

Tratnyek, P.G., Bauman, B.J., and Zogorski, J.S., (organizers), 1997, Extended Abstracts of the Symposium on Environmental Fate and Effects of Gasoline Oxygenates, in 213th National Meeting, San Francisco, CA, Division of Environmental Chemistry, American Chemical Society, p. 366-432.

Yeh, C.K., and Novak, J.T., 1994, Anaerobic biodegradation of gasoline oxygenates in soils: Water Environment Research, v. 66, no. 5, p. 744-752.

ACKNOWLEDGEMENTS

This work was supported primarily by the United States Geological Survey Toxic Substances Program through Cooperative Agreement No. 1434-WR-96-AG-00003. Collaboration with the University of Waterloo on the MTBE plume at Base Borden, Ontario, was supported by the American Petroleum Institute. In addition, Clinton D. Church was supported by an EPA STAR Graduate Fellowship.

AUTHOR INFORMATION

Clinton D, Church, Paul G, Tratnyek, and James F. Pankow; Oregon Graduate Institute, Portland, Oregon

James E. Landmeyer, U.S. Geological Survey, Charleston, South Carolina

Arthur Baehr, U.S. Geological Survey, Trenton, New Jersey

Mary Ann Thomas, U.S. Geological Survey, Columbus, Ohio

Mario Schirmer, University of Waterloo, Waterloo, Ontario, Canada

Equilibrium Vapor Method to Determine the Concentration of Inorganic Carbon And Other Compounds in Water Samples

by Ronald J. Baker, Arthur L. Baehr, and Matthew A. Lahvis

ABSTRACT

The total concentration of dissolved carbon dioxide, bicarbonate, and carbonate (C_T) in water is a fundamental parameter in studies of natural and contaminated systems. A new method (the equilibrium vapor method) for determining C_T that involves the measurement of carbon dioxide concentration in the headspace of a water sample by gas chromatography and calculation of C_T by using the equilibrium relations of the carbonate system is presented. The method is most accurate when sample pH is low (near the alkalinity titration endpoint, about 4.3) when the standard titration method is least accurate or inapplicable. The method is also advantageous over the standard titration method when the water contains other alkaline species, such as salts of organic acids, which can occur as metabolites of microbial activity. The presence of such species can result in overestimation of C_T with the standard titration method because they contribute to alkalinity. An additional advantage of the equilibrium vapor method is that aqueous concentrations of volatile compounds, such as hydrocarbons, methyl-tert-butyl ether (MTBE), and dissolved gases, such as oxygen, nitrogen, methane, and carbon disulfide, can be calculated from the headspace analysis of a single sample by using Henry's law.

Ground-water samples from two gasoline-spill sites were analyzed to demonstrate the method and compare the results with those obtained by using the standard titration method. The two methods provided comparable estimates of C_T for samples with pH values above 5.0. For low-pH samples, C_T was obtainable only with the equilibrium vapor method. Filtration and acidification of samples did not affect the accuracy of the equilibrium vapor method for samples from these sites; however, acidification of samples from sites with significant amounts of carbonate minerals may result in overestimation of C_T. The concentrations of gasoline hydrocarbons in several samples also were determined.

INTRODUCTION

Carbonates are ubiquitous solutes in natural freshwater, and commonly represent a major fraction of inorganic dissolved solids. Most carbonates originate from atmospheric carbon dioxide (CO_2), carbonate minerals, and biochemical reactions (Bolin and Cook, 1983). Four carbonate species are present in all natural waters: dissolved CO_2, carbonic acid (H_2CO_3), bicarbonate (HCO_3^-), and carbonate (CO_3^{2-}) (Stumm and Morgan, 1996). Carbonate concentrations and speciation are inseparably linked to the pH and buffering characteristics of freshwater, and carbonate species are involved in many biochemical and abiotic reactions. Total inorganic carbon (C_T) refers to the sum of concentrations (moles per liter) of all carbonates, including free and complexed forms:

$$C_T = [H_2CO_3^*] + [HCO_3^-] + [CO_3^{2-}], \quad (1)$$

where $[H_2CO_3^*]$ is the sum of aqueous $[CO_2]$ and $[H_2CO_3]$, and all concentrations are in moles per liter.

C_T is traditionally determined by alkalinity titration (Eaton and others, 1995). The alkalinity of water is defined as its acid-neutralizing capacity, and is the sum of all the titratable bases (Eaton and others, 1995). Most alkalinity in freshwater is contributed by hydroxide, bicarbonate, and carbonate. Relative contributions of these species to the

water's alkalinity can be calculated from the pH (Stumm and Morgan, 1996). At the pH range of most surface and ground water (5-8), bicarbonate is the dominant form of alkalinity. For water whose pH is near the titration endpoint (about 4.3), nearly all C_T is in the form of H_2CO_3, and alkalinity titration is inaccurate or even impossible. Measured alkalinity values also may include contributions from inorganic and organic bases other than carbonates, such as borates, phosphates, silicates, ammonia, and salts of organic acids. Therefore, assuming that all alkalinity in a sample is contributed by carbonates may lead to overestimation of C_T. Also, the titration endpoint may be difficult to discern when weak acids with dissociation constants near that of carbonate ($10^{-6.3}$) are present. Direct measurement of dissolved CO_2 would eliminate these sources of error in C_T determination.

This paper introduces the equilibrium vapor method for quantifying C_T in natural waters. It describes the method, which is an alternative to alkalinity titration, in which equilibrated headspace above a water sample is analyzed by using gas chromatography (GC); and C_T is determined from vapor-phase [CO_2], pH, and carbonate relations.

Application of the method to the analysis of environmental samples is demonstrated by using ground-water samples from two gasoline spill-sites. Determination of C_T in clean background, lightly contaminated, and heavily contaminated samples by alkalinity titration and by equilibrium vapor analysis is presented, and results of the two methods are compared. Use of the equilibrium vapor method to quantify concentrations of volatile hydrocarbons also is demonstrated.

EQUILIBRIUM VAPOR METHOD

A 125-mL (milliliter) glass sampling bulb with Teflon stopcocks and a syringe sampling port (fig. 1) is used (#CG-1808-01, Chemglass, Inc., Vineland, N.J.)[1]. The sample is collected in the field by holding the sampling bulb vertically and pumping water into the lower end until the bulb is filled, then allowing water to continue flowing until five or more bulb-volumes have passed through the bulb. The sample must have no headspace. Because microbial and abiotic processes that change C_T continue in the sample, immediate analysis is desirable. If sample storage is unavoidable, stability tests can be conducted to determine whether C_T changes noticeably during the anticipated holding time. The filled bulb is then clamped vertically to a ring stand. A gas-tight syringe is filled with 62.5 mL (milliliters) of ultrapure helium, which is injected into the bulb's upper stopcock, while an equal volume of water is gravity-drained through the lower stopcocks. The bulb is removed from the stand and shaken for 3 minutes.

The vapor phase is sampled by reinjecting 20 mL of water through the lower stopcock, while extracting 20 mL of vapor through the upper stopcock. The vapor sample is analyzed by direct injection into a gas-sampling port on the GC. A GC (Varian Model 3600 GC and a Tracor 540 GC) with a flame ionization detector (FID) and a thermal conductivity detector (TCD) was used. A gas-sampling port is attached to each of the two injectors, one for the TCD analysis for fixed gases (O_2, N_2, CO_2, CH_4), the other for the FID analysis for volatile hydrocarbons. Each port consists of a sample loop that holds a fixed volume of vapor sample, and an air- actuated valve mounted in a heated zone that is opened automatically at the beginning of the GC analysis. Fixed gases are separated on a stainless-steel packed column (6.10-m (meter) length x 5.7-mm (millimeter) i.d. (inside diameter), 100- percent Carbopack, 20-40 mesh). The GC oven is programmed from 35 °C (held 8 minutes) to 220 °C at 35 °C per minute (held 5 minutes). The injector and TCD temperatures are 200 °C. Volatile hydrocarbons are separated on a megabore capillary column in the Varian 3600 GC (60-m length x 0.75-mm i.d. Vocol, 1.5-µ (micrometer) film, Supelco, Inc., Bellefonte, Pa.) or a capillary column in the Tracor 540 GC (30-µ length x 0.53-mm i.d. DB-1, 3.0-µ film, J&W Scientific, Folsom, Cal.). The GC oven is programmed from 35 °C (held 4 minutes) to 220 °C at 4 °C per minute (held 5 minutes). The injector and FID temperatures are 200 °C. External stan-

[1]Use of brand, trade, or firm names is for identification purposes only and does not constitute endorsement by the U.S. Geological Survey

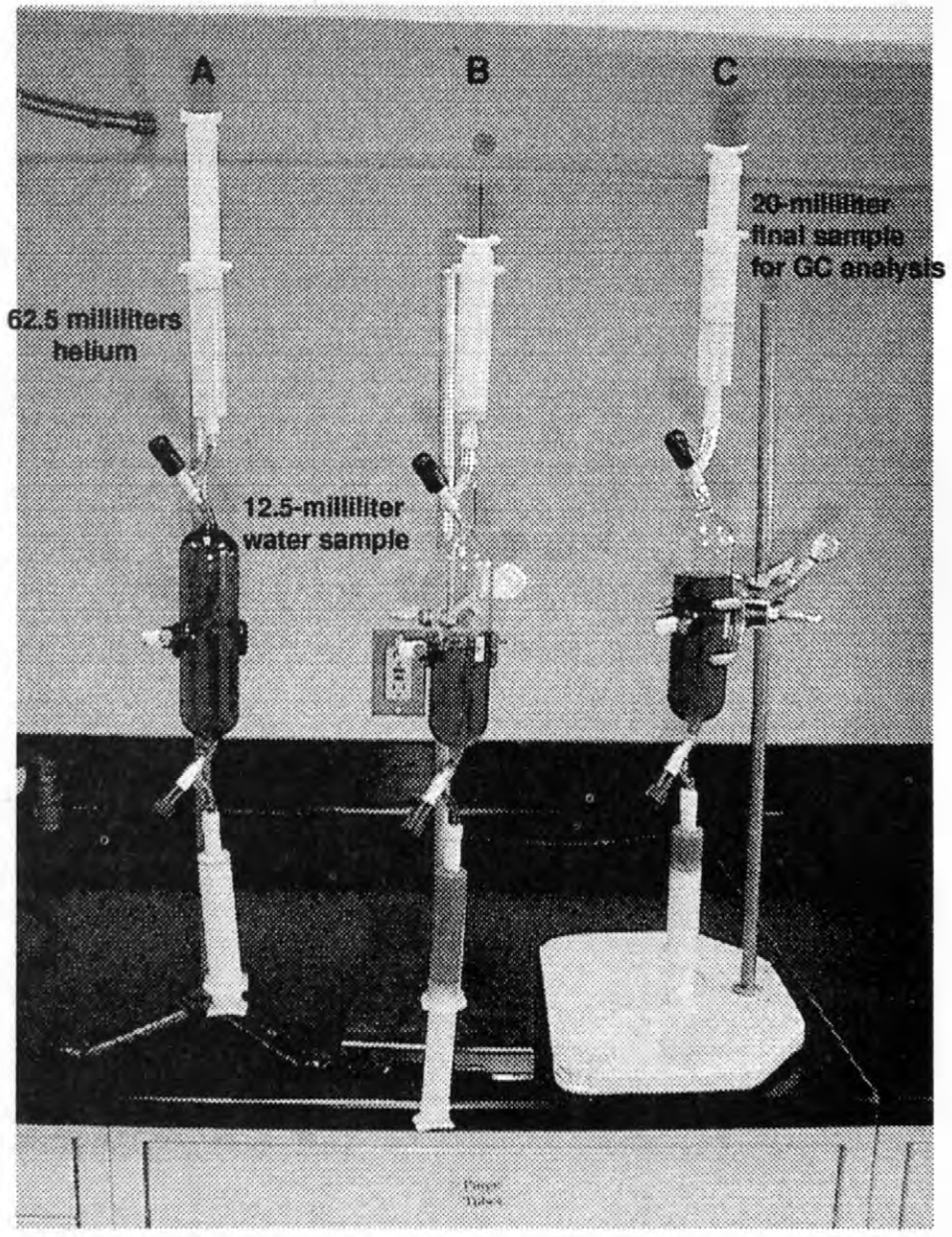

Figure 1. Preparation of water sample for analysis by equilibrium vapor method: (A) Syringes are attached to bulb containing water sample; (B) Helium is injected while water is withdrawn; (C) a portion of the water is reinjected whiile helium is withdrawn for gas-chromatographic (GC) analysis.

Table 1. Total-carbon concentration (C_T) in water samples from the Galloway and Beaufort sites determined by using the titration method and equilibrium vapor method

[Sample depths are in feet below land surface and are listed only for nested wells; well names in bold type represent background (not gasoline-contaminated) samples; --, data unobtainable because pH is at or near titration endpoint; n.d., not detected; n.a., not analyzed]

Well name (depth)	Sampling date	pH	C_T, in milligrams per liter as CO_2		
			Titration filtered	Vapor method filtered	Vapor method unfiltered
Galloway site:					
VW7 (11.5)	6/8/95	5.37	109	98	113
VW8 (11.0)	6/8/95	5.22	128	98	105
VW9 (15.5)	6/8/95	5.88	172	125	121
VW9 (12.5)	6/8/95	5.37	109	n.a.	120
VW10 (12.5)	6/8/95	4.34	--	71	81.2
VW15 (18.5)	6/8/95	4.49	208	n.a.	74.3
DEP1	8/28/96	4.98	--	6.9	n.d.
USGS2	8/27/96	4.75	65	10.4	10.7
USGS4	8/28/96	4.56	--	16.9	4.18
USGS5	8/27/96	4.92	--	10.3	10.0
USGS8	8/26/96	5.58	25.7	17.2	17.2
VW12 (22)	8/26/96	4.46	--	8.37	6.41
VW19 (11)	8/26/96	5.58	6.43	12.4	10.1
VW8 (11)	8/28/96	5.79	19.8	13.8	9.66
Beaufort site:					
NJVWB (11.7)	6/21/95	5.31	47.1	73.1	45.4
NJVW1 (14.4)	6/21/95	5.98	361	298	301
NJVW2 (13.0)	6/21/95	5.81	172	239	274
NJVW3 (14.0)	6/21/95	5.53	348	183	158
NJVW1 (13.0)	3/27/97	6.11	199	n.a.	169
NJVW2 (13)	3/27/97	5.65	294	n.a.	241
NJVW3 (12)	3/27/97	5.59	290	n.a.	173
NJVW5 (19)	3/27/97	5.79	83.9	n.a.	204
NJVWB (10)	3/27/97	5.03	37.0	n.a.	42.6
NJVW2 (13)	7/17/97	5.65	224	n.a.	334
NJVWB (10)	7/17/97	5.65	57.9	n.a.	73.3

dards are used for peak identification and quantification of fixed gases and volatile hydrocarbons. Linear-regression standard curves are prepared by using several concentrations of each analyte of interest. Additional details on the analytical methods are provided in Baker (1993).

C_T in the original water sample is determined from the CO_2 concentration in the equilibrated headspace as follows: Because the CO_2 in the headspace originated from the water remaining in the sampling bulb,

$$C_T = (H_{CO2})(P_{CO2})(Vg/Vw) + [H_2CO_3^*] + [HCO_3^-] + [CO_3^{2-}] , \quad (2)$$

where H_{CO2} is the Henry's law constant, P_{CO2} is the partial pressure of CO_2 in the headspace, V_g is the headspace volume, and V_w is the volume of water remaining in the sampling bulb ($V_g + V_w = 125$ mL = volume of sampling bulb), and $[H_2CO_3^*]$ is the sum of dissolved $[CO_2]$ and $[H_2CO_3]$. Equilibrium relations for the carbonate system (Stumm and Morgan, 1996) are as follows:

$$[H_2CO_3^*] = H_{CO2}[CO_2]_g , \quad (3)$$

$$[H^+][HCO_3^-] = K_1[H_2CO_3^*] , \text{ and} \quad (4)$$

$$[H^+][CO_3^{2-}] = K_2[HCO_3^-] , \quad (5)$$

where K_1 and K_2 are dissociation constants (at STP $K_1 = 10^{-6.3}$, $K_2 = 10^{-10.3}$).

Equations 2 to 5 imply that:

$$C_T = (H_{CO2})(P_{CO2})(V_g/V_w + 1/\alpha_0) \quad (6)$$

where α_0 is the fraction of total carbonates in the equilibrated aqueous phase that is represented by $[H_2CO_3^*]$ and that is calculated from the pH of the equilibrated water as follows:

$$\alpha_0 = (1 + K_1/[H^+] + K_1K_2/[H^+]^2)^{-1} ; \quad (7)$$

where K_1 and K_2 are dissociation constants for H_2CO_3 and HCO_3^-, respectively.

Volatile species that do not undergo such speciation in solution (for example, O_2, N_2, hydrocarbons) can be quantified by analyzing the bulb headspace and applying Henry's law:

$$C_X = (H_X)(P_X)(1 + V_g/V_w) , \quad (8)$$

where X is any volatile species.

The Galloway gasoline-spill site is located on a farm in Galloway Township, N.J. An unknown quantity of gasoline leaked from an underground gasoline tank over a period of several years. The unsaturated zone, the ephemeral perched water, and the shallow ground water contain gasoline-range hydrocarbons. Hydrocarbon distribution and biodegradation rates at this extensively studied site have been quantified (Baehr and Fisher, 1996). The pH of uncontaminated ground water at the site is low and, therefore, C_T in some samples could not be determined with the standard alkalinity titration method. The pH of contaminated samples averaged 5.3, compared to 4.6 for uncontaminated samples.

Samples were also obtained from the site of a gasoline spill that contains gasoline-range hydrocarbons in the Laurel Bay Exchange, Marine Corps Air Station, Beaufort, S.C. This site is characterized by highly permeable, homogeneous sandy sediment and a shallow (3- to 5-m-deep) water table. Unsaturated-zone-gas composition and fluxes are being monitored at this site to determine aerobic hydrocarbon biodegradation rates (Landmeyer and others, 1996). The pH of contaminated and uncontaminated samples averaged 5.9 and 5.2, respectively. Water samples from both sites were analyzed for total-inorganic-carbon content (C_T) by using both the alkalinity titration method and the equilibrium vapor method.

Evaluation of the Equilibrium Vapor Method and Comparison to other Analytical Methods

Total-Inorganic-Carbon Concentrations

C_T values for water samples from the Galloway and Beaufort sites as determined by using the two methods are shown in table 1. Both filtered and unfiltered samples were analyzed by using the equi-

Table 2. Error in total-carbon concentration (CT) (in percent) resulting from pH measurement error, equilibrium vapor method

	Error in total-carbon concentration (C_τ) (in percent)								
	pH measurement error (pH units)								
pH	-0.20	-0.10	-0.03	-0.01	+0.00	+0.01	+0.03	+0.10	+0.20
3.6	+0.1	0.0	0.0	0.0	0.0	0.0	0.0	-0.1	-0.1
4.0	+0.2	0.1	0.0	0.0	0.0	0.0	0.0	-0.1	-0.3
4.4	+0.5	0.3	0.1	0.0	0.0	0.0	-0.1	-0.3	-0.7
4.8	+1.1	0.6	0.2	0.1	0.0	-0.1	-0.2	-0.8	-1.8
5.2	+2.8	1.5	0.5	0.2	0.0	-0.2	-0.5	-1.9	-4.1
5.6	+6.5	3.5	1.1	0.4	0.0	-0.4	-1.2	-4.1	-8.9
6.0	+14.1	7.4	2.3	0.8	0.0	-0.8	-2.3	-8.0	-16.3
6.4	+25.9	13.0	3.9	1.3	0.0	-1.3	-3.8	-12.6	-24.6
6.8	+39.0	18.5	5.3	1.8	0.0	-1.7	-5.2	-16.5	-30.8
7.2	+48.8	22.4	6.3	2.1	0.0	-2.0	-6.0	-18.7	-34.2
7.6	+54.4	24.5	6.8	2.2	0.0	-2.2	-6.4	-19.9	-35.9
8.0	+57.3	25.5	7.1	2.3	0.0	-2.3	-6.6	-20.5	-36.8

librium vapor method, but all samples analyzed by the titration method were filtered with a 0.45-μ glass fiber filter as recommended in standard field procedures (Radtke and others, 1998).

C_T values from titration-method filtered samples were compared to those from equilibrium-method filtered samples. Results of analysis of 11 such sample pairs are plotted in figure 2. Reasonable agreement is evident for most sample pairs. The regression line has a slope of 1.11 and a a coefficient of determination (r^2) of 0.78; supporting a correlation between the methods, but indicates that the titration method may yield slightly higher C_T values than the equilibrium vapor method. Paired t statistics (Zar, 1974) were used to test for differences between C_T values determined by the two methods. Paired hypothesis testing is more powerful than Student's t-test for comparing two populations where each member of one population is paired with a member of the other. In this analysis, each filtered and titrated sample was matched with an identical filtered vapor-method sample. The Student's t-test would compare the two method populations without pairing the data; omitting this information from the null hypothesis would make the Student's t-test less able to distinguish between differing populations (less powerful) than a paired approach. Paired-t comparison of C_T values was unable to distinguish between results obtained by using the titration and equilibrium vapor methods (t=1.45, critical t=2.23) at the 95-percent probability level.

Although the two populations are correlated, it is apparent from table 1 and figure 2 that the methods yielded different C_T values for some sample pairs. The titration method is highly sensitive to pH when the initial sample pH is near the titration endpoint (about 4.3). Therefore, a slight error in the pH measurement can lead to a large error in C_T. This may explain why the titration C_T value obtained for samples from the well USGS2 (pH=4.75) was much higher than the value obtained with the equilibrium vapor method. C_T could not be calculated for five samples from the Galloway site because they contained no alkalinity as a result of the low sample pH (near the endpoint). In contrast, accuracy of the equilibrium vapor method would be expected to increase as pH approaches 4.3, because a greater portion of C_T would be in the form of dissolved CO_2, the species that is directly measured in this method. Therefore, it is likely that the equilibrium vapor value for C_T is more reliable than the titration value for low-pH samples.

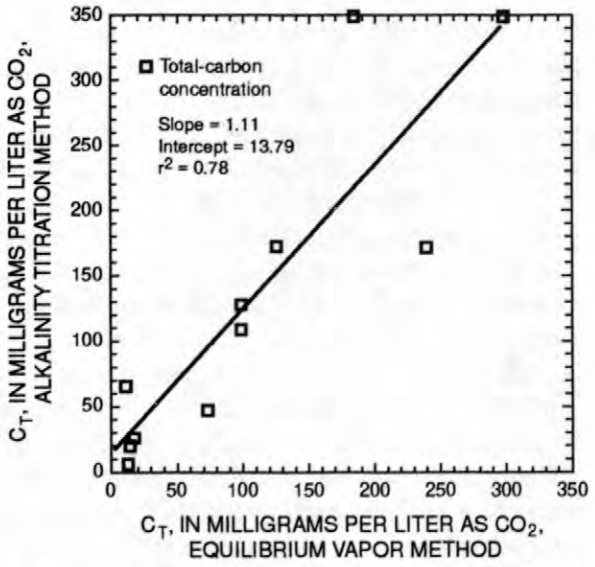

Figure 2. Relation between total-carbon concentrations (C_T) in filtered water samples determined by the alkalinity titration method and those determined by the equilibrium vapor method.

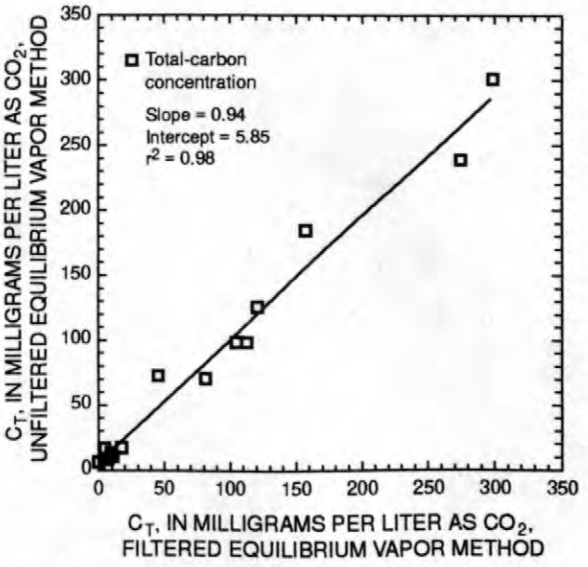

Figure 3. Relation between total-carbon concentrations (C_T) determined in filtered and nonfiltered water samples by the equilibrium vapor method.

C_T in several samples from the Beaufort site (NJVW1 (14.4) and NJVW3 (14.0), 6/21/95; NJVW3 (12), 3/27/97) was higher for the titration method than for the equilibrium vapor method. These samples may have contained salts of organic acids and other alkaline species resulting from hydrocarbon biodegradation. Any species that consumes H^+ as the sample is titrated to the alkalinity endpoint will artificially increase the calculated C_T value. These species may include a fraction of the natural background organic matter, salts of organic acids produced by microorganisms, and some inorganic salts. The equilibrium vapor method is not subject to these errors.

Sixteen pairs of samples were analyzed with the equilibrium vapor method with and without filtration. Filtration could be advantageous where suspended carbonaceous sediments are present in samples; this is because dissolution or precipitation of carbonate minerals can change C_T during sample storage. Filtering had little effect on measured C_T values (fig. 3). A paired t value of 0.27 indicated that filtration of samples analyzed by using the equilibrium vapor method did not make a significant difference in C_T at the 95-percent probability level (critical t = 2.31). This result is reasonable because Henry's law partitioning, upon which the equilibrium vapor method is based, is not significantly affected by the presence of particulates.

Samples can be acidified prior to analysis by the equilibrium vapor method for sample preservation. Lowering the pH also increases $[H_2CO_3^*]$ for a given C_T; this increases the accuracy of the method and lowers the quantitation limit. Moreover, at pH less than 3, pH is no longer a factor in calculating C_T (equation 8), and pH measurement is removed as a source of error. Possible errors introduced by inaccurate pH measurement are shown in table 2. An error greater than 30 percent may be introduced when the pH measurement is in error by 0.2 units for true pH values greater than 6.8. No apparent difference was found in C_T in four pairs of samples from the Beaufort site analyzed with and without acidification (fig. 4); therefore, acidification could be used for preservation or enhancing method accuracy in samples from this site. Acidification when carbonaceous suspended solids are present, however, may cause C_T to be overestimated.

Determination of Concentrations of Volatile Organic Compounds with the Equilibrium Vapor Method

Selected hydrocarbon-concentration data from ground-water samples from the Beaufort site

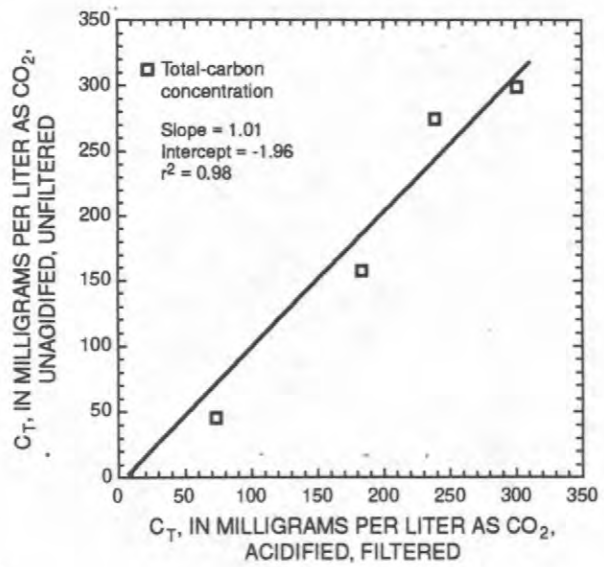

Figure 4. Relation between total-carbon concentrations (C_T) in filtered, acidified water samples and those in nonfiltered, nonacidified water samples determined by the equilibrium vapor method.

analyzed by the equilibrium vapor method are shown in table 3. Water samples from the hydrocarbon source area (NJVW2) and within the BTEX (benzene, toluene, ethylbenzene, and xylenes) plume (NJVW1) contained high concentrations of dissolved hydrocarbons, but hydrocarbons were virtually absent in samples from the well farthest from the source (NJVW5). Observed hydrocarbon concentrations obtained by using the equilibrium vapor method were generally lower than, but of the same order of magnitude as, those obtained by purge-and- trap GC/MS analysis of equivalent samples. A controlled laboratory experiment would help to verify the equivalence of the two methods for hydrocarbon quantitation.

The equilibrium vapor method can be compared to liquid-liquid solvent extraction and purge-and-trap, two alternative methods of processing water samples for analysis of volatile hydrocarbons. A comparison of detection limits associated with the three methods of analysis is shown in table 4. In each case, an instrument detection limit of 1 nanogram of toluene, n-octane, and MTBE (typical for analyses performed in the laboratory of the U.S. Geological Survey, New Jersey District) is assumed for GC/FID analysis. A 5-mL purge-and-trap sample and a 1:1 water:solvent extraction ratio are assumed for the comparison.

The equilibrium vapor method is less effective than the purge-and-trap method for detecting compounds with low vapor pressures, such as hydrocarbons with carbon numbers greater than about 10, and (or) low Henry's law constants, such as low-molecular-weight alcohols and some aldehydes and ketones. The detection limit of the equilibrium vapor method is higher for MTBE than for toluene or n-octane, which are less water-soluble. Even so, the detection-limit advantage of the equilibrium vapor method over the liquid-liquid solvent extraction method is evident (table 4). Another disadvantage of extraction methods, in general, is the presence of the solvent, which may interfere with subsequent analysis, particularly GC/FID; large solvent peaks interfere with peaks of other compounds. Although the work presented here is limited to the quantification of C_T and hydrocarbons, the equilibrium vapor method can be used to quantify any species that partition significantly from a water sample into the vapor phase, including N_2, O_2, CH_4, CS_2, N_2O, H_2S, CO, and chlorinated hydrocarbons.

CONCLUSIONS

The equilibrium vapor method provides measurements of total dissolved carbonates (C_T) in water samples that are similar to those obtained by alkalinity titration. This method avoids many interferences intrinsic in the titration method, in which all alkalinity is assumed to be from carbonate species, and is especially applicable to samples with pH near the titration endpoint (about 4.3). Further, the equilibrium vapor method is applicable for low-pH samples where no C_T value is obtainable from the titration method. Accuracy of the equilibrium vapor method depends on the accuracy of the pH measurement and the GC/TCD analysis. A comparison of results obtained by using each of the two methods to analyze ground-water samples from two gasoline-spill sites showed reasonable agreement; in those cases where there is disagreement, the equilibrium vapor method probably is more reliable.

The versatility of this method is indicated by the quantitation of C_T and concentrations of dissolved hydrocarbons in the same sample with no additional sample processing. Furthermore, although no other constituents were determined as part of this study, many other volatile species in addition to CO_2 and gasoline hydrocarbons,

Table 3. Hydrocarbon concentrations determined by equilibrium vapor method (GC/FID) and purge-and-trap (GC/MS) in ground-water samples from a gasoline-spill site, Beaufort, South Carolina, March 27, 1997

[Concentrations in micrograms per liter; n.d., not detected]

Well name and depth in feet	Method of analysis	Benzene	Toluene	Total xylenes	Total BTEX
1NJVW1 10	Vapor method	4,865	6,995	5,738	18,857
	Purge and trap	8,230	21,900	16,900	58,470
2NJVW2 13	Vapor method	5,091	10,657	17,532	36,527
	Purge and trap	7,800	24,900	20,800	58,470
3NJVW5 17	Vapor method	n.d.	0.4	n.d.	0.4
	Purge and trap	n.d.	n.d.	n.d.	n.d.

[1]Downgradient from source, within BTEX plume
[2]Location from which the leaking tank was removed
[3]Downgradient from source, beyond BTEX plume

Table 4. Estimated minimum detection limits in micrograms per liter[1] of three hydrocarbons for three analytical methods[2]

Compound	Purge-and trap[3] (5 milliliters water)	Vapor method: equal water and gas volumes (2 milliliters vapor injection)	Liquid-liquid extraction: equal water and solvent volumes (10 microliters solvent injection)
Toluene	0.2	2.35	100.0
n-Octane	0.2	0.50	100.0
MTBE	0.2	21.32	100.0

"[1]Detection limit is with respect to the original water sample, not the vapor or solvent extract
[2]Minimum instrument detection limit for all three compounds is assumed to be 1 nanogram, which typically gives a response of 1400 millivolt-seconds for GC/FID analysis for hydrocarbons on the Varian GC, set for maximum sensitivity, in the laboratory of the New Jersey District, U.S. Geological Survey.
[3]Assuming 100-percent recovery

including N_2, O_2, CH_4, CS_2, N_2O, H_2S, CO, and chlorinated hydrocarbons, can be quantified from a single equilibrium vapor sample.

REFERENCES

Baehr, A.L., and Fisher, J.M., 1996, Overview of research on the transport, microbial degradation, and remediation of hydrocarbons at a subsurface gasoline-spill site in Galloway Township, N.J., in Morganwalp, D.W., and Aronson, D.A., eds., U.S. Geological Survey Toxic Substances Hydrology Program--Proceedings of the technical meeting, Colorado Springs, Colo., Sept. 20-24, 1993: U.S. Geological Survey Water- Resources Investigations Report 94-4015, p. 1-6.

Baker, R.J., 1993, Hydrocarbon microbial degradation rate determination in columns of unsaturated porous media using vapor transport modeling: unpublished Ph.D. thesis, Philadelphia, Pa., Drexel University, Environmental Studies Institute, 235 p.

Bolin, B., and Cook, R.B., eds., 1983, The major biogeochemical cycles and their interactions: SCOPE Report 21, Chichester, Eng., John Wiley and Sons, chap. 2.

Eaton, A.D., Clesceri, L.S., and Greenberg, A.E., eds., 1995, Standard methods for the examination of water and wastewater: Washington, D.C., American Public Health Association, 10 sections.

Landmeyer, J.E., Chapelle, F.H., and Bradley, P.M., 1996, Assessment of intrinsic bioremediation of gasoline contamination in the shallow aquifer, Laurel Bay Exchange, Marine Corps Air Station, Beaufort, South Carolina: U.S. Geological Survey Water-Resources Investigations Report 96-4026, 50 p.

Radtke, D.B., Wilde, F.D., Davis, J.V., and Popowski, T.J., 1998, Alkalinity and acid neutralizing capacity, in U.S. Geological Survey, National field manual for the collection of water-quality data: U.S. Geological Survey Techniques of Water-Quality Investigations, book 9, chap. A6, 33 p.

Stumm, W., and Morgan, J.J., 1996, Aquatic chemistry: New York, John Wiley and Sons, Inc., 1,022 p.

Zar, J.J, 1974, Biostatistical analysis: Englewood Cliffs, N.J., Prentice-Hall, 620 p.

Transport of Methyl Tert-Butyl Ether (MTBE) and Hydrocarbons to Ground Water from Gasoline Spills in the Unsaturated Zone

By Matthew A. Lahvis and Arthur L. Baehr

ABSTRACT

At point-source gasoline-release sites, methyl tert-butyl ether (MTBE), a fuel oxygenate, is commonly found in ground water at concentrations that exceed those of benzene, toluene, ethylbenzene, and xylenes (BTEX). A mathematical model is developed to explain such occurrences. Type curves are developed to predict benzene and MTBE transport across the water table and to evaluate the relative importance of the advection, diffusion, and biodegradation pathways. In general, the mass flux of benzene is several orders of magnitude less than that of MTBE, if biodegradation of MTBE is assumed to be negligible. Consequently, ground-water plumes of MTBE could potentially extend several orders of magnitude farther downgradient than BTEX plumes at a gasoline-spill site. Depth to the water table has the greatest effect on the selective removal of hydrocarbons in the unsaturated zone.

INTRODUCTION

Gasoline releases from underground storage tanks (USTs) are a primary source of ground-water contamination by MTBE (Garrett and others, 1986). These releases can occur in large volumes as a result of tank defects, or in smaller quantities, but more frequently, during tank refilling. Ground water at these sites can exhibit high concentrations of MTBE independent of BTEX (Mace and Choi, 1998). These occurrences can be accounted for by considering aqueous- and vapor-phase partitioning from a near-surface, immiscible liquid source and subsequent migration by aqueous infiltration and vapor diffusion to the water table (see fig. 1). Spills of MTBE pose a greater threat to ground-water resources than spills of BTEX because MTBE is more soluble and far less degradable than BTEX (Zogorski and others, 1997).

In this paper, a mathematical model is presented to help explain the MTBE/hydrocarbon-concentration ratios found in ground water, which exceed those expected solely on the basis of solubility considerations. The model is used to simulate groundwater infiltration, vapor-phase diffusion, and biodegradation. A dimensionless type-curve analysis is presented to compare concentration and mass-flux estimates for various hydrologic characteristics of the unsaturated zone.

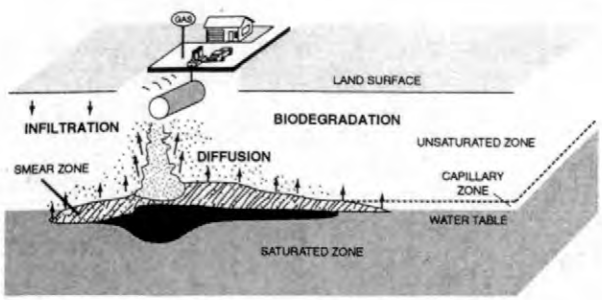

Figure 1. Conceptualization of a gasoline spill at an underground storage tank site.

MATHEMATICAL MODEL

A one-dimensional, steady-state mathematical model to simulate transport of volatile organic compounds in the unsaturated zone was developed by Baehr and others (1999). The model is based on conservation of mass principles, and is defined in terms of dimensionless parameters as:

$$\frac{\partial^2 C}{\partial x^2} - P_e \frac{\partial C}{dx} - D_m C = 0 \quad , \qquad (1)$$

at $x = 0$ $\quad C = C_o = C^*\chi$, and (1a)

at $x = 1$ $\quad \frac{dC}{dx} = 0$, (1b)

where C = aqueous-phase concentration (g/cm^3),
C_o = aqueous-phase concentration at source (g/cm^3),
C^* = solubility (g/cm^3),
χ = mole fraction of constituent in immiscible phase (dimensionless), and
x = distance (dimensionless).

P_e is a dimensionless grouping of parameters referred to as the Peclet Number, defined as follows:

$$P_e = \frac{qL}{D} \quad , \tag{2}$$

where q = ground-water infiltration rate (cm/sec),
D = effective diffusion coefficient (cm^2/sec), and
L = length of the model domain (cm).

D_m is a dimensionless grouping of parameters referred to as the Damkohler Number, defined as follows:

$$D_m = \frac{kL^2}{D} \quad , \tag{3}$$

where k = first-order biodegradation-rate constant (1/sec).

The Peclet Number scales advection and dispersion. The higher the value of P_e the more dominant advective transport is relative to diffusion. The Damkohler Number scales biodegradation and dispersion. The higher the value of D_m, the more dominant biodegradation is relative to diffusion. Sauty (1980), Garges and Baehr (1998), and Baehr and others (1999) have presented similar dimensionless formulations for transport analysis. Use of dimensionless parameters is advantageous for comparing transport of MTBE with that of other gasoline compounds in various hydrologic settings.

If aqueous-phase diffusion is assumed to be negligible, the effective diffusion coefficient (D) in equation (3) can be simplified to:

$$D = D_a H \quad , \tag{4}$$

where H = Henry's law coefficient (dimensionless), and
D_a = effective diffusion coefficient for the gaseous phase (cm^2/sec).

Gaseous-phase diffusion (D_a) is constituent-specific and defined as:

$$D_a = d_a \theta_a \tau_a \quad , \tag{5}$$

where d_a = gaseous-phase diffusivity (cm^2/sec),
θ_a = volumetric content of the gaseous phase (dimensionless), and
τ_a = tortuosity of the gaseous phase (dimensionless).

Tortuosity (τ_a) is determined from Millington (1959) as:

$$\tau_a = \frac{\theta_a^{7/3}}{\phi^2} \quad , \tag{6}$$

where ϕ = total porosity (dimensionless).

As written, (1) implies that the unsaturated zone is uniform and constituent transport is uncoupled. The model cannot be applied, therefore, to simulate transport in the capillary zone unless the capillary zone is treated as an equivalent porous medium and mass transport is coupled at the unsaturated/capillary-zone interface. In addition, the model incorporates the assumptions of a constant q, first-order biodegradation kinetics, and equilibrium partitioning of mass among immiscible, aqueous, and gaseous phases.

The upper model boundary (1a) represents a constant-concentration source (C_o) located at land surface ($x = 0$). The lower model boundary (1b) represents a boundary impermeable to vapor diffusion located at the top of the capillary zone ($x = 1$). As a result, the following condition applies at $x = 1$:

$$J_{wat} = qC_{wat} \quad , \tag{7}$$

where J_{wat} = the mass flux at $x = 1$ (g/cm^2-sec), and

C_{wat} = the aqueous-phase concentration at x = 1 (g/cm^3).

The mass flux J_{wat} calculated for the top of the capillary zone is assumed to represent the mass flux at the water table. This assumption may result in overestimation of the mass flux across the water table for benzene and other aromatic constituents that may be subject to further degradation in the capillary zone.

The solution to (1), subject to boundary conditions (1a) and (1b), is given by Baehr and others (1999):

$$\frac{C(x)}{C_o} = \frac{[r_2 \exp(r_2) \exp(r_1 x) - r_1 \exp(r_1) \exp(r_2 x)]}{[r_2 \exp(r_2) - r_1 \exp(r_1)]} \quad , \tag{8}$$

where

$$r_1 = \frac{P_e}{2} + \left(\frac{P_e^2}{4} + D_m \right)^{0.5} \quad , \text{and} \tag{8a}$$

$$r_2 = \frac{P_e}{2} - \left(\frac{P_e^2}{4} + D_m \right)^{0.5} \tag{8b}$$

Substituting x = 1 into (8) provides an expression for the concentration at the water table, C_{wat}:

$$\frac{C_{wat}}{C_o} = \frac{\exp(P_e)\,(r_2 - r_1)}{[r_2 \exp(r_2) - r_1 \exp(r_1)]} \quad , \tag{9}$$

Solving (9) for various values of D_m and P_e allows for the determination of type curves (C_{wat}/C_o) to assess constituent concentrations at the water table in various hydrologic settings (see fig. 2). The type curves are not applied for MTBE because degradation of MTBE is assumed to be negligible (D_m= 0). Although the type curves can be used to evaluate a wide range of transport conditions, values of $D_m$and P_e exist for which the transport model no longer applies. These conditions occur when oxygen (O_2) concentrations within the unsaturated zone are < 0. To assess this limitation, O_2 transport is modeled according to the following conservation of mass equation:

$$\frac{\partial C_{O2}}{\partial x^2} - P_{e_{O2}} \frac{\partial C_{O2}}{dx} = \left(\frac{L^2}{D_{O2}} \right) R_{O2} \quad , \tag{10}$$

where C_{O2} = aqueous-phase concentration of O_2 (g/cm^3),
Pe_{O2} = Peclet Number of O_2 (dimensionless),
D_{O2} = effective diffusion coefficient of O_2 (cm^2/sec),
R_{O2} = the rate of O_2utilization (g/cm^3-sec).

The rate of O_2 utilization is proportional to the rate of total hydrocarbon degradation as follows:

$$R_{O2}(x) = \sum_{k=1}^{N} r_k k_k C_k(x) \quad , \tag{11}$$

where r_k = stoichiometric mass coefficient relating the mass of oxygen utilization to the mass of the kth reactive hydrocarbon constituent (dimensionless),
k_k = biodegradation rate of the kth reactive hydrocarbon constituent (1/sec),
C_k = aqueous-phase concentration of the kth reactive hydrocarbon constituent (g/cm^3), and
N = total number of reactive hydrocarbon constituents.

Computation of R_{O2} is simplified by assuming a composite hydrocarbon consisting of an ideal mixture of remaining gasoline constituents (less benzene and MTBE). The constituent properties (H, D, k_k, C_k, r_k) for the composite hydrocarbon are calculated by assuming a weighted average based on the mole-fraction gasoline composition defined by Johnson and others (1990) and 15 percent MTBE by volume. The properties of the composite hydrocarbon, benzene, and MTBE are listed in table 1. Finite-difference approximations were required to solve (10) because R_{O2} is spatially dependent. The O_2 limitation defined by the one-dimensional transport model (10) may be overestimated, however, because lateral transport is not considered.

Table 1. Summary of input parameters for rerence hydrologic settings

PARAMETER	VALUE	UNITS
Hydrologic Properties		
Length of model domain (L)	100 - 1000	cm
Ground-water infiltration rate (q)	0 - 50	cm/yr
Air-filled porosity (θ_a), sand	0.34	dimensionless
Air-filled porosity (θ_a), clay	0.15	dimensionless
Gaseous-phase tortuosity (τ_a), sand	0.41	dimensionless
Gaseous-phase tortuosity (τ_a), clay	0.073	dimensionless

	Benzene	MTBE	Composite	
Constituent Properties				
Aqueous solubility (C^*)	1.8E-03	4.8E-02	8.3E-05	g/cm^3
Mole fraction in immiscible phase (χ)	0.009	0.111	0.595	dimensionless
Gaseous-phase diffusivity (d_a)	0.10	0.094	0.10	cm^2/sec
Henry's Law constant (H)	0.17	0.018	34	dimensionless
Effective diffusion coefficient (D), sand	2.4E-03	3.2E-04	4.8E-01	cm^2/sec
Effective diffusion coefficient (D), clay	2.8E-04	4.0E-05	5.7E-02	cm^2/sec
First-order rate constants (k), aerobic	0.10	0	0.10	1/d
First-order rate constants (k), anaerobic	0.005	0	0.01	1/d
Stoichiometric constant (r)	3.08	2.43	3.43	dimensionless
SAND (L = 300, q = 50 cm/yr):				
Peclet Number (Pe)	0.20	1.5	0.00098	dimensionless
Damkohler Number (D_m), aerobic	44	0	0.22	dimensionless
Damkohler Number (D_m), anaerobic	2.2	0	0.022	dimensionless
CLAY (L = 300, q = 50 cm/yr):				
Peclet Number (Pe)	2.6	19	0.013	dimensionless
Damkohler Number (D_m), aerobic	570	0	2.8	dimensionless
Damkohler Number (D_m), anaerobic	28	0	0.28	dimensionless

As implied by (11), the O_2 limitation is a function of the source mass. Furthermore, value of D_m that is necessary to cause an O_2 limitation is constituent-specific. For example, if the maximum source strength for benzene (C_o = 1.60E-5 g/cm^3) is defined by (1a), the O_2 limitation for benzene occurs at a $D_m > 38$ (see fig. 2). A $D_m > 38$ for benzene corresponds to a biodegradation rate of k > 1.2E-06 1/sec (0.105 1/d) if it is assumed that D = 2.4E-03 cm^2/sec (sand) and L = 300 cm (9.8 ft). For the composite hydrocarbon, the O_2 limitation would occur at $D_m > 0.19$ for equivalent L and k values, because D = 4.8E-01 cm^2/sec (sand) is much greater than the D for benzene. Given that aerobic biodegradation rates for BTEX compounds typically range from 0.024 to 0.72 1/d (DeVaull and others, 1997), and that the

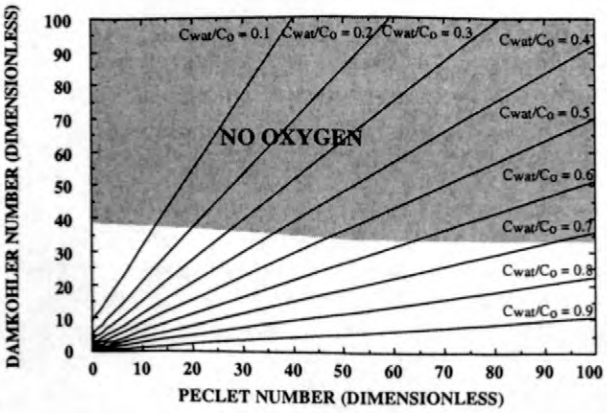

Figure 2. Plot of dimensionless type curves to determine source attenuation (C_{wat}/C_o) of benzene at the water table as a function of Damkohler and Peclet Numbers.

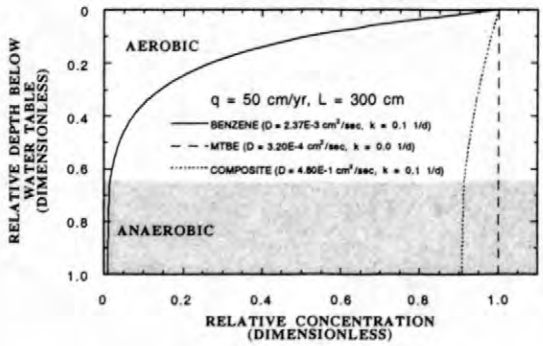

Figure 3. Concentration profiles of benzene, MTBE, and the composite hydrocarbon as a function of depth below land surface.

values of D and L used to characterize the reference hydrologic setting are relatively large and small, respectively, anaerobic conditions are likely to develop within most unsaturated-zone systems provided that source concentrations approach aqueous solubilities. Anaerobic degradation rates are applied in the transport model at depths where the O_2 concentrations are < 0, with the assumption of first-order kinetics.

RESULTS AND DISCUSSION

Hydrologic settings were characterized by sand or clay unsaturated zones ranging in thickness from 100 to 1,000 cm (3.3 - 33 ft), q between 0.01 and 50 cm/yr, and biodegradation or no biodegradation. These conditions were chosen to predict a range of concentrations and mass fluxes that could occur at the water table at gasoline-spill sites. The reference parameter values used as input to the transport model are listed in table 1. The steady-state distributions of benzene, MTBE, and the composite hydrocarbon for a sand unsaturated zone where L = 300 cm and q = 50 cm/yr are shown in figure 3. Changes in concentration with depth are attributed solely to biodegradation, which is anaerobic at depths of hydrocarbon consists mainly of constituents that partition to the gaseous phase (as indicated by a high Henry's Law constant). Over the entire range of input values listed in table 1, C_{wat} estimates range from approximately 0 to 16 mg/L for benzene and from 15 to 49 mg/L for the composite hydrocarbon. The lower limits represent ground-water concentrations obtained by assuming a 1,000-cm- (33-ft) thick, clay unsaturated zone, minimal ground-water infiltration (q = 0.01 cm/yr), and k = 0.1 1/d for both compounds. The upper limits represent the conditions obtained by assuming no biodegradation, regardless of the values input for L, q, or D. For MTBE, C_{wat} = 5,300 mg/L because biodegradation is assumed to be negligible. Ground water may, therefore, exhibit high concentrations of MTBE relative to those of benzene for sources above the water table. Estimates of J_{wat} range from approximately 0 to 0.008 kg/m^2-yr for benzene, 0 to 0.025 kg/m^2-yr for the composite hydrocarbon, and 0 to 2.7 kg/m^2-yr for MTBE. The lower limits represent estimates obtained by assuming the lower limit of ground-water infiltration (q = 0.01 cm/yr). Estimates of C_{wat} and J_{wat} are summarized in table 2. Source attenuation as a function of the input parameters (k, L, q, and D) for benzene, MTBE, and the composite hydrocarbon is shown in figure 4. Source attenuation is most sensitive to the depth to the water table (L), as implied by (3) and demonstrated by greater model sensitivity to D_m than to P_e (see fig. 5), where model sensitivity is given by J_{wat}/J_o and J_o is the mass flux (g/cm^3) defined at the source ($J_o = qC_o$).

Table 2. Summary of the aqueous-phase concentration (C_{wat}) and mass-flux (J_{wat}) estimates at the water table

[All concentrations are in milligrams per liter, and all mass fluxes are in kilograms per square meter per year]

Model Calibrated Parameter	Constituent		
	Benzene	MTBE	Composite
Aqueous-phase concentration (C_{wat})	0 - 16	5,300	15 - 49
Mass flux (J_{wat})	0 - 0.0080	0 - 2.7	0 - 0.025

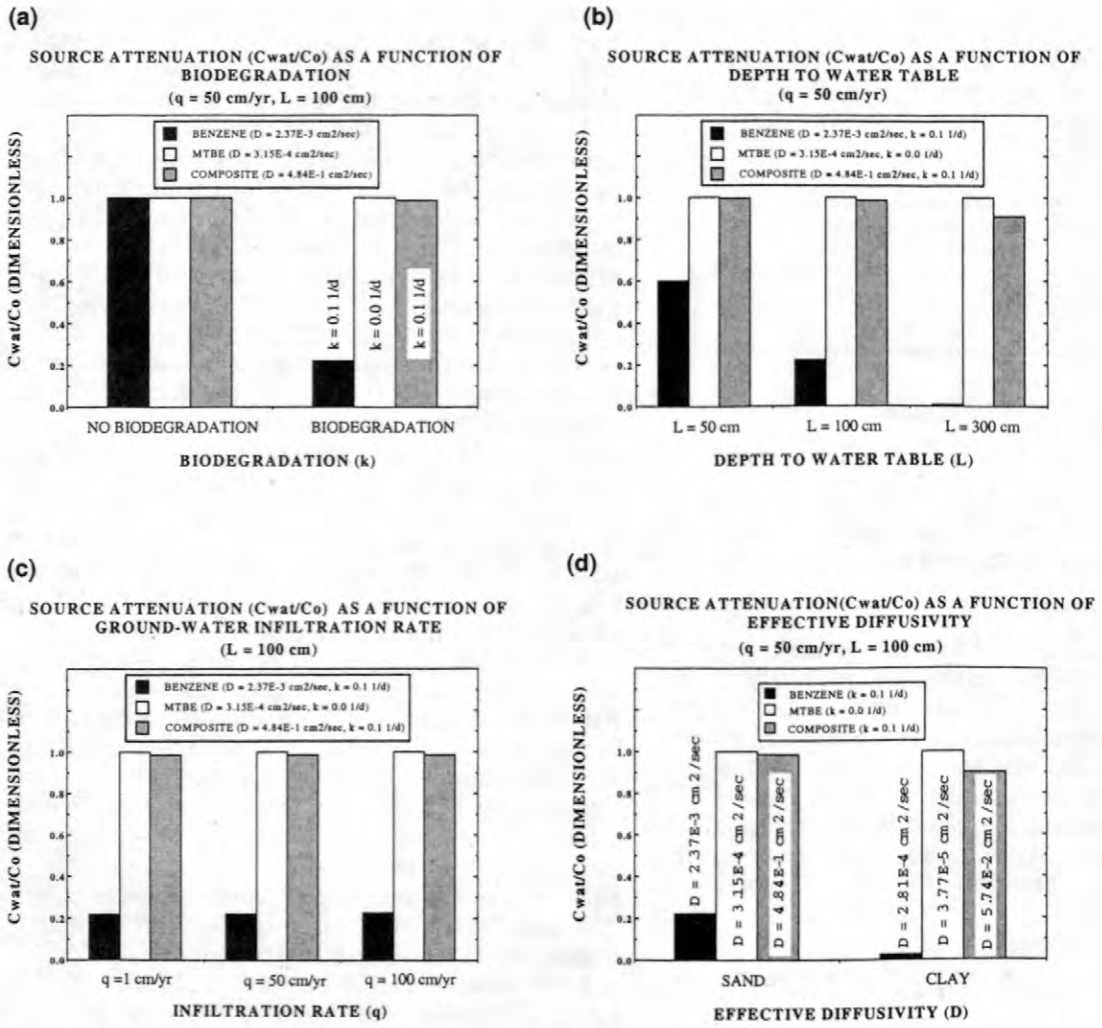

Figure 4. Plots of source attenuation of benzene, MTBE, and the composite hydrocarbon as a function of (a) biodegradation, (b) depth below land surface, (c) infiltration rate, and (d) effective diffusivity.

CONCLUSIONS

The results of this study indicate that surface or near-surface spills of gasoline can result in high concentrations of MTBE relative to those of benzene and other hydrocarbons at the water table. MTBE concentrations in ground water are several orders of magnitude higher because of the higher source concentration of MTBE (more than 300 times greater than that of benzene) and its resistance to biodegradation. Even if aerobic biodegradation of MTBE was considered, ground water would remain susceptible to high concentrations of MTBE because anaerobic conditions would develop closer to the source. Benzene flux to ground water is minimal because the hydrocarbon is biodegraded before it reaches the water table. Concentrations of other aromatic hydrocarbons (such as toluene, ethylbenzene, and xylenes) in ground water are assumed to be similar in magnitude to those of benzene. Ground-water concentrations of the composite hydrocarbon are small because the compound partitions mainly to the gaseous phase and the water table is assumed to be impermeable to vapor transport. These findings are consistent with observations at UST-release sites (Harley Hopkins, American Petroleum Institute, written commun., 1998).

Dimensionless type curves are used to assess constituent concentrations and mass fluxes at the water table for transport in various hydrologic settings. Simulation results indicate that steady-state concentrations and mass fluxes are several orders of magnitude higher for MTBE than for other gasoline hydrocarbons. This result

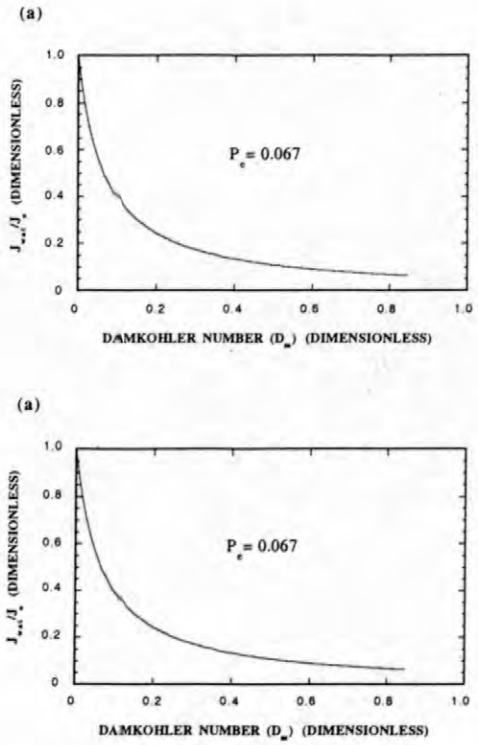

Figure 5. Plots of model sensitivity of benzene as a function of (a) Damkohler and (b) Peclet Numbers, where (J_{wat}/J_o) is the mass-flux attenuation at the water table.

implies that high concentrations of MTBE in ground water can occur independently of the other gasoline constituents. In addition, solute plumes of MTBE resulting from gasoline spills in the unsaturated zone potentially could be several orders of magnitude larger than solute plumes of other gasoline constituents. In addition, estimates of mass transport across the water table may be high because source concentrations are assumed to remain constant over time. This assumption may not be valid for small-volume spills. Nonetheless, the model is useful for approximating transport conditions at the water table and evaluating the role of the unsaturated zone in the natural attenuation of gasoline spills above the water table. The mass-flux estimates determined by applying the model could be used as input to a ground-water transport model to assess subsequent downgradient migration of the contaminants. More refined estimates of mass transport at the water table could be obtained by applying a numerical model, such as R-UNSAT (Lahvis and Baehr, 1997), especially in heterogeneous unsaturated-zone systems.

REFERENCES

Baehr, A. L., Stackelberg, P. E., and Baker, R. J., 1999, Evaluation of the atmosphere as a source of volatile organic compounds in shallow ground water: Water Resources Research, v. 35, p. 127-136.

DeVaull, G. E., Ettinger, R. A., Salanitro, J. P., and Gustafson, J. B., 1997, Benzene, toluene, ethylbenzene, and xylenes (BTEX) degradation in vadose zone soils during vapor transport: First order rate constants, in Proceedings of the NWWA-API Conference on Petroleum Hydrocarbons and Organic Chemicals in Ground Water--Prevention, Detection, and Remediation, Houston, Texas, November 12-14, 1997: National Water Well Association, Westerville, Ohio, p. 365-379.

Garges, J. A., and Baehr, A. L., 1998, Type curves to determine the relative importance of advection and dispersion for solute and vapor transport: Ground Water, v. 36, p. 959-965.

Garrett, P., Moreau, M., and Lowry, J. D., 1986, MTBE as a groundwater contaminant, in Proceedings of the NWWA-API Conference on Petroleum Hydrocarbons and Organic Chemicals in Ground Water--Prevention, Detection, and Restoration, Houston, Texas, November 12-14, 1986: National Water Well Association, Westerville, Ohio, p. 227-238.

Johnson, P. C., Kemblowski, M. W., and Colthart, J. D., 1990, Quantitative analysis for the cleanup of hydrocarbon-contaminated soil by in-situ soil venting: Ground Water, v. 28, p. 413-429.

Lahvis, M. A., and Baehr, A. L., 1997, Documentation of R-UNSAT, a computer model for the simulation of reactive, multispecies transport in the unsaturated zone: U.S. Geological Survey Open-File Report 97-630, 104 p.

Mace, R. E., and Choi, W., 1998, The size and behavior of MTBE plumes in Texas, in Proceedings of the NWWA-API conference on Petroleum Hydrocarbons and Organic Chemicals in Ground Water--Prevention, Detection, and Restoration, Houston, Texas, November 11-143 1998: National Water Well Association, Westerville, Ohio, p. 1-11.

Millington, R. J., 1959, Gas diffusion in porous media: Science, v. 130, p. 100-102.

Sauty, J. P., 1980, Computerized stratified random site-selection approaches for design of a ground-water quality sampling network: U.S. Geological Survey Water Resources Investigations Report 90-4101, 109 p.

Zogorski, J. S., Baehr, A. L., Bauman, B. J., Conrad, D. L., Drew, R. T., Korte, N. E., Lapham, W. W., Morduchowitz, A., Pankow, J. F., Washington, E., 1997, Fuel oxygenates and water quality--Current understanding of sources, occurrence in natural water, environmental behavior, fate, and significance, Chapter 2: Office of Science and Technology Policy Report, Executive Office of the President, Washington, D.C., p. 2.1 - 2.80.

AUTHOR INFORMATION

Matthew A. Lahvis, U.S. Geological Survey, West Trenton, New Jersey, (mlahvis@usgs.gov)

Arthur L. Baehr, U.S. Geological Survey, West Trenton, New Jersey, (abaehr@usgs.gov)

Ground Water Contamination By Crude Oil

Ground water contamination by crude oil, and other petroleum-based liquids, is a widespread problem. An average of 83 crude-oil spills occurred per year during 1994-96 in the United States, each spilling an average of about 50,000 barrels of crude oil (U.S. Office of Pipeline Safety, electronic commun., 1997). An understanding of the fate of organic contaminants (such as oil and gasoline) in the subsurface is needed to design innovative and cost-effective remedial solutions at contaminated sites.

A long-term, interdisciplinary research project by the U.S. Geological Survey (USGS) Toxic Substances Hydrology Program began in 1983 at a crude-oil spill site near Bemidji, Minnesota. The project involves research by scientists from the USGS and several academic institutions. Research at the site is directed toward understanding physical, chemical, and biological processes controlling the migration and fate of hydrocarbon contaminants in the subsurface. The goal is to provide information and methods to help evaluate the potential for, and long-term performance of, natural and enhanced bioremediation of hydrocarbons.

The crude-oil spill site near Bemidji is one of the better characterized sites of its kind in the world. Results of research conducted on processes affecting the migration and fate of crude oil at the site have provided fundamental knowledge that has been used to remediate similar sites worldwide. The Bemidji research project was first to document that the extent of crude-oil contamination can be limited by natural attenuation. Scientists studying natural attenuation at other contaminated sites have used many of the methods and approaches developed at the site.

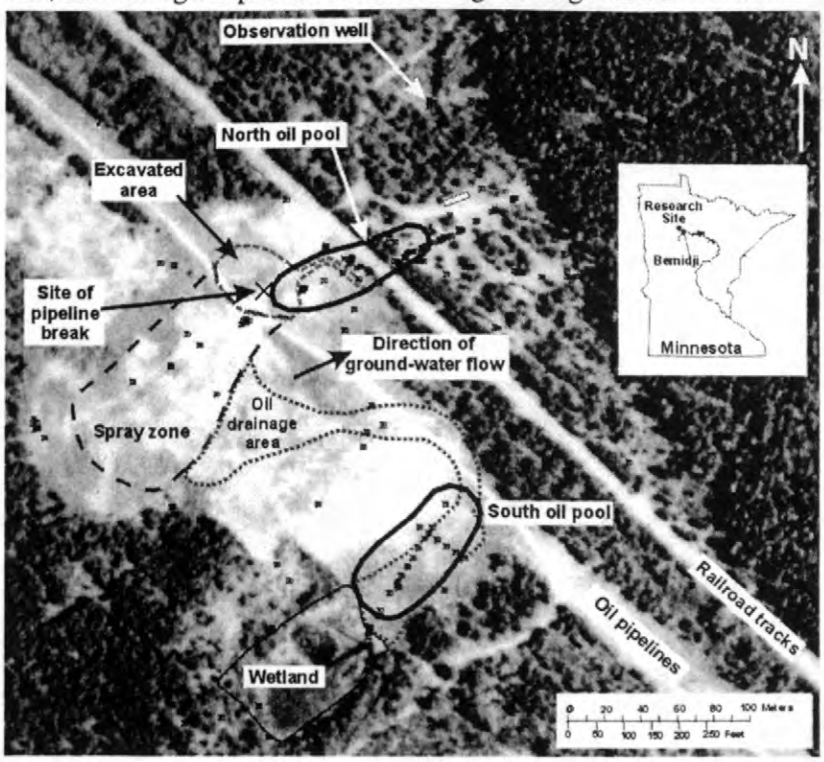

Figure 1. Features of the Bemidji, Minnesota crude-oil spill research site superimposed on a 1991 aerial photograph.

DESCRIPTION AND HISTORY OF THE BEMIDJI SITE

On August 20, 1979, approximately 16 kilometers northwest of Bemidji, Minnesota, the land surface and shallow subsurface were contaminated when a crude-oil pipeline burst. About 1,700,000 L (liters) (about 10,700 barrels) of crude oil spilled onto a glacial outwash deposit. Crude oil also sprayed to the southwest covering an approximately 7,500-m^2 (square meters) area of land (spray zone, figure 1). After cleanup efforts were completed, about 400,000 L (about 2,500 barrels) of crude oil remained in the ground. Some crude oil percolated through the unsaturated zone to the water table near the rupture site (North oil pool). Some of the sprayed oil flowed over the surface toward a small wetland forming a second area of significant oil infiltration (South oil pool).

Ground water affected by the oil spill discharges to a small lake 400-m east of the pipeline. The land surface is a glacial outwash plain underlain by stratified glacial outwash deposits. At a depth of about 25 m, a regionally persistent and uniform layer of low permeability sediment restricts vertical ground-water movement. The water table ranges from near land surface to about 11 m below the land surface. About 370 wells and test holes had been installed at the Bemidji research site as of 1998.

ONGOING AND FUTURE RESEARCH

The fate of hydrocarbons depends on the processes of transport, multiphase flow, volatilization, dissolution, geochemical reactions, biodegradation, and sorption (figure 2). An interdisciplinary investigation of these processes is critical for successful evaluation of the potential for migration of hydrocarbons in the subsurface. The investigation at the Bemidji site has involved the collection and analysis of crude oil, water, soil, vapor, and sediment samples. The oil phase that occurs as floating product on the water table and as residuum on sediment grains provides a continuing source of hydrocarbons to the ground water and vapor plumes. Studies have also been conducted to document the concentrations of gases in the unsaturated zone.

Numerical models are useful for integrating information collected in the field and have been used at the site for studying the importance of the simultaneously occurring processes. Multiphase flow modeling was used to study the oil movement after the spill. Transport and biodegradation modeling was used to simulate the evolution of the plume, to evaluate factors limiting biodegradation, and to develop a mass balance for contaminants at the site and thus evaluate the amount and rate of removal of hydrocarbons by biodegradation.

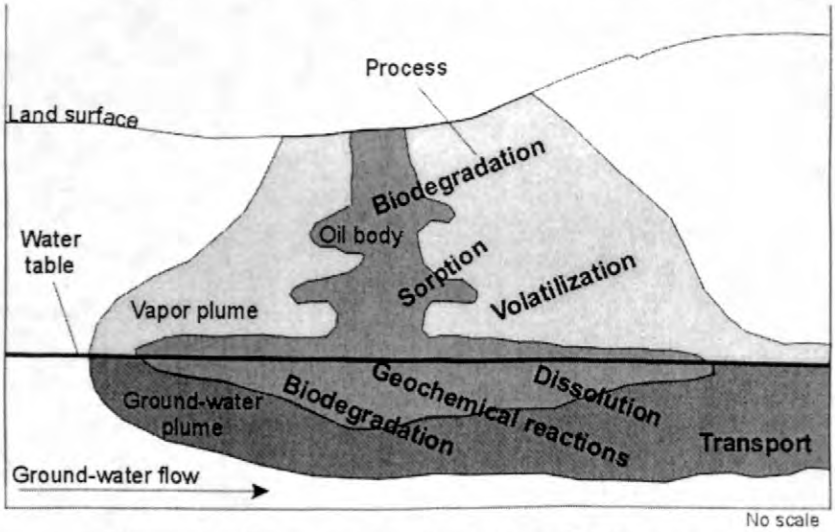

Figure 2. Processes critical to understanding the fate and transport of hydrocarbons in the subsurface at the Bemidji site.

Although initial remediation of the research site was completed more than 15 years ago, a State regulatory agency has required the pipeline company to remove more of the remaining oil. While this renewed remediation may result in termination of ongoing research documenting natural attenuation, it has also provided an opportunity to work with industry in documenting the effects of the renewed remediation. One goal of ongoing research is to add to the published literature a thorough documentation of the remediation of this site; very few remediation efforts at crude-oil contamination sites are documented in the literature.

For additional information contact:

Geoffrey N. Delin, USGS, Mounds View, Minnesota, (email: delin@usgs.gov), or

William N. Herkelrath, USGS, Menlo Park, California, (email: wnherkel@usgs.gov)

Long-Term Geochemical Evolution of a Crude-Oil Plume at Bemidji, Minnesota

By Isabelle M. Cozzarelli, Mary Jo Baedecker, Robert P. Eganhouse, Mary Ellen Tuccillo, Barbara A. Bekins, George R. Aiken, and Jeanne B. Jaeschke

ABSTRACT

The long-term study of the development of the contaminant plume at the Bemidji site has provided an excellent opportunity to determine how natural attenuation of hydrocarbons is affected by evolving redox conditions in the aquifer. During the 16 years that data have been collected the shape and extent of the contaminant plume have changed as redox reactions, most notably iron reduction, have progressed over time. The downgradient extent of the Fe^{2+} and BTEX plume did not change between 1992 and 1995, indicating that, at the plume scale, the supply of these compounds from the upgradient contaminated water is balanced by the attenuation processes. However, depletion of the unstable Fe (III) oxides near the subsurface crude-oil source has caused the maximum dissolved iron concentration zone within the plume to spread at a rate of approximately 3 m/year. The zone of maximum benzene, toluene, ethylbenzene, and xylene (BTEX) concentrations has also spread within the anoxic plume. Analysis of sediment and water, collected at closely spaced vertical intervals, from cores in the contaminant plume provide further insight into the evolution of redox zones at a smaller scale. Contaminants that appeared not to be moving downgradient from the oil based on observation well data, such as ortho-xylene, are migrating in thin layers as the aquifer evolves to methanogenic conditions.

INTRODUCTION

Concern over the contamination of groundwater resources combined with the realization that engineered clean up of contaminated sites is limited by technological and monetary constraints has lead to an interest in remediation by natural attenuation (National Research Council, 1994). The processes that control the attenuation of organic compounds in contaminated aquifers are complex. The prevalence of hydrocarbon-contaminated sites and the high degree of toxicity and aqueous mobility of hydrocarbons has resulted in numerous investigations into the fate of hydrocarbons in the subsurface. It is well known that aromatic hydrocarbons can be degraded under both aerobic and anaerobic conditions, but the rates of degradation can vary significantly under different electron accepting conditions (e.g. Krumholz and others, 1996). It has been demonstrated that closely spaced sampling is required to identify microbiological processes in contaminated aquifers (e.g., Smith and others, 1991). Characterization of the small-scale spatial variability of biogeochemical processes provides insight into how naturally occurring microbes degrade hydrocarbons in contaminated aquifers and may improve estimates of hydrocarbon degradation rates.

A number of electron acceptors in subsurface environments can be utilized by bacteria to mediate the oxidation of hydrocarbons. In the absence of oxygen, the oxidized forms of inorganic species are used by microorganisms as electron acceptors. In most sand and gravel aquifers, Fe (III) oxides are abundant, yet the spatial distribution of sedimentary iron may be heterogeneous at scales ranging from the entire formation, which may be tens of meters thick, to individual depositional layers that may be only a few centimeters (cm) thick (e.g. Knapp, 1997). The heterogeneity of iron oxides demonstrates the non-uniform availability of solid-phase electron acceptors in sedimentary aquifers. As degradation reactions progress in a contaminated aquifer, the distribution of solid iron phases can change over time and space, altering the

biogeochemical processes that affect the fate and transport of hydrocarbons.

Previous results (Baedecker and others, 1993; 1996) indicated that between 1984 and 1992, a ground-water contamination plume developed near the oil body and evolved from aerobic to manganese reducing to iron reducing and finally methanogenic conditions. The long-term study of the development of the contaminant plume at the Bemidji site has provided an excellent opportunity to look at how natural attenuation of hydrocarbons is affected by the evolving redox conditions in the aquifer. This paper describes the continued evolution of the contaminant plume over time and examines changes in aquifer geochemistry and the potential for hydrocarbon transport that occur at a small spatial scale. Detailed sampling of ground water and aquifer solids, on a centimeter scale, has allowed a more precise determination of the important oxidation-reduction reactions involved in the degradation of hydrocarbons at this site than would have been possible with ground-water sampling at a larger spatial scale.

SITE DESCRIPTION

The field site is near Bemidji, Minnesota, in the Bagley outwash plain in north central Minnesota. Location maps are given in Bekins and others (1999). In 1979, a high-pressure oil pipeline burst, spraying oil over the land surface. Crude oil percolated through the unsaturated zone to the water table, creating two main subsurface oil bodies. One oil body, termed the "north pool", where a layer of oil approximately 1 meter (m) thick remains floating on the water table, has been an area of extensive research since 1984. The contaminated surficial aquifer is approximately 20 m thick, with the water table located 6-10 m below land surface. The aquifer sediment is glacially deposited, moderately calcareous, silty sand with local lenses of silty material and lenses of coarser sand and pebbles. The mineralogy of the sediments is roughly 50% quartz, 30% feldspar, 5-6% calcite and dolomite, and about 5% heavy minerals (Bennett and others, 1993).

STUDY METHODS

Field Procedures

Ground-water samples were collected from water-table wells and deeper wells along a transect in the direction of ground-water flow (fig. 1). Ground-water samples for analysis of unstable constituents (e.g. dissolved oxygen (DO)) were collected with a submersible pump, and ground-water samples for analysis of organic compounds were collected with a Teflon bailer by the methods of Baedecker and others (1993) and Eganhouse and others (1993). Cores were collected by drilling with a hollow-stem auger to the top of the desired coring interval, followed by driving of the core barrel beneath the augers to the desired depth.

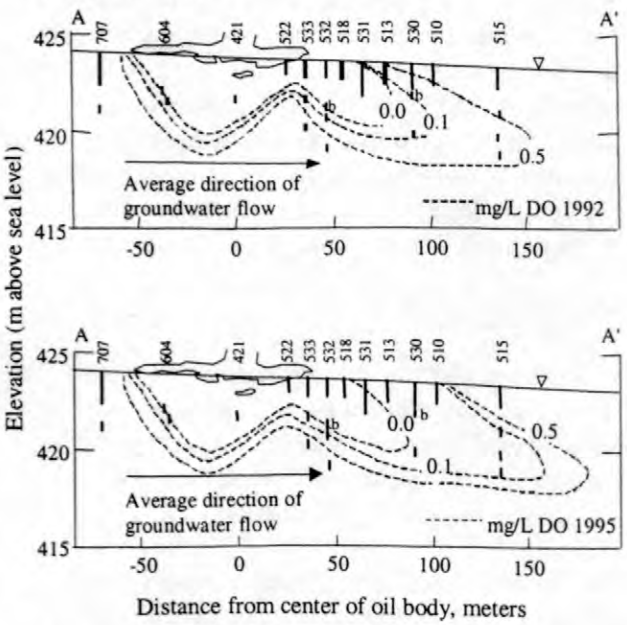

Figure 1. Dissolved oxygen (DO) contours in ground water downgradient from the crude oil source in 1992 and 1995. The location of the water table and observation wells are shown.

The coring method uses a piston that creates suction on saturated sediment within the core barrel as the barrel is driven into the sediment (Murphy and Herkelrath, 1996). The bottom of the core is frozen *in situ* to prevent loss of fluids out the core bottom. The 47-millimeter (mm) diameter cores were collected in clear

polycarbonate liners. The cores were removed from the core barrel and immediately sealed with plugs at the top and bottom after retrieval. The top plug was connected to N_2 gas, which was at a pressure of less than 30 kPa during sampling of the core.

Water from the cores was immediately collected at 15-cm intervals beginning at the top of the core. The core was drained at each interval by drilling a 4-mm-diameter hole in the polycarbonate liner and then inserting a luer-tip syringe snugly into the hole. Approximately 10 to 15 milliliters (mL) of pore water were collected at each interval. Glass syringes were used for the hydrocarbon sample; polycarbonate syringes were used for all other samples.

Concentrations of DO were measured in the field using a modified Winkler titration (Baedecker and Cozzarelli, 1992) and field-test kits available from CHEMetrics (Calverton, Virginia). Samples for monoaromatic hydrocarbon and methane (CH_4) analyses were collected from wells and cores without filtration. Water samples collected for measurement of CH_4 concentrations were collected in glass syringes and transferred from the syringe into 25-mL serum bottles containing enough mercuric chloride ($HgCl_2$) to produce a Hg concentration of 0.2 millimolar (mM). Ground water for determination of volatile hydrocarbons was transferred from the syringe into 1.8-mL glass vials containing $HgCl_2$. Samples collected for cations, including total iron, and ferrous iron (Fe^{2+}) were filtered through 0.2-micrometer (μm) filters. Samples collected for Fe^{2+} analysis were fixed with reagents in the field and cation samples were preserved with nitric acid. Samples for volatile dissolved organic carbon (VDOC) were filtered through 0.4 μm Nuclepore filters and preserved with mercuric chloride ($HgCl_2$). Samples for determination of $\delta^{13}C$ of inorganic carbon were filtered through 0.4 μm Nuclepore filters and the carbon was precipitated as strontium carbonate in the field.

The drained cores were sectioned and subsamples of the sediments were transferred to airtight containers under a CO_2-N_2 atmosphere. Sediment samples were stored frozen until they could be extracted for iron content (see sediment extraction procedure below).

Analytical Procedures

Water Chemistry

Concentrations of Fe^{2+} were determined colorimetrically by a modified bipyridine method as described in Baedecker and Cozzarelli (1992). Cation samples were analyzed with an ARL Spectraspan V Direct Current Plasma spectrometer. Carbon isotopes were analyzed using an isotope-ratio mass spectrometer (Baedecker and others, 1993). Dissolved CH_4 concentrations were measured by headspace analysis and gas chromatography (Baedecker and Cozzarelli, 1992). Concentrations of volatile monoaromatic hydrocarbons were measured by purge-and-trap capillary gas chromatography using a DB-5 bonded-phase fused-silica capillary column, as described by Eganhouse and others (1999).

Sediment Extractions

Sediment extractions were performed as described in Tuccillo and others (1999). To perform the extractions, 0.6 grams (g) to 1.5 g of sediment were placed in 30-mL serum bottles. Anoxic sediment samples were transferred to the bottles while the headspace of the sediment storage vial was flushed with N_2. After adding samples to bottles, 30 mL of 0.5 molar (M) HCl was added, and the bottles were crimped, capped, covered with foil, and placed on a shaker table for 3 days. After removal from the shaker table, the liquid was then filtered through a 0.2 μm filter and analyzed for Fe(II) and Fe(total) using Ferrozine (Gibbs, 1979). The concentrations of Fe(III) were determined by difference.

RESULTS AND DISCUSSION

2-D Plume-Scale Changes in Aquifer Chemistry

The distribution of DO in ground water along a transect downgradient from the oil body indicates that the anoxic plume extended

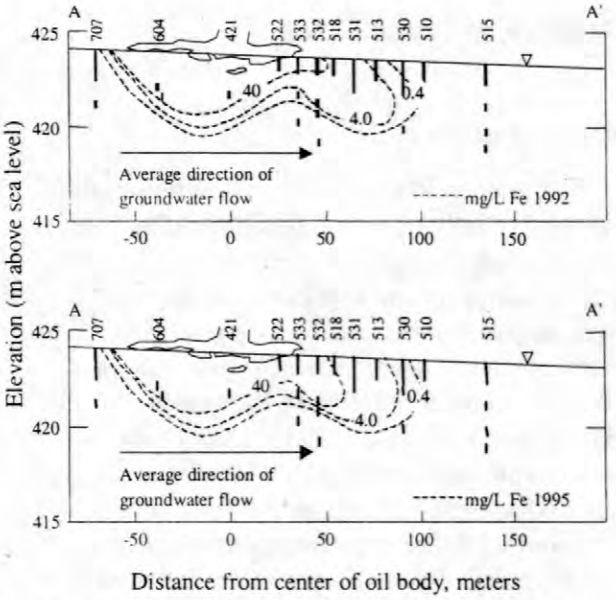

Figure 2. Dissolved iron (Fe) contours in ground water downgradient from the crude oil source in 1992, and 1995. The locations of the water table and observation wells are shown.

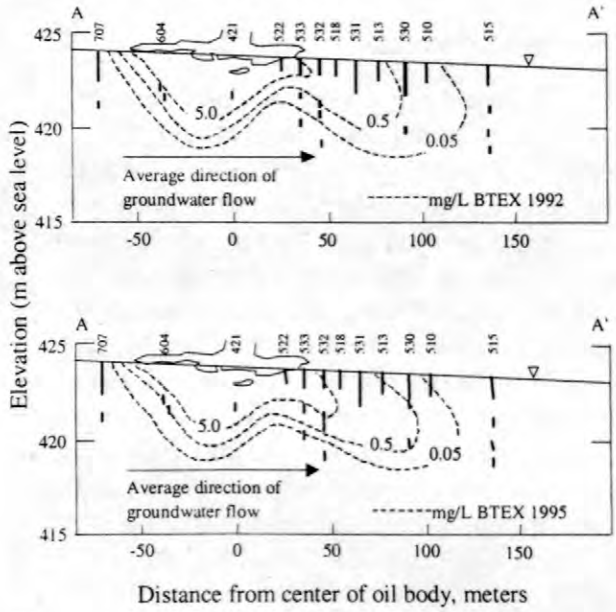

Figure 3. BTEX contours in ground water downgradient from the crude oil source in 1992, and 1995. The locations of the water table and observation wells are shown.

approximately 80 m downgradient from the crude oil in 1992 (fig. 1). The zone containing anoxic ground water and high Fe^{2+} and BTEX concentrations continues to spread (fig. 1-3), consistent with previous results for earlier years (Baedecker and others, 1993, 1996, Baedecker and Cozzarelli, 1994). Changes in chemistry observed at the plume scale are defined in this paper as those changes that can be determined on the basis of data from the observation well network. Although the shape of the anoxic plume has remained the same, the zero D.O. contour line (D.O. below detection) is now several meters further downgradient (fig. 1). Within the anoxic plume, the zone with high dissolved-iron concentrations increased in vertical extent over time and the maximum benzene, toluene, ethylbenzene, and xylene (BTEX) concentrations have also spread in this zone. The rate of movement of the high dissolved Fe^{2+} plume (defined by the 40 milligrams (mg)/L contour, fig. 2) was approximately 3 m/year. The downgradient extent of the Fe^{2+} and BTEX (fig. 3) plumes, however, has not noticeably changed, indicating that the supply of these compounds from the upgradient contaminated water is balanced by the processes that impede the movement of these compounds. It has been well established that microorganisms degrade BTEX compounds in this aquifer (Baedecker and others, 1993, Cozzarelli and others, 1994, Lovley and others, 1989). The rate of degradation has been such that, in 11 years of study, the plume-scale movement of BTEX compounds has been much slower than would have been predicted by conservative transport. The downgradient edge of the BTEX plume moved about 8 meters per year from 1987 to 1992 (Baedecker and Cozzarelli, 1994) and appears to have moved even more slowly from 1992 to 1995 (fig. 3).

The balance between microbial iron reduction and precipitation and/or oxidation of Fe^{2+} controls the movement of the dissolved iron plume (fig. 2). Depth profiles of the Fe (III) concentrations (determined from the 0.5M HCl extraction) from several cores (fig. 4) show that Fe (III) is depleted, relative to background, in the anoxic zone and underneath the oil due to microbial reduction of iron coupled to degradation of the hydrocarbons (fig. 5). The dashed line in each panel represents the mean concentration of Fe (III) for that core. At the edge of the anoxic zone reduced iron that has been transported downgradient is oxidized. In this oxic/anoxic transition zone sediment Fe (III) accumulates and concentrations reach high levels (significantly greater than background) as the

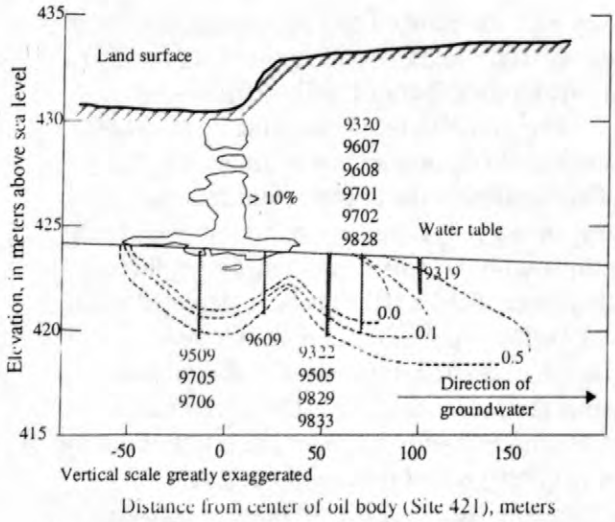

Figure 4. Location of cores collected underneath and downgradient from the crude oil source from 1993 through 1998. The locations of the DO contours in 1992 and the oil saturation values greater than 10 percent are shown.

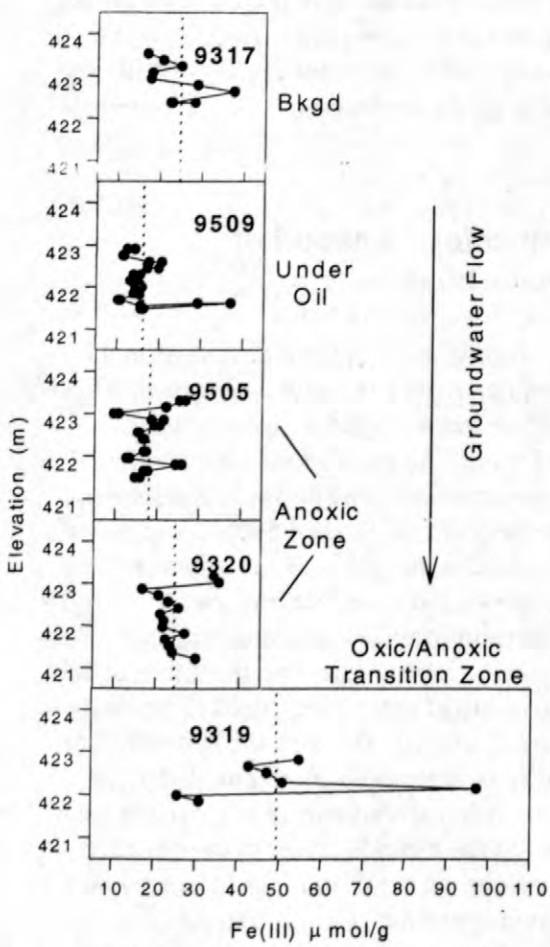

Figure 5. The concentration of Fe(III) in cores (located in fig. 4) collected downgradient from the oil body. The dashed lines represent the mean concentration of Fe (III) for that core.

aqueous Fe^{2+} oxidizes and precipitates. Plots of the Fe (II)concentrations (fig. 6) from the same cores show Fe (II) is very low in background sediments and highest underneath the oil where Fe^{2+} in the water precipitates as iron carbonates or in iron-rich clays (Tuccillo and others, 1999).

Temporal Changes in Vertical Profiles

Analyses of water chemistry from cores collected from the center of the anoxic plume (fig. 7), and from the edge of the anoxic plume (fig. 8), indicate that significant changes are occurring at particular locations within the plume that are more difficult to see when chemistry is examined at the larger plume scale. The concentrations of Fe^{2+}, CH_4, and BTEX indicate that the plume is increasing in vertical thickness over time. In the center of the anoxic plume,

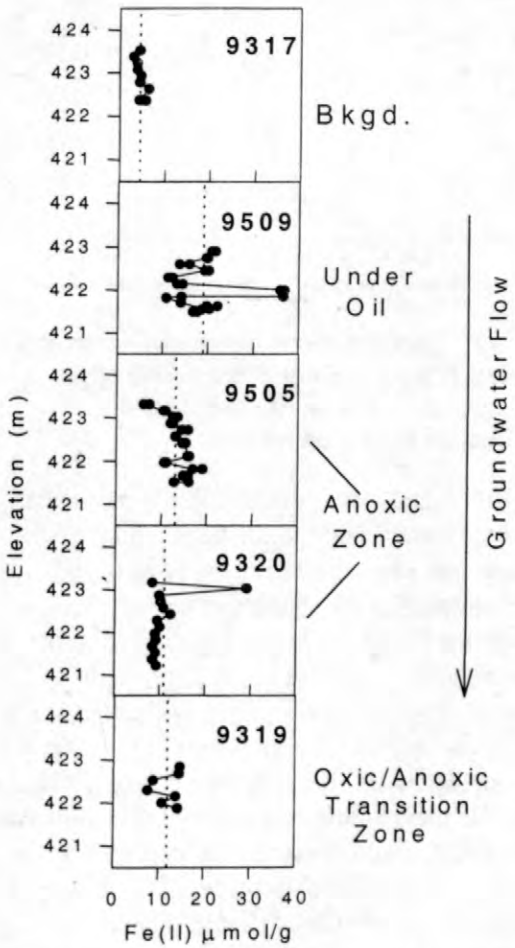

Figure 6. The concentration of Fe(II) in cores (located in fig. 4) collected downgradient from the oil body. The dashed lines represent the mean concentration of Fe (II) for that core.

although the maximum concentrations of methane and iron are approximately the same, the depths over which these high concentrations are observed have increased (fig. 7). A similar pattern was seen in the core profiles collected at the edge of the anoxic zone (fig. 8). The continued spreading of the dissolved methane and iron plumes indicate that iron reduction and methanogenesis continue to be important processes in the aquifer close to the oil body.

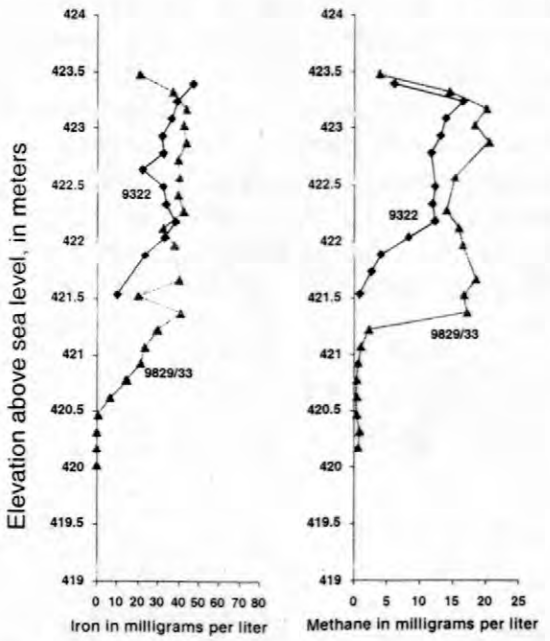

Figure 7. Concentrations of dissolved iron and methane in ground water in the center of the anoxic plume in 1993 and 1998. Core locations are shown on figure 4.

Prolonged iron reduction in the plume has caused measurable temporal changes in the sediment iron chemistry near the edge of the anoxic plume (fig. 8). Sediment extractions indicate that Fe (III) is being depleted from the sediment, while Fe (II) is being deposited. Scanning electron microscopy showed that some of the reduced iron is being stored in the plume sediments as Fe (II)-bearing minerals (e.g. ferroan calcite, Baedecker and others, 1993, Tuccillo and others, 1999). Additional pyrophosphate extractions by Tuccillo and others (1999) indicated that a portion of the Fe(II) may be present as organically bound iron. Reoxidation and precipitation of iron is taking place near the water table, as the anoxic plume mixes with oxygenated recharge water, resulting in consistently higher concentrations of Fe (III) near the top of the core profiles (fig. 8).

The availability of reducible Fe (III) in the sediments is important for the continued biodegradation in the contaminant plume. Sediment Fe (III) is clearly being removed from the anoxic plume sediments (fig. 8), yet there is no evidence that Fe (III) has been depleted to the point of limiting iron reduction. There is evidence of methanogenesis near the oil body despite the presence of Fe (III) concentrations of 15-20 μmoles per gram under the oil. Bekins and others (1999) found that areas of high contaminant flux near the oil body contained the greatest numbers of culturable methanogens. Methanogenesis occurs concurrent with iron reduction in thin layers of sediment (on the order of 25 cm) beneath the oil body, indicating that the redox zones evolve on a small spatial scale. Further downgradient, within the anoxic plume, this evolution is likely slower since a greater amount of readily reducible Fe (III) is still available for iron reduction.

Potential for Transport of Hydrocarbons

The evolution of the redox zones in the contaminant plume can have a significant effect on the fate and transport of hydrocarbons in ground water. Analysis of the hydrocarbon concentrations over time in two wells located within the plume (532b and 530b, locations on fig. 1) indicate that the concentrations of hydrocarbons vary in space and over time (fig. 9). The transport of different hydrocarbons is dependent to a large extent on the differences in degradability of these compounds (Eganhouse and others, 1993). Although the hydrocarbons appear to be attenuated at the plume scale, specific hydrocarbons appear to persist in local zones. At the location closer to the oil, 532b (fig. 9), hydrocarbon concentrations have gradually increased over time. Concentrations of all the hydrocarbons are higher after 10 years than they were in 1986 (by a factor ranging from 1.4 for ethylbenzene to 11.6 for benzene), indicating that

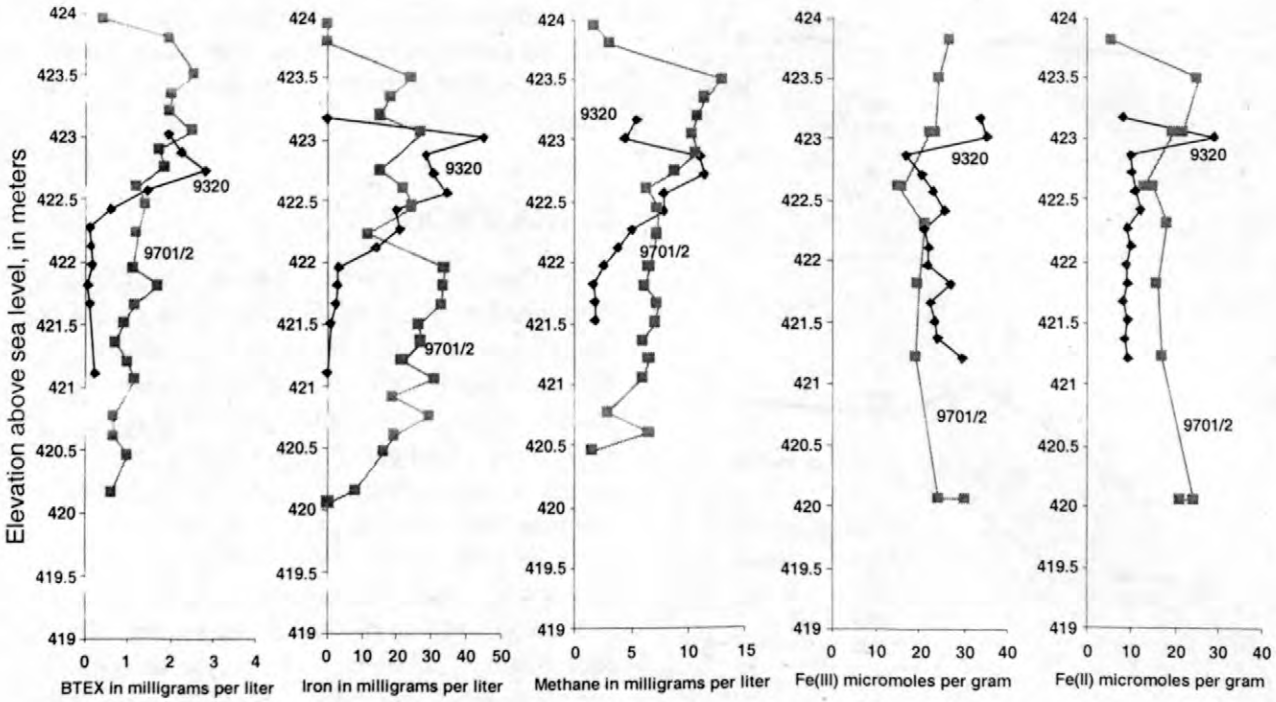

Figure 8. Concentrations of dissolved BTEX, iron and methane in ground water and Fe(III) and Fe(II) in aquifer solids at the edge of the anoxic plume in 1993 and 1997. Core locations are shown on figure 4.

the crude oil continues to provide a source for these compounds at a rate slightly above the rate at which they are attenuated. Less persistent compounds show greater temporal fluctuations in removal rates than more stable species. For example, the concentrations of *ortho*-xylene show the highest degree of variability. Benzene and ethylbenzene have consistently been shown to be stable in the anoxic plume, while toluene and ortho-xylene are consistently unstable (Eganhouse and others. 1996).

In ground water farther downgradient (well 530b), concentrations of most hydrocarbons are still increasing 16 years after the crude-oil spill (fig. 9). The more stable compounds increase in concentration earlier than the least stable compounds. The different hydrocarbons show markedly different transport rates in this part of the aquifer. The more stable compounds, such as ethylbenzene, appear to be approaching concentration levels similar to those found in the upgradient well. The concentrations of the least stable compound, *ortho*-xylene, are below detection 16 years after the original spill. Attenuation processes, most likely microbial degradation, remove this contaminant from the ground water within a short distance from the source. It has been well documented that microorganisms in anaerobic aquifers can degrade *ortho*-xylene.

Examination of the data from the closely-spaced sampling of water from the cores indicates that there is potential for *ortho*-xylene transport despite the relatively stable patterns observed in the data from the ground-water wells. The cores (locations on fig. 4) at the edge of the anoxic plume, approximately 70 m from the center of the oil body (fig. 10), were collected just upgradient from well 530b. Analyses of the hydrocarbon concentrations in this profile (fig. 10) show that *ortho*-xylene moved into this part of the aquifer between 1993 and 1997. The very thin *ortho*-xylene plume corresponds to the zone of maximum concentrations of methane and iron (fig. 8). This thin zone has been identified as a methanogenic zone by Bekins and others (1999) on the basis of geochemical evidence combined with the evolution of microbial populations of different physiological types. The long-term potential for *ortho*-xylene transport, and perhaps

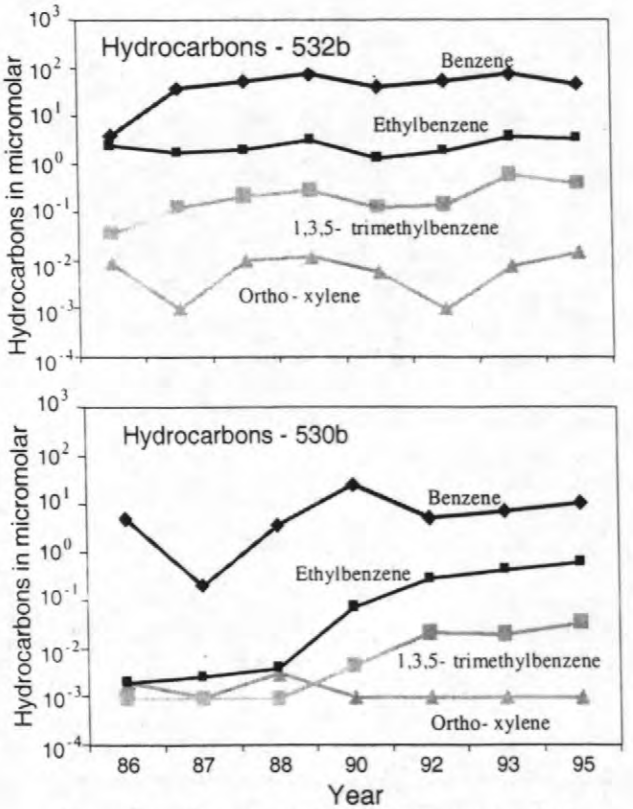

Figure 9. Concentrations of benzene, ethylbenzene, 1,3,5 trimethylbenzene and *ortho*-xylene in ground water from two wells between 1986 and 1996. Wells located on figure 1.

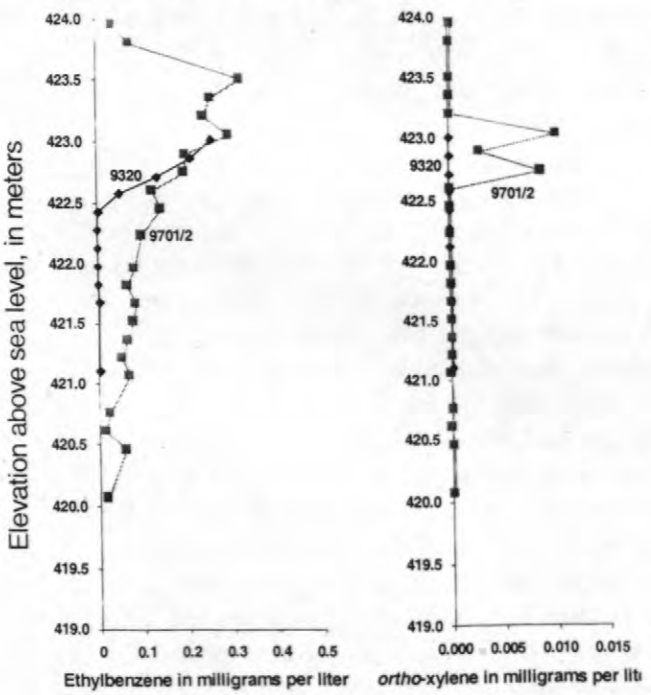

Figure 10. Concentrations of ethylbenzene and *ortho*-xylene in ground water at the edge of the anoxic plume in 1993 and 1997. Core locations are shown in figure 4.

transport of other hydrocarbons that show similar potential for degradation, is tied to the evolution of the redox zones in the plume. It is apparent that this evolution occurs at a small scale (on the order of tens of centimeters) in the contaminated aquifer.

CONCLUSIONS

This study shows the importance of long-term monitoring and examination of processes at a small spatial scale when assessing the natural attenuation of hydrocarbons in a contaminated aquifer. Examination of the patterns in the hydrocarbon well data for the crude-oil contaminated aquifer at Bemidji, Minnesota show that there were periods of several years, for example 1988 through 1992, during which hydrocarbon concentrations in the heart of the contaminant plume showed decreases for many compounds. If these were the only data available, one might have concluded that hydrocarbons near the source were being depleted and the long-term potential for hydrocarbon transport would have been underestimated. Temporal data collected at closely spaced vertical intervals, however, indicate that hydrocarbon concentrations (e.g. ethylbenzene) have spread out, consistent with a vertical thickening of the plume. It is apparent that the availability of an electron acceptor such as Fe (III) oxides in this system has a significant impact on the transport of hydrocarbons downgradient and away from the crude-oil source. Examination of changes in the distribution of this electron acceptor at the plume scale and at the core scale provides insight into the progression of biogeochemical zones. This type of information is needed in order to predict the long-term impact of hydrocarbon spills on aquifer chemistry and to assess the potential for hydrocarbon transport through the aquifer.

REFERENCES

Baedecker, M.J., and Cozzarelli, I.M., 1992, The determination and fate of unstable constituents in contaminated groundwater in Lesage, S., and Jackson, R.E., eds, Groundwater Quality and Analysis at

Hazardous Waste Sites, Marcel Dekker, p. 425-461.

Baedecker, M.J., and Cozzarelli, I.M., 1994, Biogeochemical processes and migration of aqueous constituents in ground water contaminated with crude oil. in Dutton, A.R., ed, Toxic Substances and the Hydrologic Sciences, American Institute of Hydrology, p. 69-79.

Baedecker, M.J., Cozzarelli, I.M., Eganhouse, R.P., Siegel, D.I., and Bennett, P.C., 1993, Crude oil in a shallow sand and gravel aquifer-III. Biogeochemical reactions and mass balance modeling in anoxic groundwater: Applied Geochemistry, v. 8, p. 569-586.

Baedecker, M.J., Cozzarelli, I.M., Bennett, P.C., Eganhouse, R.P., and Hult, M.F., 1996, Evolution of the contaminant plume in an aquifer contaminated with crude oil, Bemidji, Minnesota, *in* Morganwalp, D.W., and Aronson, D.A., eds, U.S. Geological Survey Toxic Substances Hydrology Program-Proceedings of the technical meeting, Colorado Springs, Colorado, September 20-24, 1993: U.S. Geological Survey Water-Resources Investigations Report 94-4015, p. 613-620.

Bekins, B.A., Cozzarelli, I.M., Godsy, E.M., Warren, Ean, Tuccillo, M.E., Essaid, H.I., and Paganelli, V.V., 1999, Chemical and physical controls on microbial populations in the Bemidji Toxics Site crude-oil plume, Morganwalp, D.W., and Buxton, H.T., eds, U.S. Geological Survey Toxic Substances Hydrology Program—Proceedings of the Technical Meeting, Charleston, South Carolina, March 8-12, 1999-- Volume 3 -- Subsurface Contamination from Point Sources: U.S. Geological Survey Water-Resources Investigations Report 99-4018C.

Bennett, P.C., Siegel, D.E., Baedecker, M.J., and Hult, M.F., 1993, Crude oil in a shallow sand and gravel aquifer - I. Hydrogeology and inorganic geochemistry: Applied Geochemistry, v. 8, p. 529-549.

Cozzarelli, I.M., Baedecker, M.J., Eganhouse, R.P., and Goerlitz, D.F., 1994, The geochemical evolution of low-molecular-weight organic acids derived from the degradation of petroleum contaminants in groundwater: Geochimica et Cosmochimica Acta, v. 58, p. 863-877.

Eganhouse, R.P., Baedecker, M.J., Cozzarelli, I.M., Aiken, G.R., Thorn, K.A., and Dorsey, T.F., 1993, crude oil in a shallow sand and gravel aquifer - II. Organic geochemistry: Applied Geochemistry, v. 8, p. 551-567.

Eganhouse, R.P., Dorsey, T.F., Phinney, C.S., and Westcott, A.M., 1996, Processes affecting the fate of monoaromatic hydrocarbons in an aquifer contaminated by crude oil: Environmental Science and Technology, v. 30, p. 3304-3312.

Eganhouse, R.P., Matthews, L.L., Cozzarelli, I.M., and Scholl, M.A., 1999, Evidence for natural attenuation of volatile organic compounds in the leachate plume of the Norman, Oklahoma landfill, Morganwalp, D.W., and Buxton, H.T., eds, U.S. Geological Survey Toxic Substances Hydrology Program—Proceedings of the Technical Meeting, Charleston, South Carolina, March 8-12, 1999-- Volume 3 -- Subsurface Contamination from Point Sources: U.S. Geological Survey Water-Resources Investigations Report 99-4018C.

Gibbs, M.M., 1979, A simple method for the rapid determination of iron in natural waters: Water Resources Research, v. 13, p. 295-297.

Knapp, E. P, 1997, The influence of redox conditions on sorption to aquifer sediments: Transport of reactive solutes in groundwater. Ph.D. thesis, University of Virginia, Charlottesville, Virginia, USA.

Krumholz, L.R., Caldwell, M.E., and Suflita, J.M., 1996, Biodegradation of "BTEX" hydrocarbons under anaerobic conditions, Crawford, R.L., and Crawford, D.L., eds, Bioremediation: Principles and Applications, Cambridge University Press, p. 61-99.

Murphy, F. and Herkelrath, W.N., 1996, A sample-freezing drive shoe for a wire line piston core sampler: Ground Water Monitoring and Remediation, v. 16, p. 86-90.

NRC, 1994, Alternatives for Ground Water Cleanup: Washington, D. C., National Academy Press, p. 315.

Lovley, D.R., Baedecker, M.J., Lonergan, D.J., Cozzarelli, I.M., Phillips, E.J.P., and Siegel,

D.I., 1989, Oxidation of aromatic compounds coupled to microbial iron reduction: Nature, v. 339, p. 297-299.

Smith, R. L., Harvey, R. W., and LeBlanc, D. R., 1991, Importance of closely spaced vertical sampling in delineating chemical and microbiological gradients in groundwater studies: Journal of Contaminant Hydrology, v. 7, p. 285-300.

Tuccillo, M.E., Cozzarelli, I.M., and Herman, J.S., 1999, Applied Geochemistry, v. 14, no. 5, p. 71-83.

AUTHOR INFORMATION

Isabelle M. Cozzarelli (icozzare@usgs.gov), Mary Jo Baedecker, Robert P. Eganhouse, Jeanne B. Jaeschke U.S. Geological Survey, Reston, Virginia

Mary Ellen Tuccillo, Department of Environmental Sciences, University of Virginia, Charlottesville, Virginia

Barbara A. Bekins, U.S. Geological Survey, Menlo Park, California

George R. Aiken, U.S. Geological Survey, Boulder, Colorado

Chemical and Physical Controls on Microbial Populations in the Bemidji Toxics Site Crude-Oil Plume

By Barbara A. Bekins, Isabelle M. Cozzarelli, E. Michael Godsy, Ean Warren, Mary Ellen Tuccillo, Hedeff I. Essaid, and Victor V. Paganelli

ABSTRACT

Processes controlling the establishment of aquifer microbial populations that degrade organic ground-water contaminants are poorly understood. We provide insight into this problem with a combined data set that includes microbial populations, grain size, pore-water chemistry, and sediment iron content. Data from three vertical profiles through the anaerobic portion of the Bemidji crude-oil plume show similar patterns in the microbial populations. Within each profile, numbers of iron-reducers vary from lows of 10^2-10^4/g sediment to highs of 10^5-10^6/g. Areas that are evolving from iron-reducing conditions to methanogenic conditions are indicated by lower numbers of iron-reducers and the presence of culturable methanogens (10^1-10^2/g). These conditions are found in areas of high contaminant flux either in the vicinity of the non-aqueous oil or where higher concentrations in the contaminant plume are associated with local increases in aquifer permeability. In all locations where methanogens are found, lower numbers of culturable iron reducers are also present. Moreover, in these areas, significant extractable Fe(III) (>10 μmol/g) is still present, suggesting that the remaining iron on the sediments may be less available for microbial reduction. The methanogenic zones are vertically narrow, ranging from 0.25-1 m thick, but they are laterally continuous extending from the source area to at least 60 m downgradient.

INTRODUCTION

Although it is well known that aquifer microbes degrade dissolved hydrocarbons under both aerobic and anaerobic conditions (see Wiedemeier and others, 1995, for a review), the ecology of the microbial populations performing the degradation reactions is poorly understood. As electron acceptors are depleted, a succession of physiologic types occurs. The spatial distribution of the physiologic types is generally inferred from aqueous concentrations of redox indicators such as dissolved oxygen, Fe(II), and dissolved methane. Although, these chemical species indicate that a particular reaction is occurring, measured concentration distributions do not accurately demarcate the regions of the aquifer where the specific microbial processes are active. This is because the concentrations are affected not only by microbial activity but also by advective transport, dispersion, and inorganic reactions. For example, methane can be transported downgradient from zones where methanogenesis occurs, complicating the use of methane concentrations for determining the exact location and extent of the methanogenic zone. Moreover, because the anaerobic cores of plumes can be extremely narrow in vertical extent (e.g., Smith and others, 1991; Cherry, 1996), pore-water samples from wells with long screens may be sampling ground water from two or more redox zones.

The goal of this work was to examine the processes that control microbial redox zones in a ground-water plume at a crude-oil spill. Characterizing distribution of microbial physiologic types together with pore-water chemistry, sediment iron content, and sediment permeability provides insight into the patterns of ecological succession at the plume scale. Using the most probable number (MPN) method, the microbial population distributions

were estimated for six physiologic types: aerobes, iron-reducers, heterotrophic fermenters, methanogens, sulfate-reducers and denitrifiers. We concentrated on the anaerobic portion of the plume because anaerobic processes probably account for the majority of the hydrocarbon degradation at this site (Essaid and others, 1995). Moreover, anaerobic processes are estimated to be important at 90% of sites contaminated by non-aqueous phase petroleum hydrocarbons (T. Wiedemeier, Parsons Engineering Science, Inc., oral. comm., 1998).

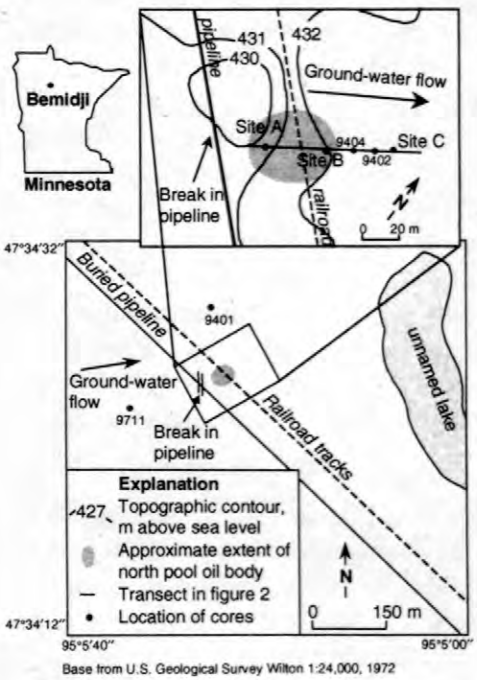

Figure 1. Site of 1979 crude oil spill near Bemidji, Minnesota, with locations of cores.

SITE DESCRIPTION

The study aquifer, located near Bemidji, Minnesota, is a surficial formation of pitted and dissected glacial outwash sediments (fig. 1). It was contaminated with crude oil when a pipeline ruptured in August, 1979. After clean-up operations by the pipeline company, residual spilled oil infiltrated into the aquifer forming bodies of oil floating on the water table (Hult, 1984). The largest oil body (the "north pool") is estimated to contain 147,000 liters of oil (Herkelrath, 1999).

A set of papers (Baedecker and others, 1993; Bennett and others, 1993; Eganhouse and others, 1993) described the geochemistry of the contaminant plume emanating from the north pool. Starting in 1984, concentrations of both reduced iron and methane began to increase in the anoxic zone immediately downgradient from the oil body. From 1986 to 1989, profiles of dissolved organic compounds indicated the plume reached a quasi steady-state in which dissolution from the non-aqueous oil was approximately balanced by biotransformation by iron-reduction (Lovley and others, 1989) and methanogenesis (Baedecker and others, 1993). Recent results on the continued chemical evolution of the plume are presented by Cozzarelli and others (1999).

METHODS

Using the existing geochemical data, locations for three vertical profiles were chosen to characterize the microbial population in the anaerobic portion of the plume (A, B, and C in figure 1). In September of 1996, two cores with a horizontal separation of 1 m were collected from Site B with a freezing drive shoe (Murphy and Herkelrath, 1996). Each core was 2.3 m long, which was sufficient to span the entire vertical extent of the anaerobic plume at this location. One core was analyzed for the microbial population on the sediments, along with extractable iron [Fe(III) and Fe(II)], and grainsize. The second core was used for pore-water chemical analyses. Because the drill rig depth measurements were imprecise, data from the two cores were aligned vertically using the grainsize distributions.

In August of 1997, five additional cores were collected. Three cores were needed to span a vertical interval from the oil body to the base of the contaminant plume at Site A, and two cores were sufficient to obtain a vertical profile of the plume at Site C. In these cores, the pore water was drained for chemical analyses and the sediments were analyzed for microbial numbers, grain-size distributions and extractable iron. Five additional cores were collected in 1994-

Table 1. Log_{10} of microbial numbers from seven locations marked in figure 2 plus two uncontaminated background locations (fig. 1). Abbreviations: Dist – Distance from center of oil body, meters; Elev – Elevation above mean sea level, meters; Fe-red – Iron-reducers; Aer – Aerobes; Ferm – Heterotrophic fermenters; Meth – Methanogens; and Bkgd – Background.

Sample	Dist	Elev	Fe-red	Aer	Ferm	Meth
9510-22s	19.8	421.5	<0.3	2.43	2.32	<0.3
9402-1s	55.3	423.0	4.00	4.00	<0.3	<0.3
9402-2s	55.3	422.1	4.46	3.32	1.53	2.32
9402-3s	55.3	421.3	4.03	3.03	1.70	<0.3
9404-1s	40.4	423.3	3.23	2.23	0.30	<0.3
9404-2s	40.4	422.5	4.38	2.90	2.15	0.90
9404-3s	40.4	421.7	2.70	1.85	<0.3	1.23
9711	Bkgd		1.15	2.85	<0.3	<0.3
9401	Bkgd		<0.3	1.76	1.98	<0.3

1997 and from these, nine samples were analyzed for sediment microbial numbers (figs. 1 and 2 and table 1).

For pore-water chemical analyses, water was drained from the core at 15 centimeter (cm) intervals. The pH was measured in the field and the water samples were preserved for laboratory analyses of hydrocarbons, dissolved organic carbon, methane, and major cations, according to the methods described by Cozzarelli and others (1999). Sediment samples were collected at 20-70 cm intervals and analyzed for populations of aerobes, iron-reducers, heterotrophic fermenters, methanogens, sulfate-reducers, and denitrifiers, using the MPN method. The methods of sediment sampling and MPN determination are described by Essaid and others (1995). The sediment grain-size analyses were performed using the method described by Hess and others (1992). The extractable iron method, described by Tuccillo and others (1999), was expected to extract the bioavailable Fe(III) as well as poorly crystalline Fe(II) from the sediments.

RESULTS

Figure 2 shows the vertical profile MPN data for the four major physiologic types found in the aquifer: aerobes, iron-reducers, fermenters, and methanogens. Data for sulfate reducers and denitrifiers are not presented here because these organisms were present in low numbers in the plume. This observation is consistent with the low concentrations of sulfate and nitrate in the uncontaminated ground water (Baedecker and others, 1993; Bennett and others, 1993). The populations of aerobes and iron-reducers vary by two to three orders of magnitude over short vertical distances of 10-20 cm. The peak populations of the methanogens are only 10^2/gram (g) of sediment but these contrast sharply with nondetectable background numbers. These results are similar to those of Godsy and others (1992) who reported a 100-fold increase in methanogens in a plume of dissolved creosote compounds compared to an uncontaminated background location. Like the aerobes and iron-reducers, the methanogenic populations vary vertically on a scale of 10-20 cm.

In all three profiles it appears that peaks in iron-reducer numbers alternate with those of methanogens. A Pearson correlation analysis of the combined data set from the three profiles shows that there is an inverse correlation between iron-reducers and methanogens of -0.62 ($p<0.0007$; 24 samples). In the Site A profile, located below the oil, iron-reducers are dominant at three levels: 424.0 meters (m), 421.8 m, and 419.0 m above sea level. At these same levels, there are lower numbers of fermenters, methanogens, and aerobes. Conversely, locations with lower numbers of iron-reducers, found at levels 424.5 m and 420.0-421.5 m, correspond to higher numbers of fermenters, methanogens, and aerobes. The increase in culturable aerobes at the same horizons where methanogens are present suggests that these are facultative organisms that can survive either aerobically or anaerobically.

The profile from Site B, located in the upwelling area, shows small-scale oscillations between methanogenic and iron-reducing conditions. Two levels in the aquifer (422.7 m and 422.3 m) have peak iron-reducing numbers together with relatively low numbers of aerobes and methanogens. At two other levels, peak values of aerobes and methanogens are found together with lower numbers of iron-reducers.

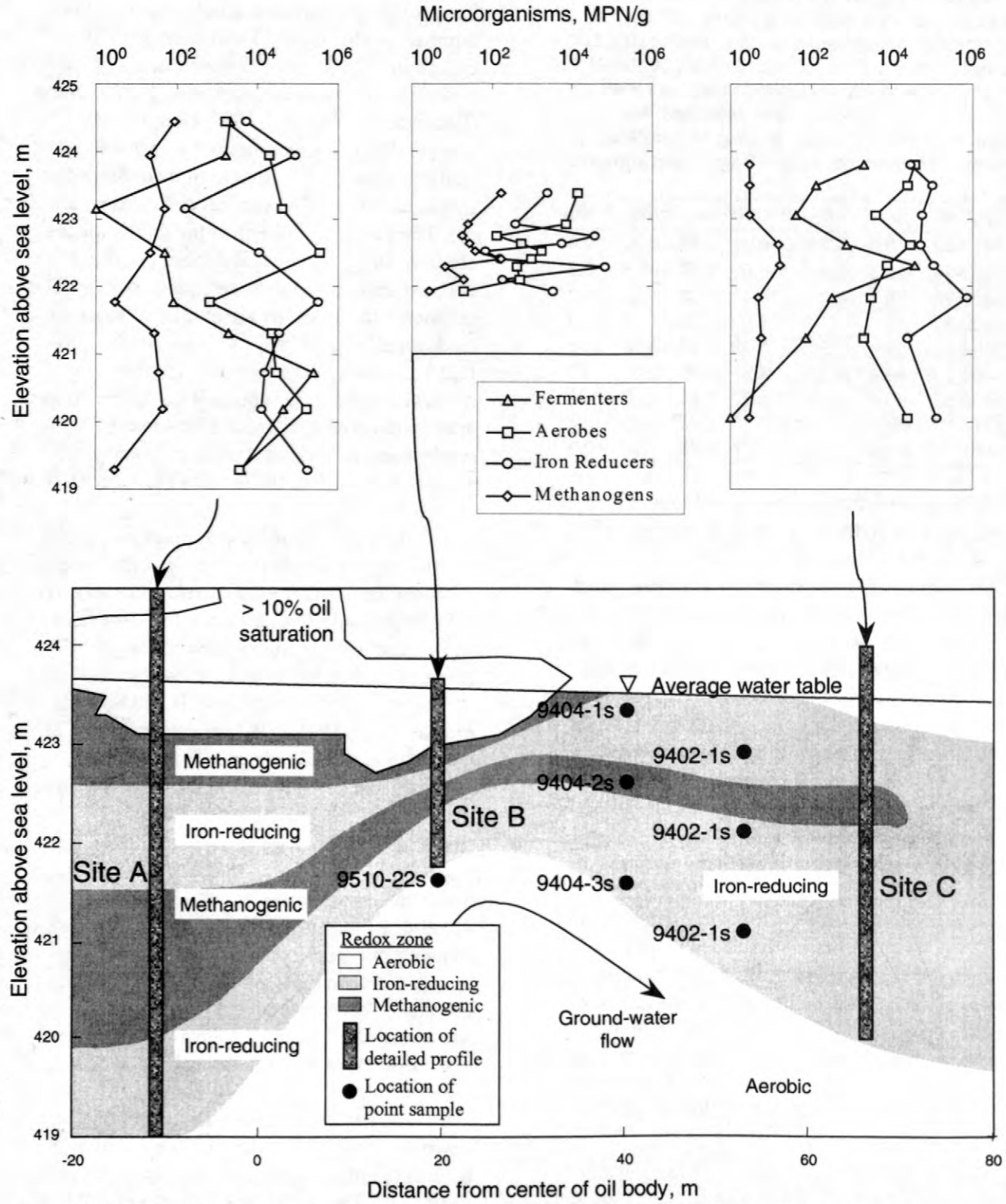

Figure 2. Vertical MPN profiles and interpreted cross section showing the distribution of microbial physiologic types in the anaerobic portion of the Bemidji plume. The vertical profiles correspond to Site A, B, and C locations in figure 1. The interpreted cross-section is based on the vertical profile data combined with data for point samples from seven locations marked on the section.

One level is located within the oil body at 423.4 m and the other is at 422.6-422.3 m in the core of the plume. A third level exhibiting this pattern is possibly also present at 422.1 m. Thus, this profile has methanogenic zones alternating with iron-reducing zones on a scale of only 25 cm.

The profile from Site C, located downgradient from the oil body, shows signs of being less evolved toward methanogenic conditions. Peak aerobe numbers are found at the top and base of the profile where aerobic conditions exist at the edge of the plume. A third peak in aerobes also exists between 422-423 m above sea level, where methanogens and fermenters increase, and iron-reducers decline. The maximum number of methanogens found is almost 10 times lower than at the sites below the oil. Moreover, the number of culturable iron-reducers still present in the evolving methanogenic zone exceeds 10^4/g compared to values as low as 10^2/g in methanogenic zones closer to the oil. These data suggest that this location may be in the early stages of switching from iron-reducing to methanogenic conditions.

Although the MPN method is not reliable for determining absolute numbers, the consistent pattern in relative numbers among the three profiles is significant. We have taken the vertical profile data together with microbial data from seven broadly-spaced sediment samples (fig. 2 and table 1) and interpolated them to provide a qualitative picture of the redox zones in the aquifer (fig. 2). A location was classified as methanogenic if more than 10/g total methanogens were present on the sediments and the iron-reducer numbers were relatively low compared to other locations in the same vertical profile. Where iron-reducer populations achieved maximum values and numbers of attached methanogens declined, the location was classified as iron-reducing. Finally, if only aerobes and fermenters were found, the location was classified as aerobic.

Within the contaminant plume, the contours of the population distribution appear to generally conform to the ground-water flow lines. Our results indicate that the anaerobic core of the plume attains a minimum vertical thickness of about one meter at the downgradient edge of the non-aqueous oil body. Essaid and others (1995) hypothesized that restricted recharge through a low permeability horizon causes the observed upwelling of oxygenated water in this location. Upwelling of the flow at Site B causes vertical focussing of the contaminated ground water, creating an especially narrow methanogenic zone centered at 422.5 m that spans a distance of only 25 cm. This contrasts with the thicker profiles upgradient at Site A and downgradient at Site C. Methanogenic zones have evolved in two places: one within the area where separate-phase oil is present, and a second below the oil in the laterally migrating plume of contaminated ground water. In the laterally migrating plume there is a classic pattern of a methanogenic core progressing with depth to iron-reducing and then aerobic conditions.

Controls on the Microbial Population Distribution

For each site, figure 3 shows the microbial data for iron-reducers and methanogens together with plots of the extractable Fe(II) and Fe(III) concentrations from the sediments; pore-water concentrations of ethylbenzene and *m*- and *p*-xylene; permeabilities estimated from sediment grain-size distributions (Krumbein and Monk, 1942), and pore-water Fe(II) concentrations.

Extractable Iron on Sediments

In general, extractable concentrations of sediment Fe(III) are lower, and Fe(II) are higher in the area of the aquifer affected by the plume than background values. Sediment Fe(III) values at the base of the core at Sites B and C are consistent with background concentrations indicating that the profiles span the entire anoxic portion of the plume. The overall picture is consistent with the results of Tuccillo and others (1999) who found that microbial iron-reduction of the petroleum hydrocarbons has resulted in depletion of solid phase Fe(III) and precipitation of authigenic Fe(II) minerals on the sediments in the anoxic zone.

Within the areas where culturable methanogens are found, extractable Fe(III) and

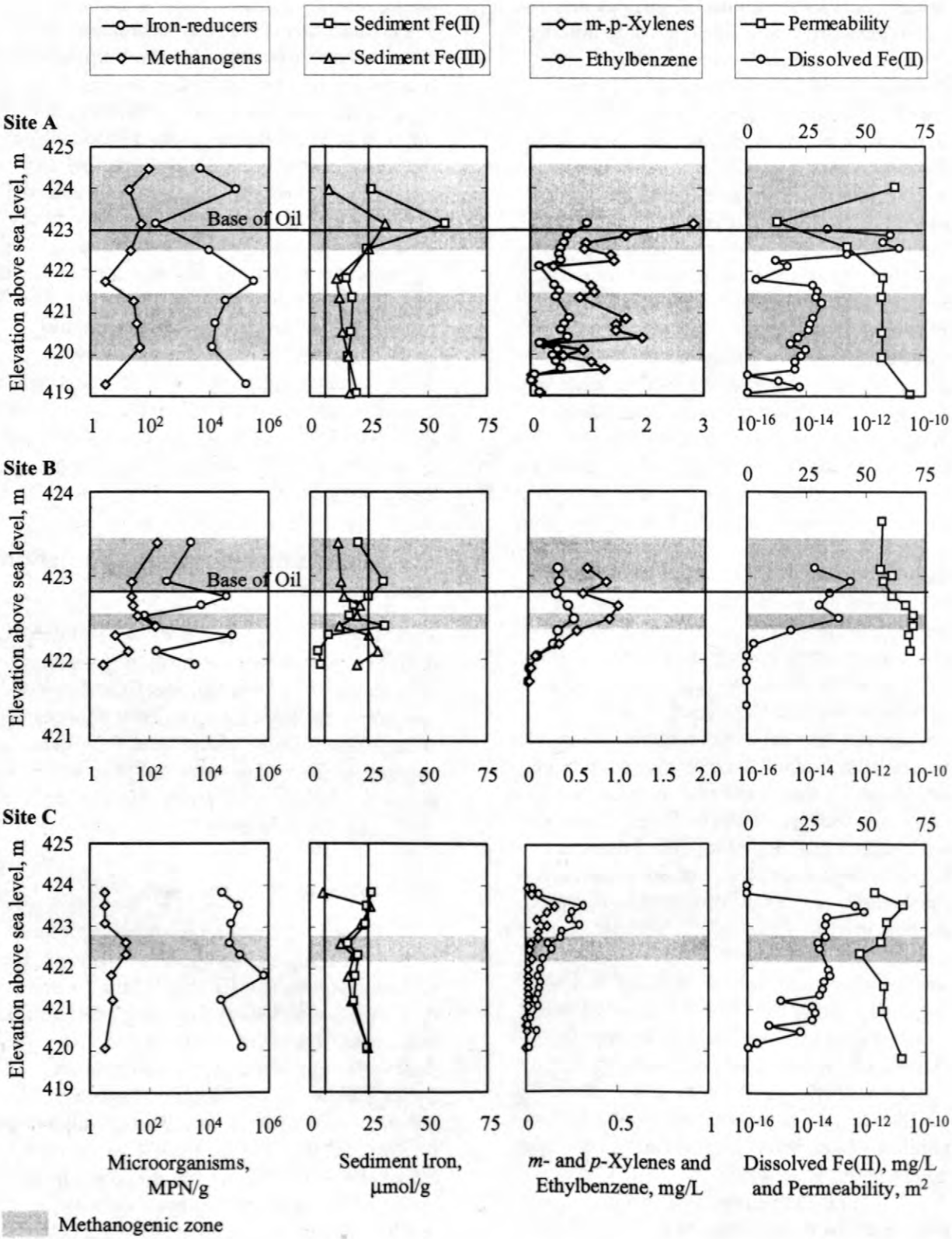

Figure 3. Vertical profiles for Sites A, B, and C of microbial data for iron-reducers and methanogens together with plots of the Fe(II) and Fe(III) concentrations from the sediments; pore-water concentrations of ethylbenzene and *m*- and *p*-xylene; and permeabilities estimated from sediment grain-size distributions and pore-water Fe(II) concentrations. Uncontaminated background concentrations of sediment Fe(II) and Fe(III) are shown in the sediment iron plots, averaging 6 and 25 µmol/g, respectively.

culturable iron-reducing organisms are still present. The lowest value of extractable Fe(III) found in all of the cores is 11 micromole/g (μmol/g) which is almost 50% of the average background concentration. Apparently, only about half of the Fe(III) available on the aquifer sediments is used before methanogenesis begins. Postma (1993) showed that simultaneous methanogenesis and iron-reduction is thermodynamically feasible if microorganisms are forced to use less soluble Fe phases than the poorly crystalline material that typically comprises hydroxypolymer coatings on mineral grains.

A detailed examination of the iron and microbial data shows that solid-phase Fe(III) depletion alone cannot explain the succession of iron-reducers by methanogens. For example, in the center of the dissolved plume at Site B (422.5 m) very low numbers of Fe-reducers are found with high values of extractable Fe(III). Also, high numbers of iron-reducers exist where Fe(III) values are low below the base of the oil body at Sites A (421.8 m) and B (422.7 m). Other factors are important that are not apparent from consideration of the extractable Fe(III) concentrations alone.

In several cases, peak values in Fe(II) are associated with low numbers of iron-reducers, and peaks in active methanogens (fig. 3: Site A, 423.2 m; Site B, 422.4 m and 422.9 m). This suggests that coating of the Fe(III) phases by Fe(II) precipitates is inhibiting iron-reduction and providing an advantage to the methanogens in these locations.

Organic concentrations

To illustrate the influence of the organic contaminants on the microbial populations the concentrations of ethylbenzene and *m*- and *p*-xylene for the three sites are shown in figure 3. Ethylbenzene was selected because it has similar biodegradability to benzene but is present at concentrations similar to *m*- and *p*-xylene. The behavior of *m*- and *p*-xylene is intermediate compared to toluene, which is highly degradable, and benzene, which is less degradable (Eganhouse and others, 1993). Between Sites B and C the average concentration of ethylbenzene drops slightly from about 0.4 to 0.3 milligrams per liter (mg/L). In contrast, the concentration of *m*- and *p*-xylene drops from 1-2 mg/L at Sites A and B to ~0.1 mg/L at Site C.

At Sites A and B, the methanogenic zones are associated with higher concentrations of ethylbenzene, *m*- and *p*-xylene, and dissolved iron (fig. 3). The correspondence between methanogenic zones and higher concentrations of contaminants suggests that these areas have been subjected to greater cumulative hydrocarbon fluxes over time. A comparison of the permeability profiles and the aqueous concentration data for Sites A and B indicates that there are two types of high organic concentration areas in the aquifer below the oil body. One is a relatively low permeability zone in the vicinity of the separate-phase oil where the flux rate is probably controlled by dissolution and diffusion. The second is a high permeability zone below the oil where the hydrocarbon flux is probably controlled by horizontal advection of water contaminated by separate-phase oil located upgradient.

The dissolved iron concentration profiles at Sites A and B closely correspond to the shapes of the hydrocarbon concentration profiles in this contaminant plume. Because total dissolved concentration can be quickly determined in the field with a portable spectrophotometer, it was useful as a field indicator to formulate our 1997 microbial sampling scheme. The peaks in the dissolved iron plume gave a good indication of where the methanogenic zones were located.

At Site C, near the edge of the anoxic zone (Cozzarelli and others, 1999), the picture is more complex. In the top two meters below the water table, the profiles of hydrocarbon concentrations correspond closely to the permeability profile. However, the peak in methanogens is found about a meter below the maximum hydrocarbon concentrations and the sediment Fe(III) is only slightly depleted. It is also not clear from the MPN data alone where transitions between iron-reducing and aerobic conditions are located. The MPN data show that iron-reducers and aerobes coexist at both the top and base of the profile. However, at both levels

dissolved Fe(II) is below detection and the cores were visually more orange colored compared to the center of the profile. These observations suggest that DO is at least intermittently present on the fringes of the profile. It seems possible that temporal changes in the ground water flow may create conditions that alternate between aerobic and iron-reducing on the fringes of the plume. Intermittent replenishing of the Fe(III) supply near the water table by oxidation of dissolved Fe(II) during water table fluctuations. might also explain the off-center position of the methanogenic zone at this location.

DISCUSSION AND CONCLUSIONS

The data set provides a consistent picture of methanogenic zones at various levels of development at the Bemidji site. The dominant physiologic type of the microbial population changes from iron-reducing to methanogenic over vertical scales as small as 25 cm. Near the oil body, methanogenic zones have evolved in two high-flux areas. One zone is found within the non-aqueous oil where high fluxes are due to local dissolution and diffusion of contaminants from the oil. A second zone exists along high permeability horizons in a laterally migrating contaminant plume. This zone appears to be continuous for more than 60 m downgradient.

Calculations based on the dissolution rate and total mass of the non-aqueous oil at the Bemidji site, indicate that the oil body may provide a continuous contaminant source for hundreds of years (Bekins and others, 1999). During this period, the methanogenic zones will continue to develop as sediment Fe(III) is depleted along the high permeability horizons. Although some recycling of Fe is expected, it is clear from the data (fig. 3) that some of the dissolved Fe(II) precipitates as Fe(II) solids in the anoxic zone.

The development of laterally continuous methanogenic zones along high permeability horizons has implications for risk analysis at sites where petroleum hydrocarbon contaminants are degrading by iron-reduction and methanogenesis. Because the hydrocarbon flux is greatest along high permeability horizons, worst-case migration scenarios should be based on two assumptions: first, continued iron reduction over the long term requires plume growth into previously uncontaminated aquifer sediments with fresh or recycled Fe(III); second, any projections of steady-state behavior should be based on methanogenic degradation capabilities and on estimated flow rates in the highest permeability horizons.

High permeability zones where methanogenic conditions develop may be very thin vertically, making them difficult to locate. At Site B, the methanogenic niche spans an interval of only 25 cm. This aspect of the plume also complicates interpretations of terminal electron processes. Cozzarelli (1993) noted that geochemical indicators became mixed when redox zones were very thin at a gasoline-contaminated site. At the Bemidji site, the strategy of collecting pore waters over 15 cm intervals and analyzing dissolved iron in the field was useful in locating the methanogenic zones.

Several aspects of the data warrant further investigation. Although Fe(III) is generally depleted in the methanogenic zones, significant extractable iron and culturable iron-reducers are still present, suggesting ongoing low levels of iron-reduction. At Sites A and B, high numbers of iron-reducers are present just below the oil at locations where the sediment Fe(III) is highly depleted. In contrast, very low numbers of iron-reducers are found at the center of the plume at Site B in spite of moderate levels of sediment Fe(III). Preferential use of favorable Fe(III) phases, along with natural variability of the Fe(III) phases on the sediments, may play a role in these observations. Another possibility is that proximity to the oil provides access to more favorable substrates such as toluene or to organic ligands. Cozzarelli and others (1994) demonstrated that organic ligands are present in higher concentrations near the oil body and Lovley and others (1994) demonstrated that organic ligands facilitate chelation of solid Fe(III) phases.

REFERENCES

Baedecker, M.J., Cozzarelli, I.M., Eganhouse, R.P., Siegel, D.I., and Bennett, P.C., 1993,

Crude oil in a shallow sand and gravel aquifer-III. Biogeochemical reactions and mass balance modeling in anoxic groundwater: Applied Geochemistry, v. 8, p. 569-586.

Bekins, B.A., Baehr, A.L., Cozzarelli, I.M., Essaid, H.I., Haack, S.K., Harvey, R.W., Shapiro, A.M., Smith, J.A., and Smith, R.L., 1999, Capabilities and challenges of natural attenuation in the subsurface: Lessons from the U. S. Geological Survey Toxics Substances Hydrology Program, in U.S. Geological Survey Toxic Substances Hydrology Program--Proceedings of the Technical Meeting, Charleston, South Carolina, March 8-12, 1999-- Volume 3 -- Subsurface Contamination from Point Sources: U.S. Geological Survey Water-Resources Investigations Report 99-4018C.

Bennett, P.C., Siegel, D.E., Baedecker, M.J., and Hult, M.F., 1993, Crude oil in a shallow sand and gravel aquifer-I. Hydrogeology and inorganic geochemistry: Applied Geochemistry, v. 8, p. 529-549.

Cherry, J.A., 1996, Conceptual models for chlorinated solvent plumes and their relevance to intrinsic remediation, in Proceedings of the Symposium on Natural Attenuation of Chlorinated Organics in Ground Water: Dallas, Texas, US EPA, p. 29-31.

Cozzarelli, I.M., Baedecker, M.J., Eganhouse, R.P., and Goerlitz, D.F., 1994, The geochemical evolution of low-molecular-weight organic acids derived from the degradation of petroleum contaminants in groundwater: Geochimica et Cosmochimica Acta, v. 58, p. 863-877.

Cozzarelli, I.M., Baedecker, M.J., Eganhouse, R.P., Tuccillo, M.E., Aiken, G.R., Bekins, B.A., and Jaeschke, J.B., 1999, Long-term geochemical evolution of the Bemidji Toxics site crude-oil plume, in U.S. Geological Survey Toxic Substances Hydrology Program--Proceedings of the Technical Meeting, Charleston, South Carolina, March 8-12, 1999-- Volume 3 -- Subsurface Contamination from Point Sources: U.S. Geological Survey Water-Resources Investigations Report 99-4018C

Cozzarelli, I.M., 1993, The biogeochemical fate of organic acids in a shallow aquifer contaminated with gasoline: Charlottesville, University of Virginia, 240 p.

Eganhouse, R.P., Baedecker, M.J., Cozzarelli, I.M., Aiken, G.R., Thorn, K.A., and Dorsey, T.F., 1993, Crude oil in a shallow sand and gravel aquifer-II. Organic geochemistry: Applied Geochemistry, v. 8, p. 551-567.

Essaid, H.I., Bekins, B.A., Godsy, E.M., Warren, Ean, Baedecker, M.J., and Cozzarelli, I.M., 1995, Simulation of aerobic and anaerobic biodegradation processes at a crude oil spill site: Water Resources Research, v. 31, no. 12, p. 3309-3327.

Godsy, E.M., Goerlitz, D.F., and Grbic-Galic, D., 1992, Methanogenic biodegradation of creosote contaminants in natural and simulated ground water ecosystems: Ground Water, v. 30, no. 2, p. 232-242.

Herkelrath, W.N., 1999, Impacts of remediation at the Bemidji oil spill site, in U.S. Geological Survey Toxic Substances Hydrology Program--Proceedings of the Technical Meeting, Charleston, South Carolina, March 8-12, 1999-- Volume 3 -- Subsurface Contamination from Point Sources: U.S. Geological Survey Water-Resources Investigations Report 99-4018C.

Hess, K.M., Herkelrath, W.N., and Essaid, H.I., 1992, Determination of subsurface fluid contents at a crude-oil spill site: Journal of Contaminant Hydrology, v. 10, p. 75-96.

Hult, M.F., 1984, Groundwater contamination by crude oil at the Bemidji, Minnesota, research site-An introduction, in Groundwater Contamination by Crude Oil at the Bemidji, Minnesota, Research Site: U.S. Geological Survey Water-Resources Investigations Report 84-4188, p. 1-15.

Krumbein, W.C. and Monk, G.D., 1942, Permeability as a function of the size parameters of unconsolidated sand: Transactions of the American Institute of Mining and Metallurgical Engineering, v. 151, p. 153-163.

Lovley, D.R., Baedecker, M.J., Lonergan, D.J., Cozzarelli, I.M., Phillips, E.J.P., and Siegel, D.I., 1989, Oxidation of aromatic

compounds coupled to microbial iron reduction: Nature, v. 339, p. 297-299.
Lovley, D.R., Woodward, J.C., and Chapelle, F.H., 1994, Stimulated anoxic biodegradation of aromatic hydrocarbons using Fe(III) ligands: Nature, v. 370, no. 14, p. 128-131.
Murphy, Fred and Herkelrath, W.N., 1996, A sample-freezing drive shoe for a wire line piston core sampler: Ground Water Monitoring and Remediation, v. 16, p. 86-90.
Postma, D., 1993, The reactivity of iron oxides in sediments: A kinetic approach: Geochimica et Cosmochimica Acta, v. 57, p. 5027-5034.
Smith, R.L., Harvey, R.W., and LeBlanc, D.R., 1991, Importance of closely spaced vertical sampling in delineating chemical and microbiological gradients in groundwater studies: Journal of Contaminant Hydrology, v. 7, p. 285-300.
Tuccillo, M.E., Cozzarelli, I.M., and Herman, J.S., 1999, Iron reduction in the sediments of a hydrocarbon-contaminated aquifer: Applied Geochemistry, v. 4, no. 5, p. 71-83.
Wiedemeier, Todd, Wilson, J.T., Kampbell, D.H., Miller, R.N., and Hansen, J.E., 1995, Technical protocol for implementing intrinsic remediation with long-term monitoring for natural attenuation of fuel contamination dissolved in groundwater, Volume I: Air Force Center for Environmental Excellence, Technology Transfer Division, Brooks Air Force Base.

AUTHOR INFORMATION

Barbara A. Bekins, Hedeff I. Essaid, E. Michael Godsy, Victor V. Paganelli, Ean Warren, U.S. Geological Survey, Menlo Park, California

Isabelle M. Cozzarelli, U.S. Geological Survey, Reston, Virginia

Mary Ellen Tuccillo, University of Virginia, Charlottesville, Virginia

Long-Term Monitoring of Unsaturated-Zone Properties to Estimate Recharge at the Bemidji Crude-Oil Spill Site

By Geoffrey N. Delin and William N. Herkelrath

ABSTRACT

Ground-water recharge is an important factor affecting the Bemidji, Minnesota crude-oil spill site. About 400,000 liters of crude oil remained in the ground after remediation was completed following the 1979 pipeline break. An automated data logging system was used to measure unsaturated zone properties relevant to estimating recharge and to evaluate their effects on dissolution of the oil. Laboratory and field testing of several soil-moisture probes indicated that the CS615 probe was better suited to estimating recharge in the glacial outwash at the Bemidji crude-oil spill site than the CS605 probes. Both probes are manufactured by Campbell Scientific Inc. The CS615 probe provided dependable and accurate data over long time periods, using a limited power supply, under the extreme weather conditions typical of northern Minnesota. Based on results of the testing, arrays of the CS615 probes, zero-maintenance tensiometers, and thermocouples were installed in the unsaturated zone at the north oil pool in the fall of 1998. Computer simulations indicated that the rate of dissolution from the oil body is linearly related to the recharge rate. Additional multiphase flow model analyses are being conducted to quantify this increased dissolution. Additional model analyses are also being conducted to evaluate how dissolution is affected by recharge that varies in relation to the presence of crude oil in the unsaturated and saturated zones, discontinuous lenses of lacustrine silt and clay, and topography. The VS2DT code is also being used to estimate recharge rates and to evaluate the movement of water through the oil.

INTRODUCTION

Ground-water recharge is an important factor affecting the Bemidji, Minnesota crude-oil spill site. Although most recharge occurs as a result of spring snowmelt, its spatial and temporal variability at the site is complex and poorly understood. Recharge varies spatially in relation to the presence of crude oil in the unsaturated and saturated zones, discontinuous lenses of lacustrine silt and clay, and topography. Little is known of how ground-water recharge (in relation to these factors) affects the dissolution, transport, and degradation of oil at the site. Preliminary model analyses have indicated that ground-water recharge is a critical factor affecting the transport and dissolution rates of oil at the site.

This paper presents preliminary results of an investigation to better understand the effects of recharge on the dissolution and movement of oil through the unsaturated and saturated zones at the Bemidji, Minnesota crude-oil spill site. Included are selected results of measurements being used to monitor water movement through the unsaturated zone and to quantify ground-water recharge. Recharge estimates based on unsaturated-zone measurements are compared to estimates based on hydrograph analysis.

Site Description

On August 20, 1979, approximately 16 kilometers northwest of Bemidji, Minnesota, the land surface and shallow subsurface were contaminated when a crude-oil pipeline burst, spilling about 1,700,000 L (liters) (about 10,700 barrels) of crude oil onto a glacial outwash deposit. Crude oil also sprayed to the southwest covering an approximately 7,500 m^2 (square meter) area of land. After cleanup efforts were completed about 400,000 L (about 2,500 barrels)

of crude oil remained at the site. Some crude oil percolated through the unsaturated zone to the water table near the rupture site (north oil pool, fig. 1). Some of the sprayed oil flowed over the land surface toward a small wetland forming a second area of oil infiltration (south oil pool).

Ground water affected by the oil spill discharges to a small lake 400-m east of the pipeline. The land surface is a glacial outwash plain underlain by stratified glacial outwash deposits. Sediments at the test site consist of poorly sorted glacial outwash sand of fine to very coarse grain size, with some fine gravel and cobbles. One- to 10-mm (millimeter) thick iron-cemented laminations occur between depths of 0.3 and 1.0 m. At a depth of about 25 m, a regionally persistent and uniform layer of low permeability sediment (till) restricts vertical ground-water movement. Crude oil (about 0.4-0.5- m thick) floats on the water table, which is about 2.7 m below land surface at the south oil pool. The water table is about 6 m below the land surface at the north oil pool.

Methods

An automated data logging system was installed near Well 981 (south oil pool) in late 1996 primarily to compare the performance of several different soil-moisture probes manufactured by Campbell Scientific Inc.[1] Three different soil-moisture probes were compared to determine which was the most appropriate for evaluating recharge at the north oil pool, which is the primary area of research interest. Other data collected at the site included soil temperature (at ½ -meter depth intervals), ground-water level, and precipitation. The soil moisture and other data were collected 6 times per day from late 1996 to present. Solar-charged batteries initially powered the CR10X data logger and time-domain reflectometry (TDR) system. The batteries were replaced in the fall of 1997 with 110-volt AC power.

Three types of Campbell Scientific soil-moisture probes were compared at the Well 981 site (fig. 2). The CS615 probes were 30-cm (centimeter) long and had 2 prongs. The CS615 is a self-contained "reflectometer" that does not require a TDR cable tester to determine water content. This probe was compared to two CS605 three-prong TDR probes (30-cm long and 50-cm long) that require a cable tester. An array of 4

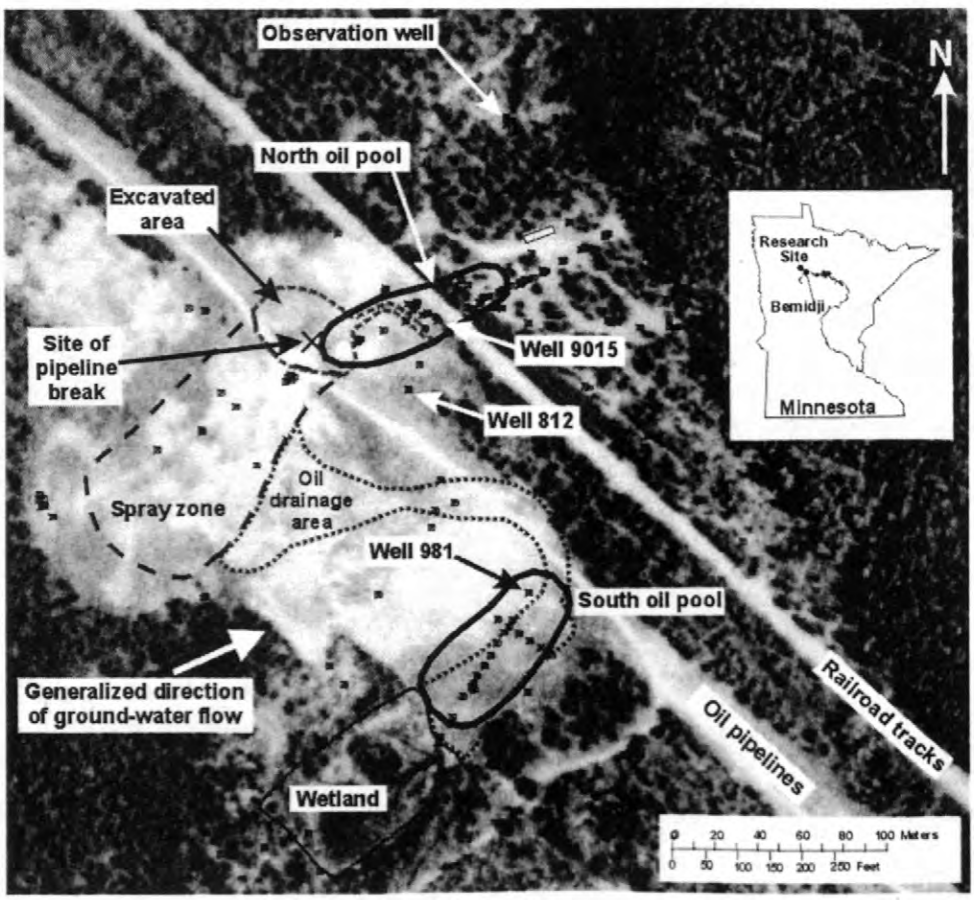

Figure 1. Features of the Bemidji crude-oil spill research site superimposed on a 1991 aerial photograph.

[1] The use of brand names herein is for identification purposes only and does not constitute endorsement by the U.S. Government.

probes of each type was installed horizontally at ½ -meter depth intervals in the wall of a 2-meter-deep pit. A fourth array of vertically oriented

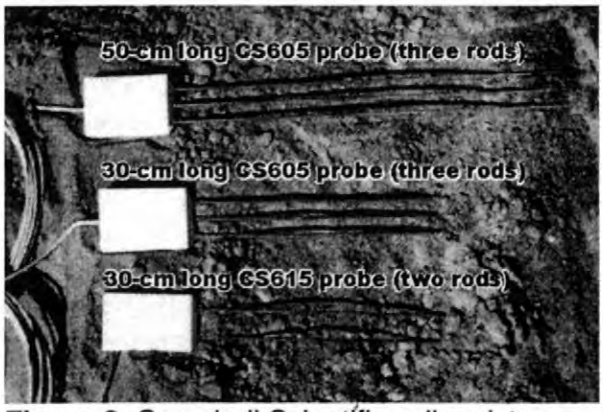

Figure 2. Campbell Scientific soil moisture probes used at the Bemidji crude-oil spill site.

CS605 30-cm long probes was also installed at ½-m depth intervals in small-diameter boreholes to evaluate how probe orientation affected soil-moisture measurements.

Using the methods described in Herkelrath and others (1991), the three types of soil-moisture probes were calibrated in the laboratory using repacked columns of sandy sediments obtained from the field site. The columns were saturated from the bottom through a tube. Relative permittivity of the sediments was determined for the saturated sample using each soil-moisture probe. The column mass was determined by weighing. Water was removed incrementally through the bottom of the column by suction with permittivity and mass being measured for each increment. Total water content corresponding to each measurement was calculated from the difference between the measured column mass and the oven-dry mass. Volumetric water contents were determined by the ratio of total water content to soil volume.

Ground-water recharge estimated using the soil-moisture data near Well 981 was based on a rudimentary water balance. The primary assumption is that water in the soil above a certain depth (boundary) in the unsaturated zone moves upward in response to evapotranspiration and water below that boundary drains to the water table. Seasonal movement of the evapotranspiration/drainage boundary is typically measured directly using soil-water tensiometers. Several tensiometers were installed at the site, but the instruments failed, and the measured data could not be reliably used. Therefore, the depth of the boundary was assumed to be 50 cm during the summer months based on previous research (unpublished data). These recharge estimates were compared to estimates based on the method of hydrograph analysis (Rasmussen and Andreason, 1959). The hydrograph analysis method is based on relating changes in water-table elevation measured in a well with changes in the amount of water stored in the aquifer. The change in storage is attributed to ground-water recharge. Recharge is equivalent to the water table rise over a given time period multiplied by the aquifer specific yield of 0.3.

RESULTS AND DISCUSSION

Results of laboratory tests indicated that the moisture content calculated using the factory-supplied calibration for the CS615 probe was accurate to within about +/- 0.02 cc/cc (cubic centimeters per cubic centimeter) of the actual value over the whole moisture content range (fig. 3). This error was deemed acceptable and the field data were not adjusted. The moisture content values calculated using the factory-supplied calibration for the CS605 probes were generally higher than the actual moisture content. Therefore, the field data were shifted downward

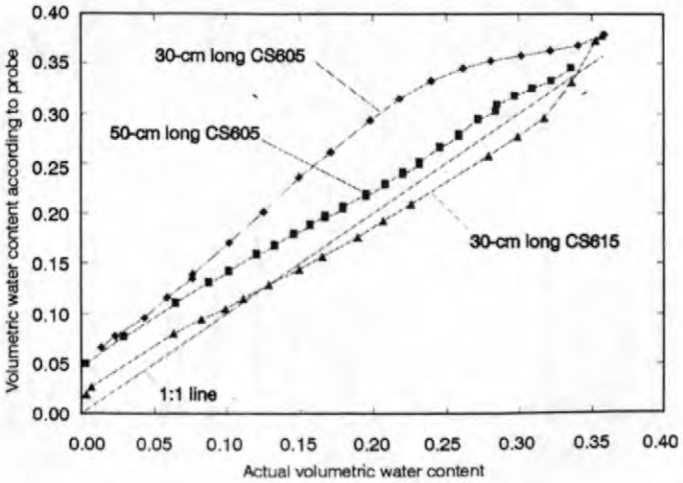

Figure 3. Calibration results for the Campbell Scientific soil moisture probes used at the Bemidji crude-oil spill site.

0.07 and 0.02 cc/cc, respectively, for the 30-cm-long and 50-cm-long CS605 probes.

Temperature Measurements

Analysis of the temporal variation in soil temperature was both qualitatively and quantitatively useful in estimating the timing, depth, and duration of recharge events. The typical profile of soil temperature with depth is observed in figure 4 where the normal summer pattern of decreasing temperature with depth becomes inverted during October, followed by increasing temperatures with depth during the winter months. The thermocouples detected wetting front movement following precipitation events that exceeded about 2 cm, most noticeably the event during early July 1997 (fig. 4). Soil temperatures generally decreased following each of these precipitation events, with slightly smaller decreases at greater depths. The shifting low temperature with depth following the July precipitation (recharge) event is evidence of movement of the recharge water through the unsaturated zone. This shift in temperature with depth and time is not noticeable for precipitation events that did not result in ground-water recharge, such as the one on August 19th. In addition to the late summer and fall time period represented in figure 4, the temperature data also proved very useful in determining the timing of recharge from spring snowmelt.

Comparison Of Soil-Moisture Probes

Each type of soil-moisture probe simultaneously detected wetting front movement at the 150-cm depth following precipitation events (fig. 5). The greatest difference in measured soil moisture between the probes occurred during precipitation events when the magnitude of the soil-moisture changes for the vertically oriented CS605s were much greater than that for the other probes. This phenomonon was observed at both the 100- and 150-cm depths. The vertical probe orientation caused the wetting fronts to be detected for a much longer period of time than for the horizontally oriented probes.

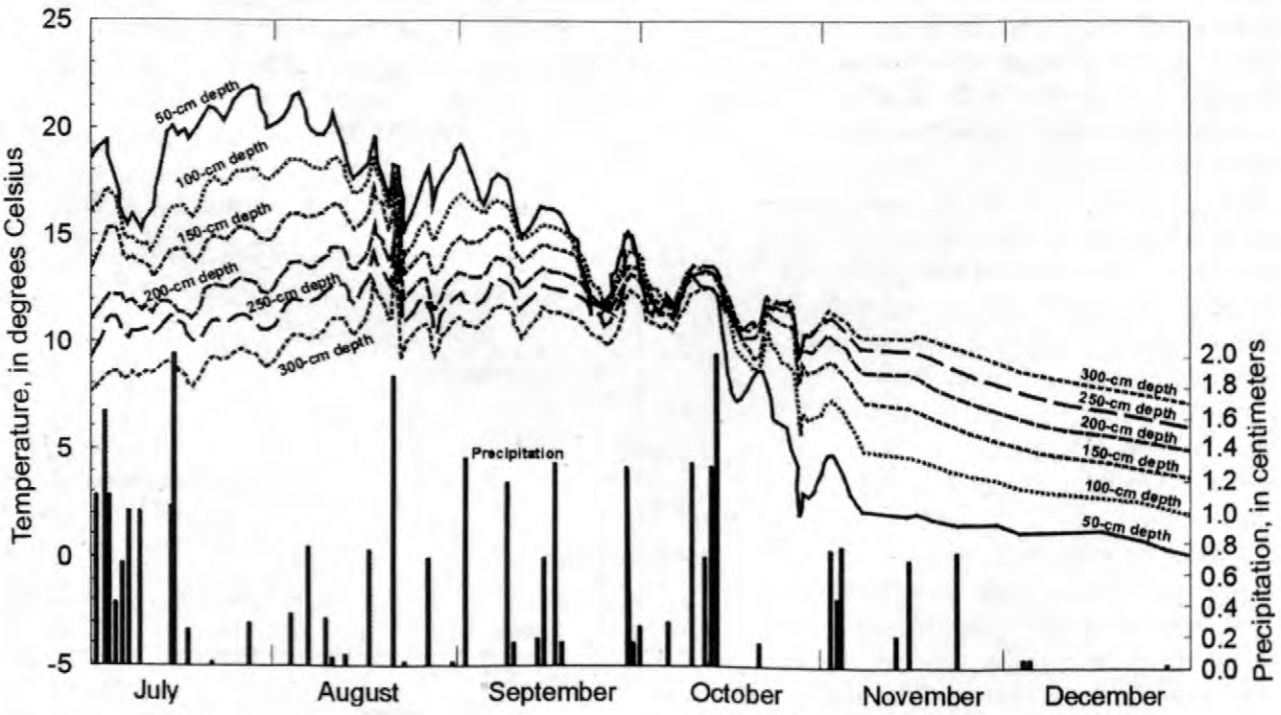

Figure 4. Soil temperature and precipitation near Well 981, July – December 1997.

The resultant apparent soil moisture during these recharge periods was necessarily greater. The slightly greater soil moisture measured by the CS615s than the horizontally oriented CS605s likely is due to localized differences in soils. Soil moisture measured with the 50-cm long CS605s did not fluctuate as much as for the 30-cm long CS605s. This may be an indication that a longer probe provides a more stable response to changes in soil moisture.

Soil-moisture values measured with the CS615s were much more stable and "clean" (less data fluctuation and data loss) than those measured with the CS605s, which were comparatively "noisy" (figs. 5 and 6). Data loss for the CS615s was less than 1 percent, with virtually all losses being unrelated to the probe itself. In contrast, data loss for the CS605s was notable with each of the CS605 probes having lost at least 5 percent of the data during each year of operation. During the first 6 months of 1997, for example, data loss for the CS605s was as follows: 12 percent for the 30-cm long (horizontally oriented) probes; 15 percent for the 30-cm long (vertically oriented) probes; and 22 percent for the 50-cm long (horizontally oriented) probes. During the same time period in 1998 these data losses were about two times greater, indicating a progressive increase of data loss in time.

Data collected with all three of the CS605s at the 300-cm depth were very sparse, with data losses of greater than 80 percent per probe. A comparison of figures 5 and 6, which have the same vertical scales, provides a good indication of the "noise" in the CS605 probes at this depth. Each of the probes at this depth was located below the water table and thus the soil moisture should not have changed significantly over time. Some of the data loss for the CS605s likely resulted from variations in power supply voltage and line noise that caused out-of-range (positive and negative) values. Loss of data with the CS605s critically affects recharge estimates resulting in inaccurate or missing recharge estimates.

During the time when the monitoring system was initially powered by solar-charged batteries, data loss for the CS605s increased

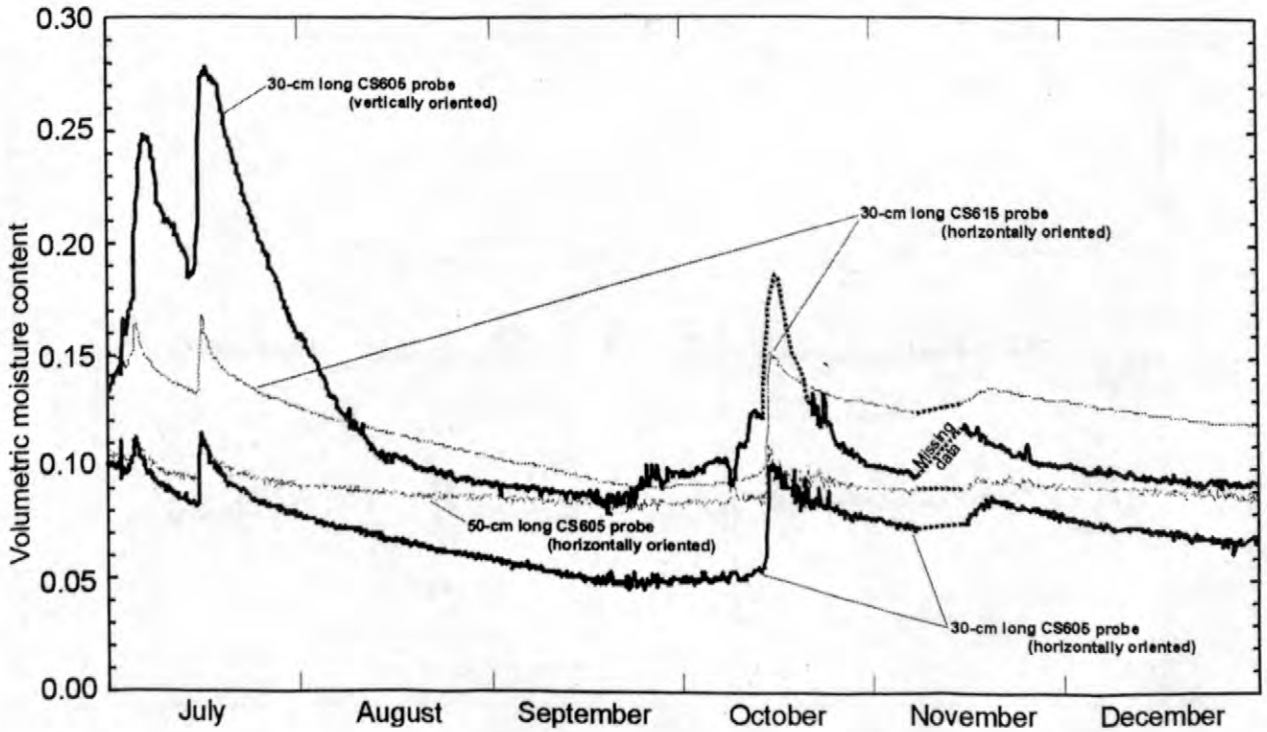

Figure 5. Soil moisture at the 150-cm depth near Well 981 measured with the different probes, July – December 1997.

during the winter months when air temperatures were below -10°C. This increased data loss was likely due to insufficient solar radiation during the winter to charge the batteries to power the cable tester. Conversely, the CS615 probes had sufficient power to make their measurements during the winter months.

The two-pronged CS615 probe was easier to install than the three-pronged CS605 probe, largely because of increased friction and the enhanced likelihood of hitting gravel with the third prong. However, greater care was required during installation of the CS615s to ensure that the internal circuitry was not damaged. The 50-cm long CS605s were most difficult to install because of their greater length, which increased friction and the likelihood of hitting gravel.

Recharge Estimates

Ground-water recharge was estimated using the soil moisture data and by the hydrograph analysis method for all events where precipitation exceeded about 2.0 cm. For the three precipitation events that occurred during the last six months of 1997 (fig. 7), for example, recharge based on data from the horizontally oriented 30-cm long CS615 and CS605 probes were similar. Small-scale soil heterogeneity rather than differences in the way soil moisture is measured by each probe likely cause the slightly different recharge estimates for these probes.

Recharge based on the vertically oriented 30-cm long CS605 probes during the early July event was about 70 percent greater than for the other probes (fig. 7). This greater recharge for the vertically oriented probe was typical during the study. The vertical probe orientation caused the wetting fronts to be detected for a much longer period of time than for the horizontally oriented probes, which generally resulted in a higher estimated recharge rate. This was not always the case, however, as evidenced by the less than average recharge estimate for the vertically oriented probes during the mid October 1997 event (fig. 7). These inconsistent results are further evidence that the vertical probe orientation is not appropriate for recharge estimation at this site.

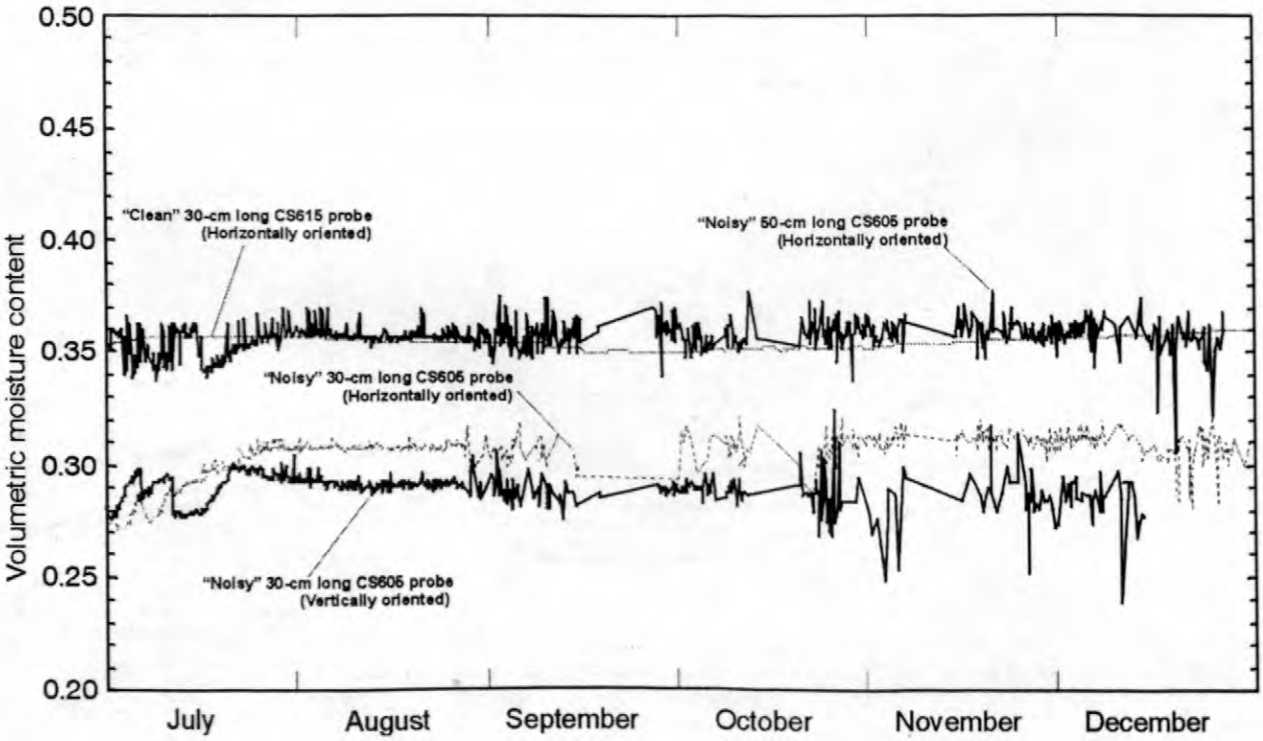

Figure 6. Soil moisture at the 300-cm depth near Well 981 measured with the different probes, July – December 1997.

The method of hydrograph analysis was applied to the three recharge events that occurred during the second half of 1997. Because the two July precipitation events occurred only about two weeks apart (fig. 5) the effects of both events were superimposed in the ground-water hydrograph response (figs. 7 and 8). Thus, only one recharge estimate is presented for the two July events. The well used for hydrograph analysis at the 981 site was installed in August 1997. Thus, data from a nearby datalogger at Well 812 were used for estimating recharge during the July recharge event (fig. 8). Use of water-level data from the two different wells shown in figure 8 may have introduced some error when comparing the recharge estimates for this time period.

Recharge estimates based on hydrograph analysis were generally 20-40 percent less than estimates based on the soil-moisture probes for events in 1997 and 1998. For example, total recharge based on hydrograph analysis for the three 1997 events shown in figure 7 was 11 cm or about 30 percent less than estimates based on the horizontally oriented probes. The several limiting assumptions behind both of the recharge estimation methods are the most likely causes for the differing estimates. Application of other methods such as tritium/helium (Solomon and others, 1993) is being employed at the site to obtain a more accurate recharge estimate.

Model Analyses

Computer simulations indicate that the rate of dissolution from an oil body is linearly related to the recharge rate. Water permeabilities estimated from a multiphase flow model (Essaid and others, 1995) were used in MODFLOW (McDonald and Harbaugh, 1988; Harbaugh and McDonald, 1996) and MODPATH (Pollock, 1994) simulations to evaluate steady state water movement through the oil body. When there is no recharge, most of the ground water flows around the oil body and does not come in contact with the oil. However, recharge water flows

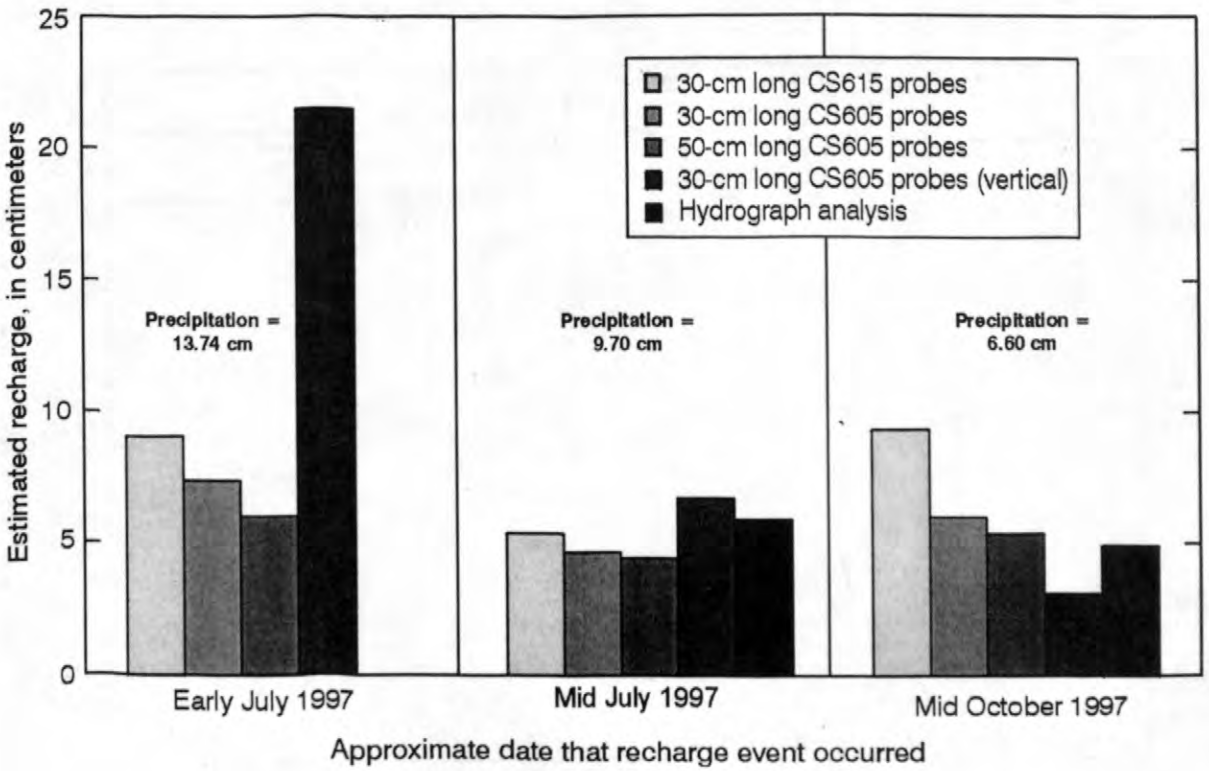

Figure 7. Recharge estimates based on the different probes near Well 981 compared to estimates based on hydrograph analysis, July – December 1997.

downward through the oil body and increases the contact between ground water and the oil, increasing the rate of dissolution.

SUMMARY AND CONCLUSIONS

Ground-water recharge is an important factor affecting the Bemidji, Minnesota crude-oil spill site where about 400,000 liters of crude oil remained in the ground after remediation was completed following the 1979 pipeline break. An automated data logging system was used to measure unsaturated zone properties relevant to estimating recharge and evaluating their effects of the dissolution of oil. The performance of several different soil-moisture probes manufactured by Campbell Scientific Inc. was evaluated. Analysis of the temporal variation in soil temperature was both qualitatively and quantitatively useful in estimating the timing, depth, and duration of recharge events.

Laboratory and field testing of the soil-moisture probes indicated that the Campbell Scientific CS615 probe was better suited to estimating recharge at the Bemidji crude-oil spill site than the CS605 probes, given the local soil and climatic conditions. Field testing indicated that the CS615 probes are better suited to the needs at the Bemidji site for the following reasons: (1) the CS615 probes provided a dependable and accurate means for long-term monitoring of soil moisture in the glacial outwash being studied; (2) the CS615 probe is somewhat easier to install in sandy soils than the standard CS605 probe; (3) data from the CS615 probes had less "noise" than data from the standard CS605 probes; and (4) the CS615 probe provided dependable and accurate data using limited power under the extreme weather conditions typical of northern Minnesota. The greater soil moisture measured by some of the vertically-oriented CS605 probes is somewhat surprising. Further

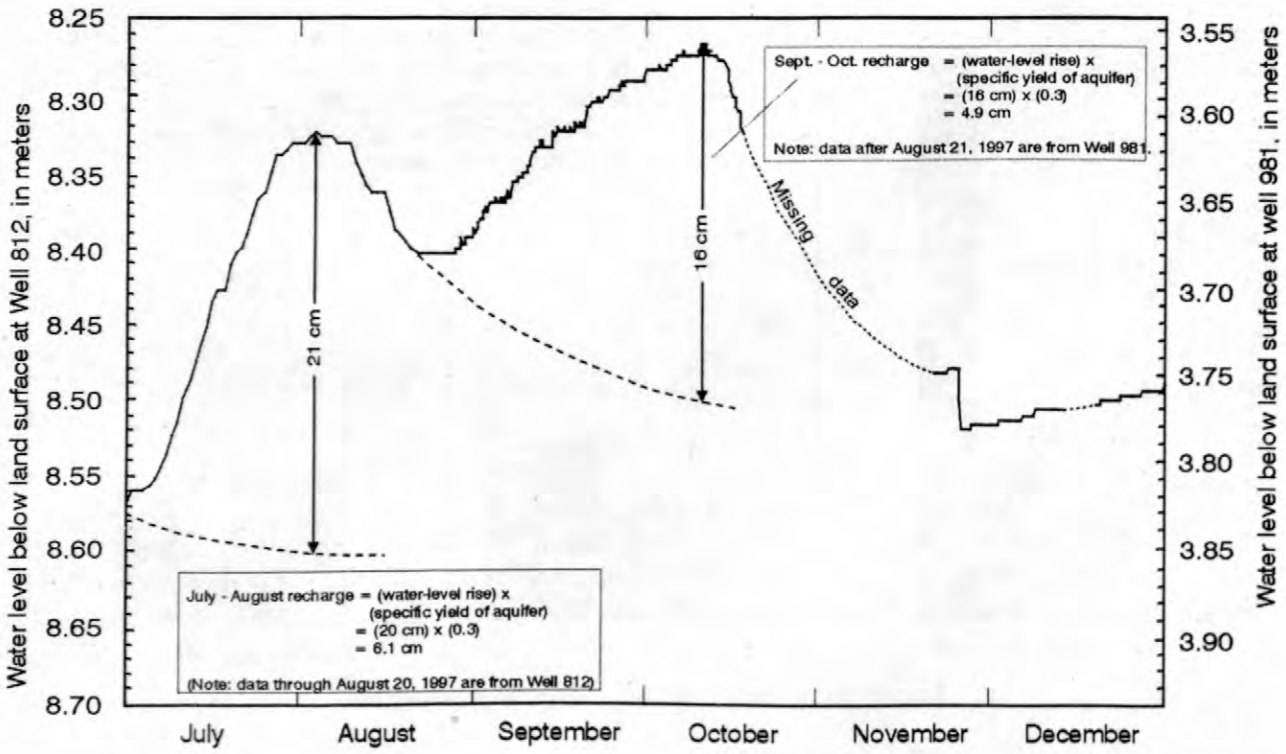

Figure 8. Water-level hydrograph and recharge calculations, July – December 1997.

laboratory or field research into this phenomenon may be warranted, the results of which would have transfer value to unsaturated-zone research using similar instrumentation.

Based on results of the preliminary testing, an array of CS615 soil-moisture probes, thermocouples, and zero-maintenance tensiometers were installed in the unsaturated zone near Well 9015 (north oil pool) in the fall of 1998. Seven CS615 probes and thermocouples were installed between the depths of 0.5 and 6.0 m. Four zero-maintenance tensiometers were installed between the depths of 1.0 and 2.5 m. The soil moisture and pressure data will be used to estimate ground-water recharge based on the zero flux plane method and to evaluate the effects of the dissolution of oil.

Computer simulations indicated that the rate of dissolution from the oil body is linearly related to the recharge rate. Additional multiphase flow model analyses are being conducted to quantify this increased dissolution. Additional multiphase flow model analyses are also being conducted to evaluate how dissolution is affected by recharge that varies in relation to the presence of crude oil in the unsaturated and saturated zones, discontinuous lenses of lacustrine silt and clay, and topography. The VS2DT code (Lappala and others, 1987; Healy, 1990) is also being used to estimate recharge rates and to evaluate the movement of water through the oil.

CITED REFERENCES

Essaid, H.I., Herkelrath, W.N., and Dillard, L.A., 1995, The influence of spatial variability of hydraulic properties on the flow of water near a subsurface oil body: EOS, Transactions, American Geophysical Union, v. 76, no. 46, p. F266.

Harbaugh, A.W., and McDonald, M.G., 1996, User's documentation for MODFLOW-96, an update to the U.S. Geological Survey modular finite-difference ground-water flow model: U.S. Geological Survey Open-File Report 96-485, 56 p.

Healy, R.W., 1990, Simulation of solute transport in variably saturated porous media with supplemental information on modifications to the U.S. Geological Survey's Computer Program VS2D: U.S. Geological Survey Water-Resources Investigations Report 90-4025, 125 p.

Herkelrath, W.N., Hamburg, S.P., and Murphy, Fred, 1991, Automatic, real-time monitoring of soil moisture in a remote field area with time-domain reflectometry: Water Resources Research, v. 27, no. 5, p. 857-864.

Lappala, E.G., Healy, R.W., and Weeks, E.P., 1987, Documentation of computer program VS2D to solve the equations of fluid flow in variably saturated porous media: U.S. Geological Survey Water-Resources Investigations Report 83-4099, 184 p.

McDonald, M.G., and Harbaugh, A.W., 1988, A modular three-dimensional finite-difference ground-water flow model: U.S. Geological Survey Techniques of Water-Resources Investigations, book 6, chap. A1, 586 p.

Pollock, D.W., 1994, User's Guide for MODPATH/MODPATH-PLOT, Version 3—A particle tracking post-processing package for MODFLOW, the U.S. Geological Survey finite-difference ground-water flow model: U.S. Geological Survey Open-File Report 94-464, 6 ch.

Rasmussen, W.C., and Andreason, G.G., 1959. Hydrologic budget of the Beaver Dam Creek Basin Maryland. U.S. Geological Survey Water-Supply Paper 1472, 106 p.

Solomon, D.K., Schiff, S.L., Poreda, R.J., and Clarke, W.B., 1993, A validation of the $^{3}H/^{3}He$ method for determining groundwater recharge: Water Resources Research, v. 29, no. 9, p. 2951-2962.

AUTHOR INFORMATION

Geoffrey N. Delin, U.S. Geological Survey, Mounds View, Minnesota (delin@usgs.gov)

William N. Herkelrath, U.S. Geological Survey, Menlo Park, California (wnherkel@usgs.gov)

Coupled Biogeochemical Modeling of Ground-Water Contamination at the Bemidji, Minnesota, Crude Oil Spill Site

By Gary P. Curtis, Isabelle M. Cozzarelli, Mary Jo Baedecker, and Barbara A Bekins

ABSTRACT

Fully-coupled multicomponent reactive solute transport simulations were preformed for the groundwater contamination at the Bemidji, MN crude oil spill site. The simulations included the oxidation of the dissolved crude oil constituents by microorganisms using four different terminal electron acceptors: O_2, MnO_2, $Fe(OH)_3$ and CO_2. The simulations also accounted for the dissolution of reactive phases resulting from the limited amount of each reactant, the formation of new phases containing Mn^{2+} and Fe^{2+}, and the outgassing of CO_2 and CH_4. The simulations assumed that O_2 was used preferentially and that all other terminal electron acceptors were used in parallel. Simulation results are presented that reproduce many of the features illustrated by the field data including the disappearance of the O_2, the appearance of Mn^{2+}, Fe^{2+}, and CH_4, the pH values, the diminished concentrations of solid phases Fe^{+3} beneath the oil body as well as the increase in Fe^{+3}-containing solid phase concentrations in the dow

INTRODUCTION

The dissolution and biodegradation of crude oil in an unconfined aquifer near Bemidji, MN has caused a diverse range of geochemical changes. Baedecker and others (1993) identified five geochemical zones that have developed as a result of these biodegradation reactions. These zones are depicted in figure 1 as zones I-V. Briefly, these zones have been described as: (I) the background water which is a Ca-Mg-HCO_3 water with a pH 7.6 to 7.8, that is saturated with oxygen, (II) a mixed zone characterized by low O_2 and elevated dissolved organic carbon (DOC), (III) an anaerobic zone with high concentrations of DOC, Fe^{2+}, Mn^{2+} and CH_4, and a pH of 6.8, (IV) a transition zone between highly reducing conditions and oxidized conditions, and (V) an impacted zone, that shows elevated concentrations of Ca and Mg.

There have been at least three previous reports on modeling the geochemical changes in the Bemidji aquifer but none have conducted fully coupled modeling. Bennett and others (1993) matched the water composition in the anoxic core of the plume by conducting reaction path calculations that mixed water from a silty layer near zone II with water from the boundary between zones II and III followed by oxidation of DOC by goethite. Baedecker and others, (1993) reported on a reaction-path model along a flow path from the zone III toward zone IV. The simulations required outgassing of CO_2 and CH_4 even though the flow path was 2 meters below the water table surface. Although these mixing and reaction path calculations can account for some geochemical changes, they do not account for any limitations imposed on the hypothesized mixing by the flow system.

Essaid and others (1995) conducted two dimensional reactive transport simulations that accounted for the biodegradation of crude oil, the consumption of O_2, solid phase Mn(IV) and solid phase Fe(III) and the production of dissolved Mn^{2+}, Fe^{2+}, and CH_4. These rate-controlled simulations showed that many of the features of the plume could be reproduced including the disappearance of O_2, the appearance of Mn^{2+}, Fe^{2+}, CH_4 and the disappearance of DOC, and volatile DOC, the two forms of dissolved crude oil

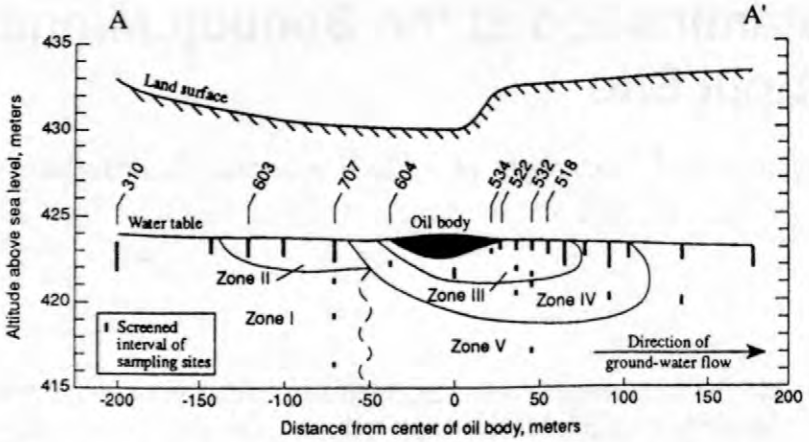

Figure 1. A cross section of the Bemidji aquifer (after Baedecker and others, 1993).

considered. These simulations did not include inorganic reactions including the carbonate system or the redox reactions involving O_2 and the reduced forms of Mn and Fe. In addition, precipitation of new phases containing reduced Fe and Mn was accounted for using a single constant for each metal and the formation of new phases containing oxidized Fe and Mn in the transition zone was ignored. Accurately accounting for these reactions may be important because they involve the electron acceptors for the biodegradation reactions which cause the geochemical changes in the aquifer.

The objectives of this work were to demonstrate the use of RATEQ (Curtis, in preparation), a fully coupled model for simulating biogeochemical transport, and to reproduce the field observations for multiple inorganic and organic species.

CONCEPTUAL MODEL

Geochemical Reactions

Modeling reactions involving the degradation of dissolved crude oil is difficult, in part, because crude oil is a complex mixture of many individual compounds. In view of this complexity, the dissolved crude oil is represented here as a generic hydrocarbon and denoted as CH (Baedecker and others, 1993; Bennett and others, 1993). This approach establishes the nominal redox-state of the crude oil and allows one to express the degradation reactions as stoichiometrically balanced reactions. Formulating these reactions is critical for both mathematically coupling the oxidation of the electron donors (CH) to the different terminal electron acceptors, and for formulating the fully-coupled, multicomponent mass balance model. The half-reaction for the formation of CH is

$$0.2\ CO_{2(g)} + H^+ + e^- = 0.2\ CH + 0.4\ H_2O \qquad (1)$$

The logarithm of the equilibrium constant (log K) for this reaction was found to be 2.1 using the approach of MacFarlane and Sims (1993).

In the aquifer at Bemidji, the dominant electron acceptors available for the oxidation of CH are O_2, solid phase Mn(IV), solid phase Fe(III), and CO_2. Neither NO_3^- nor SO_4^{-2} are significant electron acceptors in this system because the concentration is too small (Baedecker and others, 1993, Bennett and others, 1993). The half-reactions for the electron acceptors are coupled with that for the electron donor (eqn 1) to give the final, stoichiometrically balanced reaction for the oxidation of the hydrocarbon (table 1). Each reaction in table 1 is written for the oxidation of 0.2 moles of CH. Thus, the log K values illustrate the thermodynamic basis for the sequential use of electron acceptors that is often observed for microbial processes.

In addition to the reactions involving the biodegradation of the dissolved crude oil, many other geochemical reactions occur in the aquifer.

Table 1: Reactions for the oxidation of CH by various electron acceptors.

Reactions		log K
.2 CH + .25 O_2(g) + .1 H_2O	= .2 HCO_3^- + .2 H^+	18.6
.2 CH + .5 $MnO_{2(s)}$ +.8 H^+	= .2 HCO_3^- + .5 Mn^{2+} + .4 H_2O	18.6
.2 CH + $Fe(OH)_{3(s)}$ + 1.8 H^+	= 2 HCO_3^- + Fe^{2+} + 2.4 H_2O	13.9
.2CH + .225 H_2O	= .075 HCO_3^- +.125 CH_4 +.075 H^+	.9

The bulk mineralogy of the Bemidji aquifer consists primarily of quartz, feldspars, calcite and dolomite, (Bennett and others, 1993). For the simulations presented here, calcite and dolomite were included in the simulations, as were the aqueous carbonate and hydroxide species. In addition, a number of other redox reactions, sometimes called secondary reactions (Hunter and others, 1998), such as the oxidation of Fe^{+2} by MnO_2 or O_2 have been included.

One-dimensional reactive transport simulations were conducted along a 400m flow tube that extends from A to A' on figure 1. The initial conditions and the influent boundary condition were taken to match the average groundwater chemistry at well 310. The reactive phases and their relative amounts, expressed in units of moles of solid per liter of groundwater were; calcite (2M), dolomite (.25M), MnO_2 (0.001M) and $Fe(OH)_3$ (0.12M). Given that the O_2 concentration in the aquifer was $2.5x10^{-4}$M, $Fe(OH)_3$ clearly has the potential to be one of the most important electron acceptors in the aquifer. Note that if all of $Fe(OH)_3$ was reduced by CH, there would be a consumption of approximately 0.2 mole of H^+ per liter of aquifer (table 1). Extractions of cores taken from the site showed that after approximately 14 years half of the initial of $Fe(OH)_3$ present beneath the oil body had been removed (Tuccillo and others, 1998) suggesting that there was a large consumption of H^+. Because of this large consumption of H^+, which tends to increase the pH, matching the observed decrease in the field pH was difficult.

REACTIVE TRANSPORT SIMULATIONS

The crude oil was assumed to dissolve into the groundwater according to a first order dissolution process:

$$\frac{\partial C}{\partial t} = k_{diss}(C_s - C) \qquad (2)$$

where

C is the concentration of CH

C_s is the concentration of the CH in equilibrium with the crude oil, and

k_{diss} is the first order dissolution constant.

The dissolution rate used in the simulations varied with distance along the flow path. The first order dissolution rate constant was zero except in Zone II (25 to 100 m upgradient from the center of the oil body) where the value was $5x10^{-4}$ d^{-1} and in Zone III (25 upgradient to 25m down gradient from the center of the oil body) where the value was $5x10^{-2}$ d^{-1}. Outside of the zones where oil was assumed to be dissolving into the groundwater, the system was assumed to be in contact with atmospheric concentrations of O_2. This was included downgradient of the oil body as an approximation to the annual water table fluctuations of approximately 0.5 m.

Degradation Rates

The reactive transport simulations presented here assumed that the microbial populations were constant in space and time. This assumption simplified the parameter estimation because it was difficult to obtain

growth and decay parameters that gave acceptable simulation results. This difficulty may have been because of the autocatalytic nature of the reaction stoichiometry; if the biomass is allowed to vary, then the rate of the biodegradation reaction depends on the biomass produced by the reaction. A second difficulty encountered with simulating microbial growth was that the populations tended to grow unbounded which contrasts with moderate populations observed in the field (Essaid and others 1995). The actual growth may be limited by nutrients such as phosphorous (Rodgers and others, 1999), or nitrogen (Essaid and others, 1995), although in the latter study it was found that it was still necessary to artificially limit growth. The assumption of a constant biomass is consistent with the approach used to simulate biodegradation with very low amounts of biomass produced per mole of carbon oxidized for methanogens at a creosote spill at Pensacola, FL (Bekins and others, 1993).

Although the biomass was assumed to be constant in time, a dual Monod kinetics fromulation was used to simulate the reaction between the electron donor and the electron acceptor. For example, the oxidation of CH by $Fe(OH)_3$, has a rate law of the following form:

$$r = v_{\max}\left(\frac{C_{CH}}{C_{CH}+K_{CH}}\right)\left(\frac{C_{Fe}}{C_{Fe}+K_{Fe}}\right)\left(\frac{I_{O2}}{C_{O2}+I_{O2}}\right)$$

where

- v_{max} the maximum rate of substrate utilization,
- C_{CH} is the concentration of CH,
- K_{CH} is the half-velocity coefficient for the oxidation of CH by $Fe(OH)_3$,
- C_{Fe} is the concentration of $Fe(OH)_3$,
- K_{Fe} is the half-velocity coefficient for the reduction of $Fe(OH)_3$ by CH,
- I_{O2} is the inhibition constant for the effect of O_2 on the Fe reduction rate, and
- C_{O2} is the concentration of O_2.

Rate expressions of this form are used for each of the reactions listed in table 1.

Results and Discussion

The simulation results are presented in figure 2 and are compared with data obtained in 1987 (Baedecker and others, 1993, Cozzarelli and others, 1999). The Monod parameters used in these simulations were obtained by setting the half velocity coefficient to the initial concentration of the electron acceptor, or the saturated concentration in the case of CH, and adjusting the value of v_{max} to obtain an acceptable visual fit to the data. The values used in the final simulations are summarized in Table 2. Note that only anaerobic processes were inhibited by using an inhibition constant of 10^{-7} M O_2. $Fe(OH)_3$ reduction was not inhibited by MnO_2 because Fe^{2+} produced can be oxidized back to Fe^{+3} by an equilibrium controlled redox reaction with MnO_2. Methanogensis was not inhibited by the presence of $Fe(OH)_3$ for reasons discussed below.

The simulations in figure 2 reproduce the observed trends illustrated by the data. These trends include the appearance of CH, Fe^{2+}, Mn^{2+} and CH_4, and the disappearance of O_2. For CH_4, only about 10% of the quantity produced by methanogensis is illustrated in figure 2. The balance of the methane was removed in the model as a gas. A gas phase containing both $CH_{4(g)}$ and $CO_{2(g)}$ in equilibrium with aqueous solution was assumed to form when the sum of the partial pressures of $CH_{4(g)}$ and $CO_{2(g)}$ exceeded 1 atmosphere. The simulations also reproduce the observed decrease in the field pH, as well as increases in Ca^{2+}, Mg^{2+}, and alkalinity. The simulated solid phase $Fe(OH)_3$ is not completely depleted which agrees with observations from sediments samples taken from cores obtained at the site (Tuccillo and others, 1999). For CH, the simulations show little migration downgradient

Table 2: Reaction constants used for RATEQ simulation. Values not used in simulations are denoted by a '–'

Acceptor	$v_{max}(d^{-1})$	$K_{CH}(M)$	$K_{Acc}(M)$	$I_{O2}(M)$
O_2	$1x10^{1}$	$1x10^{-3}$	$1x10^{-4}$	-
MnO_2	$5x10^{-3}$	$1x10^{-3}$	$1x10^{-4}$	10^{-8}
$Fe(OH)_3$	$4x10^{-5}$	$1x10^{-3}$	$6x10^{-2}$	10^{-8}
CO_2	$2x10^{-4}$	$1x10^{-3}$	-	10^{-8}

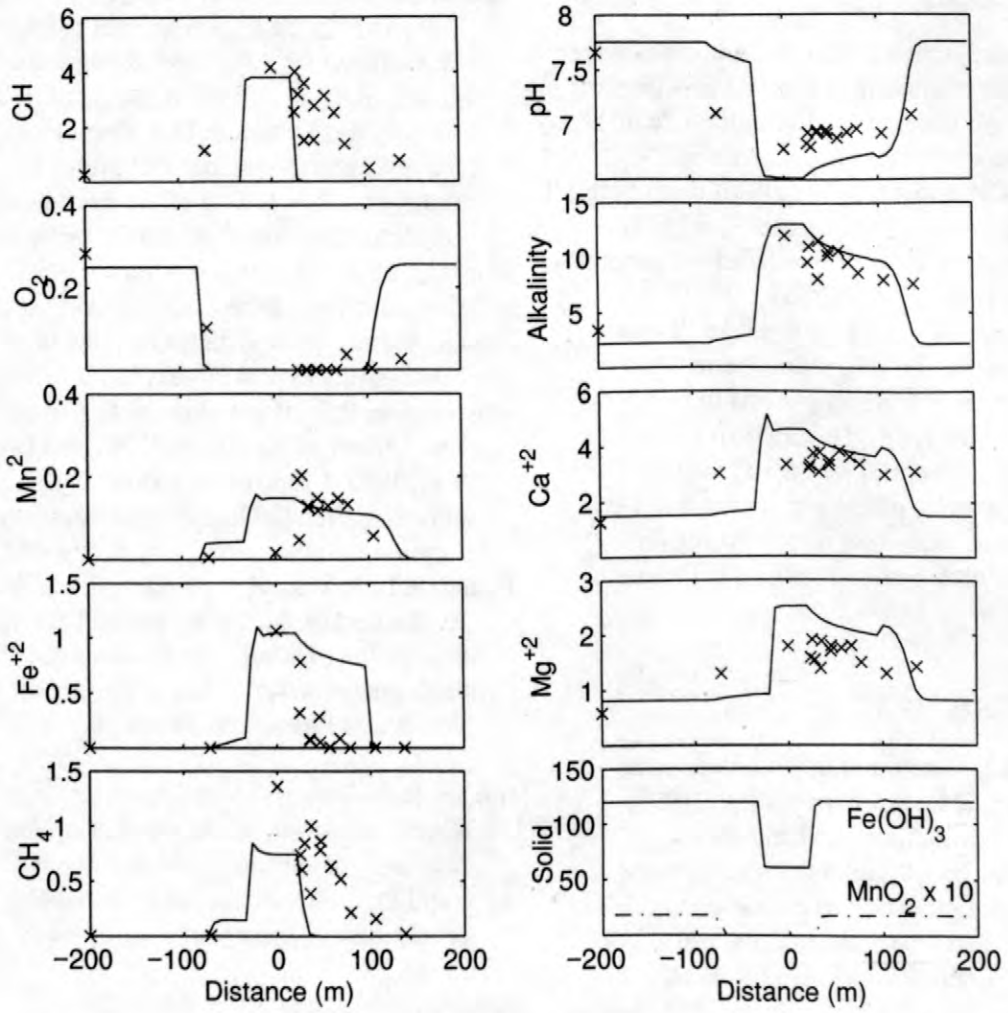

Figure 2. Comparison of observed (x) and simulated concentrations (lines) 8 years after the crude oil spill except for solid concentrations where only simulated values are shown. All concentrations are in units of millimoles per liter of water except pH which is in standard units.

from the source area probably because the crude oil has been approximated in these initial simulations by a single compound which is assumed to be completely biodegradable. It is known that even slight structural differences of individual compounds has a large impact on the extent of degradation (Eagenhouse and others, 1993). Similarly, the O_2 concentration increased to saturated values 100 meters downgradient from the source to reflect reoxygenation of the groundwater, possibly from fluctuations of the water table.

The simulations illustrated in figure 2 were obtained by assuming that iron reduction and methanogensis occurred simultaneously. This approach contradicts the often assumed process of sequential use of electron acceptors by microorganisms, but is supported by the observed co-occurrence of iron reducing and methanogenic bacteria (Bekins and others, 1999). This was the only set of reaction constants that was found that matched the observed decrease in pH and gave relatively close agreement for dissolved Fe^{2+} and solid phase Fe^{+3}. The protons consumed in the oxidation of $Fe(OH)_3$ are balanced by protons produced simultaneously by methanogenesis.

CONCLUSIONS

Coupled reactive transport simulations were performed to reproduce the observed geochemical trends in ground water at the Bemidji crude oil spill site. The simulations accounted for oxidation of CH, a dissolved crude oil constituent, by four electron acceptors: O_2, MnO_2, $Fe(OH)_3$ and CO_2. The simulations reproduced the general observed trends in CH, Fe^{+2}, Mn^{+2}, CH_4, Ca^{+2}, Mg^{+2}, alkalinity, and pH. In this model, it was necessary to allow $Fe(OH)_3$ reduction to occur simultaneously with methanogenesis to match the pH observed in the field. This approach contradicts the concept of sequential use of electron acceptors by micro-organisms, but it is supported by the coexisting iron-reducing and methanogenic microbial populations at the site (Bekins and others, 1999).

REFERENCES

Baedecker, M.J., Cozzarelli, I.M., Eganhouse, R.P, Siegel, D.I., and Bennett, P.C., 1993, Crude oil in a shallow sand and gravel aquifer, III– Biogeochemical reactions and mass balance modeling in anoxic groundwater: Applied Geochemistry, v8, p529-549.

Bekins, B.A. Cozzarelli, I.M., Godsy, E.M. Warren, E., Tuccillo, M.E., Essaid, H.I., and Paganelli, V.V., 1999, Chemical and Physical Controls on Microbial Populations in the Bemdiji Toxics Site Cured-Oil Plume, in U.S. Geological Survey Toxic Substances Hydrology Program—Proceeding of the Technical Meeting, Charleston, South Carolina, March 8-12, 1999—Volume 3—Subsurface Contamination from Point Sources: U.S. Geological Survey Water Resources Investgatins Report 99-4018C.

Bekins, B.A., Godsy, E.M. and Goerlitz, D.F., 1993, Modeling Steady-State Methanogenic Degradation of Phenols in Groundwater: Journal of Contaminant Hydrology, v. 14, no. 3-4, p. 279-294.

Bennett, P.C., Siegel, D.I., Baedecker, M.J. and Hult, M.F., 1993, Crude oil in a shallow sand and gravel aquifer, I – Hydrogeology and inorganic geochemistry; Applied Geochemistry, v8, p529-549.

Cozzarelli, I.M., Baedecker, M.J., Eganhouse, R.P., Tucillo, M.E., Aiken, G.R., Bekins, G.A., Jaeschke, J.B., 1999, Long-term geochemical evolution of the Bemidji Toxics site cured-oil plum, in U.S. Geological Survey Toxic Substances Hydrology Program—Proceeding of the Technical Meeting, Charleston, South Carolina, March 8-12, 1999—Volume 3—Subsurface Contamination from Point Sources: U.S. Geological Survey Water Resources Investgatins Report 99-4018C.

Eagenhouse, R.P., Baedecker, M.J., Cozzarelli, I.M., Aiken, G.R., Thorn, K.A., and Dorsey, T.F., 1993, Crude oil in a shallow sand and gravel aquifer-II. Organic geochemistry: Applied Geochemistry, v. 8, p. 551-557.

Essaid, H.I., Bekins, B.A., Godsy, E.M., Warren., E., Baedecker, M.J. and Cozzarelli, I.M., Simulation of aerobic and anaerobic biodegradation processes at a crude oil spill site, Water Resources. Research., 31, p3309-3327.

Hunter, K.S., Wang,Y, Van Cappellen, P., 1998, Kinetic modeling of microbially-driven redox chemistry of subsurface environments: coupling transport, microbial metabolism and geochemistry, Journal of Hydrology, v 209, p 53-80.

McFarlane, M.J. and Sims, R.C., 1991, Thermodynamic framework for evaluating PAH degradation in the subsurface, Ground Water, 29, p 885-896.

Rodgers, J.R., P.C. Bennett, and W.J. Choi, 1998, Feldspars as a source of nutrients for microorganisms, American Mineralogist, v. 83, 1532-1540.

Tuccillo, M.E., Cozzarelli, I.M., and Herman, J.S., 1999, Iron reduction in the sediments of a hydrocarbon-contaminated aquifer: Applied Geochemistry,v. 4, no. 5, p. 71-83.

AUTHOR INFORMATION

Gary P. Curtis and Barbara A. Bekins, U.S. Geological Survey, Menlo Park, California

Isabelle M. Cozzarelli and Mary Jo Baedecker, U.S. Geological Survey, Reston, Virginia

Determining BTEX Biodegradation Rates Using In Situ Microcosms at the Bemidji site, Minnesota: Trials and Tribulations

By E. Michael Godsy, Ean Warren, Isabelle M. Cozzarelli, Barbara A. Bekins, and Robert P. Eganhouse

ABSTRACT

In situ microcosms (ISMs) were installed in an aquifer contaminated by crude oil to study the in situ biodegradation of monoaromatic hydrocarbons. One was placed in an area where iron reduction predominates (ISM-Fe) and the other in an area where methanogenesis predominates (ISM-CH_4). Numerous problems were encountered during installation and operation of the ISM-CH_4 microcosm and therefore monitoring of it has been temporarily discontinued. Biodegradation rates determined from field concentrations suggested that degradation for the ISM-Fe should proceed in the following order: (1) toluene and *o*-xylene – ~12 days; (2) *m*-, *p*-xylene – ~400 days; (3) benzene – 700 days; (4) ethylbenzene – ~1600 days. Samples taken from the ISM-Fe at days 36 and 68 indicated that toluene biodegradation was occurring. Iron, manganese, CO_2, alkalinity, and low molecular weight volatile fatty acids increased while toluene concentration decreased by approximately 20 percent. All other organic and inorganic compounds remained at initial levels including the tracer with the exception of sodium, chloride, and sulfate. These species increased sharply starting at approximately day 8 and have remained elevated since then for an unknown reason.

INTRODUCTION

On August 20, 1979, approximately 1.7×10^6 liters (L) of crude oil was released in northern Minnesota due to a high-pressure pipeline rupture. At the completion of cleanup, 4.0×10^5 L of the oil remained. The majority of the oil pooled near the rupture site in the north pool while a smaller amount flowed overland to the southeast to a local depression and pooled to the south (fig. 1). At both sites, the remaining oil percolated through the unsaturated zone and pooled on the water table (Hult, 1984).

The fate, transport, and multiphase flow of the hydrocarbons present in the oil depend not only on geochemical processes, but also on volatilization, dissolution, biodegradation, transport, and sorption. All of these processes have been studied in detail by an interdisciplinary team from the U.S. Geological Survey and a number of universities.

The natural attenuation of water-soluble crude-oil organic due to biodegradation in the subsurface plume at Bemidji, Minn. is now well documented (Baedecker and others, 1993; Eganhouse and others, 1993, Essaid and others, 1995). In this paper we focus on the fate of a subset of the monoaromatic hydrocarbons: benzene, toluene, ethylbenzene, and *ortho*-, *meta*-, and *para*-xylene (BTEX). The major factor in the natural attenuation of the BTEX compounds is the ubiquitous degradative activity of the resident microbial populations. In order to formulate numerical models that simulate the transport and biodegradation processes, the biodegradation potentials and rates must be determined under naturally-occurring redox conditions.

The availability of electron acceptors is believed to determine the biodegradation potentials and rates of BTEX compounds. Availability and thermodynamic principles predict the sequence of electron acceptors used for biodegradation (Stumm and Morgan, 1981). The theoretical sequence is

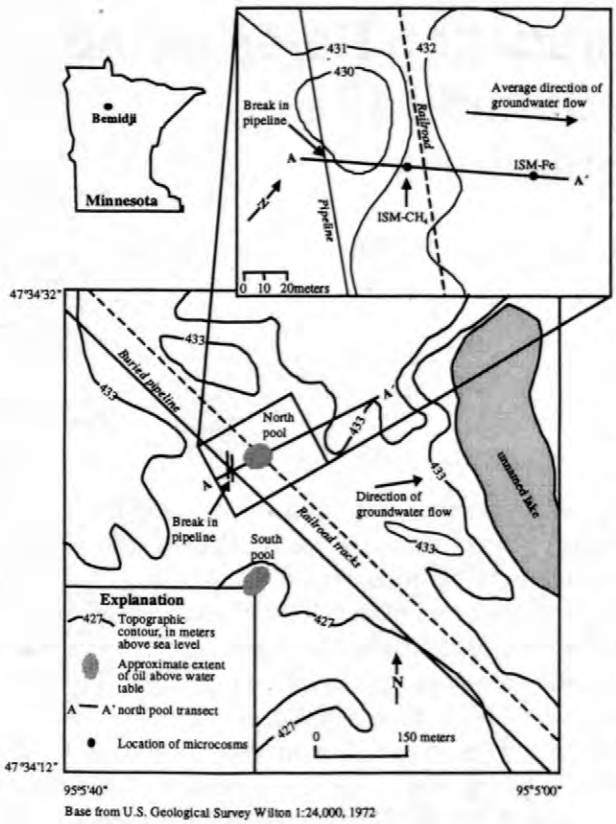

Figure 1. The study site at Bemidji, Minnesota, showing A-A´ transect, oil bodies, and oil pipeline.

aerobic biodegradation, followed by denitrification, manganese and iron reduction, sulfate reduction, and methanogenesis. This sequence has been shown to cause zonation in a contaminant plume with different electron accepting biodegradation processes dominating in different redox zones. At Bemidji, over fifteen years of observations have demonstrated that three redox zones predominate in the contaminant plume: (1) aerobic, (2) iron reducing, and (3) methanogenic (Baedecker and others, 1993; Bekins and others, 1999).

In situ biodegradation rates of the volatile organic carbon fraction at the site have been determined by fitting field concentrations using a two-dimensional reactive solute transport model with Monod biodegradation kinetics (Essaid and others, 1995). Monod kinetic constants for the individual BTEX compounds, determined by fitting field concentrations to a steady-state one-dimensional advective equation that incorporates Monod kinetics (Parlange and others, 1984), were used to predict time required for biodegradation of the individual BTEX compounds. We report here the results of an ongoing BTEX biodegradation experiment conducted with in situ microcosms (ISMs).

IN SITU MICROCOSM TECHNIQUE

The in situ microcosm (ISM) technique to determine biodegradation potentials and rates was developed at the University of Waterloo (Gillham and others, 1990a; Gillham and others, 1990b). The ISM consists of a stainless steel cylinder that encloses a volume of the aquifer that, once loaded with ground water spiked with specific hydrocarbon compounds, can be monitored over time for degradation. Unlike a field injection-tracer test where there is of the contaminant plume encountering areas of different redox potentials, differing microbial populations, and heterogeneity in the aquifer, this technique isolates a portion of the aquifer assuring the same conditions throughout the experiment.

Location of ISM

Both ISMs were placed along the A-A transect (figs. 1 and 2). The microcosm identified as ISM-CH_4 (borehole 9828) was placed in an area of the contaminant plume where biodegradation processes were predominately methanogenic. The

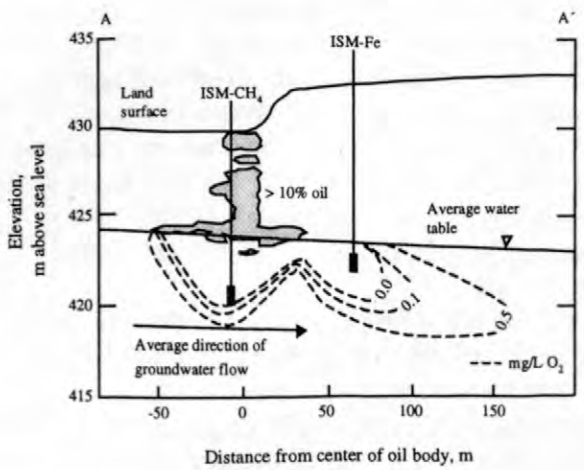

Figure 2. Cross section along transect A-A´ showing locations of the oil body, microcosms and concentrations of dissolved oxygen within the saturated zone, Bemidji, Minnesota.

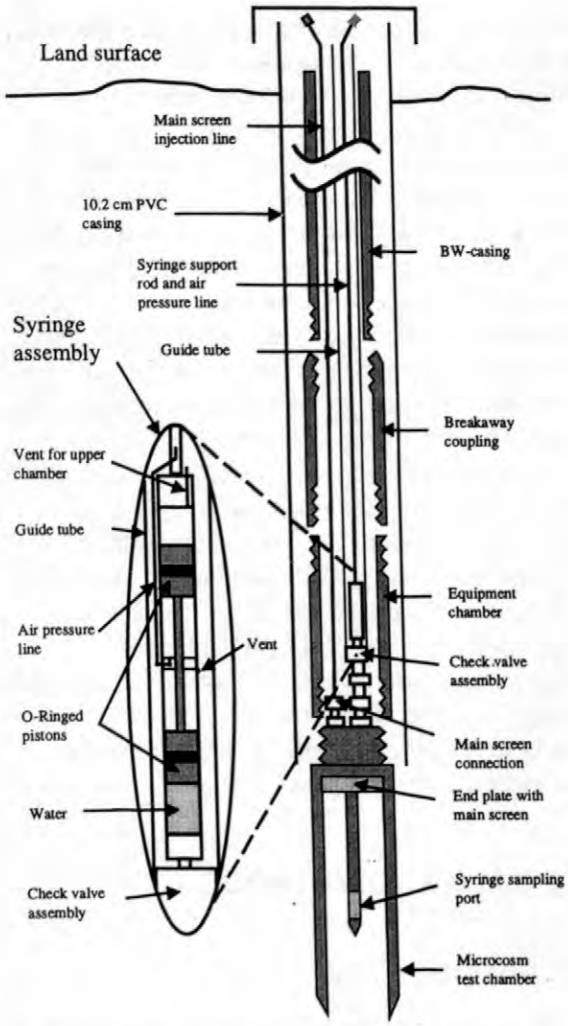

Figure 3. Cross section of the in-situ microcosm with an exploded view of the sampling syringe. Drawing not to scale.

top of the microcosm test chamber was set at an elevation of 421.1 meters (m) above sea level. ISM-Fe (borehole 9825) was placed in an area where biodegradation was predominantly by iron-reduction and set at an elevation of 432.3 m above sea level (Bekins and others, 1999).

Description of ISM

The ISM consists of an 8.3 centimeter (cm) inside diameter (id) x 88 cm stainless steel cylindrical test chamber open at the bottom and bounded at the inside-top by a set of coarse and fine stainless steel mesh screens (fig. 3). The main screens are used to remove and reinject spiked ground water into the test chamber. The design allows even flow through the screens assuring plug flow into the test chamber during reinjection. The test chamber isolates a total aquifer volume of 4.76 L or 1.43 L of ground water (assuming a porosity of 0.3). A depth adjustable, stainless steel sampling port, with a fine mesh screen, extends 26 cm into the test chamber. Water samples are collected from the central port with a syringe assembly (see expanded section of figure 3).

The stainless steel syringe is 70 cm x 1.5 cm outside diameter (od) and was developed by Fred Murphy (U.S. Geological Survey, Menlo Park, Calif.). It is divided into two chambers – a lower 30 cm x 1.2 cm id water sampling camber and an upper compressed air chamber. The bottom of the syringe is fitted with a nipple (not shown in figure 3) that fits into and releases the spring-loaded ball in the check valve assembly for sample collection from the central spike port. Connected to the top of the syringe are 2 m lengths of 0.6 cm (od) stainless steel tubing that act as both the syringe support rod and the compressed air line.

An equipment chamber, threaded onto the top of the test chamber, protects the tubing connector and the syringe check valve assembly. A breakaway coupling with reverse threads adapts the equipment chamber to the lengths of BW-casing. A 6.4 millimeter (mm) Teflon tube for spiking and a polypropylene syringe guide tube (2.5 cm) connect to the ISM and pass through the large diameter metal (BW) casing to the surface.

Installation of ISM

The ISM and the attached BW casing were installed through the center of 15.2 cm hollow stem augers equipped with a wire-line, surface-connected knockout-plug in the cutting bit to prevent the cuttings from being carried up the interior of the augers. After drilling to the desired depth, the ISM was lowered through the augers until it rested on the knockout plug. The augers were pulled up slightly to allow the displacement of the knockout plug by the ISM. After the knockout plug was opened, the ISM was advanced into the undisturbed aquifer sediment using an electric vibrating hammer until the top of the test chamber was just below the bottom of the augers. A 10.2 cm PVC casing was then installed to the bottom of the augers and the augers removed leaving the ISM with sampling tubes and both the

BW and PVC casings in place. The space between the PVC casing and the aquifer sediment was filled with the drill cuttings.

Loading of ISM

Ground water was pumped from a nearby well that was screened at the target depth of the ISM (532 B for the ISM-CH_4 and 531 B for the ISM-Fe) until temperature and pH stabilized (approximately 5 casing volumes). At this time, 10 L of ground water was pumped into a 20 L Tedlar gas-sampling bag that was immersed in an ice filled picnic cooler. This was equivalent to approximately 7 ISM test chamber volumes. Prior to filling, the sampling bag was flushed five times with O_2-free Argon. The hydrocarbon and conservative tracer spike compounds were added carefully to the ground water in the sampling bag to exclude O_2. The hydrocarbon solution was thoroughly mixed and introduced by gravity into the ISM through the main screen injection line.

Sampling of ISM

Prior to sampling, the pistons were pushed to the bottom of each chamber by a set rod inserted in the upper chamber vent. The stainless steel syringe was then attached to the support tubing and adjusted to withdraw 10 milliliters (mL) of water. This was accomplished by placing a set rod in the upper chamber vent to stop the piston from travelling the complete 30 cm distance. Ten mL was determined to be the dead volume of the sampling port and check valve assembly. The syringe was lowered down the guide tube until reaching the check valve assembly. The syringe was then raised approximately 30 cm and jammed down into the check valve assembly. Approximately 400 kilopascals (kPa) of pressure was applied to the syringe from a portable air compressor. This compressed air displaced the pistons to the top of each chamber of the syringe. The lower chamber was simultaneously filled with a water sample from the microcosm. The dead volume was discarded. The set rod was removed and the syringe was again lowered to the ISM and a full 30 mL water sample was taken. The syringe was detached from the ISM by a gentle pull, elevated to land surface, and aliquots of the sample were transferred to the appropriate bottle by manually depressing the upper piston with a metal rod passed through the upper vent.

MATERIALS AND METHODS

BTEX Solution

The spiked ground-water solution could not

Table 1. Concentations of compounds used in the BTEX solution for the ISM-Fe compared to the observed maximum field concentation in well 531 B at the Bemidji site, Minnesota.

	Concentration (µg/L)	
Compound	Maximum field	Spike solution
Benzene-D6	2100	2000
Toluene	10	1000
Ethylbenzene	323	650
m-xylene	78	250
p-xylene	78	250
o-xylene	20	150
isopropylbenzene	36	200
1-methyl-3-ethylbenzene	29	150
1-methyl-2-isopropylbenzene	6	100
1-methyl-4-isopropylbenzene	10	100
1,3-dimethyl-2-ethylbenzene	26	100
1,3-dimethyl-4-ethylbenzene	17	100
1,2,3,5-tetramethylbenzene	34	150
1,2,3,4-tetramethylbenzene	58	150

Table 2. Sampling scheme and methods for the ISM-Fe.

Parameter	Container	Bottle volume (mL)	Sample volume (mL)	Preservation (all chilled)	Analysis method
pH	Vial	5	2	None	Electrode
Alkalinity	Vial	5	2	0.2 µm nylon filter	Titration
Dissolved gases	Serum bottle, evacuated	10	2	$HgCl_2$	Headspace GC
Organic intermediates	Vial	5	10	Zero headspace	Acid ether extracct, GC/MS
BTEX compounds	Glass vial	5	5	$HgCl_2$, zero headspace	Purge & trap GC/MS
Fatty acids	Vial	5	2.5	$HgCl_2$	IC
Cations	Plastic bottle	10	4	0.2 µm nylon filter, 0.5% nitric acid	ICP/MS
Anions	Vial	5	2.5	0.2 µm nylon filter	IC

be loaded into the ISM-CH_4 for unknown reasons; therefore, the composition of the solution is given only for the ISM-Fe (table 1). A hydrocarbon mixture was prepared in the laboratory by mixing the desired volumes of the neat compounds in an ampoule. A concentrated hydrocarbon solution was prepared in the field by injecting 59.5 microliters of this mixture into 200 mL of the ground water and mixing in a sonication bath for 60 min. Then, all of the concentrated solution was injected into approximately 10 L of ground water from well 531B. A conservative tracer, KBr was then added to a final concentration of 30 milligrams/liter (mg/L) as Br.

Sampling Protocol

Samples from ISM-Fe were analyzed for pH, alkalinity, intermediate organic acids, anions including low molecular weight volatile fatty acids (VFAs), cations, hydrocarbons, and dissolved CH_4 and CO_2 as outlined in table 2. Biodegradation rates determined from field concentrations suggested that the BTEX compounds for the iron reducing ISM should degrade in the following order: (1) toluene and *o*-xylene – ~12 days; (2) *m*-, *p*-xylene – ~400 days; (3) benzene – ~700 days; (4) ethylbenzene – ~1600 days. The sampling scheme was designed to obtain as many samples as possibly for each compound with in the limits of the total volume present in the ISM.

Analytical Techniques

Alkalinity was determined in the laboratory with an automatic titrator and pH was determined in the field with an electrode. The cations were determined using an ICPMS. Dissolved gasses were determined according to the method described Godsy and others (1992). The hydrocarbons were analyzed by purge and trap capillary gas chromatography with ion trap detection as described by Eganhouse and others (1999).

The anions and low-molecular weight fatty acids (formate, acetate, propionate, and butyrate; VFA) were determined using a Dionex Ion Chromatography System equipped with an advanced gradient pump with a conductivity detector, an anion self-regenerating suppressor with an autosuppression external water mode, and a 4 mm Dionex AS15 analytical column. The system was equipped with a guard column, a column heater set at 30°C, and an anion trap column.

Intermediate organic acids were determined by a single 2:1 acid extraction into diethylether. The extract was injected in a Finnigan GCQ GC/MS equipped with a 30 m x 0.25 mm (0.25 micrometer film) DB-WAXETR fused silica column (J&W Scientific, Folsom, Calif.). The oven temperature was programmed from 35 to 245°C at 8°C/min and held at the final temperature for 5 min. The injection port temperature was 265°C and helium carrier gas velocity was 40 cm/sec.

Table 3. Selected parameters and cations from the iron reducing ISM at the Bemidji site, Minnesota. All concentrations are in mg/L except for pH. Alk = laboratory alkalinity.

Time	pH	Alk	CO_2	CH_4	Fe	Mn	Na	K
Prespike	*6.95*	*503.7*	*233.7*	*4.90*	*1.30*	*3.07*	*4.91*	*2.56*
0	6.78	485.7	397.5	7.96	33.60	0.66	3.01	15.10
1	*6.90*	*497.0*	*357.1*	*5.58*	*15.90*	*0.70*	*3.83*	*16.13*
2	6.75	491.7	263.2	6.38	13.10	0.99	4.31	15.50
5	6.74	497.0	235.6	6.64	11.40	1.02	4.46	15.60
8	6.78	500.6	383.2	6.03	10.70	1.08	15.30	17.90
13	6.80	491.2	342.9	6.09	8.64	1.08	20.40	19.00
18	7.21	413.2	404.7	4.78	NS	NS	NS	NS
36	6.89	515.8	351.4	3.54	13.80	1.39	29.50	22.70
69	6.66	576.2	479.3	6.07	28.60	1.69	15.10	17.30

italics = average of 3 analyses
ND = not detected
NS = no sample

RESULTS

Anions and Cations

The pH, alkalinity, and concentrations of anions and cations for ISM-Fe are given in tables 3 and 4. Evidence that biodegradation was occurring by day 36 is given by the increase from day 13 in the terminal electron accepting cations Fe and Mn, and the increase from day 18 in alkalinity. The concentration of CH_4 remained constant over the experiment, but the VFAs, acetate, and formate, increased by day 36, and propionate increased at day 69.

The concentrations of the conservative tracers, K and Br, show some variability but did not decrease significantly over the experiment. It is of interest to point out that the concentrations of Na, Cl, and SO_4 increased dramatically after day 5. It is unknown why the concentration of these species would increase while the conservative tracers do not increase.

Table 4. Selected anions and low-molecular weight volatile fatty acids from the iron reducing ISM at the Bemidji site, Minnesota. All concentrations are in mg/L. Ace = acetate, For = formate, and Pro = propionate.

Time	SO_4	Cl	Br	Ace	For	Pro
Prespike	*4.58*	*3.13*	ND	*0.31*	*0.60*	ND
0	0.68	0.95	28.95	0.27	0.44	ND
1	*0.70*	*1.87*	*29.04*	*0.23*	*0.47*	ND
2	0.74	2.27	29.31	0.25	0.44	ND
5	0.71	2.31	28.82	0.26	0.44	ND
8	8.55	19.05	34.13	ND	ND	ND
13	11.97	30.65	37.56	ND	1.87	ND
18	17.52	NS	28.75	3.06	1.51	ND
36	19.51	43.47	32.20	ND	ND	ND
69	11.44	16.73	33.32	2.51	ND	0.74

italics = average of 3 analyses
ND = not detected
NS = no sample

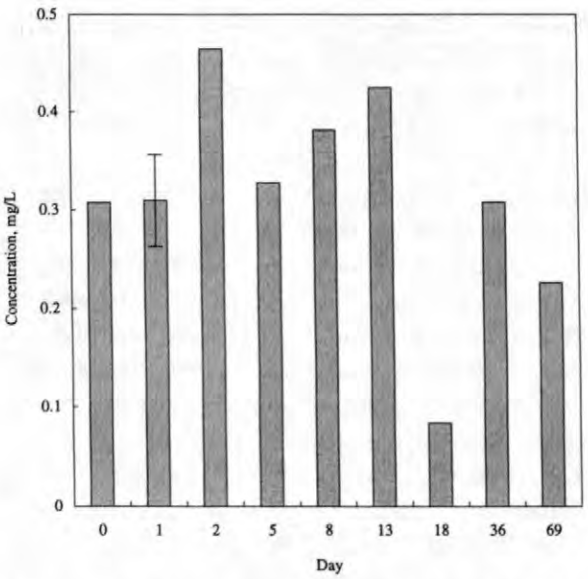

Figure 4. Concentrations of toluene in the ISM at the Bemidji site, Minnesota. Prespike concentrations were at method detection limit (MDL). Bar on day 1 represents the range of 3 replicates.

Organic Compounds

Over the course of the experiment only toluene showed any perceptible signs of biodegradation. Between days 13 and 69, there appeared to be a significant decrease in the amount of this compound (fig. 4) relative to the Br tracer. We have not established a sampling error at this time, and the next sampling is not scheduled until approximately day 170, at which time toluene degradation potential should be understood.

Benzoic acid, the major monoaromatic intermediate in the methanogenic biodegradation of monoaromatic compounds (Godsy and others, 1996) and presumably under iron reducing conditions, was detected on day 36, suggesting that biodegradation of monoaromatic hydrocarbons may be occurring in this time frame.

DISCUSSION AND CONCLUSIONS

The biodegradation of monoaromatic and polynuclear aromatic compounds under methanogenic conditions has been studied in detail in the last several years (Godsy and others, 1992; Godsy and others, 1996) and recently has been the subject of investigations under iron reducing conditions (Lovley and others, 1989). One of the questions surrounding the microbial ecology of the contaminant plume at the Bemidji site is the role of the individual members and the terminal member of the microbial consortia in different redox zones of the plume. Previous studies have shown that anaerobic iron reducing microorganisms can degrade some of the BTEX compounds in pure culture (Lovley and others, 1989; Lovley and Lonergan, 1990) while a consortia is required for these hydrocarbons under methanogenic conditions.

Investigations by Bekins and others (1999) into the nature of the microbial consortia at the Bemidji site have shown that iron-reducing microorganisms capable of utilizing acetate and H_2 as substrates are prevalent throughout the contaminant plume. They are present in both methanogenic and iron reducing redox zones, but are at lower numbers in the methanogenic zones. This finding, coupled with the appearance of VFAs and benzoate in the ISM-Fe suggests that the iron reducing microorganisms are acting as a terminal member of the consortium by utilizing the acetate and H_2 produced and not degrading the BTEX compounds directly. If the iron reducing microorganisms were degrading the BTEX directly, VFAs and benzoic acid would not appear as intermediates. Proof of this observation will require further study in the ISMs and in laboratory investigations.

Microorganisms in the zone of the plume where the iron-reducing ISM was placed have not previously encountered toluene or *o*-xylene in significant concentrations. In the past, these compounds have been degraded before reaching this distance down gradient in the aquifer (Eganhouse and others, 1993; Cozzarelli and others, 1994, Cozzarelli and others, 1999). The time elapsed for toluene biodegradation to begin, may be the time required for the microbial consortia to adapt to this compound. In addition, disturbance of aquifer material during installation may effect the degradation rate. It is not clear at this time whether a single microorganism is responsible for the ring cleavage of a single compound or its analogs or if a microorganism can open the ring structure of several classes of compounds. The preliminary results of the ISM suggest that the individual microorganism or consortia of microorganisms might be specific for a

limited number of compounds as was observed for creosote derived compounds (E.M. Godsy, unpub. data, 1993)

The reasons for the failure of the methanogenic ISM to accept the spike solution will remain a mystery until the ISM is recovered in the spring.

REFERENCES

Baedecker, M.J., Cozzarelli, I.M., Eganhouse, R.P., Siegel, D.I., and Bennett, P.C., 1993, Crude oil in a shallow sand and gravel aquifer-III. Biogeochemical reactions and mass balance modeling in anoxic groundwater: Applied Geochemistry, v. 8, p. 569-586.

Bekins, B.A., Cozzarelli, I.M., Godsy, E.M., Warren, Ean, Tuccillo, M.E., Essaid, H.I., and Paganelli, V.V., 1999, Chemical and physical controls on microbial populations in the Bemidji Toxics Site crude-oil plume, Morganwalp, D.W., and Buxton, H.T., eds., U.S. Geological Survey Toxic Substances Hydrology Program—Proceedings of the Technical Meeting, Charleston, South Carolina, March 8-12, 1999-- Volume 3 -- Subsurface Contamination from Point Sources: U.S. Geological Survey Water-Resources Investigations Report 99-4018C, this volume.

Cozzarelli, I.M., Baedecker, M.J., Eganhouse, R.P., and Goerlitz, D.F., 1994, The geochemical evolution of low-molecular-weight organic acids derived from the degradation of petroleum contaminants in groundwater: Geochemica et Cosmochimica Acta, v. 58, no. 2, p. 863-877.

Cozzarelli, I.M., Baedecker, M.J., Eganhouse, R.P., Tuccillo, M.E., Aiken, G.R., Bekins, B.A., and Jaeschke, J.B., 1999, Long-term geochemical evolution of the Bemidji Toxics site crude-oil plume, Morganwalp, D.W., and Buxton, H.T., eds., U.S. Geological Survey Toxic Substances Hydrology Program—Proceedings of the Technical Meeting, Charleston, South Carolina, March 8-12, 1999-- Volume 3 -- Subsurface Contamination from Point Sources: U.S. Geological Survey Water-Resources Investigations Report 99-4018C, this volume.

Eganhouse, R.P., Baedecker, M.J., Cozzarelli, I.M., Aiken, G.R., Thorn, K.A., and Dorsey, T.F., 1993, crude oil in a shallow sand and gravel aquifer - II. Organic geochemistry: Applied Geochemistry, v. 8, p. 551-567.

Eganhouse, R.P., Matthews, L.L., Cozzarelli, I.M., and Scholl, M.A., 1999, Evidence for natural attenuation of volatile organic compounds in the leachate plume of the Norman, Oklahoma landfill, Morganwalp, D.W., and Buxton, H.T., eds., U.S. Geological Survey Toxic Substances Hydrology Program—Proceedings of the Technical Meeting, Charleston, South Carolina, March 8-12, 1999-- Volume 3 -- Subsurface Contamination from Point Sources: U.S. Geological Survey Water-Resources Investigations Report 99-4018C, this volume.

Essaid, H.I., Bekins, B.A., Godsy, E.M., Warren, Ean, Baedecker, M.J., and Cozzarelli, I.M., 1995, Simulation of aerobic and anaerobic biodegradation processes at a crude oil spill site: Water Resources Research, v. 31, no. 12, p. 3309-3327.

Gillham, R.W., Robin, M.L., and Ptacek, C.J., 1990a, A device for in situ determination of geochemical transport parameters 1. Retardation: Ground Water, v. 28, no. 6, p. 666-672.

Gillham, R.W., Starr, R.C., and Miller, D.J., 1990b, A device for in situ determination of geochemical transport parameters 2. Biochemical reactions: Ground Water, v. 28, no. 6, p. 858-862.

Godsy, E.M., Goerlitz, D.F., and Grbić-Galić, Dunja, 1992, Methanogenic biodegradation of creosote-derived contaminants in natural and simulated ground water ecosystems: Ground Water, v. 30 no. 2, p. 232-242.

Godsy, E.M., Goerlitz, D.F., and Grbić-Galić, Dunja, 1996, Pathways of methanogenic biodegradation of creosote-derived aromatic compounds, Morganwalp, D.W., and Aronson, D.A., eds., U.S. Geological Survey Toxic Substances Hydrology Program—Proceedings of the Technical Meeting, Colorado Springs, Colorado, September 20-24, 1993-- Volume 2: U.S. Geological Survey Water-Resources Investigations Report 94-4015, p. 835-841.

Hult, M.F., 1984, Groundwater contamination by crude oil at the Bemidji, Minnesota, Research Site - An Introduction, in Groundwater Contamination by Crude Oil at the Bemidji, Minnesota, Research Site: U.S. Geological Survey Water-Resources Investigations Report 84-4188, p. 1-15.

Lovley, D.R., Baedecker, M.J., Lonergan, D.J., Cozzarelli, I.M., Phillips, E.J.P., and Siegel, D.I., 1989, Oxidation of aromatic contaminants coupled to microbial iron reduction: Nature, v. 339, p. 297-300.

Lovley, D.R. and Lonergan, D.J., 1990, Anaerobic oxidation of toluene, phenol, and p-cresol by the dissimilatory iron-reducing organism, GS-15: Applied and Environmental Microbiology, v. 56, no. 6, p. 1858-1864.

Parlange, J.Y., Starr, J.L., Barry, D.A., and Braddock, R.D., 1984, Some approximate solutions of the transport equation with irreversible reactions: Soil Science, v. 137, no. 6, p. 434-442.

Stumm, Werner and Morgan, J.J, 1981, Aquatic Chemistry: New York, N.Y., J. Wiley and Sons, 780 p.

AUTHOR INFORMATION

E. Michael Godsy, Ean Warren, and Barbara A. Bekins, U.S. Geological Survey, Menlo Park, California (emgodsy@usgs.gov)

Isabelle M. Cozzarelli and Robert P. Eganhouse, U.S. Geological Survey, Reston, Virginia

Mineralogy and Mineral Weathering: Fundamental Components of Subsurface Microbial Ecology

By Philip C. Bennett, Jennifer Roberts Rogers, Franz K. Hiebert, and Wan Joo Choi.

ABSTRACT

This is an investigation of the interplay between mineral chemistry, microbial ecology, and mineral weathering in the oil-contaminated Bemidji aquifer using field and laboratory observations and experiments over a period of 8 years. We observed microbe-mineral interactions at two scales of interaction: a *macroscale* interaction where the metabolism of both attached and planktonic organisms perturb the bulk groundwater chemistry and therefore, the mineral-water equilibria; and a *microscale* interaction where attached organisms perturb mineral-water equilibria only in the near vicinity of the organism or biofilm. The two scales reveal a tightly linked system whereby the microbial ecology controls mineral weathering, while the mineralogy and mineral chemistry control microbial colonization.

In this aquifer, carbonate chemistry is influenced primarily at the macroscale, With few native microorganisms observed on carbonate surfaces. In the upgradient oxidizing zone aerobic hydrocarbon oxidation produces excess carbon dioxide, accelerating the dissolution of calcite and dolomite, but with little weathering of silicates. Under the anoxic, leading edge, of the oil pool calcite (but not siderite) precipitates on uncolonized surfaces, while under the trailing edge of the oil, iron reduction dominates over methanogenesis and here siderite precipitates in addition to calcite. As molecular oxygen begins to diffuse into the aquifer, aerobes again dominate and residual hydrocarbons and ferrous iron are oxidized, resulting in macroscale carbonate mineral dissolution and iron precipitation.

Feldspars, in contrast, are weathered exclusively near attached microorganisms, and only at the leading edge of the anoxic sub-oil pool zone. Here native organisms preferentially colonize only those feldspars that contain trace phosphorus as apatite inclusions, apparently as a consequence to the P-limiting environment. These feldspars are rapidly weathered, while nearby feldspars without trace P are uncolonized and unweathered. The weathering of feldspars results in the release of dissolved silica which increases to near-equilibrium with amorphous silica. Comparison of the distribution of dissolved silica between 1990 and 1998 shows that the area of most intense feldspar weathering has moved downgradient, parallel with the area of most intense iron reduction.

We hypothesize that the weathering of the P-rich feldspar releases the limiting phosphate, offering the colonizing population a competitive advantage over planktonic organisms or organisms that occupy other mineral surfaces. This suggests that minerals, and the nutrient content of minerals can influence microbial processes, microbial colonization, and contaminant degradation efficiency, while the microbial ecology directly influences the mineral weathering rate and sequence.

INTRODUCTION

At the Bemidji site, native microorganisms rapidly consume dissolved components of the petroleum, but with little addition of biomass. While there is abundant carbon substrate, and sufficient abundance of electron acceptor in the saturated zone under the oil, there is scant available phosphorus or nitrogen, and the microbial community appears to be nutrient limited. In this same region, where iron reduction and methanogenesis are the dominant microbial processes, silicates rapidly weather, while carbonates precipitate, apparently in response microbial perturbation of specific mineral-water equilibria.

The role of microorganisms in feldspar weathering, however, is not well established or or documented. Mounting evidence suggests that bacteria attached to feldspar surfaces can greatly accelerate the rate of feldspar dissolution (Barker, Welch, and others, 1998; Bennett and Hiebert, 1992; Bennett, Hiebert, and Choi, 1996; Ullman, Kirchman, and others, 1996), but two important questions remain - why, and how. Here we report the results of geochemical analysis of ground waters and field microcosm experiments that help constrain the question of how, and suggests a hypothesis for why; the native microorganisms in the Bemidji aquifer may destroy feldspars to gain access to trace or limiting nutrients.

Site Background

The aquifer at the Bemidji site was contaminated by crude petroleum in 1979 when a high pressure pipeline ruptured, contaminating ~0.65 hectares of the surface, with both surface and subsurface accumulations of petroleum. The oil spilled at Bemidji is a light aliphatic crude (Eganhouse, Baedecker, and others, 1993), and dissolved aromatic hydrocarbons are present in the anoxic ground water under the oil, and are being rapidly degraded. Hydrocarbons in this zone are being biodegraded primarily by iron (III) reduction (Baedecker, Cozzarelli, and others, 1993; Lovley and Lonergan, 1990) and by secondary methanogenesis.

The contaminated aquifer consists of ~20 m of moderately calcareous, silty sand deposited as glacial morainal and outwash material overlying clayey till of unknown thickness, with thin discontinuous lacustrine silt layers interbedded with sand near the water table (Bennett, Siegel, and others, 1993). The native aquifer material is composed of ~ 57% quartz, 29% feldspars, 4-6% carbonates 2% hornblende, <1% clays, and < 0.2 % organic carbon. Degradation of the contaminating petroleum has produced a plume of inert and reactive organic and inorganic solutes, including a variety of organic acids (Baedecker, Cozzarelli, and others, 1993; Cozzarelli, Baededecker, and others, 1994; Cozzarelli, Eganhouse, and Baedecker, 1990), and etching of native quartz and feldspar grains has been documented (Bennett and Casey, 1994; Bennett and Siegel, 1987).

METHODS

For this study we used parallel field and laboratory methods to examine the role of mineralogy in microbial ecology. Complete sampling of ground waters at the Bemidji site wells were completed in September 1990 and July 1998, with additional selected wells sampled annually. Water was collected from up to 90, 5 cm OD PVC wells with stainless screens positioned to intersect the water table (1.5 meter screen length), and at specified intervals below the water table (0.15 meter length screens). Samples were collected using down-hole submersible pumps after evacuation of approximately 3 well volumes (see Bennett and others, 1993). During the 1990 sampling dissolved oxygen, pH, temperature, and specific conductance were measured at the surface using a flow cell. For the 1998 sampling, these constituents were measured *in situ* using down-hole data probes (Hydrolab Data Sonde), with readings recorded before and after sample collection. Analysis of very low dissolved oxygen (<20 ppb) was done at the surface using colorimetric techniques (Chemetrics) with a portable "Spec-20" spectrophotometer. Dissolved ferrous and ferrous+ferric iron were also determined immediately in the field using the bipyridine colorimetric method, and rechecked in the laboratory using a Perkin-Elmer Lambda 6 double-beam spectrophotometer. Alkalinity was determined on a 0.2 um filtered unpreserved sample by endpoint seeking titration with calibrated 0.1 N HCl.

Dissolved metals and silicon were determined by ICP on an acid-preserved sample filtered to 0.1 um, while ammonia was determined by single column ion chromatography (detection limit 10 ppb). Dissolved anions (F, Cl, NO_2, NO_3, SO_4) were determined from a filtered unpreserved sample by single-column ion chromatography (Detection limit 20-50 ppb). Reactive orthophosphate was determined in the laboratory by standard colorimetric methods on a filtered sample preserved with $HgCl_2$, with selected samples analyzed for total P by ICP-MS.

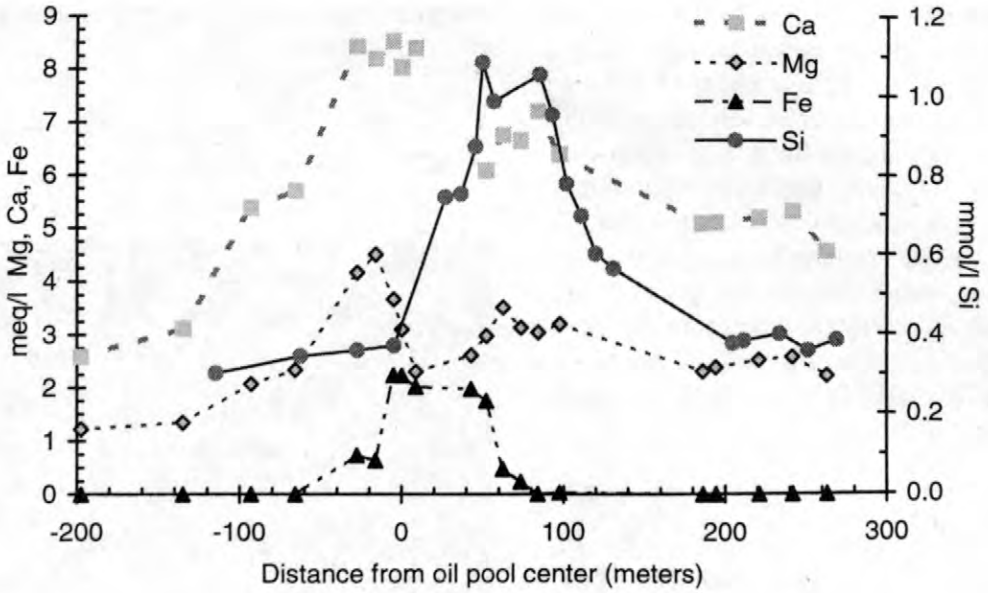

Figure 1: Solute concentrations along the primary transect. Ground water flow is from negative to positive distance.

Inorganic carbon was by measured using a Dohrman DC180 carbon analyzer.

Field microcosms of selected mineral chips were placed in different areas of a microbiologically active petroleum-contaminated aquifer for periods up to 12 months (Bennett, Hiebert, and Choi, 1996; Hiebert and Bennett, 1993; Rogers, Bennett, and Choi, 1998). In the aquifer the mineral chips were exposed to the native microbial population, and after recovery the pattern of colonization and the extent of reaction of the surface was characterized using SEM and related techniques (Rogers and others, this volume). At the time of microcosm placement and recovery, the ground water chemistry and microbiology were characterized and compared to over 15 years of record established for this site (Bennett, Siegel, and others, 1993).

Using the same mineral specimens, we also examined some of the fundamental controls on feldspar dissolution kinetics within the context of a limited experimental question - how can a microorganism accelerate the dissolution rate of a feldspar orders of magnitude over the rate of an uncolonized surface? Specimens of Bancroft albite and a South Dakota microcline were ground to a uniform size fraction, cleaned, and dissolved in an all-Teflon mixed flow reactor system (Bennett, Hiebert, and Choi, 1996; Choi, 1997; Choi and Bennett, 1995). Dissolution rate was examined as a function of pH, ionic strength, and the concentration of 3 target organic ligands: citrate, dihydroxy benzoate, and tropolone. The effect of these variables was monitored by measuring the change in absolute dissolution rate and *apparent* activation energy (the observed relationship between dissolution rate and temperature not corrected for the enthalpy of proton adsorption, (Casey and Sposito, 1992).

FIELD OBSERVATIONS AND EXPERIMENTAL FINDINGS

Macroscale Calcite Diagenesis

Upgradient of the oil pool oxidation of vadose-zone petroleum proceeds by aerobic beta-oxidation and oxygenlytic cleavage of simple aromatic compounds depleting the reservoir of dissolved oxygen. This produces substantial acidity from carbon dioxide as well as minor and transient quantities of simple and complex organic acids, resulting in a downward trend in pH along the flow path. The acid production is buffered by carbonate dissolution, resulting in an

increase in the concentration of dissolved Ca, Mg, and HCO3 along the flow path, but little increase in dissolved silica or iron (Figure 1).

Examination of mineral surfaces reacted in this region shows evidence of a macroscale perturbation in mineral water equilibria, and both calcite and dolomite show evidence of aggressive chemical weathering, with distinct etch pits and solution channels (Figure 3). Microorganisms were rarely found on the carbonate mineral surfaces, and the weathering appears to be a macroscale effect: microbial production of acidity from hydrocarbons dissolves calcite, but the microorganism itself is distant from the region of weathering:

$$2CH_2+3O_2 +CaMg(CO_3)_2 \rightarrow Ca^{2+} +Mg^{2+} +4HCO_3^- \quad (1)$$

where CH_2 represents an average mid-chain alkyl carbon (C^{-II}) and dolomite as the reacting carbonate. We found no evidence of significant feldspar weathering in the aerobic oxidation region, either from changes in the geochemistry, or from direct examination of mineral surfaces.

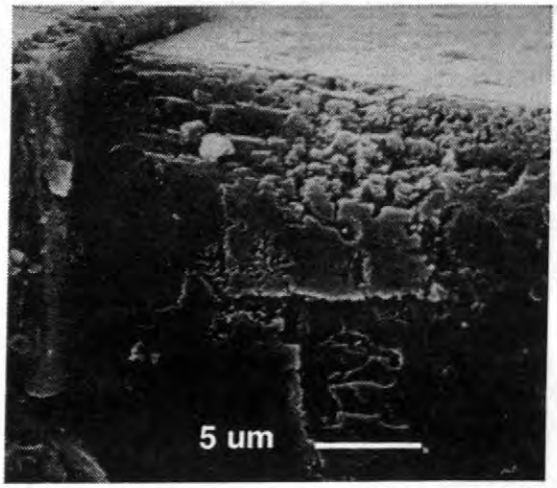

Figure 2. SEM micrograph of dolomite reacted in the oxic region of the aquifer for 1 year. Extensive etching without attached organisms is found on all surfaces.

In the anoxic region beneath the oil pool calcite had sparse dissolution pitting, but only at the microscale associated with microbial colonization. In this region, calcite were typically covered with a variety of precipitation features (Figure 4). Spikes appear to nucleate along cleavage, forming regular rows and rhombic outlines, eventually filling to form rhombic "mesas". The measured geochemical trends in this region support precipitation, probably driven by iron reduction:

$$C_7H_7 +36Fe(OH)_3 +58HCO_3^- +65Ca^{2+} \rightarrow 65CaCO_3 + 36Fe^{2+} +87H_2O \quad (2)$$

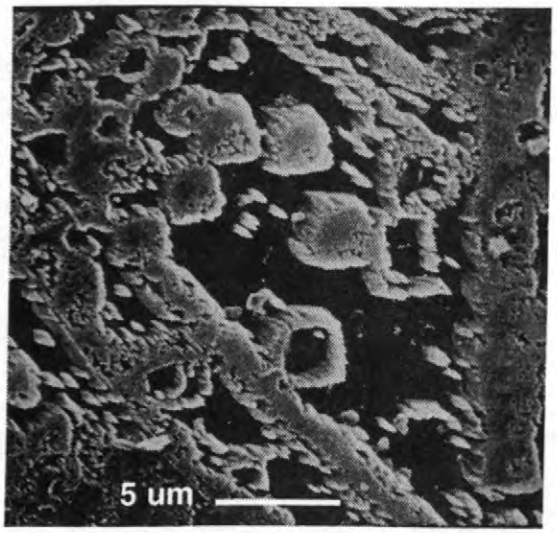

Figure 3. SEM micrograph of calcite reacted in the anoxic region of the aquifer for 1 year. Extensive precipitation without attached organisms is found on all surfaces.

Sequential leaching experiments suggests that the precipitated mineral in the upgradient anoxic region is pure calcium carbonate, with only trace magnesium, strontium, and iron (Hiebert, 1994). In the upgradient portion of the anoxic zone, where methanogenesis may dominate over iron reduction in some regions, in situ experiments show that siderite is uncolonized, and generally dissolving, not precipitating. Further downgradient, however, where iron reduction dominates over methanogenesis, siderite may also precipitate in addition to calcite.

Microscale Silicate Weathering

In the most organic-rich area of this aquifer, the ground water is extremely reducing, and dissolved ferrous iron increases along the principle flow path, while pH decreases from ~7.8 to ~6.5 (Figure 1). Dissolved silica increases

from 0.3 mmole l^{-1} to > 1 mmole l^{-1} associated with the greatly accelerated dissolution of quartz and feldspars (Bennett and Casey, 1994; Bennett and Siegel, 1987).

In 1990, the highest silica concentration was found under the center of the floating oil pool, where the greatest iron reduction activity was found (Figure 2). In 1998, the original contaminated area is increasingly dominated by methanogenesis as the available iron is consumed, and the greatest iron reduction activity was found down gradient toward the trailing edge of the oil pool. Concurrent with the downgradient shift in iron reduction activity is documented a shift in the highest silica concentration, which in 1998 exceeded 1.3 mmole l^{-1} and was also found downgradient of the trailing edge of the oil. From the geochemical data it appears that the feldspar weathering follows the iron reducing bacteria.

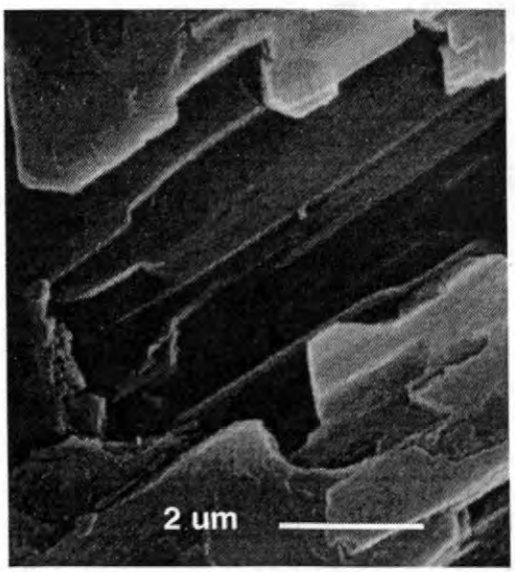

Figure 4. SEM micrograph of a single etch pit on South Dakota Microcline reacted in the anoxic region of the aquifer for 1 year, and then cleaned by brief ultrasonification. The pit is probably the result of the dissolution of an apatite inclusion..

The field microcosms experiments suggest that mineral weathering is primarily associated with surface colonizing bacteria, and that there is significant variability in colonization pattern and density (See Rogers and others, this volume), and density and depth of etch-pits, on different silicates. Significant colonization of feldspars is only observed in the very anaerobic zone, and those feldspars that are colonized all show evidence of rapid and extensive dissolution. Other feldspars in the same location, however, are uncolonized and unweathered. The apparent rate of dissolution of the colonized surfaces, based on etch pit depth is *at least* a factor of 100 greater than the uncolonized surfaces (Bennett, Hiebert, and Choi, 1996).

We found that the feldspars that are colonized in this system all contain minor phosphorus, while virtually identical feldspars without phosphorus are uncolonized and unweathered (Rogers, Bennett, and Choi, 1998; Rogers, Bennett, and Ullman, 1998). The P is present as apatite inclusions, and based on simple leaching experiments appears to be in a form available to the microorganisms. Some etch features on the microcline surface appear to be the remnant of an apatite blade (Figure 5).

Feldspar Dissolution Kinetics

The weathering pattern on the colonized feldspars suggest that the microorganisms are dissolving the feldspar matrix in addition to the exposed apatite inclusion. This is reasonable considering the exposed surface area of silicate vs. the surface area of exposed apatite inclusion. Assuming the organism is colonizing these surfaces to gain access to limiting P (and no other systematic difference has been identified to date) feldspar matrix must eventually be removed to expose new P. There are, however, a limited number of mechanisms available to accelerate silicate dissolution. Principally this can accomplished by perturbing temperature, pH or ionic strength, or by the production of metal chelating ligands (Brady and Walther, 1989; Welch and Ullman, 1993; Welch and Vandevivere, 1995).

In the laboratory experiments, we examined the dissolution dynamics of one feldspar that consistently is colonized and weathered (microcline) and one feldspar that consistently is uncolonized and unweathered (albite). The results of our experiments were then compared to other published results using similar material to try and identify possible mechanisms for the microbial acceleration of weathering. We found

that the dissolution rate of both feldspars is nearly independent of proton activity between pH 6.5 (the ground water pH) and pH 4.5, while the rate of dissolution only increases by a factor of ~3.3 between pH 4.5 and 3.0 for the microcline. Dissolution rate *decreases* with increasing ionic strength (using LiCl as an ionic strength buffer) by 50-75% up to I = 0.05 molar, with a larger effect found at lower temperature. These results suggest that ionic strength is not a factor, and the pH around the attached microorganism would have to be substantially less than 3.0 to achieve the observed field rate of microcline dissolution, an unreasonable expectation (Barker, Welch, and others, 1998).

The dissolution rate of both the albite and microcline, however, increased by a factor of 10-50 with even low (0.1-1.0 mM) concentrations of the iron-chelating ligands, while the apparent activation energy is substantially lower (decreasing from 50 kJ/mol to 32 kJ/mol for microcline). The increase in rate, and decrease in the apparent activation energy suggests that these organic ligands can substantially increase feldspar weathering rate, particularly at low temperature or under a biofilm layer where ligand concentration could be quite high.

IMPLICATIONS

We propose that microorganisms attached to feldspars in this environment are producing reactive ligands, potentially as a mechanism to scavenge scarce ferric iron for metabolic processes. While the concentration of these ligands in the aquifer is only 0.1-1.0 uM, the concentration would be much higher near the attached organism. The result of this ligand excretion therefore is the accelerated weathering of the feldspar, and in some cases, the release of a limiting nutrient. The presence of a limiting nutrient will act as a positive feedback for further metabolism, and possibly, additional colonization. The end result of this interaction is the selective weathering of only those feldspars that provide a nutritive advantage to the microorganism, while almost identical feldspars without nutritive benefit will be left untouched, and presumably preserved in the rock record.

These results represent a unique observation of the interaction of microorganisms with minerals *in situ* and the influence of microbial metabolism on mineral weathering and secondary mineral precipitation. Destruction of silicate minerals to access limiting inorganic nutrients appears to be a fundamental aspect of subsurface microbial ecology, and of the natural attenuation of oil by native microorganisms. This also has implications for our conceptual understanding of mineral diagenesis and the time-sequence of mineral weathering. A basic tenet of sediment diagenesis is the "Goldich Weathering Sequence" (Goldich, 1938), which states that the most unstable silicate mineral will weather (dissolve) first, with more resistant silicates taking progressively longer to dissolve. The ideal weathering sequence for the minerals examined in this study (from most to least rapidly weathered) *should* be: Olivine > Plagioclase > Albite > Anorthoclase > Microcline > Quartz, But the weathering sequence observed here is almost opposite, with olivine stable with respect to quartz and microcline. The evidence from this study suggests that in *some* environments the indigenous microorganisms may significantly alter weathering patterns as they aggressively scavenge limiting nutrients.

If microorganisms are colonizing and destroying specific feldspars in order to release limiting nutrients, then feldspar weathering is not simply a random event controlled by simple abiotic kinetic rate laws and mechanisms. In this microbial weathering scenario, colonized feldspars containing trace nutrients of value may weather very quickly and early, leaving only a clay residuum and those feldspars without nutritive value.

REFERENCES

Baedecker, M.J., Cozzarelli, I.M., Siegel, D.I., Bennett, P.C., and Eganhouse, R.P., 1993, Crude oil in a shallow sand and gravel aquifer-III. Biochemical reactions and mass balance modeling in anoxic groundwater: Applied Geochemistry, v. 8, p. 569-586.

Barker, W.W., Welch, S.A., Chu, S., and Banfield, J.F., 1998, Experimental observations of the effects of bacteria on

aluminosilicate weathering: American Mineralogist, v. 83, p. 1551-1563.

Bennett, P.C., and Casey, W.H., 1994, Organic acids and the dissolution of silicates, *in* Pittman, E.D., and Lewan, M., eds., The role of organic acids in geological processes, Springer-Verlag, p. 162-201.

Bennett, P.C., and Hiebert, F.K., 1992, Microbial mediation of silicate diagenesis in organic-rich natural waters: Proceedings International Symposium on Water Rock Interaction, p. 7; Pages 267-270.

Bennett, P.C., Hiebert, F.K., and Choi, W.J., 1996, Rates of Microbial Weathering of Silicates in Ground Water: Chemical Geology, v. 132, p. 45-53.

Bennett, P.C., and Siegel, D.I., 1987, Increased solubility of quartz in water due to complexation by dissolved organic compounds: Nature, v. 326, p. 684-687.

Bennett, P.C., Siegel, D.I., Baedecker, M.J., Cozzarelli, I., and Hult, M., 1993, The fate of crude oil in a sand and gravel aquifer I. Inorganic geochemistry: Applied Geochemistry, v. 8, p. 529-549.

Brady, P.V., and Walther, J.V., 1989, Controls on silicate dissolution rates in neutral and basic pH solutions at 25 C.: Geochimica et Cosmochimica Acta, v. 53, p. 2823-2830.

Casey, W.H., and Sposito, G., 1992, On the temperature dependence of mineral dissolution rates: Geochim. Cosmochim. Acta, v. 56, p. 3825-3830.

Choi, W.J., 1997, Silicate dissolution kinetics in organic electrolyte solutions: Austin, Texas, The University of Texas at Austin, Ph.D. Dissertation.

Choi, W.J., and Bennett, P.C., 1995, Dynamics of silicate dissolution in organic and inorganic electrolyte solutions: GSA Abstracts with Programs, v. 27, p. A-44.

Cozzarelli, I.M., Baededecker, M.J., Eganhouse, R.P., and Goerlitz, D.F., 1994, Geochemical evolution of low-molecular-weight organic acids derived from the degradation of petroleum contaminants in ground water: Geochimica et Cosmochimica Acta, v. 58, no. 2, p. 863-877.

Cozzarelli, I.M., Eganhouse, R.P., and Baedecker, M.J., 1990, Transformation of monoaromatic hydrocarbons to organic acids in anoxic groundwater environment: Environmental Geology and Water Science, v. 16, p. 135-41.

Eganhouse, R.P., Baedecker, M.J., Cozzarelli, I.M., Aiken, G.R., Thorn, K.A., and Dorsey, T.F., 1993, Crude oil in a shallow sand and gravel aquifer-II. Organic geochemistry: Applied Geochemistry, v. 8, p. 551-567.

Goldich, S.S., 1938, A study in rock weathering: Journal of Geology, v. 46, p. 17-58.

Hiebert, F.K., 1994, Microbial Diagenesis in Terrestrial Aquifer Conditions: Laboratory and Field Studies.: Austin, TX, University of Texas, Dissertation, 198 p.

Hiebert, F.K., and Bennett, P.C., 1993, Microbial diagenesis of silicates and calcite in an organic-rich aquifer: Abstracts with Programs Geological Society of America, v. 25, no. 6, p. 202.

Lovley, D.R., and Lonergan, D.J., 1990, Anaerobic oxidation of toluene, phenol, and *p*-cresol by the dissimilatory iron reducing organism GS-15: Applied Environmental Microbiology, v. 56, no. 1858-1864.

Rogers, J.R., Bennett, P.C., and Choi, W.J., 1998, Feldspars as a source of nutrients for microorganisms: American Mineralogist, v. 83, p. 1532-1540.

Rogers, J.R., Bennett, P.C., and Ullman, W.J., 1998, Biochemical release of a limiting nutrient from feldspars, *in* Goldschmidt Conference, Toulouse, France.

Ullman, W.J., Kirchman, D.L., Welch, S.A., and Vandevivere, P., 1996, Laboratory evidence for microbially mediated silicate mineral dissolution in nature: Chemical Geology, v. 132, no. 1-4, p. 11-17.

Welch, S.A., and Ullman, W.J., 1993, The effect of soluble organic acids on feldspar dissolution rates and stoichiometry: Geochimica et Cosmochimica Acta, v. 57, p. 2725-2736.

Welch, S.A., and Vandevivere, P., 1995, Effect of microbial and other naturally occurring polymers on mineral dissolution: Geomicrobiology Journal, v. 12, p. 227-238.

AUTHOR INFORMATION

Philip C. Bennett, Jennifer Roberts Rogers, and Wan Joo Choi, Dept. of Geological Sciences, University of Texas, Austin, TX 78712
pbennett@mail.utexas.eduj

Franz K. Hiebert, RMT Inc. 912 Captial of Texas Hwy, Suite 300, Austin, TX 78746-5210

Aromatic and Polyaromatic Hydrocarbon Degradation under Fe(III)-Reducing Conditions

Robert T. Anderson, Juliette N. Rooney-Varga, Catherine V. Gaw, Derek R. Lovley
University of Massachusetts, Amherst, MA 01003

ABSTRACT

Investigations of the Bemidji aquifer have demonstrated that important ground water contaminants such as benzene and naphthalene can be degraded under Fe(III)-reducing conditions found in situ. Mineralization of both compounds occurred without a lag period suggesting that Fe(III)-reducers found in the sediment were oxidizing these contaminants in situ. The area of greatest mineralization activity was confined to a narrow region at the downgradient edge of the Fe(III)-reducing zone. Microbial community analysis using 16S rRNA-based techniques indicated that members of the *Geobacter* family were enriched in sediments collected from this active zone. Furthermore, phylogenetic analyses of DNA sequences recovered from benzene-degrading sediments and enrichment cultures clustered with *Geobacteraceae* known to degrade aromatic compounds while sequences from uncontaminated, background sediments did not. These results could lead to the development of a rapid assay for assessing anaerobic benzene degradation potential at petroleum-contaminated sites.

INTRODUCTION

Petroleum hydrocarbon contamination of aquifers presents a serious threat to ground water resources. While most hydrocarbon compounds are known to be degraded under aerobic conditions many petroleum-contaminated aquifers contain large areas where anaerobic processes are dominant (Anderson and Lovley, 1997; Lovley, 1997b). Specifically, microbial Fe(III) reduction is predicted to be a dominant anaerobic process because Fe(III) is generally the most abundant potential electron acceptor found in aquifer sediments (Lovley, 1997a; Lovley, 1997b). Large decreases in ground water contaminant concentrations are observed in many aquifers where large areas of Fe(III) reduction are observed (Borden and others, 1995; Cozzarelli and others, 1990).

Benzene, a known carcinogen, is relatively mobile in ground water and is often observed to persist in anaerobic environments (Barbaro and others, 1992; Flyvbjerg and others, 1993). Laboratory incubations of sediment have indicated a potential for anaerobic benzene degradation under a variety of anaerobic conditions but the onset of degradation activity is often preceded by long lag periods suggesting that benzene degradation was not occurring in situ (Edwards and Grbic-Galic, 1992; Kazumi and others, 1997; Lovley and others, 1996). Evidence of in situ benzene degradation has been demonstrated in contaminated harbor sediments under sulfate reducing conditions (Coates and others, 1996) and recently in contaminated aquifer sediments under Fe(III)-reducing conditions (Anderson and others, 1998).

Polyaromatic hydrocarbons (PAHs) are also potential ground water contaminants found in petroleum contaminated environments. Many PAHs are known to be carcinogenic and when present in aquifers tend to be associated with the sediment. However some PAHs such as naphthalene do migrate with the ground water and can pose a threat to downgradient water resources (Goerlitz and others, 1985). Most low molecular weight PAH compounds are known to be degraded under aerobic conditions and until recently PAHs were generally thought to persist under anaerobic conditions (Cerniglia, 1992).

Anaerobic PAH degradation has been observed under a variety of electron-accepting conditions. Naphthalene degradation has been observed in laboratory sediment incubations where nitrate was supplied as the electron acceptor (Langenhoff and others, 1996; Thierry and others, 1996) and in contaminated harbor sediments under sulfate reducing conditions (Coates and others, 1996). While naphthalene degradation has also been observed in enrichment cultures established from aquifer sediment under sulfate reducing conditions (Bedessem and others, 1997) and in sulfate reducing ground water downgradient from a leaking underground storage tank (Thierrin and others, 1993), PAH degradation has not been previously observed under Fe(III)-reducing conditions.

This paper describes the results of a study to further examine anaerobic aromatic and polyaromatic degradation within petroleum-contaminated aquifers. The results demonstrate that benzene and naphthalene can be degraded under Fe(III)-reducing conditions found in some but not all petroleum-contaminated aquifers. When this activity is found it may be largely restricted to narrow regions of the aquifer at the downgradient edge of the Fe(III) reduction zone. Furthermore, the detection of specific Fe(III)-reducing microorganisms could lead to the development of a rapid assay to assess benzene degradation potential in petroleum-contaminated aquifers.

MATERIALS AND METHODS

Sediment Collection and TEAP Determination

Sediment samples were collected from a variety of petroleum-contaminated aquifers and evaluated for the potential to anaerobically degrade aromatic and polyaromatic compounds as previously described (Anderson and Lovley, 1999; Anderson and others, 1998; Murphy and Herkelrath, 1996). All sediment samples were collected using either a truck mounted drill rig or hand augers. Sediments collected at the Bemidji aquifer in 1997 are from sites shown in Figure 1.

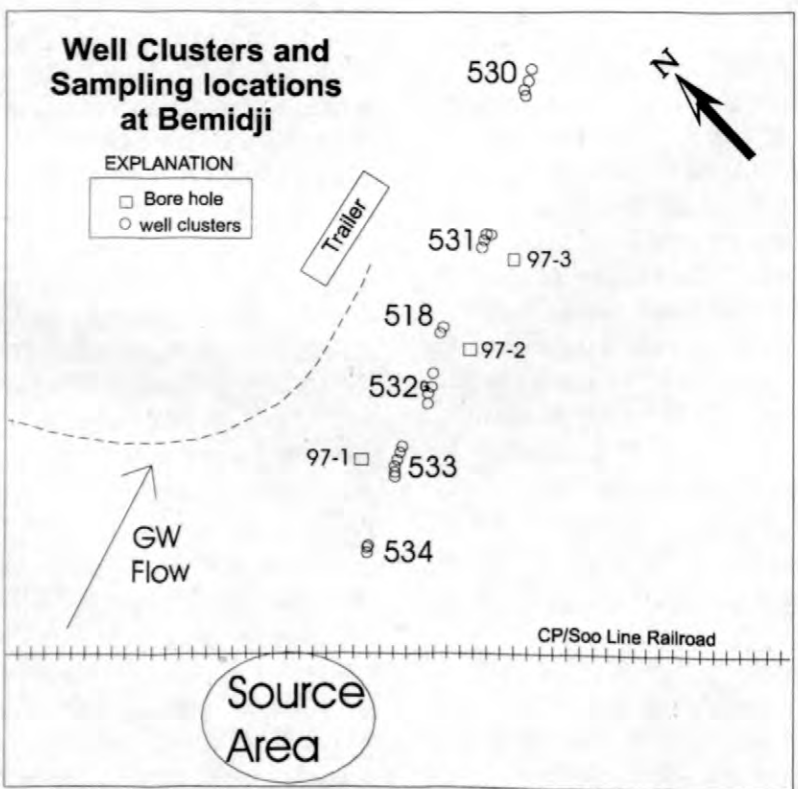

Figure 1. Well clusters and sediment sampling locations at the Bemidji site (adapted from Anderson and others, 1998).

The dominant terminal electron accepting process (TEAP) in collected sediments was assessed using [2-^{14}C]acetate as previously described (Anderson and others, 1998). Fe(III)-reducing conditions are confirmed as the dominant anaerobic process in sampled sediments if the following criteria are met: 1) ground water is depleted of nitrate, 2) Fe(II) is present in the sediments, 3) mineralization of [2-^{14}C]acetate is not inhibited by molybdate, 4) no $^{14}CH_4$ production observed when sediments are incubated with [2-^{14}C]acetate. The Fe(II) content of the sediments was evaulated using a 0.5N HCl extraction followed by measurement with ferrozine.

Ground Water Analysis

Ground water samples for anion analysis were collected in 40 mL vials or 58 mL serum bottles, chilled on ice and sent via overnight carrier to the laboratory. Once in the laboratory, the samples were immediately analyzed for nitrate and sulfate by ion chromatography (Dionex, DX-100, Sunnyvale, CA). Ground water samples for benzene analysis were placed into no-headspace 40 mL vials and preserved with HCl prior to overnight shipment to the laboratory. Benzene samples were analyzed by gas chromatography (HP6890, Wilmington, DE) coupled with a purge and trap autosampler (OI-Analytical, DPM-16, College Station, TX) according to a modification of EPA method 8015/8020.

Mineralization of Radiolabeled Substrates

The potential for benzene, toluene, naphthalene and phenanthrene degradation in sediments was assessed using [^{14}C]-labeled substrates as previously described (Anderson and Lovley, 1999; Anderson and others, 1998). Sediments (30g) were dispensed into triplicate sets of serum bottles inside an N_2-filled glove bag and stoppered with thick butyl rubber stoppers. Anaerobic stock solutions of [^{14}C]-labeled benzene and toluene were prepared using an adaptation of the manufacturer's recommended method of transfer and were added to provide 1μCi of labeled substrate to each sediment bottle.

Radiolabeled naphthalene and phenanthrene, supplied in methanol stocks, were first applied to sediment pellets prepared from the tested sediments and the methanol allowed to evaporate (Anderson and Lovley, 1999). The sediment pellets were then added to serum bottles while under a stream of anaerobic N_2. The bottles were vigorously shaken to break up and disperse the pellets inside the bottles.

Headspace samples (1ml) of bottles containing radiolabeled substrates were removed over time and analyzed for $^{14}CO_2$ and $^{14}CH_4$ using gas chromatography and gas proportional counting detection. Total mineralization percentages were calculated based on the partitioning of $H^{14}CO_2$ between bottle headspaces and the sediment.

Analysis of Microbial Populations in the Sediment

Analyses of the microbial subsurface community was performed using 16S rRNA-based techniques as previously described (Anderson and others, 1998; Rooney-Varga and others, 1999). Since cultivation-based community analyses can selectively bias the results, a more direct approach was applied at the Bemidji site. DNA was extracted directly from sediments and analyzed using both DGGE and MPN-PCR. Briefly, DNA was extracted from triplicate sediment samples using a freeze-thaw method of cell disruption followed by phenol-chloroform extraction or with the FastDNA soil extraction kit (Bio 101, Vista, CA). For bacterial community analyses, portions of the 16S rDNA sequences were amplified using the PCR and primers 338F-GC and 907R. For analysis of the *Geobacteraceae* community within sediments, 16S rDNA sequences were amplified using primers 338F-GC and Geo825R. The resulting PCR products were subsequently separated on a denaturing gradient electrophoresis gel and resolved with ethidium bromide/transillumination. Excised bands were later sequenced for identification. For MPN-PCR analyses, the extracted DNA was first serially

diluted 10-fold into sterile Milli-Q water and portions of each dilutions were used as template in the PCR. In these analyses, *Geobacteraceae* sequences were amplified using primers 8F and Geo825R. Resulting PCR products were analyzed by gel electrophoresis in agarose (1%) containing ethidium bromide and visualized by transillumination.

RESULTS AND DISCUSSION

Anaerobic Aromatic and Polyaromatic Degradation

Of several sites investigated (Anderson and others, 1998), Bemidji aquifer sediments were the only samples collected that demonstrated a potential for benzene degradation under Fe(III)-reducing conditions. While all sediments from all sites demonstrated a potential for toluene degradation only sediments from a narrow region at the downgradient edge of the Fe(III) reduction zone (site 97-3) at Bemidji readily mineralized [^{14}C]benzene to $^{14}CO_2$ (Figure 2). No lag period was observed prior to the onset of mineralization suggesting that the organisms within the sediment were preadapted for benzene oxidation and therefore must be oxidizing benzene in situ. No benzene mineralization was observed in uncontaminated, background sediments from Bemidji implying that the observed benzene degradation is associated with petroleum contamination.

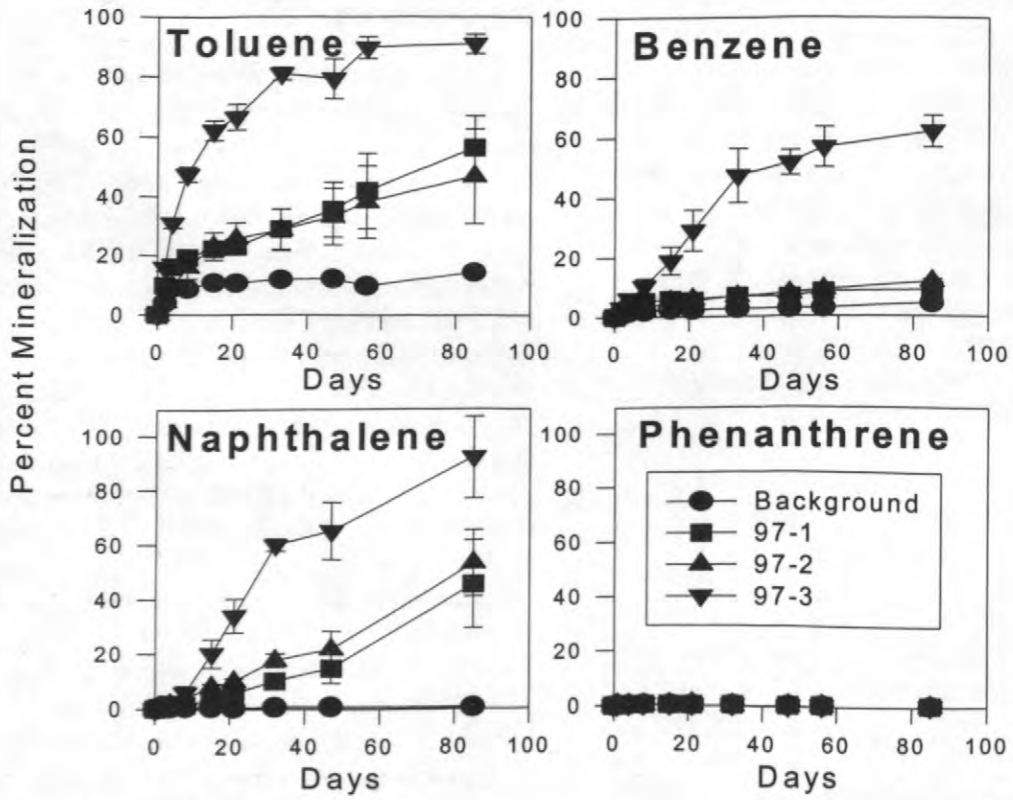

Figure 2. Mineralization [^{14}C] toluene, benzene, naphthalene and phenanthrene in sediments collected from the Bemidji aquifer (adapted from Anderson and Lovley, 1999; Anderson and others, 1998). Results are averages of triplicate analyses.

Bemidji sediments not only rapidly mineralized benzene under Fe(III)-reducing conditions but also readily mineralized [^{14}C]naphthalene to $^{14}CO_2$. Again, the onset of mineralization was immediate with no lag period suggesting that organisms present within the subsurface were preadapted for naphthalene degradation and were likely mineralizing this compound in situ. No naphthalene degradation was observed in uncontaminated sediments again indicating that this activity is associated with petroleum contamination. In addition, no mineralization of [^{14}C]phenanthrene was observed in any Bemidji sediments under Fe(III)-reducing conditions demonstrating that oxygen contamination could not account for the observed benzene or naphthalene degradation in contaminated sediments. Phenanthrene is readily oxidized under aerobic conditions but its anaerobic degradation potential may be hindered due to solubility limitations.

These results are the first documented evidence of the potential for *in situ* oxidation of benzene and naphthalene under Fe(III)-reducing conditions found in petroleum-contaminated aquifers. The greatest rates of toluene, benzene and naphthalene degradation were restricted to a narrow region at the downgradient edge of the Fe(III) reduction zone. These observations indicate that the downgradient edge of Fe(III) reduction zone at Bemidji is an area of intense microbial activity. Detection of similar zones in other petroleum-contaminated aquifers could lead to better understanding of the contribution of anaerobic process to the natural attenuation of ground water contaminants.

Association of *Geobacteraceae* with Anaerobic Benzene Degradation

Investigation of the microbial communities within the Bemidji aquifer focused on organisms involved in the degradation of benzene under Fe(III)-reducing conditions because benzene is frequently the contaminant of greatest concern when present in ground water. DGGE analysis of Bemidji sediments using *Bacteria* primers indicated that relatively few species dominated at each site, particularly the background site (Figure 3).

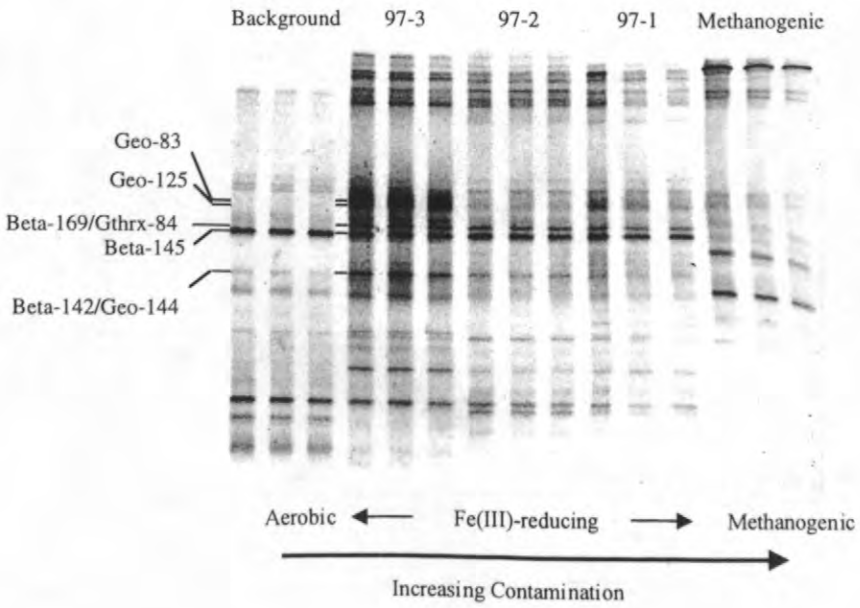

Figure 3. DGGE analysis of DNA extracted from triplicate samples of Bemidji sediment and amplified using *Bacteria* specific primers (adapted from Rooney-Varga and others, 1999). Methanogenic sediments were collected near well cluster 534.

Differences in community composition between background sediments and contaminated sediments were clearly evident as well as differences among the different TEAP zones. More bands were recovered from sediments within contaminated portions of the aquifer than in uncontaminated portions suggesting that the presence of crude oil in the subsurface stimulated the growth of microorganisms that were not previously dominant in the sediments

Previous cultivation-based results suggested that *Geobacteraceae* were enriched in benzene-degrading sediments collected at site 97-3 (Anderson and others, 1998). While the DGGE results using primers specific for *Bacteria* indicated no dramatic differences among the three Fe(III)-reducing sites investigated, a few bands of much higher intensity corresponding to *Geobacteraceae* (Geo-83, Geo-125) were found in sediments from site 97-3 (Figure 3) suggesting that these organisms were selectively enriched in 97-3 sediments. Members of the *Geobacteraceae* are strict Fe(III)-reducers many of which are known to completely oxidize aromatic compounds. Bands corresponding to *Geothrix* species (Gthrx-84) were found among all Fe(III)-reducing sites while a sequence from the β-proteobacteria (Beta-145) was found in both the background and all Fe(III)-reducing sites. These organisms are not known to oxidize aromatic compounds.

MPN-PCR analysis of DNA extracted from sediments provides an unbiased analysis of the numerical abundance of microbial species relative to cultivation-based techniques. When Fe(III)-reducing sediments collected from the Bemidji aquifer were analyzed by MPN-PCR, *Geobacteraceae* were found to be enriched in sediments known to degrade benzene (Figure 4). *Geobacteraceae* sequences enumerated in benzene-degrading sediments from site 97-3 were more than four orders of magnitude greater than background sediments and more than three orders of magnitude greater than other Fe(III)-reducing sediments that did not degrade benzene (97-1, 97-2). Site 97-3 is located near wells where the concentration of benzene in the ground water sharply decreases with downgradient distance (Figure 5). These results suggest that elevated numbers *Geobacteraceae* detected in benzene-degrading sediment play an important role in removing benzene from the ground water.

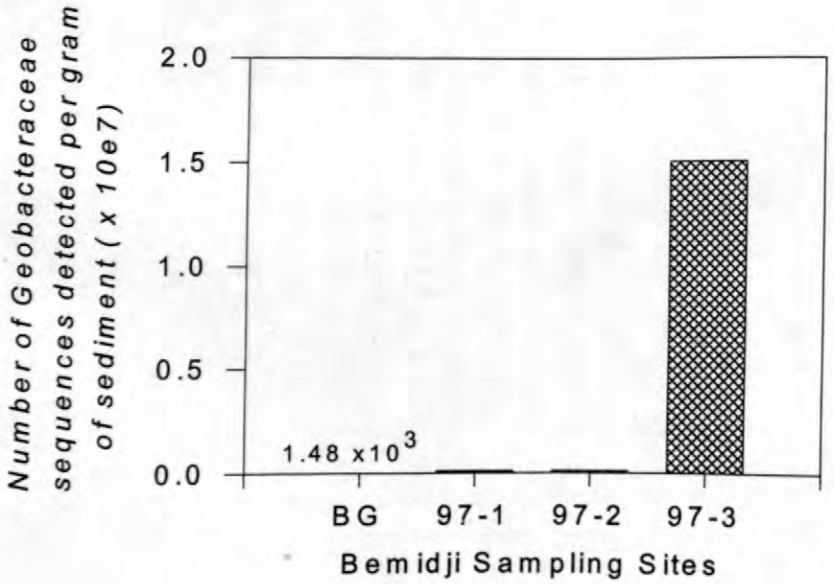

Figure 4. Enumeration of *Geobacteraceae* by MPN-PCR in sediments collected from the Bemidji aquifer (adapted from Anderson and others, 1998). BG is the background site.

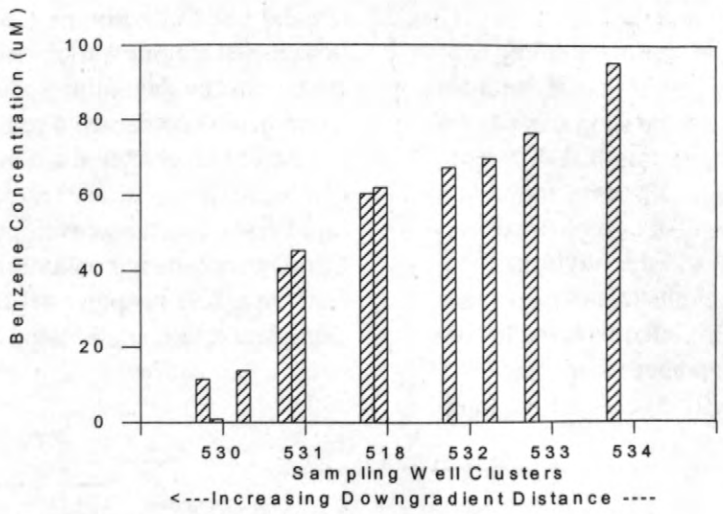

Figure 5. Ground water benzene concentrations in wells at increasing distances downgradient from the source area. Results are averages of triplicate analyses. Sediments sampling site 97-3 is near well cluster 531.

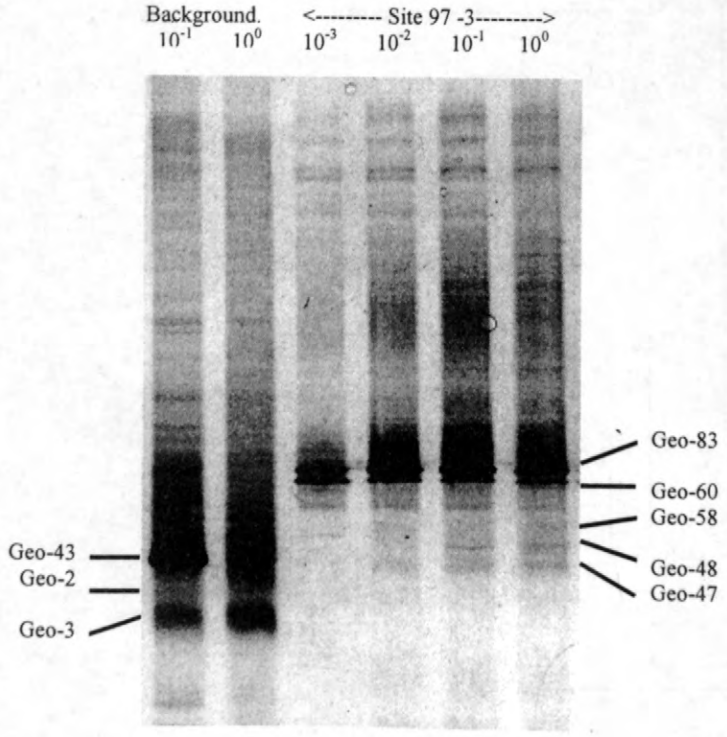

Figure 6. Comparison of *Geobacteraceae* detected in benzene-degrading sediment from site 97-3 and an uncontaminated background sediment (adapted from Rooney-Varga and others, 1999).

More intensive DGGE analysis contrasted the differences between *Geobacteraceae* recovered from site 97-3 and the background sites (Figure 6). Bands from benzene-degrading sediment were clearly different than those from background sediments with no shared bands between the two sites suggesting that different populations of *Geobacteraceae* were found in each sediment. When sequences recovered from both sites were analyzed to infer phylogenetic relationships, two distinct clusters of organisms were observed which correlated with the location of sediment samples. Sequences from the benzene-degrading site (97-3) clustered among *Geobacteraceae* known to degrade aromatic compounds while sequences from the background site did not. Furthermore, DNA extracted from a benzene-degrading enrichment culture established from benzene-degrading sediment collected at Bemidji also contained a sequence (Benz-76, Figure 7) that clustered among the *Geobacteraceae*. These results suggest that a rapid assay could be developed to detect *Geobacteraceae* in contaminated sediments in order to assess the potential for anaerobic benzene degradation in contaminated aquifers.

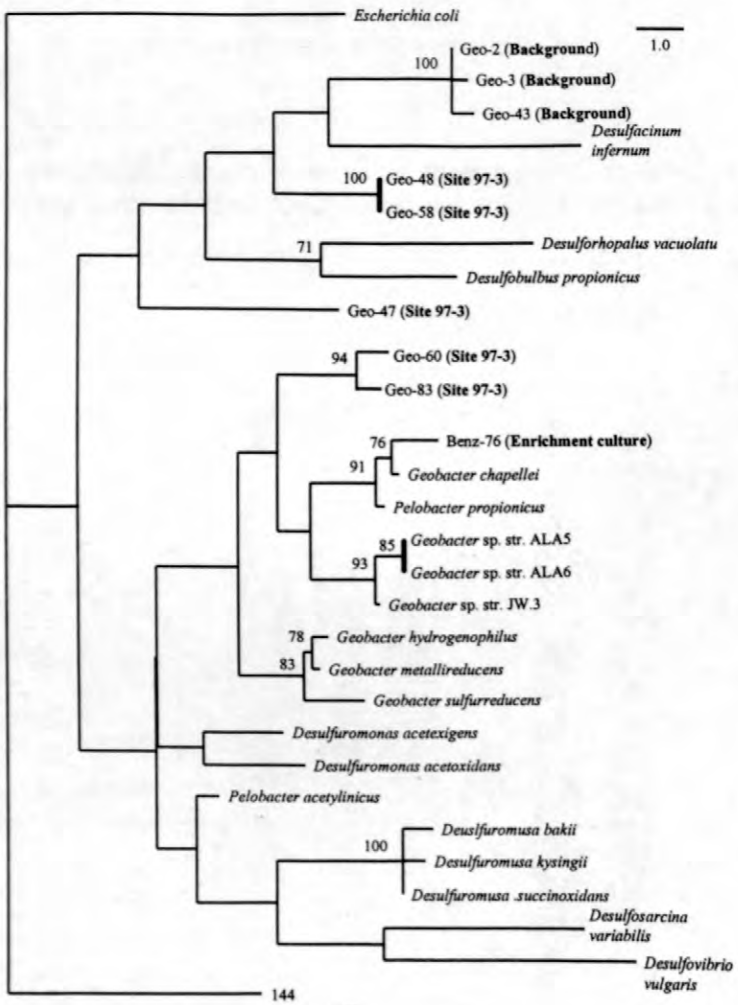

Figure 7. Phylogenetic relationship of sequences detected in benzene-degrading sediment from site 97-3, from an background site and a benzene-degrading enrichment culture developed from benzene degrading sediment collected at the Bemidji site (adapted from Rooney-Varga and others, 1999).

REFERENCES

Anderson, R.T. and Lovley, D.R. 1997. "Ecology and biogeochemistry of in situ groundwater bioremediation." In: (J. G. Jones, ed.) *Advances in Microbial Ecology.*, vol. 15, pp. 289-350, Plenum Press, New York.

Anderson, R.T. and Lovley, D.R. 1999. "Naphthalene and benzene degradation under Fe(III)-reducing conditions in petroleum-contaminated aquifers." *Bioremediation Journal,* (in press).

Anderson, R.T., Rooney-Varga, J.N., Gaw, C.V., Lovley, D.R., 1998. "Anaerobic benzene oxidation in the Fe(III) reduction zone of petroleum-contaminated aquifers." *Environmental Science and Technology, 32*(9):1222-1229.

Barbaro, J.R., Barker, J.F., Lemon, L.A., Mayfield, C.I., 1992. "Biotransformation of BTEX under anaerobic, denitrifying conditions: field and laboratory observations." *Journal of Contaminant Hydrology, 11*:245-272.

Bedessem, M.E., Swoboda-Colberg, N.G., Colberg, P.J.S., 1997. "Naphthalene mineralization coupled to sulfate reduction in aquifer-derived enrichments." *FEMS Microbiology Letters, 152*:213-218.

Borden, R.C., Gomez, C.A., Becker, M.T., 1995. "Geochemical indicators of intrinsic bioremediation." *Ground Water, 33*:180-189.

Cerniglia, C., E. 1992., "Biodegradation of polycyclic aromatic hydrocarbons." *Biodegradation, 3*:351-368.

Coates, J.D., Anderson, R.T., Lovley, D.R., 1996. "Oxidation of polycyclic aromatic hydrocarbons under sulfate-reducing conditions." *Applied and Environmental Microbiology, 62*(3):1099-1101.

Cozzarelli, I.M., Eganhouse, R.P, Baedecker, M.J., 1990. "Transformation of monoaromatic hydrocarbons to organic acids in anoxic groundwater environment." *Environmental Geology and Water Science, 16*(2):135-141.

Edwards, E.A. and Grbic-Galic, D., 1992. "Complete mineralization of benzene by aquifer microorganisms under strictly anaerobic conditions." *Applied and Environmental Microbiology, 58*:2663-2666.

Flyvbjerg, J., Arvin, E., Jensen, B.K., Olsen, S.K., 1993. "Microbial degradation of phenols and aromatic hydrocarbons in creosote-contaminated groundwater under nitrate-reducing conditions." *Journal of Contaminant Hydrology, 12*:133-150.

Goerlitz, D.F., Trouman, D.W., Godsy, E.M., Franks, B.J. 1985. "Migration of wood-preserving chemicals in contaminated groundwater in a sand aquifer at Pensacola, Florida." *Environmental and Science Technology, 19*:955-961.

Kazumi, J., Caldwell, M.E., Suflita, J.M., Lovley, D.R., Young, L.Y., 1997. "Anaerobic degradation of benzene in diverse anoxic environments." *Environmental Science and Technology, 31*:813-818.

Langenhoff, A.A.M., Zehnder, A.J.B., Schraa, G., 1996. "Behavior of toluene, benzene and naphthalene under anaerobic conditions in sediment columns." *Biodegradation, 7*:267-274.

Lovley, D.R. 1997a. "Microbial Fe(III) reduction in subsurface environments." *FEMS Microbiology Reviews, 20*:305-313.

Lovley, D.R. 1997b. "Potential for anaerobic bioremediation of BTEX in petroleum-contaminated aquifers." *Journal of Industrial Microbiology, 18*:75-81.

Lovley, D.R., Woodward, J.C., Chapelle, F.H., 1996. "Rapid anaerobic benzene oxidation with a variety of chelated Fe(III) forms." *Applied and Environmental Microbiology, 62*:288-291.

Murphy, F. and Herkelrath, W.N. 1996. "A sample-freezing drive shoe for a wire line piston core sampler." *Ground Water Monitoring and Remediation, 16*(3):86-90.

Rooney-Varga, J., Anderson, R.T., Fraga, J. L., Ringelberg, D., Lovley, D.R., 1999. "Microbial communities associated with anaerobic benzene degradation in a petroleum-contaminated aquifer." *Applied and Environmental Microbiology,* (submitted).

Thierrin, J., Davis, G.B., Barber, C., Patterson, B.M., Pribac, F., Power, T.R., Lambert, M., 1993. "Natural degradation rates of BTEX compounds and naphthalene in a sulphate reducing groundwater environment." *Hydrological Sciences, 38*:309-322.

Thierry, P.-A.B., Hohener, P., Haner, A., Zeyer, J., 1996. "Degradation of weathered diesel fuel by microorganisms from a contaminated aquifer in aerobic and anaerobic microcosms." *Environmental Toxicology and Chemistry, 15*(3):299-307.

Electrical Geophysics at the Bemidji Research Site

By Robert J. Bisdorf

ABSTRACT

Self-potential (SP), induced polarization (IP), and direct-current (DC) resistivity electrical geophysical methods were used to study the effect of crude oil on the resistivity of a sand and gravel aquifer near Bemidji, Minnesota. The SP measurements do not show any trends that correspond with the oil spill. The IP data show resistivities consistent with the DC measurements, but only a slight polarization effect. Direct-current resistivity measurements made into maps and cross sections, detect lower resistivities associated with the oil spill, especially in areas where the oil soaked into the sand and gravel. The observed resistivity measurements show a larger resistivity decrease than can be explained by laboratory measurements made on selected samples of the sand and oil.

INTRODUCTION

In 1979 a crude oil pipeline burst spilling about 1,700,000 L of oil onto the glacial outwash aquifer about 16 km northwest of Bemidji, Minnesota. Initial cleanup efforts recovered about 1,300,000 L of crude oil leaving about 400,000 L in the aquifer. Figure 1 shows the general location of the research site, the spray zone, the oil drainage area, and the excavated area. The broken pipeline sprayed crude oil to the northwest. This oil drained from the topographic high through the drainage are to the south oil pool. The excavated area is the area around the pipeline excavated for repair of the pipe as well as for oil recovery.

The glacial outwash sand and gravel is about 8m thick and is underlain by other stratified glacial deposits. A uniform glacial till underlies the stratified glacial deposits at a depth of about 25 meters (Smith and Hult, 1993). In 1998 the U.S. Geological Survey made surface electrical geophysical measurements at this site to determine the effect of crude oil on the electrical properties of the sand and gravel aquifer. Self-potential (SP), induced polarization (IP), and Direct-current (DC) resistivity electrical geophysical methods were used. The site is generally clear of cultural features except for many metallic well casings, the crude oil pipelines, a buried telephone line, and buried power cables.

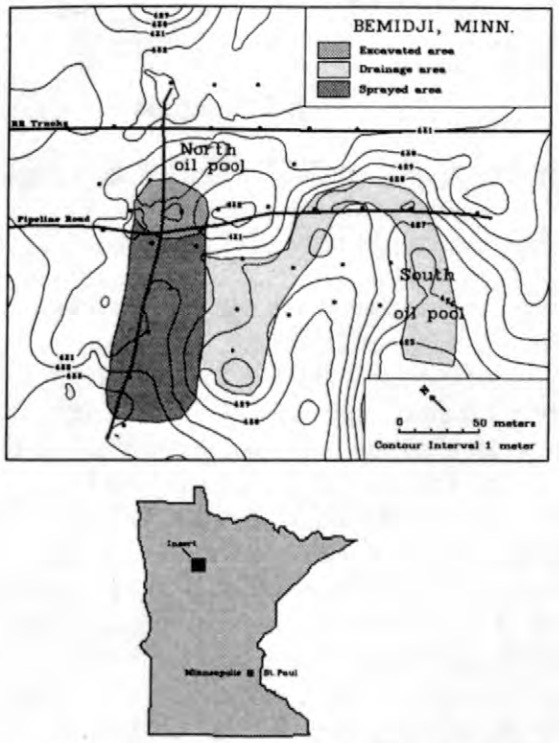

Figure 1. Location of research site near Bemidji, Minnesota (modified from Smith and Hult, 1993) including the location of the north and south oil pools, the excavated area, the spray zone, and the oil drainage area.

SP MEASUREMENTS

The SP method measures natural potential fields in the earth caused by electrokinetic coupling, thermoelectric coupling, and electrochemical reactions (Corwin, 1990). Man made sources of potential from electric power lines and associated equipment are the main source of noise for this method. About 180 total-field SP measurements were made in two sets of

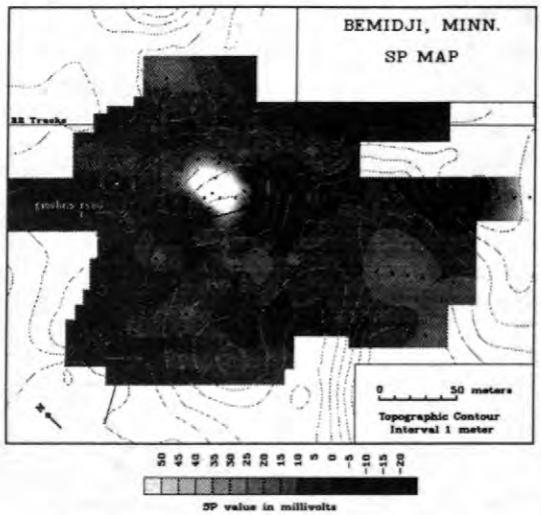

Figure 2. Map of SP values. Black dots indicate measurement locations. Gray scale represents measured voltage in millivolts.

semi-orthogonal lines each with its own zero reference electrode. The 2 data sets were consistent enough to combine into one map. Figure 2 shows a map of the combined data sets. The small black dots represent the measurement locations. Contours of elevation and road locations are overlain for reference. The main feature of the map is a small area of very high (190 mv) SP that occurs just north of the pipeline road. This anomaly is close to the pipeline break and the subsurface oil pool, but I think that the anomaly is generated by electric power lines that were installed to power the automated data loggers. In general the SP trends/anomalies shown on the map can not be correlated with the pooled oil, the oil spray zone, the areas of oil flow, or topography.

INDUCED POLARIZATION

Induced polarization (IP) is a technique that measures the delay in the response of earth materials to an electrical signal. The delay is caused by the build up of charge on metal in an electrolyte or due to membrane effects in clays (Sumner, 1976). The IP response is frequency dependent and measurements made using multiple frequencies are called complex resistivity (CR) or spectral IP (SIP). The frequency domain measurements made for this survey express the IP effect as phase in milliradians. Because the IP response is also dependent on the resistivity/conductivity of the rock, conductivity measurements are also made. Measurements were made at multiple frequencies, but results will only be presented for the lowest frequency (0.125 Hz). The IP measurements were made to detect variations in the clay content of the aquifer, and possible reactions of the crude oil with the clays. Because of its greater signal generation, measurements were made to an "n" of 10, using the pole-dipole array instead of the more conventional dipole-dipole array. The "infinite" current electrode was placed about 245 meters away from the close current electrode. Data were inverted using a computer program licensed from the University of British Columbia-Geophysical Inversion Facility under a consortium research project "Joint/cooperative inversion of geophysical and geological data". The program is based on the work of Oldenburg and Li (1994).

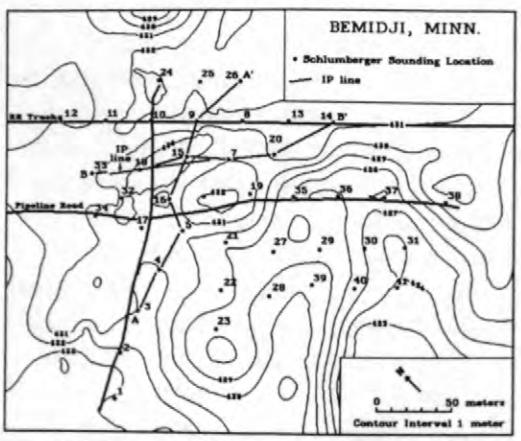

Figure 3. Map showing the location of the Schlumberger soundings, the IP line, and cross sections A-A' and B-B'.

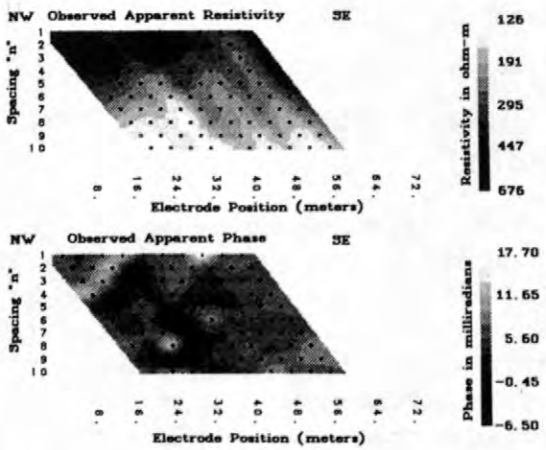

Figure 4. Pseudo sections of apparent IP resistivity and phase.

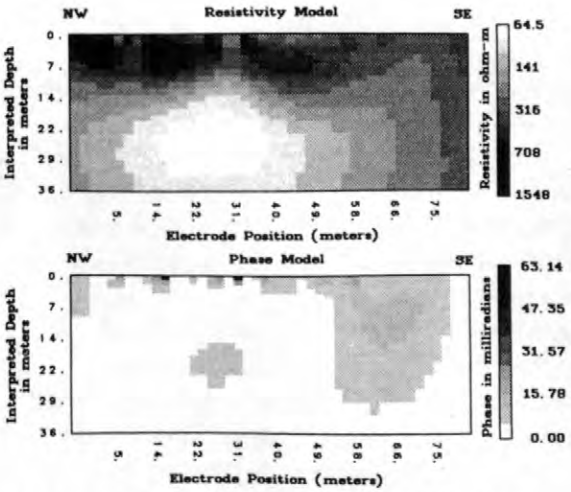

Figure 5. Cross sections of interpreted IP resistivity and phase.

Figure 3 is a location map that shows the location of the IP cross section, and the DC resistivity sounding locations. Contours of elevation, and road locations are displayed for reference. Figure 4 shows pseudo sections of the IP resistivity and phase measurements. The apparent resistivities are high (greater than 700 ohm-m) at the surface and decrease with depth. In addition, the apparent resistivities get lower to the southeast toward the north oil pool. The apparent phase pseudo section shows a phase increase in the area of "n" of 8 to 10 and at an electrode position of 40 to 46 meters. Small phase anomalies are present in the near surface.

Figure 5 shows the IP resistivity and phase models. The resistivity model shows a high resistivity (greater than 700 ohm-m) layer over a zone of dome shaped lower resistivity (less than 100 ohm-m). The phase model shows a low phase layer (less than 5 milliradians) over a dome shaped zone of slightly higher phase (greater than 5 milliradians). To the southeast of electrode position 58 exists a higher phase (7 to 16 milliradians) anomaly that is near the main portion of the north oil pool. This may be caused by the oil pool, but, unfortunately, the anomaly is on the edge of the data set and may not be directly related to the data, but only to initial model parameters and boundary values.

DC RESISTIVITY SOUNDINGS

DC resistivity sounding is a geophysical technique that uses variations in the electrical resistivity of earth materials to help detect buried geologic structures. Resistivity (the inverse of conductivity) is a fundamental rock property that varies due to rock type, clay content, porosity and the quantity and quality of the pore water. Resistivity is normally expressed in ohm-m. Generally speaking, higher clay content and/or poorer quality (more dissolved solids) ground water lowers the rock resistivity.

For this survey the Schlumberger array (Zohdy and others, 1974) was used to vertically explore the subsurface. The name Schlumberger derives from Conrad Schlumberger, an early proponent of the array geometry. Schlumberger soundings are processed by computer modeling of the sounding data as a series of horizontal layers (Zohdy, 1989 and Zohdy and Bisdorf, 1989). More detailed explanations of the processing and automatic interpretation procedure can be found in Bisdorf (1985) and Zohdy and others (1993). A series of individual soundings can be combined to generate either a geoelectrical cross section or a map view of interpreted resistivity. Cross sections, which can be thought of as vertical slices through the ground similar to a road cut, show lateral as well as vertical variations of resistivity. Maps of interpreted resistivity show areal distributions at a particular depth or

elevation and can be thought of as horizontal slices through the earth.

The resistivity of selected samples of sand and crude oil from the site was measured in the laboratory. Table 1 summarizes the results. The resistivity of the crude oil is as expected, very high, but the fact that the resistivity of the wet sand/oil mix was not much different than that of water saturated sand came as a surprise. In fact the resistivity of the oil/water-saturated sand was lower than that of the water-saturated sand. These measurements need to be repeated to verify this result, but as it stands it appears that the oil somehow increases conduction, possibly by forcing the water into more coherent paths. These data indicate that the oil floating on the water table should not be detectable as a resistivity anomaly since the resistivity contrast is small (376/320). Of course mixing oil, sand and water in the lab may not accurately reflect conditions in situ.

Table 1. Measured resistivity of selected samples.

sample description	resistivity (ohm-m)
6/17/98 crude oil	13 meg
moist uncontaminated sand 6/17/98	820
sand saturated with distilled water	376
wet sand saturated with crude oil	320
dry oil contaminated sand	20 meg

Figure 3 shows the Schlumberger sounding locations. The locations of 2 interpreted resistivity cross sections are indicated by the heavy lines labeled A-A' and B-B'. Sounding expansion was limited to a maximum of about 600 meters between the current electrodes (300 meters AB/2). In general, neither the well casings nor the pipeline influenced the Schlumberger sounding measurements. Surface areas of dry, oil coated sand caused some contact resistance problems that were solved by adding water to the electrode holes and stirring to lower the contact resistance.

CROSS SECTIONS OF INTERPRETED RESISTIVITY

Resistivity cross sections are generated from individual sounding interpretations. Each sounding interpretation is sampled in a manner to approximate a continuous vertical distribution of resistivity with depth (Bisdorf, 1982). These vertical distributions are then horizontally interpolated to create a grid. Shades of gray are assigned based on the interpolated resistivity values and the desired contour levels. Triangles on the upper surface of the cross section designate the sounding locations. Topographic information, input as sounding elevations, is represented by connecting the surface location of the soundings by straight lines.

Figure 6 shows the geoelectrical cross section labeled A-A' in Figure 3. This cross section extends across the northern oil pool from southwest to northeast. High resistivities (greater than 700 ohm-m) dominate the upper 10 to 12 meters of this cross section except under soundings 15 and 16 where resistivities are moderate (300 to 700 ohm-m). These high resistivity sediments are similar in resistivity to the moist uncontaminated sand in Table 1. The moderate resistivities are in the area of the oil pool . Sounding 15 is the area where the early oil recovery was done and sounding 16 is close to where the pipeline broke. These moderate resistivities could be due to the oil-recovery/pipeline-repair activities or to some effect of the oil on the sand that would reduce the resistivity of the material. The water table in the area is between 423 and 424 meters in elevation (Smith and Hult, 1993). Under soundings 15 and 16 low resistivity material becomes shallower, with the 150 ohm-m contour rising almost 10 meters. This low resistivity material could be the underlying till, but wells 606 and 607, shown on the cross section, encountered the till between the elevations of 405 and 410 meters. Since this shallowing of the deeper low resistivity zone is in the area of the oil plume, it is possible that it is due, in some unknown fashion, to the effect of the oil.

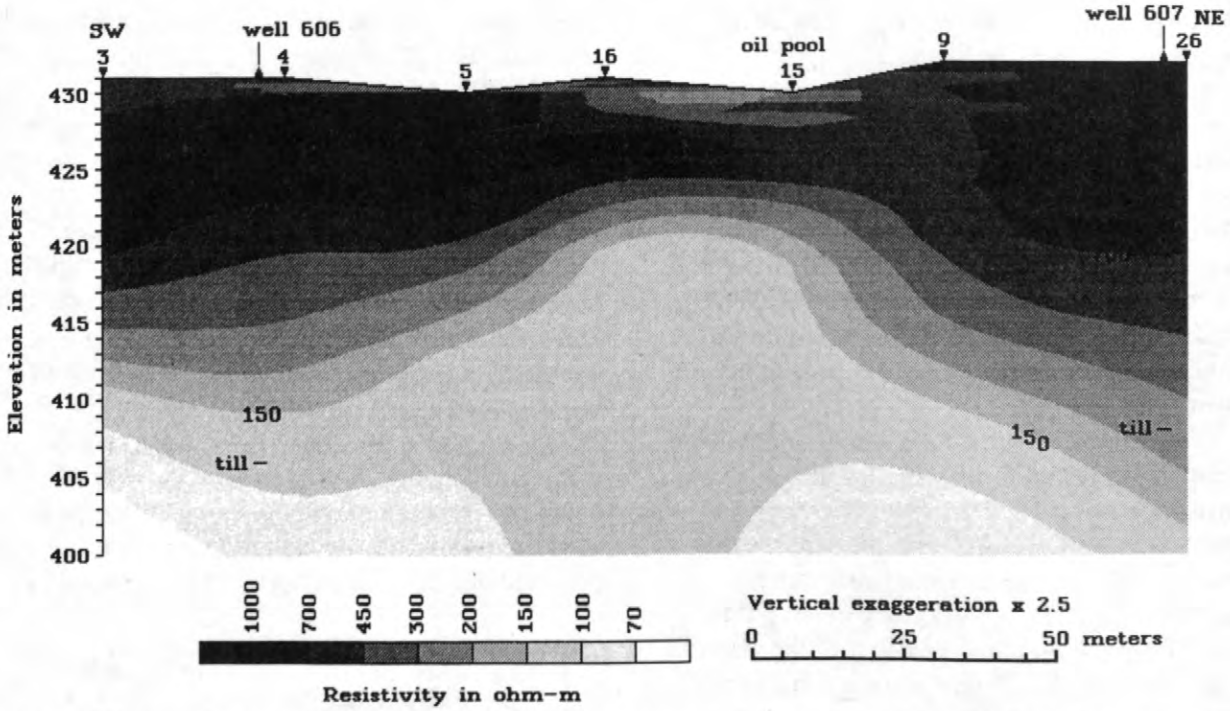

Figure 6. Cross section of interpreted resistivity designated A-A' on figure 3. The gray scale represents interpreted resistivity values in ohm-m. The surface location of the soundings are indicated by the triangles.

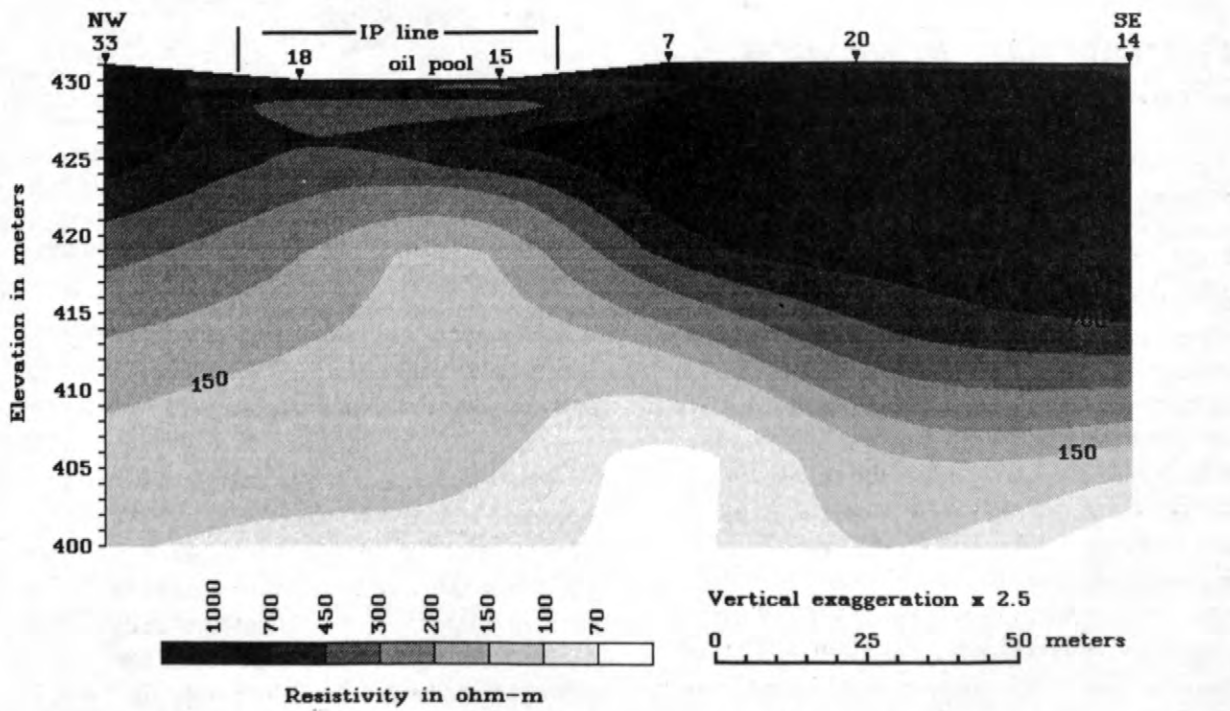

Figure 7. Cross section of interpreted resistivity designated B-B' on figure 3. The gray scale represents interpreted resistivity values in ohm-m. The surface location of the soundings are indicated by the triangles.

Figure 7 shows the geoelectrical cross section labeled B-B' in Figure 3. This cross section extends across the northern oil pool from northwest to southeast. High resistivities of greater than 700 ohm-m dominate the upper 10 to 12 meters of the cross section except under soundings 18, 15, and 7 where resistivities are moderate (300 to 700 ohm-m). This is the area where oil pooled and much of the early oil recovery was done. As in cross section A-A', the 150 ohm-m contour rises to about 10 meters under sounding 15.

It is interesting to note that the water table is not delineated on the eastern portions of these cross sections. High resistivity continues to an elevation of as low as 415 meters. This may be due to coarser sand and gravel being more predominate to the east and south of the plume area effectively masking the effect of the water table. The modeled IP data shown in figure 5 corresponds well with the applicable portion of cross section B-B'. High resistivities to the northwest moderating onto the oil pool area. At depth, low resistivities become more shallow just southeast of sounding 18.

RESISTIVITY MAPS AT SELECTED ELEVATIONS

Maps of interpreted resistivity at a particular elevation are generated by sampling the sounding interpretations at depths determined by the difference between the surface elevation at that sounding and the desired elevation. The resultant sampled interpreted resistivities and the corresponding location values are gridded using a minimum-curvature algorithm (Webring, 1981). To prevent possible interpolated resistivities of less than zero, the logarithm of the resistivities is used for gridding. Shades of gray are assigned based on the grid value and the desired logarithmically spaced contour levels. Since these maps are raster (pixel) based, a bicubic interpolation program is used to increase the size of the resultant image. An interpolating program is used to resample the grid, as opposed to simply gridding the data at the desired final interval, because the minimum-curvature algorithm generates undesirable results if the data are over sampled. The Kolor-map and section program (Zohdy, 1993) uses similar procedures and provides a discussion of the nuances of resistivity map generation.

Figure 8 shows a map of interpreted resistivity made at an elevation of 424 meters. This elevation is just at or above the water table. High resistivities are associated with topographic highs and low resistivities are associated with topographic lows. The area of the north oil pool is designated by "A" in the figure. Letter "B" is associated with moderate to low resistivities in the area where the oil drained after the pipeline break and the southern oil pool. Again, moderate and low resistivities are associated with the presence of a very high resistivity crude oil.

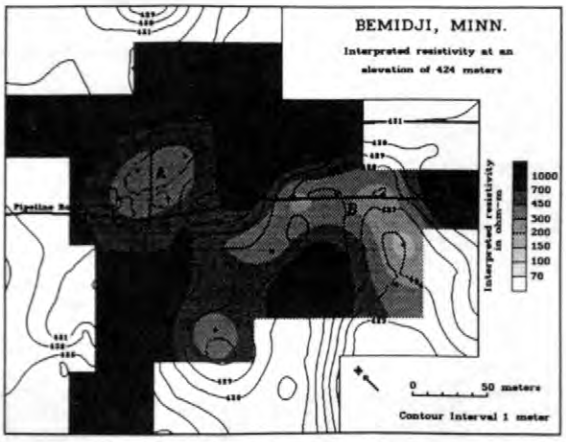

Figure 8. Map of interpreted resistivity at an elevation of 424 meters. The gray scale represents interpreted resistivity in ohm-m. The sounding locations are indicated by the black dots.

SUMMARY

SP data did not show anomalies that correlated with pooled oil, or areas of oil contamination. IP measurements showed an area of low resistivity at depth in the area of the northern oil pool. A small phase anomaly is also associated with this oil pool, although the anomaly is not very large. Additional frequencies need to be modeled to confirm the phase information. DC resistivity sounding data showed a lower resistivity anomaly in areas were

the crude oil had soaked into the sand and in the known pool areas. This is surprising because lab measurements made on selected sand, oil, and sand-oil mixture indicated only a small resistivity contrast. Some mechanism lowering resistivities is in place at the site that is not reflected in my sand samples. It is possible that by products of bacterial activity are lowering the in situ resistivities, or possibly that some fraction of the oil has gone into solution and is lowering the resistivity.

REFERENCES

Bisdorf, R.J., 1982, Schlumberger sounding investigations in the Date Creek Basin, Arizona: U.S. Geological Survey Open-File Report 82-953, 55 p.

___, 1985, Electrical techniques for engineering applications: Bulletin of the Association of Engineering Geologists, v. XXII, no. 4, p. 421-433.

Corwin, R.F., 1990, The self-potential method for environmental and engineering applications in Ward, Stanley H., ed., Geotechnical and environmental geophysics, Vol. I, Review and tutorial: Investigations in Geophysics, 5, p. 127-145.

Lucius, J. E., and Bisdorf, R. J., 1995, Results of geophysical investigations near the Norman, Oklahoma, municipal landfill, 1995: U.S. Geological Survey Open-File report 95-825, 125 p.

Oldenburg, D.W., and Li, Yaoguo. 1994, Inversion of induced polarization data: Geophysics, v. 59, p 1327-1341.

Smith, S.E., and Hult, M.F., 1993, Hydrogeologic data collected from a crude-oil spill site near Bemidji, Minnesota, 1983-91: U.S. Geological Survey Open-File Report 93-496, 158 p.

Sumner, J.S., 1976, Principles of induced polarization for geophysical exploration: Elsevier Scientific Publishing Company, New York, NY, 277 p.

Webring, Michael, 1981, MINC: A gridding program based on minimum curvature: U.S. Geological Survey Open-File Report 81-1224, 12 p.

Zohdy, A.A.R., 1989, A new method for the automatic interpretation of Schlumberger and Wenner sounding curves: Geophysics, v. 54, p. 245-253.

___, 1993, Program Kolor-Map & Section, Amiga Version: U.S. Geological Survey Open-File Report 93-585, 113 p.

Zohdy, A.A.R., and Bisdorf, R.J., 1989, Programs for the automatic processing and interpretation of Schlumberger sounding curves in QuickBASIC 4.0: U.S. Geological Survey Open-File Report 89- 137 A&B, 64 p., + disk.

Zohdy, A.A.R., Eaton, G.P., and Maybey, D.R., 1974, Application of surface geophysics to ground-water investigations, Techniques of ground water investigations of the U.S. Geological Survey, Book 2, Chapter D1:U.S. Geological Survey, Denver, CO, 116 p.

Zohdy, A.A.R., Bisdorf, R.J., and Martin, Peter, 1993, A study of sea-water intrusion using Schlumberger soundings near Oxnard, California: U.S. Geological Survey Open-File Report 93-524, 139 p.

Impacts of Remediation at the Bemidji Oil-Spill Site

By William N. Herkelrath

ABSTRACT

The U.S. Geological Survey has conducted a multidisciplinary investigation of the fate and transport of subsurface petroleum hydrocarbons at the site of crude-oil spill near Bemidji, Minnesota, since 1983. For 19 years, the Bemidji site provided a unique natural laboratory for scientists to study a subsurface oil spill that was virtually undisturbed. However, in order to ensure compliance with the law, Minnesota State authorities have recently mandated oil-recovery remediation of the site. The aim of the remediation is to remove the separate-phase oil that is presently located near the water table. In this paper, simple models were used to obtain first-order estimates of how much subsurface oil is now present at the Bemidji site, and how much oil is likely to be recovered during the remediation. These preliminary results indicate that about 241,000 liters of oil are now present, and about 41,000 liters (17% of the present oil volume) will be recovered during the remediation.

INTRODUCTION

The U.S. Geological Survey, in cooperation with several academic institutions, has conducted a multidisciplinary investigation of the fate and transport of petroleum hydrocarbons within an aquifer at the site of a crude-oil spill near Bemidji, Minnesota, since 1983. A wide range of research has been conducted at the site. Much of the research focused on understanding processes that lead to the natural bioremediation of dissolved hydrocarbons. Work also was done on studying the complex, interrelated inorganic and organic geochemical reactions that occur within a contaminated aquifer. The factors that influence the oil-saturation distribution and the rate of dissolution of separate-phase oil within the aquifer and in the unsaturated zone also were investigated. In the process of the research, a large number of sediment cores were obtained and analyzed in order to create a large database of particle-size and porosity distributions that is useful in developing model representations of the heterogeneous aquifer.

In the past, remediation efforts at the site were limited to a cleanup that was carried out within one month of the pipeline break that caused the spill in August, 1979. Because the site is located in a remote area, there was little demand for further remediation. For 19 years, the Bemidji site provided a unique natural laboratory for scientists to study a subsurface oil spill that was virtually undisturbed. However, in order to ensure compliance with state law, the Minnesota Pollution Control Agency has recently mandated further remediation. The aim of the remediation is to remove the separate-phase oil that is located near the water table at the Bemidji site. Installation of remediation equipment began in 1998, and it is anticipated that oil removal will begin in 1999.

Remediation activities will disrupt much of the ongoing research at the site. It is anticipated that large amounts of water will be pumped out of several wells, which will change the ground-water flow regime and alter the subsurface conditions that have resulted in natural biological degradation of the dissolved contaminants. However, the remediation of the Bemidji site provides an important opportunity to investigate the impact and efficacy of remediation at a well-characterized site. Although the Nation has made a large investment in research, development, and implementation of remediation techniques for petroleum spill sites, very few well-documented field-scale case studies have been published.

This paper reports preliminary quantitative estimates of the anticipated impacts of the proposed remediation on the amount and distribution of subsurface oil at the Bemidji oil-spill site.

Subsurface Oil Prior to Remediation

The primary goal of the remediation will be the removal of some of the separate-phase oil. In order to estimate how much oil is likely to be removed, I first estimated the amount and distribution of oil present prior to remediation. Since 1989, sediment cores were periodically obtained within the two major subsurface oil pools (the "north" and "south" pools) at the Bemidji site. Using the methods described in Hess and others (1992) and Murphy and Herkelrath (1996), the cores were analyzed in order to measure the vertical distribution of oil, air, and water saturation within each core. Because the oil is less dense than water, the oil tends to "float" on the water table. Oil saturation rapidly decreases below the water table. Oil also was found in the unsaturated zone above the water table. Essaid and others (1993) and Dillard and others (1997) published detailed analyses of the oil saturation data.

In order to estimate the total amount of oil present in the north and south pools at the site, I first calculated L_o, the total volume of oil per unit cross-sectional area in each borehole. L_o has dimensions of length, and is equivalent to the length that the oil phase would occupy if the oil were present in a core liner without any sediment. I then interpolated between values of L_o measured at the boreholes in order to create a matrix of estimated values of L_o on a uniform grid. A contour map of the interpolated total volume of oil per unit cross section at the Bemidji north oil pool is shown in figure 1. A contour map of the L_o distribution at the south pool is shown in figure 2. By integrating over the interpolated matrices, I estimated that the total amount of oil present at the north and south pools is 147,000 and 94,000 liters, respectively.

A significant fraction of the oil at the north pool is located above the water table in the unsaturated zone. The water table at the north pool is about six meters below the surface. The "unsaturated zone" oil is probably located beneath areas where the oil originally infiltrated into the soil, and represents a "residual" saturation of oil that is "trapped" or flows very slowly downward. This oil probably will not be mobilized in the proposed "pump and treat" remediation.

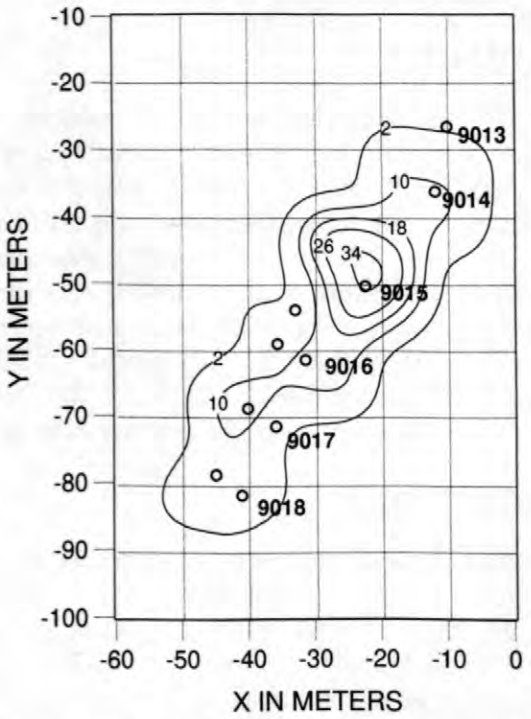

Figure 1. Contour map of the total volume of oil per unit cross section (in centimeters) at the Bemidji north oil pool. Circles indicate borehole locations. USGS well numbers are shown in bold print.

In order to estimate the total amount of oil that may be influenced by the north pool remediation, I assumed that oil that is more than one meter above the water table (or above an elevation of 424.5 meters above sea level) will not be influenced. The cutoff elevation was somewhat arbitrarily selected to roughly correspond to the top of the "capillary fringe," a zone in which both the water and oil saturation rapidly declined above the water table. I calculated L_1, the total volume of oil per unit cross sectional area below 424.5 m in each borehole. A contour map of the interpolated distribution of L_1, which illustrates the areal distribution of oil at the water table at the north pool, is shown in figure 3. By integrating over the interpolated matrix, I

estimated that the total amount of oil near the water table at the north pool is 88,000 liters, and the total amount of oil in the unsaturated zone at the north pool is 59,000 liters.

At the Bemidji south oil pool, the water table is only 2 meters below the surface, and almost all of the oil is near the water table. I assume that all of the oil at the south pool will be influenced by remediation.

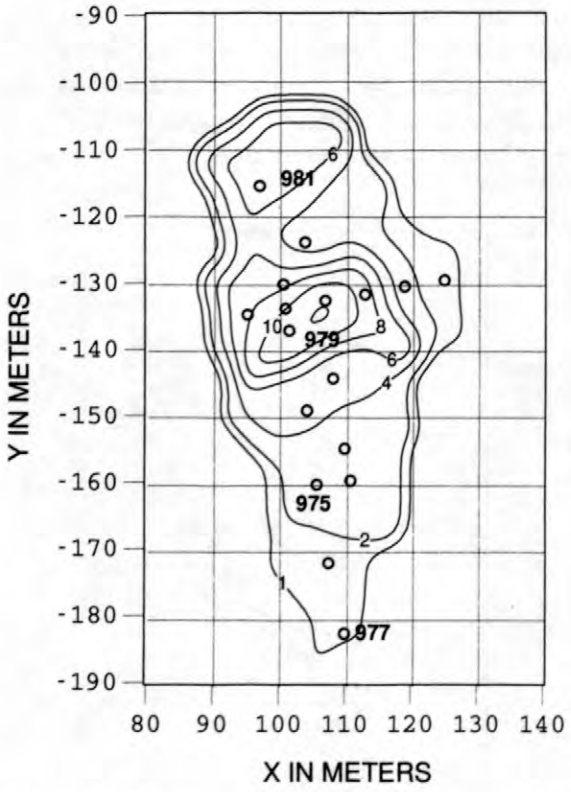

Figure 2. Contour map of the total volume of oil per unit cross section (in centimeters) at the Bemidji south oil pool. Circles indicate borehole locations. USGS well numbers are shown in bold print.

In a reconnaissance carried out in 1998, Lakehead Pipe Line Company discovered another, smaller subsurface oil pool (the "middle pool"), which is located between the north and south pool. The USGS has not cored the middle pool, and I cannot estimate the amount of oil present.

The Remediation Plan

A plan for remediating the Bemidji site was developed by the Lakehead Pipe Line Company (1998). According to the plan, two oil-recovery wells (RW-1N and RW-2N) will be installed at the north oil pool (figure 3). Each of these wells will have a 254-mm diameter and a 3-m long screen that straddles the water table. The plan is to pump water from each well at a rate of 45 liters/minute for 5 years. The idea is to create a depression in the water table near the wells within which oil will tend to collect. It is expected that oil will slowly flow into the wells, where it will be skimmed off of the surface of the water and injected into a nearby oil pipeline. Water removed from the wells will be pumped into an infiltration gallery that is located upgradient.

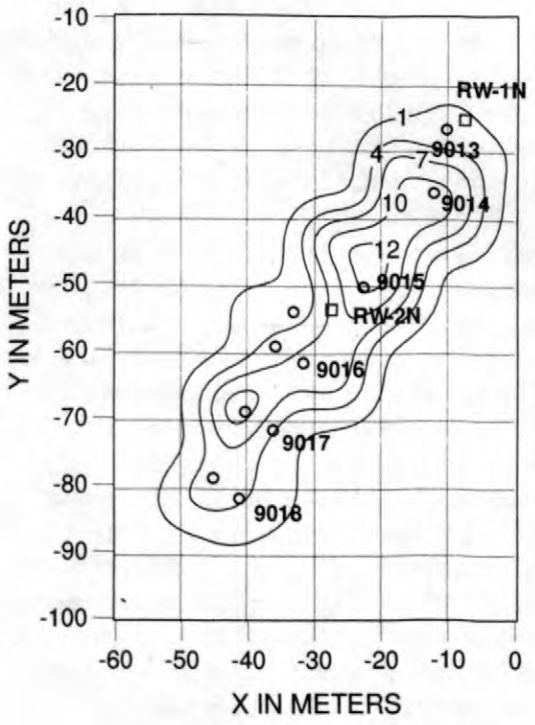

Figure 3. Contour map of the volume of oil per unit cross section (in centimeters) that is located less than one meter above the water table at the Bemidji north oil pool. Circles indicate borehole locations, and squares indicate oil-recovery well locations.

Two oil-recovery wells will also be placed at the middle pool. A total of about 70 liters of water per minute will be pumped from the middle pool area.

A drain tile that is approximately 30 meters long will be installed along the main axis of the south oil pool just below the water table. Water will be pumped from the drain tile at a rate of 80 liters/minute in order to create a linear depression in the water table. It is anticipated that oil will flow into the drain tile and be skimmed off of the surface of the water.

Predicted Oil Recovery

In order to obtain a first-order estimate of the amount of oil that can be recovered by remediation, I adopted the concept of "residual oil saturation," which is commonly used in petroleum engineering (Dullien, 1992). I assumed that wherever the oil saturation is initially above a "residual" value of S_{or}, oil would be removed until the oil saturation was reduced to S_{or}. Therefore, I assumed that the maximum oil saturation after remediation would be S_{or}. Wherever the initial oil saturation was below S_{or}, the oil was assumed to be immobile, and the oil saturation would not change during the remediation.

Residual oil saturation is difficult to estimate. S_{or} has been found to depend on many factors and to vary widely from site to site. For example, Abdul (1992) reported that S_{or} ranged from 0.08 to 0.32 (8 to 32% of the pore space) in small funnels of sand and can be higher in a heterogeneous field environment. At the Bemidji site, one indicator of S_{or} is the level of oil saturation found in the unsaturated zone beneath the location where oil infiltration occurred. After 19 years of drainage, the very oily sediments found in the unsaturated zone near the center of the north oil pool have drained to an oil saturation of 0.25 +/- 0.05. In order to cover the probable range indicated by this data, I calculated oil recovery assuming both $S_{or} = 0.2$ and 0.3.

The "recoverable" oil volume, V_{rec}, that was found in each 75-mm-long core section was used to estimate total oil recovery. V_{rec} was calculated from

$$V_{rec} = V\phi(S_o - S_{or}) \quad (\text{for } S_o > S_{or}), \qquad (1)$$

where

V is the volume of the core section,

ϕ is the porosity of the core section, and

S_o is the oil saturation in the core section.

V_{rec} was assumed to be zero if $S_o < S_{or}$.

Individual V_{rec} values were summed in order to obtain an estimate of the recoverable oil volume per unit cross section, L_{rec}, at each borehole location. For $S_{or} = 0.3$, a contour map of interpolated L_{rec} values at the north pool is shown in figure 4. By integrating over the interpolated L_{rec} matrices, I estimate that 23,000 ($S_{or} = 0.3$) to 37,000 ($S_{or} = 0.2$) liters of oil can be recovered from the north oil pool. Similar calculations using the south pool data indicate that 6,000 to 16,000 liters of oil can be recovered there.

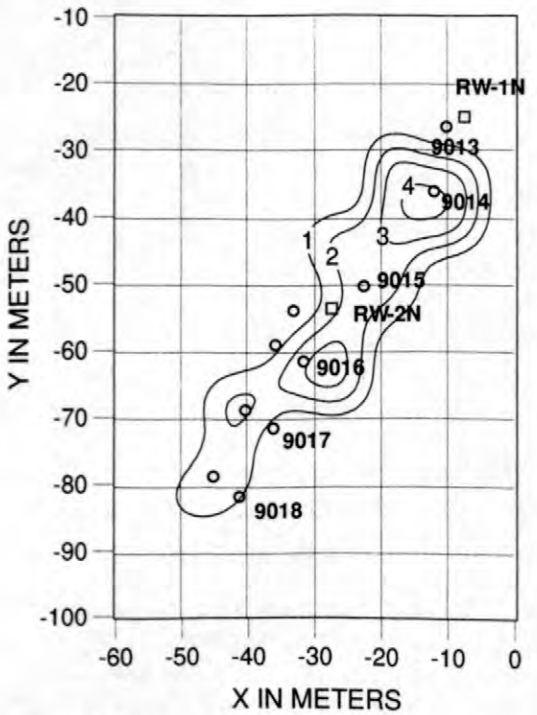

Figure 4. Contour map of the volume of oil per unit cross section (in centimeters) that is likely to be recovered by remediation at the Bemidji north oil pool. Circles indicate borehole locations, and squares indicate oil-recovery well locations.

Subsurface Oil after the Remediation

These preliminary estimates indicate that after the oil-recovery remediation there will still be 110,000 to 124,000 liters of oil at the Bemidji north oil pool. I estimate that 16 to 25% of the

original oil in place will be removed during the north pool remediation. The oil that remains should be spread over roughly the same area outlined by contours in figure 1. At the south pool, I estimate that 7 to 17% of the oil will be removed, and there should still be 78,000 to 88,000 liters in place after the remediation.

SUMMARY AND CONCLUSIONS

The State of Minnesota has mandated oil-recovery remediation of the Bemidji oil-spill site. The USGS has carried out research into the fate and transport of hydrocarbons in the subsurface at this site since 1983. The aim of the remediation, which is scheduled to begin in 1999, is to recover and remove separate-phase oil that is presently located near the water table. The remediation plan calls for pumping large amounts of water out of several recovery wells. Oil will be drawn into the wells, where it will be skimmed off of the water surface and injected into an oil pipeline. Because the natural ground-water flow regime will be greatly changed, most of the ongoing research at the site will be disrupted.

Using extensive data obtained from field cores, I estimated the amount of oil in place at the Bemidji site at present. By applying a simple model based on the concept of residual oil saturation, I obtained a first-order estimate of the amount of oil that can be recovered by the remediation. Oil volumes estimated in this analysis are summarized in table 1. The low oil recoveries predicted (16 to 25% at the north oil pool; 7 to 17% at the south oil pool) are in good agreement with other case studies (Abdul, 1992), and with the experience of the oil industry. These calculations reemphasize how difficult it is to remove separate-phase oil from sediments using pump-and-treat technology.

Table 1. Summary of Bemidji oil volume estimates. All volumes are in liters.

North oil pool:

Total initial volume of oil in the unsaturated zone	59,000	Liters
Total initial volume of oil near the water table	88,000	liters
Total initial volume of oil at the north pool	147,000	liters
Assumed residual oil saturation	0.3	0.2
Estimated recoverable oil volume	23,000	37,000
Recoverable oil volume/initial oil volume	16%	25%

South oil pool:

Total initial volume of oil at the south pool	94,000	liters
Assumed residual saturation	0.3	0.2
Estimated recoverable oil volume	6,000	16,000
Recoverable oil volume/initial oil volume	7%	17%

REFERENCES

Abdul, Abdul S., 1992, A new pumping strategy for petroleum product recovery from contaminated hydrogeologic systems: Laboratory and field evaluations: Ground Water Monitoring Review, v. 12, no. 1, p. 105-114.

Dillard, L.A., Essaid, H.I., and Herkelrath, W.N., 1997, Multiphase flow modeling of a crude-oil spill site with a bimodal permeability distribution: Water Resources Research, v. 33, no. 7, p. 1617-1632.

Dullien, F.A.L., 1992, Porous media fluid transport and pore structure (2nd ed.): San Diego, Academic Press, 574 p.

Essaid, H.I., Herkelrath, W.N., and Hess, K.M., 1993, Simulation of fluid distributions observed at a crude oil spill site incorporating hysteresis, oil entrapment, and spatial variability of hydraulic properties: Water

Resources Research, v. 29, no. 6, p. 1753-1770.
Hess, K.M., Herkelrath, W.N., and Essaid, H.I., 1992, Determination of subsurface fluid contents at a crude-oil spill site: Journal of Contaminant Hydrology, v. 10, p. 75-96.
Lakehead Pipe Line Company, 1998, Remedial investigation and corrective action design report, milepost 926.53, Pinewood, Minnesota, 30 p.
Murphy, Fred and Herkelrath, W.N., 1996, A sample-freezing drive shoe for a wire line piston core sampler: Ground Water Monitoring & Remediation, v. 16, no. 3, p. 86-90.

AUTHOR INFORMATION

William N. Herkelrath, U.S. Geological Survey, Menlo Park, California (wnherkel@usgs.gov)

Ground Penetrating Radar Research at the Bemidji, Minnesota, Crude-Oil Spill Site

By Jeffrey E. Lucius

ABSTRACT

At the Bemidji, Minnesota, crude-oil spill site, the USGS collected ground penetrating radar (GPR) data to determine the distribution of oil concentrated in two subsurface pools, which remained after cleanup efforts. Physical property information from analysis of mixtures of sand and crude oil assisted in the interpretation of the GPR data. Laboratory measurements show that the crude oil is still very electrically resistive (greater than 10^6 ohm-m). Mixing clean sand with crude oil does not significantly change the relative dielectric permittivity (RDP) or electrical conductivity of the mixture. Four GPR lines were selected, from the large number of radar lines collected at the spill site since 1984, as typical examples of 80 MHz and 300 MHz data collected over the oil pools. At the spill site, GPR is sensitive to changes in electrical conductivity and RDP related to variations in water content, due to grain size and porosity, rather than variations in the oil saturation distribution (fraction of pore space occupied by oil). The oil pools at the Bemidji site are not easily detected using GPR. Nonetheless, GPR can detect those geologic features, such as silt or gravel layers in sand, that may affect the transport and fate of petroleum in the subsurface.

INTRODUCTION

In 1979 near Bemidji, Minnesota, one of three buried pipelines broke releasing approximately 1.7 million liters of crude oil contaminating the land surface and shallow subsurface (Hult, 1984; Delin and others, 1998). After cleanup efforts were completed, about one-quarter of the oil remained, mostly concentrated in two subsurface pools near the water table (fig. 1). Since 1979, the oil at the north pool has advanced about 80 m away from the pipelines down the hydrologic gradient (Dillard and others, 1997).

The site of the crude-oil spill is located approximately 16 km northwest of Bemidji. The site is located on a glacial outwash plain consisting of medium- to coarse-grained, calcareous, quartz-rich sand with silt and fine-grained sand lenses, dissected by gravel-filled channels, and underlain by glacial till at a depth of about 25 m (Hult, 1991). Local topographic depressions in the area may be caused by the melting of stagnant ice blocks during the retreat of the glacial ice front.

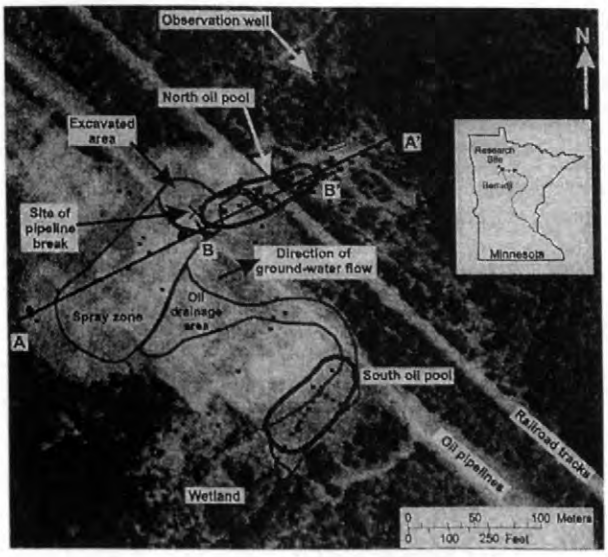

Figure 1. Aerial photograph from 1991 showing features of the Bemidji crude-oil spill research site (from Delin and others, 1998).

The overall objectives for U.S. Geological Survey (USGS) research at the site are to acquire a more complete understanding of the mobilization, transport, and fate of petroleum and petroleum derivatives in the shallow subsurface and to develop predictive models of contaminant behavior (Hult, 1984). Specific objectives for the use of geophysics are to (1) determine the distribution of hydrocarbons using GPR and other electrical methods, (2) characterize the vadose zone in terms of geometry, structure, and scale lengths, and (3) correlate GPR measurements with site hydrogeologic properties.

The USGS has collected ground penetrating radar (GPR) data and other geophysical information at the research site since 1984. This paper describes the use of GPR data and petrophysical information to map the subsurface distribution of oil. A brief overview of the GPR method and data imaging is presented and GPR data collected over the oil pools are displayed and discussed.

GPR METHOD OVERVIEW AND DATA DISPLAY

The GPR data were collected with Subsurface Interface Radar (SIR) Systems 7 and 10 manufactured by Geophysical Survey Systems, Inc. (GSSI, North Salem, NH, USA). The radar systems operate by periodically transmitting radio-frequency electromagnetic (EM) pulses, or waves, into the earth. Under the right conditions, the radiated wave propagates through the near surface. When changes in electromagnetic properties are encountered, the wave partially reflects back toward the surface where it can be detected by the GPR system. Electromagnetic properties of the earth include dielectric permittivity (ε), electrical conductivity (σ), and magnetic permeability. For a good overview of the GPR method, see Daniels (1989).

Changes in EM properties of the earth are controlled dominantly by water content, water quality, lithology, and porosity. Pore water is important because it is highly polarizable (a high value of ε) and holds free ions in solution. The propagation velocity of radar waves is controlled mostly by ε, which is often presented as relative dielectric permittivity (RDP), the ratio of ε to the dielectric permittivity of free space. Intrinsic attenuation of radar waves is controlled mostly by the σ of the medium. Conductivity is always a GPR loss mechanism as EM field energy is converted to heat due to resistance to transport. Most common earth materials have very low magnetic permeability, but where iron, cobalt, or nickel are present, as for example in magnetite, the magnetic permeability can significantly affect the velocity and attenuation of GPR energy.

From the large collection of GPR data, four typical lines near the oil pools were selected. Locations of the radar lines discussed in this paper are shown in figure 2 along with selected USGS observation wells along the lines. The images displayed here are of GPR data that have been processed to remove system noise and to add a geometric correction factor. The radar images are approximate depth sections based on an average velocity for radar waves in material above the water table. The vertical scale is exaggerated by a factor of two or three to better show features in the records. There is also a time-dependent amplitude gain applied to the data to enhance signal strength from deeper features.

PHYSICAL PROPERTIES

Several physical properties of various mixtures of distilled water with sand and oil from the Bemidji site were measured in the USGS Petrophysics Lab. Table 1 summarizes the laboratory measurements. The two oil samples were collected from wells in the north pool, Oil1 from well 301 in 1983 and Oil2 from well 412B in 1998. See Smith and Hult (1993) for locations of observation wells at this site. Sand1 is oily and dry sand collected in 1987 in the spray zone (fig. 1) near well 708. Also collected in 1987 is an oil-free sand and gravel mixture, Sand2, from well 701 at a depth of about 2.7 m. Sand3 is moist, fine-grained sand collected near the Benchmark (fig. 2) in 1998 at 0.3 m depth. The average in situ porosity of sand at the site is probably less than that measured in the lab for sample Sand3, and is likely to be around 40 percent, which agrees favorably to the value used in Dillard and others (1997). Distilled water did not mix readily with the contaminated sample, Sand1 from the

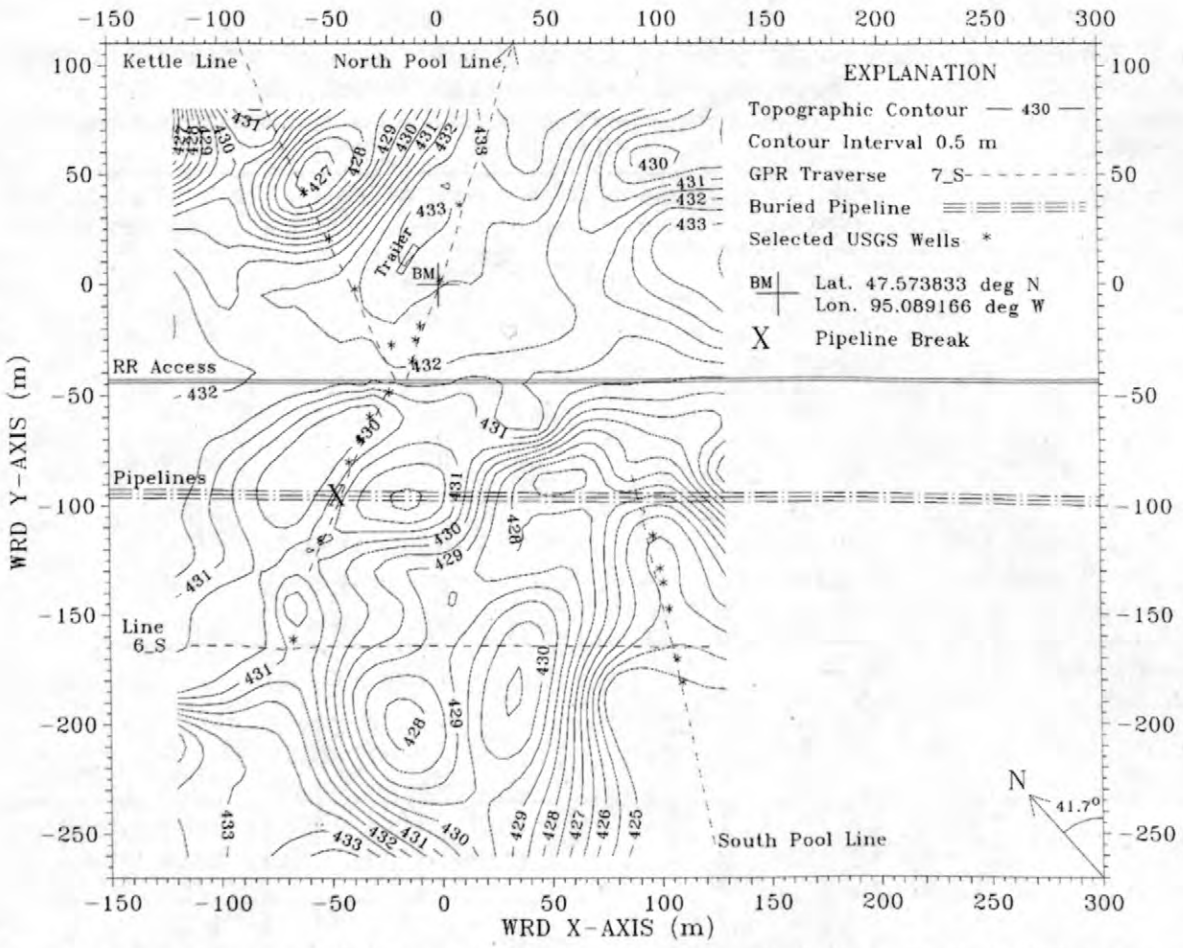

Figure 2. Topographic map of the Bemidji, Minnesota, crude-oil spill site showing selected GPR lines and observation wells.

spray zone, and required vigorous shaking and stirring.

The laboratory measurements show the oil is very resistive (very low electrical conductivity). Dry sand, whether contaminated or not, also has a low to very low conductivity. Sand saturated with water, or water and oil, has a low conductivity of less than 3.2 mS/m.

Bulk electrical conductivity at the site was measured using EM induction meters and dc resistivity soundings (Bisdorf, 1999). Both methods indicate the near surface has a conductivity of about 1 mS/m and the saturated zone conductivity is about 3 to 10 mS/m. These in situ values are similar to the laboratory values shown in table 1.

Dielectric permittivity can be approximated by a 3-phase mixing formula based on the 2-phase formulas of Sen and others (1981). Figure 3 shows calculated RDP for mixtures of sand, water, and air and for mixtures of sand, water, and oil. Note the similarity of the curves. It is assumed that the materials do not elctrochemically interact and that the RDP for water, quartz sand, crude oil, and air are, respectively, 80, 4.5, 2.3, and 1. Predicted values of RDP at various water saturation levels are listed for porosities of 30 and 40 percent. At 100 percent saturation, water fills all pore space. At saturation levels less than 100 percent, air or oil occupies some portion of the pore space.

As an example with conditions similar to that found at the Bemidji site, if quartz sand with a porosity of 40 percent is saturated with water, RDP of 25 is predicted. In that same sand, if a mixture of equal amounts of water and oil occupies pore space, an RDP is predicted to be 9.9. If air is substituted for oil, the predicted RDP only drops to 8.4. If porosity were only 30 percent in this same example, predicted RDP for 50/50 mixtures of water and oil and water and air in pore space would drop to 8.6 and 7.8 respectively.

Table 1. Summary of physical properties of various mixtures of distilled water with sand and oil from the Bemidji crude-oil spill site, determined in the USGS Petrophysics Lab. "Wet/oil" means the sample was saturated with distilled water, then gravity drained, then filled with oil. NA indicates data are not available or not applicable.

Sample Description	Conductivity (mS/m)	Resistivity (Ohm-m)	Wgt. % H_2O	Wgt. % Oil	Porosity	Bulk Density (g/cc)
Oil1	$6.6x10^{-8}$	$15x10^{6}$	0.0	100.0	NA	NA
Oil2	$7.6x10^{-8}$	$13x10^{6}$	0.0	100.0	NA	0.906
Sand1 dry	$5x10^{-8}$	$20x10^{6}$	0.0	NA[1]	NA	1.52
Sand1 sat	2.04	489	14.8	NA[1]	>0.26[1]	1.79
Sand2 dry	0.18	5444	0.0	0.0	NA	1.60
Sand3 dry	$<10^{-9}$	$>10^{9}$	0.0	0.0	0.44	1.61[2]
Sand3 moist	0.12	820	5.37	0.0	0.44	1.70
Sand3 sat	2.66	376	21.5	0.0	0.44	2.05
Sand3 wet/oil	3.13	320	20.8	3.5	0.44	2.02

[1]Amount of adsorbed oil unknown
[2]Calculated

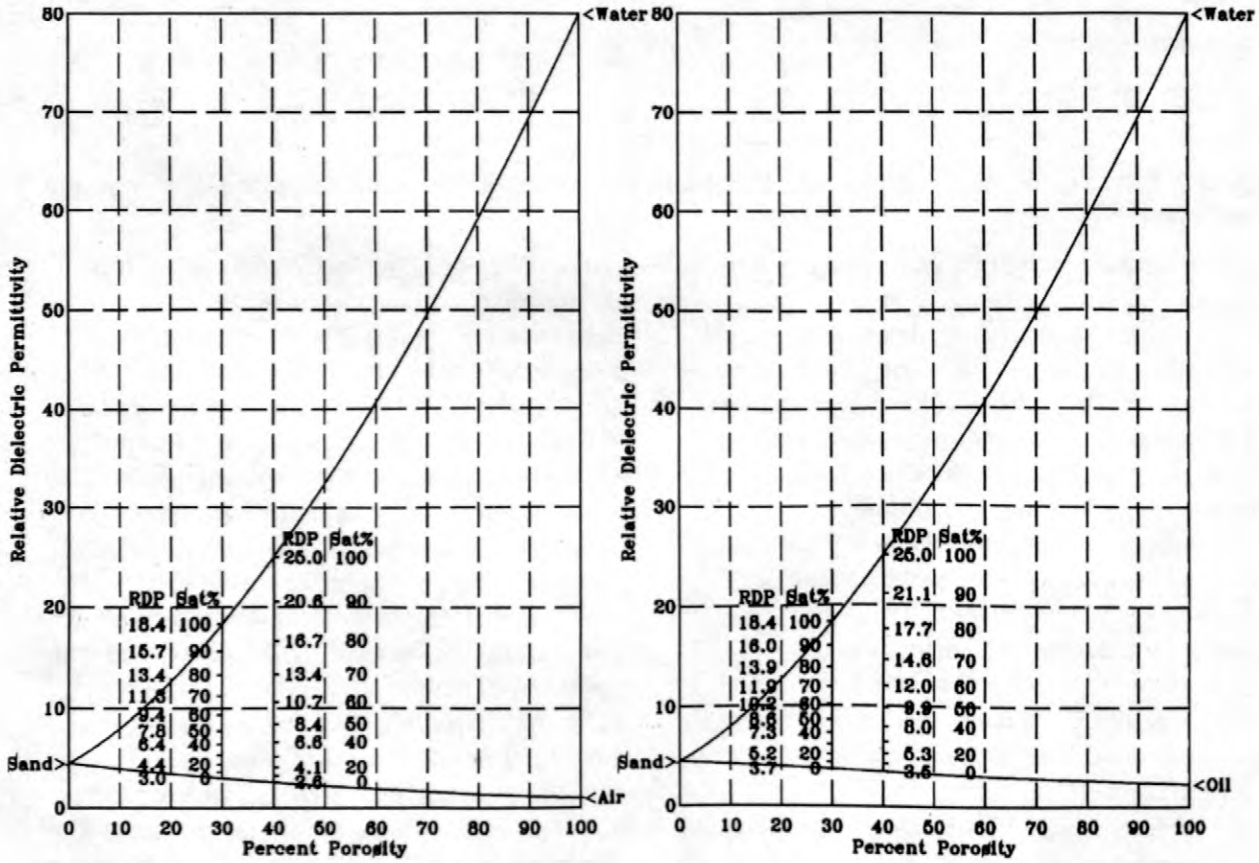

Figure 3. Calculated relative dielectric permittivity versus porosity are shown for sand-water-air mixtures and sand-water-oil mixtures

This example shows that variations in porosity and saturation levels can mask the effect of changes in oil saturation on the RDP of sand mixtures at the site.

DATA INTERPRETATION

Kettle Line

Figure 4 shows processed GPR data using 3 different antenna configurations collected along the Kettle Line in May 1987. The water table (WT) elevation, at 423 m, was established using data from Smith and Hult (1993). The data collected with the 80 MHz dual antennas (fig. 4c) readily show the top of saturated zone (SZ) as the discontinuous series of sub-horizontal reflections, near the WT level, that cross reflections from stratigraphic sequences. The top of saturated zone, rather than the water table, can generate radar reflections because EM waves are sensitive to water content, not barometric pressure, within the earth. A radar reflection from the top of SZ is much less apparent in data collected with the 80 MHz single antenna (fig. 4b) and 300 MHz dual antennas (fig. 4a).

In the topographic depression near well 702A, all three data images show dipping

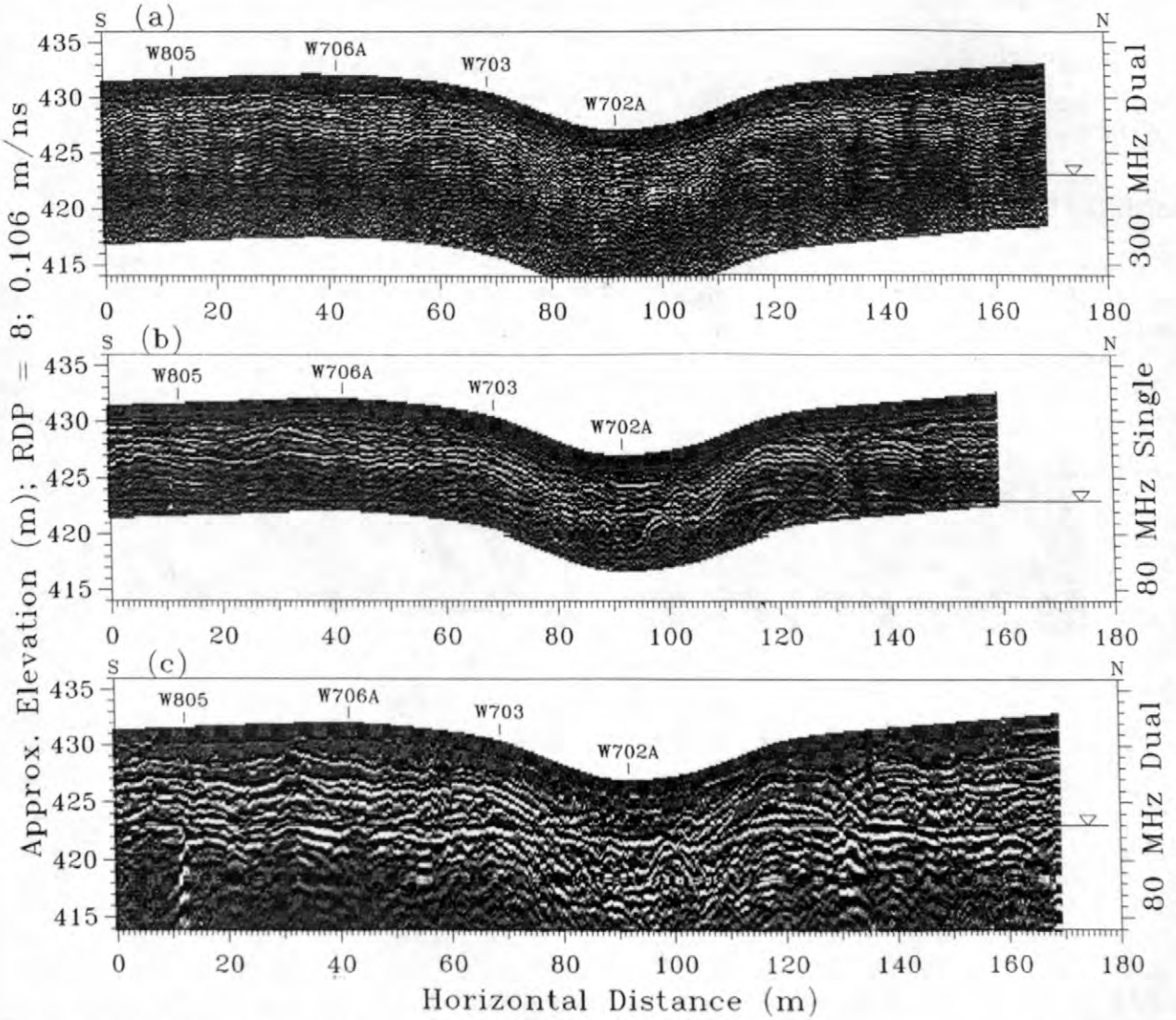

Figure 4. GPR data collected along the Kettle Line at the Bemidji, Minnesota, crude-oil spill site (see figs. 1 and 2 for location) using 3 different antenna configurations. Vertical exaggeration is 2. Selected USGS observation wells along the line are indicated for reference.

reflections indicating deposition, subsidence, and collapse related to the formation of a kettle. The oil pool extends a short distance beyond well 805 (from the left side of the figures) but does not reach well 706A (Smith and Hult, 1993). The location of the oil pool cannot be determined easily from data in figure 4.

In the unsaturated zone, GPR is mostly sensitive to changes in water content. When all water has been removed, most earth materials (including sand and clay) have a low relative dielectric permittivity of 7 or less (Telford and others, 1976; Keller, 1966). The RDP of oil is also within this range. Clay has a relatively high conductivity when wet, but lab and field measurements indicate that electrical conductivity is low for the materials at this site, and so clay content must be low. Water, however, has a RDP of about 80. Small changes in water content, not oil content, cause radar reflections above the water table.

North Oil Pool Line

Data in figure 5 were collected above the long axis of the north pool (see location in figures 1 and 2) in June 1998 using 300 MHz dual antennas. The horizontal scale shows distance from the pipelines. The gap between records is due to the railroad access. The water table, determined at the time of data collection, is shown as the sloping line at about 424-m elevation. Beneath the radar image is a cross section produced by Dillard and others (1997) that shows the oil saturation distribution (the fraction of pore space occupied by oil) determined from cores. The cross section is at the same horizontal and vertical scale as the radar image. For reference, selected well locations are shown in both the cross section and in the radar image.

The three pipelines are indicated in the radar image by the hyperbolic reflections near the origin. Curved reflections of this sort are generated because objects are detected both in front of and behind the antennas as they move across the earth. Other hyperbolic reflections present near the surface are due to wires associated with instruments at the site and are missing from data collected before 1991. The edges of the trench constructed in 1979 (fig. 1) to remove oil from the subsurface can be identified by the radar reflections sloping downward near wells 9017 and 9015.

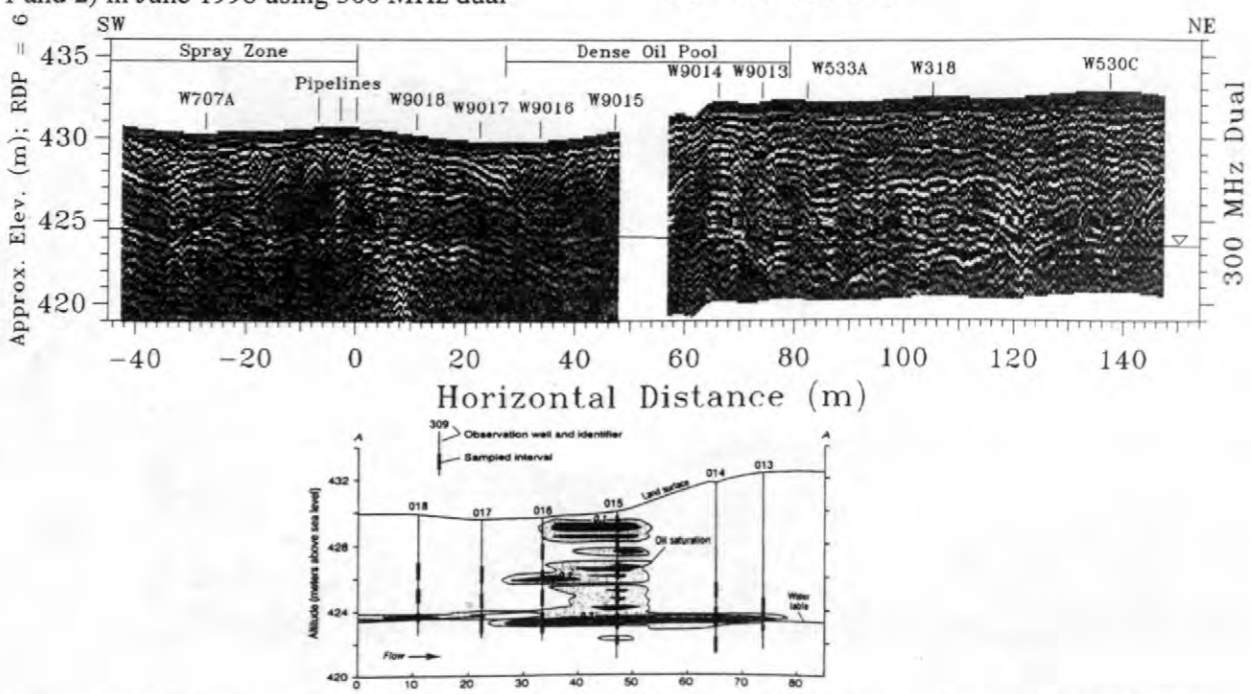

Figure 5. GPR data collected above the north oil pool at the Bemidji, Minnesota, crude-oil spill site (see figs. 1 and 2 for location). Vertical exaggeration is 3. Selected USGS observation wells along the line are indicated for reference. The cross section showing oil saturation distribution (from Dillard and others, 1997) is at the same scale as the radar image.

Using core samples, Dillard and others (1997) determined there are many fine-grained lenses in the unsaturated zone plus a distinct fine-grained layer at an elevation of about 423 m. The water table also occurs at about this elevation or slightly higher. Radar reflections from these two features cannot be distinguished in figure 5, and combine to produce a discontinuous reflection across the record. Correlation of oil saturation with grain size in Dillard and others (1997) suggests that the fine-grained lenses impede oil migration and trap the oil.

The cross section from Dillard and others (1997) in figure 5 shows that the densest part of the oil pool is between wells 9017 and 9013. Oil can be found in a few wells beyond these limits. The radar reflections are not significantly different in this area as compared to others at about the same depth.

SOUTH OIL POOL LINE AND LINE 6_S

GPR data shown in Figure 6 were collected above the long axis of the south pool (see location in figs. 1 and 2). A single 80 MHz antenna was used in January 1985 and 300 MHz dual antennas were used in October 1996. The elevation of the

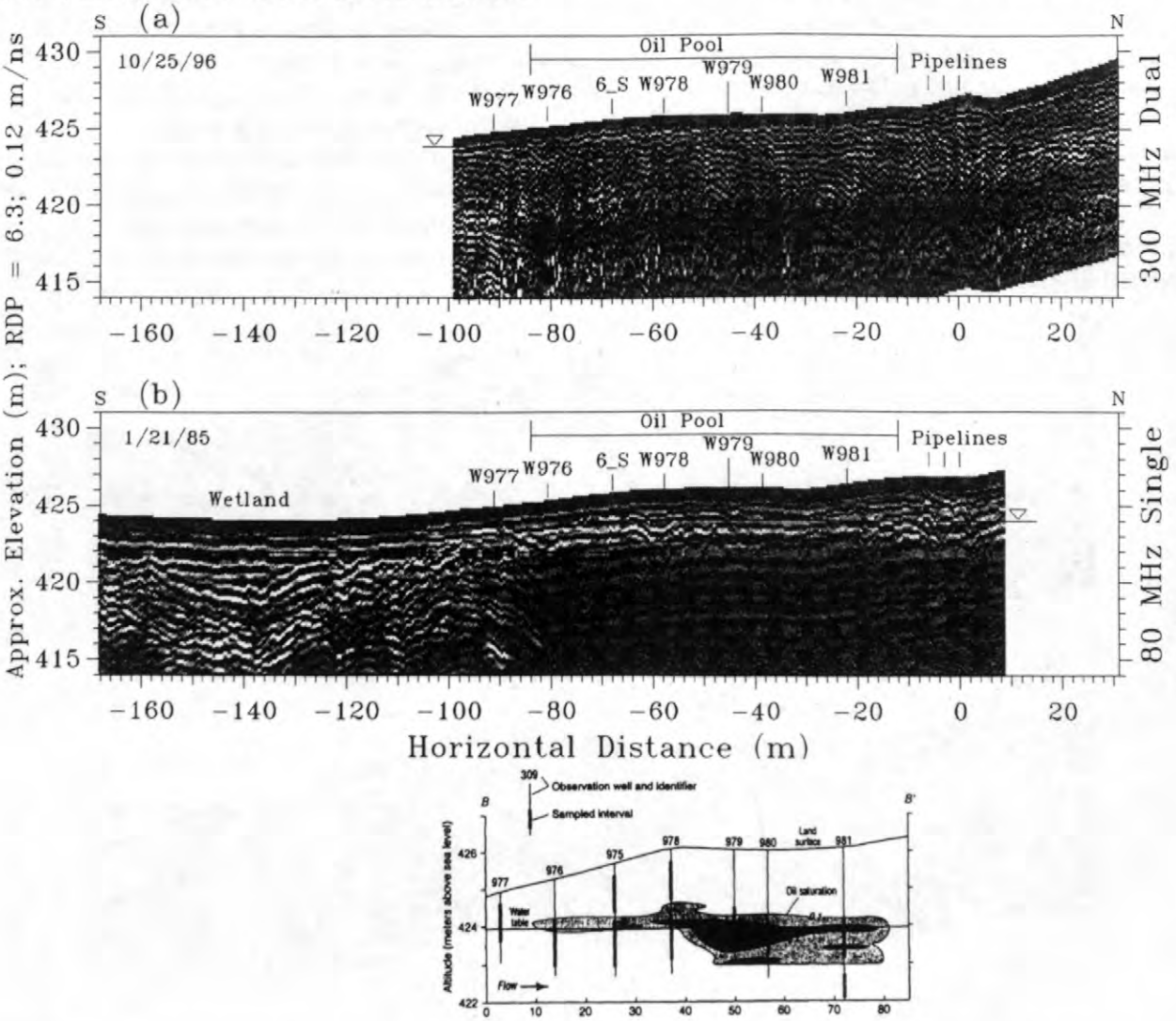

Figure 6. GPR data collected above the south oil pool at the Bemidji, Minnesota, crude-oil spill site (see figs. 1 and 2 for location) using two antenna configurations. Vertical exaggeration is 3. Selected USGS observation wells along the line and the location of Line 6_S are indicated for reference. The cross section showing oil saturation distribution (from Dillard and others, 1997) is at the same horizontal scale as the radar images, but has a different vertical scale.

water table, determined from Smith and Hult (1993), is shown at approximately 424 m. The horizontal scale for the radar images shows distance from the pipelines. Locations of selected wells next to the line are noted for reference. The cross section showing oil distribution is from Dillard and others (1997) and is at the same horizontal scale, but different vertical scale, as the radar images above it.

Radar reflections from sedimentary structures associated with kettle formation are evident in both images in the topographic low to the left of well 976. GPR reflections from below the water table are muted (attenuated) to the right (north) of well 976 in the 80 MHz data (fig. 6b). Reflections are also muted in the 300 MHz data (fig. 6a), but at a depth of about 5m below the land surface. It is tempting to correlate the oil pool location with the muted reflections in the 80 MHz data. However, this is not the case. The cross section below figure 6b shows that the oil pool, at oil saturation levels greater than 10 percent, does extend south to about well 976 but does not extend north past the pipelines to correlate with the attenuated reflections. The attenuation of radar reflections appears to be caused by differences in penetration depth related to changes in stratigraphy related to formation of the kettle.

Radar reflections away from kettle structures at the Bemidji site are often attenuated near the water table. This may be caused by the increase in electrical conductivity in the saturated zone and associated loss in radar signal strength. Figure 7 shows radar data along line 6_S that crosses the south pool line at the location shown in figure 6. The water table elevation, determined from Smith and Hult (1993), is at approximately 424 m. The 80-MHz data sets, figures 6b and 7b, were collected on the same day and have the same amplitude gain function applied. The two 300-MHz data sets, figures 6a and 7a, were collected in different years with different antenna configurations. The muted reflections clearly are related to lithologic and conductivity changes within the saturated zone and to antenna configuration, not to the distribution of the crude oil.

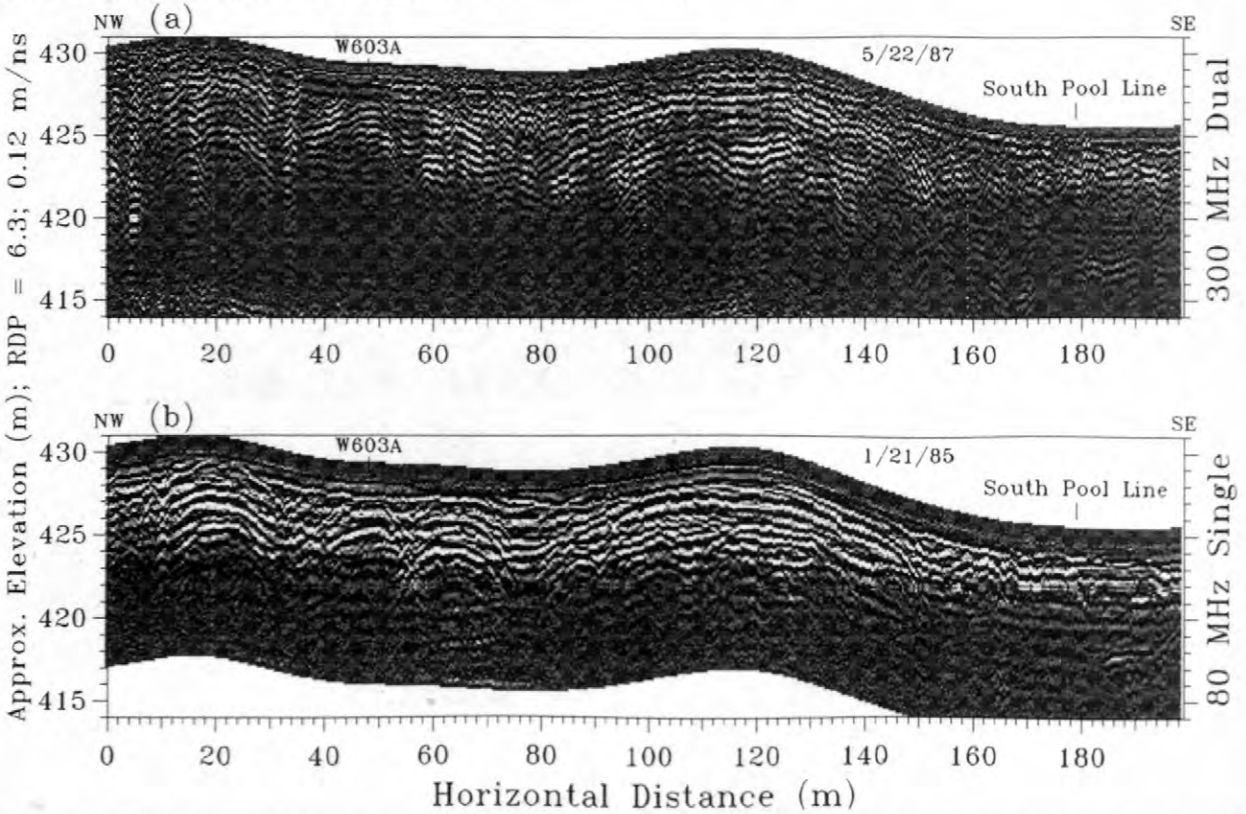

Figure 7. GPR data collected along Line 6_S at the Bemidji, Minnesota, crude-oil spill site (see figs. 1 and 2 for location). Vertical exaggeration is 3. Selected USGS observation wells along the line and the location of the South Pool Line are indicated for reference. The water table is at an elevation of about 424 meters.

CONCLUSIONS

Laboratory measurements of Bemidji crude oil indicate that the oil is still very resistive (greater than 10^6 ohm-m) even after 20 years of biodegradation, geochemical reactions, and dissolution. Mixing the crude oil with sand does not significantly affect the electrical conductivity or dielectric permittivity of the mixture, whether at the surface in the spray zone or at depth above the water table. This is illustrated by comparing GPR images with cross sections of oil saturation distribution.

Silt and gravel units within the sandier, glacial-outwash material can be imaged and mapped using GPR. Deposition, subsidence, and collapse features related to glacial kettle formation are identified in both 80 MHz and 300 MHz data. The top of the saturated zone can be detected and mapped easier with 80 MHz dual antennas than with other configurations. The GPR data do not show any reflections from the glacial till at about 25-m depth.

Because electromagnetic properties of oil and air are similar, small changes in water content, not oil content, cause radar reflections above the water table. GPR does not easily detect the oil pools at depth or the oil-contaminated sand near the surface. Nonetheless, GPR can detect those geologic features likely to impede oil migration or trap oil, for example, layers of silt or clay within the sand.

REFERENCES

Bisdorf, R.J., 1999, Electrical geophysics at the Bemidji research site, in Morganwelp, D.W., and Buxton, H.T., eds., U.S. Geological Survey Toxic Substances Hydrology Program -- Proceedings of the Technical Meeting, Charleston, SC, March 8-12, 1999 -- Volume 3 -- Subsurface Contamination from Point Sources: U.S. Geological Survey Water-Resources Investigations Report 99-4018C, this volume.

Daniels, J.J., 1989, Fundamentals of ground penetrating radar, *in* Proceedings of the Symposium on the Application of Geophysics to Engineering and Environmental Problems (SAGEEP '89), March 13-16, 1989, Golden, CO, USA: The Society of Engineering and Mineral Exploration Geophysicists, p. 62-142.

Delin, G.N., Essaid, H.I., Cozzarelli, I.M., Lahvis, M.H., and Bekins, B.A., 1998, Ground water contamination by crude oil near Bemidji, Minnesota: U.S. Geological Survey Fact Sheet 084-98, 4 p.

Dillard, L.A., Essaid, H.I., and Herkelwrath, W.N., 1997, Multiphase flow modeling of a crude-oil spill site with a bimodal permeability distribution: Water Resources Research, v. 33, no. 7, p. 1617-1632.

Hult, M.F., ed., 1984, Ground-water contamination by crude oil at the Bemidji, Minnesota, Research Site -- U. S. Geological Survey Toxic Waste -- Ground-Water Contamination Study: U.S. Geological Survey Water-Resources Investigations Report 84-4188, 107 p.

Hult, M.F., 1991, Overview of research on contamination of the subsurface by crude oil at the Bemidji, Minnesota, Toxic Substances Research Site, *in* Mallard, G.E. and Aronson, D.A., eds., U.S. Geological Survey Toxic Substances Hydrology Program -- Proceedings of the technical meeting, Monterey, California, March 11-15, 1991: U.S. Geological Survey Water-Resources Investigations Report 91-4034, p. 611-613.

Keller, G.V., 1966, Electrical properties of rocks and minerals, *in* Clark, S.P., ed., Handbook of Physical Constants: Geological Society of America Memoir 97, p. 553-577.

Sen, P.N., Scala, C., and Cohen, M.H., 1981, A self-similar model for sedimentary rocks with application to the dielectric constant of fused glass beads: Geophysics, vol. 46, no. 5, p. 781-795.

Smith, S.E., and Hult, M.F., 1993, Hydrogeologic data collected from a crude-oil spill site near Bemidji, Minnesota, 1983-91: U.S. Geological Survey Open-File Report 93-496, 158 p.

Telford, W.M., Geldhart, L.P., Sheriff, R.E., and Keys, D.A., 1976, Applied Geophysics: New York, Cambridge University Press, p. 456.

AUTHOR INFORMATION

Jeffrey E. Lucius, U.S. Geological Survey, Lakewood, Colorado, USA (lucius@usgs.gov)

Investigating the Potential for Colloid- and Organic Matter-Facilitated Transport of Polycyclic Aromatic Hydrocarbons in Crude Oil-Contaminated Ground Water

By Joseph N. Ryan, George R. Aiken, Debera A. Backhus, Karen G. Villholth, and Christine M. Hawley

ABSTRACT

The potential for colloid- and organic matter-facilitated transport of polycyclic aromatic hydrocarbons (PAHs) was investigated at a crude oil-contaminated field site near Bemidji, Minnesota. Field tests focused on sampling and characterization of the ground water colloids and assessment of the partitioning of PAHs to the colloids. The colloids were mostly iron-rich spheres of 100-300 nm diameter. Their concentration reached a maximum of about 2×10^{10} particles per liter (0.75 NTU) at a distance 50 m down-gradient from the oil spill and decreased with distance to a background concentration of about 7×10^{8} particles per liter at a distance of 140 m. During well purging, stable colloid concentrations decreased slightly with increasing pumping rate. Fluorescence quenching experiments revealed that partitioning of perylene to organic matter in the unaltered ground water was significant. Laboratory tests examined the effect of ferrous iron, present in high concentrations near the oil spill, on the partitioning of phenanthrene to aliphatic and aromatic carboxylic acids typical of crude oil degradation and hydrophobic acid fractions of natural organic matter. Ferrous iron increased the partitioning of phenanthrene to the organic acids by 11 to 250%, with the largest increase occurring for aromatic carboxylic acids. The data suggest that ferrous iron increased the partition coefficient by causing aggregation of the organic acids.

INTRODUCTION

Colloids, both organic and inorganic, have been implicated in the transport of metals, radionuclides, and certain ionizable organic pesticides in laboratory and field tests (Jury and others, 1986; Buddemeier and Hunt, 1988; Amrhein and others, 1993; de Jonge and others, 1998). Laboratory tests also indicate that colloids facilitate the transport of hydrophobic organic compounds (Vinten and others, 1983; Magee and others, 1991; Dunnivant and others, 1992); however, colloid-facilitated transport of hydrophobic organic compounds has only infrequently been observed in the field (Villholth, in press). To assess the potential for colloid-facilitated transport of hydrophobic organic compounds in the field, we examined the association of colloids and polycyclic aromatic hydrocarbons (PAHs) in a crude oil-contaminated ground water at Bemidji, Minnesota.

The Bemidji site was considered a good candidate for detecting colloid-facilitated transport of hydrophobic organic compounds. Phenanthrene and fluorene, two PAHs in the crude oil, were measured in the ground water down-gradient of the oil spill at concentrations 26% and 300% greater than concentration estimates based on equilibrium between the crude oil and the surrounding water (Aiken and others, 1991). The transport distances for phenanthrene and fluorene also exceed expections based on two-phase transport estimates (Hawley, 1995). These observations suggest sorption of the PAHs to a third phase -- a mobile colloid phase.

We suspected that organic and inorganic colloids would be abundant near the oil spill. The dissolved organic matter concentration of the

ground water increased to 50 mg C L^{-1} adjacent to the oil spill. Degradation of the oil produced an anoxic plume of ground water and high ferrous iron concentration. These conditions have been associated with colloid mobilization in iron oxide-coated sediments (Ryan and Gschwend, 1990; 1992).

Our investigation included both field and laboratory components. In the field, we tested the dependence of the stable colloid concentration on the pumping rate and characterized the colloids collected in the samples. Using the field samples, we measured the partitioning of perylene, a five-ring PAH, to the colloids at *in situ* concentrations. In the laboratory, we tested the effect of ferrous iron on the partitioning of phenanthrene, a three-ring PAH, to different types of organic matter ranging from high molecular weight aliphatic and aromatic carboxylic acids to isolated fractions of natural organic matter.

MATERIALS AND METHODS

In this section, we describe the field site, the methods of sampling the ground water, the measurement of partition coefficients by fluorescence quenching, and the measurement of partition coefficients by solubility enhancement in the presence and absence of ferrous iron.

Field Site

The field tests were conducted at the U.S. Geological Survey Toxic Substances Hydrology research site at Bemidji, Minnesota. In August 1979, a pipeline near Bemidji burst and sprayed light crude oil on the ground surface. After cleanup, an estimated 400,000 L of oil remained in the unsaturated zone of the soil perched in a lens on the water table (Hult, 1987). Since the spill, the oil body has migrated about 30 m down-gradient and oil dissolution and degradation products have traveled at least 200 m down-gradient (Hult, 1989).

The saturated sediment at the site is a calcareous silty sand deposited as glacial moraine and outwash. The sand and silt fraction is composed of quartz, feldspar, dolomite, calcite, hornblende, and ilmenite. The clay fraction (<1%) is composed of kaolinite, smectite, and chlorite (Bennett and others, 1993). Ground water flow is advancing at a rate of about 0.08 m d^{-1} (Baedecker and others, 1993).

The supply of oil degradation products to the ground water has created five distinct zones of ground water chemistry (Baedecker and others, 1993) (fig. 1). Near the oil body, dissolved oxygen decreases to zero from near saturation, dissolved organic matter increases to 50 mg C L^{-1} from 2 mg C L^{-1}, and ferrous iron increases to about 1 mM from micromolar levels.

Ground Water Sampling

Ground water was sampled from five monitoring wells aligned with the axis of ground water flow past the oil body (fig. 1) in July 1995. These wells provided samples from the uncontaminated background zone, near the oil body, and down-gradient of the oil body. The sampling apparatus and procedures were designed to minimize suspension of colloids by pumping and preserve sample chemistry.

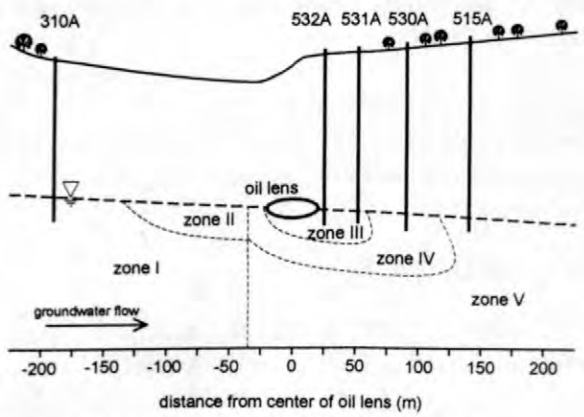

Figure 1. Locations of the monitoring wells sampled in this investigation shown with oil body and geochemical zones of contamination designated by Baedecker and others (1993). The ground water zones have the following characteristics: (I) native uncontaminated ground water, oxic; (II) high organic and inorganic carbon, sub-oxic; (III) high hydrocarbons, Mn^{2+}, Fe^{2+}, methane, anoxic; (IV) transition zone between III and V, sub-oxic; and (V) slightly elevated benzene, toluene, ethylbenzene, and xylenes, oxic. The water table depth ranges from 8 to 9 m for the wells shown.

Ground water was removed from the wells using a positive-displacement gear-driven pump

made of stainless steel and Teflon. The pumping zone was partially isolated by a packer inflated with argon above the pump. Aluminum and stainless steel tubing (pre-rinsed with acetone and deionized water) was used to connect the pump with the surface. A low flow rate (about 0.1 L min^{-1}) was used to minimize suspension of colloids.

In one well (532A), ground water sampling was conducted at 4 different pumping rates (0.15, 0.35, 1.1, and 1.8 L min^{-1}) on successive days to test the effect of pumping rate on colloid sampling. These pumping rates span the range commonly used in ground water sampling. After sampling at the highest pumping rate on the fourth day, the pumping rate was decreased to the medium and low rates to determine the effect on turbidity.

Flow from the pump tubing was directed to the bottom of an inverted, overflowing glass funnel for measurement of pH, specific conductance, and dissolved oxygen (colorimetric vacuum ampoules; Chemetrics, Inc.). Flow was also diverted to glass vials for frequent turbidity (Hach, model Ratio X/R) and total iron measurement (Hach, field titration) during well purging. Samples were collected when the field parameters stabilized. This purging of the wells required removal of 100 well volumes over 7 h. Ground water was collected in ground glass-stoppered bottles pre-filled with argon and contained in sealed plastic bags after allowing approximately one volume of overflow. The bottles were capped, covered with plastic caps, and stored on ice in coolers.

Colloids were sampled by collecting 20 to 60 mL of ground water in glass syringes and filtering through 0.1 µm membranes. The membranes were rinsed with 10 mL of deionized water and stored in sealed petri dishes.

Laboratory Analysis

Ground Water Chemistry

Samples were analyzed for major cations and metals (Al, Ca, Fe, K, Mg, Mn, Na, and Si) in whole and 0.1 µm-filtered samples by inductively coupled plasma-atomic emission spectrophotometry (ICP-AES). Sample handling and filtering was conducted in an argon-filled glove box. Total and dissolved organic carbon concentrations were determined by ultrafiltration (500 molecular weight cutoff), high-temperature platinum catalyst combustion of the samples from which inorganic carbon and volatile organic carbon had been purged, and infrared detection of carbon dioxide.

Colloid Characterization

The abundance of inorganic colloids on gold-coated filters was determined by scanning electron microscopy (SEM) at 20,000 times magnification and 30 kV accelerating voltage. From 40 to 100 randomly located fields were counted. Fields with colloids too numerous to count were excluded; these fields were photographed. Elemental composition of the colloids was estimated by energy-dispersive x-ray (EDX) analysis with count times of 60 s.

Fluorescence Quenching

Fluorescence quenching (Backhus and Gschwend, 1990) was used to determine the partitioning of a probe PAH, perylene, to the organic colloids present in ground water samples examined under in situ conditions. Organic colloids were operationally defined as organic matter that did not pass through a 500 molecular weight ultrafiltration membrane.

Solubility Enhancement

Solubility enhancement experiments (e.g., Chiou and others, 1986) were performed to determine the effect of ferrous iron on the partitioning of a PAH, phenanthrene, to various types of high molecular weight organic acids. The organic acids tested included the hydrophobic acid fractions of organic matter isolated by XAD-8 resin (Aiken and others, 1992) from the site ground water and the Suwannee River and high molecular weight aliphatic and aromatic carboxylic acids (table 1). The carboxylic acids (fig. 2) were chosen to represent typical oil degradation products found at the site (Eganhouse and others, 1993). The hydrophobic acid fractions were added at a concentration of 50 mg L^{-1}. The carboxylic acids were added at a concentration of

20 mg L^{-1}, an order of magnitude below the critical micelle concentration of any of the carboxylic acids (Mukerjee and Mysels, 1971).

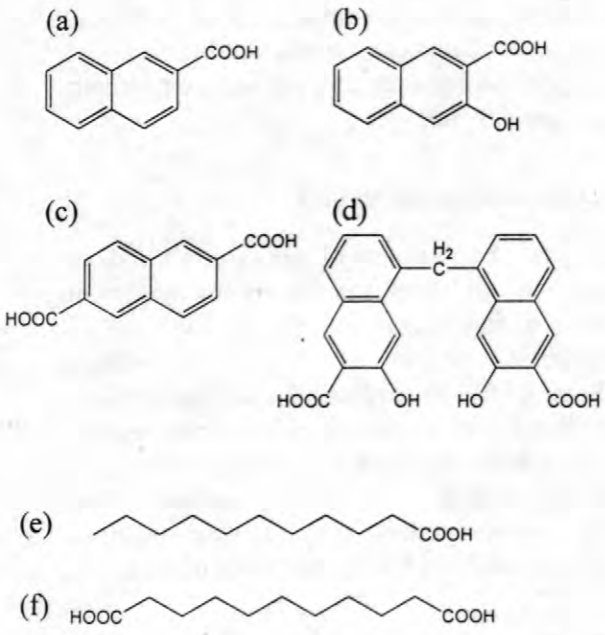

Figure 2. The aromatic and aliphatic carboxylic acids used in the solubility enhancement experiments: (a) 2-naphthoic acid, (b) 3-hydroxy-2-naphthoic acid, (c) 2,6-naphthdioic acid, (d) pamoic acid, (e) undecanoic acid, and (f) 1,11-undecanedioic acid.

Ferrous iron was added as $Fe_2SO_4 \cdot 4H_2O$ at concentrations of 0.9 and 2.7 mM. The lower concentration is about 25% higher than the maximum total iron concentration measured in the contaminated Bemidji ground water. Potassium nitrate was added to control ionic strength at a concentration of 0.01 M, approximately the ionic strength of the contaminated Bemidji ground water. Phenanthrene was added in a radiolabeled form (phenanthrene-9-^{14}C).

The phenanthrene was placed in glass centrifuge tubes with plastic caps and Teflon-lined septa. The organic acid/potassium nitrate solutions were sparged with argon to remove oxygen (<10 ppb) and added to the tubes. Sparged ferrous iron solution was spiked into the tubes and pH was adjusted to 6.5 with a sodium hydroxide solution. This pH was at least 1.5 pH units above the pK_a values of the carboxylic acids. The headspace in the tubes was replaced with argon and sealed for 14 d (an equilibration time chosen by kinetic tests) at room temperature (20±2°C). The vials were centrifuged (1750 g, 1 h) to force the excess phenanthrene to the argon-water interface. An aliquot of the aqueous solution was withdrawn by syringe for determination of phenanthrene concentration by liquid scintillation counting. All solution preparation was performed in an argon-filled glove box. Duplicate experiments were conducted for all data reported.

Table 1. Characteristics of the hydrophobic acid fractions (XAD-8) of the natural organic matter and the carboxylic acids used in the solubility enhancement experiments. The Number-averaged molecular weight (M_n), aromaticy, carboxyl content, and oxygen/carbon (O/C) ratio are shown. Aromaticity and carboxyl content calculated for the carboxylic acids and measured by ^{13}C-nuclear magnetic resonance analysis for the hydrophobic acid fractions.

organic acid	M_n (Da)	aroma-ticity (%)	carboxyl content (%)	O/C ratio
well 310A[1] (XAD-8)	536	18	15	0.66
well 532A[2] (XAD-8)	350	n.d.	n.d.	n.d.
well 530A[3] (XAD-8)	362	19	14	0.47
SR FA[4] (XAD-8)	826	25	21	0.71
2-naphthoic	160	91	9.1	0.24
2,6-naphthdioic	204	83	17	0.44
3-hydroxy-2-naphthoic	200	91	9.1	0.36
pamoic	388	91	9.1	0.35
undecanoic	186	0	9.1	0.24
1,11-undecanedioic	216	0	18	0.48

[1]Aiken and Thorn (unpublished data)
[2]Eganhouse and others (1993)
[3]Aiken (unpublished data)
[4]SR FA is Suwannee River fulvic acid (Aiken and Malcolm, 1987)

RESULTS

Pumping Rates during Sampling

Well 532A was purged at increasing pumping rates before sampling on four successive days. Turbidity and dissolved oxygen decreased

during purging, while pH and specific conductance were fairly constant (fig. 3).

The purging time required to reach a stable turbidity level decreased as the pumping rate increased (fig. 4). The stable turbidity values were highest at the lowest pumping rate. On the fourth day, when the pumping rate was decreased to medium and low rates after purging and sampling at 1.8 L min^{-1}, turbidity increased by 15 to 35% above the stable turbidity level. Only turbidity showed a significant variation as the pumping rate was increased.

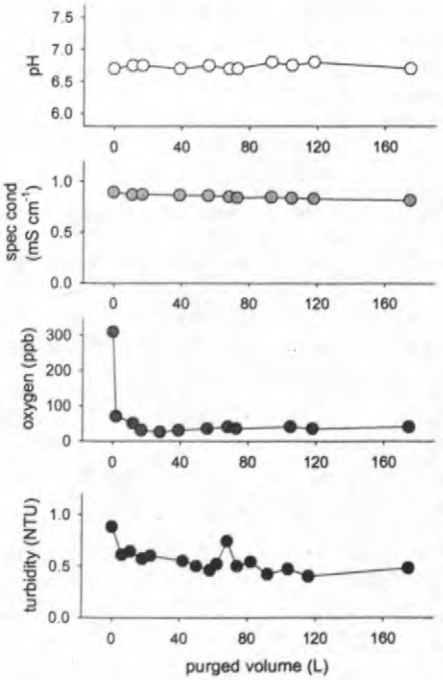

Figure 3. Changes in pH, specific conductance (spec cond), dissolved oxygen, and turbidity during the purging of well 532A at 0.35 L min^{-1}.

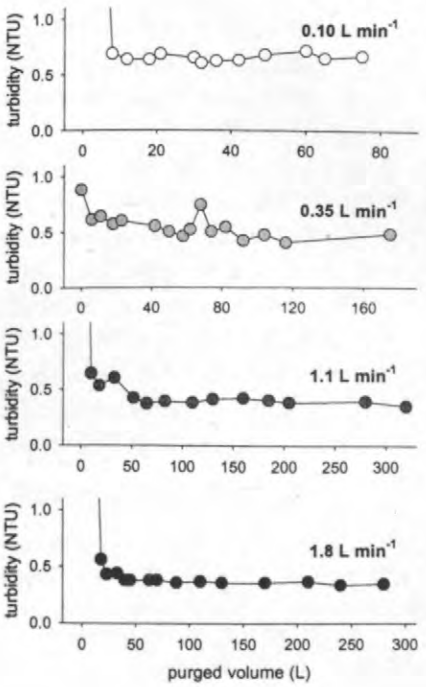

Figure 4. Changes in turbidity during purging of well 532A at four different pumping rates on four different days.

Ground Water Chemistry

The ground water sampling conducted during this study echoed results obtained in previous studies (Baedecker and others, 1993; Eganhouse and others, 1993) as shown in fig. 5. Near the oil body, pH decreased slightly and specific conductance roughly doubled. Dissolved oxygen decreased from near saturation to undetectable levels (<0.1 mg L^{-1}). Dissolved iron increased from undetectable levels (<2 μM) to 0.72 mM. Ground water from the background well (310A) was similar to ground water from the well most down-gradient (515A). Filtered (0.1 μm) and unfiltered ground water samples displayed no significant difference in major cation and metal concentrations. Field measurements of total iron agreed well with laboratory measurements by ICP-AES. In contrast, the organic carbon concentration of material trapped on 500 molecular weight cutoff ultrafilters ranged from 0.4 to 5.9 mg C L^{-1} (table 2).

Inorganic Colloids

Turbidity measurements ranged from near zero in the background and distant downgradient wells to 0.75 NTU in the wells near the oil body (fig. 5). Estimates of particle number concentrations revealed about 30 times higher colloid concentrations in ground water near the oil body. Assuming an inorganic colloid density range of 2-4 g cm^{-3}, colloid mass concentrations ranged from about 1-2 μg L^{-1} in the background

ground water to about 20-40 μg L^{-1} near the oil body. These mass concentrations are much less than the organic colloid concentration (table 2).

The inorganic colloids were roughly uniform in size (100-300 nm diameter) and shape (spherical) (fig. 6). Iron predominated the EDX scans of the colloids. Very few larger particles (approximately 1%) with elemental compositions similar to clay minerals (Al, Si, K) and organic matter (no elements above F) were also detected.

Fluorescence Quenching

The fluorescence quenching experiments showed that perylene associates signficantly with the organic colloids in the ground water down-gradient from the oil body (wells 531A, 530A, and 515A; table 2). No perylene binding was observed for the background ground water (well 310A). The extent of solubility enhancement decreased with distance down-gradient of the oil body. Some of this decrease may be attributed to the decrease in colloidal organic matter concentration with distance from the oil body; however, the organic matter partition coefficient (K_{om}) also decreased slightly with distance from the oil body.

Table 2. Fluorescence quenching results for the partitioning of perylene to colloids in the Bemidji ground water. Solubility enhancement is the ratio of the apparent solubility to the predicted solubility. K_{om} is the organic matter-normalized partition coefficient.

well	distance from oil (m)	organic colloid (mg C L^{-1})	solubility enhance-ment	K_{om} (mL g^{-1})
310A	-190	0.4	1.0	no quench
531A	25	5.9	2.2	4.0×10^5
530A	50	3.3	1.5	3.2×10^5
515A	140	2.2	1.3	3.0×10^5

Solubility Enhancement

The results of the solublility enhancement experiments are shown in table 3. The aliphatic carboxylic acids (undecanoic and 1,11-undecanedioic acids) and pamoic acid were most effective at binding phenanthrene, but ferrous iron did not significantly improve their ability to bind phenanthrene. The hydrophobic acid fractions and the remaining aromatic carboxylic acids were roughly equal in their ability to bind phenanthrene. At a concentration of 0.9 mM, ferrous iron somewhat improved phenanthrene binding of the hydrophobic acid fractions of the natural organic matter (11 to 55% increase in K_{om}). For the aromatic carboxylic acids (except pamoic acid), ferrous iron approximately doubled phenanthrene binding (205 to 250% increase in K_{om}).

Table 3. Solubility enhancements and organic matter-water partition coefficients (K_{om}) for phenanthrene with various organic acids in the absence and presence of ferrous iron at a concentration of 0.9 mM.

organic acid	relative solubility enhancement		K_{om} (mL g^{-1})	
	without Fe^{2+}	with Fe^{2+}	without Fe^{2+}	with Fe^{2+}
blank[1]	1 (±0.008)	1.03 (±0.010)	--	$10^{3.16}$
well 310A (XAD-8)	1.36 (±0.015)	1.55 (±0.017)	$10^{3.85}$	$10^{4.05}$
well 532A (XAD-8)	1.51 (±0.022)	1.62 (±0.024)	$10^{4.01}$	$10^{4.10}$
SR FA[2] (XAD-8)	1.40 (±0.015)	1.45 (±0.020)	$10^{3.90}$	$10^{3.95}$
2-naphthoic	1.14 (±0.022)	1.35 (±0.028)	$10^{3.85}$	$10^{4.25}$
3-hydroxy-2-naphthoic	1.21 (±0.022)	1.44 (±0.017)	$10^{4.03}$	$10^{4.34}$
2,6-naphth-dioic	1.19 (±0.025)	1.45 (±0.010)	$10^{3.99}$	$10^{4.35}$
pamoic	1.40 (±0.008)	1.39 (±0.011)	$10^{4.30}$	$10^{4.30}$
undecanoic[3]	1.44 (±0.006)	1.34 (±0.015)	$10^{4.34}$	$10^{4.24}$
1,11-undecane-dioic	1.34 (±0.008)	1.41 (±0.010)	$10^{4.23}$	$10^{4.31}$

[1]The solubility enhancement caused by Fe^{2+} alone was used to correct the organic acid solubility enhancements.
[2]SR FA is Suwannee River fulvic acid.
[3]black precipitate was observed.

For the undecanoic acid, repeated trials at a ferrous iron concentration of 0.9 mM produced a black precipitate after centrifugation. We suspect that the black precipitate reduced the solution concentration of phenanthrene, resulting in a solubility enhancement and K_{om} value lower than

expected in the presence of ferrous iron. At the higher ferrous iron concentration, 2.7 mM, black precipitates were produced in all of the solutions. The solubility enhancement caused by the higher ferrous iron concentration was 1.03±0.010, the same value observed at the lower ferrous iron concentration.

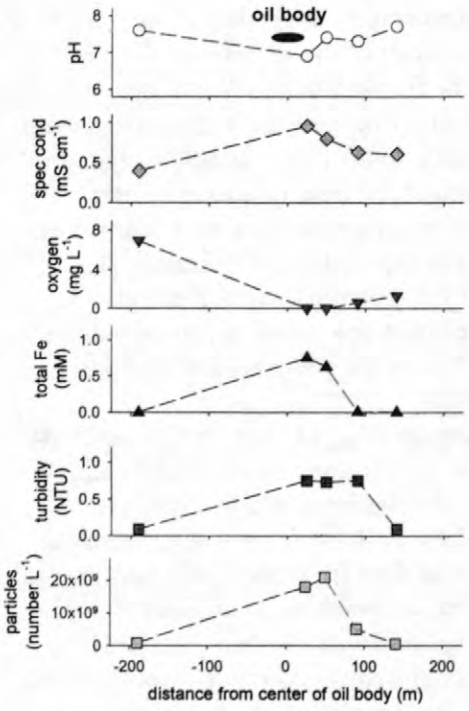

Figure 5. Variations in pH, specific conductance (spec cond), dissolved oxygen, turbidity, and particle number concentration as a function of distance from the oil body.

DISCUSSION

Pumping Rates during Sampling

Ground water sampling protocols have typically required the removal of three to five well volumes of ground water prior to sample collection. This purging of the well is meant to assure collection of ground water representative of the ground water in the formation, unaffected by the presence of the well. From this study and others (Puls and others, 1992; Backhus and others, 1993), it is clear that turbidity is still decreasing at three to five well volumes, while parameters like pH and specific conductance have reached steady levels. At this site, as many as 100 well volumes were removed before reaching a stable turbidity level.

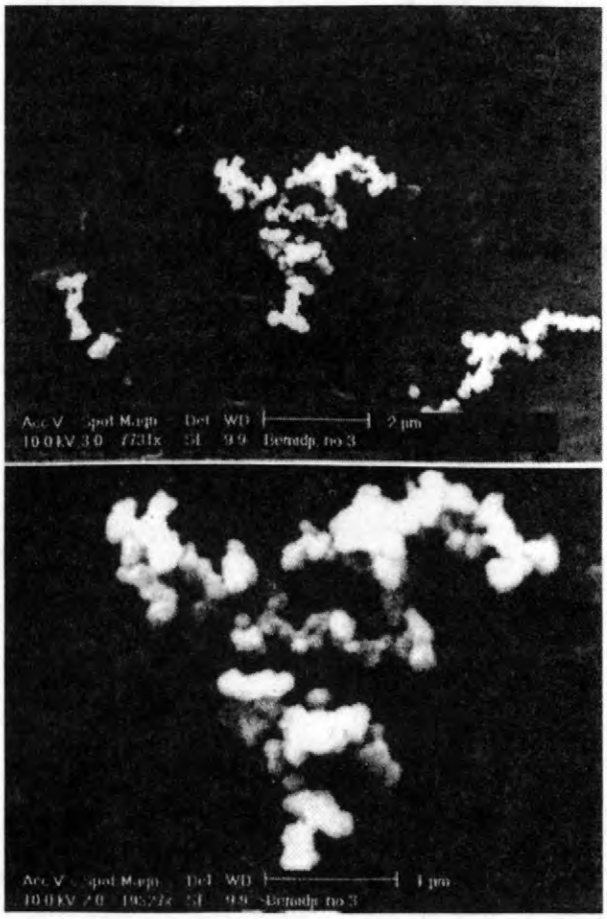

Figure 6. SEM images of colloids from well 532A (25 m down-gradient from oil body) trapped on 0.1 μm filters. Colloids are composed mostly of iron. Magnification of 7,700 times (top) and 19,000 times (bottom). Scale bars of 1 μm are shown.

Previous research on the effect of pumping rate on colloid concentrations concluded that higher pumping rates resulted in higher stable colloid concentrations (Puls and others, 1992; Backhus and others, 1993). Higher pumping rates produce greater shear on colloids attached to the framework grains. In this study, however, there was a slight decrease in the stable turbidity level as the pumping rate was increased. We suspect that the slight decrease may have resulted from depletion of the supply of colloids that could be mobilized by shear. Note that the stable turbidity level decreased with successive tests (from low to

high pumping). Inexplicably, decreases in the pumping rate after purging and sampling at a high rate also caused a decrease in the stable turbidity level. The higher stable turbidity level measured on the first day (at the lowest rate) may also be attributable to disturbance of colloids in the well. After the first day, the pump was left in the well. Puls and others (1992) observed the same effect in their studies and recommended that dedicated sampling equipment be used to more accurately sample colloids in ground water.

Colloid Mobilization and Transport

Given the significant difference between the colloid concentrations of the background well (310A) and the wells near the oil body (532A, 531A) (fig. 5), we surmise that the change in ground water chemistry caused by the oil spill is responsible for the mobilization of colloids near the oil body. A coincidence of reducing conditions and high colloid concentrations was observed by Ryan and Gschwend (1990; 1992) in Atlantic Coastal Plain sediments below an organic matter-rich swamp. At Bemidji, the degradation of oil is responsible for the onset of reducing conditions (Cozzarelli and others, 1994).

For the Atlantic Coastal Plain sediments, Ryan and Gschwend (1990; 1992) hypothesized that the mobilization of colloids (mainly clay minerals) was caused by the reductive dissolution of ferric oxyhydroxide coatings binding clay colloids to the framework grains. At Bemidji, ferric oxyhydroxides were not listed as significant components of the sediments, but ilmenite ($FeTiO_3$) is present in the heavy mineral fraction (Bennett and others, 1993). Ilmenite is also present in the Atlantic Coastal Plain sediments examined by Ryan and Gschwend (1992) and its weathering under oxidizing conditions released ferric iron that accumulated as oxyhydroxide coatings on grains. It is likely that the native Bemidji sediments are also coated by iron oxyhydroxides. The high concentrations of ferrous iron in the anoxic, organic carbon-rich ground water near the oil body also indicates that iron oxyhydroxide coatings must be present on the Bemidji sediments.

Despite the apparent similarity in colloid mobilization conditions, far fewer inorganic colloids were mobilized in the Bemidji ground water than in the Atlantic Coastal Plain ground waters. At Bemidji, the colloids mobilized (up to an estimated 30 $\mu g\ L^{-1}$) are primarily small amorphous iron-rich spheres with a few clay colloids. In the Atlantic Coastal Plains sediments, the mobilized colloids (up to 60 $mg\ L^{-1}$) were mainly clay minerals with a few crystalline goethite particles. The difference in colloid concentrations may be attributed to the difference in the clay content of the sediments. The clay content of the Bemidji sediments in less than 1% and the Atlantic Coastal Plain sediments contain nearly 4% clay. In addition, the relatively high ionic strength of the Bemidji ground water (estimated at approximately 10 mM near the oil body) may prevent colloid mobilization. The ionic strengths of the Atlantic Coastal Plain ground waters were about one to two orders of magnitude lower than that of the contaminated Bemidji ground water.

The morphology of the iron-rich colloids suggests that they formed by relatively rapid oxidation of ferrous iron. While it may seem likely that these colloids formed after sampling, we believe that they are present in the ground water because we assiduously avoided exposure of the samples to the atmosphere. Colloid abundance on the filters correlated well with the turbidity of the samples and turbidity was measured in the field before any significant ferrous iron oxidation could occur at the pH of these samples (6.5 to 7.0). Samples returned to the laboratory and filtered in an argon-filled glove box contained the same colloids at similar concentrations. We surmise that these colloids were formed by ferrous iron oxidation brought on by the diffusion of trace levels of oxygen (<10 ppb) into the Zone III and IV ground water (fig. 1). The wells sampled were screened within one meter of the water table.

Perylene Binding in Bemidji Ground Water

The fluorescence quenching experiments indicate that the oil degradation products present near the oil body enhance the apparent solubility of perylene. The natural organic matter in the background well (310A) is not present at sufficiently high concentration to enhance

perylene solubility. If the oil degradation products are mobile, they could facilitate the transport of perylene and other PAHs of similar hydrophobicity down-gradient. Given the low concentrations of inorganic colloids, it appears that the oil degradation products may be responsible for the observation of phenanthrene and fluorene concentrations above solubility at the site and the detection of these PAHs at distances down-gradient further than expected (Aiken and others, 1991).

The perylene K_{om} values measured by fluorescence quenching ($10^{5.5}$ to $10^{5.6}$ mL g^{-1}) are slightly lower than the K_{om} value predicted using the K_{om}-K_{ow} linear free energy relationship (LFER) developed by Karickhoff (1981) for PAH binding by soil organic matter. Using a K_{ow} value of $10^{6.50}$ for perylene, this LFER predicts a K_{om} value of $10^{5.85}$ mL g^{-1}. This difference may reflect a difference in the aromaticity of the organic matter responsible for perylene binding. The oil degradation products are predominantly aliphatic (Eganhouse and others, 1993) and the soil organic matter used by Karickhoff (1981) is probably more aromatic. Chin and others (1997) showed that the K_{om} values of PAHs decrease with increasing aliphatic content of the organic matter.

Phenanthrene Binding by Organic Matter

The organic matter partition coefficients for phenanthrene measured in the absence of ferrous iron compare favorably with K_{om} values estimated for aromatic hydrocarbons with K_{ow} values (Karickhoff, 1981). This LFER produces a K_{om} estimate of $10^{3.90}$ mL g^{-1} using a K_{ow} value of $10^{4.57}$. The K_{om} values for the hydrophobic acid fractions (well 310A, SR FA) were within 10% of this estimate; however, the hydrophobic acid fraction from ground water near the oil body (well 532A) was about 30% more effective at binding phenanthrene. Given the predominance of aliphatic oil degradation products in the well 532A ground water (Eganhouse and others, 1993), we expected a lower K_{om}, similar to the effect observed for perylene binding measured by fluorescence quenching.

The binding of hydrophobic organic compounds by organic matter generally increases with the molecular weight of the organic matter (Chin and others, 1997). In contrast, we observed that the lower molecular weight carboxylic acids were at least as or more effective at binding perylene than the higher molecular weight hydrophobic acid fractions. On the basis of these differences, it appears that K_{om} increases with increasing aliphatic content and decreasing oxygen/carbon ratios. To enhance phenanthrene binding, the long hydrocarbon chains of the aliphatic carboxylic acids must provide more accessible hydrophobic surface area than the hydrophobic acid fractions.

Effect of Ferrous Iron on Phenanthrene Binding

The presence of ferrous iron alone in solution very slightly enhanced the solubility of phenanthrene. While this solubility enhancement was subtracted from the solubility enhancements caused by the organic acids as a blank correction, some association between ferrous iron and PAHs is not unexpected. Metal ions can form charge transfer complexes with pi electrons in aromatic rings (e.g., the Ag^{+}-naphthalene binding constant is log K = 0.49; Smith and Martell, 1989). To check this effect, a higher concentration of ferrous iron, 2.7 mM, was added to the aqueous solution and equilibrated with phenanthrene. The solubility enhancement, however, was not significantly different than that measured at 0.9 mM ferrous iron.

The presence of ferrous iron had no significant effect on the K_{om} values for the aliphatic carboxylic acids, although the black precipitate that appeared in the undecanoic acid solution may have artificially lowered the measured K_{om} value. Ferrous iron slighly increased the K_{om} values of the hydrophobic acid fractions and roughly doubled the K_{om} values of the aromatic carboxylic acids, with the exception of pamoic acid. We surmise that ferrous iron is promoting greater association of the organic acids with each other, resulting in an effective increase in the molecular weight of the organic acids. This increase in molecular weight would provide a more hydrophobic partitioning environment and higher K_{om} values.

Bivalent cations that do not bind strongly with carboxyl groups promote the aggregation of humic substances by charge suppression. Cations

that bind to carboxyl groups more strongly, like Cu^{2+}, are thought to form multiligand complexes that more effectively promote organic matter aggregation (Underdown and others, 1985). If ferrous iron behaved as Cu^{2+} did for fulvic acid, we would expect the solubility enhancement caused by ferrous iron for 3-hydroxy-2-naphthoic acid to be greater than that for 2-naphthoic acid because the 3-hydroxy-2-naphthoic acid can form a strong bidentate complex. Ferrous iron complexation constants are not available for these compounds, but we know that hydroxybenzoic acid (log K = 10.13) forms much stronger copper(II) complexes than benzoic acid (log K = 1.76) (Smith and Martell, 1989). Contrary to the stong multiligand aggregation hypothesis, the solubility enhancement for 2-naphthoic acid was slightly greater than that for the 3-hydroxy-2-naphthoic acid. It appears to be more likely that ferrous iron is increasing the solubility enhancement by allowing organic acid association through charge suppression.

CONCLUSIONS

The geochemical changes caused by oil degradation have mobilized a small amount of iron-rich colloids in the Bemidji ground water. The organic colloids in the contaminated ground water are capable of enhancing the solubility of very hydrophobic PAHs. Potentially, this solubility enhancement may have contributed to the transport of such PAHs over distances greater than expected (Aiken and others, 1991). The presence of high ferrous iron concentrations in the contaminated Bemidji ground water may increase the ability of the the oil degradation products to enhance the solubility of PAHs.

REFERENCES

Aiken, G.R., Capel, P.D., Furlong, E.T., Hult, M.F. and Thorn, K.A. , 1991, Mechanisms controlling the transport of organic chemicals in subsurface environments, Mallard, G.E., and Aronson, D.A., eds., U.S. Geological Survey Toxic Substances Hydrology Program--Proceedings of the Technical Meeting, Monterey, California, March 11-15, 1991: U.S. Geological Survey Water-Resources Investigation Report 91-4034, p. 633-637.

Aiken, G.R. and Malcolm, R.L. , 1987, Molecular weight of aquatic fulvic acids by vapor pressure osmometry: Geochimica Cosmochimica Acta, v. 51. p. 2177-2184.

Aiken, G.R., McKnight, D.M., Thorn, K.A., and Thurman, E.M., 1992, Isolation of hydrophilic organic acids from water using nonionic macroporous resins: Organic Geochemistry, v. 18, p. 567-573.

Amrhein, C., Mosher, P.A. and Strong, J.E., 1993, Colloid-assisted transport of trace metals in roadside soils receiving deicing salts: Soil Science Society of America Journal, v. 57, p. 1212-1217.

Backhus, D.A. and Gschwend, P.M., 1990, Fluorescent polycyclic aromatic hydrocarbons as probes of studying the impact of colloid on pollutant transport in groundwater: Environmental Science & Technology., v. 24, p. 1214-1223.

Backhus, D.A., Ryan, J.N., Groher, D.M., MacFarlane, J.K. and Gschwend, P.M., 1993, Sampling colloids and colloid-associated contaminants in ground water: Ground Water, v. 31, p. 466-479.

Baedecker, M.J., Cozzarelli, I.M., Eganhouse, R.P., Siegel, D.I. and Bennett, P.C., 1993, Crude oil in a shallow sand and gravel aquifer--III. Biogeochemical reactions and mass balance modeling in anoxic groundwater: Applied Geochemistry, v. 8, p. 569-586.

Bennett, P.C., Siegel, D.I., Baedecker, M.J. and Hult, M.F, 1993, Crude oil in a shallow sand and gravel aquifer--I. Hydrogeology and inorganic geochemistry: Applied Geochemistry, v. 8, p. 529-549.

Buddemeier, R.W. and Hunt, J.R., 1988, Transport of colloidal contaminants in groundwater: Radionuclide migration at the Nevada Test Site: Applied Geochemistry, v. 3, p. 535-548.

Chin, Y.-P., Aiken, G.R. and Danielsen, K.M., 1997, Binding of pyrene to aquatic and commercial humic substances: The role of molecular weight and aromaticity: Environmental Science & Technology, v. 31. p. 1630-1635.

Chiou, C.T., Malcolm, R.L., Brinton, T.I. and Kile, D.E., 1986, Water solubility enhancement of some organic pollutants and pesticides by dissolved humic and fulvic acids: Environmental Science & Technology, v. 20, p. 502-508.

Cozzarelli, I.M., Baedecker, M.J., Eganhouse, R.P., and Goerlitz, D.F., 1994, Geochemical evolution of low-molecular weight organic acids derived from the degradation of petroleum contaminants in groundwater: Geochimica Cosmochimica Acta, v. 58, p. 863-877.

De Jonge, H., Jacobsen, O.H., de Jonge, L.W. and Moldrup, P., 1998, Particle-facilitated transport of prochloraz in undisturbed sandy loam soil columns: Soil Science Society of America Journal, v. 27, p. 1495-1503.

Dunnivant, F., Jardine, P.M., Taylor, D. and McCarthy, J.F., 1992, Cotransport of cadmium and hexachlorobiphenyl by dissolved organic matter through columns containing aquifer material: Environmental Science & Technology, v. 26, p. 360-368.

Eganhouse, R.P., Baedecker, M.J., Cozzarelli, I.M., Aiken, G.R., Thorn, K.A. and Dorsey, T.F. , 1993, Crude oil in a shallow sand and gravel aquifer--II. Organic geochemistry: Applied Geochemistry, v. 8, p. 551-567.

Hawley, C. M., 1995, A field and laboratory study of the mechanisms of facilitated transport of hydrophobic organic contaminants: Boulder, Colorado, University of Colorado, Department of Civil, Environmental, and Architectural Engineering, unpublished M.S. thesis, 119 p.

Hult, M. F., 1987, Movement and fate of crude oil contaminants in the subsurface environment at Bemidji, Minnesota, Franks, B. J., ed., U.S. Geological Survey. U.S. Geological Survey Program on Toxic Waste -- Ground-Water Contamination Proceedings of the Third Technical Meeting, Pensacola, Florida, March 23-27, 1987: U.S. Geological Survey Open-File Report 87-109, p. C3-C5.

Hult, M. F., 1989, Mobilization, transport, and, and fate of hydrocarbons in the unsaturated zone, Mallard, G. E. and Ragone, S. E., eds., U.S. Geological Survey Toxic Substances Hydrology Program -- Proceedings of the Technical Meeting, Phoenix, Arizona, September 26-30, 1988: U.S. Geological Survey Water-Resources Investigation Report 88-4220, p. 53-53.

Jury, W.A., Elabd, H. and Resteko, M.. 1986, Field study of napromide movement through unsaturated soil: Water Resources Research., v. 22, p. 749-755.

Karickhoff, S.W., 1981, Semi-empirical estimation of sorption of hydrophobic pollutants on natural sediments and soils: Chemosphere, v. 10, p. 833-846.

Magee, B.R., Lion, L.W. and Lemley, A.T., 1991, Transport of dissolved organic macromolecules and their effect on the transport of phenanthrene in porous media: Environmental Science & Technology, v. 25, p. 323-331.

Mukerjee, P. and Mysels, K. J., 1971, Critical micelle concentrations of aqueous surfactant systems: National Bureau of Standards Report NSRDS-NBS 36, 227 p.

Puls, R.W., Clark, D.A., Bledsoe, B., Powell, R.M. and Paul, C.J., 1992, Metals in ground water: sampling artifacts and reproducibility: Hazardous Waste and Hazardous Materials, v. 9, p. 149-162.

Ryan, J.N. and Gschwend, P.M., 1990, Colloid mobilization in two Atlantic Coastal Plain aquifers: Field studies: Water Resources Research, v. 26, p. 307-322.

Ryan, J.N. and Gschwend, P.M., 1992, Effect of iron diagenesis on the transport of colloidal clay in an unconfined sand aquifer: Geochimica Cosmochimica Acta, v. 56, p. 1507-1521.

Smith, R.M. and Martell, A.E., 1989, Critical Stability Constants: New York:Plenum Press.

Underdown, A.W., Langford, C.H. and Gamble, D.S., 1985, Light scattering studies of the relationship between cation binding and aggregation of a fulvic acid: Environmental Science & Technology, v. 19, p. 132-136.

Villholth, K.G., in press, Colloid characterization and colloidal phase partitioning of polycyclic aromatic hydrocarbons in two creosote-containing aquifers in Denmark: Environmental Science & Technology, to appear in February 1999.

Vinten, A.J.A., Yaron, B. and Nye, P.H., 1983, Vertical transport of pesticides into soil when adsorbed on suspended particles: Journal of

Agriculture and Food Chemistry, v. 31, p. 662-664.

AUTHOR INFORMATION

Joseph N. Ryan and Christine M. Hawley, Department of Civil, Environmental, and Architectural Engineering, University of Colorado, Campus Box 428, Boulder, Colorado 80309 (joe.ryan@colorado.edu)

George R. Aiken, U.S. Geological Survey, 3215 Marine Street, Boulder, Colorado 80303

Debera A. Backhus, School of Public and Environmental Affairs, Bloomington, Indiana 47405

Karen G. Villholth, VKI, Agern Alle 11, DK-2970 Hoersholm, Denmark.

Inhibition of Acetoclastic Methanogenesis by Crude Oil from Bemidji, Minnesota

By Ean Warren, Barbara A. Bekins, and E. Michael Godsy

ABSTRACT

The shallow ground water at a site near Bemidji, Minnesota is contaminated with crude oil spilled from a broken pipeline in 1979. With a continued source of dissolved crude oil components, the geochemical conditions in the aquifer have evolved into aerobic, iron-reducing, and methanogenic redox zones. The methanogenic zone starts within the crude oil-contaminated region and extends more than 60 meters downgradient. The methanogenic numbers in the aquifer are low, but variable, depending on the subpopulation of methanogen. In areas close to the crude-oil source, hydrogen- and formate-utilizing methanogens are found in numbers more than one hundred times higher than acetate-utilizers. The acetate-utilizers are found only well below the non-aqueous phase oil and further downgradient. This pattern of methanogen distribution suggests that growth of acetate-utilizers is limited near the source. Laboratory results suggest that toxicity of the dissolved crude-oil is an explanation.

Serum bottle assays were conducted using crude oil in a mineral salts solution inoculated with an enriched methanogenic consortia from a creosote-contaminated site in Pensacola, Florida. Acetate, hydrogen, and formate were added and gas volume change was monitored. Hydrogen- and formate-utilization were unaffected by the crude oil whereas acetate utilization was significantly inhibited. The distribution of aquifer methanogens together with the toxicity assays form a consistent picture with the hypothesis that acetoclastic methanogenesis is inhibited in the vicinity of the oil at the Bemidji site. Because acetate degradation has been widely documented as the rate-limiting step in anaerobic waste treatment processes, it is likely that the inhibition of acetoclastic methanogenesis by the crude oil affects the overall methanogenic degradation rates of the petroleum hydrocarbon contaminants.

INTRODUCTION

In August 1979, a crude oil pipeline near Bemidji, Minnesota (fig. 1) burst, spilling about 1,700,000 L (liters) of crude oil. Cleanup efforts removed all but an estimated 400,000 L of crude oil (Hult, 1984). The crude oil has moved through the unsaturated zone contaminating the sediments down to the water table. A plume of the water-soluble components (including benzene, toluene, ethylbenzene, xylenes, and polynuclear aromatic hydrocarbons) has formed under the crude oil. In the past 20 years, the plume has changed the geochemical conditions in the aquifer near the oil body from aerobic to iron-reducing and methanogenic (Baedecker and others, 1993; Bekins and others, 1999).

A model of the plume using a two-dimensional, multispecies reactive solute transport model with sequential aerobic and anaerobic degradation processes was successful in predicting the evolution of geochemical conditions in the plume (Essaid and others, 1995). However, the use of Monod kinetics to model microbial growth in the aquifer resulted in simulated microbial numbers that far exceeded the observed aquifer microbial numbers. One process that would act to limit the net growth is inhibition of crude-oil biodegradation due to contaminant toxicity.

Specific methanogens may be inhibited by the increased contaminant concentration near the crude oil or even by the non-aqueous phase of the crude oil itself. Several authors have found that acetoclastic methanogens are inhibited by toxic compounds [Hickey and others, 1987 (chloroform, bromoethanesulfonic acid, tricloroacetic acid, and formaldehyde); Patel and

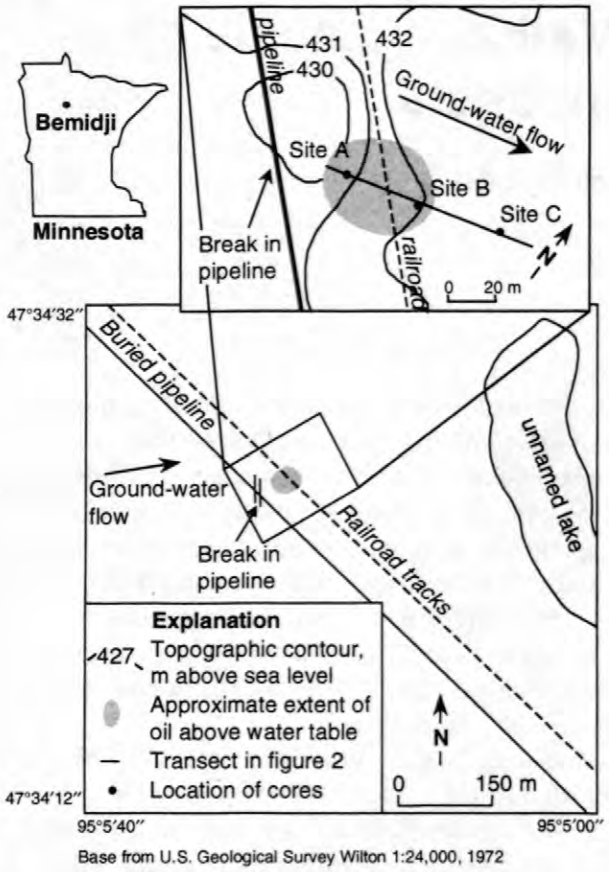

Figure 1. Site of 1979 crude oil spill near Bemidji, Minnesota, showing location of cores along a flow line.

others, 1991 (benzene ring compounds); Sierra-Alvarez and Lettinga, 1991 (monosubstituted benzenes, chlorobenzene, methoxybenzene, and benzaldehyde); Colleran and others, 1992 (chlorinated and fluorinated low molecular weight aliphatic and aromatic compounds); Davies-Venn and others, 1992 (chlorophenols and chloroanilines); van Beelen and Fleuren-Kemilä, 1993 (pentachlorophenol); and Donlon and others, 1995 (N-substituted aromatics)]. This is important because about 70 percent (%) of the methane produced comes from acetate fermentation by acetoclastic methanogens as opposed to carbon dioxide reduction by hydrogenophilic methanogens (Jeris and McCarty, 1965; Cappenberg, 1974; Cappenberg and Prins, 1974). Thus acetate fermentation is known to be the rate-limiting step in anaerobic wastewater-treatment processes. Parkin and Speece (1982) were able to model concentration-dependent inhibition of methanogenic degradation of a variety of toxic compounds by modeling inhibition of the acetate utilization step.

Very little research has compared the inhibition of acetoclastic methanogens to other subpopulations. Colleran and others (1992) found acetoclastic species were significantly more inhibited by halogenated aliphatics than hydrogenophilic subpopulations. Bhattacharya and others (1995) found that whereas acetoclastic methanogens were inhibited by 4-nitrophenol, hydrogenophilic methanogens were not. Bekins and others (1997) found that acetoclastic methanogens were more susceptible to toxicity of water-soluble creosote compounds than were hydrogen- or formate-utilizing methanogens.

In this paper, we present evidence that inhibition can explain some aspects of methanogenic microbial numbers at the crude-oil spill site near Bemidji, Minnesota.

METHODS

Most Probable Number (MPN) determinations were done on sediment from cores at three sites and compared with laboratory crude oil toxicity experiments. Inhibition of methanogens was measured by an anaerobic toxicity assay (Owen and others, 1979) in which the volume of gas produced in a methanogenic microcosm with crude oil was compared to that in a microcosm without crude oil.

Most Probable Number Determination

Most Probable Number determinations were done on sediments from three sites located within the anoxic portion of the plume, labeled A, B, and C in figure 1. Cores containing aquifer sediments and the contaminated groundwater were collected with a 2.4 m (meter) freezing drive shoe (Murphy and Herkelrath, 1996). Data from sites A, B, and C were obtained from vertical profiles consisting of 3, 1, and 2 cores, respectively. The single core from site B was collected in 1996 while the five cores from sites A and C were collected in 1997. The method was the same for each core. The core was cut with a large tubing cutter exposing the aquifer material. Under a flow of oxygen-free nitrogen gas, the first few centimeters of the core material at the

cut were removed with a sterile spatula exposing an uncontaminated surface.

Approximately 10 g (grams) of sediment from the center of the core was added to a 25 x 142 mm (millimeter) anaerobic isolation roll streak tube (Bellco Glass Inc., Vineland, N.J. Note: Any use of trade, product, or firm names in this paper is for descriptive purposes only and does not imply endorsement by the U.S. Government.) filled with 20.0 mL (milliliter) of pre-reduced mineral salts solution. The mineral salts were prepared as follows (per liter): 0.75 g of KH_2PO_4; 0.89 g of K_2HPO_4; 0.36 g of $MgCl_2 \cdot 6H_2O$; 0.9 g of NH_4Cl; 9.0 mL of trace metal solution (Zeikus, 1977); 5.0 mL of vitamin solution (Wolin and others, 1963); and 10 mg (milligram) of Tween 80® [a nonionic surfactant added to remove microbes from the sediment (Yoon and Rosson, 1990)]. The pH was adjusted to 7.0 with phosphoric acid, and the solution was then boiled, cooled, and dispensed under a stream of oxygen-free nitrogen gas. The solution was sterilized at 121°C (degrees Celsius) [100 kPa (kilopascal)] for 15 minutes. All mineral salts solutions were amended with ferrous sulfide (FeS) as a reducing agent (Brock and O'Dea, 1977) to a final concentration of 1% by volume. Oxygen-free nitrogen gas was allowed to flow over the surface of the mineral salts solution as the sediment sample was added. The tube was then sealed, mixed well, and allowed to stand for 2 hours to allow penetration of Tween 80® into the sample. The tubes were then opened and sonicated [10 watts for 30 seconds] to dislodge the bacteria into the mineral salts using a Branson Sonifier®, Model 200, with the microtip attached (Branson Ultrasonics Corporation, Danbury, Conn.) with a flow of sterile oxygen-free nitrogen gas over the surface. The sediment samples in mineral salts were stored for not more than 4 hours at 20°C before inoculation of the growth media.

Microbial concentrations in sediment samples were determined using a five-tube MPN analysis. Samples were serially diluted by orders of magnitude into dilution mineral salts solutions that were pre-reduced and anaerobically sterilized as described by Holdeman and Moore (1972). Aliquots of the dilutions were inoculated into three different media, designed to promote growth and the enumeration of acetate-, hydrogen-, and formate-utilizing methanogenic microorganisms. Acetoclastic and formate-utilizing organisms were enumerated with the addition to mineral salts of 2.5 g of sodium acetate·$3H_2O$ or 2.5 g sodium formate per liter, respectively. Hydrogen oxidizers were enumerated by aseptically pressurizing the serum bottles after inoculation with a 70:30 mix of H_2:CO_2 to 140 kPa. The serum bottles were allowed to incubate for a minimum of six weeks at room temperature. The presence of the methanogen subpopulation was established by the detection of methane using a gas chromatograph with flame ionization detection (Godsy, 1980). Subsamples of sediments from site B (fig. 2) were taken for analysis of oil content using the method described by Hess and others (1992). Values for oil content at a site near site A were determined by Dillard and others (1997).

Anaerobic Toxicity Assays

Anaerobic toxicity assays followed an adaptation of a protocol described by Owen and others (1979). Microcosms in 120 mL serum bottles were prepared to evaluate the toxicity of crude oil to formate-, hydrogen-, and acetate-utilizing methanogens. The serum bottles contained a total of 100 mL comprised of crude oil (10% by volume), mineral salts (70%), and an enriched methanogenic consortia suspended in

Table 1.. Contents of serum bottles. Number indicates number of replicates. Check mark indicates either bottle was autoclaved or crude oil was present.

Bottle	Energy Source	Autoclaved	Crude Oil	No.
1	Acetate		√	2
2	Formate		√	2
3	Hydrogen		√	2
4	Acetate			1
5	Formate			1
6	Hydrogen			1
7	Acetate	√	√	1
8	Formate	√	√	1
9	Hydrogen	√	√	1
10	None		√	2
11	None	√		1

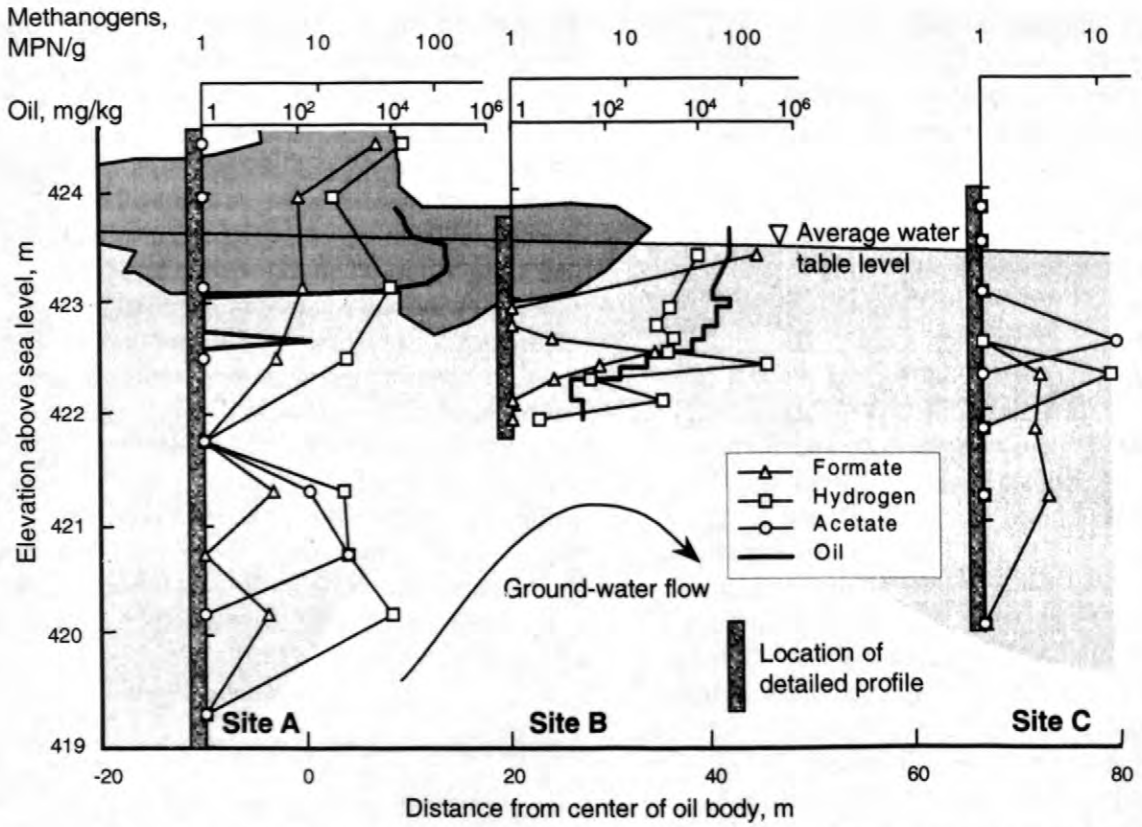

Figure 2. Formate-, hydrogen-, and acetate-utilizing microbial numbers [upper scale in graphs, shown in MPN/g (Most Probable Number per g)] from cores taken at sites A, B, and C, along with oil content [lower scale, shown in mg/kg (milligrams per kilogram of sediment)] at sites A and B. The dark gray area denotes greater than 10% oil saturation of pore space. Oil content for site A was determined by Dillard and others (1997). The light gray area corresponds to the anaerobic area of the plume (Bekins and others, 1999).

mineral salts (20%). The bottles were prepared in an anaerobic atmosphere and amended with ferrous sulfide (FeS) as a reducing agent (Brock and O'Dea, 1977) to a final concentration of 1% by volume. The bottles were sealed with solid butyl rubber stoppers and aluminum crimp seals. They were stored on their sides to reduce the possibility of gas leakage. Change of gas volume in the headspace was measured using a horizontal manometer.

Formate, hydrogen, or acetate were added to the bottles (table1). The acetate and formate microcosms contained, respectively, 110 mg/L (milligrams per liter) acetate or 330 mg/L formate in mineral salts. The headspace of the formate and acetate microcosms were flushed with oxygen-free nitrogen and carbon dioxide at a 80:20 ratio by volume. The hydrogen microcosms were flushed with 80% hydrogen and 20% carbon dioxide. At the start of the experiment, each microcosm was brought to equilibrium with atmospheric pressure using oxygen-free nitrogen.

Active microcosms were compared to controls to determine inhibition. Each active bottle containing crude oil was made in duplicate. Positive controls were made with acetate, hydrogen, and formate and no crude oil. Negative controls consisted of just the methanogenic consortium in mineral salts with the crude oil (in duplicate) as well as autoclaved bottles with acetate, hydrogen, and formate and the crude oil. The headspace was brought to atmospheric pressure with each measurement and any consumption of gas was replaced with nitrogen. All volume data were adjusted to standard temperature and pressure. Volumes from hydrogen microcosms were further normalized to

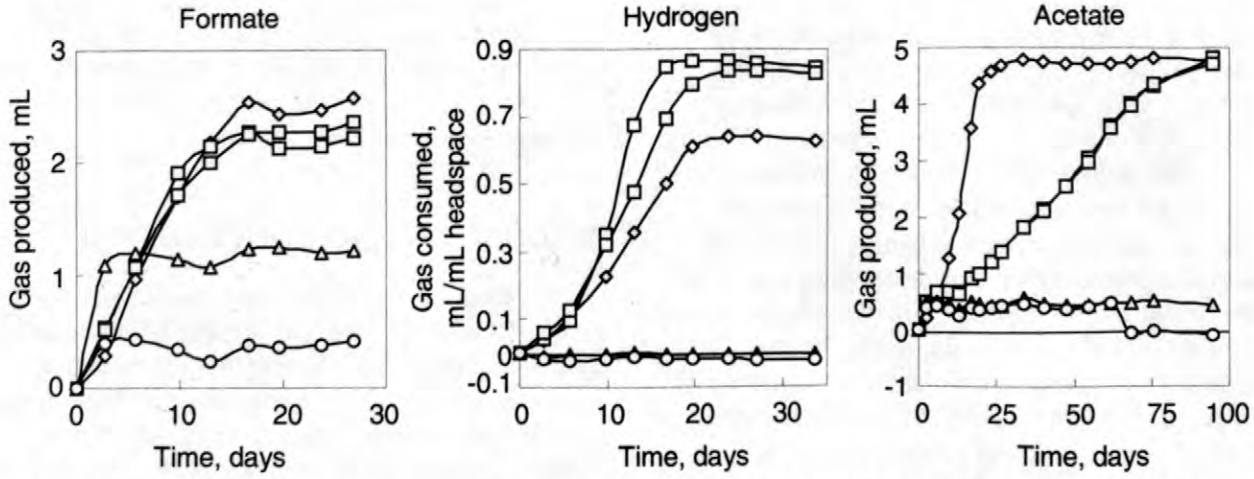

Figure 3. Gas production or consumption in microcosms fed with formate, hydrogen, or acetate. The legend is as follows: Active culture with crude oil (□), in duplicate; active culture without crude oil (◇); active culture with crude oil only (O); and average of two autoclaved cultures without crude oil (Δ).

the headspace volume to account for differing amounts of initial hydrogen mass.

RESULTS

Most Probable Numbers from the site reveal that acetoclastic methanogens are not found near the oil body. In contrast, hydrogenophilic and formate-utilizers are found in similar numbers both within the oil body and outside it in the aqueous plume. The anaerobic toxicity assays show that the acetoclasts are inhibited significantly by the crude oil whereas the hydrogenophiles and formate-utilizers are not (figs. 2 and 3).

Vertical Profiles of Methanogens

Vertical profiles of numbers of methanogens and oil concentrations through the plume of dissolved crude-oil compounds are shown in figure 2. The figure shows the microbial numbers of three subpopulations of methanogens at each location, along with oil content on sediments from sites A and B. Acetate-utilizing methanogens were found under the crude oil body at site A but only at a vertical distance of greater than 1 meter below the oil. At the center site, B, the anaerobic part of the plume is very narrow due to upwelling of oxygenated water below a low-permeability horizon. At this location there is apparently no niche sufficiently distant from the oil for the acetate-utilizers to occupy. At the down-gradient site where there is no non-aqueous oil, acetate utilizers are again present. Hydrogen- and formate-utilizers are found both in the vicinity of the oil and also downgradient. All MPNs were below 100/g sediment. At site A, there were relatively high numbers of hydrogenophiles and formate-utilizers starting in the unsaturated zone in the oil. They remained high until about 1 meter below the oil where they dropped to less than 1/g. They were found again over the next 1.5 m, but hydrogenophiles were found in greater abundance in this interval than formate-utilizers. At site B, there was a peak of formate-utilizers in the oil and another at 422.5 m near the center of the aqueous plume. The hydrogenophiles were relatively high throughout the core. The hydrogen- and formate-utilizers do not seem to be affect by the oil. Site C contained all three subpopulations of methanogens, but at very low numbers (note the scale on the site C plot).

Anaerobic Toxicity Assays

The results from the toxicity experiment are shown in figure 3. Formate-utilizing methanogens produced 2.5 mL of gas after 26 days. The microcosms with crude oil closely paralleled the active control indicating no detectable toxicity effect. After the first reading, gas in the killed

control increased. Since the microcosm remained inactive for the duration of the experiment, the likely source is due to an experimental error, possibly incomplete equilibrium with atmospheric pressure at the start of the experiment.

When hydrogen is utilized by methanogens, the net effect is a reduction of the gas volume in the headspace. The rates of hydrogen utilization in the microcosms with crude oil were similar to the active control indicating no discernable toxicity effect. Surprisingly, the hydrogen-utilizing methanogens used about 20% more gas in the presence of crude oil than in its absence. This indicates a slightly greater level of activity in the presence of the crude oil. The difference may be due to an initial excess of hydrogen in the headspace. Because hydrogen and carbon dioxide were added in stoichiometric amounts (table 2), if the hydrogen:carbon dioxide ratio in the headspace is too low, carbon dioxide-limiting conditions will occur when the as the hydrogen is exhausted. The microcosms with crude oil may have produced enough carbon dioxide from the degradation of organics to eliminate this limitation. Further studies including tighter controls of the headspace gas are planned to verify the possibility of carbon dioxide limitation.

The behavior of the acetate microcosms contrasts sharply with that of the hydrogen and formate microcosms. Production of methane and carbon dioxide in the acetate microcosms was affected significantly by the crude oil. All active microcosms produced 4.8 mL of gas. However, while the microcosm without crude oil took 30 days, the microcosms with crude oil took 100 days to reach completion.

Table 2. Reactions and energy yields (kilojoules per mole) for acetate fermentation and carbon dioxide reduction using formate and hydrogen.

Acetate
$CH_3COOH \rightarrow CH_4 + CO_2$
–28.3 kJ/mol acetate
Hydrogen
$4H_2 + CO_2 \rightarrow CH_4 + 2H_2O$
–32.7 kJ/mol hydrogen
Formate
$4HCOOH \rightarrow CH_4 + 3CO_2 + 2H_2O$
–36.1 kJ/mol formate

DISCUSSION AND CONCLUSIONS

Serum-bottle toxicity assays using crude oil and enriched methanogenic cultures with formate, hydrogen, and acetate showed that formate- and hydrogen-utilization were unaffected by the crude oil whereas acetate utilization was significantly inhibited. This result is consistent with observed numbers of methanogens found in the aquifer. Microbial numbers at the site indicate that formate- and hydrogen-utilizing methanogens are present near the non-aqueous oil whereas acetoclastic methanogens are found only at distances greater than 1 meter from the oil.

Anaerobic-toxicity experiments using water-soluble components from creosote also showed that acetoclastic methanogens were more susceptible to inhibition than the others were. This observed inhibition may be due to the lower energy yield (table 2) from the degradation of acetate. The energy gained from acetate fermentation may be inadequate to compensate for the toxicity near the oil. Methanogens from the two carbon dioxide reduction pathways may get just enough energy to overcome the toxic effects of the oil (Bekins and others, 1997).

Because the inhibition of acetoclastic methanogenesis by the crude oil would affect the overall methanogenic degradation rates of the petroleum hydrocarbon contaminants, it is important to identify sources and extent of inhibition.

REFERENCES

Baedecker, M.J., Cozzarelli, I.M., Eganhouse, R.P., Siegel, D.I., and Bennett, P.C., 1993, Crude oil in a shallow sand and gravel aquifer-III. Biogeochemical reactions and mass balance modeling in anoxic groundwater: Applied Geochemistry, v. 8, p. 569-586.

Bekins, B.A., Cozzarelli, I.M., Godsy, E.M, Warren, Ean, Tuccillo, M.E., Essaid, H.I., and Paganelli, V.V., 1999, Chemical and physical controls on microbial populations in the Bemidji Toxics Site crude-oil plume, Morganwalp, D.W., and Buxton, H.T., eds., U.S. Geological Survey Toxic Substances Hydrology Program—Proceedings of the Technical Meeting, Charleston, South Carolina, March 8-12, 1999-- Volume 3 -- Subsurface Contamination from Point Sources: U.S. Geological Survey Water-Resources Investigations Report 99-4018C, this volume.

Bekins, B.A., Godsy, E.M., and Warren, Ean, 1997, Inhibition of acetoclastic methanogenesis by complex mixtures of hydrocarbons: Eos, Transactions, American Geophysical Union, v. 78, no. 46, supplement, p. F289.

Bhattacharya, S.K., Sluder, J.L., Jr., and Uberoi, V., 1995, Effects of 4-nitrophenol and H_2 and CO levels in anaerobic propionate systems: Water Research, v. 29, no. 5, p. 1249-1258.

Brock, T.D. and O'Dea, K., 1977, Amorphous ferrous sulfide as a reducing agent for culture of anaerobes: Applied and Environmental Microbiology, v. 33, p. 254-256.

Cappenberg, T.E., 1974, Interrelations between sulfate-reducing and methane-producing bacteria in bottom deposits of a fresh-water lake. II. Inhibition experiments: Antonie van Leeuwenhoek Journal of Microbiology and Serology, v. 40, no. 2, p. 297-306.

Cappenberg, T.E. and Prins, R.A., 1974, Interrelations between sulfate-reducing and methane-producing bacteria in bottom deposits of a fresh-water lake. III. Experiments with ^{14}C-labeled substrates: Antonie van Leeuwenhoek Journal of Microbiology and Serology, v. 40, no. 3, p. 457-469.

Colleran, Emer, Concannon, F., Golden, T., Geoghegan, F., Crumlish, B., Killilea, E., Henry, M., and Coates, J., 1992, Use of methanogenic activity tests to characterize anaerobic sludges, screen for anaerobic biodegradability and determine toxicity thresholds against individual anaerobic trophic groups and species: Water Science and Technology, v. 25, no. 7, p. 31-40.

Davies-Venn, Christian, Young, J.C., and Tabak, H.H., 1992, Impact of chlorophenols and chloroanilines on the kinetics of acetoclastic methanogenesis: Environmental Science and Technology, v. 26, no. 8, p. 1627-1635.

Dillard, L.A., Essaid, H.I., and Herkelrath, W.N., 1997, Multiphase flow modeling of a crude-oil spill site with a bimodal permeability distribution: Water Resources Research, v. 33, p. 1617-1632.

Donlon, B.A., Razo-Flores, Elías, Field, J.A., and Lettinga, Gatze, 1995, Toxicity of N-substituted aromatics to acetoclastic methanogenic activity in granular sludge: Applied and Environmental Microbiology, v. 61, no. 11, p. 3889-3893.

Essaid, H.I., Bekins, B.A., Godsy, E.M., Warren, Ean, Baedecker, M.J., and Cozzarelli, I.M., 1995, Simulation of aerobic and anaerobic biodegradation processes at a crude oil spill site: Water Resources Research, v. 31, no. 12, p. 3309-3327.

Godsy, E.M., 1980, Isolation of *Methanobacterium bryantii* from a deep aquifer by using a novel broth-antibiotic disk method: Applied and Environmental Microbiology, v. 39, no. 5, p. 1074-1075.

Hess, K.M., Herkelrath, W.N., and Essaid, H.I., 1992, Determination of subsurface fluid contents at a crude-oil spill site: Journal of Contaminant Hydrology, v. 10, p. 75-96.

Hickey, R.F., Vanderwielen, J., and Switzenbuam, M.S., 1987, The effects of organic toxicants on methane production and hydrogen gas levels during the anaerobic digestion of waste activated sludge: Water Research, v. 21, no. 11, p. 1417-1427.

Holdeman, L.V. and Moore, W.E.C., 1972, Anaerobe Laboratory Manual: Blacksburg, Virginia, Virginia Polytechnic Institute and State University, 156 p.

Hult, M.F., 1984, Groundwater contamination by crude oil at the Bemidji, Minnesota, research site - An introduction, Hult, M.F. ed., Groundwater Contamination by Crude Oil at the Bemidji, Minnesota, Research Site: U.S. Geological Survey Water-Resources Investigations Report 84-4188, p. 1-15.

Jeris, J.S. and McCarty, P.L., 1965, The Biochemistry of methane fermentation using C^{14} tracers: Journal of the Water Pollution Control Federation, v. 37, no. 2, p. 178-192.

Murphy, Fred and Herkelrath, W.N., 1996, A sample-freezing drive shoe for a wire line piston core sampler: Ground Water Monitoring and Remediation, v. 16, no. 3, p. 86-90.

Owen, W.F., Stuckey, D.C., Healy, J.B., Jr., Young, L.Y., and McCarty, P.L., 1979, Bioassay for monitoring biochemical methane potential and anaerobic toxicity: Water Research, v. 13, p. 485-492.

Parkin, G.F. and Speece, R.E., 1982, Modeling toxicity in methane fermentation systems: Journal of Environmental Engineering, v. 108, no. EE3, p. 515-531.

Patel, G.B., Agnew, B.J., and Dicaire, C.J., 1991, Inhibition of pure cultures of methanogens by benzene ring compounds: Applied and Environmental Microbiology, v. 57, no. 10, p. 2969-2974.

Sierra-Alvarez, Reyes and Lettinga, Gatze, 1991, The effect of aromatic structure on the inhibition of acetoclastic methanogenesis in granular sludge: Applied Microbiology and Biotechnology, v. 34, no. 4, p. 544-550.

van Beelen, P. and Fleuren-Kemilä, A.K., 1993, Toxic effects of pentachlorophenol and other pollutants on the mineralization of acetate in several soils: Ecotoxicology and Environmental Safety, v. 26, no. 1, p. 10-17.

Wolin, E.A., Wolin, M.J., and Wolfe, R.S., 1963, Formation of methane by bacterial extracts: Journal of Biological Chemistry, v. 238, p. 2882-2886.

Yoon, W.B. and Rosson, R.A., 1990, Improved Method of enumeration of attached bacteria for study of fluctuation in the abundance of attached and free-living bacteria in response to diel variation in seawater turbidity: Applied and Environmental Microbiology, v. 56, no. 3, p. 595-600.

Zeikus, J.G., 1977, The biology of methanogenic bacteria: Bacteriological Reviews, v. 41, no. 2, p. 514-541.

AUTHOR INFORMATION

Ean Warren, Barbara A. Bekins, and E. Michael Godsy, U.S. Geological Survey, Menlo Park, California (ewarren@usgs.gov)

Polar Metabolites of Crude Oil

By Kevin A. Thorn and George R. Aiken

ABSTRACT

Polar metabolites of crude oil in the form of nonvolatile organic acids were isolated from wells downgradient from the North oil pool and from the spray zone at the Bemidji site. The nonvolatile organic acids were subjected to spectroscopic and other characterization methods. The nonvolatile organic acids were distinguishable from naturally occurring ground-water humic substances in the aquifer, and appear to represent the partial oxidation products of the C_{18} or greater alkylaromatic, naphthenoaromatic, and sulfur-containing constituents of the crude oil.

INTRODUCTION

At the study site near Bemidji, Minnesota, biodegradation has resulted in a plume of dissolved organic carbon (DOC) that extends into zones III, IV, and V downgradient from the North oil pool (fig. 1). Ground-water in the spray zone (zone II) has also been contaminated from vertical infiltration of DOC resulting from biodegradation of crude oil in the overlying unsaturated zone, or from vertical infiltration of crude oil constituents followed by degradation in the saturated zone. The majority of DOC in zones II, III, IV, and V is comprised of nonvolatile organic acids (NVOA's) in the approximate molecular weight range from 360 to 410 daltons that represent the partial oxidation products (i.e. polar metabolites) of crude oil constituents. A study was undertaken to determine to what degree of resolution these NVOA's could be differentiated from the naturally occurring ground-water DOC in the aquifer, and to determine from which constituents in the crude oil the NVOA's are derived, using spectroscopic and other characterization techniques. The results from this study (Thorn and Aiken, 1998) are summarized here.

Hydrophilic acids, hydrophobic acids, and the hydrophobic neutral fraction of organic acids were isolated on XAD resins in samples from well 530 in zone IV (transition zone, DOC=21 mg C/L), well 603 in zone II (spray zone; DOC=15 mg C/L), and well 310 in zone I (background well; DOC= 2.9 mg C/L) that were collected during the 1986-1989 field seasons. These were characterized using liquid phase ^{1}H and ^{13}C NMR spectroscopy, elemental analyses, molecular weight determinations, $\delta\ ^{13}C$'s, and ^{14}C ages. The characterization data are presented in table 1. The naturally occurring ground-water humic substances isolated from well 310 were distinguishable from the NVOA's isolated from contaminated water in wells 530 and 603. Based upon molecular weights, sulfur contents, carbon aromaticities, and the presence of methyl groups bonded to aromatic rings, the characterization data suggest that the NVOA's in wells 530 and 603 originate from the C_{18} or greater alkylaromatic, naphthenoaromatic, and sulfur-containing constituents of the crude oil, including possibly the resins and asphaltenes. A scheme for the origin of the NVOA's in well 530 is shown in figure 2.

The generation and fate of the partial oxidation products of crude oil constituents is one of the least understood processes in the biodegradation of petroleum in ground-water. Some fundamental questions need to be addressed in future research. The hydrophobic neutrals are the least polar (i.e. least oxidized) fraction of dissolved organic acids isolated from the ground-water. The possibility that metabolites of petroleum constituents less polar than the hydrophobic neutrals are sorbed to the sediment grains within the vicinity of the oil body needs to be investigated. The concentration of total dissolved organic carbon (TDOC) downgradient from the North oil pool has remained relatively stable suggesting that degradation of the plume has reached equilibrium (Delin and others, 1998). This suggests three possible fates for the NVOA's: further degradation into lower molecular weight organic acids with subsequent microbial re-assimilation; mineralization to CO_2; sorption onto aquifer sediments, possibly via ligand exchange complexation reactions.

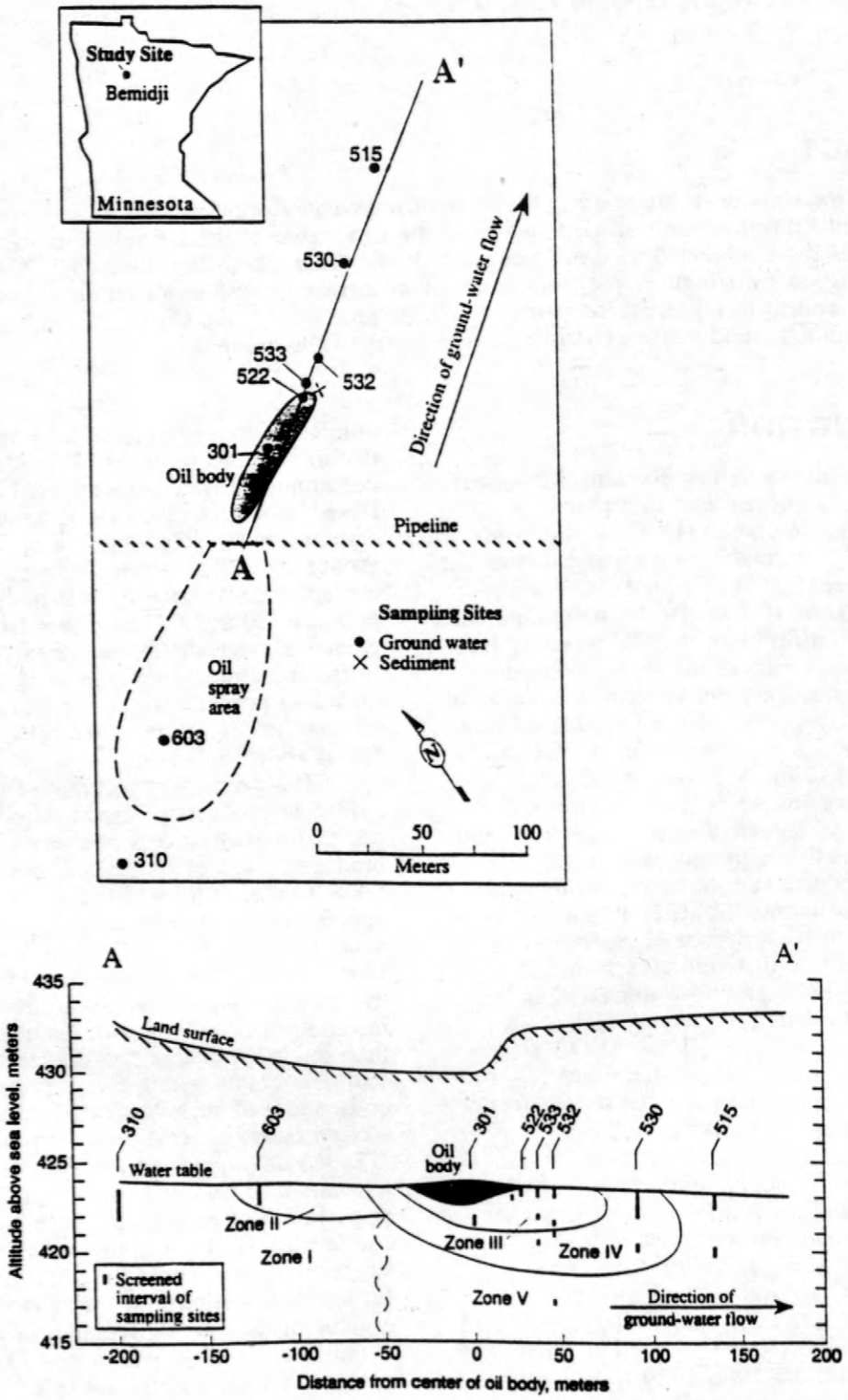

Figure 1. Bemidji study site showing locations of water table wells, North oil pool, and geochemical zones. Modified from Baedecker and others, 1993.

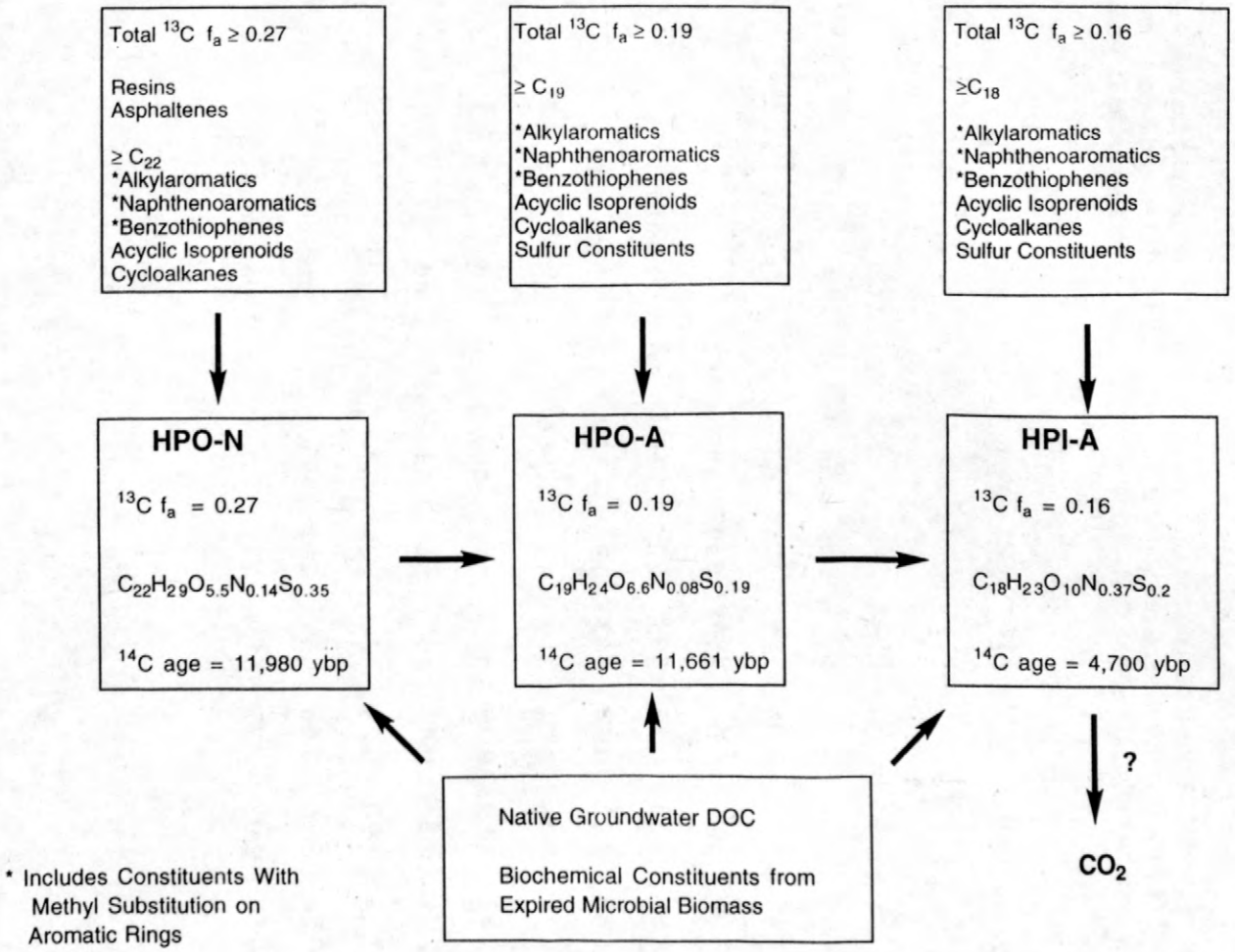

Figure 2. Scheme for the formation of NVOA's in well 530, using characterization data for the 530 NVOA's. f_a = carbon aromaticity determined from C-13 NMR, ybp = years before the present.

Table 1. Elemental Analyses, Molecular Weights, $\delta^{13}C$ values, and ^{14}C Ages for Crude Oil, Crude Oil Fractions, and Nonvolatile Organic Acids. HPI-A = hydrophilic acids; HPO-A = hydrophobic acids; HPO-N = hydrophobic neutral fraction of acids. Elemental C,H,O,N, and S contents reported on moisture free and ash free basis. M_n = number average molecular weight; C/M = number of carbons per average molecule; nd = not determined.

SAMPLE	C	H	O	N	S	ASH	O/C	M_n	C/M	$\delta^{13}C$ (%)	^{14}C Age (ybp)
Crude Oil	86.41	12.83	0.47	0.38	0.64	<0.01	0.01	nd	nd	-28.4	
Aromatic	86.45	9.42	1.20	0.36	2.54	1.27	0.01	nd	nd	nd	
Resin	80.02	9.59	5.12	1.37	2.86	0.28	0.06	586	39	nd	
Asph.	86.45	7.22	2.58	1.39	3.09	<0.1	0.03	3598	259	nd	
530 HPO-N	67.47	7.27	22.56	0.49	2.85	3.53	0.33	395	22	-27.0	11,980 ± 105
530 HPO-A	62.18	6.75	29.09	0.32	1.66	2.32	0.47	362	19	-27.7	11,661 ± 89
530 HPI-A	52.66	5.52	38.99	1.27	1.56	3.26	0.74	412	18	-25.9	4,700 ± 55
603 HPO-N	64.32	7.63	24.44	0.18	3.42	19.92	0.38	nd	nd	nd	nd
603 HPO-A	62.5	6.4	27.8	0.4	2.71	3.8	0.44	nd	nd	nd	nd
603 HPI-A	50.62	5.8	39.69	0.72	3.13	4.20	0.78	nd	nd	nd	nd
310 HPO-A	55.95	5.88	37.08	0.71	0.39	5.06	0.66	536	25	-27.0	post bomb
310 HPI-A	52.20	5.05	40.34	1.75	0.67	2.02	0.77	513	22	-26.4	post bomb

REFERENCES

Baedecker, M.J., Cozzarelli, I.M., Siegel, D.I., Bennett, P.C., and Eganhouse, R.P., 1993, Crude oil in a shallow sand and gravel aquifer. III. Biogeochemical reactions and mass balance modeling in anoxic groundwater: Applied Geochemistry, v. 8, p. 569-586.

Delin, G.N., Essaid, H.I., Cozzarelli, I.M., Lahvis, M.H., and Bekins, B.A., 1998, Ground water contamination by crude oil near Bemidji, Minnesota: U.S. Geological Survey Fact Sheet 084-98.

Thorn, K.A., and Aiken, G.R., 1998, Biodegradation of crude oil into nonvolatile organic acids in a contaminated aquifer near Bemidji, Minnesota: Organic Geochemistry, v. 29, no. 4, p. 909-931.

AUTHOR INFORMATION

Kevin A. Thorn and George R. Aiken, U.S. Geological Survey, Denver, Colorad

Patterns of Microbial Colonization on Silicates

By Jennifer Roberts Rogers, Philip C. Bennett, and Franz K. Hiebert

ABSTRACT

Several factors influence the attachment of microorganisms to mineral surfaces, such as surface charge, solution and mineral composition, and the types of organisms present in the ground water. In dilute groundwater systems inorganic nutrients can represent limiting components for growth of subsurface microorganisms and in these systems mineral composition may be an important factor in microbial colonization. In this study we examined microbial colonization of silicate minerals *in situ* using field microcosms, as well as in controlled laboratory microcosms. We found that in the petroleum-contaminated aquifer near Bemidji, MN where P is scarce, feldspars that contain inclusions of P-minerals such as apatite are preferentially colonized over similar feldspars without P. A microcline from S. Dakota, for example, which contains 1220 ppm P, was heavily colonized and deeply weathered after one year, while a similar microcline without detectable P was barren of attached organisms and completely unweathered. Anorthoclase (1050 ppm P) was very heavily colonized and weathered, whereas plagioclase specimens (<50 ppm) were uncolonized and unweathered. However, compositional differences in a limiting nutrient may not be the only controlling factor. In a stressed environment such as the aquifer near Bemidji, toxic elements may also influence colonization. Using silicate glasses, one with 4500 ppm Al and the other with 450 ppm Al, we found that Al appeared to be a deterrent to surface colonization, nor was olivine, with~3000 ppm Ni, colonized. Quartz however was sparsely colonized and is most likely the result of no positive or negative compositional effects. Quartz with an iron hydroxide coating was heavily colonized with microorganisms remaining even after the iron was utilized. We propose that colonization in this system is particularly sensitive to the availability of P, and the native subsurface microorganisms tend to colonize and weather silicates, which contain apatite. Colonization may also be increased when more than one scarce nutrient is present. The result of this interaction is that nutrient-bearing silicates will be colonized, and preferentially destroyed, as the subsurface microbial community scavenges a limiting nutrient, while colonization of non-nutrient bearing minerals are colonized based on surface charge and toxic elements effects.

INTRODUCTION

The influence of microorganisms on mineral-water interactions can be viewed at several scales, from a macro-scale examination of groundwater chemistry, to a micro-scale examination of the microbe-mineral interface. At the micro-scale, organisms that attach to surfaces can create reactive microenvironments due to the production of mineral and organic acidity and organic ligands, resulting in a perturbation of the mineral-water equilibria that may not be accurately reflected in the groundwater chemistry. In this study we examine the attachment of subsurface microorganisms to mineral surfaces both in situ and in the laboratory, and the possible controls on which mineral is colonized, and which is weathered, in the microbial microenvironment.

There are several potential controls on microbial attachment to a mineral surface, both positive and negative. A mineral's surface charge can influence initial reversible attachment due to simple coulombic attraction or repulsion (e.g. Marshall, 1980; Scholl and others, 1990). Feldspar and quartz surfaces, for example, are uniformly negatively charged at environmental pHs, as are bacteria (e.g. Stumm and Morgan, 1996; Madigan and others, 1997), so attachment to that surface must overcome some degree of coulombic repulsion. Coulombic attraction or repulsion, however, is not an absolute control; bacteria can and will overcome an apparent

repulsion and attach to a negatively charged surface if that surface offers a competitive advantage.

The importance of other factors, such as surface roughness, and surface composition on initial colonization or subsequent growth is not well known. Potential influences might be the presence of adsorbed organic carbon, limiting nutrients, adsorbed iron or manganese oxides that alter surface charge, or toxic metals. The result however is a difference in colonization between two mineral surfaces that might otherwise be considered geologically similar, such as two different K-feldspars.

We are investigating specifically the presence of trace phosphorus in feldspars as a positive control on colonization. Most organisms require phosphorus as an essential macronutrient, and P is needed for the synthesis of nucleic acids, nucleotides, phosphoproteins and phospholipids (e.g., Ehrlich, 1996; Madigan and others, 1996). In many subsurface aqueous environments P is scarce, and tightly cycled within the community, limiting the size and growth of indigenous microbial populations (Ghiorse and Wilson, 1988).

Some microorganisms can extract phosphorus from insoluble mineral sources such as apatite, variscite, strengite and vivianite, by using organic acidity or chelators (e.g. Duff and others, 1963; Halder and Chaktabartty 1993; Goldstein, 1986). Many microorganisms, particularly those associated with soil rhizopheres are capable of solubilizing mineral phosphates. The mechanism of solubilization is typically by the formation of organic acids, such as gluconic and ketogluconic acid, and the resultant decrease in pH near the organism (e.g. Kim and others, 1997; Goldstein, 1986.). Subba Rao (1982a, 1982b) found that bacteria isolated from the soil zone had the ability to solubilize mineral phosphates, and the expression of the mineral phosphate solubilizing (MPS) gene is suppressed with increasing concentration of dissolved orthophosphate (Goldstein, 1986). Solubilization of mineral phosphates by microorganisms has been primarily documented in soil zones where phosphates are applied as fertilizer however, these detrital phosphates are rarely abundant in the subsurface.

While phosphate minerals may not be widely distributed, phosphorus is a trace or minor constituent in many rocks. Pegmatitic feldspars can contain up to 2000 ppm phosphorus in the crystal matrix, while many igneous rocks including feldspars contain apatite as minor or trace inclusions. While the feldspar-bound P has not previously been considered a viable source of phosphorus, in very nutrient-limited environments silicate-bound nutrients may be an attractive source to colonizing microorganisms.

We propose that microorganisms extract phosphorus from apatite inclusions in feldspars, scavenging the nutrient while destroying the silicate matrix. We have observed this in carbon-rich, but phosphorus-poor, anaerobic groundwater.

METHODS

We used both *in situ* and laboratory microcosms to examine the relationship between the P-content of feldspars and the microbial colonization of the mineral surface. We also examined the effects this interaction had on microbial biomass, substrate degradation, and mineral weathering.

In situ Microcosms

Using *in situ* field microcosms (e.g. Hiebert and Bennett, 1992) we characterized the microbial colonization and weathering of a variety of feldspars, silicate glasses, quartz and iron-coated quartz (e.g. Grantham and Dove, 1996). An *in situ* microcosm consists of clean sterile mineral chips in a flow-through container that is suspended in a well for periods of months to years. For this study the microcosms were left in both aerobic and anaerobic zones in the petroleum-contaminated aquifer near Bemidji, Minnesota for periods up to one year. The anaerobic water has a pH of ~6.8, with very high DOC, ferrous iron and silica, while the aerobic region pH ranges from 6.2 to 7.0, and is dominated by the products of carbonate dissolution, with less DOC, little silica and no ferrous iron. The native microbial population in the anaerobic ground water consists of iron reducers, fermenters and methanogens, while the

aerobic groundwater is host to a variety of aerobes. Approximately 95% of the microorganisms are sessile, but the planktonic distribution is a good representation of the sessile population (Bekins, personal communication).

After microcosm removal, the biological tissue was fixed using a field critical point drying method (Nation, 1983; Vandevivere and Bevaye, 1993). Scanning electron microscopy was then used to characterize the types of microorganisms present, colonization patterns and weathering on the feldspar surfaces.

Laboratory Microcosms

Laboratory microcosms were constructed from sterile glass bottles containing sterile mineral chips and native sediment and formation water. Sediments were collected using a freezing shoe core barrel (Murphy and Herkelrath, 1996), and the sealed core liner was moved immediately into a nitrogen-purged glove bag where the microcosms were constructed. To maintain anaerobic conditions the microcosms were also stored in an anaerobic chamber during the course of the experiment. The microcosms were amended with toluene at the start of the experiment, and reaction progress was characterized by chemical analysis of the microcosm water and vapor head-space. Production of methane and loss of toluene was determined by gas-solid gas chromatography (GC). Silicate dissolution was characterized by analysis of dissolved silica by ICP-OES and the reduced molybdate colorimetric method (Greenberg and others, 1992). Dissolved iron and orthophosphate were also measured colorimetrically as well as by ICP-OES. Minerals from sacrificed microcosms were fixed (as described above) then imaged using scanning electron microscopy (also described above) to observe differential colonization, extent of weathering and secondary phase generation.

Total viable microbial biomass and community structure were determined by PLFA analysis (Microbial Insights, Inc.) on samples of native anaerobic groundwater, sediment core from beneath the oil pool and anorthoclase chips left in situ in the anaerobic groundwater for 3 months.

SILICATE CHEMISTRY

In this study five different feldspars as well as quartz, iron-coated quartz, olivine and two silicate glasses were exposed to the microbially active groundwater environment. It is assumed that the feldspars and quartz, as well as the two glasses, had similar starting surface charge and surface character, but with differing compositions. Whole rock, trace element, microprobe and light microscope analysis of all feldspars were used to determine compositional and mineralogical variations. The plagioclase ($\sim Ab_{60}$) is a mixture of plagioclase, albite, and muscovite, with no detectable phosphorus, while oligoclase ($\sim Ab_{75}$) had trace phosphorus, (<50ppm P) and iron of unknown redox state. The Ontario microcline was homogeneous with no detectable phosphorus, but trace iron.

The South Dakota microcline is more heterogeneous, with less iron than the Ontario microcline, but with 1220 ppm P, occurring as small apatite inclusions, intergrown with albite. The anorthoclase is also very heterogeneous, with 1050 ppm P occurring as mixed phosphate mineral inclusions. Inclusions are typically pure apatite, but some yttrium and barium were also detected. The anorthoclase also contained plagioclase and biotite, with iron/titanium oxides intergrown with apatite crystals. The apatite in both the South Dakota microcline and the anorthoclase was extractable with a weak acid solution and should be available to microorganisms. The aquifer sediment had 90 to 220 ppm total phosphorus of which only 0.9 to 3.6 ppm was available. Quartz had no impurities, while olivine contained ~3000 ppm Ni. Iron coatings on quartz were pure ferric hydroxide. The silicate glasses were obtained from NIST (standard 1830 and 1831) and had similar compositions with small differences in Al and K. The 1830 glass contained 450 ppm Al and 86 ppm K, while the 1831 glass contained 4500 ppm Al and 700 ppm K.

SURFACE COLONIZATION

We found that microorganisms colonized some silicate surfaces to a greater degree than others, with weathering correlating directly with

the extent of colonization. Only those feldspars, which contain phosphorus were colonized, only colonized feldspars were weathered, and this only occurred in the anaerobic groundwater (e.g. Rogers and others, 1998).

SEM examination of mineral surfaces after reaction in the aquifer showed that quartz had colonization by a variety of microorganisms (based on morphological differences) and was lightly etched near attached organisms. The two glasses showed different colonization density, with biomass inversely correlated to the aluminum content of the glass. Olivine had little or no colonization, and this may be due to its high Ni content. The albite (Figure 1) and the Ontario

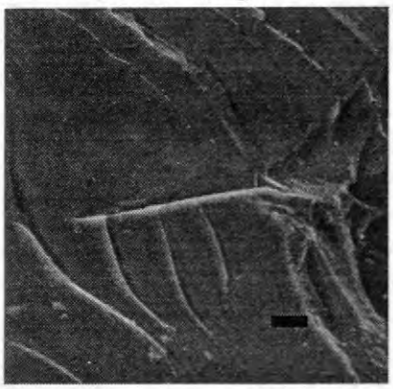

Figure 1. Photomicrograph of an albite surface after 1 year in the anaerobic groundwater at Bemidji. Scale bar is 5 μm.

microcline had little or no colonization by microorganisms and no etching. The oligoclase had minor etching and a few microorganisms were detected. In contrast the South Dakota microcline and the anorthoclase (Figure 2) were

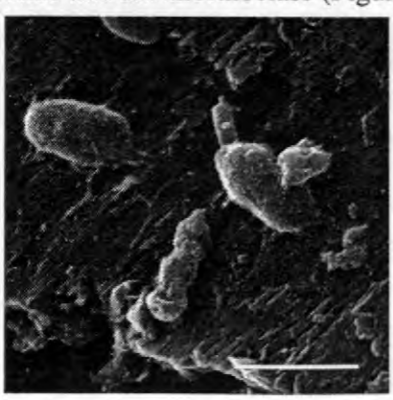

Figure 2. Photomicrograph of anorthoclase after 3 month in the aquifer. Attached organisms and etching are visible. Scale bar is 2 μm.

both heavily colonized and etched.

Anorthoclase was the most heavily colonized and weathered possibly due to the presence of both P as apatite and Fe as iron oxides. The anaerobic groundwater is dominated by iron reducers and as Fe(III) is depleted iron may become limiting as a nutrient/TEA. Colonization of anorthoclase may be advantageous to this population by providing two necessary nutrients in one place.

While the colonization and weathering of the feldspars appears to be driven by P, colonization of quartz is anomalous to the theory that silicate colonization is nutrient controlled. Quartz may be a neutral surface on which microorganisms can attach although nutrients are not available. Conversely, surfaces such as olivine may contain a toxic factor, such as Ni, which interferes with microbial viability and may be particularly acute in stressed environments such as the anaerobic groundwater at Bemidji. The lack of colonization on the silicate glass, which contains Al, also suggests that even Al can have a negative effect on microorganisms. While Al is obviously present in the colonized feldspars, it may be tolerated by the attached organism if P is present as well. However, when P is not present the Al may be a deterrent to colonization, perhaps by chelating with ligands produced by the microorganism for sequestering essential metals such as iron.

Alteration of the quartz surface by precipitation of thin layer of amorphous iron sesquioxide, enhanced the colonization on that surface substantially, with thick colonization by organisms after only a few months. Here, unlike most surfaces examined to date, distinct colonies and biofilms are apparent. The change in colonization behavior with surface character is partly related to surface charge. Initial reversible attachment to the iron-coated quartz is enhanced by coulombic attraction between the positively charged iron sesquioxide surface and the negatively charged bacterial cell wall (Marshall, 1980). On the iron-coated surfaces the surface-attached organisms also form substantial colonies with evidence of attachment and glycocalyx development (Figure 3). This finding is in conflict with one prevalent hypothesis that iron reducing

organisms directly reduce the iron solid phase via membrane-bound iron reductase, and so must continuously move to fresh iron surfaces (Grantham and Dove, 1996). We observe the colony morphology even where no detectable iron coating remains.

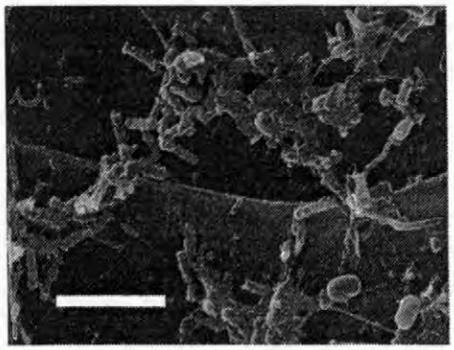

Figure 3. Photomicrograph of iron-coated quartz surface after 3 months in the aquifer. Several types of microorganisms and glycocalyx are visible. Scale bar is 6 μm.

SUBSTRATE UTILIZATION

Preliminary results from laboratory microcosm experiments suggest that P is released to the water when P-bearing feldspars are present. Further, microcosms containing anorthoclase as the sole source of P degraded toluene 90% faster than microcosms containing other feldspars or quartz, with no P. This suggests that not only is P released from the feldspars, but it is also available to the microorganisms, and the addition of P increases the rate of toluene degradation. It is not clear if an increase in the metabolism of the population or an increase in the size of the microbial population is responsible for the observed loss of toluene.

MICROBIAL BIOMASS

Biomass determinations support the laboratory microcosm results. Anorthoclase chips colonized in the Bemidji aquifer for 3 months had approximately 15 times more biomass as aquifer sediment from the same interval. This suggests that biomass is actually increased by the presence of P as apatite in the mineral. The larger amount of biomass may be due to an increase in the population size as a result of the addition of a limiting nutrient or may be a result of chemotaxis, where more organisms are attracted as the apatite is dissolved.

IMPLICATIONS

We hypothesize that phosphorus in feldspars is released secondary to microbial production of ligands, which interact with the silicate matrix, dissolve it and expose the apatite inclusions in it. The release of phosphorus secondary to the silicate weathering provides a limiting nutrient to colonizing microorganisms, which promotes growth and in turn increases mineral weathering. However, nutrient limitation is not the sole factor in determining microbial colonization on mineral surfaces, though one of the more compelling ones. Colonization also depends on the composition of the mineral surface, and this may be more important in stressed or nutrient-limited environments.

REFERENCES

Duff, R.B., Webley, D.M., and Scott, R.O., 1963, Solubilization of minerals and related material by 2-ketogluconic acid producing bacteria: Soil Science, v. 95, p. 105-114.

Ehrlich, H.L., 1996, Geomicrobiology: New York, Marcel Dekker, 719 p.

Ghirorse, W.C. and Wilson, J.L., 1988, Microbial ecology of the terrestrial subsurface: Advances in Applied Microbiology, v. 33, p. 107-172.

Grantham, M.C., and Dove, P.M., 1996, Investigation of bacterial-mineral interactions using Fluid Tapping Mode Atomic Force Microscopy: Geochimica Cosmochimica Acta, v.60, p. 2473-2480.

Greenberg, A.E., Clesceri, L.S., and Eaton, A.D., 1992, Standard Methods for Examination of Water and Wastewater: Washington, D.C., APHA, 809 p.

Halder, A.K., and Chakrabartty, P.K., 1993, Solubilization of inorganic phosphate by *Rhizobium*: Folia Microbiolology, v. 38, p. 325-330.

Goldstein, A.H., 1986, Bacterial solubilization of mineral phosphates: American Journal of Alternative Agriculture, v. 1, p. 51-57.

Hiebert, F.K. and Bennett, P.C., 1992, Microbial control of silicate weathering in an organic-rich ground water: Science, v. 258, p. 278-281.

Kim, K.Y., Jordan, D., and Krishnan, H.B., 1997, *Rahnella aquatilis*, a bacterium isolated from soybean rhisosphere, can solubilize hydroxyapatite: FEMS Microbiology Letters, v. 153, p. 273-277.

Madigan, M.T., Marinko, J.M., and Parker, J., 1997, Brock Biology of Microorganisms: Englewood Cliffs, Prentice Hall, 986 p.

Marshall, K.C., 1980, Adsorption of Microorganisms to Surfaces: New York, John Wiley and Sons, p. 317-330.

Murphy, F., and Herkelrath, W.N., 1996, A sample-freezing drive shoe for a wire-line piston core sampler: Ground Water Monitoring and Remediation, v. 16, p. 86-90.

Nation, J.L., 1983, A new method for using hexamethyldisilazane for preparation of insect soft tissues for scanning electron microscopy: Stain Technology, v.58, p. 347-351.

Rogers, J.R., Bennett, P.C., and Choi, W.J., 1998,American Mineralogist: v. 83, p. 1532-1540.

Scholl, M.A., Mills, A.L., Herman, J.S., and Hornberger, G.M., 1990, Journal of Contaminant Hydrology, v.6, p. 321-330.

Stumm, W., and Morgan, J.J., 1996, Aquatic Chemistry: New York, John Wiley and Sons, Inc., 780 p.

Subba Rao, N.S., 1982a, Biofertilizers: Interdisciplinary Science Reviews, v. 7, p. 220-229.

———1982b, Phosphate solubilization by soil microorganisms, in Subba Rao, N.S. ed., Agricultural Microbiology: Boston, MA, Butterworth, p. 295-305.

Vandivivere, P. and Bavaye, P., 1993, Improved preservation of bacterial exopolymers for scanning electron microscopy: Journal of Microscopy, v. 167, p. 323-330.

AUTHOR INFORMATION

Jennifer Roberts Rogers and Philip C. Bennett, Department of Geological Sciences, The University of Texas at Austin, Austin, Texas, 78712, (jaroberts@mail.utexas.edu and pbennett@mail.utexas.edu)

Franz K. Hiebert, RMT, Jones and Neuse, Inc., Austin, Texas.

The Fate of Complex Contaminant Mixtures From Treated Wastewater Discharges

Sewage wastes are sources of ground-water contamination worldwide. The sources range from individual septic systems discharging a few hundred gallons per day to large municipal systems discharging millions of gallons per day. Common to all these sources is the complex mixture of nutrients, trace metals, microbes and other inorganic and organic compounds that compose typical sewage wastewater. Natural physical, chemical, and biological processes interact to transport, transform, and dilute these wastes in the subsurface.

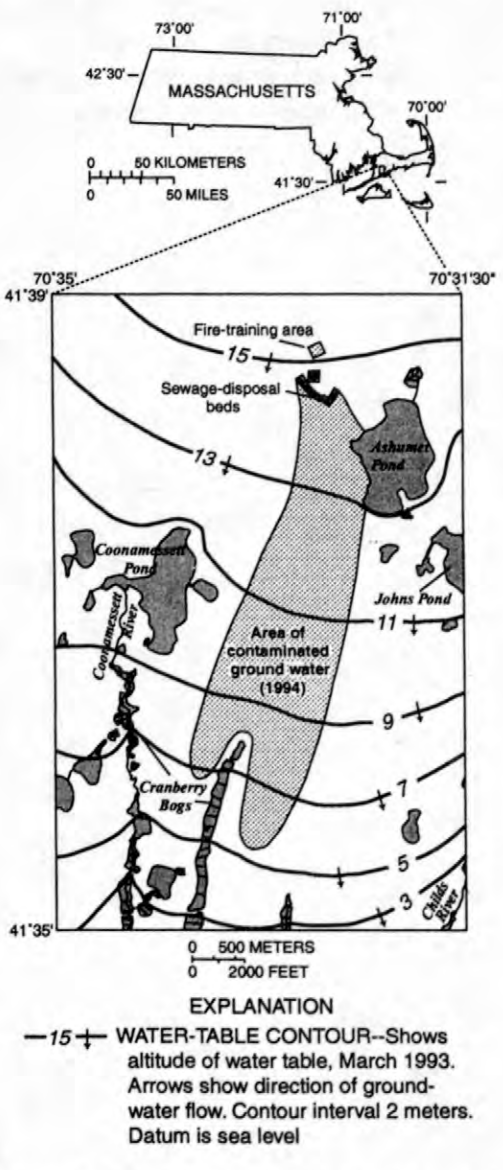

Figure 1. Location of sewage plume, western Cape Cod, Massachusetts.

During the past several decades, we have improved our understanding of these subsurface processes by studying specific sites of contamination. The sewage plume at the Massachusetts Military Reservation (formerly Otis Air Force Base) on Cape Cod is one of these sites (figure 1). Disposal of treated sewage for more than 60 years to the sand and gravel aquifer has formed a plume that is more than 3.5 miles long. The plume is characterized by distinct geochemical zones caused by biodegradation of the contaminants in the aquifer. In 1983, the sewage plume was chosen as a ground-water field site of the U.S. Geological Survey Toxic Substances Hydrology Program.

Since 1983, USGS scientists and their university colleagues have studied the Cape Cod sewage plume to understand how complex mixtures of contaminants interact with the subsurface biota and sediments. The studies initially focused on defining the plume's contaminant distributions, geochemical zones, and microbial populations. From these studies, the scientists formed hypotheses about the physical, chemical, and biological processes affecting the contaminants, and developed field and laboratory methods to study these processes. In the late 1980's, the research team began to use field experiments to examine the factors controlling these processes. The sewage plume and its distinct geochemical zones became a field-sized laboratory where the team has run more than 60 tracer experiments. This experimental work has led recently to a re-examination of the sewage plume. The scientists are using results from the field tests and new observations of the plume to improve models of how complex mixtures of contaminants move and attenuate in the subsurface. In December 1995, sewage disposal ended after 60 years of continuous discharge to the ground-water system.

The change has provided the research team with a unique opportunity to observe the natural restoration of the plume and to test the ideas and models developed during the past 16 years.

The papers in this section reflect the diversity of interdisciplinary research at the Cape Cod Toxic Substances Hydrology research site. Five papers describe the first 3 years of the natural restoration of the sewage plume. Several papers describe the fate of specific contaminants, such as phosphorus and zinc, in the plume. Other papers report on research concerning specific physical, chemical, and biological processes, such as dispersion, adsorption, and nitrification, and the simulation of these processes with geochemical models. Tracer experiments are described in several papers, including tests that used trace metals, protozoa, viruses, colloids, and nutrients as tracers. New methods to measure hydrologic and chemical variables are reported in other papers. Three papers describe a remediation experiment being conducted on a nearby plume of solvents on the military base.

The papers in this section reflect the common theme that contaminants in the subsurface are affected by complex interactions of physical, chemical, and biological processes. The studies demonstrate that an understanding of the subsurface fate of complex mixtures of contaminants, such as sewage wastewaters, requires an interdisciplinary investigative approach that links together field observations, field and laboratory experiments, and predictive modeling.

For additional information contact:

Denis R.LeBlanc, USGS Marlborough, Massachusetts, (email dleblanc@usgs.gov)

Kathryn M. Hess, USGS Marlborough, Massachusetts, (email kmhess@usgs.gov)

Natural Restoration of a Sewage Plume in a Sand and Gravel Aquifer, Cape Cod, Massachusetts

By Denis R. LeBlanc, Kathryn M. Hess, Douglas B. Kent, Richard L. Smith, Larry B. Barber, Kenneth G. Stollenwerk, and Kimberly W. Campo

ABSTRACT

Land disposal of treated sewage to infiltration beds at the Massachusetts Military Reservation on Cape Cod for 60 years has formed a plume of contaminated ground water in the sand and gravel aquifer that is more than 3.5 miles long. Sewage disposal ended in December 1995, and no action has been taken to restore the ground-water quality near the disposal site. In the first 30 months after disposal ended, the trailing edge of the conservative constituents in the plume, such as boron, moved more than 800 feet downgradient from the abandoned beds. Concentrations of dissolved oxygen remained at or near zero near the disposal beds, however, even though uncontaminated ground water that contains dissolved oxygen had been flowing into the sewage-contaminated zone from upgradient areas for 30 months. Biodegradation of organic matter associated with the sewage-contaminated sediments is probably the primary cause of the continuing suboxic to anoxic conditions. Nitrate concentrations in the center of the sewage-contaminated zone decreased to below detectable levels as nitrate moved away from the abandoned beds along with the ground-water flow or was converted to nitrogen gas by denitrification. As nitrate levels decreased to zero, the geochemical environment beneath the beds became more reducing, and dissolved-iron concentrations increased because insoluble ferric iron oxide coatings on the sediments were reduced to soluble ferrous iron. Ammonium had been expected to be oxidized to nitrate as oxygen re-entered the sewage-contaminated zone. Ammonium concentrations decreased, however, as ammonium desorbed from the sediments by cation exchange and was transported away from the disposal site in the reducing geochemical environment. pH did not change significantly because of the buffering effects of sorption on the sediment surfaces and anaerobic biodegradation. As a result, the concentrations of sorbed trace metals, such as zinc and copper, did not change significantly after disposal ended. Phosphorus concentrations remained elevated in the sewage-contaminated zone because of slow desorption from the sediments. Results of geochemical modeling of the natural restoration process indicate that restoration of ground-water quality to pre-contamination conditions will be slow because of the persistent oxygen demand in the sewage-contaminated zone.

INTRODUCTION

The cleanup of contaminated aquifers has proven to be a difficult technical challenge (National Research Council, 1994). The heterogeneity of geologic materials, sorption of contaminants to sediments, and slow degradation rates complicate efforts to implement engineered remedial solutions. Thus, natural restoration, also referred to as natural attenuation, has received increased attention as a remedial option (U.S. Environmental Protection Agency, 1997). This option relies on natural physical, chemical, and biological processes to restore the quality of ground water to acceptable levels.

Interest in natural restoration has created the need for increased understanding of the restoration process. Research on contaminant plumes has focused primarily on the processes that cause contaminants to attenuate and disperse as they migrate from source areas. Less attention has been paid to the processes that restore ground-water quality after a source has been removed. Many field investigations have shown that disposal of substances, such as sewage, that

contain degradable organic materials creates a subsurface environment characterized by distinct geochemical zones (Lovley and others, 1989). Little is known, however, about how these environments evolve and affect contaminant fate and transport after the source is removed.

Treated sewage was disposed of for about 60 years to a sand and gravel aquifer at the Massachusetts Military Reservation (MMR) on western Cape Cod (fig. 1). The disposal created an extensive plume of sewage-contaminated ground water (LeBlanc, 1984; Hess and others, 1996; Savoie and LeBlanc, 1998). The plume has been studied since 1983 as part of the U.S. Geological Survey (USGS) Toxic Substances Hydrology Program (LeBlanc, 1996; Morganwalp, 1994).

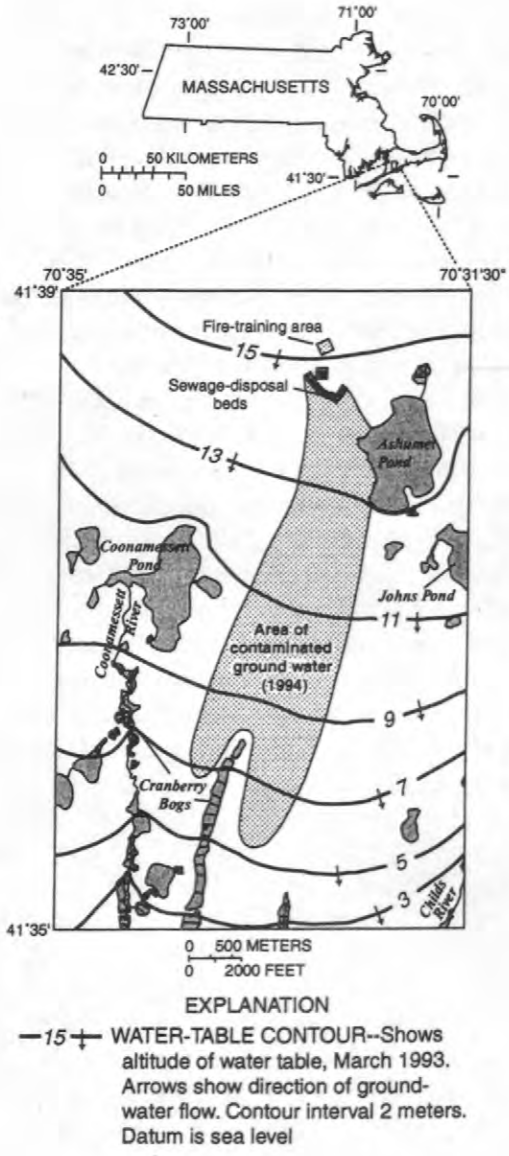

Figure 1. Location of the sewage-disposal beds, area of contaminated ground water, fire-training area, and water-table contours, western Cape Cod, Massachusetts.

On December 13, 1995, the MMR ended disposal of treated sewage at the site. Wastewater from the base is now treated at a newly built treatment facility, and effluent from the plant is pumped about 8 miles north to a disposal site near the Cape Cod Canal. The abandoned treatment plant was demolished in 1996-97, and surface pipes that carried the effluent to the disposal beds were removed. No further action, such as soil removal, was taken at the abandoned beds, which still receive natural recharge from precipitation.

The abrupt cessation of disposal without additional actions to remediate the aquifer at the disposal site provided a unique opportunity to observe the geochemical evolution of the plume as natural processes restore the water quality. This paper describes observations of ground-water quality made during the first 30 months after the disposal ended and interprets the changes in water quality that occurred. Other papers in this volume, by Kent and others (1999), Smith and others (1999), Barber and Keefe (1999), Campo and Hess (1999), and Stollenwerk and Parkhurst (1999), describe specific aspects of the natural restoration process.

DESCRIPTION OF THE SEWAGE PLUME

The disposal of secondarily treated sewage to infiltration beds on the MMR (fig. 2) for about 60 years created a plume of contaminated ground water that extended more than 3.5 miles from the disposal site in 1994. The plume was about 4,000 feet wide and about 80 feet thick. Downgradient accretion of recharge from precipitation formed an uncontaminated zone above the plume that increased in thickness with distance downgradient from the disposal site.

Hydrogeologic Setting

The treated sewage recharged the permeable, unconfined sand and gravel aquifer

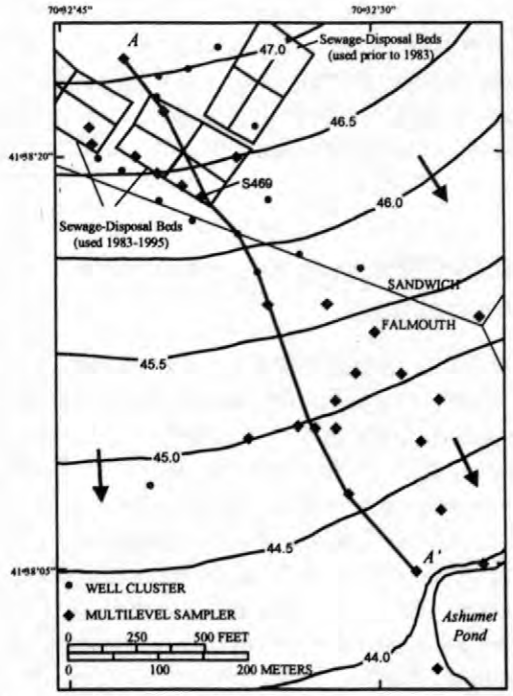

Figure 2. Location of the sewage-disposal beds, well clusters, multilevel samplers, vertical section A-A', water-table contours, and inferred direction of ground-water flow, western Cape Cod, Massachusetts. Water-table contours are in feet above sea level in January 1994.

that underlies western Cape Cod. The aquifer receives about 26 inches per year of natural recharge from precipitation (Masterson and others, 1998). At the sewage-disposal site, the aquifer is about 350 feet thick and has a hydraulic conductivity of 150 to 380 ft/d (feet per day). The depth to water varies as a function of land-surface altitude and is about 20 feet beneath the disposal beds. The water table slopes southward near the disposal site with an average hydraulic gradient of 0.0015 (fig. 2). The porosity is 35 to 40 percent, and the average ground-water velocity is 1 to 2 ft/d (LeBlanc, 1984; LeBlanc and others, 1991; Bohlke and others, 1999).

Disposal of Treated Sewage

The secondarily treated sewage was discharged to the infiltration beds from about 1936 until December 13, 1995. The rate of discharge varied over time with population at the MMR from 0.1 to 1.8 Mgal/d (million gallons per day) and was 0.1 to 0.5 Mgal/d in the 1990's prior to cessation of sewage disposal. During 1983-95, the treated sewage was applied to eight infiltration beds located along the Sandwich-Falmouth town boundary (fig. 2). The disposal history prior to 1983 is not well known, although it is known that treated sewage was discharged to four beds located at the northeastern corner of the plant for at least several years prior to 1983 (fig. 2).

The rate of sewage disposal to the beds during 1983-95 was about 30 times greater than the natural recharge rate from precipitation to the beds. The resulting water-table mound caused significant vertical flow beneath the beds. At the downgradient edge of the beds, the sewage-contaminated zone was about 80 feet thick. Ground water flowing from upgradient areas was diverted beneath and to the sides of the sewage plume, as shown schematically in figure 3A.

The treated wastewater contained generally elevated levels of dissolved substances, including nitrate, ammonium, phosphorus, and trace metals (Savoie and LeBlanc, 1998). During 1994-95, the treated wastewater was characterized by a specific conductance of about 500 µS/cm (microsiemens per centimeter), dissolved-oxygen concentrations of about 9 mg/L (milligrams per liter), dissolved-organic-carbon concentrations of about 17 mg/L, and nearly neutral pH (about 6.5). In contrast, uncontaminated ground water at the site contains low levels of dissolved substances (LeBlanc, 1984) and is characterized by a specific conductance of less than 100 µS/cm, dissolved-oxygen concentrations of 6 to 12 mg/L, less than 1 mg/L dissolved organic carbon, and acidic pH (less than 5.7).

Geochemistry of the Plume

Biodegradation of organic matter in the zone of contaminated ground water resulted in the creation of distinct geochemical zones (Hess and others, 1996). The zones were characterized by steep geochemical and microbiological gradients (Smith and others, 1991a). The plume had a core that contained little or no dissolved oxygen, and elevated concentrations of dissolved iron and manganese, which are indicative of a reducing

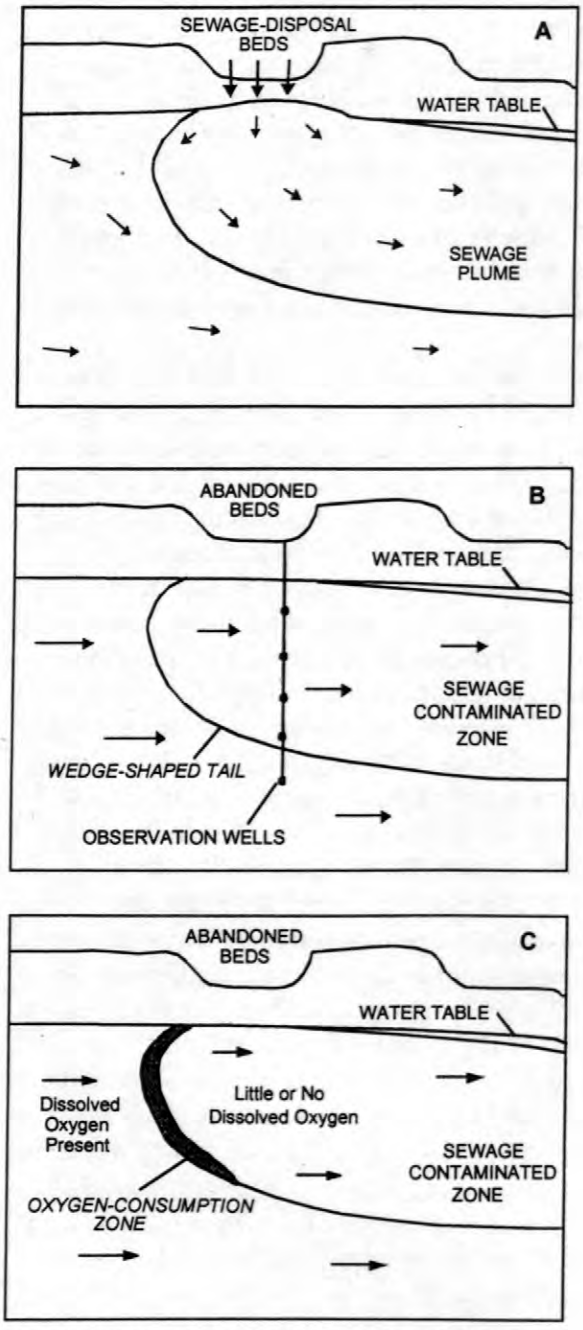

Figure 3. Schematic vertical sections through the sewage-contaminated zone (A) before and (B) after sewage disposal was stopped and (C) the hypothesized oxygen-consumption zone at the trailing edge of the plume.

geochemical environment (Kent and others, 1994). Nitrate was absent in the anoxic core because of denitrification, and transport of ammonium and phosphorus was retarded by sorption to the sediments (Ceazan and others, 1989; Smith and others, 1991b; Walter and others, 1996). Hess and others (1996) document the spatial and temporal variability of concentrations of boron, dissolved oxygen, and phosphorus near the beds that reflects historical variations in sewage-disposal patterns and rates at the site.

Predicted Changes After Sewage Disposal Ended

Hess and others (1996) predicted that ground-water-flow patterns would change after the sewage disposal ended, and that uncontaminated ground water would flow into the sewage-contaminated zone. The reintroduction of dissolved oxygen into the sewage-contaminated zone was expected to cause ammonium to oxidize to nitrate and ferrous iron to oxidize to ferric iron as the anoxic zone became smaller and eventually disappeared. The lower pH of the uncontaminated ground water was expected to cause desorption of contaminants, such as zinc and copper, that were bound to the sediments. These geochemical changes were expected to cause concentrations of some contaminants to increase temporarily in parts of the sewage-contaminated zone following the cessation of disposal.

STUDY METHODS

Ground-water samples were collected synoptically to observe the spatial distributions of constituents at specific times before and after disposal ended. Water-table altitudes were measured to estimate ground-water-flow directions.

Collection and Analysis of Water Samples

Water samples were collected periodically from observation wells and multilevel samplers (MLS) to observe water-quality changes during the natural restoration of the sewage plume. The wells are typically constructed of 2-inch-diameter polyvinyl chloride (PVC) pipe and 2-foot-long screens, and are arranged in clusters of two to eight wells screened at different depths. The

MLS include 15 individual 0.25-inch polyethylene sampling tubes bundled together and open to the aquifer at different depths. The methods used to collect water samples from the wells and MLS are described in Savoie and LeBlanc (1998).

The sampling sites are located near the abandoned disposal beds and in an area between the beds and Ashumet Pond (fig. 2). The sites near the beds include 68 wells and 14 MLS located mostly in the beds loaded during 1983-95 (fig. 2). Water-quality changes following cessation were expected to occur first at these sites, so the sampling points are closely spaced vertically and horizontally. Several sites were located upgradient from the recently loaded beds so that inflowing ground water could be sampled.

The sampling sites between the disposal beds and Ashumet Pond include 48 wells and 29 MLS located in the direction of ground-water flow from the beds (fig. 2). Water-quality changes were expected to propagate into this heavily instrumented area within about 1 year of cessation of disposal of sewage. Several of the well clusters and MLS are located along a transect (A-A' in figure 2) that is aligned with the direction of flow.

The full set of wells and MLS (fig. 2) was sampled in spring 1996, 1997, and 1998. A subset of the sites, including those near the beds and along transect A-A', was also sampled each year in the fall. Selected wells and MLS in and near the sewage beds were sampled biweekly to bimonthly with decreasing frequency from September 1995 until about February 1997. Samples were collected most frequently during the 6 months following the end of sewage disposal.

Ground-water samples were analyzed in the field for specific conductance, pH, dissolved oxygen, and turbidity. Samples were analyzed at USGS National Research Program laboratories in Boulder, Colorado, and Menlo Park, California, for dissolved species, including dissolved organic carbon (DOC), nitrate, ammonium, trace metals, phosphorus, and other selected cations and anions.

Measurement of Ground-Water Levels

Water-table altitudes were measured periodically in a network of 29 observation wells near the sewage-disposal beds and Ashumet Pond. The well locations (not shown in this report) and the three-point triangulation method used to estimate the slope of the water table are described by McCobb and others (1999).

NATURAL RESTORATION OF THE SEWAGE PLUME

The sampling described in the previous section documents the natural restoration process observed to date. In this paper, the observations are summarized by means of profiles showing water quality at MLS S469 at the downgradient edge of the disposal beds, and vertical sections showing water quality along section A-A' aligned with the direction of flow (fig. 2). Section A-A' passes through the center of the plume and intersects the anoxic zone downgradient from the disposal beds.

Water Levels and Ground-Water-Flow Direction

Water levels in the observation-well network near the disposal site were measured a few hours prior to cessation of disposal on December 13, 1995, and about 7 days after disposal ended. Water levels declined as much as 0.2 feet during this time, with the maximum decline measured at the center of the beds (Hess and others, 1996). Ground water from upgradient areas that previously had been displaced by the treated sewage could now pass unperturbed hydrologically through the sewage-contaminated zone (fig. 3B). This interpretation is supported by the detection of trace concentrations of volatile organic compounds in shallow wells in the beds during 1996-98 that are believed to originate from an abandoned fire-training area (fig. 1) located upgradient from the sewage-disposal site (Campo and Hess, 1999).

Conservative, Nonreactive Chemical Constituents

The water-quality observations indicate that the inflow of uncontaminated ground water from upgradient areas has begun to flush conservative, nonreactive chemical constituents away from the disposal site. Decreases in concentrations are evident in several water-quality profiles at MLS S469 (fig. 4). Specific conductance and boron concentrations in November 1995 show that the plume at the downgradient edge of the beds was about 80 feet thick during the plant operation. Specific conductance and boron concentrations had decreased in the bottom half of the plume by May 1996, 6 months after disposal ended, and were near background levels at all depths by June 1998 (figs. 4A and 4B).

The apparent cleanup from the bottom up shown in figure 4 may be evidence that the sewage plume had a wedge-shaped trailing edge (fig. 3B). The field data were too sparse to delineate this shape, but the northward flow of some treated sewage for a short distance because of the water-table mound and the accretion of treated sewage along the several-hundred-foot-long flowpath across the beds both could have contributed to development of a wedge-shaped tail.

The flushing of the conservative, nonreactive constituents is also evident in the longitudinal sections showing boron concentrations in June 1996 and June 1998 (fig. 5). By June 1998, 30 months after cessation of disposal, the trailing edge of elevated boron concentrations was more than 800 feet downgradient from the edge of the disposal beds. This observed rate of movement, about 1 ft/d, is consistent with the estimated average ground-water velocity of 1 to 2 ft/d.

Dissolved Oxygen and Dissolved Organic Carbon

Hess and others (1996) predicted that concentrations of dissolved oxygen in the plume would increase as uncontaminated ground water flowed into the sewage-contaminated zone from upgradient areas. Dissolved-oxygen concentrations in the plume did not change significantly, however, during the first 30 months after disposal ended (figs. 4 and 6). Concentrations beneath the disposal beds were less than 0.2 mg/L (referred to as suboxic conditions) in June 1998 and were zero (referred to as anoxic conditions) in some zones (fig. 4C). Although dissolved-oxygen concentrations at the bottom of the plume increased from June 1996 to June 1998, the zone of low dissolved-oxygen levels at the downgradient edge of the disposal beds was still 70 feet thick in June 1998 (fig. 4C).

The persistence of low dissolved-oxygen levels near the disposal beds indicates that oxygen continues to be consumed in the sewage-contaminated zone beneath the beds by biodegradation of organic matter or other chemical reactions. The oxygen may be consumed in a narrow zone where oxygen-containing ground water from upgradient areas enters the area contaminated by the treated sewage (fig. 3C). This zone may move slowly downgradient as the oxygen demand is depleted.

The concentrations of dissolved organic carbon (DOC) decreased significantly near the disposal beds after disposal ended (Barber and Keefe, 1999). By June 1998, the trailing edge of decreasing DOC concentrations was more than 800 feet downgradient from the edge of the beds. Readily mobile DOC is being flushed away from the beds by the uncontaminated ground water; however, DOC levels beneath the beds remained above background levels 30 months after cessation (Barber and Keefe, 1999). Organic matter stored on the sediments in the sewage-contaminated zone may be slowly biodegrading, a process that could maintain the suboxic and anoxic conditions near the disposal beds for many years.

Ammonium, Nitrate, and Dissolved Iron

Ammonium concentrations in the sewage-contaminated zone decreased during the first 30 months after disposal ended (Smith and others, 1999). Prior to cessation, some of the ammonium in the treated sewage was converted to nitrate by nitrification as it entered the aquifer beneath the disposal beds. Nitrification occurred because the treated sewage contained as much as 9 mg/L

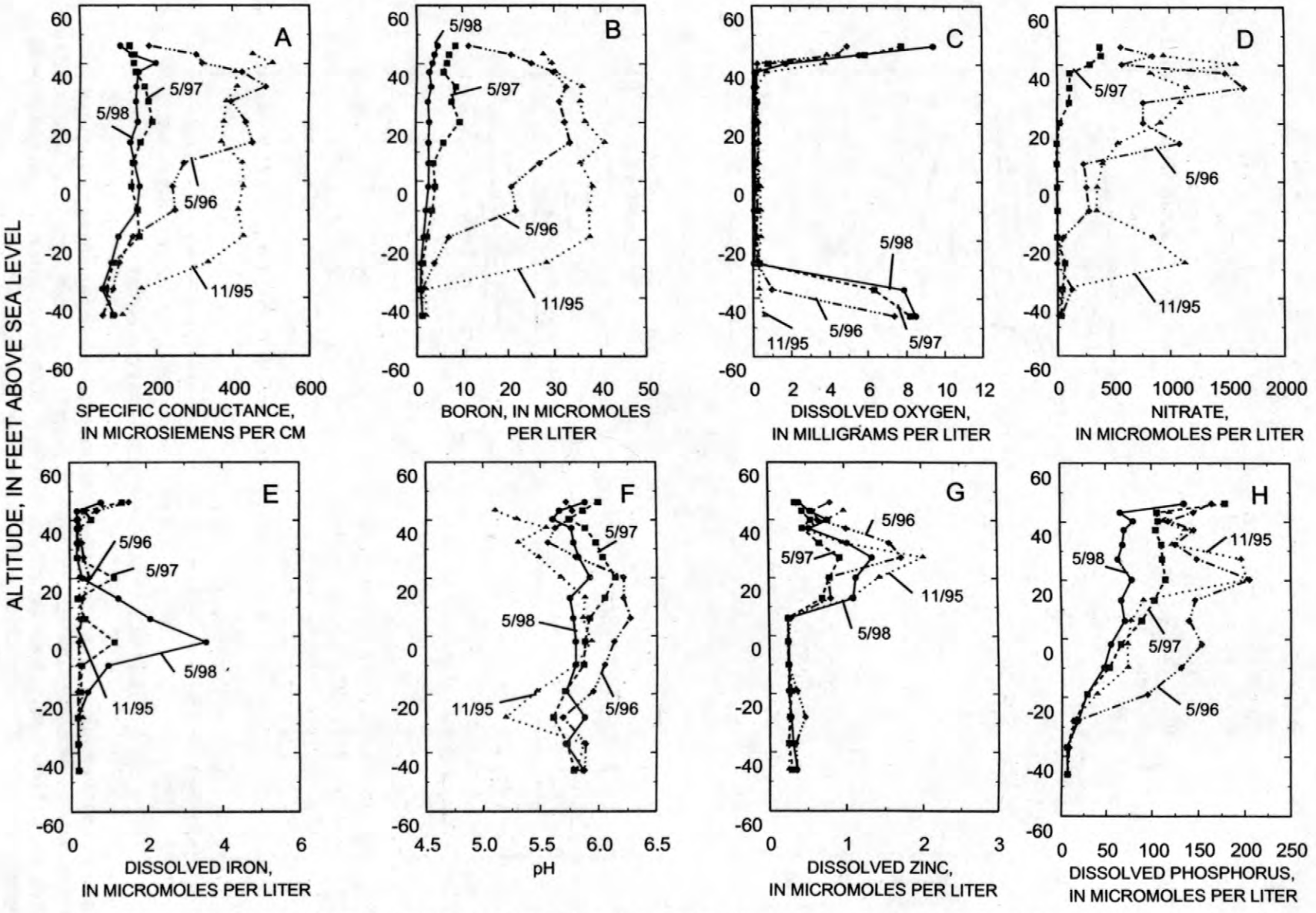

Figure 4. Vertical profiles of specific conductance, boron, dissolved oxygen, nitrate, iron, pH, zinc, and phosphorus at multilevel sampler S469, western Cape Cod, Massachusetts, 1995-98. Location of sampler shown in figure 2.

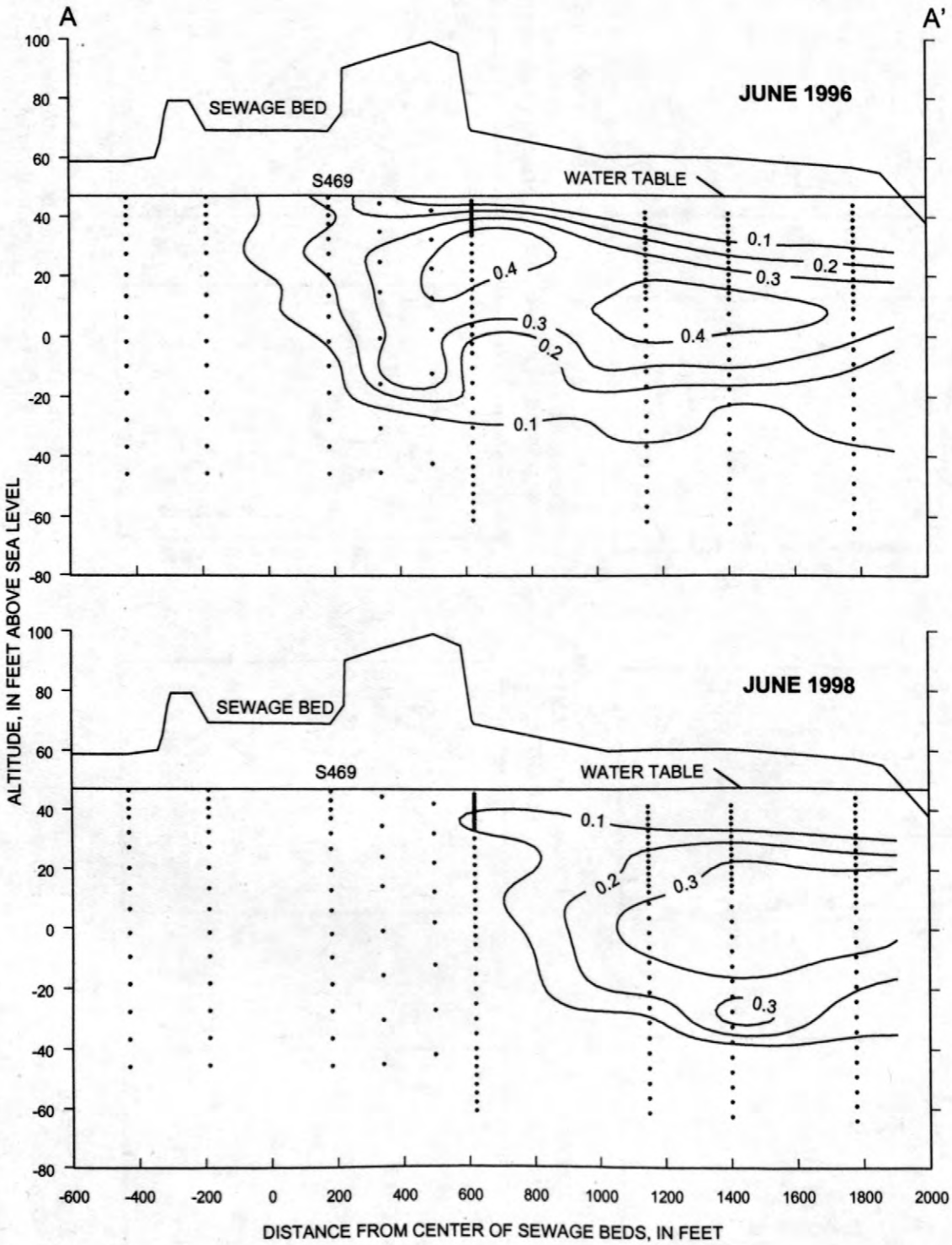

Figure 5. Longitudinal sections showing the distribution of boron concentrations between the sewage-disposal beds and Ashumet Pond, western Cape Cod, Massachusetts, June 1996 and June 1998. Lines of equal concentration in milligrams per liter. Dots show positions of well screens and multilevel-sampler ports. Location of section line shown in figure 2.

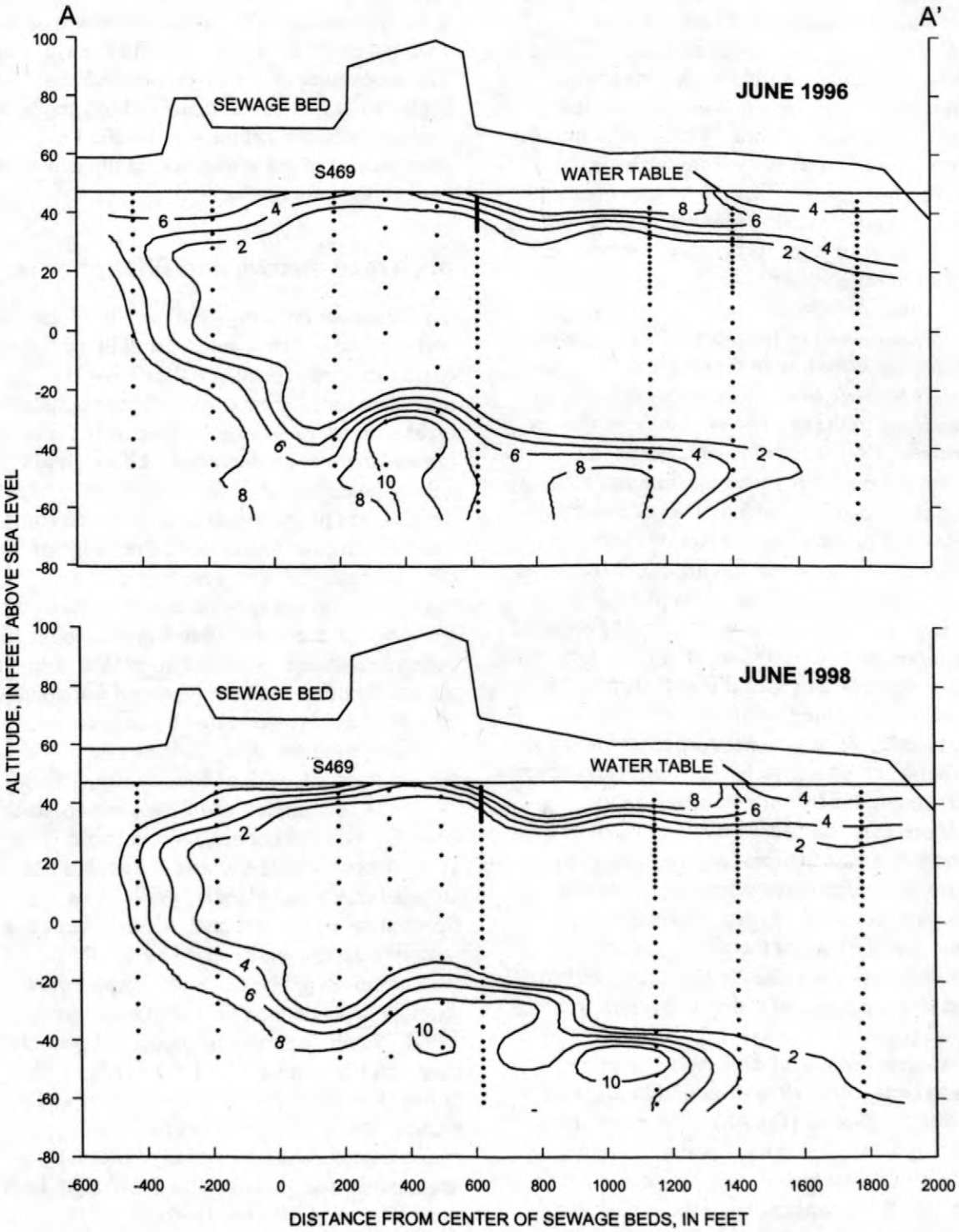

Figure 6. Longitudinal sections showing the distribution of dissolved-oxygen concentrations between the sewage-disposal beds and Ashumet Pond, western Cape Cod, Massachusetts, June 1996 and June 1998. Lines of equal concentration in milligrams per liter. Dots show positions of well screens and multilevel-sampler ports. Location of section line shown in figure 2.

dissolved oxygen. Ammonium that was not nitrified was transported downgradient from the beds at a slower rate than that of ground-water flow because of sorption by cation exchange on the sediments (Ceazan and others, 1989).

Hess and others (1996) predicted that the sorbed ammonium would be converted to nitrate as uncontaminated ground water entered the sewage-contaminated zone. The ammonium was desorbed and moved away from the beds, however, because nitrification of ammonium to nitrate was not occurring in the persistent suboxic and anoxic environments near the disposal beds (Smith and others, 1999).

Concentrations of nitrate were elevated at the top and bottom of the plume during sewage disposal, but were low in the center of the plume (fig. 4D) because of denitrification of nitrate to nitrogen gas in the suboxic environment (Smith and others, 1991a). Nitrate concentrations decreased significantly near the bottom of the plume at the beds within 5 months of cessation. By May 1997, nitrate concentrations had decreased to below detection limits through much of the sewage-contaminated zone at MLS S469 (fig. 4D). The presence of a thin zone of elevated concentrations of nitrate near the water table beneath the beds indicates that nitrate, possibly formed by continuing nitrification in the unsaturated zone, was being carried down to the water table by natural recharge. Smith and others (1999) concluded that nitrate beneath the abandoned disposal beds was being removed by transport downgradient and by denitrification because of the decreased nitrate input and the absence of dissolved oxygen. In suboxic zones surrounding the core of the plume, nitrate concentrations approached levels characteristic of uncontaminated ground water upgradient from the disposal site.

Concentrations of dissolved iron at the disposal beds were below detection limits prior to cessation of disposal (fig. 4E). The dissolved oxygen in the treated sewage was sufficient to maintain suboxic conditions in the plume within 400 feet of the downgradient edge of the beds. The core of the plume was anoxic farther downgradient, where dissolved oxygen and nitrate had been completely consumed by biodegradation of organic materials.

After nitrate in the center of the plume beneath the disposal beds had been depleted (fig. 4D), dissolved-iron concentrations steadily increased (fig. 4E), probably because insoluble ferric iron oxide on the sediments was reduced to soluble ferrous iron (Lovley and others, 1989). The appearance of dissolved iron and the depletion of nitrate and dissolved oxygen beneath the beds indicate that the geochemical environment in the sewage-contaminated zone has become more reducing.

pH, Trace Metals, and Phosphorus

Hess and others (1996) predicted that sorbed trace metals would be mobilized following cessation of sewage disposal as low-pH uncontaminated ground water from upgradient areas entered the sewage-contaminated zone and organic matter was degraded. Although pH values have fluctuated slightly (fig. 4F), large decreases in pH have not been observed (fig. 7). The pH values at the downgradient edge of the disposal beds (fig. 4F) were greater than 5.7 throughout the sewage-contaminated zone, most likely because anaerobic biodegradation reactions consume hydrogen ions and, therefore, counteract the acidity of the inflowing ground water and the additional acidity generated by aerobic biodegradation occurring in the oxygen-consumption zone (Kent and Maeder, 1999).

The concentrations of trace metals, such as zinc (fig. 4G) and copper, have changed little since disposal ended because the pH has not changed (Kent and Maeder, 1999). The fluctuations of zinc concentrations at individual sampling depths were caused by small fluctuations in pH because zinc sorption is strongly dependent on pH (Kent and others, 1999). Small decreases in copper concentrations observed from November 1995 to May 1997 probably were caused by desorption of weakly sorbing copper complexes as the sewage-contaminated zone was initially flushed by uncontaminated ground water from upgradient areas (Kent and Maeder, 1999).

Concentrations of phosphorus beneath the disposal beds were elevated, but decreased with depth prior to cessation (fig. 4H). Phosphorus sorbs strongly to the sediments, and a large

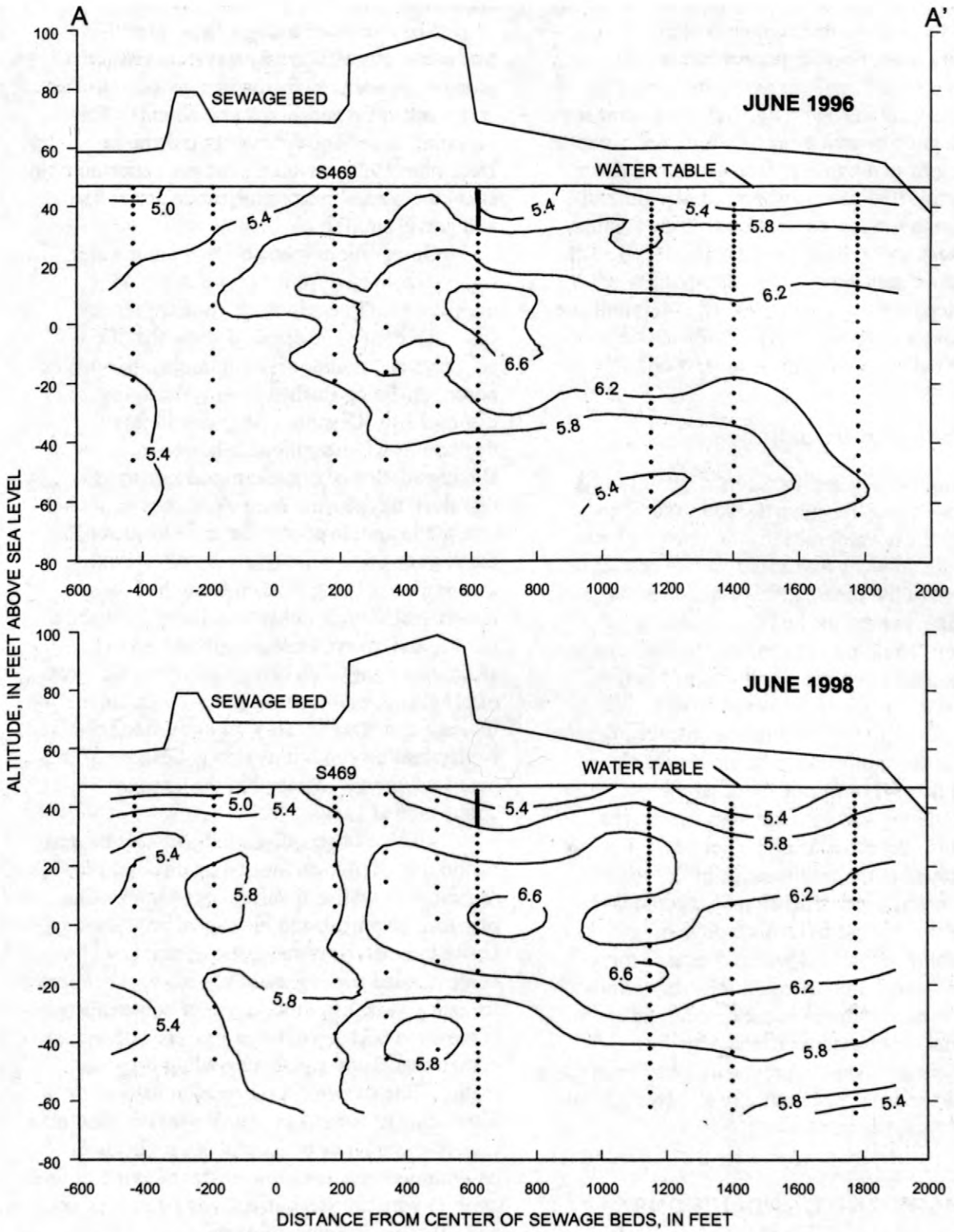

Figure 7. Longitudinal sections showing the distribution of pH between the sewage-disposal beds and Ashumet Pond, western Cape Cod, Massachusetts, June 1996 and June 1998. Lines of equal value in standard pH units. Dots show positions of well screens and multilevel-sampler ports. Location of section line shown in figure 2.

reservoir of sorbed phosphorus was associated with the dissolved phosphorus (Walter and others, 1996). During the first 6 months after sewage disposal ended, phosphorus concentrations increased significantly in the lower part of the plume beneath the beds (fig. 4H). This increase was probably caused by desorption of phosphorus resulting from a transient increase in pH as uncontaminated ground water initially flushed through the sewage-contaminated zone (Walter and others, 1999; Kent and Maeder, 1999). The small but steady decreases in phosphorus concentrations since May 1996 (fig. 4H) indicate that phosphorus will slowly desorb and be transported away from the disposal beds.

Geochemical Modeling

Stollenwerk and Parkhurst (1999) used a one-dimensional reaction-transport model to simulate the development of the sewage plume during the 60 years of disposal and to predict the evolution of the plume after cessation of disposal. Simulation results showed that reducing conditions could persist near the disposal site for more than 60 years during natural restoration, although the prediction was sensitive to the estimated reactivity and amount of sorbed organic matter in the aquifer. Simulation results also showed that pH buffering by anaerobic biodegradation and sorption reactions on the sediments may retard the advance of the low-pH environment at the trailing edge of the sewage-contaminated zone. Therefore, pH could take decades to decrease to levels typical of uncontaminated ground water. Because ionic-strength, redox, and pH conditions change at different rates, changes in concentrations of individual contaminants affected by these parameters are likely to propagate away from the disposal site in correspondingly complex spatial and temporal patterns.

SUMMARY AND CONCLUSIONS

Natural restoration has received increased attention as an option for the cleanup of contaminated aquifers. This option relies on the natural physical, chemical, and biological processes to restore the quality of ground water to acceptable levels.

Sixty years of sewage disposal at the Massachusetts Military Reservation created a plume characterized by distinct geochemical zones and steep geochemical gradients. The cessation of sewage disposal at the site in December 1995 provided a unique opportunity to study the natural restoration processes in a sand and gravel aquifer.

Observations made by analyzing water samples collected from 116 wells and 43 multilevel samplers in the 30 months since cessation of sewage disposal show that the conservative, nonreactive contaminants, such as boron, are being flushed from beneath the disposal site. Organic matter continues to degrade slowly near the site, however. Biodegradation of organic matter consumes dissolved oxygen and nitrate and thus maintains suboxic to anoxic conditions and elevated pH in the sewage-contaminated zone. As a result, ammonium is being flushed from the sewage-contaminated zone rather than being oxidized to nitrate, and trace metals remain sorbed to the sediments rather than being desorbed as a result of pH changes. Results of geochemical modeling indicate that water quality will return to pre-contamination conditions slowly because of the persistent oxygen demand in the sewage-contaminated zone.

These observations indicate that natural restoration of plumes formed by disposal of organic-rich wastes involves many interacting physical, chemical, and biological processes. Uncontaminated ground water entering contaminated zones may be altered geochemically for many years after the source of contamination is removed because of the persistence of sorbed contaminants and slowly degrading organic matter. The successful reliance on natural restoration to remediate aquifers will depend on understanding how the complex geochemical environment that is characteristic of many plumes evolves with time and affects the fate of redox- and pH-sensitive contaminants.

REFERENCES

Barber, L.B., and Keefe, S.H., 1999, Evolution of a ground-water sewage plume after removal of the 60-year-long source, Cape Cod, Massachusetts: Organic contaminants, *in* Morganwalp, D.W., and Buxton, H.T., eds., U.S. Geological Survey Toxic Substances Hydrology Program—Proceedings of the Technical Meeting, Charleston, South Carolina, March 8-12, 1999—Volume 3—Subsurface Contamination from Point Sources: U.S. Geological Survey Water-Resources Investigations Report 99-4018C, this volume.

Bohlke, J.K., Smith, R.L., Coplen, T.B., and LeBlanc, D.R., 1999, Recharge conditions and flow velocities of contaminated and uncontaminated ground waters at Cape Cod, Massachusetts: Evaluation of δ^2H, $\delta^{18}O$, and dissolved gases, *in* Morganwalp, D.W., and Buxton, H.T., eds., U.S. Geological Survey Toxic Substances Hydrology Program—Proceedings of the Technical Meeting, Charleston, South Carolina, March 8-12, 1999—Volume 3—Subsurface Contamination from Point Sources: U.S. Geological Survey Water-Resources Investigations Report 99-4018C, this volume.

Campo, K.W., and Hess, K.H., 1999, Evolution of a ground-water sewage plume after removal of the 60-year-long source, Cape Cod, Massachusetts: Fate of volatile organic compounds, *in* Morganwalp, D.W., and Buxton, H.T., eds., U.S. Geological Survey Toxic Substances Hydrology Program—Proceedings of the Technical Meeting, Charleston, South Carolina, March 8-12, 1999—Volume 3—Subsurface Contamination from Point Sources: U.S. Geological Survey Water-Resources Investigations Report 99-4018C, this volume.

Ceazan, M.L., Thurman, E.M., and Smith, R.L., 1989, Retardation of ammonium and potassium transport through a contaminated sand and gravel aquifer: The role of cation exchange: Environmental Science and Technology, v. 23, no. 11, p. 1402-1408.

Hess, K.M., LeBlanc, D.R., Kent, D.B., and Smith, R.L., 1996, Natural restoration of a sewage-contaminated aquifer, Cape Cod, Massachusetts, *in* Hydrology and hydrogeology of urban and urbanizing areas, proceedings of the conference, Boston, Mass., April 21-24, 1996: Minneapolis, Minnesota, American Institute of Hydrology, p. WQE13-WQE25.

Kent, D.B., Davis, J.A., Anderson, L.C.D., Rea, B.A., and Waite, T.D., 1994, Transport of chromium and selenium in the suboxic zone of a shallow aquifer: Influence of redox and adsorption reactions: Water Resources Research, v. 30, no. 4, p. 1099-1114.

Kent, D.B., Abrams, R.H., Davis, J.A., and Coston, J.A., 1999, Modeling the influence of adsorption on the fate and transport of metals in shallow ground water: Zinc contamination in the sewage plume on Cape Cod, Massachusetts, *in* Morganwalp, D.W., and Buxton, H.T., eds., U.S. Geological Survey Toxic Substances Hydrology Program—Proceedings of the Technical Meeting, Charleston, South Carolina, March 8-12, 1999—Volume 3—Subsurface Contamination from Point Sources: U.S. Geological Survey Water-Resources Investigations Report 99-4018C, this volume.

Kent, D.B., and Maeder, Valerie, 1999, Evolution of a ground-water sewage plume after removal of the 60-year-long source, Cape Cod, Massachusetts: pH and the fate of phosphate and metals, *in* Morganwalp, D.W., and Buxton, H.T., eds., U.S. Geological Survey Toxic Substances Hydrology Program—Proceedings of the Technical Meeting, Charleston, South Carolina, March 8-12, 1999—Volume 3—Subsurface Contamination from Point Sources: U.S. Geological Survey Water-Resources Investigations Report 99-4018C, this volume.

LeBlanc, D.R., 1984, Sewage plume in a sand and gravel aquifer, Cape Cod, Massachusetts: U.S. Geological Survey Water-Supply Paper 2218, 28 p.

LeBlanc, D.R., 1996, Overview of research at the Cape Cod site--Field and laboratory studies of physical, chemical, and microbiological processes affecting transport in a sewage-contaminated aquifer, *in* Morganwalp, D.W., and Aronson, D.A., eds., U.S. Geological Survey Toxic Substances Hydrology

Program--Proceedings of the technical meeting, Colorado Springs, Colorado, September 20-24, 1993: U.S. Geological Survey Water-Resources Investigations Report 94-4015, v. 1, p. 179-189.

LeBlanc, D.R., Garabedian, S.P., Hess, K.M., Gelhar, L.W., Quadri, R.D., Stollenwerk, K.G., and Wood, W.W., 1991, Large-scale natural-gradient tracer test in sand and gravel, Cape Cod, Massachusetts: 1. Experimental design and observed tracer movement: Water Resources Research, v. 27, no. 5, p. 895-910.

Lovley, D.R., Baedecker, M.J., Lonergan, D.J., Cozzarelli, I.M., Philips, E.J.P., and Siegel, D.J., 1989, Oxidation of aromatic contaminants coupled to microbial iron reduction: Nature, v. 339, p. 297-300.

Masterson, J.P., Walter, D.A., and LeBlanc, D.R., 1998, Delineation of contributing areas to selected public-supply wells, western Cape Cod, Massachusetts: U.S. Geological Survey Water-Resources Investigations Report 98-4237, 45 p.

McCobb, T.M., LeBlanc, D.R., and Hess, K.M., 1999, Determination of temporal and spatial variability of hydraulic gradients in an unconfined aquifer using three-point triangulation, Cape Cod, Massachusetts, *in* Morganwalp, D.W., and Buxton, H.T., eds., U.S. Geological Survey Toxic Substances Hydrology Program—Proceedings of the Technical Meeting, Charleston, South Carolina, March 8-12, 1999—Volume 3—Subsurface Contamination from Point Sources: U.S. Geological Survey Water-Resources Investigations Report 99-4018C, this volume.

Morganwalp, D.W, compiler, 1994, Bibliography of publications from the Toxic Substances Hydrology Program, U.S. Geological Survey: U.S. Geological Survey Open-File Report 94-91, 156 p.

National Research Council, 1994, Alternatives for ground water cleanup: Washington, D.C., National Academy Press, 315 p.

Savoie, Jennifer, and LeBlanc, D.R., eds., 1998, Water-quality data and methods of analysis for samples collected near a plume of sewage-contaminated ground water, Ashumet Valley, Cape Cod, Massachusetts, 1993-94: U.S. Geological Survey Water-Resources Investigations Report 97-4269, 208 p.

Smith, R.L., Harvey, R.W., and LeBlanc, D.R., 1991a, Importance of closely spaced vertical sampling in delineating chemical and microbiological gradients in groundwater studies: Journal of Contaminant Hydrology, v. 7, no. 3, p. 285-300.

Smith, R.L., Rea Kumler, B.A., Peacock, T.R., and Miller, D.N., 1999, Evolution of a ground-water sewage plume after removal of the 60-year-long source, Cape Cod, Massachusetts: Inorganic nitrogen species, *in* Morganwalp, D.W., and Buxton, H.T., eds., U.S. Geological Survey Toxic Substances Hydrology Program—Proceedings of the Technical Meeting, Charleston, South Carolina, March 8-12, 1999—Volume 3—Subsurface Contamination from Point Sources: U.S. Geological Survey Water-Resources Investigations Report 99-4018C, this volume.

Smith, R.L., Howes, B.L., and Duff, J.H., 1991b, Denitrification in nitrate-contaminated ground water: Occurrence in steep vertical geochemical gradients: Geochimica et Cosmochimica Acta, v. 55, no. 7, p. 1815-1825.

Stollenwerk, K.G., and Parkhurst, D.L., 1999, Modeling the evolution and natural remediation of a ground-water sewage plume, *in* Morganwalp, D.W., and Buxton, H.T., eds., U.S. Geological Survey Toxic Substances Hydrology Program—Proceedings of the Technical Meeting, Charleston, South Carolina, March 8-12, 1999—Volume 3—Subsurface Contamination from Point Sources: U.S. Geological Survey Water-Resources Investigations Report 99-4018C, this volume.

U.S. Environmental Protection Agency, 1997, Use of monitored natural attenuation at Superfund, RCRA corrective action, and underground storage tank sites: Washington, D.C., U.S. Environmental Protection Agency, Office of Solid Waste and Emergency Response Directive 9200.4-17, 25 p.

Walter, D.A., LeBlanc, D.R., Stollenwerk, K.G., and Campo, K.W., 1999, Phosphorus transport in sewage-contaminated ground

water, Massachusetts Military Reservation, Cape Cod, Massachusetts, *in* Morganwalp, D.W., and Buxton, H.T., eds., U.S. Geological Survey Toxic Substances Hydrology Program—Proceedings of the Technical Meeting, Charleston, South Carolina, March 8-12, 1999—Volume 3—Subsurface Contamination from Point Sources: U.S. Geological Survey Water-Resources Investigations Report 99-4018C, this volume.

Walter, D.A., Rea, B.A., Stollenwerk, K.G., and Savoie, Jennifer, 1996, Geochemical and hydrologic controls on phosphorus transport in a sewage-contaminated sand and gravel aquifer near Ashumet Pond, Cape Cod, Massachusetts: U.S. Geological Survey Water-Supply Paper 2463, 89 p.

AUTHOR INFORMATION

Denis R. LeBlanc, Kathryn M. Hess, and Kimberly W. Campo, U.S. Geological Survey, Marlborough, Mass. (dleblanc@usgs.gov)

Kenneth G. Stollenwerk, U.S. Geological Survey, Lakewood, Colorado

Richard L. Smith and Larry B. Barber, U.S. Geological Survey, Boulder, Colorado

Douglas B. Kent, U.S. Geological Survey, Menlo Park, California

Evolution of a Ground-Water Sewage Plume after Removal of the 60-Year-Long Source, Cape Cod, Massachusetts: Changes in the Distribution of Dissolved Oxygen, Boron, and Organic Carbon

by Larry B. Barber and Steffanie H. Keefe

ABSTRACT

Sewage effluent consists of a complex mixture of biogenic and synthetic organic compounds with a range of environmental behaviors. Sixty years of disposal of secondary treated sewage effluent into a sand-and-gravel aquifer on Cape Cod, Massachusetts, has resulted in an extensive plume of ground water contaminated by organic and inorganic compounds. In December 1995, the source was discontinued and a monitoring program was initiated that involved collection of about 500 samples below and down-gradient from the infiltration beds every 6 months for 3 years. The samples were analyzed for a variety of constituents including dissolved boron, dissolved oxygen (DO), and dissolved organic carbon (DOC). Removal of the source resulted in rapid flushing of boron and re-distribution of the organic compounds between the ground water and aquifer sediments. Prior to cessation, a portion of the organic carbon in the aquifer existed as DOC with concentrations ranging from 0.1 milligram per liter in the uncontaminated ground water to greater than 5 milligrams per liter in the sewage plume. The DOC was complex and had a range of solubility characteristics resulting in transport rates from conservative to highly retarded. Sediment organic carbon (SOC) concentrations (0.01 to 1.0 percent, or 100 to 10,000 milligrams per kilogram) were significantly higher than DOC concentrations. Thirty months after cessation, concentrations of boron and DOC had decreased beneath the infiltration beds, but DO concentrations remained relatively unchanged. The SOC reservoir appears to undergo desorption into the uncontaminated water moving into the zone of contamination, and considerable time will be required for ground water DOC concentrations to reach background levels. The DOC and SOC function as a pool of oxygen-consumption capacity, which will extend the period of time needed for DO concentrations to return to uncontaminated conditions.

INTRODUCTION

Natural attenuation is receiving considerable attention as an alternative means of dealing with contaminated ground water (Renner, 1998). Part of the motivation for passive remediation techniques is the difficulty in attaining cleanup goals using traditional pump and treat technology (Mackay and Cherry, 1989). Invasive remediation actions may be suitable for relatively small-scale, heavily contaminated sites, but they become cost prohibitive for large-scale contamination plumes. Therefore, natural attenuation of contaminated ground water by hydrological, chemical, and biological processes needs to be considered as a possible means of achieving water quality improvements.

To evaluate the diverse processes involved in natural attenuation of contaminants, a multidisciplinary investigation was conducted into the short-term evolution of the chemistry of a plume of sewage contaminated ground water located on Cape Cod, Massachusetts (fig. 1) after the 60-year-long source was shut off. The contamination plume is the result of disposal of secondary treated sewage effluent into sand and gravel infiltration beds. Once the sewage constituents reached the water-table aquifer, they were transported along with the regional ground water flow, at about 1.4 feet per day (Garabedian

and others, 1991; LeBlanc and others, 1991). Sixty years of wastewater disposal has resulted in a plume of contamination that is over 3.5 miles long, about 0.8 miles wide, and about 80 feet thick.

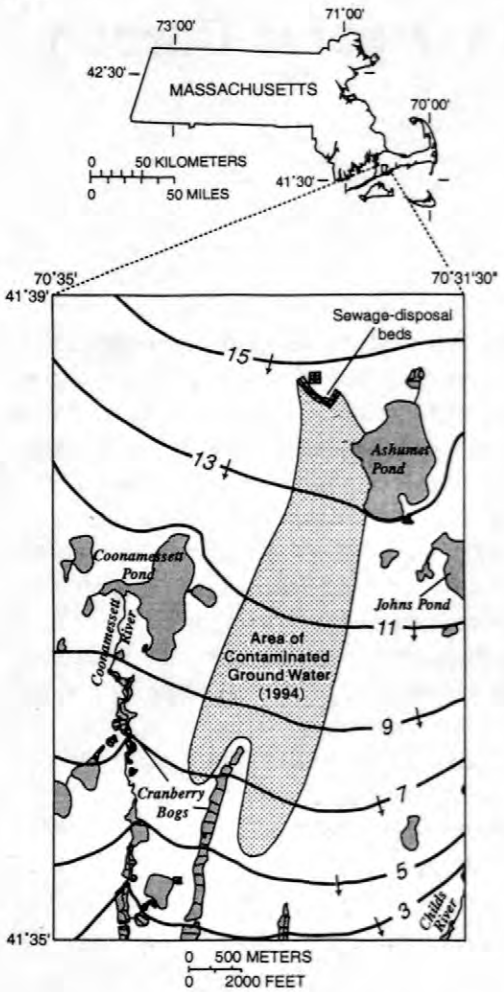

Figure 1. Location of plume of sewage-contaminated ground water on Cape Cod, Massachusetts (After Savoie and LeBlanc, 1998).

The plume is a complex mixture of organic and inorganic compounds. The inorganic components (LeBlanc, 1984) include major anions and cations (chloride, sulfate, bicarbonate, sodium, potassium, magnesium), trace elements (iron, manganese, boron, zinc), and nutrients (nitrate, ammonium, phosphate). The organic composition of the plume includes surfactant degradation products, volatile chlorinated hydrocarbons, and humic substances (Barber and others, 1988; Barber, 1992; Field and others 1992a,b). The source of contamination was removed in December 1995, after continuous wastewater disposal into the infiltration beds since 1936.

METHODS

Prior to cessation, an extensive 3-dimensional array of monitoring wells and multilevel samplers (fig. 2) was installed to monitor ground-water quality. During the cessation study, the monitoring network (about 500 sampling points) was sampled approximately every 6 months from November 1995 (prior to cessation) to November 1998. The samples were analyzed for a variety of constituents including field parameters (temperature, specific conductance, pH, and dissolved oxygen - DO), dissolved inorganic chemicals including boron, and dissolved organic carbon (DOC). Details on the sampling and analytical protocols are given in Savoie and LeBlanc (1998). The results of the analyses were used to evaluate short-term changes in the composition of the ground water as the wastewater source was stopped and uncontaminated ground water moved into the aquifer near the infiltration beds.

RESULTS

The distribution of boron was used to indicate the extent of contamination by a conservative inorganic chemical that can be traced directly to the sewage source (Barber and others, 1988). Between June 1996 and June 1998 the plume of boron contamination moved out of the region below the infiltration beds (fig. 3), indicating flushing by water coming from up-gradient. Note that the boron plume maintained the same general shape as it moved down-gradient about 900 feet. Similar results were observed for specific conductance, chloride, and other non-reactive mobile constituents. The observed changes in boron concentrations were consistent with conservative transport at the

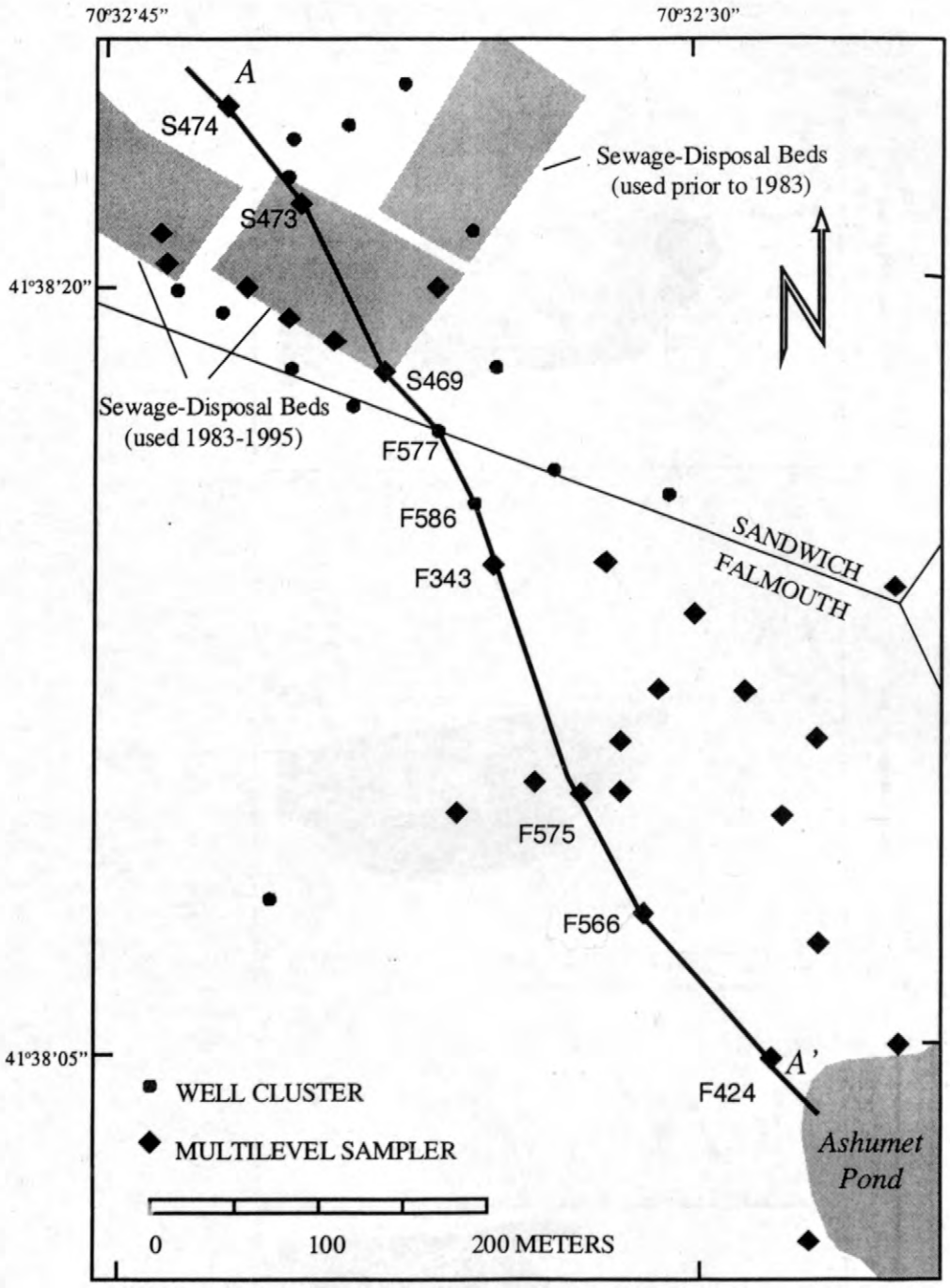

Figure 2. Site map showing location of sampling points used in this study.

regional ground water flow velocity (about 500 feet per year). In contrast to boron, DO distributions changed little between sampling rounds (fig. 4), indicating buffering of DO concentrations by the oxygen consumption capacity of the aquifer sediments near the contamination source. The most likely candidates for consuming the incoming DO are sediment organic matter, sorbed ammonium, and sorbed iron (Fe^{+2}).

Dissolved organic carbon decreased significantly following cessation (figs. 5 and 6), and after 2.5 years, DOC concentrations were less than 1 milligram per liter in a portion of the

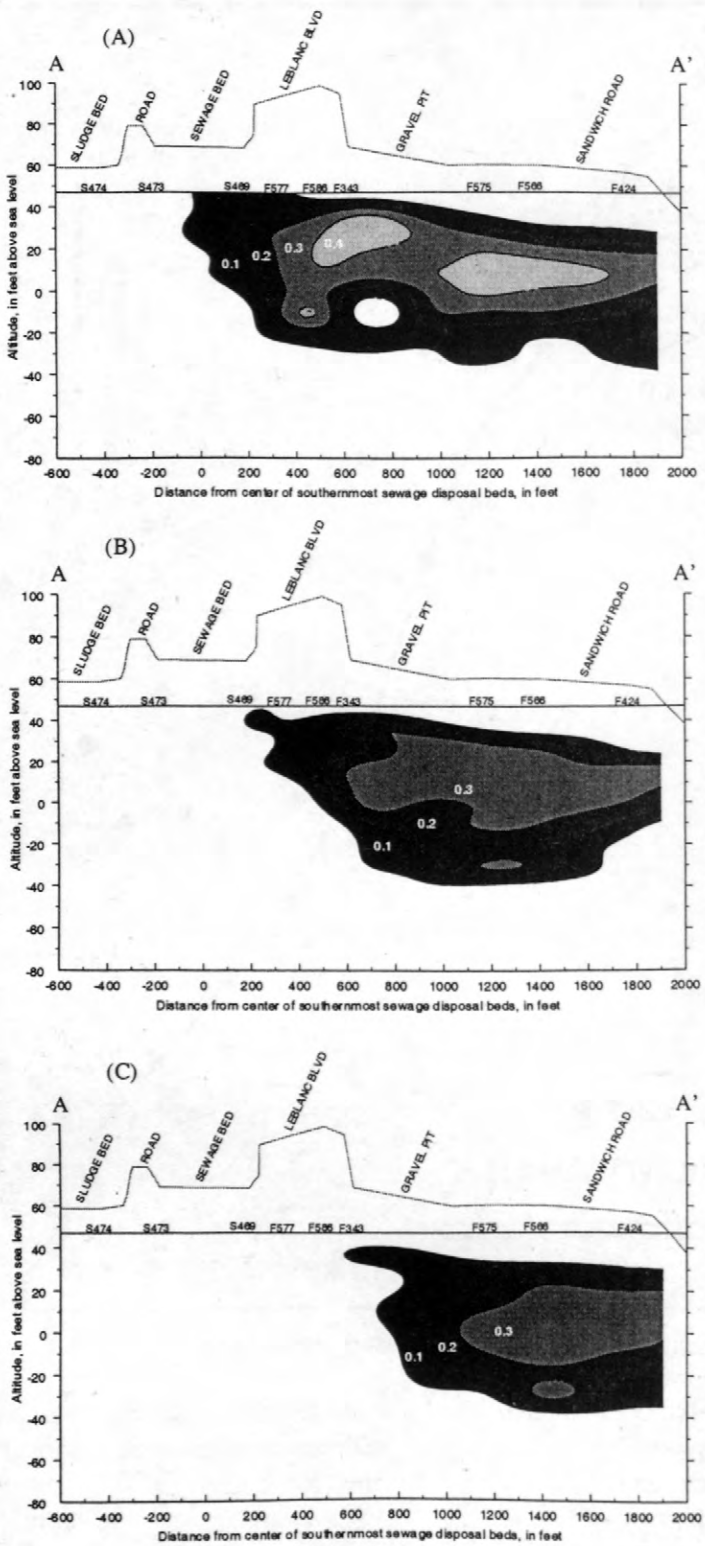

Figure 3. Distribution of boron (in milligrams per liter) along a longitudinal transect of the sewage plume in (A) June 1996 (6 months after cessation), (B) June 1997 (18 months after cessation), and (C) June 1998 (30 months after cessation).

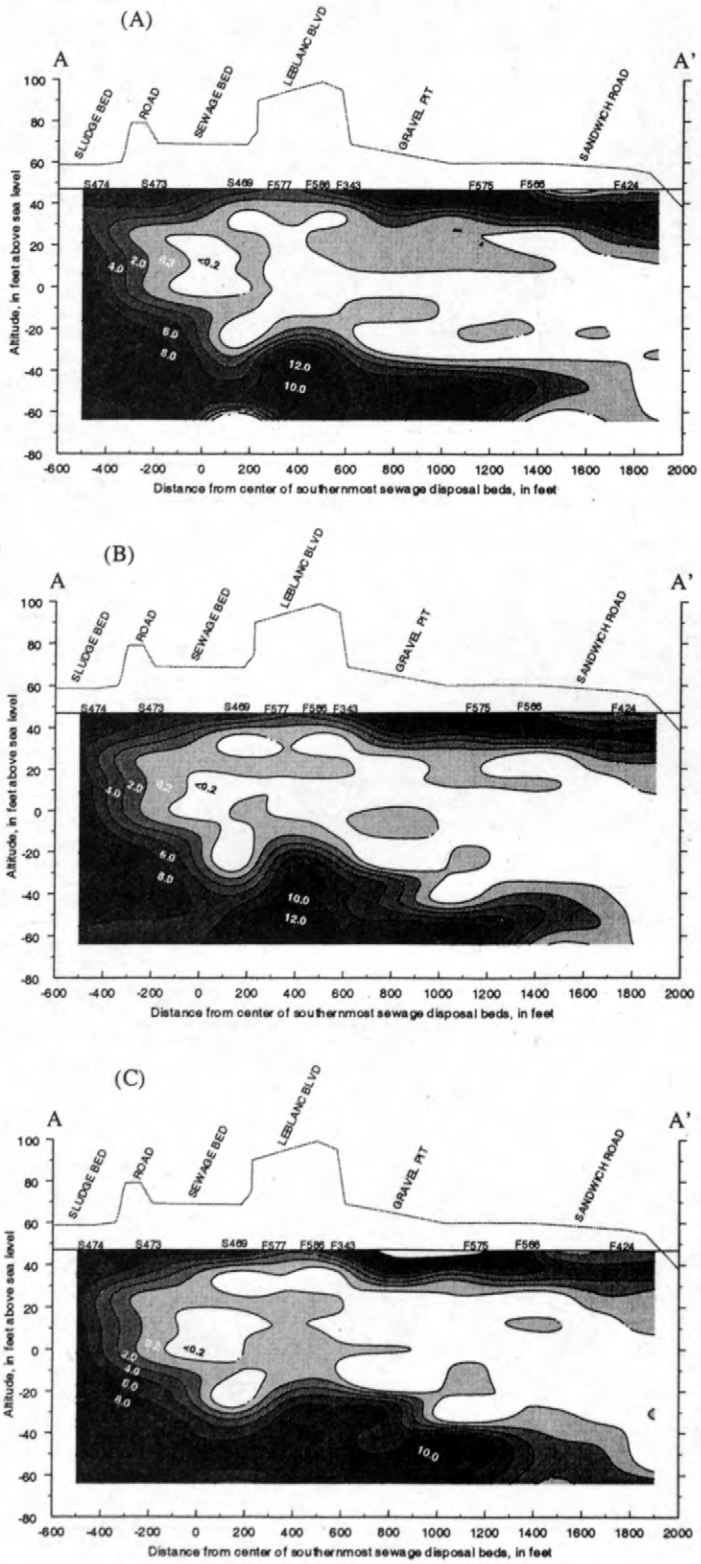

Figure 4. Distribution of dissolved oxygen (in milligrams per liter) along a longitudinal transect of the sewage plume in (A) June 1996 (6 months after cessation), (B) June 1997 (18 months after cessation), and (C) June 1998 (30 months after cessation).

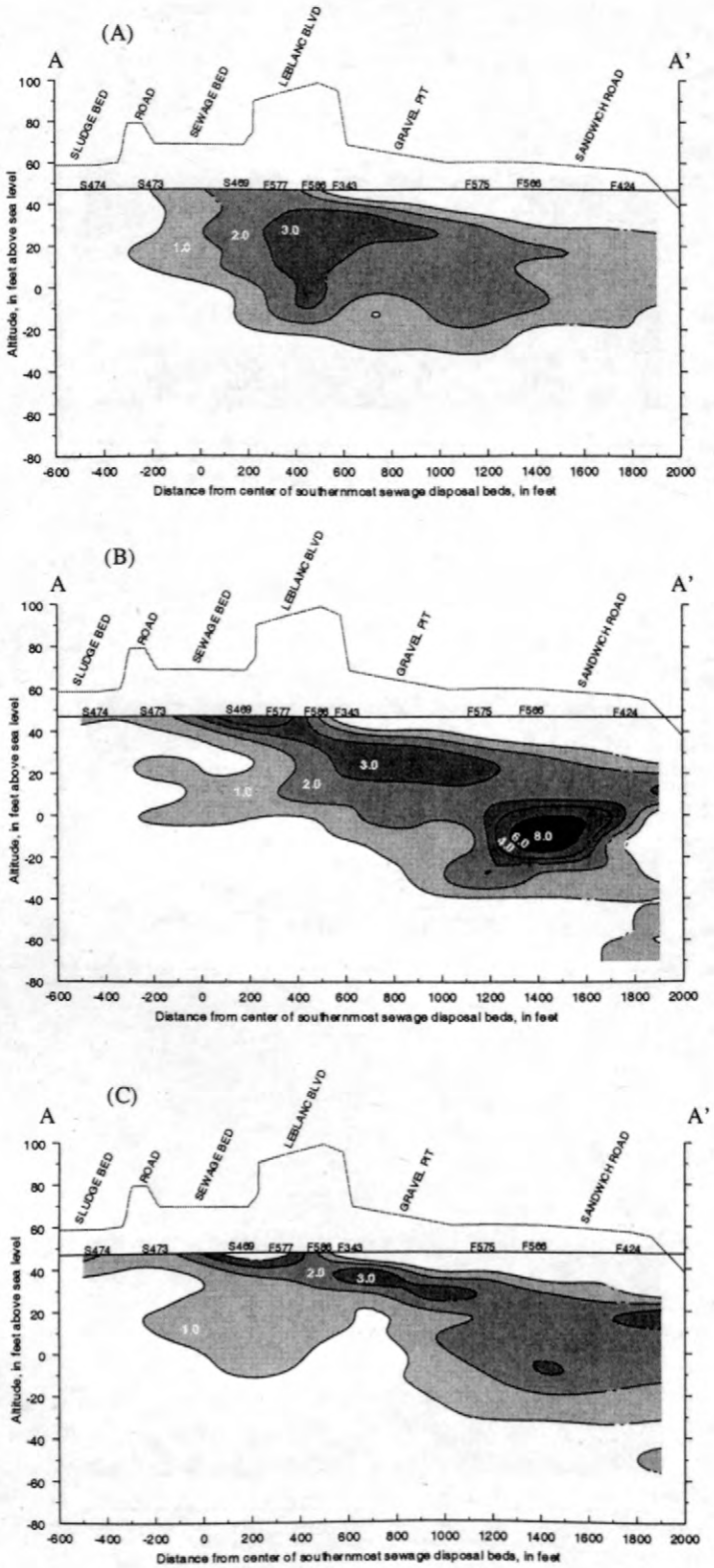

Figure 5. Distribution of dissolved organic carbon (in milligrams per liter) along a longitudinal transect of the sewage plume in (A) June 1996 (6 months after cessation), (B) June 1997 (18 months after cessation), and (C) June 1998 (30 months after cessation).

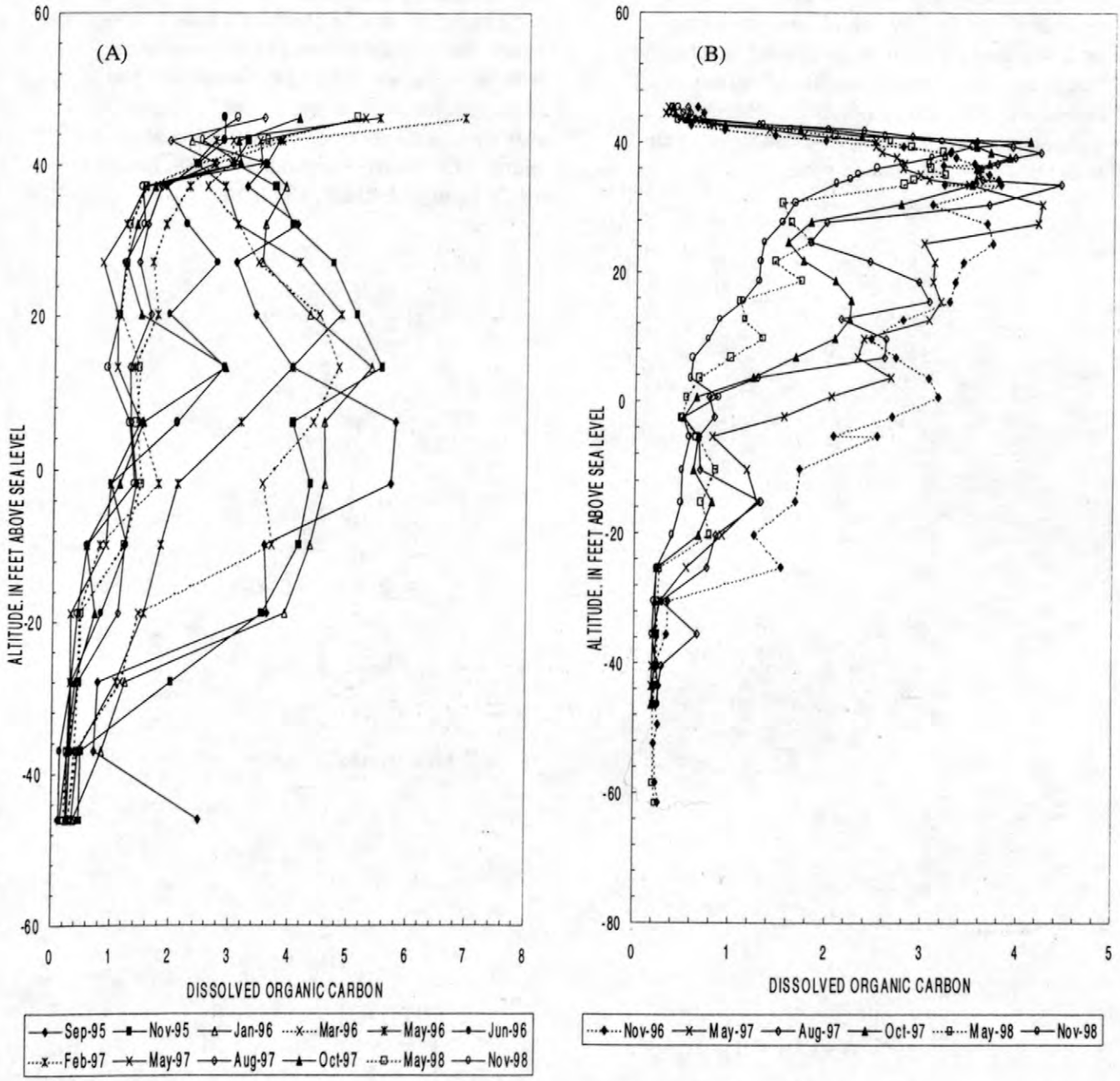

Figure 6. Vertical distribution of dissolved organic carbon (in milligrams per liter) in multilevel samplers (A) S469 and (B) F343, November 1995 to November 1998.

contaminated aquifer beneath the infiltration beds (sea level and below). These results are in contrast to boron, which reached background concentrations (less than 0.1 milligrams per liter) at all depths beneath the infiltration beds. The persistent elevated DOC concentrations in the shallow portion of the plume indicates a continuous input of organic matter, probably the result of DOC leaching from the aquifer sediments near the infiltration beds. Sediment organic carbon (SOC) concentrations ranged from 0.01 to 1.0 percent (100 to 10,000 milligrams per kilogram) and were significantly higher than DOC concentrations. The SOC reservoir can undergo desorption into the uncontaminated water, and extend the time required for DOC concentrations to reach background levels (less than 1.0 milligram per

liter). The DOC and SOC are pools of oxygen-consumption capacity, which can extend the time required for DO concentrations to return to uncontaminated conditions. Microbial activity consumes DOC and DO during biodegradation, and can maintain low DO concentrations even with incoming oxygenated water.

Secondary-treated wastewater contains a wide range of organic chemicals with varying molecular characteristics and environmental behaviors. Figure 7 shows the structures and acronyms for some of the organic compounds that are significant components of the sewage plume DOC (Barber and others, 1988; Barber, 1992; Field and others, 1992a,b).

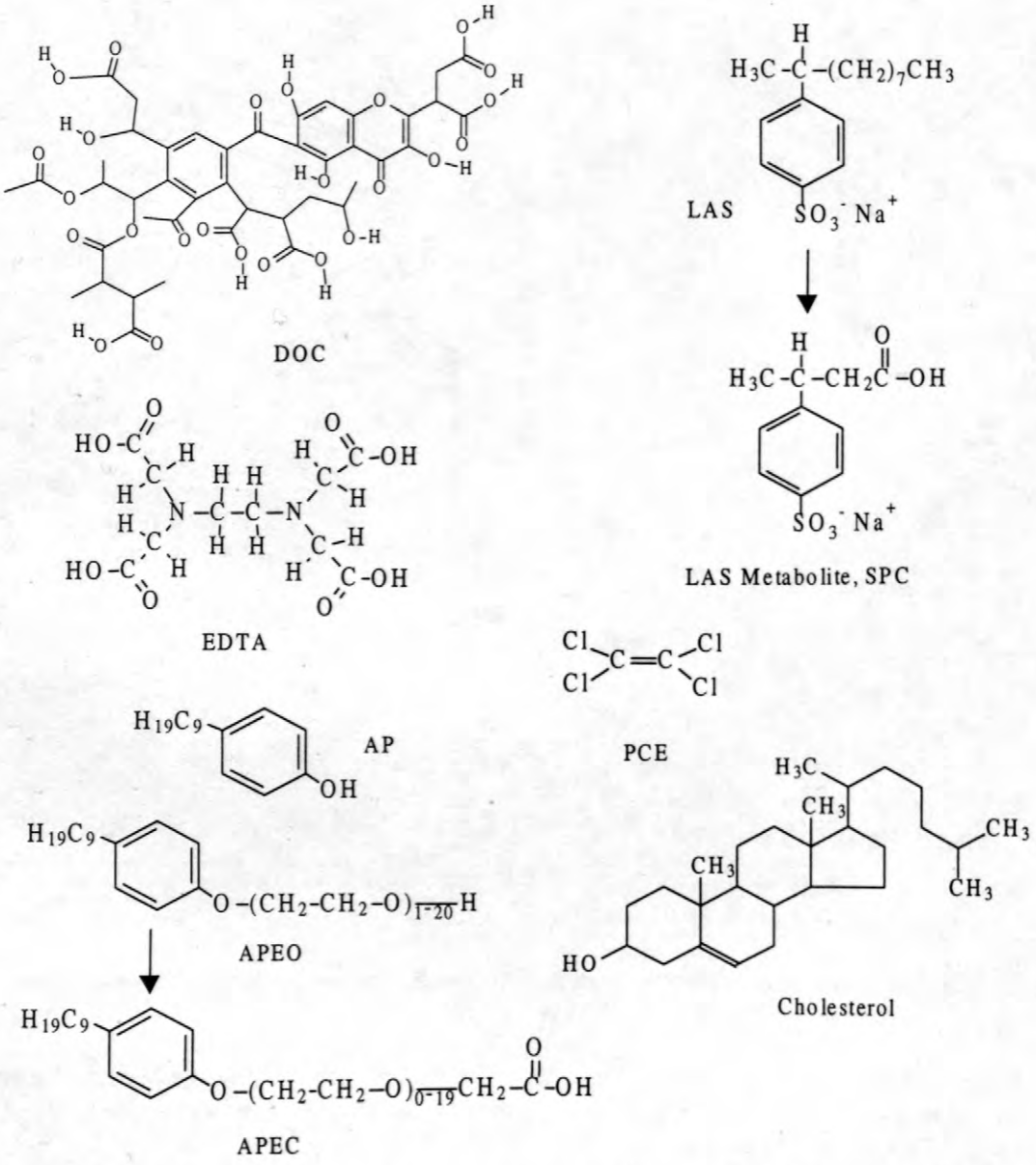

Figure 7. Chemical structures of specific organic compounds present in sewage contaminated ground water. [DOC, natural dissolved organic carbon such as fulvic acid; LAS, linear alkylbenzenesulfonate; SPC, sulfophenylcarboxylate degradation product of LAS; EDTA, ethylenediaminetetraacetic acid; PCE, tetrachloroethene; AP, alkylphenol; APEO, alkylphenolpolyethoxylate; APEC, alkylphenolethoxycarboxylate]

The physico-chemical characteristics of particular importance for this investigation are water solubility and biodegradability. The anionic surfactant LAS and fulvic acid DOC provide a comparison of environmental behaviors. Both compounds are water soluble, but fulvic acid is resistant to biodegradation (Thurman, 1985) whereas LAS is rapidly biodegraded under aerobic conditions (Barber, 1992; Field and others, 1992a; Krueger and others, 1998a,b). In situ tracer experiments with LAS indicate that although it is potentially biodegradable, biodegradation is oxygen limited in the contamination plume (Krueger and others, 1998a,b). Biodegradation is a stepwise process, and when LAS was introduced into a location within the plume containing about 1 milligram per liter DO, biodegradation proceeded until the available oxygen was consumed, after which additional degradation did not occur. The SPC metabolites of LAS persisted under the suboxic and anoxic conditions of the plume. The molar oxygen consumption capacity of LAS is greater than for fulvic acid, EDTA, and PCE, and thus is likely to have more effect on DO buffering conditions in the aquifer.

Water soluble compounds such as LAS, SPC, EDTA, PCE, and APEC are transported at rates similar to the ground water flow, whereas less soluble compounds such as AP, APEO, and cholesterol are sorbed to the sediments and transported at slower rates (Barber and others, 1988; Barber 1992; Krueger and others, 1998a,b). It is likely that LAS was sorbed to the aquifer sediments near the infiltration beds (the sediment/water distribution coefficient ranged from 0.00 to 0.14 liters per kilogram for the various isomers, Krueger and others, 1998a). Desorption of LAS and similar sewage-derived compounds from the aquifer sediments followed by biodegradation can consume DO introduced by transport of up-gradient ground water.

CONCLUSIONS

Elimination of the source of sewage contamination into the Cape Cod aquifer has initiated significant short-term changes in the ground-water chemistry of the plume. Mobile chemical species such as boron were rapidly flushed through the aquifer and have decreased to background values. A portion of the DOC, representing water-soluble compounds such as LAS, SPC, PCE, and EDTA, also was rapidly transported down-gradient. However, a significant amount of DOC is moving much more slowly, and concentrations are still elevated beneath the infiltration beds after 2.5 years. Following cessation, sediment organic matter was exposed to a changing geochemical environment resulting in desorption, reaction, and transport of SOC. The sediment derived DOC continued to maintain low DO concentrations in the aquifer after 2.5 years. The extensive plume of contaminated ground water down-gradient from the infiltration beds represents 60 years of wastewater disposal and continues to move through the aquifer without the attenuation observed for boron and DOC at the tailing edge of the plume.

REFERENCES

Barber, L.B., II, 1992, Hierarchical analytical approach to evaluating the transport and biogeochemical fate of organic compounds in sewage contaminated groundwater, Cape Cod, Massachusetts, Chapter 4 in Lesage, Suzanne and Jackson, R.E., eds., Groundwater Contamination and Analysis at Hazardous Waste Sites: New York, Marcel Dekker, p. 73-120.

Barber, L.B., II, Thurman, E.M., Schroeder, M.P., and LeBlanc, D.R., 1988, Long-term fate of organic micropollutants in sewage contaminated groundwater: Environmental Science and Technology, v. 22, p. 205-211.

Field, J.A., Barber, L.B., II, Thurman, E.M., Moore, B.L., Lawrence, D.L., and Peake, D.A., 1992a, Fate of alkylbenzenesulfonates and dialkyltetralinsulfonates in sewage-contaminated groundwater: Environmental Science and Technology, v. 26, p. 1140-1148.

Field, J.A., Leenheer, J.A., Thorn, K.A., Barber, L.B., II, Rostad, Colleen, Macalady, D.L., and Daniel, S.R., 1992b, Identification of persistent anionic-surfactant derived chemicals in sewage effluent and

groundwater: Journal of Contaminant Hydrology, v. 9, p. 55-78.
Garabedian, S.P., LeBlanc, D.R., Gelhar, L.W., and Celia, M.A., 1991, Large-scale natural gradient tracer test in sand and gravel, Cape Cod, Massachusetts 2. Analysis of spatial moments for a nonreactive tracer: Water Resources Research, v. 27, p. 911-924.
Krueger, C.J., Barber, L.B., Metge, D.W., and Field, J.A., 1998a, Fate and transport of linear alkylbenzenesulfonate in a sewage-contaminated aquifer: A comparison of natural–gradient and pulsed tracer tests: Environmental Science and Technology, v. 32, p. 1134-1142.
Krueger, C.J., Radakovich, K.M., Sawyer, T.E., Barber, L.B., Smith, R.L., and Field, J.A., 1998b, Biodegradation of the surfactant linear alkylbenzenesulfonate in sewage-contaminated groundwater: A comparison of column experiments and fields tracer tests: Environmental Science and Technology, v. 32, p. 3954-3961.
LeBlanc, D.R., 1984, Sewage plume in a sand and gravel aquifer, Cape Cod, Massachusetts: U.S. Geological Survey Water-Supply Paper 2218, 28 p.
LeBlanc, D.R., Garabedian, S.P., Hess, K.M., Gelhar, L.W., Quadri, R.D., Stollenwerk, K.G., and Wood, W.W., 1991, Large-scale natural-gradient tracer test in sand and gravel, Cape Cod, Massachusetts: 1. Experimental design and observed tracer movement: Water Resources Research, v. 27, p. 895-910.
Mackay, D.M. and Cherry, J.A., 1989, Groundwater contamination: Pump-and-treat remediation: Environmental Science and Technology, v. 23, p. 630-636.
Renner, Rebecca, 1998, Intrinsic remediation under the microscope: Environmental Science and Technology, v. 32, p. 180A-182A.
Savoie, Jennifer and LeBlanc, D.R., eds., 1998, Water-quality data and methods of analysis for samples collected near a plume of sewage contaminated ground water, Ashumet Valley, Cape Cod, Massachusetts, 1993-1994: U.S. Geological Survey Water-Resources Investigations Report 97-4269, 208 p.
Thurman, E.M., 1985, Organic Geochemistry of Natural Waters: Boston, Martinus Nijhoff/Dr W. Junk Publishers, 497 p.

AUTHOR INFORMATION

Larry B. Barber (lbbarber@usgs.gov) and Steffanie H. Keefe (shkeefe@usgs.gov), U.S. Geological Survey, 3215 Marine Street, Boulder, CO, 80303

Evolution of a Ground-Water Sewage Plume After Removal of a 60-Year-Long Source, Cape Cod, Massachusetts: Fate of Volatile Organic Compounds

By Kimberly W. Campo and Kathryn M. Hess

ABSTRACT

Evolution of a plume of contaminated ground water is being observed following the cessation in December 1995 of disposal of treated sewage onto rapid-infiltration beds at the Massachusetts Military Reservation, Cape Cod, Massachusetts. Concentrations of nonreactive species are decreasing as cleaner ground water from upgradient enters the contaminated aquifer. Oxygen concentrations in the contaminated aquifer remain low. The cessation of sewage disposal altered ground-water-flow patterns beneath the beds, allowing ground water contaminated with volatile organic compounds upgradient of the sewage-treatment plant to enter the sewage-contaminated zone beneath the beds. This new flow path has implications for natural attenuation of volatile organic compounds.

INTRODUCTION

Secondarily treated sewage was discharged onto rapid-infiltration beds at the Massachusetts Military Reservation (MMR), Cape Cod, Massachusetts, from 1936 to 1995 (fig. 1). Sixty years of sewage disposal onto these beds resulted in a plume of sewage-contaminated ground water in the underlying sand-and-gravel aquifer that extends 3 miles southward from the MMR (LeBlanc, 1984). The U.S. Geological Survey (USGS) has studied this sewage plume since the plume was first characterized 20 years ago. The sewage-treatment plant stopped the disposal of sewage onto the infiltration beds in December 1995. The Installation Restoration Program at the MMR had no immediate plans to remediate the sewage plume. Scientists at the USGS saw this as a unique opportunity to study the evolution of the plume after the source was shut off.

Ground-Water Sewage Plume

Major differences in ground-water chemistry in the study area distinguish sewage-contaminated ground water from uncontaminated ground water. Uncontaminated ground water in the study area typically has pH values less than 6, specific conductance values of around 50 µS/cm (microsiemens per centimeter at 25 degrees Celsius), and concentrations of dissolved oxygen up to 11 mg/L (milligrams per liter). Concentrations of boron, a constituent commonly found in sewage from cleaning agents and household and industrial chemicals, are less than 50 µg/L (micrograms per liter), and concentrations of volatile organic compounds (VOCs), are below analytical detection limits (typically 0.2 µg/L) in uncontaminated ground water. Sewage-contaminated ground water typically has pH values greater than 6, little or no dissolved oxygen, and a specific conductance that is up to 10 times higher than that of uncontaminated ground water in the study area. The sewage plume contains high concentrations (100–400 µg/L) of boron, as well as elevated concentrations of phosphorus and metals, such as zinc, copper, and lead. Ammonium, iron, and manganese are present in areas in the plume that have little to no dissolved oxygen. VOCs are also present throughout the downgradient portions of the plume, most likely the result of solvents

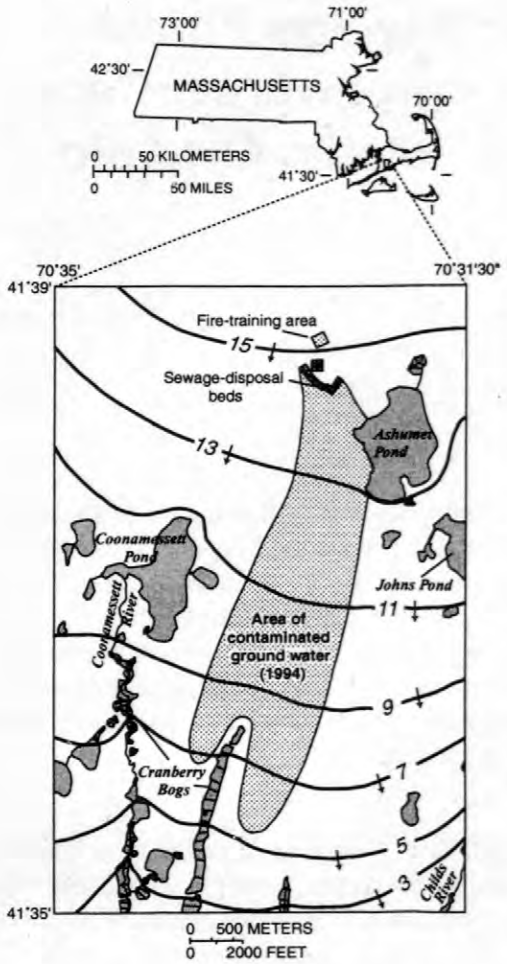

Figure 1. Location of sewage infiltration beds, fire training area, and area of sewage-contaminated ground water, western Cape Cod, Massachusetts.

discharged through the sewage-treatment plant (Barber and others, 1988; Barber, 1992) during the last couple of decades, before the recognition of the potential for contamination of ground water through deficient disposal practices.

Upgradient Source of Volatile Organic Compounds

Former Fire Training Area No. 1 (FTA-1) is located 1,300 ft (feet) upgradient of the MMR sewage-treatment plant (fig. 1). The MMR fire department conducted 6-16 fire-training exercises in designated areas in FTA-1 annually from 1958-85 (ABB Environmental Services, 1992). Flammable waste liquids were burned and extinguished during these exercises. The waste liquids included jet fuel, aviation and motor gasoline, diesel fuels, waste oils, solvents, paint thinners, transformer oils, and used hydraulic fluids. The materials were burned on the ground surface until 1983, when a concrete pad was constructed. The fire-training area was closed in November 1985 resulting from air emission permitting difficulties.

Fuel-related contaminants and chlorinated solvents were present in shallow soils at the FTA-1 site and in ground water beneath and downgradient of the site, as a result of the fire-training activities. The plume of contaminated ground water consists primarily of the chlorinated solvents tetrachloroethylene (PCE), trichloroethylene (TCE), and cis-1,2 dichloroethene (DCE), as well as other VOCs, such as benzene. The FTA-1 plume extends from the FTA-1 site to beyond the MMR sewage-treatment plant and follows a similar flow direction as the sewage plume. The FTA-1 plume is distinguished from the sewage plume because it does not contain organic and inorganic constituents associated with the sewage plume and is located at a lower altitude in the aquifer than the sewage plume.

Source Removal

Sewage disposal onto the infiltration beds at the MMR was stopped in December 1995. It was predicted that the shut off of sewage disposal would have an immediate effect on the hydrologic system, which would allow ground water from upgradient to enter the sewage-contaminated aquifer beneath the infiltration beds (Hess and others, 1996). As cleaner ground water enters the contaminated aquifer, nonreactive contaminants such as boron would be flushed downgradient. The influx of cleaner ground water has implications for transport of reactive species as decreasing ionic strength causes transient pH increases and desorption of sorbed species. Ammonium and iron will be oxidized as

concentrations of dissolved oxygen increase in the plume.

The soils at FTA-1 were excavated and stripped of volatile organic compounds before being returned to the site in 1997. Prior to 1997, these soils remained a source of VOC contamination in the ground water. The VOC-contaminated ground water from the site was not remediated as part of this effort. Scientists at the USGS have been monitoring the ground-water quality near both the FTA-1 source area and the sewage-treatment plant to provide field evidence of aquifer restoration that may be occurring due to the removal of the source of contamination at the FTA-1 site. These investigations include examining potential natural attenuation of VOCs as VOC-contaminated ground water from the FTA-1 site enters the sewage-contaminated aquifer beneath the infiltration beds after sewage disposal onto the beds ceased.

Purpose and Scope

The purpose of this paper is to describe the fate of VOCs in ground water near FTA-1 and the abandoned infiltration beds since 1995. The distribution of VOCs in 1997–98 is compared to that observed in 1994, and the differences are related to physical, chemical, and biological changes that have occurred in the aquifer following the cessation of sewage disposal in 1995.

HYDROLOGY

The MMR is located on a broad glacial outwash plain on western Cape Cod. The ground-water-flow system is bounded to the north, west, and south by saltwater, and to the east by a ground-water divide. Precipitation is the sole source of natural recharge to the aquifer, and seasonal variations in recharge cause the water-table altitude to fluctuate 1 to 3 ft each year. The aquifer is unconfined, and ground water flows radially outward from a water-table mound near the northern region of the MMR. The mound has a maximum hydraulic head of 70 ft above sea level (Savoie, 1995). In the study area, water-table altitudes ranges from 44 to 50 ft above sea level, and ground-water flow is generally southward.

For 60 years treated sewage artificially recharged the aquifer at the infiltration beds. The influx of sewage produced a strong downward component of flow at the beds, which displaced ground water from downward or laterally as the upgradient water approached the area beneath the beds (fig. 2). This upgradient ground water included the FTA-1 plume.

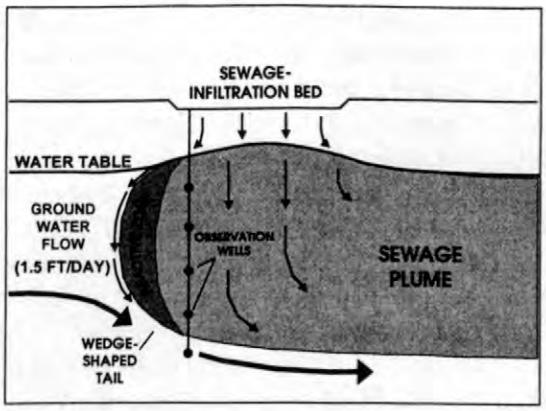

Figure 2. Schematic diagram of hydrologic system beneath the infiltration beds.

The cessation of disposal had an immediate effect on the hydrologic system. Regional ground-water-flow paths were no longer locally perturbed by the treated sewage influx. Ground-water-flow simulations conducted by the USGS show that the path of contaminants from FTA-1 should be higher in the aquifer now that the inflow of water at the infiltration beds has ceased (Masterson and others, 1996). This new flow path would move VOC-contaminated ground water from the FTA-1 source into the part of the aquifer that was contaminated by sewage.

GROUND-WATER SAMPLING

Ground-water samples were collected from observation wells and multilevel samplers (MLSs) in and around the infiltration beds. Water-quality changes were expected to first occur in the aquifer directly below the beds when disposal was stopped. Therefore, monitoring has been focused near the beds.

A network of observation wells and MLSs was established to sample at regular intervals (fig. 3). Water-quality samples were collected weekly immediately following the shutoff because it was not known how quickly changes in the aquifer would occur. Fourteen MLSs and 68 wells, located in and around the beds, are currently sampled twice per year. An additional 29 MLSs and 48 wells, located further downgradient from the sewage-treatment plant, are sampled once per year.

VOC samples were collected from a small network of observation wells that extends from the FTA-1 site to 1,000 ft downgradient of the infiltration beds (fig. 3, table 1). Ground-water samples were collected from 54 wells in November 1997 and from 15 additional wells in March 1998 to observe the distribution of VOCs. In June 1998, 42 of the 69 wells were re-sampled to monitor small-scale temporal changes in the VOC distribution. In addition, samples were collected in June 1998 from 3 new wells that were installed in 1998. Field parameters (specific conductance, pH, and dissolved oxygen) were measured at all sites sampled.

The observation wells are constructed of 2-inch diameter polyvinyl chloride (PVC) pipe with 2- or 5-ft long PVC screens, and typically installed in clusters of up to 8 wells, each screened at a different altitude. Multilevel samplers consist of 15, 0.25-inch color-coded polyethylene tubes, each screened with fine-meshed nylon fabric and set at a different altitude. Ground-water samples are collected from observation wells using a submersible pump with an inflatable packer. Samples are collected from MLSs using a peristaltic pump.

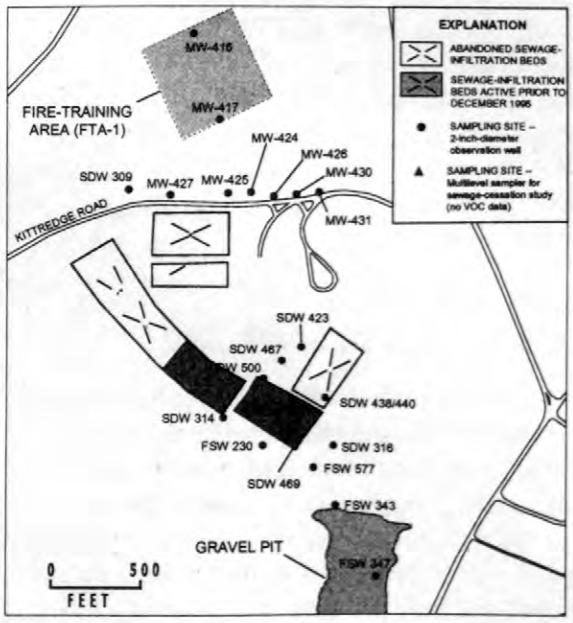

Figure 3. Location of water-quality-sampling sites.

CHANGES IN GROUND-WATER QUALITY

Nonreactive species and pH

Concentrations of nonreactive species beneath the infiltration beds are near background concentrations three years after sewage disposal ceased. Figure 4 shows vertical profiles of specific conductance, boron, and pH relative to altitude for site SDW 469 located in the southernmost infiltration beds (fig. 3). Specific conductance decreased from about 500 to 100 µS/cm and boron concentrations have decreased from about 400 to 50 µg/L. The pH has remained relatively unchanged however, despite the influx of lower pH ground water from upgradient. This is perhaps due to the pH buffering properties of the aquifer sediments. Flushing of nonreactive species has been observed as far as 500 ft downgradient of the infiltration beds based on specific conductance values (table 1) at site FSW 343 (fig. 3).

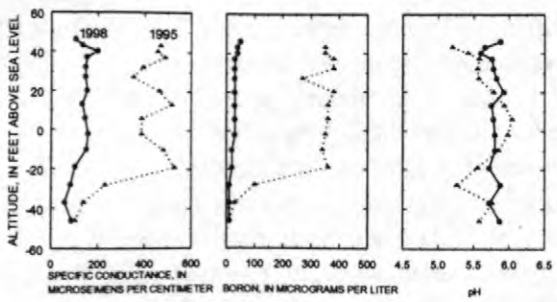

Figure 4. Vertical profiles of the distribution of specific conductance, boron, and pH in ground water at SDW 469 before (1995) and three years after (1998) sewage disposal was stopped.

Dissolved Oxygen

Dissolved oxygen concentrations in the sewage plume have remained relatively unchanged near the beds in the three years since sewage disposal ceased. Notable changes in dissolved-oxygen concentrations, however, have been observed at certain individual sites. Minor fluctuations in dissolved-oxygen concentrations near the top of the sewage plume at some sites (fig. 5) are most likely due to seasonal variations in the water-table altitude. Dissolved-oxygen concentrations near the bottom of the plume appear to have increased since 1995 (fig. 5). Oxygen values at these sites were below 1 mg/L before sewage disposal was stopped and rose steadily after cessation to values as high as 8 mg/L in November 1998. Dissolved-oxygen values at some sites in the core of the contaminated area under the beds increased within one year after cessation. These values remained relatively high until 1998, when concentrations of dissolved oxygen decreased at these sites. Figure 6 presents this trend by showing vertical profiles of dissolved oxygen relative to altitude from 1995–98 for site SDW 472, a multilevel sampler located in one of the infiltration beds (fig. 3). Dissolved-oxygen concentrations increased from 1995 to 1997 within an altitude range of 0-30 ft above sea level

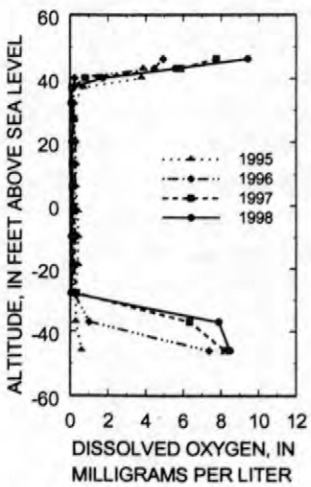

Figure 5. Vertical profiles of the distribution of dissolved oxygen in ground water at SDW 469, 1995-98.

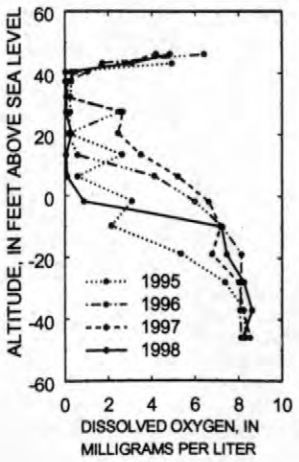

Figure 6. Vertical profiles of the distribution of dissolved oxygen in ground water at SDW 472, 1995-98.

at site SDW 472. In 1998, oxygen concentrations decreased to values less than 1 mg/L. The reason for this trend is unknown, however, it is theorized that the microbial communities are continuing to consume any available oxygen, without a renewing food supply.

It is postulated that a reactive zone with a high level of biological activity exists near the boundary between the sewage-contaminated aquifer and the uncontaminated aquifer, or what is considered the tail end of the sewage plume (fig. 2). The microbial communities persist here despite the lack of the renewing food supply that had been previously available for 60 years. The dimensions of this highly reactive zone are unknown, however, its location is theorized to be slightly upgradient of the infiltration beds, near site SDW 467 (fig. 3). As upgradient ground water containing high concentrations of dissolved oxygen passes through this reactive zone, the oxygen is removed before reaching the core of the sewage plume, thus preventing oxygen concentrations from increasing in the contaminated aquifer.

Iron

An increase in iron concentrations was observed at some sites. Figure 7 presents this trend by showing vertical profiles of dissolved

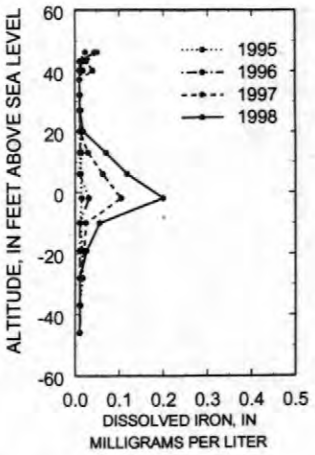

Figure 7. Vertical profiles of the distribution of dissolved iron in ground water at SDW 469, 1995-98.

iron relative to altitude from 1995-98 for site SDW 469. Iron concentrations increased from 0.01 mg/L in 1995 up to 0.2 mg/L in 1998, within an altitude range of –10 to 20 ft above sea level. The dissolved oxygen and iron trends suggest that as the sewage plume is being naturally remediated, conditions in some areas of the aquifer are becoming more reducing.

Volatile Organic Compounds

The VOC results (table 1) were compared to VOC data from a 1994 study (ABB Environmental Services, 1995; Savoie and LeBlanc, 1997) at several well clusters around the sewage-treatment plant to investigate changes in the vertical and horizontal distributions of VOCs. Vertical profiles (fig. 8) show VOC concentrations (PCE, TCE, and DCE) relative to altitude for 4 well clusters located near the infiltration beds (fig. 3). In 1994, FTA-1 VOC concentrations were located mostly within an altitude range of about 20 to –20 ft above sea level near the infiltration beds. Also plotted in figure 8 are the 1994 profiles of specific conductance. In 1994, most VOCs were at the bottom or below the sewage-contaminated zone, as outlined by the specific conductance profiles. The pattern for SDW 316 is not as clear because this site is located east of the most recently active infiltration beds (fig. 3). SDW 316 is at the edge of the sewage plume, where VOCs from FTA-1 were pushed aside instead of downward, and therefore VOCs are located at higher altitudes than at the other three sites shown in figure 8.

Data from the 1997 sampling show VOC concentrations at these same sites are at least 20 ft higher in altitude two years after the cessation of sewage disposal (fig. 8). This pattern is most evident at site SDW 314 where in 1994 VOCs were located at an altitude of about –25 ft below sea level. In 1997, VOCs were located at an altitude of about 30 ft above sea level, approximately 55 ft higher.

Volatile organic compounds were present at levels above Maximum Contaminant Levels (MCL) (U.S. Environmental Protection Agency, 1996) in and around the FTA-1 site in 1994. MCLs for PCE, TCE, and DCE are 5 µg/L, 5 µg/L, and 70 µg/L, respectively. The contaminated ground water extends southward from the southern boundary of the FTA-1 site. The areal distributions of PCE and DCE for 1994 and 1997-98 are presented in figures 9 and 10, respectively. The areal distributions were defined on the basis of the maximum concentration of these constituents at each sampling site. TCE was not included in the figures because the constituent was not present at levels above the MCL, with the exception of well SDW 314-0098 in 1994 (table 1). The data show that VOCs were still present at levels above their MCLs in ground water in the FTA-1 area, near site MW 417. The cessation of sewage disposal occurred two years prior to the November sampling, and VOCs from the FTA-1 plume were flowing into the sewage-contaminated aquifer. The microbial communities that persisted on the sediments were predicted to naturally degrade the VOCs. The geochemical conditions in this biologically active area may promote natural bioremediation of VOCs from the FTA-1 plume, especially as this area becomes more reducing (Chapelle, 1993), as indicated by the increase in iron (fig. 7). The degradation pathway of the selected constituents is PCE to TCE to DCE to vinyl chloride. Apparent degradation products, however, were observed only at site SDW 469, which had DCE concentrations as high as 140 µg/L and a trace of vinyl chloride. Unfortunately, SDW 469 is a new site and no VOC data exists at the site prior to 1997.

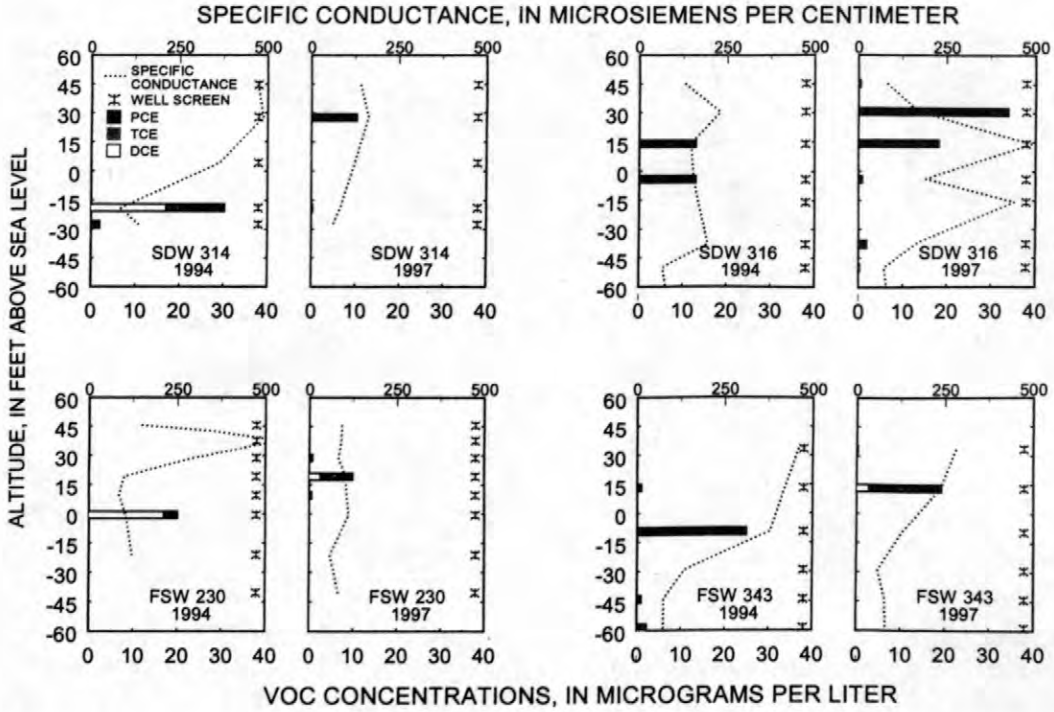

Figure 8. Vertical profiles of the distributions of volatile organic compounds and specific conductance in ground water one year before (1994) and two years after (1997) sewage disposal was stopped.

In June 1998, ground-water samples were collected from a subset of the wells sampled in November 1997 and March 1998 (table 1). The data showed that VOCs are still present in ground water in the FTA-1 area, however concentrations are below MCLs. VOC concentrations decreased or stayed the same downgradient of FTA-1 near Kittredge Road in the 3 to 7-month period between samplings. The concentrations in the one well that showed an increase (MW-425B) were less than the MCLs and were similar to levels observed in 1994.

Downgradient of the infiltration beds at the two sites in the gravel pit (fig. 3), the results of two recent samplings show little change in concentrations over the 7 months (table 1). Localized changes were observed at individual wells. For example, at FSW 347-0046, PCE was detected at 16 µg/L in March 1998. Previously, no PCE was detected (1994) or the concentration was below the MCL (1997) at this well. At well FSW 347-0067, PCE was detected at 5.44 µg/L in March 1998. Previous PCE concentrations were as high as 12 µg/L (1994).

In June 1998, DCE concentrations at site SDW 469 dropped below the MCL to 57 µg/L and vinyl chloride was no longer detected. The other sites sampled did not contain any significant concentrations of degradation products.

The cessation of sewage disposal was predicted to have an effect on the hydrologic system in the study area. One effect was a restoration of the regional ground-water-flow path. There is no longer a strong downward component of flow at the beds produced by the influx of sewage, therefore upgradient ground water is not pushed downward or aside as it enters the area beneath the beds. This change in flow paths also changed the path of contaminants from FTA-1. VOC-contaminated ground water from the FTA-1 source now flow into part of the aquifer that was contaminated by 60 years of sewage disposal and has a higher level of biological activity compared to parts uncontaminated by sewage. VOC concentrations should decrease and degradation products may be detected if natural attenuation is occurring. However, the complex short-term temporal changes observed were probably reflecting spatial variability in the VOC distribution that was not well defined with the limited number of samples collected.

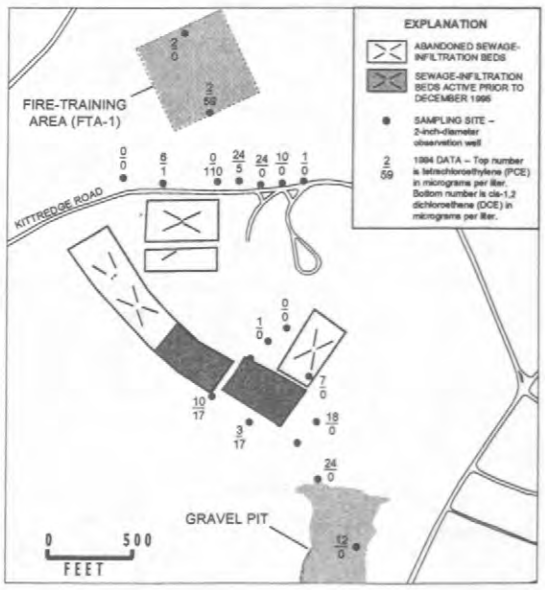

Figure 9. Distribution of maximum concentrations of tetrachloroethylene (PCE) and cis-1,2 dichloroethene (DCE) in ground water, 1994.

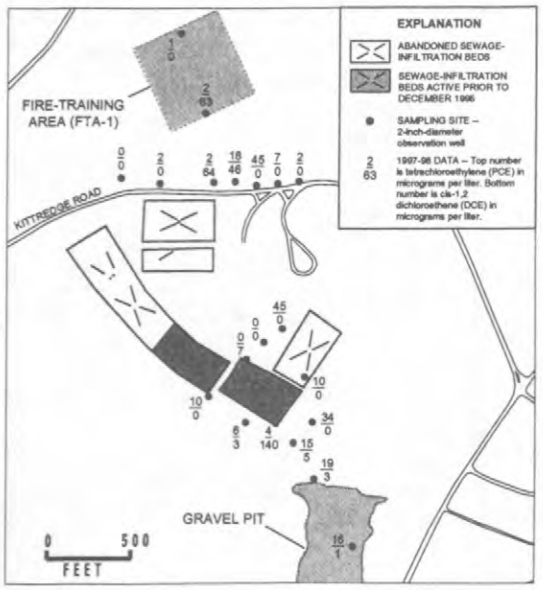

Figure 10. Distribution of maximum concentrations of tetrachloroethylene (PCE) and cis, 1,2-dichloroethylene (DCE) in ground water, 1997-98.

SUMMARY

Secondarily treated sewage was discharged onto rapid-infiltration beds for a period of 60 years, resulting in a plume of sewage-contaminated ground water in the underlying sand-and-gravel aquifer that extends 3 miles downgradient from the MMR. Major differences in ground-water chemistry in the study area distinguish sewage-contaminated ground water from uncontaminated ground water. The sewage plume overlaid a plume of volatile organic compounds (VOCs) in the vicinity of the infiltration beds. The source of the VOCs is a former fire training area (FTA-1) located 1,300 ft upgradient of the infiltration beds. The FTA-1 plume is distinguished from the sewage plume because it does not contain organic and inorganic constituents associated with sewage.

The sewage-treatment plant stopped the disposal of sewage onto the infiltration beds at the MMR in December 1995. Concentrations of nonreactive species beneath the infiltration beds have decreased to near background concentrations three years after sewage disposal ceased. The pH has remained unchanged, however, possibly due to the pH buffering properties of the aquifer sediments. Dissolved-oxygen concentrations in the sewage plume have remained relatively unchanged possibly because of a high level of biological activity that occurs at the upgradient boundary between the sewage-contaminated aquifer and the uncontaminated aquifer. Notable changes, however, have been observed at some sites indicating that as the sewage plume is being naturally remediated, conditions in part of the sewage-contaminated aquifer are becoming more reducing.

The cessation of sewage disposal also affected the hydrologic system in the study area. Regional ground-water-flow paths are no longer perturbed in the vicinity of the infiltration beds by the influx of treated sewage. Upgradient ground water is no longer pushed downward or aside as it enters the area beneath the beds. Contaminated ground water from the FTA-1 site is flowing into the part of the aquifer that was contaminated by 60 years of sewage disposal.

The contaminated soils at FTA-1 were excavated and stripped of VOCs in 1997, essentially removing the source of ground-water contamination. Ground-water samples were collected between November 1997 and June 1998 to observe the current distribution of VOCs. The 1997-98 VOC data were compared to VOC data

from a 1994 study at several well clusters around the infiltration beds. The results show that VOC concentrations at these sites are located at least 20 ft higher in altitude in 1997, two years after the cessation of sewage disposal, due to the redirected flow paths. In general, the data show that VOC concentrations are the same or diminishing. Although VOC concentrations are lower at particular sites, it remains inconclusive if natural bioremediation is occurring due to the lack of apparent degradation products and clear temporal trends. Additional ground-water monitoring is needed to determine if VOCs are being naturally removed from the aquifer as they flow into the highly-reducing zone developed from 60 years of disposal of treated sewage.

REFERENCES

ABB Environmental Services, Inc., 1992, Area of contamination Fire-Training Area No. 1 (AOC FTA-1) groundwater operable unit interim remedial investigation report – Task 2-5, Massachusetts Military Reservation, Cape Cod, Mass. (Draft): Oak Ridge, Tenn., Hazardous Waste Remedial Actions Program, April 1992 [various pagination].

——— 1995, Ashumet Valley groundwater operable unit remedial investigation report, Massachusetts Military Reservation, Cape Cod, Mass. (Draft): Oak Ridge, Tenn., Hazardous Waste Remedial Actions Program, April 1995 [various pagination].

Barber, L.B., II, Thurman, E.M., Schroeder, M.P., and LeBlanc, D.R., 1988, Long-term fate of organic micropollutants in sewage-contaminated groundwater: Environmental Science and Technology, v. 22, no. 2, p. 205-211.

Barber, L.B., II, 1992, Hierarchical analytical approach to evaluating the transport and biogeochemical fate of organic compounds in sewage-contaminated groundwater, Cape Cod, Massachusetts, *in* Lesage, Suzanne, and Jackson, R.E., eds., Groundwater Contamination and Analysis at Hazardous Waste Sites: New York, Marcel Dekker, p. 73-120.

Chapelle, F.M., 1993, Ground-Water Microbiology and Chemistry: New York, John Wiley & Sons, 424 p.

Hess, K.M., LeBlanc, D.R., Kent, D.B., and Smith, R.L., 1996, Natural restoration of a sewage-contaminated aquifer, Cape Cod, Massachusetts, *in* Hydrology and hydrogeology of urban and urbanizing areas, proceedings of the conference, Boston, Mass., April 21-24, 1996: Minneapolis, Minnesota, American Institute of Hydrology, p. WQE13-WQE25.

LeBlanc, D.R., 1984, Sewage plume in a sand and gravel aquifer, Cape Cod, Massachusetts: U.S. Geological Survey Water-Supply Paper 2218, 28 p.

Masterson, J.P, Walter, D.A., and Savoie, Jennifer, 1996, Use of particle tracking to improve numerical model calibration and to analyze ground-water flow and contaminant migration, Massachusetts Military Reservation, Cape Cod, Massachusetts: U.S. Geological Survey Water-Supply Paper 2482, 50 p.

Savoie, Jennifer, 1995, Altitude and configuration of the water table, western Cape Cod, Massachusetts, March 1993: U.S. Geological Survey Open-File Report 94-462, 1 plate, scale 1:50,000.

Savoie, Jennifer, and LeBlanc, D.R., eds., 1997, U.S. Geological Survey Water-quality data and methods of analysis for samples collected near a plume of sewage-contaminated ground water, Ashumet Valley, Cape Cod, Massachusetts, 1993-94: Water-Resources Investigations Report 97-4269, 208 p.

U.S. Environmental Protection Agency, 1996, Drinking water regulations and health advisories: EPA 822-R-96-001, February 1996.

AUTHOR INFORMATION

Kimberly W. Campo and Kathryn M. Hess, U.S. Geological Survey, Marlborough, Massachusetts (kcampo@usgs.gov)

Table 1. Field water-quality analyses and major volatile organic compounds analyses for water samples from wells, Cape Cod, Massachusetts, 1993–94 and 1997–98

[Location of wells are shown in figure 3. µS/cm, microsiemens per centimeter at 25 degrees Celsius; µg/L, micrograms per liter; <, actual value is less than method detection limit; --, no data available; Source of 1993–94 data: ABB Environmental Services, Inc., 1995; Savoie and LeBlanc, 1998]

Well cluster site and well number	Altitude, middle of screen (feet)	Date field parameters collected	Specific conductance (µS/cm)	pH (standard units)	Oxygen, dissolved (mg/L)	Date samples collected	cis-1,2-Dichloroethene µg/L)	Trichloroethylene µg/L)	Tetrachloroethylene µg/L)
FSW 230-0042	45.7	7-20-94	148	4.58	--	4-05-94	<1	<1	<1
		11-17-97	92.3	5.38	6.33	11-17-97	<0.2	<0.2	<0.2
FSW 230-0048	42.8	7-20-94	345	5.68	--	7-20-94	<.2	<.2	<.2
FSW 230-0049	37.7	7-20-94	537	5.40	--	4-05-94	<1	<1	<1
		11-17-97	91.2	5.97	0.28	11-17-97	<.2	<.2	<.2
FSW 230-0058	28.9	7-20-94	297	5.52	.5	4-05-94	<1	<1	<1
		11-17-97	83.1	5.71	2.35	11-17-97	<.2	<.2	.769
FSW 230-0068	19.2	7-21-94	100	5.40	.2	4-05-94	<1	<1	<1
		11-17-97	103	5.34	.3	11-17-97	2.58	1.1	6.23
FSW 230-0078	9.5	7-22-94	85	5.69	.2	4-05-94	<1	<1	<1
		11-17-97	107	5.58	1.15	11-17-97	<.2	<.2	.608
FSW 230-0088	-0.7	7-21-94	104	5.63	.2	4-06-94	17	<1	3
		11-17-97	112	5.71	6.15	11-17-97	<.2	<.2	<.2
FSW 230-0108	-21.0	7-21-94	122	5.57	--	4-06-94	<1	<1	<1
		11-17-97	59.2	5.84	10.2	11-17-97	<.2	<.2	<.2
FSW 230-0127	-40.3	7-22-94	63	5.49	--	4-06-94	<1	<1	<1
		11-17-97	82.6	5.63	11.2	11-17-97	<.2	<.2	<.2
FSW 343-0036	33.5	8-31-94	460	5.93	.15	3-25-94	<1	<1	<1
		11-20-97	282	6.01	.23	11-20-97	<.2	<.2	.25
		6-25-98	181	6.01	.08	6-25-98	<.2	<.2	.636
FSW 343-0057	13.1	8-31-94	422	6.55	0	5-12-93	<1	<1	1
		11-20-97	238	6.42	.305	11-20-97	2.78	.637	15.9
		6-25-98	186	6.38	.14	6-25-98	1.72	.529	19.3
FSW 343-0079	-9.4	8-30-94	379	6.52	0	5-12-93	<1	1	24
		11-20-97	129	6.44	.015	11-20-97	<.2	<.2	<.2
		6-25-98	109	6.49	0	6-25-98	<.2	<.2	<.2
FSW 343-0099	-29.1	8-30-94	136	5.73	--	5-12-93	<1	<1	<1
		11-20-97	60.7	5.84	10.8	11-20-97	<.2	<.2	<.2
		6-25-98	61.8	5.82	9.57	6-25-98	<.2	<.2	<.2
FSW 343-0114	-43.9	8-30-94	76	5.74	--	3-25-94	<1	<1	<1
		11-20-97	81	5.69	11.2	11-20-97	<.2	<.2	<.2
		6-25-98	80.8	5.71	9.81	6-25-98	<.2	<.2	<.2
FSW 343-0129	-58.5	8-30-94	76	5.72	--	8-30-94	<.2	2.2	<.2
		11-20-97	83.1	5.63	7.67	11-20-97	<.2	<.2	<.2
FSW 343-0145	-74.8	8-31-94	92	5.60	--	3-26-94	<1	<1	<1
		11-20-97	92.2	5.58	10.9	11-20-97	<.2	<.2	<.2
		6-24-98	83.1	5.98	9.88	6-24-98	<.2	<.2	<.2
FSW 347-0020	41.0	10-18-94	94	5.01	8	3-29-94	<1	<1	<1
		11-21-97	71	5.34	10.6	11-21-97	<.2	<.2	.334
		6-24-98	44.4	5.49	11.1	6-24-98	<.2	<.2	<.2

Table 1. Field water-quality analyses and major volatile organic compounds analyses for water samples from wells, Cape Cod, Massachusetts, 1993–94 and 1997–98–*Continued*

Well cluster site and well number	Altitude, middle of screen (feet)	Date field parameters collected	Specific conduct-ance (µS/cm)	pH (standard units)	Oxygen, dissolved (mg/L)	Date samples collected	cis-1,2-Dichloro-ethene µg/L)	Trichloro-ethylene µg/L)	Tetrachloro-ethylene µg/L)
FSW 347-0031	29.9	10-18-94	221	5.94	0.1	3-29-94	<1	<1	<1
		11-21-97	176	6.12	.265	11-21-97	<0.2	<0.2	0.401
		6-24-98	119	6.14	1.79	6-24-98	<.2	<.2	1.95
FSW 347-0038	22.9	10-18-94	410	5.94	.2	3-29-94	<1	<1	<1
		11-21-97	378	6.10	.25	11-21-97	<.2	<.2	<.2
		6-24-98	234	6.20	.23	6-24-98	<.2	<.2	.27
FSW 347-0046	14.9	10-18-94	224	6.20	.2	3-29-94	<1	<1	<1
		11-20-97	369	6.13	.185	11-20-97	<.2	<.2	1.04
		6-24-98	247	6.35	.2	6-24-98	.958	.445	16
FSW 347-0067	-5.9	10-19-94	179	6.28	0	5-11-93	<1	<1	12
		11-21-97	260	6.39	0	11-21-97	1.11	.401	8.84
		6-24-98	206	6.50	0	6-24-98	.538	.202	5.44
FSW 347-0101	-40.2	10-19-94	96	5.38	5	5-11-93	<1	2	3
		11-20-97	112	5.45	10.6	11-20-97	<.2	.59	<.2
		6-24-98	91.1	5.57	7.12	6-24-98	<.2	.521	<.2
FSW 347-0116	-55.0	10-18-94	69	5.56	6.5	3-30-94	<1	2	7
		11-20-97	62.4	5.62	9.62	11-20-97	<.2	.88	<.2
		6-24-98	76.6	5.58	9.39	6-24-98	<.2	<.2	<.2
FSW 347-0131	-70.0	10-18-94	83	5.47	8	3-30-94	<1	4	<1
		11-20-97	95.4	5.63	9.43	11-20-97	<.2	.21	<.2
		6-24-98	87.1	5.63	8.67	6-24-98	<.2	<.2	<.2
FSW 347-0145	-83.7	10-19-94	89	5.71	8	3-30-94	<1	<1	<1
		11-20-97	88.1	5.75	10.5	11-20-97	<.2	<.2	<.2
		6-24-98	83.8	5.82	7.89	6-24-98	<.2	<.2	<.2
FSW 577-0051	44.4	3-23-98	125	5.69	2.21	3-24-98	<.2	<.2	<.2
FSW 577-0061	34.7	3-23-98	162	5.98	.33	3-24-98	<.2	<.2	5.21
FSW 577-0071	24.5	3-23-98	184	6.28	.12	3-24-98	2.04	.248	15.4
FSW 577-0081	14.4	3-23-98	167	6.32	.13	3-24-98	4.51	<.2	1.86
FSW 577-0097	-0.8	3-23-98	178	6.34	.48	3-24-98	<.2	<.2	<.2
FSW 577-0111	-16.0	3-23-98	92.9	6.01	6.98	3-24-98	<.2	<.2	<.2
FSW 577-0126	-30.9	3-23-98	70.9	5.85	10.3	3-24-98	<.2	<.2	<.2
FSW 577-0142	-45.6	3-23-98	73	5.60	10.6	3-24-98	<.2	<.2	<.2
MW-416A	19.9	3-23-94	52	5.4	--	3-23-94	<1	<1	<1
		11-25-97	78.3	5.69	11.2	11-25-97	<.2	<.2	<.2
MW-416B	29.5	3-23-94	137	5.2	--	3-23-94	<1	<1	<1
		11-25-97	218	5.55	9.79	11-25-97	<.2	<.2	<.2
MW-416C	49.1	3-23-94	69	4.9	--	3-23-94	<1	<1	2
		11-25-97	128	5.13	10.1	11-25-97	<.2	<.2	.614
MW-417A	17.9	3-24-94	89	5.2	--	3-24-94	<1	<1	<1
		3-24-98	150	5.09	10.6	3-24-98	<.2	<.2	<.2
		6-22-98	111	5.54	10.5	6-22-98	<.2	<.2	<.2

Table 1. Field water-quality analyses and major volatile organic compounds analyses for water samples from wells, Cape Cod, Massachusetts, 1993–94 and 1997–98–*Continued*

Well cluster site and well number	Altitude, middle of screen (feet)	Date field parameters collected	Specific conduct-ance (µS/cm)	pH (standard units)	Oxygen, dissolved (mg/L)	Date samples collected	cis-1,2-Dichloro-ethene µg/L)	Trichloro-ethylene µg/L)	Tetrachloro-ethylene µg/L)
MW-417B	31.0	3-24-94	98	5.2	--	3-24-94	59	<1	2
		3-24-98	156	5.34	10	3-24-98	<0.2	<0.2	<0.2
		6-22-98	215	5.33	10.2	6-22-98	<.2	<.2	<.2
MW-417C	46.1	3-24-94	128	5.8	--	3-24-94	<1	<1	<1
		3-24-98	172	6.00	0.165	3-24-98	62.9	<.2	1.66
		6-22-98	180	6.11	.32	6-22-98	11	<.2	1.75
MW-424A	21.6	3-24-94	91	5.7	--	3-24-94	<1	<1	<1
		11-24-97	166	5.78	10.8	11-24-97	<.2	<.2	<.2
		6-22-98	148	5.49	10.0	6-22-98	1.7	<.2	<.2
MW-424B	45.0	3-24-94	69	--	--	3-24-94	5	.6	24
		11-24-97	98	5.40	5.06	11-24-97	46	.501	18.1
		6-22-98	78.8	5.16	6.08	6-22-98	19	<.2	10.8
MW-425A	21.0	3-24-94	124	--	--	3-24-94	<1	<1	<1
		11-24-97	155	5.47	10.5	11-24-97	<.2	<.2	<.2
		6-22-98	295	6.35	0	6-22-98	<.2	<.2	<.2
MW-425B	37.3	3-24-94	138	6.8	--	3-24-94	110	.1	<1
		11-24-97	191	6.56	0	11-24-97	.353	<.2	.202
		6-22-98	190	5.50	10.3	6-22-98	63.7	<.2	1.9
MW-426A	31.5	3-24-94	73	--	--	3-24-94	<1	<1	2
		11-21-97	96	5.45	9.61	11-21-97	<.2	<.2	2.4
MW-426B	41.7	3-24-94	52	6.2	--	3-24-94	.7	.5	24
		11-21-97	78	5.36	9.34	11-21-97	<.2	.332	45
MW-427	41.5	3-24-94	53	5.1	--	3-24-94	.9	.8	6
		11-24-97	82.4	5.21	9.45	11-24-97	<.2	<.2	2.4
MW-428A	-8.2	11-04-94	125	5.55	11	3-28-94	<1	<1	<1
		11-18-97	109	5.77	10.9	11-18-97	<.2	<.2	<.2
		6-23-98	178	5.46	10.8	6-23-98	<.2	<.2	<.2
MW-428B	31.6	11-04-94	95	5.35	10	3-28-94	<1	<1	<1
		11-18-97	76.4	5.67	8.96	11-18-97	<.2	.717	45
		6-23-98	88.5	5.52	6.97	6-23-98	<.2	.272	21.2
MW-430	42.1	3-25-94	49	6.0	--	3-25-94	<1	.2	7
		11-24-97	71	5.70	10.6	11-24-97	<.2	<.2	10.5
MW-431	49.0	--	--	--	--	4-07-94	<1	<1	.9
		11-24-97	65.2	5.85	11.0	11-24-97	<.2	<.2	1.58
SDW 309-0055	49.4	--	--	--	--	3-25-94	<1	<1	<1
		11-19-97	70.7	5.55	11.1	11-19-97	<.2	<.2	.499
SDW 314-0035	44.7	6-16-94	473	5.69	--	3-28-94	<1	<1	<1
		11-18-97	140	6.00	3.83	11-18-97	<.2	<.2	<.2
		6-25-98	185	5.81	3.86	6-25-98	<.2	<.2	<.2
SDW 314-0051	27.8	6-16-94	488	5.94	.1	3-28-94	<1	<1	<1
		11-18-97	163	5.95	.46	11-18-97	<.2	.734	9.61
		6-25-98	159	5.85	.1	6-25-98	<.2	.265	.789

Table 1. Field water-quality analyses and major volatile organic compounds analyses for water samples from wells, Cape Cod, Massachusetts, 1993–94 and 1997–98–*Continued*

Well cluster site and well number	Altitude, middle of screen (feet)	Date field parameters collected	Specific conduct-ance (µS/cm)	pH (standard units)	Oxygen, dissolved (mg/L)	Date samples collected	cis-1,2-Dichloro-ethene µg/L)	Trichloro-ethylene µg/L)	Tetrachloro-ethylene µg/L)
SDW 314-0075	4.3	6-16-94	364	5.98	0.3	3-28-94	<1	<1	<1
		11-18-97	124	5.73	7.12	11-18-97	<0.2	<0.2	<0.2
		6-25-98	152	5.64	2.81	6-25-98	<.2	<.2	<.2
SDW 314-0098	-18.9	6-16-94	84	5.73	--	6-16-94	17	3.3	10
		11-18-97	82.6	5.65	10.3	11-18-97	<.2	<.2	.271
		6-25-98	102	5.51	9.56	6-25-98	<.2	<.2	<.2
SDW 314-0108	-27.5	10-07-94	134	5.43	6	4-08-94	<1	<1	2
		11-18-97	62	5.76	11.1	11-18-97	<.2	<.2	<.2
		6-25-98	57.1	5.74	10.9	6-25-98	<.2	<.2	<.2
SDW 316-0051	45.3	10-31-94	129	4.74	8.6	6-23-94	<1	<1	<1
		11-19-97	82.1	5.13	9.56	11-19-97	<.2	<.2	.444
		6-23-98	84.6	5.05	10.3	6-23-98	<.2	<.2	<.2
SDW 316-0066	30.7	11-01-94	230	5.90	.1	6-23-94	<1	<1	<1
		11-19-97	172	6.02	.22	11-19-97	<.2	.394	33.5
		6-23-98	326	5.90	.25	6-23-98	<.2	<.2	2.74
SDW 316-0082	14.1	10-31-94	148	5.83	.1	6-23-94	<1	<1	13
		11-19-97	490	5.53	.24	11-19-97	<.2	.245	18
		6-23-98	129	5.84	.27	6-23-98	<.2	.707	19.3
SDW 316-0100	-4.1	10-31-94	156	6.39	0	6-23-94	<1	<1	13
		11-19-97	191	6.47	.01	11-19-97	<.2	<.2	.907
		6-23-98	160	6.56	0	6-23-98	<.2	<.2	3.54
SDW 316-0114	-15.8	11-01-94	169	5.55	6.9	4-13-94	<1	<1	<1
		11-19-97	442	5.31	5.87	11-19-97	<.2	<.2	<.2
		6-23-98	188	5.62	8.4	6-23-98	<.2	<.2	<.2
SDW 316-0134	-37.6	10-31-94	197	5.75	4.7	6-23-94	<1	<1	<1
		11-19-97	163	5.68	9.38	11-19-97	<.2	<.2	1.84
		6-23-98	186	5.71	8.86	6-23-98	<.2	<.2	<.2
SDW 316-0148	-50.0	11-01-94	68	5.79	10.3	4-13-94	<1	<1	<1
		11-19-97	72.8	5.63	10.9	11-19-97	<.2	.276	<.2
		6-23-98	77.7	5.73	10.6	6-23-98	<.2	<.2	<.2
SDW 316-0163	-65.3	11-01-94	81	5.52	10.2	4-13-94	<1	<1	<1
		11-19-97	81.9	5.51	10.8	11-19-97	<.2	<.2	<.2
		6-23-98	78.7	5.66	10.5	6-23-98	<.2	<.2	<.2
SDW 438-0041	43.0	11-18-97	142	5.82	2.3	11-18-97	<.2	<.2	<.2
		6-26-98	152	5.68	3.5	6-26-98	<.2	<.2	.723
SDW 440-0078	2.8	10-19-94	113	5.96	.2	3-27-94	<1	<1	7
		11-18-97	115	5.47	2.95	11-18-97	<.2	<.2	1.29
		6-26-98	164	5.13	3.74	6-26-98	<.2	<.2	9.63
SDW 467-0058	24.1	6-30-94	85	5.41	--	6-30-94	.3	<.2	.9
		3-24-98	134	5.39	9.95	3-24-98	<.2	<.2	<.2
SDW 469-0036	34.4	3-23-98	144	5.84	.065	3-24-98	<.2	<.2	.325
		6-26-98	145	5.78	.2	6-26-98	<.2	<.2	.332

Table 1. Field water-quality analyses and major volatile organic compounds analyses for water samples from wells, Cape Cod, Massachusetts, 1993–94 and 1997–98–*Continued*

Well cluster site and well number	Altitude, middle of screen (feet)	Date field parameters collected	Specific conduct-ance (µS/cm)	pH (standard units)	Oxygen, dissolved (mg/L)	Date samples collected	cis-1,2-Dichloro-ethene µg/L)	Trichloro-ethylene µg/L)	Tetrachloro-ethylene µg/L)
SDW 469-0051	19.2	3-23-98	165	6.02	0.08	3-24-98	19.2	<0.2	4.27
		6-26-98	135	5.96	.04	6-26-98	11.9	<.2	1.75
SDW 469-0066	4.5	3-23-98	148	5.85	.135	3-24-98	140	.241	0.325
		6-26-98	154	5.78	.08	6-26-98	56.7	<.2	<.2
SDW 500-0060	20.6	6-26-98	120	6.04	.07	6-26-98	1.51	<.2	<.2
SDW 500-0070	10.9	6-26-98	131	5.90	.07	6-26-98	0.451	<.2	<.2
SDW 500-0080	0.7	6-26-98	167	5.77	.13	6-26-98	7.08	<.2	.237

Evolution of a Ground-Water Sewage Plume After Removal of the 60-Year-Long Source, Cape Cod, Massachusetts: Inorganic Nitrogen Species

By Richard L. Smith, Brigid A. Rea Kumler, Thomas R. Peacock, and Daniel N. Miller

ABSTRACT

High concentrations of nitrate and ammonium in ground water are often associated with sewage disposal practices. However, little is known about the combined effect of physical and biological processes upon the long-term fate of inorganic nitrogen in ground water, particularly after the source of contamination has been removed. Discharge of treated sewage onto surface infiltration beds at the Massachusetts Military Reservation on Cape Cod for 60 years created a ground-water contaminant plume more than 3 miles long. This plume is characterized by a suboxic to anoxic, ammonium-containing core surrounded by an oxic to suboxic, nitrate-containing outer zone. Historically, the sewage effluent contained varying amounts of nitrate and ammonium (200-2000 micromolar (μM)), oxygen (about 350 μM), and dissolved organic carbon (about 1000 μM). The geochemical evolution of the up-gradient portion of the plume has been extensively monitored for 2 years following the cessation of disposal in December 1995. Although nitrate concentrations in the core of the plume increased initially after cessation, nitrate levels have gradually decreased in and below the core of the plume. Nitrate concentrations have remained elevated (about 1 millimolar (mM)) near the water table, however, well after non-reactive solutes were flushed from this zone. Ammonium concentrations initially increased after cessation, then gradually decreased to low levels. These observations indicate that, while the effluent was being discharged, nitrification of ammonium to nitrate was occurring in the aquifer under the infiltration beds and was fueled by the oxygen in the treated sewage. Following the shutoff, nitrification stopped because oxygen was no longer being introduced with the treated sewage, and oxygen consumption up-gradient of the ammonium zone prevented oxygen in uncontaminated water from reaching the ammonium zone. Thus, ammonium moved down-gradient away from the disposal area, even though ammonium transport was slowed by cation exchange.

INTRODUCTION

A major source of ground-water contamination in the United States is sewage disposal, with several million septic systems currently in operation. Sewage contamination is typically associated with high concentrations of nitrate, ammonium, and organic carbon. Although several studies have examined sewage-related ground-water contaminant plumes, little is known about the recovery of an aquifer once the contaminant source has been removed.

The composition of a contaminant plume is the result of the complex interaction between physical, biological, and hydrological processes. Often, large reservoirs of sorbed or insoluble phases associated with the aquifer solids may serve key contributory roles to this interaction. The latter is the case for organic carbon and ammonium in sewage-related plumes. Important questions, then, are: (1) how will the contamination associated with the solids continue to affect aquifer restoration after the contaminant source is removed and, (2) what will the short-term and long-term production, consumption, and migration patterns for nitrate, ammonium, and organic carbon be in such a system?

In 1995, the disposal of treated sewage at a site on Cape Cod, Massachusetts, was stopped after 60 years of continuous discharge. The major processes that are known to be affecting nitrogen species in the aquifer, either directly or indirectly, are shown in table 1. Ground-water chemistry at this site was monitored before and after cessation in considerable detail, both spatially and temporally, to follow the natural restoration of the contaminated aquifer. Particular emphasis was placed on each of these processes to determine their combined effect upon the post-cessation evolution of the contaminant plume.

Table 1. Major processes affecting nitrogen species at Cape Cod study site.

Process	Reactants	Products
Aerobic heterotrophic respiration	O_2 + organic C	CO_2
Nitrification	$NH_4^+ + O_2$	NO_3^-
Denitrification	NO_3^- + organic-C	$N_2 + CO_2$
Ammonium cation exchange	NH_4^+ + solids	retarded transport

STUDY SITE

The study site is an unconfined sand and gravel aquifer located on Cape Cod, Massachusetts (fig. 1) that has been contaminated by the disposal of treated wastewater for 60 years. The sewage was discharged onto infiltration sand beds and percolated down to the water table. The practice produced a contaminant plume that is currently greater than 3 miles long and consists of a suboxic to anoxic ammonium-containing core, surrounded by an oxic to suboxic, nitrate-containing outer zone. In December 1995 the sewage discharge to the sand beds was stopped. A long-term study was initiated by the U.S. Geological Survey to follow the dissipation of the up-gradient portion of the contaminant plume near the disposal site and to examine key processes affecting the evolution of that portion of the plume. Methods for sample collection, preservation, and analyses are detailed in Savoie and LeBlanc (1998). Wells used to construct a transect aligned with the direction of ground-water flow are shown in figure 1.

Table 2. Composition of sewage effluent in February 1995 [µS/cm, microsiemens per centimeter at 25 degrees Celsius; µM, micromolar].

Specific Conductance	516 µS/cm
Oxygen	>300 µM
Dissolved Organic Carbon	1300 µM
Chloride	1500 µM
Nitrate	1500 µM
Ammonium	180 µM
Organic nitrogen	140 µM
Nitrite	1.5 µM

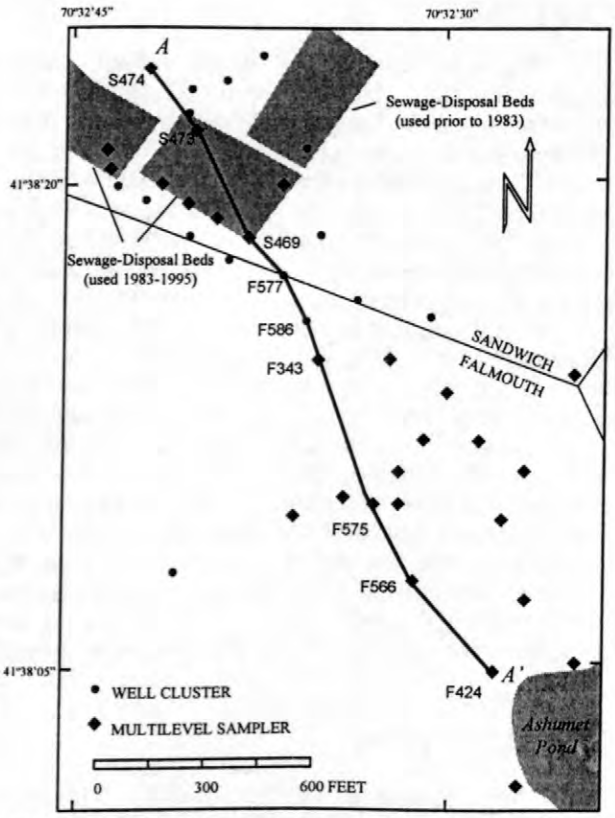

Figure 1. Ground-water study site on Cape Cod, Massachusetts, showing location of wells sampled for this study. The line depicts the longitudinal transect shown in Figures 3 and 5.

OBSERVATIONS OF GROUND-WATER QUALITY

The sewage effluent entering the aquifer prior to shutoff was well oxygenated, being in near-equilibrium with the atmosphere, and it contained dissolved nitrogen, primarily as nitrate but also as ammonium and organic nitrogen (table 2). At the time of shutoff, ground water under the infiltration beds was characterized by vertical gradients of dissolved solutes, such as oxygen, nitrate, and ammonium. The oxygen gradient at

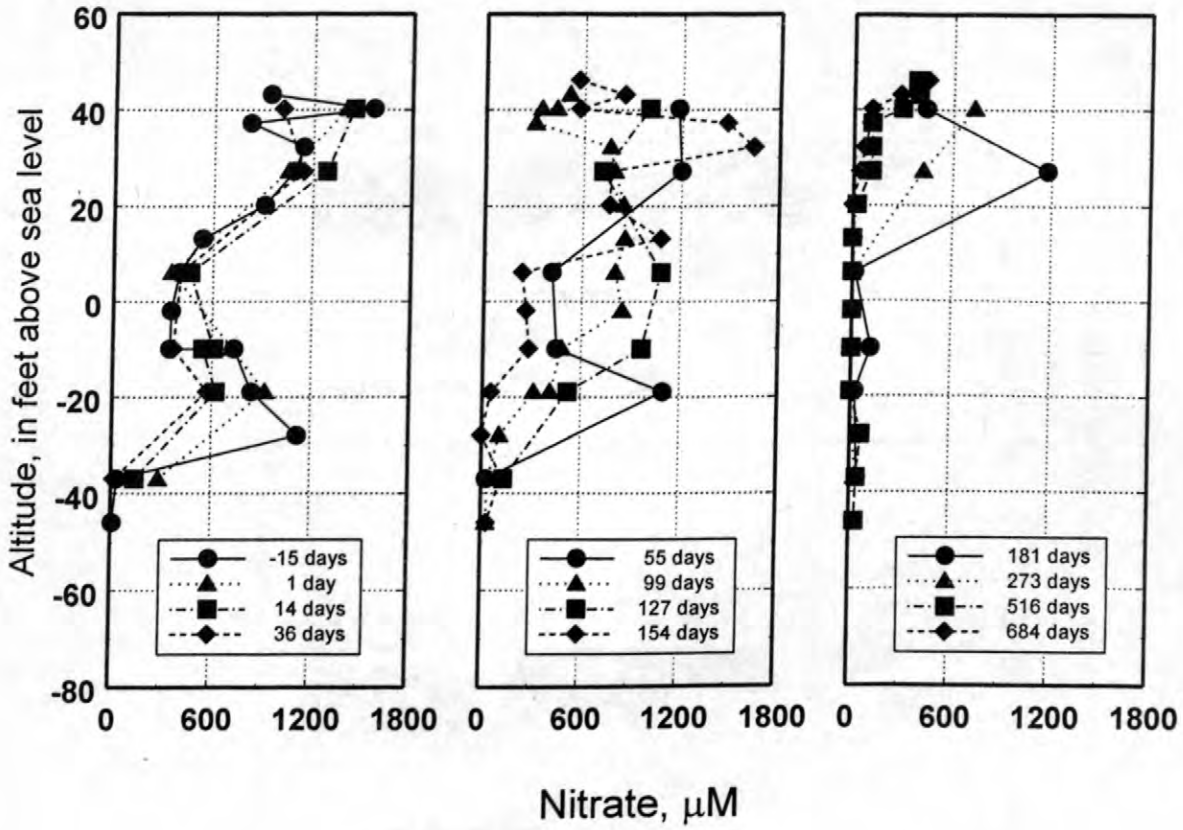

Figure 2. Depth profiles of ground-water nitrate concentrations at well site S469 relative to the date of sewage disposal cessation (December 13, 1995).

the top of the plume was approximately 10 feet thick; concentrations varied from air equilibrium (about 350 μM) at the water table to suboxic levels (less than 100 μM; data not shown) in the plume. After cessation, this gradient became narrower with time, and a second oxygen gradient, from suboxic levels in the core of the plume to oxic levels below the core, developed at the bottom of the plume (LeBlanc and others, 1999).

There was a pre-shutoff bimodal distribution of nitrate with depth under the infiltration beds. The lowest nitrate concentrations occurred in the center of the plume, with higher concentrations above and below (fig. 2). After shutoff, nitrate concentrations under the infiltration beds initially increased in the center of the plume before gradually decreasing from the bottom upward. After 273 days, nitrate concentrations exceeded 200 μM only in the shallowest samples. Along the longitudinal transect shortly after shutoff, nitrate was present at most depths throughout the contaminant plume (fig. 3), except in a zone in the center of the plume (at approximately sea level). During steady state loading prior to cessation, this zone of low nitrate concentration increased in size with downgradient transport as a result of denitrification (Smith and others, 1991, 1996). In June 1997, more than 500 days after shutoff, nitrate concentrations within 700 ft down-gradient of the infiltration beds had significantly decreased below an altitude of 30 feet, but had increased in the shallow horizons (fig. 3).

At shutoff, ammonium was present only in the center of the contaminant plume (fig. 4), even though it was present in the sewage effluent (table 2). However, ammonium concentrations increased with distance down-gradient to at least 500 feet from the beds (fig. 5). Ammonium concentrations under the infiltration beds after shutoff increased to high values at some depths (for example, 20-foot altitude), before subsequently decreasing. At greater depths, ammonium concentrations varied, but remained below 200 μM. The longitudinal transect shows that ammonium concentrations generally decreased within 700 feet of the infiltration beds by 500 days after shutoff (fig. 5).

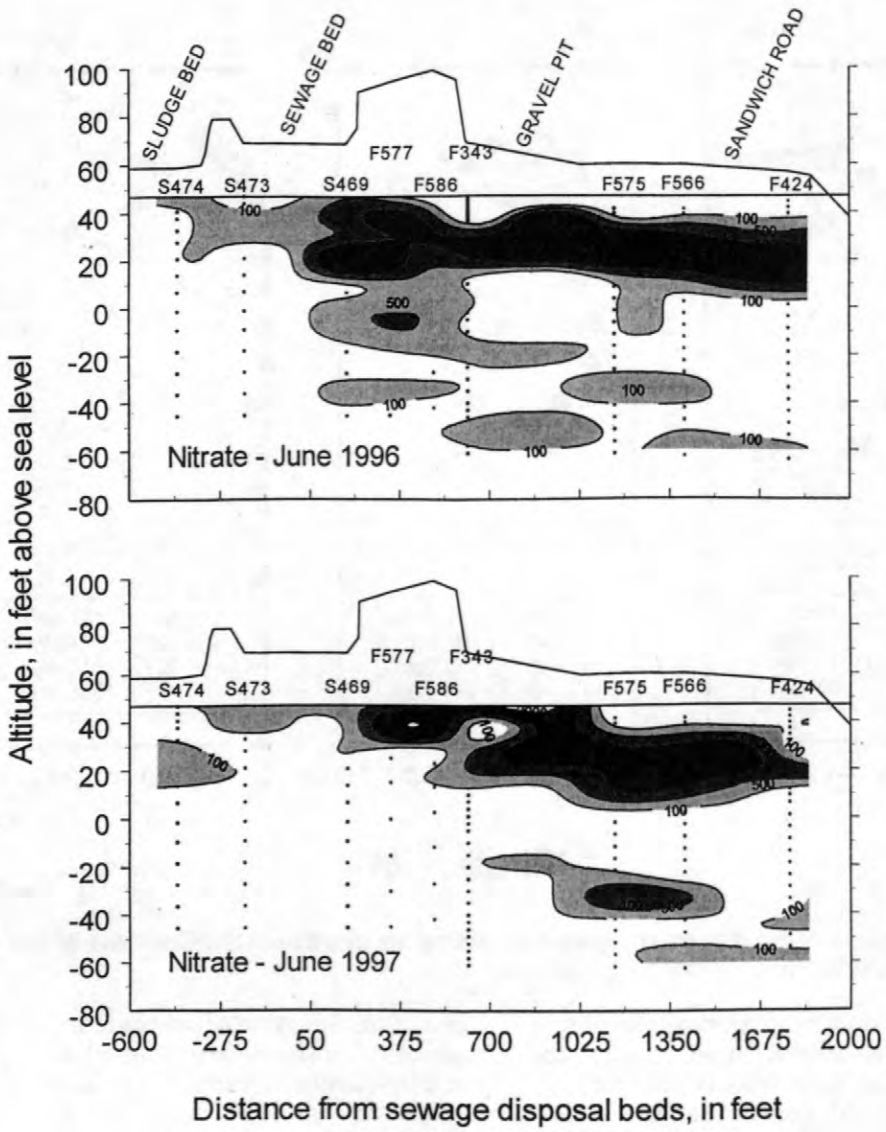

Figure 3. Longitudinal vertical section showing nitrate concentrations (μM) in ground water in June 1996 and June 1997.

PROCESSES AFFECTING INORGANIC NITROGEN SPECIES

Prior to shutoff, nitrate entered the aquifer with the sewage effluent and increased in concentration as a result of nitrification in the aerobic zone. Nitrate and any ammonium that were not oxidized were transported down-gradient, but at different rates, because ammonium transport was slowed by sorption due to cation exchange (Ceazan and others, 1989). The total ammonium pool in the contaminant plume was actually larger than indicated from ground-water concentrations alone because of the sorption. Prior to shutoff, the largest ammonium reservoir was deep below the water table. When oxygen became depleted along the flowpath, denitrification began to consume the large nitrate pool. This pool was cumulatively diminished in the core of the contaminant plume by denitrification during transport away from the beds. Ammonium persisted in this same zone because nitrification was limited by oxygen availability.

After shutoff, nitrate was still being leached from the unsaturated zone by natural recharge, but at a much lower loading rate. The combination of lower oxygen-loading and lower nitrate-loading rates allowed denitrification and ground-water flushing to significantly decrease the nitrate pool below an altitude of 10 feet (fig. 3). The denitrification was likely fueled by sorbed organic carbon. On the other hand, the remaining ammonium in the plume was transported down-gradient (fig. 5). The ammonium-containing zone remained anoxic, so nitrification did not contribute to the observed decrease in ammonium concentration. It appears

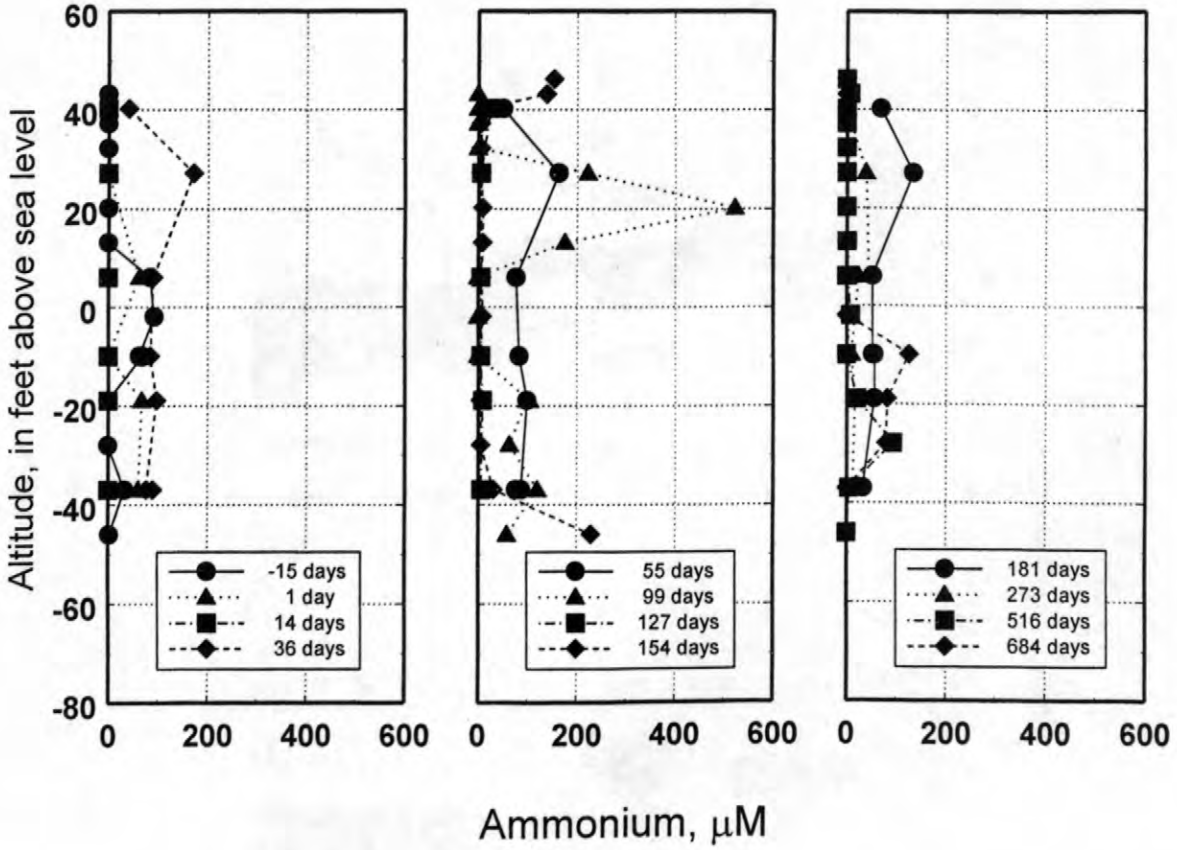

Figure 4. Depth profiles of ground-water ammonium concentrations at well site S469 relative to the date of sewage disposal cessation (December 13, 1995).

that oxygen demand at the up-gradient edge of the contaminated area was more than sufficient to remove oxygen from in-coming uncontaminated ground water, thus preserving the anoxic core. Later, as an iron reduction zone developed at well site S469 (Kent and others, 1999), ammonium was produced in the center of the plume by mineralization of organic nitrogen.

CONCLUSIONS

1) Shutoff of the contaminant source decreased the amount of oxygen delivered to the contaminant zone. Thus, the plume geochemistry became more reduced, not more oxidized as might have been predicted.

2) Although the transport of ammonium was slowed by cation exchange, the desorption and transport rates were sufficient to flush the dissolved and sorbed ammonium down-gradient away from the beds after shutoff. Nitrification was a significant process under the loading beds prior to shutoff, but not after shutoff as the geochemical environment became more reducing.

3) The total nitrate loading was significantly decreased by shutoff. However, nitrate continues to leach from the unsaturated zone 2 years later.

4) The zone of denitrification under the loading beds diminished to a rather narrow vertical interval after shutoff due to the decrease in ground-water nitrate concentrations.

REFERENCES

Ceazan, M.L., Thurman, E.M., and Smith, R.L., 1989, Retardation of ammonium and potassium transport through a contaminated sand and gravel aquifer: The role of cation exchange: Environmental Science and Technology, v. 23, p. 1402-1408.

Kent, D.B., Abrams, R.H., Campo, K.W., Rea Kumler, B.A., Stollenwerk, K.W., and Wilke, J.A., 1999, Evolution of a ground-water sewage plume after removal of the 60-year-long source, Cape Cod, Massachusetts: pH and the fate of phosphate and metals, in Morganwalp, D.W., and Buxton, H.T., eds., 1999, U.S. Geological Survey Toxic

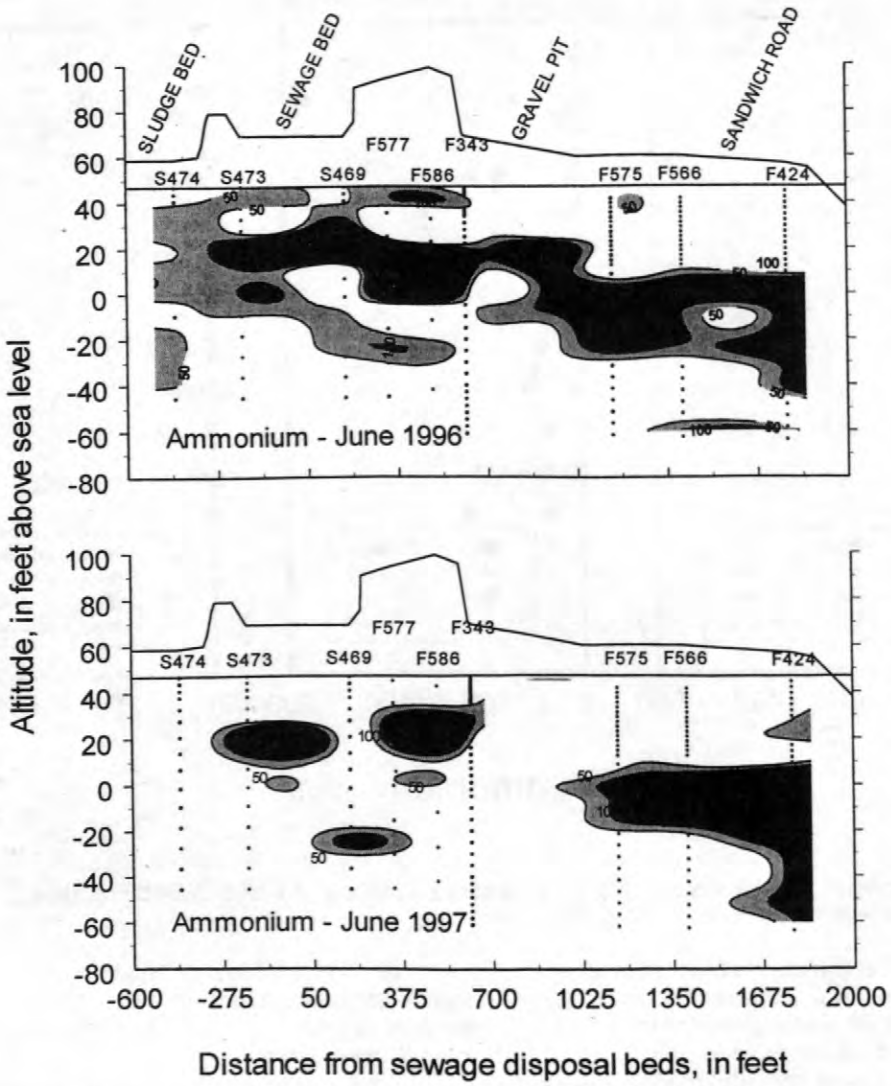

Figure 5. Longitudinal vertical section showing ammonium concentrations (μM) in ground water in June 1996 and June 1997.

Substances Hydrology Program--Proceedings of the Technical Meeting, Charleston, South Carolina, March 8-12, 1999-- Volume 3 – Subsurface Contamination from Point Sources: U.S. Geological Survey Water-Resources Investigations Report 99-4018C, this volume.

LeBlanc, D.R., Hess, K.M., Kent, D.B., Smith, R.L., Barber, L.B., and Campo, K.W., 1999, Natural restoration of a sewage plume in a sand and gravel aquifer, Cape Cod, Massachusetts, in Morganwalp, D.W., and Buxton, H.T., eds., 1999, U.S. Geological Survey Toxic Substances Hydrology Program--Proceedings of the Technical Meeting, Charleston, South Carolina, March 8-12, 1999-- Volume 3 – Subsurface Contamination from Point Sources: U.S. Geological Survey Water-Resources Investigations Report 99-4018C, this volume.

Savoie, J., and LeBlanc, D.R., eds., 1998, Water-quality data and methods of analysis for samples collected near a plume of sewage-contaminated ground water, Ashumet Valley, Cape Cod, Massachusetts, 1993-94: U.S. Geological Survey Water-Resources Investigations Report 97-4269, 208 p.

Smith, R.L., Howes, B.L., and Duff, J.H., 1991, Denitrification in nitrate-contaminated ground water: Occurrence in steep vertical geochemical intervals: Geochimica et Cosmochimica Acta, v. 55, p. 1815-1825.

Smith, R.L., Garabedian, S.P., and Brooks, M.H., 1996, Comparison of denitrification activity measurements in ground water using cores and natural-gradient tracer tests:

Environmental Science and Technology, v. 30, p. 3448-3456.

AUTHOR INFORMATION

Richard L. Smith, Brigid Rea Kumler, Thomas R. Peacock, U.S. Geological Survey, Boulder, Colorado

Daniel N. Miller, U.S. Department of Agriculture, U.S. Meat Animal Research Center, Clay Center, Nebraska

Evolution of a Ground-Water Sewage Plume After Removal of the 60-Year-Long Source, Cape Cod, Massachusetts: pH and the Fate of Phosphate and Metals

By Douglas B. Kent and Valerie Maeder

ABSTRACT

The distribution of copper (Cu), phosphorus (P), and zinc (Zn), whose fate and transport are controlled by pH-dependent adsorption, was examined as part of a multidisciplinary study of the evolution of ground-water quality in a sewage-contaminated aquifer following source cessation. Prior to source cessation, Cu and Zn were observed 10 to 20 meters below the water table under the sewage-disposal beds; most of the dissolved Cu was likely present as strongly complexed species. Down gradient of the beds, these metal ions were only observed in a narrow region near the upper boundary of the sewage plume. The initial distribution of P under the disposal beds showed considerable spatial variability and was similar to that of boron, which is assumed to be non-reactive. Examination along a flow path showed a region where dissolved P apparently was absent even though it was present both up and down gradient. After source cessation, it was anticipated that ground water under the disposal beds would become more acidic, which would lead to major changes in the mobility of these contaminants. However, pH values under the disposal beds exhibited only minor fluctuations, between 5.8 and 6.2 in the core of the contaminated region, during the 2.5 years since source cessation. This is likely related to the continued importance of anaerobic biodegradation reactions under the disposal beds. Minor changes in the distribution of Cu resulted from transport of weakly adsorbing Cu complexes away from the contaminated zone under the disposal beds. Small but consistent decreases in P concentrations suggest that P was slowly being transported away from the contaminated zone under the beds. The distribution and concentrations of both free Zn and Cu under the disposal beds did not change significantly over the 2.5 years of the study, consistent with extensive adsorption of these metal ions onto the aquifer sediments at the observed pH values.

INTRODUCTION

On December 13, 1995, disposal of secondary sewage effluent to a group of rapid infiltration beds (from here on referred to as disposal beds) was ended after nearly 60 years. Sewage disposal had caused a plume of sewage-contaminated ground water that was, at the time of source cessation, approximately 5,500 meters long, 900 to 1,700 meters wide, and 30 to 45 meters thick (Savoie and LeBlanc, 1998).

Major characteristics of the sewage plume were first described in the seminal paper by LeBlanc (1984). Since that time, a large number of investigators spanning a range of disciplines have conducted studies of the fate and transport of contaminants in the sewage plume. Source cessation provided an opportunity to study the processes that influence the evolution of ground-water quality as uncontaminated ground water flushes through the contaminated aquifer (Hess and others, 1996). This is one in a series of papers based on the results of the first 2.5 years of these investigations (see LeBlanc and others, 1999).

In this paper, we present data on the distribution of phosphorus (P), copper (Cu), zinc (Zn), and pH before and after source cessation. The fate and transport of these contaminants in

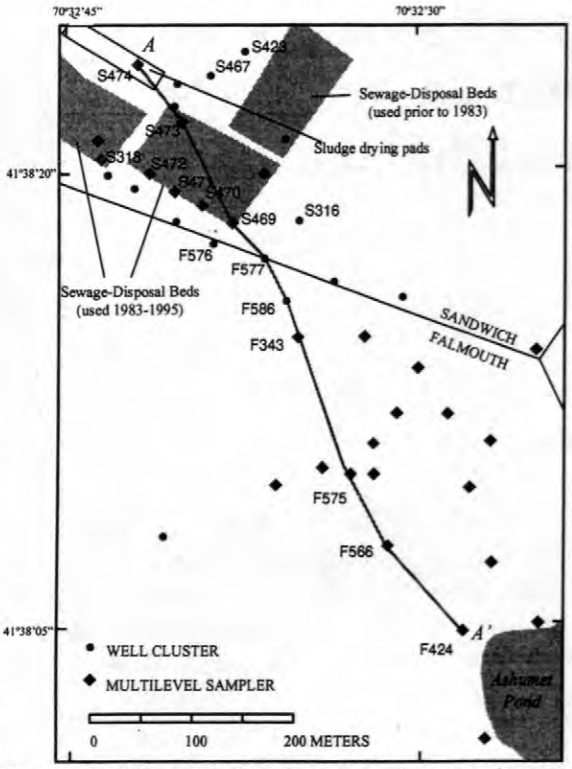

Figure 1. Site map showing sampling locations discussed in this paper. Principal line of section is also shown, along with disposal beds, sludge drying pads, boundaries between Sandwich and Falmouth townships, and a portion Ashumet Pond.

this aquifer were controlled by adsorption (Walter and others, 1996; Stollenwerk, 1996; Rea and others, 1991). The extent of adsorption of each of these contaminants is dependent on aquifer chemistry, especially pH. Boron (B) is used as a non-reactive indicator of sewage contamination (LeBlanc, 1984). It is anticipated that geochemical processes that result from the flushing of ground water up-gradient of the disposal beds through the sewage contaminated zone will profoundly influence the fate of these contaminants (Hess and others, 1996). The data are presented with the objective of illustrating the patterns that are developing, the underlying processes causing the emerging patterns, and potential complications arising from spatial and temporal variability in the source.

SITE DESCRIPTION

The network of wells established to monitor changes in water quality following source cessation is shown in figure 1 (LeBlanc and others, 1999). The line of section A-A' (fig.1) ran generally parallel to the direction of ground-water flow, which was from northwest to southeast (LeBlanc and others, 1999). It was anticipated that major changes in the distribution of many of the reactive constituents would occur slowly (Hess and others, 1996). Consequently, it was decided to install monitoring instrumentation in the disposal beds. Two sets of disposal beds (each set, shown as a block in fig. 1, was comprised of 4 individual beds) were actively used from 1983 until source cessation. A few wells already existed in one of the sets of disposal beds (the set with S317 and S318, fig. 1). It was decided to instrument the other set of four beds, which are directly to the east, because this set of disposal beds lies directly up gradient of a heavily instrumented area for which a considerable body of knowledge of ground-water composition and processes influencing transport had been accumulated.

METHODS

Ground-water samples were collected as described in Savoie and LeBlanc (1998) and filtered through a 0.45 micrometer Millex filter (Millipore Corp, the use of trade or product names in this report is for identification purposes only and does not constitute endorsement by the U. S. Geological Survey). All samples were preserved by acidification to pH 2 with trace-metal grade hydrochloric or nitric acid. Dates on which the ground-water samples used in the various figures in this report were collected are given in Table 1.

In order to provide additional information about metal ion speciation, filtered ground-water samples from selected locations were passed through cartridges packed with Chelex (Alltech brand cartridge columns) and preserved by acidification as described above. Chelex is a cation exchange resin with a high specificity for multivalent cations. Laboratory tests showed that free Cu, manganese (Mn), Zn, and other metals were removed from water samples passed through the cartridges at flow rates less than 20 ml/min, in agreement with the manufacturer's recommendations. Higher flow rates often resulted in some passage of free metal ions

Table 1. Sampling dates for the data presented in figure 2 through 5 (Month/Day/Year)

Location.	Figure Number	Date Sampled
F343	4	6/17/96
F577	4	6/21/96
F586	4	6/15/96
S318	3	11/29/95, 5/14/96
		5/07/97, 5/11/98
S469	2, 5	11/28/95
	4, 5	5/15/96
	5	5/12/97, 5/07/98
S470	2	11/29/95
S471	2	11/29/95
S472	2	11/30/95
S473	4	5/16/96
S474	4	5/16/96

through the cartridges. In addition, use of a cartridge whose capacity to take up free metal ions had been exhausted could result in passage of free metal ions through the Chelex. An examination of the data set (91 samples as of June 1998) showed that approximately 10 percent of the Chelexed samples likely exhibited artifacts related to one of these causes. Over the entire data set, Mn and Zn were either both absent (approximately 90 percent of the samples) or both present at low concentrations in Chelexed samples. Thus, it was concluded that the presence of Mn and Zn in Chelexed samples indicated that the speciation data were suspect and should not be given further consideration.

Considerable care was required to obtain pH values that were reliable and reproducible. Using the methods described in Busenberg and Plummer (1987), it was found that flushing-junction Ross electrodes (Orion) consistently were capable of making accurate pH determinations in the poorly buffered, low-ionic strength ground-water samples from the sewage plume. Experience had shown that reproducible pH values required relatively large sample volumes and moderately long equilibration times, and often required preconditioning of the electrode in the field. The following standard protocol achieved these objectives and was applied to all samples collected after September 1995. Two, 250 ml (milliliter) samples were collected and capped so that headspace was minimized. The pH electrode was calibrated in the field against standard buffers that were stored at or near 12 °C (degrees Celcius), which is close to the temperature of the ground water. The electrodes were not considered calibrated until the pH of the buffers could be reproduced, which sometimes required several calibration cycles. After calibration, the pH electrode was placed in the first 250 ml ground-water sample for approximately 5 minutes. This eliminated memory effects from the buffers. The pH electrode was then placed in the second 250 ml sample, after rinsing with the sample and allowed to equilibrate. Stable pH values were usually achieved within 2 or 3 minutes, but occasionally required up to 5 minutes. The reproducibility of pH values determined using this protocol was excellent (generally within 0.03 pH units).

Ground-water samples were analyzed for a suite of inorganic solutes using inductively coupled plasma atomic absorption spectroscopy (ICAP-AES) as described elsewhere (Coston and others, 1998). Values of the relative precision and accuracy for concentrations of Cu, P, and Zn were better than 10 percent, which is sufficient for the conclusions drawn in this paper (Coston and others, 1998).

RESULTS AND DISCUSSION

Spatial heterogeneity in contaminants prior to source cessation

Vertical profiles of pH and concentrations of B, P, Cu, and Zn from the four wells along a transect across the eastern set of disposal beds active at the time illustrate the complications owing to spatial and possibly temporal heterogeneity of the source (fig. 2). (All concentrations refer to total dissolved concentration, unless specified as referring to a particular species or set of species.) Profiles in figure 2 are arranged according the position of the wells along a northwest-southeast trending boundary of the set of disposal beds (fig. 1). The B-contaminated region (indicated by

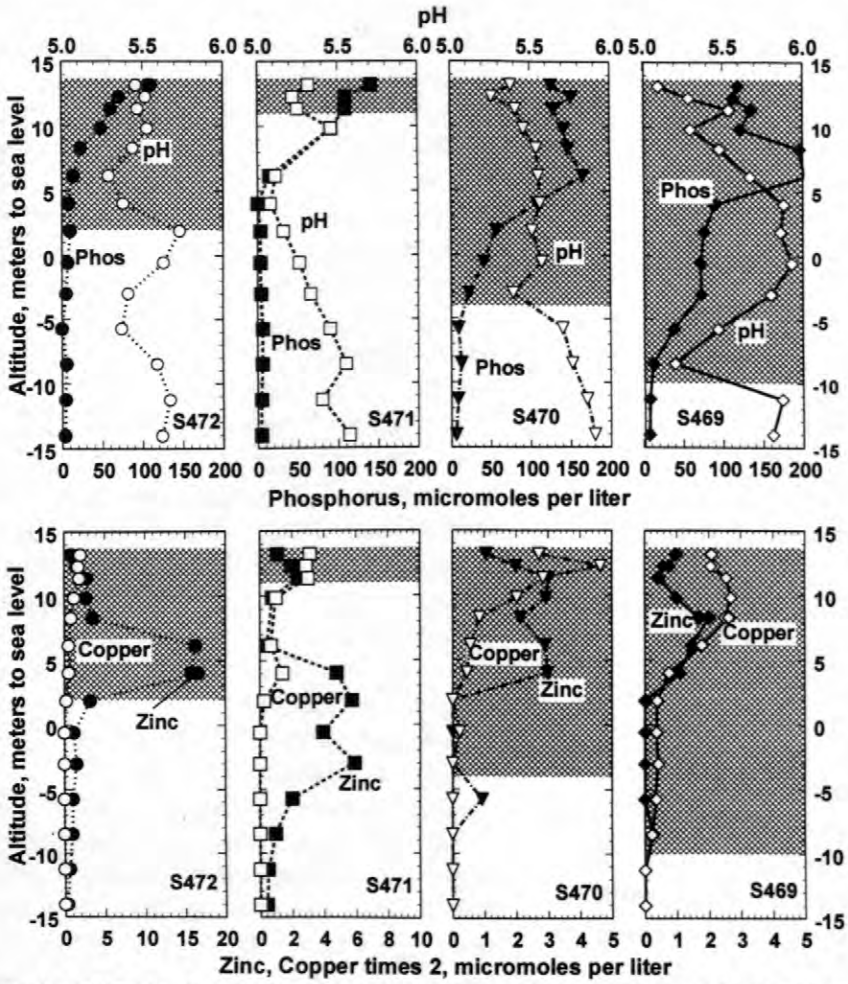

Figure 2. Vertical profiles for P, pH, Zn, and Cu at S472, S471, S470, and S469 in November 1995, before source cessation. Shaded areas show B-contaminated region. Note scale changes between different wells.

shading in fig. 2) at S469 shows that the sewage plume extended from the water table to approximately 10 meters below sea level in November 1995. The depth of the lower boundary of the B-contaminated region decreased to the west from S469 to S471 and then increased from S471 to S472. Similar results were obtained from an examination of the profiles of specific conductance determined in September 1995 (Hess and others, 1996).

The distribution of P contamination differed somewhat from that of B. Ortho phosphate constituted all of the dissolved P determined by ICAP-AES in sewage effluent and sewage-contaminated ground water. At S469 and S470, P was observed throughout the zone with significant B concentrations (fig. 2). At S472, P concentrations decreased to very low values approximately 4 meters above the current lower boundary of the sewage-contaminated zone. The data from S471 suggest that P contamination may have extended below the current boundary of the sewage contaminated zone. Similar relationships between P and specific conductance were evident during September 1995 (Hess and others, 1996).

The distribution of total dissolved Cu and Zn provide a different picture of the distribution of sewage contaminants (fig.2). A set of field tests conducted in September 1994 showed that particulate and colloidal material did not contribute to the observed concentrations of Cu and Zn in ground-water samples collected from under the disposal beds (Savoie and LeBlanc, 1998). Thus, Cu and Zn concentrations presented

in this paper can be considered to represent truly dissolved species of these metals. In contrast to B and P, dissolved Cu was observed down to a similar depth at S472, S471, and S470; Cu was observed throughout the B-contaminated region at S469. Maximum concentrations of Cu exceeded published values for dissolved Cu in the effluent, which are in the range 0.5 to 0.8 μM (micromoles per liter) (Vaccaro and others, 1979; Savoie and LeBlanc, 1998). At S469 and S470, dissolved Zn was observed down to the same depth as Cu; maximum Zn concentrations were greater than those reported for the sewage effluent (0.5 to 0.7 μM). Farther west, at S471 and S472, dissolved Zn was observed deeper in the aquifer. Maximum Zn concentrations were about 6 μM at S471 and 16 μM at S472, were associated with low pH values, and were located at or below the lower boundary of the current sewage-contaminated zone.

In all samples collected prior to or shortly after source cessation with detectable concentrations of Cu, a significant fraction of Cu passed through Chelex. Speciation data for Cu and Zn from selected samples from S469 at an altitude of 8.3 meters to sea level are presented in Table 2. The complexed and free concentrations were determined operationally from the concentration in the Chelexed sample and difference in concentrations between the filtered and Chelexed samples, respectively. Prior to and for the first month after source cessation, concentrations of complexed and free Cu remained constant near 1 μM and 0.4 μM, respectively. These data suggest that most of the dissolved Cu detected early in the study was in the form of strong complexes. Speciation data from S469 at an altitude of –5.8 meters to sea level showed that 100 percent of the Cu detected was in the form of strong complexes. The ligands complexed with Cu were not identified and could have been synthetic ligands in the sewage effluent, products of organic matter diagenesis, or microbial exudates. Synthetic ligands such as ethylenediaminetetraacetic acid (EDTA) and nitrilotriacetic acid (NTA), which have high affinities for Cu, have been detected in sewage-contaminated ground water in the vicinity of the disposal beds at concentrations in the range 0.1 to 1 μM (Barber, 1998). These synthetic ligands generally have greater affinity for Cu than for Zn, which may account for the absence of strongly complexed Zn in the sewage-contaminated ground water.

Table 2. pH and concentrations of free zinc and copper (micromoles per liter) in samples taken at various times (Month/Day/Year) from S469 at an altitude of 8.3 meters to sea level.

Date	pH	Zn (μM)	Cu (μM)	
		Free	Free	Complexed
11/28/95	5.48	2.02	0.40	0.92
12/27/95	5.62	2.26	0.34	0.97
1/4/96	5.54	2.26	0.37	0.99
2/6/96	5.79	2.05	0.23	0.72
3/21/96	5.63	1.71	0.23	0.66
5/15/96	5.80	1.74	0.33	0.75
9/11/96	6.00	1.04	0.10	0.29
2/3/97	6.01	0.93	0.13	0.14
10/27/97	5.94	1.04	0.17	0
5/7/98	5.82	1.36	0.14	0

The pH is a critical factor in understanding the fate and transport of P, Cu, and Zn (Rea and others, 1991; Stollenwerk, 1996; Davis and others, 1998). This is because most of the sewage-derived P, Cu, and Zn in the aquifer was adsorbed to the sediments at the time of source cessation (Rea and others, 1991; Coston and others, 1995; Walter and others, 1996; B. A. Rea, U. S. Geological Survey, unpublished data). Adsorption of P decreases with increasing pH (Stollenwerk, 1995) and adsorption of both Zn and Cu increase with increasing pH (Rea and others, 1991; Coston and others, 1995; Davis and others, 1998).

Values of pH at the 4 wells under the eastern set of disposal beds were between 5 and 6 (fig. 2). The highest pH values in the current sewage-contaminated zone were observed near sea level at S469, which was in the core of the current sewage-contaminated region. The lowest pH values in the sewage-contaminated zone were observed near its lower boundary at S472.

The association of low pH values with high concentrations of Zn relatively deep in the sewage plume is consistent with the results of reactive

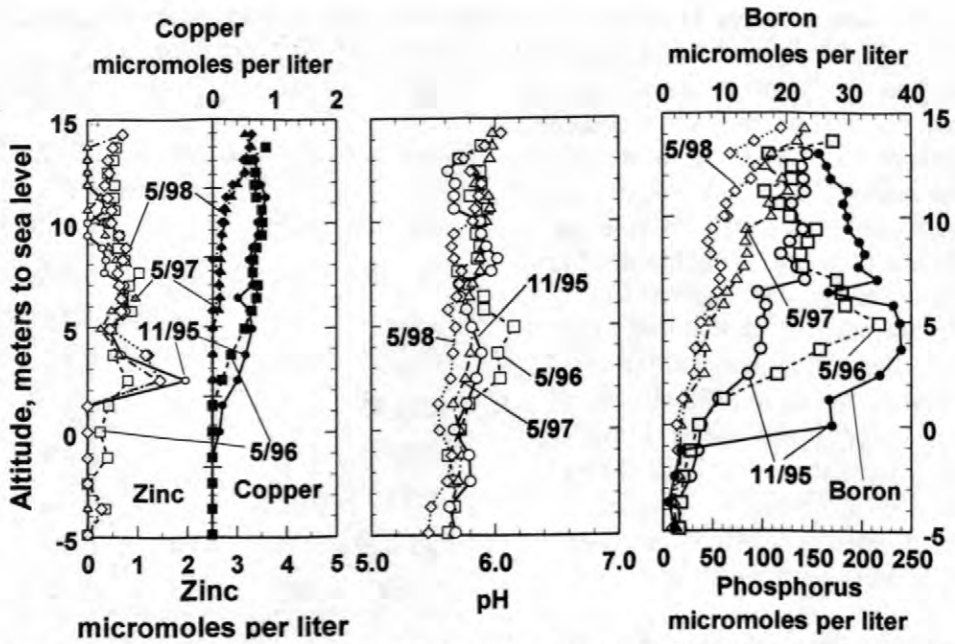

Figure 3. Vertical profiles for Zn, Cu, pH, and P for various times from S318; a vertical profile for B from November of 1995 is also shown.

transport model calculations (Kent and others, 1999). These calculations suggest that prolonged exposure of sewage-contaminated sediments to the mildly acidic pH values characteristic of uncontaminated ground water can lead to mobilization of Zn and the occurrence of high concentrations of Zn after tens of meters of transport through Zn-contaminated sediments. Plausible sources up gradient of S472 include the sludge drying pads (fig. 1) and a set of disposal beds that were used in the middle-to-late 1970's (Vaccaro and others, 1979; see also the areal photograph in LeBlanc, 1984).

The distribution of contaminants at S318, which is located at the southeast corner of the western set of disposal beds that had been active prior to source cessation, is shown in figure 3. The B concentration profile from November 1995 shows that the sewage contaminated zone at S318 was not as thick as at S469. Phosphorus concentrations decreased to low values near the lower boundary of the B-contaminated zone, in agreement with what was observed at S469 and S470. Dissolved Cu and Zn were observed down to an altitude of approximately sea level. There is a striking contrast between the similarity in thickness of the regions contaminated with Cu and Zn at S318, S469, and S470 and the difference in thickness of the regions contaminated with B at the 3 sites. This contrast suggests that at least some of the observed Cu and Zn originated from adsorbed reservoirs of these metal ions resulting from prior disposal practices. Values of pH at S318 in November 1995 varied between 5.6 and 5.8. These results are similar to those from samplings conducted throughout the 1990's (Rea and others, 1991, Savoie and LeBlanc, 1998; Hess and others, 1996).

Evolution of ground-water chemistry along a flow path through the disposal beds

Ground-water quality parameters for a line of wells generally situated along a flow line are shown in figure 4. The data came from samplings conducted approximately 6 months after source cessation (Table 1) because F586 and F343 were not sampled until this time. Minor differences in pH and the concentrations Cu, P, and Zn were observed during the first six months under the disposal beds (see discussion below). It would take ground water greater than 6 months to travel from the disposal beds to F586, so conditions

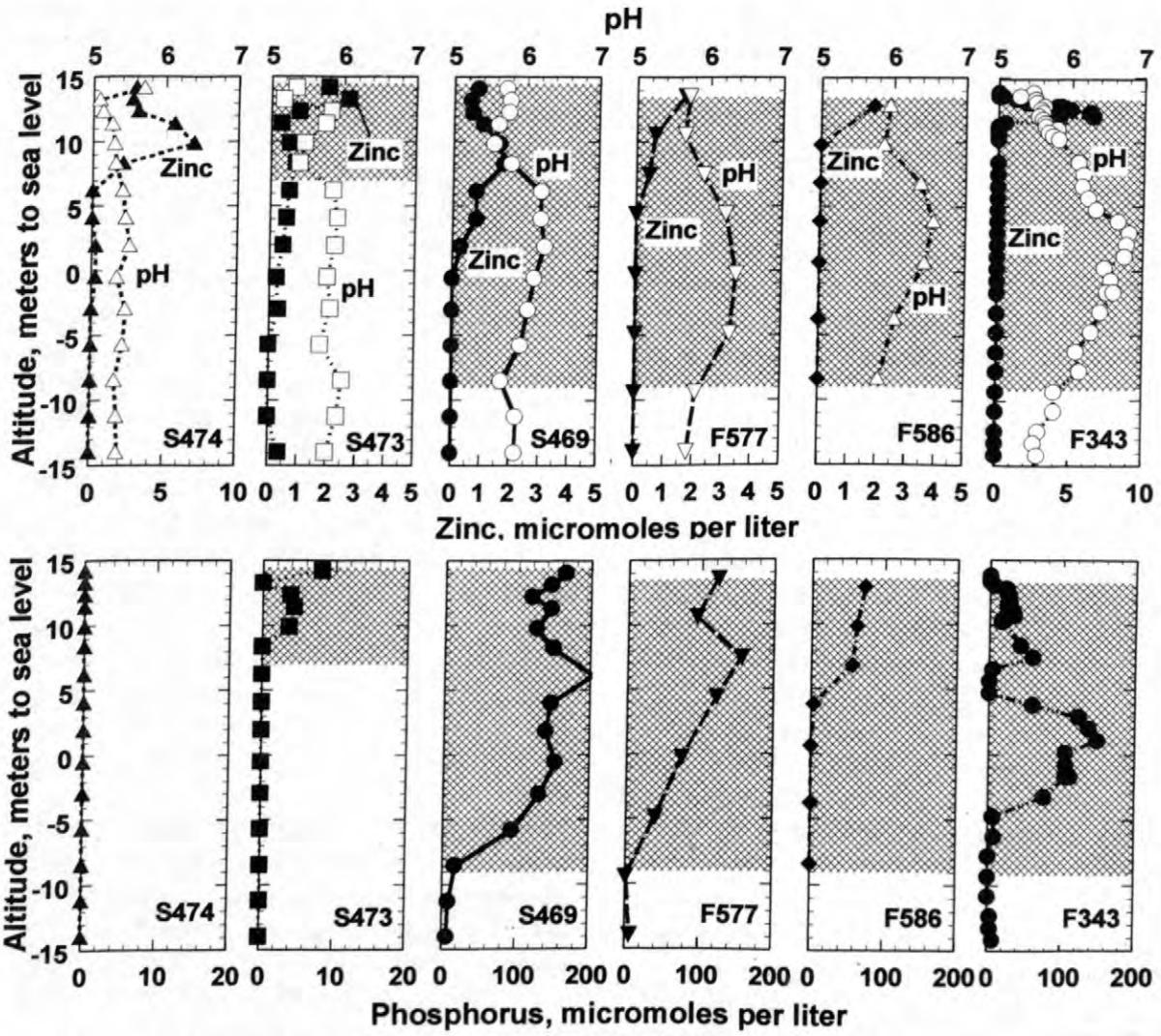

Figure 4. Vertical profiles for P, pH, and Zn for wells situated along a transect approximately parallel to a flow line. All data were from samples collected in May-June 1996 (Table 1). Panels are arranged such that distance down gradient increases from left to right. Shading shows region contaminated with B. Note scale changes for P and Zn.

there and at F343, which is located farther down gradient, should not have been affected by source cessation.

The thickness of the B-contaminated region increased across the disposal beds from S473 to S469. Boron concentrations at S474 were uniformly less than those indicative of sewage-contamination. The thickness of the B-contaminated region showed little change with distance down gradient of S469. The B concentration profile from F343 was similar to those published previously from samplings conducted between 1991 and 1995 (Kent and others, 1994; Walter and others, 1996; Busey and Walter, 1996).

The reactivity of P in the sewage plume is illustrated by the changes in its distribution with distance down gradient shown in figure 4. Phosphorus concentrations were below detection at S474 and at other locations up-gradient of the sewage disposal beds (fig.1), such as S467 (single well screened at 7.3 meters to sea level) and S423 (two wells, screend at 9.6 and –2.5 meters to sea level, respectively). Low concentrations of P were detected at S473 above an altitude of 8.4 meters (fig. 4). In the upper part of the sewage plume

(above about 6 meters to sea level), P concentrations decreased with distance down gradient from S469 to F343. In the vertical center of the sewage plume, P concentrations first decreased with distance down gradient from S469 to F586, where P was not detected below 4 meters to sea level, and then increased from F586 to F343. At F343, the 10-meter-thick region centered at sea level where the peak in P was observed corresponds to the region where concentrations of Fe(II) (iron in the plus 2 oxidation state) greater than 100 μM were observed. Low concentrations (0.3 to 1 μM) of Fe, presumably present as Fe(II), were detected at both F586 and F577 in this region of the aquifer.

Changes in P concentrations between F577 and F343 in the core of the sewage plume suggest the existence of a "phosphorus hole" in the sewage plume. This observation is probably not a result of the way in which the section was drawn. It is unlikely that F586 intersects flow paths that traveled through a region of the aquifer with significantly different P concentrations near sea level than were observed at F577. Profiles from well clusters on either side of F577 (F576 and S316, fig. 1) showed that there were significant concentrations of P near sea level at these locations. Similar P concentration profiles have been observed repeatedly at all of these locations during the 2.5 years of this investigation, thus, these results are not anomalous. The results suggest that there was a sink for P up gradient of F586 and a source of P down gradient of F586. Alternatively, it is possible that P was traveling through this region of the aquifer as filterable material. Colloidal ferrous phosphate was identified at F343 during a study conducted in 1985 (Gschwend and Reynolds, 1987), although subsequently, in 1994, it was shown that colloidal P did not account for a significant fraction of the total P in ground-water samples from F343 (Savoie and LeBlanc, 1998). Furthermore, turbidity determinations in samples from F586 were not significantly higher than those determined elsewhere in the sewage-contaminated zone. Identifying the processes responsible for the phosphorus hole will require further investigation.

Significant concentrations of Zn were observed up gradient of the disposal beds (S474 in fig. 4). Similar concentrations of Zn were reported previously in ground-water collected from a cluster of wells nearby S474 sampled in September 1992. However, Zn was below detection in ground water from S467 and S423, which also are up gradient of the disposal beds (fig. 1). The distribution of Zn at S473 was similar to that at S469 (fig. 4). Down gradient from S469, the thickness of the Zn-contaminated region decreased. At F577, Zn was observed down to an altitude of about +7 meters. At F586 and F343, Zn was observed only in a narrow region near the top of the sewage plume.

Vertical profiles for Cu at S474, S473, and S469 were similar to those for Zn shown in figure 4, except that Cu concentrations generally were lower (see fig. 2 for Cu at S469). At F577 and F586, Cu was detected only above an altitude of +13 meters; concentrations were 0.7 and 0.4 μM at F577 and F586, respectively. Copper was not detected at F343. As with Zn, Cu was not detected at either S467 or S423.

Values of pH in the sewage plume varied significantly with distance down gradient (fig. 4). The pH profile from S474 showed that ground water up gradient of the disposal beds was acidic. Similar pH values were observed at S467 and S423. Profiles of pH from S473 and S469, located at the up-gradient and down-gradient corners of disposal beds, were similar (fig. 4). From S469, pH values in the sewage-contaminated zone generally increased with distance down gradient.

Changes in pH with distance down gradient are consistent with those expected from the principal redox (oxidation-reduction) reactions associated with microbial metabolism of organic matter. Abrams and others (1998) calculated the pH changes expected in ground water initially at pH 5.5 during a series of biodegradation reactions. After metabolism of sufficient organic matter to consume 250 μM dissolved oxygen, the pH had decreased from 5.5 to 5.3. Subsequent consumption of 250 μM nitrate by denitrification resulted in a pH of 5.9. Subsequent production of 250 μM Fe(II) by microbial reduction of ferric hydroxide resulted in a pH of 6.5. The pH data through the core of the plume (near sea level) show this same trend. Water quality data from May-June 1996, in agreement with those from prior to source cessation (LeBlanc and others, 1999), suggested that denitrification prevailed in the core of the plume from S473 to F586 where pH values

increased from 5.8 to 6.2 (fig. 4). Down gradient of F586, the data suggest that Fe-reduction prevailed. Concentrations of Fe(II) at F343 in the core of the plume, where pH values were about 6.8 (fig.4), were in the range 200 to 500 μM.

Changes in water quality after cessation of the source

Flushing of uncontaminated ground water through the sewage-contaminated zone resulted in significant decreases in concentrations of non-reactive constituents. Six months after source cessation, B concentrations at S469 had decreased by 50 percent at sampling ports near sea level to 80 percent at ports near the lower boundary of the plume; B concentrations at sampling ports above sea level had not changed significantly (see LeBlanc and others, 1999). This phenomenon, where non-reactive constituents disappeared from "the bottom up," was observed consistently throughout the study, and is interpreted as being indicative of the shape of the sewage plume prior to source cessation (LeBlanc and others, 1999). By May 1997, B concentrations at S469 had decreased to less than 10 μM throughout the profile. By May 1998, B concentrations at S469 were similar to those at S474 (data not shown).

Changes in B concentrations and specific conductance over the 2.5-year period since source cessation were observed throughout the study area (LeBlanc and others, 1999). Changes in the distributions of Cu, P, and Zn, however, have thus far only been observed at sampling locations in the sewage disposal beds. In the following paragraphs, the principal changes observed at S469 and S318 are presented.

Values of pH increased throughout the profile at S469 from November 1995 to May 1996 (fig. 5). Over the next two years, pH values generally decreased. By May 1998, pH values were approximately 5.8 throughout the profile (fig. 5). Similar changes in the pH profile were observed at S318 (fig. 3). During the same period, pH values at S474 remained constant except near the water table. The absence of major pH changes in the sewage-contaminated zone under the disposal beds likely was related to the absence of major changes in microbial redox processes.

During the first 6-month period after source cessation, P increased in the middle and lower parts of the sewage contaminated zone at S469 (fig.5). Over the following 2-year period, P concentrations decreased throughout the profile. Similar changes in P were observed at S318 (fig. 3).

No significant changes in the distribution of Zn contamination were observed over the 2.5-year period following source cessation at either S469 or S318 (figs. 3 and 5). At individual sampling ports, fluctuations in Zn concentrations were observed. These fluctuations generally mirrored fluctuations in pH. For example, at the sampling port in S469 located at an altitude of +8.3 meters, the Zn concentrations were 2.0 μM, 0.9 μM, and 1.4 μM in November 1995, May 1997, and May 1998, respectively. During the same period, pH values were 5.48, 6.03, and 5.82, respectively (Table 2). These changes are consistent with those expected from changes in Zn adsorption with pH for a system with approximately 100 μM total Zn, most of which is adsorbed to the aquifer sediments.

In contrast to Zn, decreases in Cu concentrations were observed at both S469 and S318 (figs. 3 and 5). Concentrations of Cu decreased from November 1995 to May 1997, after which time little if any decrease can be discerned. This is surprising considering that Cu should adsorb more strongly to aquifer sediments than Zn and, therefore, should be less mobile. The speciation data at +8.3 meters to sea level at S469 provide a hypothesis to explain this observation (Table 2). Concentrations of Cu complexes decreased from approximately 1 μM to below detection from the time of source cessation to October 1997. After this time, only uncomplexed Cu was observed. These data show that decreases in Cu concentrations between November 1995 and May 1997 resulted primarily from decreases in the concentration of complexed Cu. Complexes of Cu with EDTA are weakly adsorbed under the chemical conditions in the sewage-contaminated zone and, therefore, are mobile. Thus, changes in Cu concentrations with time could result from mobilization of Cu in the form of weakly adsorbing complexes.

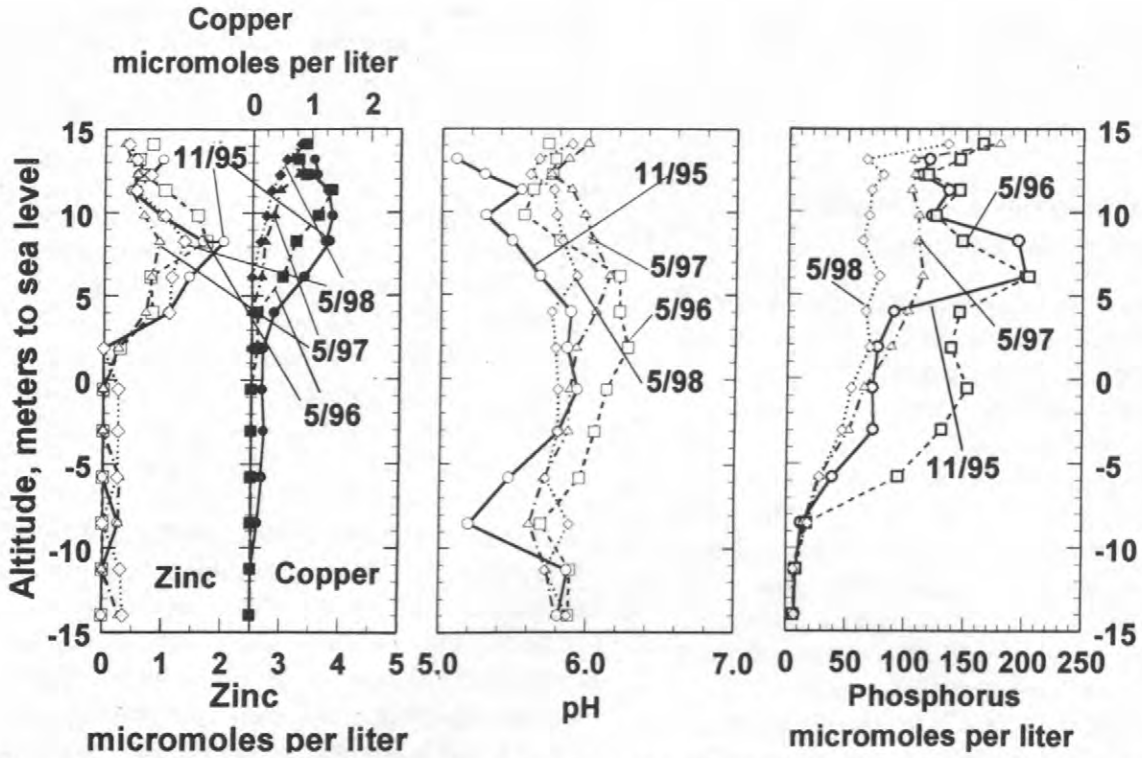

Figure 5. Vertical profiles for Zn, Cu, pH, and P for various times from S469. See Table 1 for sampling dates.

CONCLUDING REMARKS

The distribution of Cu, P, and Zn under the disposal beds prior to source cessation reflects the adsorption properties of the solutes, the spatial variability in effluent loading to the beds since their reactivation in 1983 (Hess and others, 1996), and, possibly, variability in the location and composition of disposal over the 60-year history of operation of the sewage treatment facility. Phosphorus was not present at significant concentrations in ground water up gradient of the beds. Its depth of penetration in the aquifer depended on vertical transport, as retarded by adsorption, associated with vertical flow under the disposal beds caused by effluent loading. In contrast, Cu and Zn were present in ground water up gradient of the disposal beds. Transport along flow paths pushed underneath the disposal beds by effluent loading provides an additional possible mechanism for transporting these metals to the depths they were observed. Because extensive adsorption of these metal ions greatly limits their mobility, their existence deeper in the aquifer than P and B may be a vestige of disposal to these beds prior to their reactivation, or to slow transport from abandoned disposal beds located farther up gradient. These various hypotheses will be tested using 1- and 2-dimensional flow and transport models.

Major changes in the distributions of Cu, P, and Zn were not observed during the first 2.5 years following source cessation. Speciation data suggest that the observed decreases in Cu concentrations resulted from the transport of weakly adsorbing Cu complexes away from the disposal beds. The data also suggest that minor decreases in P concentrations have occurred as a result of desorption of P from sediments in response to exposure of sewage-contaminated sediments to ground water with lower P concentrations from up gradient. The distribution of Zn has not changed significantly.

Decreasing pH values should result in mobilization of Zn from the sewage-contaminated sediments (Kent and others, 1999). Two processes should eventually lead to decreasing pH in the

sewage-contaminated zone under the disposal beds. First, ground water from up gradient of the disposal beds has lower pH values than ground water under the disposal beds. Second, biodegradation of organic matter by oxygen generates carbonic acid (Abrams and others, 1998). Two sets of processes counteract the acidification of ground water under the disposal beds. Weakly acidic and basic functional groups on sediment surfaces should act as pH buffers in the system. Preliminary modeling conducted by K. G. Stollenwerk, (U. S. Geological Survey, oral communication, 1998), suggests that the pH buffering capacity of the sediments is sufficient to retard the front of low-pH ground water somewhat, but not nearly as much as has been observed. Second, the principal anaerobic microbial biodegradation reactions (denitrification, Mn reduction, and Fe reduction) consume acid (Abrams and others, 1998). The low concentrations of dissolved oxygen in the sewage-contaminated zone under the disposal beds observed prior to source cessation (Hess and others, 1996) have not increased significantly over the 2.5 years since source cessation (LeBlanc and others, 1999). Indeed, there is evidence that the disappearance of nitrate from the sewage-contaminated region under the eastern set of disposal beds has lead to the onset of Fe reduction (LeBlanc and others, 1999). It appears that microbial biodegradation reactions in the sewage-contaminated zone under the disposal beds result in a net consumption of acid, which contributes to the neutralization of acid being transported into the system from up gradient. This underscores the importance of careful consideration of the principal biodegradation reactions in predictive models of the fate of these strongly adsorbed contaminants.

REFERENCES

Abrams, R.H., Loague, Keith, and Kent, D.B., 1998, Development and testing of a compartmentalized reaction network model for redox zones in contaminated aquifers: Water Resources Research, v. 34, no. 6, p. 1531-1541.

Barber, L. B., 1998, Organic carbon fractionation and specific organic compounds, in Savoie, J., and LeBlanc, D. R., eds., Water-quality data and methods of analysis for samples collected near a plume of sewage-contaminated ground water, Ashumet Valley, Cape Cod, Massachusetts, 1993-94: U.S. Geological Survey Water-Resources Investigations Report 97-4269, p. 16-19.

Bussey, K.W., and Walter, D.A., 1996, Spatial and temporal distribution of specific conductance, boron, and phosphorus in a sewage-contaminated aquifer near Ashumet Pond, Cape Cod, Massachusetts: U.S. Geological Survey Open-File Report 96-472, 44 p.

Busenberg, E. and Plummer, L. N., 1987, pH measurement of low-conductivity waters. U. S. Geological Survey Water-Resources Investigations Report 87-4060, 22 p.

Coston, J. A., Abrams, R. H., and Kent, D. B., 1998, Selectd inorganic solutes, in Savoie, J. , and LeBlanc, D. R., eds., Water-quality data and methods of analysis for samples collected near a plume of sewage-contaminated ground water, Ashumet Valley, Cape Cod, Massachusetts, 1993-94: U.S. Geological Survey Water-Resources Investigations Report 97-4269, p. 19-21

Coston, J.A., Fuller, C.C., and Davis, J.A., 1995, Pb^{2+} and Zn^{2+} adsorption by a natural aluminum- and iron-bearing surface coating on an aquifer sand: Geochimica et Cosmochimica Acta, v. 59, p. 3535-3547.

Davis, J. A., Coston, J. A., Kent, D. B., and Fuller, C. C., 1998, Application of the surface complexation concept to complex mineral assemblages, Environmental Science and Technology, v. 32, p. 2820-2828

Gschwend, P.M., and Reynolds, M.D., 1987, Monodisperse ferrous phosphate colloids in an anoxic groundwater plume: Journal of Contaminant Hydrology, v. 1, no. 3, p. 309-327.

Hess, K.M., LeBlanc, D.R., Kent, D.B., and Smith, R.L., 1996, Natural restoration of a sewage-contaminated aquifer, Cape Cod, Massachusetts, in Hydrology and hydrogeology of urban and urbanizing areas, proceedings of the conference, Boston, Mass., April 21-24, 1996: Minneapolis, Minnesota,

American Institute of Hydrology, p. WQE13-WQE25.

Kent, D. B., Davis, J. A., Abrams, R. H., and Coston, J. A., 1999, Modeling the influence of adsorption on the fate and transport of metals in shallow ground water: Zn contamination in the sewage plume on Cape Cod, Massachusetts, Morganwalp, D.W., and Buxton, H.T., eds., U.S. Geological Survey Toxic Substances Hydrology Program--Proceedings of the Technical Meeting, Charleston, South Carolina, March 8-12, 1999 -- Volume 3 -- Subsurface Contamination from Point Sources: U.S. Geological Survey Water-Resources Investigations Report 99-4018C, this volume.

Kent, D.B., Davis, J.A., Anderson, L.C.D., Rea, B.A., and Waite, T.D., 1994, Transport of chromium and selenium in the suboxic zone of a shallow aquifer: Influence of redox and adsorption reactions: Water Resources Research, v. 30, no. 4, p. 1099-1114.

LeBlanc, D.R., 1984, Sewage plume in a sand and gravel aquifer, Cape Cod, Massachusetts: U.S. Geological Survey Water-Supply Paper 2218, 28 p.

LeBlanc, D. R., Hess, K. M, Kent, D. B., Smith, R. L., Barber, L. B., and Campo, K. W., 1999, Natural restoration of a sewage plume in a sand and gravel aquifer, Cape Cod, Massachusetts, Morganwalp, D.W., and Buxton, H.T., eds., U.S. Geological Survey Toxic Substances Hydrology Program--Proceedings of the Technical Meeting, Charleston, South Carolina, March 8-12, 1999 -- Volume 3 -- Subsurface Contamination from Point Sources: U.S. Geological Survey Water-Resources Investigations Report 99-4018C, this volume.

Rea, B.A., Kent, D.B., LeBlanc, D.R., and Davis, J.A., 1991, Mobility of zinc in a sewage-contaminated aquifer, Cape Cod, Massachusetts, in Mallard, G.E., and Aronson, D.A., eds., U.S. Geological Survey Toxic Substances Hydrology Program--Proceedings of the technical meeting, Monterey, California, March 11-15, 1991: U.S. Geological Survey Water-Resources Investigations Report 91-4034, p. 88-95.

Savoie, J., and LeBlanc, D.R., eds., 1998, Water-quality data and methods of analysis for samples collected near a plume of sewage-contaminated ground water, Ashumet Valley, Cape Cod, Massachusetts, 1993-94: U.S. Geological Survey Water-Resources Investigations Report 97-4269, 208 p.

Stollenwerk, K.G., 1995, Modeling the effects of variable groundwater chemistry on adsorption of molybdate: Water Resources Research, v. 31, no. 2, p. 347-357.

Stollenwerk, K.G., 1996, Modeling phosphate transport in sewage-contaminated groundwater, Cape Cod, Massachusetts: Applied Geochemistry, v. 11, p. 317-324.

Vaccaro, R. F., and others, 1979, Waterwater renovation and retrieval on Cape Cod, Environmental Protection Agency Report EPA-600/2-79-176, 174 p.

Walter, D.A., Rea, B. A., Stollenwerk, K.G., and Savoie, Jennifer, 1996, Geochemical and hydrologic controls on phosphorus transport in a sewage-contaminated sand and gravel aquifer near Ashumet Pond, Cape Cod, Massachusetts: U.S. Geological Survey Water-Supply Paper 2463, 89 p.

AUTHOR INFORMATION

Douglas B. Kent and Valerie Maeder, U.S. Geological Survey, Menlo Park, California (dbkent@usgs.gov)

Phosphorus Transport in Sewage-Contaminated Ground Water, Massachusetts Military Reservation, Cape Cod, Massachusetts

By Donald A. Walter, Denis R. LeBlanc, Kenneth G. Stollenwerk, and Kimberly W. Campo

ABSTRACT

The disposal of secondarily treated sewage effluent at the Massachusetts Military Reservation on western Cape Cod, Massachusetts, between 1936 and 1995 has created a plume of contaminated ground water in the underlying sand and gravel aquifer in which dissolved phosphorus concentrations can exceed 10 mg/L (milligrams per liter). Ground water with phosphorus concentrations as high as 2 mg/L is currently (1998) discharging into nearby Ashumet Pond. Phosphorus is transported in two geochemical environments in the plume--an anoxic environment in which phosphorus is closely associated with dissolved iron and no dissolved oxygen, and a more extensive suboxic environment in which there is low, but detectable, dissolved oxygen and no dissolved iron. The adsorption of phosphorus onto iron and aluminum oxides has greatly retarded the movement of phosphorus relative to ground-water velocities. Continued loading of phosphorus onto the sediments, however, has created a large reservoir of sorbed phosphorus and allowed for the breakthrough and significant transport of dissolved phosphorus. Concentrations of phosphorus in ground water in the center of the plume have remained generally unchanged since 1993, whereas phosphorus concentrations along the eastern edge of the plume, where the highest concentrations are observed, have changed significantly. High concentrations of dissolved phosphorus along the eastern and western edges of the plume are associated with low specific conductances. This suggests that phosphorus desorption may be occurring in the aquifer in response to an influx of clean water and that phosphorus could remain in solution for long periods of time after other plume constituents have been flushed from the aquifer.

INTRODUCTION

The discharge of secondarily treated sewage effluent onto sand disposal beds at the Massachusetts Military Reservation (MMR) on western Cape Cod, Massachusetts, between 1936 and 1995 has resulted in a plume of sewage-contaminated ground water in the underlying glacial sand and gravel aquifer, known as the Ashumet Valley sewage plume, that extends about 18,000 ft (feet) downgradient from the disposal beds (Savoie and LeBlanc, 1998) (fig. 1). Previous sampling of the sewage plume in 1978-79, at a limited number of sampling sites, first identified phosphorus contamination at the site and showed that dissolved phosphorus had migrated about 2,000 ft downgradient from the disposal beds (LeBlanc, 1984). Concerns that the discharge of phosphorus-contaminated ground water into nearby Ashumet Pond could adversely affect the ecology of the pond prompted the U.S. Geological Survey (USGS), in cooperation with the National Guard Bureau (NGB), to conduct a more detailed investigation of the distribution of phosphorus and the hydrologic and geochemical controls on phosphorus transport in the aquifer. The ongoing study, which began in 1993, included the collection of water and soil samples, column experiments, core extractions, and batch experiments. Results of the investigation have

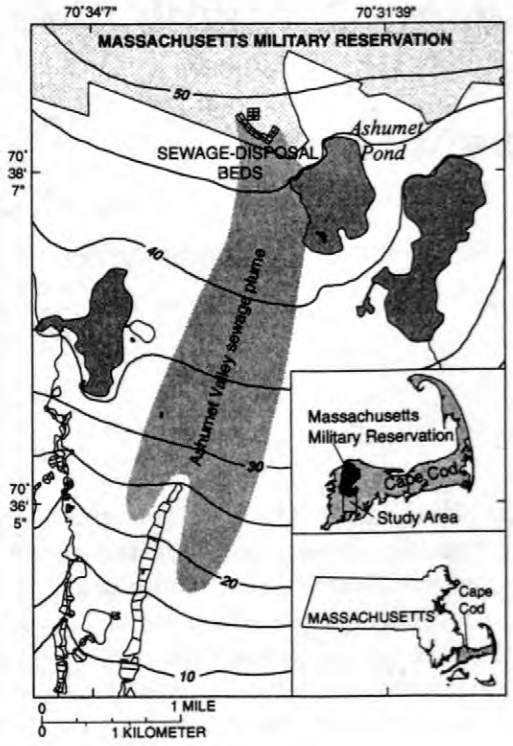

Figure 1. Location of Massachusetts Military Reservation, sewage-disposal beds, Ashumet Valley sewage plume, Ashumet Pond, and water-table contours on western Cape Cod, Massachusetts.

been reported in Stollenwerk (1994), Stollenwerk (1996), Bussey and Walter (1996), Walter and others (1996), and Walter and LeBlanc (1997).

The purpose of the water and soil sampling components of the investigation was to determine the distribution of phosphorus and related constituents in the aquifer, geochemical environments in which phosphorus transport occurs, and changes in phosphorus concentrations in the aquifer with time. Data from laboratory experiments and from water and soil sampling were used to develop conceptual models of phosphorus transport in the aquifer under different geochemical conditions before and after the cessation of sewage disposal. This paper summarizes water-quality data collected as part of the ongoing investigation of phosphorus transport in the sewage plume and presents conceptual models of phosphorus transport during sewage disposal (1936-1995) and following the cessation of sewage disposal (after 1995) that are based on onsite and laboratory data.

Hydrogeologic setting

The study area is on western Cape Cod on a broad, gently sloping glacial outwash plain that is bounded to the north and west by terminal glacial moraines and to the south by coastal embayments. The glacial outwash deposits show a fining downward sequence with coarse-grained glaciofluvial deposits consisting of sand and gravel underlain by finer grained glaciolacustrine deposits consisting of fine sand and silt. The contact between the two hydrogeologic units is about 100 ft below sea level in the study area. The coarse-grained sand and gravel sediments comprise an important aquifer for western Cape Cod and are about 150 ft thick in the study area.

The ground-water flow system of western Cape Cod, which is unconfined, is bounded to the north, west, and south by saltwater, to the east by a regional ground-water divide, and below by relatively impermeable bedrock. The sole source of water to the aquifer is areal recharge; ground water discharges naturally to streams and coastal embayments. Ground-water flow directions, which generally are to the south in the study area, are strongly affected by Ashumet Pond (fig. 1). Ground-water flow converges toward the pond in upgradient areas where ground water discharges into the pond, including the study area, and diverges away from the pond in downgradient areas where the pond recharges the aquifer. Most ground-water flow occurs in the coarse-grained sand and gravel deposits.

Ground-water sampling

The water-quality network sampled in 1993 consisted of 24 sites (fig. 2). A total of 373 samples were collected between June 1993 and January 1994: 81 samples from observation wells, 276 samples from nineteen 15-port multilevel samplers (MLS), and 16 samples from pond-bottom drive points. An additional 183 water samples also were collected from nine screened-auger borings within the study area as part of a separate investigation of volatile organic compounds in the plume conducted by the MMR

Installation Restoration Program. Wells were sampled using a stainless-steel submersible pump with a packer; screened-auger borings were also sampled using a submersible pump. Multilevel samplers and drive points were sampled using a peristaltic pump. Field parameters (temperature, pH, dissolved oxygen, and specific conductance) were measured on site and samples were collected following evacuation of a minimum of three casing volumes of water. Dissolved samples were filtered through 0.45 µm (micrometer) filters. Samples were sent to the USGS National Water-Quality Laboratory in Arvada, Colorado, for analysis, and duplicate samples for phosphorus and iron were analyzed at an onsite laboratory by USGS personnel. A more detailed description of the sampling and analytical methodology is presented in Walter and others (1996).

An additional 11 observation wells and six MLS were installed in 1995 during a second phase of the investigation to improve definition of the distribution of phosphorus in the eastern part of the plume where it was determined that phosphorus concentrations were highest and phosphorus was most likely to move toward and discharge into Ashumet Pond. A total of 297 samples were collected in 1995 using the same methodology described above. Since 1995, water-quality samples have been collected twice a year from a subset of 37 wells and eight MLS as part of an ongoing USGS investigation of natural aquifer restoration in the sewage plume (LeBlanc and others, 1999).

OCCURRENCE OF PHOSPHORUS IN GROUND WATER

Background water quality in the study area generally is characterized by high concentrations of dissolved oxygen (greater than 9 mg/L (milligrams per liter)), low pH values (5 to 6 standard units), low alkalinities (less than 10 mg/L), low organic carbon concentrations (less than 0.1 mg/L), low specific conductances (less than 80 µS/cm (microsiemens per centimeter)), and low or undetectable concentrations of cations and anions. Phosphorus concentrations in the uncontaminated ground water typically are less than 0.01 mg/L. A 1994 synoptic sampling of the sewage plume indicated that the plume was about 18,000 ft long and a maximum of 3,000 ft wide and 100 ft thick (Savoie and LeBlanc, 1998). The sewage-contaminated ground water varies in chemical character as a function of location from the source and prevailing redox conditions, but typically is characterized by low concentrations of dissolved oxygen (less than 1.0 mg/L), elevated pH values (greater than 6 standard units), elevated alkalinities (greater than 10 mg/L), elevated concentrations of organic carbon (greater than 1.0 mg/L), and high specific conductances (300 to 500 µS/cm). High concentrations of iron (1 to 25 mg/L), manganese (1 to 10 mg/L), and ammonia (greater than 1 mg/L) occur in reducing environments, and high concentrations of nitrate (greater than 10 mg/L) occur in more oxidizing environments. Phosphorus concentrations in the sewage-contaminated ground water ranged from 0.01 to more than 10 mg/L.

Distribution of phosphorus in sewage-contaminated ground water

In 1993, dissolved phosphorus was detected in ground water at a distance of more than 3,500 ft downgradient from the sewage-disposal beds. Concentrations exceeded 0.1 and 1.0 mg/L for distances of 2,500 and 2,200 ft from the beds, respectively (fig. 2). Phosphorus concentrations generally decreased with distance between the most recently used sewage-disposal beds and Ashumet Pond--from about 4 to 5 mg/L beneath the beds to 1 to 2 mg/L along the pond. Phosphorus concentrations in the center of the plume were typically 3 to 4 mg/L. The highest phosphorus concentration observed in the study area was 11 mg/L at a location about 100 ft downgradient from the westernmost disposal beds (site S590, fig. 2). An area of high phosphorus concentrations also was observed along the eastern edge of the plume; concentrations exceeded 6 mg/L at a site that is located about 1,400 ft downgradient from the four easternmost disposal beds (site F567, fig. 2).

Phosphorus concentrations exceeded 0.1 mg/L in a zone that was about 100 ft thick between the disposal beds and the pond. The area

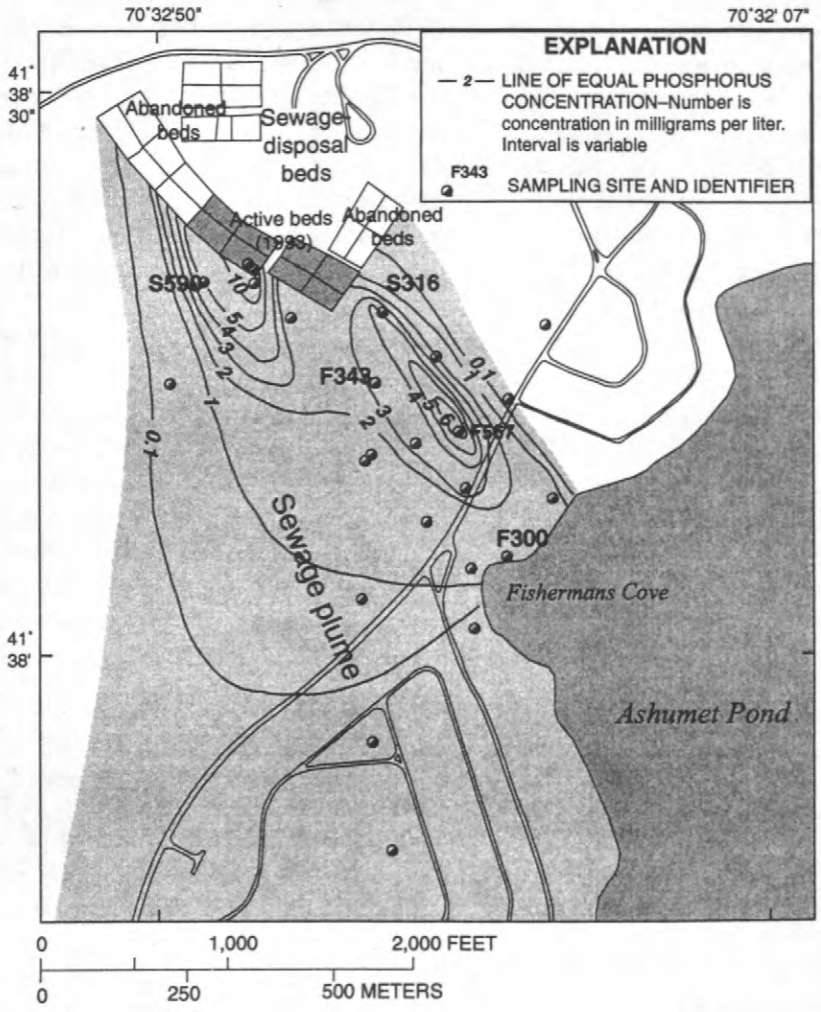

Figure 2. Distribution of dissolved phosphorus concentrations between the sewage-disposal beds and Ashumet Pond, June 1993 to February 1994, and the locations of sampling sites F300, F343, F567, S316, and S590

of ground water between the active disposal beds (1993) and the pond that contained greater than 1 mg/L of phosphorus decreased in thickness from about 45 feet beneath the disposal beds to 25 ft along the pond. Water samples collected in December 1993 from temporary in-pond drive points installed near the shore indicated that dissolved phosphorus was discharging into Ashumet Pond; the maximum concentration in discharging ground water was 1.9 mg/L.

Geochemical environments within the phosphorus plume

Dissolved phosphorus was observed in two geochemical environments in the plume--(1) an anoxic environment that had no detectable dissolved oxygen and dissolved iron concentrations as high as 25 mg/L, and (2) a suboxic environment where there was low but detectable dissolved oxygen and no detectable dissolved iron. Dissolved phosphorus in the anoxic environment was closely associated with dissolved iron, as illustrated in the chemical

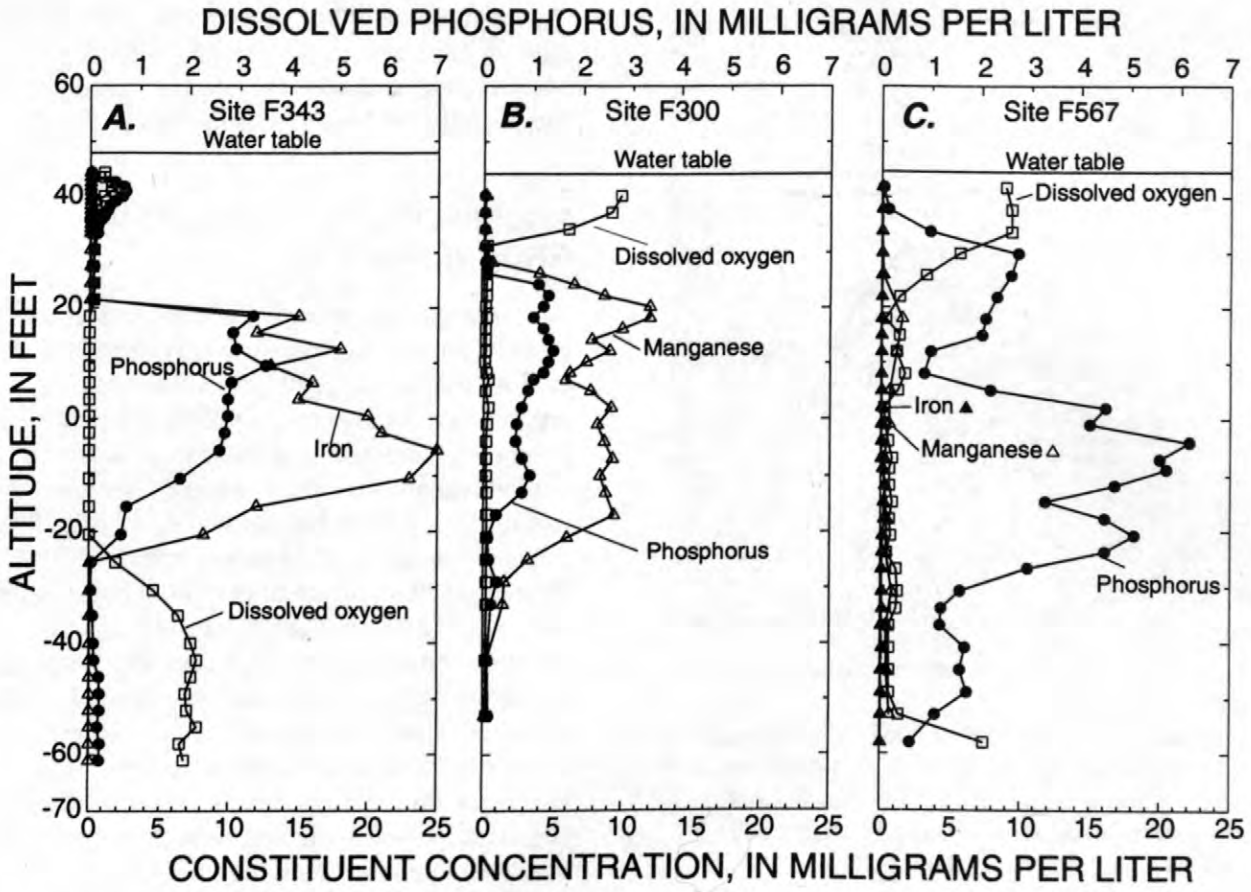

Figure 3. Vertical distribution of dissolved phosphorus, dissolved iron and (or) manganese, and dissolved oxygen concentrations at sampling sites ***A.*** F343 (center of plume), ***B.*** F300 (near Ashumet Pond), and ***C.*** F567 (along eastern edge of plume), June 1993 to February 1994.

profile from site F343 (fig. 3*A*). Dissolved phosphorus at site F343 occurred mostly in the part of the plume that had no detectable dissolved oxygen (less than 0.05 mg/L). Dissolved phosphorus in the suboxic environment was not associated with any dissolved iron, as illustrated in chemical profiles from sites F300 and F567 (figs. 3*B* and 3*C*). Dissolved phosphorus at both sites occurred in environments with geochemically significant concentrations of dissolved oxygen. Phosphorus from the suboxic environment along Ashumet Pond (site F300) was associated with high concentrations of dissolved manganese. Dissolved phosphorus along the eastern edge of the plume (site F567) was not associated with either dissolved iron or manganese. The profile indicates that the phosphorus plume is bifurcated at site F567 with distinct upper and lower concentration peaks (fig. 3*C*).

The suboxic environment is more extensive than the anoxic environment, which is limited to areas within the center of the plume (fig. 4). Suboxic conditions in the plume occupy almost the full width and thickness of the sewage plume and extend beyond the downgradient extent of phosphorus contamination (more than 3,500 ft). Anoxic conditions occur in an area that is about 750 ft wide and a maximum of about 45 feet thick, and extend about 1,400 ft downgradient from the disposal beds (fig. 4).

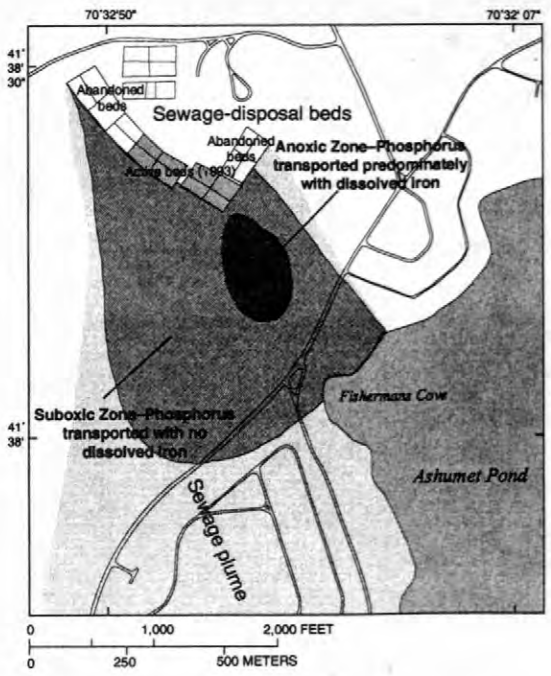

Figure 4. Areal extent of anoxic and suboxic zones within the phosphorus plume where phosphorus is associated with and without dissolved iron, June 1993 to February 1994.

Temporal changes in phosphorus concentrations and specific conductance

Annual sampling conducted since 1993 indicates that phosphorus concentrations vary significantly with time at some locations within the plume, but remain relatively constant at other locations. Maximum phosphorus concentrations in the plume near the pond (site F300) increased slightly from 1.4 mg/L in 1993 to 2.1 mg/L in 1998 (fig. 5*A*). The vertical distribution of dissolved phosphorus and the thickness of the plume generally remained unchanged at the site. Specific conductance, a conservative indicator of sewage contamination, also has remained generally unchanged at the site between 1993 and 1998 (fig. 5*B*). The distribution of phosphorus along the eastern edge of the plume (site F567) changed significantly between 1993 and 1998 (fig. 5*C*). Maximum concentrations in the lower part of the plume occurred at the same horizon, but varied from a low of 3.1 mg/L in 1994 to a high of 6.2 mg/L in 1993. Concentrations in the upper part of the plume ranged from a low of 2.7 mg/L in 1993 to a high of 7 mg/L in 1996. Specific conductance at the site also varied significantly between 1993 and 1998 (fig. 5*D*).

PHOSPHORUS TRANSPORT IN GROUND WATER

Phosphorus strongly sorbs to the surfaces of iron and aluminum oxyhydroxide minerals, such as those that are commonly found coating sediment grains in glacial aquifers, causing phosphorus transport in ground water to be retarded relative to ground-water movement (Hem, 1992; Isenbeck-Schroter and others, 1993). Synoptic sampling of the sewage plume in 1978-79 and in 1993-94 showed that phosphorus in the Ashumet Valley sewage plume had migrated about one-fifth as far as more conservative plume indicators such as boron and specific conductance (LeBlanc, 1984; Savoie and LeBlanc, 1998). Batch experiments using uncontaminated soil samples from the study area showed that the sediments, which are noncalcareous and contain iron and aluminum oxyhydroxide coatings, readily sorb phosphorus (Brigid Rea, USGS, written commun., 1993; Walter and others, 1996). Data from core extractions conducted for seven sites within the sewage plume in 1993 and 1994 indicated that 90 to 99 percent of the phosphorus within a unit volume of aquifer was sorbed to the sediment surfaces and that dissolved concentrations represented a small fraction of the total amount of phosphorus contamination in the aquifer (Walter and others, 1996).

Previous investigations of phosphorus mobility in sand and gravel aquifers reported that phosphorus transport occurs primarily in reducing environments as a result of reductive dissolution of iron-oxide mineral coatings and transport with dissolved ferrous iron (Hem, 1992). Although phosphorus can occur in oxidizing environments within calcareous sand aquifers, phosphorus typically is thought to be immobile in the presence of dissolved oxygen, particularly in noncalcareous soils where phosphorus concentrations are controlled by low-solubility iron-phosphorus and aluminum-phosphorus mineral phases (Robertson and others, 1998).

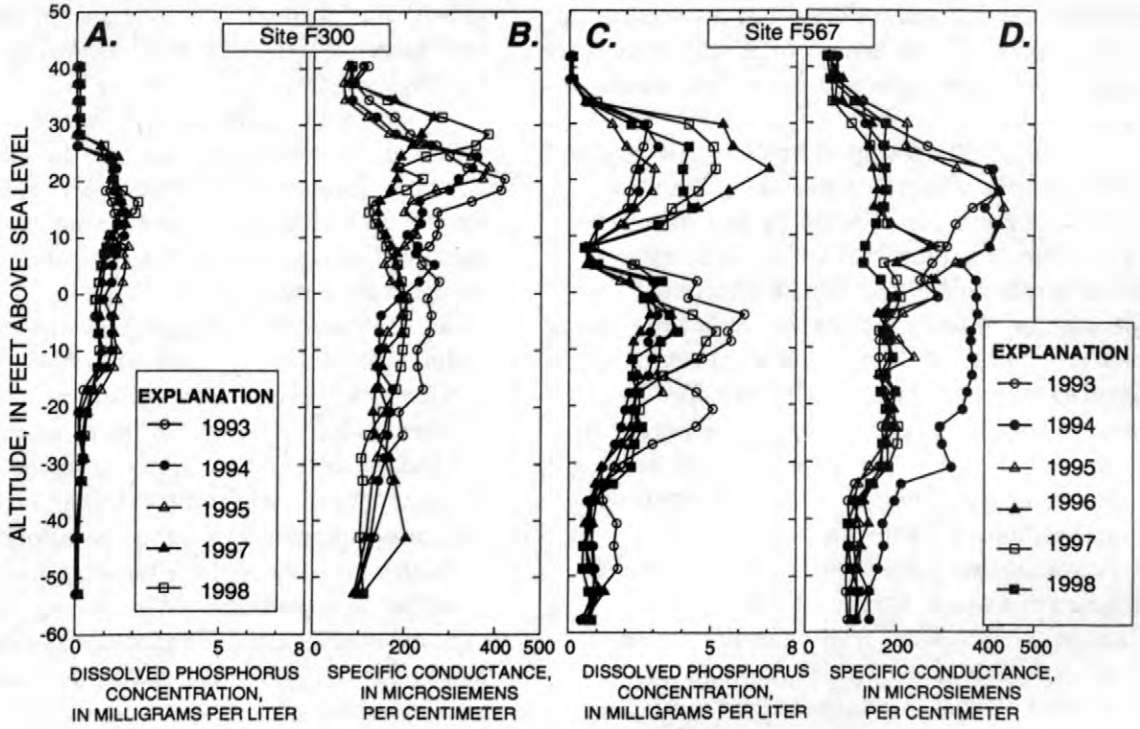

Figure 5. Vertical distribution of dissolved phosphorus (***A.*** and ***C.)*** and specific conductance (***B.*** and ***D.)*** at sampling sites F300 (near Ashumet Pond) and F567 (along eastern edge of plume) for period 1993-98

Phosphorus transport during sewage disposal (1936-1995)

Phosphorus transport under anoxic geochemical conditions in the aquifer occurs in the core of the sewage plume (figs. 3 and 4); the association of phosphorus with dissolved ferrous iron in this geochemical environment is consistent with previous investigations of phosphorus mobility. Phosphorus transport also occurs under suboxic and oxic conditions (fig. 3); transport of phosphorus under these geochemical conditions predominates in most of the sewage plume (fig. 4) and the highest phosphorus concentrations are observed in this environment (fig 5*C*).

Column experiments indicate that oxic and suboxic sediments from the aquifer have the capacity to completely adsorb inflowing phosphorus for long periods of time. Prolonged loading of phosphorus, however, diminishes the capacity of the sediments in the columns to sorb additional phosphorus for a specified pH and inflowing phosphorus concentration, resulting in the breakthrough and transport of dissolved phosphorus through the column (Stollenwerk, 1994; Stollenwerk, 1996;Walter and others, 1996). As more phosphorus is adsorbed onto the aquifer sediments, the concentration of dissolved phosphorus in equilibrium with the adsorbed phosphorus increases and approaches phosphorus concentrations in the sewage effluent. Under these conditions, there is little net mass transfer of phosphorus from ground water to the sediments, resulting in the transport of dissolved phosphorus. As this dissolved phosphorus is transported downgradient to areas with less adsorbed phosphorus, additional adsorption occurs and the process is repeated (Douglas B. Kent, USGS, written commun., 1999). The prolonged exposure of aquifer sediments to phosphorus-contaminated sewage effluent has resulted in extensive loading

of mineral surfaces with adsorbed phosphorus and allowed the transport of dissolved phosphorus in the suboxic and oxic zones of the aquifer for more than 3,500 ft downgradient from the source in about 60 years.

Phosphorus transport in the anoxic zone of the aquifer is affected by the same adsorption processes but is complicated by iron chemistry. The increase in dissolved ferrous iron resulting from the microbially mediated reductive dissolution of ferric iron oxyhydroxide may result in the formation of ferrous phosphate minerals, such as vivianite, which could limit dissolved phosphorus concentrations and cause phosphorus to be transported as iron-phosphate colloids (Gschwend and Reynolds, 1987). Analysis of water samples collected in 1993 and 1994, however, showed that the fraction of colloidal phosphorus was insignificant (Savoie and LeBlanc, 1998). Conversely, the dissolution of iron oxyhydroxide minerals may enhance dissolved phosphorus transport by (1) releasing phosphorus previously sequestered by the iron minerals and (2) decreasing the number of available sorption sites in the aquifer. The importance of the latter mechanism may not be significant because aluminum oxide minerals would not be dissolved under neutral-pH, anoxic conditions (Douglas B. Kent, USGS, written commun., 1999).

Phosphorus transport following cessation of sewage disposal (after 1995)

Geochemical conditions in the aquifer likely will change as low-ionic-strength, oxygenated recharge water flows into contaminated parts of the aquifer following the cessation of sewage disposal in December 1995. The resultant changes would be expected to vary spatially and temporally depending on local geochemical conditions in the sewage plume.

Column experiments conducted using core material from the anoxic environment showed that dissolved phosphorus, which was associated with dissolved ferrous iron, was rapidly immobilized as ferrous iron was oxidized and phosphorus was coprecipitated with iron oxide minerals. following the introduction of oxygen into the columns. The data indicate that dissolved phosphorus in anoxic environments in the aquifer may be naturally immobilized following an influx of oxygenated water into the aquifer.

Column experiments conducted using artificially contaminated, oxic aquifer material and core material from suboxic parts of the aquifer showed a rapid, transient increase in dissolved phosphorus that was associated with a transient increase in pH following the influx of clean, low-ionic-strength ground water into the sediment columns (Stollenwerk, 1994; Stollenwerk, 1996; Walter and others, 1996). Further analysis showed that the rapid increase in pH and subsequent increase in dissolved phosphorus resulted from the desorption of major cations accompanied by increased sorption of hydrogen ions, and that fluctuations in pH and dissolved phosphorus could be propagated significant distances downgradient (Stollenwerk and Parkhurst, 1999). This desorption mechanism also was observed during a clean-water tracer test, conducted within the phosphorus plume in 1997, in which pH and dissolved phosphorus were observed to increase and specific conductance was observed to decrease following the injection of clean water into a phosphorus-contaminated part of the aquifer (Kenneth G. Stollenwerk, USGS, written commun., 1998). The data indicate that an influx of recharge water following the cessation of sewage disposal could result in an increase in phosphorus concentrations in the aquifer and that phosphorus could remain in solution for long periods of time after the sewage plume has been flushed from the aquifer (Stollenwerk, 1994; Stollenwerk, 1996; Walter and others, 1996; Stollenwerk and Parkhurst, 1999).

Water-quality data collected in 1993-94 from two sites along the eastern edge of the plume (sites S316 and F567) and from one site located along the western edge of the plume (site S590) indicate that the desorption mechanism observed in the column and onsite field experiments may be occurring at some locations in the aquifer (fig. 6). Data from the three sites show that high concentrations of dissolved phosphorus occur in parts of the aquifer where low specific conductances indicate that the

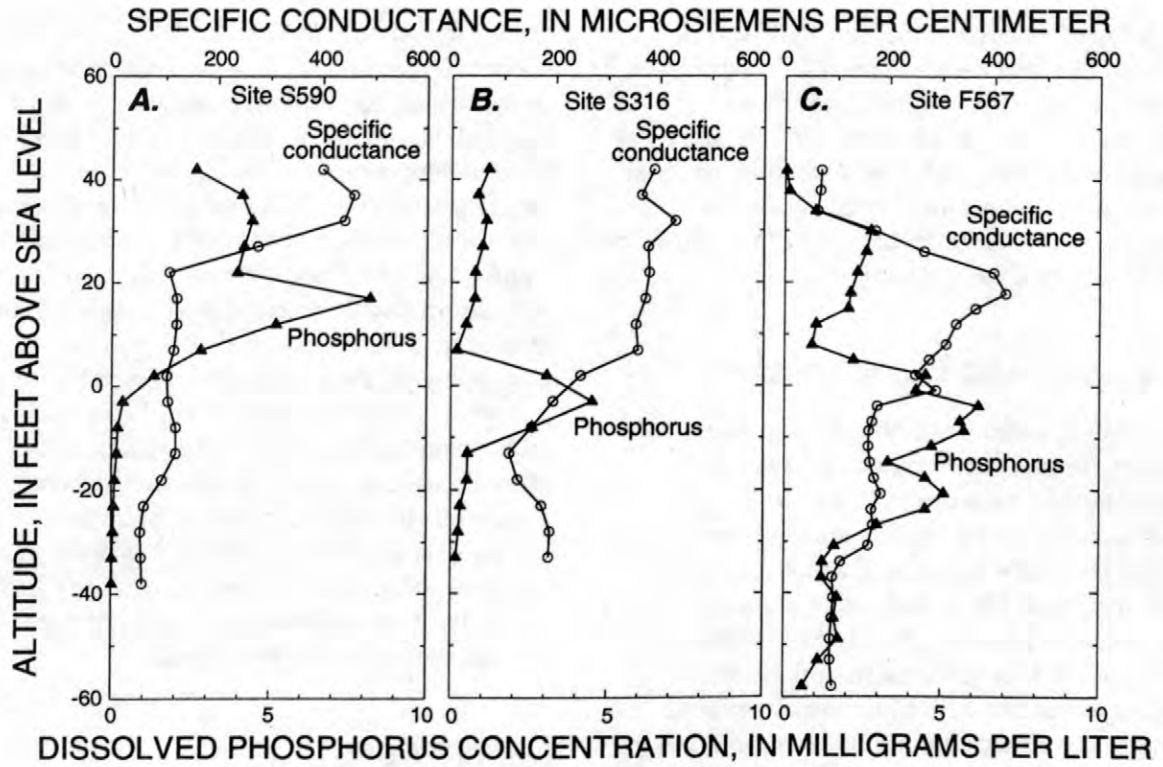

Figure 6. Vertical distribution of dissolved phosphorus and specific conductance at sampling sites ***A.*** F567 and ***B.*** S316 (along the eastern edge of plume) and ***C.*** S590 (along western edge of plume), June 1993 to February 1994

sewage plume is flushing from the aquifer. All three sites are downgradient from abandoned sewage-disposal beds where the sewage plume is flushing from the aquifer. Phosphorus concentrations at site S590, which is along the western edge of the sewage plume, had concentrations of phosphorus as high as 9 mg/L in a vertical horizon where specific conductances were about 100 µS/cm, which is close to background levels (fig. 6*A*). Similarly, phosphorus concentrations at site S316, along the eastern edge of the sewage plume, had phosphorus concentrations exceeding 5.0 mg/L in a vertical horizon where specific conductances were between 150 and 200 µS/cm, which is less than the 300 to 500 µS/cm typical of sewage-contaminated ground water. Phosphorus concentrations farther downgradient along the eastern edge of the plume (site F567) exceeded 4.0 mg/L in a zone where specific conductances also were between 150 and 200 µS/cm.

The changes in phosphorus concentrations along the edges of the plume may be a model for changes that could occur throughout the plume now that sewage disposal at the site has ceased. A study of the natural restoration of the aquifer has shown that the sewage plume has been nearly flushed from beneath the disposal beds in 1998 (Campo and Hess, 1999). Following the cessation of sewage disposal, the specific conductance of ground water beneath the most recently used disposal beds decreased from more than 400 to less than 150 µS/cm within one year, indicating that the sewage plume was rapidly flushed from the aquifer (LeBlanc and others, 1999). Concentrations of phosphorus, however, increased significantly in several zones (from less than 2 to more than 4.5 mg/L) during the same period. The increase in phosphorus was associated with an increase in pH (Kent and Maeder, 1999). Numerical modeling of the sewage plume has shown that the transient pH

increase and associated increase in dissolved phosphorus could be propagated for a significant distance downgradient (Stollenwerk and Parkhurst, 1999). Time-series data from site F300 (fig. 5*A* and 5*B*) indicate that downgradient areas of the sewage plume, such as along Ashumet Pond, have not been affected yet by the inflow of clean water into the system.

SUMMARY AND CONCLUSIONS

Sewage disposal at the Massachusetts Military Reservation on western Cape Cod, Massachusetts, between 1936 and 1995 has resulted in a plume of phosphorus-contaminated ground water that is discharging into nearby Ashumet Pond. The leading edge of phosphorus-contaminated ground water has migrated more than 3,500 ft downgradient from the disposal beds, or about one-fifth as far as conservative sewage constituents. Maximum concentrations of phosphorus in the plume exceed 10 mg/L, and ground water with concentrations of almost 2 mg/L discharges into the pond. The phosphorus is transported in two geochemical environments in the plume: (1) an anoxic environment in which there is no dissolved oxygen and phosphorus is transported in association with dissolved iron and (2) a more areally extensive suboxic environment in which there is low but detectable dissolved oxygen and no associated dissolved iron. Phosphorus concentrations within the plume upgradient from the pond generally have remained unchanged since 1993; however, phosphorus concentrations along the eastern edge of the plume have varied considerably.

Phosphorus strongly sorbs to iron and aluminum oxyhydroxide coatings on aquifer sediments. Most phosphorus in the aquifer (90 to 99 percent) is sorbed to the surfaces. Adsorption has greatly retarded the transport of phosphorus relative to the rate of ground-water movement in the aquifer. The front of dissolved phosphorus has moved in the aquifer, however, because the prolonged loading of phosphorus onto aquifer sediments has exhausted the sorptive capacity of the sediments, given the pH conditions and inflowing phosphorus concentrations. Laboratory and field experiments indicate that the fate and transport of phosphorus in the aquifer could change in response to an influx of uncontaminated recharge water into the sewage-contaminated zone after the cessation of sewage disposal. Dissolved phosphorus in the anoxic environment could be immobilized rapidly by coprecipitation with iron oxyhydroxide minerals following the influx of oxygenated water into the aquifer. Dissolved phosphorus in the suboxic environment could increase rapidly and remain mobile for long periods of time due to the desorption and remobilization of sorbed phosphorus following the influx of clean water into contaminated parts of the aquifer. This phosphorus desorption is related to a decrease in ionic strength and an increase in pH. Water-quality data suggest that phosphorus desorption already is occurring in some areas of the plume, particularly along the edges of the plume and beneath the sewage-disposal beds.

REFERENCES

Bussey, K.W., and Walter, D.A., 1996, Spatial and temporal distribution of specific conductance, boron, and phosphorus in a sewage-contaminated aquifer near Ashumet Pond, Cape Cod, Massachusetts: U.S. Geological Survey Open-File Report 96-472, 44 p.

Campo, K.W., and Hess, K.M., 1999, Evolution of a ground-water sewage plume following the removal of a 60-year-long source, Cape Cod, Massachusetts: Fate of volatile organic compounds, *in* Morganwalp, D.W., and Buxton, H.T., eds., 1999, U.S. Geological Survey Toxic Substances Hydrology Program--Proceedings of the Technical Meeting, Charleston, South Carolina, March 8-12, 1999 -- Volume 3 – Subsurface Contamination from Point Sources: U.S. Geological Survey Water-Resources Investigations Report 99-4018C, this volume.

Gschwend, P.M., and Reynolds, M.D., 1987, Monodisperse ferrous phosphate colloids in an anoxic groundwater plume: Journal of Contaminant Hydrology, v. 1, p. 309-327.

Kent, D.B., and Maeder, Valerie, 1999, Evolution of a ground-water sewage plume following the removal of a 60-year-long source, Cape Cod, Massachusetts: pH and the fate of

phosphate and metals, *in* Morganwalp, D.W., and Buxton, H.T., eds., 1999, U.S. Geological Survey Toxic Substances Hydrology Program--Proceedings of the Technical Meeting, Charleston, South Carolina, March 8-12, 1999-- Volume 3 – Subsurface Contamination from Point Sources: U.S. Geological Survey Water-Resources Investigations Report 99-4018C, this volume

Hem, J.D., 1992, The study and interpretation of the chemical characteristics of natural water (3d ed.): U.S. Geological Survey Water-Supply Paper 2254, 225 p.

Isenbeck-Schroter, Margot, Doring, Ute, Moller, Andreas, Schroter, Jurgen, and Matthes, George, 1993, Experimental approach and simulation of the retention processes limiting orthophosphate transport in groundwater: Journal of Contaminant Hydrology, v. 14, p. 143-161.

LeBlanc, D.R., Hess, K.M., Kent, D.B., Smith, R.L., Barber, L.B., Stollenwerk, K.G., and Campo, K.W., 1999, Natural restoration of a sewage plume in a sand and gravel aquifer, Cape Cod, Massachusetts, *in* Morganwalp, D.W., and Buxton, H.T., eds., 1999, U.S. Geological Survey Toxic Substances Hydrology Program--Proceedings of the Technical Meeting, Charleston, South Carolina, March 8-12, 1999-- Volume 3 – Subsurface Contamination from Point Sources: U.S. Geological Survey Water-Resources Investigations Report 99-4018C, this volume.

LeBlanc, D.R., 1984, Sewage plume in a sand and gravel aquifer, Cape Cod, Massachusetts: U.S. Geological Survey Water-Supply Paper 2218, 28 p.

Robertson, W.D., Schiff, S.L., and Ptacek, C.J., 1998, Review of phosphate mobility and persistence in 10 septic system plumes: Ground Water, v. 36, no. 6, p. 1000-1009.

Savoie, Jennifer, and LeBlanc, D.R., eds., 1998, Water-quality data and methods of analysis for samples collected near a plume of sewage-contaminated ground water, Ashumet Valley, Cape Cod, Massachusetts, 1993-94: U.S. Geological Survey Water-Resources Investigations Report 97-4269, 208 p.

Stollenwerk, K.G., 1994, Potential long-term effects of phosphate contamination in a sand and gravel aquifer, Cape Cod, Massachusetts, *in* Morganwalp, D.W., and Aronson D.A., eds., U.S. Geological Survey Toxic Substances Hydrology Program -- Proceedings of the Technical Meeting, September 20-24, 1993: U.S. Geological Survey Water Resources-Investigations Report 94-4015, p. 199-205.

Stollenwerk, K.G., 1996, Modeling phosphate transport in sewage-contaminated groundwater, Cape Cod, Massachusetts: Applied Geochemistry, v. 11, p. 317-324.

Stollenwerk, K.G., and Parkhurst, D.L., 1999, Modeling the evolution and natural remediation of a ground-water sewage plume, *in* Morganwalp, D.W., and Buxton, H.T., eds., 1999, U.S. Geological Survey Toxic Substances Hydrology Program--Proceedings of the Technical Meeting, Charleston, South Carolina, March 8-12, 1999-- Volume 3 – Subsurface Contamination from Point Sources: U.S. Geological Survey Water-Resources Investigations Report 99-4018C, this volume

Walter, D.A. and LeBlanc, D.R., 1997, Geochemical and hydrologic considerations in remediating phosphorus-contaminated ground water in a sewage plume near Ashumet Pond, Cape Cod, Massachusetts: U.S. Geological Survey Open-File Report 97-202, 20 p.

Walter, D.A., Rea, B.A., Stollenwerk, K.G., and Savoie, Jennifer, 1996, Geochemical and hydrologic controls on phosphorus transport in a sewage-contaminated sand and gravel aquifer near Ashumet Pond, Cape Cod, Massachusetts: U.S. Geological Survey Water-Supply Paper 2463, 90 pp.

AUTHOR INFORMATION

Donald A. Walter, Denis R. LeBlanc, and Kimberly W. Campo, U.S. Geological Survey, Marlborough, MA.

Kenneth G. Stollenwerk, U.S. Geological Survey, Denver, Colorado.

In situ Assessment of the Transport and Microbial Consumption of Oxygen in Ground Water, Cape Cod, Massachusetts

By Richard L. Smith, John Karl Böhlke, Kinga M. Revesz, Tadashi Yoshinari, Paul B. Hatzinger, Cecilia T. Penarrieta, and Deborah A. Repert

ABSTRACT

Oxygen is a key ground-water constituent, controlling both the geochemistry and microbiology of an aquifer. Accordingly, aerobic respiration, the microbial metabolic process that consumes oxygen, is fundamentally important to the overall functioning of the aquifer. However, despite its significance, few studies have directly examined this process in the subsurface. This study has used several different approaches to investigate oxygen consumption on several different scales in parts of a large (> 5 kilometers) plume of dilute sewage contamination in a sand and gravel aquifer on Cape Cod, Mass. First, oxygen concentration profiles and stable isotope ratios were used to infer the net effect of aerobic respiration on the aquifer scale. Second, natural gradient tracer tests were used at an intermediate scale to measure in situ rates of aerobic respiration within different contours of the ground-water oxygen gradient. Third, two different types of laboratory incubations using aquifer core material, potential electron transport activity (ETS) and oxygen uptake activity, were used for small-scale examination of the process. The latter methods yield estimates of rates and kinetic parameters, which can be compared with the tracer test and isotope results. The sum of these approaches views the aquifer within the context of a subsurface ecosystem, integrating the combined effects of the hydrology, geochemistry and microbiology on the process of oxygen consumption.

INTRODUCTION

While it is actually part of a hydrologic continuum, an aquifer can also be viewed as a discrete ecosystem. Processes that occur in an aquifer involve a complex interaction of biotic and abiotic components. To fully comprehend and predict the effects of this ecosystem on solutes of natural and anthropogenic origin (and vice versa), it is necessary to study the system from a holistic perspective, with the environmental conditions intact. This has been done many times in surface systems. However, in situ assessment of key microbial processes in ground water has been difficult, and thus rarely attempted.

The importance of oxygen as a ground-water constituent is widely recognized. The processes that consume oxygen are of fundamental importance to the overall functioning of an aquifer, both as an ecosystem and as a hydrologic unit. However, there have been relatively few integrated studies of oxygen respiration in ground water, especially from a process-oriented perspective.

This paper is an overview of a project that has examined aerobic respiration in a sand and gravel aquifer at several different scales. The aquifer is characterized by both vertical and horizontal gradients of dissolved oxygen, providing a range of electron acceptor demand from low in the uncontaminated zone of the aquifer, to moderate in the contaminated zone. The study combined recent developments for using ground-water tracer tests to measure biogeochemical processes in situ, improved analytical capabilities both for quantifying low level oxygen concentrations and determining oxygen stable isotope ratios, and laboratory incubations using artificial electron acceptors to assess microbial electron transport system (ETS) activity. These techniques were employed to study oxygen consumption within the aquifer at the kilometer-, meter-, and centimeter-scale. The results provide a better understanding of aerobic respiration as a process in the subsurface, facilitate interpretation of $\delta^{18}O_2$ natural abundance data from this and other field studies, and examine whether the respiration assays that were developed for other environments have utility for ground-water environments.

STUDY SITE

The study was conducted in an unconfined sand and gravel aquifer located on Cape Cod, Mass.

(fig. 1). The aquifer has been contaminated by the disposal of dilute sewage since 1936 (LeBlanc, 1984), which has resulted in a contaminant plume that is more than 5 kilometers long and 25 meters thick, vertically.

A 150-meter-long transect at a site about 2 years travel time from the contaminant source exemplifies ground-water oxygen profiles within the contaminant plume (fig. 2). Sharp vertical gradients of oxygen are evident within the plume. Dissolved oxygen concentrations decrease with depth from levels near atmospheric equilibrium in shallow uncontaminated ground water to anoxia in the core of the plume. There also is a relatively thick vertical interval in which oxygen concentrations persist in the 1-10 micromolar (μM) range. Sampling and analytical procedures for measuring dissolved oxygen in these concentration ranges have been previously described (Kent and others, 1994; Smith, 1997).

The depth of the oxygen gradient sinks relative to the water table as the contaminant plume moves down-gradient, but is evident even after several kilometers of transport. Similar vertical gradients of many other solutes, including dissolved organic and inorganic carbon, as well as microbial populations, coincide with the oxygen gradient, usually increasing in value where the oxygen is decreasing (Smith and others, 1991).

OXYGEN ISOTOPE FRACTIONATION BY AEROBIC RESPIRATION

Microbial processes commonly fractionate low molecular weight molecules because of the tendency of lighter isotopes to react faster than heavier isotopes during enzyme-mediated reactions. The result is an enrichment of the heavier isotopes in the substrate and lighter isotopes in the products. Fractionation of oxygen isotopes by aerobic respiration has been demonstrated in laboratory experiments and open oceans, but has not been examined in detail in ground-water environments. Oxygen isotope fractionation factors for shallow ground-water systems could prove useful to infer relations among mixing, diffusion, and reaction parameters for aerobic respiration, thus yielding aquifer-scale (i.e. up to kilometer-scale) information regarding oxygen consumption along a given flow path. The isotopic ratio of $^{18}O/^{16}O$ in dissolved molecular oxygen changes in the Cape Cod aquifer as a function of the oxygen concentration (fig. 3). As the oxygen concentration decreased, the oxygen became increasingly enriched in ^{18}O; $\delta^{18}O$ values ranged from about +25 per mil (‰) for near air saturation to +45 ‰. These results are consistent with kinetic isotope fractionation by aerobic respiration. However, when fit to the Rayleigh fractionation equation, the apparent

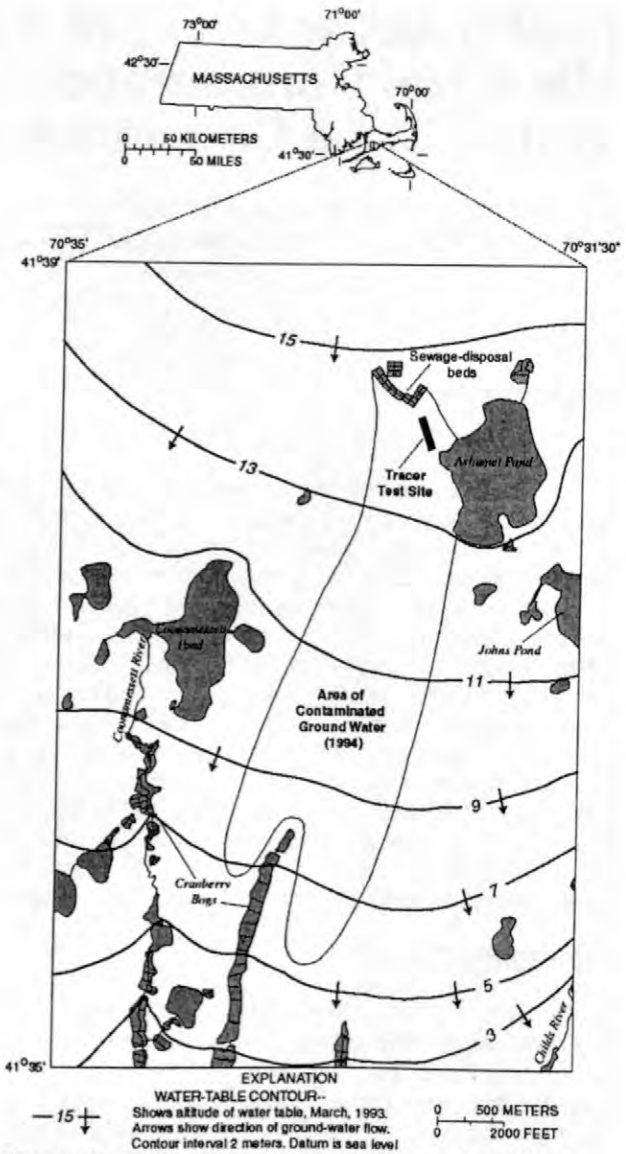

Figure 1. Ground-water study site on Cape Cod, Mass., showing location of the contaminant plume and the large-scale multilevel sampler array used in this study.

fractionation factors (ε = -2 to -10 ‰) are somewhat smaller than many values derived from closed-system experiments or field studies (ε = -20 ‰). This is due, in part, to dilution of oxygen via dispersion and diffusion during the reaction process (Revesz and others, 1999).

NATURAL GRADIENT TRACER TESTS TO ASSESS AEROBIC RESPIRATION IN SITU

Intermediate scale, in situ assessment of aerobic respiration was accomplished using natural gradient tracer tests. These tests were conducted using 15-port multilevel samplers

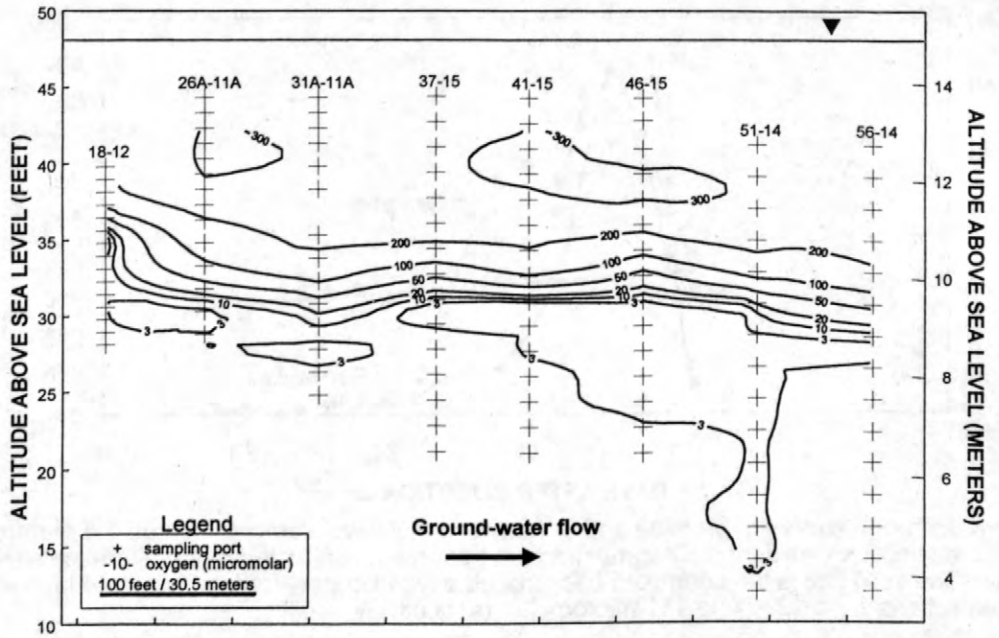

Figure 2. Longitudinal cross section of dissolved oxygen concentrations within the large-scale multilevel sampler array in November 1996. Multilevel sampler identification code is given for each well sampled.

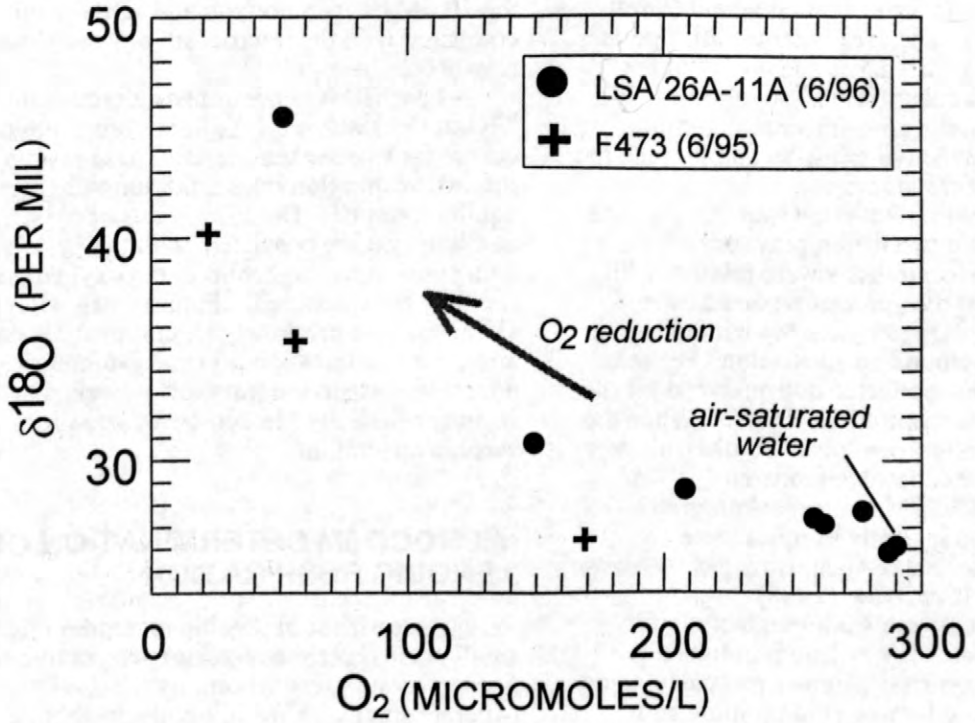

Figure 3. Isotopic content of dissolved oxygen as a function of concentration for ground water from two multilevel samplers located near the large-scale multilevel sampler array.

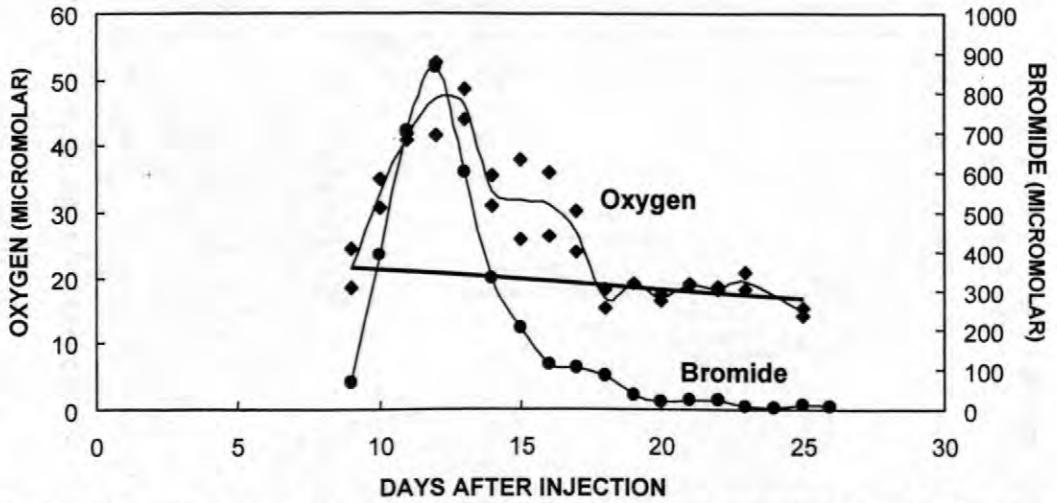

Figure 4. Breakthrough curves of bromide and oxygen at a multilevel sampler located 5.5 meters down-gradient from the injection well during a natural gradient tracer test conducted in the large-scale multilevel sampler array. The solid line is the computed background oxygen concentration. Injectate bromide and oxygen concentrations were 1290 and 111 micromolar, respectively.

(MLS) to introduce a tracer solution (200 liters) into a selected location within the oxygen gradient. The tracer cloud was transported down-gradient by natural ground-water flow and intercepted with rows of MLSs situated perpendicular to the water-table gradient (Smith and others, 1996). The grid of target MLS ports was sampled on a daily basis and analyzed for each of the tracer constituents. Sodium bromide was used as a conservative tracer to determine dispersion and advective transport and to track the path of the tracer cloud.

Aerobic respiration in the Cape Cod aquifer was assessed using two different types of tracers. When oxygen concentrations were relatively high (>30 μM), natural oxygen was replaced by exchange using $^{18}O_2$ (98 atom %) without altering the background concentration. For these tests, samples were collected and analyzed for the product of aerobic respiration, $H_2{}^{18}O$. When the oxygen concentration was low (<20 μM), air was used to increase the dissolved oxygen concentration 20-80 μM above background. Ground-water and injectate samples were analyzed for dissolved oxygen using gas chromatography (Penarrieta, 1998).

A representative breakthrough curve for one of the air tracer tests is shown in figure 4. The amount of oxygen consumed was calculated from the difference between the bromide and oxygen results, after normalizing each to the respective injectate concentration. For the data shown, the rate of oxygen consumption was 1.1 μmoles (liter aquifer x day)$^{-1}$ for 5.5 meters of transport (Penarrieta, 1998). This rate must be considered a potential rate because the in situ oxygen levels were increased above background. However, other in situ conditions were not altered. So the rate is relevant within the context of organic carbon (i.e. available supply of electron donor), microbial populations, and hydrologic flow. The rate can be viewed as an estimate of V_{max} for aerobic respiration within the 20 μM oxygen horizon and subsequently compared with the microcosm oxygen uptake results (see below).

For the $^{18}O_2$ tracer tests, enrichment of ^{18}O in H_2O was ≤ 0.1 ‰ in the breakthrough curves for two separate tests. These results indicate respiration rates ≤ 0.8 μmoles (liter aquifer x day)$^{-1}$. The lower rates of oxygen consumption are consistent with the $^{18}O_2$ test being conducted higher up in the oxygen gradient (i.e. less contaminated). Future work will entail simulating the breakthrough curves for the $^{18}O_2$ and air tracer tests using 1- and 2-dimensional advection-dispersion transport models that include Michaelis Menten-based equations for aerobic respiration.

MICROCOSM DETERMINATION OF AEROBIC RESPIRATION

Assessment of aerobic respiration from the small-scale (centimeter-scale) perspective was accomplished using laboratory incubations (microcosms) with freshly-collected aquifer core material. A variety of incubation techniques have been developed for surface-water systems to measure oxygen consumption and heterotrophic activity for indigenous microbial communities. Two of these were adapted for use in this ground-water study.

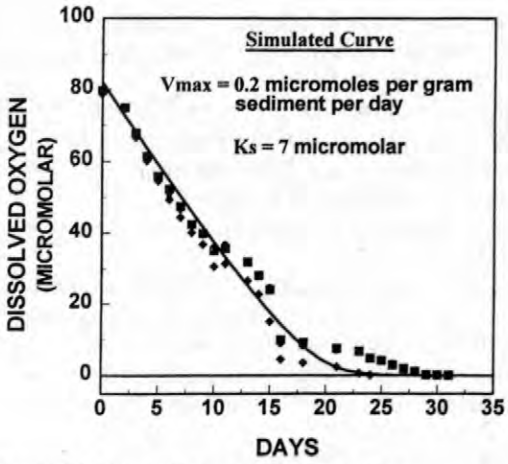

Figure 5. Progress curve of oxygen consumption by slurried aquifer core material collected from the large-scale multilevel sampler array at the 30 micromolar oxygen horizon. Incubations were conducted in triplicate (squares, diamonds and circles) at 15 °C. The line is a best-fit simulation calculated using the kinetic parameters shown in the inset.

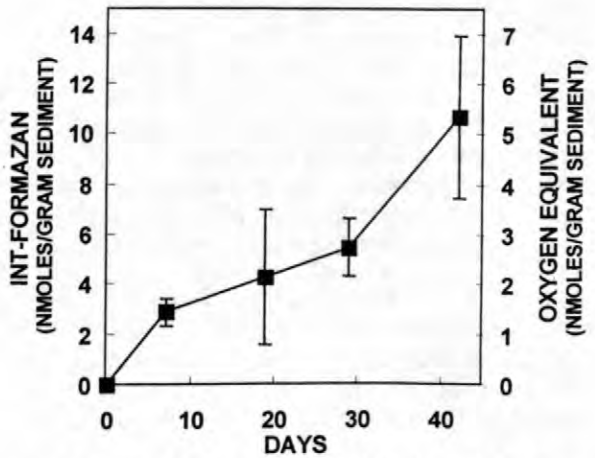

Figure 6. Production of INT-formazan by slurried aquifer core material collected from the large-scale multilevel sampler array at the 6 micromolar oxygen horizon and amended with 1 millimolar INT. Incubations were conducted at 15 °C. Error bars are standard deviation.

The first method is the direct determination of the Michaelis Menten kinetic parameters for aerobic respiration using substrate depletion progress curves. Aquifer core material was slurried with ground water in sealed serum bottles, to which varying amounts of oxygen were added (see Penarrieta, 1998, for details). The bottles were incubated with slow rotational mixing (~6 rpm) at in situ temperatures and oxygen concentrations monitored with time using gas chromatography.

Oxygen uptake in these microcosm incubations was slow, but measurable (fig. 5). Shown are the results for a core sample collected from the 30 μM oxygen horizon. Kinetic parameters were determined using best-fit simulations with a fourth-order Runge Kutta numerical approximation of the Michaelis Menten equation (Smith and others, 1994). The shape of the oxygen uptake curve is dictated by the kinetic parameters for oxygen consumption. Because there was little chemical oxygen demand in these samples, all oxygen uptake was assumed to be due to aerobic respiration. When converted to comparable units, these microcosm rates are >100-fold higher than the tracer test rate estimates. Microcosm replication within a mixed core sample was usually very good, but there was considerable variability between cores. The latter reflects the heterogeneity within the aquifer on this small scale and the disruptive effects that obtaining the core material had upon the attached microbial communities.

The second microcosm incubation method used was the determination of bacterial ETS activity using tetrazolium salts. Tetrazolium salts act as artificial electron acceptors, preferentially intercepting electrons from a cell's electron transport system prior to molecular oxygen, thus functioning as a measure of aerobic respiration. ETS activity assays have been used almost exclusively in surface-water systems; little is known regarding the utility in ground water. In this study the reduction of tetrazolium salt, 2-(p-iodophenyl)-3-(p-nitrophenyl)-5-phenyltetrazolium chloride (INT) to INT-formazan was measurable in aquifer microcosms, indicating microbial respiratory activity (fig. 6). However, rates of aerobic respiration calculated from INT reduction were 4-10-fold lower than rates obtained from the direct measurement of oxygen consumption in the laboratory microcosms. Additional studies with bacterial cultures isolated from the Cape Cod aquifer revealed that INT is toxic to many ground-water bacteria. Thus, the low rates of aerobic respiration calculated from the INT assay probably reflect the toxicity of INT to some portion of the resident microbial population.

SUMMARY AND CONCLUSIONS

A multi-scale, integrated approach is the best choice for studying a microbial process in the saturated subsurface. This study has demonstrated that aerobic respiration within an aquifer does influence the isotopic signature of molecular oxygen in ground water. That signature is an integrated result of the processes

influencing oxygen concentration along a flow path. More detail about the in situ function of the microbial process relative to transport can be obtained on an intermediate scale using natural gradient tracer tests. These tests provide the in situ quantification of the rates of oxygen consumption and provide a means to compare consumption to oxygen dispersion and diffusion across the oxygen gradient. Finally, mechanistic information, such as the reaction kinetic parameters can be obtained using small-scale laboratory incubations. These incubations also enable the assessment of the short-term responses of the ground-water ecosystem to enviromental perturbations or changes in electron donor supply.

ACKNOWLEDGEMENT

This work was funded in part by a grant (R824787) funded by an Environmental Protection Agency/National Science Foundation Partnership for Environmental Research.

REFERENCES

Kent, D.B., Davis, J.A., Anderson, L.C.D., Rea, B.A., and Waite, T.D., 1994, Transport of chromium and selenium in the suboxic zone of a shallow aquifer: Influence of redox and adsorption reactions: Water Resources Research, v. 30, p. 1099-1114.

LeBlanc, D.R., 1984, Sewage plume in a sand and gravel aquifer, Cape Cod, Massachusetts: U.S. Geological Survey Water-Supply Paper 2218, 28 p.

Penarrieta, C.T., 1998, Assessment of microbial oxygen consumption in a Cape Cod aquifer using a natural gradient tracer test and core incubations: Boulder, University of Colorado, Department of Civil, Environmental and Architectural Engineering, unpublished M.S. thesis, 131 p.

Revesz, K.M., Bohlke, J.K., Smith, R.L., and Yoshinari, T., 1999, Stable isotope composition of dissolved O_2 undergoing respiration in a ground-water contamination gradient, in Morganwalp, D.W., and Buxton, H.T., eds., 1999, U.S. Geological Survey Toxic Substances Hydrology Program--Proceedings of the Technical Meeting, Charleston, South Carolina, March 8-12, 1999-- Volume 3 – Subsurface Contamination from Point Sources: U.S. Geological Survey Water-Resources Investigations Report 99-4018C, this volume.

Smith, R.L., Ceazan, M.L., and Brooks, M.H., 1994, Autotrophic, hydrogen-oxidizing denitrifying bacteria as potential agents for bioremediation of nitrate contamination: Applied and Environmental Microbiology, v. 60, p. 1949-1955.

Smith, R.L., Garabedian, S.P., and Brooks, M.H., 1996, Comparison of denitrification activity measurements in ground water using cores and natural-gradient tracer tests: Environmental Science and Technology, v. 30, p. 3448-3456.

Smith, R.L., Harvey, R.W., and LeBlanc, D.R., 1991, Importance of closely spaced vertical sampling in delineating chemical and microbiological gradients in ground water studies: Journal of Contaminant Hydrology, v. 7, p. 285-300.

Smith, R.L., 1997, Determining the terminal electron-accepting reaction in the saturated subsurface, in Hurst, C.J., Knudsen, G.R., McInerney, M.J., Stetzenbach, L.D., and Walter, M.V., ed., Manual of Environmental Microbiology: Washington, D.C., ASM Press, p. 577-585.

AUTHOR INFORMATION

Richard L. Smith, Cecilia T. Penarrieta, and Deborah A. Repert, U.S. Geological Survey, Boulder, Colorado

John Karl Bohlke and Kinga M. Revesz, U.S. Geological Survey, Reston, Virginia

Tadashi Yoshinari and Paul B. Hatzinger, New York State Dept. Health, Albany, New York

Stable Isotope Composition of Dissolved O_2 Undergoing Respiration in a Ground-Water Contamination Gradient

By Kinga Révész, John-Karl Böhlke, Richard L. Smith, and Tadashi Yoshinari

ABSTRACT

Dissolved oxygen is a key ground-water constituent, controlling both the geochemistry and microbiology of an aquifer. Two methods were developed to analyze isotopes of dissolved O_2: a traditional method, that uses dual inlet mass spectrometry for analyzing CO_2 previously converted from O_2, and a newly developed method, that uses continuous flow isotope-ratio mass spectrometry for analyzing directly the isotopes of dissolved O_2. The major differences between the two methods are in the sample size and sample handling in the field and laboratory. Isotope analyses of dissolved O_2 were used to document the occurrence of microbial respiration near the boundary of an anoxic ground-water plume consisting of treated wastewater at the Massachusetts Military Reservation on Cape Cod. The upper boundary of the plume was a mixing zone between contaminated, anoxic plume water and uncontaminated, oxic local recharge water. Concentrations of dissolved oxygen decreased downward near the top of the plume and were inversely correlated with $\delta^{18}O$. Apparent oxygen isotope fractionation factors (ε) were -1 to -10 per mil (‰) in the absence of a dilution correction, whereas values as low as -20 ‰ were obtained by adjusting for the effects of dilution.

INTRODUCTION

Microorganisms are important factors in controlling the geochemistry of ground water. One of the most significant microbial processes is oxygen respiration, which controls ground-water redox conditions by altering concentrations of dissolved oxygen. In contaminated environments, oxygen demand and aerobic versus anaerobic pathways of degradation largely determine whether remediation of a particular set of contaminants occurs and what kind of additional *in situ* reclamation approaches might be possible.

Because molecular oxygen is a terminal electron acceptor, it is indicative of total microbial community metabolism. Because microbial processes fractionate low molecular weight molecules owing to the tendency of lighter isotopes to react faster than heavier isotopes, the fractionation of oxygen isotopes can be used to identify oxygen respiration in aquatic systems. The importance of oxygen as a ground-water constituent is widely recognized. But despite the reported fact that aerobic respiration results in fractionation of oxygen isotopes in the ocean (Bender, 1990; Quay, and others, 1993), the fractionation of oxygen isotopes in ground-water environments has not been widely investigated.

For the study of isotopic variation by oxygen respiration upon the residual oxygen pool, we developed two methods to analyze the $\delta^{18}O$ of dissolved oxygen. The major differences between the two methods are the requirements for amount of dissolved O_2, and procedures for handling samples in the field and laboratory. The traditional method requires a dual inlet isotope ratio mass spectrometry (DI-MS) to measure the isotope ratio of oxygen in CO_2 obtained by quantitative conversion of O_2 to CO_2. Sample size requirements are such that 500 mL of water with at least 1 mg/L dissolved oxygen is required for the off-line separation and conversion of oxygen to CO_2. The newly developed method uses continuous flow isotope

ratio mass spectrometry (CF-IRMS) with on-line separation and direct isotope-ratio measurement of dissolved gas constituents (i.e. O_2 and N_2). This allows a smaller sample size, about 125-mL, with a minimum concentration of 0.2 mg/L of dissolved O_2 . This paper describes the 2 methods and gives an application at a USGS test site.

STUDY SITE

The study site is a freshwater, unconfined aquifer located on western Cape Cod, Massachusetts (figure 1)

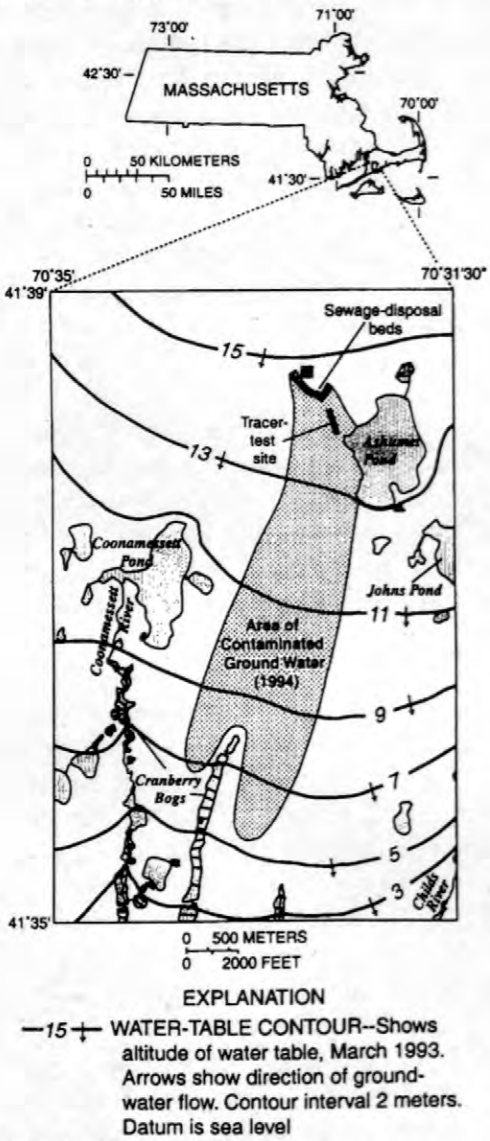

Figure 1. Study area location.

A plume of contaminated ground water was formed by continuous discharge of dilute, treated sewage to the land surface between 1936 and 1995 (LeBlanc, 1984). The plume is roughly 5 km long, 1.5 km wide, and 25 m thick. There are vertical and horizontal gradients of various properties in and around the plume, such as specific conductance (50 to 400 µS), dissolved oxygen (0 to 8 mg/L), dissolved organic carbon (1 to 4 mg/L), chloride (0 to 28 mg/L), sulfate (4 to 30 mg/L), and nitrate (0 to 16 mg of N /L) (Smith and others, 1991). The test site is equipped with an array of multi-level samplers (MLS). The MLS allow sampling of the ground water at closely spaced intervals in vertical and horizontal directions (LeBlanc and others, 1991). Each MLS consists of 15 color-coded polyethylene tubes (0.47 cm inside diameter, 0.64 cm outside diameter). The tubes run from the land surface down the inside of a 3.17-cm diameter PVC casing exiting through holes drilled through the PVC at various depths. This sand and gravel aquifer, characterized by both vertical and horizontal gradients of dissolved oxygen, shows a wide range of electron acceptor demand from pristine to moderately contaminated conditions.

SAMPLING

Based on preliminary oxygen concentration measurements, water samples were collected at the depth range that showed the steep oxygen gradient. Samples were collected by a peristaltic pump after stabilization of the chemistry of the well water. The concentrations of dissolved oxygen (O_2) were remeasured in the field by colorimeter (Chemetrics, Inc.), and water samples for $\delta^{18}O$ measurement of O_2 were collected promptly.

Samples for the traditional method were collected in approximately 500-mL"side arm"(2-chamber) evacuated vessels as described by Pearson and others (1978). Samples for the new method were collected in 125-mL serum bottles without headspace (Busenberg and others, USGS, unpublished data). Immediately before closing the bottle with a thick blue butyl rubber stopper, one KOH pellet (~100 mg) was dropped into each sample as a preservative. Samples were stored at 4 °C.

Samples for anions were filtered in the field (0.45 μm) and were analyzed by ion chromatography at the USGS, in Reston,VA., except for nitrate which was analyzed using a flow-injection autoanalyzer at the USGS laboratory in Boulder CO.

Water samples, which were saturated with air at 24 °C, and air samples were collected as control samples for both methods.

METHODS

For the traditional method, low pressure dissolved gases containing O_2 were extracted from the headspace under vacuum by a Toepler pump through a capillary to minimize water vapor in the gas phase. The oxygen gas was separated by gas chromatography (Révész and others, 1995) and converted to CO_2 by reaction with graphite at sufficiently low temperature (550-600 °C) to prevent CO formation. CO_2 was continuously frozen out in a liquid nitrogen-cooled trap to prevent its decomposition to CO in the presence of hot carbon. Yields of CO_2 were determined manometrically and isotope analysis was performed on a DuPont double collecting dual inlet mass spectrometer. The precision of this method was better than 0.2 per mil (1 σ), but it required large samples (500 mL with a minimum of 1 mg/L of dissolved O_2). In addition, it required relatively complex procedures in the field and laboratory.

The objectives of the new method were to (1) to simplify the procedures for sample collection and preparation, and (2) reduce the size of samples. In the laboratory, low-pressure headspace was created in each serum bottle by extracting about 10 percent of the water with a vacuum pump. The sample was re-equilibrated for 24 hours at room temperature. Then, constant-volume aliquots of the headspace were extracted through a syringe needle (23G1 gauge) into a He carrier gas equipped with a Nafion tube to remove water vapor. The He carrier gas was directed through a gas chromatograph for separation of its components (30-m long GS-Molesieve Plot GC Column) to the General-Purpose Interface inlet system of a Finnigan Delta Plus CF-IRMS. The CF-IRMS integrates masses 32 and 34 of the headspace aliquots, each containing about 1 μmol of O_2. The reproducibility of the method was better than 0.2 per mil (1σ). Because the isotopic compositions of air oxygen and nitrogen are constant (Dole, 1954), we used pressurized air, collected in an aluminum cylinder with an oil-free air compressor (Révész 1993), as a reference gas. In this manner, we could determine not only the isotopic composition of O_2, but also the isotopic composition of dissolved nitrogen relative to air.

Both methods were tested with air and air-saturated water samples for precision and accuracy.

RESULTS AND DISCUSSION

For the traditional method, the precision for $\delta^{18}O$ isotope measurement was better than 0.2 per mil (1σ). $\delta^{18}O$ values of the control air samples averaged 0.79 per mil more negative than those in air-saturated water (ASW), which is in good agreement with the theoretical value (Klots and Benson, 1961). With the CF-IRMS method, we monitored not only the $\delta^{18}O$ value of the O_2 component of the gas mixture, but the $\delta^{15}N$ of the N_2 component. The one-sigma standard deviation for n=3 of the isotope ratio measurements was 0.16 for $\delta^{18}O$ and 0.10 for $\delta^{15}N$. $\delta^{18}O$ and $\delta^{15}N$ of air samples were 0.75 per mil and 0.49 per mil more negative, respectively, than those in air-saturated water, in good agreement with the published values.

Samples from the Cape Cod test site were analyzed by the traditional method (DI-IRMS).

The concentrations of O_2 at all sites decreased from about 250 - 340 μM (80 - 90% of air-saturation) in the overlying wedge of local recharge water to less than 10 μM in the contaminated plume. High O_2 concentrations also occurred beneath the plume.

The $\delta^{18}O$ of O_2 ranged from about +24 per mil with respect to VSMOW reference water to +45 per mil, and the $\delta^{18}O$ of O_2 was correlated inversely with O_2 concentrations (figure 2).

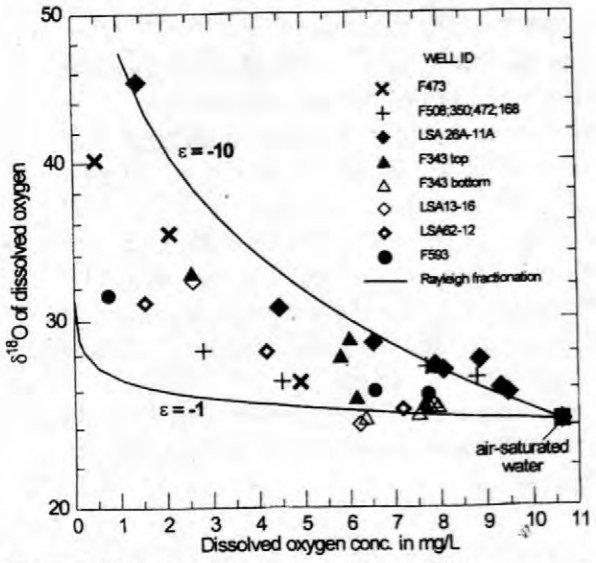

Figure 2. Isotopic composition of the diminishing oxygen reservoir as a function of the remaining fraction of dissolved oxygen reservoir.

The minimum $\delta^{18}O$ values of O_2 were near air-saturation, but sometimes higher than atmospheric equilibrium values. It is possible that the ground waters were recharged with 80-90 percent air saturation values, or that they lost 10-20 percent of their O_2 during transport through the unsaturated zone (Böhlke and others, 1999). The isotopic-ratio and concentration results of O_2 are qualitatively consistent with kinetic isotope fractionation by microbial O_2 reduction and indicate clearly that some O_2 reduction has occurred within the transition zone. The data were evaluated by using Rayleigh fractionation equation ($\ln(R/R_1)=\varepsilon\ln(C/C_1)$), where R and R_1 are the measured and initial $^{18}O/^{16}O$ ratios and C and C_1 are corresponding O_2 concentrations. Results indicate that the apparent oxygen isotopic fractionation factors (ε = -10 ‰) (figure 3) are somewhat smaller than most reported values derived from closed-system experiments or field studies (ε = -20 ±10‰) (Lane and Dole, 1956,Bender 1990, Quay and others, 1993).

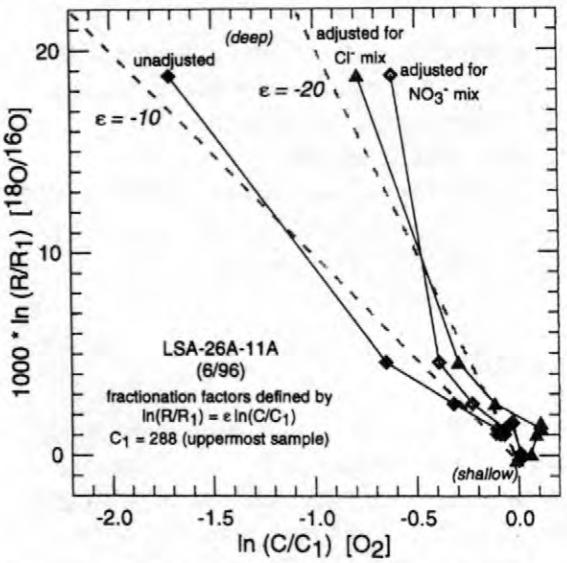

Figure 3. Isotope fractionation during O_2 reduction near the upper boundary of the contaminated plume at well LSA 26A-11A. The Rayleigh distillation equation yields linear arrays with slopes equal to apparent isotope fractionation factors (epsilon). The apparent epsilon value obtained by assuming a constant value for the un-reacted O_2 concentration (C_1) was around -10 per mil; larger epsilon values (around -20 per mil) were obtained by using C_1 values adjusted to account for conservative mixing between plume water and non-plume water, with mixing fractions determined from gradients in either NO_3^- or Cl^-(see figure 4).

At well LSA 26A-11A, the specific conductance and the concentrations of NO_3^-, Cl^-, and SO_4^{--} all increase from near background (uncontaminated) values to much higher values in the plume between about 10 and 13 m elevation (figure 4). By using those constituents as conservative indicators of the mixing fractions of anoxic plume water and oxic overlying ground-water, it is possible to adjust the values of $C[O_2]$ for individual samples to derive a more accurate relation between $\delta^{18}O$ of dissolved oxygen and the progress of the O_2 reduction reaction (figure 3). With that adjustment, the value of ε at well 26A-11A is around -20 per mil more like the closed-system values. A similar adjustment of data from Site F473-M011 altered the apparent value of ε from about -7 to -11 per mil.

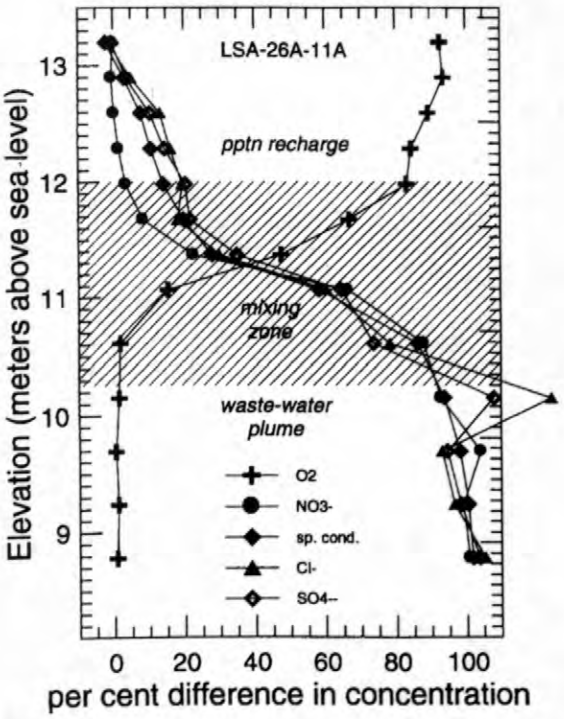

Figure 4. Concentration fraction of selected constituents, in well LSA-26A-11A. The per cent difference implicates the fraction of plume water (high NO_3^-, sp.cond., Cl^-, and SO_4^{--}) in mixtures of plume water and overlying precipitation recharge.

REFERENCES

Bender, M.L. 1990, The $\delta^{18}O$ of dissolved O_2 in seawater: a unique tracer of circulation and respiration in the deep sea: Journal of Geophysical Research. 95: p. 22243-22252.

Böhlke, J.K., Smith, R.L., Coplen, T.B., Buesenberg, E.,LeBlanc, D.R., 1999, Recharge conditions and flow velocities of contaminated and uncontaminated ground waters at Cape Cod, Massachusetts: Evaluation of δ^2H, and $\delta^{18}O$, and dissolved gases: Morganwalp, D.W., and Buxton, H.T., eds., U.S.Geological Survey Toxic Substances Hydrology Program--Proceedings of the Technical Meeting, Charleston, South Carolina, March 8-12, 1999--Volume 2--Contamination of Hydrologic Systems and Related Ecosystems: U.S. Geological Survey Water-Resources Investigations Report 99-4018B, this volume.

Coplen, T.B., 1996, Editorial: More uncertainty than necessary: Paleoceanography, v. 11, No. 4, p. 369-370.

Dole, M., Lane, G.A., Rudd, D.P., Zaukelies, D.A., 1954, Isotopic composition of atmospheric oxygen and nitrogen: Geochimica et Chomochimica Acta, v.6, p. 65-78.

Klots, C.E. and Benson, B.B., 1961, Isotope effect in the solution of oxygen and nitrogen in distilled water: Journal of Chemistry, v. 38, p. 890-892.

Lane, G.A. and Dole, M., 1956, Fractionation of oxygen isotopes during respiration. Science, v. 123,p. 574-576.

LeBlanc, D.R., 1984, Movement and fate of solutes in a plume of sewage-contaminated ground water Cape Cod, Massachusetts: U.S. Geological Survey Toxic Waste Groundwater Contamination Program, U.S. Geological Survey Open-File Report 84-475.

Pearson, F.J., Ficher, D.W. and Plummer, L.N., 1978, Correction of ground-water chemistry and carbon isotopic composition for effects of CO_2 outgassing: Geochimica et Cosmochimica Acta, v. 42, p. 1799-1807.

Quay, P.D.,Emerson, S., Wilbur, D.O., and Stump, 1993, The $\delta^{18}O$ of dissolved O_2 in the surface waters of the subarctic Pacific: a tracer of biologic productivity: Journal of Geophysical Research. 98: p. 8447-8458.

Révész, K., Coplen, T.B., Baedecker, M.J., Glynn, P.D. and Hult, M., 1995, Methane production and consumption monitored by stable H and C isotope ratios at a crude oil spill site, Bemidji, Minnesota: Applied Geochemistry, Vol. 10, p. 505-516.

Smith, R.L., Harvey, R.W. and LeBlanc, D.R., 1991, Importance of closely spaced vertical sampling in delineating chemical and microbiological gradients in groundwater studies. Journal of Contaminant Hydrology. 7: p. 285-300

Acknowledgment

We thanks T.B.Coplen and J.Hannon for reviewing this manuscript, and K.Hess for preparing the test site map for publication.

AUTHOR INFORMATION

Kinga Révész and John-Karl Böhlke, U.S. Geological Survey, Reston, Virginia
Richard L. Smith, U.S. Geological Survey, Boulder, Colorado
Tadashi Yoshinari, New York State Dept. Health Albany, New York

Nitrification in a Shallow, Nitrogen - Contaminated Aquifer, Cape Cod, Massachusetts

By Daniel N. Miller, Richard L. Smith, and John Karl Böhlke

ABSTRACT

Little is known about nitrification in ground-water environments when compared to marine systems and surface soils. Ground-water geochemistry near the upper boundary of a shallow, sewage-contaminated ground-water plume on Cape Cod, Mass., indicated a transition zone where O_2 [24 micromolar (μM)] and NH_4^+ (37 μM) coexist. The occurrence and rate of nitrification in this zone were investigated by a combination of isotopic, biogeochemical, microbial, and molecular techniques. $\delta^{15}N$ values of the NH_4^+ increased from +13 per mil (‰) within the NH_4^+ plume to +31‰ in the transition zone consistent with partial nitrification of the NH_4^+. Core incubations under nitrifying conditions demonstrated that nitrifying organisms were present and indicated a low, but measurable potential activity. Molecular analysis of core DNA also specifically detected *Nitrosomonas eutropha* DNA in sediment extracts. A small-scale, natural-gradient tracer test was conducted with ^{15}N-enriched NH_4^+ and Br^- as tracers. Transport of NH_4^+ was at least four times slower than transport of the conservative Br^- tracer. A low nitrification rate (13 to 96 nanomole per liter aquifer per day) was calculated from the natural-gradient tracer test data. From this study, we conclude that nitrification can occur in ground-water environments and can play a significant role in the speciation and transport of nitrogen.

INTRODUCTION

Nitrate and NH_4^+ contamination of freshwater aquifers and soils is a serious problem and affects watersheds throughout the United States. Ground-water nitrogen contamination is commonly associated with septic wastes, landfill leachates, and agricultural activities (Barcelona and Naymik, 1984; Bjerg and Christensen, 1993; Pederson and others, 1991). Ultimately, the movement of NO_3^- and NH_4^+ is controlled largely by aquifer geochemistry, the rate of ground-water flow, and by microbial nitrogen transformations within the aquifer.

Microbial transformation of NH_4^+ to NO_3^- (nitrification) plays an important role in surface soils and affects the speciation, transport, and fate of NO_3^- and NH_4^+ in watersheds (Fisk and Fahey, 1990; Hill and Shackleton, 1989). Ammonium transport is normally retarded in sediments and soils, but its conversion in microaerobic environments to NO_3^-, a highly mobile compound, can lead to widespread nitrogen contamination. Nitrification in soils is well documented, but this process is poorly characterized in ground-water ecosystems. The purpose of this study was to use a variety of microbial, molecular, biogeochemical, and isotopic techniques to detect, characterize, and measure the *in situ* activity of nitrifying organisms in an NH_4^+ and NO_3^- contaminated aquifer in Cape Cod, Mass.

METHODS

The study site is a shallow sand and gravel aquifer characterized by an extensive NO_3^- and NH_4^+ contamination plume that developed over sixty years as a result of continuous discharge of dilute, treated sewage (LeBlanc, 1984). An on-going research project at this field site has documented nitrogen cycling (Smith and Duff 1988), and studies have indicated that there are overlapping vertical NO_3^-, O_2, and NH_4^+ gradients within the contamination plume, suggesting that there are zones where nitrification may be occurring (Ceazan, 1987; Ceazan and others, 1989). Well site F168 (fig. 1) was selected for

this study because of its pronounced O_2, NO_3^-, and NH_4^+ gradients (see below) and its close proximity to tracer-test well array F593. This array consists of 16 multilevel sample (MLS) wells, each having 15 evenly spaced [vertical spacing = 31.75 centimeters (cm)] sampling ports at altitudes from –5.18 to –10.52 meters (m) relative to mean sea level (MSL). One MLS well (F593M02-07) served as the injection well. Thirteen downgradient MLS wells were arranged in three rows 3.05, 6.10, and 9.15 m from the injection sampler, each row roughly perpendicular to the direction of ground-water flow.

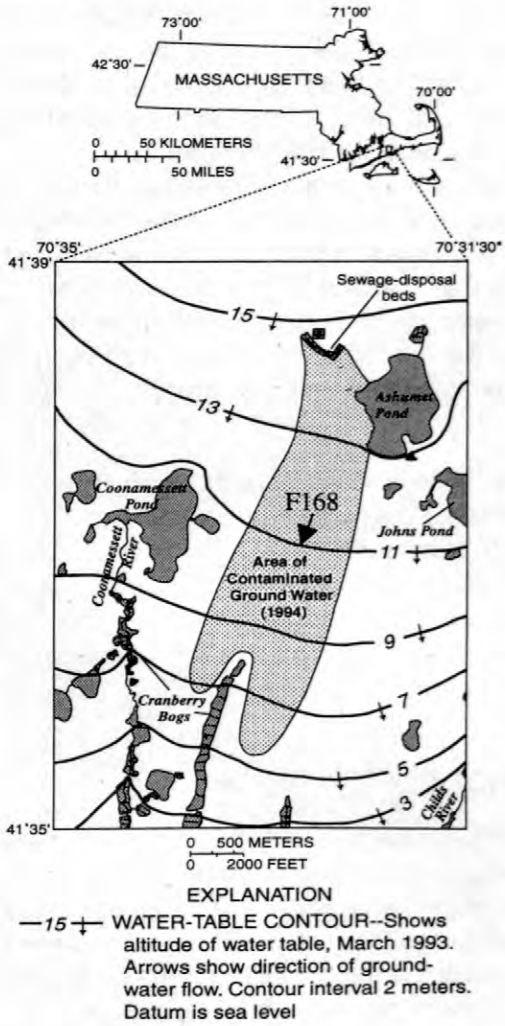

Figure 1. Ground-water study site on Cape Cod, Mass., showing the location of the contaminant plume and multilevel sampler site F168 used in this study.

Sample Collection and Incubations

Ground-water samples were collected, preserved, and analyzed as detailed by Savoie and LeBlanc, (1998). Six core samples from an elevation of –5.85 to –9.25 m relative to MSL from well site F168 were each sub-divided into three portions. One portion was used to measure nitrification potential. This portion was slurried and amended with NH_4Cl [final conc. 0.14 millimolar (mM)] and ground water. Nitrifying organisms were enumerated in the second portion of core by most probable number (MPN) technique (Schmidt and Belser, 1994). The third core portion was frozen for deoxyribonucleic acid (DNA) extraction.

Molecular Analysis of Extracted DNA

DNA was extracted from 40 grams (g) of core in 10 milliliters (ml) of TE buffer [10 mM Tris[hydroxymethyl]aminomethane (Tris), 1 mM ethylenediaminetetraacetic acid (EDTA), pH 8] containing 0.9% sodium dodecyl sulfate (SDS) during a 70 °C, 1 hour incubation with occasional mixing. Extract was separated from the core, and the DNA was precipitated by adding 1/10 volume of 3 molar (M) sodium acetate and 2 volumes ethanol. The DNA pellet was resuspended in TE buffer and purified on a Sephadex G-200 spin column (Boccuzzi and others, 1995). Two primer sequences, NITB (5'-ACCCATCCCGAAGTGTGCATT) (Voytek and Ward, 1995) and Nso190R (5'-GGAGAAAAGCAGGGGATCG) (Mobarry and others, 1996) were used to amplify ammonium-oxidizer 16S ribosomal ribonucleic acid (rRNA) genes. Polymerase Chain Reaction (PCR) amplifications were in 25 microliters (µl) and contained 1.5 mM $MgCl_2$, 50 mM KCl, 10 mM Tris (pH 8.8), 0.1 milligrams per milliliter bovine serum albumin, 0.05% Tween 20, 0.5 µM each primer, 50 µM deoxynucleotidetriphosphates, and 1 unit Taq polymerase. The following PCR temperature cycle was used to amplify nitrifying bacterial 16s rRNA genes: 80 °C hot start followed by 35 cycles of 95 °C (1 min), 60 °C (1 min), and 72 °C (1.5 min). After cycling, the reactions were subjected to a final 5 min extension at 72 °C.

A qualitative estimate of the diversity of nitrifying organisms in core material was made by comparing the restriction fragment (RFLP) patterns of the PCR-amplified 16s rRNA genes. PCR amplifications (100 µL) were purified using a BioRad DNA purification kit and resuspended in 50 µl TE buffer. The restriction endonuclease *Mbo I* was used to digest the PCR product according to the manufacturer's protocol (Promega, Milwaukee, WI). Restriction fragments were separated on a 3% agarose gel at four volts per centimeter. The gel was stained with ethidium bromide and visualized under short-wave, ultraviolet illumination. Banding patterns were compared to the banding patterns from control strains.

Tracer Injection and Sampling

A small-scale, natural-gradient tracer test was performed from June to September 1997. Approximately 200 liters (L) of ground water was withdrawn from two sampling ports with a peristaltic pump outfitted with gas impermeable tubing. The ground water was withdrawn from a zone of putative nitrification -6.3 m relative to MSL and pumped into a gas impermeable bladder that had been previously flushed with argon and contained 25.76 g NaBr and 0.46 g $(^{15}NH_4)_2SO_4$ dissolved in 1 L distilled water. After mixing the ground water and tracer in the bladder, the liquid was injected back into the aquifer (approx. 1.5 liters per min) at a single sample port -6.3 m relative to MSL. Samples (60 ml and 1 L) were collected and analyzed for Br^-, NH_4^+, NO_3^-, NO_2^-, $^{15}NH_4^+$ and $^{15}NO_3^-$ during injection from the bladder, post injection from the injection well, and during the next 10 weeks from downgradient wells. All samples were filtered (0.45 micron) and preserved in the field by freezing (60 ml NO_3^-/NO_2^-), acidification (60 ml and 1 L NH_4^+), or by adding approximately 100 mg KOH (1 L NO_3^-). Bromide was analyzed on the day of collection with an ion-specific electrode. Temperature and O_2 measurements (CHEMetrics, Calverton, VA) made during injection and post injection showed that there was only a slight increase in either of these factors during tracer injection.

RESULTS AND DISCUSSION

Groundwater Chemistry

A series of narrow vertical chemical gradients consistent with nitrification was observed in ground-water samples from F168 (fig. 2). A zone where O_2 and NH_4^+ coexist is a prerequisite for nitrification, and both O_2 and NH_4^+ are present –6.3 meters relative to MSL in ground-water samples. High concentrations of NO_3^-, a product of nitrification, were also measured in this zone. $\delta^{15}N$ values as high as +21‰ and +31‰ were measured in the transition zone in nearby wells. In contrast, $\delta^{15}N$ values below the transition zone averaged less than +13‰.

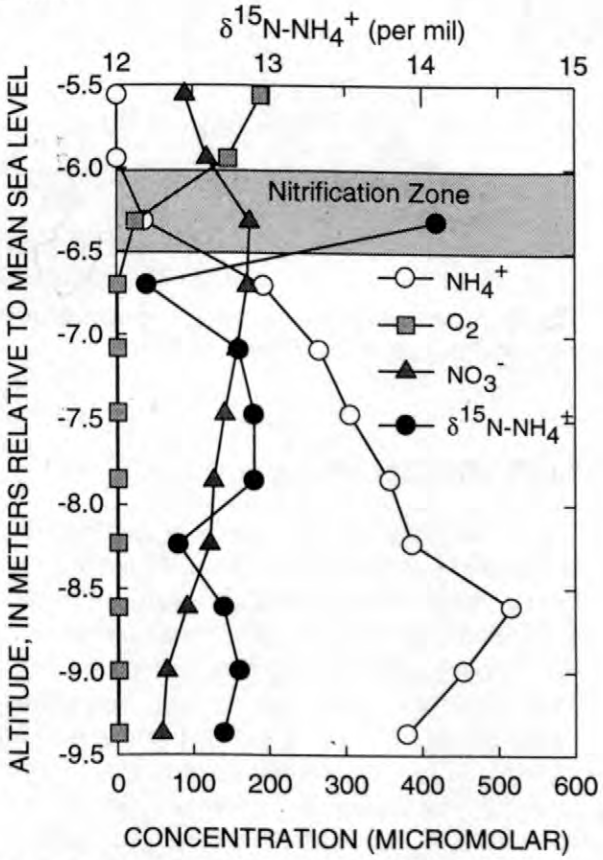

Figure 2. Concentration of dissolved nitrogen species and O_2 at tracer injection well in June 1997. Delta (δ) values are given in units of parts per thousand (‰, or per mil), as defined by $\delta = 1000*[R/R_{air} - 1]$, where R and R_{air} are the ratios $^{15}N/^{14}N$ of the sample and of atmospheric nitrogen, respectively.

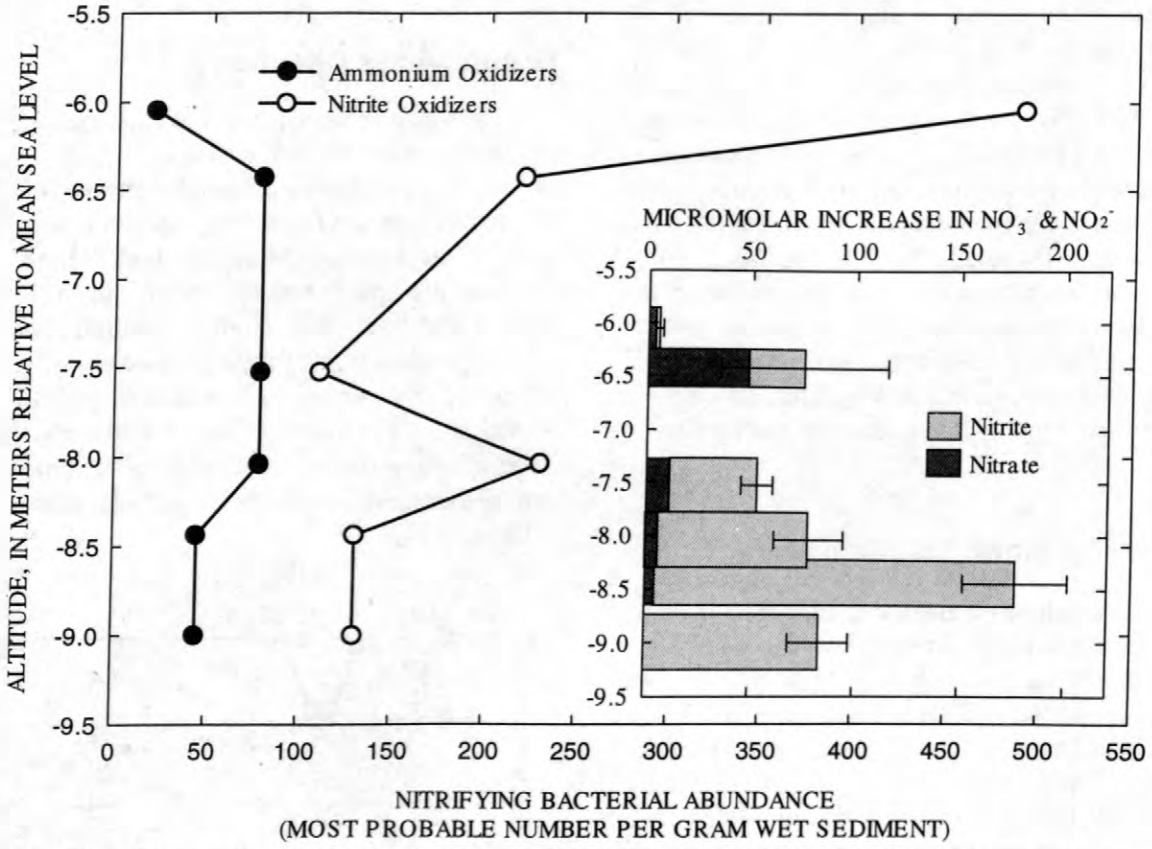

Figure 3. Abundance of nitrifying organisms and nitrification potential (inset figure) in sediment cores collected from well site F168.

Sediment Core Experiments

Nitrification is a biologically mediated, two step process where NH_4^+ is first oxidized to NO_2^- by one group of bacteria (ammonium oxidizers), and then a second group of bacteria (nitrite oxidizers) complete the transformation by oxidizing NO_2^- to NO_3^-. Ammonium- and nitrite-oxidizing bacteria were found throughout the core profile (fig. 3). The abundance of nitrite-oxidizers was consistently higher than the abundance of ammonium-oxidizers. Although nitrifier abundance was lower than expected, their presence accounts for nitrification potential observed in aerobic sediment slurries spiked with NH_4^+ (fig 3., inset). Very little NO_2^- or NO_3^- accumulated in sediment slurries above –6.25 m even though nitrifying organisms present in this core material. This is due in part to the very low numbers of ammonium oxidizers. Surprisingly, even cores taken from anaerobic zones could produce NO_2^- and NO_3^- from NH_4^+.

DNA was successfully extracted and purified from the -6.5 m core section. PCR amplification with ammonium-oxidizer specific primers produced a PCR product of the expected size (1 kilobase). Restriction analysis of the PCR product was used to (i) verify that the PCR product generated from core DNA was from nitrifying organisms and not from a closely related, non-nitrifier like *Spirillum volutans*, and (ii) determine the nitrifier species responsible for generating the PCR product. When the PCR product was restricted with *Mbo I*, a 4-cutter endonuclease, several smaller fragments were produced (fig. 4). The resultant bands corresponded exactly to the bands generated from the nitrifier strain *Nitrosomonas eutropha*.

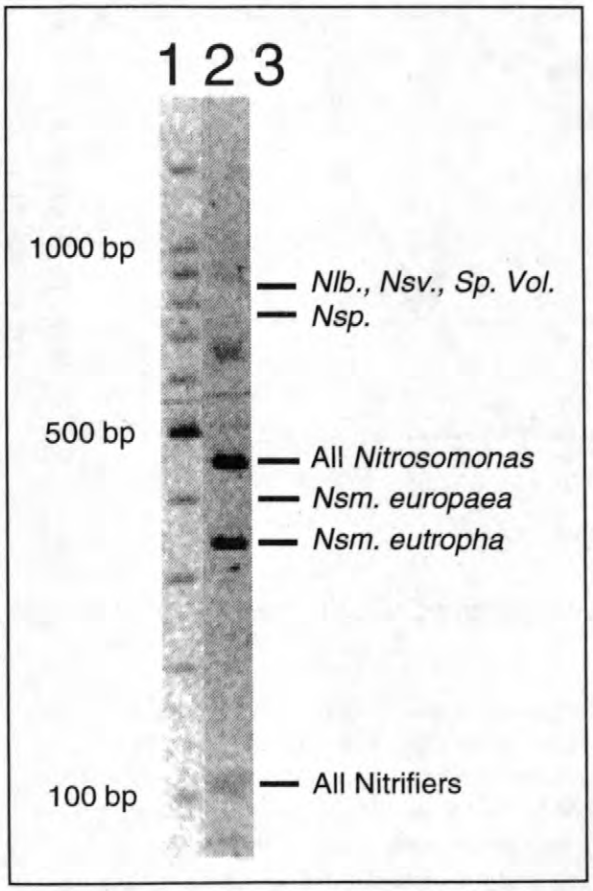

Figure 4. Endonuclease restriction analysis of the ammonia oxidizer polymerase chain reaction product with *Mbo I*. DNA fragments were separated on a 3% agarose gel, stained with ethidium bromide, and viewed under ultraviolet light. Lane 1: 100 base pair DNA ladder. Lane 2: Sediment core PCR product restricted with *Mbo I*. Lane 3: Potential restriction pattern from available nitrifying organisms and *Spirillum volutans*, a closely related non-nitrifier. Abbreviations: *Nsm* = genera *Nitrosomonas*, *Nlb* = general *Nitrosolobus*, *Nsv* = genera *Nitrosovibrio*, *Nsp* = genera *Nitrosospira, and Sp. vol* = *Spirillum volutans.*

Natural-Gradient Tracer Test

A conceptualization of the natural-gradient tracer test is presented in fig. 5. A mixture of ground water, Br^-, and $^{15}NH_4^+$ is injected in the aquifer. Because the movement of $^{15}NH_4^+$ is retarded by sorption to aquifer sediments, its movement is much slower than Br^-, which moves with ground-water flow. As $^{15}NH_4^+$ is nitrified, a cloud of $^{15}NO_3^-$ is formed. Since NO_3^- moves much faster than the NH_4^+, $^{15}NO_3^-$ will move out of the $^{15}NH_4^+$ cloud trailing behind the Br^- cloud.

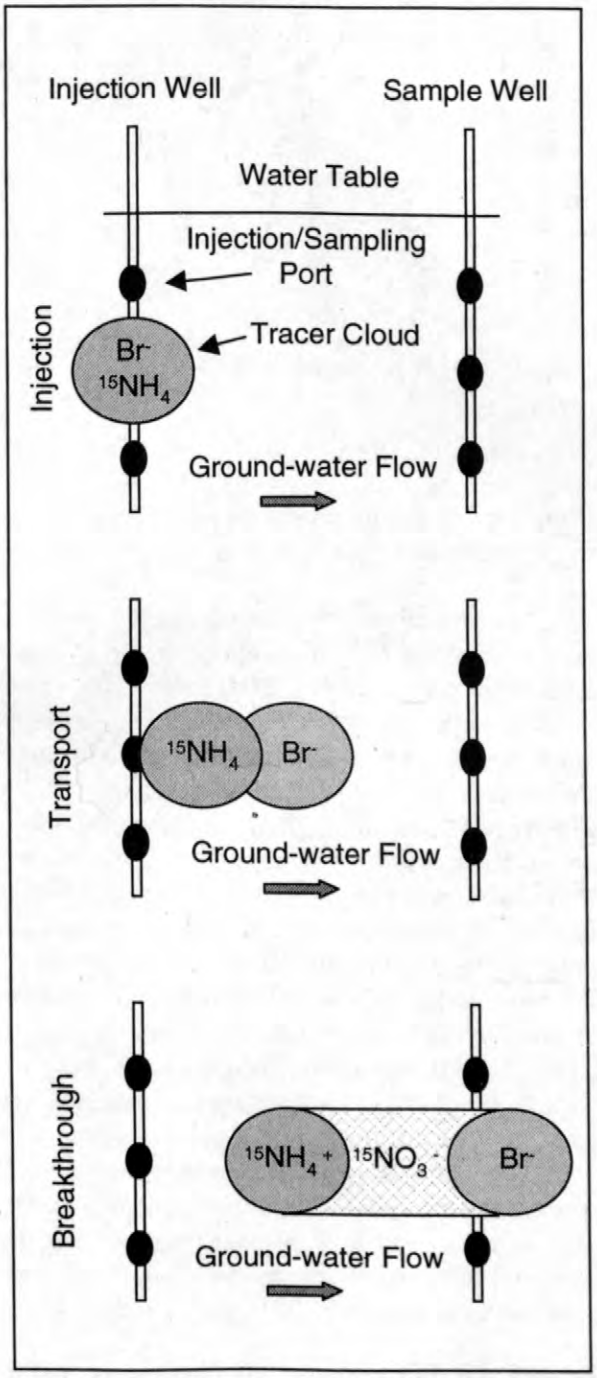

Figure 5. Idealized model of $^{15}NH_4^+$ and Br^- natural-gradient tracer test. Tracer clouds overlap immediately after injection. Clouds separate during transport owing to the slower transport of NH_4^+ compared to Br^-. Tracer clouds completely separated during breakthrough with $^{15}NO_3^-$ (formed in the $^{15}NH_4^+$ cloud) transported faster than the $^{15}NH_4^+$.

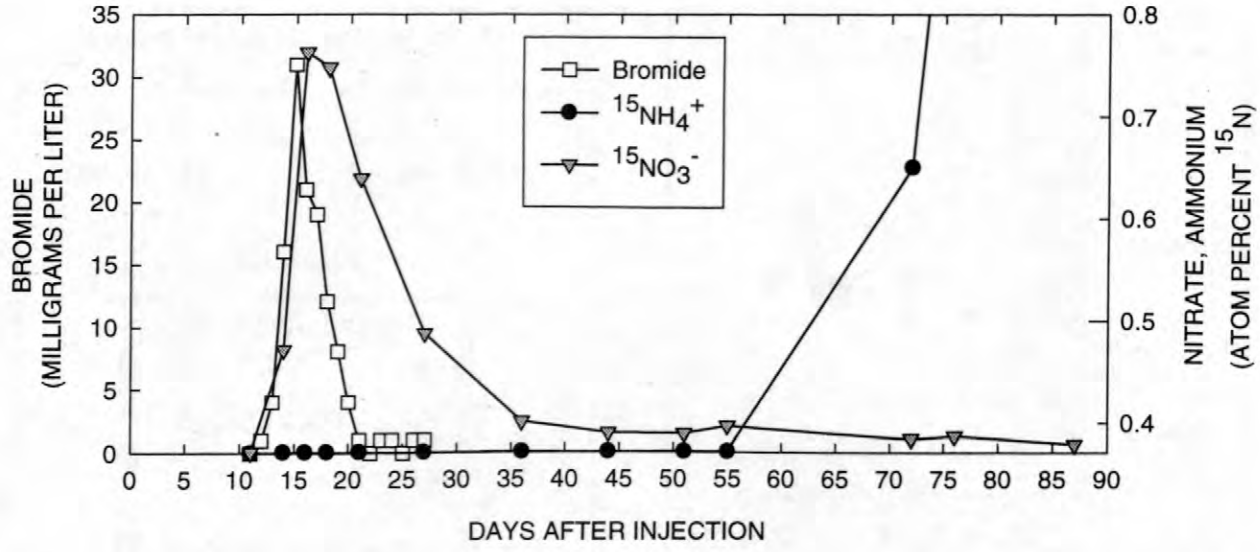

Figure 6. Breakthrough curves for Br^-, $^{15}NH_4^+$, and $^{15}NO_3^-$ at a sampling well 9.15 meters downgradient of the injection well

The initial concentration of tracer constituents was 103 milligrams (mg) $Br^- L^{-1}$ and 53.6 Atom percent (At%) $^{15}NH_4^+$. Peak Br^- breakthrough (31 mg $Br^- L^{-1}$) occurred 15 days after injection at well F593 M08-06 (9.15 m from the injection well) at a depth of –6.2 m (fig. 6). Initial $^{15}NH_4^+$ breakthrough began more than 55 days after injection. A large peak of $^{15}NO_3^-$ is seen immediately after Br^- at the sampling well. We interpret this large peak as an injection artifact, possibly because nitrification was stimulated by the two-fold increase in NH_4^+ concentration and/or by additional O_2 (concentrations increased from 24 to 27 µM). However, $^{15}NO_3^-$ did not return to background levels. It is this low concentration of $^{15}NO_3^-$ that we attribute to *in situ* nitrification.

A rough estimate of the *in situ* nitrification rate in the transition zone can be calculated based upon ground-water flow rate, the mass of $^{15}NO_3^-$ produced immediately before the $^{15}NH_4^+$ breakthrough, assumed $^{15}NH_4^+$ peak width and shape, the porosity of the aquifer, and a constant nitrification rate. A minimum and maximum nitrification rate of 13 and 96 nanomoles of NO_3 per L aquifer per day was calculated (table 1). Given these rates, it would take from 2 to 16 years to consume the NH_4^+ in the nitrification zone. In that amount of time, NO_3^- would have traveled from 500 to 3800 m while the NH_4^+ would have traveled 63 to 480 m. Our interpretation of these results is that nitrification plays a significant role in nitrogen speciation and transport in the transition zone between the sewage plume and uncontaminated ground water. A second tracer test, with complete Br^-, $^{15}NO_3^-$, and $^{15}NH_4^+$ breakthrough curves, is currently under way. This new data set will allow us to accurately measure *in situ* nitrification rates and predict the fate and transport of nitrogen species at this site.

Table 1. Nitrification natural-gradient tracer test results.

Nitrogen Species	Transport Rate (centimeters/day)	Retardation Factor	Oxidation Rate (nanomoles per liter aquifer per day)
NH_4	8 - 16	3.8	13 – 96
NO_3	32 - 64	1.0	NA

ACKNOWLEDGEMENTS

This work was funded in part by USDA grant #95-37101-1713 and a National Research Council postdoctoral fellowship. We would also like to thank Brigid Kumler for her technical support.

REFERENCES

Barcelona, M.J. and Naymik, T.G., 1984, Dynamics of a fertilizer contaminant plume in groundwater: Environmental Science and Technology, v. 18, p. 257-261.

Bjerg, P.L. and Christensen, T.H., 1993, A field experiment on cation exchange-affected multicomponent solute transport in a sandy aquifer: Journal of Contamination Hydrolology, v. 12, p. 269-290.

Boccuzzi, V.M., Straube, W.L., Ravel, J., Colwell, R.R., and Hill, R.T., 1995, Removal of contaminating substances from environmental samples prior to PCR using Sephadex G-200 spun columns, in Abstracts of the 95th General Meeting of the American Society for Microbiology, May 21-25, 1995, American Society for Microbiology, Washington, D.C., p. 361.

Ceazan, M.L, 1987, Migration and transformations of ammonium and nitrate in a sewage-contaminated aquifer at Cape Cod, Massachusetts: Golden, Colo., Colorado School of Mines, unpublished Master's Thesis, 145 p.

Ceazan, M.L., Thurman E.M., and Smith, R.L., 1989, Retardation of ammonium and potassium transport through a contaminated sand and gravel aquifer: the role of cation exchange: Environmental Science and Technology, v. 23, p. 1402-1408.

Fisk, M., and Fahey, T, 1990, Nitrification potential in the organic horizons following clearfelling of northern hardwood forests: Soil Biology and Biochemistry, v. 22, p. 277-279.

Hill, A.R., and Shackleton, M., 1989, Soil N mineralization and nitrification in relation to nitrogen solution chemistry in a small forested watershed: Biogeochemistry, v. 8, p. 167-184.

LeBlanc, D.R., 1984, Sewage plume in a sand and gravel aquifer, Cape Cod, Massachusetts: U.S. Geological Survey Water-Supply Paper 2218, 28 p.

Mobarry, B.K., Wagner, M., Urbain, V., Rittmann, B.E., and Stahl, D.A., 1996, Phylogenetic probes for analyzing abundance and spatial organization of nitrifying bacteria: Applied and Environmental Microbiology, v. 62, p. 2156-2162.

Pederson, J.K., Bjerg, P.L., and Christensen, T.H., 1991, Correlation of nitrate profiles with groundwater and sediment characteristics in a shallow sandy aquifer: Journal of Hydrology, v. 124, p. 263-277.

Savoie, J., and LeBlanc, D.R., 1998, Water-quality data and methods of analysis for samples collected near a plume of sewage-contaminated ground water, Ashumet Valley, Cape Cod, Massachusetts, 1993-94: U.S. Geological Survey Water-Resources Investigations Report 97-4269, 208 p.

Schmidt, E.L., and Belser, L.W., 1994, Autotrophic nitrifying bacteria, in Weaver, R.W., Angle, J.S., and Bottomley, P.S., eds., Methods of Soil Analysis, Part 2--Microbiological and Biochemical Properties: Madison, Wis, Soil Science Society of America, p. 159-177.

Smith, R.L., and Duff, J.H, 1988, Denitrification in a sand and gravel aquifer: Applied and Environmental Microbiology, v. 54, p. 1071-1078.

Voytek, M.A., and Ward, B.B., 1995, Detection of ammonium-oxidizing bacteria of the beta-subclass of the class Proteobacteria in aquatic samples with the PCR: Applied and Environmental Microbiology, v. 61, p. 444-1450.

AUTHOR INFORMATION

Daniel N Miller, U.S.D.A., A.R.S., U.S. Meat Animal Research Center, Clay Center, Nebraska

Richard L. Smith, U.S. Geological Survey, Boulder, Colorado

John Karl Bohlke, U.S. Geological Survey, Reston, Virginia

Recharge Conditions and Flow Velocities of Contaminated and Uncontaminated Ground Waters at Cape Cod, Massachussetts: Evaluation of δ^2H, $\delta^{18}O$, and Dissolved Gases

John-Karl Böhlke, Richard L. Smith, Tyler B. Coplen, Eurybiades Busenberg, and Denis R. LeBlanc

ABSTRACT

The isotopes of H and O in H_2O, and the concentrations of dissolved Ar, N_2, and O_2, were used to investigate recharge conditions and flow velocities in parts of a ground-water contaminant plume originating from disposal of treated domestic waste water and in surrounding uncontaminated ground water at the Massachusetts Military Reservation on Cape Cod. Contrasting patterns of isotope and gas abundances in the two water types are attributed to their different recharge sources and conditions: a low rate of areally distributed recharge of precipitation producing closely spaced, horizontal isochrons above the plume resulted in significant vertical variation in the H_2O isotope ratios but relatively little variation in atmospheric gases; conversely, a high rate of local recharge of recycled ground water producing more widely spaced, tilted isochrons in the plume resulted in significant horizontal variation in atmospheric gases but almost no variation in the H_2O isotope ratios. In addition, waters enriched in heavy isotopes by evaporation were detected in a pond and in the aquifer downgradient from the pond.

Concentrations of Ar and N_2 were consistent with recharge at temperatures ranging from about 8-24°C, followed by varying amounts of denitrification within the plume. Plume waters were anoxic, but O_2 concentrations above and below the plume averaged about 80-90 % of air saturation values at the temperatures implied by corresponding Ar concentrations, indicating relatively little O_2 reduction at time scales of up to at least 25 years. Vertical variations in ground-water isotope ratios above the plume at a site 140 m from the source in November 1996 were consistent with a precipitation recharge rate of 0.6-1.0 m/yr, an age of 1.0-1.5 yrs at the top of the plume, and a horizontal flow velocity of 140-210 m/yr. Longitudinal variations in Ar concentrations and H_2O isotopes in March 1998 were consistent with the position and age of the trailing edge of the plume following cessation of waste-water disposal in December 1995, and with horizontal flow velocities between about 120 and 240 m/yr. The isotope and dissolved-gas results are consistent (to within about ± 50 %) with travel times indicated by $^3H/^3He$ dating, injected tracer tests, regional flow modeling, and passage of other conservative tracers representing the trailing edge of the plume.

INTRODUCTION

Conditions of ground-water recharge and short-term ground-water velocities commonly are reflected in the stable isotopic composition of H_2O and the concentrations of dissolved atmospheric gases. The H and O isotopes in atmospheric moisture vary systematically as air masses move away from moisture sources, cool, condense, and precipitate rain or snow (Craig, 1961; Rozanski and others, 1993). A common result is that the δ^2H and $\delta^{18}O$ values of precipitation are positively correlated with temperature, so that winter values are more negative than summer values. Regular seasonal variations in the δ^2H and $\delta^{18}O$ values of precipitation may be evident at the water table if recharge occurs by piston flow, and they may persist for some distance downward within the saturated zone if vertical ground-water dispersion is limited. In favorable situations, seasonal isotope signals can be used to determine ground-water flow velocities within a few years of recharge (Stichler and Moser, 1979). Similarly, the concentrations of dissolved atmospheric gases vary inversely with the temperature of equilibration at the water table (Weiss, 1970) and, if recharge and isolation occur rapidly enough, seasonal variations in concentrations of Ar and other stable gases may be used to determine ground-water flow velocities (e.g., Sugisaki, 1961). Dispersion may be expected to reduce the

amplitudes of seasonal variations in the gas concentrations and isotopic compositions of recharging ground waters as they flow through aquifers, but the rate at which this occurs is not well known from direct evidence and may be expected to vary depending on the geometry of recharge and flow.

Applications of the isotope and gas methods to determining recharge conditions and ground-water velocities are most likely to succeed where recharge is rapid and(or) dispersion is limited. In unconfined aquifers where recharge is areally distributed, isochrons are approximately parallel to the water table, and seasonal variations in water isotopes or gas concentrations are most likely to be found in short vertical profiles near the water table. In confined aquifers or in unconfined aquifers with high local recharge rates, isochrons are spaced more widely in the vertical dimension and seasonal variations in recharge characteristics may be detectable in longitudinal (subhorizontal) transects. The Toxic Substances Hydrology Program research site at the Massachusetts Military Reservation (MMR) on Cape Cod includes both types of recharge environments. In addition, the MMR includes numerous surface-water bodies in which isotope signals related to evaporation and(or) seasonal precipitation may originate. The current study is a preliminary evaluation of the distribution of H and O isotopes of water and the concentrations of Ar, N_2, and O_2 in those different environments. The data were collected as a result of two major projects investigating the transport and reaction of N and O species in a contaminated waste-water plume (Böhlke and others, 1997; Smith and others, 1997; Smith and others, 1999; Miller and others, 1999; Revesz and others, 1999).

CONTAMINATED AND UNCONTAMINATED GROUND WATERS

The surficial aquifer at the MMR study site consists largely of fluvial-deltaic sands and gravels deposited from glacial melt waters in Late Wisconsin time. Distributed recharge to the surficial aquifer from precipitation in the vicinity of the MMR was estimated to be about 0.55 m/yr based on water balance calculations (LeBlanc and others, 1986), and 0.66 m/yr based on a calibration of a ground-water flow model (Masterson and others, 1998). Those distributed recharge rates would result in annual isochrons roughly parallel to the water table with a vertical spacing of around 1.4-1.7 m near the water table (for the average porosity of 0.39). Most of the natural precipitation recharge occurs in late fall and early winter (LeBlanc and others, 1986).

The Ashumet Valley ground-water contaminant plume was formed in the surficial aquifer by artificial recharge of treated domestic waste water starting in 1936 and ending on December 13, 1995 (LeBlanc, 1984; Hess and others, 1996). The high rate of artificial recharge beneath the waste-water disposal beds caused water-table mounding and rapid downward vertical movement of contaminated water, which then joined the regional flow system and moved more horizontally to the south (Masterson and others, 1997; Figures 1 and 2). The result after 60 years was a plume of contaminated ground water approximately 5000 m long, 500-1000 m wide, and 20-25 m thick. The plume was overlain by a wedge of uncontaminated locally-recharged ground water that increased in thickness to the south, and it was underlain by relatively uncontaminated ground water from recharge areas north of the disposal beds. The contaminated plume was anoxic ($O_2 < 10$ μM) and had relatively high concentrations of NO_3^-, Cl^-, SO_4^{--}, dissolved organic C, dissolved inorganic C, B, and other constituents; whereas, the surrounding ground waters generally were oxic. Vertical chemical gradients between the plume and the surrounding ground waters above and below were fairly abrupt. Since cessation of waste-water recharge in December, 1995, the trailing edge of the plume has been replaced by ground waters recharged under more normal conditions (LeBlanc and others, 1999).

The 8 southernmost (downgradient) disposal beds were active from 1983 until the end in 1995 (Hess and others, 1996; Figure 1). The amount of treated waste water discharged to the disposal beds averaged approximately 950 m^3/d spread over an area of about 2000 m^2 at any given time, or 16,000 m^2 overall). The normal rotation cycle for disposal among the individual beds was in the order of 1 day; for time scales longer than a few days, the 950 m^3/d recharge may be considered to have been distributed evenly over 16,000 m^2, corresponding to a local recharge rate of about 6 cm/d or 22 m/yr. At that rate, the 20-25 m thickness of the plume would have been filled vertically in less than half a year. The horizontal travel time from the upgradient edge to the downgradient edge of the southern disposal area could be as much as 1 yr, consistent with

significant lateral spreading of the plume beneath the source. In recent years, rates of water use and disposal at the site averaged around 10-20 % higher in summer months than in winter months (F. Creighton, Otis ANG Base, written commun., 1998).

From the longitudinal $^3H/^3He$ age gradient in the core of the plume, Shapiro (1998) estimated that the long-term average velocity of the plume was 126 ± 2 m/yr., but the data also indicate significant variations in the vertical age gradients within the plume. Horizontal velocities estimated from aquifer hydraulic properties and from injected tracer tests range from about 0.2-0.6 m/d (70-220 m/yr) (LeBlanc, 1984; LeBlanc and others, 1991). Because of seasonal and other variations in water use at the MMR, and because of variations in aquifer hydraulic properties, it is possible that age gradients within the plume exhibit significant irregularities with a resolution of months to years (Figure 2). Nevertheless, limited data support the conceptual model that calls for annual isochrons within the plume generally to dip downward toward the point source of recharge (Shapiro, 1998).

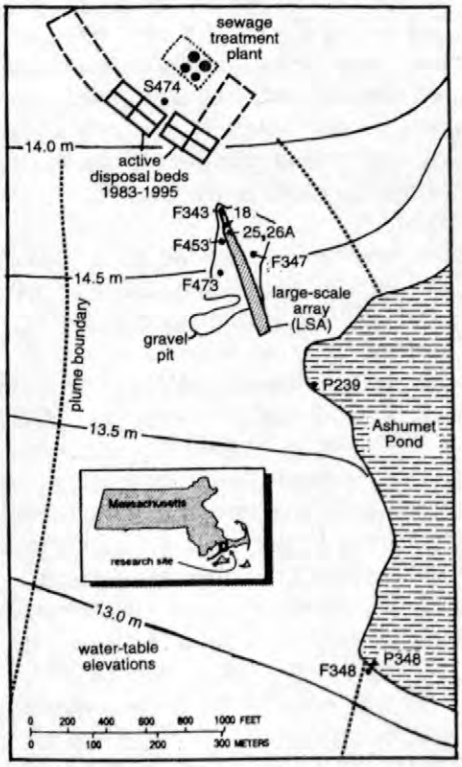

Figure 1. Map showing the location of sampling sites in the northern (proximal) part of the study area. Average water table contours are from LeBlanc (1984). Sites F168 and F593 (Appendix) are off the map approximately 2600 m downgradient (south) from the disposal beds.

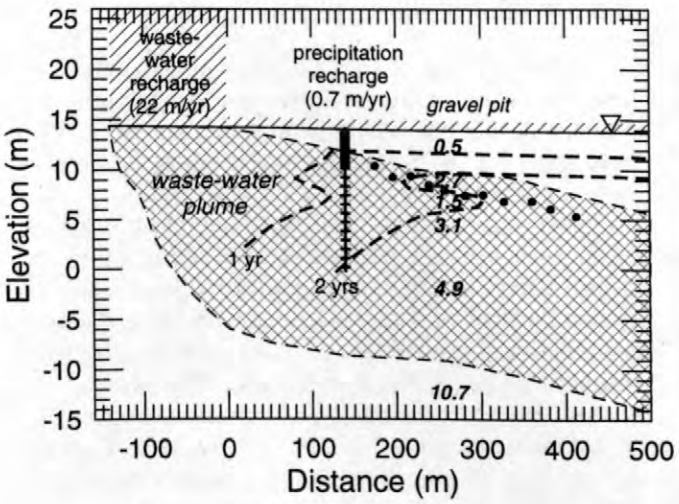

Figure 2. Schematic longitudinal vertical section through the waste-water plume showing the locations of sample profiles. The boundaries of the plume (shaded area) correspond approximately to the limits of anoxia. Dashed lines indicate approximate configuration of isochrons. $^3H/^3He$ ages (in years) are given for samples collected in October, 1994 from F347 (Shapiro, 1998). Filled circles indicate samples in the longitudinal dissolved gas transect in the LSA multiports (see Figure 6); crosses indicate samples in the vertical isotope profile in F343 (see Figure 4).

METHODS

Ground-Water Sampling

Most of the ground-water samples were collected from multilevel sampling devices located either within the gravel pit (about 140-420 m down-gradient from the nearest waste-water infiltration bed) or in Ashumet Valley (about 2600 m downgradient) (Figure 1). A multilevel sampler (LeBlanc and others, 1991) is a 3.2-cm diameter PVC pipe containing a bundle of 6-mm diameter polyethylene tubes that exit the pipe at 15 discrete elevations separated by 0.25-1.0 m intervals. Samples were pumped from the polyethylene tubes through Norprene tubing by a peristaltic pump at the land surface, approximately 4-7 m above the water table. Other ground waters were obtained with submersible pumps from 5-cm diameter PVC observation wells with screens ≤ 1 m long.

Stable Isotopes of Water

Samples for H and O isotope analysis were obtained from multilevel samplers, observation wells, a MMR water-supply well, faucets in the laboratory and living quarters of the MMR, and Ashumet Pond. The isotope samples were collected unfiltered in glass bottles with polyseal caps. For hydrogen isotope measurement, a 2-mL split from each sample was equilibrated with H_2 gas at 30°C and 1 atm for 1 hour. The H_2 gas was then admitted to a dedicated mass spectrometer for analysis against a H_2 reference gas. For oxygen isotope measurement, a 2-mL split from each sample was equilibrated with CO_2 gas at 25°C and 0.5 atm for 7 hours. The CO_2 was then admitted to a dedicated mass spectrometer for analysis against a CO_2 reference gas. The hydrogen and oxygen isotope analyses were calibrated by interspersed analyses of laboratory standard waters whose values are known with respect to the normalized scale defined by the Vienna Standard Mean Ocean Water (VSMOW) and Standard Light Antarctic Precipitation (SLAP) reference waters (Coplen, 1988). The stable isotope ratios are reported relative to a standard as delta (δ) values in units of parts per thousand (‰), as defined for each element by $\delta_x = 1000 \bullet [R_x/R_s - 1]$, where R_x and R_s are the ratios $^2H/^1H$, or $^{18}O/^{16}O$ of the sample and standard, respectively. δ^2H and $\delta^{18}O$ values are reported relative to VSMOW, with overall uncertainties of around ± 1.5 ‰ and ± 0.1 ‰, respectively. H_2O isotope data are given in the Appendix; the data for F453 are from Reilly and others (1996).

Dissolved Gases

Dissolved O_2 was measured in the field by electronic probe ($O_2 > 30$ µmol/L) or by colorimetry ($O_2 < 30$ µmol/L; Chemetrics, Inc.). Samples for laboratory analysis of N_2, Ar, O_2, and CH_4 were collected in 125 mL glass serum bottles with no headspace. A dry KOH pellet (approximately 100 mg) was added to each bottle as a preservative (pH > 12), and a rubber stopper was inserted with a syringe needle in place to allow excess water to escape. In the laboratory, low-pressure headspace was created by vacuum-extraction of approximately 10 % of the water, the remaining water and headspace were equilibrated for several days at constant temperature, then the concentrations of gases in the headspace were measured by gas chromatography and converted to aqueous concentrations with corrections for the lab solubilities (E. Busenberg, M. Doughten, and P. Widman, USGS, unpublished data). Overall uncertainties, including sampling artifacts, leakage, and GC analysis, generally were less than ± 2-4 %, except for low O_2 concentrations. All samples analyzed by GC had $CH_4 < 0.1$ µmol/L.

RESULTS AND DISCUSSION

Water Sources from H and O Isotopes

In most vertical profiles, the H and O isotopic compositions of water in the plume were significantly different from those of overlying and underlying oxic ground waters and there were abrupt vertical gradients in the water isotope values between the two water types (see Appendix for data). Plume waters had relatively uniform isotopic compositions (Figure 3): at sites under the gravel pit (140-270+ m from the source) between 1995 and 1998, plume samples had $\delta^2H = -41.5 \pm 1.5$ ‰ and $\delta^{18}O = -6.8 \pm 0.2$ ‰ (± σ, n=59); at F168 and F593 under Ashumet Valley (2600 m from the source) in 1997, plume samples had $\delta^2H = -44.0 \pm 1.0$ ‰ and $\delta^{18}O = -7.3 \pm 0.1$ ‰ (n=28). Seasonal variations in the isotopic composition of precipitation were not detected within the plume, which consisted almost entirely of recycled waste water (the normal precipitation recharge rate was only 2 % of the waste-water recharge rate in the disposal beds).

Plume samples from beneath the gravel pit in 1995-1998 were similar isotopically to water samples collected from a water-supply well (J-well) in 1998 and from tap waters collected at several locations and times at the MMR in 1996 and 1998, all of which had $\delta^2H = -43.0 \pm 1.0$ ‰ and $\delta^{18}O = -6.9 \pm 0.1$ ‰ (Appendix). Those data indicate that the isotopic composition of the water was not altered significantly between the time it was extracted from the ground and the time it was re-introduced to the aquifer after having been used. That is, there is no evidence for isotopic fractionation caused by any parts of the anthropogenic hydrologic cycle including (1) extraction, (2) treatment for human consumption, (3) consumption or other use on the MMR, (4) sewage treatment including aeration, or (5) disposal in the infiltration beds.

Oxic ground waters above, below, upgradient from, and elsewhere in the vicinity of the waste-water plume (e.g., S474, S313) had relatively variable isotopic compositions, with δ^2H

= -61 ‰ to -37 ‰ and $\delta^{18}O$ = -9.9 ‰ to -6.4 ‰. In several profiles beneath the gravel pit, the δ^2H and $\delta^{18}O$ values of the overlying oxic waters decreased immediately above the plume. At F343, the isotopes varied cyclically with depth above the plume (Figure 4). The relatively large isotopic variations in the oxic ground waters are consistent with those of meteoric waters in which $\delta^2H = 8 \bullet \delta^{18}O$ + "^{2}H-excess" (Dansgaard, 1964), where ^{2}H-excess = 15 ± 2 (Figure 3). Though no precipitation measurements were made locally for this study, it is considered likely that seasonal isotope variations at the MMR were somewhat larger than those at a coastal site at Lewes, DE (around 40 ‰ in δ^2H and 5 ‰ in $\delta^{18}O$), but not as large as those at an inland site at Underhill, VT (around 70 ‰ in δ^2H and 9 ‰ in $\delta^{18}O$) (T.B. Coplen, unpublished data). Thus, the magnitude of the isotope variation in the MMR ground waters (about 24 ‰ in δ^2H and 3.5 ‰ in $\delta^{18}O$) probably was somewhat less than that of local precipitation.

Surface-water samples collected from Ashumet Pond in December, 1996 were relatively enriched in ^{2}H and ^{18}O and also were relatively far from the meteoric-water trend, with low apparent ^{2}H-excess values of 8 ± 2 (Figure 3). Those features are consistent with evaporation having altered the isotopic composition of the pond water. The apparent degree of heavy-isotope enrichment was slightly more for a sample taken near F348 at the southwest (downgradient) shore of the pond and less for a sample taken near F239 at the mid-western (upgradient) shore, possibly because of ground-water discharge near the upgradient shore. Ground waters from the F348 well nest had isotope ratios similar to the pond values, indicating that evaporated pond water recharged the aquifer and moved to depths of at least 30 m near the down-gradient edge of the pond (Figure 1).

The reason for the small apparent enrichment of ^{2}H and ^{18}O in the MMR treated waste-water plume with respect to the average of the overlying oxic ground waters is not known. Other examples have been reported of ground-water contaminant plumes having δ^2H and(or) $\delta^{18}O$ values slightly different from those of surrounding ground waters, but the reasons for the differences have not been clear. Fritz and others (1976) reported relative enrichment of ^{2}H and ^{18}O in a leachwater plume from a sanitary landfill, and speculated that the contrast might be due to evaporation in the landfill, different water sources, CO_2-H_2O exchange, or organic matter decomposition.

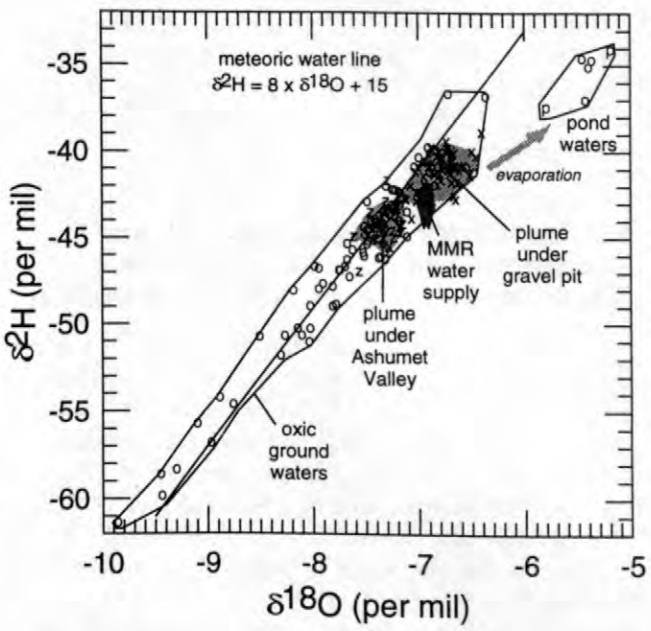

Figure 3. Relation between δ^2H and $\delta^{18}O$ in ground waters, tap waters, and pond waters. Oxic ground waters are indicated by symbol "o"; anoxic plume waters are indicated by symbols "x" and "z" (Appendix); pond waters are indicated by symbol "p".

Aravena and others (1993) attributed a small relative depletion in ^{2}H and ^{18}O in a domestic septic tank drainage water plume to the fact that the domestic water source was a relatively deep confined aquifer with an isotopic composition different from that of the surficial aquifer. Enrichment of ^{2}H caused by methanogenesis is common in ground waters from some types of sources (e.g., Hackley and others, 1996), but is not consistent with the plume data. The plume data (with ^{2}H excess = 13 ± 2) could be consistent with a minor component of evaporated pond water in the MMR water supply that was not present in the ground-water wedge overlying the plume (Figure 3). However, Masterson and others (1998) indicate that the source area for the J-well does not include major surface-water bodies.

Though the data are sparse, the slightly lower δ^2H and $\delta^{18}O$ values of the older (downgradient) plume waters at Sites 168 and 593 under Ashumet Valley could indicate a long-term (decade-scale) shift in the isotopic composition of the shallow ground-water source of the MMR water supply, possibly due to a shift in the local climatic conditions affecting recharge to the water-supply aquifer, or possibly because of a

shift in the amount of pond-evaporated water in the aquifer being used. By interpolation between the ^3H-^3He ages of plume waters at F411 (14 yrs) and F350 (26 yrs) (Shapiro, 1998), the ages of waters in the core of the plume at F168 and F593 are estimated to be about 22 yrs.

Vertical Ground-Water Velocity and Recharge Rate from Variations in Stable Isotope Ratios Above the Plume

At F343, the vertical distributions of H and O isotope ratios in oxic ground waters above the plume (Figure 4) appear to be consistent qualitatively with seasonal cycles in precipitation contributing to recharge (though damped significantly in amplitude compared to likely precipitation variations). If so, then it would appear that the multiports sampled about 1.0-1.5 years of recharge in a vertical distance of 2.5 m, corresponding to a vertical linear velocity of about 1.7-2.5 m/yr. Multiplied by the average porosity at the site (0.39), those velocities would correspond to recharge rates between about 0.6 and 1.0 m/yr, similar to the value used recently in a regional ground-water flow model (0.66 m/yr; Masterson and others, 1998). Differences between long-term regional recharge estimates and the isotope recharge rate at F343 could be due to local deviations from average recharge conditions, or to non-average precipitation in the period between Summer, 1995 and Fall, 1996, which may have been somewhat higher than usual (McCobb and others, 1999). The isotope pattern at F343 also is consistent with the timing of the sampling in November, 1996, as the $\delta^{18}O$ values near the water table may be interpreted to have just begun to decrease after the summer high values (sampled between 13 and 14 m elevation). The water at the bottom of the oxic wedge (11.5 m elevation) would have been recharged during the previous summer, perhaps 3-6 months before the waste-water disposal ended in December, 1995. These results indicate that closely spaced vertical profiles of δ^2H and $\delta^{18}O$ values of H_2O may yield reasonable estimates of ground-water vertical velocity and recharge rate in the parts of the flow system that are not affected by the waste-water plume to a depth of at least 2.5 m, corresponding to at least 1 yr of precipitation recharge. Similar techniques cannot be used within the plume because the isotopic composition of the MMR water supply was relatively homogeneous.

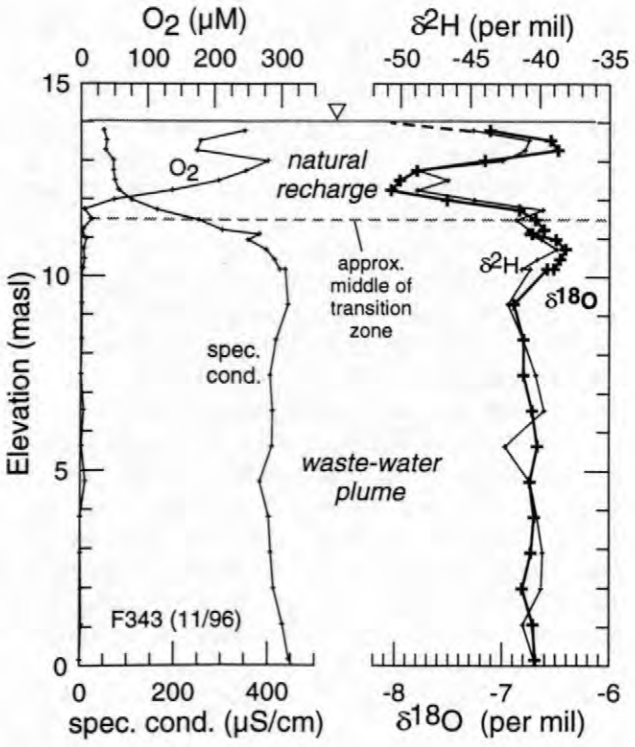

Figure 4. Vertical profiles of specific conductance, O_2 concentration, δ^2H, and $\delta^{18}O$ values near the top of the contaminated plume in F343 (Figures 1 and 2). The transition zone between plume water and overlying natural recharge is indicated by the specific conductance gradient between 11 and 12 m elevation. The upper plume boundary is shown at 11.5 m elevation near the middle of the transition zone.

Recharge Temperatures from Dissolved Nitrogen and Argon Concentrations

Concentrations of Ar and N_2 (Figure 5) and $\delta^{15}N[N_2]$ values (Böhlke and others, 1997), in oxic ground waters above and below the waste-water plume were similar to those of air-saturated waters at approximately 12-20°C (Weiss, 1970) with 0 ± 2 cm^3/L of excess air (Heaton and Vogel, 1981), some of which could have been gained (positive values) or lost (negative values) during sampling. Plume waters had slightly more variable Ar concentrations corresponding to those of air-saturated waters at approximately 8-24°C. Plume waters also had more variable N_2 concentrations and $\delta^{15}N[N_2]$ values that are attributed in part to denitrification (Smith and others, 1991; Böhlke and others, 1997).

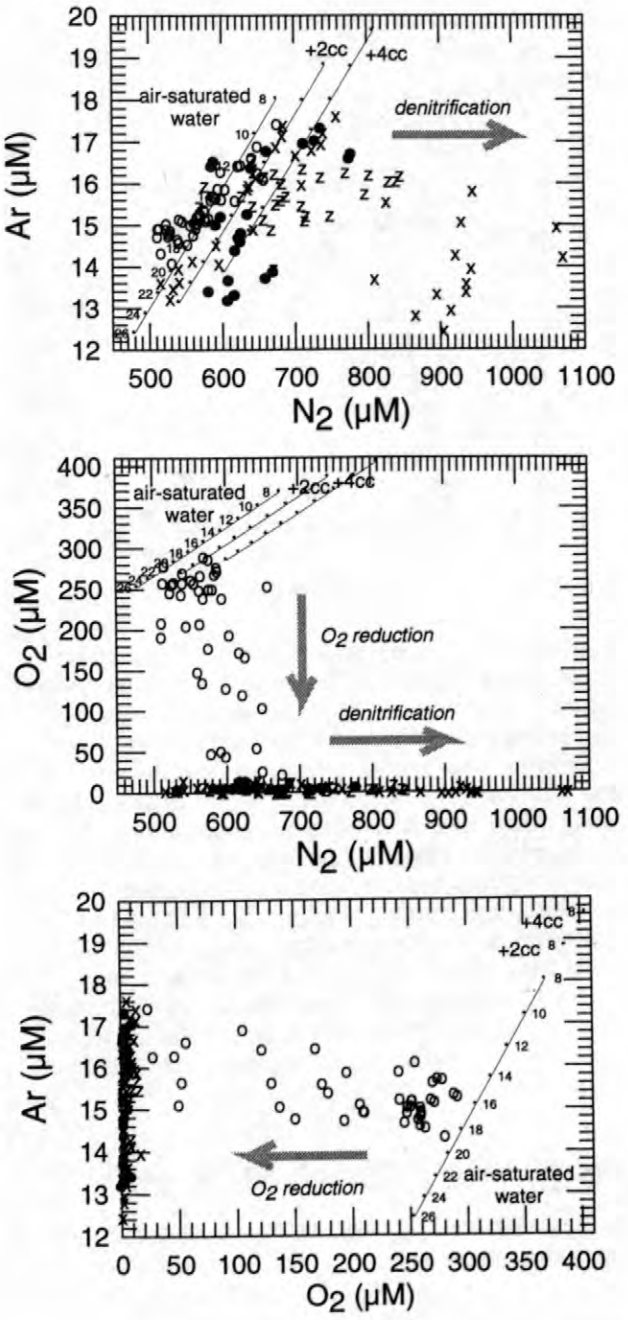

Figure 5. Ar, N_2, and O_2 concentrations in contaminated and uncontaminated ground waters. Oxic ground waters are indicated by symbol "o"; anoxic plume waters are indicated by symbols "x" and "z" (Appendix 1); filled circles indicate samples in the longitudinal dissolved gas transect (see Figure 6); curves indicate concentrations of gases in equilibrium with air (Weiss, 1970) at 100 % humidity, 14 m elevation, over a range of temperatures (8-24°C) and with varying amounts of excess air (0- 4 cm^3/L).

Variations in the concentrations of Ar may be attributed largely to seasonal variations in the temperatures of recharge. Relatively large variations in apparent recharge temperatures were recorded and preserved within the plume near its source, possibly because the high local rate of recharge and the relatively large distances between isochrons minimized the effects of dispersion or re-equilibration on the Ar concentrations. Ar concentrations at F168 and F593 (2600 m downgradient from the disposal beds) indicate more uniform recharge temperatures (13-17°C), consistent with dispersion of the seasonal signal over long travel times. The relatively small variations in the apparent recharge temperatures of the oxic waters may indicate effects of vertical dispersion or of partial equilibration with changing temperatures near the water table.

Whereas the majority of precipitation recharge is believed to have occurred in the colder months, there may have been a slightly higher rate of waste-water disposal in the summer months. However, the Ar concentrations do not indicate that recharge temperatures were systematically higher in the plume than outside the plume, possibly because the variability of both groups is large and the sample set is not representative, or because of delay or partial re-equilibration between infiltration and isolation.

Horizontal Ground-Water Velocity from Variations in Apparent Recharge Temperatures and H_2O Isotopes

A one-dimensional survey of Ar concentrations in ground waters just below the upper boundary of the contaminated plume in March, 1998 indicates a range of apparent recharge temperatures from about 10 to 22°C (Figure 6), similar to the range observed in other samples from various localities at the site. The systematic cyclic variation of apparent recharge temperatures in the 240 m longitudinal transect could be consistent with a 1.0-1.1 year-long record of seasonal changes in recharge temperature of the plume, in which case the Ar transect would indicate a horizontal flow velocity of around 220-240 m/yr. However, because those samples were collected 2.2 yrs after the cessation of waste-water disposal, it is possible that upgradient ground waters may have replaced plume waters in parts of the transect. This is supported by significant deviations of δ^2H and $\delta^{18}O$ from plume values about half-way through the transect (Figure 6),

indicating that the trailing edge of the plume water was around 250-300 m downgradient from the edge of the disposal beds (around LSA rows 40-50). The isotope data are in agreement with the distributions of other conservative tracers such as B, which indicate the trailing edge of the plume was about 250-300 m downgradient in May-June, 1998 (LeBlanc and others, 1999). As the isotope samples were taken about 1-3 m below the top of the plume (that is, at plume depths between 5 and 15 % of the total plume thickness of 20 m), their recharge points may be assumed to have been upgradient from the southern edge of the infiltration beds by 5-15 % of the total distance across the infiltration beds (about 100 m), yielding total flow-path distances about 5-15 m longer than those given in Figure 6. In that case, allowing time for waste-water recharge, the H_2O isotope data would indicate a minimum velocity of about 120-140 m/yr for the trailing edge of the plume. This interpretation is supported by the observation that the trailing edge of the plume defined by the H_2O isotopes occurs where Ar concentrations are relatively high, consistent with the timing of source cessation in December, 1995.

The plume transect results can be compared with several other independent indicators of the horizontal ground-water flow velocities beneath the gravel-pit area. For example, the ground-water age at the top of the plume indicated by the H_2O isotope profile in F343 in 1996 was 1.0-1.5 yrs, which, for a travel distance of 140 m, would correspond to a horizontal velocity of 140-210 m/yr. In a large-scale tracer experiment monitored from July, 1985 to December, 1986 (LeBlanc and others, 1991), the trailing and leading edges of a Br^- cloud advanced at rates ranging from 0.2 to 0.9 m/d (70-330 m/yr); whereas the center of mass of the cloud moved with an average velocity of 0.42 m/d (153 m/yr). The shape of the cloud was irregular and the apparent velocities varied spatially, being relatively high near the water table (LeBlanc and others, 1991). The overall average velocity of the contaminated plume estimated from the distribution of ^3H-^3He ages was 126 ± 2 m/yr (Shapiro, 1998). However, an apparent age reversal at F347 beneath the gravel pit may indicate significant variations in the velocities at different depths (Figure 2). The apparent ages and corresponding velocities from estimated recharge points within the disposal beds to the sample elevations in F347 are: to 4.5 m elevation, 310 m in 3.1 yrs = 100 m/yr; to 7.0 m elevation , 290 m in 1.6 yrs = 180 m/yr; to 9.1 m elevation, 270 m in 2.7 yrs = 100 m/yr. The elevation of the dissolved gas transect at Row 41 (nearest F347) was 7.9 m, possibly within a zone of relatively rapid flow (Figure 2).

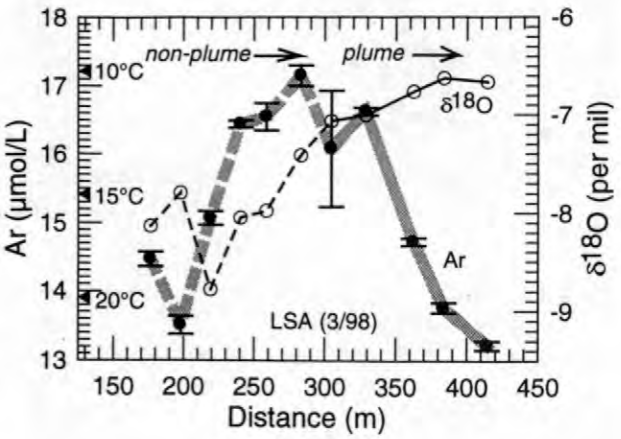

Figure 6. Ar concentrations and $\delta^{18}O$ values in a longitudinal transect in the upper part of the waste-water plume (Figure 2). Samples were collected in the large-scale array (LSA) in March, 1998. The horizontal flow-path distances are measured from the nearest edge of the waste-water disposal beds. Data points and error bars represent averages and ranges for analyses of duplicate samples. Temperatures are indicated for Ar concentrations in equilibrium with air at 100 % humidity, 14 m elevation, with no excess air (Weiss, 1970). The solid lines indicate the part of the transect in which H and O isotopes are consistent with plume water; the dashed lines indicate the part of the transect in which plume water may have been replaced by upgradient ground water.

Distribution of Dissolved Oxygen

Dissolved O_2 concentrations were high in uncontaminated ground waters both above and below the contaminated plume (Figure 2; Appendix). Maximum O_2 concentrations in samples collected for Ar and N_2 analyses averaged about 260 µM, approximately 85 % of the saturation value (310 µM) at the average Ar recharge temperature of 16°C. Larger sets of field measurements at the site indicate maximum O_2 concentrations ranging between about 250 and 340 µM (Savoie and LeBlanc, 1998), equal to or slightly less than saturation values over the range of apparent recharge temperatures. O_2 concentrations of at least 250 µM occur in ground waters at least as old as 25 yrs (Savoie and LeBlanc, 1998; Shapiro, 1998), indicating that the glacial-fluvial sediments in the surficial aquifer

were not capable of supporting a high rate of O_2 reduction outside the plume. Corresponding cumulative reaction rate constants derived from some of the relatively old oxic ground waters (assuming maximum recharge concentrations of around 340 µM) would be less than 0.013/yr (first-order) or less than 4 µM/yr (zero-order). The data do not indicate systematic decreases in O_2 concentrations with age; instead it is possible that the oxic ground waters were recharged with 80-90 % of the air-saturation values owing to O_2 reduction in the unsaturated zone, or that they lost 10-20 % of their O_2 relatively quickly after recharge, perhaps by oxidation of small amounts of reactive DOC. In this case, reaction rates after the first few years may have been significantly smaller than the estimated maximum values for the cumulative rates.

O_2 concentrations decreased abruptly in the dispersive transition zones at the upper and lower boundaries of the plume (Figures 2 and 4), and were consistently low (< 10 µM) within the plume. O_2 reduction apparently was associated with oxidation of reduced constituents in the plume water, and occurred at a relatively high rate near the source beds. Complete loss of O_2 within 1 year of recharge implies O_2 reduction rates within the plume greater than 1/yr (first-order) or greater than 350 µM/yr (zero-order), at least two orders of magnitude higher than the rates outside the plume. O_2 reduction rates in the transition zone between the plume and overlying ground water apparently were intermediate between those above and below (Smith and others, 1999).

SUMMARY

Evidence was found for seasonal variations in the stable isotope ratios and dissolved atmospheric gas concentrations of recharging ground waters at the MMR. In the vicinity of the waste-water treatment plant, the distributions of stable isotopes and dissolved gases were consistent with 2 contrasting isochron configurations caused by the high local recharge rate in the waste-water disposal beds: Outside the plume, isochrons were parallel to the water table and closely spaced. Inside the plume, isochrons were at a higher angle to the water table (with some apparent reversals) and more widely spaced. Seasonal variations in stable isotope ratios with depth below the water table were used to determine vertical velocities and recharge rates outside the plume, while seasonal variations in atmospheric gas concentrations with horizontal distance from the source beds were consistent with horizontal velocities within the trailing edge of the plume. There is approximate agreement on travel times and velocities in the first few years of flow near the top of the plume derived from (1) $^3H/^3He$ dating, (2) vertical recharge from H_2O isotopes, (3) displacement of the plume after cessation of waste-water disposal indicated by H_2O isotopes and other conservative tracers, (4) horizontal gradients in dissolved gas concentrations in the plume, (5) injected tracer tests, and (6) regional flow simulations. Discrepancies or uncertainties of around ± 50 % may be due in part to incorrect assumptions in some of the methods (including the configuration of the flow field under the disposal beds), but real variations of the same magnitude are also evident. Specifically:

1. Three sources of ground-water recharge were distinguishable within the surficial aquifer on the basis of H and O isotope values of the H_2O: Local recharge water overlying the treated waste-water plume and elsewhere in the vicinity had variable δ^2H (-61 ‰ to -37 ‰) and $\delta^{18}O$ (-9.9 ‰ to -6.4 ‰) values that were consistent with meteoric waters with ^2H-excess values of 15 ± 2. Waters in and downgradient from Ashumet Pond but outside the plume had relatively high δ^2H (to -34 ‰) and $\delta^{18}O$ (-5.2 ‰) and significantly lower apparent ^2H-excess values (8 ± 2) indicating isotopic enrichment by evaporation. Plume waters within 420 m of the disposal beds had relatively constant and generally higher average δ^2H (-43.0 ± 1.0 ‰) and $\delta^{18}O$ (-6.9 ± 0.1 ‰) with slightly lower apparent ^2H-excess values (13 ± 2), consistent with a relatively homogeneous source and possibly indicating a minor component of evaporated pond water in the MMR ground-water supply.
2. The artificial hydrologic cycle of H_2O at the MMR, involving ground-water extraction, purification, use, treatment, disposal, and infiltration, had little or no effect on the H and O isotope ratios of the water ($\Delta\delta^2H \leq 2$ ‰; $\Delta\delta^{18}O \leq 0.2$ ‰).
3. A ground-water isotope profile at F343 indicated a vertical ground-water flow velocity of around 1.7-2.5 m/yr, corresponding to a recharge rate of around 0.8 ± 0.2 m/yr, roughly consistent with other estimates of the local natural recharge rate.
4. Concentrations of dissolved atmospheric gases indicate that plume waters were recharged at

temperatures ranging from about 8 to 24°C with 0 ± 2 cc/L of excess air.

5. A March, 1998 transect near the top of the plume beneath the gravel pit was truncated as a result of source cessation in 1995. Changes in gas recharge temperatures and H_2O isotopes indicated horizontal ground-water flow velocities in the order of 120-240 m/y, near the high end of the range of velocities derived from tracer tests and $^3H/^3He$ dating.

ACKNOWLEDGMENTS

This study was supported in part by the USDA (National Research Initiative Competitive Grants Program), EPA (NSF/EPA Water and Watersheds Program), and the USGS-WRD National Research Program and Toxic Substances Hydrology Program, in collaboration with T. Yoshinari (NY State Health Dept.) and K. Revesz (USGS). T. Peacock, M. Nimiroski, K. Revesz, J. Hannon, and T. Yoshinari assisted with field sampling. P. Widman, M. Doughten, B. Baldridge, I. Hamblen, and K. Plummer assisted with laboratory analyses. T. Councell and K. Revesz reviewed the manuscript.

REFERENCES

Aravena, R., Evans, M.L., and Cherry, J.A., 1993, Stable isotopes of oxygen and nitrogen in source identification of nitrate from septic systems. Ground Water, v. 31, p. 180-186.

Böhlke, J.K., Revesz, K.M., Smith, R.L., and Yoshinari, T., 1997, Multispecies investigation of nitrogen and oxygen isotopes in a contaminated ground-water plume undergoing dilution, oxygen consumption, and denitrification, Cape Cod, Massachusetts. EOS, Transactions of the American Geophysical Union, v. 78, p. F211.

Coplen, T.B., 1988, Normalization of oxygen and hydrogen isotope data. Chemical Geology (Isotope Geoscience Section), v. 72, p. 293-297.

Craig, H., 1961, Isotopic variations in meteoric waters. Science, v. 133, p. 1702-1703.

Dansgaard, W., 1964, Stable isotopes in precipitation. Tellus, v. 16, p. 436-468.

Fritz, P., Matthess, G., and Brown, R.M., 1976, Deuterium and oxygen-18 as indicators of leachwater from a sanitary landfill. In: Interpretation of Environmental Isotope and Hydrochemical Data in Groundwater Hydrology, International Atomic Energy Agency, Proceedings of an Advisory Group Meeting, January, 1975, p. 131-142.

Hackley, K.C., Liu, C.L., and Coleman, D.D., 1996, Environmental isotope characteristics of landfill leachates and gases. Ground Water, v. 34, p. 827-836.

Heaton, T.H.E., and Vogel, J.C., 1981, "Excess air" in groundwater. Journal of Hydrology, v. 50, p. 201-216.

Hess, K.M., LeBlanc, D.R., Kent, D.B., and Smith, R.L., 1996, Natural restoration of a sewage-contaminated aquifer, Cape Cod, Massachusetts. In: Hydrology and Hydrogeology of Urban and Urbanizing Areas, American Institute of Hydrology, p. WQE13-WQE25

LeBlanc, D.R., 1984, Sewage plume in a sand and gravel aquifer, Cape Cod, Massachusetts. U.S. Geological Survey Water-Supply Paper 2218, 28 p.

LeBlanc, D.R., Guswa, J.H., Frimpter, M.H., and Londquist, C.J., 1986, Ground-water resources of Cape Cod, Massachusetts. U.S. Geological Survey, Hydrologic Investigations Atlas HA-692, 4 sheets.

LeBlanc, D.R., Garabedian, S.P., Hess, K.M., Gelhar, L.W., Quadri, R.D., Stollenwerk, K.G., and Wood, W.W., 1991, Large-scale natural-gradient tracer test in sand and gravel, Cape Cod, Massachusetts-1. Experimental design and observed tracer movement. Water Resources Research, v. 27, p. 895-910.

LeBlanc, D.R., Hess, K.M., Kent, D.B., Smith, R.L., Barber, L.B., and Campo, K.W., 1999, Natural restoration of a sewage plume in a sand and gravel aquifer, Cape Cod, Massachusetts (this volume).

Masterson, J.P., Walter, D.A., and Savoie, J., 1997, Use of particle tracking to improve numerical model calibration and to analyze ground-water flow and contaminant migration, Massachusetts Military Reservation, western Cape Cod, Massachusetts. U.S. Geological Survey Water-Supply Paper 2482, 50 p.

Masterson, J.P., Walter, D.A., and LeBlanc, D.R., 1998, Delineation of contributing areas to selected public-supply wells, western Cape Cod, Massachusetts. U.S. Geological Survey Water-Resources Investigations Report 98-4237, 45 p.

McCobb, T.D., LeBlanc, D.R., and Hess, K.M., 1999, Temporal variability of hydraulic gradients in an unconfined aquifer determined using the three-point triangulation method, Cape Cod, Massachusetts (this volume).

Miller, D.N., Smith, R.L., and Böhlke, J.K., 1999, Nitrification in a shallow, nitrogen-contaminated aquifer, Cape Cod, Massachusetts (this volume).

Reilly, T.E., LeBlanc, D.R., Bussey, K.W., Councell, T.B., Smith, R.L., and Böhlke, J.K., 1996, Chemical and stable-isotope data from an experiment to examine temporal variability in water samples from screened wells on Cape Cod, Massachusetts, 1994. U.S. Geological Survey Open-File Report 95-734, 21 p.

Revesz, K.M., Böhlke, J.K., Smith, R.L., and Yoshinari, T., 1999, Reduction and isotope fractionation of dissolved oxygen in contaminated ground water, Cape Cod, Massachusetts (this volume).

Rozanski, K., Araguas-Araguas, L., and Gonfiantini, R., 1993, Isotopic patterns in modern global precipitation. In: Climate Change in Continental Isotopic Records, American Geophysical Union, Geophysical Monograph 78, p. 1-36.

Savoie, J., and LeBlanc, D.R. (editors), 1998, Water-quality data and methods of analysis for samples collected near a plume of sewage-contaminated ground water, Ashumet Valley, Cape Cod, Massachussetts, 1993-1994. U.S. Geological Survey Water Resources Investigations Report 97-4269, 208 p.

Shapiro, S.D., 1998, Evaluation of the ^{3}H-^{3}He dating technique in complex hydrologic environments. PhD Dissertation, Columbia University, 253 p.

Smith, R.L., Howes, B.L., and Duff, J.H., 1991, Denitrification in nitrate-contaminated ground water: Occurrence in steep vertical geochemical gradients. Geochimica et Cosmochimica Acta, v. 55, p. 1815-1825.

Smith, R.L., Böhlke, J.K., Revesz, K., Yoshinari, T., and Garabedian, S.P., 1997, Assessing denitrification in ground water using in situ tracer tests with 15N. EOS, Transactions of the American Geophysical Union, v. 78, p. F202.

Smith, R.L., Böhlke, J.K., Revesz, K.M., Yoshinari, T.D., Hatzinger, P., Penarrieta, C.T., and Repert, D.A., 1999, In situ assessment of the transport and microbial consumption of oxygen in ground water, Cape Cod, Massachusetts (this volume).

Stichler, W., and Moser, H., 1979, An example of exchange between lake and groundwater. In: Isotopes in Lake Studies, International Atomic Energy Agency, Vienna, p. 115-119.

Sugisaki, R., 1961, Measurement of effective flow velocity of ground water by means of dissolved gases. American Journal of Science, v. 259, p. 144-153.

Weiss, R.F., 1970, The solubility of nitrogen, oxygen, and argon in water and seawater. Deep-Sea Research, v. 17, p. 721-735.

AUTHOR INFORMATION

John Karl Böhlke, U.S. Geological Survey, 431 National Center, Reston, VA 20192 [jkbohlke@usgs.gov]

Richard L. Smith, U.S. Geological Survey, 3215 Marine St., Boulder, CO 80303 [rlsmith@usgs.gov]

Tyler B. Coplen, U.S. Geological Survey, 431 National Center, Reston, VA 20192 [tbcoplen@usgs.gov]

Eurybiades Busenberg, U.S. Geological Survey, 432 National Center, Reston, VA 20192 [ebusenbe@usgs.gov]

Denis R. LeBlanc, U.S. Geological Survey, 28 Lord Road, Marlborough, MA 01752 [dleblanc@usgs.gov]

Appendix 1. Specific conductance, dissolved oxygen, and water isotope data

sample ID	elev. m	H2O d18O	H2O d2H	**	O2 µM (field)	sp. cd. µS/cm (field)
S474 (3/22/96)						
PT	14.1	-7.34	-44.2	o	322	123
GNT	13.2	-8.51	-50.6	o	227	84
RT	12.3	-9.86	-61.3	o	262	84
BUT	11.4	-8.15	-50.1	o	240	105
BKT	9.8	-7.75	-46.7	o	233	124
WT	8.3	-8.31	-51.7	o	60	93
O	6.2	-6.77	-40.0	o	19	132
GY	4.0	-6.90	-41.1	o	214	138
Y	1.9	-7.49	-45.2	o	245	144
Y	1.9	-7.48	-45.0	o	245	144
P	-0.6	-7.82	-47.7	o	273	154
GN	-3.0	-7.31	-41.9	o	303	77
R	-5.8	-6.72	-36.6	o	301	56
BU	-8.5	-6.91	-39.7	o	301	52
BK	-11.3	-7.31	-43.8	o	298	65
W	-14.0	-7.23	-43.0	o	311	82
F343 (11/18/96)						
M03-PT	13.8	-7.11	-44.8	o	245	49
M03-GNT	13.5	-6.55	-40.8	o	179	55
M03-RT	13.3	-6.48	-41.1	o	173	52
M03-BUT	13.0	-7.16	-42.7	o	280	69
M03-BKT	12.8	-7.79	-48.7	o	247	69
M03-WT	12.5	-7.95	-46.6	o	206	72
M03-O	12.2	-8.03	-48.8	o	137	80
M03-GY	12.0	-7.51	-44.7	o	49	108
M03-Y	11.7	-6.84	-39.8	o	5	163
M03-P	11.5	-6.69	-41.7	x	16	252
M03-GN	11.2	-6.61	-40.8	x	3	303
M02-PT	11.1	-6.72	-41.0	x	2	383
M03-R	11.0	-6.50	-39.9	x	8	359
M03-BU	10.7	-6.41	-38.8	x	4	398
M03-BK	10.5	-6.46	-40.2	x	5	416
M03-W	10.2	-6.52	-41.3	x	3	427
M02-GNT	10.2	-6.58	-40.7	x	2	439
M02-RT	9.3	-6.89	-42.3	x	1	445
M02-BUT	8.4	-6.80	-41.2	x	2	419
M02-BKT	7.5	-6.80	-40.3	x	1	407
M02-WT	6.6	-6.72	-39.7	x	4	412
M02-O	5.6	-6.67	-42.5	x	2	410
M02-GY	4.7	-6.74	-40.7	x	7	384
M02-Y	3.8	-6.70	-40.2	x	0	403
M02-P	2.9	-6.73	-39.8	x	1	407
M02-GN	2.0	-6.81	-39.9	x	2	413
M02-R	1.1	-6.71	-41.2	x	2	432
M02-BU	0.2	-6.69	-40.4	x	0	446
M02-BK	-0.8	-6.71	-40.9	x	1	411
M02-W	-1.7	-7.02	-42.8	x	0	317
M01-PT	-1.7	-6.79	-41.6	x	1	392
M01-GNT	-3.2	-6.77	-40.3	x	1	349
M01-RT	-4.7	-6.95	-41.4	x	6	292
M01-BUT	-6.3	-6.88	-42.7	x	11	223
M01-BKT	-7.8	-6.88	-39.7	x	5	251
M01-WT	-9.3	-7.70	-46.5	o	210	124
M01-O	-10.8	-7.53	-45.7	o	193	110
M01-GY	-12.4	-6.94	-40.5	o	248	74
M01-Y	-13.3	-7.34	-45.2	o	271	61
M01-P	-14.2	-7.28	-43.5	o	260	59
M01-GN	-15.1	-7.33	-44.1	o	259	59
M01-R	-16.0	-7.26	-43.0	o	250	69
M01-BK	-17.8	-7.17	-42.3	o	251	75
M01-W	-18.8	-7.11	-43.4	o	252	84
LSA-18-12 (2/26-29/96)					2/26/96	
PT	12.1	-7.46		o	213	191
GNT	11.9	-7.11		o	169	173
RT	11.6	-6.96		o	109	179
BUT	11.4	-6.72		o	47	294
BKT	11.1	-6.72		x	8	355
WT	10.9	-6.66		x	6	363
O	10.6	-6.67		x	6	385
GY	10.3	-6.63		x	8	412
Y	10.1	-6.55		x	6	429
P	9.8	-6.43		x	6	420
GN	9.6	-6.64		x	6	443
R	9.3	-6.62		x	6	463
BU	9.1	-6.77		x	6	452
BK	8.8	-6.79		x	6	461
W	8.6	-6.66		x	6	467

sample ID	elev. m	H2O d18O	H2O d2H	**	O2 µM (field)	sp. cd. µS/cm (field)
LSA-25-13A (6/13/96)						
PT	13.5	-9.45	-58.5	o	275	
GNT	13.2	-9.10	-55.7	o	325	
RT	12.9	-8.89	-54.2	o	278	
BUT	12.6	-8.19	-47.9	o	234	
BKT	12.3	-7.68	-45.2	o	188	
WT	12.0	-7.37	-43.5	o	163	
O	11.7	-7.18	-43.0	o	175	
GY	11.4	-7.00	-40.3	o	109	
Y	11.1	-6.88	-40.9	o	38	
P	10.6	-6.82	-41.1	x	18	
GN	10.2	-6.78	-40.9	x	9	
R	9.7	-6.79	-40.8	x	11	
BU	9.2	-6.81	-40.0	x	17	
BK	8.8	-6.74	-39.3	x	17	
W	8.1	-6.79	-41.6	x	15	
LSA-26A-11A (6/13/96)						
PT	13.5	-9.44	-59.8	o	288	41
GNT	13.2	-9.30	-58.3	o	288	32
RT	12.9	-8.27	-50.5	o	291	52
BUT	12.6	-7.68	-46.1	o	278	70
BKT	12.3	-7.34	-43.4	o	263	82
WT	12.0	-7.24	-42.1	o	259	95
O	11.7	-7.22	-42.1	o	209	118
GY	11.4	-7.19	-43.9	o	150	149
Y	11.1	-6.89	-40.0	o	52	267
P	10.6	-6.85	-41.2	x	10	376
GN	10.2	-6.81	-40.4	x	9	406
R	9.7	-6.67	-40.0	x	6	423
BU	9.2	-6.68	-40.5	x	8	432
BK	8.8	-6.69	-39.9	x	7	437
F453-M2 (9/21/94)						
PT	13.7	-8.97	-56.7	o		63
GNT	13.1	-8.76	-54.5	o		59
RT	12.1	-6.91	-40.8	x		299
BUT	11.1	-6.70	-40.8	x		443
BKT	10.1	-6.66	-40.9	x		462
WT	9.1	-6.66	-40.7	x		462
O	8.1	-6.69	-40.5	x		462
GY	7.1	-6.65	-42.7	x		444
Y	6.1	-6.70	-40.6	x		436
P	5.0	-6.62	-41.0	x		462
GN	4.0	-6.64	-41.7	x		385
R	3.0	-6.81	-41.3	x		431
BU	2.0	-6.82	-41.9	x		430
BK	1.0	-6.89	-41.9	x		322
W	0.0	-6.95	-41.9	x		397
F473-M011 (6/15/95)						
PT	12.1	-7.52	-44.2	o	168	193
GNT	11.9	-7.45	-43.9	o	105	234
RT	11.6	-7.49	-44.4	o	56	270
BUT	11.4	-7.52	-45.9	o	23	309
BKT	11.1	-7.28	-45.4	x	13	344
WT	10.9	-7.16	-42.2	x	13	383
O	10.6	-7.02	-42.3	x	9	402
GY	10.3	-6.99	-42.3	x	13	421
Y	10.1	-7.03	-41.1	x	9	396
P	9.8	-7.07	-43.8	x	9	187
GN	9.6	-7.01	-40.8	x	11	311
R	9.3	-7.08	-41.9	x	8	268
BU	9.1	-7.12	-42.7	x	5	299
BK	8.8	-6.87	-40.6	x	5	214
W	8.6	-6.83	-40.2	x	5	211

sample ID	elev. m	H2O d18O	H2O d2H	**	O2 µM (field)	sp. cd. µS/cm (field)
F593 (6/9/97)						
PT		-7.63	-45.6	o	251	89
GNT		-7.38	-46.0	o	195	94
RT		-7.25	-42.1	o	130	93
BUT		-7.36	-45.9	o	27	111
BKT		-7.46	-43.4	z	5	111
WT		-7.41	-44.3	z	3	126
O		-7.35	-44.3	z	13	136
GY		-7.34	-43.4	z	5	147
Y		-7.33	-44.9	z	2	153
P		-7.30	-41.6	z	6	184
GN		-7.24	-44.9	z	10	205
R		-7.25	-44.5	z	3	204
BU		-7.18	-44.3	z	4	214
BK		-7.21	-43.2	z	4	205
W		-7.21	-43.7	z	4	198
F168 (6/8-9/97)						
M15-PT	6.3	-6.37	-36.7	o	142	71
M15-GNT	3.3	-7.16	-42.6	o	240	90
M15-RT	0.2	-7.32	-46.1	o	271	89
M15-BUT	-1.3	-7.76	-46.7	o	254	91
M15-BKT	-2.8	-7.95	-47.8	o	257	88
M16-PT	-4.0	-8.11	-50.5	o	259	147
M16-GNT	-4.3	-7.99	-46.5	o	270	133
M15-WT	-4.4	-8.04	-50.9	o	259	93
M16-RT	-4.6	-8.03	-50.1	o	268	119
M16-BUT	-4.9	-7.82	-48.8	o	274	122
M16-BKT	-5.5	-7.66	-47.1	o	241	122
M16-WT	-5.8	-7.42	-43.8	o	121	136
M15-O	-5.9	-7.42	-44.3	o	46	98
M16-O	-6.1	-7.17	-44.1	z	3	138
M16-GY	-6.5	-7.14	-42.6	z	5	135
M16-Y	-7.1	-7.40	-44.9	z	8	133
M15-GY	-7.4	-7.35	-45.0	z	8	123
M16-P	-7.4	-7.31	-43.3	z	5	132
M16-GN	-7.7	-7.25	-43.6	z	6	132
M16-R	-8.0	-7.33	-44.4	z	15	155
M16-BU	-8.6	-7.31	-42.8	z	3	161
M15-Y	-8.9	-7.22	-43.1	z	6	185
M16-BK	-8.9	-7.29	-45.7	z	4	178
M16-W	-9.2	-7.30	-44.5	z	1	186
M15-P	-10.5	-7.17	-44.6	z	3	209
M15-GN	-12.0	-7.15	-44.1	z	0	183
M15-R	-13.5	-7.18	-42.6	z	0	175
M15-BU	-15.0	-7.44	-45.0	z	1	155
M15-BK	-16.5	-7.57	-46.8	z	1	147
M15-W	-18.1	-7.62	-44.8	z	0	167
Water Supply (4/15/98)						
J-well		-6.93	-44.1	w		
Tap Water (12/4/96)						
bldg 1146 (lab)		-6.91	-42.0	w		
bldg 5526 (BOQ)		-6.89	-43.2	w		
Tap Water (4/15/98)						
bldg 1146 (lab)		-6.93	-43.1	w		
bldg 5526 (BOQ)		-6.98	-43.0	w		
Ashumet Pond (12/4/96)						
near F239		-5.80	-37.4	p		
near F348		-5.19	-34.0	p		
S313 (8/6/98)						
20'		-7.91	-47.5	o		
38'		-7.04	-40.8	o		
60'		-7.41	-44.0	o		
80'		-7.49	-42.8	o		
S348 (8/6/98)						
21'		-5.46	-34.5	o		
43'		-5.43	-36.9	o		
73'		-5.37	-34.6	o		
98'		-5.40	-35.0	o		

**
o = oxic ground water
x = plume water under gravel pit
z = plume water under Ashumet Valley
w = MMR water supply
p = pond water

Determination of Temporal and Spatial Variability of Hydraulic Gradients in an Unconfined Aquifer Using Three-Point Triangulation, Cape Cod, Massachusetts

By Timothy D. McCobb, Denis R. LeBlanc, and Kathryn M. Hess

ABSTRACT

Three-point triangulation of ground-water levels for two observation-well networks was used to estimate horizontal hydraulic gradients in an unconfined aquifer on Cape Cod, Massachusetts. Hydraulic gradients were estimated during times of low and high water levels. Increasing gradient magnitudes and changes in gradient directions with rising water levels in both networks show the strong effects of ponds and streams on the ground-water-flow system. In the regional network, gradients shifted towards streams as water levels rose, reflecting an increased divergence of flow at high water levels away from the hydraulic divide between the streams. In the local network, the magnitude and direction of gradients near a glacial kettle pond were closely correlated to water levels and proximity to the pond. Gradient estimates at one element for over 15 years demonstrated that hydraulic gradient can vary temporally and is not a constant that can be determined with a single water-table snapshot. The accuracy of gradient estimates determined by three-point triangulation depends on network elements that are appropriately sized to capture the curvature of the water table and accurate measurements of water levels.

INTRODUCTION

The horizontal hydraulic gradient in an unconfined aquifer commonly is considered constant throughout a hydrologic investigation. An average gradient typically is estimated from sparse measurements of ground-water levels, which may have been made at times of low, average, or high water-table conditions. These estimated gradients can vary greatly depending on the hydrologic conditions at the time and location, and the size of the area for which the estimates are made. Cole and Silliman (1996) provided theoretical analysis of two three-point triangulation methods used in a heterogeneous, unconfined aquifer. Little work has been done, however, to quantify the temporal and spatial variability of hydraulic gradients in unconfined aquifers on the basis of actual water-level measurements.

Water-level measurements in an unconfined aquifer at the Cape Cod Toxic Substances Hydrology research site in Falmouth and Sandwich, Massachusetts (fig. 1), were used to evaluate the temporal variability of horizontal hydraulic gradients during times of high and low water levels for two well networks of different sizes. Water-level measurements at an element from the local network provided long-term data from which trends in estimated gradient magnitude and direction can be determined.

The purpose of this paper is to quantify and illustrate the temporal and spatial variability of hydraulic gradients on the basis of estimates from a three-point triangulation method applied to Cape Cod water-level data. The results show the importance and utility of collecting hydraulic-head data in a well-distributed observation-well network on a regular basis to accurately determine ranges in hydraulic-gradient magnitude and direction as opposed to considering average values.

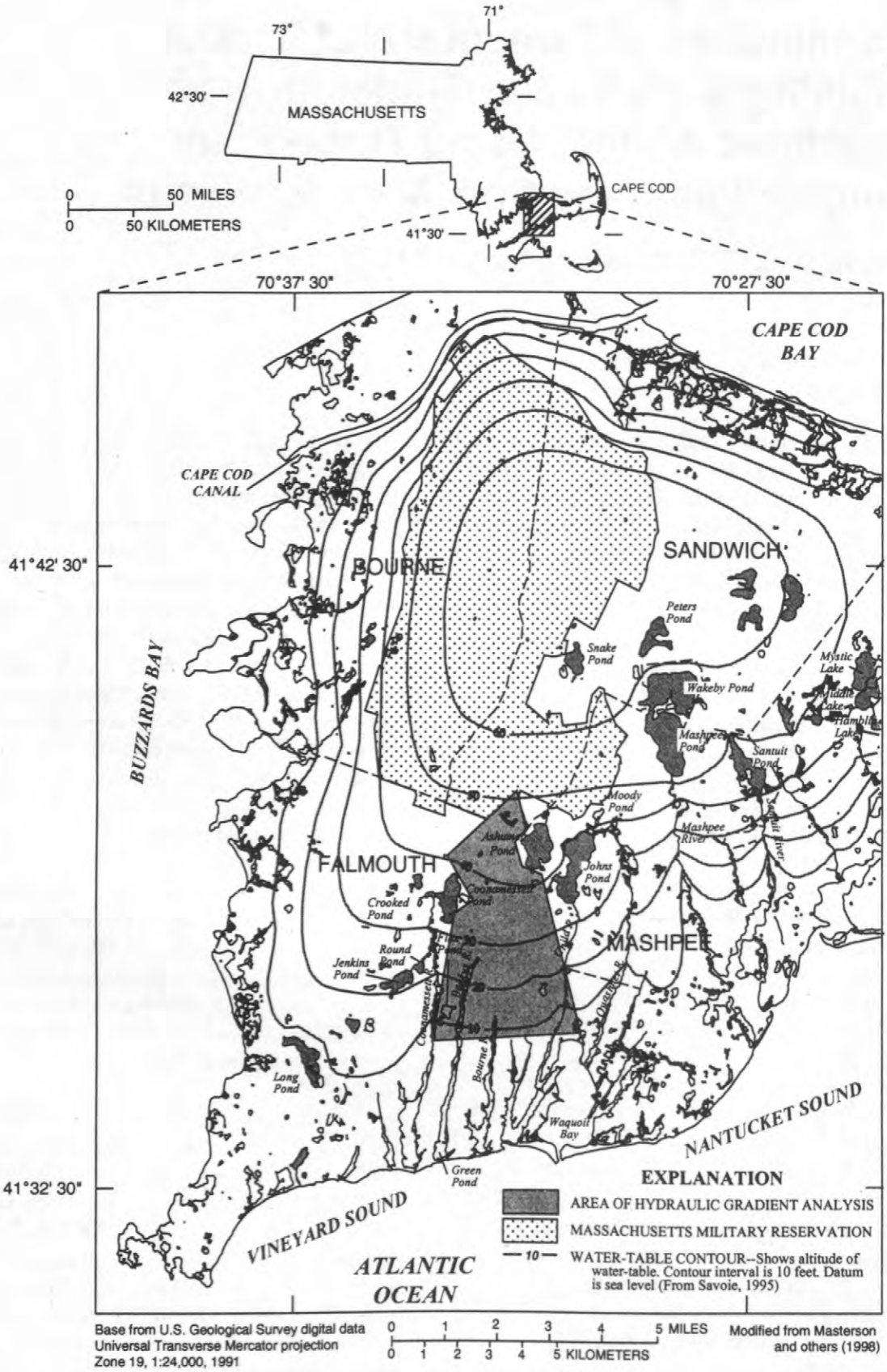

Figure 1. Area of hydraulic-gradient analysis and water-table configuration on March 23-25, 1993, western Cape Cod, Massachusetts.

HYDROGEOLOGIC SETTING

The Cape Cod Toxic Substances Hydrology research site is on a sand-and-gravel glacial-outwash plain in western Cape Cod (fig. 1). The outwash-plain sediments consist of medium- to coarse-grained glaciofluvial sand and gravel underlain by deposits of fine-to-medium glaciolacustrine sand and silt. The underlying bedrock consists of granodiorite and is considered impermeable to ground-water flow (Masterson and others, 1997a). Horizontal hydraulic conductivity of the sand and gravel on the research site averages 300 to 380 feet per day; the hydraulic conductivity of the finer underlying sediments is estimated to be about one-tenth that of the sand and gravel (LeBlanc and others, 1988; Hess and others, 1992; Moench, 1994). Land-surface altitude ranges from 50 to 110 feet above sea level, and water-table altitudes range from about 41 to 57 feet above sea level.

The regional flow system is bounded by Vineyard and Nantucket Sounds to the south, Buzzards Bay to the west, the Cape Cod Canal to the north (fig. 1), and a ground-water divide to the east (not shown in figure 1). Ground water is unconfined (water-table conditions) and generally flows to the south towards Vineyard and Nantucket Sounds. Most of the ground water flows through the upper coarse-grained deposits; the saturated thickness of the coarse-grained deposits is about 150 feet.

Areal recharge from precipitation is the sole source of freshwater to the aquifer system, at a rate of about 26 inches per year. Ground water leaves the system through discharge to streams, coastal embayments, the ocean, and public-supply wells (Masterson and others, 1998). The altitude of the water table fluctuates as much as 7 feet annually, with highest levels during the early spring when recharge rates are high and water use is low. The lowest levels occur in the late summer and early fall when recharge rates are low and water use is high (LeBlanc and others, 1986; Masterson and others, 1997b).

Many glacial kettle ponds, including Ashumet, Johns, and Coonamessett Ponds (fig. 1), strongly affect the regional and local flow systems. Ground water discharges into each pond at the upgradient end, and water flows from the pond back into the aquifer system at the downgradient end. This pattern of inflow and outflow causes ground-water flow to be focused through the ponds.

Horizontal hydraulic gradients at the Cape Cod research site are calculated regularly at a variety of scales to assist studies of the physical, chemical, and microbiological processes affecting the transport of sewage contaminants in the aquifer (LeBlanc, 1996). Determination of the magnitude and orientation of the gradient is critical for the design of many types of experiments at the site. For example, accurate estimation of the ground-water flow path and the rate of flow is essential for designing a successful sampling strategy in a tracer test (see, for example, LeBlanc and others, 1991).

THREE-POINT TRIANGULATION TO ESTIMATE HYDRAULIC GRADIENT

The three-point triangulation method discussed by Fetter (1994) can be used to estimate horizontal hydraulic gradients in an unconfined aquifer by fitting a planar surface to three measurement points to approximate the curved surface of the water table (fig. 2). Slope and direction of the planar surface can be calculated to yield estimates of the magnitude and direction of the horizontal hydraulic gradient using basic trigonometry:

$$\text{Magnitude} = [(dh/dx)^2 + (dh/dy)^2]^{1/2} \quad \text{(in feet/feet), and} \qquad (1)$$

$$\text{Direction} = \arctan[(dh/dx)/(dh/dy)] \quad \text{(in degrees),} \qquad (2)$$

where

dh/dx is $1/2A\,[h_1(y_2-y_3) + h_2(y_3-y_1) + h_3(y_1-y_2)]$,

dh/dy is $1/2A\,[h_1(x_3-x_2) + h_2(x_1-x_3) + h_3(x_2-x_1)]$,

A is $[x_2y_3 - x_3y_2 + x_3y_1 - x_1y_3 + x_1y_2 - x_2y_1]/2$,

x_i is x coordinate of the location of well i, relative to a common datum,

y_i is y coordinate of the location of well i, relative to a common datum,

h_i is measured hydraulic head in well i, relative to a common datum, and

i is well 1, 2, and 3.

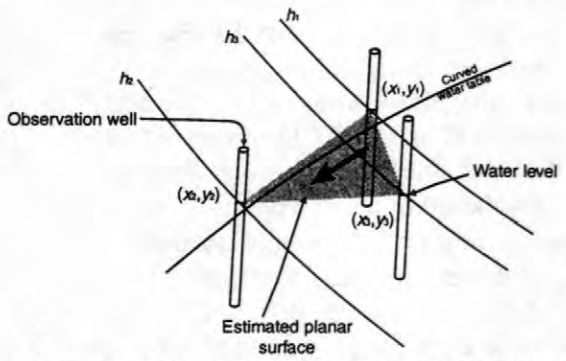

Figure 2. Schematic of gradient approximation.

The magnitude of the error in approximating the curved water-table surface by a plane is small if the wells are sufficiently close together because the curvature of the water table is typically small (Bear, 1979).

Two overlapping well networks of different sizes were selected for the purpose of evaluating the temporal variability of the horizontal hydraulic gradient. Observation wells were selected from several well networks that were established at the Cape Cod site for other purposes, such as predicting the paths of tracer tests (LeBlanc and others, 1991), monitoring the movement and fate of sewage-contaminated ground water (LeBlanc, 1984), calibrating ground-water flow models (Masterson and others, 1997b), and mapping the regional water table (Savoie, 1995). The two networks (fig. 3) include (1) a regional network used to map a sewage plume (LeBlanc, 1984) and (2) a local network in the vicinity of the decommissioned sewage-treatment plant used to monitor the start of natural restoration of the plume (Hess and others, 1996).

The regional network consists of 29 observation wells screened within 20 feet of the water table. This network contains 31 triangular estimation elements. The regional network spans the area from the sewage-treatment plant to approximately 2.5 miles to the south and is bounded by the Coonamesset River to the west and the Childs River to the east. The mean element area of the regional network is about 7.7×10^6 square feet. Water levels in the regional network were measured 17 times from May 1989 through May 1998.

The local network consists of 29 water-table wells that provide 41 estimation elements. The local network is a dense set of wells spanning the area from slightly upgradient of the sewage-treatment plant to approximately 2,500 feet downgradient of the plant. The mean element area of the local network is 4.5×10^5 square feet. The local network water levels were measured 16 times from November 1995 through May 1998. One element within the local network that encompasses a large-scale tracer test site (LeBlanc and others, 1991) was measured 135 times over the period from June 1984 through December 1998.

Comparisons between the two networks were made for high and low water-table-altitude conditions. Both networks were measured on May 11, 1998, at a time of historically high levels (water-level altitude of well FSW 343-0036 = 49.48 feet). The lowest water levels at the local network were measured on November 30, 1995 (water-level altitude of well FSW 343-0036 = 44.50 feet). The regional network was not measured on that date. For the purpose of comparing variations in gradients during similar low water-level conditions, data for the regional network from December 17, 1991, were used (water-level altitude of well FSW 343-0036 = 44.39 feet). The long-term mean water-level altitude for well FSW 343-0036 is 46.28 feet.

TEMPORAL AND SPATIAL VARIABILITY OF HYDRAULIC GRADIENTS

Regional Network

Regional ground-water flow is generally in a southerly direction with local deviations caused by the effects of adjacent ponds and streams (fig. 4). At low water levels, the hydraulic gradients have a median magnitude of 0.00163 foot per foot and a median direction of 193.8° (east of true north). At high water levels,

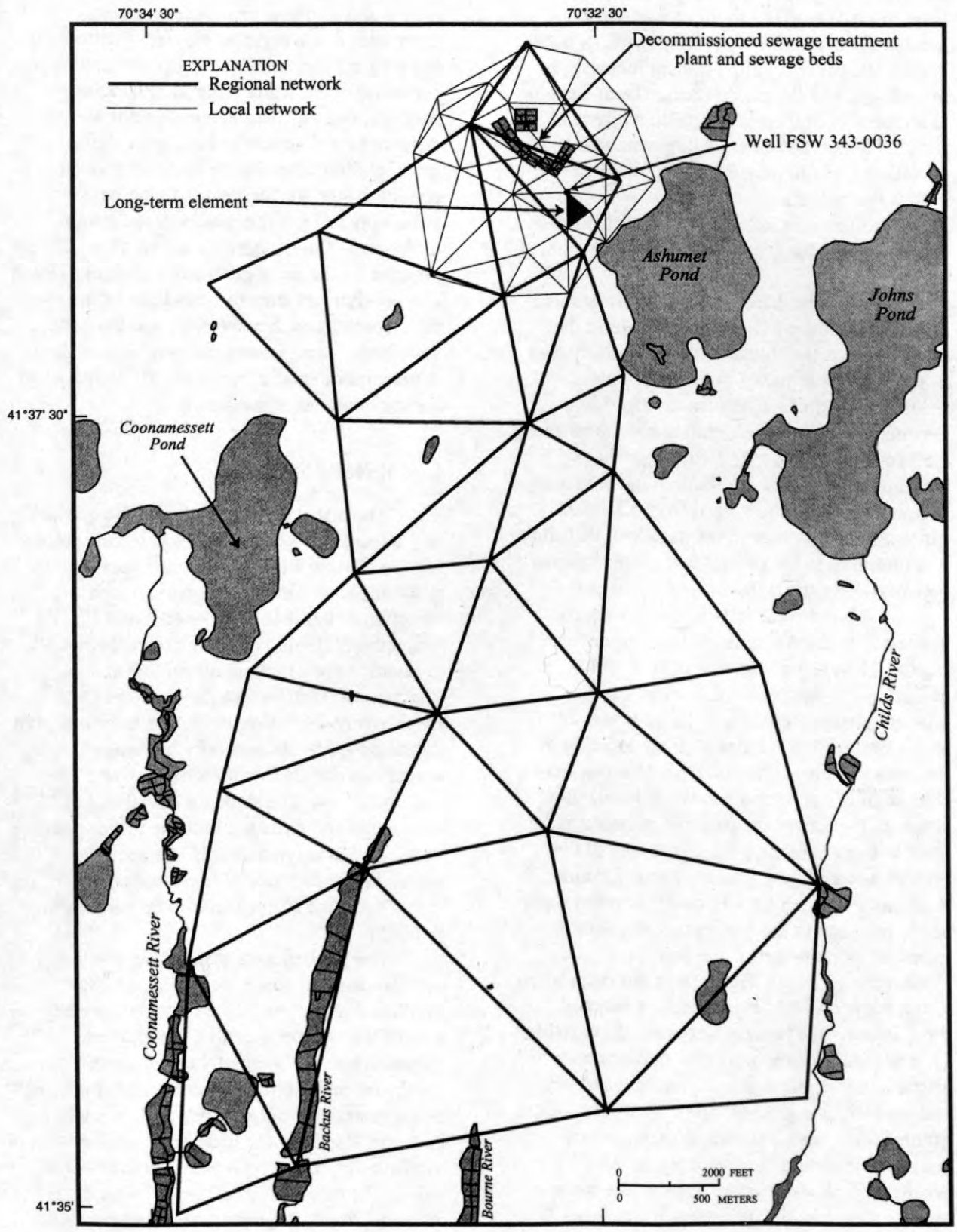

Figure 3. Regional and local hydraulic-gradient networks, Cape Cod, Massachusetts.

the hydraulic gradients have a median magnitude of 0.00195 foot per foot and a median direction of 193.4°. In general, as water levels rise, the hydraulic gradient increases in magnitude, and directions change from element to element even though the median direction remains about the same. A larger standard deviation for both magnitude and direction at high water levels as compared to low water levels indicates increasing spatial variability in gradient at higher water-table conditions (table 1).

The largest differences in the magnitude of the hydraulic gradient are observed in the elements directly upgradient from and adjacent to surface-water bodies in the area. This confirms the strong hydraulic connection between the unconfined aquifer and the adjacent surface-water bodies. Typical values of maximum difference in direction in the vicinity of ponds and streams ranged from 15 to 20°. Little or no difference in magnitude or direction was observed in the central part of the regional network along the Ashumet Valley (fig. 4).

A ground-water divide that is roughly aligned with the Ashumet Valley is defined regionally by the divergence of hydraulic-gradient directions (fig.4). The line of zero gradient change between high and low water levels generally coincides with the location of the ground-water divide (fig. 4). This line may shift slightly east or west as water levels vary, although the size of the regional elements is too large to track subtle shifts. To the east of the ground-water divide, gradients shift towards Ashumet Pond and the Childs River when water levels rise, and to the west, gradients shift towards Coonamessett Pond and the Coonamessett River. The shift in direction with rising water levels is evident in the range of directions for the two measurement dates (table 1). The median direction for both dates is aligned almost due south because the easterly and westerly components on the two sides of the ground-water divide tend to be balanced by the median calculation. But the range is 23.4° greater at high water levels than at low water levels because of the increased divergence of flow and discharge to surface-water bodies during high water levels.

Local hydrologic features, such as pond inflow and outflow, can cause apparent anomalies in the regional gradient estimates if the network elements are large compared to the curvature of the water table. In the regional network, two adjacent elements southwest of Ashumet Pond appear to have converging gradient directions for the high water-level condition (fig. 4). Element A to the west accurately reflects the generally southward direction of flow, whereas element B is strongly affected by the steep gradients at Ashumet Pond and poorly represents the curvature of the water-table contours as they wrap around the pond. The result is an apparent convergence of flow. A network of smaller elements would represent the curvature more accurately.

Local Network

The orientation of the hydraulic gradient in the local network is to the south and southeast (fig. 5). At low water levels, the hydraulic gradients have a median magnitude and direction of 0.00148 foot per foot and 171.1°, respectively (table 1). At high water levels, the gradients have a median magnitude and direction of 0.00184 foot per foot and 157.0°, respectively. As water levels rise, the calculated hydraulic gradients generally increase in magnitude and shift in direction toward Ashumet Pond. The standard deviations of magnitude and direction indicate more spatial variability in magnitude and less spatial variability in direction at high water-table conditions than at low water-table conditions (table 1).

The gradients estimated from the local network indicate three areas of hydraulic-gradient distribution (fig. 5). On the western side of the network (area 1), the gradient direction remains generally to the south-southwest under both hydraulic conditions, with slight variations in magnitude and direction. Ashumet Pond has the least effect on the gradient direction in this area. On the eastern side of the network (area 3), northwest of Ashumet Pond, elements under both hydraulic conditions had the least change in direction and the largest change in magnitude, as much as 1.5

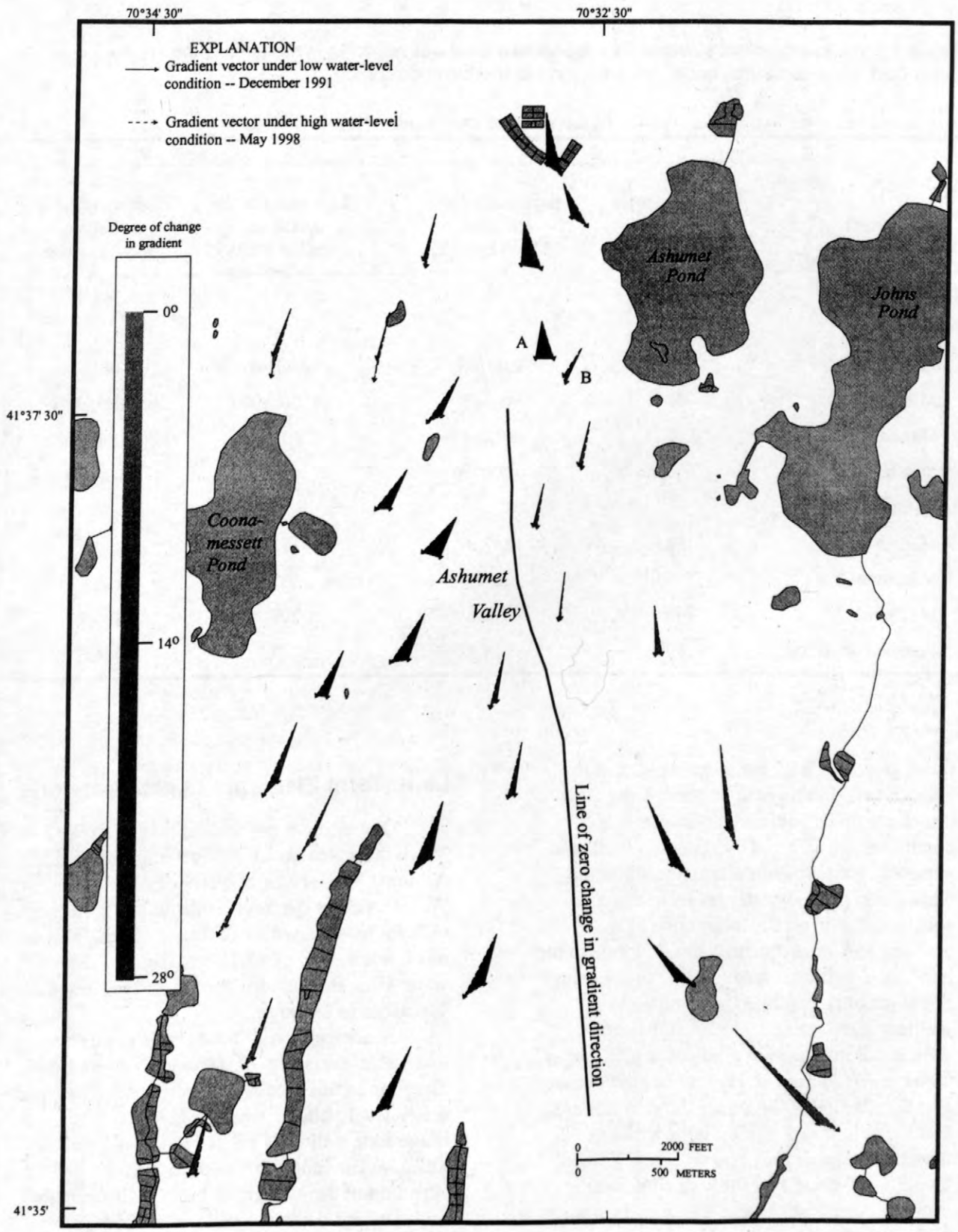

Figure 4. Regional gradient vectors under low and high water-level conditions.

Table 1. Hydraulic-gradient statistics for regional and local well networks in the unconfined aquifer on Cape Cod, Massachusetts, under low and high water-table conditions.

[magnitude in units of foot/foot, direction in units of degrees (east of true north), location of networks on figure 3]

Statistic	Regional Network		Local network	
	Low water-table condition, December 17, 1991	High water-table condition, May 11, 1998	Low water-table condition, November 30, 1995	High water-table condition, May 11, 1998
Number	31	31	41	41
Magnitude				
Median	0.00163	0.00195	0.00148	0.00184
Minimum	.00116	.00107	.000800	.00123
Maximum	.00423	.00484	.00198	.00244
Standard deviation	.000566	.000710	.00281	.000354
Direction				
Median	193.8	193.4	171.1	157.0
Minimum	138.0	134.0	137.9	129.5
Maximum	204.2	223.6	203.7	189.9
Standard deviation	16.5	24.4	17.1	14.6

times greater at high water levels than at low water levels. In this case, ground-water flow directions under low and high water-table conditions are affected by Ashumet Pond and generally are perpendicular to the shoreline. Changes in ground-water levels in this area substantially affect the magnitude of the gradient and, consequently, the flow rate to the pond. A transitional area (area 2) in the center of the network exhibited large changes in gradient direction (a 19 to 27° shift) and substantial increases in gradient magnitude as water levels increased. Hydraulic gradients are greatly affected by Ashumet Pond in this area. Gradients in area 2 exhibit large shifts in direction towards the pond with rising water levels, suggesting that the area contributing ground-water discharge to the pond is greatest at high water levels.

Long-Term Element in Local Network

One element in the local network (fig. 3), which is located about 900 feet upgradient from Ashumet Pond, has a 15-year-long record. Water levels in the three wells defining the element have varied more than 5.70 feet, with a mean water level of 45.71 feet (fig. 6). The water-table fluctuations correspond to seasonal variations in recharge.

A comparison of water-table gradients and water levels (fig. 6) indicates that gradient direction in this area is inversely related to water-level altitude, whereas gradient magnitude is directly related to water-level altitude. The long-term median gradient direction of the element is 149.5°, with a range and standard deviation of 21.5° and 4.9°,

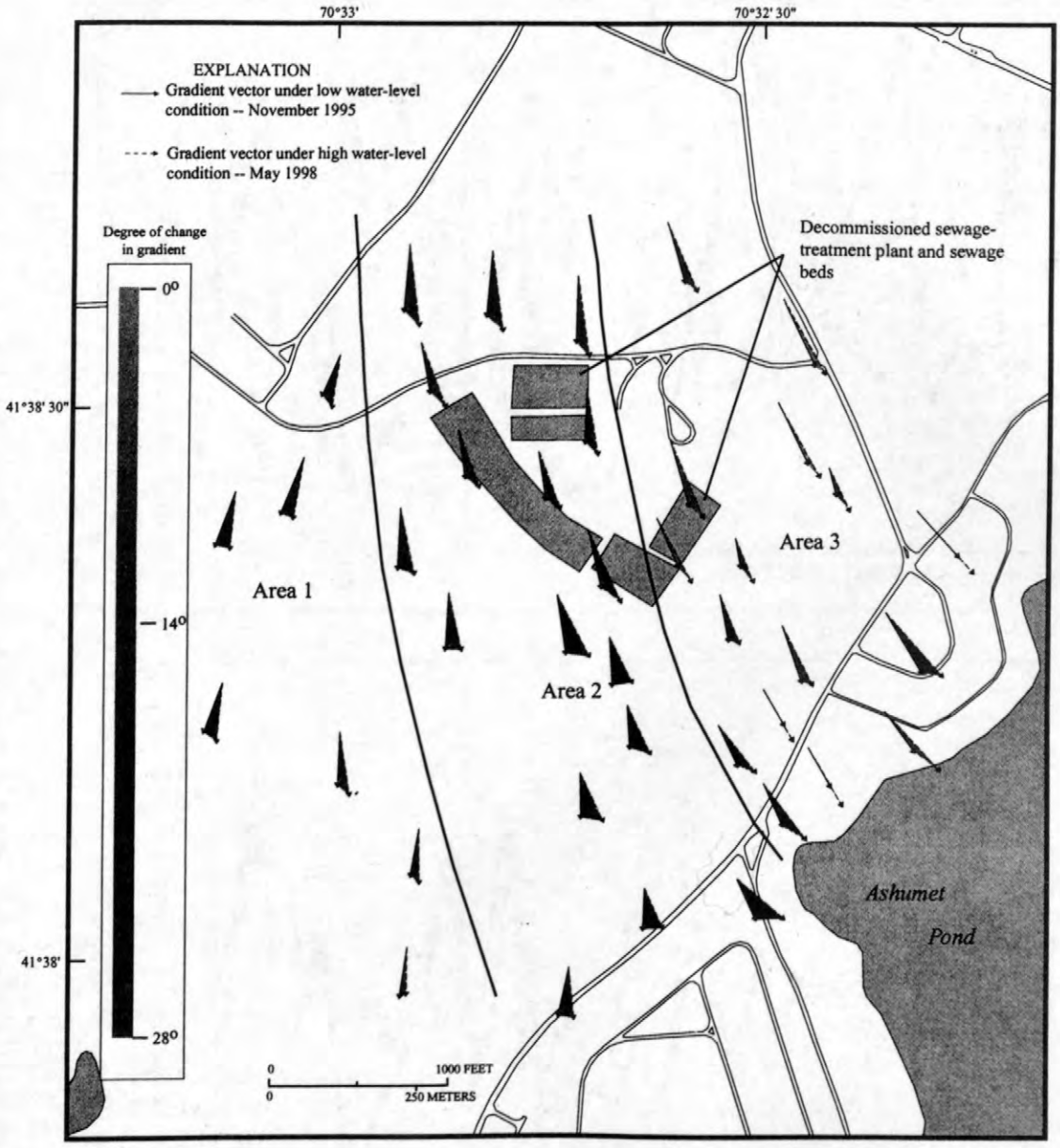

Figure 5. Local gradient vectors under low and high water-level condition.

respectively. The long-term median gradient magnitude of the element is 0.00142 foot per foot, with a range and standard deviation of 0.000630 and 0.000132 foot per foot, respectively.

The large fluctuations during the period of record at this element show that a single set of measurements to determine gradient would not represent the total variation in hydraulic gradient at this site. The magnitude and direction vary as much as 46 and 14 percent, respectively, with time. Gradient calculations based on single measurements made during periods of high or low water levels will inaccurately represent long-term average gradients. Long-term monitoring is essential to confirm that a single set of hydraulic-head measurements at a given site is representative of long-term conditions.

DISCUSSION

Hydraulic-gradient estimates for two observation-well networks on Cape Cod show that the flow-through kettle ponds and streams

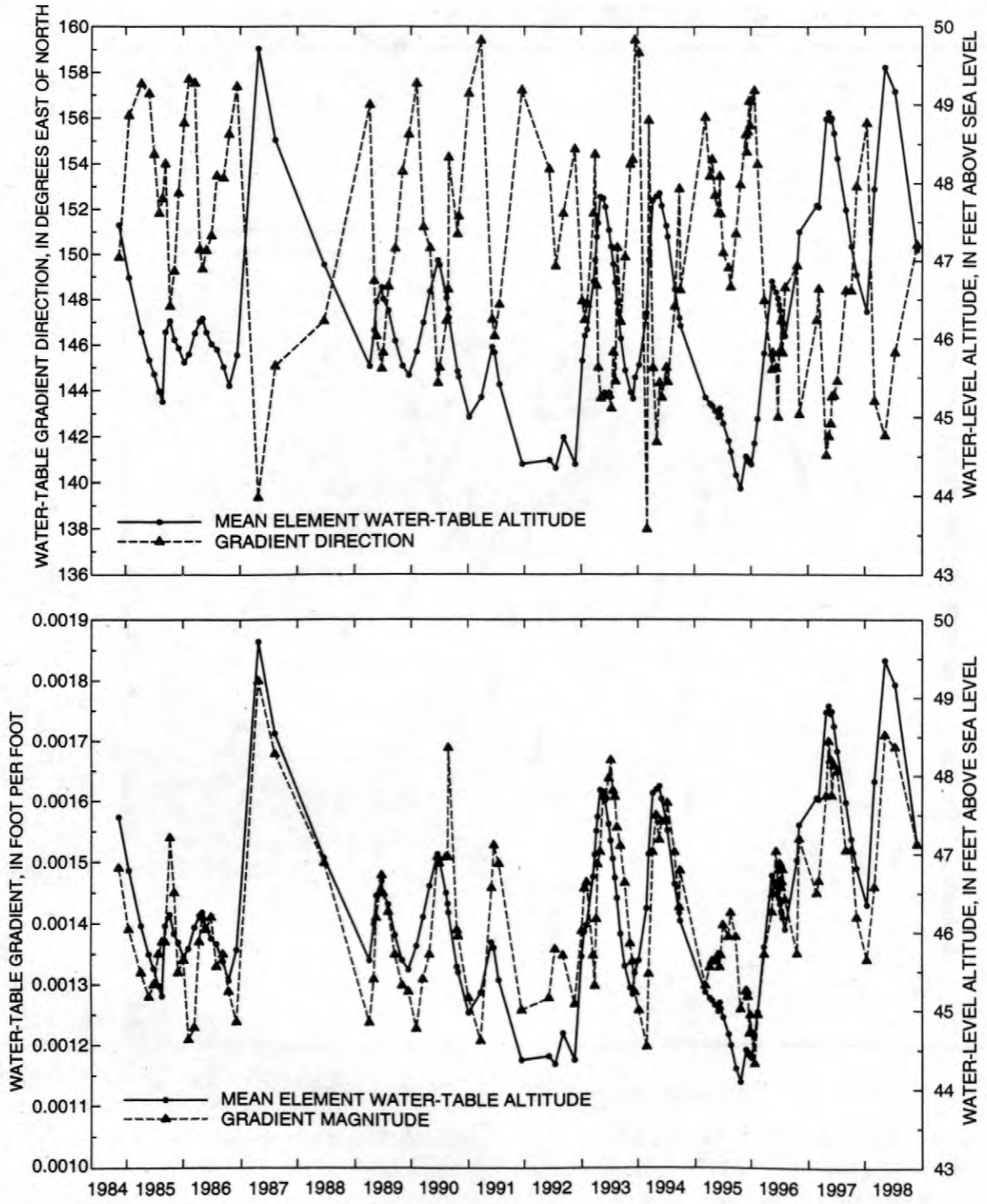

Figure 6. Hydraulic-gradient trends in a long-term element in the local network, Cape Cod, Massachusetts.

strongly affect regional and local flow directions. This is particularly evident in temporal gradient trends at the long-term element shown in figure 6. As ground-water levels rise, the level of Ashumet Pond also rises, but at a slower rate, owing to the larger storage capacity of the pond. In addition, pond dimensions do not change significantly as water

levels rise, so the pond, which is essentially an expression of the flat surface of the water table, cuts more deeply into the surrounding water table. The result is that the pond focuses ground-water flow more effectively during high water levels and causes shifts in flow directions toward the pond in the upgradient areas and away from pond in downgradient areas.

The variation in direction and magnitude of the estimated gradient is dependent on the size of the network elements and the proximity of the observation wells to surface-water bodies. The estimated gradients can be significantly in error and poorly represent the curvature of the water table if the elements are too large. This problem arises in areas near surface-water bodies, such as ponds. A comparison of estimated gradients for the local and regional network in the area where they overlap shows that the standard deviation increased as the size of the elements increased because of these estimation errors.

At smaller scales, the accuracy of onsite measurements is important. Small errors in measurements, as small as 0.01 feet, can significantly skew the magnitude and direction of the gradient estimate. For example, if an element area is 2×10^6 square feet and water levels at three wells are 46.00, 45.92, and 45.85 feet, the gradient magnitude and direction would be 0.0392 foot per foot and 190.97°, respectively. If the third well's water-level measurement was changed by 0.01 foot to 45.84 feet, the gradient magnitude and direction would change to 0.0413 foot per foot and 188.75°, respectively. Considering that typical measurement errors are about 0.005 to 0.01 foot, accurate water-level measurement and surveying of the well measuring points are critical for accurate gradient estimations.

SUMMARY

Three-point triangulation of ground-water levels is a useful method for estimating horizontal hydraulic gradients in unconfined aquifers. Hydraulic gradients were estimated at the Cape Cod site in two networks during times of low and high water levels. Increasing gradient magnitudes and changes in gradient directions with rising water levels in both the regional and local networks show the strong effects of ponds and streams on the ground-water flow system.

The gradient calculations in the regional network showed the strong regional effects of surface-water bodies, with the largest gradient changes taking place in the vicinity of the ponds and streams. A line of zero gradient change approximately coincided with the ground-water divide along the Ashumet Valley.

Results from the local network showed three areas of hydraulic-gradient response to changes in water levels. Far from Ashumet Pond, there was little variation in magnitude and direction. Northwest and upgradient of the pond, there were large increases in magnitude, but little variation in direction. Large variations in gradient magnitude and direction were observed where ground water flows to the pond at high water levels and passes to the southwest of the pond at low levels.

The long-term element in the local network showed that temporal trends in gradient can be related to water-level altitude and the hydraulic effect of a nearby flow-through kettle pond. This assessment demonstrates that hydraulic gradient can vary temporally and is not a constant value determined by water-level measurements made at a single point in time.

Results showed that the size of the network elements must be small enough for gradient estimates to accurately reflect the curvature of the water table. For small elements, water levels and relative measuring-point altitudes must be accurately measured to obtain meaningful estimates of the temporal and spatial variability of the hydraulic gradient.

REFERENCES

Bear, Jacob, 1979, Hydraulics of groundwater: New York, McGraw-Hill, 569 p.

Cole, B.E., and Silliman, S.E., 1996, Estimating the horizontal gradient in heterogeneous, unconfined aquifers--comparison of three-point schemes: Ground Water Monitoring and Remediation, v. 16, no. 2, p. 84-91.

Fetter, C.W., 1994, Applied hydrogeology (3d ed.): Columbus, Ohio, Merrill, 691 p.

Hess, K.M., LeBlanc, D.R., Kent, D.B., and Smith, R.L., 1996, Natural restoration of a sewage-contaminated aquifer, Cape Cod, Massachusetts, *in* Conference on Hydrology and Hydrogeology of Urban and Urbanizing Areas, Boston, Mass., April 21-24, 1996, Proceedings: Minneapolis, Minnesota, American Institute of Hydrology, p. WQE13-WQE25.

Hess, K.M., Wolf, S.H., and Celia, M.A., 1992, Large-scale natural gradient tracer test in sand and gravel, Cape Cod, Massachusetts--3. Hydraulic-conductivity variability and calculated macrodispersivities: Water Resources Research, v. 28, no. 8, p. 2011-2027.

LeBlanc, D.R., 1984, Sewage plume in a sand and gravel aquifer, Cape Cod, Massachusetts: U.S. Geological Survey Water-Supply Paper 2218, 28 p.

_____1996, Overview of research at the Cape Cod site--field and laboratory studies of physical, chemical, and microbiological processes affecting transport in a sewage-contaminated aquifer, *in* Morganwalp, D.W., and Aronson, D.A., eds., U.S. Geological Survey Toxic Substances Hydrology Program—Proceedings of the technical meeting, Colorado Springs, Colorado, September 20-24, 1998: U.S. Geological Survey Open-File Report 94-4015, p. 179-189.

LeBlanc, D.R., Garabedian, S.P., Hess, K.M., Gelhar, L.W., Quadri, R.D., Stollenwerk, K.G., and Wood, W.W., 1991, Large-scale natural-gradient tracer test in sand and gravel, Cape Cod, Massachusetts--1. Experimental design and observed tracer movement: Water Resources Research, v. 27, no. 5, p. 895-910.

LeBlanc, D.R., Garabedian, S.P., Quadri, R.D., Morin, R.H., Teasdale, W.E., and Paillet, F.L., 1988, Hydrogeologic controls on solute transport in a plume of sewage-contaminated ground water, *in* Ragone, S.E., ed., U.S. Geological Survey Program on Toxic Waste--Ground-Water Contamination--Proceedings of the second technical meeting, Cape Cod, Massachusetts, October 21-25, 1985: U.S. Geological Survey Open-File Report 86-481, p. B-7 to B-12.

LeBlanc, D.R., Guswa, J.H., Frimpter, M.H., and Londquist, C.J., 1986, Ground-water resources of Cape Cod, Massachusetts: U. S. Geological Survey Hydrologic-Investigations Atlas HA-692, 4 sheets, scale 1:48,000.

Masterson, J.P., Stone, B.D., Walter, D.A., and Savoie, Jennifer, 1997a, Hydrogeologic framework of western Cape Cod, Massachusetts: U. S. Geological Survey Hydrologic-Investigations Atlas HA-741, 1 sheet, scale 1:50,000.

Masterson, J.P, Walter, D.A., and LeBlanc, D.R., 1998, Delineation of contributing areas to selected public-supply wells, western Cape Cod, Massachusetts: U.S. Geological Survey Water-Resources Investigation Report 98-4237, 42 p.

Masterson, J.P, Walter, D.A., and Savoie, Jennifer, 1997b, Use of particle tracking to improve numerical model calibration and to analyze ground-water flow and contaminant migration, Massachusetts Military Reservation, Cape Cod, Massachusetts: U.S. Geological Survey Water-Supply Paper 2482, 50 p.

Moench, A.F., 1994, Specific yield as determined by type-curve analysis of aquifer-test data: Ground Water, v. 32, no. 6, p. 949-957.

Savoie, Jennifer, 1995, Altitude and configuration of the water table, western Cape Cod aquifer, Massachusetts, March 1993: U.S. Geological Survey Open-File Report 94-462, 1 sheet, scale 1:50,000.

AUTHOR INFORMATION

Timothy D. McCobb, Denis R. LeBlanc, and Kathryn M. Hess, U.S. Geological Survey, Marlborough, Massachusetts (tmccobb@usgs.gov, dleblanc@usgs.gov, and kmhess@usgs.gov)

Modeling the Influence of Adsorption on the Fate and Transport of Metals in Shallow Ground Water: Zinc Contamination in the Sewage Plume on Cape Cod, Massachusetts

By Douglas B. Kent, Robert H. Abrams, James A. Davis, and Jennifer A. Coston

ABSTRACT

Land disposal of sewage effluent at the Massachusetts Military Reservation on Cape Cod, Massachusetts, for nearly 60 years resulted in contamination of the aquifer with zinc (Zn). In contrast to non-reactive constituents of the sewage plume, which were observed greater than 5,500 meters down gradient of the source, Zn contamination was observed only within approximately 400 meters of the source. Under the disposal beds, Zn contamination was observed 12-25 meters below the water table. Greater than 200 meters down gradient of the source, Zn contamination was only observed in a 2-4 meter-thick region near the top of the sewage plume. The fate and transport of Zn in the aquifer most likely was controlled by pH-dependent adsorption onto aquifer sediments. A model that coupled flow, transport, and equilibrium adsorption was used to examine the influence of variable pH on the fate and transport of Zn. Adsorption was described using a semi-empirical surface complexation modeling approach; model parameters were determined from laboratory batch experiments. Model results captured the principal features of the distribution of Zn contamination in the aquifer after nearly 60-years of disposal. The model also was used to predict that acidification of ground water under the disposal beds, which should occur as a natural consequence of source cessation, would cause significant increases in Zn concentration and mobility.

INTRODUCTION

Historically, predictive simulations of the transport of inorganic contaminants that undergo adsorption during transport in ground water have incorporated empirical parameters, such as distribution coefficients or isotherm parameters, to describe adsorption (Cherry and others, 1984). Empirical parameters have been used successfully to predict the influence of adsorption on the transport of contaminants under constant chemical conditions (Dzombak and Ali, 1993; Burgisser and others, 1993; Cernik and others, 1994; Friedly and others, 1995; Szecsody and others, 1998). For a large number of inorganic contaminants, the extent of adsorption varies with chemical conditions, such as pH (Davis and Kent, 1990). Variability in chemical conditions over the spatial or temporal domain of the model can lead to large variations in the values of such empirical parameters (Reardon, 1981; Kohler and others, 1996; Davis and others, 1998). Thus, this approach is unlikely to produce satisfactory predictive simulations under variable chemical conditions.

A new approach to modeling the influence of adsorption on contaminant transport under variable chemical conditions recently has been proposed (Westall and others, 1995; Davis and others, 1998). The approach is based on using surface complexation models (SCMs) to describe quantitatively the influence of variable chemistry on adsorption in batch systems (Davis and Kent, 1990; Dzombak and Morel, 1990, and references therein). One or more mass action expressions are written between the solute of interest and surface sites, such as:

$$M^{n+} + >S_{\alpha}OH = >S_{\alpha}OM^{n-1} + H^{+}, \quad (1)$$

where

M^{n+} is a metal ion and

$>S_{\alpha}OH$ is one of a series of adsorption sites with different affinities for the metal ion M^{n+}.

Reactions with different stoichiometries also may be required. Mass action quotients, which have the form of equilibrium constants, are written for each reaction. Mass action quotients and site densities for the reactions are obtained by optimizing fits to experimental data (Westall and others, 1995; Davis and others, 1998). The mass action quotients and site densities derived from fitting experimental adsorption data on natural materials are best regarded as semi-empirical parameters. No rigorous procedures for determining the optimal number of reactions have been described. In contaminant transport applications, the optimal number of reactions depends on the objectives of the modeling exercise (Kohler and others, 1996).

The semi-empirical SCM approach has been successfully applied to experimental data on reactive transport under variable chemical conditions. Kohler and others (1996) obtained excellent predictions of the transport of uranium through columns packed with silica in the presence of different concentrations of fluoride at different, but constant, pH values. Stollenwerk (1998) successfully applied this approach to predicting the effects of vertical gradients in pH and concentrations of competing adsorbing anions on the transport of molybdate in a large-scale ground-water tracer test.

In this paper, we apply the semi-empirical SCM approach to predicting the effect of spatial and temporal variations in pH on the fate and transport of Zn (zinc) in the sewage plume at the USGS research site on Cape Cod, Massachusetts (fig. 1). Zinc contamination in the aquifer resulted from disposal of sewage effluent to rapid infiltration beds over a period of nearly 60 years (Kent and Maeder, 1999). Sewage disposal also resulted in a vertical gradient in pH, from mildly acidic values in uncontaminated ground water above the plume to near-neutral values in the core of the sewage plume (Kent and others, 1994). A combination of field and laboratory studies demonstrated that the fate and transport of Zn was controlled by adsorption onto metal

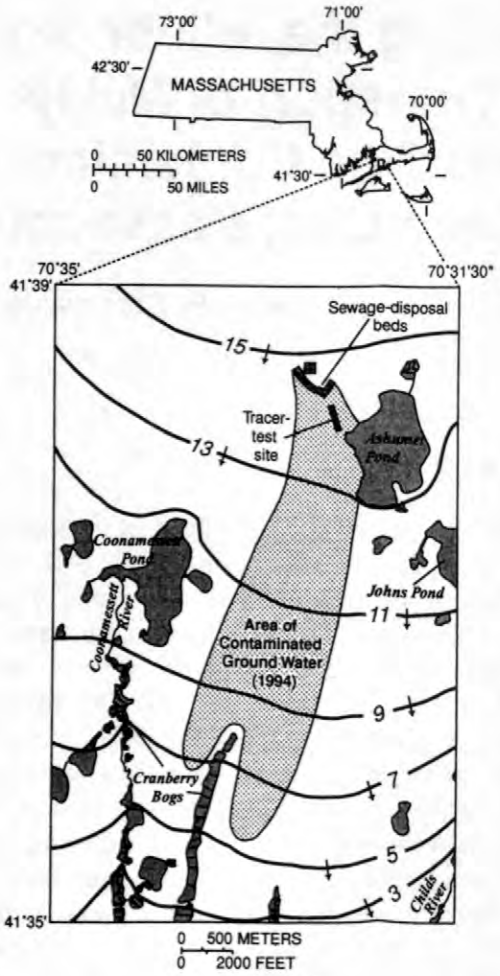

Figure 1. Map showing area of sewage-contaminated ground water (based on a synoptic sampling conducted in 1994, Savoie and LeBlanc, 1998) in relation to the hydraulic gradient and the major hydrologic features that influence ground-water flow (ponds, bogs, and rivers). The sewage disposal beds and the tracer test site are also shown.

hydroxypolymer coatings on the surfaces of mineral grains (Rea and others, 1991; Davis and others, 1993; Coston and others, 1995).

ADSORPTION MODELING

Two different SCMs were used to fit batch experimental data for Zn adsorption onto aquifer sediments for this transport modeling application

(Davis and others, 1998). The experimental data were collected over the range of pH values (4.9 to 7.4) and Zn concentrations (0.1 to 100 μM, micromoles per liter) relevant to the field application (Davis and others, 1998). In a one-site SCM, Zn adsorption data were modeled with a single reaction:

$$Zn^{2+} + >SOH = >SOZn^{+} + H^{+}, \quad (2)$$

In a two-site SCM, Zn adsorption was modeled with two chemical reactions:

$$Zn^{2+} + >S_sOH = >S_sOZn^{+} + H^{+}, \quad (3a)$$

$$Zn^{2+} + >S_wOH = >S_wOZn^{+} + H^{+}, \quad (3b)$$

where

$>S_sOH$ is a strong adsorption site and

$>S_wOH$ represents the remainder of the sites.

The fit to the batch experimental data was much better with the two-site SCM than with the one-site SCM (Davis and others, 1998).

DISTRIBUTION OF ZINC CONTAMINATION IN THE SEWAGE PLUME

The distribution of Zn contamination in the sewage plume under the sewage beds was fundamentally different than that down gradient of the beds. Under the sewage disposal beds, dissolved Zn, at concentrations less than 2 μM, was observed 12 to 25 meters below the water table. Under the disposal beds, pH values varied with location but generally increased to approximately 5.9 with depth in the sewage-contaminated zone (see figs. 2 and 3 in Kent and Maeder, 1999).

At distances greater than 200 meters down gradient from the disposal beds (200 meters down gradient corresponds to the up-gradient end of the tracer test array shown in fig. 1), dissolved Zn was observed only in a narrow zone near the upper boundary of the sewage plume (see fig. 4 in Kent and Maeder, 1999). The pH was relatively constant at 5.6 to 5.8 across the top of the plume and then increased steadily with depth to 6.8 in the core of the plume. Zinc concentrations increased with depth across the upper boundary of the sewage plume and then decreased rapidly with further increases in depth. The sharp decrease in Zn concentrations with depth in the sewage plume coincided with the increase in pH above approximately 6.0. Profiles with similar characteristics were observed farther down gradient.

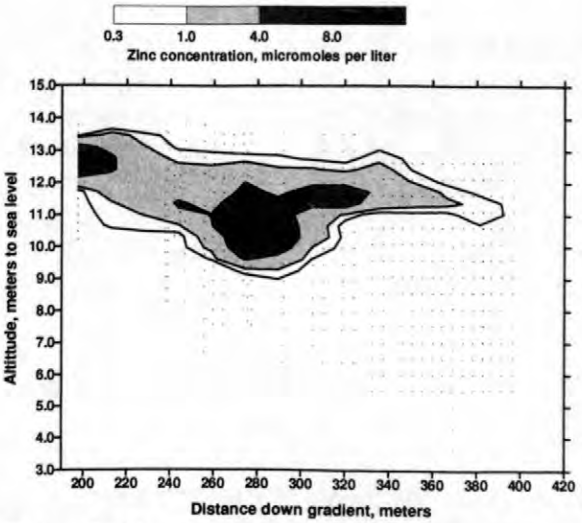

Figure 2. Dissolved Zn concentrations along a longitudinal profile through the tracer test array shown in figure 1. Zn concentrations (micromoles per liter) are shaded according to the scale shown at the top. Samples were collected in 1993-1994 at points shown.

The longitudinal cross section shown in figure 2, which runs through the tracer test array (fig. 1) and is described later in this paper, illustrates several characteristics of the down-gradient portion of the Zn-contaminated region. Distance down gradient was calculated relative to the center of the disposal beds directly up gradient of the large-scale tracer test array (fig. 1). An abrupt leading edge was observed approximately 400 meters down gradient from the disposal beds. In contrast, non-reactive constituents of the sewage plume were detected 5,500 to 6,000 meters down gradient (fig. 1). The Zn-contaminated region was 2 to 4 meters thick. Areas with Zn concentrations much greater than those under the beds were observed.

A large mass of Zn adsorbed to the sediments was observed in the regions with detectable concentrations of dissolved Zn. Extractions of sediments collected down gradient of the disposal beds showed that a significant mass of adsorbed Zn was observed only where dissolved Zn was detected in ground water (Rea and others, 1991). Comparison of the concentrations of adsorbed Zn and dissolved Zn showed that greater than 95 percent of the Zn-contamination was adsorbed (Rea and others,

1991). Similar results have been obtained on sediments from the disposal beds (B. A. Rea, USGS, unpublished data, 1993). The presence of adsorbed Zn on sediments in the Zn-contaminated region and absence below it was corroborated by the results of field transport experiments (Kent and others, 1991; Wilkie and others, 1998; Davis and others, 1999).

REACTIVE TRANSPORT MODELING

Simulation of 59-year history of sewage disposal

Reactive transport simulations were conducted to test the influence of pH-dependent adsorption on the mobility of Zn. We hypothesized that Zn introduced at the disposal beds was transported along the flow field; the increase in pH with depth caused an increase in the extent of Zn adsorption and, therefore, a decrease in Zn mobility. This conceptual framework was tested using a numerical model that coupled flow with advection, dispersion, and equilibrium adsorption in a two-dimensional (2-D) vertical cross section constructed along a flow line.

A simplified steady-state flow model was constructed and the resulting flow field was used to set up the reactive transport simulations. The model included horizontal flow across the up-gradient boundary and uniform areal recharge across the upper boundary. The flow model was calibrated using known head distributions, hydraulic conductivity measurements, and groundwater flow rates. Longitudinal and vertical transverse dispersivities were taken from Garabedian and others (1991). The pH gradient was simulated by fixing the total dissolved CO_2 concentration of inflowing groundwater at 1 mM (millimoles per liter) and adjusting the ratio of H_2CO_3 to HCO_3^- at each altitude to give the desired pH. The H_2CO_3/HCO_3^- ratio in the recharge water was chosen to give a pH of 5.6. A constant and uniform concentration of dissolved Zn was input along the up-gradient boundary.

The modeling approach requires that equilibrium be achieved on the time-scale of transport. Several lines of evidence support the validity of this assumption. Batch studies have shown that Zn adsorption onto the sediments is fast and reversible (Coston and others, 1995). Field-scale tracer tests involving the injection of EDTA (ethylenediaminetetraacetic acid) into the down-gradient portion of the Zn-contaminated region have shown that desorption of Zn occurs on the time-scale of transport (Kent and others, 1991; Davis and others, 1993, 1999). Another recent field-scale tracer test showed that injecting low pH ground water into the Zn-contaminated region caused large increases in Zn concentrations and mobility, as expected from predictions based on the local equilibrium assumption (Wilkie and others, 1998).

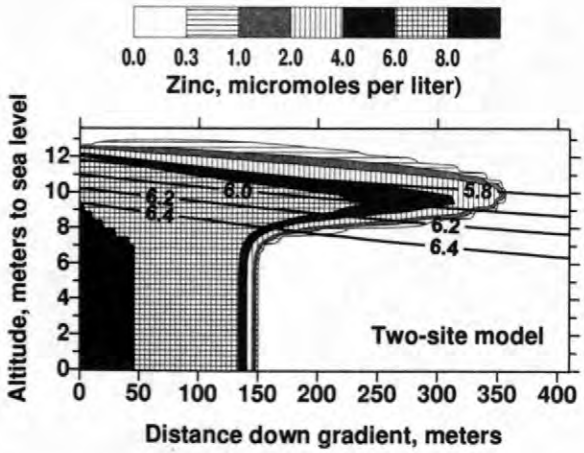

Figure 3. Results of a 59-year simulation using the two-site SCM to describe Zn adsorption. Zinc concentrations are shaded according to the scale shown at the top. Labeled contour lines show pH values.

The reactive transport simulations capture the major features of the distribution of Zn contamination in the aquifer. Results of a 59-year simulation, with an input concentration of 8 μM Zn, computed using the two-site SCM are shown in figure 3. Simulations using the two-site SCM and lower input concentrations of Zn were nearly identical to the results shown in figure 3. Results of simulations conducted with the one-site SCM were similar except that the leading edge of the Zn-contaminated region was more diffuse and extended farther down gradient (fig. 4A). Zinc contamination migrated much farther at the lower pH values near the top of the sewage plume than

at higher pH values deeper in the plume. Down-gradient, the simulated Zn-contaminated region was relatively thin. The leading edge was sharp and was located about 350 meters down gradient from the effluent disposal beds. This is somewhat less than was observed in the field (fig. 2). However, considering that non-reactive constituents of the sewage plume migrated more than 5 kilometers during this time, the overall amount of retardation of Zn was very close to that observed in the field. The simulated amount of retardation at the higher pH values deeper in the sewage plume also was in reasonable agreement with that observed in the field (Kent and Maeder, 1999).

Simulation of the effect of source cessation

In December 1995, sewage disposal onto the beds ended upon completion of a new treatment plant (LeBlanc and others, 1999). Flushing of the sewage-contaminated zone with pristine ground water should lead to decreasing pH values because pristine ground water up gradient of the disposal beds had lower pH values than existed in the sewage-contaminated zone (Hess and others, 1996). In addition, the up-gradient ground water was oxygenated; oxygen metabolism should lead to further decreases in pH (Abrams and others, 1998).

A model calculation was done to illustrate the consequences of acidic ground water flushing through Zn-contaminated sediments. The simulation was done along a 2D vertical cross section that extended to 600 meters, which is the distance between the disposal beds and Ashumet Pond (fig. 1). Otherwise the model was similar to that described above. The one-site SCM was used to describe Zn adsorption because of numerical problems encountered with the two-site SCM in this simulation. Numerical problems were, in part, a result of the coarser grid that was used to avoid excessive computation times. For the first 59 years, 2 μM Zn was input, along with the imposed pH gradient, at the up-gradient boundary. A Zn concentration of 2 μM was used rather than 8 μM to match more closely Zn concentrations observed under the disposal beds (Kent and Maeder, 1999). After 59 years, the Zn concentrations were set to 0 and the pH was set to 5.3 all along the up-gradient boundary.

Model calculations showed large increases in Zn concentrations as pH values decreased (fig. 4). Eight years after source cessation, Zn concentrations had increased by at least a factor of 10 in the deeper part of the Zn-contaminated region (fig. 4B). The pH in this part of the aquifer had decreased from greater than 6.2 to approximately 5.7. The magnitude of the increase in Zn concentration diminished with decreasing depth (fig. 4B). Thus, smaller differences between the pH during sewage disposal and the pH after source cessation resulted in smaller increases in Zn concentration.

The large increases in Zn concentration predicted by the model resulted from desorption of Zn from the sediments in response to decreasing pH. The increased mobility of Zn caused by lower pH values allowed Zn concentrations to build up as ground water moved through the region that had a large reservoir of adsorbed Zn. Thus, Zn concentrations increased with transport distance through the region of the aquifer originally contaminated with Zn (fig. 4A). The model results shown in figure 4B represent the maximum concentrations of Zn observed in the simulation results (the temporal resolution was approximately 1 year). Once the pulse of high Zn concentrations was transported out of the original Zn-contaminated region, Zn concentrations began to decrease (fig. 4C). Despite this attenuation, decades later and after several hundred meters of transport, Zn concentrations remained greater than those in the sewage-effluent itself and in the sewage-contaminated zone prior to source cessation (fig. 4D). It is noteworthy that high concentrations of Zn associated with low pH values have been observed at locations down gradient from an abandoned set of disposal beds (Kent and Maeder, 1999).

These simulations illustrate one possible origin for the areas down gradient of the disposal beds with Zn concentrations much greater than those observed under the disposal beds (fig. 2). Abandonment of a particular set of disposal beds could have resulted in a situation similar to that shown in figure 4B. Subsequent reactivation of these disposal beds would have

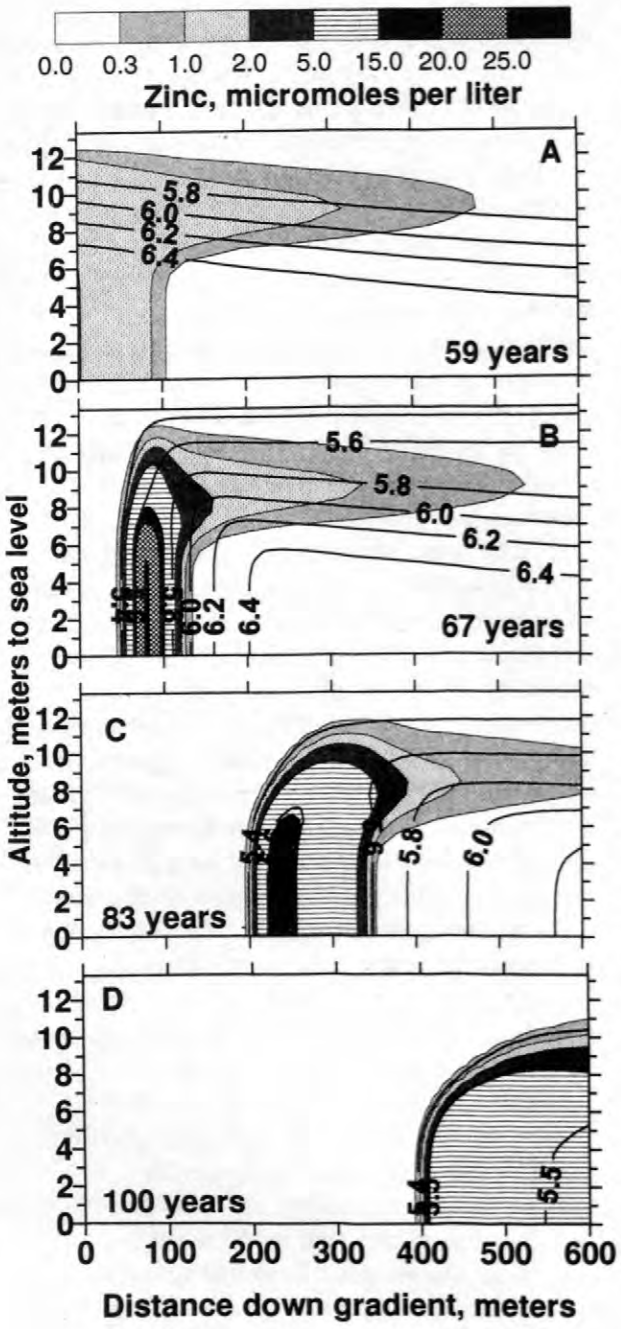

Figure 4. Simulation of the effect of acidic ground water flushing through the Zn-contaminated zone just prior to source cessation (A), 8 years after source cessation (B), 24 years after source cessation (C), and 41 years after source cessation (D). Zn concentrations (micromoles per liter) are shaded according to the scale shown at the top. Contour lines show pH values. Sequence of conditions is described in the text.

reestablished the pH gradient. Reestablishment of higher pH values deeper in the aquifer should "cut off" the lower region of elevated Zn concentrations. Propagation down gradient of a region with relatively high Zn concentrations would be expected only near the upper boundary of the sewage plume (fig. 3).

Quantitative predictions from these simulations, particularly the Zn concentration and timing of the changes, are highly uncertain. These quantitative predictions are strongly dependent on the imposed pH profile and assumed pH buffering properties of the sediments, which may differ somewhat from those assumed in the model. The observed pH values directly under the disposal beds were not as high as those imposed in the model calculations (Kent and Maeder, 1999). Consequently, the reservoir of adsorbed Zn available for mobilization directly under the disposal beds was likely to be less than that predicted in the model calculations. On the other hand, aerobic biodegradation of the particulate organic matter that has accumulated under the disposal beds may result in decreases in pH below 5.3 (Abrams and others, 1998). These uncertainties do not, however, call into question the main qualitative predictions of the model calculations. First, dissolved Zn concentrations will increase over those observed prior to source cessation as a result of flushing of the Zn-contaminated region with more acidic ground water. Second, elevated concentrations of Zn likely will be transported hundreds of meters. Third, it is likely that decades will be required for Zn contamination to be flushed from the aquifer.

CONCLUDING REMARKS

A reactive transport model incorporating a semi-empirical surface complexation modeling (SCM) approach to account for pH-dependent adsorption achieved remarkable success in predicting the distribution of Zn contamination resulting from approximately 60 years of disposal of sewage effluent to the aquifer. Similar approaches have been successfully applied to laboratory column experiments (Kohler and others, 1996) and field transport experiments (Stollenwerk, 1998) under variable chemical conditions. Because the SCM-approach accounted for the influence of variable pH on

adsorption, model calculations could be used to predict that acidification of the aquifer under the disposal beds following source cessation should result in significant increases in Zn concentrations and mobility. These predictions are being tested as part of the investigation of the impact of source cessation on water quality in the sewage-contaminated aquifer (LeBlanc and others, 1999).

These successes could not have been easily achieved with modeling approaches based on empirical parameters like K_ds or constant-pH isotherm parameters (such as Freundlich isotherm parameters). Isotherm parameters do not account for the influence of pH on adsorption and K_ds do not account for either pH or Zn-concentration effects on adsorption. Based on the range of pH values and Zn concentrations relevant to this field application, Davis and others (1998) showed that chemical variability observed in the sewage-plume would cause K_ds to vary by least a factor of 100 within the spatial domain of the model. Incorporating the effects of chemical variability into predictive simulations utilizing empirical parameters would require referring to tables of conditional parameters or fitting a spline to the empirical parameters and incorporating the spline into the model. Either approach likely would be more cumbersome than the SCM-based approach, which explicitly incorporates the influence of variable chemistry.

The fate and transport of Zn was controlled by the pH gradient, which, in turn, was largely controlled by microbial biodegradation processes (Abrams and others, 1998; Kent and Maeder, 1999). From a modeling perspective, this illustrates how processes controlling the fate and transport of reactive contaminants can be nested inside the geochemical processes that control plume-scale chemical variability. Models that account for the influence of microbial redox reactions on plume-scale geochemical variability are steadily improving. Unlike the use of K_ds or other empirical parameters, the SCM approach to modeling adsorption facilitates linking models that describe contaminant transport with those that describe the development and evolution of the geochemistry of contaminant plumes.

REFERENCES

Abrams, R.H., Loague, Keith, and Kent, D.B., 1998, Development and testing of a compartmentalized reaction network model for redox zones in contaminated aquifers: Water Resources Research, v. 34, no. 6, p. 1531-1541.

Buergisser, C. A. M., Cernik, C. A., Borkovec, M., and Sticher, H., 1993, Determination of nonlinear adsorption isotherms from column experimnets: An alternative to batch studies, Environmental Science and Technology, v. 27, p. 943-948.

Cernik, C. A., Federer, P., Borkevic, M., and Sticher, H., 1994, Modeling of heavy metal transport in a contaminated soil, Journal of Environmental Quality, v. 23, p. 1239-1248.

Cherry, J. A., Gillhwm, R. W., and Barker, J. F., 1984, Contaminants in groundwater, in Groundwater Contamination, National Academy Press, Washington, D. C., p. 46-64.

Coston, J.A., Fuller, C.C., and Davis, J.A., 1995, Pb2+ and Zn2+ adsorption by a natural aluminum- and iron-bearing surface coating on an aquifer sand: Geochimica et Cosmochimica Acta, v. 59, no. 17, p. 3535-3547.

Davis, J. A., Coston, J. A., Kent, D. B., and Fuller, C. C., 1998, Application of the surface complexation concept to complex mineral assemblages, Environmental Science and Technology, v. 32, p. 2820-2828.

Davis, J. A., and Kent, D. B., 1990, Surface complexation modeling in aqueous geochemistry, in H. F. Hochella and A. F. White, eds., Mineral-Water Interface Geochemistry, Reviews in Mineralogy, v. 23, p. 177-260.

Davis, J. A., Kent, D. B., Coston, J. A., Hess, K. M., and Joye, J. L., 1999, Multispecies tracer test in an aquifer with spatially variable chemical conditions: An overview, Morganwalp, D.W., and Buxton, H.T., eds., U.S. Geological Survey Toxic Substances Hydrology Program--Proceedings of the Technical Meeting, Charleston, South Carolina, March 8-12, 1999 -- Volume 3 -- Subsurface Contamination from Point Sources: U.S. Geological Survey Water-Resources Investigations Report 99-4018C, this volume.

Davis, J.A., Kent, D.B., Rea, B.A., Maest, A.S., and Garabedian, S.P., 1993, Influence of redox environment and aqueous speciation on metal transport in groundwater: Preliminary results of tracer injection studies, in Allen, H.,E. Perdue, E.M., and Brown, D.S., eds., Metals in Groundwater: Chelsea, Mich., Lewis Publishers, p. 223-273.

Dzombak, D. A. and Ali, M. A., 1993, Hydrochemical modeling of metal fate and transport in fresh water environments, Water Pollution Research Journal of Canada, v. 28, p. 7-50.

Dzombak, D., and Morel, F.M.M., 1990, Surface Complexation Modeling: Hydrous Ferric Oxide, John Wiley, 393 p.

Friedly, J.C., Davis, J.A., and Kent, D.B., 1995, Modeling hexavalent chromium reduction in ground water in field-scale transport and laboratory batch experiments, Water Resources Research, v. 31, no. 11, p. 2783-2794.

Garabedian, S.P., LeBlanc, D.R., Gelhar, L.W., and Celia, M.A., 1991, Large-scale natural-gradient tracer test in sand and gravel, Cape Cod, Massachusetts: 2. Analysis of spatial moments for a nonreactive tracer: Water Resources Research, v. 27, no. 5, p. 911-924.

Hess, K.M., LeBlanc, D.R., Kent, D.B., and Smith, R.L., 1996, Natural restoration of a sewage-contaminated aquifer, Cape Cod, Massachusetts, in Hydrology and hydrogeology of urban and urbanizing areas, proceedings of the conference, Boston, Mass., April 21-24, 1996: Minneapolis, Minnesota, American Institute of Hydrology, p. WQE13-WQE25.

Kent, D. B., Davis, J. A., Anderson, L. C. D., and Rea, B. A., 1991, Transport of zinc in the presence of a strong complexing agent in a shallow sand and gravel aquifer on Cape Cod, Massachusetts, , in Mallard, G.E., and Aronson, D.A., eds., U.S. Geological Survey Toxic Substances Hydrology Program--Proceedings of the technical meeting, Monterey, California, March 11-15, 1991: U.S. Geological Survey Water-Resources Investigations Report 91-4034, p. 78-83.

Kent, D.B., Davis, J.A., Anderson, L.C.D., Rea, B.A., and Waite, T.D., 1994, Transport of chromium and selenium in the suboxic zone of a shallow aquifer: Influence of redox and adsorption reactions: Water Resources Research, v. 30, no. 4, p. 1099-1114.

Kent D. B. and Maeder, V., 1999, Evolution of a ground-water sewage plume after removal of the 60-year-long source, Cape Cod, Massachusetts: pH and fate of phosphate and metals, Morganwalp, D.W., and Buxton, H.T., eds., U.S. Geological Survey Toxic Substances Hydrology Program--Proceedings of the Technical Meeting, Charleston, South Carolina, March 8-12, 1999 -- Volume 3 -- Subsurface Contamination from Point Sources: U.S. Geological Survey Water-Resources Investigations Report 99-4018C, this volume.

Kohler, M., Curtis, G. P., Kent, D. B., and Davis, J. A., 1996, Experimental investigation and modeling, of uranium(VI) transport under variable chemical conditions, Water Resources Research, v. 32, p. 3539-3551.

LeBlanc, D. R., Hess, K. M, Kent, D. B., Smith, R. L., Barber, L. B., and Campo, K. W., 1999, Natural restoration of a sewage plume in a sand and gravel aquifer, Cape Cod, Massachusetts, Morganwalp, D.W., and Buxton, H.T., eds., U.S. Geological Survey Toxic Substances Hydrology Program--Proceedings of the Technical Meeting, Charleston, South Carolina, March 8-12, 1999 -- Volume 3 -- Subsurface Contamination from Point Sources: U.S. Geological Survey Water-Resources Investigations Report 99-4018C, this volume.

Rea, B.A., Kent, D.B., LeBlanc, D.R., and Davis, J.A., 1991, Mobility of zinc in a sewage-contaminated aquifer, Cape Cod, Massachusetts, in Mallard, G.E., and Aronson, D.A., eds., U.S. Geological Survey Toxic Substances Hydrology Program--Proceedings of the technical meeting, Monterey, California, March 11-15, 1991: U.S. Geological Survey Water-Resources Investigations Report 91-4034, p. 88-95.

Reardon, E. J., 1981, K_d's-Can they be used to describe reversible ion sorption reactions in contaminant migration?, Ground Water, v. 19, p. 279-286.

Savoie, J., and LeBlanc, D.R., eds., 1998, Water-quality data and methods of analysis for samples collected near a plume of sewage-

contaminated ground water, Ashumet Valley, Cape Cod, Massachusetts, 1993-94: U.S. Geological Survey Water-Resources Investigations Report 97-4269, 208 p.

Stollenwerk, K.G., 1998, Molybdate transport in a chemically complex aquifer: Field measurements compared with solute-transport model predictions, Water Resources Research, v. 34, p. 2727-2740.

Szecsody, J. E., Chilakapati, A., Zachara, J. M., and Garvin, A. L., 1998, Influence of iron oxide inclusion shape on Co(II/III)EDTA reactive transport through spatially heterogeneous sediment, Water Resrouces Research, v. 34, p. 2501-2514.

Westall, J.C., Jones, J. D., Turner, G. D., Zachara, J. M., 1995, Enironmental Science and Technology, v. 29, p. 951-959.

Wilkie, J. W., Kent, D. B., and Davis, J. A., 1998, Effect of pH on metal transport in a contaminated sand and gravel aquifer, Cape Cod, Massachussets, Eos, Transactions of the American Geophysical Union, v. 79, no. , p S123.

AUTHOR INFORMATION

Douglas B. Kent, James A. Davis, and Jennefer A. Coston, U.S. Geological Survey, Menlo Park, California (dbkent@usgs.gov)

Robert H. Abrams, Stanford University, Stanford, California.

Modeling the Evolution and Natural Remediation of a Ground-Water Sewage Plume

By Kenneth G. Stollenwerk and David L. Parkhurst

ABSTRACT

A one-dimensional reaction-transport model was used to simulate the 60-year chemical development of a plume of sewage-contaminated ground water at the Massachusetts Military Reservation on Cape Cod, Massachusetts. The dominant biogeochemical reactions in the model were oxidation of organic carbon by dissolved oxygen, nitrate, manganese oxides and iron oxyhydroxides. Sorption controlled transport of phosphate, ammonium, potassium, calcium, magnesium, iron(II), and manganese(II). Reaction parameters were chosen to fit the observed concentration profiles of solutes along the longitudinal axis of the core of the plume. The model was then used to predict the evolution of the plume for the first 60 years following cessation of sewage disposal. Based on estimates of the reactivity of sorbed organic carbon, the model predicted that reducing conditions could be maintained for the next 60 years. Sorbed cation concentrations will decrease slowly and move downgradient; pH will remain at pre-cessation levels throughout much of the aquifer. As low ionic strength, uncontaminated ground water elutes through the aquifer, a transient increase in pH is predicted to cause a spike in phosphate concentrations. Phosphate concentrations at the shore of Ashumet Pond could increase for the next 10-15 years.

INTRODUCTION

Active remediation of the large number of toxic waste sites in the United States requires significant resources. Therefore, natural remediation is an attractive alternative. Natural remediation of an aquifer generally implies that the source of contamination is either removed or sequestered from the environment. As uncontaminated ground water flows through the aquifer, various processes act to reduce the concentration of contaminants. These processes include, but are not limited to, dispersive dilution, fixation by solid phases, and biotransformation to less toxic compounds.

The decision to use natural remediation must be based on a thorough understanding of the processes affecting the behavior of contaminants at a particular site. Such knowledge is essential to the design of appropriate models which can be used to help predict future contaminant behavior and aid in making regulatory decisions.

The goals of this study were to model the chemical development of a plume of sewage-contaminated ground water and predict the future evolution of the plume after the source of contamination was terminated. The first step was to calibrate a reaction-transport model by simulating the development of the sewage plume from its inception to the time when sewage discharge ceased. The calibrated model was then used to simulate how sewage-plume constituents will react to the influx of uncontaminated ground water for 60 years following the cessation of sewage discharge.

Site Description

Disposal of secondarily treated sewage onto rapid infiltration beds at the Massachusetts Military Reservation on Cape Cod, Massachusetts, began in 1936. By 1995 a plume of contaminated ground water had formed that was about 30 m (meters) thick, 900 m wide, and more than 5500 m long. The sewage plume can be divided into two distinct geochemical environments. There is an anoxic core characterized by little to no O_2 (dissolved oxygen) and greater than 200 µmol/L (micromoles per liter) Fe(II) (ferrous iron). The anoxic core extends from approximately 200 to 500 m from the sewage beds. Surrounding the anoxic core is a suboxic zone that contains little or no Fe, low but detectable O_2, NO_3 (nitrate), and Mn (manganese).

METHODS

Modeled Flow Path

A reaction-transport model was used to simulate the evolution of the sewage plume along a 1D (one dimensional) flow path. The modeled flow path extends along the longitudinal axis of the core of the sewage plume from the sewage beds to near the toe of the plume (fig. 1). Location of the plume core was based on concentration data from an extensive sampling of well clusters and multilevel samplers in 1994 (Savoie and LeBlanc, 1998). Measured concentrations used to define the core of the plume are from 14 multilevel sampler locations and 6 nested well locations. The flow path through the anoxic portion of the plume (200-500 m) was defined by the zone of highest Fe(II) concentration at each site. The flow path for the suboxic portion of the plume (0 -200 m and 500-4000 m) was defined by the highest specific conductance and highest concentrations of boron.

Description of the Geochemical Model

A modified version of PHREEQC (Parkhurst, 1995), a 1D reaction-transport model, was used to simulate the chemical development of the sewage plume while the sewage plant was operated and to predict the evolution of the plume during the first 60 years following the cessation of sewage discharge. The chemical composition of sewage effluent used to model the development of the plume is listed in table 1. The composition of uncontaminated ground water used to initialize the model and simulate post-cessation evolution of the plume is also listed in table 1. The chemical reactions and physical processes that are proposed to describe the evolution of the plume are based on interpretation of the chemical data from synoptic samples of the water and sediments in the aquifer, field experiments at the site, and laboratory experiments on water and sediment samples from the site.

Computer Model

PHREEQC (Parkhurst, 1995) has the capability to model advective transport of water in combination with a variety of chemical reactions including homogeneous aqueous reactions, mineral equilibria, and surface-complexation reactions. The modified version of PHREEQC has added capabilities to simulate kinetic reactions (Appelo and Parkhurst, 1998; Parkhurst and Appelo, 1997), which were used to model the kinetic degradation of dissolved and sorbed organic carbon.

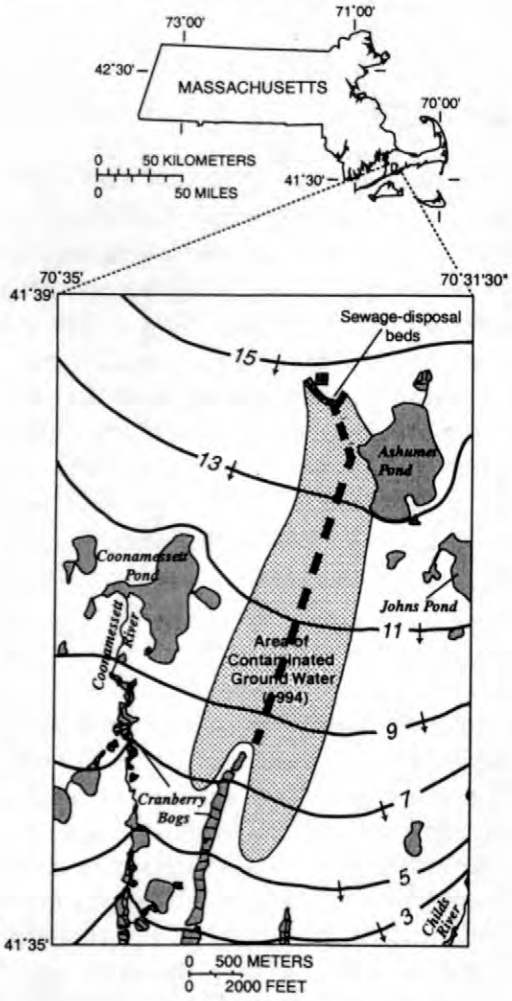

Figure 1. Location of sewage plume and the modeled one-dimensional flow path along the longitudinal axis of the core of the plume.

Geochemical Reactions and Dilution

The primary biogeochemical reaction in the sewage plume is the oxidation of organic carbon by a succession of electron acceptors: O_2, NO_3, MnO_2 (manganese oxide), and FeOOH (iron oxyhydrox-

ide). No sulfate reduction has been observed in the plume.

The natural geochemical reactions in the aquifer are assumed to be minor relative to the reactions that occurred as a result of the introduction of sewage effluent. In addition, the silicate and alumino-silicate minerals that comprise the aquifer are assumed to be relatively inert even in the presence of the sewage effluent. Thus, the only reactive constituents in the aquifer included in the conceptual model of geochemical reactions are iron and manganese oxyhydroxides which coat the silicate minerals. Analysis of total Fe and Mn in the sediment indicates that the amount present in an aquifer volume that contains one liter of water is about 0.080 moles of FeOOH and 0.0007 moles of MnO_2 (Coston and others, 1995).

The surfaces of minerals are known to sorb dissolved constituents and sorption reactions are important in the sewage plume. The diffuse double-layer model of sorption (Dzombak and Morel, 1990) is included in PHREEQC and was used to model sorption reactions in the aquifer. Surface sites were hypothesized to react with cations and anions including NH_4 (ammonium), K (potassium), Ca (calcium), Mg (magnesium), Fe(II), Mn(II), and PO_4 (phosphate). A separate kinetic reaction was hypothesized to sorb organic carbon. These two processes were modeled separately to simplify the modeling and because the interaction of the sorbed carbon with the mineral surface sites is unknown. Organic carbon has been sorbed on aquifer sediments while sewage effluent was introduced into the aquifer. The amount and continued reactivity of this pool of sorbed carbon are important factors in the evolution of the plume after sewage discharge has ceased (Barber and Keefe, this volume).

One additional reaction was hypothesized to account for the rapid decrease in phosphate concentration over the first few meters of the flow path. Saturation indices for strengite (ferric phosphate) indicate that this mineral could form in the initial part of the flow path. Thus, the formation of strengite is used to model the initial depletion of phosphate, while recognizing that the real chemical process may be more complicated, such as the formation of a solid solution of iron oxyhydroxide and iron phosphate or formation of a solid only at iron oxyhydroxide surfaces.

Table 1. Chemical composition of sewage effluent and uncontaminated ground water

[Concentrations are in micromoles per liter unless otherwise noted]

Chemical constituent or property	Sewage effluent	Uncontaminated ground water
pH, unitless	6.0	5.6
pe, unitless	7.0	7.0
Temperature, °C	14.0	11.0
Ca	335	29
Mg	170	31
Na	2100	200
K	240	10
Fe	4.5	0
Mn	0.4	.64
Al	1.9	0
Si	210	102
Cl	990	140
Sulfate	290	86
Dissolved inorganic carbon	1200	28
Ammonium	180[a]	0
Nitrate	1050	0
P	190	2.3
F	33	0
Dissolved oxygen as O_2	100	175
Reactive organic carbon	1667[b]	0
Sorbing organic carbon	250[c]	0
B	56	1

[a]Concentration of ammonium of 682 µmol/L for first 40 years was estimated by parameter fitting.

[b]Concentration of reactive carbon of 1464 µmol/L was estimated by parameter fitting.

[c]Estimate of organic carbon that sorbed and will react after cessation of sewage discharge based on assumption that about one quarter of sorbed organic carbon will react.

Sorption of sodium appears to be minimal; however, the profile of sodium within the plume shows a decrease in concentration by a factor of two

beginning at approximately 600 m. With no plausible reaction that consumes sodium, the decrease in sodium is attributed to dilution. The direction of flow is known to vary up to 18 degrees (Leblanc and others, 1991; McCobb and others, this volume), and it is hypothesized that this variation in flow direction is sufficient to mix approximately equal amounts of contaminated and uncontaminated water within a zone ranging from 600 to 1200 m downgradient. The concentration of B (boron), which also exhibits minimal sorption, also decreased by a factor of two over the same distance.

Model Fitting Parameters

Fourteen model parameters were adjusted to obtain a fit between modeled and observed concentration profiles along the flow path. Each of these parameters is identified by a number in the following discussion. The organic carbon entering the system is arbitrarily divided into two fractions: dissolved organic carbon that reacts rapidly over the first 500 m of the flow path and organic carbon that is sorbed onto the sediments and will eventually react. Organic carbon that does not react is ignored. The dissolved organic carbon that reacts rapidly is modeled with first-order reaction kinetics with respect to dissolved organic carbon. The parameters for this reaction are (1) the average concentration of reactive organic carbon that enters the flow system and (2) the rate constant for the first-order decay reaction. The sorbing organic carbon is assumed to accumulate for 60 years as the sewage treatment plant is operated. Once sewage discharge ceases, the sorbed organic carbon is assumed to begin to react. A first-order rate expression is used to describe sorption over the 60 years of plant operation. Two rate expressions are used to describe the rate of decay of the sorbed organic carbon as the system is flushed with uncontaminated water: one rate expression is first order with respect to sorbed organic carbon and has a Monod factor for oxygen with a half-saturation constant of 1e-8; the other rate expression is also first order with respect to sorbed organic carbon and has a Monod factor for amorphous iron hydroxide with a half-saturation constant of 1e-5. One parameter for the sorption of organic carbon is the average concentration of organic carbon in the sewage effluent that sorbs and eventually reacts. Simulations indicate that a concentration of about 1,000 µmol/L organic carbon is needed to produce amounts consistent with two measurements of sorbed organic carbon along the flow path (L.B. Barber, USGS, oral commun.). Arbitrarily, one quarter of that amount was considered to be potentially reactive. The rate constant for the sorption reaction was arbitrarily set to 6e-8 1/s, so that the carbon sorbed over roughly the same zone in which the reactive organic carbon oxidized. The two rate constants for post-cessation reaction of the sorbed organic carbon with O_2 and FeOOH were fitting parameters (3 and 4).

The constants for surface complexation reactions in this media are unknown and were used as fitting parameters in the model. Constants for (5) NH_4, (6) K, (7) Ca, (8) Mg, (9) Fe(II), (10) Mn(II), and (11) PO_4 were fit. The surface area used for the sorption model was at 0.4 m^2/g and the number of grams of sediment per liter of water was 4140 g/L. The number of sorption sites per liter of water (12) was a fitting parameter.

All thermodynamic data except the equilibrium constants for surface complexation and strengite were taken directly from the database for PHREEQC (Parkhurst, 1995). However, ammonium was separated from the rest of the nitrogen species so that ammonium would not oxidize to N_2(aq) or nitrate nor would ammonium form by reduction of nitrate or N_2. The equilibrium constant for strengite (13) was used as a fitting parameter to reduce the incoming concentration of phosphate.

Dilution was modeled by mixing the contents of appropriate sewage plume cells with uncontaminated water such that the product of the mixing fractions for the cells was approximately 0.6. In other words, the concentration of a conservative constituent present in only contaminated water would be reduced by a total of 40 percent in cells that represented distances between 600 and 1200 m.

Finally, the shape of the ammonium profile--low concentrations for the first 1000 m and large concentrations for the next 2000 m--could not be modeled with a constant input concentration of 180 µM, the average value measured over the last 15 years. It is proposed that concentrations of ammonium were greater during the first 40 years of operation, when the plant had greater use and treatment practices probably were less effective. Consequently, the average concentration of ammonium in the sewage effluent during the first 40 years of plant operation (14) was a fitting parameter.

Table 2. Parameters used in reactive transport modeling

[Parameter: d, day; g, gram; L, liter; m, meter; mol, mole; s, second; K_1 indicates no hydrogen ion is released in the association reaction; K_2 indicates one hydrogen ion is released in the association reaction; K_3 indicates that one hydrogen ion is consumed in the association reaction. Adjusted: "Yes" indicates that the parameter was fit or adjusted; "No" indicates the parameter was not changed]

Parameter	Value	Adjusted
Column length, m	4000	No
Number of cells	160	No
Dispersivity	0	No
Velocity, m/d	.43	No
Simulation period, years	60	No
$Fe(OH)_3$, mol/L	.08	No
MnO_2, mol/L	.0007	No
Strengite, mol/L	0	No
Strengite log K	-25.5	Yes
Ammonium, 1978-cessation, µmol/L	180	No
Ammonium, 1938-1977, µmol/L	682	Yes
Surface complexation		
Log K_1, NH_4^+	1.8	Yes
Log K_1, K^+	2.0	Yes
Log K_2, Mn^{2+}	-3.2	Yes
Log K_2, Fe^{2+}	-2.5	Yes
Log K_2, Ca^{2+}	-5.6	Yes
Log K_2, Mg^{2+}	-5.6	Yes
Log K_3, PO_4^{3-}	18.8	Yes
Log K_1, H^+	-6.3	No
Surface sites, µmol/L	8,300	Yes
Solids, g/L	4140	No
Surface area, m^2/g solid	.4	No
Reactive organic carbon, µmol/L	1,465	Yes
Rate constant for reactive organic carbon, 1/s	8.2e-8	Yes
Sorbing reactive organic carbon, µmol/L	250	No
Sorption rate constant for sorbing organic carbon, 1/s	6.0e-8	No
Oxygen rate constant for decay of sorbed organic carbon, 1/s (post-cessation)	3.0e-9	Yes
Iron rate constant for decay of sorbed organic carbon, 1/s (post-cessation)	1.0e-10	Yes

The parameters were fit by a combination of trial and error and parameter estimation with UCODE (Poeter and Hill, 1998). In the parameter-estimation process, some parameters were combined or simply set to fixed values if simulation results were not sufficiently sensitive to the parameters. The calculations proved to be insensitive to the log K values for calcium and magnesium sorption, and these parameters were fixed at a value that produced a small amount of sorption. The model parameters are summarized in table 2.

RESULTS AND DISCUSSION

Sewage Plume Evolution

The observed concentrations of O_2, NO_3, Mn, and Fe in the core of the sewage plume after 60 years of sewage discharge are compared with the model-calculated concentrations in figure 2. These are the principal electron acceptors for oxidation of organic carbon. The measured concentration of O_2 in sewage effluent has varied. For this modeling exercise, an initial concentration of 100 μM was used. The model calculated that O_2 should completely react within the first 25 m (size of one model cell) downgradient of the sewage beds, which matches the field measurements.

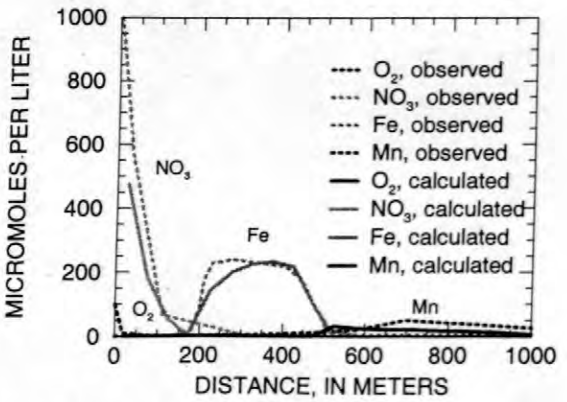

Figure 2. Observed and calculated concentrations of dissolved oxygen, nitrate, iron, and manganese along the longitudinal axis of the core of the sewage plume prior to cessation.

When O_2 concentrations become sufficiently small, NO_3 becomes the dominant electron acceptor for organic carbon. Smith and Duff (1998) have shown that the mechanism of NO_3 reduction in this aquifer is denitrification to N_2, rather than NO_3 reduction to NH_3. Denitrification is kinetically controlled and carbon limited; the rate was highest near the sewage beds and decreased with increasing distance downgradient (Smith and others, 1996).

Nitrate concentrations decrease from about 1000 μM below the sewage beds to below detection between 150 m and 300 m along the flow path. The model calculates that NO_3 should be gone by about 150 m. The rate constant used in the model for oxidation of organic carbon was comparable to the in-situ rate measured in the aquifer by Smith and others (1996).

When available NO_3 has been depleted, organic carbon begins to reductively dissolve MnO_2. As MnO_2 becomes depleted, FeOOH is reduced. Ferrous iron concentrations in the sewage plume begin to increase about 175 m down gradient, in the approximate area where NO_3 concentrations approach zero (fig. 2). The length of the Fe zone, about 350 m, is controlled by a combination of reactions. Decreasing organic carbon concentrations limit the amount of iron oxides that are reduced. Transport of Fe(II) is slowed by sorption. At the leading edge of the Fe(II) zone, equilibrium thermodynamics predict that Fe(II) is oxidized by MnO_2 causing precipitation of FeOOH, and dissolution of Mn. This oxidation process can explain the increase in Mn near the leading edge of the Fe(II) zone. Manganese concentrations in solution are further controlled by sorption.

The calculated location of the initial increase in Fe(II) concentration and the location of the leading edge matches the measured extent of the Fe(II) zone reasonably well. Calculated peak concentrations are also comparable to those measured in the anoxic zone. The model correctly simulated the plateau in Mn concentration downgradient from the Fe zone.

Figure 3 shows the distribution of Na along the flow path. Although there is variability in Na concentration at different observation points, observed concentrations overall are relatively constant between 0 and 600 m, and 1200 and 4000 m. The decrease in concentration between 600 and 1200 m was used to calculate the amount of mixing between the sewage plume and uncontaminated ground water.

Ammonium and potassium are sorbed by aquifer solids (fig. 3). The equilibrium constants for both the NH_4 and K surface complexation reactions

were fit to the measured concentrations along the defined flow path. To match the zone of high NH_4 concentrations between about 1000 m and 3000 m, higher sewage effluent concentrations were used in the model for the first 40 years.

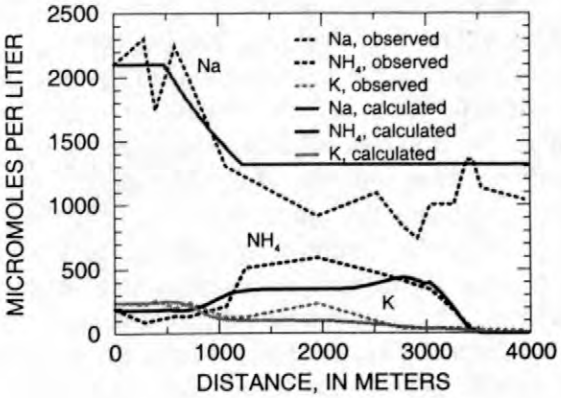

Figure 3. Observed and calculated concentrations of sodium, ammonium, and potassium along the longitudinal axis of the core of the sewage plume prior to cessation.

The pH of treated sewage was generally about 6.5, yet the pH at the water table in 1994 was 6, decreasing to 5.7 in the first 100 m (fig. 4a). This section of aquifer is where O_2 reduction takes place, which can result in a decrease in pH.

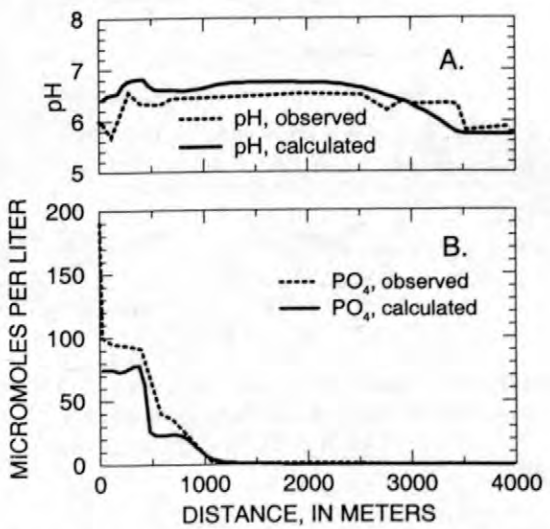

Figure 4. Observed and calculated pH and phosphate concentrations along the longitudinal axis of the core of the sewage plume prior to cessation.

$$O_2 + CH_2O = H_2CO_3 \quad (1)$$

$$H_2CO_3 = H^+ + HCO_3^- \quad (2)$$

The pH increases after 200 m to about 6.5. This coincides with the zone where reductive dissolution of manganese and iron oxides begin. Both reactions consume H^+.

$$2MnO_2 + CH_2O + 3H^+ = 2Mn^{2+} + 2H_2O + HCO_3^- \quad (3)$$

$$4Fe(OH)_3 + CH_2O + 7H^+ = 4Fe^{2+} + 10H_2O + HCO_3^- \quad (4)$$

The pH of the sewage plume remains near 6.5 for most of its length, decreasing near the toe of the plume.

Ground-water pH is buffered by sorption reactions on aquifer solids (Stollenwerk, 1996). The model does a reasonable job of simulating the observed pH, although the model pH is about 0.2 units higher than the measured pH. The model did not simulate the decrease in pH observed in the first 100 m. The calculated decrease in pH, from 6.8 to 6.6, near 500 m coincides with oxidation of Fe(II) by MnO_2 and precipitation of FeOOH.

Phosphorus in the sewage plume occurs predominantly as orthophosphate. The dominant species is the $H_2PO_4^-$ anion. Phosphate is sorbed by the iron and aluminum oxyhydroxides coating aquifer solids (Walter and others, 1996). As a result, the leading edge of the PO_4 plume is only 1000 m downgradient from the sewage beds (fig. 4b). Two processes were used to model PO_4 reaction. Strengite precipitated PO_4 within the first 25 m of transport from the sewage beds, and is undersaturated downgradient. After the first 25 m, calculated PO_4 concentrations in ground water were controlled by sorption. The model calculated slightly lower concentrations for the first 500 m, but did simulate the decrease in PO_4 between 500 and 1100 m as well as the location of the leading edge of the PO_4 plume.

Aquifer Remediation

The combination of measured and adjusted parameters used in the geochemical model were reasonably successful in simulating the reactions that resulted in the distribution of sewage-plume constituents after 60 years of sewage discharge. Therefore, the model should be able to provide

some insight on how this aquifer will respond to the cessation of sewage discharge. Figures 5-6 show the model predictions of sewage-plume constituent concentrations for 0, 20, and 60 years after cessation of sewage discharge.

The rate of removal of sewage plume constituents from the aquifer will depend on several factors. The concentration of non-reacting solutes would be expected to rapidly decrease as uncontaminated ground water flushes through the aquifer. After 20 and 60 years, the front between uncontaminated and contaminated ground water should be about 3000 and 9000 m from the sewage beds. Removal of other solutes will depend on reaction rates and concentrations in the solid-phase.

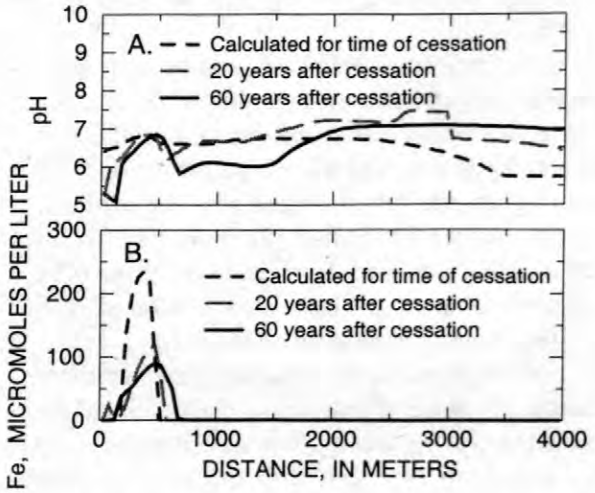

Figure 5. Predicted pH and iron concentrations along the longitudinal axis of the core of the sewage plume, 20 and 60 years after cessation.

The model predicted that the pH of ground water could take decades to decrease to pre-contaminant levels (fig. 5a). The influent pH of uncontaminated ground water is 5.6. After 20 years, pH near the infiltration beds should decrease to uncontaminated levels. Further downgradient, pH is predicted to increase from 6.5 to near 7. After 60 years, the uncontaminated pH zone extends about 200 m from the sewage beds, and lower pH values are predicted as far out as 1500 m.

The length of time that will be required to reestablish oxic conditions within the aquifer will depend in part on the reactivity of the sorbed organic carbon pool. For modeling purposes it was assumed that 25 percent of the sorbed organic carbon would eventually react. The rate of organic carbon oxidation used in the model was based on laboratory column experiments using contaminated cores collected downgradient from a landfill (Stollenwerk, 1998). Aquifer chemistry and sorbed organic carbon content at this site were comparable to the Cape Cod site, although the composition of the organic carbon compounds probably differs.

Model calculations indicate that aerobic conditions will reestablish slowly. The front of the O_2 zone is located at the beginning of the Fe zone (fig. 5b). After 60 years, only the first 100 m of aquifer contain O_2. Iron concentrations are expected to slowly decrease with time as the reservoir of organic carbon in the aquifer is oxidized and the rate of FeOOH reduction decreases (fig. 5b). Based on the assumed reactivity of organic carbon used in this model, the most dramatic decrease is expected within the first 20 years. There is little difference between 20 and 60 years. The leading edge of the Fe(II) zone could also move slightly downgradient. Closer to the beds, the 20-year simulation predicts that Fe(II) concentrations could increase. Increases in Fe have been observed near the sewage beds three years after cessation (LeBlanc and others, this volume).

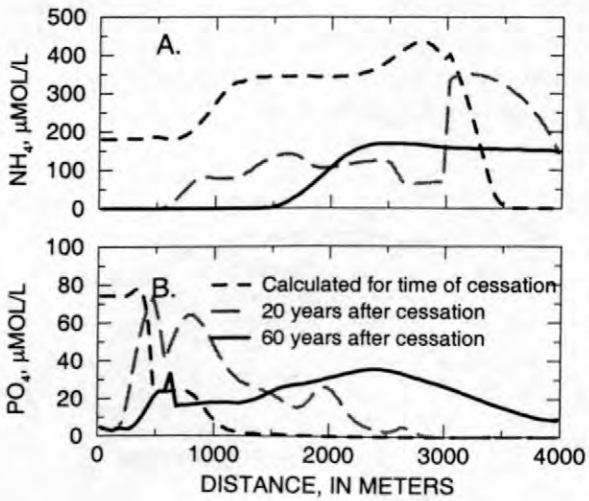

Figure 6. Predicted phosphate and ammonium concentrations along the longitudinal axis of the core of the sewage plume, 20 and 60 years after cessation.

The post cessation profile for NH_4 is typical of other sorbing cations (fig. 6a). Concentrations should gradually decrease as the high concentration pulse moves downgradient. The rate of travel of the trailing edge of the NH_4 plume, where concentrations approach zero, is about 6 times slower than the ground water velocity.

Phosphate is one of the constituents of concern in the sewage plume because part of the plume discharges to Ashumet Pond. A study by K.V. Associates (1991) concluded that Ashumet Pond is mesotrophic but on the border of becoming eutrophic. Addition of PO_4 from the sewage plume could shift the balance toward eutrophication. Concern centers not only on the dissolved PO_4 between Ashumet Pond and the sewage beds, but also on the pool of sorbed PO_4. Laboratory column experiments predict that eluting uncontaminated ground water through sewage-contaminated sediments can release substantial amounts of sorbed PO_4 over many years (Stollenwerk, 1996).

The model predicts that natural remediation of PO_4 from the aquifer will be a slow process. Even after 60 years, only the first 500 m have PO_4 concentrations near uncontaminated levels (fig. 6b). Spikes in PO_4 are also evident, especially after 20 years.

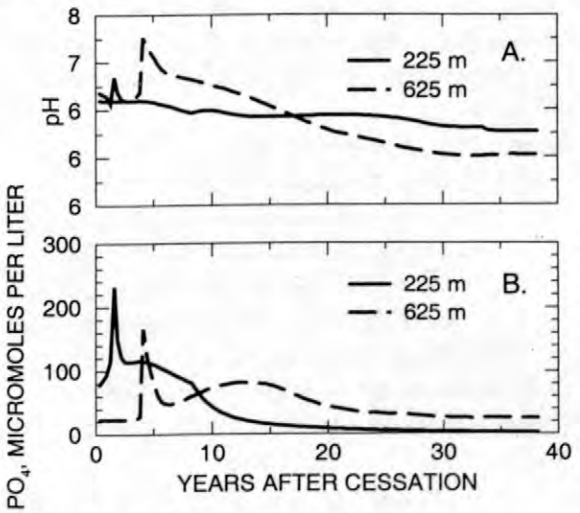

Figure 7. Predicted pH and phosphate concentrations at distances of 225 and 625 m from the sewage beds with time.

Phosphate desorption in the aquifer is affected by pH. The sharp valley in the PO_4 profile at about 600 m after 20 years (fig. 6b) coincides with a decrease in pH (fig. 5a). The predicted pH and PO_4 concentration over time at 225 m and 625 m from the sewage beds are plotted in figures 7a and 7b. A spike increase in pH to 6.7 is predicted at 225 m two years after cessation. Concurrent with the pH spike is an increase in PO_4 concentration to more than twice the pre-cessation concentration. Phosphate concentrations and pH at 225 m then gradually decrease. The pH spike, up to 7.3, arrives at 625 m four years after cessation. The increase in PO_4 concentration at 625 m is also evident. This is potentially significant because 625 m is the approximate location of the shore of Ashumet Pond.

The spike in PO_4 concentration at 225 and 625 m is the result of a combination of reactions. Sewage-contaminated sediments contain large concentrations of sorbed cations such as K^+, NH_4^+, Ca^{2+}, and Mg^{2+} compared to uncontaminated sediments. As uncontaminated ground water flows through the sewage-contaminated sediments, cations are desorbed, and replaced by H^+. This results in an increase in pH which enhances desorption of PO_4. This phenomena has been observed in laboratory column experiments (Stollenwerk, 1996) and in small-scale field experiments (data unpublished).

CONCLUSIONS

A 1D reaction-transport model was used to simulate most of the principal geochemical reactions in the sewage plume at the Massachusetts Military Reservation, Cape Cod. The primary biogeochemical reaction in the aquifer is oxidation of organic carbon by a succession of electron acceptors: dissolved oxygen, nitrate, manganese oxides, and iron oxyhydroxides. Transport of most other solutes is controlled by sorption onto the surfaces of aquifer solids. Parameters for most of the reactions included in the model were adjusted to give the best fit to measured concentration profiles along the longitudinal axis of the core of the plume.

The model was then used to simulate the fate of sewage plume constituents for 60 years after discharge of sewage stopped. Modeling results predict that concentrations of the reactive solutes will decrease with time, although slowly. The reservoir of reactive sorbed organic carbon could reduce dissolved oxygen in uncontaminated water, resulting in little change in the current anoxic conditions in the aquifer for the next 60 years. Cations will move downgradient at velocities less than the groundwater velocity and concentrations will slowly decrease; pH is predicted to remain at pre-cessation levels and only gradually decrease near the sewage beds. Phosphate will also decrease; however, during the near term, it is likely that phosphate concentrations could increase in the first few hundred meters in response to a transient spike increase in pH. Model results indicate that phosphate concentra-

tions in the sewage plume entering Ashumet Pond may remain high for 10 - 15 years.

REFERENCES

Appelo, C.A.J., and Parkhurst, D.L., 1998, Enhancements to the geochemical model PHREEQC--1D transport and reaction kinetics, *in* Arehart, G.B, and Hulston, J.R., eds., Water-Rock Interaction: Rotterdam, Balkema, p. 873-876.

Barber, L.B., and Keefe, S.H., 1999, Evolution of a ground-water sewage plume after removal of the 60-year-long source, Cape Cod, Massachusetts: Organic contaminants, *in* Morganwalp, D.W., and Buxton, H.T., eds., U.S. Geological Survey Toxic Substances Hydrology Program -- Proceedings of the Technical Meeting, Charleston, South Carolina, March 8-12, 1999-- Volume 3 -- Subsurface Contamination from Point Sources: U.S. Geological Survey Water-Resources Investigations Report 99-4018C, this volume.

Coston, J.A., Fuller, C.C., and Davis, J.A., 1995, Pb^{2+} and Zn^{2+} adsorption by a natural aluminum- and iron-bearing surface coating on an aquifer sand: Geochimica et Cosmochimica Acta, v. 59, no. 17, p. 3535-3547.

Dzombak, D.A., and Morel, F.M.M., 1990, Surface Complexation Modeling: New York, John Wiley & Sons, 393 p.

K.V. Associates, 1991, Ashumet Pond, Falmouth/ Mashpee, Massachusetts - A diagnostic/feasibility study, Prepared for the towns of Falmouth and Mashpee, Barnstable County, Massachusetts, 158 p.

LeBlanc, D.R., Garabedian, S.P., Hess, K.M., Gelhar, L.W., Quadri, R.D., Stollenwerk, K.G., and Wood, W.W., 1991, Large-scale natural gradient tracer test in sand and gravel, Cape Cod, Massachusetts, I. Experimental design and observed tracer movement: Water Resources Research, v. 27, no. 5, p. 895-910.

LeBlanc, D.R., Hess, K.M., Kent, D.B., Smith, R.L., Barber, L.B., and Campo, K.W., 1999, Natural restoration of a sewage plume in a sand and gravel aquifer, Cape Cod, Massachusetts, *in* Morganwalp, D.W., and Buxton, H.T., eds., U.S. Geological Survey Toxic Substances Hydrology Program -- Proceedings of the Technical Meeting, Charleston, South Carolina, March 8-12, 1999-- Volume 3 -- Subsurface Contamination from Point Sources: U.S. Geological Survey Water-Resources Investigations Report 99-4018C, this volume.

McCobb, T.D., LeBlanc, D.R., and Hess, K.M., 1999, Three-point triangulation method to evaluate the temporal variability of hydraulic gradients in an uncontaminated aquifer, Cape Cod, Massachusetts, 1999, *in* Morganwalp, D.W., and Buxton, H.T., eds., U.S. Geological Survey Toxic Substances Hydrology Program -- Proceedings of the Technical Meeting, Charleston, South Carolina, March 8-12, 1999-- Volume 3 -- Subsurface Contamination from Point Sources: U.S. Geological Survey Water-Resources Investigations Report 99-4018C, this volume.

Parkhurst, D.L., 1995, Users's guide to PHREEQC--A computer program for speciation, reaction-path, advective-transport, and inverse geochemical calculations: U.S. Geological Survey Water-Resources Investigations Report 95-4227, 143 p.

Parkhurst, D.L., and Appelo, C.A.J., 1997, Enhancements to the geochemical model PHREEQC--1D advection and dispersion, diffusion to stagnant zones, and reaction kinetics: Supplement to EOS, April 29, 1997, p. S167.

Poeter, E.P., and Hill, M.C., 1998, Documentation of UCODE, a computer code for universal inverse modeling: U.S. Geological Survey Water-Resources Investigations Report 98-4080, 116 p.

Savoie, Jennifer, and LeBlanc, D.R., 1998, Water-quality data and methods of analysis for samples collected near a plume of sewage-contaminated ground water, Ashumet Valley, Cape Cod, Massachusetts, 1993-94: U.S. Geological Survey Water-Resources Investigations Report 97-4269, 208 p.

Smith, R.L., Garabedian, S.P., and Brooks, M.H., 1996, Comparison of denitrification activity measurements in groundwater using cores and natural-gradient tracer tests: Environmental Science and Technology, v. 30, no. 12, p. 3448-3456.

Smith, R.L., and Duff, J.H., 1998, Denitrification in a sand and gravel aquifer: Applied Environmental Microbiology, v. 54, no. 5, p. 1071-1078.

Stollenwerk, K.G., 1996, Simulation of phosphate transport in sewage-contaminated groundwater, Cape Cod, Massachusetts: Applied Geochemistry, v. 11, p. 317-324.

Stollenwerk, K.G., 1998, Natural remediation of arsenic-contaminated groundwater: Eos, v. 79, no. 45.

Walter, D.A., Rea, B.A., Stollenwerk, K.G., and Savoie, Jennifer, 1996, Geochemical and hydrologic controls on phosphorus transport in a sewage-contaminated sand and gravel aquifer near Ashumet Pond, Cape Cod, Massachusetts: U.S. Geological Survey Water-Supply Paper 2463, 89 p.

AUTHOR INFORMATION

Kenneth G. Stollenwerk and David L. Parkhurst,
U.S. Geological Survey, Lakewood, Colorado
(kgstolle@usgs.gov and dlpark@usgs.gov)

Multispecies Reactive Tracer Test in an Aquifer with Spatially Variable Chemical Conditions: An Overview

By James A. Davis, Douglas B. Kent, Jennifer A. Coston, Kathryn M. Hess, and Jennifer L. Joye

ABSTRACT

A field investigation of multispecies reactive transport was conducted in a well-characterized, sand and gravel aquifer on Cape Cod, Massachusetts. Ten thousand liters of ground water with added tracers (Br, Cr(VI), and EDTA complexed with Pb, Zn, Cu, and Ni) were injected into the aquifer and the distributions of tracers were monitored for 15 months. Most of the tracers were transported more than 200 meters; transport was quantified using spatial moments computed from the results of a series of synoptic samplings. The aquifer is characterized by different geochemical regimes caused by sewage contamination; the interactions of the reactive tracers with the aquifer sediments varied due to the differing chemical conditions. For example, retardation of the tracers varied with pH and Cr(VI) reduction varied with the concentration of dissolved oxygen. Transport of the metal-EDTA complexes was affected by the extent and rates of various metal exchange reactions, especially those involving Fe(III) dissolution and complexation with EDTA. These reactions also were influenced by the spatial distribution of Zn contamination in the aquifer from sewage disposal. The results of the field experiment provide a well-characterized, chemically complex data set that can be used for future development and testing of hydrogeochemical transport models of flow coupled with chemical reactions.

INTRODUCTION

Chemical reactions can have a major influence on the transport of inorganic solutes (Abrams and others, 1998; Walter and others, 1994a,b; Yeh and Tripathi, 1991), and the reactivity generally depends strongly on chemical speciation. For example, many metal ions are extensively retarded in ground water when present as a free (uncomplexed) cation at circumneutral pH values (Kent and others, 1999a; von Gunten and others, 1991). In contrast, the formation of weakly adsorbing, anionic complexes with organic ligands may greatly increase the mobility of metal ions or radionuclides (Zachara and others, 1995; Jardine and Taylor, 1995; Szecsody and others, 1994; Killey and others, 1984). Inorganic ligands, such as fluoride and carbonate, have been shown to increase the mobility of uranium(VI) (Kohler and others, 1996; Waite and others, 1994). Changes in pH along ground-water flow paths can cause shifts in metal ion speciation from soluble to sparingly soluble species. In addition to complexation and acid-base reactions, redox (electron transfer) reactions may cause changes in speciation that have a marked effect on transport. For example, aqueous chromium(VI) species are generally mobile in ground water (Kent and others, 1995), however, chromium(III), if uncomplexed, should be highly retarded in ground water because its aqueous species are extensively adsorbed or insoluble (Kent and others, 1994).

Many reactive transport models have been developed to describe the effects of chemical and biological reactions on the transport of solutes (e.g., Stollenwerk, 1998; Yeh and Salvage, 1995; Parkhurst, 1995; Walter and others, 1994a,b). Application of these models and computer codes to real-world problems is limited by a lack of relevant kinetic and thermodynamic data for describing appropriate reactions in the environment, particularly data for sorption and

redox processes. Further advances in this area will require the development of operational paradigms for field applications, perhaps including approaches for estimating a distribution of values for significant model parameters in the laboratory using site-specific materials (Fuller and others, 1996).

This paper presents an overview of the results of a tracer test conducted at the U. S. Geological Survey (USGS) Toxic Substances Hydrology Research site on Cape Cod, Massachusetts (fig. 1). Ground water was injected into the aquifer with bromide, chromium (as Cr(VI)), lead-ethylenediaminetetraacetic acid (EDTA) , copper-EDTA, zinc-EDTA, and nickel-EDTA complexes added as tracers (table 1). The tracers were chosen based on their relative reactive properties and the chemical conditions present at the field site. LeBlanc and others (1991) concluded that bromide (Br) was a suitable choice for a nonreactive tracer. Adsorption of the injected anionic tracers was known to be pH dependent and a function of the concentration of competing anions from previous small-scale tracer tests (Kent and others, 1994; 1995) and laboratory studies (Nowack and Sigg, 1996). The lead (Pb)-, copper (Cu)-, zinc (Zn)-, and nickel (Ni)-EDTA complexes were chosen as tracers based on available thermodynamic data for metal exchange reactions with iron [as Fe(III)]. EDTA was chosen as a ligand for metal complexation because it was known to be resistant to biodegradation in the Cape Cod aquifer (Davis and others, 1993; Kent and others, 1999b).

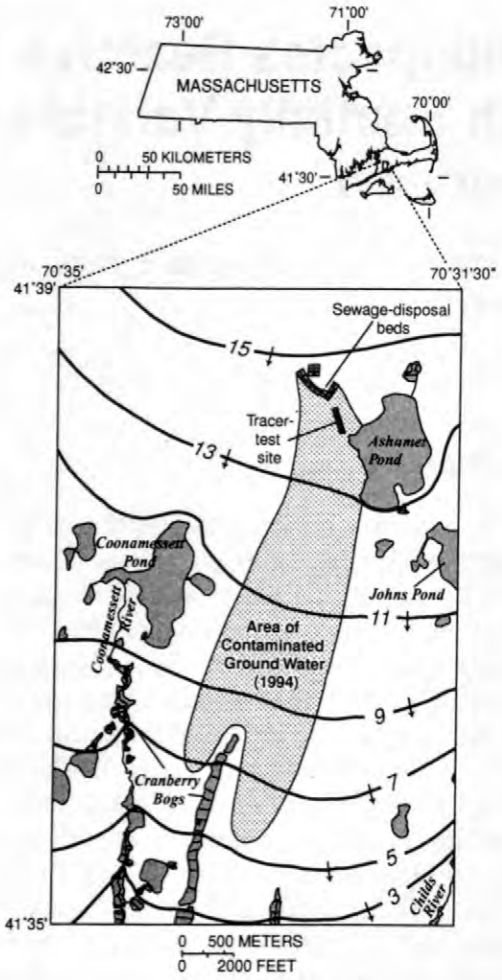

Figure 1. Location of tracer-test site, area of sewage-contaminated ground water, and water-table contours, western Cape Cod, Massachusetts.

SITE CHEMISTRY AND TRACER TEST METHODS

At the time of the tracer test, shallow ground water at the site was contaminated by secondary sewage effluent that had been disposed since 1938 onto infiltration beds located about 200 meters (m) upgradient of the tracer test injection site (Savoie and LeBlanc, 1998). Steep vertical concentration gradients in dissolved oxygen, pH, the concentration of Zn^{2+}, and other water quality parameters were observed near the water table, caused by limited vertical mixing of the sewage effluent with ambient ground water (Smith and others, 1991; Kent and others, 1994). For purposes of discussion, the ground water can be characterized in terms of three different geochemical zones (Davis and others, 1999). The pristine zone, near the water table, had high concentrations of DO (dissolved oxygen), pH values in the range 5.4-5.7, and low concentrations of dissolved salts. The sewage-contaminated, suboxic zone was mildly reducing, with low concentrations of DO (<10 micromolar) and dissolved manganese, pH values in the range 6.0-6.5, increased concentrations of dissolved salts, and sewage-derived contaminants, such as

Table 1. Description of the injectate and injection conditions

Constituent	Reagent	Concentration	Concentration/DL*
pH	-----	5.6	-----
Br^-	KBr	3.43 mM⊥	1143
$EDTA^{4-}$	Na_4EDTA	1.112 mM	139
CrO_4^{2-}	$K_2Cr_2O_7$	0.506 mM (as Cr)	2663
Cu	$CuCl_2 \cdot 6H_2O$	0.266 mM	4222
Ni	$NiCl_2 \cdot 6H_2O$	0.256 mM	502
Pb	$Pb(NO_3)_2 \cdot 6H_2O$	0.248 mM	517
Zn	$ZnCl_2 \cdot 6H_2O$	0.266 mM	1773
Volume	9884 L		
Altitude of Injection ports	13.17, 12.18, 11.18 meters		
Rate of Injection	1.02 L/min/port		
Duration of Test	449 days		

*DL = Method Detection Limit

⊥mM = millimolar

phosphate and Zn. A transition zone approximately 2.5 m thick between the pristine and suboxic zones enclosed most of the dissolved chemical gradients. Ground water in the transition zone at the injection location contained elevated concentrations of dissolved and adsorbed Zn, derived from the sewage effluent. Laboratory studies have shown that Zn^{2+} is adsorbed primarily by Fe and Al oxyhydroxide coatings on the aquifer sediment grains (Coston and others, 1995). The increase in pH with depth causes an increase in Zn^{2+} adsorption to the sediments and increased Zn^{2+} retardation during transport (Kent and others, 1999a). The Zn-contaminated region was approximately 3 m thick near the injection location but decreased in thickness with distance downgradient, until at 150 m downgradient of the injection, no Zn contamination in the aquifer could be detected.

On April 20, 1993, about 10,000 liters of pristine ground water were withdrawn from a well 400 m downgradient of the injection site and transported to a holding tank near the injection point. The ground water was mixed with the tracers in the tank and injected into the aquifer over a nine-hour period. The injection was designed to utilize an existing array of multi-level samplers installed in the aquifer for a previous tracer test (LeBlanc and others, 1991). The vertical extent of the tracer injection spanned the vertical concentration gradients in DO, pH, and Zn^{2+}. In this way, the mobility of the tracers under different chemical conditions could be compared and the fate of the tracers in response to different chemical processes could be contrasted.

EDTA was injected at a concentration in slight excess (7%) of the sum of concentrations of Ni, Cu, Pb, and Zn. Speciation of the four metals was dominated by the complex, $MeEDTA^{2-}$, in the injectate water, where Me represents one of the four injected metal ions. According to available thermodynamic data (Smith and Martell, 1989), only minor amounts of complexes other than $MeEDTA^{2-}$ were present under the chemical conditions present in the aquifer. To simplify the discussion, we shall use the general term of metal-EDTA complexes to refer to all of the EDTA complexes formed. For the four metals, concentrations of species other than the metal-EDTA complexes were below detection in the injected water.

Transport of the tracers was quantified using spatial moments computed from a series of comprehensive synoptic samplings of the tracer cloud and temporal moments of concentration data collected frequently at two multi-level samplers (breakthrough curves) located 37 and 52 m downgradient of the injection. Three-dimensional spatial moments were used to calculate the total mass (zeroth moment), center of mass (first moment), and higher moments of each tracer, according to the methods given in Garabedian and others (1991). Other details about

the site and tracer test methods are given in Davis and others (1999).

RESULTS

Observed distributions of Br showed an increase in the size of the tracer cloud with time due to dispersion, a sinking trend with time due to density differences between the tracer cloud and the ambient ground water, and a slightly curved path of transport due to changes in the hydraulic-gradient direction (Hess and others, 1999). Figure 2 shows the results of the zeroth moment analysis for Br, Ni, and Cr for each synoptic sampling, normalized by dividing the calculated mass by the injected mass for each tracer. The normalized mass for Br averaged 1.03 for eight synoptic samplings.

Chemical interactions between the reactive tracers and the aquifer sediments varied among the different solutes and the different geochemical zones. Figure 3 shows typical breakthrough curve data in the pristine, transition, and suboxic zones at a multi-level sampler 52 m downgradient of the injection site. In agreement with the results of Kent and others (1994), total dissolved Cr was equal to the concentration of Cr(VI) within experimental error in all samples tested. Cr(III) is very strongly sorbed at the pH values present in the aquifer, thus any Cr(III) that formed would not likely be detected in the ground-water samples. Retardation of Cr(VI) was greatest in the pristine zone and decreased with decreasing altitude (fig. 3), due to the increase in pH and concentrations of other anions in the ground water (Kent and others, 1994; Kent and others, 1995). Figure 4 shows how the retardation factor of Cr(VI) varied with altitude at the two multi-level samplers where breakthrough data were collected. Retardation factors are not shown for the lowest altitudes because Cr(VI) was reduced and irreversibly sorbed in the suboxic zone before reaching 37 m downgradient. Dissolved Cr mass decreased to less than 50% of the injected Cr mass during the first 100 days of the tracer test, and then declined at a slower rate for the remainder of the test (fig. 2). The slower decline in Cr mass began after all Cr(VI) in the suboxic zone had been reduced.

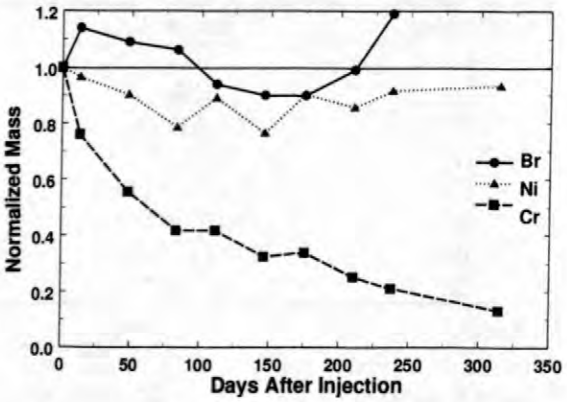

Figure 2. Calculated masses (zeroth moment) of Br, Ni, and Cr for each synoptic sampling normalized by dividing by the initial injected mass of each tracer.

Dissolved Fe (fig. 3) and Al appeared within the tracer cloud shortly after its introduction into the aquifer (Davis and others, 1999). This was due to partial dissolution of the oxyhydroxide phases present as grain coatings (Coston and others, 1995). Exchange reactions of the metal-EDTA complexes with Fe(III) dissolved from oxyhydroxide phases can be expected to be accompanied by adsorption of the dissociated metal ion according to the following reaction:

$$MeEDTA^{2-} + Fe(OH)_{3,s} + \equiv SOH + 2H^{+} = FeEDTA^{-} + \equiv SOMe^{+} + 3H_2O \qquad (1)$$

where Me represents a divalent metal ion initially complexed with EDTA in the injectate, $Fe(OH)_{3,s}$ is an iron oxyhydroxide phase, and $\equiv SOH$ represents a surface site for adsorption on the aquifer sediments.

The overall result of the metal exchange reactions that occurred as the tracer cloud moved downgradient was a shift in the EDTA speciation among the metals. EDTA speciation was dominated by the Fe- and Ni-EDTA complexes by the end of the experiment. Figure 5 shows the masses (in moles) of the four metals injected as EDTA complexes, that is, Ni, Pb, Cu, and Zn_{tot} (total dissolved Zn), and the two metals (Al and Fe(III)) derived from dissolution. Dissolved Al and Pb disappeared completely from the tracer

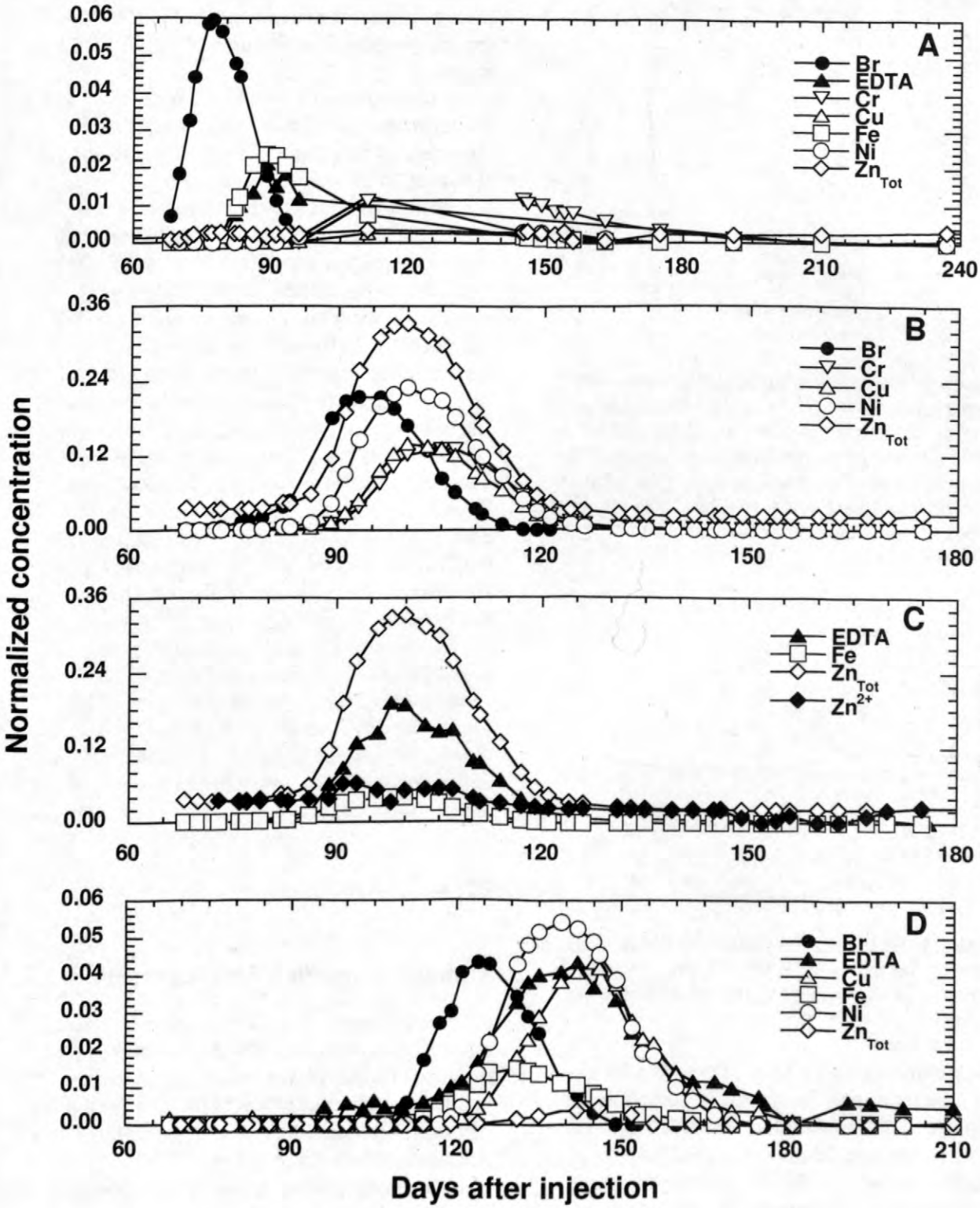

Figure 3. Normalized tracer concentrations (concentration divided by injected concentration) at 52 m downgradient of the injection; Fe concentration divided by the injected EDTA concentration. (a) pristine zone, 12.6 m altitude, pH=5.6; (b and c) transition zone, Zn^{2+}-contaminated, 10.6 m altitude, pH=5.85 (d) suboxic zone, below Zn^{2+} contamination, 8.6 m altitude, pH=6.1.

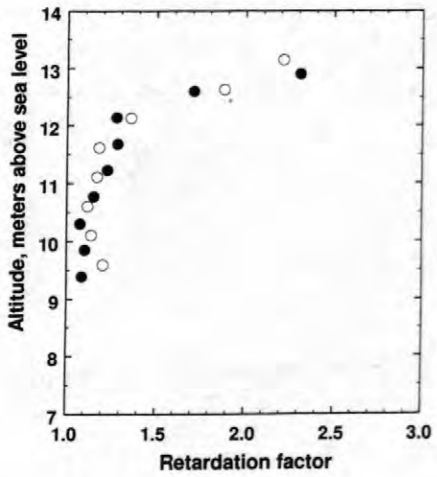

Figure 4. Retardation factors for Cr calculated from the breakthrough-curve data plotted as a function of the altitude of the sampling port at which the breakthrough curve was collected. The filled circles are for a multi-level sampler located 37 m downgradient of the injection. The open circles are for a multi-level sampler 52 m downgradient.

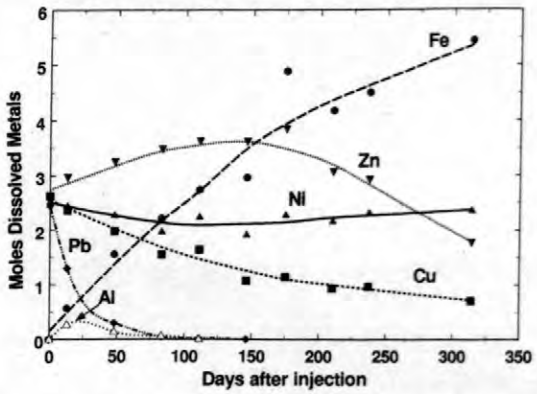

Figure 5. Results of the spatial moments analysis showing the moles of Ni, Pb, Cu, Zn_{tot}, Fe, and Al in the tracer cloud as a function of time after the injection.

cloud within about 100 days. Dissolved Pb was not detected during breakthrough curve sampling at either of the breakthrough multi-level samplers.

Ni normalized mass averaged 0.88 for nine synoptic samplings (fig. 2). No temporal trend was observed. The retardation of Ni transport relative to Br (fig. 3) shows that Ni-EDTA complexes were reversibly adsorbed onto the aquifer sediments. However, the fact that Ni mass remained essentially constant throughout the tracer test indicates that little Ni-Fe exchange occurred via the reaction in Eq. 1. Thus, the primary chemical reaction that influenced Ni in the experiment was adsorption of the Ni-EDTA complexes.

In the pristine and suboxic zones, Zn_{tot} and Cu concentrations during breakthrough were considerably less than that of Ni (figs. 3a and 3d). However, in the transition zone, Zn_{tot} concentrations were greater than both Ni and Cu, and Fe exchange reactions were less significant than in the pristine zone (figs. 3b and 3c). Only small fluctuations in Zn^{2+} concentration were observed in the transition zone, suggesting that adsorbed Zn^{2+} buffered the aqueous Zn^{2+} concentration (fig. 3c). Dissolved Zn_{tot} mass increased during the first 111 days of the tracer test but then decreased significantly toward the end of the test (fig. 5). In the portions of the tracer cloud that were above and below the Zn^{2+}-contaminated region, Zn_{tot} concentrations decreased as a result of metal exchange reactions with Fe(III) leached from the sediments (Eq. 1). However, at the beginning of the test, the decreases in Zn_{tot} concentrations in these zones were apparently offset by greater increases in Zn_{tot} concentrations in the transition zone (fig. 3b), causing an increase in dissolved Zn_{tot} mass (fig. 5). By the end of test, the tracer cloud was moving beyond the region of Zn contamination, and the dissolved Zn_{tot} mass began to decrease via the Fe exchange reaction (Eq. 1).

DISCUSSION

Transport Coupled with Adsorption

Based on the results of small-scale tracer tests (Kent and others, 1999b), adsorption of the metal-EDTA complexes was expected in the aquifer, causing retardation of the transport of the metal-EDTA complexes relative to Br (fig. 3). Adsorption of the divalent metal-EDTA complexes was greater in the pristine zone near the water table, because the pH was lower (around 5.5) than in the suboxic zone of the aquifer. In addition, the concentrations of other anions which compete with the metal-EDTA for

available adsorption sites, such as sulfate and phosphate, are low in the pristine zone.

As was shown in previous small-scale tracer tests, the transport of Cr(VI) was affected by reversible adsorption as well as reduction to Cr(III). At a site 2 km downgradient of the tracer test, it was found that Cr(VI) transport was controlled by weak reversible adsorption in the pristine zone (Kent and others, 1995), similar to the results presented here. At the same site described in this paper, Cr(VI) and molybdate adsorption were very weak in the suboxic zone due to the higher pH and the presence of competing anions (Stollenwerk, 1995; Kent and others, 1994). Transport of Cr(VI) in the transition zone had not been previously studied, but the retardation trends observed in this tracer test as a function of altitude (fig. 4) are consistent with the previous results.

Kent and others (1994) showed that the decrease in dissolved Cr in the suboxic zone was due to reduction of Cr(VI) and subsequent strong sorption of Cr(III). The breakthrough curve data show that Cr(VI) reduction occurred relatively quickly in the suboxic zone [Cr(VI) was below detection, fig. 3d], but proceeded at a slower rate in the transition zone (fig. 3b). Considerable dissolved Cr mass was lost in the suboxic region within 13 days (Davis and others, 1999). As the test progressed, vertical transport of the tracers to the suboxic zone may have controlled or greatly influenced the overall rate of Cr(VI) reduction. For example, by 83 days, a considerable portion of the Br mass had sunk from the oxic region into the suboxic region (Hess and others, 1999).

Transport Coupled with Dissolution, Aqueous Complexation, and Adsorption

In the regions of the aquifer without Zn^{2+} contamination, the observed rate of metal exchange decreased in the order Pb>>Zn>Cu. There was no evidence that a significant mass of Ni was lost from the tracer cloud beyond that which was reversibly adsorbed as Ni-EDTA complexes (fig. 2).

Understanding the overall result of the metal exchange reactions requires a consideration of complexation, dissolution, and adsorption reactions (Eq. 1). It is instructive to break Equation 1 into two separate reactions for metal adsorption and exchange as follows:

$$MeEDTA^{2-} + Fe(OH)_{3,s} + 3H^{+} = FeEDTA^{-} + Me^{2+} + 3H_2O \quad (2)$$

$$Me^{2+} + \equiv SOH = \equiv SO_sMe^{+} + H^{+} \quad (3)$$

where Me represents Pb, Zn, Cu, or Ni. The thermodynamic affinity for the metal exchange reaction of Eq. 2 decreases in the order Zn>>Pb>Ni>Cu, as shown in Table 2 (Smith and Martell, 1989). In other words, if the influence of adsorption (Eq. 3) is ignored, the thermodynamic data lead to the conclusion that $ZnEDTA^{2-}$ exchange with Fe(III) is most favored thermodynamically, followed by $PbEDTA^{2-}$, $NiEDTA^{2-}$, and then $CuEDTA^{2-}$. However, the stability constants for Eq. 3 can also influence the order of the metal exchange reactions. To illustrate this point, consider the stability constants for adsorption of metal ions onto ferrihydrite, a commonly found Fe oxyhydroxide coating on sediment surfaces (table 3, tabulated from Dzombak and Morel, 1990). The constants illustrate that the affinity for adsorption decreases in the order Pb>>Cu>>Zn>Ni. This general preference among the metal ions for adsorption on oxide surfaces likely is true for the Cape Cod sediments, although the values of stability constants for adsorption reactions on the Cape

Table 2. Stability Constants of Fe(III) Exchange Reactions with Metal-EDTA Complexes

Me	Log K
Cu^{2+}	9.5
Ni^{2+}	9.9
Pb^{2+}	10.3
Zn^{2+}	11.8

Table 3. Stability Constants for Metal Ion Adsorption on Ferrihydrite

Me	Log K
Ni^{2+}	0.4
Zn^{2+}	1.0
Cu^{2+}	2.9
Pb^{2+}	4.7

Cod aquifer sediments are only known well for Zn^{2+} at this point in time (Davis et al, 1998).

By combining Eqs. 2 and 3, one obtains Eq. 1, and the stability constants can be determined as the product of the constants of the reactions in Eqs. 2 and 3. Using ferrihydrite as an analogue for the Cape Cod sediment, one obtains the stability constants in Table 4 for Eq. 1. With the two reactions combined, one obtains the same

Table 4. Stability Constants of Fe(III) Exchange Reactions Including Metal Ion Adsorption

Me	Log K
Ni^{2+}	10.3
Cu^{2+}	12.4
Zn^{2+}	12.8
Pb^{2+}	15.0

order in affinity of metal exchange that was observed in the tracer test (in the absence of Zn^{2+} contamination): Pb>>Zn>Cu>>Ni (fig. 3d). Thus, adsorption reactions are critical components of the reaction network affecting the transport of Pb, Zn, Cu, and Ni during the tracer test.

Evaluation of the critical issues in predictive transport modeling for reactive contaminants in ground water awaits the testing of such models with well constrained experimental data. The design and execution of the reactive solute tracer test described here were conducted with this in mind. The chemical complexity and heterogeneity encountered within the spatial and temporal domain of the experiment were well characterized. Experimental data that describe the temporal and spatial distribution of the dissolved tracers were collected to the extent feasible, along with supplementary data, such as that describing metal speciation. Additional investigations will continue to determine which chemical reactions and processes were most important, in order to further enhance the usefulness of these experimental data in testing approaches to predictive modeling of the transport of reactive contaminants under spatially variable chemical conditions.

REFERENCES

Abrams, R. H., Loague, K., and Kent, D. B., 1998, Development and testing of a compartmentalized reaction network model for redox zones in contaminated aquifers, Water Resources Research, 34, 1531-1541.

Coston, J.A., Fuller, C.C., and Davis, J.A., 1995, Pb^{2+} and Zn^{2+} adsorption by a natural aluminum- and iron-bearing surface coating on an aquifer sand, Geochimica et Cosmochimica Acta, 59, 3535-3547.

Davis, J. A., Kent, D. B., Coston, J. A., Hess, K. M., and Joye, J. L., 1999, Multispecies reactive tracer test in an aquifer with spatially variable chemical conditions: 1. Experimental design and observed tracer movement, Water Resources Research, submitted.

Davis, J. A., Coston, J. A., Kent, D. B., and Fuller, C. C., 1998, Application of the surface complexation concept to complex mineral assemblages, Environmental Science and Technology, 32, 2820-2828.

Davis, J.A., Kent, D.B., Rea, B.A., Maest, A.S., and Garabedian, S.P., 1993, Influence of redox environment and aqueous speciation on metal transport in groundwater: Preliminary results of tracer injection studies, in Allen, H.E., Perdue, E.M, and Brown, D.S., Eds., Metals in Groundwater, Chelsea, Mich., Lewis Publishers, 223-273.

Dzombak, D.A., and Morel, F.M.M., 1990, Surface complexation modeling: Hydrous ferric oxide, New York, Wiley-Interscience, 393 pp.

Fuller, C.C., Davis, J.A., Coston, J.A., and Dixon, E., 1996, Characterization of metal adsorption variability in a sand and gravel aquifer, Cape Cod, Massachusetts, U.S.A., Journal of Contaminant Hydrology, 22, 165-187.

Garabedian, S. P., Leblanc, D. R., Gelhar, L. W., and Celia, M. A., 1991, Large-scale natural gradient tracer test in sand and gravel, Cape Cod, Massachusetts, 2. Analysis of spatial moments for a nonreactive tracer, Water Resources Research, 27, 911-924.

Hess, K. M., Davis, J. A., Kent, D. B., and Coston, J. A., 1999, Multispecies reactive tracer test in an aquifer with spatially variable chemical conditions: 2. Bromide and Nickel Tracers, this proceedings.

Jardine, P. M. and Taylor, D. L., 1995, Fate and transport of ethylenediaminetetraacetate chelated contaminants in subsurface environments, Geoderma, 67, 125-140.

Kent, D. B., Abrams, R. H., Davis, J. A., Coston, J. A., and LeBlanc, D. R., 1999a, Modeling the fate and transport of zinc under variable chemical conditions in a sewage-contaminated aquifer, Water Resources Research, submitted.

Kent, D.B., Davis, J.A., Anderson, L.C.D., Rea, B.A., and Coston, J.A., 1999b, Effect of adsorbed metal contaminants on the transport of Zn- and Ni-EDTA complexes in a sand and gravel aquifer, Environmental Science and Technology, submitted.

Kent, D.B., Davis, J.A., Anderson, L.C.D., and Rea, B.A., 1995, Transport of chromium and selenium in a pristine sand and gravel aquifer: Role of adsorption processes, Water Resources Research, 31, 1041-1050.

Kent, D.B., Davis, J.A., Anderson, L.C.D., Rea, B.A., and Waite, T.D., 1994, Transport of chromium and selenium in the suboxic zone of a shallow aquifer: Influence of redox and adsorption reactions, Water Resources Research, 30, 1099-1114.

Killey, R.W.D., McHugh, J.O., Champ, D.R., Cooper, E.L., and Young, J.L., 1984, Subsurface cobalt-60 migration from a low-level waste disposal site, Environmental Science and Technology, 18, 148-157.

Kohler, M., Curtis, G.P., Kent, D.B., and Davis, J.A., 1996, Experimental investigation and modeling of uranium(VI) transport under variable chemical conditions, Water Resources Research, 32, 3539-3551.

LeBlanc, D.R., Garabedian, S.P., Hess, K.M., Gelhar, L.W., Quadri, R.D., Stollenwerk, K.G., and Wood, W.W., 1991, Large-scale natural gradient tracer test in sand and gravel, Cape Cod, Massachusetts: 1. Experimental design and observed tracer movement, Water Resources Reseach, 27, 895-910.

Nowack, B. and Sigg, L., 1996, Adsorption of EDTA and metal-EDTA complexes on goethite, Journal of Colloid and Interface Science, 177, 106-121.

Parkhurst, D. L., 1995, User's guide to PHREEQC: A computer program for speciation, reaction-path, advective-transport, and inverse geochemical calculations, U.S. Geological Survey Water- Resources Investigation Report, 95-4227, 143 pp.

Savoie, J. and LeBlanc, D. R., 1998, Water-Quality data and methods of analysis for samples collected near a plume of sewage-contaminated ground water, Ashumet Valley, Cape Cod, Massachusetts, 1993-94, U.S. Geological Survey Water-Resources Investigations Report, 97-4269.

Smith, R. L., Harvey, R. W., and LeBlanc, D. R., 1991, Importance of closely spaced vertical sampling in delineating chemical and microbiological gradients in groundwater studies, Journal of Contaminant Hydrology, 7, 285-300.

Smith, R.M. and Martell, A.E., 1989, Critical Stability Constants, Vol. 6, Second Supplement, New York, Plenum, 643 pp.

Stollenwerk, K.G., 1995, Modeling the effects of variable groundwater chemistry on adsorption of molybdate, Water Resources Research, 31, 347-357.

Stollenwerk, K. G., 1998, Molybdate transport in a chemically complex aquifer: Field measurements compared with solute-transport model predictions, Water Resources Research, 34, 2727-2740.

Szecsody, J. E., Zachara, J. M., and Bruckhart, P. L., 1994, Adsorption-dissolution reactions affecting the distribution and stability of Co(II)-EDTA in iron oxide-coated sand, Environmental Science and Technology, 28, 1706-1716.

von Gunten, H.R., Karametaxas, G., Krahenbuhl, U., Kuslys, M., Giovanoli, R., Hoehn, E., and Keil, R., 1991, Seasonal biogeochemical cycles in riverborne groundwater, Geochimica et Cosmochimica Acta, 55, 3597-3609.

Waite, T.D., Davis, J.A., Payne, T.E., Waychunas, G.A., and Xu, N., 1994, Uranium(VI) adsorption to ferrihydrite: Application of a surface complexation model, Geochimica et Cosmochimica Acta, 58, 5465-5478.

Walter, A. L., Frind, E. O., Blowes, D. W., Ptacek, C. J., and Molson, J. W., 1994a, Modeling multicomponent reactive transport

in groundwater, 1. Model development and evaluation, Water Resources Research, 30, 3137-3148.

Walter, A. L., Frind, E. O., Blowes, D. W., Ptacek, C. J., and Molson, J. W., 1994b, Modeling multicomponent reactive transport in groundwater, 2. Metal mobility in aquifers impacted by acidic mine tailings discharge, Water Resources Research, 30, 3149-3158.

Yeh, G. T. and Salvage, K., 1995, HYDROGEOCHEM 2.1: A coupled model of hydrologic transport and geochemistry with both equilibrium and kinetic reactions, Tech. Rept., Pennsylvania State Univ., Dept. of Civil and Environ. Eng., State College, PA.

Yeh, G.T. and Tripathi, V.S., 1991, A model for simulating transport of reactive multispecies components: Model development and demonstration, Water Resources Research, 27, 3075-3094.

Zachara, J.M., Smith, S.C., and Kuzel, L.S., 1995, Adsorption and dissociation of Co-EDTA complexes in iron oxide-containing subsurface sands, Geochimica et Cosmochimica Acta, 59, 4825-4844.

Multispecies Reactive Transport in an Aquifer with Spatially Variable Chemical Conditions: Dispersion of Bromide and Nickel Tracers

By Kathryn M. Hess, James A. Davis, Jennifer A. Coston, and Douglas B. Kent

ABSTRACT

Dispersion of ground-water solutes was investigated as part of a multispecies reactive tracer test conducted under spatially varying chemical conditions in an unconfined, sewage-contaminated, sand-and-gravel aquifer on Cape Cod, Massachusetts. The fate and transport of two tracers, nonreactive bromide and reactive nickel (complexed with ethylenediaminetetraacetic acid (EDTA)), are reported here. About 14 percent of the aqueous nickel mass was lost throughout the test, probably due to reversible adsorption of the nickel-EDTA complex onto the iron and aluminum oxyhydroxide minerals coating the aquifer sediments. The two tracers traveled through the aquifer at constant velocities, but the nickel was retarded relative to the bromide (retardation factor, 1.2). The tracers showed little dispersion transverse to the direction of flow (vertical dispersivity, 0.5–3.8 millimeters; lateral dispersivity, 1.4–1.5 centimeters) and great dispersion in the direction of flow (longitudinal dispersivity, 1.1–2.2 meters). The nickel tracer cloud showed smaller longitudinal dispersion than the bromide cloud, possibly due to nonlinear adsorption that led to proportionally greater removal of mass at the edges of the tracer cloud where concentrations were lower. This smaller dispersion also may have resulted from greater adsorption in the shallow uncontaminated part of the aquifer that coincidentally had a higher flow velocity than the deep part of the aquifer. The bromide dispersion results are similar to those obtained in a test conducted previously in this aquifer. The similarity suggests that physical dispersion in this aquifer was spatially stationary at the scale of about 300 meters covered by these two overlapping tests.

INTRODUCTION

A ground-water tracer test was initiated in 1993 to investigate the fate and transport of reactive species under spatially variable chemical conditions. About 10,000 L (liters) of traced ground water were injected and monitored for about 450 d (days) as the tracers traveled through the shallow, unconfined, sand-and-gravel aquifer on western Cape Cod, Massachusetts (fig. 1). The chemical conditions in the aquifer varied spatially due to a plume of sewage-contaminated ground water (LeBlanc, 1984) that has been the focus of study under the U.S. Geological Survey's Toxic Substances Hydrology Program since 1983.

The transport behavior of the two tracers, bromide and nickel, was expected to differ. Bromide is conservative and nonreactive, whereas nickel was injected as a complex with EDTA (ethylenediaminetetraacetic acid) forming an anionic complex ($NiEDTA^{2-}$) that weakly adsorbs onto the iron and aluminum oxyhydroxide minerals coating the aquifer sediments. The purpose of this paper is to compare the manner in which the two tracers were transported and, in particular, how they dispersed. A tracer test of similar magnitude was conducted at this site in 1985–88 (Garabedian and others, 1991; LeBlanc and others, 1991) to investigate dispersion of bromide.

Site Chemistry

The tracer test was conducted about 250 m (meters) downgradient of the sewage-disposal beds (fig. 1) on the Massachusetts Military Reservation. Treated sewage was disposed onto

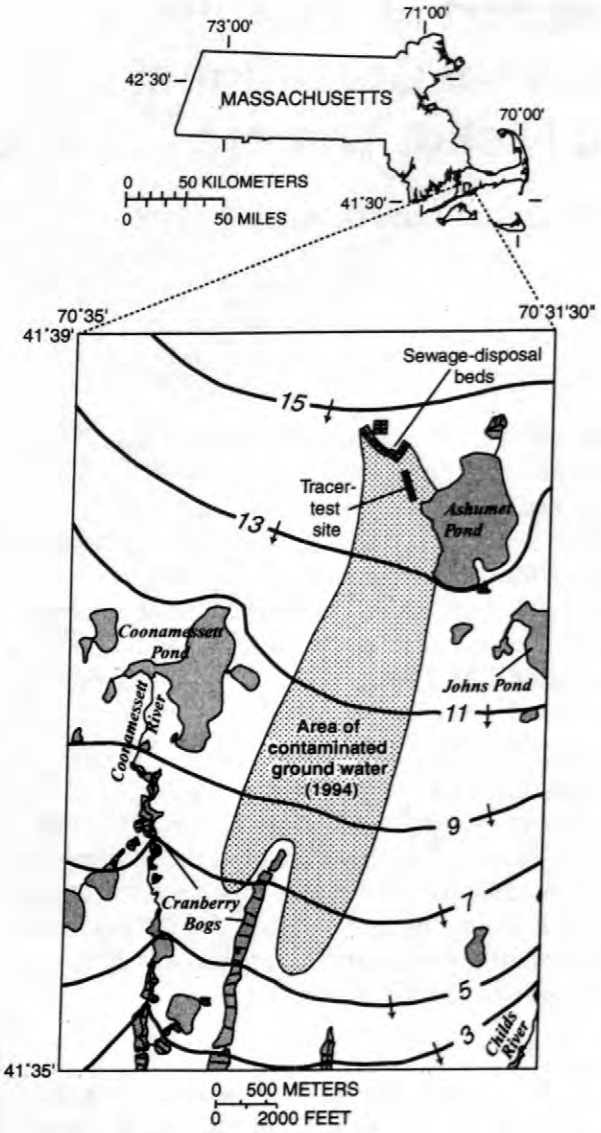

Figure 1. Location of tracer-test site, area of contaminated ground water, and general water-table contours, western Cape Cod, Massachusetts.

these rapid-infiltration beds for about 60 years; the disposal practice ceased in 1995 after the tracer test described here was completed.

The long-term disposal of sewage created geochemical zones whose characteristics depend on vertical location within the aquifer and on distance downgradient from the disposal beds. At the site of the tracer test, clean, uncontaminated water from recharge overlies the sewage-contaminated ground water. This upper pristine zone is characterized by saturated oxygen levels of 8–10 mg/L (milligrams per liter), pH values in the range of 5–5.5, and low amounts of dissolved constituents leading to specific conductance values typically below 80 µS/cm (microsiemens per centimeter at 25 degrees Celsius). The suboxic zone has dissolved oxygen levels below 1 mg/L, pH values greater than 6, and specific conductance values greater than 300 µS/cm. Between the pristine and suboxic zones is a transition zone where the chemistry changes considerably over a vertical distance of only 1 to 2 m. In the transition zone, contaminant levels are high enough and pH levels are low enough that dissolved zinc has been transported as far downgradient as the middle of the tracer test site (Rea and others, 1991; Kent and others, in press).

Tracer-Test Design

The test began on April 21, 1993, with the injection of about 10,000 L of tracer solution. Several chemicals were mixed with uncontaminated ground water that was removed from a site about 400 m downgradient of the injection location and the solution was injected into the aquifer over a 9-hour period. The tracers included nonreactive bromide (3.43 mM (millimolar)) and reactive nickel (0.256 mM). The nickel and three other less reactive metals (lead, zinc and copper) were injected as complexes with EDTA.

Ground-water samples were collected every month from an array of multilevel samplers (LeBlanc and others, 1991) installed downgradient of the injection site. Samplers were constructed of 15 tubes, each of which was open to a different level in the aquifer. The ports on a sampler typically spanned the vertical extent of the tracers. Chemical analyses of the samples were used to define the three-dimensional distribution of the tracers at the time of the sampling. Ten synoptic sampling rounds were completed between 13 and 449 d after the injection. By the time of later sampling rounds,

some of the tracers had traveled outside the region instrumented with multilevel samplers. Therefore, the results reported here were collected during time intervals 237 d and 314 d for the bromide and nickel distributions, respectively.

TRACER TRANSPORT

Bromide was expected to travel freely through the aquifer without chemically reacting with the aquifer sediments. In contrast, the nickel-EDTA complex was expected to adsorb reversibly to the iron and aluminum oxyhydroxide minerals that coat the quartz-dominated aquifer sediments. Nickel is believed to be thermodynamically the least reactive of the four complexed metals (Davis and others, 1999). The transport behavior of nickel was expected to depend upon altitude within the aquifer because of the vertical variability in the background chemistry within the aquifer. The increase in pH and the increase in concentrations of adsorbing anions, especially phosphate, with increasing depth, should favor a decrease in the tendency for the nickel-EDTA complex to adsorb onto aquifer sediments (Novak and Sigg, 1996). Davis and others (1999) describe the fate and transport of EDTA and the other injected metals.

The bromide and nickel tracer clouds spread out in the direction of ground-water flow. Figure 2 shows the mapped distributions of the maximum bromide and nickel concentrations observed at each multilevel sampler 13 and 83 d after injection. At 83 d, the leading edge of the nickel appears to trail slightly the leading edge of the bromide. Otherwise, the mapped distributions appear similar.

Vertical longitudinal slices through the same distributions (fig. 3) provide different views of the transport of the two tracers. By 83 d the bromide tracer cloud has obtained an asymmetric shape with the leading edge high near the water table and the trailing edge lower in the aquifer. This asymmetric distribution resulted from variability in velocity caused by variability in aquifer hydraulic conductivity.

Unexpectedly, the vertical distribution of nickel at 83 d is more symmetrical than the bromide distribution, even though nickel is the reactive tracer. Relative to bromide, the nickel tracer is more retarded near the water table in the pristine zone, where pH and competition for adsorption sites are low (Davis and others, 1999) and less retarded in the lower suboxic zone where pH and competition are higher. This difference in adsorption properties results in a vertical distribution of nickel that differs from that of bromide and that somewhat masks the effects of the physical heterogeneity of the aquifer.

Quantitative Analysis

Spatial moment analysis was performed on each synoptic data set for both tracers. The linear interpolation scheme was the same as that used by Garabedian and others (1991) for the test performed earlier in this aquifer.

Figure 4 shows the bromide and nickel masses quantified by spatial analysis of each sampling (zeroth moment) plotted against the number of days from injection. The porosity used in the analysis affects the masses calculated; the assumed porosity of 0.39 is reasonable for this type of sand-and-gravel sediment and is the same as the porosity used by Garabedian and others (1991) in the analysis of the earlier test. Each mass has been normalized by dividing the calculated mass by the total mass of the specific tracer injected (fig. 4A). The normalized masses of bromide range from 0.89 to 1.19 and have an average of 1.03 (n=8). No temporal trends were observed, a result that supports the assumption that bromide transport was nonreactive and conservative.

The normalized masses of nickel range from 0.76 to 0.97 and have an average of 0.88 (n=9). A second normalization step of dividing the normalized mass of nickel by the normalized mass of bromide was done to remove error in the calculated masses that might have resulted from the spatial sampling scheme (fig. 4B). The relative masses have an average of 0.86 (n=8), which is similar to the average of the normalized nickel masses. The consistent loss in aqueous nickel mass of around 12–14 percent throughout the test suggests that nickel was reversibly adsorbed onto the aquifer sediments.

The first spatial moment defines the center of mass for each tracer cloud at each synoptic sampling. Figure 5 shows the distance from the

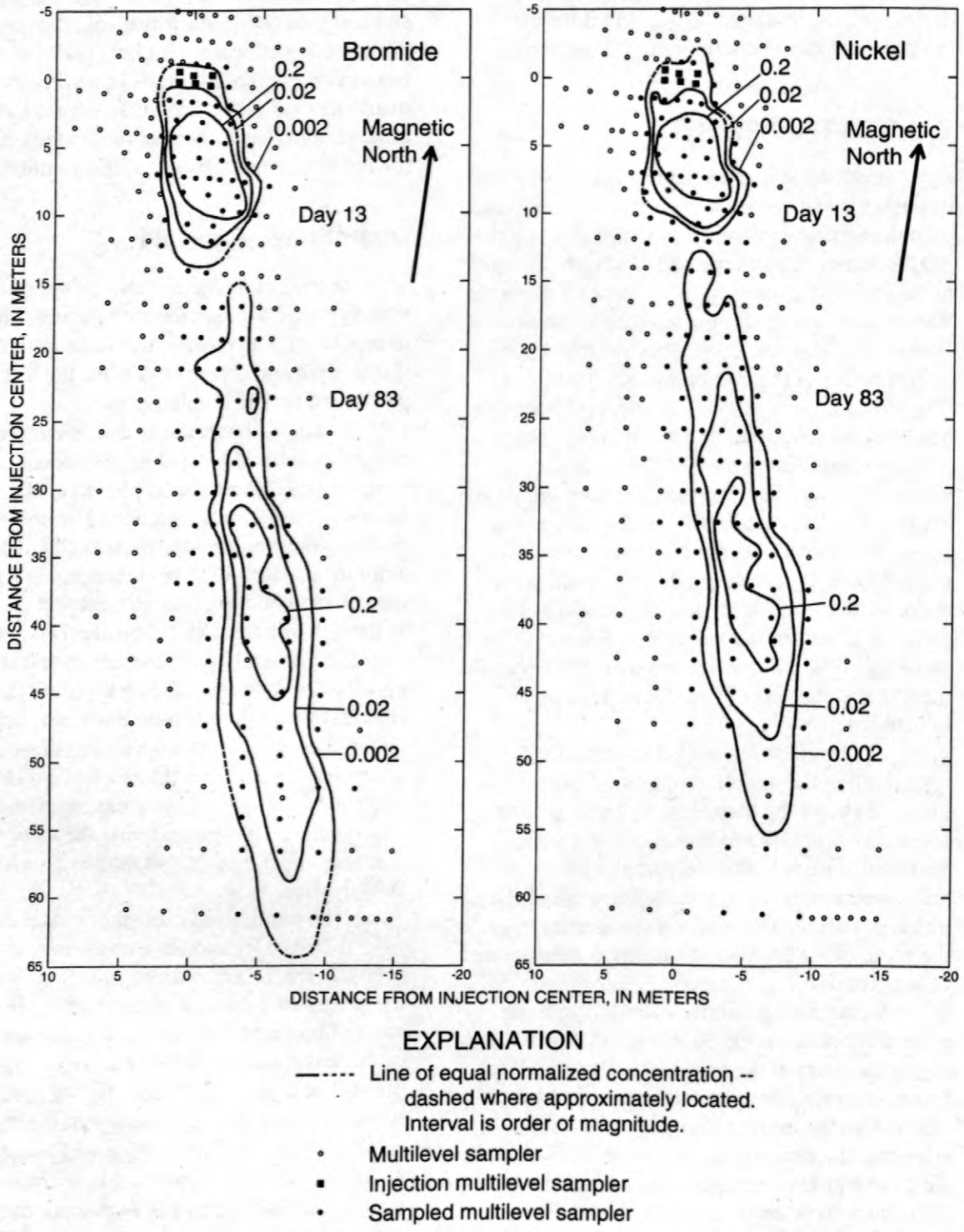

Figure 2. Mapped distributions of maximum concentrations of bromide and nickel observed 13 and 83 days after injection. Normalized concentrations are calculated by dividing measured concentrations by the injection concentration. Also shown are the locations of multilevel samplers (MLS) available for sampling during the tracer test, MLS sampled at 13 and 83 days, and the six injection MLS.

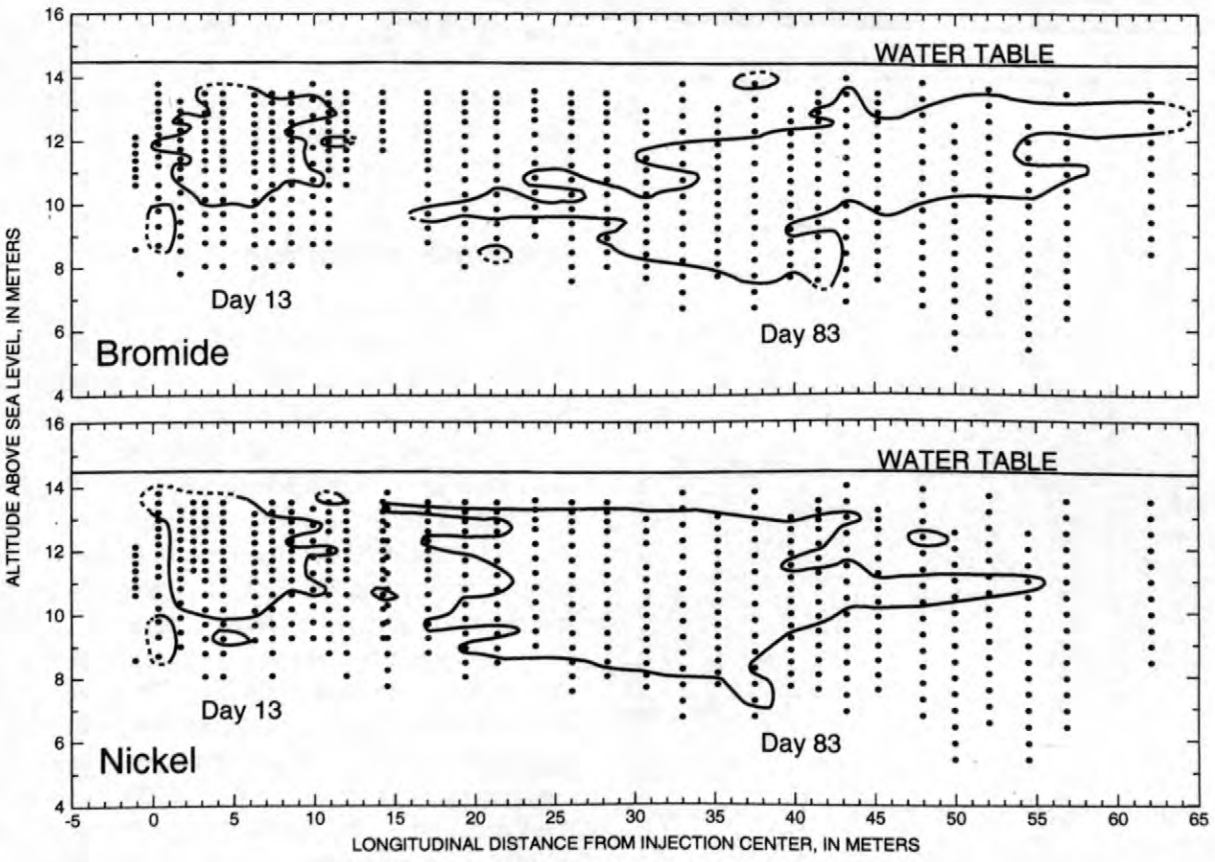

Figure 3. Longitudinal and vertical distributions of bromide and nickel tracer clouds observed 13 and 83 days after injection. Sections are aligned along the mean direction of transport. The extents of the tracer clouds are marked by the 0.002 normalized concentration contour. Normalized concentrations are calculated by dividing measured concentrations by the injection concentration.

center of the injection to the center of mass as a function of time. Nickel and bromide data sets show linear trends indicating constant transport velocities through the aquifer. Solute velocities determined by the slopes of the trend lines are 0.39 and 0.47 m/d for nickel and bromide, respectively (table 1). The lower but constant velocity for nickel is consistent with reversible adsorption of the nickel-EDTA complex onto the aquifer sediments. A retardation factor of 1.2 is calculated from these velocities. This retardation factor suggests an adsorbed mass of 16 percent, if linear adsorption is assumed (Kohler and others, 1996). This calculated adsorbed mass is similar to the 12 to 14 percent observed in the zeroth moment calculations from the synoptic data.

The retardation of nickel relative to bromide is illustrated in a map view of the positions of the centers of mass for bromide and nickel (fig. 6). By 237 d the difference between the centers of mass is about 20 m, which is about 20 percent of the entire distance traveled. Breakthrough curves constructed by frequently (every 2-5 d) collecting samples at two multilevel samplers located downgradient 37 m (data not shown) and 52 m (data shown in Davis and others, 1999) also graphically display the retarded velocity of nickel relative to bromide.

The altitude component of the centers of mass was also calculated. A plot of altitude as a function of days from injection (fig. 7A) shows that both tracer clouds sank dramatically at the beginning of the test. By 83 d the clouds had dropped about 2 m, probably due to the density difference between the injection solution and the native ground water. After 83 d the clouds remained mostly at the same altitude in the aquifer.

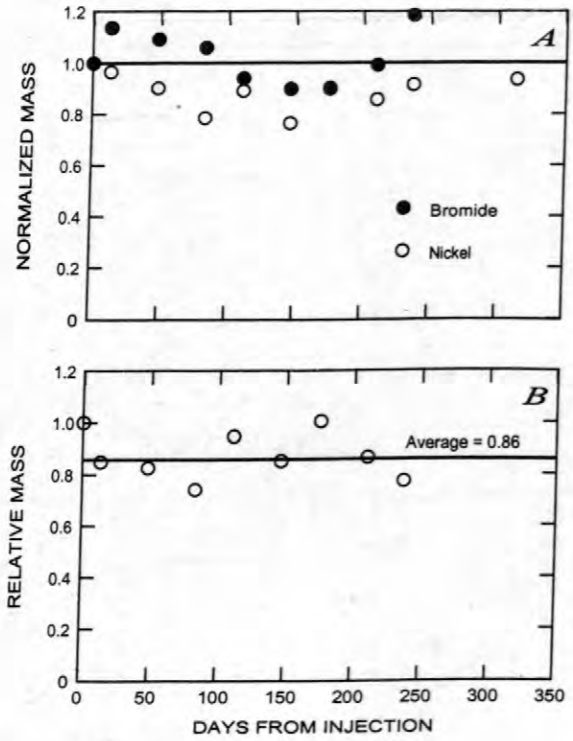

Figure 4. Spatial zeroth moment of bromide and nickel tracer clouds calculated for each monthly synoptic sampling: *A*) calculated mass is normalized by the total injected mass (note the coincident symbols at 0 and 175 days); and *B*) calculated normalized nickel mass is divided by calculated normalized bromide mass to obtain a relative mass.

In general, the nickel center of mass is slightly lower than the bromide center (fig. 7A). This consistent difference probably reflects the greater degree of adsorption of nickel in the upper pristine zone relative to the suboxic zone due to lower pH values and lower concentrations of competing adsorbing anions, such as phosphate, in the pristine zone.

Figure 7B shows the same vertical component of the centers of mass as shown in fig. 7A, but plotted against the horizontal component. Superimposed on the plot is an outline of the region of the aquifer contaminated by zinc. Background dissolved zinc is one of the indicators of the transition zone. The centers of mass eventually dropped below the zinc-contaminated region (fig. 7B). The time and distance trends indicate that the proportion of the tracer clouds in each zone varied with time, although the vertical extent of the tracer clouds spanned all three zones throughout the test. This temporal variability in the proportion of the tracer clouds in each geochemical zone complicates the quantitative analysis of reactive transport in this test.

Dispersion of Tracers

The distributions of bromide and nickel tracers at 13 and 83 d (figs. 2 and 3) graphically show the effects of dispersion on solute transport. At 13 d the tracer clouds are about 15 m long along the direction of ground-water flow. By 83 d the clouds had attained a length of about 45 m, indicating significant dispersion in the longitudinal direction. The second central moments, the variances, quantify the spread of the tracer clouds as they traveled through the aquifer.

The longitudinal variances are plotted against travel distance in fig. 8A. The increase in variance of the bromide cloud between synoptic samplings is small early in the test. A larger constant rate of increase is reached after about 70 m of transport. A longitudinal dispersivity of 2.2 m (table 1) can be calculated from one-half the slope of this later trend; see Garabedian and others (1991) for a presentation of the theoretical relationship between dispersivity and change in variance. The estimate of longitudinal dispersivity assumes that the transport velocity was constant throughout the test; fig. 5 shows that this assumption is met.

The change in nickel variance appears to reach a constant trend by a travel distance of only

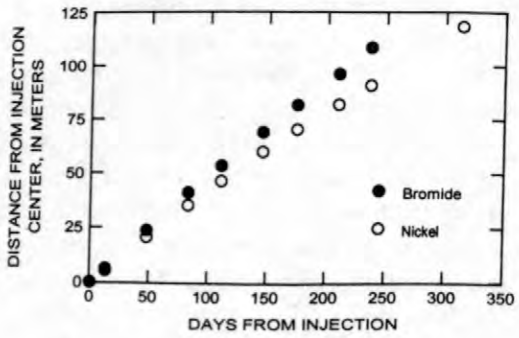

Figure 5. Distance from the center of the injection to the centers of mass of the bromide and nickel tracer clouds (first moment) calculated for each monthly synoptic sampling.

Table 1. Transport parameters estimated from tests conducted in 1985–88 (Garabedian and others, 1991) and in 1993–94 (this study), Cape Cod, Massachusetts

Parameter	1985–88	1993–94	
	Bromide	Bromide	Nickel
Velocity, meters per day	0.42	0.47	0.39
Longitudinal dispersivity, meters	0.96	2.2	1.1
Transverse horizontal dispersivity, centimeters	1.8	1.4	1.5
Transverse vertical dispersivity, millimeters	1.5	0.5	3.8

48 m. This linear relationship yields a lower dispersivity of 1.1 m (table 1). In the dispersion process the edges of the tracer clouds mix with the ambient ground water. The solute concentrations at the edges decrease and the cloud spreads. Counterbalancing the spread of tracers through the dispersion process is the adsorption process. As concentrations decrease adsorption of the nickel-EDTA complex onto the aquifer increases (Nowak and Sigg, 1996. This increased adsorption at the lower concentrations may be responsible for the smaller longitudinal dispersivity calculated for the nickel tracer relative to bromide.

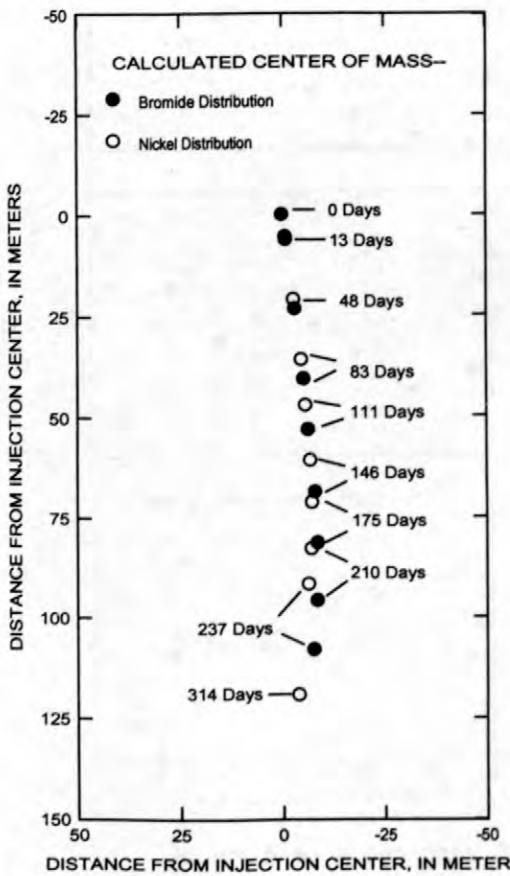

Figure 6. Mapped distance from the center of the injection to the centers of mass of the bromide and nickel tracer clouds (first moment) calculated for each monthly synoptic sampling.

Adsorption of the nickel-EDTA complex also varied vertically in the aquifer due to the geochemical zones formed from the sewage contamination. Adsorption was greatest in the pristine zone. Coincidentally, the local velocity in this zone appears to be greater than in the suboxic zone, as reflected in the skewed vertical distribution of bromide that forms with time (fig. 3). Therefore, the smaller dispersion of the nickel tracer may result from the greater adsorption in the zone were velocity is greatest. The overall dispersion of nickel probably results from both adsorption processes.

The transverse horizontal variances that were calculated for the synoptic samplings of bromide and nickel have similar trends with travel distance (fig. 8B). Linear trends through these data sets yield estimates of transverse horizontal dispersivities (one-half the slope of the trend) of 1.4 and 1.5 cm (centimeters) for bromide and nickel, respectively. If adsorption of nickel increases as concentrations decrease, as was suggested by one of the explanations for the differences in longitudinal dispersivities, then the transverse horizontal dispersivity of nickel should be less than that for bromide as well. The fact that the two transverse horizontal dispersivities are essentially the same may reflect the lack of resolution in the sampling network in the transverse horizontal direction. As shown in the mapped distributions (fig. 2), the transverse

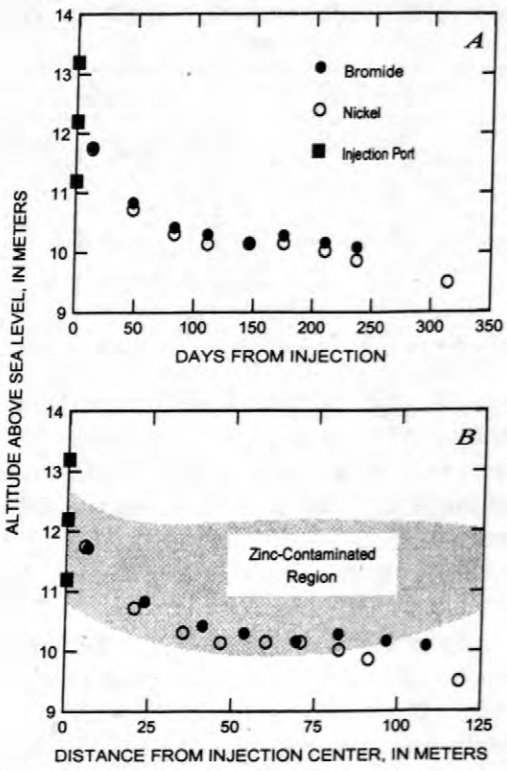

Figure 7. Altitude of the centers of mass of the bromide and nickel tracer clouds (first moment) calculated for each monthly synoptic sampling as a function of *A*) days from injection, and *B*) cumulative distance from the center of the injection. Region of aquifer contaminated with zinc is shaded gray.

horizontal dimension of the tracer clouds is usually defined by rows of about 5 sampled multilevel samplers. In contrast, a line of about 20 multilevel samplers along the longitudinal axis of each cloud (fig. 2) defined the longitudinal horizontal dimension at 83 d.

The transverse vertical variance for nickel is slightly larger than that for bromide throughout the test (fig. 8C). This slight difference probably reflects the more symmetrical nature of the nickel tracer cloud relative to the bromide cloud (fig. 3). Both tracer clouds show an increase in vertical variance with travel distance at the shorter travel distances less than 50 m. Assuming that dispersivities equal one half the slopes of these trends, vertical dispersivities of 0.5 and 3.8 mm (millimeters) are estimated for bromide and nickel, respectively (table 1). These estimates indicate that vertical dispersion in this aquifer is small at the scale of this experiment (travel distance of about 100 m).

At larger travel distances (fig. 8C), both nickel and bromide show decreasing trends in vertical variances; these trends indicate a slight decrease in the vertical extent of each tracer cloud with time. An apparent decrease in extent may result when more of the outer portion of a tracer cloud decreases to a concentration that is below the analytical detection limit, or when the cloud moves downgradient to the area where the vertical distance between sampling points is greater (fig. 3) and, therefore, vertical resolution is decreased.

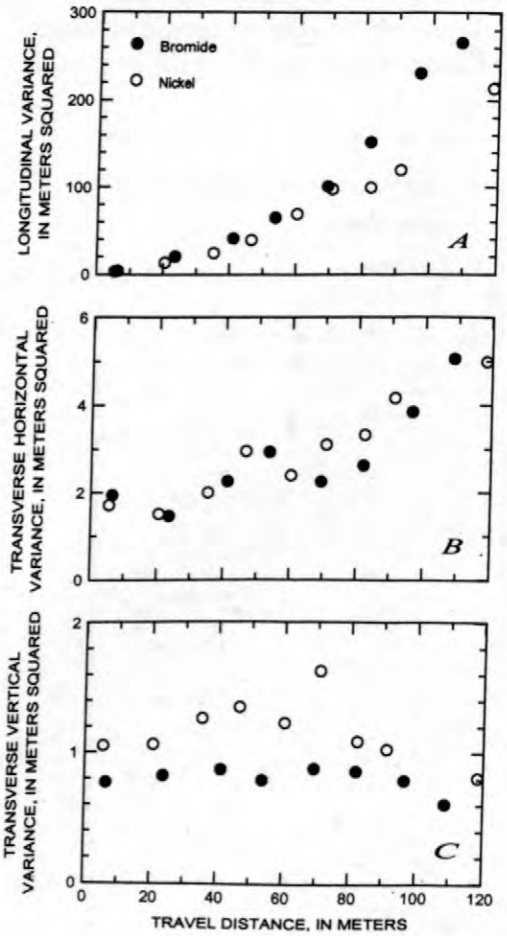

Figure 8. Variances (second central moments) of the bromide and nickel tracer clouds calculated for each monthly synoptic sampling: *A*) longitudinal, *B*) transverse horizontal, and *C*) transverse vertical.

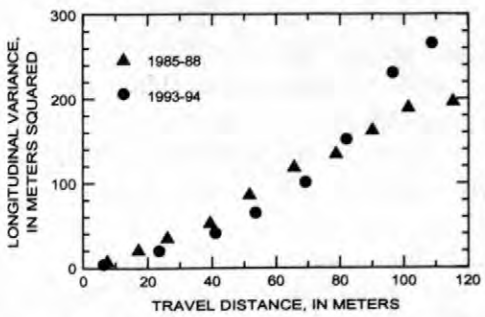

Figure 9. Longitudinal variances (second central moments) of the bromide tracer clouds calculated for each synoptic sampling in the 1993-94 and 1985-88 tracer tests.

The real vertical extent of a tracer cloud may decrease if the cloud funnels into a faster zone, if the cloud becomes skewed in the vertical transport plane, or if mass is lost at the edges of the cloud due to adsorption. Regardless of the cause, the decreases in vertical variance are not great in the later part of the test, just as the vertical spread of the clouds earlier in the test was not great. Vertical dispersion is virtually nonexistent. The estimated transverse vertical dispersivities are an order of magnitude smaller than the transverse horizontal dispersivities, which are two orders of magnitude smaller than the longitudinal dispersivities.

Implications of Observed Dispersion

The smaller longitudinal dispersivity calculated for the nickel relative to the bromide tracer was not anticipated. Previous theoretical work (Garabedian and others, 1988) suggests that a retarded solute could undergo greater dispersion relative to a conservative, nonreactive solute. The dispersion of solutes in aquifers is caused by small-scale variability in the flow field which, in turn, is caused by spatial variability in the hydraulic conductivity (Gelhar and Axness, 1983). Adsorption properties of aquifer materials may be negatively correlated with hydraulic conductivity (Robin and others, 1991); more solute adsorbs onto small-grained material of low hydraulic conductivity, while less solute adsorbs onto coarse-grained material with a high hydraulic conductivity. The negative correlation between hydraulic conductivity and adsorption could lead to an enhanced dispersion by increasing the variation in relative velocities for the reactive solutes. This theoretical model might be applicable for the fate and transport of solutes that are dominated by cation exchange reactions with clay minerals. But little data exist that can be used to elucidate this relationship between adsorption and hydraulic conductivity.

Typically, adsorption is controlled by the distribution of reactive minerals coating the aquifer sediments (Fuller and others, 1996). Consequently, adsorption of anions, such as the nickel-EDTA complex, is probably more highly correlated with the abundance of extractable coatings which, in turn, may correlate with surface area of the aquifer sediments. The abundance of the reactive coatings, such as the iron and aluminum oxyhydroxide minerals coating the sediments at Cape Cod, may positively correlate with hydraulic conductivity, which may lead to a positive correlation between hydraulic conductivity and adsorption.

If a correlation between hydraulic conductivity and adsorption properties exists in the Cape Cod aquifer, large-scale spatial patterns in adsorption may dominate. Greater adsorption at the edges would lead to a sharpening of the tracer cloud edges and a decrease in the spread of the reactive tracer cloud. The degree of this enhanced adsorption at the edges must be small, because there was no quantifiable increase in the loss in mass with time (zeroth moment, fig. 4). This enhanced adsorption may still be significant enough, however, to affect calculated variances, which are functions of each observed concentration multiplied by the square of the distance from the center of mass to each data point. Therefore, processes that affect concentration levels at the edges of the cloud, at large distances from the center of mass, affect the calculations of variance more than calculations of the mass and center of mass that do not involve squaring the distance. The basic dispersion theory also does not account for the spatial variability in adsorption due to spatial variability in background chemistry; fig. 3 clearly shows greater adsorption of nickel in the pristine zones where pH values are low and competition for adsorption sites is low. These two adsorption processes probably affect the observed dispersion of the nickel cloud as it is transported.

Comparison to Earlier Test

A bromide tracer test of similar magnitude was conducted in this aquifer in 1985–88 (LeBlanc and others, 1991; Garabedian and others, 1991). The injection point for the earlier test was 43 m upgradient from the injection point for the test described here. The sections of aquifer traversed in the two tests are spatially different, but do overlap. A comparison between the results of the two tests provides insight into the spatial stationarity of transport properties in this aquifer and tests the reproducibility of this type of large-scale field experiment.

Table 1 presents the basic transport results from the earlier test and the results of the 1993–94 test discussed in other sections of this paper. The 12 percent difference in average velocity of the two bromide tracers can be explained by a similar difference in average hydraulic gradient measured during the two tests.

In general, the trends in calculated longitudinal variances of the two bromide tracer clouds are similar (fig. 9). In the later test, the cloud traveled a larger distance before the longitudinal variance became linear with travel distance. The longitudinal dispersivities that were calculated for the two tests (2.2 and 0.96 m) are similar, however, especially because the general range of longitudinal dispersivity values from field observations is more than six orders of magnitude (Gelhar and others, 1992). Likewise, the transverse horizontal and vertical dispersivities are similar in the two tests (table 1). The similarity in the dispersivities and other transport properties between the two bromide tracer tests partially validates the results and suggests that physical dispersion of conservative, nonreactive solutes in this aquifer is spatially stationary at the combined distance of these overlapping tests of 300 m.

SUMMARY

A large-scale tracer test was conducted in an unconfined, sand-and-gravel aquifer on Cape Cod, Massachusetts, to investigate the reactive transport of multiple solute species under spatially variable chemical conditions. The chemical conditions in the aquifer varied spatially because of the presence of a plume of sewage-contaminated ground water. Monthly synoptic sampling rounds provided spatial data of the distributions of the injected tracers as they moved through the aquifer. A spatial moments analysis of these synoptic data sets quantifies this transport.

The nonreactive, conservative tracer, bromide, was transported with the flowing ground water at a constant rate of 0.47 m/d. As expected, the mass of bromide throughout the test remained close to the mass that was injected. The dispersivities calculated from the spread of the bromide with time were 2.2 m, 1.4 cm, and 0.5 mm in the longitudinal, transverse horizontal, and transverse vertical directions, respectively.

Nickel was the least reactive of the reactive tracers that were injected as a complex with EDTA. About 14 percent of the injected nickel mass was lost during the test and not captured in the distribution of aqueous nickel, suggesting reversible adsorption of the nickel-EDTA complex onto the iron and aluminum oxyhydroxide minerals that coat the aquifer sediments. The nickel was transported at an average rate of 0.39 m/d, which results in a retardation factor of 1.2 relative to the transport of bromide. The calculated longitudinal, transverse horizontal, and transverse vertical dispersivities were 1.1 m, 1.5 cm, and 3.8 mm, respectively.

The longitudinal dispersivity for the nickel was unexpectedly lower than that calculated for the bromide. Nonlinear adsorption of nickel would result in greater adsorption of nickel at lower concentrations and, therefore, at the edges of the tracer cloud. This adsorption pattern could explain the difference in longitudinal dispersivity. A similar difference is not observed, however, in the transverse dispersivities; neither is a temporal loss of nickel mass observed. The effects of spatially varying background chemistry on adsorption, with lower pH values and lower concentrations of competing anions resulting in greater adsorption in the pristine zone, probably also contributed to the unexpected longitudinal dispersivity results. The pristine zone near the water table also had higher ground-water velocities.

The quantitative results of the transport of bromide in this experiment are similar to those from an experiment of similar scale that had been conducted previously in this aquifer. The test described here spatially overlapped only part of the aquifer traversed in the earlier test. The similarity of the results that transport properties, particularly dispersion, are spatially stationary, at least at the combined distance of about 300 m covered in these two overlapping tests.

REFERENCES

Davis, J.A., Kent, D.B., Coston, J.A., Hess, K.M., and Joye, J.L., 1999, Multispecies reactive tracer test in an aquifer with spatially variable chemical conditions: An Overview, in Morganwalp, D.W., and Buxton, H.T., eds., U.S. Geological Survey Toxic Substances Hydrology Program–Proceedings of the Technical Meeting, Charleston, South Carolina, March 8–12, 1999–Volume 3–Subsurface Contamination from Point Sources: U.S. Geological Survey Water-Resources Investigations Report 99-4018C, this volume.

Fuller, C.C., Davis, J.A., Coston, J.A., and Dixon, Eleanor, 1996, Characterization of metal adsorption variability in a sand and gravel aquifer, Cape Cod, Massachusetts, U.S.A.: Journal of Contaminant Hydrology, v. 22, no. 3-4, p. 165-187.

Garabedian, S.P., Gelhar, L.W., and Celia, M.A., 1988, Large-scale dispersive transport in aquifers: Field experiments and reactive transport theory: Cambridge, Mass., Massachusetts Institute of Technology, Dept. of Civil Engineering, Ralph M. Parsons Laboratory, Hydrology and Water Resources Systems Report No. 315, 290 p

Garabedian, S.P., LeBlanc, D.R., Gelhar, L.W., and Celia, M.A., 1991, Large-scale natural-gradient tracer test in sand and gravel, Cape Cod, Massachusetts: 2. Analysis of spatial moments for a nonreactive tracer: Water Resources Research, v. 27, no. 5, p. 911-924.

Gelhar, L.W., and Axness, C.L., 1983, Three-dimensional stochastic analysis of macrodispersion in aquifers: Water Resources Research, v. 19, no. 1, p. 161-180.

Gelhar, L.W., Welty, Claire, and Rehfeldt, K.R., 1992, A critical review of data on field-scale dispersion in aquifers: Water Resources Research, v. 28, no. 7, p. 1955-1974.

Kent, D.B., Abrams, R.H., Davis, J.A., Coston, J.A., and LeBlanc, D.R., in press, Characterization and modeling of the fate and transport of zinc under variable chemical conditions in a sewage-contaminated aquifer: Water Resources Research.

Kohler, M., Curtis, G.P., Kent, D.B., and Davis, J.A., 1996, Experimental investigation and modeling of uranium(VI) transport under variable chemical conditions: Water Resources Research, v.32, no. 12, p. 3539-3551.

LeBlanc, D.R., 1984, Sewage plume in a sand and gravel aquifer, Cape Cod, Massachusetts: U.S. Geological Survey Water-Supply Paper 2218, 28 p.

LeBlanc, D.R., Garabedian, S.P., Hess, K.M., Gelhar, L.W., Quadri, R.D., Stollenwerk, K.G., and Wood, W.W., 1991, Large-scale natural-gradient tracer test in sand and gravel, Cape Cod, Massachusetts: 1. Experimental design and observed tracer movement: Water Resources Research, v. 27, no. 5, p. 895-910.

Nowak, B., and Sigg, L., 1996, Adsorption of EDTA and metal-EDTA complexes on goethite: Journal of Colloid Interface Science, v. 177, p. 106-121.

Rea, B.A., Kent, D.B., LeBlanc, D.R., and Davis, J.A., 1991, Mobility of zinc in a sewage-contaminated aquifer, Cape Cod, Massachusetts, *in* Mallard, G.E., and Aronson, D.A., eds., U.S. Geological Survey Toxic Substances Hydrology Program--Proceedings of the technical meeting, Monterey, California, March 11-15, 1991: U.S. Geological Survey Water-Resources Investigations Report 91-4034, p. 88-95.

Robin, M.J.L., Sudicky, E.A., Gillham, R.W., and Kachanoski, 1991, Spatial variability of strontium distribution coefficients and their correlation with hydraulic conductivity in the Canadian Forces Base Borden Aquifer: Water Resources Research, v. 27, no. 10, p. 2619-2632.

AUTHOR INFORMATION

Kathryn M. Hess, U.S. Geological Survey, Marlborough, Massachusetts (kmhess@usgs.gov)

James A. Davis, Jennifer A. Coston, and Douglas B. Kent, U.S. Geological Survey, Menlo Park, California

Effect of Growth Conditions Upon the Subsurface Transport Behavior of a Ground-Water Protist

By Ronald W. Harvey, Naleen A. Mayberry, Nancy E. Kinner, and David W. Metge

ABSTRACT

A low-nutrient, slightly acidic, porous-media growth procedure was used to grow *Spumella guttula*, a ground-water nanoflagellate, for an injection and recovery transport experiment involving an organically contaminated aquifer, Cape Cod, Massachusetts. The new growth procedure mimiced conditions within the aquifer and maintained the nanoflagellates' small (2-3 microns [μm]) size. This allowed assessment of its potential for advective transport through the aquifer sediments. Results from the in-situ transport experiment suggest a high transport potential, which was about two orders of magnitude greater than was observed in an earlier experiment using the same nanoflagellate grown in conventional liquid-broth media. The high degree of mobility of *S. guttula* in the aquifer sediments has important ecological implications for the protistan community within the contaminated aquifer sediments.

INTRODUCTION

New findings regarding the role of protists in the natural attenuation of organically contaminated aquifers and in the potability of ground water are leading to an increasing interest in the subsurface mobility of protozoa. A number of recent studies have examined the transport potential of *Cryptosporidium parvum* oocysts through saturated porous media in laboratory microcosms (Mawdsley and others, 1996; Harter and others, in review; Darnault and others, 1997). However, little is known about the subsurface mobility of protistan populations that are indigenous to the aquifer.

In 1991, an aquifer nanoflagellate (*S. guttula,* Kinner and others, 1998) was used in a small-scale injection and recovery study involving a sandy aquifer at Cape Cod (Harvey and others, 1995). The aquifer sediments at the test site are contaminated with treated sewage and harbor a large (up to 10^5/gram (g) dry weight; Kinner and others, 1998) and diverse (Novarino and others, 1994) protistan community dominated by 2-3 μm nanoflagellates (Kinner and others, 1998). Although flow-through column studies with microspheres indicated that the nanoflagellates may be near optimal size for transport (Harvey and others, 1993), the 1991 study suggested rather modest transport potentials for the liquid broth-grown, nanoflagellates. However, the nanoflagellates (4-5 μm at time of injection) also exhibited an increasing transport potential and a decrease in cell size as they re-adapted to aquifer conditions over the experimental time course. Therefore, it was evident that more accurate information about the true transport behavior of ground-water nanoflagellates would necessitate use of nanoflagellates that were adapted apriori to conditions within the aquifer. Also, important questions remained about the effects of culturing in liquid broth upon their mobility, retardation, and propensity for attachment in aquifer sediments.

The overall objective of the present study was to better determine the transport behavior of *S. guttula* , the ground-water nanoflagellate used in the 1991 study, in contaminated aquifer sediments from the Cape Cod site. In particular, we were interested in knowing whether nanoflagellates, which are highly-efficient predators of ground-water bacteria (Kinner and others, 1998), have the potential to respond rapidly to the spatial changes in unattached bacterial abundance that occur downgradient from sources of organic contaminants. To better address these questions, a porous-media, low-nutrient, low-pH culturing

procedure was developed (Kinner and others, 1998) that preserves the in-situ cell-size (2-3 μm) of the nanoflagellates. This report describes an injection and recovery experiment in which the transport behavior of porous-media grown *S. guttula* in Cape Cod aquifer sediments were assessed and compared to a that of a conservative tracer and to that observed in an earlier field test involving liquid-broth grown *S. guttula.*

MATERIALS AND METHODS

Nanoflagellates

Nanoflagellates were recovered from aquifer sediments taken aseptically from the U.S. Geological Survey (USGS) site within the contaminant plume using a wireline piston-type coring device (Zapico and others, 1987) in conjunction with a hollow-stem auger drill as described in the 1991 study (Harvey and others, 1995). Coring was done without the use of drilling fluids. Nanoflagellates recovered in the collection procedure were grown in acidic, low-nutrient porous-media as described by Kinner and others (1998). Briefly, the procedure involved growth in 500 g of sterile sieved (0.5 – 1.0 millimeters [mm], grain size) aquifer sediments saturated with dilute Cerophyl-Prescott medium to give a final dissolved organic carbon concentration of ~10 milligrams per liter [mg/L] in the pore fluid. The pH of the sediment was adjusted to 6.0 to match conditions in the contaminated zone of the aquifer where the injection and recovery test was performed (Pieper and others, 1997). The jars containing the sterile porous media, which contained ~ 1 centimeters [cm] of free-standing liquid above the aquifer sediment, were each inoculated with 1 g of core material, gently swirled, and held at room temperature (20 degrees Celsius [°C]).

Nanoflagellates, which grazed upon the ground-water bacteria that also grew in the cultures (Gruden, 1991), were harvested at peak abundance (4-10 days after inoculation) using a suction device described by Mayberry (1996). Nanoflagellates in the pore fluid of the porous media reached concentrations between 10^4 and 10^5/ milliliter [mL]. Most were 2-3 μm-sized *S. guttula*, a raptorial feeding chrysomonad that swims along circular lines (Novarino and others, 1997). The nanoflagellates were then fixed with 1% glutaraldehyde solution and stained with the DNA-specific fluorescent dye 4,6-diamidino-2-phenylindole (DAPI) (290 micromolar [μM], final concentration).

Injection and Recovery Study.

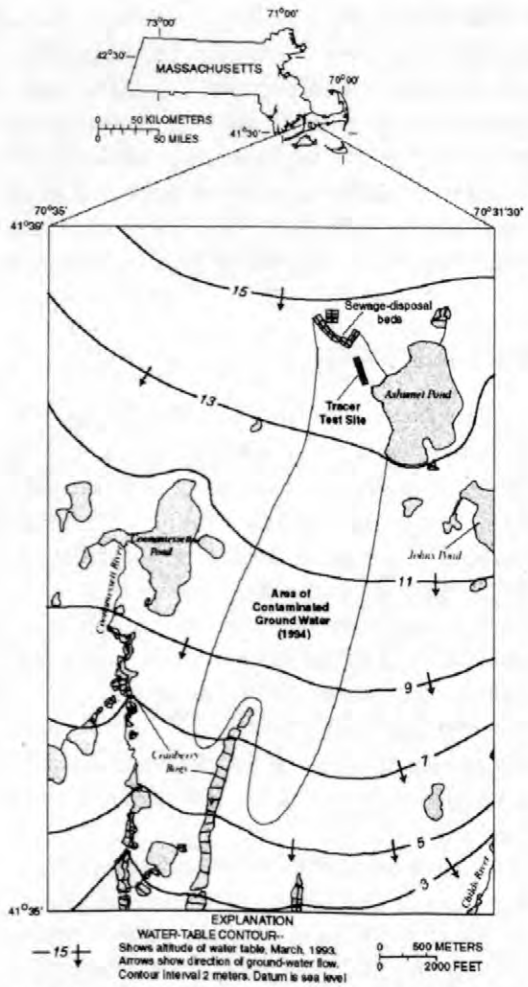

Figure 1. Location within the USGS Cape Cod study site of the multi-level samplers (MLS) used in the 1991 and 1994 tracer tests with *Spumella guttua*. The MLS used in the tests sample ground water contaminated from a 60 year discharge of treated sewage.

The field tracer investigation was conducted at the USGS Cape Cod ground-water hydrology study site (fig. 1) in Falmouth, MA. The nanoflagellate injection and recovery experiment

was performed concomitantly with a virus transport test (Pieper and others ,1997) at USGS injection well M4-15, which is within a large (50 x 200m) array of multi-level samplers (mls) constructed for the purpose of studying advective transport.

The protocol and mls array used in the field study is depicted in figure 2. The nanoflagellates harvested from pore fluid of the porous media were stained and fixed as described above and added, with bromide (1.9 millimolar [mM], final concentration), to ground water collected from the injection depths. To avoid introduction of atmospheric oxygen, the injectate was pumped into a collapsed, acid-rinsed, nitrogen-sparged, gas-impermeable fuel bladder under nitrogen headspace. The 100 liters [L] contents of the fuel bladder were mixed by agitation and pumped back (~ 1 L/min) into the suboxic contaminant plume. M4-14 sampling ports GN and R, which are, respectively, 9.8 and 10.0 meters below land surface (mbs), served as injection ports for the introduction of the injectate into the aquifer.

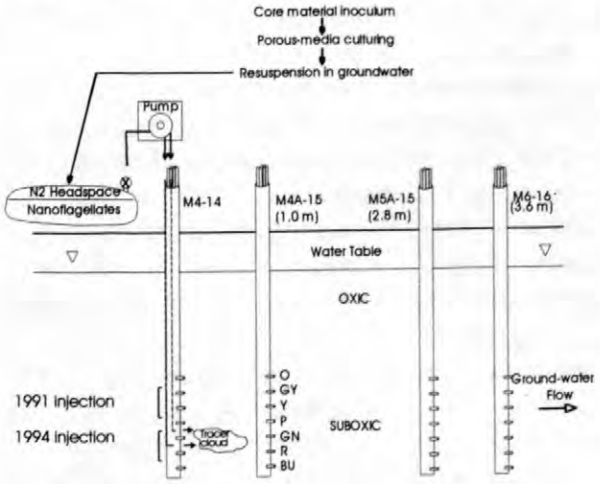

Figure 2. Schematic depiction of the 1994 injection and recovery experiment with the porous-media grown, ground-water nanoflagellate *Spumella guttua*. Wells shown are the injection well and the multi-level samplers that lay along the trajectory of the injectate cloud. The injection depths for a similar experiment performed in 1991 using liquid-broth grown S. guttula are shown for comparative purposes.

The injection ports chosen in the 1994 injection study were somewhat deeper than those used in the 1991 test, just in case the hydrologic characteristics of the strata utilized in the 1991 study (at 9.0 and 9.3 mbs) had been altered in that test (fig. 2). Concentrations of labeled nanoflagellates and bromide were monitored as they were advected downgradient by the natural flow of ground water past mls (M4A-15, M5A-15, and M6-15) that lay along the trajectory of the injectate cloud at 1.0, 2.8, and 3.6 m downgradient, respectively. Breakthrough curves (dimensionless concentration histories) were obtained at each of the three mls at depths exhibiting substantive breakthrough, i.e.: GN, R, and BU (9.8, 10.0, and 10.3 mbs, respectively).

RESULTS

The dimensionless concentrations of bromide and *S. guttula* are depicted in figure 3 for 1 m downgradient and 10.0 meters below surface (mbs) at mls 4A-15 R. For comparative purposes, dimensionless concentrations of bromide and *S. guttula* appearing at mls 4A-15 are shown in inset A for a similar injection and recovery test performed in 1991. Peak abundance of the 2-3 μm *S. guttula* at M4A-15 in the 1994 study occurred concomitantly with that of the bromide tracer. In contrast, peak abundance of labeled-nanoflagellates from the 1991 test, which employed 4-5 μm *S. guttula* grown in liquid broth, took over 3 times as long to reach mls M4A-15 as did the conservative tracer.

Dimensionless concentration histories for bromide and 2 μm carboxylated microspheres at 2 m downgradient from point of injection (M7-15) from the 1991 injection and recovery investigations is shown for comparative purposes in inset b of figure 3. The pattern of breakthrough exhibited by the 2 μm microspheres in the earlier experiment was similar to that observed for the 2-3 μm nanoflagellates in the 1994 test, i.e., a peak abundance that was coincident with that of bromide, followed by a protracted tail.

The maximum dimensionless concentrations of *S. guttula* appearing at 1.0, 2.8, and 3.6 m downgradient from M 4-15 in the 1991 and 1994 tests are shown in figure 4 for five different depths. One meter downgradient from point of injection, the maximum dimensionless concentation of porous-media grown nanoflagellates was ~ 10-fold

higher than observed for the earlier test which employed liquid-broth grown nanoflagellates. The difference in relative abundance of nanoflagellates increased to almost 100-fold by 3.6 m downgradient.

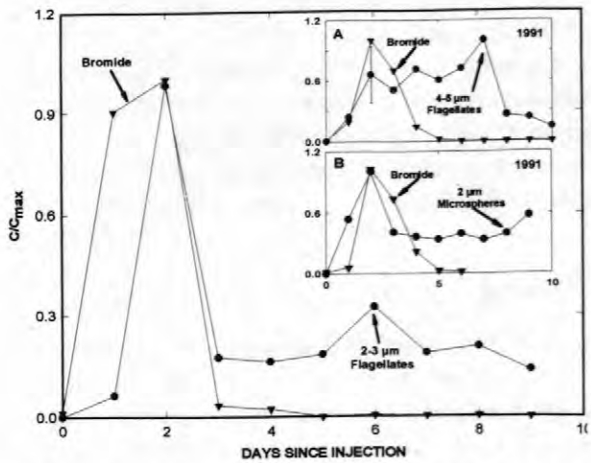

Figure 3. Dimensionless concentration histories (expressed as the concentration in samples collected daily at 1 m downgradient from point of injection normalized to the maximum concentration) for DAPI-stained, 2-3 µm *Spumella guttula* and for bromide in the 1994 tracer test. Sampling port is level R of USGS MLS M4A-15. Inset A. Dimensionless concentration histories for 4-5 µm *Spumella guttula* and bromide at level GY of MLS M4A-15 in the 1991 test. Inset B. Dimensionless concentration histories for 2 µm carboxylated microspheres and bromide at level GY of MLS M7-15 in the 1991 test.

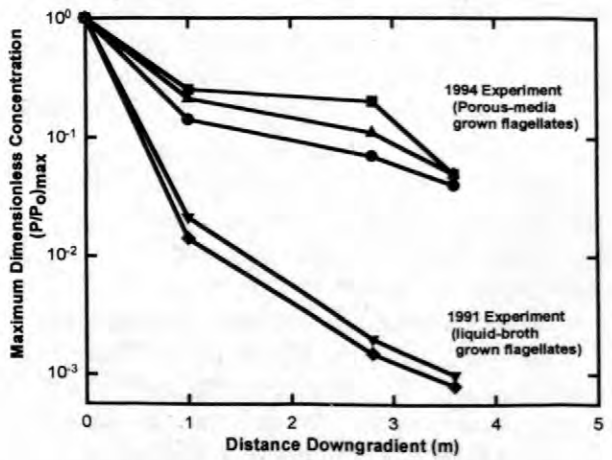

Figure 4. Maximum dimensionless concentration histories for *Spumella guttula* in the 1991 and 1994 tests at MLS M4A-15 (1 m downgradient from point of injection), M5A-15 (2.8 m downgradient) and M6-15 (3.6 m downgradient). Squares represent breakthrough at level R; triangles, level BU; circles, level GN; inverted triangles, level GY; diamonds, level Y.

DISCUSSION

The high fractional recoveries and low degree of retardation observed for labeled *S. guttula* in the 1994 experiments relative to that observed in the 1991 tests suggest that the manner in which the organisms are cultured can play an important role in their apparent subsurface mobility. The manner in which microorganisms are grown can affect several physical parameters that affect how well the microbes are advected through porous media (Harvey and others, 1997). Important considerations for transport within sandy aquifer sediments include the microbes size, buoyant density (specific gravity), and surface characteristics.

It is likely that some of the differences in transport behavior observed for the porous-media grown nanoflagellates in the 1994 test and the liquid-broth grown nanoflagellates employed in the 1991 experiment are simply due to differences in cell size. It is interesting to note that the pattern of breakthrough exhibited by the 2-3 µm *S. guttula* relative to that of the bromide tracer was more similar to that of 2 µm carboxylated microsperes than to that exhibited by the 4-5 µm *S. guttula* (fig. 3). Experiments with different size classes of carboxylated microspheres in flow-through columns of aquifer sediments suggest that an optimal cell diameter for transport of microbes with a buoyant density of ~1.05 g/cm^3 would be ~2 µm (Harvey and others, 1993). Using colloid filtration theory (Yao and others, 1970), it was calculated that the 2-3 µm flagellates are near the optimal size for transport through the aquifer sediments at the Cape Cod site (Harvey and Garabedian, 1991).

Buoyant density is another important factor controlling the ability of the nanoflagellates to be advected through the aquifer sediments. Both buoyant density and cell size depend, in part, upon the manner in which a microorganism is grown (Harvey and others, 1997). Although uncultured microorganisms from Cape Cod have buoyant

densities between 1.01 and 1.02 grams per cubic centimeter [g/cm^3] (Harvey and others, 1997), microorganisms isolated from sandy aquifers and grown in liquid broth typically exhibit buoyant densities between 1.04 and 1.12 g/cm^3, with an average of 1.09 g/cm^3 (Wan and others, 1995).

Buoyant density is particularly important in the transport behavior of larger (protist-sized) microorganisms, because the rate of sedimentation is related to the square of the microbe's diameter (Harvey and others, 1997). Wan and others (1995) have calculated that the measured settling velocities of microorganisms in saturated porous media (sand) is predictably within 90% of the free sedimentation velocity, assuming large well-rounded grains. Wan and others (1995) measured a sedimentation velocity through saturated quartz sand of 17 mm/day for a 3 μm, broth-cultured, rod-shaped, ground-water bacterium (stain OYS3). Because of their large size, protists with high buoyant densities (e.g., 1.09 g/cm^3) would predictably settle at a rate that is significant when compared with flow rates in the Cape Cod aquifer (Harvey and others, 1997). However, *S. guttula* that were cultured in low-nutrient porous media had buoyant densities less than 1.02 g/cm^3 (Harvey and others, 1997). The low buoyant densities of this nanoflagellate are comparable to those of the unattached ground-water bacteria that serve as its primary food source (Kinner and others, 1998) and contribute to its ability to be advected through aquifer sediments.

A third important factor in the subsurface transport behavior of microorganisms involves the nature of the surface. Differences in surface characteristics of *S. guttula* grown in the two different media were not measured. However, there is evidence to suggest that the manner in which *S. guttula* is handled prior to injection can have a big effect upon its subsequent subsurface mobility. For example, a-priori fixation with glutaraldehyde causes at least an order of magnitude increase in this nanoflagellates rate of immobilization in sandy aquifer sediments, judging from results of flow-through column experiments (Mayberry, 1996). The nanoflagellates injected into the Cape Cod aquifer in the 1991 field experiment had been fixed with glutaraldehyde because the fluorochrome used to stain them (4,6-diamidino-2-phenylindole [DAPI]) is lethal to protists and fixation is necessary to preclude lysis that otherwise occurs upon death of the microbe. DAPI itself appears to have little effect upon the subsurface mobility of microorganisms in subsurface sediments, judging from a recent study of its effect upon the transport of bacteria through saturated sand (Küçükçolak and others, 1998). Therefore, it is likely that DAPI-stained (killed) *S. guttula* in the 1991 injection and recovery experiment would have been transported much more efficiently if an alternative method of fixation were used that did not substantively alter the organisms surface chemistry. Had the nanoflagellates in the 1991 and 1994 experiments both been stained a-priori with hydroethidine, the difference in their transport potential would have been even greater than what is suggested in fig. 4.

In summary, the ability to grow in-situ sized (2-3μm) nanoflagellates characterized by low buoyant densities represents an important advance in that it allows more accurate information to be gathered about their in-situ transport behavior. The ability of ground-water nanoflagellates to be readily advected through aquifer sediments has important ecological implications for ground-water habitats contaminated with treated sewage. This is because it allows these important preditors of the ground-water bacteria that degrade organic contaminants (Kinner and others, 1998) to redistribute in response to spatial changes in nutrient conditions. However, more research is needed on the response of the subsurface protistan communities to changes in loading of organic contaminants.

REFERENCES

Darnault, C.J.G., Garnier, P., Steenhuis, T.S., Parlange, J.-Y., and Ghiorse, W.C., 1997, Transport and fate of *Cryptosporidium parvum* in different media (abstract); EOS, v. 78, no. 46, p. F237.

Gruden, C.L., 1991, An investigation into the role of protozoa in an organically-contaminated aquifer: Durham, University of New Hampshire, Department of Civil Engineering, unpublished M.S. thesis, 189 p.

Harter, T., Wagner, S., and Atwill, E.R., in review, Colloid transport and filtration of

Cryptosporidium parvum in sandy porous media (soils and ground water), Environmental Science and Technology.

Harvey, R.W., and Garabedian, S., 1991, Use of colloid filtration theory in modeling movement of bacteria through a contaminated sandy aquifer: Environmental Science and Technology, v. 25, p. 178-185.

Harvey, R.W., Kinner, N.E., Bunn, A., MacDonald, D., and Metge, D., 1995, Transport behavior of ground water protozoa and protozoa-sized microspheres in sandy aquifer sediments: Applied and Environmental Microbiology, v. 61, 209-217.

Harvey, R.W., Kinner, N.E., MacDonald, D., Metge, D.W. and Bunn, A., 1993, Role of physical heterogeneity in the interpretation of small-scale laboratory and field observations of microorganism, microsphere, and bromide transport through aquifer sediments: Water Resources Research v. 29, p. 2713-2721.

Harvey, R.W., Metge, D.W., Kinner, N., and Mayberry, N., 1997, Physiological considerations in applying laboratory-determined buoyant densities to predictions of bacterial and protozoan transport in ground water: Results of in-situ and laboratory tests, Environmental Science and Technology, v. 31, p. 289-295.

Kinner, N.E., Harvey, R.W., Blakeslee, K., Novarino, G., and Meeker, L.D., 1998, Size-selective predation of ground water bacteria by nanoflagellates in an organically-contaminated aquifer: Applied and Environmental Microbiology, v. 64, p. 618-625.

Küçükçolak, E., Koopman, B., Bitton, G., and Farrah, S., 1998, Validity of fluorochrome-stained bacteria as tracers of short-term microbial transport through porous media: Journal of Contaminant Hydrology, v. 31, p. 349-357.

Mawdsley, J.L., Brooks, A.E., and Merry, R.J., 1996, Movement of the protozoan pathogen Cryptosporidium parvum through three contrasting soil types: Biology and Fertility of Soils, v. 21, p. 30-36.

Mayberry, N.A., 1996, An investigation into the transport of 2-3μm protozoa through sandy aquifer sediments: Durham, University of New Hampshire, Department of Civil Engineering, unpublished M.S. dissertation, 249 p.

Novarino, G., Warren, A., Butler, H., Lambourne, G., Boxshall, A., Bateman, J., Kinner, N.E., Harvey, R.W., Mosse, R.A., and Teltsch, B., 1997, Protistan communities in aquifers: a review, FEMS Microbiological Reviews, v. 20, p. 261-275.

Novarino, G., Warren, A., Kinner, N.E., and Harvey, R.W., 1994, Protists from a sewage-contaminated aquifer on Cape Cod, Massachusetts, U.S.A: Geomicrobiology Journal, v. 12, p. 23-36.

Pieper, A.P., Ryan, J.N., Harvey, R.W., Amy, G.L., Illangasekare, T.H., and Metge, D.W., 1997, Transport and recovery of bacteriophage PRD1 in a sand and gravel aquifer: Effect of sewage-derived organic matter: Environmental Science and Technology, v. 31, p. 1163-1170.

Wan, J., Tokunaga, T.K., and Tsang, C.-F., 1995, Bacterial sedimentation through a porous medium: Water Resources Research, v. 31, p. 1627-1636.

Yao, K.M., Habibian, M.T., and O'Melia, C.R., 1971, Water and waste water filtration: concepts and applications: Environmental Science and Technology, v. 11, p. 1105-1112.

Zapico, M.M., Vales, S., and Cherry, J.A., 1987, A wireline piston core barrel for sampling cohesionless sand and gravel below the water table: Ground Water Monitoring Reviews, v. 7, p. 74-87.

AUTHOR INFORMATION

Ronald W. Harvey and David W. Metge, U.S. Geological Survey, Boulder, Colorado.

Naleen A. Mayberry, Wright Pierce, Topsham, Maine.

Nancy E.. Kinner, Dept. Civil Engineering, University of New Hampshire, Durham, New Hampshire.

Mobilization and Transport of Natural and Synthetic Colloids and a Virus in an Iron Oxide-Coated Sewage-Contaminated Aquifer

By Joseph N. Ryan, Menachem Elimelech, Rebecca A. Ard, and Robin D. Magelky

ABSTRACT

To examine the dependence of colloid transport and mobilization on chemical perturbations, we injected colloid-mobilizing agents, synthetic tracer colloids, and a virus into a geochemically heterogeneous aquifer. The transport of mineral (silica and silica-coated metal oxide) and biological (viruses) colloids were related to the surface properties of the colloids and aquifer grains (as measured by zeta potential). The extent of ferric oxyhydroxide surface coverage measured by electron microprobe and estimated by the collision efficiencies for the viruses agreed well. Increases in pH were most effective in mobilizing colloids (both natural and synthetic) and viruses because increases in pH above the pH_{pzc} were most effective in reversing the charge of the ferric oxyhydroxide coatings. In most cases, the transport of mobilized colloids was limited by the advance of the colloid-mobilizing agent (e.g., decrease in ionic strength, anionic surfactant concentration, reductant concentration). A new class of tracer colloids, silica-coated metal oxides, were developed to test the dependence of colloid transport on colloid size.

INTRODUCTION

Colloids have been implicated in the enhanced transport of radionuclides and metals in recent field studies and laboratory experiments (McCarthy and Zachara, 1989). Unfortunately, these studies have rarely delved into the genesis, nature, and abundance of the colloids responsible for the enhanced transport. Our understanding of the processes governing the association of these contaminants with colloids is realtively clear, but we have little knowledge of the potential for colloid mobilization and subsequent transport in a given aquifer.

Colloid mobilization is caused by chemical and physical perturbations to aquifer geochemistry and hydraulics (Ryan and Elimelech, 1996). Chemical perturbations of the type occurring in contaminant plumes are capable of mobilizing large quantities of colloids. In particular, the mobilizing effect of organic compounds like surfactants and reductants is well known (Ryan and Gschwend, 1994; Allred and Brown, 1994). Colloid mobilization by physical perturbations are generally limited to fracture flow and increases in groundwater flow velocity induced by pumping (Degueldre and others, 1989; Backhus and others, 1993).

The major hypothesis of this research was that the transport of the colloids in a contaminant plume is limited by the advance of the chemical agent causing colloid mobilization. In contaminant plumes, colloids are mobilized and transported with the groundwater. If the advance of the contaminant plume is retarded, the colloids will attempt to move ahead of the plume. When the colloids re-enter the pristine groundwater, they will be redeposited. As the plume catches up, the colloids will be remobilized and the cycle will begin again. These simultaneous mobilization and deposition processes have been observed in natural analogs to contaminant plumes like organic matter-rich water infiltrating from a swamp (Ryan and Gschwend, 1990) or fresh water advancing into salt water in a coastal aquifer (Goldenberg and others, 1983).

The colloid front advance hypothesis was tested by field experiments at the U.S. Geological Survey Toxic Substances Hydrology Research site on Cape Cod, Massachusetts (Ard, 1997; Magelky, 1999) and by laboratory mobilization

experiments (Ard, 1997). This paper presents the results of the field experiments.

MATERIALS AND METHODS

Site Description

The virus and silica colloid injections were conducted in the surficial aquifer at the U.S. Geological Survey's Cape Cod Toxic Waste Research Site near the Massachusetts Military Reservation on Cape Cod, Massachusetts. The aquifer was contaminated by disposal of secondary sewage effluent onto rapid infiltration sand beds for over 50 years, creating a contaminant plume characterized by low dissolved oxygen concentrations and elevated pH, specific conductivity, and organic carbon concentrations. The aquifer consists of Pleistocene glacial outwash deposits characterized by interbedded lenses of sand and gravel. The grains (average diameter 0.6 mm) consist mainly of quartz coated by ferric oxyhydroxides (Coston and others, 1995) and the porosity is 0.39 (LeBlanc and others, 1991).

Injections and Sampling

Two major sets of field experiments were conducted during the summers of 1996 (Ard, 1997) and 1997 (Magelky, 1999). Each set of experiments consisted of (1) natural colloid mobilization by chemical perturbations, (2) synthetic colloid deposition under ambient conditions, and (3) synthetic colloid mobilization by chemical perturbations. The basic experiment consisted of injections of amended groundwater into the uncontaminated and contaminated zones of the aquifer using four arrays of multi-level samplers (MLSs; Figure 1). In 1996, three identical virus and colloid injections were followed by three different chemical perturbation injections. In 1997, a variety of colloid and chemical perturbation injections were made. Injection and sampling details are provided in Ard (1997) and Magelky (1999).

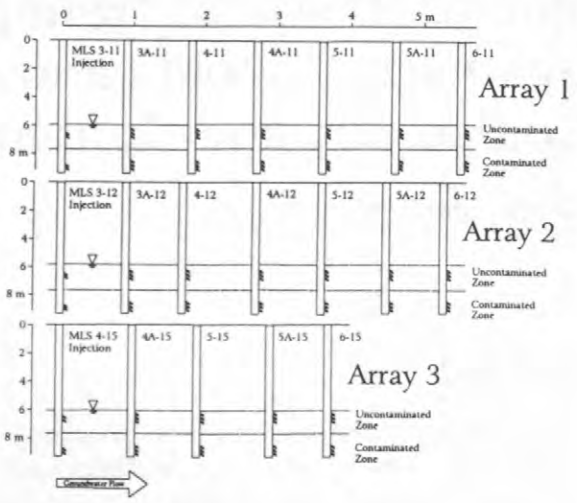

Figure 1. Schematic of multilevel sampler (MLS) arrays used in the field experiments.

Injection Constituents

Silica colloids (Nissan Chemical Industries, MP-1040) of 107±21 nm diameter were used as the synthetic colloid during the 1996 experiments. Silica colloid concentration was measured by UV spectrophotometry at 340 nm (with a detection limit of about $C\ C_0^{-1} = 0.001$) and turbidity (with a detection limit of about $C\ C_0^{-1} = 0.01$).

To improve the detection of the colloids injected during our 1997 field experiment, two "tracer" colloids composed of metal oxides (zirconia, ZrO_2; titania, TiO_2) coated by silica were developed (Table 1). Their synthesis is described in Ryan, Magelky, and Elimelech (in preparation). The concentrations of the silica-coated zirconia and titania particles were measured by inductively-coupled plasma-atomic emission spectrophotometry for zirconium and titanium, providing a much improved detection limit of $C\ C_0^{-1} < 10^{-5}$.

The virus used in the injections is the bacteriophage PRD1 (Olsen and others, 1974). The PRD1 were radiolabeled with ^{32}P-phosphate (Loveland and others, 1996). Virus concentrations were measured by liquid scintillation counting and checked by standards of known ^{32}P activity.

Colloid Characterization

The abundance of natural colloids was measured by turbidity. The natural colloids were also characterized by SEM and energy-dispersive x-ray (EDX) spectroscopy. The electrophoretic mobility of the colloids and virus were determined by microelectrophoresis in uncontaminated and contaminated groundwater and groundwaters amended by the chemical perturbations. During the elevated pH mobilization experiments in 1997, dissolved organic carbon was measured in 0.45 μm-filtered samples by combustion on a platinum catalyst. Total organic carbon concentration was also measured by absorbance of light at 254 nm in unfiltered samples.

Table 1. Size and zeta potentials of titania and zirconia particles before and after coating with silica. Size measured by dynamic light scattering reported as the mean diameter ± one standard deviation for a Gaussian distribution of particle sizes. The coating thickness estimated as one-half the difference between the silica-coated and uncoated diameters.

particle	uncoated diameter (nm)	silica-coated diameter (nm)	silica coating thickness (nm)
zirconia	110 ±34	130 ±49	10
titania	1030±140	1080±160	50

Aquifer Sediments

Cores were obtained from the uncontaminated and contaminated zones of the aquifer about 5 m east of the injection wells used in the field experiments. Thin sections were prepared for electron microprobe and SEM (backscatter electron detection) analysis. The area of surfaces covered by ferric oxyhydroxide coatings were estimated visually by microprobe. The mineralogy of the fine particles of the sediments was determined by powder x-ray diffraction (XRD). Total Fe, Al, and Mn were measured by digestion in concentrated HF/HNO_3 solutions. Free Fe, Al, Mn were measured by Ti(III)-citrate-EDTA-bicarbonate extraction (Ryan and Gschwend, 1991). Streaming potentials (Brookhaven BI-EKA) of aquifer grains were measured in the laboratory of Dr. Philip R. Johnson at Notre Dame University.

Attenuation, Collision Efficiency, Recovery, and Interaction Forces

The relative breakthrough (*RB*, %) of an injected constituent is a ratio of the time-integrated mass of the constituent relative to that of the conservative tracer. Collision efficiencies (α) were calculated with longitudinal dispersion for pulse inputs of PRD1 and silica colloids (Harvey and Garabedian, 1991). In the collision efficiency calculations, the single collector efficiencies (Rajagopalan and Tien, 1976) were calculated using only the convective-diffusion and sedimentation contributions. Fractional recoveries of virus and silica colloids following the chemical perturbations were estimated as the quantity of virus or colloid recovered during the second injection divided by the quantity of virus or colloid immobilized during the first injection (Pieper and others, 1997).

RESULTS

Colloid Characterization

The mobilized natural colloids ranged in size from <0.1 to 10 μm, were platy, and were composed primarily of Si and Al with traces of P and Fe in both zones and for all chemical perturbations. Minerals content included quartz, feldspar, kaolinite, illite/muscovite, and smectite, but no crystalline ferric oxyhydroxides. Microelectrophoresis analysis revealed a pH_{pzc} of approximately 2.2±0.3.

The silica and silica-coated colloid surfaces were negatively charged from about pH 3 to the ambient pH of the uncontaminated groundwater. The silica and silica-coated colloids were slightly more negatively charged in the contaminated groundwater than in the uncontaminated groundwater. The PRD1 surface was negatively charged from pH 3.2 to the ambient pH of the uncontaminated groundwater. PRD1 was slightly more negatively charged in the contaminated

groundwater than in the uncontaminated groundwater.

Sediment Characterization

The sediments contained quartz, feldspars, and traces of clay minerals (kaolinite, illite/muscovite, smectite) and iron oxyhydroxides. Iron-rich coatings were scattered on the quartz grains in both the uncontaminated and contaminated zones. The coating coverage was estimated at 3.0±10.0% of the uncontaminated grain surfaces and 3.5±11.1% of the contaminated grain surfaces. The zeta potential of contaminated sediments in the contaminated groundwater is significantly more negative than that of the uncontaminated sediments in the uncontaminated groundwater.

Natural Colloid Mobilization by Chemical Perturbations

Over the two field seasons, two injections of elevated pH groundwater were performed at approximate injection pH values of 11 (1997) and 12.5 (1996). The amount of colloids mobilized increased with increasing pH (Table 2). Colloid mobilization in the uncontaminated zone always exceeded colloid mobilization in the contaminated zone.

The lower concentration of NaDBS (0.57 mM, 200 mg L^{-1}), about half the critical micelle concentration, caused greater mobilization of natural colloids in the uncontaminated zone. At the lower concentration, a measurable amount of the NaDBS was attenuated, presumably by sorption to the aquifer sediments, but the overall transport of the NaDBS plume was not significantly retarded; thus, colloid mobilization coincided or slightly lagged the passage of the tracer and NaDBS pulses.

An increase in the ascorbic acid concentration produced much greater colloid mobilization in the uncontaminated zone than in the contaminated zone. Ascorbic acid was attenuated to C C_0^{-1} levels of 0.05 and 0.5 in the uncontaminated and contaminated zones of the aquifer, respectively, but no retardation was observed. The mobilized colloids appeared at the same time or slightly behind the tracer and ascorbic acid pulses. Iron(II) concentrations well above the detection limit of 1.8 µM were detected only in the contaminated zone.

A decrease in the ionic strength of the groundwater produced a small amount of colloid mobilization with slightly greater mobilization occurring in the uncontaminated zone. The deionized water "plume" moved through the array at the same rate as the bromide tracer moved through the array in later experiments and the mobilized colloids always appeared at the same time or slightly after the depression of specific conductance caused by the deionized water pulse.

Table 2. Amount of natural colloids mobilized by chemical perturbation injections. Mass of colloids mobilized reported for the first meter of transport. No significant increase in turbidity occurred during the pH 10 injections. Some NaDBS data not reported (n.r.) owing to interference in turbidity measurements by bubbles.

experiment	conditions	aquifer zone	mass of colloids mobilized[a] (mg)
elevated pH (NaOH)	11	uncontam	0.75
		contam	0.45
	12.5	uncontam	500
		contam	17
elevated surfactant NaDBS	0.57 mM	uncontam	59
		contam	20
	29 mM	uncontam	n.r.
		contam	n.r.
elevated reductant AscAc	1.0 mM	uncontam	41
		contam	2.0
decreased ionic strength deionized water	<5 µS cm^{-1}	uncontam	2.7
		contam	1.1

Synthetic Colloid and Virus Deposition

Silica colloids and bacteriophage PRD1 displayed breakthroughs over the first meter of transport (Figure 2). The silica colloids and PRD1 were less attenuated in the contaminated zone than in the uncontaminated zone (Table 3).

Collision efficiencies calculated with and without dispersion varied by up to a factor of 3.4 with the collision efficiency calculated with dispersion always the larger value. Details of these experiments are presented in Ryan and others (1999).

The transport of the silica-coated zirconia displayed similar trends in the same arrays – relative breakthroughs were higher and collision efficiencies were lower in the contaminated zone of the aquifer. In a special experiment conducted in 1997, both the silica-coated zirconia and titania particles were injected into array 4 following the injection of 29 mM (1%) NaDBS to mobilize natural colloids. Under these conditions, transport through the uncontaminated and contaminated zones was similar. The silica-coated zirconia colloids displayed collision efficiencies that were substantially lower than those of the silica-coated titania colloids.

Table 3. Summary of relative breakthroughs (*RB*) and collision efficiencies (α) calculated with dispersion for silica and silica-coated colloids and PRD1.

colloid	aquifer zone	# of arrays	*RB* (%)	α
PRD1	uncontam	3	2.5 ±1.7	0.032 ±0.016
	contam	3	4.3 ±1.4	0.016 ±0.005
silica	uncontam	3	13 ±4	0.023 ±0.009
	contam	3	37 ±16	0.0056 ±0.0034
silica-coated ZrO_2	uncontam	3	1.3 ±1.5	0.039 ±0.013
	contam	3	34 ±42	0.012 ±0.008
silica-coated ZrO_2 after 1% NaDBS	uncontam	1	78	0.0021
	contam	1	76	0.0017
silica-coated TiO_2 after 1% NaDBS	uncontam	1	11	0.0077
	contam	1	12	0.0090

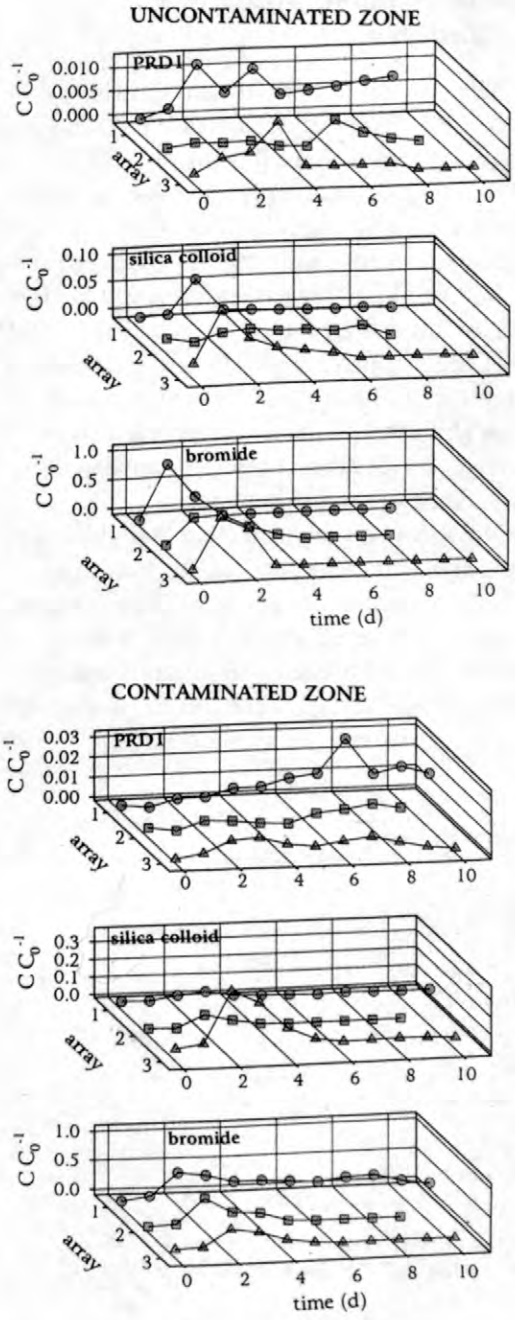

Figure 2. Breakthroughs of PRD1, silica colloids, and bromide at the 0.9 m transport distance in the uncontaminated zone (6.4 m depth) and contaminated zone (8.7 m depth) zones of array 1. Concentrations normalized by the concentration measured immediately after injection ($C\ C_0^{-1}$).

Synthetic Colloid and Virus Mobilization

The amount of colloids and viruses mobilized by pH elevation increased as the pH of the injection was increased from 10 to 12.5 (Table 4). Generally, the pH increase was more effective at mobilizing colloids in the uncontaminated zone (Figure 3). The migration of the NaOH plume lagged significantly behind the tracer, but during the pH 11 injection in 1997, some of the mobilized colloids appeared slightly ahead of the pH increase at the 1 m transport distance (Figure 4). Dissolved organic carbon mobilized by this pH increase also appeared slightly ahead of the pH increase.

NaDBS was more effective at mobilizing colloids and viruses in the contaminated zone than in the uncontaminated zone. The migration of the surfactant closely matched the tracer migration. The mobilized colloids and viruses appeared at the first MLS concurrently or slightly behind the surfactant peak concentration.

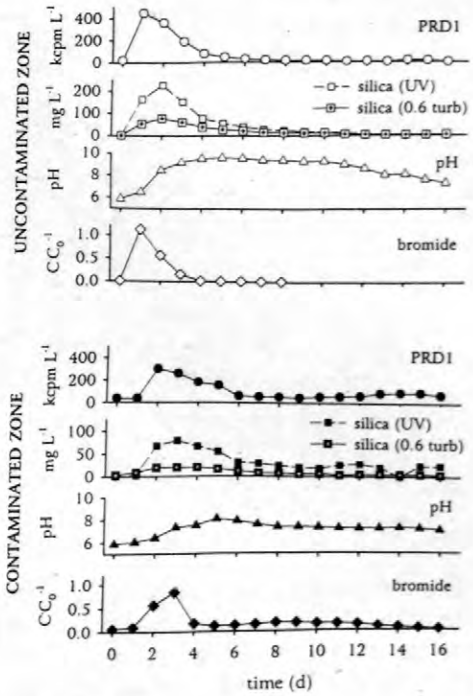

Figure 3. Release of PRD1 and silica colloids and breakthroughs of pH and bromide at the 0.9 m transport distance in the uncontaminated (6.4 m depth) and contaminated (8.7 m depth) zones of array 1 during the elevated pH recovery experiment.

Ascorbic acid was more effective at mobilizing the silica colloids than the viruses. SEM examination of filtered particles revealed at least 90% silica colloids; therefore, no correction for mobilization of natural colloids was applied. The transport of ascorbic acid was attenuated, especially in the uncontaminated zone, but no significant retardation of ascorbic acid occurred. The mobilized colloids and viruses appeared at about the same time or slightly after the appearance of the ascorbic acid peaks at the first MLS. The ascorbic acid injection produced a significant increase in the Fe(II) concentration in the contaminated zone, but no significant increase above the detection limit in the uncontaminated zone. Dissolved oxygen concentrations were slightly depressed in the uncontaminated zone during the ascorbic acid injection, but not significantly different in the contaminated zone.

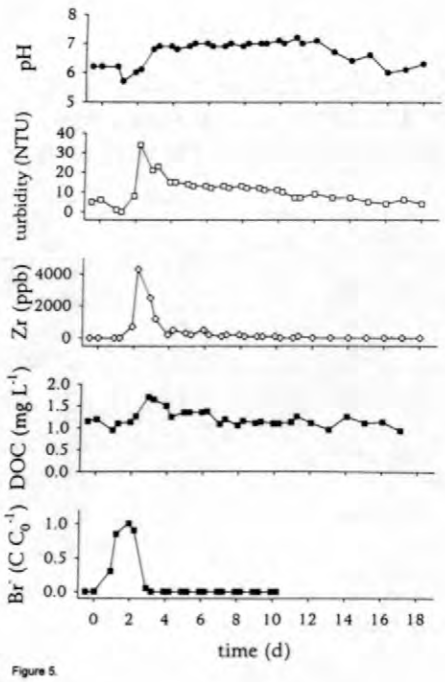

Figure 4. Release of silica-coated zirconia colloids and dissolved organic carbon at the 0.9 m transport distance in the uncontaminated zone (6.4 m depth) of array 1 during the elevated pH recovery experiment.

A decrease in ionic strength brought about by an injection of 100 L of deionized water mobilized more colloids in the uncontaminated

zone of the aquifer. The mobilized colloids appeared at the 1 m transport distance at the same time or slightly behind the deionized water pulse.

Table 4. Recovery of silica and silica-coated colloids and PRD1 over the first meter of transport. Two pairs of recoveries are listed for the silica colloids at an elevated pH of 12.5 – the first pair is for silica colloids measured by UV absorbance and the second pair is for silica colloids measured as 0.6 times the sample turbidity to account for natural colloids.

chemical change	condition	colloid	aquifer zone	recovery (%)
elevate pH NaOH	10.0	$Si\text{-}ZrO_2$	uncont	0.00
			contam	0.10
	11.0	$Si\text{-}ZrO_2$	uncont	1.5
			contam	0.70
	12.5	PRD1	uncont	100
			contam	78
		SiO_2 UV	uncont	240
			contam	120
		SiO_2 0.6 turb	uncont	103
			contam	37
elevate surfactant NaDBS	0.57 mM	PRD1	uncont	0.5
			contam	49
		SiO_2 (UV)	uncont	3.5
			contam	15
elevate reductant AscAc	1.0 mM	PRD1	uncont	3.8
			contam	24
		SiO_2 (UV)	uncont	51
			contam	27
decrease I deionized water	5 $\mu S\ cm^{-1}$	$Si\text{-}ZrO_2$	uncont	0.50
			contam	0.10

DISCUSSION

Silica and Silica-Coated Colloid, PRD1, and Aquifer Grain Zeta Potentials During Injections

The negative zeta potentials of the silica and silica-coated colloids reflect the predominance of deprotonated surface hydroxyls at pH values above the pH_{pzc} value of about 2 to 2.5 reported for silica (Parks, 1967). The similarity between the pH_{pzc} and the zeta potentials of the silica and silica-coated colloids indicate that the silica coating thickness of 10 to 60 nm was sufficient to mask the underlying surface properties of zirconia and titania.

The pH_{pzc} for PRD1 in the uncontaminated groundwater is less than 3.2, similar to a pH_{pzc} value of less than 3.9 in a calcium phosphate solution (Bales and others, 1991). On the basis of studies by Penrod and others (1996) relating the pH_{pzc} values of bacteriophage MS2 and lambda to the composition of their protein capsids, these low pH_{pzc} values for PRD1 indicate that deprotonated carboxyl groups in amino acids dominate the surface speciation of the PRD1 protein capsid.

In the contaminated groundwater, the silica and silica-coated colloids and PRD1 were slightly more negative than in the uncontaminated groundwater. For PRD1, the change in zeta potential may simply be caused by the higher pH of the contaminated groundwater, although changes in virus surface charge may also be attributed to surfactants (Small and Moore, 1987) and fulvic acid (Bixby and O'Brien, 1979). The silica colloids, however, appear to have reached a constant zeta potential at about pH 4.4, so the more negative zeta potential measured in the contaminated groundwater cannot be attributed to the higher pH of the contaminated groundwater. The zeta potential of the silica colloids must have been made more negative by adsorption of anions; e.g., organic matter and phosphate. While extensive adsorption of organic matter to silica at pH near 6.0 is unlikely owing to electrostatic repulsion (Davis, 1982), calcium and magnesium in the contaminated groundwater may enhance organic matter adsorption by reducing the negative charge of the organic matter.

The zeta potentials of the aquifer grains represent a heterogeneous surface made up of the underlying quartz grains, ferric oxyhydroxide and clay mineral coatings, and adsorbed organic matter and phosphate. At the ambient pH of the groundwater, quartz is negatively charged, ferric oxyhydroxide is positively charged, and clay minerals are negatively charged overall with positively charged edges (Parks, 1967). Adsorption of organic matter and phosphate to the positively charged surfaces reverses the surface charge (Liang and Morgan, 1990). The net negative surface potential of the uncontaminated sediment suggests that the ferric oxyhydroxide coating on the quartz grains is patchy, as suggested by thin sections of Cape Cod aquifer grains examined by Coston and others (1995) and

this study. We attribute the more negative zeta potential of the contaminated sediment to the much higher organic matter content of the contaminated sediments. The phosphate content of the contaminated sediments is also elevated, but only by a maximum factor of about 2.5.

Silica and Silica-Coated Colloid and PRD1 Deposition Behavior

Most studies of virus attachment to mineral grains conclude that electrostatic forces dominate the interaction between virus and grain surfaces (Gerba, 1984; Murray and Parks, 1980; Loveland and others, 1996). If electrostatic forces dominated colloid and virus deposition in these experiments, the zeta potential data should provide a qualitative explanation for the observed deposition behavior.

Both the silica and silica-coated colloids and viruses were transported through the contaminated zone more readily than through the uncontaminated zone. The greater abundance of organic matter in the contaminated sediments appears to have masked the ferric oxyhydroxide coatings, giving the contaminated sediments a greater negative zeta potential than the uncontaminated sediments. Consequently, when the negatively charged colloids and viruses interact with the contaminated sediments, they experience greater repulsion, resulting in collision efficiencies lower than those measured in the uncontaminated zone.

The zeta potential data and the ferric oxyhydroxide coatings detected in the thin sections indicate that ferric oxyhydroxides in the Cape Cod sediments enhance colloid and virus attachment and organic matter in the sewage plume inhibits colloid and virus attachment. The presence of positively charged oxides limits the transport of viruses and bacteria because these "biocolloids" are typically negatively charged at the ambient pH of most waters and readily attach to positively charged surfaces (Murray and Parks, 1980; Loveland and others, 1996). For mineral colloids, Johnson and others (1996) showed that the transport of silica colloids in a porous media consisting of mixtures of clean and iron oxide-coated quartz sand depends strongly on the amount of iron oxide coating. Organic matter of natural and anthropogenic (e.g., sewage, surfactants) origin hinders virus attachment to mineral surfaces (Moore and others, 1981; Fuhs and others, 1985), presumably by adsorbing to and masking virus attachment sites. Similarly, the transport of ferric oxide colloids is enhanced by natural organic matter in quartz sands (Amirbahman and Olson 1993; Kretzschmar and others, 1995).

The transport of silica-coated zirconia and titania colloids were measured in a simultaneous injection with dodecylbenzene sulfonate. The collision efficiency calculated for the silica-coated titania particles were about 4-5 times greater than that calculated for the silica-coated zirconia particles (Table 2), indicating greater repulsion between colloid and grain for the silica-coated titania particles. This result qualitatively agrees with the zeta potentials measured for the two colloids – the silica-coated titania colloids have greater negative zeta potentials than the silica-coated zirconia colloids near the ambient pH of the groundwater.

Grain Surface Heterogeneity and Collision Efficiencies

The aquifer grain surfaces are primarily made up of patchy coatings of ferric oxyhydroxides on the underlying quartz grains. At the ambient pH of the groundwaters, the negatively charged PRD1 should be collected by the ferric oxyhydroxide coating and repelled by the exposed quartz (Loveland and others, 1996). The measured collision efficiencies should reflect the summed contribution of ferric oxyhydroxide and quartz surfaces (Johnson and others, 1996). Using PRD1 collision efficiencies of $\alpha_{FeOx} \approx 1$ for ferric oxyhydroxide (owing to electrostatic attraction) and $\alpha_{qtz} \approx 6\times10^{-3}$ for quartz surfaces (Bales and others, 1991), we can estimate the fraction of the surface area coated by ferric oxyhydroxide, f_{FeOx}, using the following equation:

$$\alpha_{measured} = f_{FeOx}\,\alpha_{FeOx} + f_{qtz}\,\alpha_{qtz} \qquad (1)$$

This equation gives estimates of $f_{FeOx} = 0.026$ for the uncontaminated zone and $f_{FeOx} = 0.010$ for the contaminated zone. The uncontaminated zone f_{FeOx} estimate is in close agreement with the 3.0%

surface coverage detected by electron microprobe in the thin sections, but the contaminated zone f_{FeOx} estimate is lower than the 3.5% surface coverage detected. No significant difference between the surface coverage in the uncontaminated and contaminated zones was observed in the thin sections; therefore, the lower contaminated zone f_{FeOx} estimate is attributable to the masking of ferric oxyhydroxide coatings by organic matter and phosphate adsorption.

Colloid and Virus Mobilization by Elevated pH

The NaOH injection was designed to reverse the charge on the ferric oxyhydroxide coatings by raising pH above the pH_{pzc} of ferric oxyhydroxides (Parks, 1967). The amount of colloid and PRD1 mobilization increased with increasing pH. Although the precision of the silica colloid recovery measurement is clouded by the presence of the natural colloids, it appears that similar amounts of PRD1 and silica colloids were released and that release occurred more readily in the uncontaminated zone.

In the uncontaminated zone, the lack of buffering in the groundwater and sediments resulted in a greater increase in pH and greater release of PRD1 and silica colloids than in the contaminated zone. The pH in the uncontaminated zone peaked at nearly 10 at the 1 m distance (injection pH 11.7), while the pH in the contaminated zone peaked at only 8.5 at the 1-m distance (injection pH 11.5) (Figure 3). An increase of pH to 10 is sufficient to reverse the surface charge of any ferric oxyhydroxide, but an increase to pH 8.5 may not exceed the pH_{pzc} of some ferric oxyhydroxides. The greater release of colloids and viruses in the uncontaminated zone must be attributed to the increase in pH well in excess of the pH_{pzc} of the ferric oxyhydroxide coatings.

Colloid and Virus Mobilization by Surfactant Addition

NaDBS was added to alter the ferric oxyhydroxide surface charge and promote release. NaDBS is an anionic surfactant that readily adsorbs to positively charged oxide surfaces and reverses surface charge by hemimicelle formation (Dick and others, 1971). Similar surfactants have been shown to mobilize natural colloids (Ryan and Gschwend, 1994) and cause permeability reduction through colloid mobilization (Allred and Brown, 1994).

The high NaDBS injection concentration made it difficult to determine with any precision the amount of NaDBS lost to aquifer sediments by adsorption. Only a small fraction of the NaDBS injected would be required to saturate the ferric oxyhydroxide surfaces with adsorbed NaDBS (Pieper and others, 1997); however, NaDBS was much less effective at mobilizing PRD1 and silica colloids than the increase in pH. Similarly, Bales and others (1991) showed that 1% Tween 80 and 2.5% beef extract solutions were only marginally effective at mobilizing PRD1 and MS2, another bacteriophage, relative to an increase in pH to 8 in a sodium phosphate solution. Bales and others (1991) speculated that the high ionic strength of the surfactant and beef extract solutions inhibited virus detachment. Our addition of NaDBS to the Cape Cod groundwater caused an increase in ionic strength (0.57 mM) less than that caused by the sodium bromide tracer (about 1.5 mM).

Colloid and Virus Mobilization by Reductant Addition

Ascorbic acid was added to remove the ferric oxyhydroxide coatings by reductive dissolution, resulting in the release of PRD1 and silica colloids attached to the coatings. Ryan and Gschwend (1994) observed that reductive dissolution by ascorbate mobilized natural colloids from a similar ferric oxyhydroxide-coated quartz sand as long as increases in the ascorbate concentration did not raise ionic strength to a level too high to inhibit release. In this experiment, ascorbic acid addition promoted PRD1 and silica colloid release that was somewhat comparable to the surfactant addition, but less than that caused by the pH increase. The amount of ascorbic acid injected in this experiment was similar to the amount promoting the maximum colloid release in the experiments of Ryan and Gschwend (1994).

The amount of PRD1 and silica colloid release varied inconsistently in these experiments.

Ascorbic acid appeared to be effectively dissolving ferric oxyhydroxides in the contaminated zone because the Fe(II) concentration increased as the ascorbic acid broke through; however, Fe(II) release continued near the peak level of Fe(II) release for 15 days beyond the ascorbic acid breakthrough. In contrast, very little ascorbic acid broke through and very little Fe(II) was released in the uncontaminated zone. Some ascorbic acid may have been oxidized by oxygen, although no significant changes in the oxygen content were observed. Released Fe(II) may have been re-adsorbed by aquifer grains or by released colloids, in which case the Fe(II) would promote destabilization and deposition. Based on these results, it is difficult to assess the dependence of PRD1 and silica colloid recovery by ascorbic acid addition.

Colloid Mobilization by Ionic Strength Decrease

Decreases in groundwater ionic strength have frequently caused substantial colloid mobilization and permeability reduction during artificial recharge (Nightingale and Bianchi, 1977) and secondary oil recovery (Khilar and Fogler, 1984). When low ionic strength water replaces high ionic strength water in aquifers with substantial clay contents, an expansion of double layers leads to an increase in electrostatic repulsion between colloids and grains and colloid mobilization. In the ferric oxyhydroxide-coated sands at Cape Cod, however, we hypothesized that a decrease in ionic strength would not cause substantial colloid mobilization because most of the colloid-grain interaction is attractive (negatively charged colloids, positively charged grain coatings). A decrease in ionic strength and expansion of double layers would only serve to strengthen this attractive interaction. As hypothesized, the decrease in ionic strength caused minimal mobilization of the natural colloids and the silica-coated zirconia colloids.

CONCLUSIONS

The field experiments examined the dependence of colloid transport and mobilization on chemical perturbations and assessed the relative transport of mobilized colloids and the chemicals that caused their mobilization. The transport of mineral (silica and silica-coated metal oxide) and biological (viruses) colloids were related to the surface properties of the colloids and aquifer grains (as measured by zeta potential). Excellent agreement was found between the extent of ferric oxyhydroxide surface coverage measured by electron microprobe and estimated by the collision efficiencies for the viruses. Increases in pH were most effective in mobilizing colloids (both natural and synthetic) and viruses because increases in pH above the pH_{pzc} were most effective in reversing the charge of the ferric oxyhydroxide coatings.

In most cases, the transport of mobilized colloids was limited by the advance of the colloid-mobilizing agent (e.g., decrease in ionic strength, anionic surfactant concentration, reductant concentration). A notable exception occurred when pH was increased in one field experiment – mobilized colloids appear to have been transported ahead of the hydroxide plume owing to coating of colloids by natural organic matter. The field research led to the development of a new class of tracer colloids, silica-coated metal oxides. The size of the two types of colloids used in this research, silica-coated zirconia and titania, was controlled by varying the precipitation conditions.

ACKNOWLEDGMENTS

We thank the following people for their help during this project: Bob Puls (U.S. EPA, R.S. Kerr Laboratory), Ron Harvey, Dave Metge, and Doug Kent (U.S. Geological Survey), Denis LeBlanc, Kathy Hess, and Tim McCobb (U.S. Geological Survey, Massachusetts District), Mike Bonewitz (University of Colorado), Jenny Baeseman (University of Wisconsin, Stevens Point), Ning Sun and Chun-Han Ko (UCLA) , Jon Loveland, Dean Abadzic, John Drexler, and Jon Larson (University of Colorado), and Phil Johnson (Notre Dame University).

REFERENCES

Allred, B. and Brown, G.O., 1994, Surfactant-induced reductions in soil hydraulic

conductivity. Ground Water Monit. Remed. p. 174-184.

Amirbahman, A. and Olson, T.M., 1993, Transport of humic matter-coated hematite in packed beds. Environ. Sci. Technol., v. 27, p. 2807-2813.

Ard, R. A., 1997, Natural and artificial colloid mobilization in a sewage-contaminated aquifer: Field and laboratory experiments: Boulder, University of Colorado, Department of Civil, Environmental, and Architectural Engineering, unpublished M.S. thesis, 202 p.

Backhus D.A., Ryan J.N., Groher D.M., MacFarlane J.K. and Gschwend P.M. (1993) Sampling colloids and colloid-associated contaminants in ground water. Ground Water 31, 466-479.

Bales R.C., Hinkle S.R., Kroeger T.W., Stocking K. and Gerba C.P. (1991) Bacteriophage adsorption during transport through porous media: Chemical perturbations and reversibility. Environ. Sci. Technol. 25, 2088-2095.

Bixby R.L. and O'Brien D.J. (1979) Influence of fulvic acid on bacteriophage adsorption and complexation in soil. Appl. Environ. Microbiol. 38, 840-845.

Coston J.A., Fuller C.C. and Davis J.A. (1995) Pb^{2+} and Zn^{2+} adsorption by a natural aluminum- and iron-bearing surface coating on an aquifer sand. Geochim. Cosmochim. Acta 59, 3535-3547.

Davis J.A. (1982) Adsorption of natural dissolved organic matter at the oxide/water interface. Geochim. Cosmochim. Acta 46, 2381-2393.

Degueldre C., Baeyens B., Goerlich W., Riga J., Verbist J. and Stadelmann P. (1989) Colloids in water from a subsurface fracture in granitic rock, Grimsel Test Site, Switzerland. Geochim. Cosmochim. Acta 53, 603-610.

Dick S.G., Fuerstenau D.W. and Healy T.W. (1971) Adsorption of alkylbenzene sulfonate (A.B.S.) surfactants at the alumina-water interface. J. Colloid Interface Sci. 37, 595-602.

Fuhs G.W., Chen M., Sturman L.S. and Moore R.S. (1985) Virus adsorption to mineral surfaces is reduced by microbial overgrowth and organic coatings. Microbial Ecology 11, 25-39.

Gerba C.P. (1984) Applied and theoretical aspects of virus adsorption to surfaces. Adv. Appl. Microbiol. 30, 133-169.

Goldenberg L.C., Magaritz M. and Mandel S. (1983) Experimental investigation on irreversible changes of hydraulic conductivity on the seawater-freshwater interface in coastal aquifers. Water Resour. Res. 19, 77-85.

Harvey R.W. and Garabedian S.P. (1991) Use of colloid filtration theory in modeling movement of bacteria through a contaminated sandy aquifer. Environ. Sci. Technol. 25, 178-185.

Johnson P.R., Sun N. and Elimelech M. (1996) Colloid transport in geochemically heterogeneous porous media: Modeling and measurements. Environ. Sci. Technol. 30, 3284-3293.

Khilar K.C. and Fogler H.S. (1984) The existence of a critical salt concentration for particle release. J. Colloid Interface Sci. 101, 214-224.

Kretzschmar R., Robarge W.P. and Amoozegar A. (1995) Influence of natural organic matter on colloid transport through saprolite. Water Resour. Res. 31, 435-445.

LeBlanc D.R., Garabedian S.P., Hess K.H., Gelhar L.W., Quadri R.D., Stollenwerk K.G. and Wood W.W. (1991) Large-scale natural gradient tracer test in sand and gravel, Cape Cod, Massachusetts 1. Experimental design and observed tracer movement. Water Resour. Res. 27, 895-910.

Liang L. and Morgan J.J. (1990) Chemical aspects of iron oxide coagulation in water: Laboratory studies and implications for natural systems. Aquatic Sciences 52, 32-55.

Loveland J.P., Ryan J.N., Amy G.L. and Harvey R.W. (1996) The reversibility of virus attachment to mineral surfaces. Colloids Surf. A 107, 205-221.

Magelky, R. D. (1999) Colloid deposition and mobilization in a sewage-contaminated iron oxide-coated aquifer. M.S. Thesis, University of Colorado, Boulder, 235 pp.

McCarthy, J. F., and J. M. Zachara (1989) Subsurface transport of contaminants. Environ. Sci. Technol., 23, 496-502.

Moore R.S., Taylor D.H., Sturman L.S., Reddy M.M. and Fuhs G.W. (1981) Poliovirus

adsorption by 34 minerals and soils. Appl. Environ. Microbiol. 42, 963-975.

Murray J.P. and Parks G.A. (1980) Poliovirus adsorption on oxide surfaces. Correspondence with the DLVO-Lifshitz theory of colloid stability. In Particulates in Water. Characterization, Fate, Effects, and Removal (Kavanaugh M.C. and Leckie J.O., Eds.), p. 97. American Chemical Society, Washington, DC.

Nightingale H.I. and Bianchi W.C. (1977) Ground-water turbidity resulting from artificial recharge. Ground Water 15, 146-152.

Olsen R.H., Siak J.-S. and Gray R.H. (1974) Characteristics of PRD1, a plasmid-dependent broad host range DNA bacteriophage. J. Virology 14, 689-699.

Parks G.A. (1967) Aqueous surface chemistry of oxides and complex oxide minerals. In Equilibrium Concepts in Natural Water Systems (Stumm W., Ed.), p. 121. American Chemical Society, Washington, DC.

Penrod S.L., Olson T.M. and Grant S.B. (1996) Deposition kinetics of two viruses in packed beds of quartz granular media. Langmuir 12, 5576-5587.

Pieper A.P., Ryan J.N., Harvey R.W., Amy G.L., Illangasekare T.H. and Metge D.W. (1997) Transport and recovery of bacteriophage PRD1 in a sand and gravel aquifer: Effect of sewage-derived organic matter. Environ. Sci. Technol. 31, 1163-1170.

Rajagopalan R. and Tien C. (1976) Trajectory analysis of deep-bed filtration with the sphere-in-cell porous media model. AIChE J. 22, 523-533.

Ryan J.N., Ard R.A., Magelky R.D., and Elimelech M. (in preparation) Effect of elevated pH on the mobilization of colloids from a ferric oxide-coated quartz sand: Laboratory and field experiments.

Ryan J.N. and Elimelech M. (1996) Colloid mobilization and transport in groundwater. Colloids Surf. A 107, 1-52.

Ryan J.N., Elimelech M., Ard R.A., Harvey R.W., and Johnson P.R. (1999) Bacteriophage PRD1 and silica colloid transport and recovery in an iron oxide-coated sand aquifer. Environ. Sci. Technol., v. 33, p. 63-73.

Ryan J.N. and Gschwend P.M. (1990) Colloid mobilization in two Atlantic Coastal Plain aquifers: Field studies. Water Resour. Res. 26, 307-322.

Ryan J.N. and Gschwend P.M. (1991) Extraction of iron oxides from sediments using reductive dissolution by titanium(III). Clays Clay Min. 39, 509-518.

Ryan J.N. and Gschwend P.M. (1994) Effects of solution chemistry on clay colloid mobilization from an iron oxide-coated sand aquifer. Environ. Sci. Technol. 28, 1717-1726.

Ryan J.N., Magelky R.D., and Elimelech M. (in preparation) Using silica-coated metal oxide tracer colloids of variable size in a colloid transport field experiment.

Small D.A. and Moore N.F. (1987) Measurement of surface charge of baculovirus polyhedra. Appl. Environ. Microbiol. 53, 598-602.

Walter, D. A., Rea, B. A., Stollenwerk, K. G., and Savoie, J. (1996) Geochemical and hydrologic controls on phosphorus transport in a sewage-contaminated sand and gravel aquifer near Ashumet Pond, Cape Cod, Massachusetts. U.S. Geol. Survey Water-Supply Paper 2463, 89 pp.

AUTHOR INFORMATION

Joseph N. Ryan, Rebecca A. Ard, and Robin D. Magelky, Department of Civil, Environmental, and Architectural Engineering, University of Colorado, Boulder, Colorado 80309 (joe.ryan@colorado.edu)

Menachem Elimelech, Department of Chemical Engineering, Yale University, New Haven, Connecticut (menachem.elimelech@yale.edu)

Dual Radioisotope Labeling to Monitor Virus Transport and Identify Factors Affecting Viral Inactivation in Contaminated Aquifer Sediments from Cape Cod, Massachusetts

By David W. Metge, Theresa Navigato, Jon E. Larson, Joseph N. Ryan, and Ronald W. Harvey

ABSTRACT

The *in-situ* mobility of bacteriophage PRD-1, whose DNA was labeled with ^{32}P nucleotides and protein coat was labeled with ^{35}S methionine, was tested using small-scale (1-4 meter) injection and recovery experiments. The isotope-labeled virus and a conservative (bromide) tracer were injected into shallow (uncontaminated) and deep (treated-sewage-contaminated) sandy aquifer sediments within an unconfined glacial outwash aquifer on Cape Cod, Mass. This contaminated aquifer has sharp pH and chemical gradients and sediment heterogeneities, which influence the transport properties of microorganisms (0.05-5.0 micrometers [μm]).

In the presence of treated-sewage contaminants and the common household surfactant SDBS (sodium dodecyl benzene sulfonate), concentration histories of dual-labeled phage exhibited much different transport behavior than was observed in an earlier field experiment using a different surfactant. Peak breakthroughs of infective virus were 1 to 2 orders of magnitude greater than the earlier experiment. Also, there was little or no breakthrough of radiolabel in the absence of infective virus. This was in direct contrast to results from the earlier experiment where greater than 98% of the observed breakthrough was as noninfective virus. It is hypothesized that virus infectivity may be due to virus-sediment binding interactions.

Although virus transport properties differ somewhat from those observed for groundwater microbial populations, dual-isotope-labeled infective virus were detected several meters downgradient. The high degree of infective virus transport in the presence of environmentally relevant concentrations of SDBS suggests that this surfactant may help protect against virus inactivation and promote subsurface transport by reducing virus binding to sediment surfaces. Presence of surfactants appears to have implications in the degree of risk associated with viral pathogen transport and in the setback distances for public water supply wells close to sources of sewage contamination.

INTRODUCTION

Sewage disposal is a major cause of ground-water contamination in the United States, largely due to millions of septic systems currently in operation (USEPA, 1987). A number of studies have examined the subsurface transport behavior of sewage-derived viruses (Ryan and others, 1999;Bales and others, 1995). However, little is known about the role of ground-water chemistry, particularly surfactants, upon the fate and transport of viruses in drinking water aquifers. A better understanding of this issue

may facilitate better prediction of the transport of viral pathogens in ground water and facilitate implementation of the EPA's Ground Water Disinfection Rule (Macler, 1996).

Subsurface viral transport was investigated by introducing radiolabeled bacteriophage to contaminated and uncontaminated ground-water zones within an unconfined glacial outwash aquifer. In 1994 and 1997, injection and recovery experiments with radiolabeled virus were conducted in a surficial aquifer at the U.S. Geological Survey's Toxic Waste site on the Massachusetts Military Reservation, Cape Cod, Mass. The use of radiolabeled virus was critical since it allowed us to monitor both infective and total virus concentrations using conventional plaque assay techniques and scintillation counting of isotopes, respectively. Coupled field and laboratory experiments were used to investigate how surfactants affect subsurface viral transport and inactivation within contaminated and uncontaminated aquifer sediments.

MATERIALS AND METHODS

Study Site

The study site is a glacial outwash aquifer located on western Cape Cod, Mass. It was contaminated by a 60-year long discharge of secondarily-treated sewage effluent. The resulting ground-water plume is more than 6 kilometers (km) long and about 1 km wide; this plume contains sharp pH and chemical gradients. Studies have demonstrated that plume chemistry and sediment heterogeneities strongly influence the degree of microbial transport (e.g. Pieper and others, 1997). Relative to background conditions, low dissolved oxygen concentrations, high pH, high specific conductance, and high dissolved organic carbon (DOC) concentrations characterize the contaminated plume (see Table 1) . A pair of injection and recovery experiments was performed with radiolabeled bacteriophage within a well array south of the sewage treatment plant (tracer test site, fig. 1).

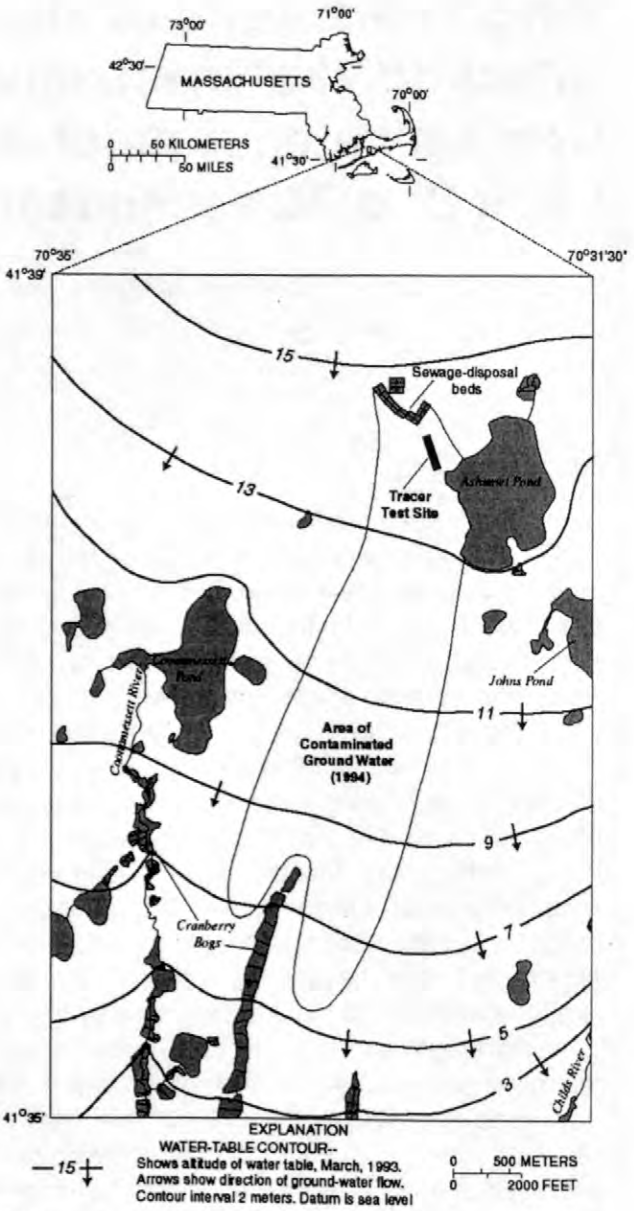

Figure 1 – Location with tracer test site, Cape Cod, Mass.

In the last 15 years, several multidisciplinary studies have focused on subsurface fate and transport of chemical and biological contaminants (Harvey and others, 1989; Harvey and Garabedian, 1991; LeBlanc and others, 1991; Smith and others, 1991; Smith and others, 1991; Hess and others, 1992; Kent and others, 1994; Bales and others, 1995; Harvey and others, 1995;

Barber and others, 1995; Pieper and others, 1997).

Table 1. Aquifer geochemical characteristics about 150 meters downgradient from sewage treatment plant.

Constituent (units)	Contaminated zone	Uncontaminated Zone
Sediment Fe(III)[b] (in micromoles per gram)	4.7 ± 1.4	3.6 ± 0.3
Sediment f_{oc}[a]	0.01	<0.0001
pH	5.8-6.1	5.4-5.8
DOC (in milligramps per liter)	2.0-4.4	0.4-1.0

[a]fraction of organic carbon present in sediments by mass spectroscopy (Scholl and Harvey, 1992).
[b]metals measured by Ti(III)-citrate-EDTA-bicarbonate reduction (Ryan and Gschwend, 1994)

Field Experiments

Previous field tracer experiments (1994, 1996) used nonspecifically labeled bacteriophage. These were radiolabeled with ^{32}P phosphate (Pieper and others, 1997). Therefore, the entire virus (protein coat and nucleic acid) contained ^{32}P. For the most recent field experiment, PRD1 bacteriophage (bacteria-specific virus) were specifically radiolabeled with ^{35}S and ^{32}P. The goal was to label the virus' protein coat with ^{35}S and its DNA with ^{32}P. This method utilized α PO_4 ^{32}P DNA nucleotides and ^{35}S methionine. Radioisotopes were incubated with PRD1 virus and a log phase bacterial host (*Salmonella typhimurium*) culture in methionine-deficient media. The virus:host ratio was about 10:1, which is an appropriate infection ratio to achieve maximal virus production. This mixture was incubated at 35°C until lysis of the bacterial host was achieved. The radiolabeled virus were purified by sequential centrifugation to remove bacterial host cell debris (3-5000 rpm, 15 min. [minute], 4°C) and pelleting (20000 rpm, 4-8 h. [hour], 4°C). After purification the virus were suspended in PBS (phosphate buffered saline) and shipped to the test site.

Injection and recovery experiments were performed in a well array with similar geochemistries to the 1994 field test. The injection site was near the head of the large-scale well field about 0.2 km downgradient from a sewage treatment plant. Injections were made into uncontaminated ground water immediately beneath the water table and into the underlying contaminant plume. To avoid changing the ground-water chemistry near the injection point, ground water collected from the injection depths was used as a suspending medium for the injectate constituents. For injection into the suboxic contaminant plume, a gas impermeable bladder with a nitrogen headspace was employed as the injectate reservoir. In the 1997 experiments, iron-oxide-containing sediments were preconditioned with surfactants. This involved a preliminary injection of SDBS (25 milligrams per liter, [mg/L]). Injectate concentrations were 10^6/milliliter [mL] of ^{35}S / ^{32}P labeled PRD1, 100 mg/L NaBr, and 25 mg/L of SDBS. Twice-a-day sampling was performed at three multilevel samplers (MLS) downgradient.

Retardation factors (R_f) were calculated using relative 1 meter (m) transport times of integrated centers of mass for conservative and reactive tracers. Collision efficiencies were calculated using equations as described in Ryan and others, (1999). The degree of immobilization is calculated as the relative amount of virus remaining attached to sediments within the transport interval.

Laboratory Experiments

Laboratory experiments were performed as previously reported (Loveland, 1995) within static mini-columns to determine viral inactivation rates. Approximately 10^6 virus /g sediment were loaded to columns containing 10 g of 0.5-1.0 millimeter (mm) sieved aquifer sediments and either unamended, LAS (linear alkyl-benzene sulfonate)-amended or SDBS- amended contaminated ground water. These columns were placed in a 10°C incubator for 7 days. Each day they were flushed with one pore

volume of unamended or surfactant-amended ground water. Viruses were assayed using a plaque assay method as described previously. Virus inactivation rates were calculated by determining linear regression slopes from log-adjusted concentrations of plaque forming units (PFU) plotted as a function of time (Yates and Yates, 1987;Yates and others, 1985).

RESULTS AND DISCUSSION

Significant differences in virus transport and inactivation rates were observed for the SDBS-treated sediments in the 1997 experiment relative to the results observed for the LAS-treated sediments in the 1994 experiment. Results from both experiments are summarized in table 2. There was coincident breakthrough of PRD1, ^{35}S, and Br^- at 1 m downgradient. Retardation factors for active virus and isotope were similar. This was in contrast to previous work using a different surfactant within the same well array where nearly 98% of the virus that appeared was noninfective. In the earlier injection and recovery experiments, the R_f for the virus and ^{32}P varied by 3 fold (Pieper and others, 1997). At 1 m downgradient from the point of injection, the transport of PRD1 was ~100 fold higher than in 1994, judging from the virus peak dimensionless concentrations at 1 m downgradient. The collision efficiencies in the 1997 test were very small (i.e.: ~10^{-3}). Finally, in contrast to the 1994 results, most of the PRD1 injected retained their infectivity during a 1 m transport distance. This suggests that PRD1 traveling through SDBS-exposed sediments retain their structural integrity in spite of the inter-surface forces during reversible attachment to sand grains. Virus-sediment interactions have been hypothesized to be the predominant factor in controlling virus infectivity (Pieper and others, 1997). Groundwater chemistry, the degree of sediment associated carbon, and sediment iron oxides (see table 1) were thought to be the predominant factors determining the degree of subsurface viral transport (Pieper and others, 1997, Ryan and others, 1999).

Table 2. Transport parameters for radiolabeled virus in 1994 and 1997 experiments, [Rf, retardation factor].

Parameter	1997[a]	1994[b]
R_f –Virus	0.8	1.3
R_f –Isotope	0.8	5.6
Collision Efficiency	0.0016	0.016
Immobilization- Virus	42%	99%

[a]SDBS surfactant used, [b] LAS surfactant used

From these results, the lowered collision efficiency and immobilization in 1997 suggest that virus-sediment grain interactions were less likely to result in inactivation. It was also evident that the predominant isotope (^{35}S) coeluted with the virus. This was in contrast to the earlier experiment.

Laboratory experiments also suggest that virus-sediment interactions are more likely to result in inactivation than in contaminated water alone. In fact, the rate is about 20 times higher in sediments. In the presence of contaminated water, sediments, and LAS surfactant, the inactivation rate is about 10% lower than water and sediments alone. These data are summarized in table 3 below. These laboratory data suggest that surfactants can protect this virus from becoming inactivated by their interaction with aquifer sediments. Therefore, one could expect viral subsurface transport (in the presence of these surfactants) over longer distances in an infective state.

Table 3. Calculated inactivation rates for PRD1 virus from static mini columns.

Experimental Matrix	Inactivation rate (in plaque forming units per day)
Unamended contaminated water	0.018
Water + sediments	0.563
Water + sediiments + LAS	0.496

A comparison of results between the 1994 and 1997 experiments suggest that high inactivation for PRD1 in Cape Cod sediments seems to correlate with increased immobilization. Lowering the degree of

immobilization by exposing the sediments to SDBS also helps protect the virus from inactivation. SDBS seems to be much more effective in this regard than LAS. It has been suggested (Ryan and others, 1999) that there may be a variety of interactive factors involved in the attachment/detachment dynamics of colloids, including viruses. SDBS was used in a 1996 field experiment with adsorbed virus to promote sediment charge reversal. However, Ryan (1999) found that SDBS was less effective at remobilizing sorbed virus than an increase in ground water pH. In our 1997 experiment, SDBS was equally effective in promoting virus transport in both the contaminated and uncontaminated zones. This may be due to the ability of SDBS to modify the surface charge of iron oxide-coated grains in the aquifer sediments.

SUMMARY

We found that low (part-per-million) concentrations of LAS and SDBS concentrations can affect viral movement and inactivation within aquifer sediments. Virus-sediment interactions appear to be the primary factor governing viral transport and inactivation. A variety of mechanisms may be present and complicated by the presence of surfactants. The presence of surfactants resulted in significantly lowered virus collision efficiency and immobilizations within both contaminated and uncontaminated aquifer sediments. The type of surfactant is important; differences were observed in viral transport behavior between a pair of injection and recovery experiments conducted in 1994 and 1997 in which different surfactants were used. Laboratory experiments suggest that surfactants may protect this virus from inactivation by sediment interactions. Therefore, the presence of certain surfactants may raise the degree of health risk because significantly more active viral pathogens could be transported to public water supply wells. This would require examination of appropriate setback distances for wells close to sources of sewage contamination.

More experiments are planned with surfactants and aquifer sediments to define mechanisms governing viral inactivation and attachment to aquifer sediments. Also, the influence of different types of organic material upon viral attachment to sediments deserves closer examination. Ultimately, we plan to compare results from column experiments with radioisotope labeled bacteriophage to these field tracer tests to determine how contaminants affect viral transport and inactivation processes in the subsurface.

REFERENCES

Bales, R.C., Li, S., Maguire, K.M., Yahya, M.T., Gerba, C.P., and Harvey, R.W., 1995, Virus and bacteria transport in a sandy aquifer, Cape Cod, MA. Ground Water, v.33, p. 653-661.

Barber, L.B., II, Kreuger, C., Metge, D.W., Harvey, R.W., and Field, J.A., 1995, Fate of linear alkylbenzene sulfonate in groundwater., Sorensen, Jan, eds., Surfactant enhanced subsurface remediation., 1995, American Chemical Society, New York, 1995.

Harvey, R.W. and Garabedian, S.P., 1991, Use of colloid filtration theory in modeling movement of bacteria through a contaminated sandy aquifer. Environmental Science & Technology, v.25, p. 178-185.

Harvey, R.W., George, L.H., Smith, R.L., and LeBlanc, D.R., 1989, Transport of microspheres and indigenous bacteria through a sandy aquifer: results of natural and forced-gradient tracer tests. Environmental Science & Technology, v.23, p. 51-56.

Harvey, R.W., Kinner, N.E., Bunn, A., MacDonald, D., and Metge, D.W., 1995, Transport behavior of groundwater protozoa and protozoa-sized microspheres in sandy aquifer sediments. Applied and

Environmental Microbiology, v.61, p. 209-217.

Hess, K.M., Wolf, S.H., and Celia, M.A., 1992, Large-scale natural gradient tracer test in sand and gravel, Cape Cod, Massachusetts 3. hydraulic conductivity variability and calculated macrodispersivities. Water Resources Research, v.28, no. 8, p. 2011-2027.

Kent, D.B., Davis, J.A., Anderson, L.C.D., and Rea, B.R., 1994, Transport of chromium and selenium in the suboxic zone of a shallow aquifer: influence of redox and adsorption reactions. Water Resources Research, v.30, p. 1099-1114.

LeBlanc, D.R., Garabedian, S.P., Hess, K.M., Gelhar, L.W., Quadri, R.D., Stollenwerk, K.G., and Wood, W.W., 1991, Large-scale natural-gradient tracer test in sand and gravel, Cape Cod, Massachusetts: 1. Experimental design and observed tracer movement. Water Resources Research, v.27, p. 895-910.

Loveland, J.P., 1995, Virus Transport in groundwater: bacteriophage PRD1 attachment to Mineral Surfaces, 120 p.

Macler, B.A., 1996, Status of the groundwater disinfection rule, in Seacrest, S. and Karlin, R., eds., Under the microscope—examining microbes in groundwater--symposium proceedings of the 1996 Groundwater Foundation, Boston, Mass., Sept. 5-6, 1996: Denver, Colo., AWWA Research Foundation, p. 75-81.

Pieper, A.P., Ryan, J.N., Harvey, R.W., Amy, G.L., Illangasekare, T.H., and Metge, D.W., 1997, Transport and recovery of bacteriophage PRD1 in an unconfined sand aquifer: effect of anthropogenic organic material. Environmental Science & Technology, v.31, p. 1163-1170.

Ryan, J.N., Elimelech, M., Aard, R.A.H.R.W., and Johnson, P.R., 1999, Bacteriophage PRD1and silica colloid transport in an iron-oxide-coated sand aquifer. Environmental Science & Technology, v.33, p. 63-73.

Ryan, J.N. and Gschwend, P.M., 1994, Effect of solution chemistry on the detachment of clay colloids from an iron oxide-coated sand. Environmental Science & Technology, v.28, p. 1717-1726.

Scholl, M.A. and Harvey, R.W., 1992, Laboratory investigations on the role of sediment surface and groundwater chemistry in transport of bacteria through a contaminated sandy aquifer. Environmental Science & Technology, v.26, p. 1410-1417.

Smith, R.L., Harvey, R.W., and LeBlanc, D.R., 1991, Importance of closely spaced vertical sampling in delineating chemical and microbiological gradients in groundwater studies. Journal of Contaminant Hydrology, v.7, p. 285-300.

Smith, R.L., Howes, B.L., and Duff, J.H., 1991, Denitrification in nitrate-contaminated groundwater: occurence in steep vertical gradients. Geochimica et Cosmochimica Acta., v.55, p. 1815-1825.

USEPA, 1987, Guidelines for delineation of wellhead protection areas. Washington, D.C.

Yates, M.V., Gerba, C.P. and Kelley. L.M., 1985, Virus persistance in groundwater. Appl. Environ. Microbiol., v.49, p. 778-781.

Yates, M.V. and Yates, S.R., 1987, A comparison of geostatistical methods for estimating virus inactivation rates in groundwater. Water Research, v.9, p. 1119-1125.

AUTHOR INFORMATION

David W. Metge and Ronald W. Harvey, U.S. Geological Survey, WRD, Boulder, Colorado (email:dwmetge@usgs.gov, rwharvey@usgs.gov) [web: http://wwwbrr.cr.usgs.gov/bacteria]

Theresa Navigato, Jon Larson, Joseph N. Ryan, University of Colorado, Boulder, Colorado

Installation of Deep Reactive Walls at MMR using a Granular Iron-Guar Slurry

By David W. Hubble and Robert W. Gillham

ABSTRACT

The primary contaminant in the CS-10 plume at a military base on Cape Cod is tetrachloroethene (PCE) and site groundwater has been shown to be treatable using granular zero-valent iron. The plume, which extends over a depth interval of 24 to 37 m near its source, is considered to be deep (i.e. > 15 m below the ground surface) and not accessible for conventional means of installing granular iron. Thus, a novel method of vertical reactive wall installation was selected for a 15 m long, full depth, trial wall at the CS-10 plume. The method (hydraulic fracturing) uses special tools to mix granular iron in a guar-based biodegradable polymer and then inject it into a hydraulically created vertical fracture. Geotechnical and geophysical test results show that iron was successfully installed in a wall having an average thickness of 80 mm and between 24 and 37 m depth. The CS-10 demonstration is thus the deepest installation of any reactive material in a wall to date. Monitoring of inorganic and organic groundwater parameters has shown the effects of 1) wall installation, 2) a delayed break of the bio-polymer cross-link and 3) an amendment injected to hasten guar breakdown.

INTRODUCTION

The Massachusetts Military Reservation (MMR) in Cape Cod, Massachusetts, has several groundwater contaminant plumes containing halogenated organic compounds such as tetrachloroethene (PCE), trichloroethene (TCE) and ethylene dibromide (EDB). The contaminants are dispersed at concentrations between their method detection limits and typically less than about 500 µg/L in a large volume of groundwater and extend off base toward ecological receptors. The University of Waterloo (UW) was contracted to demonstrate the use of granular iron in the remediation of halogenated compounds in the MMR groundwater. Most of the plumes at MMR are at depths of between 15 and 60 m below the ground surface, too deep for installation of granular iron in a permeable reactive wall or barrier (PRB) using conventional emplacement methods such as backfilling of excavations dug by backhoes or continuous trenching machines. Near its source area, the CS-10 plume extends from about 24 to 37 m below the ground surface, has a width of at least 120 m and has peak PCE and TCE concentrations of about 250 and 10 µg/L, respectively (Figure 1). Down-gradient, the plume is up to 1,200 m wide and 43 m thick and extends for a distance of about 5,200 m from the source area. MMR is located on western Cape Cod and is underlain by glacial outwash and glacial till materials (see LeBlanc, 1984, Masterson *et al.*, 1996). A thick unconfined aquifer comprising sand and gravel underlies most of MMR. This aquifer is the water supply source for MMR and several nearby communities.

The zero-valent iron technology has been shown at bench and field scales to effectively treat chlorinated aliphatic hydro-carbons through reductive dechlorination (Gillham, 1996). The material consists of granular iron or an iron and sand mixture which is placed in the ground. As groundwater passes through the reactive material, chlorinated hydrocarbons are degraded, allowing decontaminated water to emerge on the down-gradient side. Of particular importance, the treatment process is a "passive" remediation technology and has very low operating and maintenance costs.

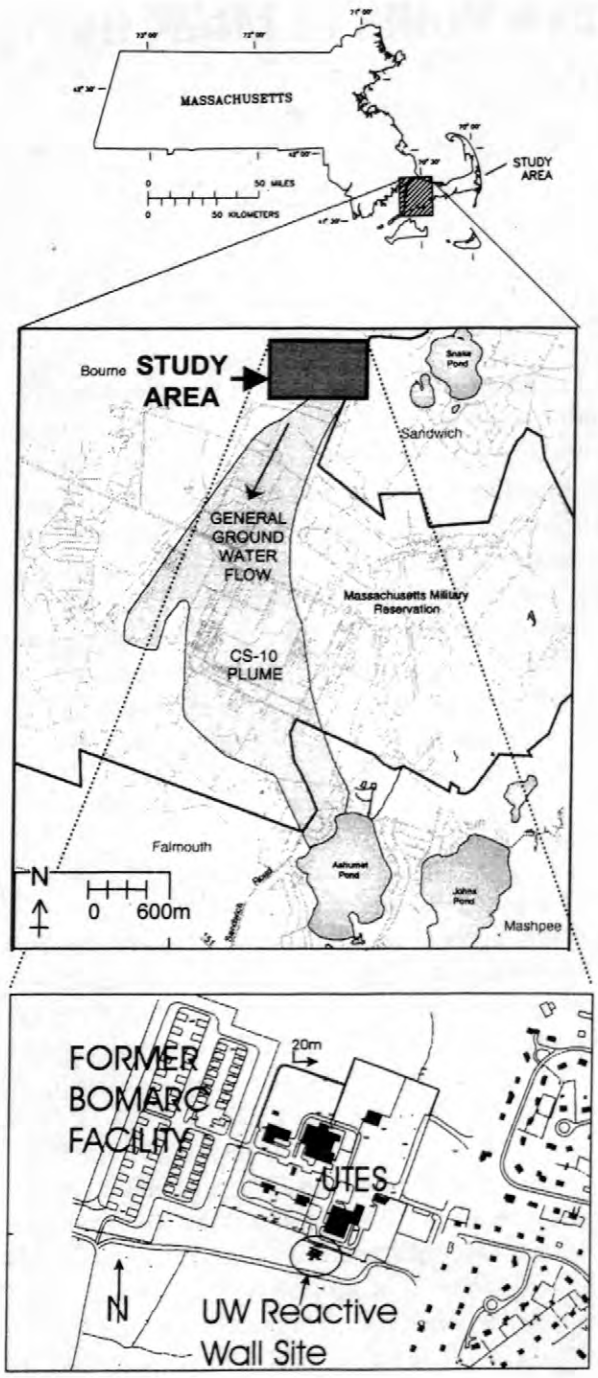

Figure 1. Location of the study area, CS-10 plume, and UW reactive wall demonstration site, MMR, Cape Cod, Massachusetts.

OBJECTIVES

The primary objective of this work was to demonstrate the use of granular zero-valent iron to remediate groundwater contaminated with chlorinated solvents at MMR. Due to the great depth of most of the solvent plumes at the site, a second objective was to advance PRB technology to depths never accomplished before. This was to be done by selecting and testing a method of emplacement that was capable of creating reactive zones of granular iron at depths of 15 to 60 m or more.

This paper addresses the progress of the work to date in meeting the objectives, including a summary of previous work:

- Laboratory experiments with granular iron (Fe^0) and site water
- An emplacement methods study and preliminary design to:
  - compare various installation methods used in the "impermeable" barrier industry to determine which could be adapted for emplacement of granular iron
  - select a feasible and cost effective method for a 15 m demonstration length wall and/or a full scale length wall

The paper then reports on:

- Installation of reactive walls in June 1998
- Quality control and assurance (verification) testing during and after installation
- Monitoring of groundwater parameters before and after emplacement of the PRB

SUMMARY OF PREVIOUS WORK

Experimental Work

A bench scale treatability study was conducted in the UW laboratory using site water collected from the CS-10 source area plume and commercial granular iron. The column setup used in the experimental work is shown in Figure 2. The concentration of PCE in the site water was in the range of 150 to 200 μg/L. The PCE was increased to about 400 μg/L for the column testing using analytical grade PCE dissolved in methanol to show the ability of the iron to treat the PCE and its degradation products.

The results of column tests (e.g. Figure 3) indicated that the site water could be treated with granular iron and that degradation was complete and sufficiently rapid such that a practical design or "treatment" thickness could be achieved. A

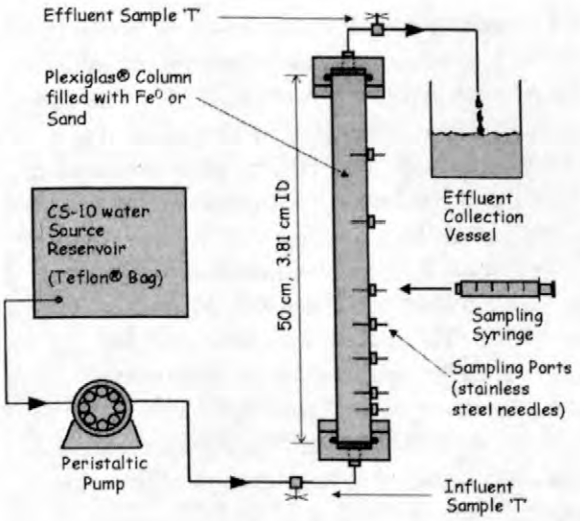

Figure 2. Laboratory Column Setup

half-life of 0.8 hr was found for PCE in the site water treated by 75 percent granular iron (equivalent to 0.6 hr for 100 percent iron). The degradation product TCE was found at low levels (<5 μg/L) and was treated, together with the TCE in the site water, within the zone of treatment of the PCE. The degradation products dichloroethene (DCE) and vinyl chloride (VC) were below method detection limits throughout the column.

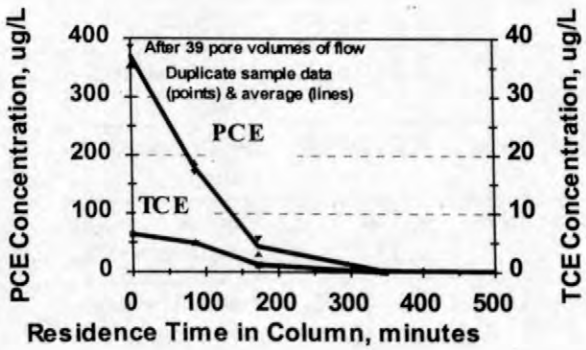

Figure 3. Column Results – 75% granular iron and 25% sand, average flow velocity of 0.4 m/day

Emplacement Methods Study and Preliminary Design

An emplacement methods study was carried out and reported to the Air Force Center for Environmental Excellence (AFCEE). A permeable reactive wall configuration was chosen rather than funnel-and-gate system, since flow modeling showed it to be more hydraulically efficient and less expensive (Hubble *et al.*, 1997). The emplacement methods that have been used in the past for civil engineering construction and "impermeable" barrier installation were evaluated, taking into consideration factors such as site geology, which comprises compact to dense glacial outwash sand and gravel. The emplacement methods selected for preliminary design and costing were:

- slurry wall construction
- driven/vibrated beam walls
- deep-soil mixing
- vertical hydrofracturing and injection of iron

One of the findings of this work was the need to convey the granular iron into the ground in a slurry. Therefore, another column test was conducted with granular iron mixed with a guar bio-polymer gel. This bench scale test indicated that the residual polymer on the iron caused an increase in half-life of PCE, at least up to 100 pore volumes of flow. This effect appears to diminish with cumulative amount of flow. To account for the effects of the guar, precipitation of inorganic solid phases and the lower temperature in the ground, a half-life value of 2.75 hr was recommended for design (Hubble *et al.*, 1997). Estimates of the quantity of iron needed for remediation were then based on the groundwater velocity (0.3 m/day), design maximum contaminant concentration (200 μg/L PCE) and the design half-life (2.75 hr).

Each method was assessed for cost of implementation and its expected performance or treatment integrity. A thickness variability factor (TVF) was defined as the average thickness of reactive material needed to be emplaced, divided by the minimum thickness that can be relied upon for treatment design. (Or the average thickness to be used for quantity and cost estimation was arrived at by multiplying the design (minimum) thickness by the TVF value). A TVF was assigned for each method to accommodate concerns about the variability in the wall thickness that would be achieved by the various installation techniques. The TVF values used were 1.2, 1.29, 1.25 and 1.5 for the four methods listed above, respectively.

For a 15 m wide, full-depth, demonstration of an iron PRB at the CS-10 source area, the emplacement method selected was vertical hydrofracturing and injection. This method had the least estimated installation cost, even with the highest TVF applied. A key recommendation was that to improve the treatment integrity of fracture-emplaced walls to an acceptable level, at least two parallel fracture walls should be used in any given application of the hydrofracturing method for full-scale remediation.

Treatment of the CS-10 source area plume (with the design variables above) would require a design treatment thickness of 183 mm of 100 percent commercial iron and an average total wall thickness of 277 mm (due to the TVF of 1.5). It was recommended that this thickness be installed in 3 walls of about 92 mm average thickness (61 mm minimum). For the 15 m demonstration project at MMR, it was decided to install

- one wall of 100 percent iron, 75 to 100 mm thickness
- a second wall consisting of a uniform mixture of sand and iron, up to 75 mm thick

The purpose of the second wall was to model the use of an "enhanced" iron with a much higher reaction rate than commercial granular iron and a sand "filler" material (Hubble *et al.*, 1997).

At the time of its selection, hydraulic fracturing had not been used in a PRB with granular iron. The MMR reactive wall was also the deepest PRB planned and remains the deepest installation of a granular iron reactive wall to date.

RESULTS

Field Installation

In June 1998, two iron walls were installed using vertical hydrofracturing performed by Golder Sierra LLC as contractor (Figure 4). The up-gradient wall contains 40 tonne of Master Builder fine to medium granular iron. Table 1 provides a summary of the timing of installation of monitoring wells, the reactive walls and other events at the site. Table 2 provides details on the construction of the two walls. The up-gradient 100 percent iron wall is comprised of a total of 38,700 L of guar-iron slurry injected in FW-A1 and A2 between June 4 and 25, 1998. The down-gradient wall is comprised of 10 tonnes of a sand/iron mixture (11,500 L of guar-iron/sand in FW-B1 and B2, totaling 4.4 tonnes of iron and 5.6 tonnes of sand).

The sand was a clean, well sorted, coarse sand from a local supplier (R.F. Morse Ltd. Well Sand 00S). The second wall was not fully completed after problems were encountered during injection in the "frac well" FW-B1. The problems included loss of frac fluid pressure and azimuth control – due to migration of fines (or "piping") into wells RW-11 and RW-12.

Table 1. Summary of Events: MMR CS-10 - University of Waterloo Demonstration Project

Date(s)	Locations	Task
Oct. 1996	RW-1 to 23	Install wells for radar survey/water sampling
Nov. 1996 - May 1998	RW-1 to 23	Periodic of water level monitoring, sampling
Jul. 1997	RW-24 to 27	Install monitoring wells
Jul. 1997 - May 1998	RW-24 to 27	Periodic "pre-wall" sampling of wells
Sep. 1997	FW-A1, A2 FW-B1, B2	Install 160 mm ID frac wells
Oct. 1997	RW-9 to 15	Install resistivity strings
May 1998	RW-28, 29	Install monitoring wells
June 1998	RW-4, 5, 11, & 12	Pre-wall borehole deflection profiles
June 1998	RW-1 to 8, RW-12	Pre-wall hydraulic pulse testing
June 1998	FW-A1, A2 FW-B1, B2	Hydraulic fracturing of walls (see Table 2)
July 1998	RW-30	Install monitoring wells
July 1998 to present	RW-24 to 30	Periodic "post-wall" sampling of wells
Sep. 1998	See Table 3	Enzyme amendment

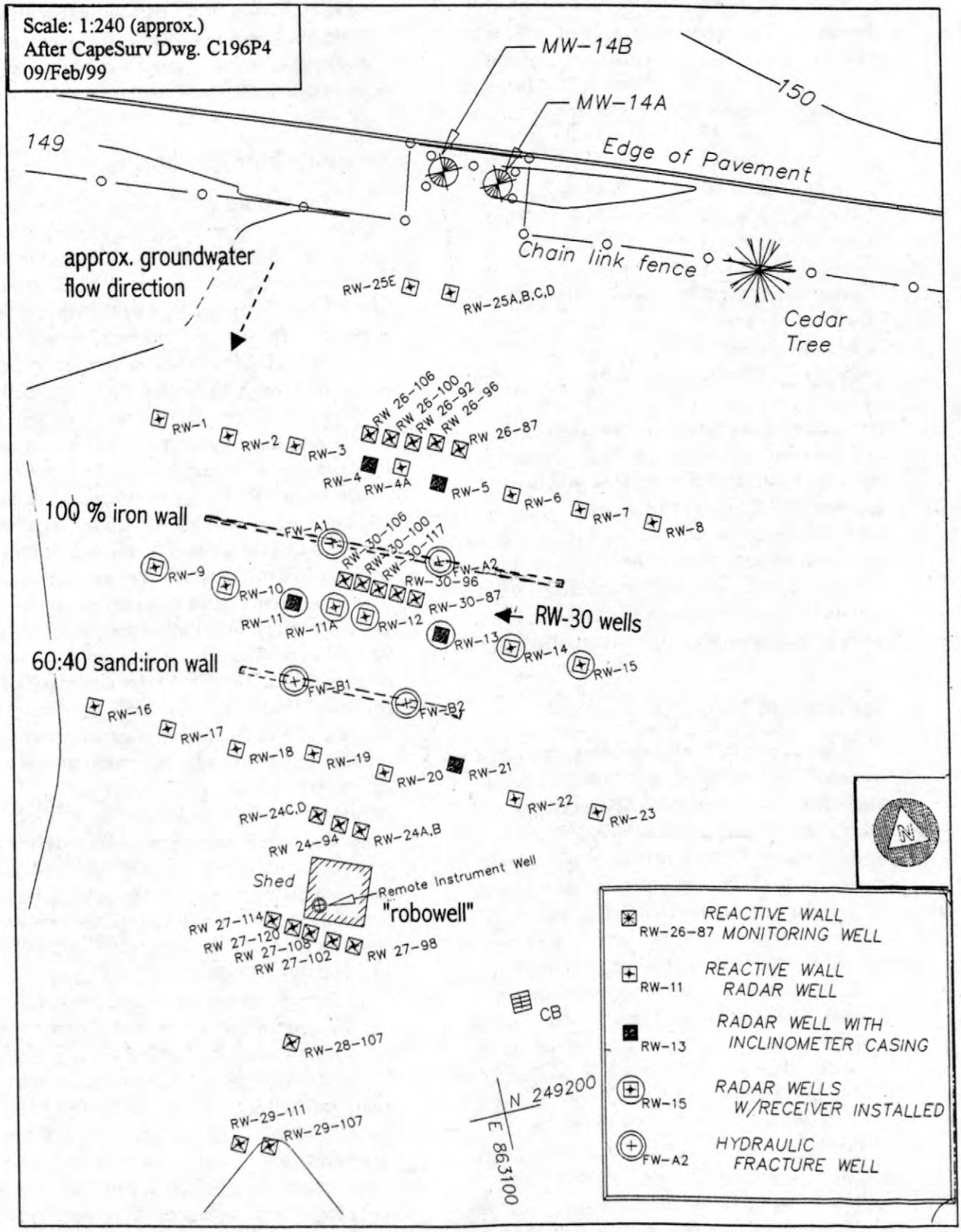

Figure 4. Site Plan showing locations of Frac Wells, monitoring wells and the approximate location of the two PRB's at the University of Waterloo reactive wall demonstration site, MMR, Cape Cod, MA.

Table 2. Summary of Iron Injection: MMR CS-10 - University of Waterloo Demonstration Project

Dates (1998)	Well No.	Weight of Iron (tonne)	Weight Sand (tonne)
Up-gradient (North) Wall - 100% iron			
June 4	FW-A1	8.51	0
June 10	FW-A1	2.50	0
June 11	FW-A2	3.29	0
June 24	FW-A2	6.58	0
June 24	FW-A1	6.01	0
June 25	FW-A2	13.04	0
Down-gradient (South) Wall - 40:60(wt.) iron/sand			
June 29	FW-B1	1.76	2.20
June 29	FW-B2	1.81	2.27
June 30	FW-B1	0.86	1.09

The piping of the natural soils into these wells was followed by flow of frac fluid – which was later found in these wells. It was decided to frac into FW-B2 only until the edge of the frac extended about 3 m beyond the frac well, before it reached the area around the RW-21 well, which was known to deviate to the north and intersect the proposed wall alignment. Thus, the down-gradient sand/iron wall is only partially complete.

Verification Monitoring

Installation of the up-gradient 100 percent iron wall was verified by active resistivity and borehole radar tomography, hydraulic pulse interference testing and borehole deflection measurements. The active resistivity mapping, together with the measurement of the iron-guar density and volume injected indicated that the up-gradient wall extends from about 14.8 m to more than 37 m depth and is about 80 mm thick on average. The average thickness is estimated based on dividing the volume of material installed by the area of wall as determined by the active resistivity. Further analysis of this data, together with the results of the hydraulic pulse testing and borehole deflection profiles, is in progress.

The down-gradient wall was studied using only the active resistivity and borehole radar methods. The active resistivity monitoring was operational, but not sufficiently constrained during the injections in FW-B1 due to the loss of the resistivity strings in two monitoring wells (RW-11 and RW-12). The results of the cross-hole radar survey of the partial south wall is reported in Lane *et al.*, 1999 (this volume). The results indicate a wall about 8 m wide and 10 m high extending from 27 to 37 m depth.

Groundwater Monitoring

The performance of the emplaced iron is being monitoring by inorganic and organic sampling and testing. Figure 5 shows the plume profile at the MW-30 cluster of wells installed about 1.5 m down-gradient of the 100 percent iron wall. The 3D coordinates of the 0.6 m screened wells have not been verified by borehole deviation testing, so it can only be assumed that they are 1.5 m from the iron wall over the depth of interest (26.5 to 35.7 m depth). Based on the PCE concentration and inorganic chemistry results to August 20, it was concluded that flow had not been re-established through the reactive zone and that the cross-link of the guar bio-polymer had not broken. This was consistent with concurrent results obtained by Golder Sierra at a commercial installation at another site using vertical hydrofracturing of the same iron and guar mixture, but at which the PRB was installed shallower than 15 m. To hasten the breakdown of the guar, it was decided to inject an amendment solution containing a higher proportion of enzyme known to break the cross-link of the hydroxypropyl guar and break the polysaccharide molecules further into sugars. The enzyme used is a proprietary blend, "Golder BE1", similar in composition to that used in the column testing described above – a blend of carbohydrate (CAS Reg. No. 63-42-3) and cellulase enzyme (CAS Reg. No. 9012-54-8).

From September 12 to 15, 1998, 9100 L of enzyme amendment was injected into each of monitoring wells RW-2 to RW-7 up-gradient of the north wall, RW-12, RW-13 up-gradient of the south wall and also the frac wells FW-A1, A2, B1 and B2 (Table 3). The solution contained enzyme blend dissolved in water obtained from the Otis water supply and adjusted to a pH of 3 to 3.5 using acetic acid. A sample of one of the injections had pH = 3.3, Eh = +205 mV and specific conductance = 630 µS/cm.

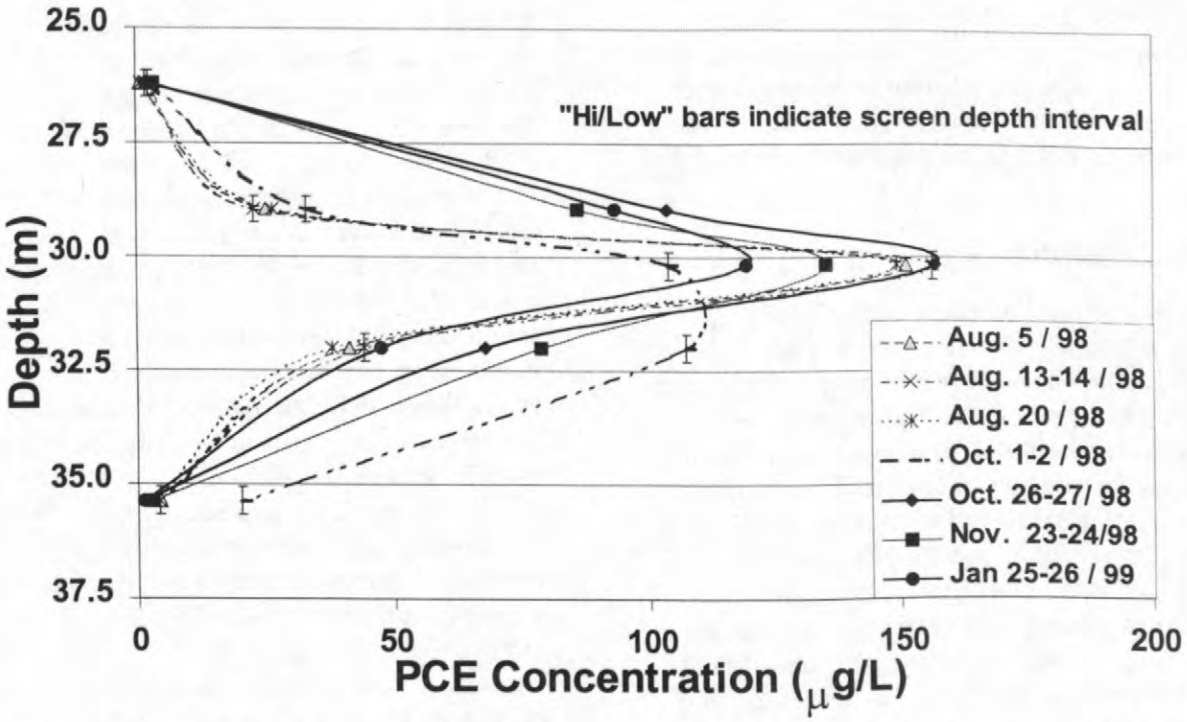

Figure 5. Profiles of CS-10 source area plume in RW-30 monitoring well cluster from August 5, 1998 to January 26, 1999.

Table 3. Enzyme Amendment Injections: MMR - University of Waterloo Demonstration Project

Date(s)	Locations	Injection Volume
Sep. 12	RW 2-5	9100 L each well
Sep. 13	RW-7, FW-A2, FW-A1	9100 L each well
Sep. 14	RW-3, 6, 13	9100 L each well
Sep. 15	RW-12, FW-B1, -B2	9100 L each well

The effects of the iron injections in June 1998 and the enzyme injection in September 1998 are being seen in the inorganic parameters measured in the down-gradient wells. The water in the cross-linked gel of the iron-guar injection was bound up and not mobile for a long period of time. The gel had a high concentration of salt (2 g/L NaCl) added for the active resistivity monitoring. Thus, the first down-gradient effects on inorganic parameters would not be that of zero-valent iron pore water coming through. Instead, complex effects would be due to a combination of:

- pressure increases during injection causing disturbance to the natural flow regime
- use of MMR water supply water in large quantities for flushing/cleaning of equipment - this water would be mobile
- enzyme/acid injections
- release of NaCl from the guar gel as it breaks

A further complication in assessing the flow regime is that the large volume associated with the enzyme amendment injection would have mounded the water table temporarily, but significantly, causing a perturbation in flow velocity and direction.

Monitoring records such as those available from an automated well (RW-24-102A) 15 m down-gradient of the 100 percent iron wall and 9 m down-gradient of the sand/iron wall (Granato and Smith, 1999, this volume) are useful in filling in data between discrete sampling dates. If the date of an activity or event is known, the "continuous" record can be used to calculate travel times. However, the data available to date from the automated well and from the other wells

at the site is not yet sufficient to conclude that flow through the treatment zone(s) has been established or that treatment in the reactive zone is occurring as expected. On-going sampling of the groundwater and monitoring and analysis of the inorganic and organic parameters is planned.

CONCLUSIONS

A method to emplace commercially available granular iron in a vertical PRB up to 75 or 100 mm thick and at depths of up to 37 m (and probably to > 60 m in some geologic formations) has been demonstrated. It has also been shown that granular iron can be emplaced as a uniform sand / iron / guar mix, which may be required for thin walls containing more highly reactive "enhanced iron". Further monitoring and analysis of groundwater chemistry down-gradient of the walls is required before estimates of field treatment rate can be made. Further testing of a revised guar-iron-enzyme mix design in field scale applications is required. At deep sites the deviation of monitoring wells and other drilled wells must be measured so that their proximity to the PRB can be accounted for in the installation procedure and the analysis of results.

ACKNOWLEDGMENTS

The authors thank AFCEE and the Army National Guard at MMR for funding the work and the U.S. Geological Survey for research cooperation and logistical support, especially Denis LeBlanc and Jennifer Savoie.

REFERENCES

Gillham, R.W., 1996, In Situ Treatment of Groundwater: Metal-enhanced Degradation of Chlorinated Organic Contaminants. In *Advances is Groundwater Pollution Control and Remediation*, p 249-274. Kluwer Academic Publishers, Netherlands.

Granato, G.E., and Smith, K.P., 1999, Robowell: A reliable and accurate automated data collection process and method applied to reactive wall monitoring at the Massachusetts Military Reservation, Morganwalp, D.W., and Buxton, H.T., eds., 1999, U.S. Geological Survey Toxic Substances Hydrology Program--Proceedings of the Technical Meeting, Charleston, South Carolina, March 8-12, 1999-- Volume 3 – Subsurface Contamination from Point Sources: U.S. Geological Survey Water-Resources Investigations Report 99-4018C, this volume.

Hubble, D.W., Gillham, R.W. and Cherry, J.A., Emplacement of Zero-valent Metal for Remediation of Deep Contaminant Plumes, Proceedings, 1997 International Containment Technology Conference and Exhibition, Feb. 9-12, St. Petersburg, Florida.

Lane, J.W., Joesten, P.K., and Savoie, J.G., 1999, Monitoring a permeable reactive wall installation in unconsolidated sediments using a cross-hole radar method. Morganwalp, D.W., and Buxton, H.T., eds., 1999, U.S. Geological Survey Toxic Substances Hydrology Program--Proceedings of the Technical Meeting, Charleston, South Carolina, March 8-12, 1999-- Volume 3 -- Subsurface Contamination from Point Sources: U.S. Geological Survey Water-Resources Investigations Report 99-4018C, this volume.

LeBlanc, D.R., 1984, Sewage plume in a sand and gravel aquifer, Cape Cod, Massachusetts: U.S. Geological Survey Water-Supply Paper 2218, 28 p.

Masterson, J.P., Walter, D.A. and Savoie J., 1996, Use of Particle Tracking to Improve Numerical Model Calibration and to Analyze Ground-Water Flow and Contaminant Migration, Massachusetts Military Reservation, Western Cape Cod, MA.

AUTHOR INFORMATION

David W. Hubble and Robert W. Gillham, Institute for Groundwater Research, Department of Earth Sciences, University of Waterloo, Waterloo, Ontario, Canada (e-mail address: dwhubble@engmail.uwaterloo.ca)

Monitoring A Permeable Reactive Iron Wall Installation In Unconsolidated Sediments By Using A Cross-Hole Radar Method

By John W. Lane, Jr., Peter K. Joesten, and Jennifer G. Savoie

ABSTRACT

Cross-hole common-depth (CD) radar scanning was used at the Massachusetts Military Reservation (MMR) in Cape Cod, Massachusetts, to monitor pilot-scale testing of a hydraulic-fracturing method to install permeable reactive zero-valent iron walls in unconsolidated sediments. The pilot-scale study was undertaken to assess the feasibility of using zero-valent iron to remediate ground water that is contaminated with chlorinated solvents at depths exceeding the range of conventional iron wall installation methods. The pilot-scale test was conducted at the site near the source area of Chemical Spill 10 (CS-10), a chlorinated-solvents plume that underlies the MMR. Two iron walls 5 meters (m) apart and 12 m long were designed to intersect the contaminated ground water at depths ranging from 24 to 37 m below land surface.

A series of post-installation cross-hole CD radar-scanning surveys were conducted in boreholes installed on opposite sides of the walls. The presence of iron significantly reduces the radar-pulse amplitude and can be identified using CD radar scanning. Significant decreases in cross-hole radar-pulse amplitude were observed in field data after the iron walls were installed. Changes in cross-hole radar-pulse amplitudes observed in the field data were compared to results of two-dimensional finite-difference time-domain models used to predict the effects of holes in the wall and wall edges. Analysis of these data from the south wall indicates the presence of an irregularly shaped wall about 8 m wide, extending from about 27 to 37 m below land surface. Analysis of data from the north wall is presently underway.

INTRODUCTION

Zero-valent iron has been used to remediate ground water that is contaminated with chlorinated solvents at more than a dozen sites in North America and Europe (Gillham and O'Hannesin, 1994). At many of these sites, a 'funnel and gate' technology has been implemented utilizing impermeable barriers to channel ground water through a permeable zone that contains zero-valent iron filings (Starr and Cherry, 1994, Smyth and others, 1996). An impermeable barrier, which often consists of sheet pilings, channels ground water towards a 'gate', which is filled with granular iron. At some sites, contaminated ground water is too deep to use the 'funnel and gate' method.

At the Massachusetts Military Reservation (MMR) at Cape Cod, Massachusetts, contaminated ground water near the source area for the Chemical Spill 10 (CS-10) plume (fig. 1), which contains tetrachloroethylene (PCE) and trichloroethylene (TCE), is located between 24 and 37 meters (m) below land surface. Because these depths exceed the practical limits of the normal 'funnel and gate' construction approach, the CS-10 site required an alternative installation approach. The method of installation that was selected was hydraulic fracturing (Hubble and others, 1997). The hydraulic-fracturing method uses a proprietary injection technology to install permeable reactive iron walls in unconsolidated sediments (Grant Hocking and S.L. Wells, Golder Sierra LLC, written commun., 1997). A pilot-scale test of their installation method was conducted near the CS-10 plume source area at MMR in which two iron walls were designed to intersect the contamination between 24 and 37 m below land surface.

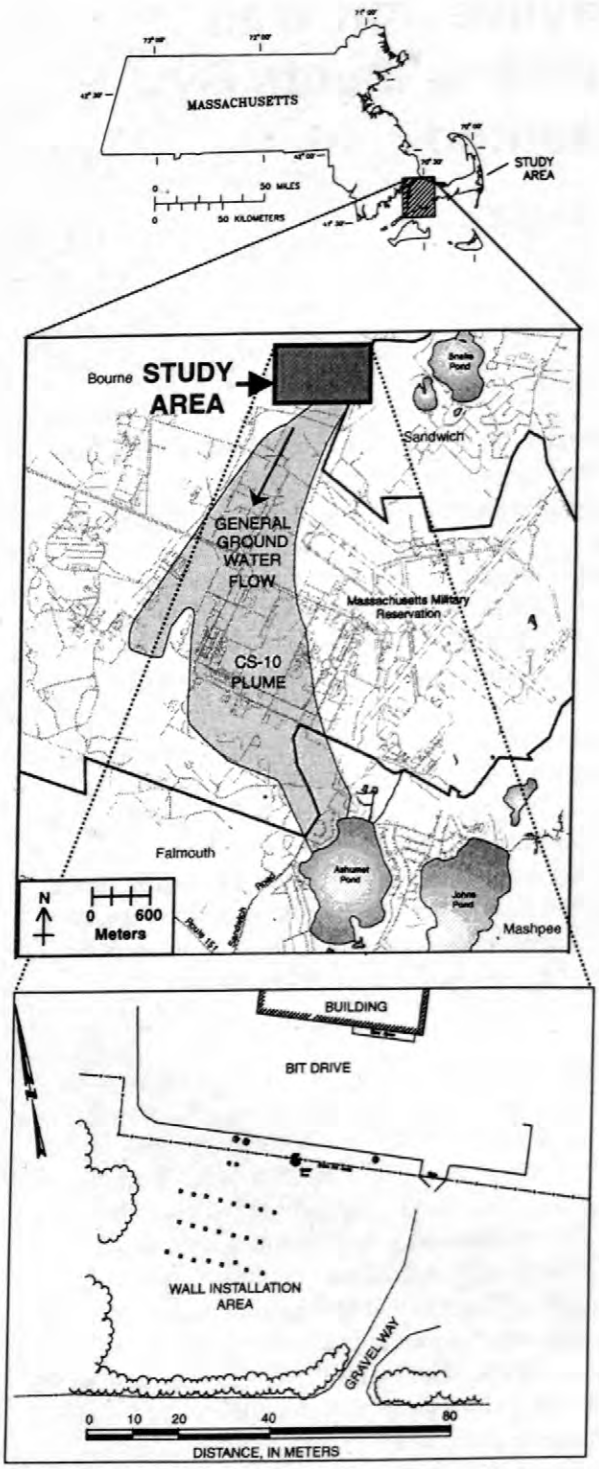

Figure 1. Location of the study area and the CS-10 plume, Massachusetts Military Reservation (MMR), Cape Cod, Massachusetts.

The geometry of the iron walls was estimated using borehole-radar surveys conducted in 21 boreholes installed on opposite sides of the iron walls (fig. 2). The presence of the iron significantly reduces the radar-pulse amplitude, and can be identified using CD radar scanning. A two-dimensional finite-difference time-domain model (Xiao and others, 1998) was used to predict the effects of holes in the wall and wall edges on cross-hole radar amplitudes. This paper presents results of numerical modeling and analysis of cross-hole CD radar field data at the south wall.

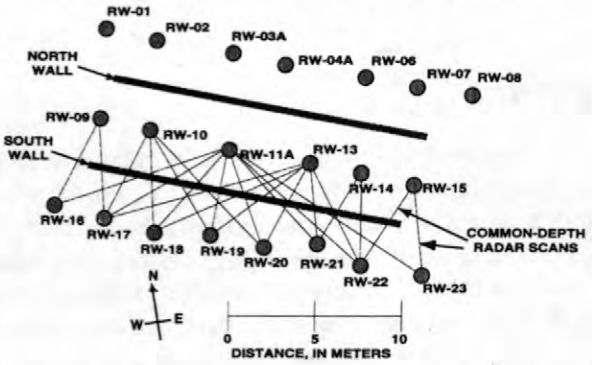

Figure 2. Map view of the 7-centimeter plastic-cased observation boreholes at the MMR reactive wall site. 250 MHz cross-hole CD radar scans collected over the south wall after installation are shown.

NUMERICAL MODELING

A cross-sectional two-dimensional finite-difference time-domain model (Xiao and others, 1998) was used to predict the effects of holes in a wall and wall edges on cross-hole radar amplitudes. The simulation grid contains 5-centimeter (cm) by 5-cm cells, and spans 12.8 m (256 cells) in the horizontal direction perpendicular to the wall, and 12.8 m (256 cells) in the vertical direction. A 2.5-m (50 cell) super-absorbing boundary surrounds the model to reduce model-edge reflection effects. The electromagnetic properties of the model interior are consistent with field measurements at the MMR site. The model simulates a saturated sand with a relative dielectric permittivity (ε_r) of 25, an electrical conductivity (σ) of 0.01 siemens per meter (S/m), and a relative magnetic permeability (μ_r) of 1. Due to the electrical conductivity of iron (1 x 10^7 S/m) (Carmichael, 1989), the wall was approximated as a 10-cm thick near-perfect reflector. The cross-hole radar pulse was simulated using a 250-Megahertz (MHz) Ricker wavelet, with a wavelength of 24 cm in the

saturated sand, which is considered a reasonable approximation of the field data. Model responses were sampled at 5270 MHz using 1024 samples per waveform.

Models were used to predict the effects of holes in the wall on cross-hole radar data. The modeled wall contains holes having apertures ranging from 0- to 60-cm (0 to 2.50 wavelengths) in 5-cm (0.208 wavelength) increments. In the simulations, the transmitting and receiving antennas are 6.30 m apart, centered over the modeled hole in the wall (fig. 3).

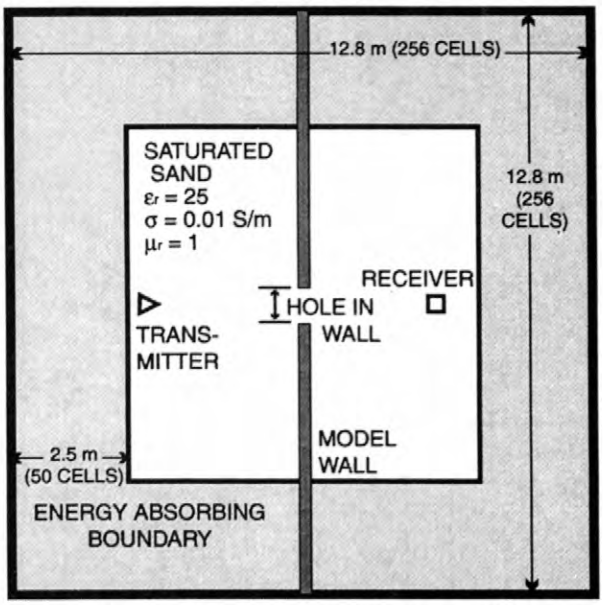

Figure 3. Model wall with hole in the wall ranging from 0 to 60 cm (0 to 2.50 wavelengths).

Numerical modeling results demonstrate the effect of the wall hole-size on radar-pulse amplitude. Radar-pulse amplitude increases as hole-size increases (fig. 4). Minor differences in radar-pulse amplitude observed for holes smaller than 10 cm suggest that the lower limit of hole-size detection is about 40 percent of the radar-pulse wavelength.

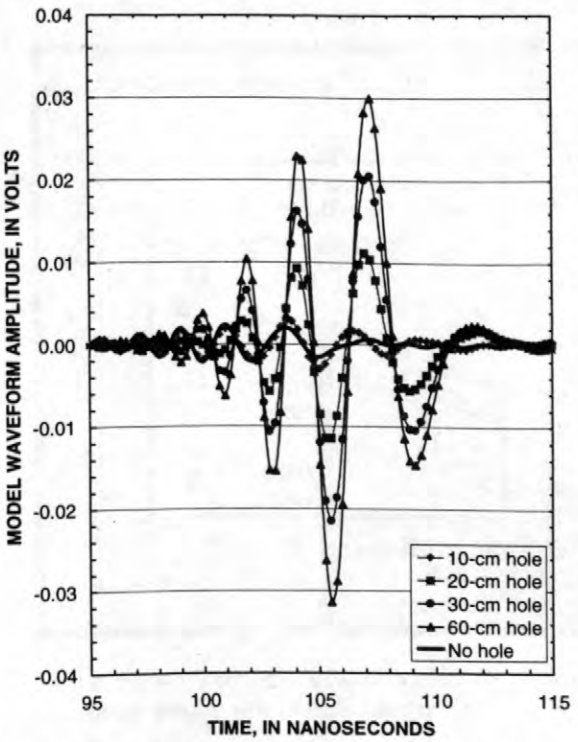

Figure 4. Radar model waveform data as a function of time with holes ranging in aperture from 0 to 60 cm (0 to 2.50 wavelengths).

Models also were constructed to predict the effects of wall edges on cross-hole radar data. These models contain a wall that extends vertically from the center of the model to the model boundary (fig. 5). The modeled separation between the radar transmitter and receiver ranges from 5.00 to 7.25 m, which is consistent with field conditions. The models simulate a CD cross-hole scan by stepping the transmitter and receiver location along the model at 10-cm intervals. Results of these simulations over the range of transmitter-receiver separations modeled show that the top of the wall consistently correlated to a depth where the pulse amplitude had decreased to about 43 percent of the normalized 'background' wave amplitude (fig. 6).

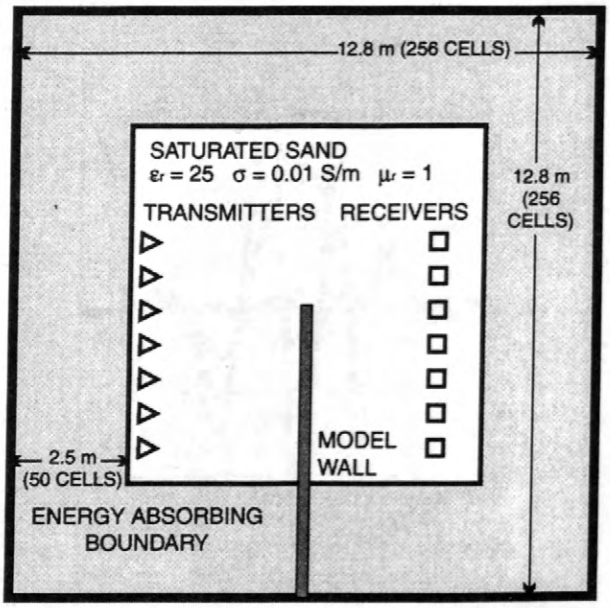

Figure 5. Model geometry used to determine the effects on radar waves due to the edges of the wall.

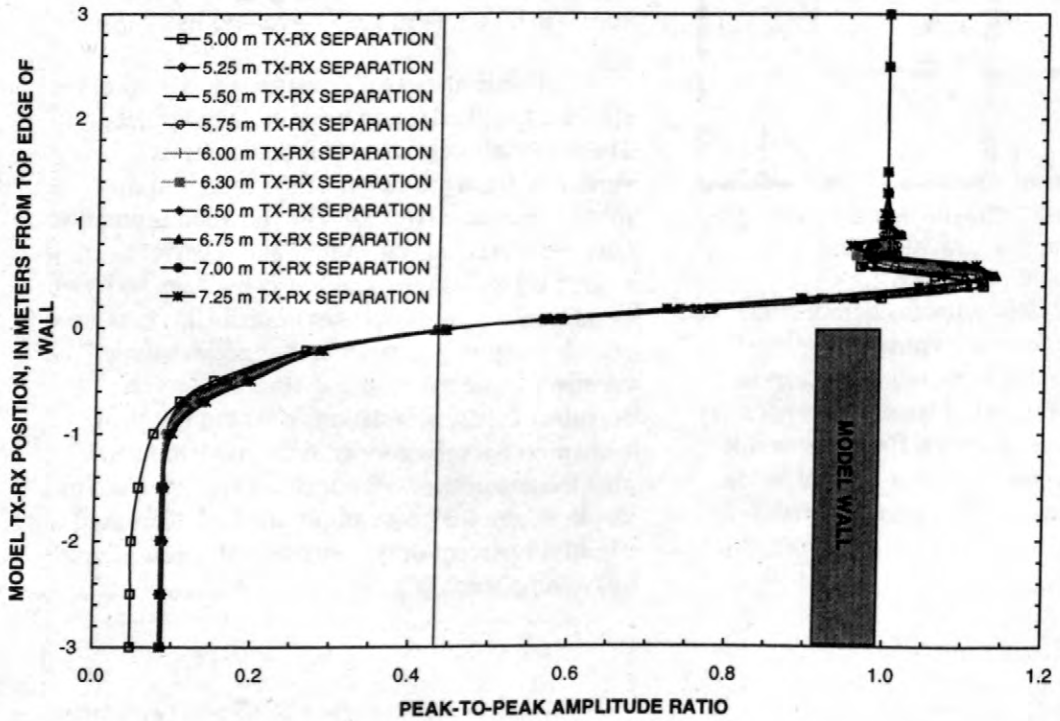

Figure 6. Model amplitudes normalized to unaffected amplitudes, for transmitter (TX) – receiver (RX) separations ranging from 5.00 to 7.25 meters plotted from 3 m above top edge to 3 m below top edge of the wall.

Results of the 'hole in the wall' models and 'edge' effect models shown in figures 4 and 6 can be used to help interpret field radar data to identify discontinuities in the wall and estimate wall dimensions.

FIELD METHODS

CD cross-hole radar surveys were conducted after iron wall installation at the MMR. Radar data were collected using a Malå GeoScience RAMAC[1] borehole radar system with electric-dipole antennas with center frequencies of 100 and 250 MHz. Electromagnetic waves of cross-hole radar are sensitive to the electrical conductivity of iron. The amplitude of an electromagnetic wave propagating between the radar transmitter and receiver that intersects a region containing iron will decrease with respect to 'background' radar-pulse amplitudes. CD cross-hole scans were conducted from boreholes on opposite sides of the wall (fig. 2). CD cross-hole scans were acquired by lowering the transmitter and receiver at 10-cm increments from the top of the 7-cm plastic casing to the bottom of the boreholes.

DATA ANALYSIS

The CD cross-hole radar-data was analyzed to identify decreases in radar-pulse amplitude induced by iron absorption. Radar-pulse amplitudes were normalized to the average amplitude of cross-hole scans below 40 m, where a normalized value of 1.00 implies a 'background' value. The scans below 40 m were used to determine the mean "background" amplitude because these scans are several meters below the expected bottom of the wall. Figure 7 shows normalized CD cross-hole data between boreholes RW-20 and RW-13 (fig. 2). Amplitude changes caused by the iron wall and the results of numerical modeling are shown (fig. 7). The numerical model results were fit to the field data by changing the length of the wall (fig. 8). Based on this analysis, the section of wall between boreholes RW-20 and RW-13 is about 3.10 m in length, and extends from 31.7 m to 34.8 m below the top of casings.

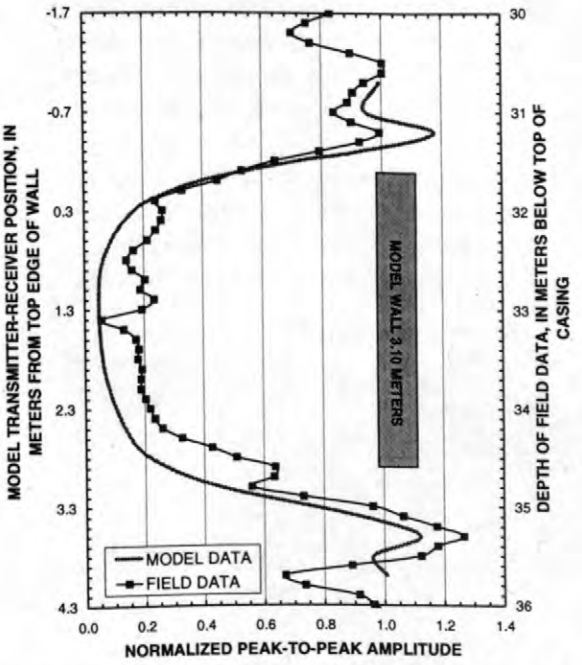

Figure 7. Comparison of normalized model wall amplitude for a 3.10-meter wall and the normalized field data amplitude from the CD radar survey between boreholes RW-20 and RW-13, MMR, Cape Cod, Massachusetts.

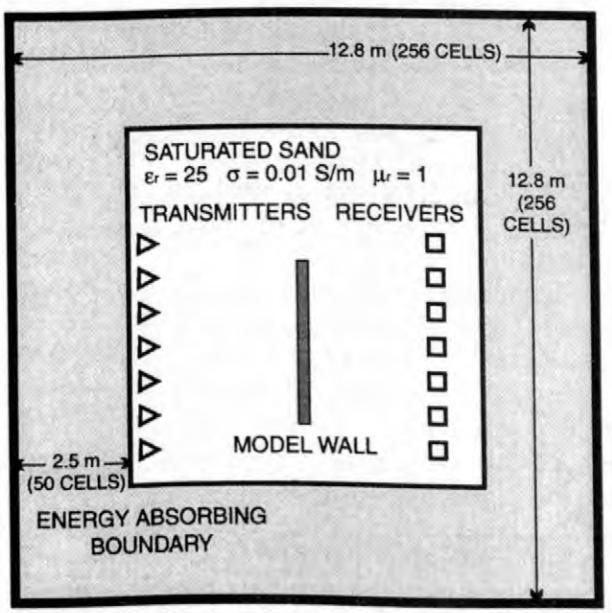

Figure 8. Model configuration to determine the extent of the wall.

After normalization, all of the field data were combined into contoured cross-section plots. Figure 9 shows data along the cross-sectional

[1] The use of trade names in this report is for identification purposes only and does not constitute an endorsement by the U.S. Geological Survey.

extent of the south wall, by use of the ray paths that cross the south wall (fig. 2). Normalized amplitudes below the value of 84 percent, which is the median value of the normalized amplitude data, outline an irregularly shaped zone about 9 m wide and 12 m high. Horizontal bands extend outward from the main zone. These 'stringers' could be a result of the presence of salt water, suspension gel used in the hydraulic-fracturing process, or iron particles moving into higher permeability zones within the saturated sediments.

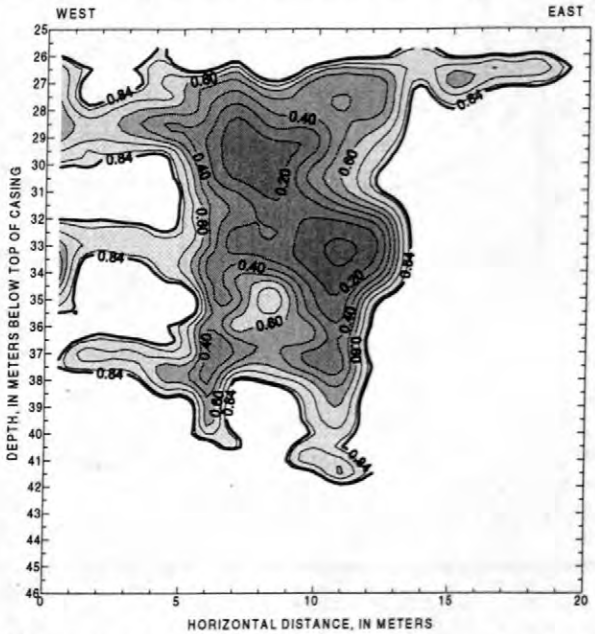

Figure 9. Cross-section plot of the normalized transmission amplitude data collected over the south iron filing wall, MMR, Cape Cod, Massachusetts. The 0.84 contour represents the median value of the normalized amplitude data.

The outline of the south wall using the results of the 'edge' model simulations are superimposed in figure 10. The wall edge is defined as the 43-percent normalized wave amplitude contour. The field data are complex, containing small-scale structures that could be interpreted as isolated small zones or stringers of iron; this demonstrates the need for additional modeling and analysis of the CD cross-hole data. However, based on numerical modeling results to date and the analysis of cross-hole radar field data from the south wall, the hydraulic fracturing produced an irregularly shaped wall that is about 8 m wide and 10 meters high and extends from about 27 to 37 m below land surface.

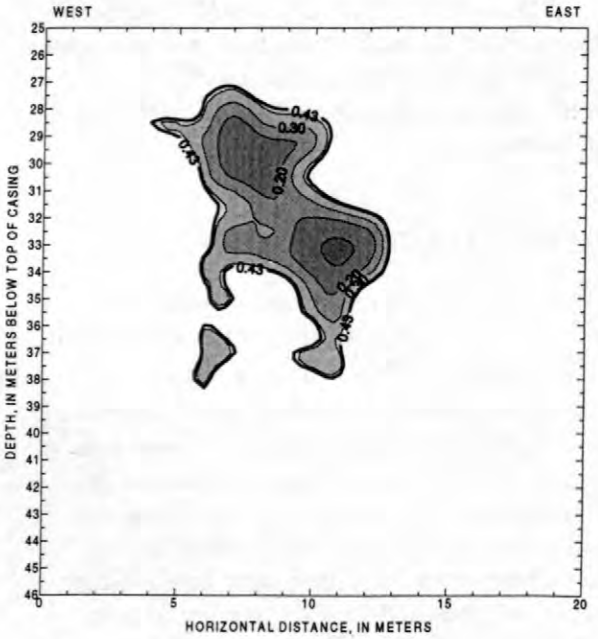

Figure 10. Cross-section plot of the normalized transmission amplitude data collected over the south iron filing wall with the estimated edges of the wall superimposed, MMR, Cape Cod, Massachusetts. The 0.43 contour represents the edges of the wall based on numerical modeling.

CONCLUSIONS

Cross-hole CD radar scanning was used at the Massachusetts Military Reservation in Cape Cod, Massachusetts, to monitor the pilot-scale testing of a hydraulic-fracturing method to install permeable reactive iron walls in unconsolidated sediments. The pilot-scale study was undertaken to assess the feasibility of using zero-valent iron to remediate ground water that is contaminated with chlorinated solvents at depths exceeding the range of conventional iron wall installation methods. The pilot-scale test site was conducted near the source area of Chemical Spill 10 (CS-10), a chlorinated-solvents plume that extends across the MMR. Two 12-m-long iron walls were designed to intersect contamination detected between about 24 and 37 m below land surface.

A series of post-installation cross-hole common-depth radar scanning surveys were conducted in rows of boreholes installed on opposite sides of the walls. Significant decreases in cross-hole radar-pulse amplitude are observed in field data after installation of the iron walls.

Changes in cross-hole radar-pulse amplitude observed in field data were compared to results of two-dimensional finite-difference models that predict the effects of holes in the wall and wall edges on radar-pulse amplitudes. Based on numerical modeling results, preliminary analysis of cross-hole radar field data from the south wall indicate the hydraulic fracturing produced an irregularly shaped wall about 8 m wide, extending from about 27 to 37 m below land surface. Interpretation of small-scale structures that may be stringers of iron will require additional modeling and analysis of the CD cross-hole data.

ACKNOWLEDGMENTS

The authors thank the Air Force Center for Environmental Excellence at the Massachusetts Military Reservation and the Army National Guard for funding the work on this project. The authors thank Lei Xiao and Dr. Lanbo Liu of the University of Connecticut for the use of the finite-difference model and for their guidance with the modeling.

REFERENCES

Carmichael, R.S., 1989, Practical handbook of Physical Properties of Rocks and Minerals: Boca Raton, Florida, CRC Press, Inc., p. 373.

Gillham, R.W., and O'Hannesin, S.F., 1994, Enhanced degradation of halogenated aliphatics by zero-valent iron: Ground Water, v. 32, no. 6, p. 958-967.

Hubble, D.W., Gillham, R.W., and Cherry, J.A., 1997, Emplacement of zero-valent metal for remediation of deep contaminant plumes: *in* International Containment Technology Conference, St. Petersburg, Florida, February 9-12, 1997, Proceedings: Tallahassee, Florida, Florida State University, p. 872-878.

Smyth, D.J.A., Shikaze, S.G., and Cherry, J.A., 1996, Hydraulic performance of permeable barriers for in situ treatment of contaminated groundwater: Rumer, R.R. and Mitchell, J.K, eds., Assessment of Barrier Containment Technologies: A Comprehensive Treatment for Environmental Remediation Applications: Springfield, Virginia, National Technical Information Service, p. 881-886.

Starr, R.C., and Cherry, J.A., 1994, In Situ Remediation of Contaminated Ground Water: The Funnel-and-Gate System: Ground Water, v. 32, no. 3, p. 465-476.

Xiao, Lei; Liu, Lanbo; and Cormier, V.F., 1998, Two dimensional finite-difference time-domain solution for Maxwell's equations using pseudo-spectral method: *in* Seventh International Conference on Ground Penetrating Radar (GPR'98), Lawrence, Kansas, May 27-30, 1998, Proceedings: Lawrence, Kansas, Radar Systems and Remote Sensing Laboratory, p. 585-589.

AUTHOR INFORMATION

John W. Lane, Jr. and Peter K. Joesten, U.S. Geological Survey, Storrs Mansfield, Connecticut (jwlane@usgs.gov, pjoesten@usgs.gov)

Jennifer G. Savoie, U.S. Geological Survey, Marlborough, Massachusetts (jsavoie@usgs.gov)

Robowell: A Reliable and Accurate Automated Data-Collection Process Applied to Reactive-Wall Monitoring at the Massachusetts Military Reservation, Cape Cod, Massachusetts

By Gregory E. Granato and Kirk P. Smith

ABSTRACT

Robowell was developed and tested by the U.S. Geological Survey (USGS) to automatically monitor ground-water quality. Robowell follows standard manual-sampling protocols that require monitoring and recording of properties and constituents in water pumped from a well or multilevel sampler until purge criteria have been met. The Robowell process can be used to identify changes in ground-water quality on a real-time basis without the cost of sample collection, processing, and analysis. This automated process can be tailored for different applications.

Six Robowell units have reliably sampled water in different well designs and geochemical environments during all four seasons of the year since 1994 to produce accurate real-time ground-water-quality records that are more than 96 percent complete. Performance has been verified with a program of regular quality-control samples obtained by using independent water-quality probes, manual measurements, and laboratory analyses throughout the period of record. Results of the quality-control program indicate that from 80 to more than 95 percent of the measurements of specific-conductance, pH, and dissolved-oxygen would be rated as good or better on the basis of draft USGS guidelines for water-quality measurements. These results verify the integrity of the automated-sampling records and demonstrate that the automated monitoring system can accurately measure ground-water quality over a large range of geochemical conditions.

A Robowell technology demonstration unit was installed and run on Cape Cod at the Massachusetts Military Reservation with the assistance of the USGS Toxic Substances Hydrology Research group. This unit was run to test the technology and to monitor geochemical changes caused by emplacement of a zero-valent, iron reactive wall designed to remediate volatile organic compounds in ground water. The monitoring unit recorded substantial changes in ground-water quality in a short period as the reaction byproducts of the wall and a subsequent enzyme/pH adjustment raised pH by almost a full unit, raised specific conductance by about 800 µS/cm (microsiemens per centimeter at 25 degrees Celsius), and completely depleted the dissolved oxygen in water from the well. The automated monitoring system demonstrated its success as a sentry well by notifying the project chief through phone calls from a voice modem that geochemical changes had been detected. Real-time records at the site define the variability in ground-water quality during the monitoring period.

INTRODUCTION

Most of the costs involved in operating a ground-water monitoring network are associated with labor and the materials required for manual water-sample collection (Zhou, 1996). Minimizing the cost of ground-water monitoring programs by using statistical strategies to reduce sampling frequency may result in data that are inadequate to (1) determine representative mean (or median) values of water-quality properties and constituents; (2) detect long-term trends, periodic fluctuations, and abrupt changes in water quality; and (3) verify the accuracy of the resulting

estimates of the trends (Johnson and others, 1996; Zhou, 1996). Process automation is an alternative to manual methods, but searches of the literature, ground-water-monitoring equipment supply catalogs, and patent records did not reveal any automated monitoring devices or processes that meet currently accepted ground-water-quality sampling protocols.

The complexity of the search for an appropriate automated monitoring system is compounded by long-standing debates about appropriate ground-water-monitoring protocols. Debate about the proper sampling methods and protocols appropriate for a given site will always exist because the ground water and aquifer materials surrounding each monitoring well have unique physical and chemical characteristics that can change through time. Sampling equipment and purging protocols appropriate to a site are necessary to obtain consistent measurements that are representative of aquifer-water quality (Herzog and others, 1991; Koterba and others, 1995; Stone, 1997). Therefore, to obtain consistent and representative measurements, automated monitoring techniques ideally would follow the same protocols selected for manual sample collection. Historically, automated ground-water-quality monitoring has been done using passive monitoring devices, but these devices do not collect data using methods that are comparable with manual-sampling protocols. Thus, the comparability of the passive-monitoring record obtained from an automatic-monitoring probe and the results of analysis of water samples obtained from a well is uncertain (Smith and Granato, 1998).

The U.S. Geological Survey (USGS) developed a process and assembled prototype sets of instrumentation and equipment that can be used to automatically monitor ground-water-quality properties and constituents using established sampling protocols. The technology was developed under a grant from the USGS Technology Enterprise Office, and a patent is pending on the process and device (Granato and Smith, 1998). This automated monitoring system provides data that are consistent with results of analysis of ground-water samples collected manually. Robowell was designed to monitor ground-water quality in real time and to provide the operators with the information needed to optimize manual sampling efforts at a ground water monitoring site. This paper briefly describes this automated process, documents results of a quality-assurance and quality-control (QA/QC) program, and presents a case study done with the assistance of the USGS Cape Cod Toxic Substances Hydrology Research Group.

ROBOWELL: THE PROCESS

Robowell is an automated process that was developed and tested by the USGS to provide a method for monitoring ground-water quality that meets accepted manual sampling protocols without incurring high labor and laboratory costs associated with frequent manual sampling efforts. The process embodies a series of programmed instructions that activate the equipment on a preset schedule to monitor and adjust the status of the system as it purges the well and records measurements. If the system is functioning properly, water-quality properties and constituents are monitored and recorded until purge criteria are met. An example of one implementation of the Robowell process is shown in figure 1. Typically, a system using the process would (1) activate itself as programmed, (2) perform a series of self-tests, (3) measure the water level in the well, (4) calculate the purge volume, (5) measure and record values of water-quality properties and constituents during the purge cycle, (6) determine and record the final values of the properties and constituents, and (7) return to an inactive mode. If errors are detected, the system records error codes along with measured values for the sampling interval before returning to the inactive mode. The system's computer program uses information from system feedback, water-quality measurements, and the internal clock to automatically control the process. Normal operations can be suspended or modified in response to errors in system feedback, remote control through a communications link, or direct control by technical staff maintaining the system.

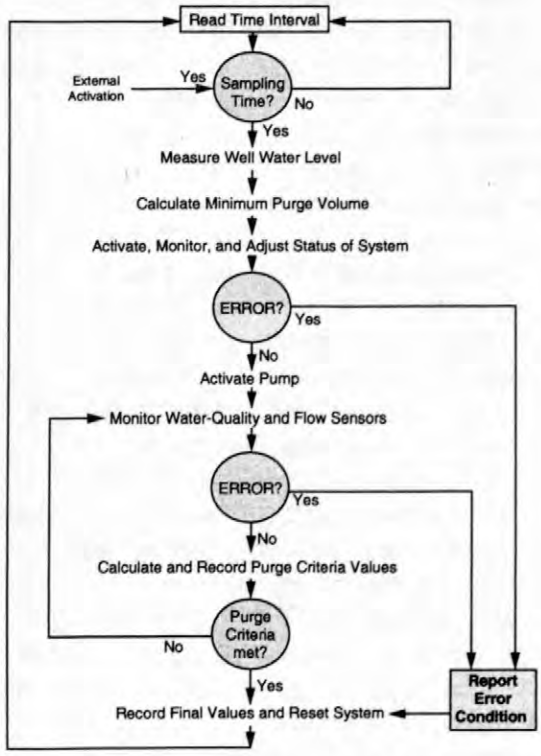

Figure 1. Generalized example of a process flow chart for the Robowell automated ground-water monitoring system.

The Robowell process is an improvement over passive automated ground-water-monitoring systems because measurements made by Robowell are directly comparable to measurements made by manual sampling. Information from periodic manual sampling events during a comparative test of active and passive automated monitoring methods indicates that passive measurements may be substantially biased in relation to measurements made using standard manual-sampling protocols, even in short-screen water-table monitoring wells (Smith and Granato, 1998). Unlike passive monitors, Robowell pumps and purges the well or multilevel sampler while measuring values of each prespecified water-quality property and constituent until standard purge criteria (Herzog and others, 1991; Koterba and others, 1995) have been met. Additionally, all measured values are recorded during the purge cycle to document that final recorded values are representative of water in the aquifer.

The Robowell process can be used to detect changes in ground-water quality on a real-time basis and at a lower cost than that required for manual sample collection with subsequent processing and analysis. Properties such as water temperature, specific conductance, and pH are indicators of ground-water quality (Hem, 1992) and, therefore, changes in these properties indicate changes in ground-water quality. A record of relatively frequent measurements of water-quality properties and(or) constituents made at a ground-water monitoring site can provide the context for the interpretation of periodic discrete samples collected for laboratory analysis. The record can be used with the discrete samples to identify an abrupt arrival of a contaminant plume, trends caused by a diffuse source of contaminants, or an analytical error in a discrete sample analysis. Detection of substantial changes in measured values by remote query can prompt a visit to the field installation for manual measurements. Independent manual field measurements and recalibration of the monitoring probes with a separate measuring device resets the system and further verifies recorded values. If changes in water quality are substantiated by calibration and independent manual field measurements, a sample can be collected for further documentation by laboratory analysis. The automated process can supply information needed to decide when the collection of a water sample for laboratory analysis would best meet the objectives and the QA/QC design of the monitoring effort.

The automated process is designed so that it can be tailored for different applications. Purge criteria appropriate for different types of chemical constituents, sampling installations, and hydrogeologic regimes (Robin and Gillham, 1987; Herzog and others, 1991; Koterba and others, 1995) can be used, and changes in purge criteria can be accommodated as new ground-water-sampling information becomes available.

The process is designed so that commercially available sampling equipment and instrumentation can be selected on the basis of the nature of the contaminants to be measured, the hydrogeology of the site, and site logistics such as available power and communications (Granato and Smith, 1998). Also, the process--if operated

from a local base station--can be used to monitor one or several closely spaced wells or multilevel sampling ports. The instruments and equipment typically used to implement the process at research sites are more complex than would be necessary for some applications. The system typically includes a Campbell Scientific Incorporated (CSI) CR10 data logger[1] as the control module for the process and a CSI SM192 solid-state storage device to store data. Because electric and phone services typically are not economically feasible at field sites, batteries recharged by solar panels are used to power the controllers and other instruments, nitrogen gas is used to inflate a packer each time the system is activated and to power the QED bladder pumps through a pneumatic logic controller, and a CSI DC112 telephone modem is used for communications. The water level in the water-table well is monitored with a Keller pressure transducer (operating range of 0-0-2.5 pounds per square inch). A hand-operated Plastomatic three-way valve is placed near the beginning of the flow train to divert water for manual collection of samples. A 1/2-inch Data Industrial flow sensor is used to monitor the flow rate of ground water pumped through the system during purge and recording cycles. A Hydrolab Multiprobe, with a flow cell, is used as a control module for the water-temperature, pH, specific-conductance, and dissolved-oxygen probes under data-logger control. For some applications, however, the process could be implemented with only a dedicated pump, a conductance probe, and a simple data logger using solar/battery power.

ROBOWELL: A RELIABLE AND ACCURATE DATA-COLLECTION PLATFORM

Six Robowell monitoring units have been in operation at one time or another since December, 1994. The units have sampled water during all four seasons of the year under various hydrogeologic conditions, well designs, and geochemical environments. In total, the six units have operated reliably for more than 881 days to produce data that were consistently verifiable when manual check measurements were performed. During these sampling periods, the units were not in operation an additional 30 days because of technical difficulties. These 30 days represent only about 3.4 percent of the period of record. About 14 of these days of lost record occurred during the operating period for the second unit and were caused by freezing conditions. Design changes in the subsequent prototypes have resolved this problem.

When each prototype is emplaced and activated, a series of QA/QC measures is initiated to ensure that the system is collecting valid measurements that are equivalent to measurements obtained by accepted manual sampling methods. Each system is constructed of inert materials that have been demonstrated to be appropriate for constituents of interest. The components of each system are washed, acid-leached, and rinsed with deionized water to ensure that the system is thoroughly clean before installation. Equipment blanks are analyzed to ensure that the system is not contributing constituents of interest to the water sampled. Once the system is emplaced, the water-quality probes are maintained by performing precalibration measurements with standard solutions, cleaning and maintaining probe components, and recalibrating with attention to changes in the slope and intercept of probe calibration data.

A program of regularly collected quality-control (QC) samples obtained by using independent water-quality probes, manual measurements, and laboratory analyses is necessary to demonstrate the accuracy and precision of the data collected. Results of the QC program for the specific-conductance measurements (fig. 2) demonstrate that the automated method produces valid, accurate, and precise measurements when compared to traditional manual measurements. Examination of the specific-conductance measurements reveals that 93 percent of the 44 QC samples were within ±5 percent and 95 percent of QC samples were within ±10 percent of manual and laboratory

[1] The use of brand/firm/trade names in this report is for identification purposes only and does not constitute endorsement by the U.S. Geological Survey.

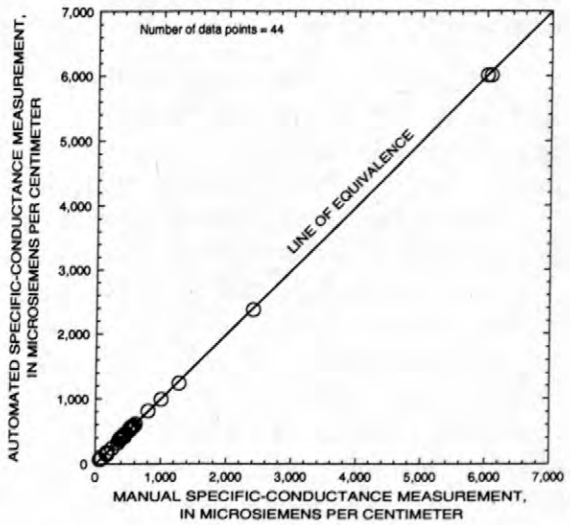

Figure 2. Relation between automated and manual quality-control measurements of specific conductance from several automated ground-water-quality monitoring stations in Massachusetts.

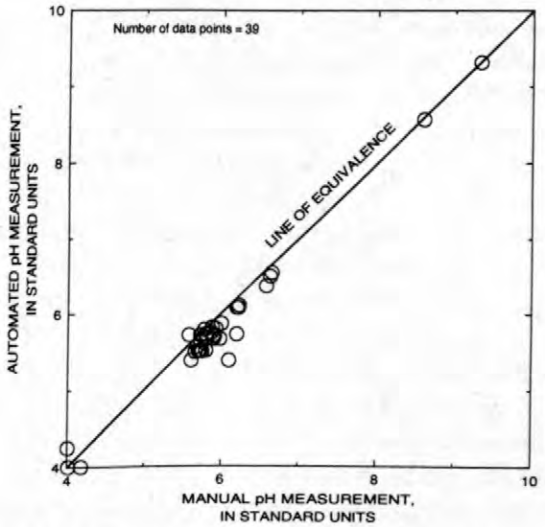

Figure 3. Relation between automated and manual quality-control measurements of pH from several automated ground-water-quality monitoring stations in Massachusetts.

measurements. These specific-conductance values would be classified as "excellent" and "good," respectively, as defined by USGS draft water-quality record ratings (H.C. Mattraw, USGS, written commun., 1998). Results of the QC program for pH measurements also indicated that that the accuracy and precision of automated measurements were equivalent to those of manual sampling efforts (fig. 3). These 39 QC measurements reveal that about 70 percent of all pH measurements were within ±0.2 pH units (an "excellent" rating by USGS draft guidelines, and the published accuracy of the probe) and 97 percent were within ±0.5 pH units of manually obtained values (a "good" rating by USGS draft guidelines). Manual measurements of pH consistently were slightly higher than those made by the automated system. The lower automated pH measurements may be an artifact of sampling in a flow cell. The automated measurements, however, may be more accurate than the manual measurements because the water in the flow train cannot degas to the atmosphere during the measurement process. The QC program for dissolved-oxygen (DO) included 26 measurements. Results indicated the accuracy and precision of individual automated measurements were equivalent to those of manual sampling efforts (fig. 4). For DO measurements,

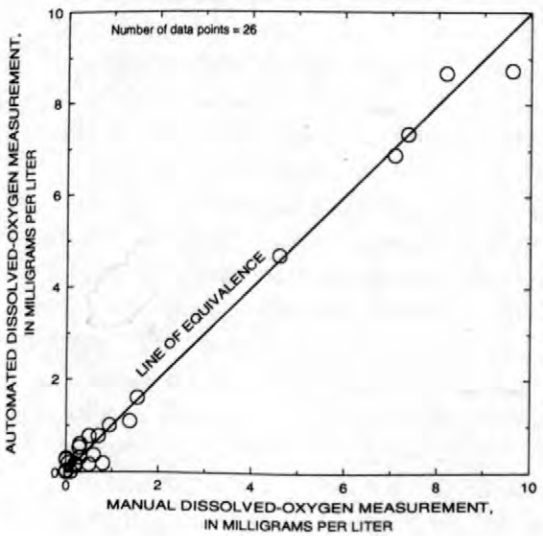

Figure 4. Relation between automated and manual quality-control measurements of dissolved oxygen from several automated ground-water-quality monitoring stations in Massachusetts.

the USGS draft guidelines define uncertainty ranges of ±5, ±10, and ±15 percent as "excellent," "good," and "fair," respectively. These classifications do not apply for values of less than 1.0 because the accuracy of most commercial DO probes is within ±0.2 mg/L (milligrams per liter). Of the population of DO measurements greater

than 1.0 mg/L (n=7), about 57 percent and 85 percent of measurements would be rated "excellent" and "good," respectively. Below a DO threshold of 1 mg/L (n=19), 61 percent of measurements were within ±0.2 mg/L (the uncertainty range of the probe), and 99 percent were within ±0.4 mg/L. By extension of the pH rating method, this means that 61 percent of these DO readings can be rated "excellent" and 99 percent can be rated "good" or better. Therefore, the QA/QC program ensures that the automated monitoring system can produce data that are as valid, accurate, and precise as comparative manual measurements. The automated system, however, can produce a detailed, real-time data record with many more individual measurements than could be obtained by manual sampling methods, which are limited by cost and personnel constraints.

Results of the QA/QC program verified the integrity of the automated sampling records and demonstrated that the automated monitoring system can accurately measure ground-water quality over a large range of geochemical conditions. Specific conductance in the QC samples ranged from about 70 to about 6,000 µS/cm, and real-time specific conductance measurements ranged from about 60 to about 8,250 µS/cm. Thus, the automated monitoring system operated successfully over a range of specific-conductance values of about two orders of magnitude, which represents the full range of ionic strength for fresh and brackish waters commonly analyzed in water-quality monitoring studies (Hem, 1982; Hem, 1992). The values of pH measured in the QA/QC program and the automated monitoring records ranged from about 4 to about 10.6 standard units. By comparison, pH values in most ground waters measured across the United States generally range from about 6.0 to about 8.0 (Hem, 1992). The automated monitoring records and the QA/QC program demonstrated that the automated monitoring system provides acceptable data over a dissolved-oxygen concentration range from nearly anoxic to nearly saturated conditions (0-8.7 mg/L). The automated monitoring system, therefore, provided accurate data over the full range of water-quality conditions expected for most ground-water-quality monitoring conditions.

CASE STUDY: REACTIVE-WALL MONITORING

A Robowell prototype was installed on Cape Cod at the Massachusetts Military Reservation (MMR) to augment and guide manual sampling and to provide a demonstration unit for the technology development process. The site is favorable for a short-term ground-water-quality investigation because the unconsolidated deposits of sand and gravel in the area form a permeable, unconfined aquifer. Expected changes in ground-water quality caused by an experimental in situ ground-water-treatment method known as the reactive wall, or the zero-valent iron wall (Hubble and others, 1997; Hubble and Gillham, this volume) would provide specific geochemical events to be monitored, and the automated monitoring prototype could provide the research team with real-time information with which to plan and implement sampling events. The automated monitoring unit was emplaced using a 2-inch-diameter polyvinylchloride well that was screened from about 99 to 101 ft (feet) below land surface at a site where the water table was about 80 ft below land surface (USGS well SDW 485-102A). This well is about 30 and 50 ft downgradient from the first and second reactive walls, respectively (Hubble and Gillham, this volume).

The reactive wall was emplaced by the MMR Installation Restoration Program (IRP). The reactive zero-valent iron wall technology consists of iron filings and a guar slurry that is injected at high pressure to form a permeable wall in a specified zone of the aquifer (Hubble and others, 1997; Hubble and Gillham, this volume). The presence of the zero-valent iron is expected to create a highly reducing environment, altering the existing ground-water chemistry and microbial population to enhance abiotic degradation of the hydrocarbons. Theoretically, as the plume moves through the permeable reactive wall, the zero-valent iron will become oxidized and reductively dechlorinate the organic compounds, producing water, hydrogen, chloride, and aliphatic hydrocarbons, such as methane and ethane, which are considered to be harmless in low concentrations (Hubble and others, 1997; Hubble and Gillham, this volume).

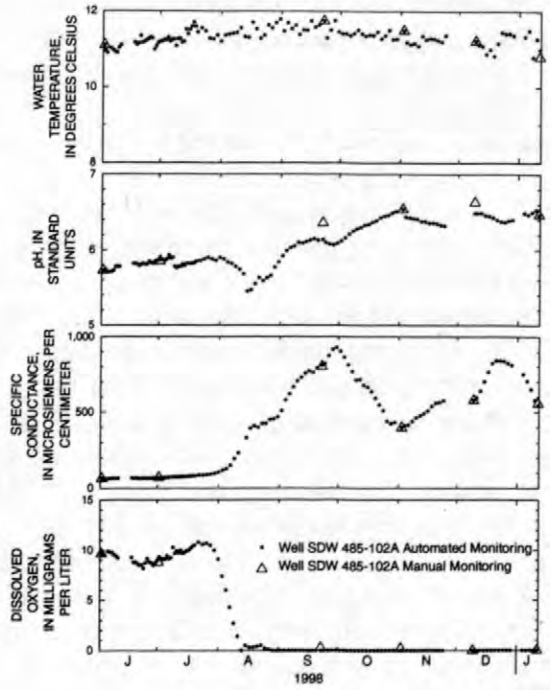

Figure 5. Ground-water quality properties measured with the automated monitoring process and manual measurements in well SDW 485-0102A, downgradient from the reactive wall, Cape Cod, Massachusetts.

Contractors for the IRP have installed two prototype walls in series in the aquifer within a plume that originates from a chemical spill source area on the MMR (Savoie and Granato, 1998). These walls are designed to be about 50 ft wide and to intercept the vertical extent of the plume from about 80 ft to about 140 ft below ground surface. The USGS, through its Toxic Substances Hydrology and National Research Programs, with cooperation from the U.S. Air Force Center for Environmental Excellence and the University of Waterloo, is studying the effects of the zero-valent iron on the ground-water chemistry and microbial population downgradient from the wall.

Application of the automated ground-water monitoring system by the Cape Cod Toxics in Hydrology monitoring project was successful and demonstrated potential applications for the technology. The automated ground-water monitoring system began measuring field parameters before the zero-valent iron walls were installed, thereby recording background ground-water-quality properties and constituents. The system successfully recorded substantial changes in ground-water quality in a short time period (fig. 5) as the plume of reaction byproducts reached the monitoring well. Although the temperature record was relatively flat, evidence of the changes in ground-water chemistry caused by the injection of the zero-valent iron wall and the subsequent injection of the enzyme/pH adjustment compound are apparent in the other measurements. The complicated pattern of different measurements apparent in the different water-quality patterns presented in figure 5 reflects the complicated schedule for injection of the reactive wall slurry and the subsequent enzyme/pH adjustment compound. The pH record indicated an increase in pH, which correlates with increasing pH and alkalinities measured in the manual sampling program (Shannon Dionne, U.S. Geological Survey, oral commun., 1999). The specific-conductance record showed a primary arrival, a secondary arrival after a short plateau, and a peak in conductance as water and solutes from the wall injection and the enzyme/pH adjustment passed the measuring point. The DO record indicated that the ground water had become anoxic in response to emplacement of the reactive wall because DO decreased at the same time as the initial increase in specific conductance.

The automated monitoring system also was successful as a sentry well. On two separate dates the demonstration unit automatically notified the project chief through phone calls from a voice modem that specific conductance had exceeded 100 and then 200 µS/cm. These preestablished criteria were designed to facilitate the timing of manual sampling efforts to characterize the geochemical changes caused by the reaction byproducts when they initially appeared in the well. The triangles that are superimposed on the automated monitoring record in figure 5 indicate the dates of service visits and the comparability of automated and manual measurements made by using independent field probes.

Automated monitoring records collected by using accepted manual sampling protocols provide detailed information that is difficult to obtain, except with intensive and costly manual

sampling programs. These detailed records present new opportunities for interpretation, and may also be helpful in determining or verifying hydrologic information for the study area. If available, a real-time record can be used to evaluate analytical results of periodic manual sampling efforts in the context of the variability in magnitude of changes in ground-water quality through time. For example, a quarterly manual sampling effort on the last day of July, October, and January would have missed both peaks in specific conductance that occurred between sampling rounds (fig. 5).

SUMMARY

Manual sampling and analysis of ground-water samples is labor- and resource-intensive. Process automation, although it will never completely replace manual methods, is an alternative because the real-time records can be used to optimize manual sampling efforts. Robowell is an automated process that was developed and tested by the USGS to provide a method for monitoring ground-water quality that meets the accepted manual-sampling protocols without incurring high labor and laboratory costs. This process is designed so that sampling equipment and instrumentation can be selected on the basis of the nature of the contaminants to be detected, site hydrogeology, and logistics such as available power and communications. The automated system can produce a detailed real-time data record with many more individual measurements than could be obtained by manual sampling methods, which are limited by cost and personnel constraints.

Six Robowell monitoring units have been in operation at one time or another since December 1994. These units have operated for more than 881 days with a loss of only about 3.4 percent of the period of record. The units have operated reliably to sample water under different hydrogeologic conditions, from different well designs, in different geochemical environments, and during all four seasons of the year. Performance was evaluated by a program of regular quality-control samples obtained by using independent water-quality probes, manual measurements, and laboratory analysis throughout the period of record. Results of this quality-control program verified the integrity of the automated sampling records and demonstrated that the automated monitoring system could accurately measure ground-water quality over a large range of geochemical conditions.

A Robowell prototype was installed at the MMR to monitor geochemical changes caused by emplacement of a zero-valent iron reactive wall. The automated ground-water monitoring system began measuring the field parameters before the zero-valent iron wall was installed, thereby recording background ground-water-quality properties and constituents. The monitoring unit recorded substantial changes in ground-water quality in a short period as the reaction by products of the wall and a subsequent enzyme/pH adjustment raised pH by almost a full unit, raised specific conductance by about 800 microsiemens per centimeter, and completely depleted the dissolved oxygen in ground water monitored in the well. The automated monitoring system also was successful as a sentry well by notifying the project chief using a voice modem that specific conductance had exceeded preset thresholds. If available, a real-time record can be used to evaluate analytical results of periodic manual sampling efforts in the context of the variability in magnitude of changes in ground-water quality through time.

REFERENCES

Granato, G.E., and Smith, K.P., 1998, Automated groundwater monitoring system and method: Patent pending: Washington, D.C., U.S. Government Patent and Trademark Office Serial Number 09/015214.

Hem, J.D., 1992, Study and interpretation of the chemical characteristics of natural water (3d ed): U.S. Geological Survey Water-Supply Paper 2254, 263 p.

Hem, J.D., 1982, Conductance: A collective measure of dissolved ions: in, Minear, R.A., and Keith, L.A., eds., Water analysis, v. 1, part 1. Inorganic species: New York, Academic Press, p. 137-161.

Herzog, B.L., Pennio, J.D., and Nielsen, G.L., 1991, Ground-water sampling: in Practical handbook of ground-water monitoring, Nielsen, D.M., ed. Chelsea, Mich., Lewis Publishers, Inc. 717 p.

Hubble, D.W., Gillham, R.W., and Cherry, J.A., 1997, Emplacement of zero-valent metal for remediation of deep contaminant plumes: Proceedings, 1997 International Containment Technology Conference and Exhibition, Feb. 9-12, St. Petersburg, Fla. p. 57-60.

Hubble, D.W., and Gillham, R.W., Installation of deep reactive walls at MMR for remediation using a granular iron-guar slurry, in Morganwalp, D.W., and Buxton, H.T., eds., 1999, U.S. Geological Survey Toxic Substances Hydrology Program--Proceedings of the Technical Meeting, Charleston, South Carolina, March 8-12, 1999-- Volume 3 -- Subsurface contamination from point sources: U.S. Geological Survey Water-Resources Investigations Report 99-4018C, this volume.

Johnson, V.M., Tuckfield, R.C., Ridley, M.N., and Anderson R.A., 1996, Reducing the sampling frequency of groundwater monitoring wells: Environmental Science and Technology, v. 30, no. 1, p. 355-358.

Koterba, M.T., Wilde, F.D., and Lapham, W.W., 1995, Ground-water data-collection protocols and procedures for the National Water-Quality Assessment Program--Collection and documentation of water-quality samples and related data: U.S. Geological Survey Open-File Report 95-399, 113 p.

Robin, M.J.L., and Gillham, R.W., 1987, Field evaluation of well purging procedures: Ground Water Monitoring Review, v. 7, no. 4, p. 85-93.

Savoie, Jennifer, and Granato, G.E., 1998, Automated monitoring for the zero-valent iron wall project at the Massachusetts Military Reservation: accessed on the world-wide web at http://ma.water.usgs.gov/automated1/a3index.html on March 15, 1999.

Smith, K.P., and Granato, G.E., 1998, Technology transfer opportunities: Automated ground-water monitoring, a proven technology: U.S. Geological Survey Fact Sheet FS-122-98, 2 p.

Stone, W.J., 1997, Low-flow ground water sampling--Is it a cure-all? Ground Water Monitoring and Remediation, v. 17, no. 2, p. 70-72.

Zhou, Y., 1996, Sampling frequency for monitoring the actual state of ground water systems: Journal of Hydrology, v. 180, p. 301-318.

AUTHOR INFORMATION

Gregory G. Granato (ggranato@usgs.gov) and Kirk P. Smith (kpsmith@usgs.gov), U.S. Geological Survey, Marlborough, Massachusetts

Factors and Processes that Affect Waste Disposal and Subsurface Transport of Contaminants in Arid Environments

In 1976, the U.S. Geological Survey (USGS) began studies of unsaturated-zone hydrology in the Amargosa Desert, near Beatty, Nevada. At that time, the research was conducted under the auspices of the USGS Low-Level Radioactive Waste Program. In 1983, agreements with the Bureau of Land Management and the State of Nevada established two field study areas for sustained study of arid-site processes: a 16-hectare (ha) area adjacent to a waste-burial facility and a 0.1-ha area about 3 kilometers farther south. The study areas are collectively known as the Amargosa Desert Research Site (ADRS). Investigations at the ADRS have produced long-term benchmark data on hydraulic characteristics and soil-water movement for undisturbed conditions and for simulated waste-disposal conditions in arid environments. In 1995, after the unexpected discovery of high concentrations of tritium and carbon-14 in the unsaturated zone beneath the ADRS, the scope of research was broadened to include the study of processes affecting radionuclide transport. The ADRS was incorporated into the USGS Toxic Substances Hydrology Program in 1997.

The goal of present research at the ADRS is improved understanding of processes controlling the migration and fate of contaminants in arid environments. Research at the site is a multidisciplinary collaboration among scientists from universities, research institutes, national laboratories, and the USGS. The papers that follow illustrate the main avenues of active research. They explore the application of new and emerging methods for characterizing hydrogeologic frameworks in desert alluvial basins; quantifying the exchanges of materials and energy across the land surface; and understanding the distribution, movement, and fate of radionuclides in deep unsaturated zones.

Information on ongoing research activities at the Amargosa Desert Research Site is available on the World Wide Web at: **http://nevada.usgs.gov/adrs/**.

For additional information contact:

Brian J. Andraski, USGS, Carson City, Nevada (email: andraski@usgs.gov), or

David A. Stonestrom, USGS, Menlo Park, California (email: dastones@usgs.gov)

Overview of Research on Water, Gas, and Radionuclide Transport at the Amargosa Desert Research Site, Nevada

By B.J. Andraski and D.A. Stonestrom

ABSTRACT

Studies at the U.S. Geological Survey Amargosa Desert Research Site have focused on characterizing factors and processes that control transport and fate of contaminants in arid environments. This paper summarizes research results that have been published through 1998. Results have improved understanding of water and gas movement through a thick unsaturated zone, including the degree to which features of the natural unsaturated-flow system can be altered by installation of a waste-disposal facility. The study of radioactive-contaminant transport at the site is at an early stage. Field data measured in association with this new component of research have generated speculation regarding the exact mechanisms that control tritium transport in arid unsaturated zones.

INTRODUCTION

Arid environments often are considered ideal for waste isolation because the natural environment has features that can minimize the risk of waste migration to the underlying water table (e.g., low precipitation, high evapotranspiration, thick unsaturated zone). On this premise, sites in the arid western United States are increasingly being sought for isolation of the Nation's radioactive and other hazardous wastes for periods ranging from hundreds to thousands of years. In addition, volumes of locally generated wastes are increasing because of rapid population growth, industrialization, and the importance of mining in the arid West. Thus, concern about the potential effect of contaminants on the environment is rising. An understanding of the factors and processes that control liquid and gas movement under desert conditions is needed to provide a strong scientific basis for developing effective waste-burial systems, monitoring systems, and remedial strategies intended to limit contaminant releases to the environment.

Investigations at the Amargosa Desert Research Site (ADRS) began in 1983 and have produced long-term benchmark data on hydraulic characteristics and soil-water movement for undisturbed conditions and for simulated waste-disposal conditions in arid environments. In 1995, as a result of unexpectedly finding high concentrations of tritium and carbon-14 in the unsaturated zone of the ADRS, the scope of research was broadened to include the study of processes affecting radionuclide transport. The ADRS was incorporated into the USGS Toxic Substances Hydrology Program in 1997. The overall research objective for the site is to improve understanding of and methods for characterizing the mechanisms that control transport and fate of contaminants in arid environments. The purpose of this paper is to provide an overview of ADRS research published through 1998. Additional information is available on the ADRS Internet page at Uniform Resource Locator http://nevada.usgs.gov/adrs/.

SITE DESCRIPTION

The two ADRS study areas are located near a waste-burial facility that is about 17 kilometers (km) south of Beatty, Nev. and 20 km east of Death Valley National Park (fig. 1A). The ADRS is in the Mojave Desert ecosystem, one of the most arid regions of the United States. Annual precipitation at the site averages about 108 millimeters (mm). About 70% of the precipitation is associated with frontal systems that cover large areas during October through April. Summer rainfall occurs predominantly during localized, short-duration, convective storms. Annual pan evaporation is about 1,900 mm (Nichols, 1987). Air temperatures average 3 degrees Celsius (°C) during December and

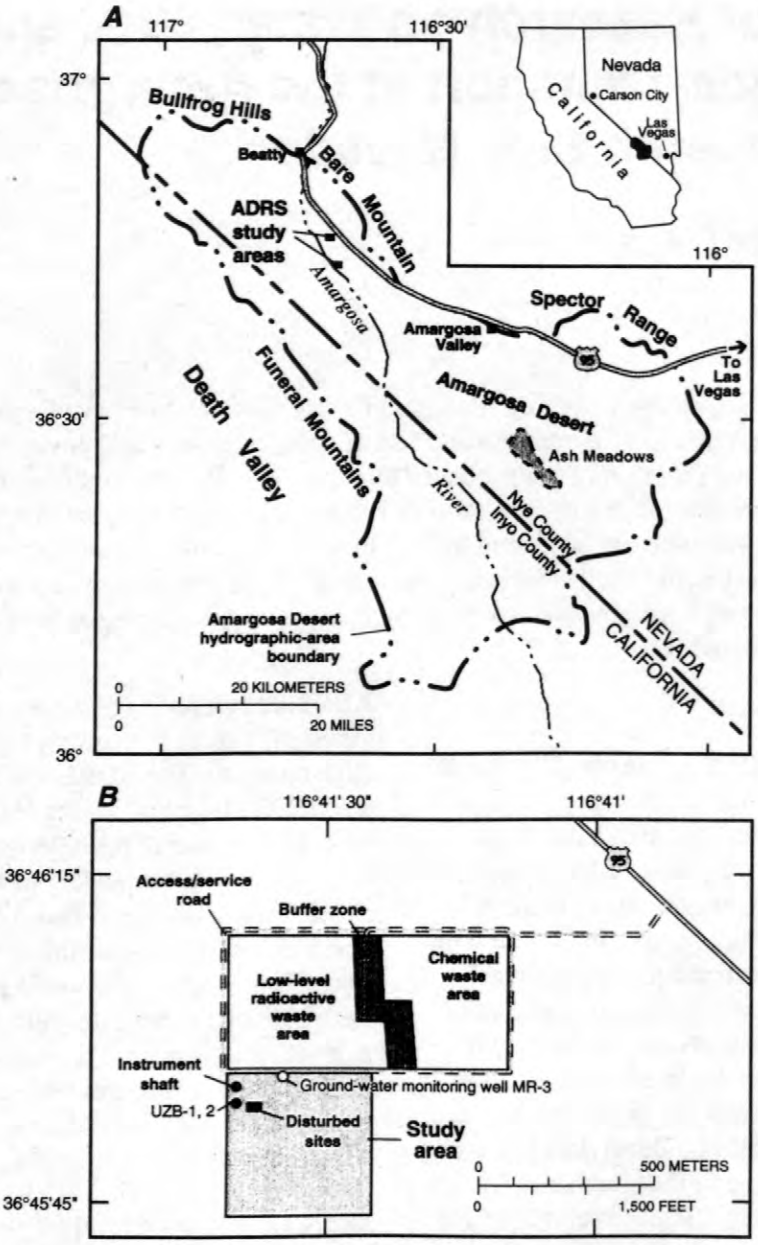

Figure 1. Location of (*A*) Amargosa Desert Research Site (ADRS) study areas near Beatty, Nev., and (*B*) 16-hectare study area adjacent to waste-burial facility. The instrument shaft and unsaturated-zone boreholes UZB-1 and UZB-2 are located in undisturbed sediments.

33°C during July (Andraski and others, 1995). Vegetation in the area is sparse; creosote bush [*Larrea tridentata* (DC.) Cov.], an evergreen shrub, is the dominant species. The Amargosa Desert is in the Basin and Range physiographic province. Sediments beneath the waste facility are primarily fluvial and alluvial-fan deposits that are more than 170 meters (m) thick (Nichols, 1987). Depth to the water table ranges from 85 to 115 m (Fischer, 1992).

The waste facility has been used for the burial of low-level radioactive waste (LLRW) (1962–92) and hazardous chemical waste (1970 to present). The LLRW facility was the first such commercially operated site in the United States. Construction of the LLRW burial trenches included excavation and stockpiling of native soil, emplacement of waste, and backfilling with stockpiled, uncompacted soil. Prior to closure of the LLRW facility, the surfaces of completed burial trenches and perimeter areas

were kept free of vegetation. Regulations governing burial of LLRW do not require that trenches be lined with impervious materials. Liquid LLRW could be shipped to the facility, but the operating license required that liquids be solidified with portland cement before disposal. However, a 1976 U.S. Nuclear Regulatory Commission (USNRC) investigation indicated that liquid wastes delivered to the site between 1962 and 1975 were disposed directly into the trenches (USNRC, 1976).

Different study areas at the ADRS have been established over the years to support research of flow and transport processes. At a 16-hectare (ha) area adjacent to the waste-burial facility, an instrument shaft was installed in 1983 to facilitate emplacement and maintenance of monitoring devices in undisturbed sediments in the upper 13 m of the unsaturated zone (figs. 1B and 2; Fischer, 1992). Meteorological data have been collected by an automated weather station next to the instrument shaft (for example, Wood, 1996). Three disturbed sites were established in 1987 to allow comparison of arid-site hydrology under undisturbed, vegetated soil (fig. 2), devegetated soil, and simulated waste-trench conditions (figs. 1B and 3; Andraski, 1990). Ground-water level has been periodically monitored since 1987 at well MR-3 (fig. 1B). Deep test holes drilled near the instrument shaft (UZB-1, 2; fig. 1B) and at a 0.1-ha study area 3 km south of the 16-ha area have been used for measurements of temperature, water potential, and air pressure, and for collection of soil gas samples throughout the thick unsaturated zone (Fischer, 1992; Prudic and Striegl, 1995; Andraski and Prudic, 1997). An array of soil-gas sampling tubes in undisturbed, near-surface sediments was installed in 1997 to allow for periodic collection and analysis of the chemical composition of unsaturated zone air to a depth of about 1.5 m (Striegl and others, 1998).

WATER AND GAS TRANSPORT

Data from beneath undisturbed, vegetated areas have provided a conceptual understanding of moisture and gas movement through the unsaturated zone. Chloride mass-balance estimates of long-term deep percolation through the unsaturated zone suggest that percolation of precipitation below a depth of 10 m has been minimal or nonexistent for at least 6,000 (Fouty, 1989) to 16,000 years (Prudic, 1994). The estimated age of 16,000 years approximates the time when climate in the area was wetter and cooler. Field measurements between 1983 and 1988 that characterized the shallow (upper 13 m) unsaturated zone and documented the dryness of the soil and sediments show that below a depth of 1 m, water potentials typically ranged between -3 and -7 megapascals (Fischer, 1992). In addition, water potential and temperature data between the depths of 9 and 13 m demonstrate persistent upward driving forces for water (liquid and vapor) flow. Subsequent measurements in the deep unsaturated zone indicate that water-potential gradients between depths of 9 and 48 m and the geothermal gradient provide upward driving forces for water flow (Prudic, 1994; Andraski and Prudic, 1997). Profiles of deuterium and oxygen-18 concentrations in soil-pore water were consistent with the hypothesis of upward movement and evaporative discharge of ground water at land surface (Prudic and others, 1997). Similarly, the distribution of carbon dioxide suggests degassing from ground water and upward movement of carbon dioxide gas to land surface (Prudic and Striegl, 1994). Results of these studies indicate that the natural hydrologic system limits the potential for deep percolation of precipitation and facilitates the upward movement of water and gases through the thick unsaturated zone.

Laboratory and multiple-year field investigations have contributed to improved understanding of the degree to which features of the natural unsaturated-flow system can be altered by installation of a waste-disposal facility. The effects of disturbance were evaluated in terms of differences between data collected under undisturbed conditions and data collected under simulated solid-waste-burial conditions. Properties and variability of the natural site environment were significantly altered by test-trench construction (Andraski, 1996). Hydraulic properties were characterized using data measured over a water-content range that is representative of arid conditions but is seldom studied. Results demonstrate that reliance on standard characterization techniques could lead to significant errors in the description of hydraulic properties of desert soils. Field data collected during a 5-year period show that the naturally stratified soil in combination with native plants provide for (1) limited percolation depth and seasonal depletion of water accumulated in the root zone and (2) episodic, deep drying

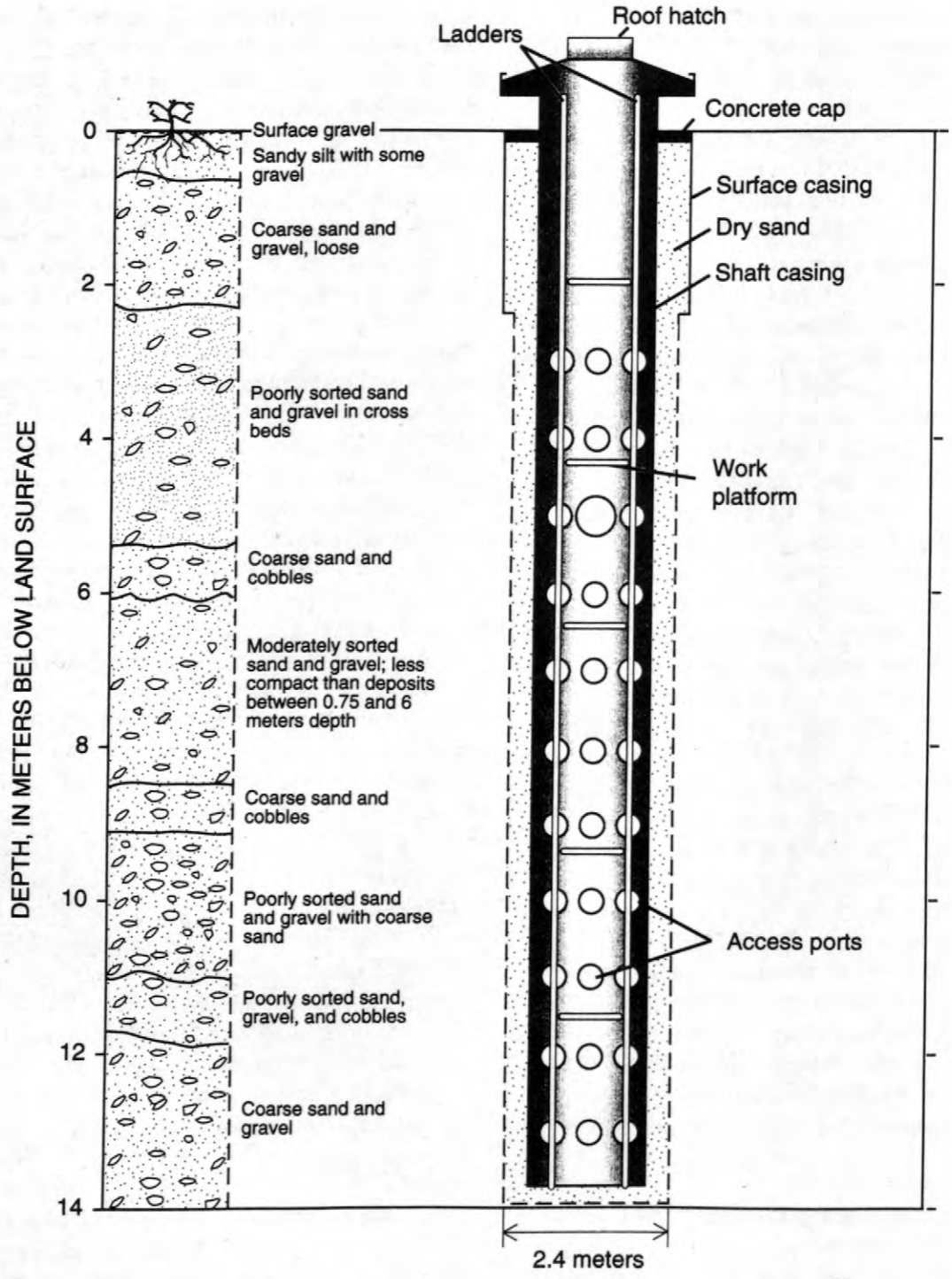

Figure 2. Diagram of instrument shaft used to study hydrologic processes under undisturbed conditions at the Amargosa Desert Research Site, near Beatty, Nev.

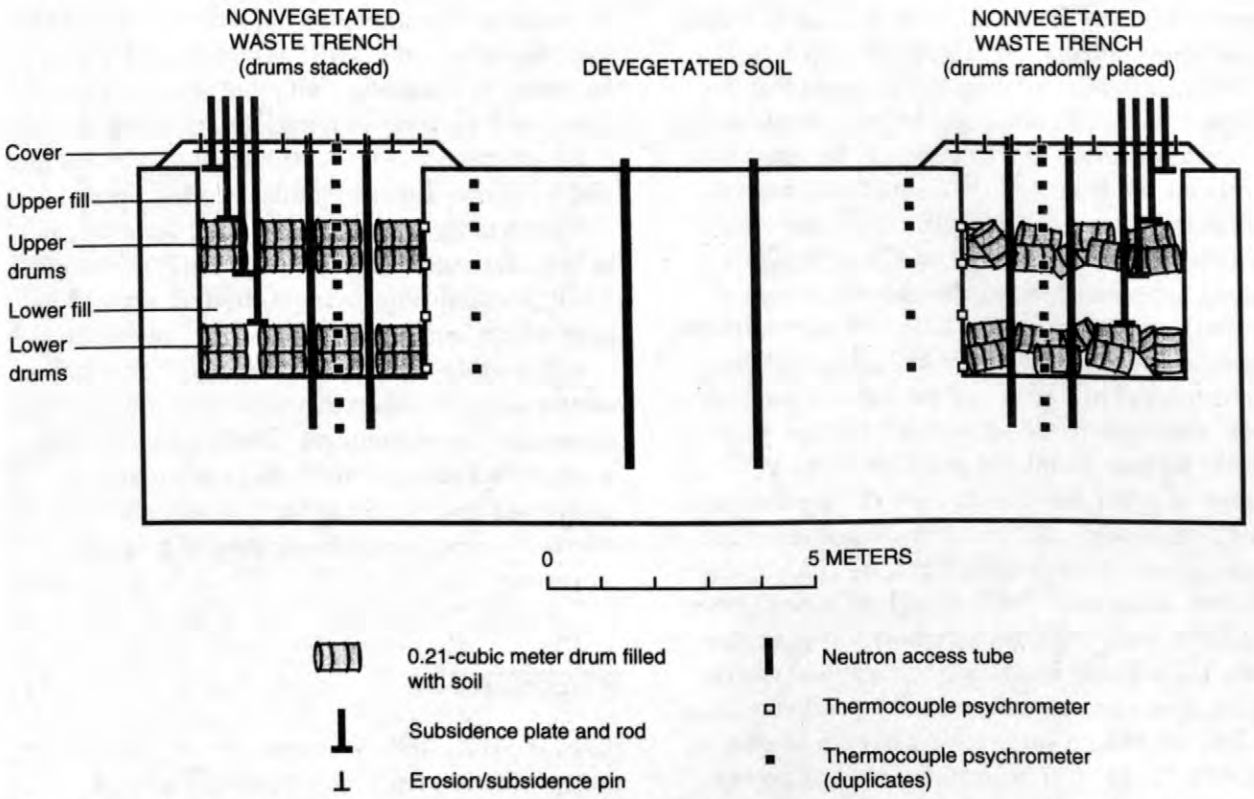

Figure 3. Diagram of instrumentation used to study hydrologic processes under devegetated soil and simulated waste-trench conditions at the Amargosa Desert Research Site, near Beatty, Nev.

of the unsaturated zone well below the apparent root zone during years with below-average precipitation (Gee and others, 1994; Andraski, 1997). Under devegetated soil and test-trench conditions, accumulation and shallow (1-2 m) penetration of infiltrated water was observed; at greater depths, however, water-potential gradients provided typically upward driving forces for water flow.

Field measurements of test-trench erosion and subsidence provided information on processes that can influence the accumulation and movement of water at a waste-burial site. Erosion of test-trench covers totaled less than 10 mm during the 5-year study (Andraski and Prudic, 1997). Most of the soil loss was attributed to deflation (wind erosion) that occurred during the first 2 years following trench construction. Subsidence of trench covers did not have a measurable influence on the water balance, but trends in subsidence did show a positive relation with cumulative precipitation (Andraski, 1997). This implies that subsidence could become a factor in the long-term water balance of the trenches, particularly if the subsidence were to result in localized ponding and the development of preferential flow paths.

Results from studies of water and gas transport suggest that the ultimate fate of contaminants buried at properly managed solid-waste sites can be strongly influenced by the interactions among climate and the near-surface features (soils, plants) of the disposal facility, and how these factors change with time. Further work is needed to define the soil-plant-atmosphere interactions that caused the deep drying at the vegetated-soil site and to evaluate how such interactions could affect the potential for release of contaminants to the terrestrial environment as well as to ground water.

RADIONUCLIDE DISTRIBUTION AND TRANSPORT

Data are being collected to improve understanding of the distribution and transport of radionuclides through the unsaturated zone. Gas samples collected in 1994 and 1995 from test hole UZB-2, about 100 m away from the waste-burial facility (fig. 1B), show elevated tritium concentrations in water vapor to a depth of 108.8 m and elevated carbon-14 concentrations in carbon-14 dioxide gas to a depth of 34 m; tritium concentration in ground

water collected from UZB-2 at the time of drilling was below detection limits (Prudic and Striegl, 1995). Evaluation of these data suggest that the carbon-14 distribution could be partly explained by gaseous diffusion or advective gas transport away from the waste facility. In contrast, all plausible mechanisms that could explain the distribution of tritiated water vapor relied on lateral liquid flow along preferential flow paths (Striegl and others, 1996). Subsequent analysis of pore water extracted from archived core samples and additional measurements of tritium in soil gas indicate that tritium concentrations in the upper 5-50 m of the unsaturated zone have stabilized with time (1992-97) in the range of 400-1,300 tritium units (TU); tritium concentrations below 50 m have increased with time to a maximum of about 1,800 TU at the 108.8-m depth (Prudic and others, 1997; Striegl and others, 1998). Samples collected from a shallow soil-gas probe near UZB-2 indicate tritium concentrations were greatest in a coarse-textured soil layer that is about 1-2 m below land surface; values were as great as 20,600 TU. In 1997, an array of soil-gas probes was installed to measure the spatial distribution of tritium in water vapor collected from this coarse-textured layer. Tritium concentrations within 300 m of the waste burial area indicate a general trend of increasing concentrations toward the burial area; values ranged from 16-36,900 TU. The coarse-textured layer is thought to provide a preferential pathway for radionuclide movement (Striegl and others, 1998).

The elevated tritium concentrations in water vapor collected at the ADRS and the time history of these concentrations have caused speculation regarding the exact mechanisms that control tritium transport in arid unsaturated zones. More detailed characterization of the waste-source and the local geology, and more data on the composition of soil gases from existing and additional sampling points are needed to advance understanding of the mechanisms that control radionuclide transport.

SUMMARY

Research at the ADRS has contributed to improved understanding of water and gas movement through the thick unsaturated zone and of the degree to which features of the natural unsaturated-flow system can be altered by installation of waste-disposal trenches. The study of radioactive-contaminant transport at the ADRS is underway. Field data measured in association with this new component of research have raised questions regarding the exact mechanisms that control tritium transport in arid unsaturated zones. Further work is needed to characterize the interactive physical, chemical, and biological mechanisms that control migration and fate of contaminants in desert environments. Such information is important to the development of effective waste-burial systems, monitoring systems, and remedial strategies that will limit contaminant releases to the environment. The research facilities at the ADRS and long-term data sets provide a foundation upon which to build collaborative efforts to further the understanding of arid-site processes.

REFERENCES

Andraski, B.J., 1990, Water movement and trench stability at a simulated arid burial site for low-level radioactive waste near Beatty, Nevada: La Grange Park, Ill., American Nuclear Society, Nuclear Waste Isolation in the Unsaturated Zone, Las Vegas, Nev., September 1989, Proceedings, p. 166-173.

———1996, Properties and variability of soil and trench fill at an arid waste-burial site: Soil Science Society of America Journal, v. 60, no. 1, p. 54-66.

———1997, Soil-water movement under natural-site and waste-site conditions—A multiple-year field study in the Mojave Desert, Nevada: Water Resources Research, v. 33, no. 8, p. 1901-1916.

Andraski, B.J., and Prudic, D.E., 1997, Soil, plant, and structural considerations for surface barriers in arid environments—Application of results from studies in the Mojave Desert near Beatty, Nevada, *in* Barrier Technologies for Environmental Management, Summary of a Workshop: Washington, D.C., National Academy Press, p. D50-D60.

Andraski, B.J., Prudic, D.E., and Nichols, W.D., 1995, Waste burial in arid environments—Application of information from a field laboratory in the Mojave Desert, southern Nevada: U.S. Geological Survey Fact Sheet FS-179-95, 4 p.

Fischer, J.M., 1992, Sediment properties and water movement through shallow unsaturated alluvium at an arid site for disposal of low-level radioactive waste near Beatty, Nye County, Nevada: U.S. Geological Survey Water-Resources Investigations Report 92-4032, 48 p.

Fouty, Suzanne, 1989, Chloride mass-balance as a method for determining long-term ground-water recharge rates and geomorphic surface stability in arid and semi-arid regions—Whiskey Flat and Beatty, Nevada: Tucson, University of Arizona, unpublished M.S. thesis, 130 p.

Gee, G.W., Wierenga, P.J., Andraski, B.J., Young, M.H., Fayer, M.J., and Rockhold, M.L., 1994, Variations in water balance and recharge potential at three western desert sites: Soil Science Society of America Journal, v. 58, no. 1, p. 63-72.

Nichols, W.D., 1987, Geohydrology of the unsaturated zone at the burial site for low-level radioactive waste near Beatty, Nye County, Nevada: U.S. Geological Survey Water-Supply Paper 2312, 57 p.

Prudic, D.E., 1994, Estimates of percolation rates and ages of water in unsaturated sediments at two Mojave Desert sites, California-Nevada: U.S. Geological Survey Water-Resources Investigations Report 94-4160, 19 p.

Prudic, D.E., Stonestrom, D.A., and Striegl, R.G., 1997, Tritium, deuterium, and oxygen-18 in water collected from unsaturated sediments near a low-level radioactive-waste burial site south of Beatty, Nevada: U.S. Geological Survey Water-Resources Investigations Report 97-4062, 23 p.

Prudic, D.E., and Striegl, R.G., 1994, Water and carbon dioxide movement through unsaturated alluvium near an arid disposal site for low-level radioactive waste, Beatty, Nevada [abs.]: Eos, American Geophysical Union Transactions, v. 75, no. 16, p. 161.

———1995, Tritium and radioactive carbon (14C) analyses of gas collected from unsaturated sediments next to a low-level radioactive-waste burial site south of Beatty, Nevada, April 1994 and July 1995: U.S. Geological Survey Open-File Report 95-741, 7 p.

Striegl, R.G., Healy, R.W., Michel, R.L., and Prudic, D.E., 1998, Tritium in unsaturated zone gases and air at the Amargosa Desert Research Site, and in spring and river water, near Beatty, Nevada, May 1997: U.S. Geological Survey Open-File Report 97-778, 13 p.

Striegl, R.G., Prudic, D.E., Duval, J.S., Healy, R.W., Landa, E.R., Pollock, D.W., Thorstenson, D.C., and Weeks, E.P., 1996, Factors affecting tritium and ^{14}carbon distributions in the unsaturated zone near the low-level radioactive-waste burial site south of Beatty, Nevada: U.S. Geological Survey Open-File Report 96-110, 16 p.

U.S. Nuclear Regulatory Commission, Office of Inspection and Enforcement, Region V, 1976, IE Inspection Report 76-02.

Wood, J.L., 1996, Selected meteorological and micrometeorological data for an arid site near Beatty, Nye County, Nevada, calendar year 1992: U.S. Geological Survey Open-File Report 96-434, 33 p.

AUTHOR INFORMATION

Brian J. Andraski, U.S. Geological Survey, Carson City, Nevada (andraski@usgs.gov)

David A. Stonestrom, U.S. Geological Survey, Menlo Park, California (dastones@usgs.gov)

Isotopic Composition of Water in a Deep Unsaturated Zone Beside a Radioactive-Waste Disposal Area Near Beatty, Nevada

By David A. Stonestrom, David E. Prudic, and Robert G. Striegl

ABSTRACT

The isotopic composition of water in deep unsaturated zones is of interest because it provides information relevant to hydrologic processes and contaminant migration. Profiles of oxygen-18 (^{18}O), deuterium (D), and tritium (^{3}H) from a 110-meter deep unsaturated zone, together with data on the isotopic composition of ground water and modern-day precipitation, are interpreted in the context of water-content, water-potential, and pore-gas profiles. At depths greater than about three meters, water vapor and liquid water are in approximate equilibrium with respect to D and ^{18}O. The vapor-phase concentrations of D and ^{18}O have remained stable through repeated samplings. Vapor-phase ^{3}H concentrations have generally increased with time, requiring synchronous sampling of liquid and vapor to assess equilibrium. Below 30 meters, concentrations of D and ^{18}O in pore water become approximately equal to the composition of ground water, which is isotopically lighter than modern precipitation and has a carbon-14 (^{14}C) concentration of about 26 percent modern carbon. These data indicate that net gradients driving fluxes of water, gas, and heat are directed upwards for undisturbed conditions at the Amargosa Desert Research Site (ADRS). Superimposed on the upward-directed flow field, tritium is migrating away from waste in response to gradients in tritium concentrations.

INTRODUCTION

The isotopic composition of pore water depends on the source water but can be modified by processes that influence the movement of water and the transport of radionuclides. Evaporation near the land-atmosphere interface shifts δD and $\delta^{18}O$ to heavier values, but on a slope less than that of the meteoric water line (MWL). In the upper Amargosa Desert, precipitation from most storms infiltrates to depths of only several millimeters (Nichols, 1987; Fischer, 1992). Infrequent, intense storms can temporarily saturate the land surface and produce runoff and deeper percolation (Fischer, 1992). Even then, hysteresis between water content and water potential tends to keep infiltrated water high in the soil profile where it is available for uptake by plant roots (Rubin, 1967).

The Amargosa Desert Research Site (ADRS) includes 16 hectares of native vegetation adjacent to a former disposal area for low-level radioactive waste about 18 kilometer (km) south of Beatty, Nevada (Andraski and Stonestrom, 1999). Potential evapotranspiration at the site is about 18 times the mean annual precipitation of 0.1 meter (m). Despite this, near-surface water balances are highly sensitive to vegetation (Nichols, 1987). Removal of native vegetation can induce accumulation and downward penetration of infiltrating rainfall, increasing the potential for water to contact and mobilize waste (Andraski, 1997).

This paper summarizes results on the isotopic composition of deep, unsaturated-zone pore water at the ADRS in the context of available hydrologic data. The results are from test facilities UZB-1, UZB-2, well MR-3, a research shaft, and research-trench facilities that are about 20 to 100 m south of a fence surrounding the disposal area. A photograph and maps of the facilities appear in Andraski and Stonestrom (1999) and Prudic and others (1999).

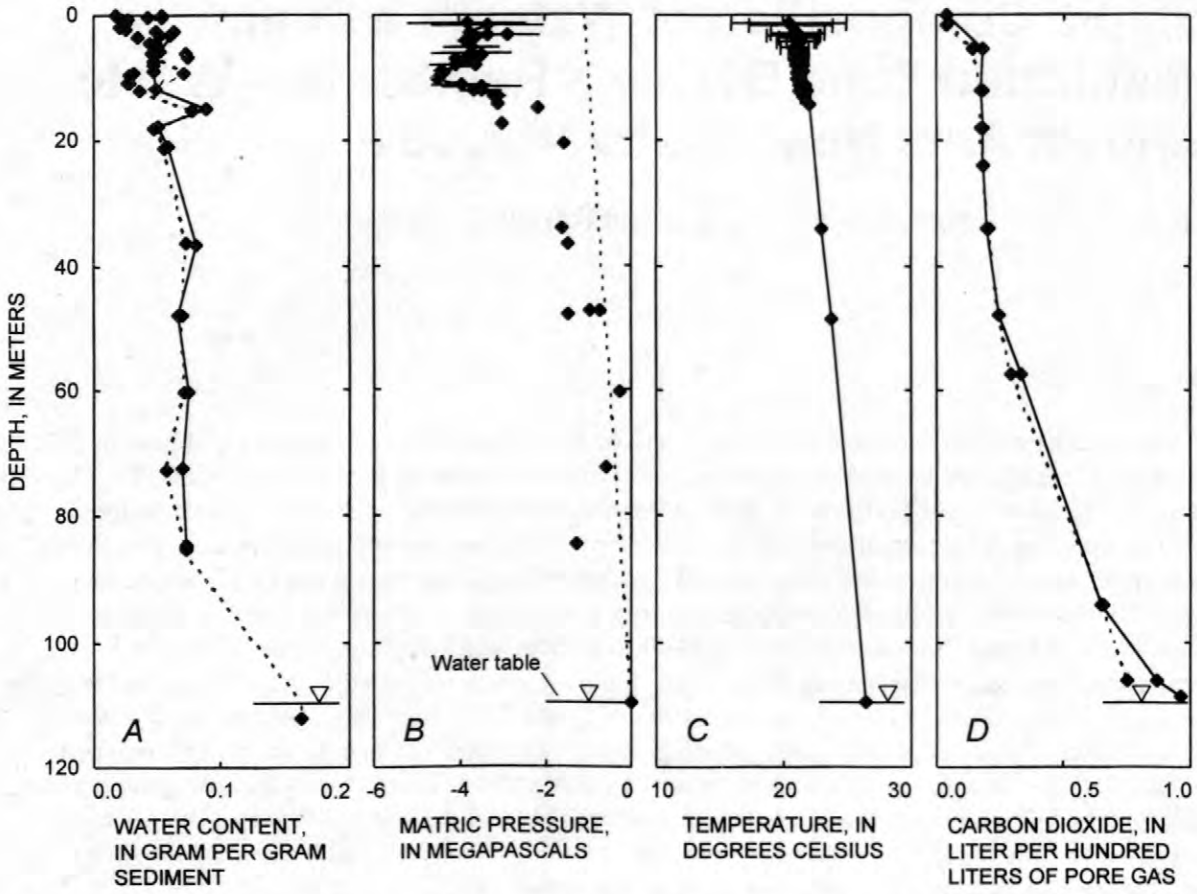

Figure 1. Profiles of water content (A), matric pressure (B), temperature (C), and carbon dioxide (D) at hydrologic test facilities at the Amargosa Desert Research Site. Carbon dioxide values were determined by W.C. Evans of the U.S. Geological Survey. Other data are from Fischer (1992), Prudic (1994), Andraski and Prudic (1997), and Prudic and others (1997). The dashed line in (B) is the matric-pressure profile representing hydrostatic equilibrium.

WATER CONTENT AND POTENTIAL

Water contents are low throughout most of the profile, generally decreasing upward from the 110-m deep water table to within a few meters of the land surface (fig. 1A). Storm-induced and seasonal fluctuations in water contents were limited to the uppermost meter at three neutron-probe boreholes separated by about 20 m near the research shaft during a 7.8-year period (Fischer, 1992; Andraski, 1997). This period included large (>25 mm) rainfall events and El-Nino related periods of higher precipitation. Measurements were made to maximum depths of 14 to 31 m. Data collected from six additional neutron-probe boreholes at the research-trench facility also indicated containment of water-content changes in the top meter over a five-year interval of the 7.8-year period (Andraski, 1997).

The attenuation of near-surface fluctuations in water content is reflected in matric-pressure and temperature profiles (fig. 1B,C). Indicated ranges are standard deviations of daily averages of data obtained every four hours over the course of one year (Fischer, 1992). The dashed line connecting the 110-m deep water table and land surface in figure 1B is the hydrostatic matric-pressure gradient that would exactly balance the gravitational-potential field. For isothermal conditions, a slope less than that of the hydrostatic line represents a net upward driving force for liquid-water flow because the upward pressure-potential gradient exceeds the downward gravitational-potential gradient. The upward-directed thermal gradient adds to the upward matric-pressure gradient and induces upward flow of water vapor as well (Fischer, 1992).

GAS COMPOSITION

The gross composition of pore gas in the unsaturated zone is approximately equal to that of air, except for elevated water-vapor and carbon-dioxide (CO_2) levels. Relative humidities measured with thermocouple pyschrometers were > 95% at depths > 1 m (Fischer, 1992; Andraski, 1997).

Figure 1D shows CO_2 profiles in May and November of 1997 at borehole UZB-2. Concentrations were determined by gas chromatography with an analytical uncertainty of about 5%. At a depth of 109 m, just above the water table, CO_2 makes up nearly 1% of pore gas. The fraction of CO_2 decreases upward toward the land surface. The CO_2 may represent outgassing of ground water (Thorstenson, and others, 1972; Prudic and Striegl, 1994) or microbial respiration (Wood and Petraitis, 1984; Wood and others, 1993). In either case, the data indicate an upward diffusive flow of CO_2 from the water table to the land surface.

ISOTOPIC COMPOSITION OF WATER IN THE DEEP UNSATURATED ZONE

Concentrations of ^{18}O, D, and ^{3}H were determined for liquid water from UZB-1 and UZB-2 cores and for water vapor from UZB-2 gas-sampling ports using methods described in Prudic and others (1997). The cryodistillation method that removed water from core samples did not substantially alter its isotopic composition. When water added to dry test samples was subsequently recovered, maximum changes in D and ^{18}O were 3 and 0.4 permil, respectively. Tritium recovered in the same tests agreed to within 5 tritium units (TU) or 10%, whichever was greater.

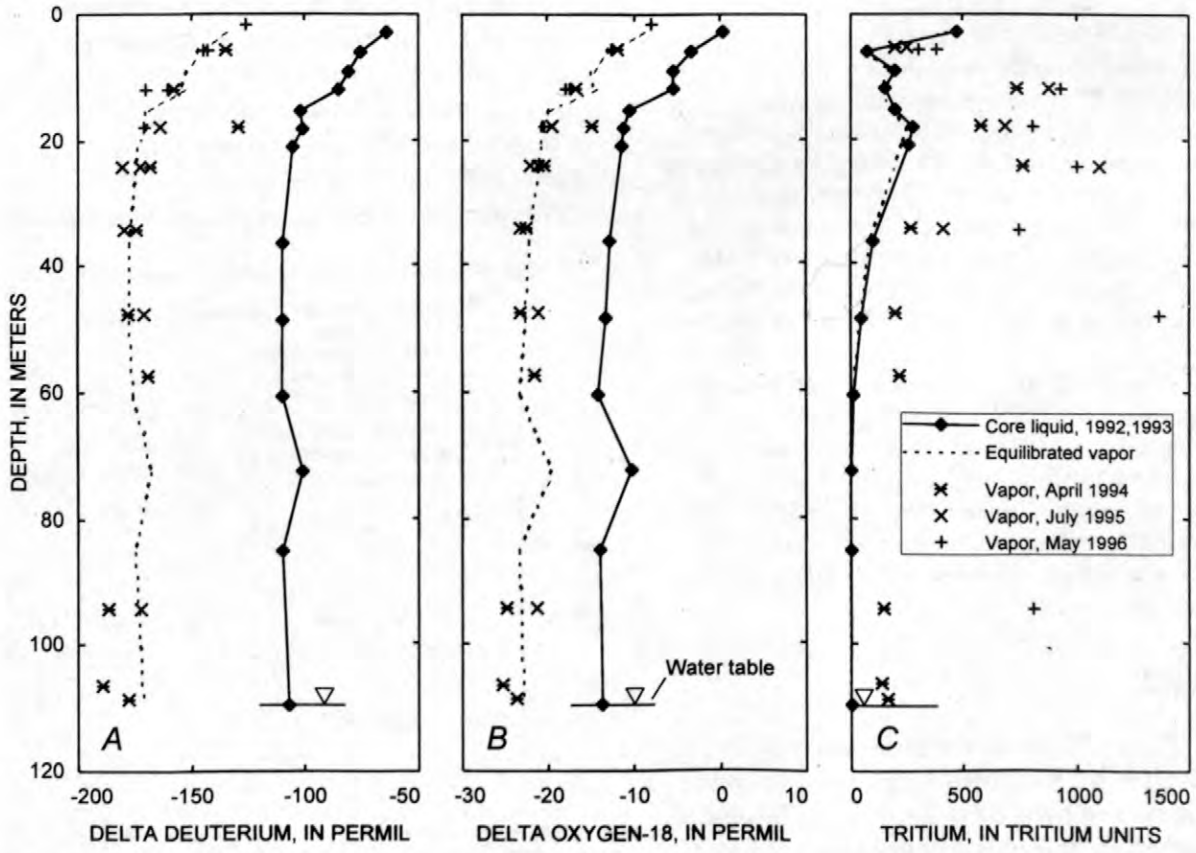

Figure 2. Profiles of deuterium (A), oxygen-18 (B), and tritium (C) from test holes UZB-1 and UZB-2 at the Amargosa Desert Research Site, about 100 meters south of a fence surrounding a former waste facility for low-level radioactive waste. Dashed lines indicate isotopic composition of water vapor in theoretical equilibrium with liquid water extracted from core samples. Data from Prudic and others (1997).

Deuterium and Oxygen-18

Figure 2A,B shows the distribution of D and ^{18}O in water extracted from core samples and in water vapor from UZB-2 air ports . The dashed lines show the theoretical composition of water vapor in isotopic equilibrium with liquid water extracted from the cores using fractionation factors compiled by Friedman and O'Neil (1977) and:

$$\delta x_v = (1{,}000 + \delta x_l)/\alpha_x \; — \; 1{,}000 \qquad (1)$$

where

δx_v is the δD or $\delta^{18}O$ value of water vapor in equilibrium with liquid water, in permil,

δx_l is the δD or $\delta^{18}O$ value of liquid water, in permil, and

α_x is the temperature-dependent fractionation factor for D or ^{18}O.

The δD and $\delta^{18}O$ values measured for water-vapor samples were close to theoretical predictions from core-water samples when temperature-dependent fractionation was taken into account (fig. 2A,B). This suggests that water vapor and liquid water are in approximate isotopic equilibrium throughout most of the unsaturated zone. Repeated samplings of water vapor produced nearly the same profiles with no clear temporal trends towards heavier or lighter values.

Core water at a depth of 3 m had a δD of –64 permil and an $\delta^{18}O$ of +0.4 permil. Concentrations of D and ^{18}O in core water decreased with depth in the upper unsaturated zone, becoming uniform below about 30 m and approximately equal to values in ground water sampled at the 110-m deep water table at UZB-2 (fig. 2A,B).

Tritium

Figure 2C shows the distribution of ^3H for water extracted from core samples and for water vapor sampled from UZB-2 air ports. The dashed line shows the theoretical composition of water vapor in isotopic equilibrium with the liquid water from the cores using fractionation factors from Ferronsky and Polyakov (1982) and:

$$C_v = C_l / \alpha_T \qquad (2)$$

where

C_v is the concentration of tritium in water vapor, in tritium units (TU),

C_l is the concentration of tritium in liquid water, in TU, and

α_T is the temperature-dependent fractionation factor for ^3H.

Tritium concentrations in water-vapor samples are in apparent disequilibrium with liquid water. The disequilibrium may only be apparent because tritium concentrations generally increased between water-vapor collections. Due to the time-dependent nature of tritium concentrations, synchronous sampling of liquid and vapor will be necessary to evaluate the degree of equilibrium between the two phases.

RELATION TO PRECIPITATION AND GROUND WATER

On the basis of 18 months of data from a station 35 km southeast of the ADRS and 9 m higher in elevation, winter precipitation at the site has an estimated volume-weighted mean δD of –87 permil and $\delta^{18}O$ of –12.0 permil (Milne and others, 1987; fig. 3). Wilshire and Friedman (1999) present δD data from six stations collected

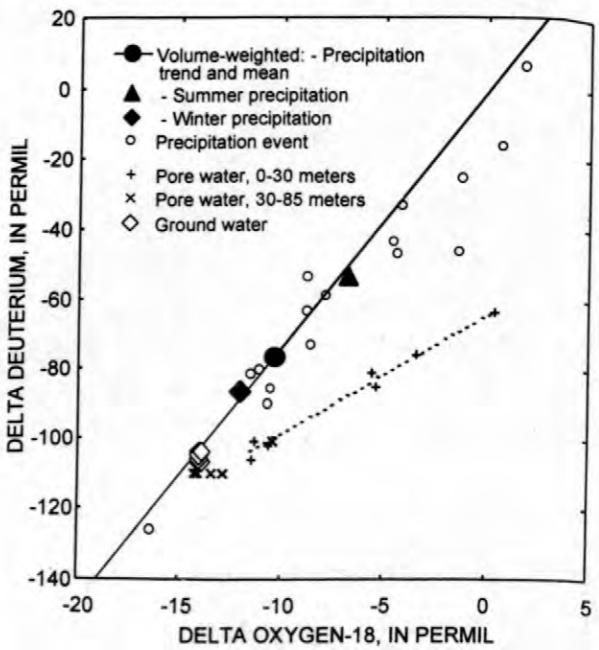

Figure 3. Stable isotopic composition of ground water, pore water, and precipitation at the Amargosa Desert Research Site. Precipitation data from Milne and others (1987); other data from Prudic and others (1997).

over a period of 14 years. These data, when corrected to the elevation of the ADRS using the dependence of δD on elevation reported by Smith and others (1979), suggest a volume-weighted mean δD of –79 permil for annual precipitation and –85 permil for winter precipitation.

Ground water at UZB-2 had a δD of –107 permil and $\delta^{18}O$ of –13.7 permil. Ground water at well MR-3 and nine additional wells within one-kilometer circle centered on the disposal area had nearly identical isotopic compositions, with δD ranging from –104 to –108 and $\delta^{18}O$ from –13.9 to –14.0 (Prudic and others, 1997; fig. 3).

The isotopically light ground water is consistent with other studies suggesting that much ground water in deep alluvial basins of the region represents recharge from an earlier climatic period (Smith and others, 1992). The carbon 14 (^{14}C) concentration in ground water from well MR-3 is about 26 percent modern carbon (Prudic and Striegl, 1995). The half life of ^{14}C is 5,730 years, giving an unadjusted age of about 11 thousand years for the ground water. Processes can modify the concentration of ^{14}C (Clark and Fritz, 1997; Bacon and Keller, 1998), thus, the degree to which this value represents the actual age of groundwater warrants further study.

On a δD-$\delta^{18}O$ plot the unsaturated zone data are approximated by a line with a slope of +3.3 (dashed line, fig. 3), considerably less than the +7.3 slope of the local meteoric water line (solid line, fig. 3). The point of departure of unsaturated zone water from the meteoric water line (MWL) is at a δD-$\delta^{18}O$ value significantly lighter than volume-weighted modern precipitation but close to that of ground water. Since evaporation produces a trajectory with a lower slope than that of the MWL, the δD-$\delta^{18}O$ data suggest upward flow of water in the unsaturated zone.

DISCUSSION AND CONCLUSIONS

Tritium concentrations at a depth of about 1.5 m did not change greatly with repeated sampling (Healy and others, 1999). Likewise, ^{14}C concentrations throughout the profile have remained relatively stationary (Prudic and others, 1999). At depths greater than five meters, in contrast, ^{3}H concentrations have changed significantly since water vapor was first sampled in 1994 (Prudic and others, 1999). The highest concentration observed to date in UZB-2, 2,570 TU, represents fewer than 3 tritium atoms in 10^{15} hydrogen atoms. The transport of ^{3}H is occuring at trace (femto-) levels. It does not necessarily follow that bulk movement of water can be inferred from these trends, as cross- and counter-current diffusion of tritium-bearing compounds are likely to occur. Oxygen-18 and D are, respectively, 11 and 12 orders of magnitude more abundant in pore water, explaining why tritium concentrations can be in apparent disequilibrium while ^{18}O and D values from the same aliquots appear stationary and in equilibrium. The absence of simultaneous liquid and vapor sampling precludes assessing the degree of isotopic equilibrium in tritiated water.

Additional drilling will be needed to test the uniformity and extent of deep trends, especially those of water content and matric potential. The proximity of high liquid contents possibly serving as a source of tritium, either from rainwater that transported waste downward and laterally from disposal trenches, or from infiltrated liquid waste, remains to be evaluated, as does the possibility that tritium is transported by compounds other than water. Nevertheless, the stable-isotope data, together with hydraulic, thermal, and gas-composition gradients provide consistent evidence of upward flow in areas of undisturbed vegetation.

REFERENCES

Andraski, B.J., 1997, Soil-water movement under natural-site and waste-site conditions--A multiple-year field study in the Mojave Desert, Nevada: Water Resources Research, v. 33, no. 9, p. 1901-1916.

Andraski, B.J., and Prudic, D.E., 1997, Soil, plant, and structural considerations for surface barriers in arid environments--Application of results from studies in the Mojave Desert near Beatty, Nevada, Barrier Technologies for Environmental Management, Summary of a Workshop: Washington., D.C., National Academy Press, p. D50-D60.

Andraski, B.J., and Stonestrom, D.A., 1999, Overview of research on water, gas, and

radionuclide transport at the Amargosa Desert Research Site, Nevada, Morganwalp, D.W., and Buxton, H.T., eds., U.S. Geological Survey Toxic Substances Hydrology Program --Proceedings for the Technical Meeting, Charleston, South Carolina, March 8-12, 1999--Volume 3--Subsurface Contamination from Point Sources: U.S. Geological Survey Water Resources Investigations Report 99-4018C, this volume.

Bacon, D.H., and Keller, C.K., 1998, Carbon dioxide respiration in the deep vadose zone: Implications for groundwater age dating: Water Resources Research, v. 34, no. 11, p. 3069-3077.

Clark, I.D., and Fritz, P., 1997, Environmental Isotopes in Hydrogeology: Boca Raton, Lewis Publishers, 328 p.

Ferronsky, V.I., and Polyakov, V.A., 1982, Environmental Isotopes in the Hydrosphere: New York, John Wiley and Sons, 762 p.

Fischer, J.M., 1992, Sediment properties and water movement through shallow unsaturated alluvium at an arid site for disposal of low-level radioactive waste near Beatty, Nye County, Nevada: U.S. Geological Survey Water-Resources Investigations Report 92-4032, 63 p.

Friedman, I., and O'Neil, J.R., 1977, Compilation of stable isotope fractionation factors of geochemical interest (6th ed.): U.S. Geological Survey Professional Paper Paper 440-KK, 12 p.

Healy, R.W., Striegl, R.G., Michel, R.L., Prudic, D.E., and Andraski, B.J., 1999, Tritium in water vapor in the shallow unsaturated zone at the Amargosa Desert Research Site, in Morganwalp, D.W., and Buxton, H.T., eds., U.S. Geological Survey Toxic Substances Hydrology Program --Proceedings for the Technical Meeting, Charleston, South Carolina, March 8-12, 1999--Volume 3--Subsurface Contamination from Point Sources: U.S. Geological Survey Water Resources Investigations Report 99-4018C, this volume.

Milne, W.K., Benson, L.V., and McKinley, P.W., 1987, Isotope content and temperature of precipitation in southern Nevada, August 1983-August 1986: U.S. Geological Survey Open-File Report 87-463, 32 p.

Nichols, W.D., 1987, Geohydrology of the unsaturated zone at the burial site for low-level radioactive waste near Beatty, Nye County, Nevada: U.S. Geological Survey Water Supply Paper 2312, 57 p.

Prudic, D.E., 1994, Estimates of percolation rates and ages of water in unsaturated sediments at two Mojave Desert sites, California-Nevada: Water-Resources Investigations Report 94-4160, U.S. Geological Survey, 19 p.

Prudic, D.E., Stonestrom, D.A., and Striegl, R.G., 1997, Tritium, deuterium, and oxygen-18 in water collected from unsaturated sediments near a low-level radioactive-waste burial site south of Beatty, Nevada: U.S. Geological Survey Water-Resources Investigations Report 97-4062, 23 p.

Prudic, D.E., and Striegl, R.G., 1995, Tritium and radioactive carbon (^{14}C) analyses of gas collected from unsaturated sediments next to a low-level radioactive-waste burial site south of Beatty, Nevada, April 1994 and July 1995: U.S. Geological Survey Open File Report 95-471, 7 p.

Prudic, D.E., and Striegl, R.G., 1994, Water and carbon dioxide movement through unsaturated alluvium near an arid disposal site for low-level radioactive waste, Beatty, Nevada [abs.]: Eos, American Geophysical Union Transactions, v. 75, no. 16, p. 161.

Prudic, D.E., Striegl, R.G., Healy, R.W., Michel, R.L., and Hass, H., 1999, Tritium and ^{14}C concentrations in unsaturated zone gases at test hole UZB-2, Amargosa Desert Research Site, 1994-1998, in Morganwalp, D.W., and Buxton, H.T., eds., U.S. Geological Survey Toxic Substances Hydrology Program -- Proceedings for the Technical Meeting, Charleston, South Carolina, March 8-12, 1999--Volume 3--Subsurface Contamination from Point Sources: U.S. Geological Survey Water Resources Investigations Report 99-4018C, this volume.

Rubin, J., 1967, Numerical method for analyzing hysteresis-affected, post-infiltration redistribution of soil moisture: Soil Science Society of America Proceedings, v. 31, no. 1, p. 13-20.

Smith, G.I., Friedman, I., Gleason, J.D., and Warden, A., 1992, Stable isotope composition of waters in southeastern California: 2.

of waters in southeastern California: 2. Groundwaters and their relation to modern precipitation: Journal of Geophysical Research, v. 97, no. D5, p. 5813-5823.

Smith, G.I., Friedman, I., Klieforth, H., and Hardcastle, K., 1979, Areal distribution of deuterium in eastern California precipitation, 1968-1969: Journal of Applied Meteorology, v. 18, p. 172-188.

Thorstenson, D.C., Mackenzie, F.T., and Ristvet, B.L., 1972, Experimental vadose and phreatic cementation of skeletal carbonate sand: Journal of Sedimentary Petrology, v. 42, p. 162-167.

Wilshire, H.G., and Friedman, I., 1999, Contaminant migration at two low-level radioactive waste sites in arid western United States -- A review: Environmental Geology, v. 37, no. 1-2, p. 112-123.

Wood, B.D., Keller, C.K., and Johnstone, D.L., 1993, In situ measurement of microbial activity and controls on microbial CO2 production in the unsaturated zone: Water Resources Research, v. 29, no. 3, p. 647-659.

Wood, W.W., and Petraitis, M.J., 1984, Origin and distribution of carbon dioxide in the unsaturated zone of the Southern High Plains of Texas: Water Resources Research, v. 20, no. 9, p. 1193-1208.

AUTHOR INFORMATION

David A. Stonestrom, U.S. Geological Survey, Menlo Park, California (dastones@usgs.gov)

David E. Prudic, U.S. Geological Survey, Carson City, Nevada (deprudic@usgs.gov)

Robert G. Striegl, U.S. Geological Survey, Denver, Colorado (rgstriegl@usgs.gov)

Tritium and ^{14}C Concentrations in Unsaturated-Zone Gases at Test Hole UZB-2, Amargosa Desert Research Site, 1994-98

By David E. Prudic, Robert G. Striegl, Richard W. Healy, Robert L. Michel, and Herbert Haas

ABSTRACT

Tritium concentrations have been determined yearly since April 1994 from water-vapor samples collected at test hole UZB-2. The hole was drilled about 100 m (meters) south of the southwest corner of a commercial burial site for low-level radioactive wastes in September 1993. UZB-2 is equipped with ten 2.5-cm (centimeters) diameter air ports permanently installed in the unsaturated zone between the depths of 5.5 and 108.8 m below land surface. Depth to ground water is about 110 m. Additional sampling ports were driven by hand to depths of 0.5, 1.0 and 1.5 m in May 1997. Initial samples of water vapor collected in April 1994 showed elevated tritium concentrations of more than 100 TU (tritium units) from all 10 air ports, with a maximum concentration of 762±10 TU from an air port at a depth of 24.1 m. Subsequent tritium concentrations increased in all air ports, although tritium concentrations at depths of less than 34.1 m have remained relatively constant since July 1995. The largest observed increase in tritium has been at a depth of 47.9 m. There, tritium concentration has increased from 198±5 TU in April 1994 to 2,570±30 TU in June 1998. Large increases also have been measured in samples collected from air ports at depths of 106.4 and 108.8 m, just above the water table.

During September and October 1998, carbon dioxide samples were collected from all ten air ports in UZB-2 and at a depth of 1.5 m, and analyzed for radioactive carbon-14 (^{14}C). ^{14}C concentrations are highest in air ports at depths less than 6 m where they exceed 2,000 pmc (percent modern carbon). Concentrations decrease rapidly in air ports at depth and are about 20 pmc below 94.2 m. However, at 47.9 meters, the ^{14}C concentration is 205±1 pmc, which is 2 to 4 times higher than concentrations in air ports immediately above and below. This depth corresponds to the largest tritium increase in UZB-2. Concentrations of both tritium and ^{14}C are greater than what could be expected from atmospheric fallout. The distribution of tritium and ^{14}C likely represent a complex pattern of lateral and vertical transport through the unsaturated zone from buried wastes to UZB-2.

INTRODUCTION

Test hole UZB-2 was drilled in September 1993, about 100 m south of the southwest corner of a commercial burial area for low-level radioactive wastes. The burial area is located in the Amargosa Desert about 18 km (kilometers) south of Beatty, Nev. (see Andraski and Stonestrom, 1999 for location map). A low angle air photograph (fig. 1) shows the relation of UZB-2 to the waste-burial area and to other research facilities at the Amargosa Desert Research Site (ADRS). A description of the research facilities at the ADRS is given by Andraski and Stonestrom (1999). UZB-2 was drilled as part of a study to determine the depth of atmospheric air circulation in the thick unsaturated zone at the ADRS (Prudic, 1996).

Sediments at UZB-2 and in the vicinity of the waste-burial area generally are coarse grained, and consist predominately of a poorly sorted mixture of silt, sand and gravel deposited by debris flows or in overbank areas. These deposits are separated by less abundant moderately sorted sand and gravel deposited in channels of the ancestral Amargosa River. A sandy silt to silty sand covers much of the land surface and ranges from 0.3 to 1 m in thickness. The silty sand is absent in active channels, where deposits are sand and gravel. A lag gravel forms a desert pavement over the silty sand.

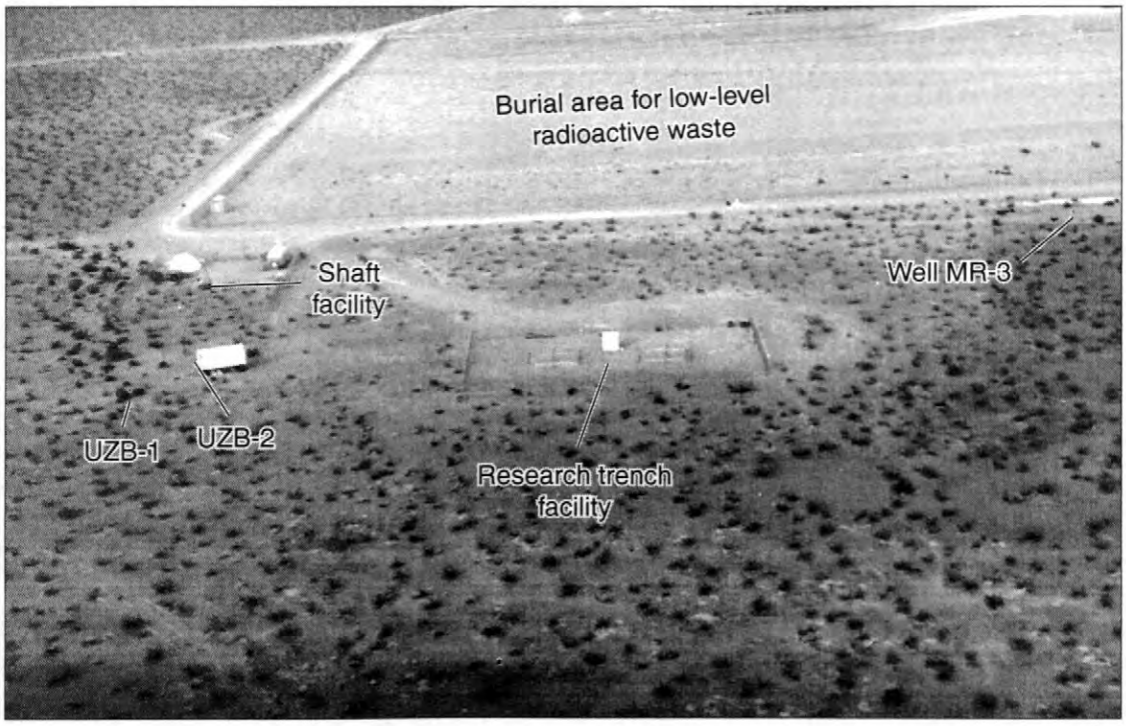

Figure 1. Oblique aerial photograph showing Amargosa Desert Research Site in relation to southwest corner of burial area for low-level radioactive wastes. The site is located about 18 kilometers south of Beatty, Nevada. View is looking north. Photograph by D. E. Prudic, December 1998.

The air ports were initially sampled for tritium and ^{14}C in April 1994. Results of these samples showed greater concentrations of tritium and ^{14}C than were expected. These concentrations were greater than what could be explained from atmospheric fallout (Prudic and Striegl, 1995; Prudic and others, 1997). Observed concentrations of tritium cannot be explained by applying current tritium transport models using reasonable ranges of geological, hydrological, and chemical conditions known for the site. However, observed concentrations of $^{14}CO_2$ could be explained by either diffusive or advective transport of the radioactive gas from the waste-burial site (Striegl and others, 1996). Data collected at UZB-2 continues to cause speculation regarding mechanisms that control lateral and vertical migration of tritium and ^{14}C through the unsaturated zone.

The purpose of this report is to present and discuss the distribution of tritium, and ^{14}C concentrations in unsaturated-zone gases at UZB-2 from the time it was drilled through the most recent samples collected in 1998. Although all tritium and ^{14}C analyses of samples collected at UZB-2 will be discussed and presented in figures, only the most recent analyses for tritium and ^{14}C of samples collected in 1998 will be tabulated in this report. Previous analyses are tabulated by Prudic and Striegl (1995), Prudic and others (1997), and Striegl and others (1998) and are not repeated herein.

Drilling UZB-2 and Sampling Air Ports

UZB-2 was drilled to a total depth of 114.6 m below land surface, and extended about 5 m below the water table. The upper 91 m was drilled using an ODEX air-hammer method (Hammermeister and others, 1985), in which casing is connected to an eccentric bit attached to a down-hole hammer. Air injected down the drill stem operates the hammer and also carries cuttings to the surface through the inside of the casing. Cores were collected at intervals of 26.7 to 27.3 m, 35.9 to 36.5 m, 48.0 to 48.6 m, 60.2 to 60.8 m, 72.5 to 73.1 m and 84.7 to 85.3 m. No cores were collected below this depth because a section of casing broke when the casing had reached 91 m. The remaining hole was drilled uncased using a rotary tricone bit and air to remove the cuttings (Prudic and Striegl, 1995). In addition

to cores collected in UZB-2, seven cores were collected between 2.3 and 21.2 m depths while drilling test hole UZB-1 in November 1992. Because the two holes are only 6 m apart, cores were not obtained in UZB-2 at depths less than 21 m.

Ten air ports were installed in UZB-2 as the hole was being backfilled. Each air port consists of a 30-cm long stainless-steel screen that has an outside diameter of 2.3 cm and slot openings of 0.2 mm in width. Each screen is connected to a nominal 6-mm diameter nylon tube that extends into a trailer parked at the test hole (fig. 1). Depths to the midpoint of each air port are 5.5, 11.9, 18.0, 24.1, 34.1, 47.9, 57.6, 94.2, 106.4, and 108.8 m. Each port is surrounded by a 60-cm thick medium gravel and separated by bentonite grout. Additional details on the drilling and backfilling of UZB-2 are presented by Prudic and Striegl (1995) and Prudic and others (1997).

In May 1996, a small-diameter steel tube was driven by hand to a depth of 1.68 m at UZB-2, sampled for tritium and removed. The tritium concentration at this depth was 20,600±200 TU (error of analyses is due to counting uncertainty and is reported at one standard deviation) and exceeded tritium concentrations from air ports in UZB-2 (Prudic and others, 1997). Subsequently in May 1997, three small-diameter steel tubes (outside diameter of 9.5 mm and inside diameter of 3.2 mm) were driven by hand to depths of 0.5, 1.0 and 1.5 m, respectively, sampled and left in place. Tritium concentrations in these tubes for May 1997 were 12,180±110, 12,000±120 and 15,510±140 TU, respectively (Striegl and others, 1998).

Water vapor was collected from air ports and the three steel tubes at UZB-2 during June 16-17, 1998. The samples were collected by connecting 6-mm inside-diameter Bevaline tubing to the exposed end of the nylon or steel tube, attaching a glass freeze trap to the free end of the Bevaline tubing, and attaching another piece of Bevaline tubing from the freeze trap to a diaphragm pump. Unsaturated-zone gas was pulled through the tubing and glass freeze trap when the pump was on. Pumping rates ranged from about 1 to 2 L (liters) of air per minute. Each freeze trap was chilled in a slurry of dry ice and ethanol or propanol. This resulted in water vapor being frozen in the trap as air passed through it (Striegl, 1988). Between 5 and 10 mL (milliliters) of water was collected from each air port or steel tube. Water frozen in each trap was thawed and the liquid was poured into glass vials and sealed. The water samples were analyzed at the USGS Water Resources Division isotope laboratory in Menlo Park, Calif. Analyses of tritium in water vapor from air ports at UZB-2 are listed in table 1.

Table 1. Tritium concentration in water vapor collected from sampling ports at UZB-2 during June 16-17, 1998.

Depth (meters below land surface)	Tritium (tritium units)	Counting uncertainty (tritium units)[1]
0.5	941	±23
1.0	10,320	±110
1.5	14,580	±150
5.5	288	±9
11.9	922	±28
18.0	543	±19
24.1	1,082	±18
34.1	940	±19
47.9	2,570	±30
57.6	1,040	±30
94.2	1,640	±40
106.4	1,488	±22
108.8	1,623	±27

[1]Uncertainty represents the counting error at one standard deviation.

A similar method was used for collecting CO_2 gas between September 29 and October 7, 1998, except unsaturated-zone air was bubbled through a gas-wash bottle containing 300 mL of 5-molar potassium-hydroxide solution to collect the CO_2 (Striegl, 1988). CO_2 gas also was collected from the atmosphere about 3.2 km (kilometers) south of UZB-2. The gas was bubbled through the potassium-hydroxide solution for 3 to 7 days to obtain a sufficient quantity of carbon. ^{14}C concentration in CO_2 was analyzed at the Radiocarbon Laboratory, Desert Research Institute, Las Vegas, Nev., using the method described by Haas and others (1983). Analyses of ^{14}C in CO_2 gas are listed in table 2.

Table 2. ^{14}C concentration in carbon dioxide collected from sampling ports at UZB-2 during September 29- October 7, 1998.

Depth (meters below land surface)	^{14}C (percent modern carbon)	Counting uncertainty (percent modern carbon)[1]
1.5	2,739	±12
5.5	2,127	±16
11.9	933	±5
18.0	407	±2
24.1	205	±2
34.1	84.4	±0.6
47.9	205	±1
57.6	42.3	±0.3
94.2	17.5	±0.3
106.4	18.8	±0.3
108.8	20.8	±0.4
Air[2]	112	±1

[1]Uncertainty represents the counting error at one standard deviation.
[2]Air sample collected 3.2 km south of UZB-2.

RESULTS

Tritium concentrations in water vapor at UZB-2 from April 1994 through June 1998 are shown in figure 2. Highest observed tritium concentrations are from air ports at depths of 1.5 to 1.68 m below land surface. These concentrations are within an area where high tritium concentrations have been observed in a near-surface sand and gravel (Striegl and others, 1998; Healy and others, 1999). At deeper depths, tritium concentrations in water vapor have increased since April 1994.

One hypothesis of the measured changes in tritium concentrations at UZB-2 is that tritium was present in the hole at the time it was drilled and that changes in tritium concentration are an artifact of the large quantities of low-tritium air injected into the hole during drilling. Substantial quantities of air could have entered the unsaturated sediments, particularly where the hole was uncased below a depth of 91 m. This air would slowly reach a new equilibrium with pore water that presumably contained elevated concentrations of tritium. If this were the case, there should have been substantial quantities of tritium in core samples collected while drilling test holes UZB-1 and UZB-2.

Pore water from core samples collected while drilling test holes UZB-1 and UZB-2 were extracted using a cyrodistillation method, and analyzed for tritium and the stable isotopes deuterium and ^{18}O (Prudic and others, 1997). Tritium in pore water was considerably less than that measured from water vapor pumped from the air ports (fig. 2). Air introduced into the core samples while drilling would not be sufficient to change the tritium concentration of pore water in cores, because the mass of water in the air-filled pore space of the cores is tens of thousands times lower than the mass of water in the core samples. Additionally, deuterium and ^{18}O concentrations of pore water are in approximate isotopic equilibrium with the water vapor (Stonestrom and others, 1999), which suggests little effect of air injected during drilling.

Implication from tritium concentrations in pore water of cores is that tritium was present to depths of 85 m at UZB-2 prior to drilling in September 1993. Assuming that tritium concentrations in water vapor were in equilibrium with pore water when the cores were collected, tritium concentrations in water vapor would be slightly less than that in the pore water (fig. 2). Estimates of water vapor in equilibrium with pore water were calculated from (Ferronsky and Polyakov, 1982):

$$C_v = \frac{C_l}{\alpha_{HTO}} \quad , \qquad (1)$$

where

C_v is tritium concentration in water vapor in equilibrium with liquid water, in tritium units,

C_l is tritium concentration in liquid water, in tritium units, and

α_{HTO} is fractionation factor for tritiated water, which varies from 1.108 to 1.103 over the temperature range corresponding to depths at which cores were collected.

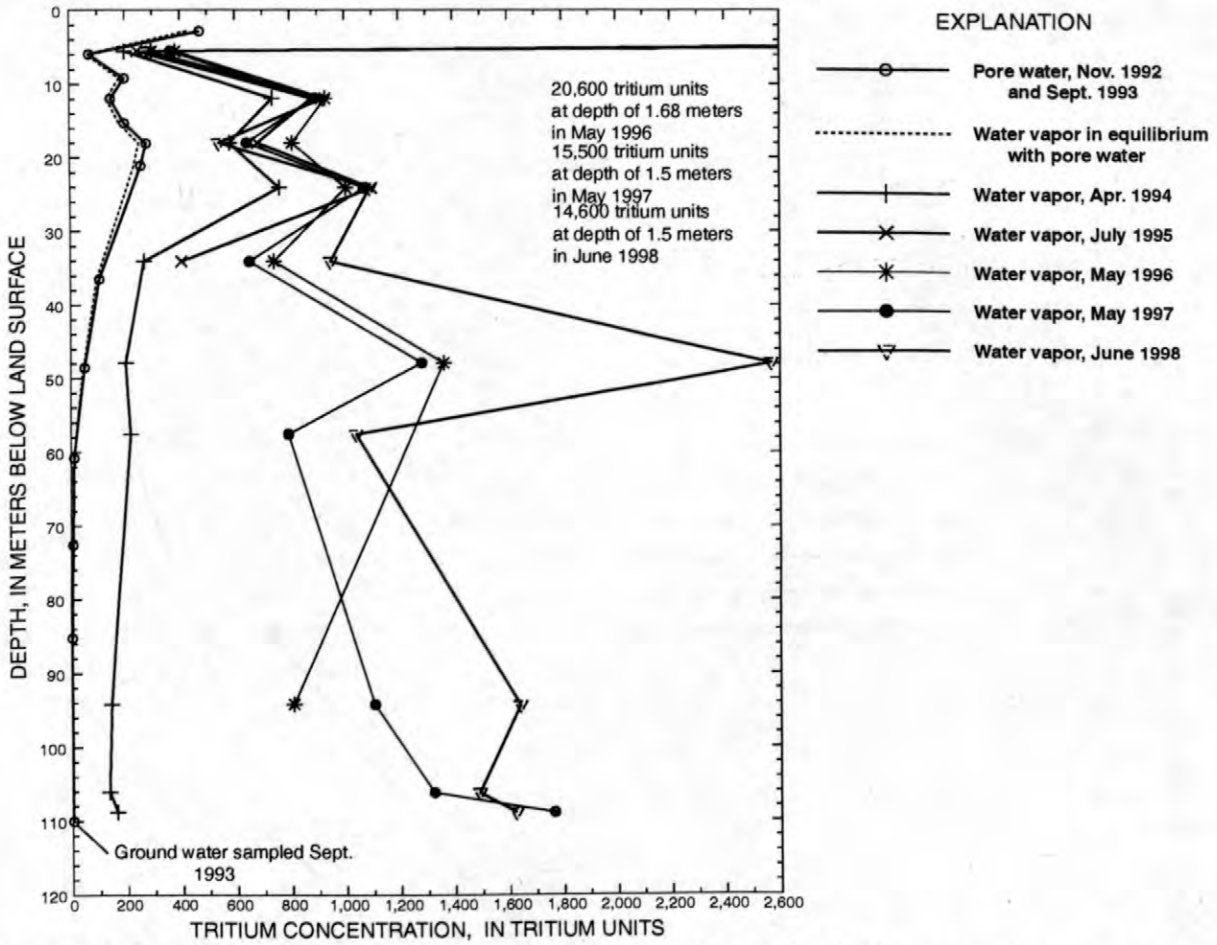

Figure 2. Tritium concentration in water extracted from UZB-1 and UZB-2 core samples collected November 1992 and September 1993, respectively, and in water vapor from UZB-2 collected April 1994, July 1995, May 1996, May 1997 and June 1998. Equilibrium values for water vapor (dotted line) were calculated on basis of temperatures measured in UZB-1 and UZB-2. Modified from Prudic and others, 1997, fig. 6, and Striegl and others, 1998, fig. 4.

The difference in tritium concentrations between pore water from cores and subsequently sampled water vapor could be due to increasing tritium concentrations throughout the profile (fig. 3). Tritium concentrations in water vapor at depths corresponding to air ports for November 1992 and September 1993 were linearly interpolated from tritium concentrations calculated from pore water in cores. Tritium concentrations for depths greater than 85.2 m were assumed below detection for September 1993 because tritium concentrations in pore water at that depth and in ground water at 110 m were below detection.

Tritium concentrations in water vapor have increased markedly in air ports at depths greater than 34 m, whereas those in air ports at depths less than 24.1 m have remained relatively constant since July 1995 (fig. 3) The greatest observed increase is at a depth of 47.9 m, where tritium concentrations in water vapor have increased from 198±5 TU in April 1994 (Prudic and Striegl, 1995) to 2,570±30 TU in June 1998 (table 1). As of May 1997, tritium concentrations in the 3 air ports at depths greater than 94 m exceeded those in the 4 air ports at depths 24.1 m and less (fig. 3).

Migration of tritium through the unsaturated zone from the waste-burial area is the most likely explanation of the presence of tritium measured at UZB-2 (Striegl and others, 1996 and Prudic and others, 1997), although processes producing tritium migration are not known. If liquid and vapor-phase water are in isotopic equilibrium with respect to tritium, and if the source of tritiated water is at least 100 m away, then the distribution of tritium at UZB-2 (including tritium at depths less than 2 m) cannot be explained by vapor transport alone (Striegl and

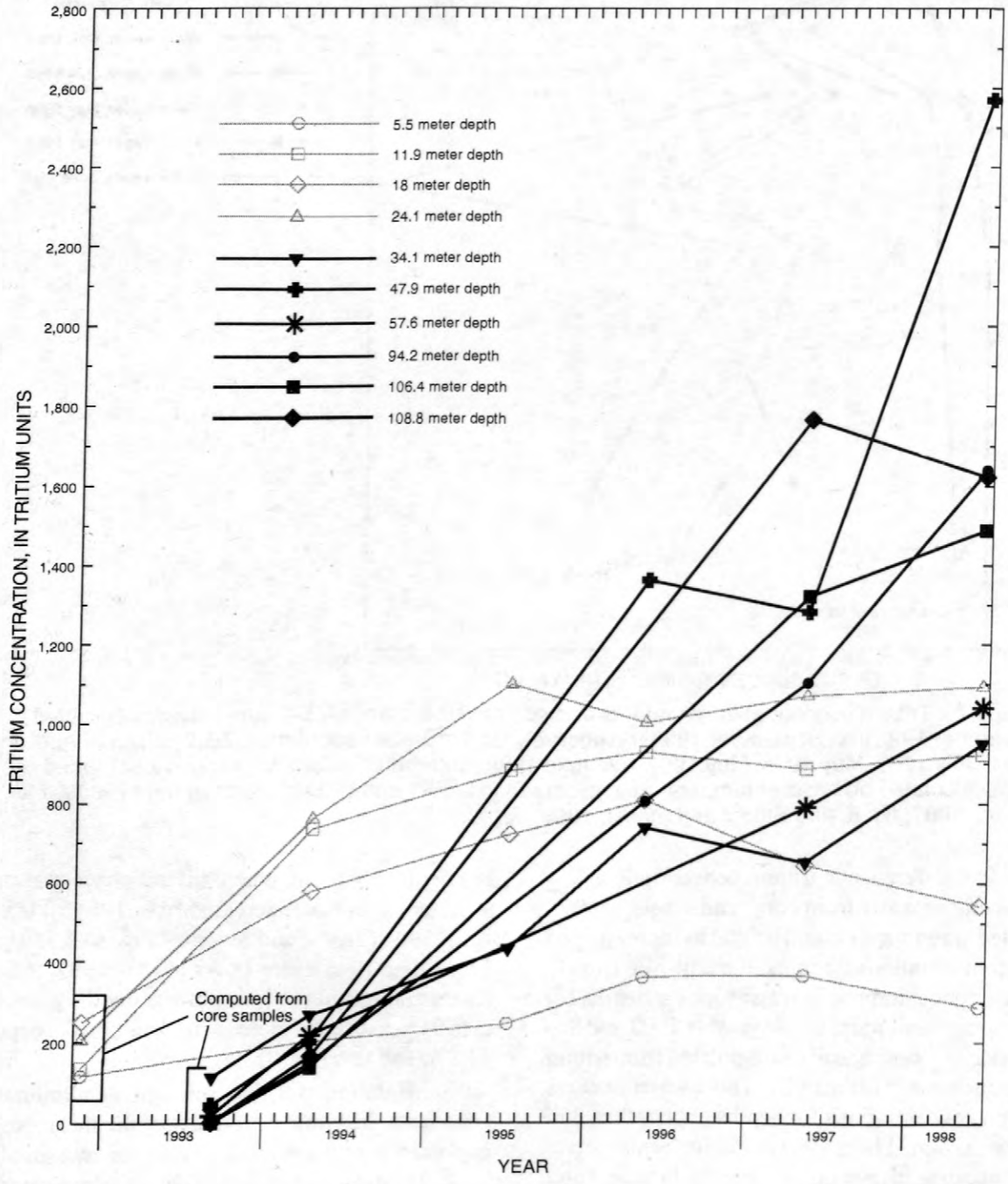

Figure 3. Concentrations of tritium in water vapor sampled from UZB-2 air ports in April 1994, July 1995, May 1996, May 1997, and June 1998, and concentrations in water vapor in November 1992 and September 1993 computed on basis of tritium concentrations in pore water extracted from core samples. Modified from Prudic and others, 1997, fig. 9.

others, 1996). Advective transport by liquid flow from the waste-burial area should produce an increase in water content at intervening points. However, water content in a 30-m deep neutron access hole between UZB-2 and the waste-burial area has not changed measurably below a depth of 1 m since 1987 (Andraski and Prudic, 1997). Low water contents and water pressures less than -3 MPa (megaPascals) measured at the nearby shaft and research trench facilities indicate little potential for rapid liquid flow.

The distribution of ^{14}C concentrations in unsaturated zone CO_2 at UZB-2 has not changed greatly since July 1995 (fig. 4). As with tritium, ^{14}C concentrations are highest at shallow depth (1.5 m) and exceed what would be expected from present-day atmospheric fallout (112± 1 pmc measured 3.2 km to south of UZB-2; table 2) or from the early 1960's peak concentration in the atmosphere of the northern hemisphere (about 180 pmc; Broecker and others, 1980). ^{14}C concentrations increase toward the waste-burial area and are in excess of 400,000 pmc at a depth of 1.68 m at two locations along the southern security fence of the waste-burial area (Prudic and Striegl, 1995), whereas ^{14}C concentrations in the unsaturated zone are at or below atmospheric concentrations 3.2 km south of UZB-2 (Prudic and Striegl, 1995). Diffusive or advective gas transport of ^{14}C as $^{14}CO_2$ can explain the observed concentrations of ^{14}C at UZB-2 (Striegl and others, 1996).

Unlike tritium concentrations at UZB-2, ^{14}C concentrations decrease rapidly with depth (fig. 4). The three air ports between 94.2 and 108.8 m depths have ^{14}C concentrations from 17.5±0.3 to 20.8±0.4 pmc (table 2). These concentrations are similar to the 26 pmc measured in ground water at a nearby well (MR-3, fig. 1). The lack of ^{14}C at depths greater than 50 m can be explained by upward diffusing CO_2 having low concentrations of ^{14}C (Prudic and Striegl, 1994, Stonestrom and others, 1999).

The air port at a depth of 47.9 m was sampled for the first time in September-October 1998 and the ^{14}C concentration was considerably higher than adjacent air ports at depths of 34.1 and 57.6 m (fig. 4 and table 2). This air port also has had the greatest increase in tritium concentration and corresponds to the highest soil-water pressure (and hydraulic head) measured from core samples (Andraski and Prudic, 1997).

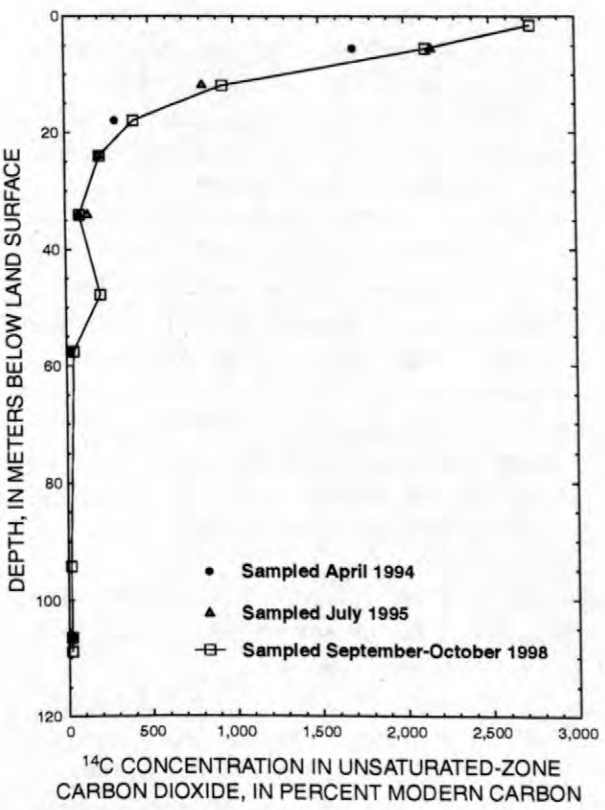

Figure 4. Concentrations of ^{14}C in carbon dioxide gas extracted from UZB-2 air ports for April 1994, July 1995, and September-October 1998. Modified from Prudic and Striegl, 1995, fig. 2.

In conclusion, Tritium and ^{14}C concentrations observed at UZB-2 likely represent a complex pattern of lateral and vertical transport through the unsaturated zone. However, mechanisms causing the migration of tritium and ^{14}C, including uncertainties in the source of each radionuclide, are not yet understood.

REFERENCES

Andraski, B.J, and Prudic, D.E., 1997, Soil, plant, and structural consideration for surface barriers in arid environments—application of results from studies in the Mojave Desert near Beatty, Nevada *in* Barrier Technologies for Environmental Management, Summary of a Workshop: Washington, D.C., National Academy Press, p. D50-D60.

Andraski, B.J., and Stonestrom, D.A., 1999, Overview of research on water, gas, and radionuclide transport at the Amargosa Desert Research Site, Nevada *in* Morganwalp, D.W., and Buxton, H.T., eds., U.S. Geological Survey Toxic Substances Hydrology Program—Proceedings for the Technical Meeting, Charleston, South Carolina, March 8-12, 1999—Volume 3. Subsurface Contamination from Point Sources: U.S. Geological Survey Water-Resources Investigations Report 99-4018C, this volume.

Broecker, W.S., Peng, T-H., and Engh, R., 1980, Modeling the carbon system *in* Stuiver, M. and Kra, R.S., eds., International ^{14}C Conference, 10th Proceedings: Radiocarbon, v. 22, no. 3, p. 565-598.

Ferronsky, V.I., and Polyakov, V.A., 1982, Environmental isotopes in the hydrosphere: New York, John Wiley and Sons, 762 p.

Haas, H., Fisher, D.W., Thorstenson, D.C., and Weeks, E.P., 1983, $^{13}CO_2$ and $^{14}CO_2$ measurements on soil atmosphere in the subsurface unsaturated zone in the Western Plains of the U.S.: Radiocarbon, v. 23, no. 2, p. 301-314.

Hammermeister, D.P., Blout, D.O., and McDaniel, J.C., 1985, Drilling and coring methods that minimize the disturbance of cuttings, core, and rock formation in the unsaturated zone, Yucca Mountain, Nevada: National Water Well Association, Conference on Characterization and Monitoring of the Vadose (Unsaturated) Zone, Denver, Colo., November 1984, Proceedings, p. 507-541.

Healy, R.W., Striegl, R.G., Michel, R.L., Prudic, D.E., and Andraski, B.J., 1999, Tritium in shallow unsaturated zone gases at the Amargosa Desert Research Site *in* Morganwalp, D.W., and Buxton, H.T., eds., U.S. Geological Survey Toxic Substances Hydrology Program—Proceedings for the Technical Meeting, Charleston, South Carolina, March 8-12, 1999—Volume 3. Subsurface Contamination from Point Sources: U.S. Geological Survey Water-Resources Investigations Report 99-4018C, this volume.

Prudic, D.E., 1996, Water-vapor movement through unsaturated alluvium in Amargosa Desert near Beatty, Nevada—Current understanding and continuing studies *in* Stevens, P.R., and Nicholson, T.J., eds., Joint U.S. Geological Survey and U.S. Nuclear Regulatory Commission Workshop on Research Related to Low-Level Radioactive Waste Disposal, May 4-6, 1993, Reston, Va., Proceedings: U.S. Geological Survey Water-Resources Investigations Report 95-4015, p. 157-166.

Prudic, D.E., and Striegl, R.G., 1994, Water and carbon-dioxide movement through unsaturated alluvium near an arid disposal site for low-level radioactive waste, Beatty, Nevada [abs.]: EOS, American Geophysical Union Transactions, v. 75, no. 16, p. 161.

——— 1995, Tritium and radioactive carbon (^{14}C) analyses of gas collected from unsaturated sediments next to a low-level radioactive-waste burial site south of Beatty, Nevada, April 1994 and July 1995: U.S. Geological Survey Open-File Report 95-471, 7 p.

Prudic, D.E., Stonestrom, D.A., and Striegl, R.G., 1997, Tritium, deuterium, and oxygen-18 in water collected from unsaturated sediments near a low-level radioactive-waste burial site south of Beatty, Nevada: U.S. Geological Survey Water-Resources Investigations Report 97-4062, 23 p.

Stonestrom, D.A., Prudic, D.E., and Striegl, R.G., 1999, Isotopic composition of water in a deep unsaturated zone beside a radioactive-waste disposal area near Beatty, Nevada *in* Morganwalp, D.W., and Buxton, H.T., eds., U.S. Geological Survey Toxic Substances Hydrology Program—Proceedings for the Technical Meeting, Charleston, South Carolina, March 8-12, 1999—Volume 3. Subsurface Contamination from Point Sources: U.S. Geological Survey Water-Resources Investigations Report 99-4018C, this volume.

Striegl, R.G., 1988, Distribution of gases in the unsaturated zone at a low-level radioactive-waste disposal site near Sheffield, Illinois: U.S. Geological Survey Water Resources Investigations Report 88-4025, 69 p.

Striegl, R.G., Healy, R.W., Michel, R.L., and Prudic, D.E., 1998, Tritium in unsaturated zone gases and air at the Amargosa Desert Research Site, and in spring and river water, near Beatty, Nevada, May 1997: U.S. Geological Survey Open-File Report 97-778, 13 p.

Striegl, R.G., Prudic, D.E., Duval, J.S., Healy, R.W., Landa, E.R., Pollock, D.W., Thorstenson, D.C., and Weeks, E.P., 1996, Factors affecting tritium and ^{14}Carbon distributions in the unsaturated zone near the low-level radioactive-waste burial site south of Beatty, Nevada: U.S. Geological Survey Open-File Report 96-110, 16 p.

AUTHOR INFORMATION

David E. Prudic, U.S. Geological Survey, Carson City, Nevada
Robert G. Striegl and Richard W. Healy, U.S. Geological Survey, Denver, Colorado
Robert L. Michel, U.S. Geological Survey, Menlo Park, California
Herbert Haas, Desert Research Institute, Water Resources Center, Las Vegas, Nevada

Tritium in Water Vapor in the Shallow Unsaturated Zone at the Amargosa Desert Research Site

By Richard W. Healy, Robert G. Striegl, Robert L. Michel, David E. Prudic, and Brian J. Andraski

ABSTRACT

Samples of water vapor in soil gas were obtained at the U.S. Geological Survey's Amargosa Desert Research Site in 1997 and 1998 from a depth of 1.5 m (meters) within a 300 m by 300 m grid that lies immediately to the south and west of a low-level radioactive-waste disposal site. The gas samples were analyzed for tritium. Fifty-eight samples were collected in May 1997; 61 samples were collected in June 1998. Measured tritium concentrations ranged from 16 ± 9 TU (tritium units) to 36,900 ± 300 TU in 1997, and from 6 ± 6 TU to 37,360 ± 450 TU in 1998. Concentrations decreased from northeast to southwest across the grid. In general, there was very little difference in tritium concentrations between the two sampling periods.

INTRODUCTION

Elevated tritium concentrations in water vapor collected from the unsaturated zone and plants at the Amargosa Desert Research Site (ADRS), south and west of a commercial burial site for low-level radioactive waste near Beatty, Nevada (Prudic and Striegl, 1995) have caused speculation regarding the exact mechanisms that control tritium transport in arid unsaturated zones. Measured tritium concentrations in the ADRS unsaturated zone are higher than concentrations predicted by applying current tritium transport models to ranges of geological, hydrological, and chemical conditions that encompass *in situ* conditions at the site (Striegl and others, 1996). Understanding of tritium transport at the ADRS is complicated by several unknown factors, including tritium source strength; form, timing, and location of tritium contamination; complex geology of the unsaturated zone; and the extent of liquid-water/water-vapor interaction that occurs in the unsaturated zone.

During May 15-24, 1997, as part of ongoing research to understand the mechanisms that control the transport of tritium in arid unsaturated zones, water-vapor samples were collected from depths of 1.5 m over an area of 250 m by 250 m that lies to the south and west of the burial site. During June 15-18, 1998, samples were again collected from the grid (which was expanded by 50 m to both the south and the west). The focus of this investigation is to determine the spatial distribution of tritium in water vapor. Spatial data on tritium concentrations can provide insight regarding the direction and extent of tritium movement at the ADRS and may help in selecting sites for new deep test holes.

The purpose of this report is to present and discuss the spatial distribution of tritium concentration in the shallow unsaturated zone at the ADRS and to compare measurements made in 1997 with those made in 1998. Tritium concentrations measured in 1997 are discussed in Striegl and others (1998), so the emphasis in this report will be on the samples obtained in 1998.

STUDY SITE

Soil-gas samples were collected within a 300 m by 300 m grid which lies directly south and west of a commercial low-level radioactive-waste burial

site in the Amargosa River Valley, approximately 17

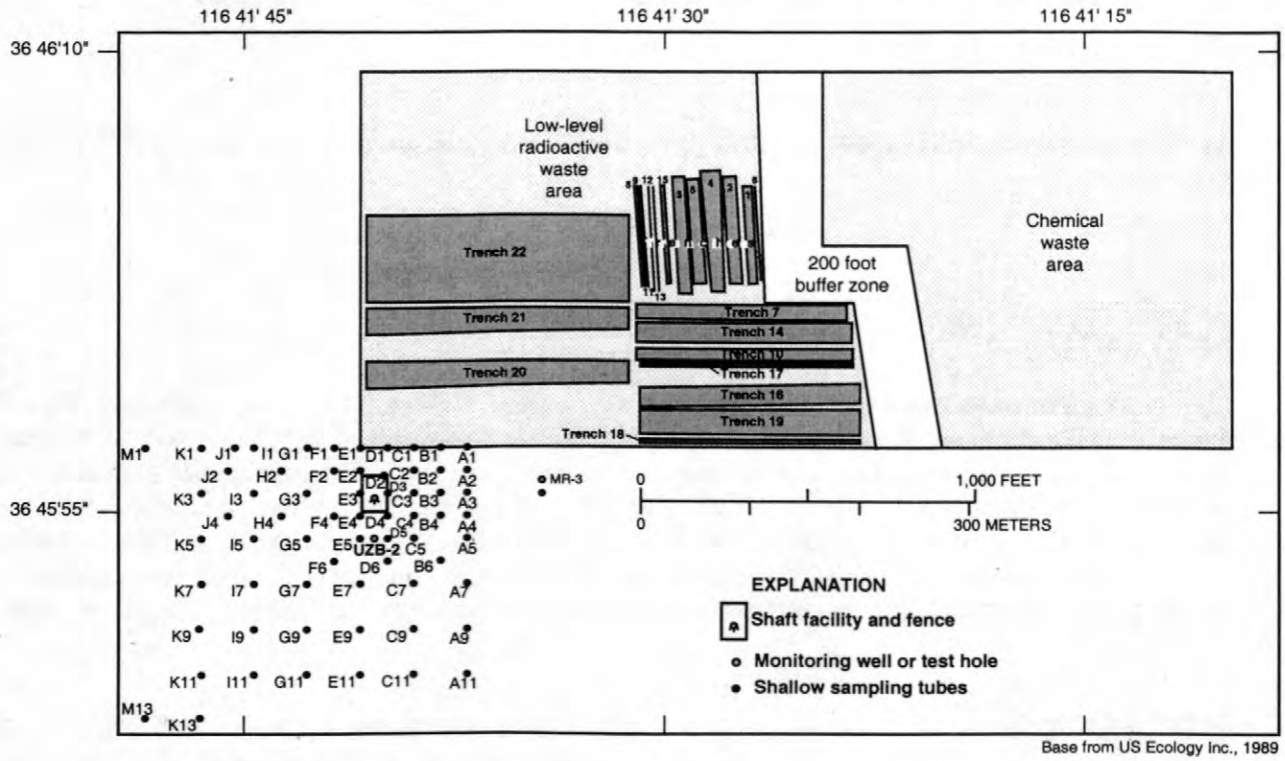

Figure 1. Map identifying node distribution within the sampling grid at the Amargosa Desert Research Site

km (kilometers) south of Beatty (see figure 1 in Andraski and Stonestrom, 1999). Sampling points within the grid are alined in an east-west and north-south fashion and are spaced at 25 m intervals (fig 1). Sampling points are identified by letter for columns, which increase from east (column A) to west (column M) and by number for rows, which increase from north (row 1) to south (row 13). Row 1 corresponds to the south fence of the burial site. In addition to the grid sampling points, shallow soil-gas samples were obtained near well MR-3, approximately 50 m east of sampling point A2 and near borehole UZB-2 (at depths of 0.5, 1.0, and 1.5 m) between grid points D5 and E5.

METHODS

At the grid nodes that were sampled, steel tubes having an outside diameter of 9.5 mm (millimeters) and an inside diameter of 3.2 mm were hand driven 1.5 m into the unconsolidated deposits or to the point of refusal, if that was slightly shallower. Prior to driving, a nail having a 9.5 mm head was inserted into the bottom end of each tube to prevent clogging of the tube with sediment as it was driven downward. After driving, the tube was pulled upward about 10 mm to free the nail and open a space at the bottom of the tube. For the purpose of reporting, the depth of sampling at the grid nodes is referred to as the "1.5 m depth". Tubes at most of the grid points were installed in 1997. Eight additional tubes were installed in June 1998: B4, H4, I11, K9, K13, M1, M13, and adjacent to well MR-3.

Water vapor was collected by attaching 6 mm inside diameter Bevaline tubing to the tops of the steel tubes, attaching a glass freeze trap to the free end of the tubing, and pulling unsaturated zone air through the sampling apparatus using a diaphragm

air-sampling pump. The freeze traps were kept

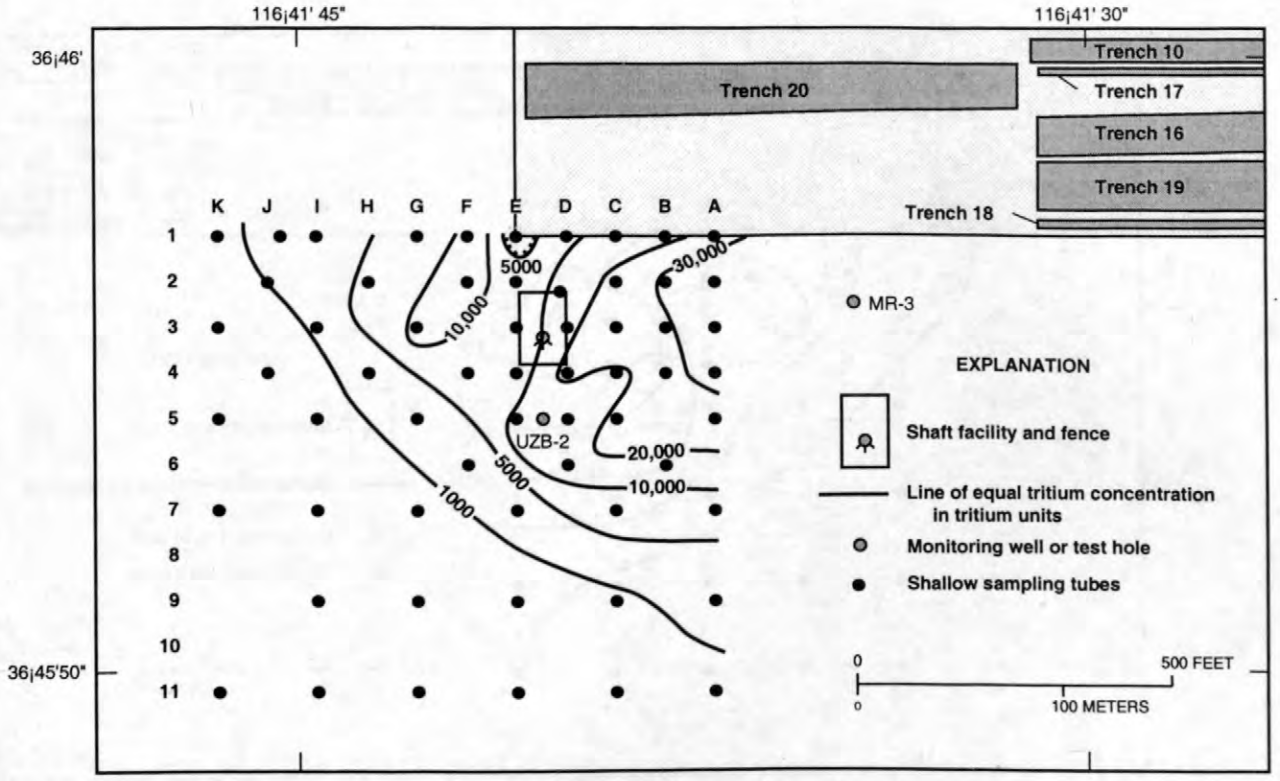

Figure 2. Map showing tritium concentration in water vapor collected at the 1.5 m depth within the sampling grid at the Amargosa Desert Research Site, May 1997.

chilled in a slurry of dry ice and ethanol or propanol, where water vapor was frozen out of the air stream into the freeze traps (Striegl, 1988). Approximately 3 to 10 milliliters of water were collected at each sampling location for tritium analysis at the USGS Water Resources Division isotope laboratory in Menlo Park, California. Sample collection times varied with location from 6 to 24 hours with a pump rate of about 1 to 2 liters of air per minute,

RESULTS

Tritium concentrations in water vapor for the May 1997 sampling dates are shown in figure 2 (these values are listed in table 1 of Striegl and others, 1998). Concentrations for the June 1998 sampling dates are listed in table 1 and displayed in figure 3. Concentrations for the 1998 samples tended to decrease from northeast to southwest across the grid, ranging from a maximum of 37,360 ± 450 TU at grid point B4 near the northeast corner of the grid to a minimum of 6 ± 6 TU at M13 in the far southwest corner. Striegl and others (1998) measured a tritium in water vapor concentration of 11 ± 7 TU at a borehole located 2 km west of the study area. Assuming that this value represents background, then most of the samples obtained from the grid have concentrations above background.

Trends in contours of tritium concentrations in water vapor for June 1998 are quite similar to those for May 1997. The average tritium concentrations for the 52 points that were sampled in both 1997 and 1998 were 10,439 TU in 1997 and 9,177 TU in 1998. This reduction is more than would be expected due to radioactive decay (tritium has a half-life of 12.33 years). It is likely that more tritium is being stored in liquid soil water in 1998 than 1997. Spring of 1998 had an unusually high amount of precipitation, most likely due to the *El Nino* effect. Even a small increase in soil moisture content should result in a measurable decrease in tritium concentrations in water vapor because the equal-volume ratio of water vapor to liquid water is very small (1.73×10^{-5} : 1 at 283 K and 100 KPa). For example, if volumetric moisture content was

0.045 in May 1997 and 0.050 in June 1998, then

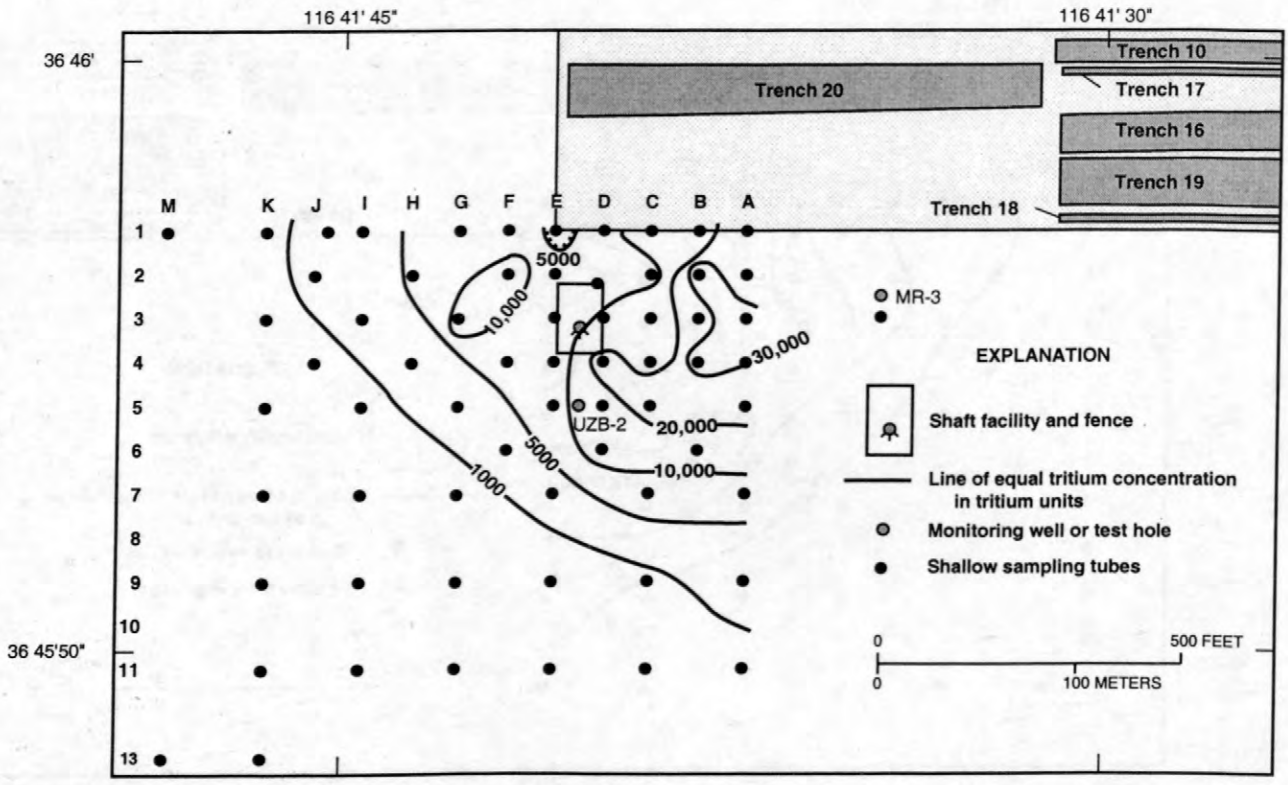

Figure 3. Map showing tritium concentration in water vapor collected at the 1.5 m depth within the sampling grid at the Amargosa Desert Research Site, June 1998.

dilution alone would account for about a 10% decrease in concentrations. Such a slight change in

Table 1. Tritium concentration in water vapor collected from a depth of 1.5 m within the sampling grid at the Amargosa Desert Research Site, June 15-18, 1998.

Grid location	Tritium concentration (tritium units)	Counting uncertainty (tritium units)
A1	19,030	± 200
A2	27,300	± 300
A3	33,800	± 300
A4	29,900	± 300
A5	24,200	± 300
A7	5,830	± 60
A9	3,840	± 40

Table 1. Tritium concentration in water vapor collected from a depth of 1.5 m within the sampling grid at the Amargosa Desert Research Site, June 15-18, 1998.

Grid location	Tritium concentration (tritium units)	Counting uncertainty (tritium units)
A11	124	± 9
B1	16,780	± 170
B2	32,900	± 300
B3	24,190	± 190
B4	37,360	± 450
B6	17,000	± 200
C1	14,290	± 150
C2	6,810	± 80
C3	18,990	± 180

Table 1. Tritium concentration in water vapor collected from a depth of 1.5 m within the sampling grid at the Amargosa Desert Research Site, June 15-18, 1998.

Grid location	Tritium concentration (tritium units)	Counting uncertainty (tritium units)
C4	16,870	± 150
C5	24,050	± 290
C7	6,150	± 70
C9	534	± 11
C11	94	± 8
D1	7,550	± 90
D2	8,710	± 90
D3	10,120	± 120
D4	20,970	± 250
D5	15,430	± 190
D6	18,200	± 200
E1	2,570	± 30
E3	6,130	± 60
E5	7,800	± 100
E7	2,920	± 30
E9	29	± 19
E11	71	± 9
F1	5,970	± 80
F2	10,350	± 130
F4	6,620	± 70
G1	6,210	± 80
G3	10,980	± 100
G5	2,070	± 26
G7	34	± 15
G9	65	± 8
G11	49	± 8

Table 1. Tritium concentration in water vapor collected from a depth of 1.5 m within the sampling grid at the Amargosa Desert Research Site, June 15-18, 1998.

Grid location	Tritium concentration (tritium units)	Counting uncertainty (tritium units)
H2	5,590	± 60
H4	1,810	± 26
I1	1,903	± 24
I5	197	± 10
I9	30	± 9
I11	20	± 7
J1	2,303	± 28
J2	1,071	± 26
K1	396	± 19
K3	65	± 8
K5	58	± 7
K7	25	± 9
K9	14	± 8
K11	30	± 7
K13	39	± 6
M1	49	± 8
M13	6	± 6
MR-3	2,380	± 30
UZB-2	14,580	± 150

moisture content would be almost impossible to measure in the field.

REFERENCES

Andraski, B.J., and Stonestrom, D.A., Overview of research on water, gas, and radionuclide transport at the Amargosa Desert Research Site,

Nevada, Morganwalp, D.W., and Buxton, H.T., eds., U.S. Geological Survey Toxic Substances Hydrology Program--Proceedings of the Technical Meeting, Charleston, South Carolina, March 8-12, 1999 -- Volume 3 -- Subsurface Contamination from Point Sources: U.S. Geological Survey Water-Resources Investigations Report 99-4018C, this volume.

Prudic, D.E., and Striegl, R.G., 1995, Tritium and radioactive carbon (^{14}C) analyses of gas collected from unsaturated sediments next to a low-level radioactive-waste burial site south of Beatty, Nevada, April 1994 and July 1995: U.S. Geological Survey Open-File Report 95-741, 7 p.

Striegl, R.G., 1988, Distribution of gases in the unsaturated zone at a low-level radioactive-waste disposal site near Sheffield, Illinois: U.S. Geological Survey Water-Resources Investigations Report 88-4025, 69 p.

Striegl, R.G., Healy, R.W., Michel, R.L., and Prudic, D.E., 1998, Tritium in unsaturated zone gases and air at the Amargosa Desert Research Site, and in Spring and River Water, near Beatty, Nevada, May 1997: U.S. Geological Survey Open-File Report 97-778, 13 p.

Striegl, R.G., Prudic, D.E., Duval, J.S., Healy, R.W., Landa, E.R., Pollock, D.W., Thorstenson, D.C., and Weeks, E.P., 1996, Factors affecting tritium and ^{14}carbon distributions in the unsaturated zone near the low-level radioactive-waste burial site south of Beatty, Nevada: U.S. Geological Survey Open-File Report 96-110, 16 p.

US Ecology, Inc., 1989, Site stabilization and closure plan for low-level radioactive waste management facility: Beatty, Nev., Radioactive Materials License State of Nevada No. 13-11-0043-02, attachment 1.

AUTHOR INFORMATION

Richard W. Healy and Robert G. Striegl, U.S. Geological Survey, Lakewood, CO
Robert L. Michel, U.S. Geological Survey, Menlo Park, CA
David E. Prudic and Brian J. Andraski, U.S. Geological Survey, Carson City, NV

Soil Respiration at the Amargosa Desert Research Site

By Alan C. Riggs, Robert G. Striegl, and Florentino B. Maestas

ABSTRACT

Automated opaque flux-chamber measurements of soil carbon dioxide (CO_2) flux (soil respiration) into the atmosphere at the Amargosa Desert Research Site show seasonal and diel cycles of soil respiration that are closely linked with soil temperature and soil moisture. During 1998, soil respiration increased with soil warming through spring, reaching a maximum rate (not counting anomalously high values scattered through the record) of about 0.055 moles CO_2 m^{-2} day^{-1} around Julian Day 120. Respiration rates then declined along with volumetric soil moisture content, tending to stay at or below about 0.02 moles CO_2 per square meter per day (m^{-2} day^{-1}) for the rest of the year, except after summer rainfalls when respiration sharply increased for short periods. The diel respiration pattern during dry spells is marked by a sharp rise in CO_2 flux coincident with steeply rising soil temperatures in the morning, then dropping back to low levels about the time of maximum soil temperature. The reason for this pattern is unclear.

INTRODUCTION

As the second largest CO_2 flux in the global carbon cycle, soil respiration has been extensively studied and measured by a wide variety of techniques in a diversity of environments. Despite the fact that deserts occupy more than 20 percent of the Earth's land surface, little is known about soil respiration in desert environments (Raich and Schlesinger, 1992). The Amargosa Desert in southern Nevada is one of the most arid areas in North America, and hence, a suitable environment to identify and quantify the processes controlling desert soil respiration. In addition to the usual relatively shallow microbial and root sources of CO_2, borehole CO_2 profiles at the Amargosa Desert Research Site (ADRS) indicate that CO_2 may continuously diffuse from the water table, through the 100 meter (m) thick unsaturated zone, and into the atmosphere.

Automated soil-CO_2-flux chambers (one clear and one opaque) were built to measure the soil-CO_2 flux from the floor of the basin. The chambers have reliably made hourly measurements of soil-CO_2 flux since mid-January 1998. Air and soil temperature, photosynthetically active solar radiation, relative humidity, rainfall, soil moisture content, barometric pressure, and wind speed and direction were measured contemporaneously. This paper presents the chronology of soil-CO_2 fluxes measured by the opaque chamber for nearly the whole, unusually wet, El Niño year of 1998. Preliminary evaluations of the controls on Amargosa soil-CO_2 fluxes are also presented.

METHODS

Figure 1 is a schematic of soil-CO_2 flux chamber design, along with the data, gas flow, power and control circuit hookups. On the right side of the figure, the 38-centimeter (cm)-diameter chamber is shown in the open position. The cylindrical bottom of the chamber (the collar) was installed by driving it 18-19 cm into the ground, leaving only a cm or two cm above ground level. A hole was dug outside the collar, so that the framework could be bolted to the collar, and the hole was refilled, leaving only the brackets that support the truss above ground. The truss, pneumatic cylinder, and chamber lid were installed and adjusted so that when the

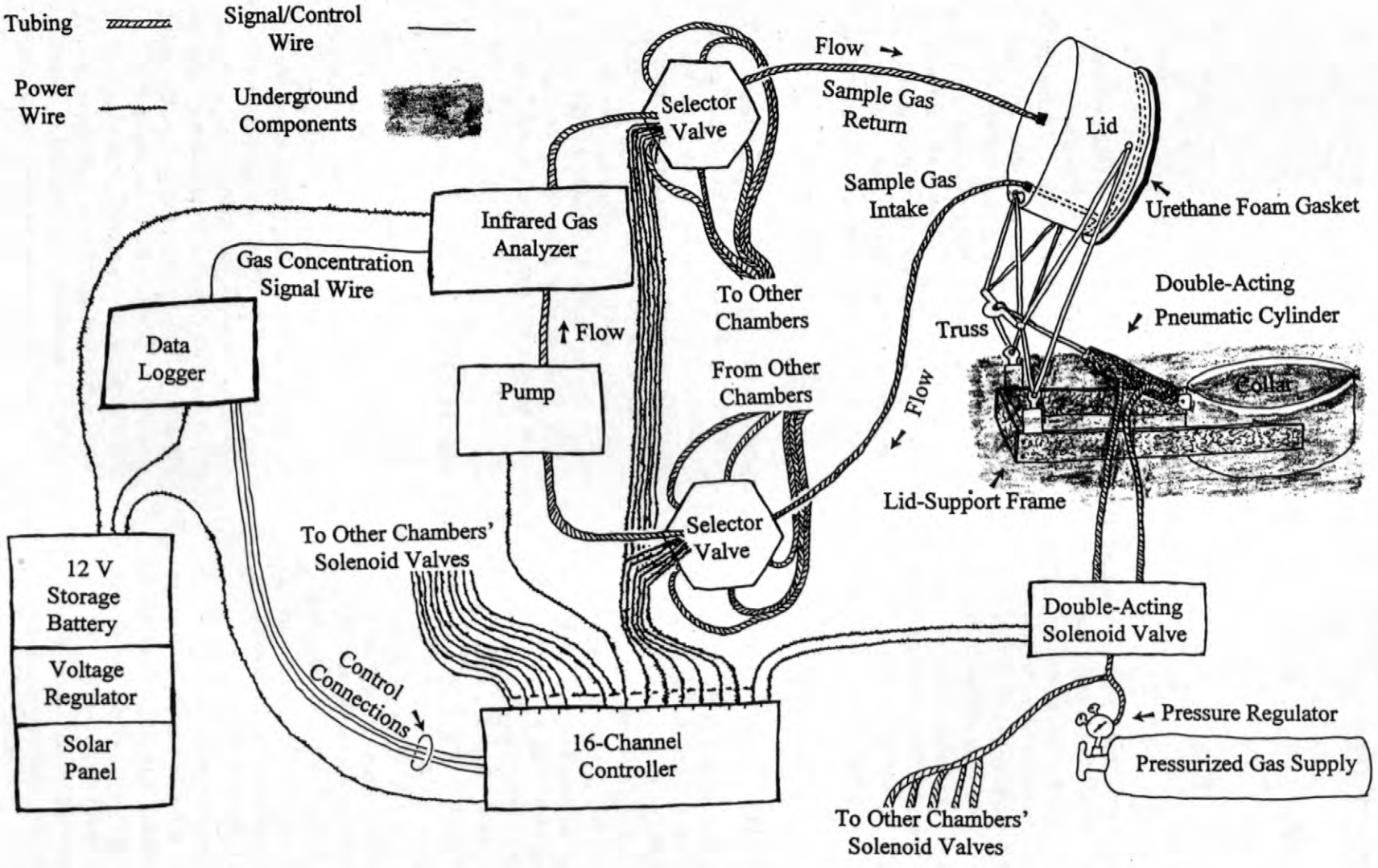

Figure 1. A schematic of the automated soil-CO_2-flux chamber system, showing chamber design, and connections for power, data, control, sample gas, and pneumatic-cylinder gas. The lid-support frame is totally buried, minimizing interference with natural air movements. The system shown can operate up to six individual chambers in sequence, though experience has shown that a maximum of four fluxes can be measured in an hour. Where there is no vegetation inside the collar, a short lid can be used to increase sensitivity.

pneumatic cylinder retracts, the lid pivots down squarely on top of the collar and makes an airtight seal. The lid is normally up: when a measurement is made, the lid is lowered to seal on the collar, air is pumped from the closed chamber, through the infrared gas analyzer (IRGA), and back to the chamber. CO_2 concentrations measured by the IRGA are stored in the data logger. After 4 minutes, the measurement interval is finished, and the lid rises, allowing conditions inside the collar to return to ambient. Recorded CO_2 concentration measurements are the average of 10 1-second measurements. A computer program evaluates the 24 recorded measurements from a typical 4-minute measurement interval to determine the maximum rate of CO_2 concentration change with respect to time. This rate is then converted to a soil respiration rate for the measurement period. The chamber system operated unattended except for visits every month or two to download data and renew the pressurized gas supply that powered the pneumatic cylinder.

Air temperature at a height of 2 m, soil temperature at depths of 5 and 10 cm, photosynthetically active solar radiation, relative humidity, rainfall, volumetric soil moisture content, barometric pressure, and wind speed and direction at a height of 2 m were measured using standard, commercially available meteorological instrumentation. All parameters except rainfall and soil moisture were measured as 15-minute averages of 10-second readings. Volumetric soil moisture content integrated over 0 to 10 cm depth was measured once every 15 minutes, and rainfall was measured as the number of 0.1-millimeter bucket tips per 15-minute interval.

RESULTS

The hourly CO_2 fluxes and mean daily volumetric soil moisture content and soil temperature values for 1998 are presented in figure 2. Three important relationships are shown in figure 2. (1) During the first 120 days of 1998, the maximum daily CO_2 flux (the upper bound of the black envelope of hourly CO_2 fluxes) and mean daily soil temperature have very similar trends. (2) From day 120 to day 160, maximum daily CO_2 flux and mean daily soil moisture content have very similar trends. (3) The rainfalls on days 162-163, 202, and 242-247 all caused dramatic and abrupt increases of CO_2 flux, which then quickly dropped back to pre-rainfall levels, even though it took many days for soil moisture to return to pre-rainfall levels.

Hourly CO_2 flux, volumetric soil moisture content, and soil temperature during and following a 0.675 cm rainfall (evident as the rapid increase in volumetric soil moisture content) on day 202 are shown in figure 3. There was a dramatically increased CO_2 flux that lasted a little more than a day after the rainfall. Increased flux occurred at night, as well as during the day. Even though the CO_2 flux quickly returned to near pre-rainfall levels, soil moisture took more than a week to return to nearly pre-rainfall levels (as in figure 2).

Figure 4 shows the relationship between the daily CO_2 flux peaks and the daily variations in soil temperature and barometric pressure, during a time of low (about 6%) soil moisture. The tendency for CO_2 flux to peak during periods of soil warming is striking. There is a slightly poorer correspondence between peak CO_2 fluxes and diel decreases in barometric pressure.

DISCUSSION

Soil CO_2 flux is derived primarily from the metabolic activity of soil flora and fauna, primarily microbial and root respiration. Like metabolic rates, soil CO_2 flux is generally strongly positively correlated with temperature (Raich and Schlesinger, 1992). In addition, there is a optimal range of soil moisture content for microbial and root metabolic activities; soil moisture contents greater or lesser than this range lead to progressively less metabolic activity and, hence, decreased CO_2 fluxes. These two relations are sufficient to explain the major features of the soil CO_2 flux chronology in figure 2, with the exception of the times following summer rainfall events. Up until about day 120, the trend of maximum daily CO_2 fluxes followed the trend of increasing soil temperature, up to maximum daily flux rates in

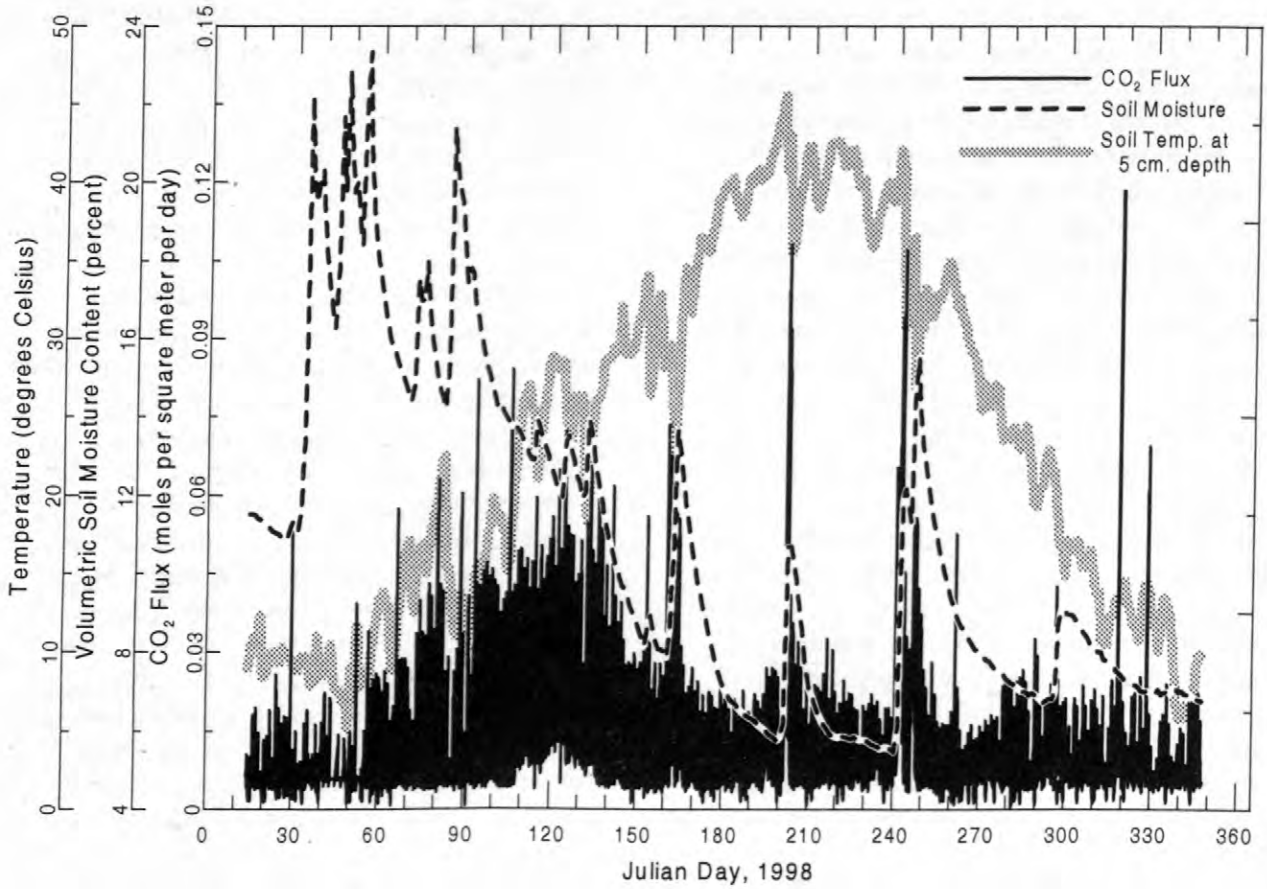

Figure 2. Hourly soil-CO_2 fluxes, and mean daily volumetric soil moisture content and soil temperature. The goodness of fit of the individual points making up the slope of increasing CO_2 concentrations from which the individual hourly fluxes are calculated was evaluated using the coefficient of determination (r^2). Only points having an r^2 greater than 0.6 were included in this plot. The limited sensitivity of the IRGA used, coupled with low night-time soil-CO_2 fluxes resulted in below-threshold values ($r^2 < 0.6$) most nights. Hence, the bottom of the soil-CO_2 flux envelope is a threshold, and not an indication of actual minimum fluxes, except between days 110 – 140, and right after the rainstorms on days 162-163, 202, and 242-247. The total amount of CO_2 respired during the period of the plot is about 3.11 moles/meter^2. This evaluation of total flux value will change with more refined analytical techniques, but the real value of the plot is in showing qualitatively how soil-CO_2 flux varies with volumetric soil moisture content and soil temperature.

the range of 0.055 moles CO_2 m^{-2} day^{-1}. The trend of maximum daily CO_2 fluxes did not follow the trend of volumetric soil moisture content, indicating that temperature was probably the primary control on CO_2 flux during that interval of relatively high (>12%) soil moisture. After day 120, soil CO_2 flux decreased, closely mimicking the decrease in soil moisture through about day 160, even though soil temperature continued to climb. This pattern indicates that soil moisture below about 12% was a limiting factor for soil respiration. Except during and after the three summer rainfalls, soil moisture stayed well below 12% for the rest of the year and soil CO_2 flux stayed at or below baseline levels, i.e. daily maximum flux rates of about 0.02 moles m^{-2} day^{-1}.

The three summer rainfalls occurring on days 162-163, 202, and 242-247 (0.925, 0.675, and 1.75 cm, respectively) triggered CO_2 emissions that departed significantly from the pattern described in the previous paragraph (figs. 2 and 3). CO_2 fluxes abruptly rose to very high levels during, or just after, the rain, then decreased to near-pre-rainfall levels after a day or two, even though soil moisture took a week or more to return to near-pre-rainfall levels (fig.

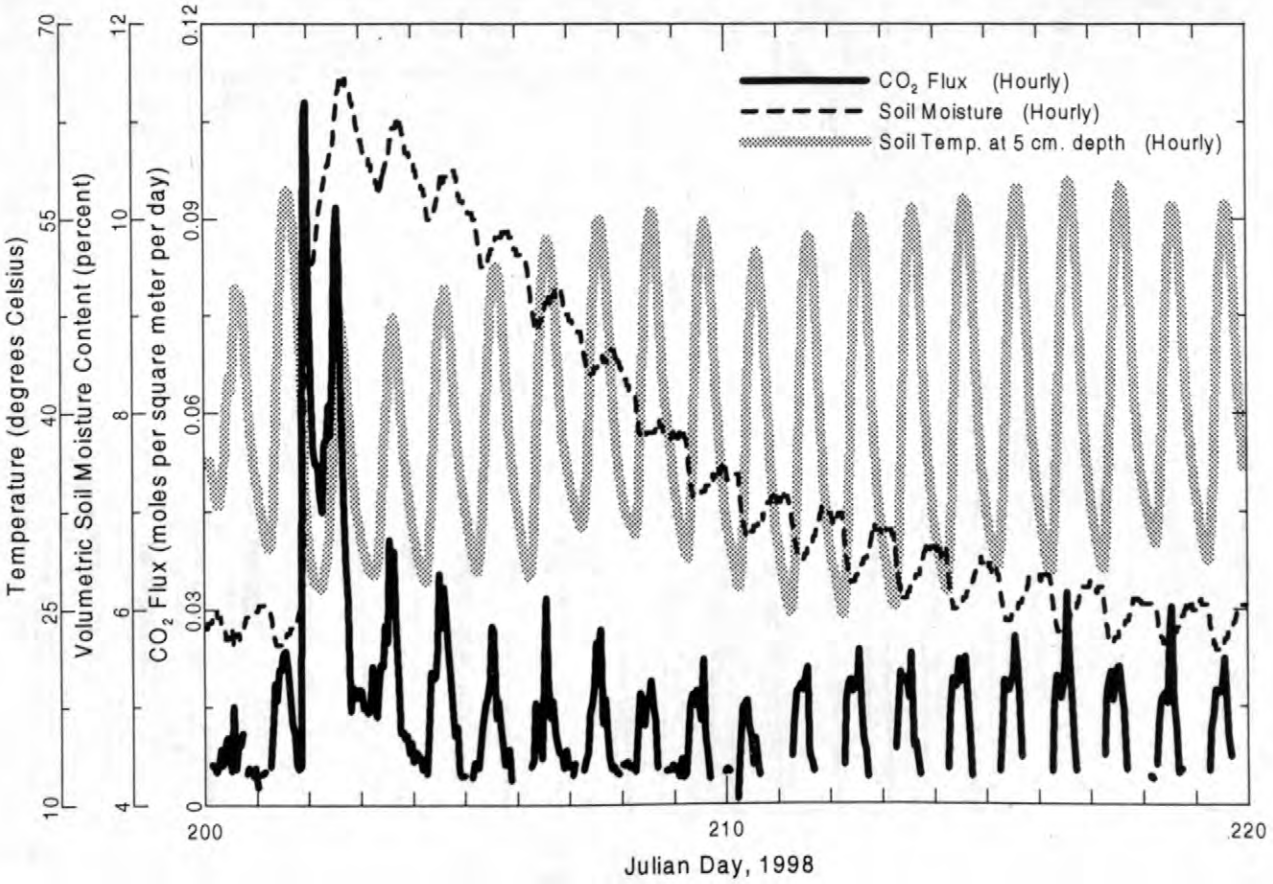

Figure 3. The effect of a 0.675 millimeter rainfall on soil-CO_2 flux after a dry period. Note that flux is temporarily radically enhanced without regard for time of day. The soil moisture monitor gives an integrated value for the top 10 cm of the soil column; diurnal fluctuations may be partly instrumental artifacts. Note that beginning on day 205, nocturnal flux values start to fall below instrumental threshold sensitivity.

3). A possible explanation for this behavior is that the rainfall triggered a major burst of microbial metabolism of organic debris left on the ground surface after the big El Niño spring bloom earlier in 1998. However, the rainfall (0.675 cm on day 202, fig. 3, for example) was capable of elevating soil moisture content above 12% only in the top few cm of the soil moisture measurement interval and only for a short time. The apparent discrepancy between volumetric soil moisture content and CO_2 flux (including the failure of the measured soil moisture content to exceed 12% during or after the rainfall) probably arose because the soil moisture monitor integrated the water content of the top 10 cm of soil, and it could not discriminate a wet surface layer (>12% soil moisture content) over dry subsurface soil (about 6% soil moisture content), as would occur immediately after a rain, from a uniformly moist, but <12% water content soil column, as might occur after the rainfall has soaked in. Another possible explanation for the abrupt increase in CO_2 flux is that organics already in place at depth in the soil column or readily metabolizable dissolved organics carried into the soil by infiltrating rain water were quickly metabolized by microbes once there was sufficient water. In these cases, the rapid infiltration of rainwater could cause a short burst of CO_2 production which would quickly stop when the readily metabolized organics were used up. The present data set provides us with no good way of choosing between these possibilities. Both may be operating simultaneously.

A couple of features of the CO_2 flux chronology in figure 2 remain unexplained. The first is that scattered through the chronology are

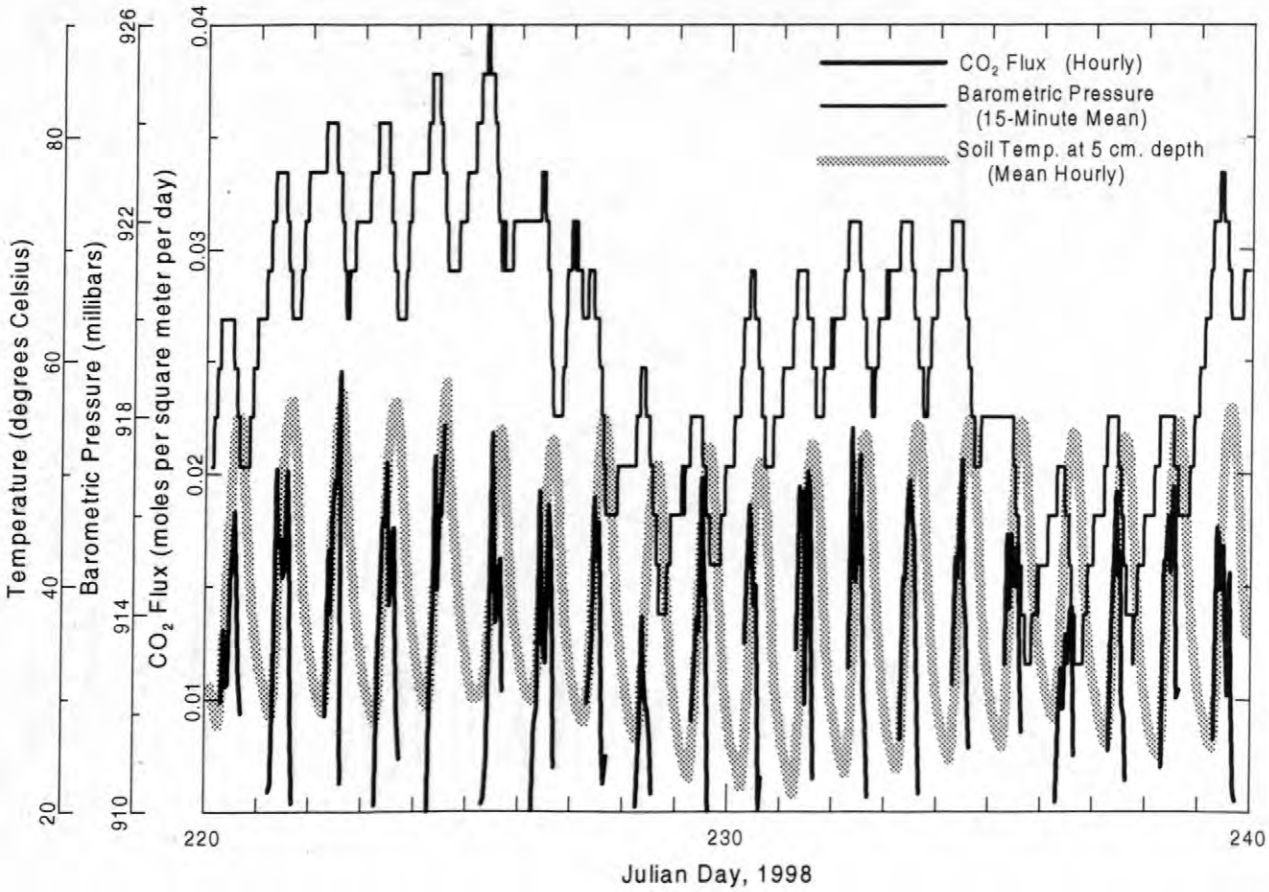

Figure 4. The relationship of soil-CO_2 flux to soil temperature and barometric pressure during a dry period (~6% volumetric soil moisture content; see figure 2). Note that soil-CO_2 flux tends to be greatest during times of rapid increase in soil temperature. Flux also tends to be correlated with decreasing barometric pressure, though in several cases, the flux begins to increase while barometric pressure is still increasing. During the twenty days shown in this plot, there also seems to be a positive correlation between the approximately weekly variations in the daily maxima of barometric pressure and soil-CO_2 flux. As in figures 2 and 3, nocturnal fluxes are below detection.

flux spikes that stand anomalously taller than adjacent fluxes. In a statistical sense, at least, many of the spikes seem to be real; some of them have coefficients of determination (a measure of the goodness of fit of the individual points making up the CO_2 concentration slope from which flux values are calculated) >0.9, whereas many of the hourly CO_2 fluxes plotted in figure 2 have coefficients of determination between 0.6 and 0.9. The second unexplained feature is the two periods between days 180-200 and days 264-282 where there are minor but distinct upward trends in daily CO_2 flux maxima during a period of decreasing soil moisture. One upward trend occurs during a period of increasing soil temperature, and the other during a period of decreasing soil temperature. Explanation of both of these phenomena awaits more in-depth data analysis, or collection of different sorts of data.

The last feature of note is the correspondence of daily CO_2 flux highs with times of rapid soil heating (fig. 4), at least when the soil volumetric moisture content is low (near 6%). This pattern of soil respiration is not easily explained as a consequence of microbial activity: there is no correlation with soil moisture, and flux variations correspond not to temperature, but more to rate of soil temperature increase. The shapes of the flux peaks are also much more complex than those of temperature. Preliminary calculations indicate that the daily flux peaks are too large to be explained solely by the efflux of soil gases caused by thermal

expansion. Diel barometric pressure cycling moves air in and out of the soil, but figure 4 shows that, on some days, the phase relations of barometric pressure cycling and soil respiration rule out barometric pressure changes as the sole cause of the effect, although figure 4 does show an apparent correspondence between the approximately weekly variations in barometric pressure and daily flux maxima. Understanding these flux patterns will require further work.

ACKNOWLEDGMENTS

We thank David Parkhurst and Don Thorstenson for fruitful discussions leading to a clearer appreciation of the subtleties of gas movement in the unsaturated zone. Reviews by Richard Healy, Alisa Mast, and Dave Stannard helped immeasurably in improving the logical flow and user friendliness of the manuscript.

REFERENCES

Raich, J.W., and Schlesinger, W.H., 1992, The global carbon dioxide flux in soil respiration and its relationship to vegetation and climate: Tellus, v. 44B, p. 81-89.

AUTHOR INFORMATION

Alan C. Riggs, Robert G. Striegl, and Florentino B. Maestas, U.S. Geological Survey, Denver, Colorado (ariggs@usgs.gov, rstriegl@usgs.gov, and fbmaestas@usgs.gov)

Geochemical and Microbiological Processes in Ground Water and Surface Water Affected by Municipal Landfill Leachate

Landfilling is the most common method of disposal of municipal waste. The United States produces more than 150 million tons of solid waste each year, over 70 percent of which is disposed of in landfills. According to the U.S. Environmental Protection Agency, 3,581 landfills were operating in the United States in 1995, down from 7,683 in 1982. Many of the now-closed landfills were unlined and sited on alluvial deposits because the land had little economic value and excavations were conveniently available from sand and gravel operations. Whereas Superfund and other hazardous-waste sites have received much attention, little is known about the hazards to ground-water resources and environmental receptors posed by a typical municipal landfill.

In 1995, the U.S. Geological Survey began an intensive investigation as part of the Toxic Substances Hydrology Program at a closed municipal landfill in Norman, Oklahoma. The Norman Landfill Research Site is located on the Canadian River alluvial plain in central Oklahoma. Due to the prevalence of landfills in this type of hydrogeologic setting, an increased understanding of the hydrologic and geochemical processes controlling the migration of organic and inorganic contaminants from the Norman landfill is applicable to many sites across the United States. The contamination of the shallow alluvial aquifer at the Norman landfill provides an excellent opportunity to study the spatial variability of biogeochemical processes and the resulting effects on the fate of degradable contaminants in the leachate plume. The existence of zones with differing anaerobic microbial processes facilitates investigations of the role of electron acceptors on the fate of organic compounds *in situ*. The influence of surface-water and ground-water interactions on contaminant degradation can be studied where the slough, a small stream and wetland, overlie the leachate plume. The shallow water table provides a setting to study how recharge and seasonal surface-water inputs affect aquifer chemistry and interaction with a leachate plume. The heterogeneous permeability structure of the alluvium provides an opportunity to study the effects of physical heterogeneities on the fate and transport of contaminants in the aquifer.

The landfill accepted solid waste from the City of Norman, Oklahoma, from 1922 to 1985, when the landfill was closed and covered with a vegetated earthen cap. The landfill never utilized liners or leachate collection systems, and a leachate plume has developed that extends at least 225 meters from the edge of the landfill. The shape and size of the plume is influenced by physical heterogeneities and changes in hydrologic conditions at the site. Several transport and reaction zones have been identified along a transect from the edge of the landfill, under the slough, and toward the Canadian River (fig. 1). The observed spatial variability of the leachate plume is due to the complex interaction between biogeochemical and hydrogeological processes, including biodegradation, sorption, dispersion, and dilution. The heterogeneity of available electron acceptors and the mixing of anoxic plume water with oxygenated recharge water have resulted in a wide range of microbial degradation rates.

The research products from the studies at the Norman landfill will include a conceptual model describing the flow system and the nature and magnitude of biogeochemical processes that occur as landfill leachate reacts with native ground water and aquifer solids. Additionally, quantitative analysis of the flow system and the biogeochemical processes affecting the fate and transport of landfill-derived contaminants will facilitate the development of a geochemical budget for iron, sulfur, and carbon in the contaminated aquifer and surface

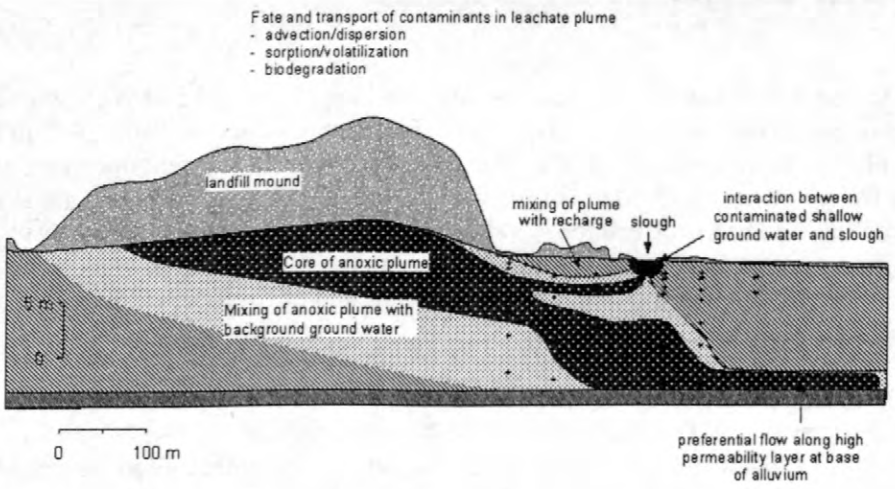

Figure 1. Conceptual model of transport and reaction zones at the Norman Landfill

water, and will further our understanding of the evolution of the contaminant plume. The emphasis of this research project is on developing an understanding of the processes controlling contaminant migration and attenuation. The knowledge gained from studying the Norman landfill will provide insight into natural biogeochemical and hydrogeologic processes that cause intrinsic bioremediation and will be of use in the design of effective bioremediation technologies.

For additional information contact:

Scott C. Christenson, USGS, Oklahoma City, Oklahoma (email: schris@usgs.gov), or

Isabelle M. Cozzarelli, USGS, Reston, Virginia (email: icozzare@usgs.gov)

Ground-Water and Surface-Water Hydrology of the Norman Landfill Research Site

By Scott Christenson, Martha A. Scholl, Jamie L. Schlottmann, and Carol J. Becker

ABSTRACT

The Norman Landfill Research Site is a closed municipal landfill located south of Norman, Oklahoma. The landfill accepted municipal solid waste from the City of Norman from the early 1920's until 1985, when the landfill was closed. The landfill never utilized liners or leachate collection systems, and a leachate plume has developed and extends at least 225 meters from the edge of the landfill.

The landfill is located on the floodplain of the Canadian River. The Canadian River alluvial aquifer consists of fluvial sediments 10 to 12 meters thick. Alluvial sediments at the site range in size from coarse gravel to clay, although medium-grained sand dominates. Hydraulic conductivity measured by slug tests ranged from 2.37×10^{-7} meters per second to 2.81×10^{-4} meters per second, with a median of 6.72×10^{-5} meters per second. Below the alluvium are Permian-age clastic sediments of low permeability that act as a basal confining layer.

Recharge to the alluvial aquifer is infiltration from precipitation, small streams, and wetlands near the landfill. Ground water discharges to the small streams and wetlands, the Canadian River, and to evapotranspiration. The eastern edge of the leachate plume discharges to small streams near the base of the landfill. Further west, the leachate plume sinks to the bottom of the aquifer and flows under a wetland and stream.

SITE HISTORY

The Norman Landfill Research Site is a closed municipal landfill located south of Norman, Oklahoma (fig. 1). The population of Norman was 80,071 in 1990. The landfill accepted municipal solid waste from the City of Norman from the early 1920's until 1985, when the landfill was closed (Dixon, 1992). The waste in the landfill is predominantly residential and commercial solid waste, although the landfill closure report documents several incidents of suspected hazardous waste disposal (Dixon, 1992). Landfill practices at this site evolved over time. Initially waste was dumped on the land surface, then in the 1960's and 1970's waste was buried in shallow trenches and covered with sand. In the final fills, waste was deposited in lifts above the land surface and covered with sand. When the landfill was closed in 1985, the final fills (shown as "East Cell" and "West Cell" in figure 1) were covered with earthen caps and vegetation was planted on the caps (Dixon, 1992). The capped landfills cover 186,000 square meters, and they rise 12-13 meters above the alluvial plain. At no time were liners or leachate-collection systems employed at the site.

Organic and inorganic contaminants are leaching into the ground water from the buried waste. A leachate plume moving through the Canadian River alluvial aquifer extends at least 225 meters from the edge of the landfill (fig. 2). This plume is being studied by researchers from the U.S. Geological Survey, the University of Oklahoma, the Colorado School of Mines, Oklahoma State University, the National Risk Management Research Laboratory of the U.S. Environmental Protection Agency, and several other academic institutions.

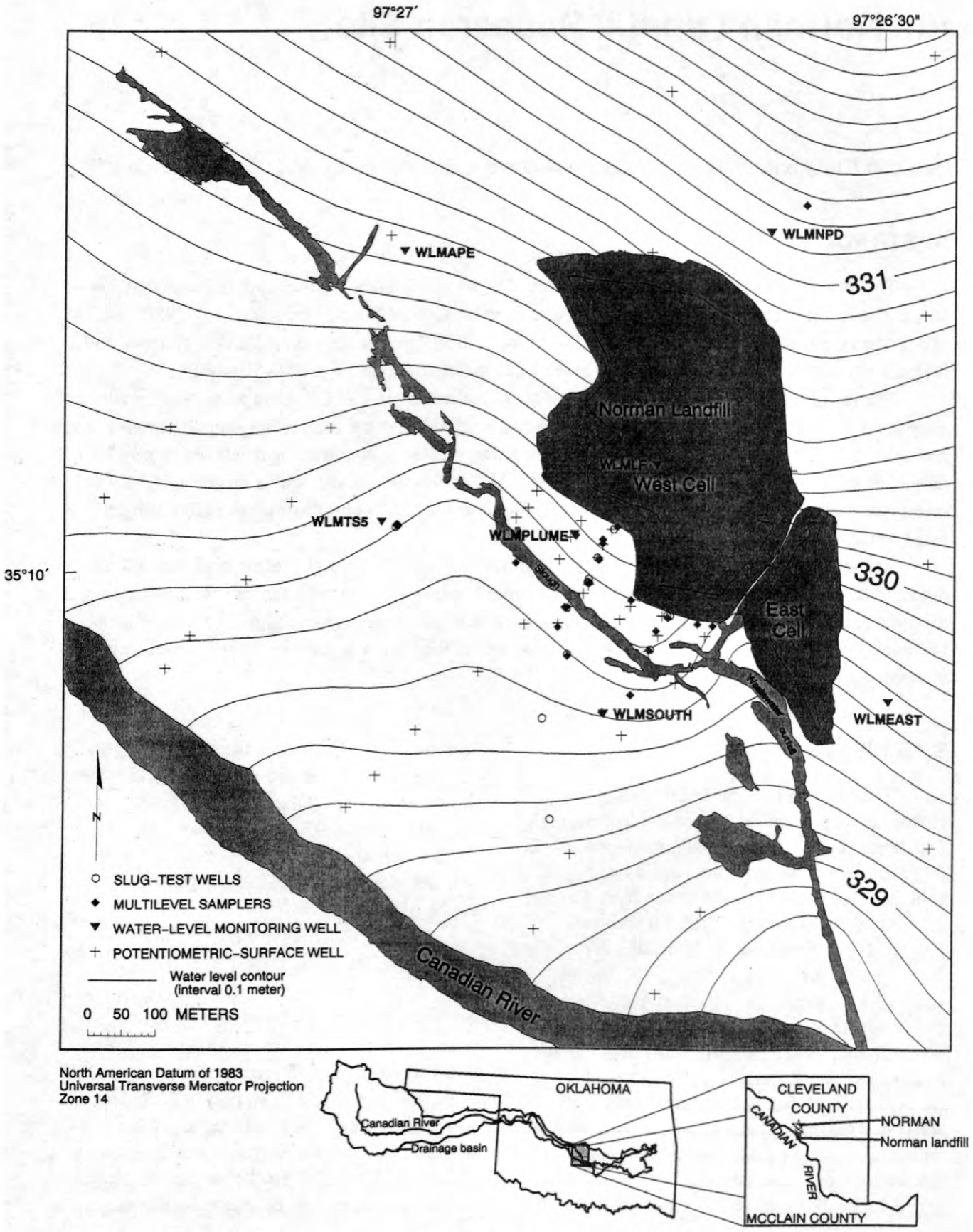

Figure 1. Locations of streams, wells, and regional potentiometric surface at Norman landfill.

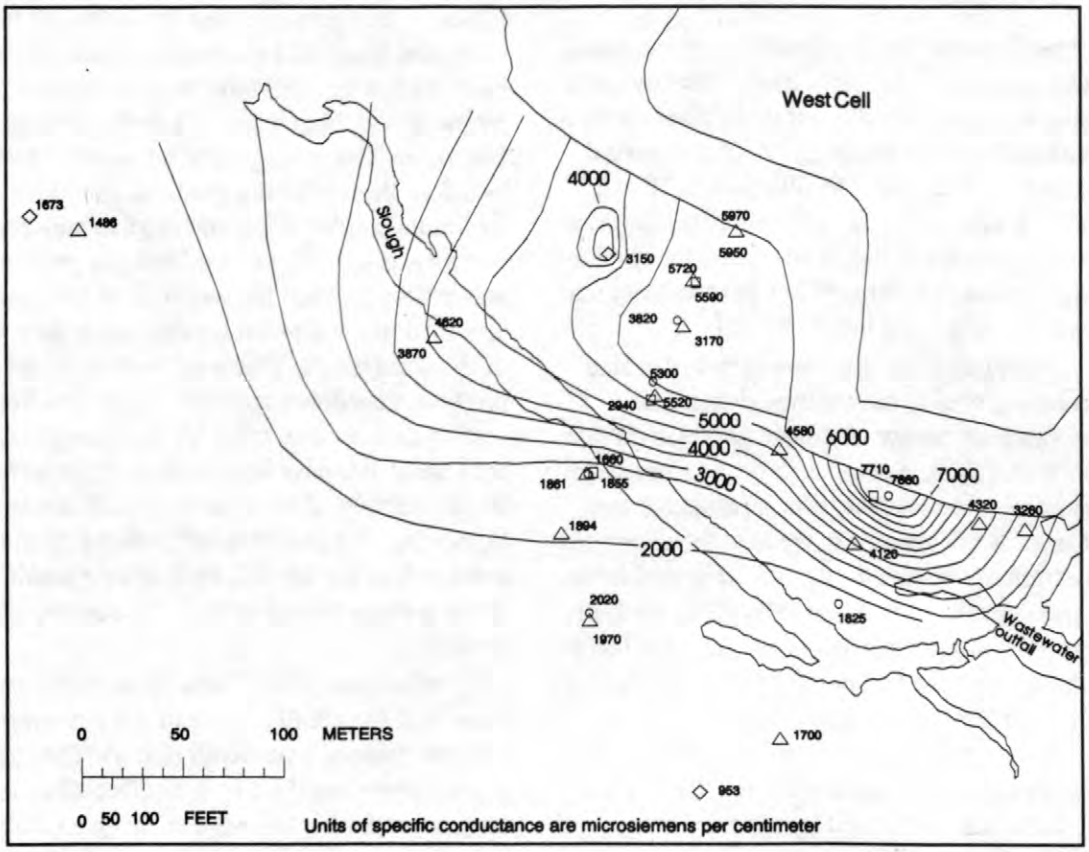

Figure 2. Distribution of specific conductance at shallow depths (less than 3 meters).

SURFACE-WATER HYDROLOGY

The landfill is located on the floodplain of the Canadian River, which has a drainage area of about 67,000 square kilometers (fig. 1). The drainage area of the river extends west from Norman across western Oklahoma into Texas and New Mexico. The drainage area includes large areas of the Ogallala Formation and includes mountainous terrain in eastern New Mexico.

Average precipitation at Norman is about 860 millimeters per year. Precipitation is greatest in the spring and least in winter. Median flow in the Canadian River at Norman is about 10 cubic meters per second, but flood discharges have exceeded 4,200 cubic meters per second (Blazs and others, 1997). Flow in the river receded to less than 0.05 cubic meter per second during drought conditions in 1998. At the present time (1999), the Canadian River is about 500 meters from the capped landfill (fig. 1), but as recently as 1985 it was in contact with the landfill.

There are several small streams near the landfill (fig. 1). An intermittent stream flows along the northeast edge of the landfill after storm events. The City of Norman wastewater treatment plant discharges effluent to a small stream at the base of the east landfill cell. This effluent stream flows south and discharges to the Canadian River. Discharge in this effluent stream is determined by inflow into the wastewater treatment plant and does not have large seasonal variation. A small intermittent stream, shown on figures 1 and 2 as "Slough," flows southeast and discharges into the wastewater effluent stream. A beaver dam elevates the head of the slough about 0.5 meter forming a wetland that contains pooled water most of the year. During most of the year, flow through the slough is minimal, less than 0.01 cubic meter per second. There was no flow in the slough during the drought of 1998, and it became dry except for two small pools. During floods, large volumes of water from the Canadian River enter the slough upstream from the landfill.

GROUND-WATER HYDROLOGY

The Canadian River alluvial aquifer consists of fluvial sediments that were transported by the Canadian River. Areas adjacent to the river are covered with eolian sand deposits, which form wind ripples and small dunes. The alluvium is 10 to 12 meters thick in and near the area where the leachate plume has developed. Below the alluvium are Permian-age clastic sediments of low permeability that act as a basal confining layer.

Alluvial sediments at the site range in size from coarse gravel to clay, although medium-grained sands dominate. A coarse gravel layer less than 0.5 meter thick is at the base of the alluvium at most sites near the leachate plume, although the gravel layer is not present in wells at the downgradient margin of the plume. Above the gravel layer, sediments consist of interbedded medium sand, silt, and clay, with minor amounts of gravel. Clay layers are common and can be laterally extensive. A clay layer about 0.5 meter thick occurs at a depth of about 4 meters in many of the cores drilled in the area underlain by the leachate plume. The bulk of sediments being transported by the river are medium-grained sand.

The regional potentiometric surface (fig. 1) indicates that ground water flows toward both the Canadian River and the wastewater outfall, which have the lowest hydraulic head in the area. The hydraulic gradient is about 1.4 to 2.2 meters per kilometer. The average ground-water velocity, based on this hydraulic gradient, median slug-test hydraulic conductivity, and median soil-zone porosity, is about 7 to 11 meters per year. A well was drilled through the west cell of the landfill and screened in the alluvial aquifer just below the base of the solid waste. This well was equipped with a pressure transducer and data logger and began collecting data in September 1998. During the limited time these data have been recorded, measured water levels in this well have been 1 to 13 centimeters higher than water levels interpolated from wells surrounding the landfill, indicating a small mound in the potentiometric surface has formed under the landfill.

Measurements of head at different depths show that the configuration of the potentiometric surface changes with depth (fig. 3). The shallow potentiometric surface is more affected by the small streams at the eastern edge of the leachate plume than the potentiometric surface at the base of the

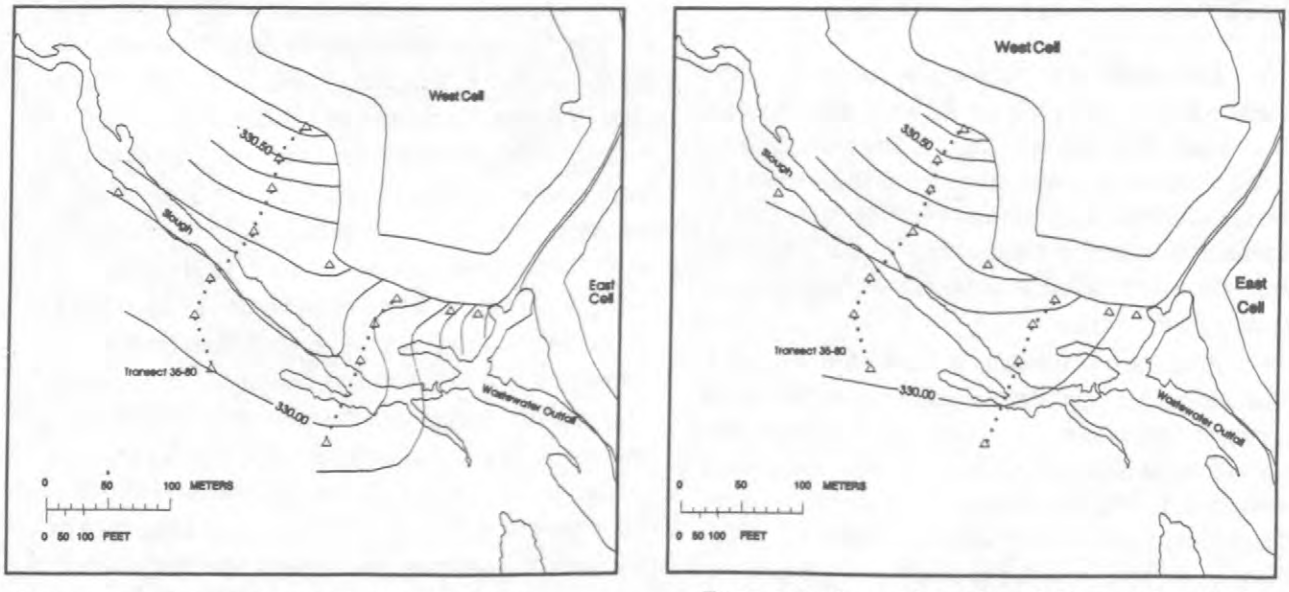

Shallow potentiometric surface (at water table)

Deep potentiometric surface (at base of aquifer)

Figure 3. Potentiometric surface at different depths on January 28, 1998.

alluvium. The configuration of the leachate plume also is affected by the streams. The eastern edge of the leachate plume discharges to the small streams near the base of the landfill. Further west, along well transect 35-80, the leachate plume sinks to the base of the alluvium and flows under a wetland and stream, shown in figure 4 as "slough." The slough contributes water to and receives water from the aquifer, as determined by oxygen and hydrogen isotopes and chloride concentration in wells downgradient from the slough.

Slug tests were performed in 96 zones in 12 wells to quantify the distribution of hydraulic conductivity in the alluvial aquifer at the site (Scholl and Christenson, 1998). Tests were conducted in temporary 2.5-centimeter diameter, drive-point wells with 0.3-meter-length screens. The wells were driven at 1-meter intervals from 1 meter below the water table to the base of the alluvium. Measured hydraulic conductivities ranged from 2.37×10^{-7} meters per second to 2.81×10^{-4} meters per second, with a median of 6.72×10^{-5} meters per second. The hydraulic conductivity of the clay layers was not measured because the slug test method used was not designed to measure very low hydraulic conductivity.

Soil properties were measured in the upper 1.5 meters of the alluvium, the zone in which the water table fluctuates. Medium-grained sands are the predominant lithology in this zone. Porosity of these sands ranged from 0.34 to 0.44 with a median of 0.40. Specific yield was computed as porosity minus the volumetric moisture content at 1/3 bar pressure (Johnson, 1967). Specific yield ranged from 0.30 to 0.35 with a median of 0.32.

Depth to water is shallow and fluctuates seasonally. The water table is at land surface in wetland areas. Where the leachate plume has developed, depth to water rarely exceeds 2 meters. Ground-water levels decline rapidly during the summer and show strong diurnal fluctuations attributable to phreatophytes (fig. 5). Phreatophyte transpiration is a major discharge of ground water from the alluvial aquifer. The area surrounding the landfill is heavily vegetated with cottonwoods, willows, and salt cedar—all considered to be phreatophytes (Robinson, 1958).

Recharge to the alluvial aquifer is from infiltration of precipitation through the unsaturated zone and from infiltration of surface water through stream beds and wetlands. Ground-water levels rise almost instantaneously in response to precipitation

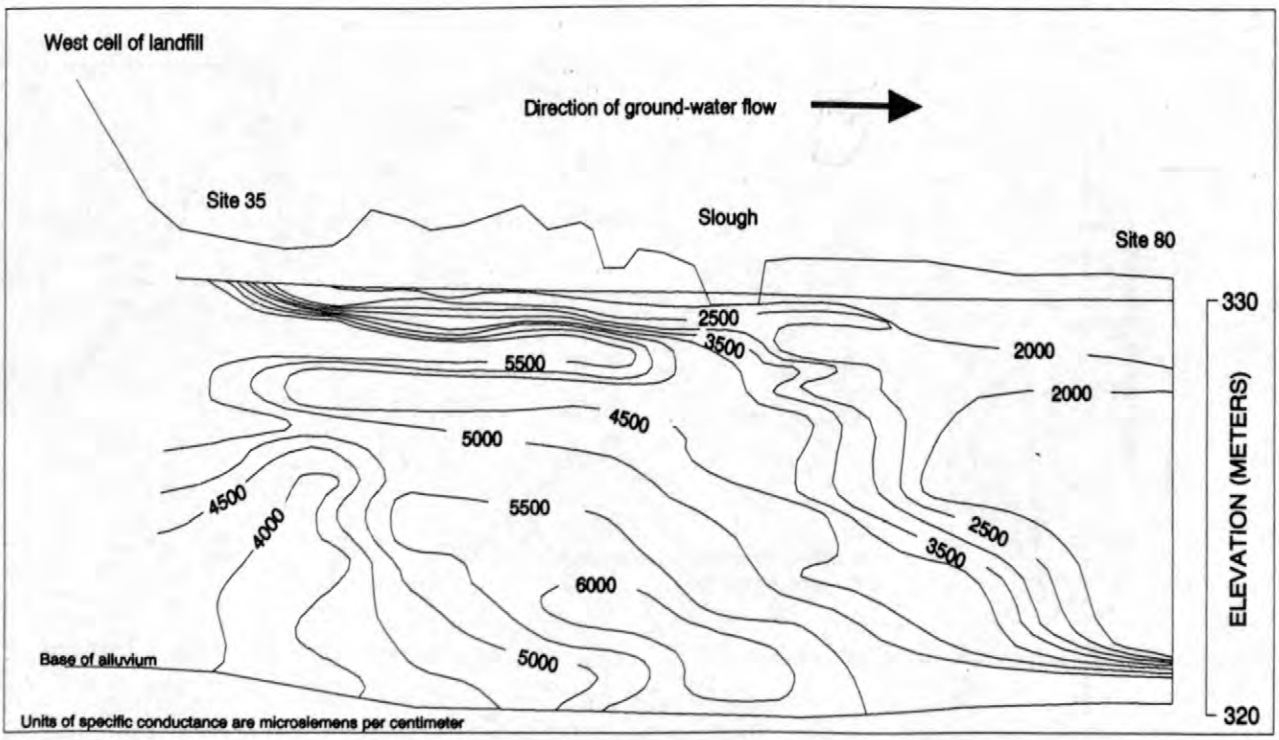

Figure 4. Cross section showing specific conducatnce in the leachate plume along well transect 35-80.

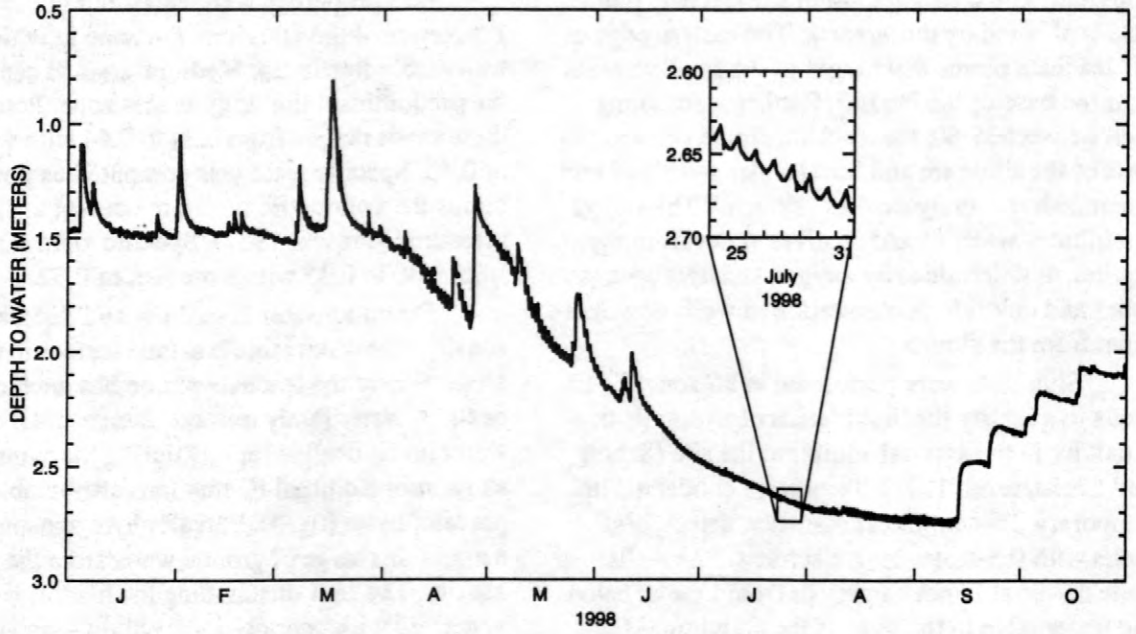

Figure 5. Ground-water level in well WLMSouth showing seasonal decline and diurnal fluctuations caused by evapotranspiration.

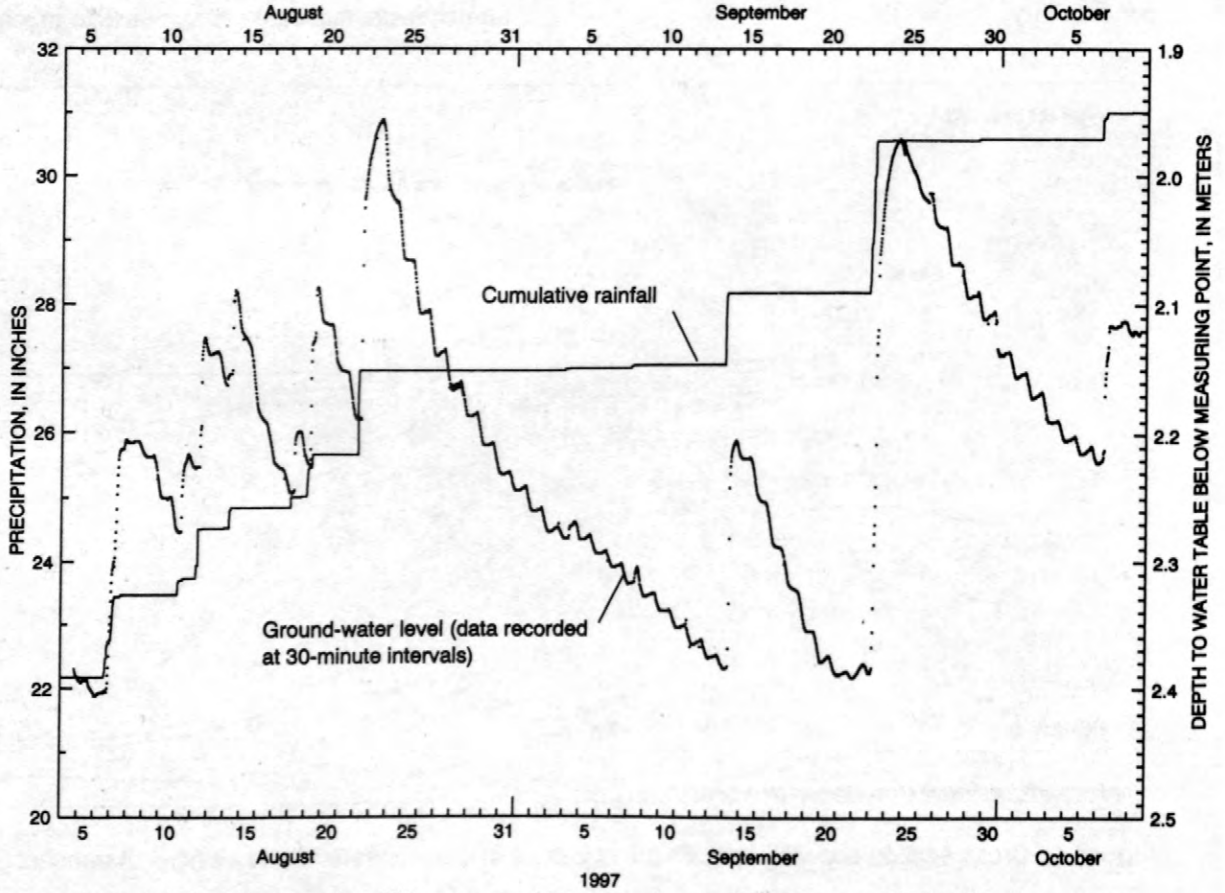

Figure 6. Rainfall at Norman landfill compared to ground-water levels at well WLMSouth.

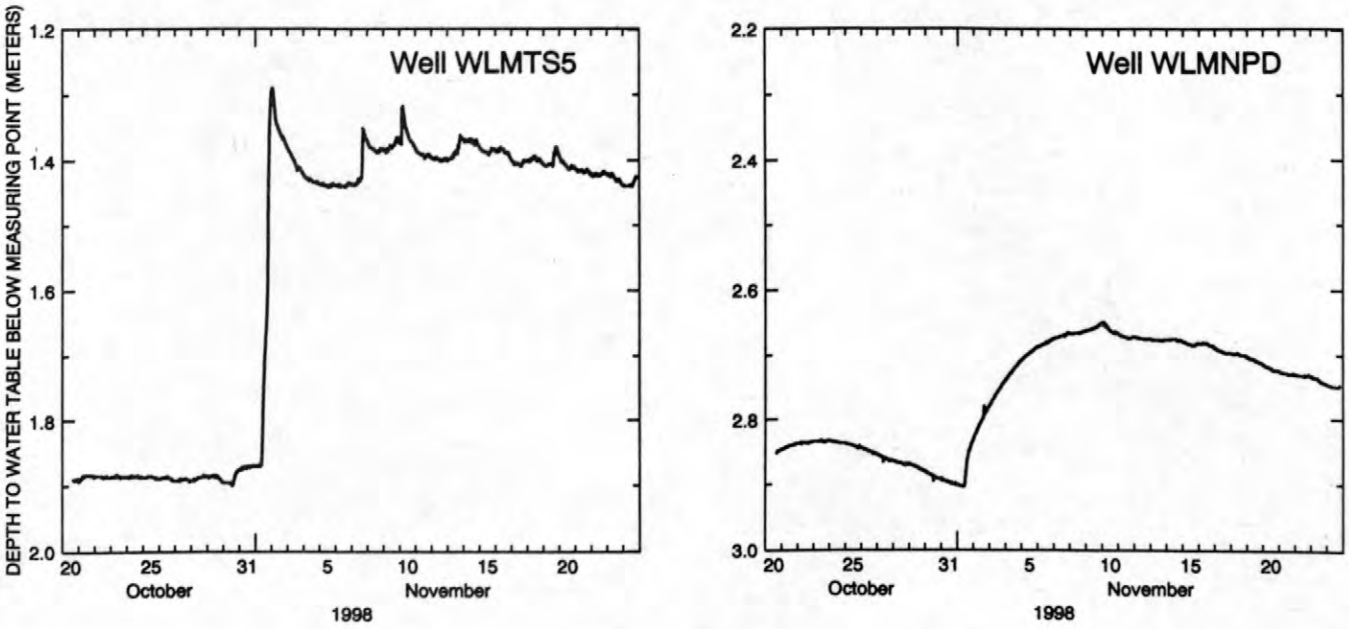

Figure 7. Water levels measured in two wells in response to a 61 millimeter rainfall event on October 31, 1998.

(fig 6). Ground-water levels near streams show much larger and more rapid rises than ground-water levels in wells that are not near streams, indicating that infiltration of surface water is a major source of recharge to the alluvial aquifer. The ground-water level in well WLMTS5, located close to the slough, rose 0.609 meter in response to a 61 millimeter rain, whereas the water level in well WLMNPD, which is not near a stream, rose only 0.255 meter and rose much more slowly (fig. 7). Recharge is seasonal, based on the rises of the water table after precipitation. Very little recharge occurs in the summer, probably due to evapotranspiration depleting soil moisture in the unsaturated zone.

REFERENCES

Blazs, R.L., Walters, D.M., Coffey, T.E., White, D.K., Boyle, D.L., and Kerestes, J.F., 1997, Water Resources Data, Oklahoma, Water Year 1997: U.S. Geological Survey Water-Data Report OK-97-1, 447 p.

Dixon, K.K., 1992, Preliminary Assessment (PA) Report for the Old Norman Landfill, Oklahoma State Department of Health, Oklahoma City.

Johnson, A.I., 1967, Specific yield—Compilation of specific yield for various material: U.S. Geological Survey Water-Supply Paper 1662-D, 74 p.

Robinson, T.W., 1958, Phreatophytes: U.S. Geological Survey Water-Supply Paper 1423, 84 p.

Scholl, M.A., and Christenson, Scott, 1998, Spatial variation in hydraulic conductivity determined by slug tests in the Canadian River alluvium near the Norman Landfill, Norman, Oklahoma: U.S. Geological Survey Water-Resources Investigations Report 97-4292, 28 p.

AUTHOR INFORMATION

Scott Christenson, Jamie L. Schlottmann, and Carol J. Becker, U.S. Geological Survey, Oklahoma City, Oklahoma

Martha A. Scholl, U.S. Geological Survey, Reston, Virginia

Identifying Ground-Water and Evaporated Surface-Water Interactions near a Landfill Using Deuterium, ^{18}Oxygen, and Chloride, Norman, Oklahoma

By Jamie L. Schlottmann, Martha A. Scholl, and Isabelle M. Cozzarelli

ABSTRACT

The composition of water discharging to a small wetland (the slough) downgradient from a closed municipal landfill was investigated using chloride concentration and enrichment in deuterium and ^{18}oxygen to determine the source waters for the slough. Potential source waters include native alluvial ground water, shallow recent recharge to the alluvium from precipitation, and leachate-contaminated ground water. Effects of evaporation from the slough on those potential source waters were calculated to determine source waters for the slough.

Deuterium and chloride are enriched in the landfill leachate relative to the native ground water. Deuterium and ^{18}oxygen have a great range and chloride concentration is low in recent recharge relative to native ground water. The initial water isotopic composition of the slough was estimated based on the range of temperature and humidity conditions under which the water was evaporated. The amount of evaporation of the potential source waters was then estimated by the change in deuterium, ^{18}oxygen, and chloride values of the slough from those in potential source waters. Results of calculating evaporation of potential source waters suggest the slough receives primarily uncontaminated native ground water but also some landfill leachate and the contribution from these sources varies over time. One of three slough samples had a suggested initial composition of leachate-contaminated water, which was diluted approximately 70 percent by recent recharge prior to entering the slough. Suggested initial compositions of other two samples included native ground water only.

INTRODUCTION

Sources of ground water discharging into a stream can be determined from the deuterium and chloride composition of the stream and the compositions of the potential source waters; however, evaporation from a ponded stream must be considered to determine the water sources. Gonfiantini (1986) has shown that deuterium and ^{18}oxygen are enriched in surface water affected by evaporation and the amount of evaporation can be estimated by the amount of enrichment. Typically, isotopes of either hydrogen or oxygen are used to estimate evaporation because in most basins the source-water compositions plot along the local precipitation line or regional ground-water line. The isotopic composition of leachate-contaminated ground water hydraulically downgradient from some landfills, such as the one studied here, is shifted upward from the precipitation line by a greater proportion of the heavier hydrogen isotope (Baedecker and Back, 1979, and Hackley and others, 1996), requiring the use of both isotopes to arrive at an evaporation estimate for one temperature and humidity.

This paper presents results of a study to identify ground-water sources discharging to a small intermittent ponded stream; referred to in this report as the slough, which is hydraulically downgradient from a closed municipal landfill. This study developed from an objective of the investigation of the Norman Landfill site to determine whether leachate-contaminated water discharged to the slough. The potential sources of ground-water discharge to the slough include native alluvial ground water, shallow recent recharge to the alluvium from precipitation, and leachate-contaminated ground water. Native alluvial ground water is

defined in this report as uncontaminated deep-circulating water in the alluvium. Deuterium, ^{18}oxygen, and chloride compositions of these waters were investigated as part of this study.

Water contaminated by leachate discharging from landfills has been observed to be enriched in deuterium (Baedecker and Back, 1979; Hackley and others, 1996; and Clark and Fritz, 1997). The enrichment is either a result of decomposition of landfill materials enriched in deuterium, or bacterial processes preferentially consuming the lighter hydrogen isotope. Hackley and others (1996) reported 30 to 60 per mil deuterium enrichment in leachate from three landfills in Illinois and speculated that most of the enrichment was a result of methanogenesis.

Leachate-contaminated water commonly is enriched in chloride (Baedecker and Back, 1979 and Nicholson and others, 1983). Water affected by evaporation also is enriched in chloride. The percentage of a source water that has evaporated can be estimated by comparing chloride concentration in the source water to the concentration in the water after evaporation. Where percentage-evaporation estimates of a selected source water to produce a known evaporated water calculated independently using δD, δ^{18}O, and chloride concentration all agree, the source water can be considered as a possible initial water.

Field site

This study focused on the slough, which is situated in alluvium of the Canadian River near Norman, Oklahoma. The slough is a small intermittent stream about 80 meters southwest and hydraulically downgradient from the capped part of a former municipal landfill (fig. 1). A beaver dam south of the capped landfill elevates the head of the slough about 0.5 meter, forming a pooled wetland. Flow through the slough typically is less than 0.01 cubic meter per second.

The landfill received waste from 1922 to 1985, at which time it closed and 186,000 square meters of the most recently deposited waste was capped with local clay, silt, and sand (fig. 1). The approximately 350,000-square meter landfill, including the capped and uncapped areas, is located on alluvial deposits of the Canadian River. The landfill was not lined and a leachate plume extends southwest from the landfill, toward the river in the direction of regional ground-water flow. The plume splits into shallow and deeper parts separated by less-contaminated ground water (Scholl and others, 1999). The shallow part extends toward the slough. The deeper part passes beneath the slough.

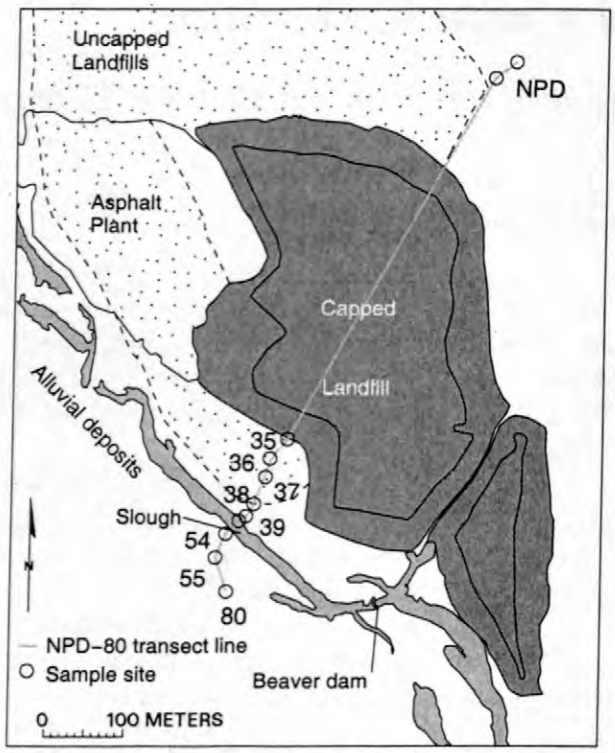

Figure 1. Detailed map of the Norman Landfill Research Site showing the NPD–80 transect and the water sampling sites.

Recharge to the alluvial aquifer is from infiltration from precipitation, small streams, and wetlands. The alluvial sediments are dominantly composed of medium-grained quartz sand, so infiltration of rainfall is rapid and substantial surface runoff does not occur in areas other than from the capped landfill and an adjacent asphalt plant.

The dominant water source for the slough is ground-water discharge, which includes native ground water, leachate-contaminated ground water, and shallow recent recharge from large precipitation events. Native ground water is characterized by (1) a narrow range in delta ^{18}oxygen (δ^{18}O) values, (2) a shift in stable isotope composition below the regional ground water line, and (3) chloride concentrations greater than those of recent recharge but less than those of leachate-contaminated water. Leachate-contaminated ground water is downgradient of the landfill and is characterized by enrichment in deuterium and chloride. Recent recharge

from precipitation is shallow alluvial ground water that is characterized by (1) a wide range in delta ^{18}oxygen ($\delta^{18}O$) values, (2) stable isotope compositions that fall along the regional ground water line, and (3) chloride concentrations lower than those of older native ground water. Ground water flowing upward from the underlying low-permeability rocks of Permian age is isotopically similar to native alluvial ground water but has a lower chloride concentration. This upward flowing water probably is a minor contributor of water to the alluvium.

Rates of ground-water discharge to the slough are unmeasured and probably vary seasonally. Discharge to the slough likely increases after large precipitation events and decreases during a drought. A mud and silt layer 3 to 4 meters beneath the slough along the transect studied may prevent deeper leachate-contaminated alluvial ground water from discharging to the slough (Scholl and others, 1999). A sediment core collected about 100 meters upstream from the transect did not intercept the clay layer, indicating deeper native ground water could discharge upstream of the sampling location.

METHODS, ASSUMPTIONS, AND MODELS

Fifty-eight ground-water samples and two slough samples were collected during November and December 1995, April 1996, and April and May, 1997. The samples were collected from wells installed in a transect along the hydraulic gradient southwest from site NPD (fig. 1). All wells were sampled using a peristaltic pump. Samples with PS and DP prefixes (table 1) were collected from stainless-steel temporary drive-point wells. MLS samples were collected from nested polyvinyl chloride multilevel sampling wells. Two point samples were collected from the base of the slough during the PS and DP well sampling in 1995 and 1996 using a peristaltic pump. Biweekly accumulated-precipitation samples, collected under mineral oil from August 1996 through June 1998, were used to generate the local isotopic precipitation line (fig. 2). Temperature, humidity, and precipitation data were collected at the Mesonet tower at station 69, Norman, Oklahoma, about 7 kilometers north of the Norman Landfill, by the Oklahoma Climatological Survey (fig. 3).

Hydrogen-isotope activity ratios relative to Vienna mean standard ocean water (VSMOW), δD, were determined by the U.S. Geological Survey National Water Quality Laboratory using a hydrogen equilibration technique at 30 degrees Celsius (Coplen and others, 1991). Oxygen-isotope ratios relative to VSMOW, $\delta^{18}O$, were measured by the U.S. Geological Survey National Water Quality Laboratory using the carbon-dioxide equilibration technique at 25 degrees Celsius (Epstein and Mayeda, 1953). Chloride determinations on PS samples were made by the U.S. Environmental Protection Agency, National Risk Management Research Laboratory, in Ada, Oklahoma, using capillary electrophoresis. Chloride determinations on DP and MLS samples were made by the U.S. Geological Survey in Reston, Virginia, using ion-exchange chromatography.

The slough is similar to a small lake or pond, therefore we consider it appropriate to use evaporation formulae for lakes (Gonfiantini, 1986) to determine the pre-evaporation deuterium and ^{18}oxygen composition of the slough. As a first approximation, evaporation in the slough was estimated with the assumption that there was no exchange of ground water with the slough during evaporation. In actuality evaporation in the slough likely occurs coincident with small steady inflows and outflows of ground water, and with periodic large inflows. The lack of ground-water flux data and accurate slough-discharge data results in a potentially large error in the evaporation calculation.

Chloride was assumed to be conserved in the slough during evaporation, although we know that chloride concentration also would be affected by ground-water fluxes. Chloride and the stable isotope composition of individual or mixed source waters were considered to be conservatively transported to the slough prior to evaporation.

Deep and shallow alluvial ground-water samples collected upgradient from the landfill were assumed to represent time-weighted average compositions of native ground water and recent recharge, despite the small number of samples (three shallow samples and five deeper samples) and the difference in sampling times relative to the slough sampling. The overall composition of native ground water was assumed to change little over time, and the isotopic composition of recent recharge was assumed to vary only along the regional ground-water line.

Table 1. Samples collected along a transect extending southwest from the upgradient site NPD to site 80

[δ D, delta deuterium; δ ^{18}O, delta ^{18}oxygen; VSMOW, Vienna standard mean ocean water; mg/L, milligrams per lier]

Site name	Sample number	Land surface elevation (meters)	Depth of screened interval (meters)	Sampling date	δ D, relative to VSMOW (per mil)	δ ^{18}O, relative to VSMOW (per mil)	Chloride, dissolved (mg/L)
			Up hydraulic gradient from the capped landfill				
NPD	MLSNPD-1	332.66	2.41–2.53	04–30–97	–30.8	–5.48	42
	MLSNPD-2	332.66	2.90–3.02	04–30–97	–33.3	–5.68	42
	MLSNPD-3	332.66	3.94–4.06	04–30–97	–30.8	–5.33	134
	MLSNPD-4	332.66	4.91–5.03	04–30–97	–31.3	–5.22	172
	MLSNPD-5	332.66	6.07–6.19	04–30–97	–31.2	–5.18	156
	MLSNPD-6	332.66	8.90–9.02	05–01–97	–32.4	–5.18	181
	MLSNPD-7	332.66	12.93–13.05	05–01–97	–30.3	–5.23	52
	DPNPDA	332.77	1.83–1.92	04–23–96	–35.5	–5.91	11
	DPNPDB	332.77	6.02–6.11	04–23–96	–31.4	–5.41	48
	DPNPDC	332.77	8.83–8.92	04–23–96	–30.6	–5.13	82
			Down hydraulic gradient from the capped landfill				
35	PS35	331.18	1.20–1.97	11–06–95	–11.9	–5.47	603
	DP35A	331.17	0 .91–1.00	04–18–96	–24.3	–5.66	373
	DP35B	331.17	1.22–1.31	04–18–96	–14.3	–5.73	528
	DP35C	331.17	1.48–1.57	04–18–96	–13.9	–5.49	642
	DP35D	331.17	1.99–2.07	04–18–96	–13.1	–5.31	662
	DP35E	331.17	3.49–3.57	04–19–96	–13.7	–5.27	783
	DP35F	331.17	5.57–5.65	04–19–96	–7.6	–5.32	925
	DP35G	331.17	11.20–11.28	04–19–96	–13.7	–5.21	649
	MLS35-3	331.29	2.56–2.67	05–03–97	–11.4	–5.46	630
	MLS35-4	331.29	3.52–3.64	05–03–97	–12.2	–5.28	713
	MLS35-5	331.29	5.52 -5.64	05–03–97	–8.1	–5.38	848
	MLS35-6	331.29	7.56 -7.68	05–04–97	–16.9	–5.12	653
	MLS35-7	331.29	10.83-10.95	05–04–97	–17.1	–5.09	593
36	PS36	331.03	2.38–3.15	11–07–95	–11.9	–5.34	723
37	PS37	331.52	2.30–3.07	11–08–95	–26.2	–5.50	281
	MLS37-2	331.18	2.20–2.32	05–01–97	–19.8	–5.31	632
	MLS37-3	331.18	3.26–3.38	05–01–97	–10.6	–5.31	813
	MLS37-4	331.18	4.10–4.22	05–01–97	–14.1	–5.44	745
	MLS37-5	331.18	6.05–6.08	05–02–97	–6.0	–5.41	895
	MLS37-6	331.18	8.01–8.13	05–02–97	–3.4	–5.52	1,108
	MLS37-7	331.18	11.39–11.51	05–02–97	–16.7	–5.13	661
38	PS38	331.33	2.37–3.14	11–13–95	–32.6	–6.38	250
	PS38B	331.33	5.84–6.57	11–30–95	–12.9	–5.54	821
	PS38BD	331.33	5.84–6.57	11–30–95	–9.4	–5.47	836
	PS38C	331.33	9.46–10.22	12–04–95	–7.4	–5.52	1,000
	PS38D	331.33	11.72–12.48	12–04–95	–10.3	–5.43	1,081
	DP38A	331.41	1.34–1.42	04–19–96	–29.2	–5.39	9
	DP38B	331.41	2.33–2.42	04–20–96	–31.9	–6.58	318
	DP38C	331.41	5.94–6.03	04–21–96	–6.8	–5.68	953
	DP38D	331.41	11.17–11.26	04–21–96	–8.9	–5.44	1,023

Table 1. Samples collected along a transect extending southwest from the upgradient site NPD to site 80—Continued

Site name	Sample number	Land surface elevation (meters)	Depth of screened interval (meters)	Sampling date	δ D, relative to VSMOW (per mil)	$\delta^{18}O$, relative to VSMOW (per mil)	Chloride, dissolved (mg/L)
			Down hydraulic gradient from the capped landfill				
38	MLS38-2	331.38	2.23–2.35	05–01–97	–26.5	–5.29	206
	MLS38-3	331.38	3.24–3.36	05–01–97	–17.5	–5.79	654
	MLS38-4	331.38	3.63–3.75	05–02–97	–13.2	–5.77	653
	MLS38-5	331.38	6.14–6.25	05–02–97	–11.2	–5.51	851
	MLS38-6	331.38	6.95–7.07	05–02–97	–5.1	–5.57	1,027
	MLS38-7	331.38	12.01–12.13	05–02–97	–12.7	–5.27	938
39	PS39	330.74	2.75–1.98	11–13–95	–34.5	–6.25	206
			Shallow ground water down hydraulic gradient from the slough				
54	PS54	330.60	1.13–1.90	11–22–95	–1.3	0.55	255
	MLS54-1	330.51	1.31–1.43	05–05–97	–16.9	–3.87	386
	MLS54-2	330.51	1.78–1.90	05–05–97	–16.2	–3.30	273
	MLS54-3	330.51	2.55–2.67	05–05–97	–18.8	–3.30	251
	MLS54-4	330.51	3.10–3.22	05–05–97	–22.0	–4.89	467
55	MLS55-1	330.53	1.23–1.35	05–05–97	–26.2	–4.59	104
	MLS55-2	330.53	1.73–1.85	05–05–97	–24.6	–3.86	151
	MLS55-3	330.53	2.76–2.88	05–05–97	–21.8	–3.39	243
	MLS55-4	330.53	3.71–3.83	05–05–97	–26.0	–4.09	263
80	MLS80-1	330.21	1.27–1.39	05–06–97	–17.3	–2.41	257
	MLS80-3	330.21	2.63–2.75	05–06–97	–27.6	–4.20	267
			Slough				
Slough	SLOUGH1	329.68	—	11–09–95	–12.1	–1.53	300
	SLOUGH2	329.68	—	04–20–96	–20.8	–2.83	184

All samples collected between the capped landfill and the slough were considered to be contaminated by leachate, because they were at least somewhat enriched in deuterium. Samples collected at site 35, adjacent to the landfill, that had greatest deuterium enrichment and chloride concentration were considered to represent the composition of leachate exiting the landfill.

Chloride concentration and deuterium and ^{18}oxygen enrichment in the slough and in ground water recharged from the slough, which we assumed represented slough water, were evaluated to determine if the slough received leachate from the landfill and to estimate the percentages of leachate-contaminated and uncontaminated ground water contributing to the slough. Ground water upgradient from the slough that had chloride concentration and δD and $\delta^{18}O$ values less than or equal to the values in slough1, slough2, and PS54 were selected as potential source waters for the slough because we assumed that chloride concentration will become concentrated or stay the same in the slough but not become more dilute. Those waters samples contained less than 300 milligrams per liter of chloride. Most of the samples were from upgradient of the landfill, and represent possible native ground-water input to the slough upstream of the capped landfill. Four were shallow samples from contaminated sites 38 and 39. Water from these contaminated sites was enriched in deuterium by only a few per mil.

Fractionation factors ($\alpha_{l\text{-}v}$*) for deuterium and ^{18}oxygen during evaporation of water are the inverse of $\alpha_{l\text{-}v}$, the enrichment factors during condensation of water. $\alpha_{l\text{-}v}$*values were calculated for the air-temperature range from 0 to 35 degrees Celsius based on formulae for $10^3 \ln \alpha_{l\text{-}v}$ determined by Horita and Wesolowski (1994):

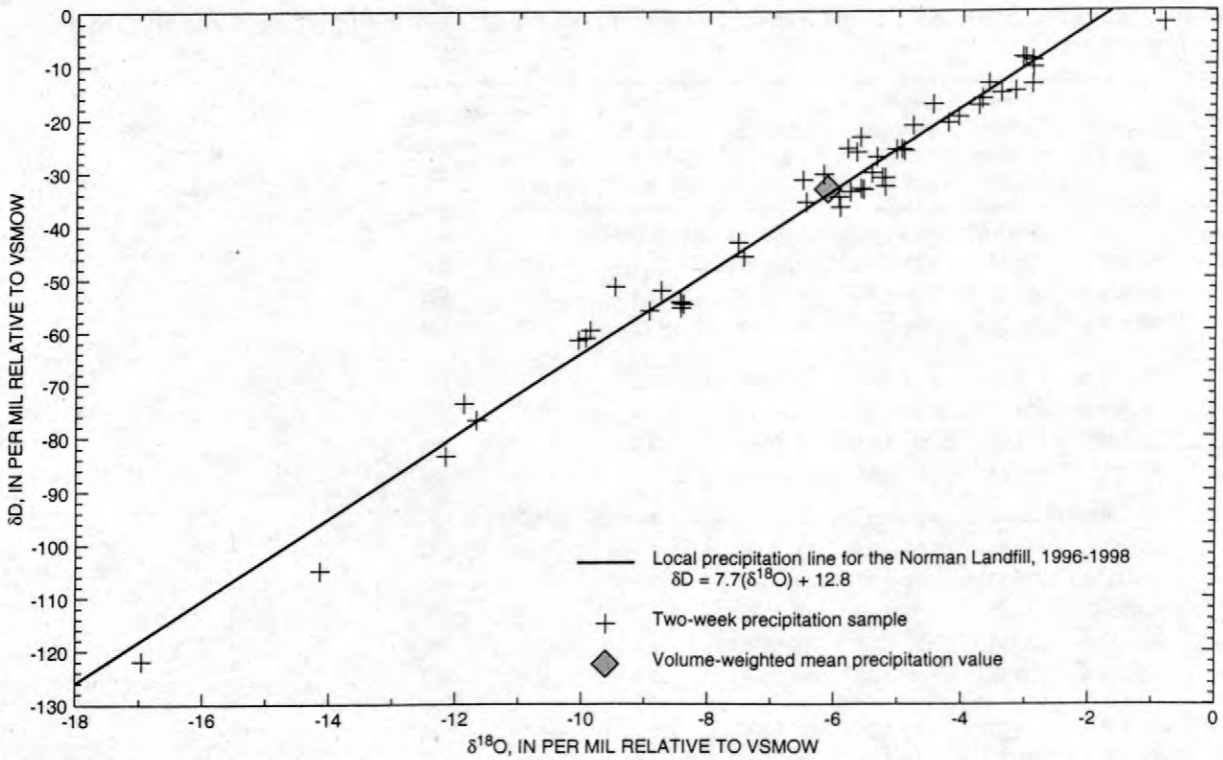

Figure 2. Average δD and $\delta^{18}O$ values for precipitation samples collected at the Norman Landfill,1996-1998.

$$10^3 \ln \alpha_{l\text{-}v}(^{18}\text{oxygen}) = -7.685 + 6.7123\,(10^3/T) - 1.6664\,(10^6/T^2) + 0.35041\,(10^9/T^3) \quad (1)$$

$$10^3 \ln \alpha_{l\text{-}v}(\text{deuterium}) = 1158.8\,(T^3/10^9) - 1620.1\,(T^2/10^6) + 794.84\,(T/10^3) - 161.04 + 2.9992\,(10^9/T^3), \quad (2)$$

where

$\alpha_{l\text{-}v}$ is the fractionation factor for the isotope exchange between the liquid (l) and the vapor (v) phase of water (unitless)

T is the air temperature (degrees Kelvin).

Water isotopic enrichment in per mil related to air temperature is described by the equilibrium fractionation factor $\varepsilon_{l\text{-}v}$:

$$\varepsilon_{l\text{-}v} = (\alpha_{l\text{-}v}{}^* - 1)\,10^3. \quad (3)$$

The isotope fractionation between water and air in per mil also is affected by kinetic factors including humidity and wind that are represented by $\Delta\varepsilon_{bl\text{-}v}$, the kinetic enrichment factor (Clark and Fritz, 1997):

$$\Delta\varepsilon_{bl\text{-}v} = (\alpha_{bl\text{-}v} - 1)\,10^3, \quad (4)$$

where

$\alpha_{bl\text{-}v}$ is the fractionation factor for the isotope exchange between the boundary layer (bl) interface of water and air and the vapor in the air (v) (per mil).

The total fractionation between water and air is described by equation 5 (Clark and Fritz, 1997):

$$\delta_l - \delta_v = \varepsilon_{l\text{-}v} + \Delta\varepsilon_{bl\text{-}v}, \quad (5)$$

where

δ_l is the delta value of the isotope in the residual water (per mil) and

δ_v is the delta value of the isotope in the evaporated vapor (per mil).

Kinetic enrichment factors between the boundary layer interface of water and air and the vapor in the air to determine the depletion of deuterium and ^{18}oxygen in the vapor were determined

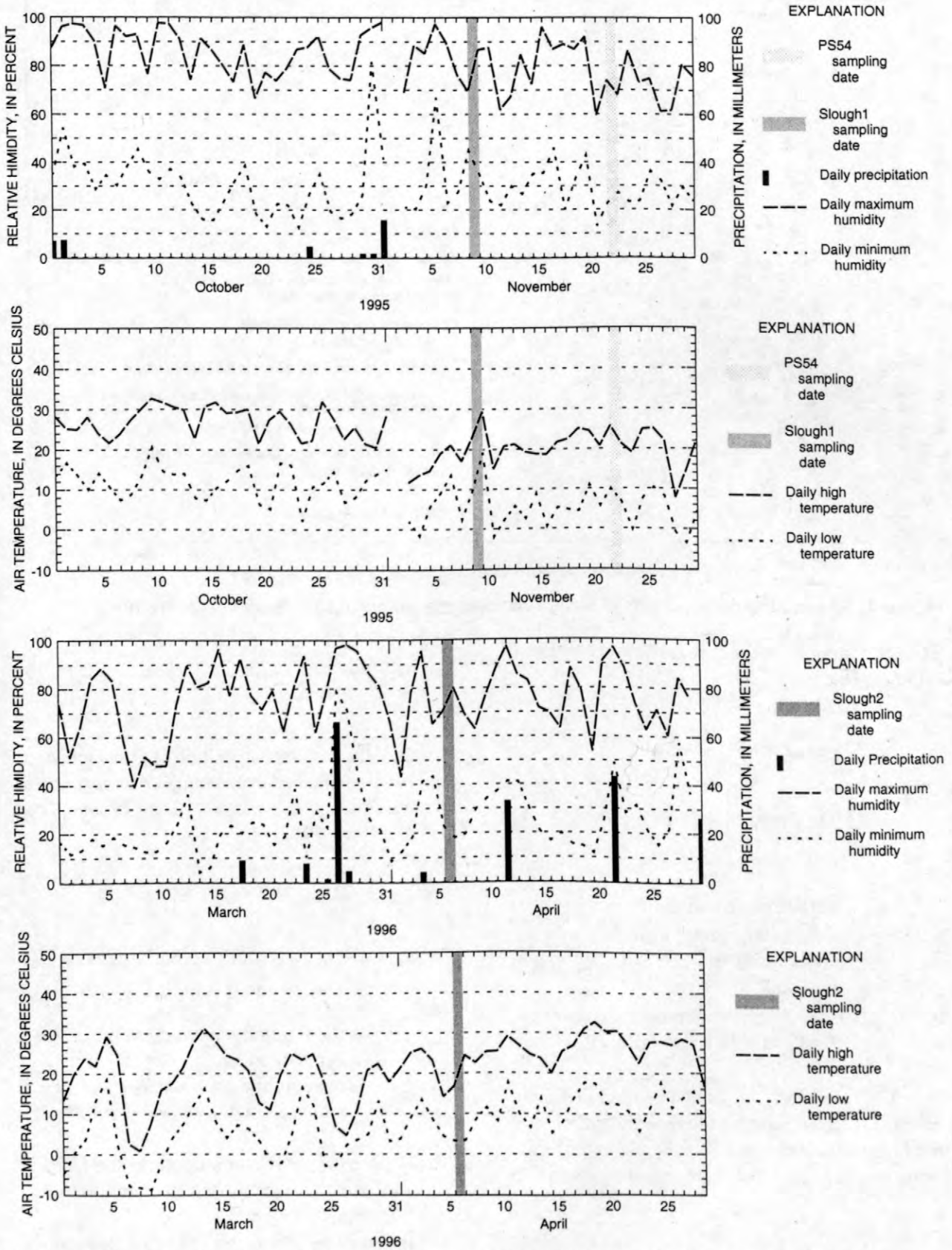

Figure 3. Daily humidity and temperature extremes measured at the Norman Mesonet site during October-November 1995 and March-April 1996.

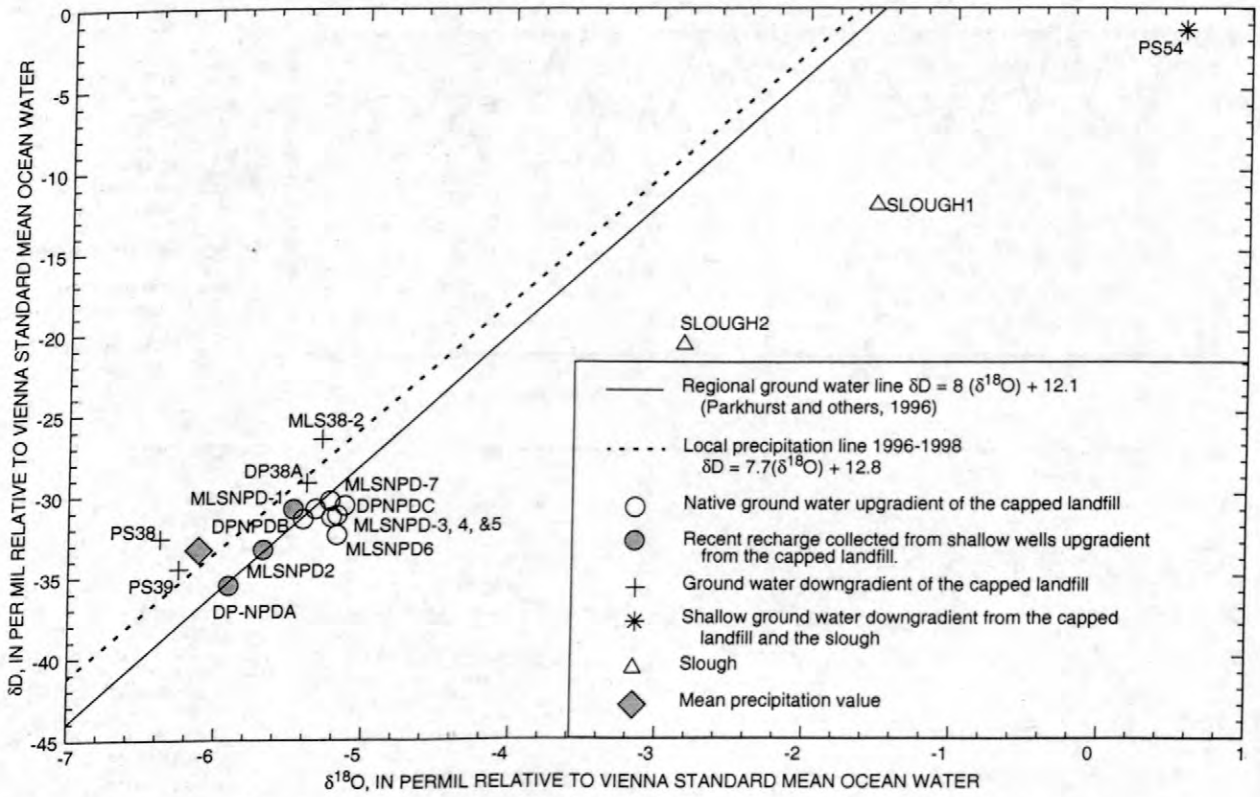

Figure 4. δD and $\delta^{18}O$ compositions of slough samples and potential source waters for the slough.

for most evaporation conditions in nature by Gonfiantini (1986):

$$\Delta\varepsilon\, D_{bl\text{-}v} \text{ per mil} = 12.5\,(1-h) \qquad (6)$$

$$\Delta\varepsilon\, {}^{18}O_{bl\text{-}v} \text{ per mil} = 14.2\,(1-h), \qquad (7)$$

where

h is the relative humidity,

$\Delta\varepsilon\, D_{bl\text{-}v}$ is the kinetic enrichment factor for deuterium (Clark and Fritz, 1997) (per mil), and

$\Delta\varepsilon\, {}^{18}O_{bl\text{-}v}$ is the kinetic enrichment factor for ^{18}oxygen (Clark and Fritz, 1997) (per mil).

The inverse of α_{bl-v} must be used in kinetic enrichment factor equations to determine the enrichment of deuterium and ^{18}oxygen in the liquid during evaporation, resulting in equations 8 and 9:

$$\Delta\varepsilon D_{bl\text{-}v}{}^{*} = 10^{3}\left(\frac{1}{((12.5(1-h))\div 10^{3})+1}-1\right) \qquad (8)$$

$$\Delta\varepsilon\, {}^{18}O_{bl\text{-}v}{}^{*} = 10^{3}\left(\frac{1}{((14.2(1-h))\div 10^{3})+1}-1\right). \qquad (9)$$

Initial isotopic composition of the evaporated water can be estimated over a range of temperatures and humidities using equations 10 and 11 (based on Clark and Fritz, 1997):

$$\delta D_{initial} = \delta D_{slough} - (\varepsilon D_{l\text{-}v} + \Delta\varepsilon D_{bl\text{-}v}{}^{*})\ln f \qquad (10)$$

$$\delta^{18}O_{initial} = \delta^{18}O_{slough} - (\varepsilon^{18}O_{l\text{-}v} + \Delta\varepsilon^{18}O_{bl\text{-}v}{}^{*})\ln f, \qquad (11)$$

where

f is the fraction remaining of the initial volume of water,

$\varepsilon D_{l\text{-}v}$, is the equilibrium fractionation factor for deuterium during evaporation (per mil), and

$\varepsilon^{18}O_{l\text{-}v}$ is the equilibrium fractionation factor for ^{18}oxygen during evaporation (per mil).

Initial deuterium and $\delta^{18}O$ values for samples slough1, PS54, and slough2 were calculated over a range of air temperatures (0–35 degrees Cel-

sius), humidities (20–90 percent) and fractions (0.65–0.95) of the original volume using equations 10 and 11. Results were graphically compared to isotopic compositions of potential source waters, that is water samples containing less chloride than the evaporated water. Percentage or fractions of water remaining and conditions under which the evaporation could have occurred were those that resulted in initial isotopic compositions that plotted within the range of the potential source waters. This calculation suggested the range of conditions under which ground water upgradient from the slough could evaporate to produce the evaporated waters.

Initial chloride concentrations were calculated using equation 12. This calculation was based on the fractions of water remaining, *f*, that were indicated by the calculation of the initial isotopic composition. Water samples that matched or approximated the calculated initial compositions were selected for further evaluation as potential sources.

$$\text{Chloride}_{\text{initial}} = f\,(\text{Chloride}_{\text{slough}}) \qquad (12)$$

After determination of the potential source waters, evaporation of each potential source water was calculated using equation 13 with the temperature and humidity range predicted by the previous calculation:

$$f = e^{\left(\frac{\delta^{18}O_{\text{slough}} - \delta^{18}O_{\text{initial}}}{\varepsilon^{18}O_{\text{l-v}} + \Delta\varepsilon^{18}O_{\text{bl-v}}}\right)}. \qquad (13)$$

The amount of evaporation needed to produce the observed change in chloride concentration was calculated for each potential initial water using the relation described in equation 12.

When the three evaporation estimates based on δD, $\delta^{18}O$, and chloride matched exactly for a sample, the sample was selected to represent a potential source. Conditions under which the estimates matched were considered to be the time-averaged evaporating conditions. Isotope compositions for simple water mixtures were calculated if none of the evaporation estimates based on the stable isotopes and chloride converged.

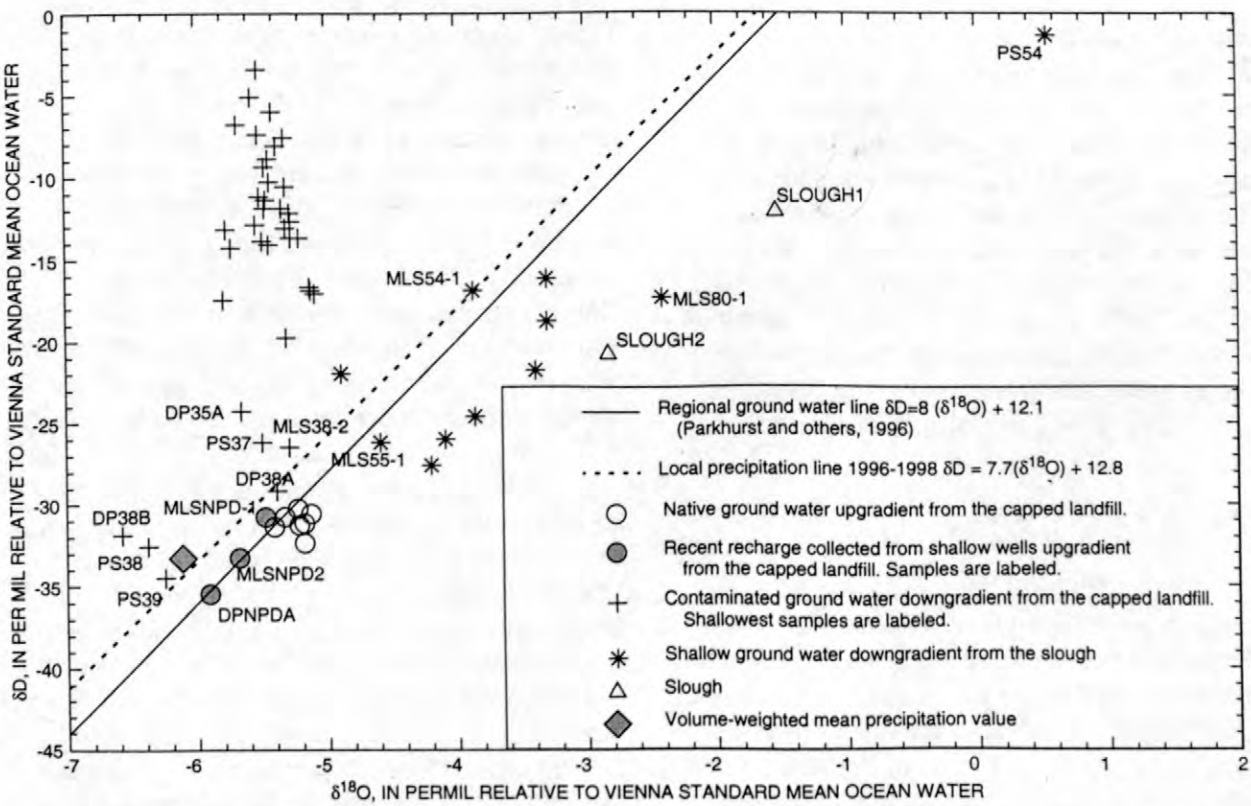

Figure 5. Comparison of δD and $\delta^{18}O$ in water from upgradient and downgradient from the capped landfill along a transect from the NPD site to site 80 and in surface water from the slough.

Table 2. Results of reverse model of slough evaporation indicating the range in initial chloride concentration, humidity, and air temperature required to produce the evaporated sample from available initial waters

[mg/L, milligrams per liter; °C, degrees Celsius]

Sample	Percentage of initial water evaporated	Range of initial chloride concentration (mg/L)	Upgradient samples with chloride concentration in or near range, and thus are potential source waters	Range of relative humidity (percent)	Range of predicted air temperature (°C)
Slough1	18 to 25	225 to 246	PS38, MLS38-2, PS39	23 to 60	0 to 35
PS54	25 to 35	166 to 230	MLSNPD-5, 4, and 6, MLS38-2, and PS39	40 to 65	0 to 32.2
Slough2	10 to 15	156 to 166	MLSNPD-3, 4, 5, and 6	0 to 60	0 to 30

Source waters for which evaporation estimates based on δD, $\delta^{18}O$, and chloride were equal at a temperature and humidity reasonable for the Norman area within a month prior to slough sampling were determined to represent sources of most of the water in the slough samples. A source was assumed to be contaminated by leachate if the source was downgradient from the capped landfill and if the source was enriched in deuterium relative to regional ground water. The percentage of leachate in any contaminated shallow source water (less than 3.6 meters depth) was estimated based on two end-member mixing of the most concentrated shallow leachate composition (DP35D, table 1) and estimated recent recharge water. The composition of estimated recent recharge had the chloride concentration of average recent recharge water (mean chloride concentration of DPNPDA, MLSNPD-1, and MLSNPD-2) and a δD and $\delta^{18}O$ composition representing the intersection of the regional ground-water line with a mixing line through DP35D and the contaminated source water.

RESULTS

Deuterium and ^{18}oxygen have unique relations in potential sources of water for the slough. Ground water contaminated with leachate from the Norman Landfill is enriched in deuterium relative to local precipitation and uncontaminated ground water by 3 to 30 per mil. $\delta^{18}O$ of leachate-contaminated water is similar to that of uncontaminated ground water upgradient of the landfill (-6.00 to -5.00 per mil, fig. 5). Recent recharge from precipitation, represented by shallow ground water upgradient of the landfill, plots along the regional ground-water line (fig. 5). The range in precipitation $\delta^{18}O$ values (-16.96 to -0.82 per mil, fig. 2) and $\delta^{18}O$ values for the shallowest ground-water samples (-6.58 to -2.41 per mil, fig. 5) indicate a potentially great range in δD and $\delta^{18}O$ values for recent recharge. Thus, waters that include some recent recharge from precipitation could have δD and $\delta^{18}O$ values that are greater or less than native ground water and leachate contaminated water. Recent recharge with values similar to those of native ground water can be differentiated by low concentrations of chloride as described below. Deeper native alluvial ground water plots slightly to the right of the regional ground water line and the mean precipitation value indicating an enrichment in δD and $\delta^{18}O$, possibly as a result of recharge from evaporated surface-water sources. Native alluvial ground water along the transect and the deepest ground water (sample MLSNPD-7), ground water upwelling from deeper Permian aged rocks, have a $\delta^{18}O$ composition of -5.23 per mil.

Chloride concentrations ranged from 11 to 42 milligrams per liter in recent recharge collected from shallow wells (MLSNPD-1 and 2, and DPNPDA) and from 48 to 181 milligrams per liter in deeper native ground water from site NPD (table 1), indicating that chloride concentration can be used to differentiate recent recharge to the alluvium from older recharge. Uncontaminated ground water flowing upward from deeper Permian aged rocks (MLSNPD-7) contained only 52 milligrams per liter of chloride. Most leachate-contaminated water contained between 600 and 1,100 milligrams per

liter of chloride. The shallowest leachate-contaminated ground-water samples at sites 35, 37, 38, and 39, contained 9 to 632 milligrams per liter of chloride. The low chloride concentration in the shallowest downgradient sample, DP38A (9 milligrams per liter), indicates that recent recharge to the plume can be differentiated by a low chloride concentration or the $\delta^{18}O$ value.

Water in the slough and in shallow ground water downgradient from the slough is enriched in deuterium and ^{18}oxygen relative to native ground water, as a result of evaporation (fig. 5). One shallow ground-water sample (PS54) collected just downgradient from the slough in November 1995 was more enriched in deuterium and ^{18}oxygen than water collected from the slough in November 1995 and April 1996. That water probably recharged the aquifer from the slough at a time when evaporation had enriched the stable isotopes and in this report is interpreted to represent slough water. Chloride concentrations in the slough water samples including PS54 ranged from 184 to 300 milligrams per liter.

Calculation of potential source waters for samples slough1, PS54, and slough2 provided probable ranges of the percentages of water evaporated, of chloride concentration, of relative humidity, and of predicted air temperature (table 2). The chloride concentrations predicted by the calculation were too great to have been in native ground water recharged by recent precipitation or from water flowing upward from the underlying Permian-aged rocks, so these waters alone were not considered potential sources for the slough. The ranges in humidity were within the range of humidity observed prior to sampling slough1 and PS54 and included percentages slightly less than those observed prior to sampling slough2. The range of predicted overall evaporation temperatures indicated by the calculation covered the entire range of temperatures observed at the site. The greatest calculated deuterium enrichment for any possible initial water was 8 per mil, which included the range of waters with chloride concentration less than 300 milligrams per liter.

Calculated evaporation of most of the potential source waters indicated in table 2 individually did not produce converging evaporation estimates. A possible explanation is that the source of water in the slough was a mixture of waters.

Initial chloride concentration estimated by the source-water calculation indicated samples PS38, MLS38-2, and PS39, downgradient of the landfill, were potential source waters for sample slough1 (table 2). However, estimates of percentage evaporation to generate δD and $\delta^{18}O$ values and chloride concentration of sample slough1 from PS38, MLS38-2, and PS39 would not converge within the expected temperature and humidity range. Evaporation of simple mixtures of equal amounts of the three potential source waters were calculated, and the calculated evaporation of a 50-50 mixture of PS38 and PS39 evaporated by 24 percent of the original volume at 40.5 percent relative humidity and 27.5 degrees Celsius resulted in the δD, $\delta^{18}O$, and chloride composition of sample slough1. This suggests that the slough was dominantly fed by water slightly contaminated by leachate prior to early November 1995. The mixture of PS38 and PS39 represents water that is about 30 percent leachate and 70 percent recent recharge based on the low δD and chloride concentrations.

The source-water calculation indicated that upgradient samples MLSNPD-5, 4, and 6, MLS38-2, and PS39 were potential source waters for sample PS54, which is considered to represent slough water. Estimates of percentage of evaporation of MLSNPD-6 based on δD and $\delta^{18}O$ and chloride concentration converged with 29 percent of MLSNPD-6 evaporated at 13.5 degrees Celsius with 55 percent relative humidity, but would not converge for any other source waters. MLSNPD-6 is a sample of uncontaminated native ground water. This result suggests that minimal leachate-contaminated water discharged to the slough before PS54 water was affected by evaporation and that the source of water discharging to the slough probably was uncontaminated native ground water that was discharged upstream of the transect.

Estimates of percentage of evaporation to produce the isotopic composition and chloride concentration of sample slough2 from samples MLSNPD-3, 4, 5, or 6, which were native ground water, would not converge. However, estimates for a simple mixture of equal amounts of MLSNPD3, 4, 5, and 6 evaporated by 13 percent at 27.0 degrees Celsius and 38 percent relative humidity did converge, indicating that the slough source was dominantly uncontaminated native ground water in early April 1996. However, this estimated evaporation temperature is high for the period prior to sample collection, indicating that perhaps the sampled

waters or the mixtures used do not precisely represent the water discharged to the slough.

CONCLUSIONS

Estimations of the pre-evaporation compositions of water samples from a small wetland (the slough) downgradient from a landfill were used to determine the probable compositions of water sources to the slough. Calculated evaporation of potential source waters for the slough indicates that the sources of ground water discharging to the slough have varied over time. The calculations suggest that the dominant source of water for the slough is uncontaminated native ground water, but there is some leachate discharged to the slough. Two of the three slough samples contained no apparent contribution from leachate. Leachate discharged to the slough prior to one sampling apparently was diluted approximately 70 percent by recent recharge before entering the slough.

REFERENCES CITED

Baedecker, M.J., and Back, William, 1979, Hydrogeological processes and chemical reactions at a landfill: Ground Water, v. 17, n. 5, p. 429–437.

Clark, I. D., and Fritz, Peter, 1997, Environmental isotopes in hydrogeology, Lewis Publishers, New York, 328 p.

Coplen, T.B., Wildman, J.D., and Chen, J., 1991, Improvements in the gaseous hydrogen-water equilibration technique for hydrogen isotope ratio analysis: Analytical Chemistry, v. 63, p. 910-912.

Epstein, S. and Mayeda, T., 1953, Variation of ^{18}O content of water from natural sources: Geochimica et Cosmochimica Acta, v. 4, p. 213-224.

Gonfiantini, Roberto, 1986, Environmental isotopes in lake studies: in Handbook of environmental isotope geochemistry, eds: P. Fritz and J.Ch. Fontes, v. 2, The terrestrial environment B, Elsevier, NY, 557 p

Hackley, K.C., Liu, C.L., and Coleman D.D., 1996, Environmental isotope characteristics of landfill leachates and gases: Ground Water, v. 34, n. 5, p. 827–836.

Horita, Juske, and Wesolowski, D.J., 1994, Liquid-vapor fractionation of oxygen and hydrogen isotopes of water from freezing to the critical temperature: Geochimica et Cosmochimica Acta, v. 58, n. 16, p. 3425–3437.

Nicholson, R.V., Cherry J.A., and Reardon, E.J., 1983, Migration of contaminants in groundwater at a landfill: a case study, 6 hydrogeochemistry: Journal of Hydrology, V. 63, p. 131–176.

Parkhurst, D.L., Christenson, S.C., and Breit, G.N., 1996, Ground-water-quality assessment of the Central Oklahoma aquifer, Oklahoma: Geochemical and geohydrologic investigations: U.S. Geological Survey Water-Supply Paper 2357–C, 101 p.

Scholl, M.A., Cozzarelli, I.C., Christenson, S.C., Breit, G.N., and Schlottmann, J.L., 1999, Aquifer Heterogeneity at Norman Landfill and its effect on observations of biodegradation processes, *in* Morganwalp, D.W., and Buxton, H.T., eds., U.S. Geological Survey Toxic Substances Hydrology Program—Proceedings of the Technical Meeting, Charleston, South Carolina, March 8-12, 1999—Volume 3—Subsurface Contamination from Point Sources: U.S. Geological Survey Water-Resources Investigations Report 99-4018A, this volume.

AUTHOR INFORMATION

Jamie L. Schlottmann, U.S. Geological Survey, Oklahoma City, Oklahoma,

Martha A. Scholl, and Isabelle M. Cozzarelli, U.S. Geological Survey, Reston, Virginia

Biogeochemical Processes in a Contaminant Plume Downgradient from a Landfill, Norman, Oklahoma

By Isabelle M. Cozzarelli, Joseph M. Suflita, Glenn A. Ulrich, Steve H. Harris, Martha A. Scholl, Jamie L. Schlottmann, and Jeanne B. Jaeschke

ABSTRACT

Studies of an alluvial aquifer contaminated with landfill leachate, at Norman, Oklahoma, indicate that the non-uniform distribution of electron acceptors and biogeochemical reactions in anoxic ground water result in steep chemical gradients and the formation of distinct reaction zones. A combined geochemical and microbiological approach was used to delineate different biogeochemical zones along a transect parallel to regional ground-water flow downgradient from the landfill. The important microbially mediated reactions in the anoxic plume are iron reduction, sulfate reduction, and methanogenesis. Dissolved H_2 measurements in ground water at several depth intervals at one location near the edge of the landfill indicate that sulfate reduction is a dominant respiratory process, but near- saturation levels of methane were detected in some intervals. Cycling of sulfur was apparent in a thin interval at the water table where the highest rates of sulfate reduction (13.2 micromoles per day (μM/day)) and sulfate concentrations well above background levels (up to 4.6 millimolar (mM)) were measured. In this zone, sulfur isotope analyses indicate that the sulfate is enriched in ^{34}S ($\delta^{34}S$ of SO_4^{2-} was 67-69 per mil). Elevated concentrations of sulfate near the water table appear to result from the oxidation of sulfides as oxygenated recharge water mixes with anoxic plume water during recharge events. Sulfate availability in this vertically thin zone near the water table appears to control the high sulfate reduction rates measured in the zone. Iron reduction occurred at the edges of the sulfate-depleted plume, whereas methanogenesis was detected only in the center of the plume. This study underscores the importance of examining the availability of electron acceptors in contaminated environments and using a combined geochemical and microbiological approach to elucidate the spatial distribution of biogeochemical processes.

INTRODUCTION

Contamination of shallow aquifers by landfill leachate is a significant environmental concern because of the sheer magnitude of the problem. More than 70 percent of the approximately 150 million tons of solid waste produced each year in the United States is disposed of in landfills (Suflita and others, 1992). The natural attenuation of organic contaminants, such as those typically found in ground water contaminated by landfill leachate, is receiving increased attention as a remedial option for pollutant-tainted aquifers where the threat to environmental receptors is minimal. The availability of electron acceptors is important for determining whether intrinsic bioremediation is a viable strategy for ground-water cleanup. Bacteria that degrade organic compounds in aquifers can utilize a range of naturally occurring electron acceptors. In sediments, Fe (III) and Mn (IV), present as oxides, are reducible by microorganisms, which results in the accumulation of high dissolved concentrations of Fe^{2+} and Mn^{2+} in ground water (e.g., Baedecker and Back, 1979b; Ehrlich and others, 1983; Chapelle and Lovley, 1992; Baedecker and others, 1993). Reduction of NO_3^- and SO_4^{2-}, supplied during recharge, result in the accumulation of sulfides and reduced nitrogen species in contaminated aquifers (e.g., Baedecker and Back, 1979a; Back and Baedecker, 1989).

Characterization of redox environments in aquifers downgradient from contaminant sources often forms the basis of identifying the important attenuation processes. As hydrologic and geochemical conditions in an aquifer change, the dominant microbial processes shift in response to these changes, resulting in different rates and pathways of biodegradation. Previous studies at U.S Geological Survey Toxic Substances Hydrology Program research sites have shown that microbial processes and the associated geochemistry can vary over distances of several centimeters in contaminated aquifers. Microbial populations in a crude-oil contaminated aquifer in Bemidji, Minn., exhibited heterogeneities on the scale of tens of centimeters and spatial zonation of physiologic types (Bekins and others, 1998; this volume). In a Coastal Plain aquifer contaminated with gasoline, Cozzarelli and others (in press) demonstrated that the availability of electron acceptors controlled the dominant hydrocarbon degradation processes in shallow ground water. Depletion of microbially reducible solid iron-oxyhydroxides in thin zones in the anoxic aquifer allowed sulfate reduction to occur.

Geochemical research has shown that ground water downgradient from the Norman, Oklahoma Landfill is contaminated with many volatile and non-volatile organic compounds (Dunlap and others, 1976; Eganhouse and others, 1998; this volume), has low dissolved oxygen concentrations, and elevated dissolved inorganic carbon and methane concentrations (Gibson and Suflita, 1986; Beeman and Suflita, 1987; 1990; Cozzarelli and others, 1997). Two spatially distinct microbiological zones were identified in the shallow aquifer near the edge of the landfill. Organic carbon degradation processes were dominated by sulfate reduction at one location and by methanogenesis at another location (Beeman and Suflita, 1987; 1990). This paper provides insight into the spatial heterogeneity of these processes, as well as iron reduction, along a transect downgradient from the landfill. Characterizing the spatial distribution of sulfate reduction and methanogenesis and elucidating how the availability of electron acceptors controls the progression of these biogeochemical reactions will ultimately provide the information needed to predict the fate and transport of organic contaminants away from the landfill.

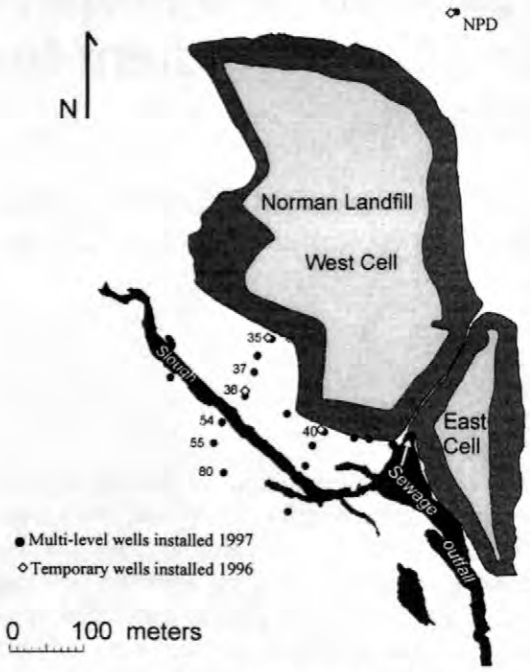

Figure 1. Map of the Norman Landfill, showing the location of the multi-level samplers and temporary wells.

DESCRIPTION OF FIELD SITE

The field site is a closed municipal landfill in Norman, Oklahoma, located in the alluvium of the Canadian River. The landfill received solid waste beginning in 1922. The waste was dumped into trenches approximately 3 meters (m) deep that contained 1.5 to 2.5 m of water because of the shallow water table, and then covered with 15 cm (centimeters) of sand. No restrictions were placed on the type of material dumped at the landfill. In 1985, the landfill was closed and the mounds, which had reached a maximum height greater than 12 m, were covered with local clay, silty-sand material.

The Canadian River alluvium is 10 to 12 m thick and consists predominantly of sand and silty sand, with interbedded mud and gravel. In the vicinity of the landfill, the water table is less than 2 m below land surface. Hydraulic conductivity measurements made using slug tests ranged from 7.3×10^{-2} m/day to 24 m/day (Scholl and Christenson, 1998). Along the transect where most data have been collected (fig. 1), a discontinuous low hydraulic conductivity, silt-clay layer is present about 3 to 4 m below the

water table. Near the base of the alluvium, at a depth of approximately 10-12 m, is a high hydraulic conductivity layer containing coarse sand and gravel (Scholl and others, this volume). A shallow slough, approximately 0.75 m deep, lies parallel to the landfill about 100 meters to the southwest (fig. 1).

STUDY METHODS

Ground Water Sampling

Ground-water samples were collected in April 1996 from a network of small diameter temporary wells set at closely spaced vertical intervals and in April 1997 from 2.54-cm diameter multilevel wells, respectively (fig. 1). The temporary wells consisted of 1.9-cm diameter, schedule-80 stainless steel line pipe, with threaded couplings, attached to stainless steel screened sandpoints with a screen length of 8.7 cm. The temporary wells were driven at sites at which 3.8-cm diameter sediment cores were collected for microcosm experiments and geological characterization of the sediment. These wells were driven with an electric jack hammer to the desired sampling depths, based on field analysis of the cores, from just below the water table (depth about 1 m) to the base of the aquifer (depth about 11 m). Teflon tubing was attached directly to the stainless steel screened sandpoints and samples were withdrawn using a peristaltic pump. Samples were collected from three vertical profiles downgradient from the landfill (sites 35, 38 and 40), at a background location, at an upgradient location (NPD), and from the slough (fig. 1).

Each well location in the permanent multi-level sampler network (MLS), installed in 1997, is comprised of 7 nested well casings set at different depths with 0.12 m-length screens. Clusters of the 1.9-cm PVC wells were installed in an 20-cm (8-inch) augered hole. The auger flights were withdrawn and the alluvial sands collapsed around the wells. In each cluster, the first six well screens were set about 0.5, 1.0, 2.0, 3.0, 4.0, 7.0 m below the water table at the time of emplacement. The seventh screen was set just above the base of the alluvium at 11 to 12 meters.

Water samples were collected for measurement of pH, conductivity, temperature, dissolved oxygen (DO), Fe^{2+}, H_2S, NH_4^+, HCO_3^-, CH_4, anions (NO_3^-, SO_4^{2-}, Cl^-, Br^-, PO_4^{3-}), cations (Ca, Mg, Na, K, Fe_T, Si, Al, B, Ba, Mn, Li, Sr, Tl), $\delta^{13}C$ of total inorganic carbon, δD of H_2O, $\delta^{34}S$ of SO_4^{2-}, and dissolved organic carbon. Samples were collected from the temporary wells in April 1996 and from the MLS network in April 1997. Cross sectional profiles of chemistry along the 35-80 transect (figs. 2-9) were generated using the 1997 data (shown as diamonds in the figures), and 1996 data (shown as triangles in the figures).

Field Collection Procedures and Analyses

Conductivity, pH, and temperature were determined in the field using specific electrodes. DO, Fe^{2+}, NH_4^+, and H_2S concentrations were determined in the field using colorimetric CHEMets kits (CHEMetrics Inc., Calverton, VA) or HACH kits. Alkalinity titrations were done using an incremental titration method in a mobile field laboratory. Water samples for measurement of CH_4 concentrations were collected in Glasspak syringes connected directly to the sample-pump outlet following the method of Baedecker and Cozzarelli (1992). The water sample was transferred from the syringe into 25-mL (milliliter) serum bottles containing mercuric chloride ($HgCl_2$, at a concentration of 0.2 mM Hg). Water collected for analyses of nonvolatile dissolved organic carbon (NVDOC) was filtered in line through a 0.4 micrometer (μm) silver filter. Samples collected for determination of anions were filtered through a 0.2 μm Nuclepore filter. Cation samples were filtered through 0.1 μm Nuclepore filters and acidified with HNO_3 to a pH of 2. Samples for analysis of $\delta^{13}C$ of total dissolved inorganic carbon (TDIC) were filtered through 0.4 μm Nuclepore filters and were collected in glass bottles to which was added a solution of 30 percent ammonium hydroxide saturated with strontium chloride (Gleason and others, 1969). Samples for analysis of $\delta^{34}S$ of SO_4^{2-} were filtered through 0.2 μm Nuclepore filters and samples collected for δD and $\delta^{18}O$ of H_2O were collected without filtration. All samples were stored on ice after collection and during transport to the laboratory.

Laboratory Analytical Procedures

Dissolved methane concentrations were measured by headspace analysis and gas chromatography (Baedecker and Cozzarelli, 1992). Anion concentrations were measured by ion-exchange chromatography. Concentrations of NVDOC were determined by the persulfate wet-oxidation technique using a carbon analyzer (Baedecker and Cozzarelli, 1992). The determination of $\delta^{13}C$ values of TDIC was made on $SrCO_3$ precipitates with an isotope ratio mass spectrometer.

Iron Reduction and Methanogenesis Experiments

Microbial activity assays were performed within 2 days after obtaining samples. Sediments were processed inside an anaerobic glove bag filled with 100% N_2. Anoxic sediment slurries (15g/15mL) were prepared in 160-mL serum bottles with sediment from cores and groundwater obtained from the adjacent monitoring wells. The slurries were incubated under a N_2/CO_2 (80/20) headspace at 18°C in the dark. Production of soluble Fe^{+2} was monitored by periodic removal of liquid samples for analysis using the ferrozine assay as previously described (Lovley and Phillips, 1986). Measurement of CH_4 concentrations in the microcosms was by GC analysis according to the procedure of Beeman and Suflita (1987).

Sulfate Reduction Activity and Iron Sulfide Analyses

For the sulfate reduction assays, small sediment samples were obtained by pushing 5-mL syringes (with distal end cut and removed) into the cores. An anoxic solution of $^{35}SO_4$ (100 microliter (μL))(20 microCurie (μCi) mL^{-1}; carrier free; ICN) was injected into the samples with a syringe and needle. The incubations were sealed with butyl rubber stoppers and placed inside ammunition boxes under an N_2/CO_2 (80:20) atmosphere. The samples incubated for 17 hours at 18°C, the approximate *in-situ* temperature of the aquifer at the time of sampling. Sulfate reduction rates, iron monosulfides extractable with 6N HCl, and iron disulfides were then determined as described by Ulrich and others (1997).

RESULTS AND DISCUSSION

Chloride and non-volatile dissolved organic carbon (NVDOC) profiles confirm that the plume extends through the entire thickness of the alluvium and has migrated beneath the slough (figs. 2 and 3). Ground water downgradient from the landfill has high concentrations of NVDOC (fig. 3) compared to upgradient ground water collected northeast of the landfill at site NPD (fig. 1) where the average concentration is <0.2mM. The high NVDOC concentrations result from the dissolution and partial degradation of organic waste components in the landfill. The maximum concentration of NVDOC, approximately 17 mM, was measured at site 40, close to the landfill edge (fig. 1). Degradation of organic compounds in the leachate has resulted in the consumption of oxidized chemical species and the accumulation of reduced products in ground water downgradient from the landfill. The entire area sampled along the transect between the landfill and the slough is anoxic (< 5 micromolar (μM) D.O.) (fig. 4). Degradation of organic matter to inorganic carbon is evident by the increase in alkalinity (up to 7 times the background concentrations) of groundwater downgradient from the landfill (fig. 5).

High Fe^{2+} concentrations in the ground water (>0.5 mM (fig. 6)) are consistent with reductive dissolution of iron oxides or dissolution of iron waste in the landfill. Hematite grain coatings remain on all samples taken within the anoxic plume (Breit and others, 1996) but more reactive iron oxides were depleted from these sediments (Suflita and others, this volume). The persistence of hematite relative to iron oxyhydroxides suggest that the microbial reduction of hematite either does not occur or occurs at very slow rates. The large ammonium plume downgradient from the landfill (fig. 7) may result from the fermentation of organic matter in the landfill. At the boundaries of the plume, ammonium concentrations decrease sharply. Ammonium may be oxidized along the plume boundary, creating local zones, such as near the water table, where nitrate may be produced and available as an electron acceptor.

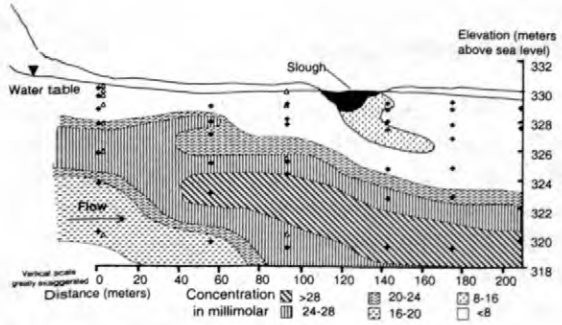

Figure 2. Distribution of chloride (Cl-) concentrations in ground water downgradient from the Norman Landfill along a transect from site 35 to 80. Diamonds are multilevel samplers, triangles are temporary wells.

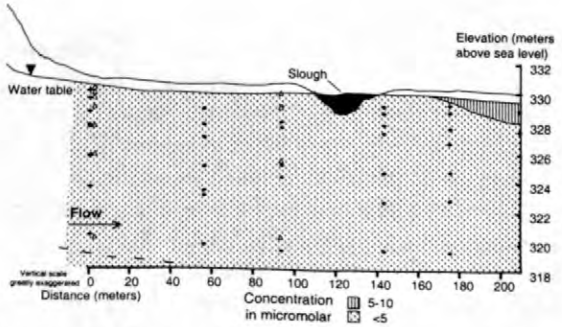

Figure 4. Distribution of dissolved oxygen (DO) concentrations in ground water downgradient from the Norman Landfill along a transect from site 35 to 80. Diamonds are multilevel samplers, triangles are temporary wells.

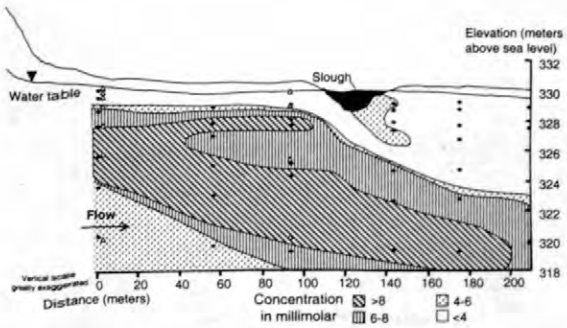

Figure 3. Distribution of non-volatile dissolved organic carbon concentrations in ground water downgradient from the Norman Landfill along a transect from site 35 to 80. Diamonds are multilevel samplers, triangles are temporary wells.

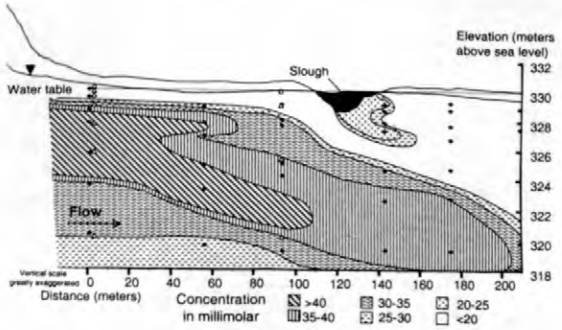

Figure 5. Distribution of alkalinity values (as bicarbonate) in ground water downgradient from the Norman Landfill along a transect from site 35 to 80. Diamonds are multilevel samplers, triangles are temporary wells.

Sulfate reduction has resulted in the depletion of sulfate from the main body of the plume (fig. 8). Analysis of the sediment cores also indicates that iron sulfides are accumulating in the aquifer within the plume (Suflita and others, this volume; Cozzarelli and others, 1997).

The oxidation of sedimentary sulfides (mainly FeS_2 and FeS) was evaluated in the laboratory. The sulfides were stable under anoxic conditions, but were oxidized rapidly when oxygen was available. The high concentrations of dissolved sulfate at the water table may result from the reoxidation of these solid sulfides or may be supplied during recharge events from the dissolution of sulfate-containing construction wastes or sulfate deposited in the unsaturated zone during dry periods. Another source of sulfate may be barite dissolution. In the sulfate-depleted zone, the ground water is undersaturated with respect to barite. Barite in the alluvial sediments dissolves, resulting in a small source of sulfate as an electron acceptor, and relatively high concentrations of barium (up to 60 μM) (Breit and others, 1996).

At the edge of the landfill, concentrations of methane are highest in the center of the anoxic plume, with the greatest methane concentrations occurring slightly beneath the top of the sulfate-depleted zone (fig. 8). The δD values for ground water downgradient from the landfill indicate that the ground water is enriched in deuterium (fig. 9). The greatest enrichment in deuterium was measured in the center of the plume, where δD values ranged from –10.6 to -3.4 per mil, compared to background values of δD of -27.9 to -45.8 per mil. Water contaminated by leachate discharging from other landfills has been observed to be enriched in deuterium (Baedecker

and Back, 1979, Hackley and others, 1996, and Clark and Fritz, 1997). Hackley and others (1996) reported 30 to 60 per mil deuterium enrichment in leachate from three landfills in Illinois, and speculated that most of the enrichment was a result of methanogenesis, with some enrichment resulting from isotopic exchange with hydrogen sulfide. Methanogenesis leads to enrichment of the deuterium content of water because bacteria preferentially use lighter isotopic species of hydrogen in water to produce methane (Clark and Fritz, 1997). The high concentrations of methane combined with the heavy δD of H_2O values right at the edge of the landfill mound indicate that methanogenesis also occurs underneath the landfill (figs. 8 and 9).

Microbial Processes

The sharp chemical concentration gradients in the ground water reflect the different microbial processes that occur in the contaminated aquifer. Concentration gradients near the landfill are steepest close to the water table. Sulfate concentrations in the leachate plume vary by more than 3 orders of magnitude downgradient from the landfill (from 0.001 mM to 5.27 mM (fig. 8)), whereas concentrations in the upgradient water vary by a factor of 2 (0.72 mM to 1.62 mM). Ferrous iron and ammonium concentrations vary by more than 2 orders of magnitude (figs. 6 and 7) in the contaminated water. The depletion of sulfate and increase in

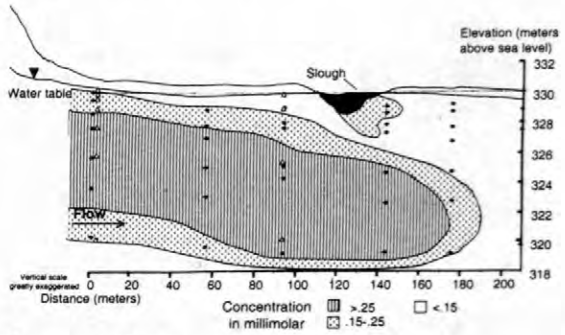

Figure 6. Distribution of ferrous iron concentrations in ground water downgradient from the Norman Landfill along a transect from site 35 to 80. Diamonds are multilevel samplers, triangles are temporary wells.

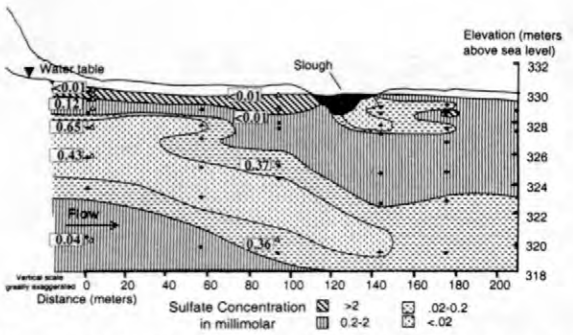

Figure 8. Distribution of sulfate concentrations in ground water downgradient from the Norman Landfill along a transect from site 35 to 80. Methane concentrations are shown on the plot as individual values at sites 35 and 38. Diamonds are multilevel wells, triangles are temporary wells.

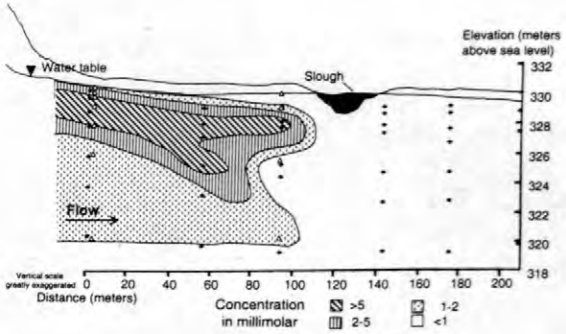

Figure 7. Distribution of ammonium concentrations in ground water downgradient from the Norman Landfill along a transect from site 35 to 80. Diamonds are multilevel samplers, triangles are temporary wells.

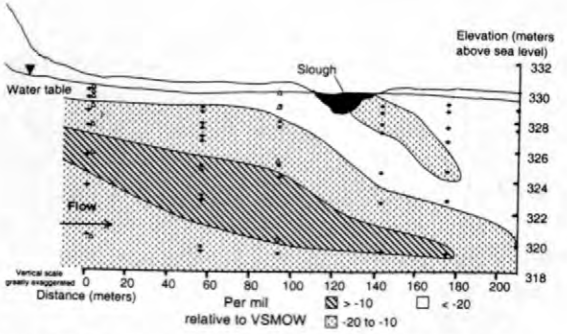

Figure 9. Distribution of delta D of H_2O values (relative to VSMOW) in ground water downgradient from the Norman Landfill along a transect from site 35 to 80. Diamonds are multilevel samplers, triangles are temporary wells.

ferrous iron and methane concentrations in the deeper water indicate that the most reduced part of the plume is within a zone 3 to 7 meters below the water table. This zone contains the highest concentrations of methane, approximately 0.65 mM (fig. 8).

The water composition data are consistent with laboratory microcosm experiments conducted with sediment collected at site 35. Microcosm results demonstrated that sulfate reduction is the dominant terminal electron-accepting process in a narrow zone just below the water table (Suflita and others, this volume; Cozzarelli and others, 1997). Sulfate reduction rates at site 35 were greatest a few centimeters below the water table where dissolved sulfate concentrations were highest (fig. 10). Dissolved H_2 concentrations measured at site 35 were in the range of 1.6-1.9 nM supporting the assumption that sulfate reduction was a dominant microbial process (Cozzarelli and others, 1997; Suflita and others, this volume). Elevated iron sulfide content of the sediment (TRIS, fig. 10), and an enrichment of isotopically heavy SO_4^{-2} in the ground water ($\delta\ ^{34}S$ of SO_4^{2-} were as heavy as 69 per mil) also suggest that significant amounts of sulfate reduction occur just below the water table.

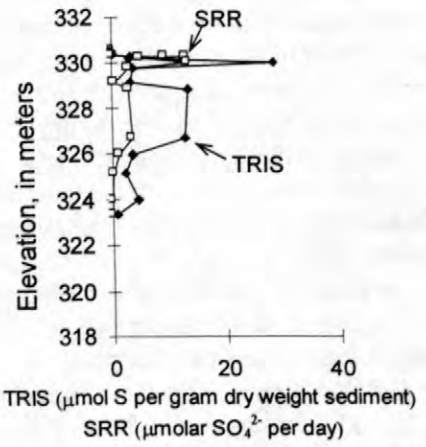

Figure 10. Sulfate reduction rates (SRR) and total reduced inorganic sulfur (TRIS) in sediment from site 35.

Below the sulfate-depleted zone, at depths greater than 7 meters below the water table, the ground water contains high concentrations of dissolved iron and sulfate. The increased concentrations are attributed to mixing of the plume with background ground water. At site 35, hydrogen concentrations are low at this depth, consistent with iron reduction as the dominant degradation reaction (Suflita and others, this volume). A small amount of iron reduction, 2 nmoles Fe^{2+}/g/day, was detected at this depth (at 324 m, fig. 11), supporting the hypothesis that iron reduction may be occurring at the boundaries of the highly reduced, sulfate-depleted plume.

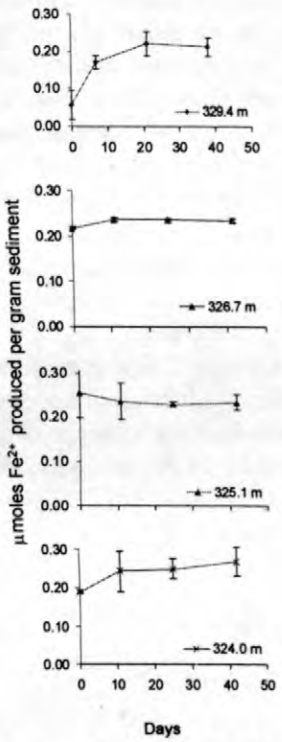

Figure 11. Iron production over time in biologically active microcosm experiment using sediments collected at four elevations from site 35.

Iron reduction was also detected near the water table at a rate of 7 nmoles Fe^{2+}/g/day (at 329.4 m, fig. 11). No iron reduction was detected in experiments designed to test abiological iron reduction. Near the water table, in the sulfate-enriched zone, oxygenated recharge water mixes with the shallow anoxic plume and iron oxyhydroxides precipitate. These iron oxyhydroxides are subsequently available for iron reduction as the water table rises. Another sample collected near the water table at 329.7 m (only a few tenths of a meter higher in the same core) showed much less iron reduction indicating that this process, and the availability of the

reducible iron oxyhydroxides, may vary over short distances near the water table.

No microbially mediated iron reduction was detected in microcosm experiments conducted with sediments from within the sulfate-depleted zone in the center of the plume (326.7 m and 325.1 m, fig. 11). The very high concentrations of Fe^{2+} in the ground water of this zone (fig. 6), coupled with the very low sulfate concentrations (fig. 8), indicates that iron reduction is an important process. However, the microcosm results indicate that it is unlikely that the dissolved Fe^{2+} is generated at this location, but rather, the source may be from reduction of iron oxyhydroxides upgradient or the dissolution of iron-containing wastes in the landfill. These data illustrate the importance of coupling geochemical and microbiological evidence when assessing active biogeochemical processes within a contaminant plume. Within the center of the plume, the stability of the remaining iron oxides, including hematite, likely limits iron reduction and may allow sulfate reduction to become energetically favorable at the expense of iron reduction, as described by Postma and Jakobsen (1996).

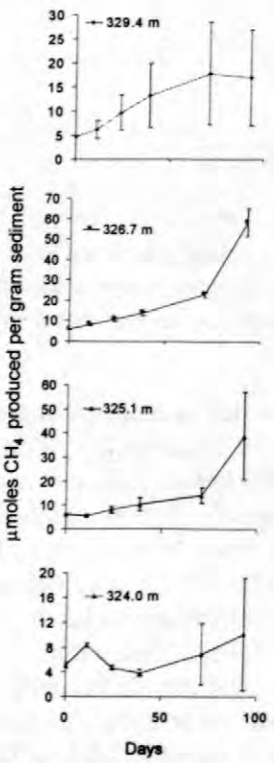

Figure 12. Methane production over time in biologically active microcosm experiment using sediments collected at four elevations from site 35.

Methane production rates measured in these same sediments showed the opposite trend from the iron reduction experiments (fig. 12). In the sediment from the center of the plume at site 35 (326.7 m and 325.1 m), the maximum methane production rate was approximately 0.5 nmoles CH_4/g/day. If these results are generalized along the transect, they support the conclusion that the core of the plume is strictly anaerobic and supports both sulfate reduction and methanogenesis. The edges of the plume appear to support iron reduction and, to a greater extent, sulfate reduction, possibly due to the increased availability of readily reactive electron acceptors at these boundaries.

CONCLUSIONS

The cycling of sulfate and iron and the formation of methane are important biogeochemical processes that affect aquifer geochemistry downgradient from the Norman, Oklahoma landfill. The non-uniform availability of electron acceptors and mixing of the contaminant plume with oxygenated water at the plume boundaries appear to have a significant impact on biogeochemical processes and result in sharp concentration gradients in the ground water. High rates of sulfate reduction near the water table appear to be controlled by the rate of supply of these electron acceptors by sulfide oxidation or dissolution of sulfate during recharge events. Although sulfate reduction and methane production occur within the anoxic core of the plume, there are high concentrations of non-volatile dissolved organic carbon transported through this zone. The availability of electron acceptors for degradation reactions is an important control on the fate of organic compounds in the plume. The geochemical and microbiological information obtained in this study will be used to understand the fate of specific organic compounds in the different redox zones. The results of this study underscore the importance of determining chemical concentration gradients along with microbiological analyses as a basis for evaluating the biogeochemical processes occurring in contaminated subsurface environments.

REFERENCES

Back, W., and Baedecker, M.J., 1989, Chemical hydrogeology in natural and contaminated environments: Journal of Hydrology, v. 106, p. 1-28.

Baedecker, M.J., and Back, W., 1979a, Hydrogeological processes and chemical reactions at a landfill: Ground Water, v. 17, no. 5, p. 429-437.

Baedecker, M.J., and Back, W., 1979b, Modern marine sediments as a natural analog to the chemically stressed environment of a landfill: Journal of Hydrology, v. 43, p. 393-414.

Baedecker, M.J. and Cozzarelli, I.M., 1992, The determination and fate of unstable constituents in contaminated ground water. *In Groundwater Quality and Analysis at Hazardous Waste Sites* (ed. S. Lesage and R. Jackson), Marcel Dekker, Inc., New York, p. 425-461.

Baedecker, M.J., Cozzarelli, I.M., Siegel, D.I., Bennett, P.C. and Eganhouse, R.P., 1993, Crude oil in a shallow sand and gravel aquifer: 3. Biogeochemical reactions and mass balance modeling in anoxic ground water: Applied Geochemistry, v. 8, p. 569-586.

Beeman, R.E., and Suflita, J.M., 1987, Microbial ecology of a shallow unconfined ground water aquifer polluted by municipal landfill leachate: Microbial Ecology, v. 14, p. 39-54.

Beeman, R.E. and Suflita, J.M., 1990, Environmental factors influencing methanogenesis in a shallow anoxic aquifer: a field and laboratory study: Journal of Industrial Microbiology, v. 5, p. 45-58.

Bekins, B.A., Cozzarelli, I.M., Godsy, E.M., Warren, E., and Tuccillo, M.E., 1998, Chemical and physical controls on shifts of microbial populations in an aquifer contaminated with crude oil: American Geophysical Union, Spring Meeting, May 26-29, 1998, EOS Transactions, v. 79, no. 17, p. S131.

Bekins, B.A., Cozzarelli, I.M., Godsy, E.M., Warren, E.M., Tuccillo, M.E., Essaid, H.I., and Paganelli, V.V., 1999, Chemical and physical controls on microbial populations in the Bemidji Toxics Site crude-oil plume, Morganwalp, D.W., and Buxton, H.T., eds., U.S. Geological Survey Toxic Substances Hydrology Program--Proceedings of the Technical Meeting, Charleston, South Carolina, March 8-12, 1999-- Volume 3 -- Subsurface Contamination from Point Sources: U.S. Geological Survey Water-Resources Investigations Report 99-4018C, this volume.

Breit, G.N., Cozzarelli, I.M., Johnson, R.D., and Norvell, J.S., 1996, Interaction of alluvial sediments and a leachate plume from a landfill near Norman, Oklahoma: Geological society of America Abstracts with Programs, v. 28, no. 7, p. A258.

Chapelle, F.H., and Lovley, D.R., 1992, Competitive exclusion of sulfate-reduction by Fe(III)-reducing bacteria: a mechanism for producing discrete zones of high-iron ground water: Ground Water, v. 30, p. 29-36.

Clark, I.D., and Fritz, Peter, 1997, Environmental isotopes in hydrogeology, Lewis Publishers, New York, 328 p.

Cozzarelli, I.M., Herman, J.S., Baedecker, M.J., and Fischer, J.M., in press, Geochemical heterogeneity of a gasoline-contaminated aquifer: Journal of Contaminant Hydrology.

Cozzarelli, I.M., Suflita, J.M., Ulrich, G., Harris, S.H., Jr., Breit, G.N., Christenson, S.C., and Norvell, J.S., 1997, Microbial processes and the availability of alternate electron acceptors in an anaerobic landfill-leachate plume: American Geophysical Union, Spring Meeting, May 27-30, 1997, EOS Transactions, v. 78, no. 17, p. S127.

Dunlap, W.J., Shew, D.C., Robertson, J.M., and Toussaint, C.R., 1976, Organic pollutants contributed to groundwater by a landfill: *in* Proceedings, Research Symposium on gas and leachate from landfills: Rutgers University Cooks College, New Brunswick, New Jersey, March 24-26, 1975, p. 96-110, U.S. Environmental Protection Agency 600/9-76-004.

Eganhouse, R.P., Cozzarelli, I.M., Scholl, M.A., and Matthews, L.L., 1998, Natural attenuation of dissolved organic compounds in the leachate plume of a municipal landfill, Norman, Oklahoma: American Geophysical Union, Spring Meeting, May 26-29, 1998, EOS Transactions, v. 79, no. 17, p. S123.

Ehrlich, G.G., Godsy, E.M., Goerlitz, D.F., and Hult, M.F., 1983, Microbial ecology of a creosote-contaminated aquifer at St. Louis park, Minnesota: Developments in Industrial Microbiology, v. 24, p. 235-245.

Gibson, S.A., and Suflita, J.M., 1986, Extrapolation of biodegradation results to groundwater aquifers: reductive dehalogenation of aromatic compounds: Applied and Environmental Microbiology, v. 52, p. 681-688.

Gleason, J.D., Friedman, I., and Hanshaw, B.B., 1969, Extraction of dissolved carbonate species from natural water for carbon-isotope analysis: U.S. Geological Survey Prof. Paper 650-D, p. D248-D250.

Hackley, K.C. Liu, C.L., and Coleman, D.D., 1996, Environmental isotope characteristics of landfill leachates and gases: Ground Water, v. 34, no. 5, p. 827-836.

Harris, S.H, Ulrich, G.A., and Suflita, J.M., 1999, Dominant terminal electron accepting processes occurring at a landfill leachate-impacted site as indicated by field and laboratory measures, in Morganwalp, D.W., and Buxton, H.T., eds., U.S. Geological Survey Toxic Substances Hydrology Program--Proceedings of the Technical Meeting, Charleston, South Carolina, March 8-12, 1999-- Volume 3 – Subsurface Contamination from Point Sources: U.S. Geological Survey Water-Resources Investigations Report 99-4018C, this volume.

Lovley, D.R., and Phillips, E.J.P., 1986, Organic matter mineralization with reduction of ferric iron in anaerobic sediments: Applied and Environmental Microbiology, v. 51, p. 683-689.

Postma, D., and Jakobsen, R., 1996, Redox zonation: equilibrium constraints on the Fe (III)/SO_4-reduction interface: Geochimica et Cosmochimica Acta, v. 60, p. 3169-3175.

Scholl, M.A., and Christenson, S.C., 1998, Spatial variation in hydraulic conductivity determined by slug tests in the Canadian River alluvium near the Norman Landfill, Norman, Oklahoma: U.S. Geological Survey Water-Resources Investigations Report 97-4292, 28 p.

Scholl, M.A., Cozzarelli, I.M., Christenson, S.C., Breit, G.N., and Schlottmann, J.L., 1999, Aquifer heterogeneity at Norman landfill and its effect on observations of biodegradation processes, Chemical and physical controls on microbial populations in the Bemidji Toxics Site crude-oil plume, Morganwalp, D.W., and Buxton, H.T., eds., U.S. Geological Survey Toxic Substances Hydrology Program--Proceedings of the Technical Meeting, Charleston, South Carolina, March 8-12, 1999-- Volume 3 -- Subsurface Contamination from Point Sources: U.S. Geological Survey Water-Resources Investigations Report 99-4018C, this volume.

Suflita, J.M., Gerba, C.P., Ham, R.K., Palmisano, A.C., Rathje, W.L. and Robinson, J.A., 1992, The worlds largest landfill—A multidisciplinary investigation: Environmental Science and Technology, v. 26, no. 8, p. 1486-1495.

Ulrich, G.A., Krumholz, L.R., and Suflita, J.M., 1997, A rapid and simple method for estimating sulfate reduction activity and quantifying inorganic sulfides: Applied and Environmental Microbiology, v. 63, p. 1627-1630.

AUTHOR INFORMATION

Isabelle M. Cozzarelli (icozzare@usgs.gov), Martha A. Scholl and Jeanne B. Jaeschke, U.S. Geological Survey, Reston, Virginia

Steve H. Harris, Glenn A. Ulrich and Joseph M. Suflita, University of Oklahoma, Dept. of Botany and Microbiology, Norman, Oklahoma

Jamie L. Schlottmann, U.S. Geological Survey, Oklahoma City, Oklahoma

Evidence for Natural Attenuation of Volatile Organic Compounds in the Leachate Plume of a Municipal Landfill near Norman, Oklahoma

By Robert P. Eganhouse, Lara L. Matthews, Isabelle M. Cozzarelli, and Martha A. Scholl

ABSTRACT

Samples of ground water collected downgradient from the Norman Landfill in 1995 and 1996 were analyzed for volatile organic compounds (VOCs) by purge-and-trap gas chromatography/mass spectrometry. More than 70 individual compounds were identified. The VOCs originate from a wide variety of natural and anthropogenic sources. This is consistent with the heterogeneous mixture of materials likely to have been buried at the site. Concentrations of VOCs are low when compared with published data for other landfills, and the dominant class (monoaromatic hydrocarbons) accounts for less than 0.1% of the total dissolved organic carbon. The low concentrations likely reflect the age of the landfill and the character of the wastes. Spatial distributions of the VOCs in ground water are variable, but concentrations of all compounds are near or below detection limits within 200 meters of the landfill. Meanwhile, the distribution of chloride ion, a putative conservative tracer, shows little dilution over the same distance. Thus, natural attentuation processes are effectively limiting migration of the VOC plume. Large differences in the spatial distribution of isomeric alkylbenzenes suggest that biodegradation is a significant, if not dominant, process contributing to the observed attenuation.

INTRODUCTION

As of 1995 there were more than 2,500 municipal landfills operating in the United States (U.S. Environmental Protection Agency, 1997). By contrast, the number of closed landfills, many of which are unlined and sited on alluvial deposits, could approach 100,000 (Suflita and others, 1992). Municipal wastes deposited on or adjacent to surface waters are subject to complex hydrologic processes that affect the transport and fate of leached contaminants.

Studies performed to date have shown that a large number of volatile organic compounds (VOCs) are typically found in ground water impacted by landfill leachate (Christensen and others, 1994). The most commonly observed VOCs include the halogenated hydrocarbons and aromatic hydrocarbons, such as BTEX (benzene, toluene, ethylbenzenes and the xylenes) and the C_3-C_5-benzenes. In some cases, extensive plumes several hundreds of meters long have developed downgradient from the source (Reinhard and others, 1984). However, some VOCs are attenuated within a short distance (Rugge and others, 1995). Compositional variations in leachate plumes have indicated that biodegradation can be an important process in the removal of certain compounds (Reinhard and others, 1984).

This paper describes initial studies of the volatile organic compounds in the main leachate plume of a municipal landfill near Norman, Oklahoma. Our objectives were: (1) to characterize the VOCs in the leachate plume and identify potential molecular tracers, (2) to determine concentrations of VOCs along a transect within the main body of the leachate plume, and (3) to evaluate processes affecting the fate of VOCs.

SITE DESCRIPTION

The study site is a closed municipal landfill located near Norman, Oklahoma adjacent to the Canadian River (fig. 1; see Christenson and others, this volume). From 1922 to 1960 solid wastes were deposited directly on the alluvium. Subsequently (1960-1972), municipal wastes were placed in trenches about 3 meters deep in association with excavation activities of a gravel company. In 1972, new state legislation required landfilling to be done 0.6 meters above the water table. This practice continued until 1985 when the landfill was closed and capped.

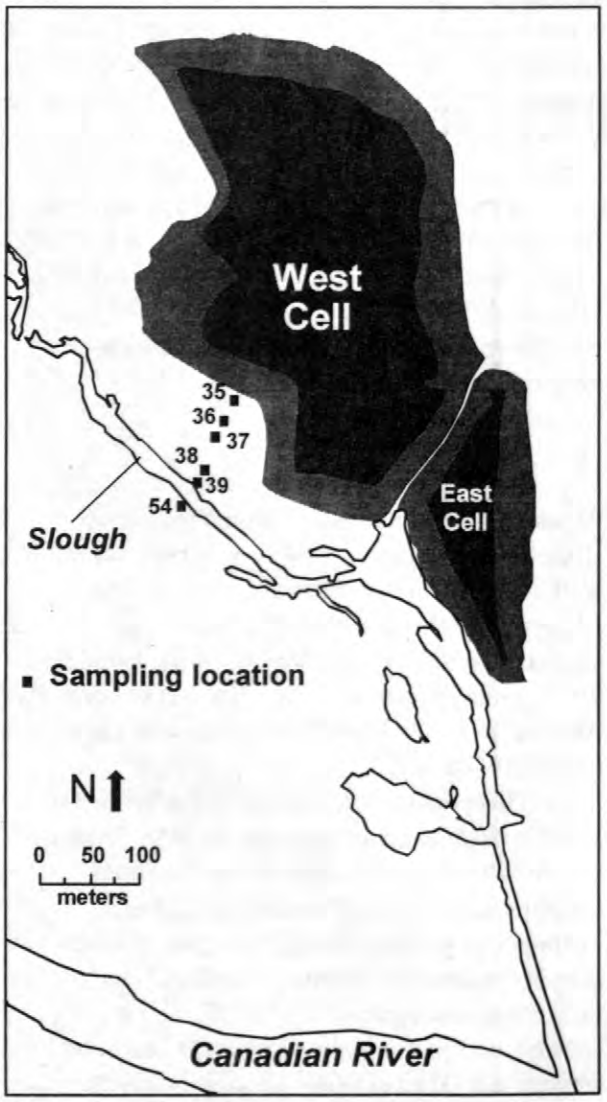

Figure 1. Map of the Norman, Oklahoma landfill showing locations where ground-water samples were collected.

The present configuration of the Norman landfill consists of two units, an east cell and a west cell. The cells rise to a maximum height of about 12-13 meters. The alluvium is 10-15 meters thick and is bounded to the southwest and northeast by terrace deposits formed by the flood plain of the river. The Canadian River is a braided stream that in 1983 was only 70 meters from the toe of the landfill. The river changed course due to a flood in 1987 and is presently 500 meters from the landfill. Underlying the alluvium is a low permeability unit (the Hennessey Group) composed of shale and mudstone. A slough located approximately 130 meters downgradient from the landfill serves as both a source and sink for materials transported in the aquifer. The slough is a remnant of the former river channel and, thus, runs parallel to the edge of the landfill. The overriding feature of the system is its heterogeneity. This heterogeneity has important consequences for the transport and fate of leachate-derived contaminants (Cozzarelli and others, this volume; Scholl and others, this volume).

Figure 2 presents a conceptual diagram of the permeability distribution in the aquifer along a transect originating at the west cell (see Scholl and others, this volume, for details). Mud-silt layers of low permeability are found at elevations of about 3-5 meters below land surface (bls). A high permeability layer, dominated by coarse sand and gravel, exists at the base of the alluvium (about 10-11 meters bls). Superimposed on the generalized permeability structure are isopleths of the non-volatile dissolved organic carbon (NVDOC) plume. The leachate plume is bifurcated by the low permeability mud-silt layer. The shallow portion of the plume appears to discharge to the slough, whereas the deeper portion extends to the base of the alluvium and is found more than 200 meters downgradient within the high permeability layer.

METHODS

Figure 1 shows locations where ground water was collected for VOC analysis during 1995-96. Samples were collected in November

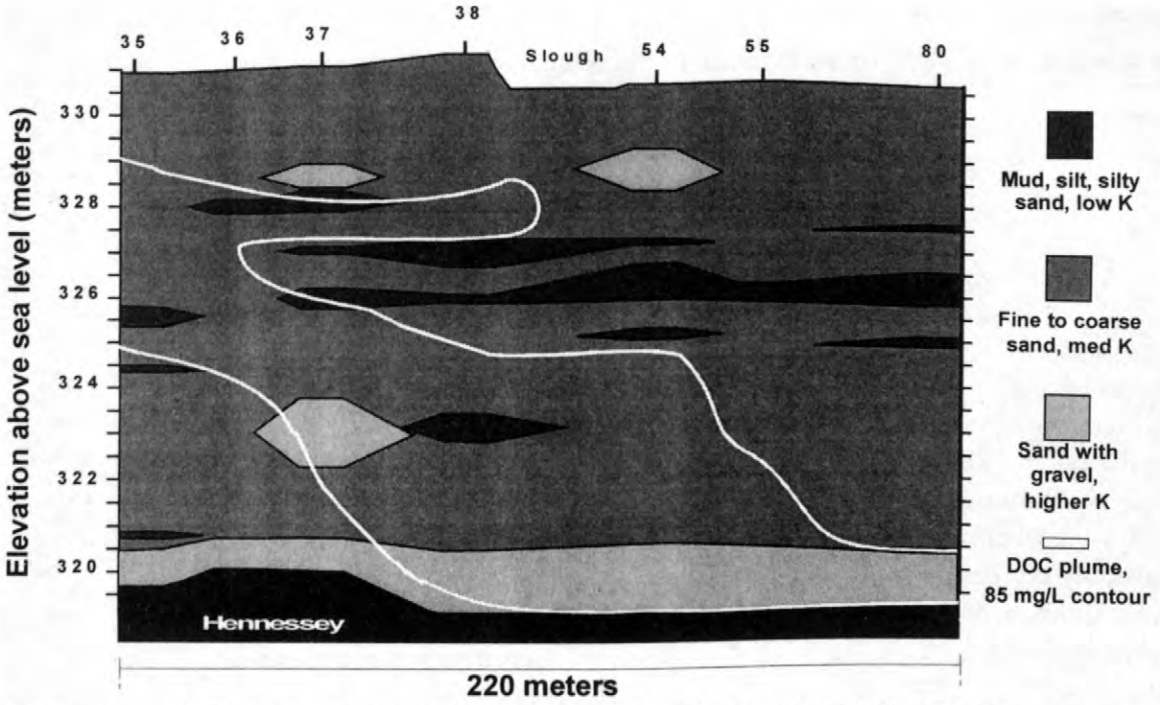

Figure 2. Generalized permeability structure in the alluvial aquifer. Sampling locations are given in figure 1. 'K' refers to hydraulic conductivity.

1995 and April 1996, using stainless steel drive point wells driven with a jackhammer. The sampling locations form a NE/SW transect that extends approximately 200 meters from the toe of the landfill in the direction of ground-water flow. Thus, it represents a path along which hydrologic and biogeochemical processes operating in the system can be examined.

After the wells were purged, samples for VOC analysis were collected by peristaltic pump/Teflon[1] tubing and transferred directly to 40 mL amber VOC vials that contained $HgCl_2$. Each sample was spiked with a recovery surrogate solution containing benzene-D_6, toluene-D_8, *o*-xylene-D_{10} and 1,3,5-trimethylbenzene-D_{12} and stored on ice until return to the laboratory. The samples were analyzed by purge-and-trap capillary gas chromatography with ion trap detection (P&T-CGC/ITD) as described by Eganhouse and others (1993). The procedure involves determination of benzene, toluene, C_{2-4}-benzenes and naphthalene by the internal standard method using a Tekmar LSC2000 P&T equipped with a Tekmar ALS2016 autosampler. The transfer line was directly connected to a fused silica capillary column (30 meter DB-5 or DB-5ms, 0.25-mm id, 0.25-m film thickness; J&W Scientific) maintained in a Varian 3500 high resolution gas chromatograph. The analytical column was interfaced to a Finnigan 800a ion trap detector *via* an uncoated length of deactivated fused silica capillary.

Just before analysis, samples were spiked with an internal standard solution containing ethylbenzene-D_{10} and 1-bromo-4-fluorobenzene. Additional quality-control procedures included continuing calibration verification and the analysis of processed laboratory blanks, field blanks, and sample duplicates. Method detection limits (MDLs) for 39 analytes ranged from 0.01 to 0.17 µg/L. Based on analysis of replicate samples, the precision of the method is estimated at $\lesssim$10% (coefficient of variation).

The concentration of non-volatile dissolved organic carbon (NVDOC) was determined as described by Baedecker and Cozzarelli (1992), and chloride ion concentrations were determined by ion chromatography.

[1] The use of brand or trade names in this paper is for identification purposes only and does not constitute endorsement by the U.S. Geological Survey.

Table 1. Compounds identified in the leachate plume of the Norman, Oklahoma landfill.

Hydrocarbons:
benzene*
toluene*
m-xylene*
p-xylene**
o-xylene*,**
ethylbenzene*
isopropylbenzene*
n-propylbenzene
1-methyl-2-ethylbenzene
1-methyl-3-ethylbenzene
1-methyl-4-ethylbenzene
1,2,3-trimethylbenzene
1,2,4-trimethylbenzene
1,3,5-trimethylbenzene
t-butylbenzene†
iso-butylbenzene
sec-butylbenzene
n-butylbenzene
1-methyl-2-propylbenzene
1-methyl-3-propylbenzene
1-methyl-4-propylbenzene†
1-methyl-2-isopropylbenzene
1-methyl-3-isopropylbenzene
1-methyl-4-isopropylbenzene
1,2-diethylbenzene
1,3-diethylbenzene
1,4-diethylbenzene
1,2-dimethyl-3-ethylbenzene
1,2-dimethyl-4-ethylbenzene
1,3-dimethyl-2-ethylbenzene
1,3-dimethyl-4-ethylbenzene
1,3-dimethyl-5-ethylbenzene†
1,4-dimethyl-2-ethylbenzene
naphthalene*
2-methylnaphthalene
1-methylnaphthalene*
α-methylstyrene
3-methylstyrene
camphene
indan
C_1-indans
C_2-indans
C_3-indans
tetralin
C_1-tetralins
C_2-tetralins

Oxygen-bearing compounds:
fenchone**,†
benzaldhehyde
1,4-cineole*
1,8-cineole
desmethylfenchone
campholine epoxide†
1-methylpropoxybenzene†
1,4-dioxane
acetone†
1,3-oxathiolane

Chlorinated hydrocarbons:
chlorobenzene*
1,2-dichlorobenzene*
1,4-dichlorobenzene*
trichloroethylene
chloroform
dichloromethane
chloromethylbenzene

* Compounds identified by the U.S. EPA (Wilson, B.H. personal communication *via* I. Cozzarelli).
** Compounds identified by Dunlap and others (1976). † Tentative identification.

RESULTS AND DISCUSSION

Identification of VOCs

Table 1 lists some of the more than 70 volatile organic compounds identified in the leachate plume samples. Many of these same compounds have been reported in other landfill studies (see references in Christensen and others, 1994) and a few have been observed previously by researchers investigating the Norman landfill leachate (Dunlap and others, 1976).

The VOCs fall into three groups: (1) hydrocarbons, (2) oxygen-bearing compounds, and (3) chlorinated hydrocarbons. The hydrocarbons are dominated by the monoaromatics (BTEX + C_{3-5}-benzenes, methylstyrenes). However, significant but variable amounts of naphthalene, substituted naphthalenes and a variety of alicyclic hydrocarbons were also found. The oxygen-bearing compounds are composed mainly of plant-derived natural products, such as fenchone, 1,4-cineole and 1,8-cineole. Several common, presumably anthropogenic, substances, such as acetone, 1,4-dioxane and benzaldehyde, were found in low abundance. The chlorinated VOCs, most of which probably arise from solvents, are few in number and occur in low abundance when compared with the other compound classes.

Table 2 summarizes some of the many possible sources of VOCs identified in the leachate plume. The most important of these are: (1) **solvents**, (2) **petroleum**/petrochemical products and processes, (3) **coal/coke** and related materials, (4) **chemicals** used as feedstock and intermediates in chemical synthesis, (5) **natural plant remains**, and (6) **resins and paints**.

Finally, we have identified several compounds that may serve as potential "leachate plume markers" (fig. 3). All of these VOCs are relatively abundant and persistent in the plume downgradient from the landfill. It is important to note, however, that the concentrations of even the most persistent VOCs are attenuated to near detection limits within 200 meters of the toe of the landfill (see below).

Table 2. Potential sources of VOCs in leachate plume.

Application → / Compound:	Solvent	Petroleum	Coal/coke	Synthetic	Pesticide	Plant Material	Inks/Dyes	Resins/Paints	Pharmaceuticals	Wood preservative	Food additive	Perfumes	Cosmetic products	Heat transfer fluid	Odor control
Bz	◆	◆	◆	◆			◆	◆							
Toluene	◆	◆	◆	◆			◆	◆							
Xylenes	◆	◆	◆	◆				◆							
EthylBz	◆	◆	◆	◆											
1,2,4-trimethylBz	◆	◆	◆	◆			◆	◆	◆						
IsopropylBz	◆	◆	◆	◆				◆							
α-methylstyrene				◆				◆							
Naphthalene		◆	◆	◆	◆		◆	◆	◆	◆					◆
Camphene				◆	◆	◆					◆	◆			
Indan		◆	◆	◆				◆							
Tetralin	◆	◆						◆							
Fenchone						◆									
Cineoles						◆			◆		◆	◆			
Benzaldehyde	◆			◆		◆	◆	◆	◆		◆	◆			
1,4-dioxane	◆						◆	◆					◆		◆
Acetone	◆			◆				◆	◆				◆		
ChloroBz	◆			◆				◆						◆	
1,2-dichloroBz	◆			◆	◆					◆				◆	◆
1,4-dichloroBz				◆	◆										◆
Trichloroethylene	◆			◆				◆						◆	
Chloroform	◆			◆	◆				◆						
Dichloromethane	◆			◆				◆						◆	
ChloromethylBz	◆			◆	◆										

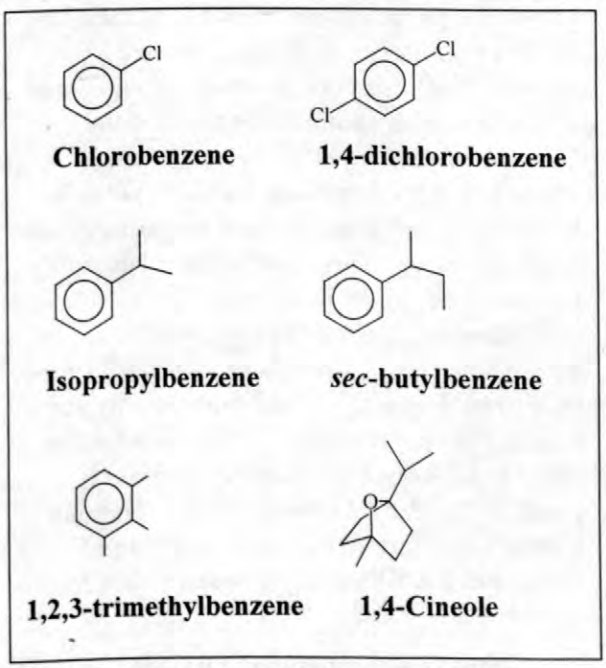

Figure 3. Potential markers of the leachate plume.

Abundance of VOCs

Table 3 lists concentration ranges for some of the compounds determined in the leachate plume samples. Also shown are

Table 3. Comparison of VOC concentrations found in Norman, Oklahoma landfill leachate plume with those reported in the literature. All concentrations are in units of μg/L.

Compound	Norman Landfill	Reported in Literature
Benzene	0-10	1-570
Toluene	0-10	1-7500
Σ xylenes	0-4	4-3500
Ethylbenzene	0-0.14	1-1100
Σ trimethylbenzenes	0-2.2	4-250
Naphthalene	0-160	0.1-260
Chloroform	0.02-0.04	1-70
1,1,1-trichloroethane	0.09	0.1-90
Vinyl chloride	0.05	---
Trichloroethylene	0.6-0.7	0.7-750
Chlorobenzene	---	0.1-110
1,4-dichlorobenzene	0.1-5.6	0.1-16

* After Christensen and others (1994). ** Σxylenes = [*o*-xylene + *p*-xylene + *m*-xylene]. *** Σtrimethylbenzenes = [1,2,3-trimethylbenzene + 1,2,4-trimethylbenzene + 1,3,5-trimethylbenzene].

ranges reported by Christensen and others (1994) for the small, but growing, literature on landfill chemistry. In all cases but one (naphthalene), the concentrations of individual and even isomer summations found at the Norman landfill are in the low μg/L range. These fall in the lower end and sometimes below the lower end of concentration ranges reported in the literature. This is not entirely surprising because some of the most elevated concentrations reported in the literature are for sites where large quantities of industrial wastes have been disposed. In addition, the literature data include results not only for ground water near landfills but also leachate samples. It is possible that the data obtained at the Norman Landfill are more representative of capped municipal landfills that have been closed for some time.

Based on quantitation of benzene + C_{1-4}-benzenes, the VOCs represent less than 0.1% of the total DOC; thus, they are not quantitatively important in fueling biogeochemical reactions in the aquifer.

The leachate plume

Figure 4 shows the distribution of chloride, a conservative tracer of the leachate plume, and NVDOC in ground water downgradient from the landfill. The core of the

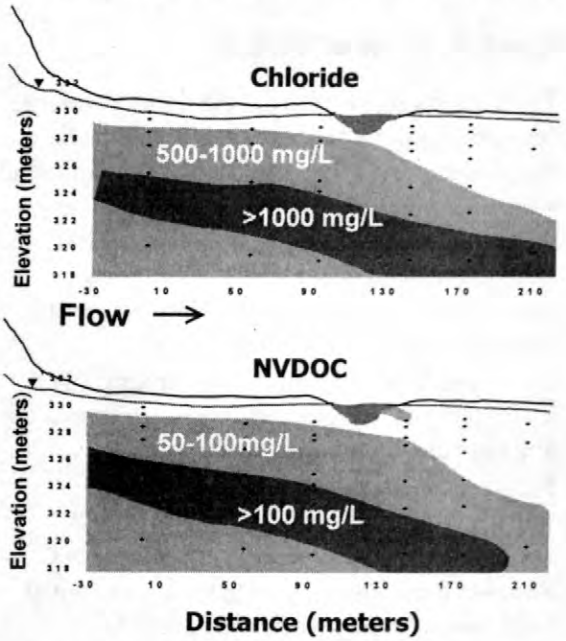

Figure 4. Distribution of chloride ion and NVDOC in leachate plume downgradient from the Norman, Oklahoma landfill. See figure 1 for locations of wells on sampling transect.

leachate plume descends with increasing distance downgradient from the landfill, reaching the base of the aquifer at a distance of 130 meters. This pattern results from dilution by recharge and discharge from the slough and the presence of the low permeability clay layers found a few meters below the land surface (see fig. 2). The NVDOC plot shows a similar pattern. Highest concentrations are present within an envelope that descends with increasing distance downgradient from the landfill. Again, the plume reaches the base of the alluvium at a distance of approximately 130 meters. Along this transect, the deeper portion of the plume extends more than 200 meters downgradient from the landfill and contains NVDOC at concentrations exceeding 150 mg/L. This compares with background concentrations of NVDOC in native ground water in the range of 2-3 mg/L. These patterns are in contrast to the observed behavior of most of the VOCs as shown in figure 5.

In the upper panel of this figure the distribution of 1,2,3,4-tetramethylbenzene

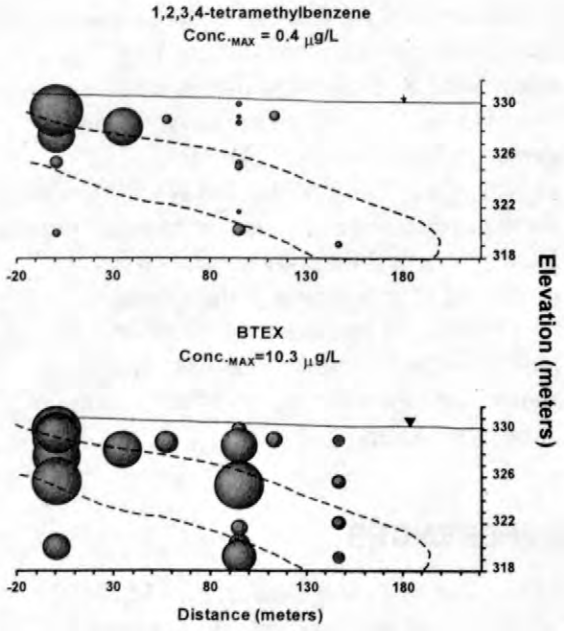

Figure 5. Distribution of 1,2,3,4-tetramethylbenzene and BTEX in leachate plume downgradient from Norman landfill. Dotted line is NVDOC plume (> 100 mg/L).

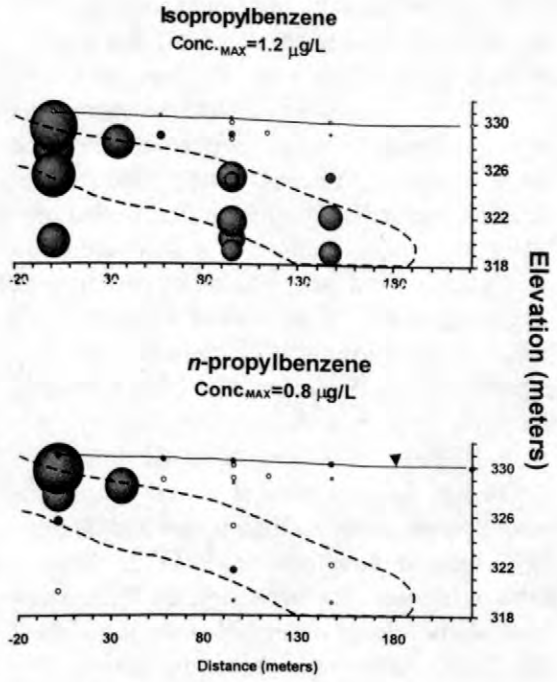

Figure 6. Distribution of isomeric C_3-benzenes in leachate plume downgradient from the Norman landfill.

(1,2,3,4-TMB) is represented in the form of a bubble plot. The area of the largest bubble corresponds to the maximum concentration. All other bubbles are scaled proportionately by concentration. Also shown for reference is the outline of the NVDOC plume (>100 mg/L). The pattern seen here is typical of many of the VOCs. Concentrations decrease rapidly with increasing distance from the landfill falling below detection limits within a distance of 200 meters. Although we presently do not have data on the temporal variability of 1,2,3,4-TMB concentrations in the leachate, it is reasonable to assume that the source term for this compound has not increased over time. Given that chloride and NVDOC concentrations show no significant change along this flow path, it can be assumed that 1,2,3,4-TMB and other VOCs are being attenuated. Thus, natural processes are limiting migration of the VOCs in this aquifer.

It is of interest to examine the distribution of BTEX because of the importance of these compounds in ground-water contamination studies. In general, concentrations of BTEX decline with distance within the main portion of the leachate plume (as defined by [Cl^-] and [NVDOC] in figure 4). However, high concentrations are found at some locations outside of the main body of the plume, and low concentrations are found within it. These apparent deviations occur because BTEX is a summation of the concentrations of six individual compounds and because of the heterogeneous nature of the aquifer. Some BTEX constituents are persistent (*e.g.* benzene, ethylbenzene), whereas others are not (toluene). Similar differences have been observed by Wilson and others (1986) who used methanogenic aquifer material from the Norman landfill in microcosm studies.

In figure 6 the distributions of two C_3-benzene isomers (*n*-propylbenzene and isopropylbenzene) are plotted. Also shown is the approximate boundary of the NVDOC plume (≥ 100 mg/L). The physical properties of these isomeric alkylbenzenes are similar (aqueous solubility = 52 and 50 mg/L, respectively; Henry's law constant = 1.0×10^3 and 1.5×10^3 Pa-m^3/mol; log K_{OW} = 3.7 and 3.6; Mackay and others, 1992), and the compounds are found at comparable maximum concentrations in ground water near the toe of the landfill (1.2 *vs.* 0.8

µg/L). Consequently, physical processes (dilution, volatilization, sorption) that could result in attenuation would be expected to affect these two compounds to nearly the same extent. Isopropylbenzene, which appears to be one of the best potential tracers of the plume at this location, has a distribution similar to that of NVDOC. Concentrations of *n*-propylbenzene, on the other hand, are reduced by two orders of magnitude within 60 meters of the landfill. This indicates that biological degradation is a significant, if not dominant process, affecting the fate of VOCs in this aquifer.

Differences in persistence of isomeric alkylbenzenes have been observed in previous ground-water studies (Eganhouse and others, 1996; Reinhard and others, 1984). In the case of these particular alkylbenzenes, the difference is most likely related to the structure of the alkyl side chain. Branching, especially terminal branching, tends to enhance resistance to biodegradation (Boethling, 1993). Thus, all things being equal, isopropylbenzene is expected to be more persistent than *n*-propylbenzene.

SUMMARY

Ground water in the surficial aquifer downgradient from the Norman Landfill is contaminated with volatile organic compounds. The spatial distribution of VOCs in the leachate plume is determined by a complex interplay of hydrologic and biogeochemical factors. Based on observations to date, the most important of these factors appear to be: (1) recharge to the shallow water table, (2) interactions with the slough, and (3) spatial heterogeneity of the aquifer. Preliminary results indicate that the monoaromatic hydrocarbons are the most abundant class of VOCs at this site. The sources of VOCs are diverse, reflecting the wide range of anthropogenic and natural materials that have historically been disposed at this site. Concentrations of all compounds identified to date appear to be in the low µg/L range and are among the lowest that have been reported in the literature. This is probably due to the age of the landfill, the presence of the cap and the fact that it was not used for disposal of large quantities of industrial solvents. Many of the VOCs are attentuated within a short distance downgradient from the landfill, and all are below or near detection limits within 200 meters. The persistence of chloride ion and NVDOC within the same distance suggests that extension of the VOC plume is limited by natural removal processes. Comparison of the spatial distributions of two isomeric alkylbenzenes indicates that biological degradation plays a significant role in the observed attenuation of these compounds.

REFERENCES

Baedecker, M.J., and Cozzarelli, I.M., 1992, The determination and fate of unstable constituents in contaminated ground water, Lesage, S. and Jackson, R., eds., Groundwater Quality and Analysis at Hazardous Waste Sites: New York, Marcel Dekker, p. 425-461.

Boethling, R.S., 1993, Biodegradation of xenobiotic chemicals, Handbook of Hazardous Materials, New York, Academic Press, p. 55-67.

Christensen, T.H., Kjeldsen, P., Albrechtsen, H-J., Heron, G., Nielsen, P.H., Bjerg, P.L., and Holm, P.E., 1994, Attenuation of landfill leachate pollutants in aquifers: Critical Reviews in Environmental Science and Technology, v. 24(2), p. 119-202.

Christenson, S., Scholl, M.A., Schlottmann, J.L., and Becker, C.J., 1999, Ground-water and surface-water hydrology of the Norman Landfill research site, Morganwalp, D.W., and Buxton, H.T., eds., U.S. Geological Survey Toxic Substances Hydrology Program--Proceedings of the Technical Meeting, Charleston, South Carolina, March 8-12, 1999--Volume 3--Subsurface Contamination from Point Sources: U.S. Geological Survey Water-Resources Investigations Report 99-4018C, this volume.

Cozzarelli, I.M., Suflita, J.M., Ulrich, G., Harris, S.H., Scholl, M.A. Norvell, J.S., and Jaeschke, J.B., 1999, Biogeochemical

processes in a contaminant plume downgradient from a landfill, Norman, Oklahoma, Morganwalp, D.W., and Buxton, H.T., eds., U.S. Geological Survey Toxic Substances Hydrology Program--Proceedings of the Technical Meeting, Charleston, South Carolina, March 8-12, 1999--Volume 3--Subsurface Contamination from Point Sources: U.S. Geological Survey Water-Resources Investigations Report 99-4018C, this volume.

Dunlap, W.J., Shew, D.C., Scalf, M.R., Cosby, R.L., and Robertson, J.M., 1976, Isolation and identification of organic contaminants in ground water, Keith, L.H., ed., Identification & Analysis of Organic Pollutants in Water, Ann Arbor, Ann Arbor Science, p. 453-477.

Eganhouse, R.P., Dorsey, T.F., Phinney, C.S., and Westcott, A.M., 1996, Processes affecting the fate of monoaromatic hydrocarbons in an aquifer contaminated by crude oil: Environmental Science and Technology, v. 30, p. 3304-3312.

Eganhouse, R.P., Dorsey, T.F., Phinney, C.S., and Westcott, A.M., 1993, Determination of C_6-C_{10} aromatic hydrocarbons in water by purge-and-trap capillary gas chromatography: Journal of Chromatography, v. 628, p. 81-92.

Mackay, D., Shiu, W.Y., and Ma, K.C., 1992, Illustrated Handbook of Physical-Chemical Properties and Environmental Fate for Organic Chemicals, Vol. 1: Monoaromatic Hydrocarbons, Chlorobenzenes, and PCBs, Boca Raton, FL, Lewis Publishers, 697p.

Reinhard, M., Goodman, N.L., and Barker, J.F., 1984, Occurrence and distribution of organic chemicals in two landfill leachate plumes: Environmental Science and Technology, v. 18, p. 954-961.

Rugge, K., Bjerg, PL., and Christensen, T.H., 1995, Distribution of organic compounds from municipal solid waste in the groundwater downgradient of a landfill (Grindsted, Denmark): Environmental Science and Technology, v. 29, p. 1395-1400.

Scholl, M.A., Cozzarelli, I.M., Christenson, S.C., Breit, G.N., and Schlottmann, J.L., 1999, Aquifer heterogeneity at Norman landfill and its effect on observations of biodegradation processes, Morganwalp, D.W., and Buxton, H.T., eds., U.S. Geological Survey Toxic Substances Hydrology Program--Proceedings of the Technical Meeting, Charleston, South Carolina, March 8-12, 1999--Volume 3--Subsurface Contamination from Point Sources: U.S. Geological Survey Water-Resources Investigations Report 99-4018C, this volume.

Suflita, J.M., Gerba, C.P., Ham, R.K., Palmisano, A.C., and Robinson, J.A., 1992, The Worlds's largest landfill: Environmental Science and Technology, v. 26, p. 1486-1495.

U.S. Environmental Protection Agency (1997) Characterization of municipal solid waste in the United States 1996 Update, Report No. EPA530-R-97-015, June 1997, 169p.

Wilson, B.H., Smith, G.B., and Rees, J.F., 1986, Biotransformations of selected alkylbezenes and halogenated aliphatic hydrocarbons in methanogenic aquifer material: A microcosm study: Environmental Science and Technology, v. 20, p. 997-1002.

AUTHOR INFORMATION

Robert P. Eganhouse, Lara L. Matthews, Isabelle M. Cozzarelli, Martha A. Scholl, U.S. Geological Survey, Reston, Virginia

Dominant Terminal Electron Accepting Processes Occurring at a Landfill Leachate-Impacted Site as Indicated by Field and Laboratory Measures

By Steve H. Harris, Glenn A. Ulrich, and Joseph M. Suflita

ABSTRACT

We used soluble and solid phase geochemical profiles as well as microbiological rate experiments to evaluate the dominant terminal electron accepting processes occurring in an aquifer polluted by leachate from the closed municipal landfill in Norman, OK. Sulfate reduction and methanogenesis were identified as dominant processes influencing the biodegradation of aquifer contaminants. Interestingly, both of these processes were governed, at least in part, by the ambient concentration of sulfate. Consequently, the supply of sulfate in the aquifer was a major determinant governing the biodegradation of contaminant materials. We were able to determine that the supply of this electron acceptor was a function of several processes including the oxidation of iron sulfides near the water table, the advective flux of sulfate from background subsurface locations, and the dissolution of barite minerals.

INTRODUCTION

Understanding the transport and fate characteristics of contaminant materials requires an accurate description of the dominant microbially catalyzed electron accepting processes occurring in an environment. This is because contaminant biodegradation pathways, and the attendant risk associated with the presence of the pollutants, is not identical under all electron accepting regimes. A variety of approaches have been used for such assessments. Examination of groundwater geochemistry is often the method of choice to describe electron accepting processes in the terrestrial subsurface due to its relative ease. However, it is well known that many redox sensitive species can migrate in aquifers and reflect past geochemical events rather than the immediate location under investigation. Further, precipitation or immobilization reactions of other geochemical species can easily confound interpretations based on groundwater measurements alone. Clearly, the analysis of groundwater geochemistry is an essential part of evaluating the dominant electron accepting conditions in an environment, but such information is most useful when it is bolstered by multiple lines of evidence on both the solid and liquid phases of an aquifer.

The Utility of Dissolved H_2 Measurements

One of the promising indicators of microbially catalyzed terminal electron accepting processes in the subsurface is the interpretation of the steady state concentration of dissolved H_2 (Lovely and Goodwin, 1988). This method is based on the observation that complex microbial communities both produce and consume H_2, eventually to a low steady state value that

correlates with the nature of the electron acceptor being primarily utilized in the system under investigation. Lower steady state H_2 concentrations are manifest when more thermodynamically favorable electron acceptors are available and in use by the resident microflora.

We evaluated how well the published theory predicted the steady state level of dissolved H_2 in leachate-impacted aquifer slurries that were experimentally amended with different electron acceptors (Figure 1).

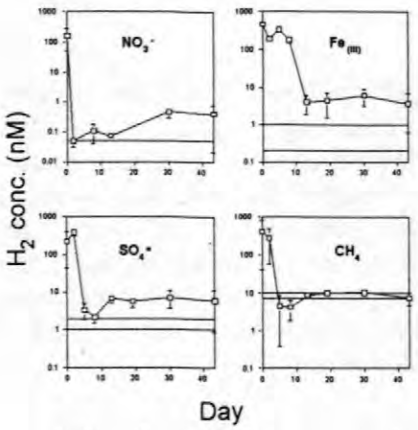

Figure 1. Steady state H_2 concentration as a function of different terminal electron accepting conditions in aquifer slurries. Dashed lines reflect the predicted hydrogen level based on Lovely and Goodwin, 1988 .

We found that the steady state H_2 values in nitrate reducing and methanogenic incubations were largely consistent with current theory, but incubations amended with sulfate or amorphous iron oxyhydroxides resulted in H_2 concentrations that were essentially indistinguishable. We then compared our laboratory findings with measurements of dissolved H_2 in the field. The latter determinations suggested that sulfate reduction (1-3 nM) occurred in the upper part of the aquifer and that iron reduction (0.1-0.5 nM) was more important with increasing depth (Figure 2). The former contention could be supported in sulfate reduction assays conducted with sediments obtained from an area immediately adjacent to the monitoring well where the H_2 determinations were made. We found that sulfate reduction was indeed positive in the upper regions of the aquifer, but this activity clearly diminished with increasing depth

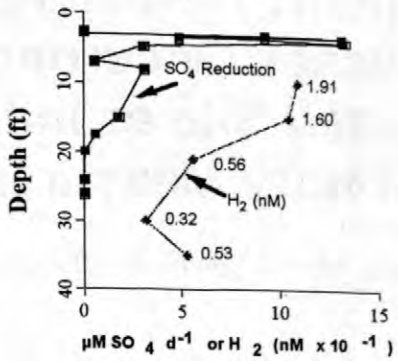

Figure 2. Relationship between sulfate reduction and the steady state concentration of dissolved H_2 in the aquifer

in the aquifer. However, the prospect of iron reduction proved much more difficult to verify. Despite repeated attempts to measure ferric iron reduction in deeper sediments from this aquifer, we consistently found that this bioconversion was below the limit of our detection. Various reasons for this finding can be offered (see below). However, we are forced to conclude that there are interpretational constraints to the information one can deduce using the steady state dissolved H_2 concentration as a measure of the dominant terminal electron accepting process in aquifers. The approach appears to be a useful tool for characterizing some anaerobic processes, but interpretational difficulties may be attendant when lower H_2 values (< 1 nM) are encountered. Comparable limitations associated with dissolved H_2 determinations have also been encountered by others (Smith, 1997, Chapelle et al, 1996).

Dissolved Geochemistry

As pointed out above, the mere detection of various geochemical species must be interpreted with a great deal of caution. However, geochemical investigations are often the obvious starting points for helping determine the dominant terminal electron accepting process. In this aquifer, dissolved oxygen concentrations were generally very low (<0.3 ppm) while nitrate was always below the limit of detection (~ 1 µM). In contrast, methane, sulfate, and ferrous iron could be found at most locations (Cozzarrelli et al, 1999). However, the sulfate concentration was generally low (< 10 µM), with the exception of the values measured at or near the water table

(see below). Such findings suggest that methanogenesis or ferric iron reduction could be important in portions of the aquifer. Of course, the concentration of a potential reactant or product alone does not argue forcefully for the importance of that chemical species to the functioning of the resident microbial community. Independent evidence on the rate of microbial processing of such materials is paramount for making such determinations.

Microbial Activity Measurements

One of the most interpretationally direct methods to determine the dominant electron accepting process in an environment is to measure the rate of that process in samples obtained from the location of interest. Such determinations are difficult to conduct in the field, but relatively straightforward in laboratory incubations. The resulting information can then be considered with other geochemical indicators that are obtained both in the field and on representative samples. We specifically evaluated the importance of iron and sulfate reduction in addition to methanogenesis in slurries of sediment and groundwater obtained from the landfill leachate-impacted aquifer and the salient results are presented below.

Iron Reduction

Dissolved H_2 values (~0.5 nM) near the base of the landfill suggested that iron reduction was an important process in deeper portions of the aquifer. This contention was also supported by the detection of relatively high concentrations of soluble $iron_{(II)}$ (Cozzarelli et al, 1999) in most groundwater samples. Of course, as a mobile species, there is no reason to assume that the ferrous iron detected in the groundwater actually originated where it was found. In consistent fashion, our attempts at the direct assay of iron reduction by monitoring the formation of $iron_{(II)}$ as a function of time were negative, with the exception of a single sample from a shallow interval. Of course, it may be that the sensitivity of our assay was limited by the relatively high levels of endogenous ferrous iron. Therefore, we conducted a detailed vertical profile in an effort to measure the "bioavailable" $iron_{(III)}$ that might be accessible to the resident microflora. However, we could garner no evidence for any bioavailable iron in any of the samples that were obtained. While $iron_{(III)}$ is likely common in the aquifer, it apparently occurs mainly as highly crystalline forms which tend to be less readily bioavailable. Consequently, the prospect of iron reduction as an important microbially catalyzed electron accepting process could not be confirmed in the aquifer.

Sulfate Reduction

As mentioned above, sulfate reduction rates were determined in aquifer samples and the rates were found to be greater in the relatively shallow intervals (Figure 2). This result confirmed the suggestion that attended the dissolved H_2 determinations. That is, dissolved H_2 values of ~2nM are consistent with the suggestion that sulfate reduction is a major electron accepting process. However, periodic monitoring revealed that the steady state H_2 values at this location did vary temporally and dropped to subnanomolar concentrations at various times of the year. Nevertheless, sulfate reduction was always easily demonstrated in samples retrieved from the aquifer and assayed in the laboratory.

Methanogenesis

High concentrations of dissolved methane were found in the center of the leachate plume but not in the shallow and deep portions of the aquifer (Cozzarelli et al, 1999). This area of elevated methane corresponds to a zone of relatively low sulfate concentration suggesting that this electron acceptor helps modulate methanogenesis. Indeed, this is consistent with previous findings (Beeman and Suflita, 1987). In consistent fashion, most probable number enumeration assays revealed relatively high numbers of methanogenic bacteria in this region relative to the bottom of the aquifer where these organisms were below detection limits (Figure 3).

Acetate-utilizing

Depth (m)	Methanogens	Sulfate Reducers
0.6	BDL	93
1.5	4.3×10^3	2.3×10^3
4.0	4.6×10^3	4.6×10^3
5.5	BDL	4.2×10^1
6.4	9.3×10^1	9.3×10^2
8.8	BDL	4.6×10^3
10.4	BDL	ND
Background	BDL	4.3×10^1

Hydrogen-utilizing

Depth (m)	Methanogens	Sulfate Reducers
0.6	BDL	2.3×10^3
1.5	1.0×10^4	2.3×10^3
4.0	1.1×10^4	4.6×10^4
5.5	9.3×10^1	BDL
6.4	2.3×10^2	4.6×10^3
8.8	BDL	1.0×10^4
10.4	BDL	1.0×10^4
Background	BDL	42.7

ND=not determined; BDL = Below Detection Limit

Figure 3. Distribution of acetate and hydrogen-metabolizing anaerobic bacteria as a function of depth

To test the importance of methanogenesis and sulfate reduction as major terminal electron accepting processes in this aquifer, we incubated intact core sections with ^{14}C-acetate, ^{14}C-bicarbonate or ^{35}S-sulfate and followed the fate of the radioactivity (Figure 4).

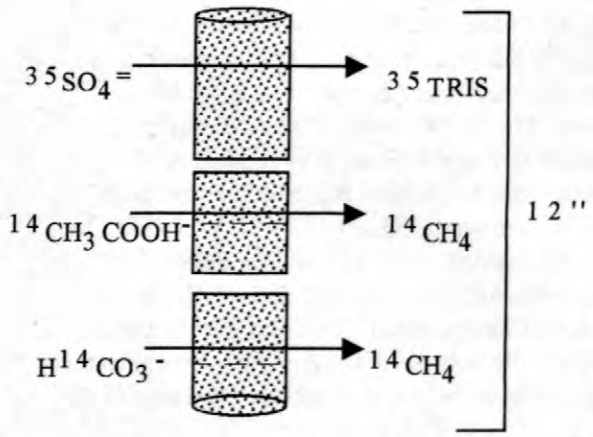

Figure 4. Radioisotopes for tracing sulfate reduction and methanogenesis in sediment cores.

The assays were designed to detect reduced sulides (TRIS) when labeled sulfate was used as a tracer and labeled methane with acetate or bicarbonate were added to the core. When cores received ^{14}C-bicarbonate, we failed to detect radiolabeled methane production (Figure 5).

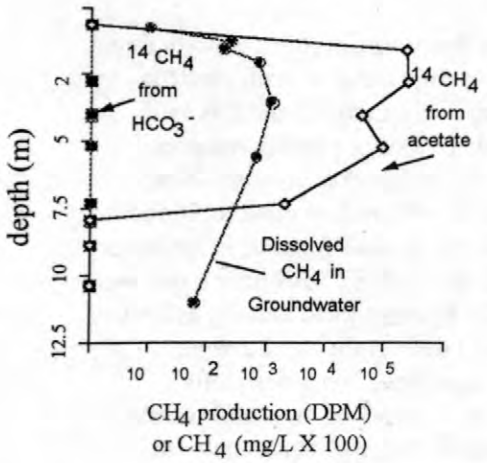

Figure 5. Depth profile of autotrophic and acetoclastic methanogenesis relative to groundwater methane.

Thus, we could not obtain evidence for autotrophic methanogenesis. In contrast, when ^{14}C-acetate was employed as a substrate, $^{14}CH_4$ resulting from acetoclastic methanogenesis was easily detected. In fact, this activity was coincident with the zone of high dissolved methane measured in the aquifer and suggested that acetate cleavage was the likely source of methane production in the aquifer.

However, the amount of radioactivity recovered as $^{14}CH_4$ did not quantitatively account for the amount of radiolabel added to the core. In fact, most of the radioactivity was recovered as $^{14}CO_2$ (data not shown), indicating that acetate oxidation was possibly coupled with the reduction of sulfate, as the latter was detected in all core samples. While it is possible that aquifer methanogens utilize other C_1 carbon sources to support their metabolism, it is probably far more

likely that a slow rate of acetoclastic methanogenesis occurs in the center of the plume and is responsible for the relatively high methane concentrations measured at those locations.

The Influence of Clay and Sulfate on Microbial Activities

We further investigated the variables that influenced sulfate reduction and methanogenesis in the aquifer. The basic procedures outlined in Figure 4 were employed to visualize where sulfate reduction occurred in cores and to quantify activity by measuring the amount of total reduced inorganic sulfides (TRIS) (Krumholz et al, 1997). A procedure that employed silver foils as sulfide traps was also used to visualize and detect sulfate reduction in near continuous core sections taken from various portions of the aqufier (Figure 6).

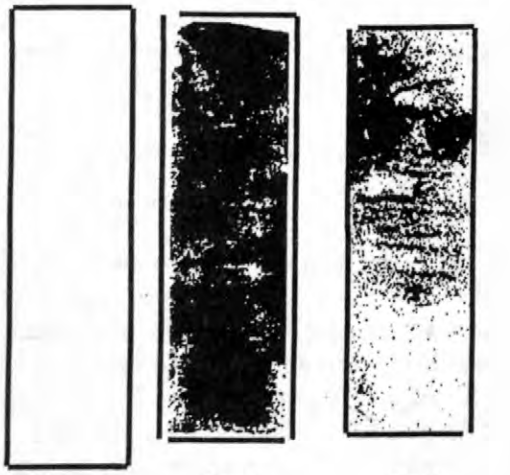

Figure 6. Autoradiograms depicting area of sulfate reduction activity in core sections from a leachate–impacted aquifer in Norman, OK: left, 4.04-4.25m; center, 5.18-5.35m; right, 5.35-5.51m (depths refer to below land surface).

In this assay, areas of sulfate reduction are visualized as radioactive spots (dark areas in Fig. 6) on the autoradiograms of the silver foils. This analysis revealed that medium-grained sands, which comprise most of the aquifer, exhibit a relatively uniform distribution of sulfate reducing activity (Figure 6, center and right). At a 0.6 m thick clay interval located about 4 m below the land surface, sulfate reduction activity was greatly diminished (Fig. 6, left). Consequently, we hypothesized that clay could inhibit sulfate reduction in the aquifer and subsequent experiments using clay as a variable supported this contention (data not shown). While the mechanism of this inhibition is not clear, the presence of clay certainly seems to be a detriment to sulfate reduction in this aquifer.

By monitoring the rate of sulfate reduction in depth profiles and comparing the results to the amount of sulfate in the pore water, we noted that the values were often correlated. This led to the hypothesis that the concentration of sulfate helped govern the amount of sulfate reduction in the aquifer. We tested this hypothesis by experimentally manipulating the concentration of sulfate in aquifer slurries and monitoring the rate of sulfate reduction (Figure 7).

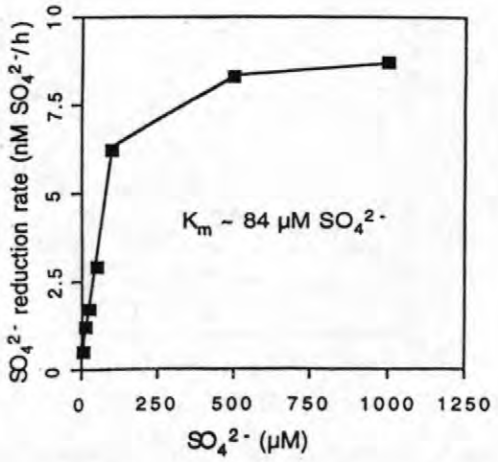

Figure 7. Sulfate reduction rate in aquifer slurries as a function of sulfate concentration

We observed Michalis-Menten saturation kinetics with an apparent Km of approximately 80 µM. It is interesting to note that the ambient concentrations of sulfate in most regions of the aquifer were generally below this apparent Km value. Thus, the concentration of sulfate was likely a major variable controlling the amount of sulfate reduction in the aquifer.

As stated above, the amount of sulfate also impacts methanogenesis in the aquifer; the latter being most evident in aquifer locations where sulfate is nearly depleted. Given the importance of sulfate as a major environmental

variable controlling the biodegradation of contaminants, a consideration of the sources of this anion are particularly germane for predicting the transport and fate of materials in the aquifer.

Sources of Sulfate

We have been able to identify at least three sources of sulfate to the aquifer (Ulrich et al, 1999). Experiments have shown that hydrogen sulfide, produced as an endproduct of sulfate reduction, precipitates rapidly as iron sulfide minerals in the aquifer (data not shown). Such minerals are rather stable and not easily oxidized under anaerobic conditions (Figure 8).

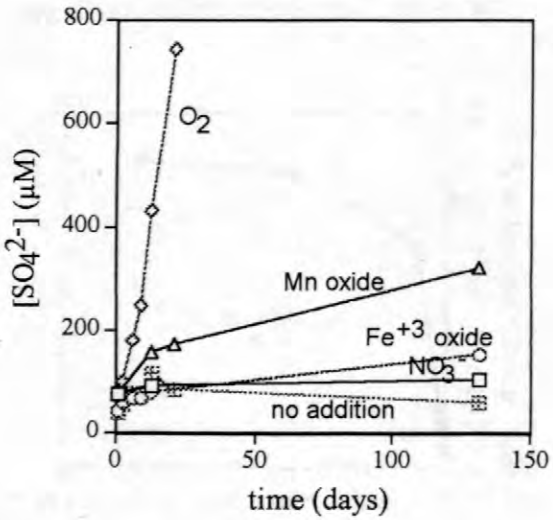

Figure 8. Iron sulfide oxidation in aquifer slurries in response to various potential electron acceptors

In the presence of a variety of potential electron acceptors, little sulfate formation was evident in these experiments except when manganese oxide was present. To our knowledge, significant manganese sources are not present in this aquifer. However, when aerobic conditions prevail, reduced sulfides can be readily reoxidized and sulfate is observed to accumulate.

In situ evidence for this process was found at the water table, where despite relatively high rates of sulfate reduction, the concentration of iron sulfides were comparatively low. We typically observed larger quantities of sulfides with increased depth and decreased levels of sulfate and sulfate reduction. Further, sulfate concentrations were highest just above and below the water table and decreased rapidly with depth. These observations suggest that the oxidation of iron sulfides occurs at the water table where periodic inputs of oxygen allow sulfate regeneration and restoration to the aquifer.

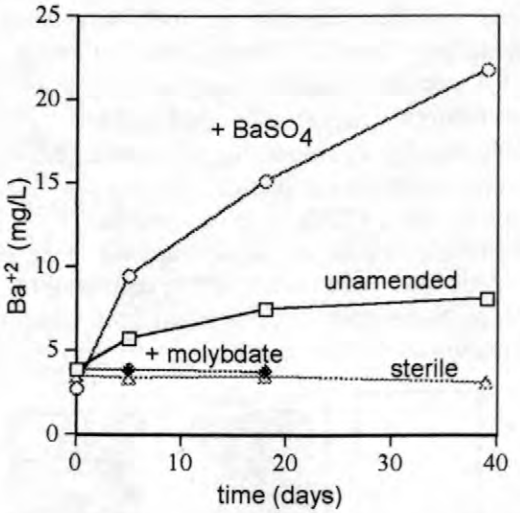

Figure 9. Ba+2 production in aquifer slurries

Another important source of sulfate in the aquifer is through advective flux occurring just above the confining layer at the bottom of the aquifer. Hydraulic conductivity is relatively high (Scholl and Christenson, 1998) in this region allowing sulfate-laden uncontaminated groundwater to mix with the sinking leachate plume. Were this the case, one might expect to find increased rates of sulfate reduction. In fact, increased rates of sulfate reduction could be measured at locations near the bottom of the aquifer where the sulfate concentration was higher.

Finally, we investigated the possibility of barite ($BaSO_4$) dissolution as an additional sulfate source based on some careful observations of the presence of this mineral by our colleague, Dr. George Breit. Under conditions of low sulfate (<10µM), as in most aquifer locations, barite will dissolve resulting in a sulfate resupply mechanism and the production of soluble barium. Barium concentrations were higher in contaminated groundwater where sulfate was depleted suggesting that active sulfate reduction

within the plume decreased sulfate to levels that allowed barite dissolution. Laboratory incubations of unamended and barite-amended landfill slurries accumulated barium as the result of sulfate consumption to low levels (~1μM) (Figure 9).

Barium did not accumulate in sterile controls or in live bottles that contained 5mM molybdate as an inhibitor of sulfate reduction. These data suggest that the activity of sulfate-reducing bacteria diminishes the *in situ* sulfate concentration to levels that favor barite dissolution, and a resupply of a low level of sulfate to the aquifer.

Conclusions

Our findings illustrate the utility of combining geochemical and microbiological investigations to clarify the important microbial processes responsible for the destruction of aquifer contaminants. In some instances, the implications based on groundwater chemistry were consistent with microbiological indicators of the dominant terminal electron accepting processes occurring in the aquifer. However, high concentrations of methane and reduced iron in groundwater did not always parallel high rates of methanogenesis and iron reduction, respectively. In a similar manner, no dissolved sulfide and very little sulfate were ever measured in groundwater despite the biogeochemical importance of sulfate reduction. Sulfate reduction and methanogenesis are now identified as the dominant microbially catalyzed redox reactions in this leachate-impacted aquifer. Iron reduction, while implicated by the low levels of steady state hydrogen concentration, could not be confirmed with other assays. Our findings suggest that the level of sulfate in the aquifer is a dominant factor modulating the destruction of contaminants linked to both sulfate reduction and methanogenesis. In addition, several resupply mechanisms serve to buffer the sulfate status in this environment. These include the oxidation of reduced sulfides with oxygen at the water table, the advective flux of sulfate from background waters, and the dissolution of sulfate containing barite minerals.

REFERENCES

Beeman, R.E., and Suflita, J.M., 1987, Microbial ecology of a shallow unconfined ground water aquifer polluted by municipal landfill leachate: Microbial Ecology,v. 14, p.39-54.

Chapelle, F. H., Haack, S. K., Adriaens, P., Henry, M. A. and Bradley, P. A., 1996, Comparison of E_h and H_2 measurements for delineating redox processes in a contaminated aquifer: Environ. Sci. Technol., v. 30, 3565-3569.

Cozzarelli, I. M., Suflita, J. M., Ulrich, G. A., Harris, S. H., Scholl, M. L., Schlottman, J. L., and Jaeschke, J. B., 1999, in Morganwalp D.W., and Buxton, H.T., eds., 1999, U.S. Geological Survey Toxic Substances Hydrology Program—Proceedings of the Technical Meeting, Charleston, South Carolina, March 8-12, 1999, Volume 3 *In* Subsurface Contamination from Point Sources:U.S. Geological Survey Water-Resources Investigations Report 99-4018C, this volume.

Krumholz, L. R., McKinley, J. P., Ulrich, G. A. and Suflita, J. M., 1997, Confined subsurface microbial communities in Cretaceous rock: Nature v. 386, 64-66.

Lovley, D. R., and Goodwin S., 1988, Hydrogen concentrations as an indicator of the predominant terminal electron-accepting reactions in aquatic sediments: Geochem. Cosmochem. Acta., v. 52, 2993-3003.

Scholl, M. A. and Christenson, S.C., 1998, Spatial variation in hydraulic conductivity determined by slug tests in the Canadian River alluvium near the Norman Landfill, Norman, Oklahoma: U.S. Geological Survey Water-Resources Investigations Report 97-4292, p.28.

Smith, R.L., 1997, Determining the Terminal Electron Accepting Reaction in the Saturated Subsurface. *In* Manual of Environmental

Microbiology (ed. C.J. Hurst, G.R. Knudsen, M.J. McInerney, L.D. Stetzenbach and M.V. Walter), ASM Press, Washington, D.C., p.577-585.

Ulrich, G. A., Breit, G. N., Cozzarelli, I. M., and Suflita, J. M., 1999, Biogeochemistry of barium and the ecology of sulfate reduction under electron acceptor limitations in a landfill leachate-contaminated aquifer: (In preparation).

AUTHOR INFORMATION

Joseph M. Suflita, Glenn A. Ulrich and Steve H. Harris, University of Oklahoma, Dept. of Botany and Microbiology, Norman, Oklahoma

Heterogeneous Organic Matter in a Landfill Aquifer Material and Its Impact on Contaminant Sorption

By Hrissi K. Karapanagioti and David A. Sabatini

ABSTRACT

Phenanthrene was used as a model chemical to study the sorption properties of Canadian River Alluvium aquifer material sampled from the closed Norman Landfill which is a USGS Toxic Substances Research Site in Norman, Oklahoma. Both equilibrium and kinetic sorption processes were evaluated through batch studies. The bulk sample was divided into subsamples with varying properties such as particle size, organic content, equilibration time, etc. in order to determine the effect of these properties on resulting sorption parameters. The data have been interpreted using the Freundlich isotherm model and a numerical solution of Fick's 2nd law in porous media. Organic matter in the subsamples was divided into two main groups based on the microscopic organic matter characterization: a) organic particles (i.e. coal, charcoal, etc.) or mature organic matter and b) organic coatings of quartz grains or young organic matter. Samples containing organic particles presented high Koc values. Samples with organic matter dominated by organic coatings on quartz grains presented low Koc values and contained a high percentage of fast sorption sites. The numerical solution of Fick's 2nd law requires the addition of two terms (fast and slow) in order to properly fit the kinetics of these heterogeneous samples. These results thus demonstrate the need for soil organic matter characterization in order to predict and explain the sorption properties of a soil sample containing heterogeneous organic matter and also the difficulty and complexity of modeling sorption in such samples. Microscopic organic matter characterization proved to be a valuable tool for characterizing the heterogeneous organic matter and explaining the results.

INTRODUCTION

Natural attenuation is currently one of the most important topics in ground water remediation. Sorption equilibria and kinetic properties are very important factors affecting natural attenuation in the subsurface. There is an extensive body of literature that discusses sorption processes; however, very limited information exists on the effects of naturally-occurring heterogeneous soil organic matter on sorption properties.

Karickhoff and others (1979) published one of the early and important studies on sorption of hydrophobic organic compounds. Their research suggested instantaneous equilibrium and linear isotherms demonstrating partition-like sorption. The organic content normalized distribution coefficient (Koc) was found to depend on chemical hydrophobicity as quantified via the chemical's octanol-water partition coefficient (Kow) and solubility. Sorption capacity was observed to be a function of soil organic carbon content and Koc.

More recent work has revealed that in addition to the organic content the nature of the organic matter has a significant impact on sorption capacity and nonlinearity (Grathwohl, 1990; Weber and Huang, 1996; Gustafsson and others, 1997; Huang and Weber, 1997; Xing and Pignatello, 1997; Kleineidam and others, 1998). Organic matter with different sorption properties

has been divided into: a) soft or rubbery and b) hard or glassy (Young and Weber, 1995; Xing and Pignatello, 1997). A critical review paper summarizes all the important soil properties and the sorption processes related to them (Luthy and others, 1997). More than one type of organic matter, as well as the presence of organic particles, can be present in the soil samples.

Recent publications summarize the slow sorption/desorption of organic compounds in natural particles that can be attributed to intraparticle diffusion (Pignatello and Xing, 1996; Luthy and others, 1997; Grathwohl, 1998). Luthy and others (1997) present a correlation between soil properties and sorption kinetics. In the past intraparticle pore diffusion models have been used to describe the long-term sorption kinetics in bulk samples (Ball and Roberts, 1991b; Grathwohl and Reinhard, 1993). Rügner and others (1998) used an empirical correlation that predicts long term sorption kinetics of organic pollutants in heterogeneous aquifer materials based on intraparticle porosity and equilibrium sorption capacity of homogeneous constituents of the sample.

The objectives of this study were to examine the effects of heterogeneous organic matter on sorption equilibria and kinetic parameters in a sandy aquifer material. Sorption parameters were explained based on organic matter characterization. This study is unique in demonstrating the presence of and petrographically characterizing organic particles in alluvial aquifer materials and in demonstrating the effect of these organic particles on sorption properties.

MATERIALS AND METHODS

Soil was sampled from the closed Norman Landfill which is a United States Geological Survey Toxic Substances Research site in Norman, Oklahoma, USA. The sampling depth was just below the water table at about 3 ft. The initial soil sample was divided into two groups with grain size: a) <0.5 mm and b) >0.5 mm. Sieve analysis was performed on the soil sample with grain size less than 0.5 mm and the sample was separated into four subsamples. Code names given to subsamples (Table 1) were based on their grain size. The organic carbon content of these subsamples was analyzed by dry combustion at 850°C (Model 183 Boat Sampling Module, Rosemount) and quantified by an infrared detector for CO_2 (Horiba PIR-2000). Surface area and intraparticle porosity were measured using N_2 and the BET method (ASAP 2010, Micromeritics).

Phenanthrene was used as the model chemical in this study. Phenanthrene ($C_{14}H_{10}$) is a three ring polycyclic aromatic hydrocarbon with: a) molecular weight: 178 g mol^{-1}, b) solubility: 1.29 mg L^{-1} at 25° C, c) Henry's law constant: $2.6x10^{-5}$ atm m^3 mol^{-1}, and d) log Kow: 4.6 (Montgomery and Welkom, 1990). The estimated log Koc of phenanthrene is 4.4 (Karickhoff and others, 1979). Phenanthrene was chosen because of its high hydrophobicity (Kow), low volatility (Henry's law constant), and simplicity of analysis. Phenanthrene was diluted to a 100 mg L^{-1} stock solution in methanol. Solutions were prepared with synthetic ground water comprised of deionized water with 44 mg L^{-1} $CaCl_2.2H_2O$, 14 mg L^{-1} $CaSO_4$, and 17 mg L^{-1} $NaHCO_3$. Sodium azide was added at a concentration of 200 mg L^{-1} to inhibit biodegradation.

All equilibrium sorption isotherm experiments were conducted in triplicate in 10 mL crimp top glass vials. The soil samples were pulverized to assure equilibrium in a reasonable time. The soil samples were mixed with variable phenanthrene concentrations and were shaken for seven days at constant temperature (20°C) in the dark. Headspace was kept at a minimum. Different solid to water ratios were used due to different sorption capacities of the subsamples.

All sorption kinetic batch experiments were conducted in triplicate in 100 mL crimp top glass vials. The initial phenanthrene concentration used was 0.1 mg L^{-1}. The solid to water ratio was different for each subsample. The vials were stored at 20°C in the dark. Measurements were taken at various time intervals.

For both isotherm and kinetic batch experiments phenanthrene concentrations were measured by a cuvette mode Perkin-Elmer LS-3B Fluorescence Spectrometer. For each batch study blank samples with phenanthrene solutions and

without soil were prepared and monitored. These blank samples did not indicate any significant phenanthrene degradation or sorption on the glassware. At the end of the kinetic experiment phenanthrene was extracted from the solids with hot methanol (60°C) for 4 days (Ball and others, 1997).

In order to characterize optical properties of organic matter thin sections of the soil subsamples were prepared. Microscopic investigations were carried out on a Leica DMRX photometer microscope. Organic matter was identified and characterized using white light and UV illumination in transmitted and reflected light mode.

MODELING OF DATA

Non- linear isotherms can be described by the Freundlich equation:

$$qe = Kfr\ Ce^{n} \quad (1)$$

where

Kfr is the Freundlich sorption constant and

n is the Freundlich exponent.

The organic content normalized distribution coefficient is described by:

$$Koc = Kd\ foc^{-1} \quad (2)$$

where

Kd is the sorption distribution coefficient that equals ***Kfr*** at chemical concentrations equal to 1 $\mu g\ L^{-1}$ and

foc is the organic content of the soil.

Solute diffusion from an aqueous phase into spherical porous grains can be described by Fick's 2nd law:

$$\partial C\ \partial t^{-1} = Da\ [(\partial^2 C\ \partial r^{-2}) + (2\partial C\ (r\partial r)^{-1})] \quad (3)$$

where

C is the concentration of the chemical,

t is time,

Da is the apparent diffusion coefficient, and

r is the radial distance from the center of the grain.

In the present study a numerical solution of Fick's 2nd law was evaluated. This numerical model is described by Jäger (1997) and is based on the finite difference method using the Crank-Nicholson approach. Input data are the grain radius, the solid to water ratio, the initial water concentration, the Freundlich parameters, the solid density and the intraparticle porosity. In this study the numerical model was used to fit the sorption kinetic curves and produce values for ***Da***. As summarized in Grathwohl (1998) the sorptive uptake curves, expressed as ***Kd*** versus time, allow comparison of sorptive uptake at different solid to water ratios in a batch experiment.

Table 1. Soil Analysis

Sample	Effective Diameter	wt	foc	Fraction foc in subsample	Porosity	Predominant Organic Matter	Maturity
Code	mm	(%)	(%)	(%)			
CRA comp.	<0.5	100	0.40	100	0.017	Mixed	Mixed
0.5	0.5-0.25	3	2.90	22	0.044	Organic Particles	Mature
0.25	0.25-0.125	28	0.51	36	0.014	Organic Particles in Clay Matrix	Mixed
0.125	0.125-0.063	58	0.20	29	0.015	AOM coatings	Young
0.063	<0.063	11	0.52	14	0.027	Charcoal	Mature

wt: weight fraction of composite; foc: organic carbon content; Porosity: for pore diameter <66.6 nm; CRA comp.: Canadian River Alluvium composite sample; AOM: Amorphous Organic Matter

Table 2. Isotherm Results

Sample	wt	foc	n	Kfr	log Koc	Confidence Interval
	(%)	(%)		($\mu g\ kg^{-1}$) ($L\ \mu g^{-1}$)^n		95%
CRA comp.	100	0.40 ± 0.092	0.65 ± 0.021	1100 ± 95	5.4	5.3 - 5.5
0.5	3	2.90 ± 0.270	0.64 ± 0.043	11000 ± 1300	5.6	5.5 - 5.7
0.25	28	0.51 ± 0.038	0.70 ± 0.013	1100 ± 55	5.3	5.3 - 5.4
0.125	58	0.20 ± 0.011	0.57 ± 0.036	400 ± 61	5.3	5.2 - 5.4
0.063	11	0.52 ± 0.048	0.53 ± 0.044	2100 ± 100	5.6	5.6 - 5.7

wt: weight fraction of composite; foc: organic carbon content; n: Freundlich exponent; Kfr: Freundlich constant; Koc: organic content normalized sorption distribution coefficient; CRA comp.: Canadian River Alluvium composite sample

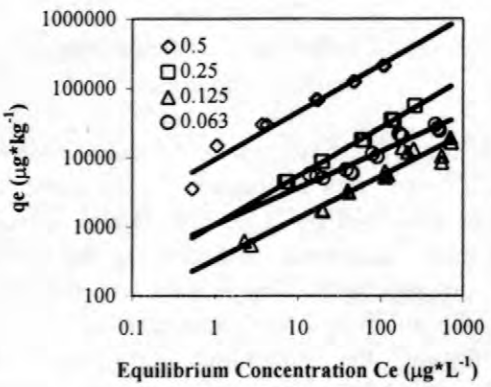

Figure 1. Size fraction subsample isotherms. qe is the amount of phenanthrene sorbed per amount of soil, Ce is the equilibrium phenanthrene concentration. The symbols denote experimental data points and the lines the Freundlich isotherm fit. Subsample code names indicate particle size (as presented in Table 1).

RESULTS AND DISCUSSION

Soil Analysis

The soil organic content (foc), surface area (SA), and porosity for each subsample and the composite soil sample are presented in Table 1. Fine sand particles (0.125) make up 58% of the composite sample amount but only contribute 29% of the organic content. A large fraction (22%) of the composite sample foc is associated with the larger grain size (0.5) which makes up only 3% of composite sample amount. While previous studies have generally shown that the finest grain size particles were associated with the highest organic content, as well as the highest Koc values (Kan and others, 1994; Barber, 1994), Ball and Roberts (1991a) did observe higher organic content for the larger size fractions using the Borden sand.

Organic petrography analysis of the different subsamples of the present study showed different types of organic matter for each subsample. The sand size fraction (0.5) includes organic particles, such as coal and phytoclast particles, as well as amorphous organic matter (AOM) in quartz aggregate clay matrices. The medium sand size fraction (0.25) mainly includes organic particles in clay matrices coating quartz grains. The fine sand size fraction (0.125) mainly includes AOM coatings of quartz grains. The fine grain size fraction (0.063) includes charcoal particles and AOM coatings of quartz grains. All subsamples are highly heterogeneous and contain coal particles. Ongoing research in our laboratory is focusing on quantification of the different organic matter characteristics and characterization of the organic carbon content into different fractions as proposed in Gustafsson and others (1997); this will be presented in a future publication.

Equilibrium sorption isotherms

The four subsample sorption isotherms are presented in Figure 1. The isotherms for phenanthrene in the composite sample and all of the subsamples have a Freundlich curvilinear shape suggesting more than just partitioning of phenanthrene into the organic matter. Table 2 presents the isotherm constants derived from equilibrium experiments. In all cases, log Koc values (5.3 - 5.6) are much higher than Kow-based estimates (Karickhoff and others, 1979; log Koc = 4.4). These results demonstrate that organic carbon content alone is not enough to predict Kfr values.

Based on the Koc values, there are two distinct groups: a) the sand (0.5) and the finest grain (0.063) size fractions, and b) the medium (0.25) and fine (0.125) sand fractions. Group (a) presented higher Koc values than group (b). Studying the previous trends, it is obvious that the presence of coal (0.5) and charcoal particles (0.063) in soil samples increases both the amount of organic carbon content present and the Koc value for this fraction. These organic particles (i.e. coal, charcoal, etc.) can generally be characterized as mature organic matter (see Table 1). Amorphous organic matter coatings of quartz grains (0.125), characterized as young organic matter, produce the lowest Koc value. Even the lowest Koc value of this study (log Koc = 5.2 - 5.4; 95% confidence interval) is higher than the value estimated by Kow (log Koc = 4.4) due to coal particles present in all subsamples.

The presence of mature organic matter in soil samples increases the Koc values of these samples. If mature and young organic matter are not considered as different sorptive media sorption potential of the soil will be underestimated (log Koc = 5.4 versus log Koc = 4.4; Table 2 and Karickhoff and others, 1979, respectively). This observation is important when trying to predict chemical transport in the subsurface. When natural attenuation is considered as a remediation scenario underestimating sorption potential causes an overestimate of the potential risk and can lead to unnecessary remediation expenses.

Sorption Kinetics

Figure 2 presents the apparent sorption coefficient at a given time (Kda) normalized by the equilibrium distribution coefficient (Kd) as a function of time for the composite sample during kinetic experiments. The apparent sorption distribution coefficient (Kda) values follow the diffusion model prediction line (solid and dashed lines representing the model without and with the adjustment for fast sorption sites, respectively) for the composite sample (CRA comp.). Some of the 30 day measurements deviated from the diffusion model. Although there was NaN_3 present in the reactors this behavior was attributed to biodegradation which, due to the presence of

Table 3. Kinetic Sorption Properties based on Numerical Solution

Sample	a	Da a^{-2}	Da	T_1 75% Eq	Xi	T_2 75% Eq
	(cm)	($1\ s^{-1}$)	($cm^2\ s^{-1}$)	(d)	(%)	(d)
CRA comp.	0.0077	7.7E-08	7.7E-12	12	20	22
0.5	0.0180	1.2E-08	3.9E-12	73	15	290
0.25	0.0089	6.4E-08	5.1E-12	16	20	84
0.125	0.0044	3.4E-07	6.6E-12	3	40	5
0.063	0.0027	4.5E-07	3.3E-12	2	25	3

a: grain radius; Da a^{-2}: apparent diffusion rate coefficient; Da: apparent diffusion coefficient; T 75% Eq: time to reach 75% equilibrium 1) without and 2) with fast sorption sites included in the numerical solution, respectively; Xi: Percent of fast sorption sites; CRA comp.: Canadian River Alluvium composite sample

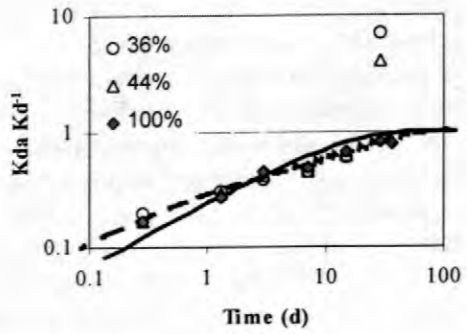

Figure 2. CRA composite sample kinetic experiment. Apparent distribution coefficient, Kda, normalized to the equilibrium distribution coefficient, Kd, versus time (d). The symbols denote experimental data points, the solid line and the dashed line the numerical solution fit without and with the fast sorption term (Xi), respectively. Numbers in the legend represent percent of amount recovery at the end of the experiment (last step only) using hot methanol extraction.

NaN_3, had a lag period of about 15-30 days. In order to prove this assumption all samples were solvent extracted with hot methanol. For the samples that followed the diffusion model the mass balance was within 90-100% recovery - the remaining samples presented only a 26-76% recovery.

Table 3 presents results of experimental and modeling work studying the kinetic sorption properties of the soil samples. In Figure 2 it is obvious that the model (solid line) does not fit all the data properly; especially longer term (slower) sorption. This is expected because the numerical model used assumes homogeneous samples. In order to fit all the data properly the introduction of a fast sorption term (Xi) that represents a percent of fast sorption sites in the sample was required (see dashed line in Figure 2 and Table 3). Table 3 also presents Xi and the time needed to reach 75% of equilibrium ($T_2$75% Eq) based on the model adjusted for fast sorption sites. The highest Xi term was estimated for the subsample that contains AOM coatings (0.125) suggesting a faster sorption mechanism that is not limited by intraparticle diffusion kinetics. More details on modeling of subsamples is discussed in another publication (Karapanagioti et al., 1999). The time needed to reach 75% of equilibrium when estimated including fast sorption sites ($T_2$75% Eq) is higher than when based on a single component ($T_1$75% Eq) in Table 3. The solid curve in Figure 2 tries to fit both fast and slow data as if they behaved the same and thus does not fit either of them properly. It both overestimates and underestimates the time required to reach equilibrium for the fast sorption sites and the slow sorption sites, respectively. Once a fast sorption term is added (see dashed line) the fast sorption points are fitted well and is better incorporated into the results resulting in longer estimated equilibration times ($T_2$75% Eq > $T_1$75% Eq; Table 3).

The presence of organic particles and coatings in the soil samples thus affected the kinetics of sorption. Kinetic models should cautiously be applied to fit the kinetic properties of soil samples containing heterogeneous organic matter. The model that assumes a homogeneous organic matter behavior by trying to fit the fast sorbing sites will overestimate the time required for sorption to reach equilibrium ($T_1$75% Eq = 12 versus $T_2$75% Eq = 22; Table 3). When incorporating sorption into natural attenuation it is thus important to consider the impacts of heterogeneous organic matter on sorption equilibria and kinetics so as to properly estimate the risk of exposure.

Ongoing research in our laboratory studies other related aspects of transport and fate of contaminants using CRA samples. Changes in sorption equilibria and kinetic characteristics with aquifer depth are being studied. Aquifer material reactors will be used to study the effect of natural heterogeneous organic matter on coupled sorption and biodegradation processes.

SUMMARY

Batch experiments were conducted to examine sorption equilibria and kinetic sorption characteristics of phenanthrene with the Canadian River Alluvium aquifer material. Sorption isotherms were non-linear and subsample Koc values were higher than estimated based on the Kow predictions. Two groups of subsamples were found: a) subsamples with high organic

content including organic particles or mature organic matter and b) subsamples with organic matter coatings on quartz grains or young organic matter. Group (a) presented a Koc value higher than group (b).

Modeling of sorption kinetics was best performed by the numerical solution of Fick's 2nd law when the fast sorbing sites were considered independently. The use of a fast sorption term was necessary for better fit especially for samples with organic coatings. These results demonstrate the importance of organic matter characteristics and heterogeneity on the resulting sorption equilibria and kinetics. Soil samples containing heterogeneous organic matter could present equilibrium and kinetic sorption properties that would be difficult to predict using models developed based on the assumption that organic matter is homogeneous. Soil organic matter characterization is thus necessary for accurate prediction of soil sorption behavior which is critical in estimating contaminant fate and risk assessment.

Acknowledgment. This study was partially funded by the U.S. National Science Foundation through the Oklahoma EPSCoR program. The authors would like to especially thank Dr. Sybille Kleineidam and Dr. Peter Grathwohl of the Universität Tübingen for their valuable input in this research. The authors would also like to thank the following people from the Universität Tübingen: Dr. Sybille Kleineidam and Dr. Bertrand Ligouis for the organic matter characterization, Renate Riehle for TOC measurements and Hermann Rügner for BET measurements. This research was conducted at the Universität Tübingen while David Sabatini was on sabbatical there as a Senior Fulbright Scholar and while Hrissi Karapanagioti, his PhD student from the University of Oklahoma, was conducting research with him at the Universität Tübingen.

REFERENCES

Ball, W.P. and Roberts, P.V., 1991a, "Long-Term Sorption of Halogenated Organic Chemicals by Aquifer Material. 1. Equilibrium", Environmental Science & Technology, V. 25, No 7, p. 1223-1237.

Ball, W.P. and Roberts, P.V., 1991b, "Long-Term Sorption of Halogenated Organic Chemicals by Aquifer Material. 2. Intraparticle Diffusion", Environmental Science & Technology, V. 25, No 7, p. 1237-1249.

Ball, W.P., Xia, G., Durfee, D.P., Wilson, R.D., Brown, M.J., and Mackay, D.M., 1997, "Hot Methanol Extraction for the Analysis of Volatile Organic Chemicals in Subsurface Core Samples from Dover Air Force Base, Delaware", Ground Water Monitoring and Research, V. 17, No 1, p. 104-121.

Barber, L.B., 1994, "Sorption of Chlorobenzenes to Cape Cod Aquifer Sediments", Environmental Science & Technology, V. 28, No 5, p. 890-897.

Grathwohl, P., 1990, "Influence of organic matter from Soils and Sediments from Various Origins on the Sorption of Some Chlorinated Aliphatic Hydrocarbons: Implications on Koc Correlations", Environmental Science & Technology, V. 24, No 11, p.1687-1693.

Grathwohl, P. and Reinhard, M., 1993, "Desorption of Trichloroethylene in Aquifer Material: Rate Limitation at the Grain Scale", Environmental Science & Technology, V. 27, No 12, p.2360-2366.

Grathwohl, P., 1998, Diffusion in Natural Porous Media: Contaminant Transport, Sorption/Desorption and Dissolution Kinetics, Kluwer Academic Publishers, Boston, Massachusetts.

Gustafsson, Ö., Haghseta, F., Chan, C., Macfarlane, J., and Gschwend, P.M., 1997, "Quantification of the Dilute Sedimentary Soot Phase: Implications for PAH Speciation and Bioavailability", Environmental Science & Technology, V. 31, No 1, p. 203-209.

Huang, W. and Weber, W.J.Jr., 1997, "A Distributed Reactivity Model for Sorption by Soils and Sediments 10. Relationships Between Desorption, Hysteresis, and the Chemical Characteristics", Environmental Science & Technology, V. 31, No 9, p. 2562-2569.

Jäger, R., 1997, Modellierung Nichtlinear Intrapartikel-Diffusion in Heterogenem Aquifermaterial, Diploma Thesis, University of Tübingen, FRG.

Kan, A.T., Fu, G., and Tomson, M.B., 1994, "Adsorption/Desorption Hysteresis in Organic Pollutant and Soil/Sediment Interaction", Environmental Science & Technology, V. 28, No 5, p.859-867.

Karapanagioti, H.K., Sabatini, D.A., Kleineidam, S., Grathwohl, P., and Ligouis, B., 1999, "Phenanthrene Sorption with Heterogeneous Organic Matter in a Landfill Aquifer Material", Journal of Physics and Chemistry of the Earth, accepted.

Karickhoff, S.W., Brown, D.S., and Scott, T.A., 1979, "Sorption of Hydrophobic Pollutants on Natural Sediments", Water Research, V. 13, p. 241-248.

Kleineidam, S., Rügner, H., Ligouis, B., and Grathwohl, P., 1998, "Organic Matter Facies and Equilibrium Sorption of Phenanthrene", Environmental Science & Technology, submitted.

Luthy, R.G., Aiken, G.R., Brusseau, M.L., Cunningham, S.D., Gschwend, P.M., Pignatello, J.J., Reinhard, M., Traina, S.J., Weber, W.J.Jr., and Westall, J.C., 1997, "Sequestration of Hydrophobic Organic Contaminants by Geosorbents", Environmental Science & Technology, V. 31, No 12, p.3341-3347.

Montgomery, J.H. and Welkom, L.M., 1990, Ground Water Chemicals Desk Reference, Lewis Publishers, Inc., Chelsea, Michigan.

Pignatello, J.J. and Xing, B., 1996, "Mechanisms of Slow Sorption of Organic Chemicals to Natural Particles", Environmental Science & Technology, V. 30, No 1, p. 1-11.

Rügner, H., Kleineidam, S., and Grathwohl, P., 1998, "Long Term Sorption Kinetics of Phenanthrene in Aquifer Materials", Environmental Science & Technology, submitted.

Weber, W.J.Jr. and Huang, W., 1996, "A Distributed Reactivity Model for Sorption by Soils and Sediments. 4. Intraparticle Heterogeneity and Phase-Distribution Relations under Nonequilibrium Conditions", Environmental Science & Technology, V. 30, No 3, p. 881-888.

Xing, B. and Pignatello, J.J., 1997, "Dual-Mode Sorption of Low-Polarity Compounds in Glassy Poly(Vinyl Chloride) and Soil Organic Matter", Environmental Science & Technology, V. 31, No 3, p. 792-799.

Young, T.M. and Weber, W.J.Jr., 1995, "A Distributed Reactivity Model for Sorption by Soils and Sediments. 3. Effects of Diagenetic Processes on Sorption Energetics", Environmental Science & Technology, V. 29, No 1, p. 92-97.

Aquifer Heterogeneity at the Norman, Oklahoma, Landfill and its Effect on Observations of Biodegradation Processes

By Martha A. Scholl, Isabelle M. Cozzarelli, Scott C. Christenson, George N. Breit, and Jamie L. Schlottmann

ABSTRACT

Biodegradation processes in the leachate plume at Norman landfill probably vary among the distinct hydrologic and chemical environments at the site. These environments include zones of mixing with surface water, rainfall recharge or background ground water, and areas of varying permeability in the part of the aquifer occupied by the contaminant plume. The alluvial aquifer at the Norman landfill site consists of sediments ranging from mud to pebbly sand, which, except for the mud layers, have a range of measured hydraulic conductivity from 2.4×10^{-7} to 2.8×10^{-4} m/s. Core descriptions from the site indicate that average aquifer composition is 75% sand (fine, medium and coarse), 10% silt and clay in discrete layers, 10% medium-grained sand matrix with pebbles or mud clasts, and 5% coarse sand with pebbles. A numerical model (BIOMOC) was used to explore how permeability might affect observed biodegradation processes and rates. Results of the simulation suggest that low-permeability areas in the aquifer may be relatively uncontaminated, and act as reservoirs of electron acceptors to the surrounding leachate-contaminated areas. A moderate permeability area in the model had relatively low contaminant concentrations and biodegradation appeared to be most efficient in that area. In the highest-permeability areas, the simulation results suggested that preferential electron acceptors are depleted very quickly, leading to higher contaminant concentrations due to less efficient degradation processes and high rates of transport.

INTRODUCTION

The Norman Landfill is a closed municipal landfill sited on the alluvial plain of the Canadian River near Norman, Oklahoma (see Christenson and others, this volume, for background information). The alluvial plain is approximately 2.1 – 2.4 km (kilometers) wide and is bordered by older, higher-elevation terrace deposits. The alluvial aquifer downgradient from the landfill is 11-12 m (meters) thick and currently extends about 500 m from the edge of the landfill mound to the riverbank (fig. 1). Sediments in the alluvial aquifer range from mud to pebbly sand, and the aquifer is underlain by low-permeability shale of the Permian Hennessey Formation. The ground-water system in the alluvium is unconfined, with water levels no more than 2 m from the land surface in the area between the river and the landfill mound. A beaver-dam-ponded stream (slough) that is a surface-water expression of the alluvial aquifer runs parallel to and about 100 m from the edge of the landfill. Ground-water levels in the aquifer change seasonally, with higher levels in winter (Christenson and others, this volume). The ground water throughout the alluvial plain is suboxic to anoxic, and a plume of landfill leachate exists in the aquifer downgradient from the landfill. The leachate plume is characterized by high levels of dissolved organic compounds and inorganic solutes (for details, see Eganhouse and others, and Cozzarelli and others, both in this volume). Biodegradation of the leachate is occurring, as indicated by the depletion of electron acceptors such as sulfate and oxygen and the increased levels of degradation products such as dissolved methane, dissolved

iron, and bicarbonate alkalinity relative to background levels.

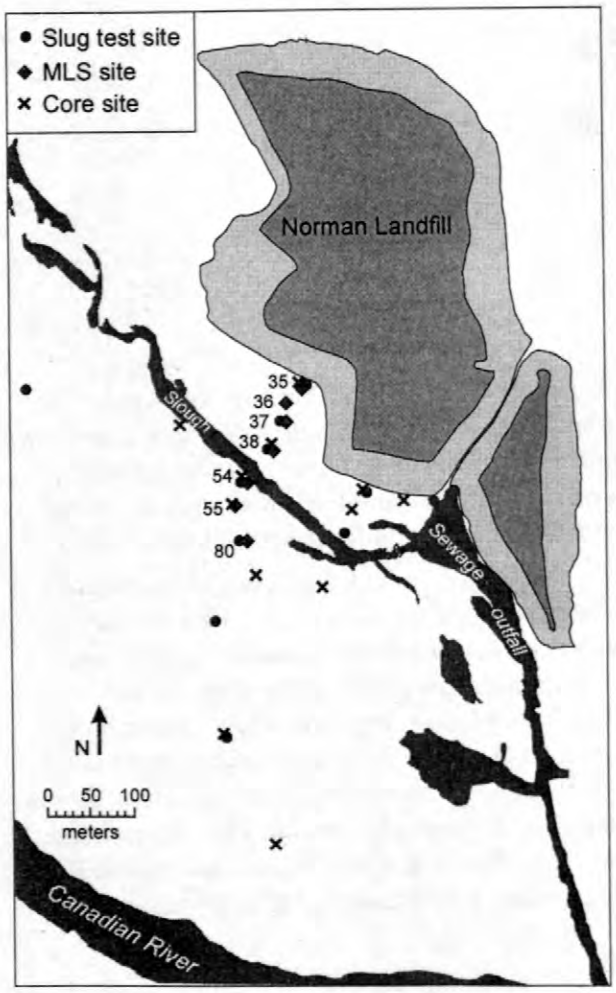

Figure 1. Location map of the Norman landfill study area, showing sites of the multi-level samplers (MLS), slug tests, and core samples that are discussed in the text.

The broad objectives of the study described here are to determine how different hydrologic environments affect biodegradation of the landfill leachate. The leachate plume travels through a relatively heterogeneous alluvial aquifer, and also interacts with surface water and the unsaturated zone above the water table in the shallow unconfined aquifer. In this paper, conceptual models of the aquifer heterogeneity and biodegradation processes are described, and an approximation of the permeability structure of the alluvial aquifer at Norman landfill is used in a numerical model to explore the effects of permeability heterogeneity on observed biodegradation processes in the core of the leachate plume.

AQUIFER CHARACTERIZATION

Cores

Cores have been taken in the alluvial aquifer around the landfill by Geoprobe™, auger, and rotosonic methods. Core logs with qualitative field descriptions of the sediments are available for 12 sites in the area downgradient from the landfill (fig. 1). (In cases where there was more than one core at a site, the most complete core was used.) These core descriptions were analyzed to obtain information on the aquifer structure at the site. The sediment descriptions were classified as one of 8 categories of sediment type and the percentages of each sediment type for all the cores are shown in Table 1. About 20% of the total cored intervals were missing (not recovered in the coring process). The most common sediment type is sand (predominantly medium-grained sand), comprising 75% of the recovered sediment. The sand is generally described in the core logs as silty sand, or sand with thin clay or silt laminae, typically moderately to poorly sorted. Mud and silt layers accounted for 10% of the recovered sediment, and coarse sand with pebbles or gravel comprised 5%. The remaining sediments were medium-grained sand matrix with either pebbles or clay (mud) clasts (10%), and plant fragments, trash or bedrock (0.3%).

The alluvial aquifer was deposited by a braided stream. As a broad generalization, the aquifer can be described as predominantly sand interbedded with mud and coarse-grained sand and gravel layers. The bedforms in the sediment are oriented roughly along the axis of the alluvial plain, so the regional direction of ground water flow toward the river is approximately perpendicular to the fabric of the sedimentary units. For the 12 cored sites considered, the average thickness of recovered clay and silt layers was 0.15 m (maximum 0.85 m), and of coarse sand with gravel layers, 0.2 m (maximum 0.6 m). The core logs from the 12 sites, taken as a group, show that the aquifer changes character with

depth. The upper part of the aquifer consists of laminated sand deposits and mud or silt layers. There is a concentration of mud layers between 3 and 5 m depth in the aquifer (nine of the 12 cores have two or more mud or silt layers greater than 0.1 meter thick in this depth interval) although mud layers are common in the aquifer from 0 to 8 m depth. All of the layers of coarse sand with pebbles that were recorded are below 6 m depth in the aquifer, with the greatest abundance in the bottom 3 m of the aquifer.

Table 1. Percentages of sediment type from core log descriptions in the alluvial aquifer at Norman landfill. Numbers are average of the 12 sites.

Sediment category	Percentage entire core length	Percentage recovered sediment
Missing	19.8	---
Fine-grained sand	7.6	9
Medium-grained sand	47.7	60
Coarse-grained sand	5.2	6
Silt	2.6	3
Clay or mud	5.3	7
Medium sand matrix with either pebbles or clay/mud clasts	7.7	10
Coarse sand with pebbles or gravel	3.7	5
Other (organics, bedrock, garbage)	0.3	0.3

Slug tests

Hydraulic conductivity (K) of the alluvium has been characterized by slug tests at 97 points in the aquifer to date (methods and results from 44 points can be found in Scholl and Christenson, 1998). At selected locations downgradient from the landfill (fig. 1), slug tests were done at successive 1-meter depth intervals until the bottom of the aquifer was reached. The hydraulic conductivity for 97 of 103 depth points was measured, and ranged from 2.4×10^{-7} to 2.8×10^{-4} m/s (meters per second). The remaining 6 points were in mud layers and the equipment was not appropriate for low-permeability slug tests, so the hydraulic conductivity is assumed to be less than about 10^{-7} m/s.

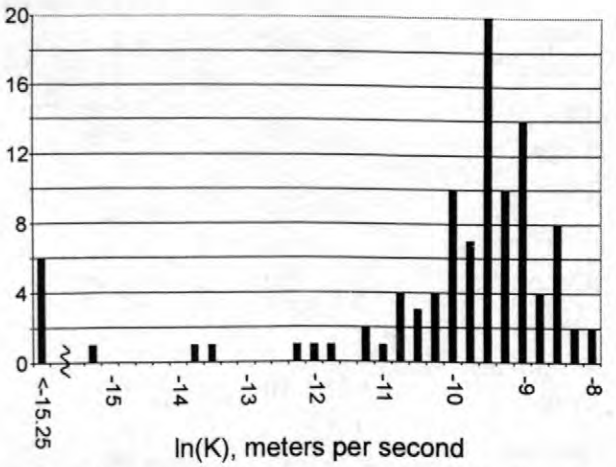

Figure 2. Frequency distribution of ln of hydraulic conductivity (K) values from slug tests at 103 points in the alluvial aquifer at Norman landfill.

The hydraulic conductivity distribution is shown in figure 2. The bulk of the hydraulic conductivity measurements from the site (values > -10.6 or 2.5×10^{-5} m/s) are lognormally distributed as indicated by a Kolmogorov-Smirnov normality test at the 90% confidence interval. The rest of the K measurements are scattered at lower values, including the 6 points from mud layers that were not measured. A lognormal distribution of K has been found for many field data sets and most of the Norman aquifer data fit this pattern, however, the excluded lower K values make up about 15% of the measured values and are an important part of the heterogeneity at the Norman site. The geometric mean and the variance of the ln K data (excluding only the 6 unmeasured points) are shown in Table 2, compared to values from the Cape Cod site (Hess and others, 1992), the Columbus Air Force Base site (Rehfeldt and others, 1992), an aquifer in western Denmark (Bjerg and others, 1992), and the Borden, Ontario aquifer (Sudicky, 1986). The comparison shows that the Norman landfill alluvial aquifer is most like the aquifer with a similar depositional environment at the Columbus, Mississippi site (note that the variance shown for the Norman site is an underestimate because the mud layers that were encountered were not measured).

Table 2. Comparison of Norman landfill hydraulic conductivity distribution with other published sites.

Site	Geometric mean K, m/s	Variance of ln K	Type of data	Number of data	Aquifer type
Norman landfill*	5.4×10^{-5}	1.3	slug tests	97	river alluvium
Otis AFB, Cape Cod	1.1×10^{-3}	0.24	flowmeter	668	glacial outwash
Otis AFB, Cape Cod	3.5×10^{-4}	0.14	permeameter	825	
Columbus AFB	5.5×10^{-5}	4.5	flowmeter	2187	river alluvium
Columbus AFB	1.65×10^{-4}	1.8	slug tests	22	
Western Denmark	5.04×10^{-4}	0.37	slug tests	274	glacial outwash
Borden, Ontario	9.75×10^{-5}	0.38	permeameter	1279	glacial, sand and silty sand

*excluding the 6 unmeasured data points from mud layers

AQUIFER HYDRAULIC CONDUCTIVITY STRUCTURE

By combining the information from the slug tests and core samples, an approximate picture of the aquifer structure can be constructed along the longest transect of multi-level samplers (MLS) at the site (fig. 1), from well MLS-35 to well MLS-80. This simple model divides the aquifer into 3 facies with similar hydrologic properties, of low, moderate and high permeability (fig. 3). These hydrologic facies explain the configuration of the landfill leachate plume fairly well, as it was measured in April of 1997. The plume appears to be divided into an upper and lower mass by a mud-silt layer at 326-327 m elevation. The upper, smaller mass of leachate appears to discharge into the slough, and the larger mass moves to the bottom of the aquifer and flows along the high-permeability layer along the bottom. Note that this transect is not assumed to be strictly parallel to ground-water flow in the area. Patterns of specific conductance (not shown) indicate that the higher permeability layers cause flow in directions other than parallel to the transect.

CONCEPTUAL MODEL OF BIODEGRADATION FOR SITE

With this model of the aquifer structure and leachate plume in mind, and with chemistry data collected thus far at the site (see Cozzarelli and others, this volume), a conceptual model of zonation of biodegradation processes at the site can be formulated (fig. 4). The complex mixture of organic chemicals that make up the landfill leachate is undoubtedly degraded by many different processes, and specific compounds are degraded at different rates. Neglecting specific compounds and processes and considering the site from the standpoint of bulk leachate transport and biodegradation, one of the major goals of this project is to identify where in the aquifer most of the degradation of the bulk leachate is occurring.

The transect discussed above has several environments in which different biodegradation processes may occur. The possible environments can be divided into five broad categories that are illustrated in figure 4 and discussed below: 1. Aerobic zone – a very thin zone at the top of the water table where oxygenated recharge enters the ground-water system. This may be present only for a brief time after a large rainfall, and may be

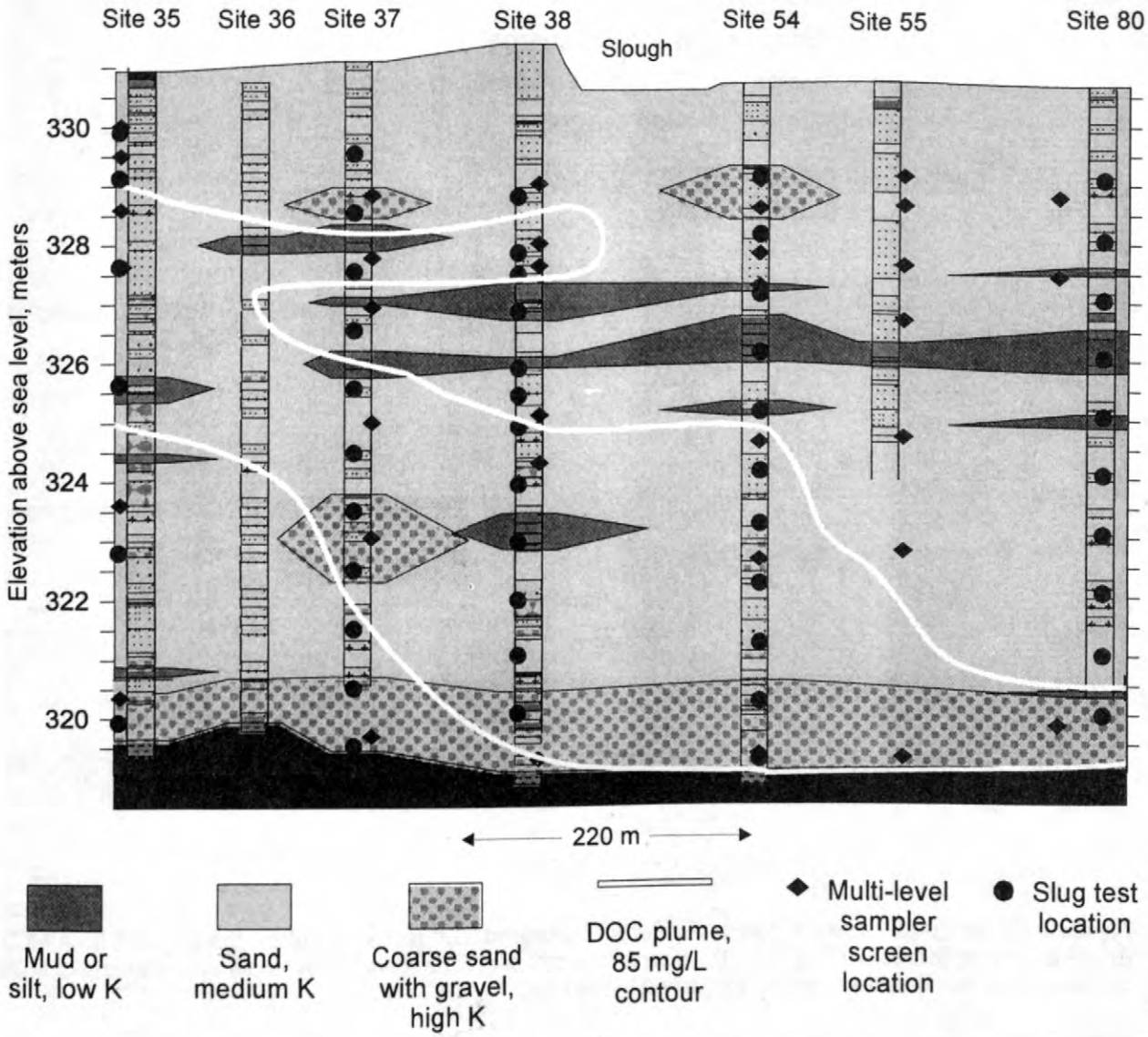

Figure 3. Generalized permeability structure in the alluvial aquifer along the multi-level sampler transect from site 35-80 at Norman landfill. The structure was formulated using core descriptions and slug test results. The outline of the contaminant plume is based on the 85 milligram per liter dissolved organic carbon (DOC) contour from samples taken in April, 1997.

an area where aerobic or facultative anaerobic bacteria are present. 2. Sulfur recycling zone – this zone is in the upper part of the water table, in the part of the aquifer where the water table fluctuates seasonally. This area likely has a relatively large influx of nutrients, carbon and electron acceptors. Sulfate reduction in anoxic water forms iron sulfides in the sediment, which may be oxidized when the area becomes unsaturated or oxygenated recharge infiltrates. As the water level rises, the water may become anoxic again and the cycle repeats. 3. Core of the plume – this area has the highest levels of dissolved organic carbon and methane. It likely has been an area of intensive microbial activity such that alternative electron acceptors are depleted and methanogenesis is an important biodegradation process. 4. Slough /ground water interaction zone – this involves two processes, upgradient leachate discharge to the slough and slough recharge to downgradient ground water. Where leachate enters the surface water, there is likely an active microbial community at the interface between the surface and ground water.

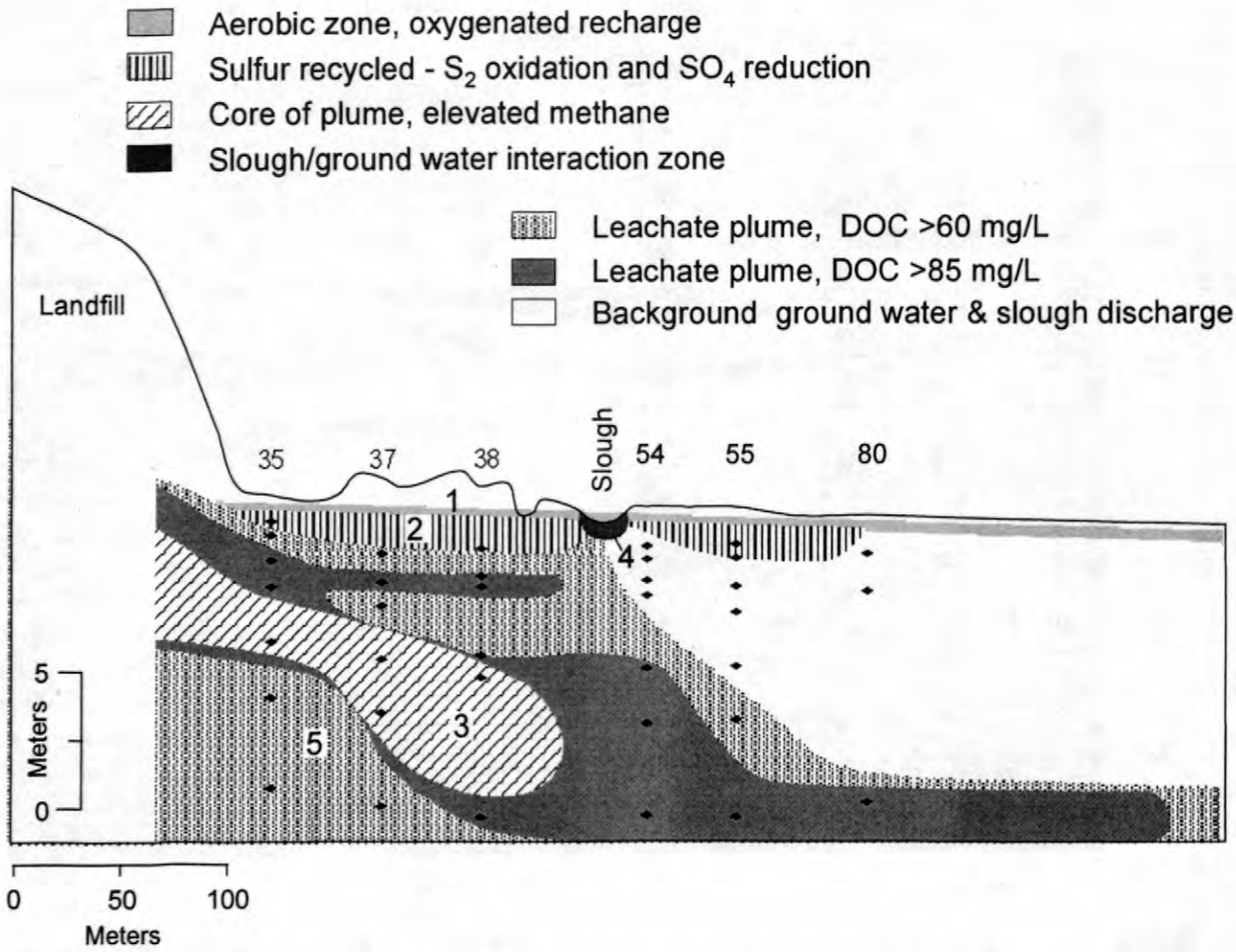

Figure 4. Conceptual model of zones of different biodegradation processes along the transect from MLS (multi-level sampler) 35 to MLS 80 at the Norman landfill site. The diamond symbols are locations of MLS screens. The numbered zones are discussed in the text.

Slough water recharges the aquifer on the downgradient side. It is unclear how contaminated the slough recharge is, and the slough water may be a source of fresh nutrients to the leachate plume below. 5. Edge of leachate plume – this is the interface between the leachate plume and background ground water or slough recharge and may occur at the leading edge of the plume, or where cleaner ground water flowing under the landfill mixes with the plume. The background ground water may contain higher levels of electron acceptors and nutrients than the core of the plume.

Superimposed upon the environments described above is another factor that affects biodegradation locations and rates – the permeability heterogeneity in the aquifer. The next section of this paper will describe the use of a numerical model to explore the effects of permeability heterogeneity on biodegradation processes in one of the environments described above, the core of the leachate plume. Questions still to be answered for the site include whether the low permeability areas are more or less contaminated than the surrounding sediments, and whether they are a source of nutrients or electron acceptors to surrounding depleted areas. For the higher permeability zones, questions involve degradation rates in these areas; degradation may be faster because of better supplies of nutrient and electron acceptors, or slower due to lower microbial populations or quick depletion of electron acceptors, leading to a less efficient degradation process.

USING A BIODEGRADATION MODEL TO GAIN INSIGHT ON PROCESSES

Previous work on how permeability heterogeneity affects biodegradation has provided some insight on possible processes at the landfill site. Studies by Aelion, 1996, Murphy and others, 1997, and Cozzarelli and others, (in press), showed that low permeability areas can act as sources of either contaminants or nutrients and electron acceptors, in contrast to the surrounding area. On the other hand, high permeability zones in a heterogeneous aquifer can transport contaminants faster than they can be degraded, leading to a large amount of dispersion in a contaminant plume. Studies using numerical models have shown that accurate determination of transport and biodegradation parameters in aquifers with heterogeneous permeability can be difficult (Ginn and others, 1995, Schafer and Kinzelbach, 1996, Miralles-Wilhelm and others, 1997).

A numerical model can help to evaluate possible effects of heterogeneity on biodegradation processes in the aquifer at the Norman site. A heterogeneous permeability distribution derived from the distribution of values shown in figure 2 was used with the BIOMOC model (Essaid and Bekins, 1997) to examine the evolution of terminal electron acceptor processes in different-permeability areas of a hypothetical contaminant plume. The model simulates the core of the plume at the landfill (zone 3 in the conceptual model above), but the model is at a larger scale and greatly simplified from the actual conditions at the site.

Model parameters

The model aquifer was two dimensional, 100 m long by 10 m deep, with 1 m by 0.25 m blocks. Hydraulic conductivity (K) ranged from 1.0×10^{-8} to 3.2×10^{-4} m/s. The K distribution was generated by sequential Gaussian simulation (Deutsch and Journel, 1992), conditioned on the Norman landfill slug test data set, which produced a permeability structure with the histogram distribution shown in figure 2. This method generates a permeability distribution with the general features of the aquifer at the site; it does not, however, reproduce the actual structure of the aquifer along the transect described above. The model domain contained low-permeability layers approximately 0.25 to 0.75 m thick and 5 to 50 m long, with a few high-permeability channels of similar dimensions in a matrix of moderate permeability. The contrasting-permeability layers at the landfill site are generally thinner, but the model discretization controlled the minimum thickness of layers.

The biodegradation processes in the model were sequential sulfate reduction and methanogenic degradation of BTEX; although there is little BTEX in the leachate, degradation reactions and rates have not yet been established for the bulk leachate or any compound in the leachate. Published information on BTEX degradation is readily available, so it works well as an example. Sequential biodegradation processes reflect that there is a limited amount of sulfate available and when it decreases below a threshold value, methanogenesis becomes the predominant degradation process. The rate of methanogenesis was one half the rate of sulfate reduction, and the assumption was made that nutrients are not limited in the system. Microbial populations were at steady state (no growth) and uniform everywhere that the hydraulic conductivity was above 1.0×10^{-6} m/s, and near zero elsewhere, so that effectively no degradation occurred in the lowest K areas. Several studies indicate that microbial populations are very low in low-permeability areas, but the studies do not agree as to whether populations in higher permeability areas are correlated in any predictable way with permeability (summarized in Scholl, written commun.).

The model boundary conditions were no flow on the top and bottom boundaries, and a head gradient of 0.0025 across the model domain. Inflow of solutes and water occurred along the entire left (upgradient) boundary and discharge occurred along the entire right (downgradient) boundary. The model included four solutes – the contaminant (substrate for degradation), sulfate (electron acceptor for sulfate reduction), bicarbonate (product of sulfate reduction), and methane (product of methanogenesis). Initial conditions in the model domain were a constant background concentration of sulfate, and no

contaminant, methane or bicarbonate. The upgradient boundary had influx of contaminant and sulfate at constant rate for the 50-year duration of the simulation.

The simulation does not use site-specific values for biodegradation processes, concentrations, or time since contamination, because degradation processes at the site have not yet been quantified. The model differs from the field situation in that leachate composition and strength in the aquifer under the landfill has certainly not been constant over the years. In most cases, there is a lag time before an indigenous microbial population 'learns' to degrade a compound; because this lag time is not included in this model, the estimates of time until steady state is reached should be considered as examples. In addition, the closed upper boundary in the model is not entirely representative of the situation in the aquifer, where influx of additional sulfate is possible. Still, if these approximations are acknowledged, the model does provide insight on how biodegradation may be affected by different permeability areas in the aquifer.

Model Results

As contaminant and sulfate entered the system at the start of the simulation, a plume of contaminant formed and sulfate reduction was the primary degradation process until sulfate became depleted. Methanogenesis then became the dominant degradation process, except near the upgradient boundary where the influx of sulfate allowed sulfate reduction to continue. At the end of the simulation (50 years), steady state had been reached in all but the lowest permeability areas, with the primary area of sulfate reduction in a narrow zone near the source at the upgradient boundary and methanogenesis predominating elsewhere. The rate of methanogenesis was low relative to the contaminant input rate, so that a plume of contaminant approximately 50 m long existed at steady state. Concentrations of biodegradation products (bicarbonate and methane) increased in the model domain until steady state was reached.

Three observation points in areas of different permeability in the model domain showed evolution of conditions through time in the simulation. The first observation point is 26 m downgradient from the source in a high-permeability zone that is well-connected to the source area. The contaminant reaches this area in about 0.7 years, and sulfate becomes depleted and methanogenesis becomes the dominant process in about 1.5 years (fig. 5A). By about 5 years, steady state has been reached. At steady state, there is a relatively high concentration of contaminant (5.5 mg/L, about 50% of the incoming concentration of 10 mg/L) since the rate of methanogenesis does not equal or exceed the rate of influx of contaminant to the area. Methane concentration is about 2 mg/L. The second observation point is also 26 m downgradient in the middle of an area of moderate permeability (fig. 5B). Here, sulfate depletion occurs and methanogenesis becomes dominant within 5 years. Steady state for all four solutes is reached in about 10-15 years. Contaminant concentration in this area is quite low (about 0.25 mg/L, less than 3% of the incoming concentration) because the rate of transport into the area does not exceed the degradation rate by very much. Methane concentration here is around 5 mg/L. The third observation point is at 14 m downgradient in the middle of a silt/mud layer with $K=1.0\times10^{-8}$ m/s. In this area, microbial populations are near zero and effectively no degradation occurs, so changes in concentration are due to flow in or out of the silt layer. It takes about 6.5 years before sulfate begins to decrease in the area in response to depleted concentrations elsewhere (fig. 5C). Sulfate concentration continues to decrease slowly but does not reach zero by the end of the 50-year simulation. Bicarbonate and methane degradation products begin to enter the silt layer at 6.5 years and appear to approach steady state concentrations in the 50 year time period. Contaminant concentrations in the silt are insignificant compared to the incoming concentration and remain low throughout the simulation, probably because contaminant is degraded quickly in the area surrounding the silt layer due to availability of sulfate from the silt layer.

The difference in contaminant and product concentrations between the high and moderate permeability areas (fig. 5A, B) shows that

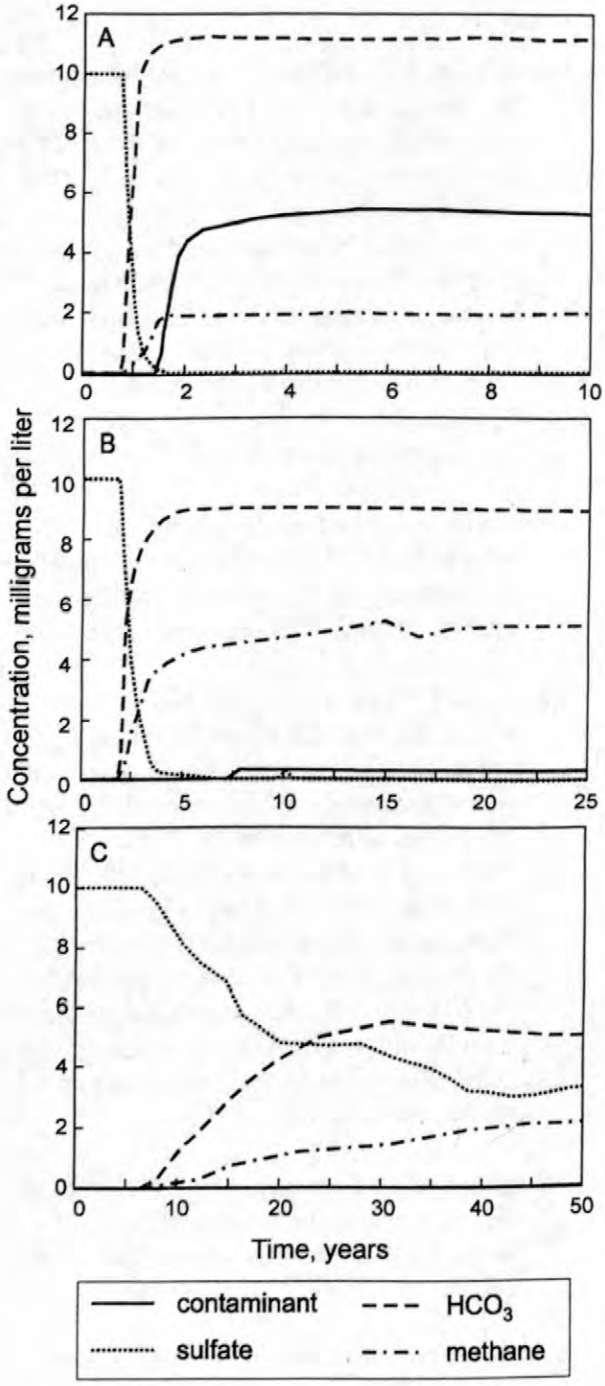

Figure 5. Simulation results from BIOMOC showing changes in average concentration of four solutes representing products and reactants in sulfate reduction and methanogenesis. Concentration changes are shown over time at three observation points in different permeability areas in the model domain. Note the different time scales on the x axis. A. high-permeability zone, B. moderate-permeability zone, C. low-permeability zone.

degradation appears to be more efficient in the moderate permeability area, with all factors except permeability being equal. The lowest permeability area stayed relatively uncontaminated throughout the simulation. The time taken to reach steady-state concentrations is also very different between the three areas. Some of the methods for determining field biodegradation rates require that concentrations be at steady state; these results illustrate that in heterogeneous aquifers, different parts of the system reach steady state at different times. Concentrations at a point are a result of both transport into the area and production or loss in the area, so in the high permeability area, input exceeds degradation whereas in the moderate permeability area, the rate of degradation nearly balances the rate of input. In the lowest permeability area, no degradation occurs, but the electron acceptor is decreasing and products are accumulating simply from transport processes. If biodegradation rates were calculated from a concentration history in one of these areas using the average hydraulic conductivity from the site and assuming uniform microbial populations, the apparent degradation rates would be very different. These results illustrate the need to measure the permeabilities and sample over the range of permeabilities at a contaminated site to determine an overall degradation rate. The number of samples needed to accurately characterize degradation rates and processes at the Norman landfill site will depend on the range of permeabilities in the area of interest and at what scale the permeability variations are compared to the scale of the plume. For the Norman site, it will be important to characterize the low permeability areas as well as the high permeability areas to see whether the low permeability areas have remained relatively clean, as in the simulation, or act as reservoirs of contaminants. In the highest permeability areas, the rate of transport may exceed the rate of degradation, leading to high contaminant concentrations in those areas.

SUMMARY

The aquifer at the Norman landfill site has sediments ranging from clay to gravel and measured hydraulic conductivity ranging from less than 2.4×10^{-7} to 2.8×10^{-4} m/s. This alluvial aquifer is relatively heterogeneous in terms of permeability, with both lower and higher permeability layers in a matrix of moderate permeability medium-grained sand. Biodegradation processes for the leachate plume are likely to vary with hydrologic and chemical heterogeneities in the environment, including permeability variations, surface water interaction, and recharge from rainfall. A conceptual model was formulated to classify these different environments, and future work at the site will result in refinement of this model. Simulation with a numerical model suggested that low-permeability areas in the aquifer may be relatively uncontaminated, and act as reservoirs of electron acceptors to the surrounding contaminated areas. The simulation also suggested that preferential electron acceptors are depleted very quickly in the highest-permeability areas, leading to higher contaminant concentrations due to less-efficient degradation processes and high rates of transport in these areas. Determination of the total amount of biodegradation occurring for the bulk leachate plume will require identification and detailed sampling of the areas where most degradation is occurring. In addition, careful measurement of variations in ground water flow parameters will be necessary to determine accurate degradation rates in those areas.

REFERENCES

Aelion, C. Marjorie, 1996, impact of aquifer sediment grain size on petroleum hydrocarbon distribution and biodegradation, Journal of Contaminant Hydrology, v. 22, p. 109-121.

Bjerg, P.L., Hinsby, Klaus, Christensen, T.H. and Gravesen, Peter, 1992, Spatial variability of hydraulic conductivity of an unconfined sandy aquifer determined by a mini slug test, Journal of Hydrology, v. 136, p. 107-122.

Christenson, S.C., Scholl, M.A., Schlottmann, J.L., and Becker, C.J., 1999, Ground-water and surface-water hydrology of the Norman landfill research site, in Morganwalp, D.W., and Buxton, H.T., eds., U.S. Geological Survey Toxic Substances Hydrology Program--Proceedings of the Technical Meeting, Charleston, South Carolina, March 8-12, 1999--Volume 3 – Subsurface Contamination from Point Sources: U.S. Geological Survey Water-Resources Investigations Report 99-4018C, this volume.

Cozzarelli I.M., Herman, J.S., Baedecker, M.J., and Fischer, J.M., in press, Geochemical heterogeneity of a gasoline-contaminated aquifer, Journal of Contaminant Hydrology.

Cozzarelli I., Suflita, J., Ulrich, G., Harris, S., Scholl, M., Norvell, J. and Jaeschke, J., 1999, Biogeochemical processes in a contaminant plume downgradient from a landfill, Norman, Oklahoma, in Morganwalp, D.W., and Buxton, H.T., eds., U.S. Geological Survey Toxic Substances Hydrology Program--Proceedings of the Technical Meeting, Charleston, South Carolina, March 8-12, 1999--Volume 3 – Subsurface Contamination from Point Sources: U.S. Geological Survey Water-Resources Investigations Report 99-4018C, this volume.

Deutsch, C.V. and Journel, A.G., 1992, GSLIB, Geostatistical software library and user's guide, Oxford University Press, New York, 340 p.

Eganhouse, R.P., Matthews, L.L., Cozzarelli, I.M., and Scholl, M.A., 1999, Evidence for natural attenuation of volatile organic compounds in the leachate plume of the Norman, Oklahoma landfill, in Morganwalp, D.W., and Buxton, H.T., eds., U.S. Geological Survey Toxic Substances Hydrology Program--Proceedings of the Technical Meeting, Charleston, South Carolina, March 8-12, 1999--Volume 3 – Subsurface Contamination from Point Sources: U.S. Geological Survey Water-

Resources Investigations Report 99-4018C, this volume.

Essaid, H.I. and Bekins, B.A., 1997, BIOMOC, A multispecies solute-transport model with biodegradation, U.S. Geological Survey Water-Resources Investigations Report 97-4022, 68 p.

Ginn, T. R., Simmons, C. S., Wood, B. D., 1995, Stochastic-convective transport with nonlinear reaction: biodegradation with microbial growth, Water Resources Research, v. 31, no. 11, p. 2689-2700.

Hess, K.M., Wolf, S.H., Celia, M.A., 1992, Large-scale natural gradient tracer test in sand and gravel, Cape Cod, Massachusetts; 3, Hydraulic conductivity variability and calculated macrodispersivities, Water Resources Research, v. 28, no. 8, p. 2011-2027.

Miralles-Wilhelm, F., Gelhar, L.W., and Kapoor, V., 1997, Stochastic analysis of oxygen-limited biodegradation in three-dimensionally heterogeneous aquifers, Water Resources Research, v. 33, no. 6, p. 1251-1263.

Murphy, E.M., Ginn, T.R., Chilakapati, Ashokkumar, Resch, C.T., Phillips, J.L., Wietsma, T.W., and Spadoni, C.M., 1997, The influence of physical heterogeneity on microbial degradation and distribution in porous media, Water Resources Research, v. 33, no. 5, p. 1087-1103.

Rehfeldt, K.R., Boggs, J.M., Gelhar, L.W., 1992, Field study of dispersion in a heterogeneous aquifer; 3, Geostatistical analysis of hydraulic conductivity, Water Resources Research, v. 28, no. 12, p. 3309-3324.

Schafer, W. and Kinzelbach, W.K.H., 1996, Transport of reactive species in heterogeneous porous media, Journal of Hydrology, v. 183, no. 1-2, p. 151-168.

Scholl, M.A. and Christenson, Scott, 1998, Spatial variation in hydraulic conductivity determined by slug tests in the Canadian River alluvium near the Norman landfill, Norman, Oklahoma, U.S. Geological Survey Water Resources Investigations Report 97-4292, 28 p.

Scholl, M.A., written commun., Effects of heterogeneity in aquifer permeability and biomass on biodegradation rates calculated from field data – results from numerical simulations, submitted to Ground Water.

Sudicky, E.A., 1986, A natural gradient experiment on solute transport in a sand aquifer: spatial variability of hydraulic conductivity and its role in the dispersion process, Water Resources Research, v. 22, no. 13, p. 2069-2082.

AUTHOR INFORMATION

Martha A. Scholl and Isabelle M. Cozzarelli, U.S. Geological Survey, Reston, Virginia (mascholl@usgs.gov)

Scott C. Christenson and Jamie L. Schlottmann, U.S. Geological Survey, Oklahoma City, Oklahoma

George N. Breit, U.S. Geological Survey, Denver, Colorado

Hydraulic Conductivity Reductions Resulting from Clay Dispersion within Alluvial Sediments Impacted by Sodium-rich Water

By Lance J. King and Harold W. Olsen, Colorado School of Mines, Golden, Colorado, and George N. Breit, U.S. Geological Survey, Denver, Colorado.

ABSTRACT

Substantial reductions in hydraulic conductivity (HC) of soils and sediment can result from dispersion of clay into flowing ground water. Smectitic clays with high amounts of exchangeable sodium are particularly likely to disperse into ground water if the ionic strength of the pore water substantially decreases. Our experimental study evaluated the HC decrease possible due to clay dispersion resulting from a sodium-rich leachate plume moving through smectite-containing alluvium near the Norman Landfill, Oklahoma. Core samples of alluvium were placed in a triaxial cell and flushed with background water, NaCl solutions and distilled water. These tests detected substantial dispersion of clay that was associated with decreases in HC of more than two orders of magnitude from 4.38×10^{-3} cm/sec to 2.05×10^{-5} cm/sec (centimeters per second) in sediments containing less than 5 percent clay-sized particles. The change in HC attributable to clay dispersion can change the distribution of hydraulic conductivity in an aquifer. Such changes need to be considered in forecasting plume migration and developing remediation strategies.

INTRODUCTION

Clays within sediments consist of books or packets of clay plates and aggregates of these packets that stick together when the attractive forces between the plates are larger than the repulsive forces associated with interactive diffuse double layers between the clay plates and packets. Clays disperse when increasing repulsive forces cause the packets in clay aggregates to separate. Interparticle repulsive forces increase with increasing percentages of sodium on the exchange sites of clay particles and with decreasing ionic strength of the pore water. Dispersion of clay and loss of hydraulic conductivity can be induced by sequentially passing sodium-rich saline water and dilute water through a sediment or soil. Within sediments and soils, the dispersed clay can move with the pore water and accumulate at pore throats permanently decreasing hydraulic conductivity (Shainberg, and others, 1981). Smectite is particularly prone to dispersion relative to other clay minerals because of its high content of exchangeable ions and generally small particle size (McNeal and Coleman, 1966). Examples in which the effect has been demonstrated include irrigated lands (Quirk and Schofield, 1955; McNeal and Coleman, 1966; Pupisky and Shainberg, 1979; and Shainberg and others, 1981) and sea water incursion (Goldenberg and others, 1983). Surfactants injected for remediation have also been demonstrated to increase clay dispersion in the subsurface, resulting in decreased hydraulic conductivity (Renshaw and others, 1997).

The objective of our research is to determine if and to what extent clay dispersion and loss of hydraulic conductivity may occur in the Canadian River alluvium surrounding the closed Norman Landfill, Oklahoma. Clay dispersion is considered possible because a sodium–rich leachate plume with a sodium concentration of 770 mg/L (milligrams per liter) (background is 31 mg/L) and dissolved-solids

concentration of 5500 mg/L is moving through the smectite-containing alluvium. The passage of a leachate plume is being simulated in the laboratory using simplified solution compositions and relatively undisturbed core samples. The intent is to determine if clay dispersion and decreased hydraulic conductivity are plausible at the landfill site. Test results demonstrate that hydraulic conductivity decreased by over two orders of magnitude and that a substantial amount of clay is dispersed even in samples with less than 5 percent clay.

GEOLOGIC SETTING

The closed Norman municipal landfill (Norman Landfill) is located on the flood plain of the Canadian River. Alluvium near the landfill is typically 11 meters thick and contains between 85 and 95 percent sand with the remaining sediment composed mainly of silt, mud, and gravel. Fine planar laminations are common in the upper 2 to 3 meters of sandy sediment. The laminations are defined by increased amounts of clay and silt, and occasionally heavy minerals. Below ten feet, the sediment is typically massive. Sand in the top 8 meters of the alluvium is typically fine to medium grained. The bottom 3 meters has some layers containing coarse sand, granules, and pebbles. Sand layers contain from 0.6 to 12 percent clay (<2 μm (micrometers)); mud layers typically contain 50 percent clay-sized particles. Discrete mud layers are distributed vertically through the sediment and vary from 0.01 to 1 meter thick. Sand ranges from well to very poorly sorted; mud layers are poorly sorted. Major framework grains include quartz, feldspar, calcite, and clay with minor amounts of dolomite and hematite. Clay minerals identified in the < 2 μm fraction include smectite, with lesser amounts of illite-smectite, kaolinite, and chlorite-smectite. Cation exchange capacity of the <2 μm fraction is about 85 milliequivalents per 100 grams. Major exchangeable cations are calcium, magnesium, and sodium. The proportion of exchangeable sodium increases in the clay fraction affected by the landfill leachate.

METHODS

Our experimental methods are designed to simulate the introduction and subsequent displacement of leachate or other sodium-rich water from a saturated sediment under a flow field that resembles natural conditions as closely as possible. This sequence of events, under natural flow conditions was expected to cause a decrease in the HC. Faster flow rates may induce dispersion due to mechanical effects (Rowel and others, 1969). The flow rate used for our tests is $4.616 \times 10^{-4} cm^3/sec$, which corresponds to an average hydraulic gradient of approximately 0.01 (cm H_2O/cm of sample thickness). Although this is approximately three times greater than the field values found near the Canadian River (approximately 0.003 (cm H_2O/cm of sample thickness)), it was the minimum necessary to obtain reliable measurements and is considered sufficiently slow to simulate natural conditions.

A triaxial cell-based system was used to establish the required low hydraulic gradients (Olsen, 1966; Olsen and others, 1994). The pressure difference across the sample under conditions of constant flow is used to determine changes in HC (fig. 1). Conventional constant head and falling head measurements of HC cause gradients of up to 3 orders of magnitude greater than those that can be achieved by this system, (ASTM, 1996). The system is constructed of 316 stainless steel to minimize corrosion and changes in the water chemistry related to the experimental system. The influent and effluent reservoirs are constructed of acrylic to allow visual observation of the influent and effluent.

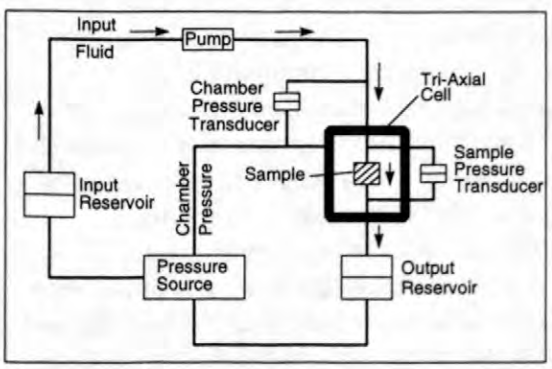

Figure 1. Schematic diagram of the experimental apparatus.

Alluvial sediment cores were collected by rotosonic drilling at locations along the hydrologic gradient and within 400 meters of the Norman landfill. Samples of the core selected for experimental study were apparently unaffected by the landfill leachate. All samples were chosen to have an initial HC between 10^{-4} cm/sec and 10^{-3} cm/sec to allow the use of a single flow rate for the entire test. The samples used were minimally disturbed prior to placement in the experimental system. Cylindrical subsamples 6.5 centimeters in diameter, and approximately 7.5 centimeters long were cut from the core using a hydraulic ram, and a circular cutting device. The subsamples were mounted in the triaxial cell with porous stones equivalent to a fine to medium grained sand at each end so that any suspended solids could pass out of the sample with the effluent. The samples were mounted to simulate flow perpendicular to the bedforms of the sediment. This orientation is intended to simulate downward movement of surface recharge, the abrupt termination of bedforms in fluvial sediments, and the observed downward movement of the leachate plume in the alluvium. Some future samples may be mounted to simulate flow parallel to bedforms. Descriptions of the samples used and the tests performed on them are presented in table 1. The samples were flushed with the different solutions for different times to try to determine how significant exposure time was to the process.

The samples mounted in the triaxial cell were flushed at a rate of 2 pore volumes per day. The number of pore volumes of the various solutions varied among the samples depending on completeness of ion exchange and conditions tested (table 1). Completeness of ion exchange was determined by measuring the concentration of calcium in the effluent, because calcium is the dominant ion on the exchange sites. The first solution simulated the cation composition of ground water distant from the leachate plume (background water). This solution was used to determine an initial HC value. Background water was followed by 0.1M, 1 M and 0.01M NaCl to exchange sodium for other ions. Maximum reported sodium concentration in Norman landfill leachate is only about 0.03 M. Higher concentrations of sodium in the permeant were used to increase the rate and degree of cation exchange. Permeation with 1M NaCl in samples 2, 3 and 4 was continued until the calcium concentration of the sample effluent was less than 1 mg/L indicating that cation exchange was largely complete. For sample 1, permeation with 1M NaCl was limited to 2 pore volumes leading to incomplete replacement of "background" cations with sodium. This was intended to assess the effect of limited exposure to sodium-rich solutions. The solutions subsequently passed through the samples were selected to test sample response to decreasing ionic strength water.

Table 1. Description of samples, composition of solutions, and number of pore volumes for each solution used in the experiments. [Background water composed of: 166 mg/L Ca^{2+}, 45 mg/L Mg^{2+}, 31 mg/L Na^{+}, and 8 mg/L K^{+} to simulate groundwater unaffected by landfill leachate. N/A, not applicable. M, molar]

	Pore Volumes			
	Sample 1	Sample 2	Sample 3	Sample 4
Sequence of solution compositions	VC-F 11.1'-11.9' Massive sand 11.4 % silt and clay	VC-I 31.0'-31.8' Massive sand 10 % silt and clay	VC-G 9.4'-10.2' Laminated sand 3-5 % silt and clay	VC-G 16.3'-17.1' Massive sand 3-5% silt and clay
1) Background	0.01	8	4	4
2) 0.1M NaCl	4	2	4	4
3) 1M NaCl	2	18	20	34
4) 0.01M NaCl	5	20	20	N/A
5) Distilled Water or	6	26	115	N/A
5) Background	N/A	N/A	N/A	78

Although the natural waters in this region have bicarbonate as the dominant anion, each of these solutions were prepared using chloride salts.This change from the natural environment was deemed necessary to avoid calcite scale formation within the test apparatus. The effect of anions on the thickness and character of clay double layers during dispersion is considered small at low ionic strengths (Bohn and others, 1985).

Samples of the effluent were collected every 2 pore volumes for analysis. The frequency of effluent sample collection was decreased to every 4 or 6 pore volumes after the sodium concentration in the effluent did not change by more than approximately 0.001M over 2 pore volumes. These samples were analyzed for pH and the concentrations of suspended solids, calcium, magnesium, potassium, and sodium.

RESULTS

The concentrations of major ions in the effluent vary during the experiments. Potassium, calcium, and magnesium concentrations rise in the effluent during flushing with 1M NaCl (fig. 2) because of cation exchange of sodium for other ions. When these concentrations drop close to zero once again, the cation exchange is close to completion. The concentrations of calcium and magnesium also increased during elution with distilled water near the end of samples 2 and 3. The increased concentrations are attributed to calcite and dolomite dissolution. Calculations indicate that approximately 3 percent of the calcite present in the sample (bulk sediment contains about 1 wt. percent calcite) would have had to dissolve to produce the concentrations of calcium observed in the effluent. This would have had the effect of slightly increasing pore space, and possibly dissolving some cement freeing slightly more dispersed clay. Both effects should have had minimal effects on our results.

In sample 4, which was flushed with background water containing both calcium and magnesium (table 1), the levels of calcium and magnesium in the effluent were lower than the background water concentrations. The decrease is attributed to exchange of these elements for sodium on the exchange sites.

The hydraulic conductivity (HC) of every sample decreased upon the passage of low ionic strength water following the NaCl solutions.

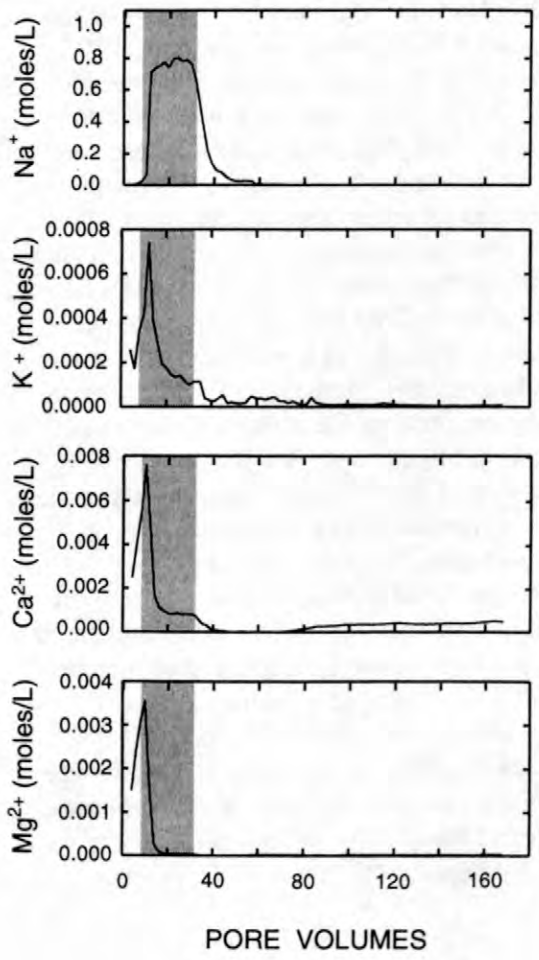

Figure 2. Profile of concentration (moles per liter) changes of sodium, potassium, calcium, and magnesium in effluent from sample 3. These results are typical of the profiels measured. Shaded interval identifies passage of 1 molar NaCl through the sample.

Figures 3 and 4 show the pattern of HC fluctuations caused by changes in the influent composition. Five stages of HC change were identified for samples in which replacement of sodium-rich water with rainwater (distilled water) was simulated (Samples 1, 2, and 3) (figs. 3, 4). Initially (stage 1) the HC increased as background water and 0.1M NaCl passed through the sample. The HC remained relatively constant during elution with 1M NaCl. Initial elution with 0.01M

NaCl decreased HC (stage 2), but this was followed by a slight increase in HC (stage 3) until elution with distilled water began. During elution with distilled water the HC dropped substantially (stage 4). In stage 5, the HC rose to a value close to the initial HC after the decrease due to distilled water. Stage 5 was only observed in sample 1, which did not undergo complete cation exchange.

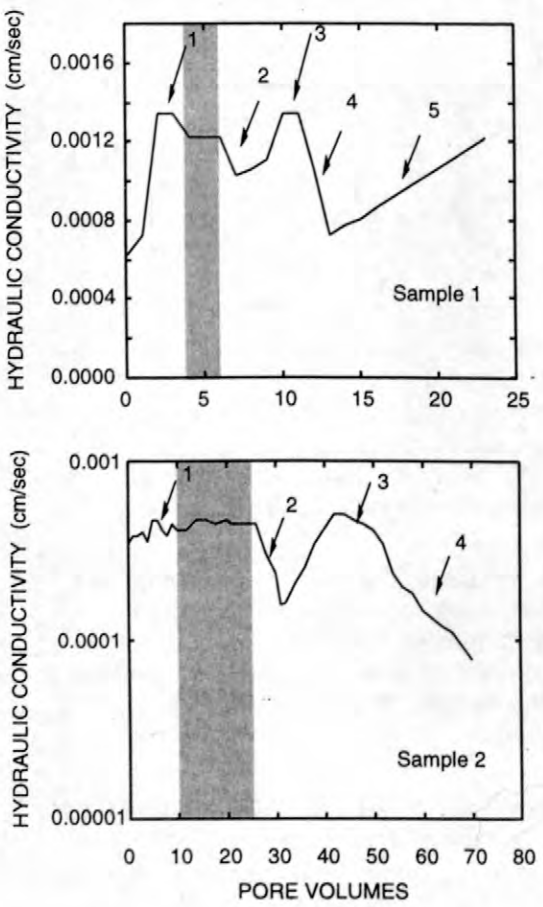

Figure 3. Hydraulic conductivity relative to the cumulative pore volumes eluted through samples 1 and 2. Shaded interval identifies passage of 1 molar NaCl through the sample. Arrows identify stages of hydraulic conductivity change. [Stage 1: Slight hydraulic conductivity increase due to increased ionic strength. Stage 2: Hydraulic conductivity drop due to 0.01 M NaCl influent. Stage 3: Hydraulic conductivity rise due to incomplete dispersion at 0.01 M NaCl. Stage 4: Hydraulic conductivity drop due to distilled water. Stage 5: Hydraulic conductivity increase (sample 1) attributed to incomplete cation exchange.]

Sample 4 differs from the above in that water simulating background ground water was used instead of distilled water following the sodium-rich water. This sample displayed only two distinct stages in its HC reduction curve (fig. 4). An intial increase in HC is similar in magnitude to the rise in HC seen during stage 1 in the other three samples. This stage ended after about 55 pore volumes with a short term rise in HC from 2.54×10^{-3} to 3.82×10^{-3} over 8 pore volumes. Following this rise, the HC proceeded to decrease by approximately 1.5 orders of magnitude over the next 66 pore volumes.

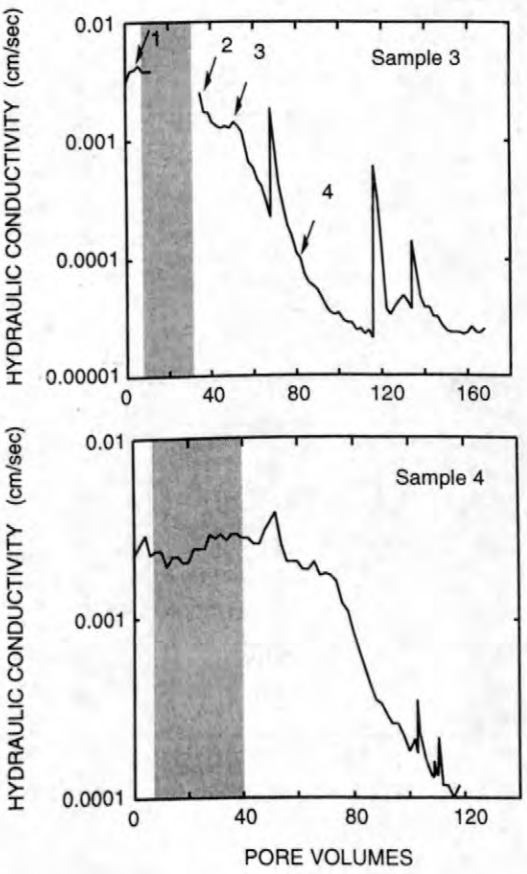

Figure 4. Hydraulic conductivity relative to the cumulative pore volumes eluted through samples 3 and 4. Shaded interval identifies passage of 1 molar NaCl through the sample. Arrows identify stages of hydraulic conductivity change. [Stage 1: Slight hydraulic conductivity increase due to increased ionic strength. Stage 2: Hydraulic conductivity drop due to 0.01 M NaCl influent. Stage 3: Hydraulic conductivity rise due to incomplete dispersion at 0.01 M NaCl. Stage 4: Hydraulic conductivity drop due to distilled water.]

This decrease is simlar to stage 4 in other samples. The end of this decrease was characterized by brief fluctuations of the HC, which are attributed to reorganizations and consolidations of the clay clogging the pores.

Figures 5 and 6 plot the concentrations of suspended solids against pore volumes of flow through each sample. Concentrations of suspended solids near 0.8 g/L were measured in sample 3 and a maximum of 1.2 g/L was measured in sample 2. Maximum concentrations of suspended solids were detected early in the passage of the distilled water following the NaCl solutions. Sample 4 showed only a slight increase in suspended solids when background water followed the NaCl solutions. However, suspended solids in sample 4 remained below detection (<0.02 g/L) during the main decrease in HC (fig. 6).

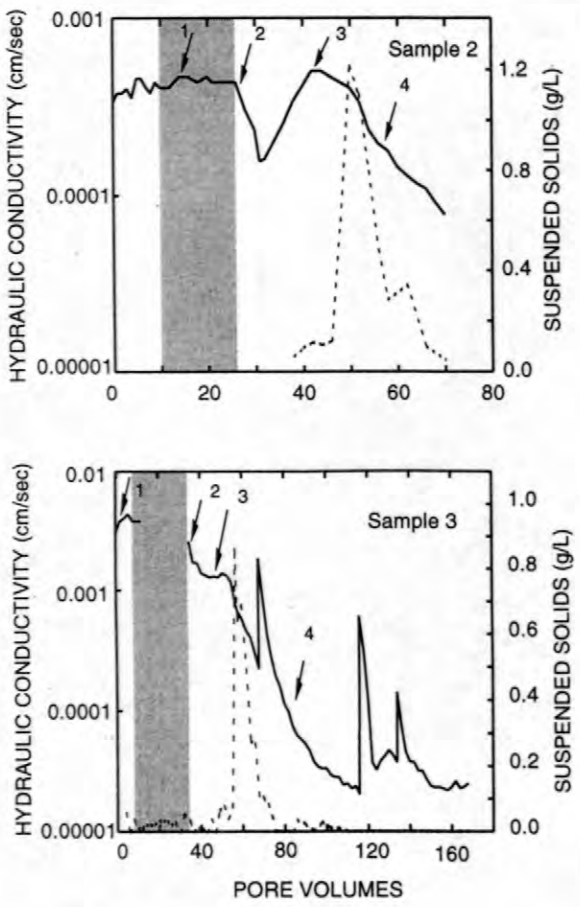

Figure 5. Hydraulic conductivity (solid line) and suspended solids concentration (dashed line) relative to the number of pore volumes eluted through samples 2 and 3. Shaded interval identifies passage of 1 molar NaCl through the sample. Arrows identify stages of hydraulic conductivity change. [Stage 1: Slight hydraulic conductivity increase due to increased ionic strength. Stage 2: Hydraulic conductivity drop due to 0.01 M NaCl influent. Stage 3: Hydraulic conductivity rise due to incomplete dispersion during elution with 0.01 M NaCl. Stage 4: Hydraulic conductivity drop due to distilled water.]

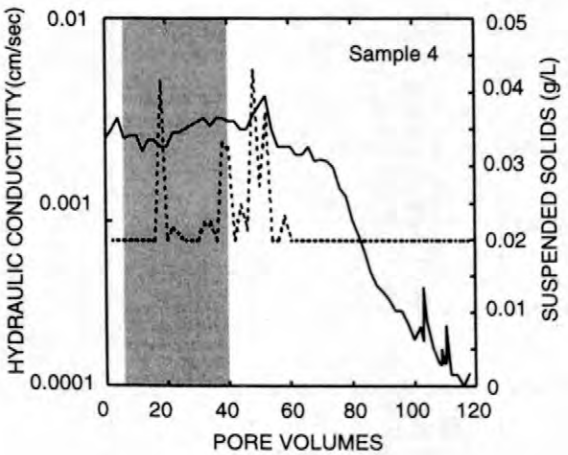

Figure 6. Hydraulic Conductivity (solid line) and suspended solids concentration (dashed line) relative to cumulative pore volumes in sample 4. Shaded interval identifies passage of 1 molar NaCl through the sample. Stages were not recognized for sample 4.

The pH of the effluent increased from the value of the influent (approximately 7) to values as large as 10 in sample 2 but remained below 8.5 in samples 3 and 4. The pH increase is attributed to corrosion of the stainless steel of the system in the presence of the strong NaCl solutions. High pH can affect the edge charge of clay particles and therefore their dispersion characteristics. Smectitic clays have a high face to edge charge ratio (Bohn and others, 1985). For this reason smectitic clays are not as strongly affected by changes to edge charge as are kaolinite and other clay minerals (Bohn and others, 1985). Clays in the Canadian River alluvium are mainly smectite, therefore the effect of pH on edge charge is unlikely to be substantial. The increase in pH may limit the application of these results to some natural environments.

DISCUSSION

Hydraulic Conductivity Changes

Five stages of hydraulic conductivity change were shown on figures 3 and 4 for the samples which were exposed to distilled water (Samples 1-3). Proposed mechanisms for each stage of the change in HC are described in detail below.

Stage 1: Slight HC Increase

During flushing with background, 0.1 M NaCl and 1 M NaCl the ionic strength of the pore fluid increased resulting in a decrease in the double layer thickness around the clay particles. This causes the clay aggregates to shrink. However, the exchange of sodium onto the exchange sites of the clays tends to thicken the clays, causing the aggregates to swell. Based on our HC observations, the net effect appears to be a slight shrinkage of the clay aggregates which opens the pore throats of the sediment, allowing more fluid flow, and therefore higher HC values.

Stage 2:HC Decrease

As the ionic strength of the influent is decreased to 0.01 M NaCl following cation exchange, the double layer thickens which increases the distance between clay particles. This swelling acts to restrict fluid flow through the pore throats. In addition, some clay is pushed to the point where interparticle attractive forces can no longer hold it together, it disperses, and moves with the pore water to collect at constrictions in the flow path. This accumulation at pore throats reduces the HC. The increase in suspended solids seen at the beginning of stage 2 (See figs. 5 and 6) is attributed to initial dispersion of the clay.

Stage 3: HC Increase

HC increases after the decrease described in stage 2, but the mechanism is uncertain. Pupisky and Shainberg (1979) proposed that the increase could result from erosion of the thin layer of clay that clogged the pore throats. No increase in suspended solids was measured concurrent with the increase in HC we observed. Therefore either the eroded clay was redeposited within the sample or the increase is related to another process.

Stage 4: Major HC Decrease

Clay dispersion increased substantially during passage of distilled water in samples 1, 2 and 3. This dispersion is attributed to increasing repulsive forces. In addition, Emerson and Bakker, (1973) suggested that osmotic gradients could develop between the center of clay aggregates equilibrated with high ionic strength water and low ionic strength pore fluids. This gradient would promote dispersion of the clay aggregates. When distilled water is first introduced to the sample, conditions favorable for such a gradient are present. The large release of dispersed clay particles causes an immediate decrease in HC followed by a long steady reduction interpreted to indicate that the amount of clay accumulating at the pore throats is increasing.

Stage 5: Linear HC Increase

After reaching a low value of approximately 1.04×10^{-3} cm/sec the HC of sample 1 increased in a linear fashion (fig. 3). This may be attributed to erosion of the clay that was clogging the pore throats. An increase in suspended solids (not shown) was observed in the effluent during this stage which verifies that clay was eroding from the sample. The clay was able to erode, as possibly occurred during stage 3 in the other samples, because the amount of dispersed clay was insufficient to permanently clog the sediment's pore throats. The lack of sufficient clay to permanently clog the pore throats is attributed to incomplete exchange of sodium for calcium and magnesium. These results for only sample 1, which was exposed to the 1M NaCl for a short time, suggest that when sodium exchange is not complete the HC reduction is reversible.

Sample 4

Changes in HC in sample 4 did not correspond to the stages defined for samples 1 through 3 and therefore are described separately. The HC reductions in sample 4 did not occur immediately upon replacement of the 1M NaCl by dilute water (background water in this sample) as in the other three samples (figs. 3 and 4). Because of the use of background water, instead of distilled water, the ionic strength of the pore water took longer to decrease. In addition, the concentration of calcium in the effluent did not reach the value of the influent until almost 80 pore volumes after the re-introduction of background water (fig. 4). This implies that calcium was exchanging for sodium. Substitution of calcium would act to inhibit clay dispersion by placing more divalent cations between the clay platelets. As sodium was replaced by calcium, the ionic strength the pore fluid needed to cause dispersion would correspondingly decrease (Emerson and Bakker, 1973). Nonetheless, in this case HC substantially decreased, indicating that the ionic strength of the pore fluid dropped low enough to cause dispersion before calcium exchange was complete enough to prevent the dispersion. In other samples under slightly differing conditions, the opposite could have been true, and possibly no reduction in HC would have taken place.

Hydraulic Conductivity, Sodium Concentration Correlation

Rapid increases in the hydraulic gradient across sample 3 took place during the distilled water phase of sample 3's testing. The hydraulic gradient increased to a maximum of approximately 3 feet H_2O/foot sample and returned to the original gradient within 0.25 to 1 seconds. In response to these spikes, the HC of the samples briefly rose then decreased once again, resuming its pre-spike HC reduction curve within a few pore volumes (fig. 6). The HC increase was likely due to erosion of the clay clogging the pores of the sample followed by redeposition, which caused the HC to resume its pre-spike value.

Investigation of this change led to the discovery of an interesting correlation.

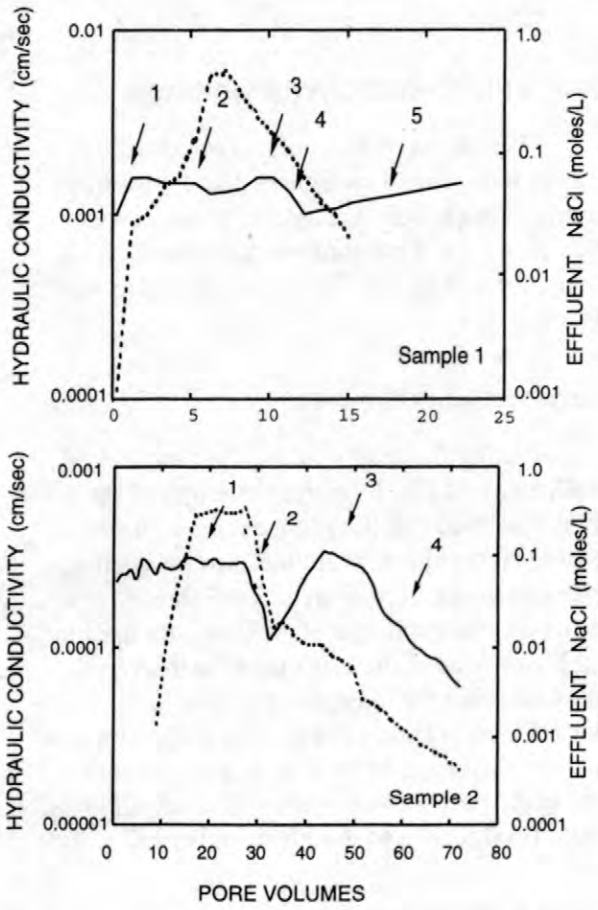

Figure 7. Hydraulic conductivity (solid line) and effluent NaCl molarity (dashed line) relative to cumulative pore volumes for samples 1 and 2. Arrows identify stages of hydraulic conductivity change. [Stage 1: Slight hydraulic conductivity increase due to increased ionic strength. Stage 2: Hydraulic conductivity drop due to 0.01 M NaCl influent. Stage 3: Hydraulic conductivity rise due to incomplete dispersion at 0.01 M NaCl. Stage 4: Hydraulic conductivity drop due to distilled water. Stage 5: Hydraulic conductivity increase (sample 1) attributed to incomplete cation exchange during 1M NaCl influent stage.]

Figures 7 and 8 plot the logarithm of the NaCl concentration of the effluent along with the logarithm of the HC for each sample. The HC decrease for sample 1 did not progress far enough to observe the relationship between these two variables, but samples 2 and 3 show a strong correlation between HC and effluent NaCl concentration. The slow decrease in the NaCl concentration and the ionic strength of the pore

fluid would slowly increase the average double layer thickness throughout the samples. This would gradually allow progressively more clay particles to disperse, and join the other particles clogging the pore throats. Sample 4 does not show a strong correlation between HC and effluent ionic strength, likely due to the delay in clay dispersion caused by calcium cation exchange as described above.

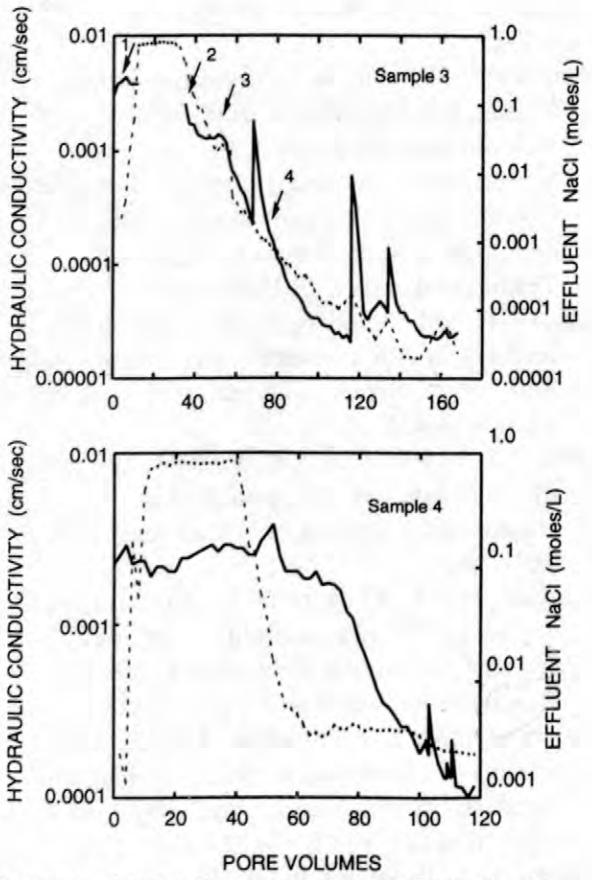

Figure 8. Hydraulic conductivity (solid line) and effluent NaCl molarity (dashed line) relative to cumulative pore volumes in samples 3 and 4. Arrows identify stages of hydraulic conductivity change. Stages were not recognized for sample 4. [Stage 1: Slight hydraulic conductivity increase due to increased ionic strength. Stage 2: Hydraulic conductivity drop due to 0.01 M NaCl influent. Stage 3: Hydraulic conductivity rise due to incomplete dispersion at 0.01 M NaCl. Stage 4: Hydraulic conductivity drop due to distilled water.]

CONCLUSIONS

When relatively undisturbed samples of Canadian River alluvium were exposed to a sequence of solutions with high contents of sodium followed by low ionic strength waters, their hydraulic conductivity (HC) decreased by more than two orders of magnitude. The magnitude of HC reduction increased as the degree of sodium substitution on the cation exchange sites increased, and as the ionic strength of the pore fluid decreased. This phenomenon is dependent on the dispersal of clays into the pore water as is indicated by the amounts of suspended solids measured in the effluent. However, the samples used for these experiments contain low contents of silt and clay (<75μm), estimated to be between 3 and 11.4 weight percent of the total specimen. The HC reductions were reversible only when the extent of clay dispersion was small. Although the experiments and solutions do not exactly mimic the conditions at the Norman Landfill, the results highlight the potential significance of clay dispersion on characterizing HC of a contaminated aquifer.

Practical implications of these results include:

- This phenomenon may occur at the edges of the present leachate plume in locations where the boundary between fresh and contaminated water is not stable. Any locations where the leachate plume retreats are subject to this phenomenon. Any return of the leachate plume, to this area would be impeded by the lowered HC of the region. If this were to take place along the edges of the leachate plume, the flow of the leachate plume may be focused with decreased dispersion of the contaminants.
- The measured decreases in hydraulic conductivity are large enough to affect the production rate of wells in affected aquifers, and change ground-water flow paths by altering the permeability distribution in the aquifer.
- The decrease in hydraulic conductivity has been shown to occur in sediments with low silt and clay contents. Water producing aquifers containing small amounts of clay can be substantially affected by clay dispersion.

- The largest HC decrease occurs when sodium substitution on cation exchange sites is close to completion (based on effluent monitoring). As complete sodium exchange takes time to complete, rapid response to and cleanup of brine spills and other high sodium contaminants may help reduce dispersion of clays.
- The dispersion of the clays does not occur until the ionic strength of the pore fluid decreases. If the ionic strength of the pore fluid is elevated with divalent ions during treatment, this phenomenon may be postponed until the sodium on the exchange sites of the clay has been removed, and dispersion is no longer likely.
- Many contaminants bind to solids in aquifers, therefore clay dispersion has implications for the mobility of contaminants bound to fine particles as shown by Grolimund and others (1998).

ACKNOWLEDGMENTS

This project was supported through Jim McNeal by the Toxic Substances Hydrology Program of the United States Geological Survey (USGS).

REFERENCES

American Society for Testing and Materials (ASTM), 1996, 1996 Annual Book of ASTM Standards, Section 4, Volume 04.09, p. 63-70.

Bohn, H. L., McNeal, B. L., and O'Connor, G. A., (1985), Soil Chemistry, 2nd ed.: John Wiley & Sons, New York, 315p.

Emerson, W.W., and Bakker, A. C., 1973, The comparative effect of exchangeable Ca, Mg, and Na on some physical properties of red brown earth subsoils. II The spontaneous dispersion of aggregates in water: Australian Journal of Soil Research, v. 11, p. 151-157.

Goldenberg, L. C., Magaritz, M., Amiel, A. J., and Mandel, S., 1983, Changes in hydraulic conductivity of laboratory sand-clay mixtures caused by a seawater-freshwater interface, Journal of Hydrology, v. 70, p. 329-336.

Grolimund, D., Elimelech, M., Borkovec, M., Barmettler, K., Kretzschmar, R., and Sticher, H, 1998, Transport of in situ mobilized colloidal particles in packed soil columns: Environmental Science and Technology, v. 32, p. 3562-3569.

McNeal, B. L., and N. T. Coleman, 1966, Effect of solution composition on soil hydraulic conductivity: Soil Science Society of America Proceedings, v. 30, p. 308-312.

Olsen, H. W., 1966, Darcy's law in saturated kaolinite: Water Resources Research, v. 2, p. 287-295.

Olsen, H.W., Willden, A.T., Kiusalaas, N.J., Nelson, K.R., and Poeter, E.P., 1994, Volume-controlled hydrologic property measurements in triaxial systems: Hydraulic Conductivity and Waste Contaminant Transport in Soils: American Society for Testing Materials STP 1142, p. 482-504.

Pupisky, H. and Shainberg, I., 1979, Salt effects on the hydraulic conductivity of a sandy soil: Soil Science Society of America Journal., v. 43, p. 429-433.

Quirk, J. P. and Schofield, R. K., 1955, The effect of electrolyte concentration on soil permeability: Journal of Soil Science, v. 6, p. 163-178.

Renshaw, Carl E., Gregory D. Zynda, and John C. Fountain, 1997, Permeability reductions induced by sorption of surfactant: Water Resources Research, v. 33, p. 371-378.

Rao, Narasimha S. and Mathew, Paul, K., 1995, Effects of exchangeable cations on hydraulic conductivity of a marine clay: Clays and Clay Minerals, v. 43, p. 433-437.

Rowell, D. L, D. Payne, and N. Ahmad, 1969, The effect of the concentration and movement of solutions on the swelling, dispersion, and movement of clay in saline and alkali soils: Journal of Soil Science, v. 20, p. 176-188.

Shainberg, I., Rhodes, J. D., and Prather, R. J., 1981, Effect of Low Electrolyte Concentration on clay dispersion and hydraulic conductivity of a sodic: Soil Science Society of America Journal., v. 45, p. 273-277.

Mapping the Norman, Oklahoma, Landfill Contaminant Plume Using Electrical Geophysics

By Robert J. Bisdorf and Jeffrey E. Lucius

ABSTRACT

The lateral extent of the electrically conductive portion of the contaminant plume emanating from the Norman Landfill was mapped using electrical geophysical measurements. EM induction and DC resistivity methods measured the apparent electrical resistivity of the subsurface. Both methods show an area of low resistivity indicating poor ground water quality in the alluvium, presumably due to leachate from the Norman Landfill. This area extends from the southwest side of the main landfill mound toward the Canadian River for no more than about 200 meters. Cross section and depth-slice maps made from the interpretation of the DC resistivity soundings and maps of measured resistivity from the EM measurements illustrate the lateral extent of the landfill contamination and show that the contaminate plume, which is about 9m thick, does not appear to extend into the bedrock. The EM induction method proved to be an easy and efficient procedure for rapidly determining the lateral extent of the leachate plume. The DC resistivity method, although more time consuming, provided better vertical resolution of the resistivity distribution.

INTRODUCTION

In 1995, 1996, and 1998 the U.S. Geological Survey made surface electrical geophysical measurements at the Norman Landfill near Norman, Oklahoma (Lucius and Bisdorf, 1995, and Bisdorf, 1996). The electromagnetic (EM) induction and direct-current (DC) resistivity methods were used. The Norman Landfill is located in central Oklahoma (figure 1) in an alluvium-filled valley made by the Canadian River. The alluvium is Quaternary in age and is underlain by the Permian mudstones and shales of the Hennessey Group (Wood and Burton, 1968). The geophysical measurements were made to determine if surface electrical techniques could delineate the horizontal and vertical extent of the conductive portion of the contaminant plume believed to be migrating from the landfill. The site is generally clear of cultural features except for the area between the slough and the landfill that has piles of debris including metallic objects.

EM INDUCTION

EM induction instruments, models EM31-D and EM34-3, manufactured by Geonics Limited[1] (Mississauga, Ontario, Canada) were used to measure the apparent electrical conductivity (conductivity is the inverse of resistivity) of the ground near the Norman Landfill. The main utility of the conductivity measurements is to map relative changes in ground conductivity rather than to determine the actual values of conductivity. The separation and orientation of the instrument coils determine the depths of investigation and sensitivity. The EM31 has a fixed coil separation of 3.66 meters and the EM34 can be used at coil separations of 10, 20 and 40 meters. When the coils are vertical (horizontal magnetic dipoles, HMD) the instruments are most sensitive to near-surface materials and have an effective depth of exploration of about 3 meters for the EM31 and about ¾ of the coil spacing for the EM34. When the coils are horizontal (vertical

[1]Any use of trade, product or firm names is for descriptive purposes only and does not imply endorsement by the U.S. Government.

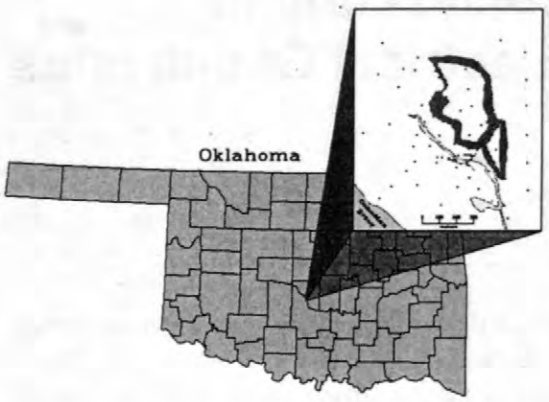

Figure 1. Map showing generalized location of the Norman Landfill area.

magnetic dipoles, VMD) the instruments have an effective depth of exploration of 6 meters for the EM31 and about 1½ times the coil spacing for the EM34 (McNeill, 1980).

EM induction measurements were made at about 700 locations (Lucius and Bisdorf, 1995) many with multiple coil configurations and spacings. Figure 2 shows a map of apparent resistivity made from EM31-D VMD data. The station locations are indicated by the black dots within the shaded areas. The outline of the landfill, the slough, the sewage outfall, and the north bank of the Canadian River (as of Feb. 1995) are shown for reference. The lowest resistivities occur within 200 meters of the landfill, suggesting that the conductive part of the leachate plume probably does not extend beyond this limit. There is an area of lower resistivity near the center of the map next to the landfill. This zone represents either shallow leachate or a higher concentration of near-surface clay. Away from the landfill, there appears to be little variation in the ground resistivity.

Figure 3 shows a map of apparent resistivity made from EM34-3 VMD 10 meter coil separation data. This map represents a deeper area than the map shown in figure 2. Again lower resistivities are present from the landfill southwest to just beyond the slough. The EM34-3 is very sensitive to coil misalignment when used in the horizontal coil mode. Inaccurate readings due to coil misalignment are probably the main cause of the blotchy appearance of parts of the map.

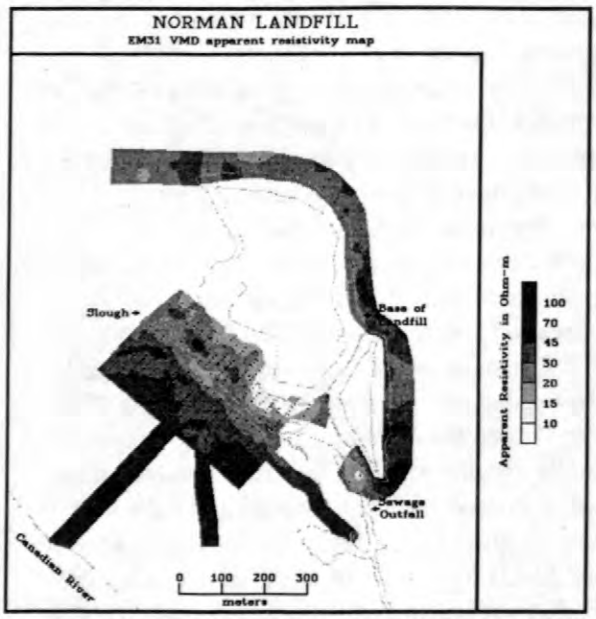

Figure 2. Map of EM 31 VMD data. Black dots represent measurement locations. The outline of the Landfill, the slough and sewage outfall, and the north bank of the Canadian River (as of Feb. 1995) are as indicated.

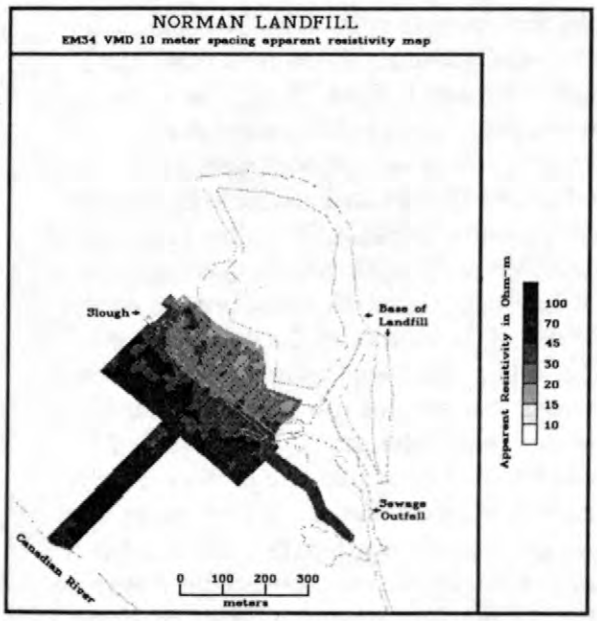

Figure 3. Map of EM 34 VMD 10 meter coil spacing data. Black dots represent measurement locations. The outline of the landfill, the slough and sewage outfall, and the north bank of the Canadian River (as of Feb. 1995) are as indicated.

DC RESISTIVITY SOUNDINGS

Schlumberger sounding is a geophysical technique that uses variations in the electrical resistivity of earth materials to help detect buried geologic structures. DC resistivity (the inverse of conductivity) is a fundamental rock property that varies due to rock type, clay content, porosity, and the quantity and quality of the water contained in the rock. Resistivity is normally expressed in ohm-m. Within a given rock type, the resistivity of the rock is primarily dependant on the quality and quantity of water and the amount of clay present. Generally speaking, higher clay content and/or poorer quality (more dissolved solids and/or chlorides) ground water lowers the rock resistivity.

Schlumberger sounding uses a symmetric electrode array to vertically explore the subsurface. The name Schlumberger derives from Conrad Schlumberger, an early proponent of the array geometry. Schlumberger soundings are processed by computer modeling of the sounding data as a series of horizontal layers (Zohdy, 1989 and Zohdy and Bisdorf, 1989). More detailed explanations of processing and automatic interpretation procedure can be found in Bisdorf (1985) and Zohdy and others (1993). A series of individual soundings can be combined to generate either a geoelectrical cross section or a map view of interpreted resistivity. Cross sections, which can be thought of as vertical slices through the ground, similar to a road cut, show lateral as well as vertical variations of resistivity. Maps of interpreted resistivity show areal distributions at a particular depth or elevation and can be thought of as horizontal slices through the earth.

Figure 4 shows the sounding locations. Seventy Schlumberger soundings were made with sounding expansion limited to a maximum of 2000 feet between the current electrodes (1000 ft AB/2). With the exception of some long (100-200 ft) sections of old metallic gas pipe, neither the metallic debris between the landfill and the slough nor other cultural features affected the Schlumberger soundings.

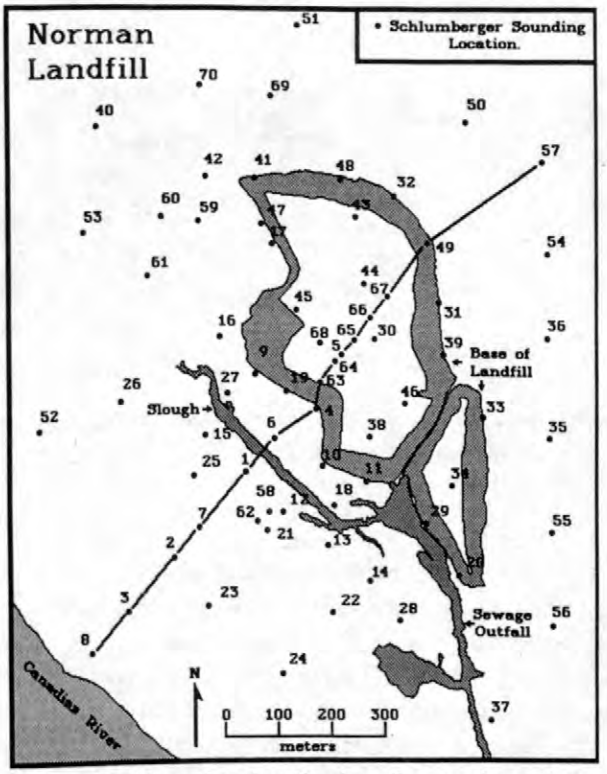

Figure 4. Map showing the location and number of the Schlumberger soundings. The cross section location is shown by the heavy black line. The outline of the landfill, the slough and sewage outfall, and the north bank of the Canadian River (as of Feb. 1995) are as indicated.

CROSS SECTIONS OF INTERPRETED RESISTIVITY

Resistivity cross sections are generated from individual sounding interpretations. Each sounding interpretation is sampled in a manner to approximate a continuous vertical distribution of resistivity with depth (Bisdorf, 1982). This vertical data is then horizontally interpolated to create a grid. Shades of gray are assigned based on the interpolated resistivity values and the desired contour levels. Triangles on the upper surface of the cross section designate the sounding locations. Topographic information, input as sounding elevations, is represented by connecting the surface location of the soundings by straight lines. The cross sections are displayed from the surface to an elevation of 280 m.

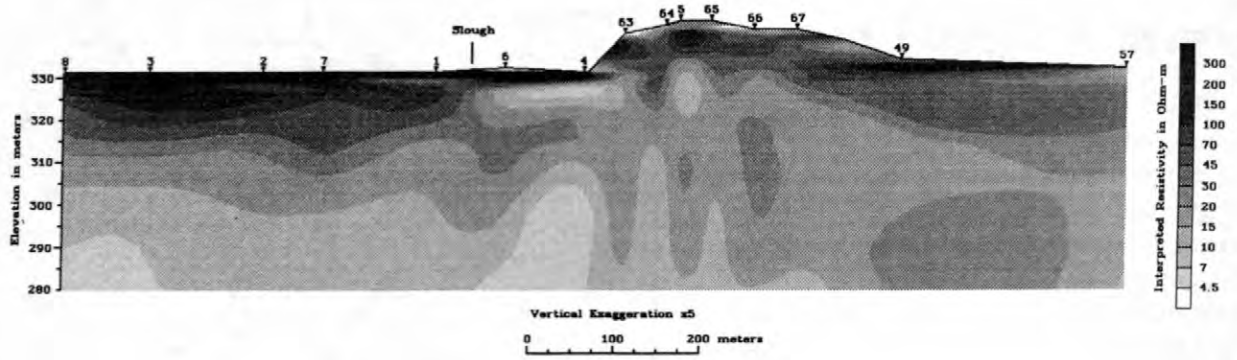

Figure 5. Interpreted resistivity cross section (see figure 4 for location). The gray scale represents interpreted resistivity values in ohm-m. The surface locations of the soundings are indicated by the triangles.

Figure 5 shows the geoelectrical cross section located as shown on Figure 4. This cross section is vertically exaggerated 5 times and extends from sounding 57 on the northeast across the landfill to sounding 8 at the Canadian River (Fig. 4). The high resistivities (>300 ohm-m) under soundings 1 through 8 represent dry sand. The intermediate resistivities (45-300 ohm-m) represent sand saturated with relatively good quality water. Low resistivities (<45 ohm-m) represent either fine grained materials such as mudstone, shales or clays, or represent sand saturated with poor quality (high TDS) water. Under soundings 4 to 6 a low resistivity layer exists from elevations 329 m to 320 m. This low resistivity layer is interpreted as the conductive portion of the contaminate plume and is estimated to be about 9 m thick. Unpublished penetrometer readings put the elevation of the Hennessey at about 319 meters (Scott Christenson, 1996, electronic communication) near sounding 6. Using this elevation as a lower limit, the leachate plume can be up to 10 m thick, which compares favorably with the 9 m estimated from the cross section.

RESISTIVITY MAPS AT SELECTED ELEVATIONS

Maps of interpreted resistivity at a particular elevation are generated by sampling the sounding interpretations at depths determined by the difference between the surface elevation at that sounding and the desired elevation. The resultant sampled interpreted resistivities and corresponding location values are gridded using a minimum curvature gridding algorithm (Webring, 1981). To prevent possible interpolated resistivities of less than zero, the logarithm of the resistivities is used for gridding. Shades of gray are assigned based on the grid value and the desired logarithmically spaced contour levels. Since these maps are raster (pixel) based, a bicubic interpolating program is used to increase the size of the resultant image. An interpolating program is used to resample the grid, as opposed to simply gridding the data at the desired final interval, because the minimum curvature algorithm generates undesirable results if the data are over sampled. The Kolor-map and section program (Zohdy, 1993) uses similar procedures and provides a discussion of the nuances of resistivity map generation.

Figure 6 shows a map of interpreted resistivity for an elevation of 330 meters. Over most of the surveyed area, with the exception of the landfill proper, this elevation is within 2 to 5 m. of the surface. The black dots represent sounding locations. The outline of the landfill, the slough, and the north bank of the Canadian River are presented for reference. The map shows an area of high resistivity (>300 ohm-m) about 150 m southwest of the slough. These high resistivities represent the dry sand present in the dune area near the river. Areas of low resistivity

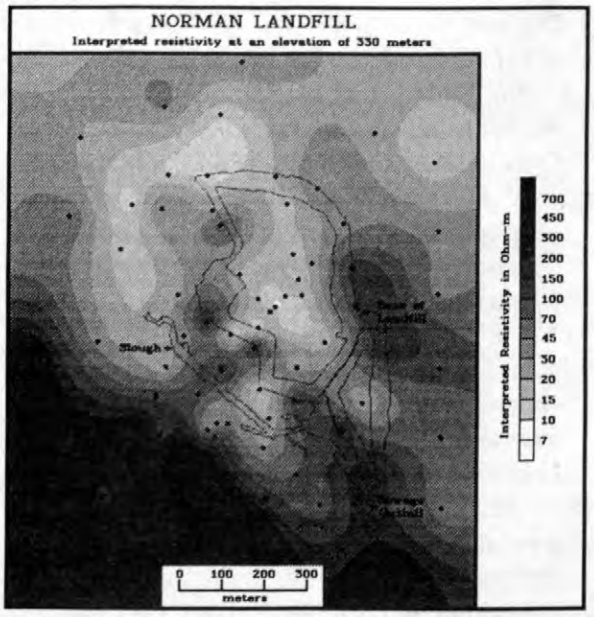

Figure 6. Map of interpreted resistivity at an elevation of 330 meters. The gray scale represents interpreted resistivity values in ohm-m. The sounding locations are indicated by the black dots.

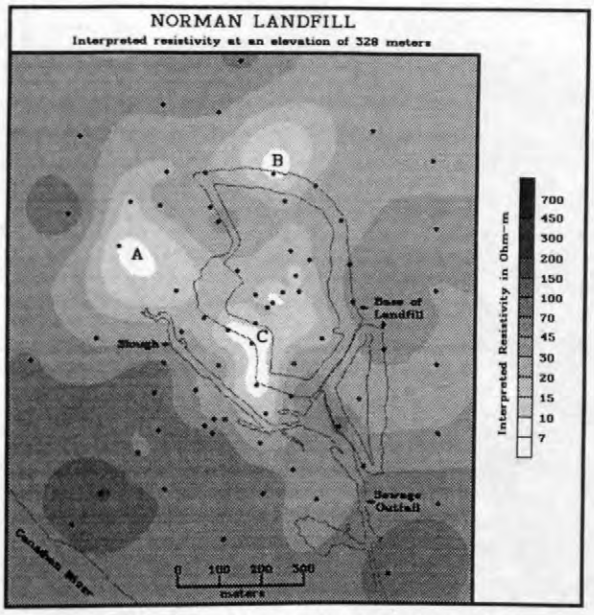

Figure 7. Map of interpreted resistivity at an elevation of 328 meters. The gray scale represents interpreted resistivity values in ohm-m. The sounding locations are indicated by the black dots.

(7 to 45 ohm-m) form coherent zones or trends and represent fine grained deposits. These may have been zones of quiet water or over bank deposits that allowed the fine grained materials to settle. These areas are generally above the water table and water quality is not thought to be a predominant factor in determining their resistivity. The low resistivities under the landfill cap are in areas that were probably excavated and filled with trash. These lower resistivities may be caused by removal of the original sand and subsequent deposits of trash. It is also possible that there is a rise in the water table under the landfill and these resistivities are water quality related.

Figure 7 shows a map of interpreted resistivity for an elevation of 328 meters. This elevation was chosen because it shows some shallow conductive features that are not considered to be related to the main portion of the contaminate plume. The low resistivity anomalies indicated by "A" and "B" on figure 7 are interesting in that they don't have the same source of contamination, if indeed they are contaminated, as the main conductive anomaly centered on the landfill ("C"). The conductive anomaly at "A" is associated with an area were the trucks from the local asphalt company are washed. The runoff from the trucks may be the cause of this conductive feature. The contaminate plume is indicated by the low resistivity anomaly near "C".

Figure 8 shows a map of interpreted resistivity for an elevation of 326 meters. This elevation was chosen because it falls near the middle of the low resistivity anomaly seen on the cross section in Figure 5. The lowest resistivities occur under and just west of the large cell of the landfill and are interpreted to represent the conductive portion of the leachate plume. The general shape of the contours to the west and south of the landfill resemble the potentiometric surface (Scholl and Christenson, 1998), implying that the low resistivity feature is caused by the ground water and not clays. This resemblance doesn't change until about 75 meters west of the slough, indicating that there is still some contamination to that point. The gradual increase in the resistivities away from the landfill indicates that the contaminant plume is either becoming less conductive (i.e. less contaminated) or thinner.

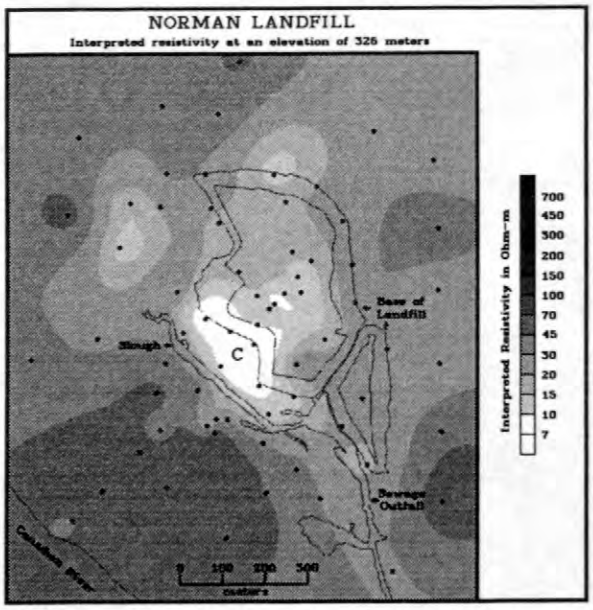

Figure 8. Map of interpreted resistivity at an elevation of 326 meters. The gray scale represents interpreted resistivity values in ohm-m. The sounding locations are indicated by the black dots.

SUMMARY

Surface electrical geophysical methods successfully delineated the vertical and areal extent of a conductive contaminate plume in the mixed alluvial sands and clays of central, Oklahoma. The EM induction maps of apparent conductivity/resistivity are a fast way to get an idea of the direction and extent of contaminate movement in this shallow (less than 20 m) environment. Although taking longer to collect and process, DC resistivity soundings and resultant maps and cross section give more depth detail and more accurate estimates of resistivity.

REFERENCES

Bisdorf, R.J., 1982, Schlumberger sounding investigations in the Date Creek Basin, Arizona: U.S. Geological Survey Open-File Report 82-953, 55 p.

___, 1985, Electrical techniques for engineering applications: Bulletin of the Association of Engineering Geologists, v. XXII, no. 4, p. 421-433.

___, 1996, Schlumberger soundings at the Norman landfill, Norman, Oklahoma: U.S. Geological Survey Open-File Report 96-668.

Lucius, J. E., and Bisdorf, R. J., 1995, Results of geophysical investigations near the Norman, Oklahoma, municipal landfill, 1995: U.S. Geological Survey Open-File report 95-825, 125 p.

McNeill, J.D., 1980, Electromagnetic terrain conductivity measurement at low induction numbers: Mississauga, Ontario, Canada, Geonics Ltd, Technical Note TN-6, 15 p.

Scholl, M.A., and Christenson, Scott, 1998, Spatial variation in hydraulic conductivity determined by slug tests in the Canadian River alluvium near the Norman Landfill, Norman, Oklahoma: U.S. Geological Survey Water-Resources Investigations Report 97-4292, 28 p.

Webring, Michael, 1981, MINC: A gridding program based on minimum curvature: U.S. Geological Survey Open-File Report 81-1224, 12 p.

Wood, P.R., and Burton, L.C., 1968, Ground-water resources, Cleveland and Oklahoma counties: Oklahoma Geological Survey Circular 71, 75 p.

Zohdy, A.A.R., 1989, A new method for the automatic interpretation of Schlumberger and Wenner sounding curves: Geophysics, v. 54, p. 245-253.

___, 1993, Program Kolor-Map & Section, Amiga Version: U.S. Geological Survey Open-File Report 93-585, 113 p.

Zohdy, A.A.R., and Bisdorf, R.J., 1989, Programs for the automatic processing and interpretation of Schlumberger sounding curves in QuickBASIC 4.0: U.S. Geological Survey Open-File Report 89- 137 A&B, 64 p., + disk.

Zohdy, A.A.R., Bisdorf, R.J., and Martin, Peter, 1993, A study of sea-water intrusion using Schlumberger soundings near Oxnard, California: U.S. Geological Survey Open-File Report 93-524, 139 p.

Shallow-Depth Seismic Refraction Studies Near the Norman, Oklahoma, Landfill

By Michael H. Powers and Wilfred P. Hasbrouck

ABSTRACT

Seismic refraction surveys were performed near the Norman, Oklahoma, landfill to determine the depth to bedrock between the landfill and the Canadian River. For two lines, one short and one longer, both compressional wave data and shear wave data were acquired. Because the compressional wave velocities are strongly influenced by the variable saturation of sand, clay, and gravel in the unconsolidated sediments, and shear wave velocities are not influenced by these features, the shear wave data lead to much more accurate models of the bedrock interface.

INTRODUCTION

As part of a large research project to study the leachate migration seeping from the Norman, Oklahoma, landfill near the north bank of the Canadian River, many geophysical surveys have been performed on and around the landfill (Hasbrouck and others, 1998; Lucius and Bisdorf, 1998, Young and Lucius, 1998). For fluid flow modeling of the landfill leachate in the area, hydrologists need to know the depth to bedrock, especially between the landfill and the river. Bedrock in the area is the Permian Hennessey group, an aquiclude primarily composed of mudstones and shales (Wood and Burton, 1968).

Depth to bedrock information is available from boreholes, and can be determined along profiles between boreholes with seismic surveys. Shallow seismic reflection surveys can provide depth to bedrock, as well as information about lateral changes in the nature of the unconsolidated overlying material (Knapp and Steeples, 1986a,b; Hoyos and others, 1998), but they are costly and time-consuming both in the field and in the office. Seismic refraction surveys can often provide excellent information on depth to bedrock, but are limited in their ability to identify and correctly account for lateral changes in the overlying material.

Because seismic surveys respond to variations in the velocity of compressional (P) and shear (S) waves, they can provide information on lithological changes that correspond to changes in material velocities. In unconsolidated sediments, changes in P-wave velocity are generally associated with changes in saturation, compaction, and material type. S-wave velocity does not respond to changes in the pore space fluid (air versus water), but only to changes in the "shear stiffness" of the matrix material. Seismic surveys cannot provide any information about the quality of the saturating fluid.

Some basic principles of the seismic refraction method are described below. This is followed by a presentation of data from two examples lines. We explain what we established as the best method for the determination of depth to bedrock in this area.

SEISMIC REFRACTION

Use of the seismic refraction method has been described at least as early as the 1930s (Thornburgh, 1930; Edge and Laby, 1931; Muskat, 1933; Partlo and Service, 1934), and has been re-examined many times between then and now (Hagedoorn, 1959; Hawkins, 1961; Barry, 1967; Palmer, 1980). It is based on the existence of increasingly higher-speed layers at successive depths below slower layers. The method measures the arrival time of energy at geophones placed in a line extending away from a source excited at the surface. As the energy moves away from the source, going out and down, its arrival

time at the first few geophones can be used to determine the velocity of the shallow material. Once the energy gets down to a higher-speed layer, it moves along the interface between the two materials at the higher velocity. This produces a "head wave" that moves into the upper low-speed layer, much like the wake of a boat moving out from the interface. When this "wake" hits the geophones at the surface, the arrival times show a change that can be used to determine the depth and velocity of the higher-speed layers.

The distance away from the energy source at which one needs to record arrival times varies with each site. As the velocity contrast between the low and high-speed layers changes, and the depth to the high-speed layers changes, the distance away from the source where the "wake" arrives at the surface will also change. For shallow high-speed layers with velocities much greater than the overlying low-speed layers, one can record the necessary data with geophones placed relatively near the source position. However, as the depth to the higher-speed layer increases, and/or as the contrast in velocity between the layers decreases, the geophones must be placed farther from the source position to record the arrival of the "wake" energy. This becomes a problem when the necessary recording distance from the source is so far away that the signal energy has fallen to the level of the background noise. In such cases, the geophysicist must try to boost his source energy (get a bigger guy to swing the hammer, use explosives, etc.) or decrease the noise (bury the geophones, work at night or on weekends, etc.).

The depth to the higher-speed layers (water table and bedrock in this case) is generally calculated assuming a laterally constant velocity through the lower-speed layers (overlying sediments, dry and wet). Lateral changes or changes with depth in the composition of an assumed layer in the overlying sediments, such as clay lenses or gravel beds in a sand deposit, will affect the energy propagation time through the sediment. This creates variations in the arrival times that are often interpreted as variations in the depths to the interfaces.

In general, it is impossible to measure only travel times and uniquely determine distance and velocity. Given either the distance or the velocity, the other can be calculated from the measured times. Errors in the velocity will always lead to errors in the distance (depth). For seismic refraction this means the determination of depth to bedrock is only as good as the velocity and depth calculations for the overlying layers. If the velocities and depths determined for the dry and wet sediment layers vary laterally along the profile due to clay lenses or gravel beds, and these variations are undetected, they will result in errors in the depth to the deeper layer (bedrock).

NORMAN LANDFILL SEISMIC REFRACTION SURVEYS

Figure 1 shows the locations of seismic refraction surveys performed on and around the landfill. The profiles on the landfill all have one end at the base of the fill material. These are P-wave surveys performed to determine the depth to the water table inside the fill. The profiles away from the landfill are S-wave surveys performed to determine depth to bedrock. In this paper, only the depth to bedrock profiles away from the landfill will be discussed.

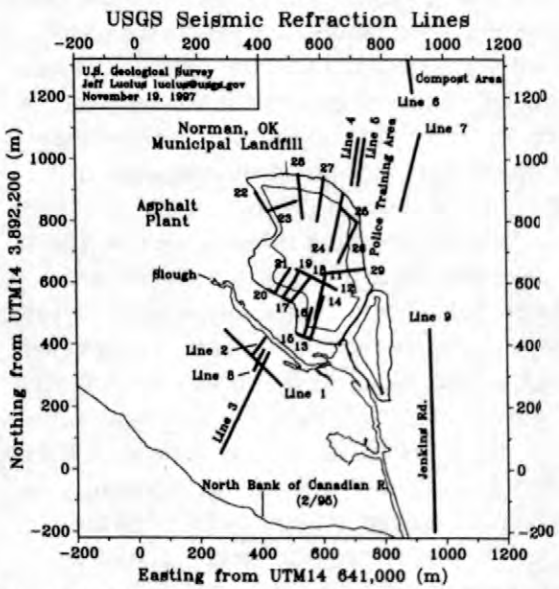

Figure 1. Plan view map of the Norman landfill area showing the locations of seismic refraction lines. Line 1 and Line 2, on the floodplain between the landfill and the Canadian river, are discussed in this paper.

Both P-wave and S-wave surveys can be used to determine the depth to bedrock off the

landfill. Lines 1 and 2 were acquired with both types of data.

Figure 2 shows a P-wave shot record from Line 2. This record shows the time history of vertical ground motion at 24 locations increasing in distance away from the source. The geophone locations vary from 3 to 72 meters from the source, with a 3 meter increment between phones. The time histories all begin at the moment of source impact. The total time of this record is 100 milliseconds, with solid gridlines drawn every 10 milliseconds. Note that the first-arrival times of the energy are fairly easy to pick, and vary from about 9 to 47 milliseconds. A reverse shot was also acquired using these same geophone plants, but with the source placed at the far geophone location.

Figure 3 is a display of the first-arrival time picks for the forward and reverse P-wave shots of Line 2. On the vertical axis is first-arrival time in milliseconds, and on the horizontal axis is lateral distance corresponding to the geophone locations on the ground. The time picks are plotted for both the forward and reverse shots. Note that because this is a plot of time and distance, the slopes ($\Delta y/\Delta x$) are direct measures of reciprocal velocity. This plot is used, along with any other information about the local geology, to create a model of the subsurface.

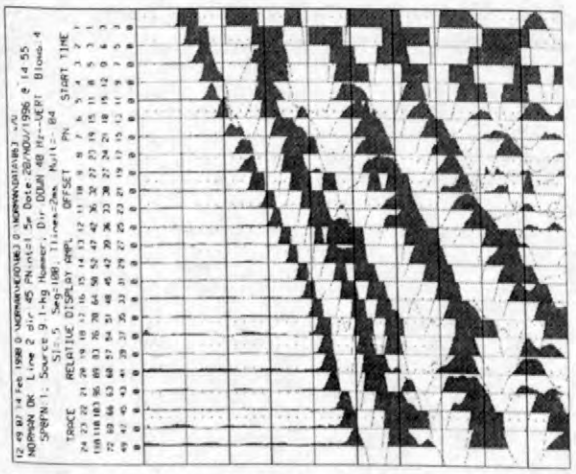

Figure 2. P-wave shot record from Line 2. Total time shown is 100 milliseconds, and solid gridlines are at 10 millisecond intervals. Geophone offset from the source varies from 3 to 72 meters. First-arrival energy time picks are not hard to determine.

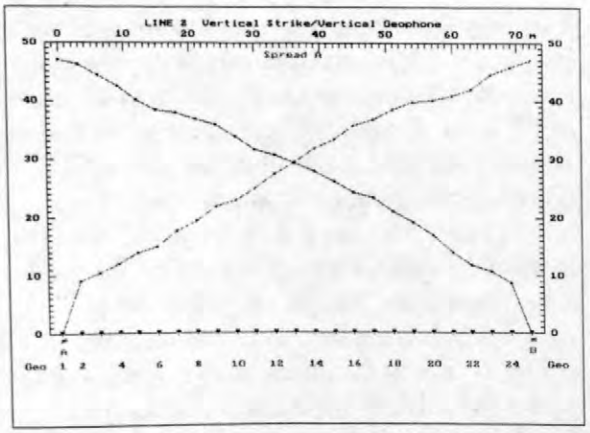

Figure 3. First-arrival time in milliseconds is on the vertical axis and lateral distance showing geophone positions is on the horizontal axis. The time picks for the forward shot (Figure 2), and reverse shot are plotted. Slopes are in units of reciprocal velocity.

Figure 4 shows the subsurface model generated for Line 2 using the P-wave data. This model was determined from the data shown in Figure 3 and the knowledge that the subsurface generally consisted of dry sediment over wet sediment over bedrock. The model in Figure 4 provides a good match to the data in Figure 3, but it is by no means the only model that will match the data. If there is a clay layer about one meter thick in the wet sediment, but pinching out halfway across the profile, it may have a higher P-wave velocity than the surrounding wet sand.

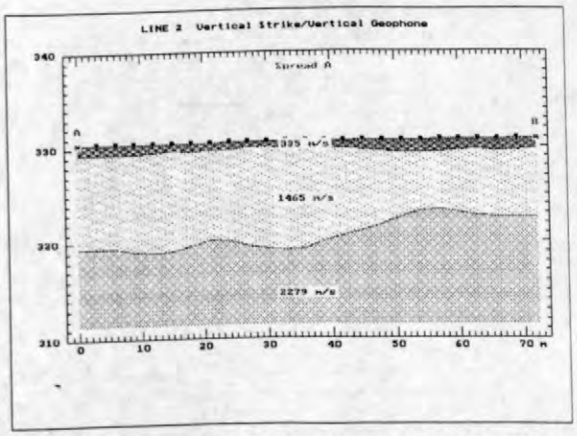

Figure 4. The subsurface model generated from the data shown in Figure 3, and knowledge that the geology consisted of dry sediment over wet sediment over bedrock. This model fits the data, but is only one of any number of models that will do so.

This may vary the arrival times to some of the geophones in the same manner as the rise in the bedrock surface shown halfway across the model of Figure 4. Geophysicists usually try to find the simplest model that fits all of the data at hand (geophysical, geological, and anecdotal).

Figure 5 shows a shot record based on the S-wave data also acquired along Line 2. Shear waves propagate with the displacement of particles occurring in a "side-to-side" fashion, perpendicular to the direction of travel. (With P-waves the particle displacement occurs in a "front-to-back" fashion, parallel to the direction of travel.) Our source used to generate shear waves is called a "golf shoe", and looks something like a heavy, steel footstool coupled to the ground with long spikes. On either end are vertical metal plates that can be struck with a hammer while standing on the device. Commonly, we collect a shot record by hitting one end, and then collect another record while hitting the other end. The shear waves generated by the two records will be reversed in polarity, while the P-waves generated unintentionally from the "golf shoe" will have the same polarity on both records. By subtracting one record from the other (reverse polarity and add), we can enhance the S-wave arrivals, and attenuate the P-wave arrivals. Figure 5 shows such a "shear pair difference" record acquired at Line 2.

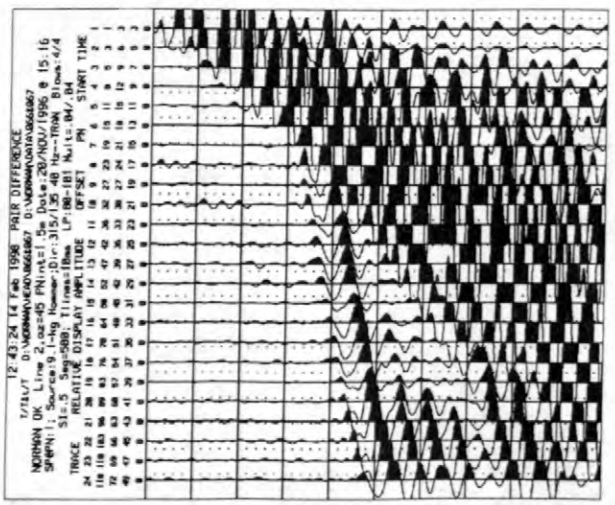

Figure 5. S-wave "pair difference" shot record. One record is reversed and added to the other. S-wave energy is enhanced and P-wave energy is attenuated. The total time shown is 500 milliseconds and the solid gridlines are drawn at 50 millisecond intervals.

Shear waves travel through earth materials at a slower velocity than compressional waves. The total time shown in Figure 5 is 500 milliseconds, with the solid grid lines representing 50 millisecond increments. The first-arrival times are not hard to pick, and vary from about 10 to just under 250 milliseconds.

Figure 6 shows the S-wave first-arrival time picks plotted for both the forward and reverse shots. A simple model that fits this data is shown in Figure 7. Note that only two layers exist, as shear wave velocity is not affected by dry versus wet sediment. Note also the simple, smooth bedrock interface in this model.

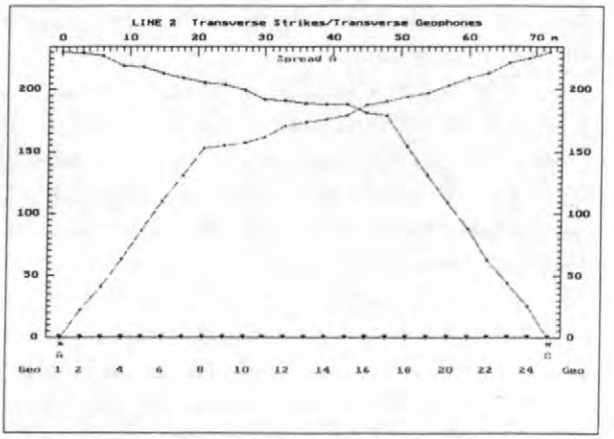

Figure 6. The time picks (milliseconds) of the shear pair data for Line 2 are plotted. The shallow layer S-wave velocity is more accurately determined than for the P-wave data.

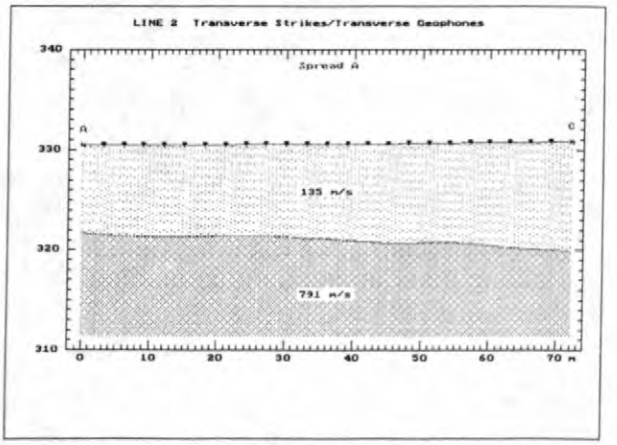

Figure 7. A simple model that matches the S-wave data of Figure 6. This model is a closer match to the geology from well data. Because the S-wave energy does not respond to dry versus wet sediments, it suffers less from the assumption of a single, average velocity for each layer.

According to well data, the S-wave model matches the geology much better than the P-wave model. There are clay lenses and gravel beds throughout the unconsolidated sediment in the vicinity of Line 2. Evidently, these inhomogeneities have a greater P-wave velocity contrast to the surrounding sand than they have S-wave velocity contrast, and this variation is enhanced as the sediments are water saturated. The S-wave data record an accurate, homogenous velocity for the entire thickness of unconsolidated sediment, leading to a better refraction interpretation.

Figures 8 and 9 show the first-arrival time picks and resultant model for the longer Line 1 oriented near and perpendicular to Line 2. The time picks are accurate, but variations in the P-wave velocity of the unconsolidated sediment again result in false undulations in the bedrock interface. Figures 10 and 11 show the S-wave data and resultant model for Line 1. Again, the insensitivity of the S-wave velocity to inhomogeneities in the unconsolidated sediments due to water saturation variations leads to a much more accurate interpretation of the bedrock interface.

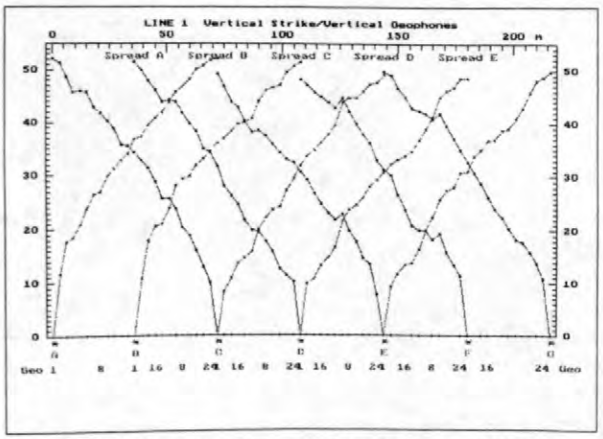

Figure 8. First-arrival travel-time plots of P-wave data collected along Line 1.

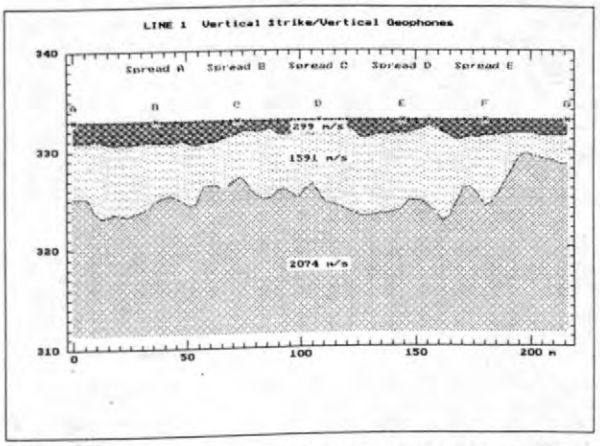

Figure 9. The simple model of Line 1 calculated to match the P-wave data of Figure 8. Variations in the arrival times of the P-wave energy lead to variations in the depth to bedrock. In fact, the travel-time variations are likely due to P-wave velocity variations in the unconsolidated sediment, but such variations are impossible to accurately determine from the data.

SUMMARY

Seismic refraction surveys near the Norman landfill have been acquired and interpreted to determine depth to the bedrock away from the landfill. The data clearly show a better interpretation when S-wave surveys are used instead of P-wave surveys. Inhomogeneities in the unconsolidated sediment above the bedrock, enhanced by variable water saturations, such as clay lenses and gravel beds within the sand deposit, have a greater P-wave velocity contrast than fluid insensitive S-wave velocity contrast. We will continue to determine depth to bedrock in this region using S-wave refraction surveys.

REFERENCES

Barry, K.M., 1967, Delay time and its application to refraction profile interpretation: in Seismic refraction prospecting: A.W. Musgrave, Ed., SEG, Tulsa, OK, p.348-361.

Edge, A.B., and Laby, T.H., 1931, The principles and practice of geophysical prospecting: London, Cambridge University Press.

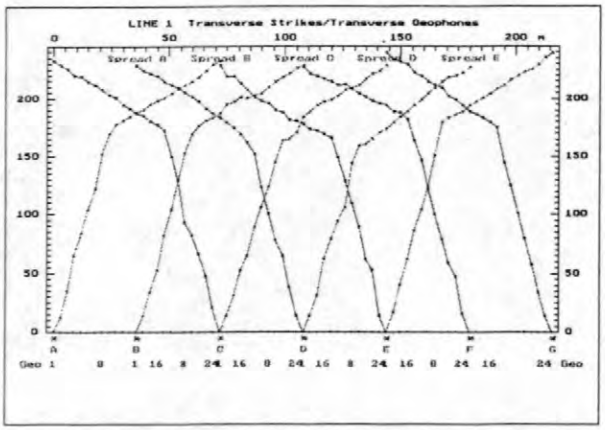

Figure 10. First-arrival travel-time plots of S-wave data collected along Line 1.

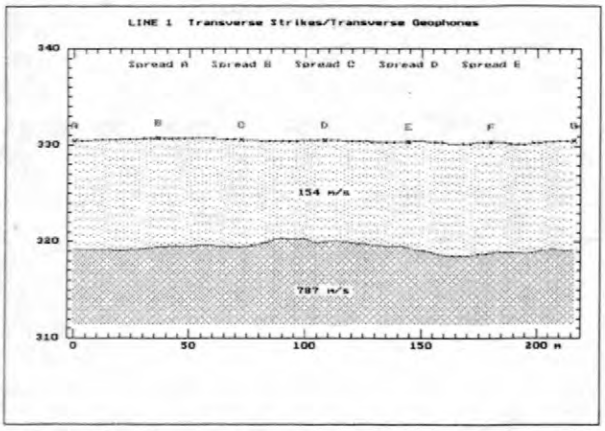

Figure 11. The simple model of Line 1 calculated to match the S-wave data of Figure 10. This model is a much more reasonable interpretation of the bedrock surface than the model of Figure 9. The S-wave velocity of the unconsolidated sediment is unaffected by variations in saturation, and is well approximated by a single average value. This leads to more accurate values of depth to the bedrock interface.

Hagedoorn, J.G., 1959, The plus-minus method of interpreting seismic refraction sections: Geophys. Prosp., v.7, p.158-182.

Hasbrouck, W.B., Lucius, J.E., and Powers, M.H., 1998, Seismic refraction investigations: in GSA Abstracts with Programs, South Central Section, v.30, n.3, p.7.

Hawkins, L.V., 1961, The reciprocal method of routine seismic refraction investigations: Geophysics, v.26, p.806-819.

Hoyos, J., Young, R., and Ahern, J., 1998, Seismic shear wave surveys at the Norman landfill site: in GSA Abstracts with Programs, South Central Section, v.30, n.3, p.8.

Knapp, R. W. and Steeples, D. W., 1986a, High-resolution common-depth-point seismic reflection profiling - instrumentation: Geophysics, v.51, n.2, p.276-282.

Knapp, R. W. and Steeples, D. W., 1986b, High-resolution common-depth-point reflection profiling - field acquisition parameter design: Geophysics, v.51, n.2, p.283-294

Lucius, J.E., and Bisdorf, R.J., 1998, Extent of the contaminant plume: in GSA Abstracts with Programs, South Central Section, v.30, n.3, p.8.

Muskat, M., 1933, The theory of refraction shooting: Physics v.4, p.14-28.

Palmer, D., 1980, The generalized reciprocal method of seismic refraction interpretation: SEG, Tulsa, OK.

Partlo, F.L., and Service, J.H., 1934, Seismic refraction methods as applied to shallow overburdens: Am. Inst. Min. Eng., Tr., v.110, p.473-492.

Thornburgh, H.R., 1930, Wavefront diagrams in seismic interpretation: AAPG Bull., v.14, p.185-200.

Wood, P.R., and Burton, L.C., 1968, Ground-water resources, Cleveland and Oklahoma Counties: Oklahoma Geological Survey Circular 71, 75p.

Young, R.A., and Lucius, J.E., 1998, Geophysical exploration strategy at the Norman landfill: in GSA Abstracts with Programs, South Central Section, v.30, n.3, p.8.

AUTHOR INFORMATION

Michael H. Powers and Wilfred P. Hasbrouck,
U.S. Geological Survey, Denver, CO
(mhpowers@usgs.gov)

Processes that Control the Natural Attenuation of Chlorinated Solvents

In the early 1980's, when the Toxic Substances Hydrology Program of U.S. Geological Survey began, chlorinated solvents like trichloroethene (TCE) were considered to be non-biodegradable. In fact, it wasn't until 1985 that a mechanism for microbial degradation of TCE was first documented. Since that time, numerous biodegradation mechanisms including reductive dechlorination, direct oxidation, and various cometabolic mechanisms have been identified. These processes act in conjunction with non-biologic processes such as adsorption, dilution, and dispersion, to limit the migration of chlorinated solvents in ground-water systems. Perhaps the best-documented example of this behavior was observed at the Toxic Substances Hydrology site at Picatinny Arsenal, New Jersey. Data collected from this site shows that a large plume of solvent-contaminated ground water had come to a steady-state condition, and that this behavior reflected the combination of biological (reductive dechlorination), geochemical (sorption), and hydrologic (dilution) processes. Because these have been so well documented, Monitored Natural Attenuation (the use of these natural processes to reach remediation goals) has become an accepted remedial strategy.

Because of the many different processes that contribute to the natural attenuation of chlorinated solvents, assessing their efficiency can be a complex task. The papers in this section reflect this complexity. Depending on the characteristics of different sites, sorption may be a controlling process (Imbrigiotta), interactions with wetlands may be significant (Lorah-Devereux), temporal changes in redox conditions may be important (Mcguire and others), uptake by trees may occur (Vroblesky and others), biodegradation may be reflected in the diversity of microbial biomass (Haack and Reynolds), or previously unknown biodegradation processes might be observed (Bradley and Chapelle).

The scope of papers presented in this section reflects the diversity of processes that affect the natural attenuation of chlorinated solvents. Considering that just 15 years ago TCE was considered to be non-biodegradable, this shear variety is astounding. However, given the impressive advances of the last 15 years, it is reasonable to presume that much remains to be learned about the behavior of these compounds. This knowledge, in turn, will help make assessments of natural attenuation that are much more reliable and technically feasible.

For additional information contact:

Francis H. Chapelle, USGS, Columbia,
South Carolina (email: chapelle@usgs.gov)

Using Molecular Approaches to Describe Microbial Populations at Contaminated Sites

By Sheridan K. Haack and Lisa A. Reynolds

ABSTRACT

Information about the distribution, numbers, types and activities of bacteria and other microorganisms at contaminated sites is important for proper site characterization, for selection of sampling sites, for development of monitoring strategies and for development of accurate site models. The nucleic acids DNA (deoxyribonucleic acid) and RNA (ribonucleic acid), extracted from sediments at contaminated sites, can provide information on the identity, biomass and biodegradative pathways of bacteria. This project employs several nucleic-acid based methods to study bacterial community and population dynamics at a representative site at which ground water is contaminated with fuel and chlorinated compounds. Using these molecular methods, bacterial community composition and population abundance at this site have been observed to vary spatially over scales of less than 1 meter and temporally over scales of months. Changes in bacterial communities and populations can be used to infer the reasons for spatial and temporal changes in aqueous geochemistry and contaminant chemistry at this site. Molecular methods provide information about bacterial biodegradative processes at contaminated sites that cannot be obtained using traditional microbiological methods.

INTRODUCTION

Prior to the mid 1980's, it was widely believed that the subsurface was sterile (Chapelle, 1993). During the past ten to fifteen years, however, studies of pristine and contaminated subsurface environments have revealed healthy and active populations of bacteria and other microorganisms. It is now widely understood that these organisms perform important biodegradative activities at contaminated subsurface sites. Biodegradation is one component of natural attenuation, that in concert with physical and chemical processes, decreases contaminant migration along ground-water flow paths. Understanding biodegradation is particularly important, because of all the processes natural attenuation encompasses, only biodegradation offers the potential to truly convert the contaminants to harmless substances.

Given the importance of biodegradation, it is clear that knowledge of the distribution, numbers, types and activities of the bacteria and other microorganisms at contaminated sites is critical. Nevertheless, little is known on this subject for two reasons. First, subsurface samples are difficult and expensive to obtain. Second, the study of bacteria and other microorganisms was historically limited to laboratory investigations of bacteria cultured from environmental samples because research methods to identify microorganisms *in situ* did not exist. It is particularly important to recognize that bacterial culturing methods result in the growth of only those bacteria that can tolerate the specific conditions the investigator provides. Although these methods have resulted in enormous advances in understanding of bacterial physiology, biochemistry and metabolic versatility, it has been unclear if this knowledge is transferrable to the true conditions found in the environment. Indeed, until recently, it was unclear if the isolated bacteria were important at all (i.e., in numbers or activity) in environments from which they were isolated (Hugenholtz and Pace, 1996).

Fortuitously, during the same time that the importance of bacteria in the subsurface became known, a revolution occurred in the discipline of microbiology. New methods, based on analysis

of deoxyribonucleic acid (DNA) extracted from environmental samples, were developed. Analysis of bacterial DNA revealed that bacteria could be categorized by the sequence of a particular segment of DNA that codes for 16S ribosomal ribonucleic acid (RNA), called the 16S rDNA gene. This discovery meant that bacterial DNA, extracted from subsurface samples, could provide information on the identities of the bacteria present. In addition, the extracted DNA could be analyzed for the presence of other DNA sequences (genes) that code for enzymes that allow certain bacteria to carry out particular biodegradative reactions.

The study described here employs some of these new DNA-based methods in order to understand how spatial and temporal variation in bacterial community structure affects the natural biodegradation of fuel and chlorinated solvents. The study sampling program is designed to:

(1) Determine the dominant terminal electron accepting process (TEAP) at multiple locations and on multiple dates in a typical contaminated aquifer;
(2) Determine patterns of bacterial community composition in sediments taken from each TEAP zone, by using two methods of bacterial DNA analysis and;
(3) Determine spatial and temporal patterns in the distribution and abundance of selected bacterial populations involved in various TEAPs or in specific biodegradation reactions, again using various DNA-based methods.

This paper describes preliminary observations on relations between bacterial communities or populations and TEAP zones in a contaminated aquifer. We have chosen to focus on TEAPs because the development of TEAP zonation is believed to be one indicator of natural biodegradation activity at contaminated sites (Hinchee and others, 1995), and because bacteria are involved in the creation of TEAP zones (Chapelle, 1993).

FIELD SITE DESCRIPTION

The study site is at the former Wurtsmith Air Force Base approximately 2 kilometers (km) west of the Lake Huron shoreline in Michigan's Lower Peninsula. The principal aquifer at the base averages 21 meters (m) thick and is comprised of glacial deposits of gravel, sand, silt and clay (U. S. Geological Survey, 1991; Huffman and others, 1995).

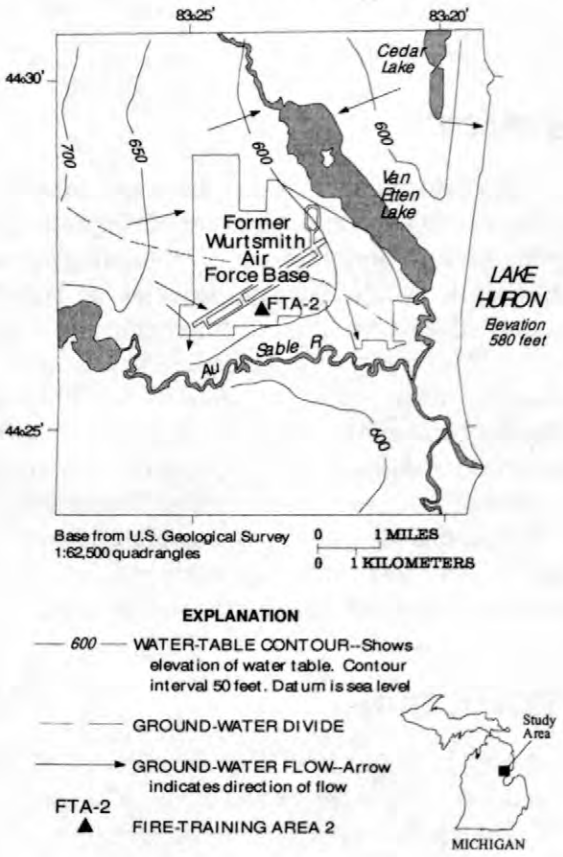

Figure 1. Location of the study site.

Surficial deposits include lacustrine sediments such as deltas, beaches and lakebed sand and clay, ice-contact sediments such as till, and alluvium near drainage channels. The silty-clay confining unit below the water table aquifer is at least 30 m thick. The water table ranges from 5-8 m below land surface (194-200 m above sea level) and water levels fluctuate 0.3-1 m annually. The average ground water velocity is 0.1-0.3 m per day. The study site (Fire-Training-Area 2; FTA-2, fig. 1) was used for fire-training exercises from 1958 until 1986, resulting in dispersal of waste fuel, solvents and fire-fighting compounds to the shallow water-table aquifer. The contaminant plume extends about 500 m downgradient from the central site of fire-training activities and the

majority of the contaminants are located on the aquifer sediments, near the water table. Groundwater contaminants detected at the site include: benzene, toluene, ethylbenzene, and xylene (BTEX), *cis* 1,2-dichloroethene, vinyl chloride, acenaphthene, and naphthalene. Chemical analyses in 1987-88 showed that total petroleum hydrocarbon and BTEX concentrations in soil ranged from nondetectable levels to 40,000 and 313 mg/kg, respectively (U. S. Geological Survey, 1991).

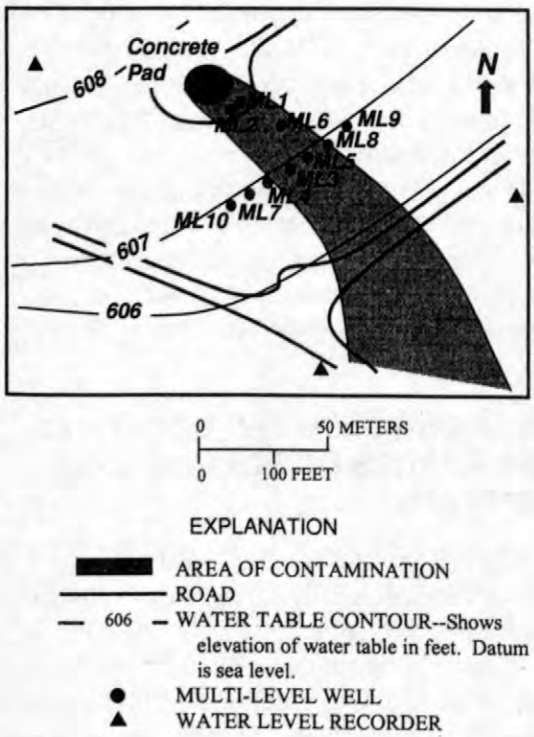

Figure 2. Plume of contaminated ground water at Fire-Training Area 2 at the former Wurtsmith Air Force Base, Michigan. The concrete pad was the site of fire-training activities.

The range in concentration or magnitude of typical water-quality constituents and properties at uncontaminated Wurtsmith sites includes the following (mg/L, milligrams per liter, unless otherwise specified): pH, 7.0-7.9; alkalinity, 75-190 (mg/L $CaCO_3$); specific conductance (SC), 200-330 microSiemens (µS); nitrate, NO_3, <1-4; ferrous iron, Fe(II), 0.0; and sulfate, SO_4, 7-12. At the FTA-2 Site, variations from background water chemistry include increases in alkalinity, specific conductance and Fe(II), and decreases in pH, NO_3 and SO_4. Aromatic acids (*m* toluic, 2.93 µmol/L and *p* toluic, 1.16 µmol/L) that are typical bacterial products of the fermentation of aromatic hydrocarbons, were detected about 90 m downgradient of the central fire training area (Barcelona and others, 1995). All of these variations in water chemistry are indicators of biodegradation (Hinchee and others, 1995).

STUDY METHODS

Field Sampling

A series of multi-level wells (PVC, 2.5 cm i.d. with 0.33 m PVC screens) are located downgradient from the central fire-training area (fig. 2). Depths range from 5.5 to 11.5 m below land surface. On three dates (October 1995, June 1996 and October 1996) water samples were collected from selected multilevel wells. Each sample was analyzed in the field for:

(1) Temperature, SC, dissolved oxygen (DO), pH and oxidation/ reduction potential (Eh) using a flow-through cell equipped with the appropriate probes;
(2) Alkalinity by titration;
(3) Fe(II) by the ferrozine assay and;
(4) Dissolved H_2 determined by the "bubble-strip" method (Chapelle and others, 1995).

CH_4 and CO_2 were determined by headspace gas analysis, and NO_3, NO_2 and SO_4 by ion chromatography (Chapelle and others, 1996) or (NO_3, NO_2) by cadmium reduction-diazotization (Fishman and Friedman, 1989). Taken together, these parameters were used to estimate the TEAP for each water sample, as described in Chapelle and others (1995). Following definition of TEAP zones, aquifer sediments were collected from specified depths, corresponding to TEAP zones, using a hydraulic punch. Cores retrieved in this manner were stored at 10 °C until they were subsampled for DNA analysis, approximately 3 weeks later.

Analysis of Community Structure

To examine patterns in microbial community structure, two methods of microbial community DNA analysis were used: Amplified

Ribosomal DNA Restriction Analysis (ARDRA; Massol-Deya and others, 1995) and Denaturing Gradient Gel Electrophoresis (DGGE; Muyzer and others, 1993). In the ARDRA procedure (fig. 3), DNA encoding the 16S rDNA genes of bacterial communities is amplified using the polymerase chain reaction (PCR; Mullis and Faloona, 1987) and analyzed by gel electrophoresis. The resulting electrophoretic patterns suggest differences or similarities in microbial community DNA composition. In the DGGE procedure (fig. 3), a smaller piece of the 16S rDNA gene is similarly amplified, and separated according to sequence on a denaturing gradient gel. Again, the resulting banding patterns suggest differences or similarities in microbial community DNA composition; however, in the case of DGGE, each band may theoretically be associated with a specific microorganism. Therefore, the DGGE procedure provides the opportunity to better understand the actual membership of the community.

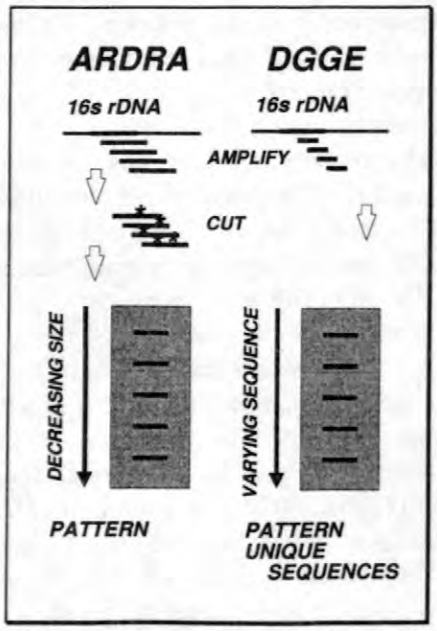

Figure 3. Comparison of two methods for analyzing bacterial community 16S rDNA.

DNA was extracted from Wurtsmith aquifer materials by the method of Zhou and others (1996). For the ARDRA procedure, the method was identical to that described by Massol-Deya and others (1995). For DGGE, we followed the methods of Muyzer and others (1993); however, we used the PCR primers described in Nubel and others (1996).

Population Studies

Population study methods are described in Dojka and others (1998) and Reynolds and Haack (1999, this Proceedings). In the study by Dojka and others (1998), the sequence was determined for the 16S rDNA gene from representative bacteria at three site locations in October of 1996. The sequence of the 16S rDNA gene can be used to determine the relationships between bacteria, thus allowing a tentative grouping of the major bacteria at the sampled locations. The work of Dojka and others (1998) showed that methane-producing bacteria are important at the sampled sites. Therefore, population studies of these bacteria are being conducted, as described in Reynolds and Haack (1999, this Proceedings).

RELATIONS BETWEEN BACTERIAL COMMUNITIES OR POPULATIONS AND TEAPS

TEAP gradients defined by H_2 gas concentrations generally changed from methane-producing to SO_4-reducing, Fe(III)-reducing, NO_3-reducing and aerobic with increasing depth. Sharp changes in the predominant TEAP occurred at less than 1 m intervals. The most reduced zone (methane-producing) occurred nearest the water table where the largest concentrations of contaminants have been detected. In contrast to H_2 analyses and the distributions of CH_4, SO_4, Fe(III) and NO_3, Eh measurements for October 1995 indicated progressively more reduced conditions with depth and all Eh values indicated iron reduction as the dominant redox process within the plume (Chapelle and others, 1996). Some additional information on geochemical gradients at the site is described in McGuire and others (1999, this Proceedings) and Reynolds and Haack (1999, this Proceedings).

On the basis of either ARDRA or DGGE analysis, communities near well ML3 formed 5 groups (C1-C5, table 1). Community groups were defined by the number and electrophoretic migration distance of 16S rDNA molecules in

each type of gel. Samples with bands in similar locations, or having similar numbers of bands, were judged more similar in community composition than those with large differences in banding patterns.

Table 1. Comparison of 16S rDNA electrophoretic banding pattern groups with TEAP zone, at five depths on three dates. [ft, feet; TEAP, terminal electron accepting process; CH_4, methane-producing zone; S, sulfate-reducing zone; Fe, Fe(III)-reducing zone; Fe/Mn, zone intermediate between Fe(III) and Mn(IV) reduction; Fe/S, zone intermediate between Fe(III) and sulfate reduction]

Depth below land surface	Date					
	October 1995		June 1996		October 1996	
	Community[1]	TEAP	Community[1]	TEAP	Community[1]	TEAP
17 ft	C1	Dry	C3	Dry	C3	Dry
19 ft	C1	Dry	C3	CH_4	C3	Fe/S
22 ft	C2	CH_4	C3	S	C3	S
30 ft	C2	S	C4	S	C4	Fe
35 ft	C2	Fe/Mn	C5	S	C5	Fe

[1] Group (C1-C5) assigned to the electrophoretic banding pattern of bacterial community 16S rDNA molecules for samples taken at the indicated depth and date.

Community groups were not differentiated by the TEAP zone from which the aquifer materials were derived (table 1). For example, the C3 community banding pattern was associated with samples that were dry at the time of sampling, as well as with samples from methane-producing, sulfate-reducing and iron-reducing TEAP zones (table 1).

Three locations in October 1996 were evaluated for dominant bacterial populations by analysis of the sequences of 16S rDNA molecules (Dojka and others, 1998). The locations were the 22 and 30 ft depths indicated in table 1, plus an additional sample from 24 ft below land surface. A total of 104 sequences was analyzed. Of these, about two-thirds could be related to cultured bacteria. At the 22 and 24 ft depths, sequences related to *Syntrophus* sp. and *Methanosaeta concillii* were dominant, comprising approximately 13% of all the sequences at these depths. These bacteria are known to be involved in anaerobic aromatic-hydrocarbon degradation and acetate-consuming methane production, respectively. It is interesting to note that these sequences were abundant where methane concentrations were relatively high, although the TEAP indicated by H_2 gas concentration was sulfate-reduction (table 1). At the 30 ft depth, other sequences were dominant, and these could not be related to TEAP processes at the site. Significantly, no sequences closely related to laboratory isolates of Fe(III)-reducing bacteria were found at any of the three depths. Likewise, few sequences related to commonly-studied sulfate-reducing bacteria were found. This is in direct contrast to the indicated TEAPs at these locations.

Perhaps most interesting was the finding that approximately one-third of the sequences at all three depths could not be related to known bacterial isolates. Some of these sequences for unknown bacteria comprised a significant proportion (approximately 15%) of the total sequences at the 22 and 24 ft depths.

CONCLUSIONS

Two lines of evidence suggest that TEAPs (as indicated by H_2 gas concentration) are not major factors influencing bacterial community composition at this site. First, community patterns were unrelated to TEAP designation for the sample. Second, populations present, as determined by 16S rDNA gene sequences, do not necessarily match the TEAP designation for the sample. It may be that other geochemical or contaminant chemistries influence bacterial community structure and population abundance more than do TEAPs. We are currently investigating such relations. In addition, further information on population distributions and dynamics is needed. It is possible that TEAP-related populations such as Fe(III)-reducers are abundant at this site, but in locations we have not analyzed. This finding is important, because TEAP measurements play an important role in site characterization and monitoring at natural attenuation sites. Recognition that certain bacterial populations may be limited to specific

locations within a plume of contaminated ground water can lead to more informed sampling strategies and improved models of plume response to various hydrologic conditions.

A second important finding is that many of the bacteria present at the Wurtsmith site belong to groups for which we have no cultured representatives. This means that we do not know anything about their metabolism, nutritional needs, biodegradative capabilities, or role in TEAPs at the site. This finding simply warns that we must be careful about assuming that we truly understand the nature and role of bacteria at contaminated sites.

ACKNOWLEDGMENTS

In addition to funding by the U.S. Geological Survey Toxic Substances Hydrology Program, a portion of this work was also funded by the National Science Foundation (EAR-9708487 and BIR 9120006), and the National Center for Integrated Bioremediation Research and Development, at Michigan University. We greatly appreciate contributions to the original experimental design by L. J. Forney, and the advice and assistance of members of the ROME lab at Michigan State University.

REFERENCES

Barcelona, M. J., Lu, J., and Tomczak, D. M., 1995, Organic acid derivatization techniques applied to petroleum hydrocarbon transformations in subsurface environments: Ground Water Monitoring and Remediation, vol. 15, no. 1, p. 114-124.

Chapelle, F. H., 1993, Ground-water microbiology and geochemistry: New York, John Wiley and Sons, 424 p.

Chapelle, F. H., McMahon, P. B., Dubrovsky, N. M., Fujii, R. F., Oaksford, E. T. and Vroblesky, D. A., 1995, Deducing the distribution of terminal electron accepting processes in hydrologically diverse groundwater systems: Water Resources Research, vol. 31, no. 1, p. 359-371.

Chapelle, F. H., Haack, S. K., Adriaens, Peter, Henry, M. A., and Bradley P. M., 1996, Comparison of Eh and H_2 measurements for delineating redox processes in a contaminated aquifer: Environmental Science and Technology, vol. 30, no. 12, p. 3565-3569.

Dojka, M. A., Hugenholtz, Philip, Haack, S. K., and Pace, N. R., 1998, Microbial diversity in a hydrocarbon- and chlorinated-solvent-contaminated aquifer undergoing intrinsic bioremediation: Applied and Environmental Microbiology, vol. 64, no. 10, p. 3869-3877.

Fishman, M. J. and Friedman, L. C., 1989, Methods for the determination of inorganic substances in water and fluvial sediments: USGS Techniques of Water Resources Investigations, Book 5, Chapter A1, 545 p.

Hinchee, R.E., Wilson, J. T., and Downey, D.C., 1995, Intrinsic Bioremediation: Columbus, Ohio, Batelle Press, 352 p.

Huffman, G. C., Cummings, T. R., Gillespie, J. L., and Brannen, J. R., 1995, Investigation of soil and ground water contamination at selected sites, Wurtsmith Air Force Base, Michigan. Installation Restoration Program Phase-II – Confirmation/Quantification Stage 2, Vol. I: U.S. Geological Survey, Lansing, Michigan, 600 p.

Hugenholtz, Philip and Pace, Norman, 1996, Identifying microbial diversity in the natural environment: a molecular approach: Trends in Biotechnology, vol. 14, no. 1, p. 190-198.

Massol-Deya, A. .A., Odelson, D. A., Hickey, R. F., and Tiedje, J. M., 1995, Bacterial community fingerprinting of amplified 16S and 16S-23S ribosomal DNA gene sequences and restriction endonuclease analysis (ARDRA), Akkermans, A. D. L., van Elsas, J. D., and deBruijn, F. J., eds., Molecular Microbial Ecology Manual, Norwell, Massachusetts, Kluwer Academic Publishers, Chapter 3.3.2, p. 1-8.

McGuire, J.T., Smith, E. W., Kolak, J. J., Long, D. T., Hyndman, D. W., Velbel, M. A., Klug, M. J., and Haack, S. K., 1999, Temporal Variations in Biogeochemical Processes that Influence Ground-Water Redox Zonation U.S. Geological Survey Toxic Substances Hydrology Program - -Proceedings of the

technical meeting, Charleston, South Carolina, March 8-12, 1999.
Mullis, K.B., and Faloona, F.A., 1987, Specific synthesis of DNA in vitro via a polymerase catalyzed chain reaction: Methods in Enzymology vol. 155, no. 2, p. 263-273.
Muyzer, G., de Waal, E. C., and Uitterlinden, A. G., 1993, Profiling of complex microbial populations by denaturing gradient gel electrophoresis analysis of polymerase chain reaction-amplified genes coding for 16S rRNA: Applied and Environmental Microbiology, vol. 59, no. 2, p. 695-700.
Nübel, U., Engelen, B., Felske, A., Snadir, J., Wieshuber, A., Amann, R. I., Ludwig, W., and Backhaus, H., 1996, Sequence heterogeneities of genes encoding 16S rRNAs in *Paenibacillus polymyxa* detected by temperature gradient gel electrophoresis: Journal of Bacteriology, vol. 178, no. 19, p. 5636-5643.
Reynolds, L. A. and Haack, S. K., 1999, Evaluation of RNA hybridization to assess bacterial population dynamics at natural attenuation sites: U.S. Geological Survey Toxic Substances Hydrology Program - - Proceedings of the technical meeting, Charleston, South Carolina, March 8-12, 1999.
U. S. Geological Survey, 1991, Investigations of groundwater and soil contamination at selected sites Wurtsmith Air Force Base, Michigan. Installation Restoration Program Phase-II – Confirmation/Quantification Stage 1, Vol. I: U.S. Geological Survey, Lansing, Michigan, 154 p.
Zhou, J.-Z., Bruns, M. A., and Tiedje, J. M., 1996, DNA recovery from soils of diverse composition: Applied and Environmental Microbiology, vol. 62, no. 1, p. 316-322.

AUTHOR INFORMATION

Sheridan K. Haack and Lisa A. Reynolds, U.S. Geological Survey, Lansing, Michigan (skhaack@usgs.gov, lreynold@usgs.gov).

Methane as a Product of Chloroethene Biodegradation under Methanogenic Conditions

By Paul M. Bradley and Francis H. Chapelle

ABSTRACT

Radiometric detection headspace analyses of microcosms containing bed sediments from two geographically distinct sites indicated that 10-39% of the radiolabeled carbon transformed during anaerobic biodegradation of [1,2-^{14}C] trichloroethene (TCE) or [1,2-^{14}C] vinyl chloride (VC) under methanogenic conditions was ultimately incorporated into $^{14}CH_4$. The results demonstrate that, in addition to ethene, ethane and CO_2, CH_4 can be a significant product of chloroethene biodegradation in some methanogenic sediments.

INTRODUCTION

Under strongly reducing, methanogenic conditions, poly-chlorinated compounds like PCE and TCE can be degraded via reductive dechlorination through the less chlorinated intermediates, *c*-DCE and VC, to the non-chlorinated compounds, ethene and ethane (Bouwer, 1994; De Bruin and others, 1992; DiStefano and others, 1991; Freedman and Gossett, 1989; Maymo-Gatell and others, 1995; 1997; McCarty and Semprini 1994). A number of investigations conducted in the laboratory using relatively well defined microbial cultures have reported stoichiometric conversion of chlorinated contaminants to ethene and ethane (De Bruin and others, 1992; DiStefano and others, 1991; Freedman and Gossett, 1989). In ground-water systems, however, where microbial communities and environmental conditions are complex, ethene and ethane accumulation rarely accounts for the total observed loss of chloroethene contaminants (Ellis and others, 1996; Weidemeier and others, 1996; Weaver and others, 1996; authors' unpublished results). This observation, in turn, suggests the possibility that in situ biodegradation of chloroethene contaminants under methanogenic conditions may yield other products like CO_2 and CH_4 which are not unique to and, therefore, not diagnostic of chloroethene biodegradation. In fact, a number of studies have demonstrated that CO_2, theoretically the ultimate endproduct of oxidative biodegradation, can be a significant product of chloroethene biodegradation even under methanogenic conditions (Bradley and Chapelle, 1997; 1998; Bradley and others, 1998; Vogel and McCarty, 1985). In contrast, significant reduction of chloroethene contaminants to CH_4, theoretically the ultimate reductive endproduct of biodegradation, has not been reported previously. The purpose of this report is to provide evidence that CH_4 can be a significant product of chloroethene biodegradation under methanogenic conditions.

METHODS

Chemicals

Biodegradation of TCE and VC under methanogenic conditions was investigated using [1,2-^{14}C] TCE (Sigma Chemical Co., St. Louis) and [1,2-^{14}C] VC (NEN Dupont, Boston). Radiometric detection gas chromatography (GC/GRD) and liquid scintillation counting analyses demonstrated that greater than 99% and 98% of the total radioactivity present in the TCE

and VC stocks used in this study was, in fact, [1,2-^{14}C] TCE and [1,2-^{14}C] VC, respectively. The chemical purity (> 99%) of the [1,2-^{14}C] TCE and [1,2-^{14}C] VC was confirmed in our lab by GC/FID and mass spectrometry gas chromatography (GC/MS) analyses.

Study Sites

Microcosm studies were conducted using bed sediments from two geographically distinct sites: the Naval Weapons Industrial Reserve Plant (NWIRP) Dallas, Texas and the Naval Air Station (NAS) Cecil Field, Jacksonville, Florida. The NWIRP Dallas bed sediments were collected from a shallow, freshwater lake which continuously receives ground water contaminated with low concentrations (≤ 20 ppb) of TCE, *c*-DCE and VC. The bed sediment was a highly reduced, soft mud composed of clay and fine silt and characterized by vigorous methanogenesis. The NAS Cecil Field bed sediments, which were described in detail previously (Bradley and Chapelle, 1997), were collected from a shallow, freshwater stream which receives ground water contaminated with low concentrations (≤ 20 ppb) of *c*-DCE. The NAS Cecil Field bed sediment samples, a coarse grained sand with a 2-5% organic content, were collected from a location where continuous methane outgasing was observed.

Microcosm Studies

Anaerobic microcosms were prepared as described previously (Bradley and Chapelle, 1997). In brief, 20 mL serum vials were amended with 15 g saturated, methanogenic bed sediment under a helium atmosphere, sealed with teflon-lined butyl rubber stoppers, and flushed with an excess (1000 mL) of high purity helium. Experimental treatments were prepared in triplicate. Duplicate killed control microcosms were prepared as described and autoclaved twice for 1 h at 15 PSI and 121 C. Sediment microcosms were pre-incubated for 5 days to reestablish active methanogenesis and then amended with approximately 0.5 μCi of [1,2-^{14}C] TCE or [1,2-^{14}C] VC. For the NWIRP Dallas microcosms, initial dissolved concentrations in equilibrium with the headspace were estimated based on experimentally determined adsorption and Henry's law coefficients to be 550 μg/L and 370 μg/L for TCE and VC, respectively. For the NAS Cecil Field microcosms, the initial dissolved concentration was estimated to be 630 μg/L for VC.

For the [1,2-^{14}C] TCE biodegradation study (NWIRP Dallas sediments only), headspace concentrations of TCE and its chlorinated daughter products (*c*-DCE and VC) were monitored periodically by removing 0.5 mL of headspace and analyzing by GC/FID. Headspace concentrations of CH_4, CO_2, ethene and ethane and the absence of O_2 were monitored in the same manner using thermal conductivity detection gas chromatography (GC/TCD). The headspace sample volumes were replaced with helium. At the end of the study, the final distribution of radioactivity in non-chlorinated products was quantified by GC/TCD coupled to GC/GRD. The GC/GRD output was calibrated by liquid scintillation counting using $H^{14}CO_3$. Because the radioactivity of the non-chlorinated products formed in the experimental treatments was not monitored throughout the study, the results of the [1,2-^{14}C] TCE biodegradation study presented in Figure 1 and Table 1 were not corrected for the loss of constituents due to headspace sample collection. Calculations based on interim TCE concentrations observed in killed control microcosms indicated that the low recovery (66%) in this treatment was entirely attributable to sample collection and headspace replacement. For the [1,2-^{14}C] VC biodegradation studies (NWIRP Dallas and NAS Cecil Field sediments), headspace concentrations of VC and its non-chlorinated daughter products were monitored as described above with the exception that the formation of radiolabeled daughter products was monitored continuously throughout the incubation using GC/GRD. The results of the [1,2-^{14}C] VC biodegradation study presented in Figure 2 and Table 2 were corrected for the loss of constituents due to headspace sample collection.

RESULTS AND DISCUSSION

As part of a remedial investigation for NWIRP Dallas, the potential for reductive dechlorination of TCE was examined in bed sediment microcosms under anaerobic conditions (Figure 1). Under these

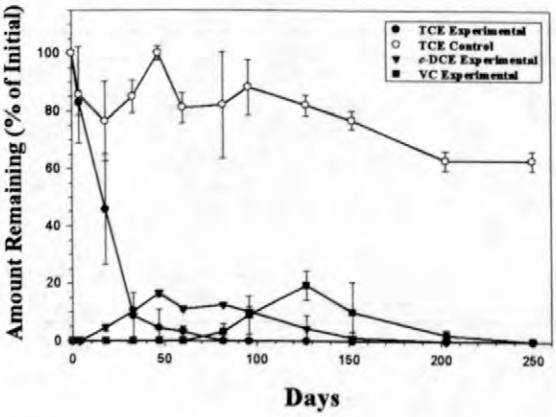

Figure 1. Total amount of TCE and its chlorinated daughter products remaining in methanogenic microcosms containing lake bed sediments from NWIRP Dallas. Data are means±SD.

conditions microbial activity resulted in vigorous methanogenesis (about 35 μmoles/L headspace or 2.1 mg/L microcosm water produced per day , data not shown) and complete disappearance of TCE within 80 days. TCE degradation was followed in turn by accumulation and subsequent disappearance of *c*-DCE and VC. By 250 days, no chloroethene compounds were detected in the experimental microcosms and the study was terminated. In contrast, TCE disappearance in the control microcosms was slow with 63±3 % of the TCE remaining after 250 days (Figure 1). No production of methane (data not shown) or chlorinated daughter products was observed in the control microcosms.

Headspace analyses conducted at day 250 using GC/GRD indicated that TCE had been degraded to non-chlorinated compounds (Table 1). The close agreement in the recovery of radioactivity between experimental and control microcosms indicates that degradation to endproducts other than those reported here was not significant. Approximately half of the radioactivity initially added as [1,2-^{14}C] TCE was recovered as ^{14}C-ethene. This result is consistent with numerous reports that chloroethene contaminants can be reductively dechlorinated to ethene under methanogenic conditions (Bouwer, 1994; De Bruin and others, 1992; DiStefano and others, 1991; Ellis and others, 1996; Freedman and Gossett, 1989; Maymo-Gatell and others, 1995; 1997; McCarty and Semprini, 1994; Weidemeier and others, 1996; Weaver and others, 1996). In addition, 12% of the radioactivity was recovered as $^{14}CO_2$ and 9% as $^{14}CH_4$, respectively. The observed recovery of radioactivity as $^{14}CO_2$ is consistent with previous reports demonstrating significant oxidation of chloroethenes to CO_2 even under methanogenic conditions (Bradley and Chapelle, 1997; 1998; Bradley and others, 1998; Vogel and McCarty, 1985). To our knowledge, however, this is the first evidence of significant degradation of a chloroethene to CH_4.

Table 1. Final distribution of ^{14}C radiolabel in methanogenic microcosms containing sediment from NWIRP Dallas. Data are final recoveries expressed as a percentage of the radioactivity added as TCE. Data are means±SD.

Compound	Experimental %	Control %
TCE	ND*	63±3
c-DCE	ND	ND
VC	ND	ND
Ethene	46±8	ND
Ethane	ND	ND
CH_4	9±2	ND
CO_2	12±2	3±1
Total Recovery	67±8	66±3

*Not detected during analysis. Minimum detection limit was equivalent to a final recovery of 2%.

The biodegradation of chloroethene compounds to CH_4 under methanogenesis was

confirmed in NWIRP Dallas sediment microcosms amended with [1,2-^{14}C] VC (Figure 2a). Consistent

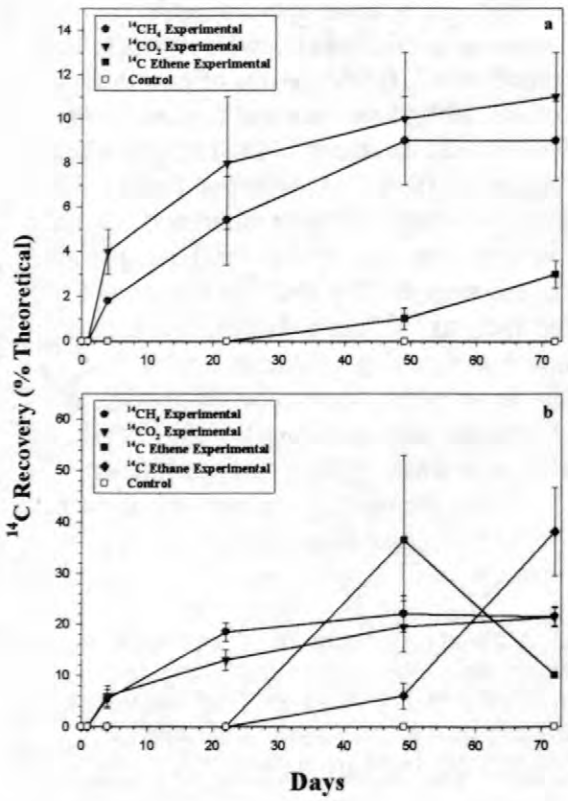

Figure 2. Percentage recvoery of [1,2-^{14}C] VC radioactivity as non-chlorinated products in methanogenic microcosms containing bed sediments from NWIRP Dallas (a) and NAS Cecil Field (b). Data are means ±SD.

with the results of the TCE experiment, biodegradation under these conditions was slow and resulted in only a 21% decline in VC concentrations in the experimental treatments after 70 days compared with a 6% decline in the control microcosms (Table 2). In this study [1,2-^{14}C] VC was degraded to ^{14}C-ethene, $^{14}CO_2$, and $^{14}CH_4$ (Figure 2a, Table 2). Significant recovery of $^{14}CO_2$ and $^{14}CH_4$ was observed within 5 days of incubation but significant production of ^{14}C-ethene was not detected until day 50. The fact that $^{14}CH_4$ represented 39% of the radiolabeled daughter products demonstrated the significance of CH_4 as a product of chloroethene biodegradation in these methanogenic sediments.

Table 2. Final distribution of ^{14}C radiolabel in methanogenic microcosms containing sediment from NWIRP Dallas or NAS Cecil Field. Data are final recoveries expressed as a percentage of the radioactivity added as VC. Data are means±SD.

Site	Compound	Experimental %	Control %
NWIRP Dallas	VC	79±5	94±4
	Ethene	3±1	ND*
	Ethane	ND	ND
	CH_4	9±2	ND
	CO_2	11±2	ND
	Total Recovery	102±5	94±4
NAS Cecil Field	VC	2±3	87**
	Ethene	10±1	ND
	Ethane	39±9	ND
	CH_4	22±1	ND
	CO_2	22±2	ND
	Total Recovery	95±8	87**

*Not detected during analysis. Minimum detection limit was equivalent to a final recovery of 2%.
**Datum for single control microcosm.

A similar production of $^{14}CH_4$ during biodegradation of [1,2-^{14}C] VC was observed in methanogenic microcosms containing stream bed sediments from NAS Cecil Field (Figure 2b). For these sediments, VC loss from experimental treatments was complete after 70 days compared to a 13% loss observed in control microcosms (Table 2). Significant recovery of $^{14}CO_2$ and $^{14}CH_4$ was observed immediately and reached maximum values of 22±2% and 22±1%, respectively. Significant ^{14}C-ethene accumulation was not observed until day 50. In contrast to the NWIRP Dallas study, ^{14}C-ethene concentrations subsequently declined as ^{14}C-ethene was further reduced to ^{14}C-ethane. By the end of the study, ^{14}C-ethene and ^{14}C-ethane represented about 50% of the recovered radioactivity. The significant degradation of [1,2-^{14}C] VC to $^{14}CH_4$ observed in this study is consistent with that observed in NWIRP Dallas

microcosms. The fact that chloroethene biodegradation to CH_4 was observed in sediments from geographically distinct sites suggests that this process may be widespread.

The results of this study have important implications for the use of natural attenuation as a component of contaminant remediation at chloroethene contaminated sites. The results demonstrate that, in addition to ethene, ethane and CO_2, CH_4 can be a significant product of chloroethene biodegradation in some methanogenic sediments. Because regulatory approval of natural attenuation as a remedial strategy at chloroethene contaminated sites typically depends on the demonstration of efficient degradation to nonchlorinated products, the potential transformation of chloroethenes to non-diagnostic, natural products is of significant interest to the field of environmental restoration. Thus, the mechanism of this process and its significance at other chloroethene contaminated sites merit further investigation.

REFERENCES

Bouwer, E. J., 1994, Bioremediation of chlorinated solvents using alternative electron acceptors, Norris and others, eds., Handbook of Bioremediation: Lewis Publishers, Boca Raton, p 149-175.

Bradley, P. M. and Chapelle, F. H., 1997, Effect of contaminant concentration on aerobic microbial mineralization of DCE and VC in stream-bed sediments: Environmental Science and Technology, v. 31, p. 2692-2696.

Bradley, P. M. and Chapelle, F. H., 1998, Microbial mineralization of VC andDCE under different terminal electron accepting conditions: Anaerobe, v. 4, p. 81-87.

Bradley, P. M., Chapelle, F. H., and Lovley, D. R., 1998, Humic acids as electron acceptors for anaerobic microbial oxidation of vinyl chloride and dichloroethene: Applied and Environmental Microbiology, v. 64, p. 3102-3105.

De Bruin, W. P., Kotterman, M. J. J., Posthumus, M. A., Schraa, G., and Zehnder, A. J. B., 1992, Complete biological reductive transformation of tetrachloroethene to ethane: Applied and Environmental Microbiology, v. 58, p. 1996-2000.

DiStefano, T. D., Gossett, and J. M., Zinder, S. H., 1991, Reductive dechlorination of high concentrations of tetrachloroethene to ethene by an anaerobic enrichment culture in the absence of methanogenesis: Applied and Environmental Microbiology, v. 57, p. 2287-2292.

Ellis, D. E., Lutz, E. J., Klecka, G. M., Pardieck, D. L., Salvo, J. J., Heitkamp, M. A., Gannon, D. J., Mikula, C. C., Vogel, C. M., Sayles, G. D., Kampbell, D. H., Wilson, J. T. and Maiers, D. T., 1996, Remediation technology development forum intrinsic bioremedation project at Dover Air Force Base, Deleware–Proceedings of the Symposium on Natural Attenuation of Chlorinated Organics in Ground Water, Dallas, Texas, September 11-13, 1996: U.S. Environmental Protection Agency, EPA/540/R-96/509, p. 93-97.

Freedman, D. L. and Gossett, J. M., 1989, Biological reductive dechlorination of tetrachloroethylene and trichloroethylene to ethylene under methanogenic conditions, Applied and Environmental Microbiology, v. 55, p. 2144-2151.

Maymo-Gatell, X., Tandoi, V., Gossett, J. M., and Zinder, S. H., 1995, Characterization of an H_2 utilizing enrichment culture that reductively dechlorinates tetrachloroethene to vinyl chloride and ethene in the absence of methanogenesis and acetogenesis, Applied and Environmental Microbiology, v. 61, p. 3928-3933.

Maymo-Gatell, X., Chien, Y-T, Gossett, J. M., and Zinder, S. H., 1997, Isolation of a bacterium that reductivley dechlorinates tetrachloroethene to ethene, Science, v. 276, p. 1568-1571.

McCarty, P. L. and Semprini, L., 1994, Ground-water treatment for chlorinated solvents, Norris and others, eds., Handbook of Bioremediation: Lewis Publishers, Boca Raton, p. 87-116.

Vogel, T. M. and McCarty, P. L., 1985, Biotransformation of tetrachloroethylene to trichloroethylene, dichloroethylene, vinyl chloride, and carbon dioxide under methanogenic conditions: Applied and Environmental Microbiology, v. 49, p. 1080-1083.

Weaver, J. W., Wilson, J. T., and Kampbell, D. H., 1996, Extraction of degradation rate constants from the St. Joseph, Michigan, trichloroethene site–Proceedings of the Symposium on Natural Attenuation of Chlorinated Organics in Ground Water, Dallas, Texas, September 11-13, 1996: U.S. Environmental Protection Agency, EPA/540/R-96/509, p. 69-73.

Weidemeier, T. H., Wilson, J. T., and Kampbell, D. H., 1996, Natural attenuation of chlorinated aliphatic hydrocarbons at Plattsburgh Air Force Base, New York–Proceedings of the Symposium on Natural Attenuation of Chlorinated Organics in Ground Water, Dallas, Texas, September 11-13, 1996: U.S. Environmental Protection Agency, EPA/540/R-96/509, p. 74-82.

AUTHOR INFORMATION

Paul M. Bradley and Francis H. Chapelle, U.S. Geological Survey, Columbia, S.C.

Chlorinated Ethenes from Ground Water in Tree Trunks

By Don A. Vroblesky, Christopher T. Nietch, and James T. Morris

ABSTRACT

The purpose of this investigation was to determine whether tree-core analysis could be used to delineate shallow ground-water contamination by chlorinated ethenes. Analysis of tree cores from baldcypress [*Taxodium distichum* (L) Rich.], tupelo (*Nyssa aquatica* L.), sweetgum (*Liquidambar stryaciflua* L.), oak (*Quercus* spp.), sycamore (*Platanus occidentalis* L.), and loblolly pine (*Pinus taeda* L.) growing over shallow ground water contaminated with *cis*-1,2-dichloroethene (*c*DCE) and trichloroethene (TCE) showed that those compounds also were present in the trees. The cores were collected and analyzed by headspace gas chromatography. Baldcypress, tupelo, and loblolly pine contained the highest concentrations of TCE, with lesser amounts in nearby oak and sweetgum. The concentrations of *c*DCE and TCE in various trees appear to reflect the configuration of the chlorinated-solvent ground-water contamination plume. Baldcypress cores collected along 18.6-meter vertical transects of the same trunks showed that TCE concentrations decline by 30 to 70 percent with trunk height. The ability of the tested trees to take up *c*DCE and TCE make tree coring a potentially cost effective and simple approach to optimizing well placement at this site

INTRODUCTION

The use of vegetation in studies of ground-water contamination has received increasing attention for a variety of reasons. Plants can remove contaminants from the subsurface by direct uptake and degradation (Briggs and others, 1982; McFarlane and others, 1987; McCrady and others, 1987; Schnabel and others, 1997; Strand and others, 1995), transpiration of volatile contaminants to the atmosphere (Newman and others, 1997; McFarlane and others, 1990; Tollsten and Muller, 1996), binding contaminants to plant tissue (Newman and others, 1997; Schnabel and others, 1997; Strand and others, 1995), and enhancing microbial growth and bioremediation in the rhizosphere (Shimp and others, 1993; Schnoor and others, 1995; Anderson and Walton, 1989; Jordahl and others, 1997; Walton and Anderson, 1990). Direct uptake of contaminants is controlled by a variety of factors, but, in general, moderately hydrophobic organic compounds (octanol-water coefficient, log K_{ow} = 0.5-3), such as trichloroethene (TCE) and *cis*-1,2-dichloroethene (*c*DCE), readily enter vegetation transpiration streams (Schnoor and others, 1995; Anderson and Walton, 1995).

This investigation shows that TCE and *c*DCE are present in tree trunks growing above contaminated shallow ground water contaminated. To our knowledge, this is the first investigation demonstrating that headspace analysis of tree cores can be an inexpensive and rapid method to delineate shallow TCE and *c*DCE ground-water contamination. In addition, this investigation presents data showing variations in concentrations of those compounds vertically upward along a tree trunk. Cores were collected from 97 mature trees growing above and in the vicinity of contaminated ground water. Six different species of trees were examined. Cores from one tree were collected at various heights along the trunk.

The study area is a forested flood plain of the Savannah River near the TNX Area, Savannah River Site, South Carolina (fig. 1). The flood plain consists of an upper and lower terrace, separated by an embankment ranging from about

1 to 2 meters (m) high. Northeast of the upper flood plain, land surface rises sharply to an upland terrace (the TNX Area) containing a former seepage basin. During a few days to a few months per year, the Savannah River inundates the lower flood plain (fig. 2). During most of the year, however, standing water is limited to low-lying areas of the upper and lower flood plains.

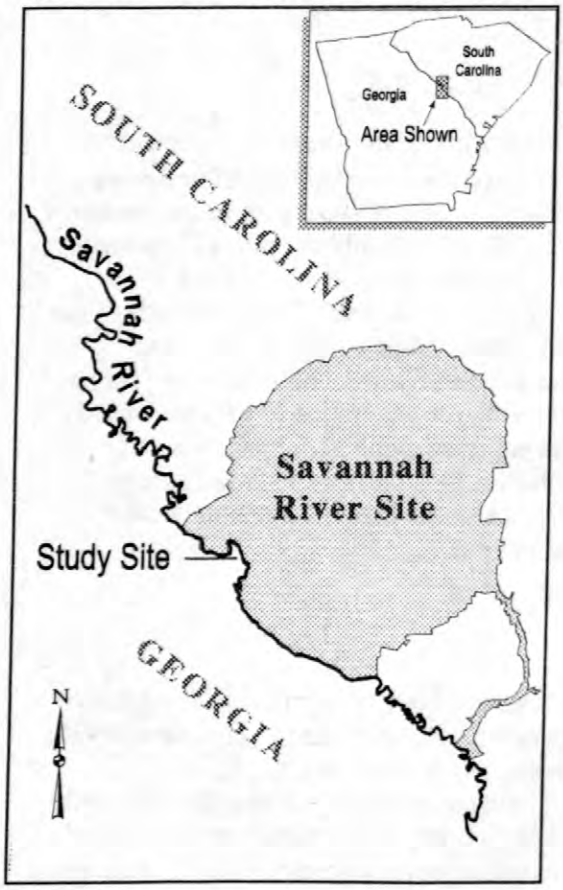

Figure 1. Location of study area.

Chlorinated solvents are present in the ground water beneath parts of the upper flood plain. The dominant contaminants are TCE and *c*DCE. The probable source of the chlorinated solvents is leakage from a former seepage basin in the TNX Area (fig. 2). Ground water flows through unconsolidated sands toward a drainage ditch that empties into the Savannah River. Depth to the water table beneath the flood plain ranges from the land surface to about 1.5 m. The ground-water-flow rate in the flood plain is approximately 0.46 meters per day (Hamm and others, 1997).

Vegetation in the swamps of the flood plain primarily consists of baldcypress [*Taxodium distichum* (L) Rich.], tupelo (*Nyssa aquatica* L.), and sweetgum (*Liquidambar stryaciflua* L.). In drier parts of the flood plain, oak (*Quercus* spp.), loblolly pine (*Pinus taeda* L.), and sweetgum are dominant, with a relatively small population of baldcypress and sycamore (*Platanus occidentalis* L.).

METHODS

Cores were collected with an increment borer from 97 trees on the Savannah River flood plain in South Carolina during January, February, July, August, September, and October 1997, and January and February 1998. The trees included 64 baldcypress, 5 tupelos, 12 loblolly pines, 3 sycamores, 6 oaks, and 7 sweetgums (fig. 2). Part of the area contained ground water contaminated with TCE and *c*DCE. Trees 11, 16, 17, and 53, were control oak, loblolly pine, sweetgum, and sycamore trees, respectively, collected from offsite areas not shown in figure 2.

The cores used to delineate contamination in Figures 3 and 4 were collected from the northeastern side of the respective tree. All cores used to examine areal distribution of contamination were collected from a height of approximately 1.5 m above ground, except for tree 7a, which was collected from 9 m on August 11, 1997 and 3 m on October 1, 1997, and trees 20z and 21z, which were collected from about 1.8 m.

At selected trees, two cores were collected approximately 25 millimeters (mm) horizontally from each other to compare replication. The average concentration difference between replicate cores was 15.2 percent for TCE in 6 replicate pairs and 2.5 percent for *c*DCE in 3 replicate pairs. A baldcypress (tree 7) also was cored at various heights along its trunk. A bucket truck was used to access the tree, which grew adjacent to an unpaved road.

Upon collection, the cores (approximately 68 mm in length) immediately were removed from the coring tools and placed in 20-milliliter (mL) glass vials. At selected sites, ambient-air

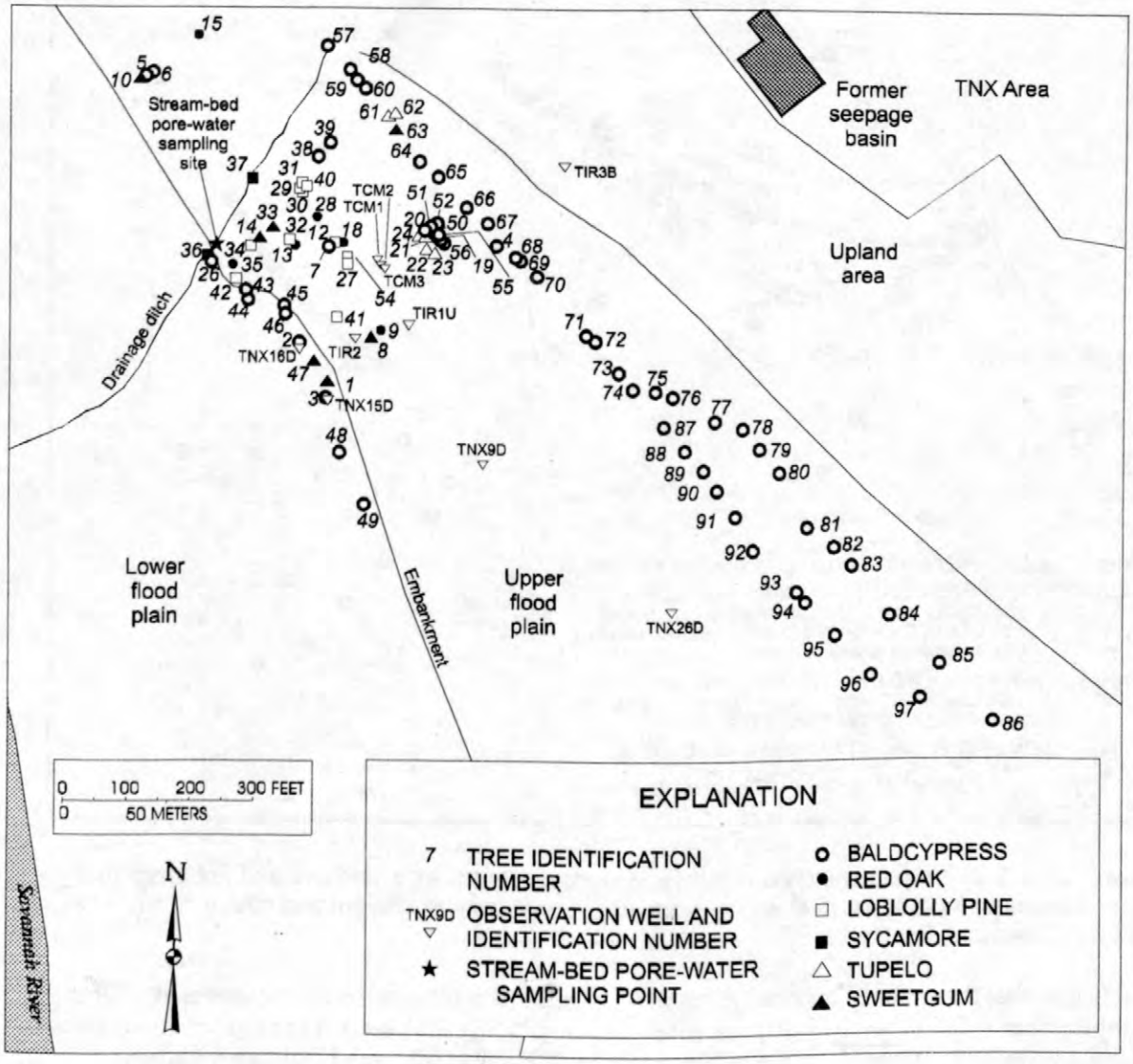

Figure 2. Location and identification numbers of test trees and observation wells on the Savannah River flood plain, TNX Area, Savannah River Site, SC.

samples also were collected by waving empty 20-mL glass vial in the air for several seconds. Teflon-coated septum caps then were crimped onto the vials. The vials were heated at 40 degrees Celsius (°C) for 12 hours to vaporize volatile compounds in the cores. The vials then were cooled to room temperature, and a 100 microliter (μL) sample of the head space was collected into a gas syringe. Gas samples were analyzed by photoionization detection on a Photovac 10S Plus gas chromatograph. Concentrations are reported here as nanomoles of gas per liter of core water (nmol/L). Statistical tests were done on concentrations based on core-water volume and the core dry weight verified that the sample normalization procedure did not significantly affect the results.

Ground-water was purged and sampled from wells using a positive-displacement submersible pump. Casing water was purged until specific conductance stabilized. Ground-water was sampled from beneath the drainage ditch by pushing a 6.35-centimeter (cm) inside-diameter (I.D.) stainless-steel sampling point into the

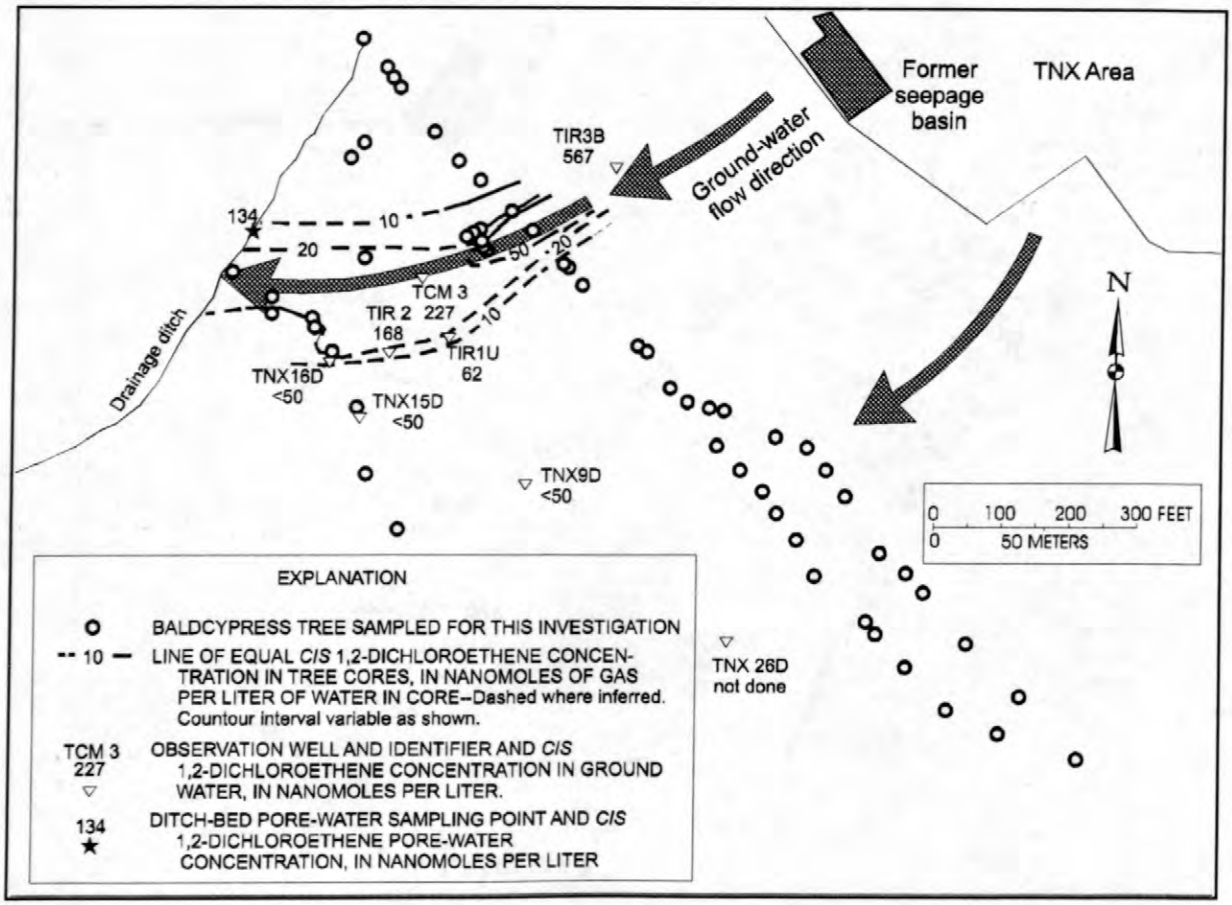

Figure 3. cis-1,2-Dichloroethene concentrations in baldcypress trunks in January and February 1998 and in ground water during August 1997 and ground-water-flow directions (Hamm and others, 1997), TNX flood plain, Savannah River Site, SC.

streambed so that the screened interval (7.8 mm) was approximately 0.6 m below the stream base. Interstitial water was pumped from the piezometer using a peristaltic pump. Water was pumped at a slow rate, and a minimum amount of water (20 mL) was removed prior to collecting a water sample for VOCs to avoid dilution effects from mixing with stream water. Water samples were collected in 40-mL glass bottles, capped with Teflon-lined bottle caps, and were analyzed using U.S. Environmental Protection Agency method 8240 (U.S. Environmental Protection Agency, 1986).

Statistics were performed using the SAS software package (SAS Institute Inc., Cary, N.C.). Analysis of variance tests (PROC GLM) were used to evaluate differences in TCE and *c*DCE concentrations among tree species and between sites (control relative to contaminated). Linear regression analysis was used to test for changes in TCE and *c*DCE with height above ground.

RESULTS AND DISCUSSION

Ground water in the vicinity of several test trees contained TCE and lesser amounts of *c*DCE . These compounds were not detected in air samples adjacent to the trees, indicating that the compounds were derived from below land surface. In May 1997, water samples from wells TIR 3B and TCM 3 contained 3,577 and 1,187 nmol/L of TCE, respectively (William Pidcoe, Westinghouse Savannah River Company, written commun., July 1997). Well TCM 3 also contained 246 nmol/L of *c*DCE. Numerical

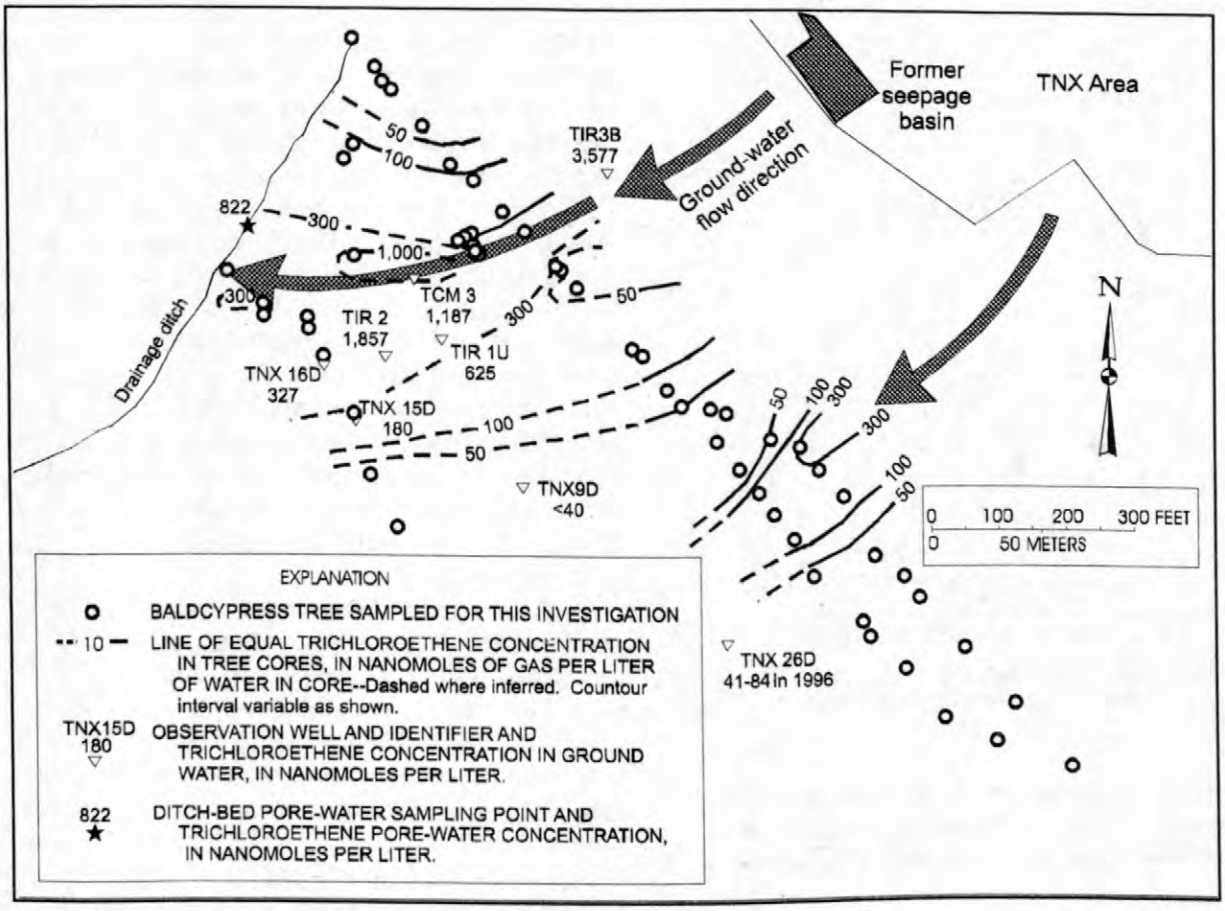

Figure 4. Tichloroethene concentrations in baldcypress trunks in January and February 1998, in ground water during May 1997 and 1996 (well TNX-26D only), and at the ditch-bed pore-water sampling point during August 1997 and ground-water-flow directions (Hamm and others, 1997), TNX flood plain, Savannah River Site, SC.

simulations (Hamm and others, 1997) suggest that the path of contaminated ground water flow from the former seepage lagoon is toward a reach of the drainage ditch near the embankment separating the upper and lower flood plains (fig. 3). Ground water beneath the ditch, collected from a drive-point well screen (fig. 2) in the probable contaminant-discharge zone, contained 134 nmol/L of *c*DCE and 822 nmol/L of TCE in August 1997, providing supporting evidence for the hypothesized path of contaminant transport.

Cis-1,2-dichloroethene was present in cores from several baldcypress trees growing in the area of *c*DCE contaminated ground water. The area where *c*DCE was found in baldcypress trees was along a path coincident with the ground-water-flow path from the former seepage basin (fig. 3) and coincided with areas where *c*DCE was found in ground water. The data strongly suggest that the *c*DCE in tree trunks is derived from the contaminated ground water originating from the former seepage basin.

TCE also was found in baldcypress trunks growing in the area of TCE contaminated ground water downgradient from the former seepage basin (fig. 4). The distribution of baldcypress containing TCE was more widespread than the distribution of baldcypress containing *c*DCE. Moreover, TCE also was found in tree 78 and the neighboring trees farther south than the flow path from the former seepage basin (fig. 4). These data suggest a second plume of TCE in the aquifer. Although no data was collected from well TNX 26D during 1997-98, 41 to 84 nmol/L of TCE were found in ground water at the well during 1996 (William Pidcoe, Westinghouse Savannah River Company, written commun., July

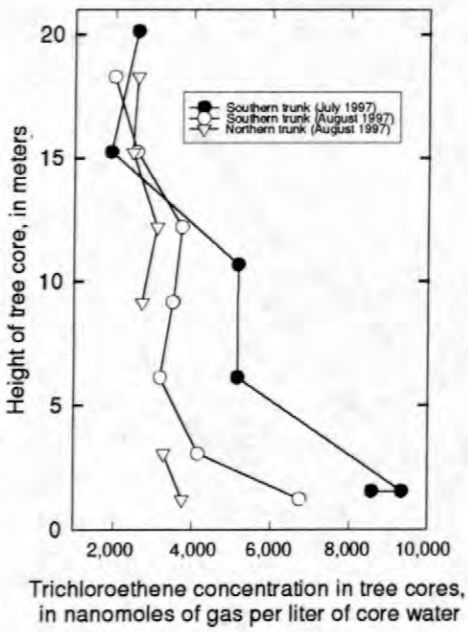

Figure 5. Trichloroethene concentrations in cores along the trunk of tree 7 (baldcypress). Cores from the northern trunk were not collected in July 1997.

1998), supporting the hypothesis that the spatial distribution of TCE among baldcypress sampled across the area reflects the distribution of TCE in the shallow aquifer.

Examination of cores collected at various trunk heights of a baldcypress (tree 7) growing in an area of ground water contaminated with TCE showed that concentrations of TCE decreased significantly with increasing trunk height ($p=0.001$) (fig. 5), although *c*DCE concentrations did not ($p=0.4$) (data not shown). Tree 7 branched into two trunks at a height of 2.1 m above ground. The two trunks are designated as southern and northern. TCE concentrations along the southern trunk of tree 7 during July and August decreased by about 70 percent and 53 percent, respectively, from near the ground to a height of about 17 to 18.6 m (fig. 4). The northern trunk of tree 7 showed an approximate 30 percent decrease in TCE concentrations over the same vertical distance in August 1997 (fig. 5).

The specific mechanism causing decreasing concentrations of TCE with increasing height in tree 7 (fig. 5) is not known. One possibility is that there is a loss mechanism for TCE along the transport pathway up the tree. Such a loss mechanism could be VOC volatilization followed by diffusion through the tree bark. The fact that water vapor is known to escape through the bark of trees, chiefly through lenticels (Kozlowski and Pallardy, 1997), is consistent with the loss of TCE through the tree bark. The Henry's Law Constant is slightly larger for smaller for TCE (0.007 m^3 atm/mol) than for *c*DCE (0.0032 m^3 atm/mol), indicating that TCE has a slightly larger tendency to volatilize that *c*DCE (Washington, 1996). Additional possible explanations include TCE degradation or sorption within the trunk, the potential for spiral transport of fluids up the trunk (Kozlowski and others, 1962), or temporal changes in ground-water contaminant concentrations.

Although all of the cores collected for this analysis were from the northeastern part of each tree, selected trees were cored at various locations around the trunk to examine directional variability. Core data from different sides of individual trees showed concentration differences ranging from 44 to 92 percent for TCE and 6 to 90 percent for *c*DCE. The relatively good replication in cores collected 25 mm apart (15.5 percent for TCE and 2.5 percent for *c*DCE) indicates that the coring approach did not contribute significant inconsistencies to the data. The source of the directional variation is not known, but may be related to a variety of factors, such as injuries (Scholander and others, 1957), disease and insect damage (Kozlowski and others, 1962), gas embolisms (Clark and Gibbs, 1957), and variations in TCE concentration taken up by root systems on differing sides of the tree.

All species of trees examined from areas of ground-water contamination showed evidence of TCE or *c*DCE in the trunks. Some species appeared to exhibit similar uptake potential. Examination of a cluster of baldcypress and tupelo (trees 19-24, 50-52, and 55) showed no significant differences in concentrations between the species. In January 1998, the TCE concentration in baldcypress 7 was approximately 2,000-3,000 nmol/L, and high concentrations of TCE also were found in nearby loblolly pines 12, 27, and 54 (1,742; 1,241; 1,324 nmol/L, respectively). Baldcypress 43 also contained similar TCE concentrations (296 nmol/L) to adjacent loblolly 42 (479 nmol/L).

Oaks, however, appeared to contain less TCE than adjacent baldcypress or loblolly pines. In September 1997, oak 11 contained <50 nmol/L of TCE while a nearby loblolly pine (tree 12) contained 730 nmol/L of TCE, and a nearby baldcypress tree (tree 7) contained 3,180 nmol/L of TCE. Similarly, in January 1997, a different oak (tree 35) contained only 69 nmol/L of TCE, whereas loblolly pines on either side of tree 35 contained 2,263 (tree 34) and 479 (tree 42) nmol/L. Likewise, oak 13 contained less than 50 nmol/L of TCE while an adjacent loblolly (tree 32) contained 764 nmol/L of TCE. The consistency of the data implies that these findings are function of tree-species differences rather than an artifact of variability due to sampling a particular side of each tree.

Sweetgum also appeared to contain less TCE than loblolly pines. Sweetgums 14 and 33 contained <50 and 74 nmol/L of TCE, respectively, in January 1998, while loblolly pines on various sides of the sweetgums contained 765 nmol/L (tree 32), 2,263 nmol/L (tree 34), 308 nmol/L (tree 29), 318 nmol/L (tree 30), and 751 nmol/L (tree 31).

Previous investigations also have noted concentration differences among species. Selected chlorinated compounds have been found to be degraded faster in the rhizosphere soil of monocot species than dicot species (Shann and Boyle, 1994). Loblolly pines have been found to take up more trichloroethene (TCE) than grasses and legumes (Anderson and Walton, 1989). In this investigation, the concentration differences also may partly be a function of the water-conduction differences between species. Conifers (such as baldcypress and loblolly pine) conduct water through more than the outermost ring, whereas in ring-porous trees (such as oak) nearly all of the water is conducted through the outermost growth ring (Ellmore and Ewers, 1986). Thus, the higher concentrations detected in conifers relative to the oaks may be because the cores, being of approximately equal length, incorporated more of the transpiration stream in conifers than in the ring-porous trees.

SUMMARY AND CONCLUSIONS

The extensive areas of swamp and periodic flooding impart difficulties in installing and maintaining effective ground-water sampling wells at this site. The large number of trees available, however, and the ability of those trees to take up *c*DCE and TCE, even in areas of standing water, make tree coring a potentially cost effective and simple approach to optimizing well siting in this type of environment.

REFERENCES

Anderson, T.A., and Walton, B.T., 1989, Microbial degradation of trichloroethylene in rhizosphere and nonvegetated soils from a contaminated field site: Abstracts, 10th Annual Meeting, Society of Environmental Toxicology and Chemistry, Toronto, Ontario, Canada, October 28- November 2, p. 69.

_____ 1995, Comparative rate of [^{14}C]trichloroethylene in the root zone of plants from a former solvent disposal site: Environmental Toxicology and Chemistry, v. 14, no. 12, p. 2041-2047.

Briggs, G.G., Bromilow, R.H., and Evans, A., 1982, Relationships between lipophicity and root uptake and translocation of non-ionized chemicals by barley: Pesticide Science, v. 13, p. 495-504.

Clark, J., and Gibbs, R.D., 1957, Studies in tree physiology, IV, Further investigations of seasonal changes in moisture content of certain Canadian forest trees: Canadian Journal of Botany, v. 35, p. 219-253.

Ellmore, G.S., and Ewers, F.W., 1986, Fluid flow in the outermost xylem increment of a ring-porous tree, Ulmus Americana: American Journal of Botany, v. 73, no. 12, p. 1771-1774.

Hamm, L.L., Aleman, S.E., and Shadday, M.A., 1997, TCE contaminant transport modeling in the TNX area (U): Westinghouse Savannah River Company Report WSRC-TR-97-0111, Westinghouse Savannah River Company, Aiken, S.C., 139 p.

Jordahl, J.L., Foster, L., Schnoor, J.L., and Alvarez, P.J., 1997, Effect of hybrid poplar trees on microbial populations important to hazardous waste bioremediation:

Environmental Toxicology and Chemistry, v. 16, no. 6, p. 1318-1321.

Kozlowski, T.T., Winget, C.H., and Torrie, J.H., 1962, Daily radial growth of oak in relation to maximum and minimum temperature: Botanical Gazette (Chicago), v. 124, p. 9-17.

Kozlowski, T.T., Hughes, J.F., and Leyton, L., 1967, Dye movement in gynmosperms in relation to tracheid alignment: Forestry, v. 40, p. 209-227.

McCrady, J.K., McFarlane, C., and Lindstrom, F.T., 1987, The transformation and affinity of substituted benzenes in soybean stems: J. Experimental Botany, v. 38, no 196, p. 1875-1890.

McCrady, J.K., McFarlane, C., and Lindstrom, F.T., 1987, The transformation and affinity of substituted benzenes in soybean stems: J. Experimental Botany, v. 38, no 196, p. 1875-1890.

McFarlane, J.C., Pfleeger, T., and Fletcher, J., 1990, Effect, uptake and disposition of nitrobenzene in several terrestrial plants: Environmental Toxicology and Chemistry, v. 9, p. 513-520.

Newman, L.A, Strand, N.C., Duffy, J., Ekuan, G., Ruszaj, M., Shurtlef, B.B., Wilmoth, J., Heilman, P., and Gordon, M.P., 1997, Uptake and biotransformation of trichloroethylene by hybrid poplars: Environmental Science and Technology, v. 31, p. 1062-1067.

Schnabel, W.E., Dietz, A.C., Burken, J.G., Schnoor, J.L., and Alvarez, P.J., 1997, Uptake and transformation of trichloroethylene by edible garden plants: Water Research, v. 31, no. 4, p. 816-824.

Schnoor, J.L., Licht, L.A., McCutcheon, S.C., Wolf, N.L., and Carreira, L.H., 1995, Phytoremediation of organic and nutrient contaminants: Environmental Science and Technology, v. 29, no. 7, p. 318A-323A.

Shann , J.N., and Boyle, J.J., 1994, Influence of plant species on in situ rhizosphere degradation, *in* Anderson, T.A., and Coats, J.N., eds., Bioremediation through rhizosphere technology: Washington D.C., American Chemical Society, p. 71-81.

Shimp, J.F., Tracy, J.C., Davis, L.C., Lee, E., Huang, W., Erickson, L.E., and Schnoor, J.L., 1993, Beneficial effects of plants in the remediation of soil and ground water contaminated with organic materials: Critical Reviews in Environmental Science and Technology, v. 23, no. 1, p .41-77.

Scholander, P.F, Ruud, B., and Leivestad, H., 1957, The rise of sap in a tropical liana: Plant Physiology, v. 32, p. 1-6.

Strand, S.E., Newman, L., Ruszaj, M., Wilmoth, J., Shurtleft, B., Grandt, M., Choe, N., Ekuan, G., Duffy, J., Massman, J.W., Heilman, P.E., and Gordon, M.P., 1995, Removal of trichloroethylene from aquifers using tress: Presented at the ASCE Annual Meeting, Pittsburgh, P.A.

Tollsten, L., and Muller, P.M., 1996, Volatile organic compounds emitted from beech leaves: Phytochemistry, v. 43, no. 4, p. 759-762.

U.S. Environmental Protection Agency, 1986, Test methods for evaluating solid waste, Physical/chemical methods, SW-846 (3rd ed.): U.S. Environmental Protection Agency, Washington, D.C., 1919 p.

Walton, B.T., and Anderson, T.A., 1990, Microbial degradation of trichloroethylene in the rhizosphere - Potential application to biological remediation of waste sites: Applied and Environmental Microbiology, v. 56, p. 1012-1016.

Washington, J.W., 1996, Gas partitioning of dissolved volatile organic compounds in the vadose zone - Principles, temperature effects and literature review: Ground Water, v. 34, no. 4, p. 707-718.

AUTHOR INFORMATION

Don A. Vroblesky is a geochemist with the U.S. Geological Survey. James T. Morris is a professor at the University of South Carolina. Christopher T. Nietch is a graduate student at the University of South Carolina.

Relative Importance of Natural Attenuation Processes in a Trichloroethene Plume and Comparison to Pump-and-Treat Remediation at Picatinny Arsenal, New Jersey

by Thomas E. Imbrigiotta and Theodore A. Ehlke

ABSTRACT

The relative importance of naturally occurring fate and transport processes that remove or introduce trichloroethene (TCE) from or to a contamination plume at Picatinny Arsenal, New Jersey, was evaluated. Anaerobic biotransformation removes the most TCE from the plume, destroying 230 kilograms per year, and accounts for approximately 70 percent of the total mass of TCE removed from the plume annually by all natural attenuation processes. Advective transport and advection-driven volatilization each remove 50 kilograms per year. Other removal processes--lateral dispersion, diffusion-driven volatilization, and sorption--are minor in comparison. Desorption is the most significant TCE input process evaluated. A mass-balance analysis shows that the removal of TCE from the plume by natural attenuation processes is of the same order of magnitude as the input of TCE to the plume. The field-scale natural-attenuation rate constants calculated from field TCE concentrations and time-of-travel data are in general agreement with anaerobic-biotransformation rate constants measured in laboratory microcosm studies. A pump-and-treat system operating at the site is removing about 20 percent as much TCE as is being removed from the plume annually by natural attenuation processes.

INTRODUCTION

Past efforts to clean up ground water contaminated with chlorinated solvents typically have relied on engineered remediation systems that were costly to build and operate and have met with limited success. Recently, environmental regulatory agencies have begun to give serious consideration to the use of natural attenuation as a more cost-effective remediation option (Wiedemeier and others, 1996). The successful use of natural attenuation to remediate chlorinated-solvent contamination sites requires an understanding of the processes that control the transport and fate of these compounds in the ground-water system. Therefore, the U.S. Geological Survey, as part of its Toxic Substances Hydrology Program, has been conducting an interdisciplinary research study of ground-water contamination by chlorinated solvents at Picatinny Arsenal, New Jersey. The objectives of the study are to (1) identify and quantify the physical, chemical, and biological processes that affect the transport and fate of chlorinated solvents, particularly trichloroethene (TCE), in the subsurface; (2) determine the relative importance of these processes at the site; and (3) develop predictive models of chlorinated-solvent transport that may have transfer value to other solvent-contaminated sites in similar hydrogeologic environments. This paper reports the results of work done to identify and quantify the natural processes that remove or introduce TCE from or to the plume at Picatinny Arsenal and to determine the relative importance of these processes on a plume-wide basis, and compares the TCE-removal effectiveness of natural attenuation processes and a pump-and-treat system operating as an interim remediation measure at the site.

Geohydrology

Picatinny Arsenal is a weapons research-and-development facility located in a narrow glaciated valley in north-central New Jersey (fig. 1). The site is underlain by a 15- to 20-m- (meter) thick unconfined aquifer consisting primarily of fine to coarse

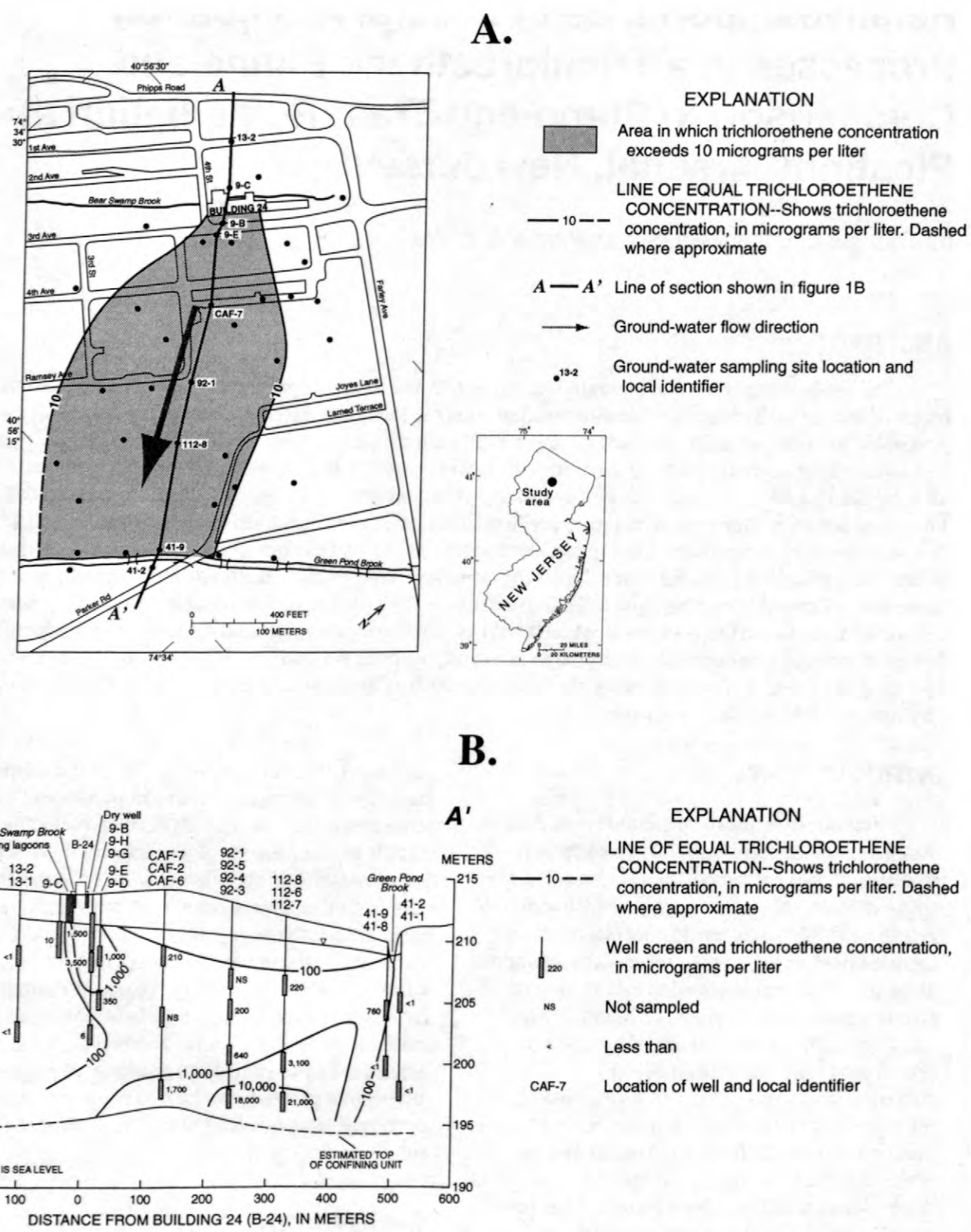

Figure 1. Location of Building 24 study area at Picatinny Arsenal, New Jersey, and (A) areal extent of ground-water trichloroethene plume, and (B) vertical distribution of ground-water trichloroethene concentrations, October and November 1991.

sand with some gravel and discontinuous layers of silt and clay. Ground water flows from the sides of the valley toward the center, where it discharges to Green Pond Brook. Within the unconfined aquifer, flow is generally horizontal, with some downward flow near the valley walls and upward flow near Green Pond Brook. Ground-water-flow velocities are estimated to range from 0.3 to 0.7 m/d (meters per day) at the site on the basis of hydraulic conductivities that range from 15 to 90 m/d, gradients that range from 1.5 to 3.0 m/500 m, and an average porosity of 0.3 (Martin, 1989; Martin, 1991; Martin, 1996; Voronin, 1991; Voronin and Rice, 1996).

Ground-Water and Surface-Water Contamination

Ground water at Picatinny Arsenal was contaminated over a period of 30 years as a result of activities associated with metal-plating and degreasing operations in Building 24 (Sargent and others, 1990; Benioff and others, 1990). The areal and vertical extent of TCE contamination at the site, determined on the basis of TCE concentrations in October and November 1991, is shown in figure 1. Areally, the plume, as defined by the 10-µg/L (microgram per liter) isoconcentration line, extends about 500 m from Building 24 to Green Pond Brook and is approximately 250 m wide where it enters the brook (fig. 1A). Vertically, TCE is found at shallow depths near the source, over the entire 15- to 20-m thickness of the unconfined aquifer in the plume center, and at shallow depths as it discharges upward to the brook (fig. 1B). Whereas TCE concentrations greater than 1,000 µg/L are found in the source area, the TCE concentrations are highest (>10,000 µg/L) near the base of the aquifer midway between the source and the discharge point.

Although TCE concentrations in shallow wells in the center of the plume near Green Pond Brook are high (760 µg/L, fig. 1B), those in the brook immediately downstream from the plume discharge point average 1 µg/L. This decrease in concentrations of dissolved TCE over this short distance is attributed to dilution by streamflow. Where the stream leaves the arsenal approximately 1 mile further downstream, all TCE concentrations are less than 1 µg/L.

GEOCHEMISTRY OF THE PLUME

Results of water-quality analyses indicate that the pH of ground water in the plume is near-neutral (6.5-7.5) and concentrations of both dissolved oxygen (<0.5 mg/L (milligram per liter)) and dissolved nitrate (<1 mg/L) are very low. Concentrations of ferrous iron(II) are greater than 1 mg/L in some areas of the plume, whereas sulfate and carbon dioxide are present in sufficiently high concentrations (>40 mg/L and >100 mg/L as bicarbonate, respectively) over most of the plume to act as terminal electron acceptors. In addition, sulfide odor was noted in water from many wells within the plume and methane was present at concentrations ranging from 1 to 85 µg/L. These findings indicate that the plume is primarily anaerobic and contains a variety of reducing environments controlled in different areas by ferric iron(III) reduction, sulfate reduction, and methanogenesis. Under these conditions, reductive dechlorination of TCE can take place if sufficient electron donors are available. Dissolved organic carbon (DOC), consisting primarily of humic and fulvic acids, may fulfill the electron-donor requirement in this system. Concentrations of DOC are highest immediately downgradient from the source area (5-14 mg/L) and also are elevated near the discharge point (1-2 mg/L).

The presence of cis-1,2-dichloroethene (cis-DCE) and vinyl chloride (VC), anaerobic TCE breakdown products, in water from 75 percent of the wells sampled in and around the plume indicates that reductive dechlorination of TCE is taking place in the aquifer. Because neither of these compounds was used in Building 24, they are believed to originate from the biologically mediated breakdown of TCE. Additional evidence for reductive dechlorination of TCE is that cisDCE and VC are found only at sites where TCE has previously been identified, although the concentrations of cisDCE and VC are highest in the downgradient part of the plume, nearer the point where the plume discharges to the brook.

TRICHLOROETHENE MASS DISTRIBUTION

The mass of TCE dissolved in the ground water in the plume was estimated on the basis of

results of six synoptic sampling events during 1987-91. By using a plume volume of 2.3×10^6 m^3 (cubic meters), a porosity of 0.3, and the assumption that each well represents a finite volume of the aquifer, the average mass of TCE dissolved in the plume was estimated to be 1,000 kg (kilograms) +/- 200 kg (Imbrigiotta and others, 1995). This estimate did not show a consistent upward or downward trend over the six sampling events, which implies that the dissolved TCE mass in the plume was essentially at steady state. Most of the dissolved TCE mass (57 percent) is found near the base of the unconfined aquifer, where TCE concentrations are greater than 10,000 µg/L (fig. 1B).

The mass of sorbed TCE within the plume was estimated from methanol-extraction analyses of sediments from six shallow sites (6- to 9-m depths) along the centerline of the plume (Koller and others, 1996). Using these data and estimates of the volume of the aquifer each site represents, Ehlke and others (1999) calculated a total sorbed TCE mass for the plume of approximately 2,500 kg. Although this value for the sorbed mass of TCE was used in calculations in this paper, it may be an underestimate because it is based on sorbed TCE concentrations in shallow sediment samples and sorbed TCE concentrations at greater depths in the aquifer (12- to 15-m depths) are known to be higher (authors' unpublished data).

TRICHLOROETHENE MASS-FLUX ESTIMATES

The major naturally occurring processes that affect the input or removal of TCE to or from the plume were identified and studied independently as part of the Toxic Substances Hydrology Program project at Picatinny Arsenal (Imbrigiotta and Martin, 1991; Imbrigiotta and Martin, 1996); the results of these studies are described briefly below. The TCE-removal processes evaluated include advective transport, lateral dispersion, anaerobic biotransformation, diffusion-driven volatilization, advection-driven volatilization, and sorption. The TCE-input processes evaluated include desorption, infiltration, and dissolution. A TCE mass flux was estimated for each of these processes (fig. 2).

Removal Processes

Dissolved TCE is removed from the plume in ground-water discharge to Green Pond Brook by advective transport. The mass flux of TCE lost to the brook was calculated by using an advective flux rate of 800 liters per square meter per week (based on modeling analyses by Voronin (1991), Voronin and Rice (1996) and Martin and Imbrigiotta (1994)), a median ground-water TCE concentration of 1,200 µg/L, and a cross-sectional area of 980 m^2 (square meters) where the aquifer discharges to the brook. On the basis of these values, approximately 50 kg/yr (kilograms per year) of TCE is removed from the plume by discharge to Green Pond Brook.

Lateral dispersion is the process that causes plume spreading by transport of TCE out of the side boundaries of the plume (defined by the 10-µg/L isoconcentration lines in figure 1A). By using Fick's Law, the lateral TCE-concentration gradient from the center of the plume to the 10-µg/L isoconcentration line, and the estimated area of the sides of the plume, it was calculated that less than 1 kg/yr of TCE is lost from the plume by this mechanism.

Anaerobic biotransformation is the biologically mediated process of reductive dechlorination whereby TCE undergoes the sequential replacement of the chlorine atoms on the molecule with hydrogen atoms to form the breakdown products cisDCE, VC, and ethene (Parsons and others, 1984; Vogel and others, 1987). Biotransformation rate constants were determined in laboratory batch microcosm studies of core samples from five sites along the centerline of the plume (Wilson and others, 1991, 1996; Ehlke and others, 1991; Wilson and others, 1996). The first-order TCE-degradation rate constants obtained in these studies range from -0.004/wk (per week) to -0.035/wk, with a median of -0.007/wk. If the rate constants at each of the five sites are applied to the estimated volume of the aquifer and, hence, the portion of the 1,000 kg of dissolved TCE each represents, then about 230 kg/yr of TCE is removed from the plume by naturally occurring anaerobic biotransformation.

Volatilization is the loss of TCE from ground water into the soil gas of the unsaturated zone across the water table. Volatilization is driven by diffusive and advective mechanisms. The rate of

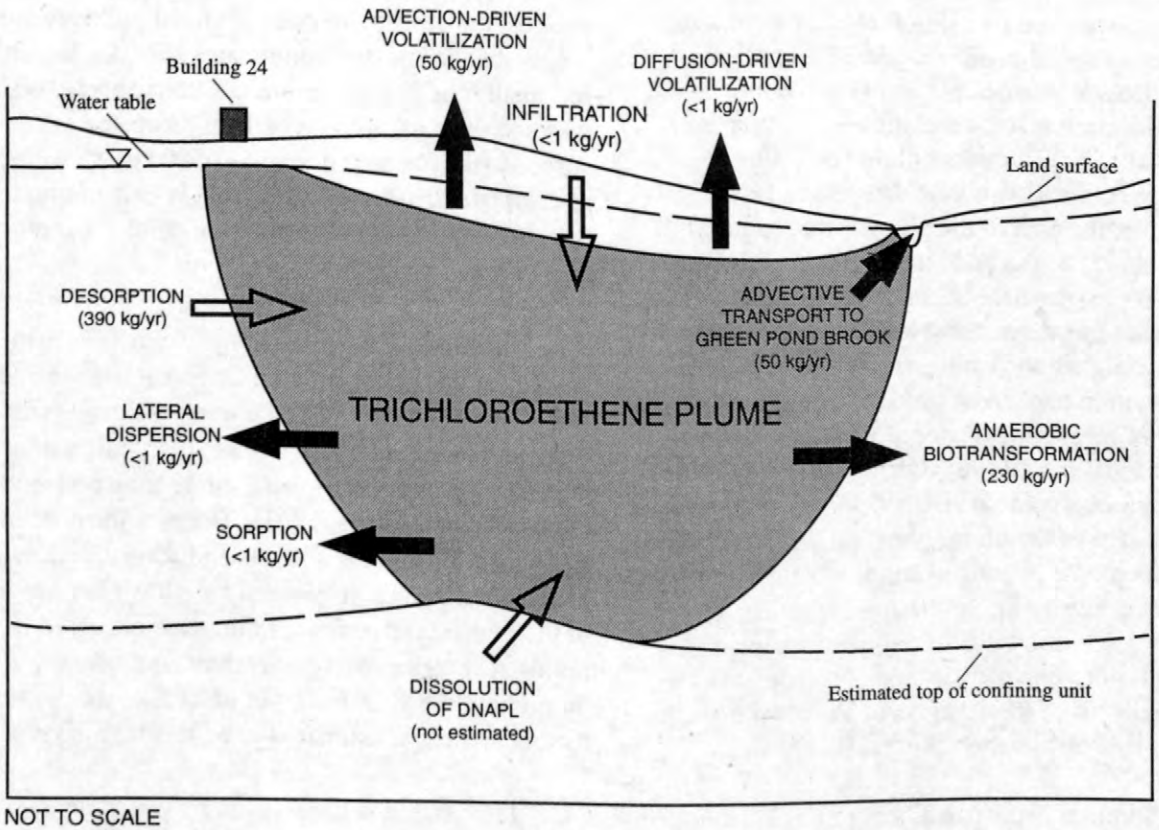

TRICHLOROETHENE MASS-BALANCE COMPONENTS

[kg/yr, kilograms per year; <, less than]

GAINS		LOSSES	
DESORPTION	390 kg/yr	ANAEROBIC BIOTRANSFORMATION	230 kg/yr
INFILTRATION	<1 kg/yr	ADVECTIVE TRANSPORT TO BROOK	50 kg/yr
DISSOLUTION OF DENSE NONAQUEOUS PHASE LIQUID	not estimated	ADVECTION-DRIVEN VOLATILIZATION	50 kg/yr
		LATERAL DISPERSION	<1 kg/yr
		DIFFUSION-DRIVEN VOLATILIZATION	<1 kg/yr
		SORPTION	<1 kg/yr
TOTAL	390 kg/yr	TOTAL	330 kg/yr

Figure 2. Mass-balance estimates of fluxes of naturally occuring processes that affect the removal or input of trichloroethene to or from the ground-water system at Picatinny Arsenal, New Jersey.

loss of TCE in diffusion-driven volatilization is determined by the TCE gradient in the soil gas of the unsaturated zone. Diffusion-driven volatilization was estimated by using Fick's Law, field-measured unsaturated-zone soil-gas TCE gradients, bulk diffusion coefficients from the literature for sites with similar soils, and the area of the plume. Removal of TCE from the plume by diffusion-driven volatilization is calculated to be less than 1 kg/yr over the area of the plume (Imbrigiotta and others, 1995; Smith and others, 1996). In advection-driven volatilization, the rate of loss of TCE is controlled by pressure and temperature changes in the unsaturated-zone soil gas. Advection-driven volatilization was investigated by using a total-vertical-flux-measuring device at Picatinny Arsenal (Smith and others, 1996). On the basis of total-flux measurements made with the device at eight sites and the area of the plume, the total TCE removed from the plume by volatilization is estimated to be approximately 50 kg/yr. Because less than 1 kg/yr is accounted for by diffusive-flux mechanisms, advection-driven volatilization is responsible for essentially all of the 50 kg/yr of TCE lost from the aquifer by volatilization processes.

Sorption is the partitioning of TCE from the ground water onto the aquifer sediments. Field partition coefficients measured at several locations within the plume (Koller and others, 1996) indicate that more TCE was sorbed to aquifer materials at all sites than would be predicted if the sorbed TCE concentrations were in equilibrium with the ground-water TCE concentrations. Therefore, desorption processes rather than sorption processes most likely predominate. Removal of TCE by sorption is estimated to be less than 1 kg/yr.

Input Processes

Desorption is the process by which TCE is removed from the contaminated aquifer sediments and resolubilized back into the ground water in response to concentration gradients. At Picatinny Arsenal, this process has two parts: an initial rapid phase of desorption in which 1 to 10 percent of the TCE is released and a second, slower phase of desorption in which most of the TCE is released over a longer period of time (Koller and others, 1996). First-order desorption rate constants ranging from -0.003/wk to -0.015/wk were measured in flow-through column experiments. Because these experiments were conducted with Picatinny Arsenal ground water stripped of all volatile organic compounds, the desorption rates obtained probably are higher than in situ desorption rates. For this reason, the smaller of the desorption rate constants (-0.003/wk) and the total amount of TCE estimated to be sorbed to the plume sediments (2,500 kg) were used to calculate that 390 kg/yr of TCE is being input to the plume by means of desorption (Ehlke and others, 1999).

Infiltration, the process by which TCE in the soil gas or on the unsaturated-zone soil is dissolved by recharge percolating to the water table, was studied with laboratory soil columns, field infiltration experiments, and multi-phase solute-transport modeling (Cho and others, 1993). Because the concentrations of TCE in the soil gas and sorbed to the unsaturated-zone soil generally are low over most of the plume, and because infiltration occurs only during recharge events rather than continuously throughout the year, the input of TCE to the plume by this process is estimated to be less than 1 kg/yr.

Dissolution is the process by which dense nonaqueous-phase liquid (DNAPL) TCE dissolves into the ground water. DNAPL TCE may be present at Picatinny Arsenal at the base of the unconfined aquifer midway between the source and the brook because concentrations of TCE in ground water in deep wells in this area consistently exceed 1 percent of saturation, which is one indication of DNAPL presence (Cohen and Mercer, 1993). DNAPL TCE has not been confirmed by measurement or observation of free-phase TCE in any water or soil sample from the arsenal. Consequently, the mass of DNAPL TCE that is input by dissolution cannot be calculated directly but can only be estimated as the difference between the sum of the mass removed by all removal processes and the sum of the mass introduced by all other input processes.

MASS-BALANCE ANALYSIS

The estimated mass balance for the TCE plume at Picatinny Arsenal is shown in figure 2. Inputs are represented with open arrows; outputs are represented with solid arrows.

Approximately 330 kg/yr of dissolved TCE is estimated to be removed from the plume by natural processes. Of this amount, 230 kg/yr, or 70 percent of the TCE removed annually, is removed as a result of anaerobic biotransformation. This is by far the most important TCE removal process operating in the Picatinny Arsenal plume. Removal by advective transport to Green Pond Brook and advection-driven volatilization are each estimated at 50 kg/yr. Therefore, each of these processes is responsible for the removal of about 15 percent of the total TCE removed annually from the plume. Lateral dispersion, diffusion-driven volatilization, and sorption are all of minor importance in comparison.

The finding that natural anaerobic biotransformation is the principal mechanism for removal of TCE from the plume at Picatinny Arsenal is significant. Anaerobic biotransformation has been reported to be a major natural removal process for TCE at only a few sites (Wilson and others, 1994), and this conclusion has not previously been reached by quantifying and comparing the magnitude of all other removal processes occurring at a site. This result is likely to have transfer value to other sites with similar geochemistry, hydrology, and geology.

Desorption is the most important input mechanism identified at Picatinny Arsenal. It accounts for the introduction of an estimated 390 kg/yr of TCE. Input by infiltration is very small in comparison (<1 kg/yr). Because the sum of the inputs is larger than the sum of the outputs, dissolution of DNAPL TCE in the system cannot be estimated.

The fact that long-term desorption is a significant continuing source of TCE to the aquifer may explain why the TCE concentrations are still relatively high in the source area (>1,000 µg/L) 16 years after the use of TCE was discontinued at the site. This finding shows that desorption can be an important input mechanism even at sites where the sediment organic content is low (<0.5 percent).

Because the mass of dissolved TCE in the ground-water plume was at steady state during these studies, the sources of TCE ideally should equal the sinks of TCE. Although the estimated inputs do not equal the estimated outputs in the mass balance, they are of the same order of magnitude. Additional study of the individual processes is necessary to refine the mass balance further.

All the mass-flux estimates are associated with some degree of error. The confidence associated with the output estimates is fairly high because each of the significant output processes was measured directly in the field or in the laboratory using standard procedures or was obtained from a well-documented, calibrated ground-water flow model. Although the desorption input mass-flux estimate also was made using standard laboratory procedures, the confidence in this estimate is not as high for the experimental-design reasons mentioned previously. In addition, because the potentially significant input process of DNAPL TCE dissolution could not be estimated, confidence in the overall input mass-flux estimate is not high. Obviously, the presence of even a small amount of DNAPL TCE would greatly alter the total TCE mass in the aquifer system and significantly lengthen any estimates of the time required for natural attenuation processes to remove the TCE from the aquifer.

FIELD-SCALE ESTIMATE OF NATURAL ATTENUATION RATE

The overall natural attenuation rate of TCE at Picatinny Arsenal can be calculated from field data and compared to the anaerobic-biotransformation rates calculated in the laboratory microcosm studies. If first-order kinetics are assumed, the decrease in median TCE concentrations in wells along a flow path from the source area to the discharge area (1,900 µg/L to 760 µg/L) and the time of travel for TCE between these two points in the plume (2.7 yr to 6.6 yr depending on the amount of sorption) can be used to compute a range of field-scale natural-attenuation rate constants of -0.003/wk to -0.007/wk (Ehlke and others, 1999). These field-calculated rate constants compare favorably to the low end of the range of rate constants determined in the five microcosm experiments (-0.004/wk to -0.035/wk) (Wilson and others, 1991). The fact that both independent procedures yield rate constants of the same order of magnitude indicates that the methods used to make these measurements and estimates are valid.

The overall field-scale natural attenuation rate is expected to be larger than the anaerobic biodegradation rate alone because it includes all the processes by which TCE is removed from the plume. The fact that the range of overall field-scale rate constants (-0.003/wk to -0.007/wk) is lower than or equal to the median microcosm-determined rate constant (-0.007/wk) results in large part from a net positive input of TCE midway down the length of the plume near the base of the aquifer, where concentrations of dissolved TCE still exceed 10,000 µg/L (fig. 1B). Recent unpublished work by the authors indicates that concentrations of sorbed TCE on sediments in this area are high (as much as 6 micrograms per gram) and that slow desorption of TCE from these sediments is taking place. The lab microcosms do not account for this input because they were constructed from discrete sediment samples from each of five sites and all showed some TCE degradation.

COMPARISON OF NATURAL ATTENUATION PROCESSES TO PUMP-AND-TREAT REMEDIATION

A pump-and-treat system was installed as an interim remediation measure in the Picatinny Arsenal TCE plume in September 1992. The system consists of a set of five withdrawal wells from which an average of 440,000 liters per day is pumped to a treatment system consisting of two stripping towers and two granulated-activated-carbon filters. On the basis of average pumpage values and ground-water TCE concentrations in each withdrawal well during 1995, the pump-and-treat system is removing about 70 kg/yr of dissolved TCE at a cost of $700,000 per year. The total dissolved TCE being removed by natural attenuation processes is estimated to be 330 kg/yr at a cost of $50,000 per year (primarily monitoring costs). Thus, the pump-and-treat system is removing only about 20 percent as much dissolved TCE as is being removed by natural attenuation processes each year, but at 14 times the cost. The mass of dissolved TCE being removed by the pump-and-treat system is about 30 percent as much as is being removed by anaerobic biotransformation alone and is just slightly more than the mass of dissolved TCE being removed by each of the processes of advective transport and advection-driven volatilization.

CONCLUSIONS

Anaerobic biotransformation is the most important process by which TCE is being removed from the plume at Picatinny Arsenal, New Jersey, by a factor of more than four (230 kg/yr compared to 50 kg/yr) over advective transport and advection-driven volatilization. Anaerobic biotransformation accounts for an estimated 70 percent of the total mass of TCE removed from the plume annually by all natural attenuation processes. Other removal processes--lateral dispersion, diffusion-driven volatilization, and sorption--are minor in comparison. Desorption is the most significant TCE input process evaluated. A mass-balance analysis shows that the annual removal of TCE from the plume by natural attenuation processes (330 kg/yr) is of the same order of magnitude as the input of TCE to the plume by desorption (390 kg/yr). The field-scale natural-attenuation rate constant calculated from field TCE concentrations and time-of-travel data is in general agreement with anaerobic-biotransformation rate constants measured in laboratory microcosm studies.

Natural attenuation processes annually remove approximately five times as much dissolved TCE as is removed by an interim pump-and-treat remediation system operating at Picatinny Arsenal. Anaerobic biotransformation itself destroys approximately three times as much dissolved TCE as is removed by the pump-and-treat system. The pump-and-treat system removes just slightly more dissolved-TCE mass per year than each of the processes of advective transport to Green Pond Brook and advection-driven volatilization.

REFERENCES

Benioff, P.A., Bhattacharyya, M.H., Biang, C., Chiu, S.Y., Miller, S., Patton, T., Pearl, D., Yonk, A., and Yuen, C.R., 1990, Remedial investigation concept plan for Picatinny Arsenal, Volume 2: Descriptions of and sampling plans for remedial investigation sites: Argonne, Ill., Argonne National Laboratory, Environmental Assessment and Information Sciences Division, p. 22-1 - 22-24.

Cho, H.J., Jaffe, P.R., and Smith, J.A., 1993, Simulating the volatilization of solvents in unsatur-

ated soils during laboratory and field infiltration experiments: Water Resources Research, v. 29, no. 10, p. 3329-3342.

Cohen, R.M., and Mercer, J.W., 1993, DNAPL site evaluation: Boca Raton, Florida, C.K. Smoley, 500 p.

Ehlke, T.A., Imbrigiotta, T.E., Wilson, B.H., and Wilson, J.T., 1991, Biotransformation of cis-1,2-dichloroethylene in aquifer material from Picatinny Arsenal, Morris County, New Jersey, *in* Mallard, G.E., and Aronson, D.A., eds., U.S. Geological Survey Toxic Substances Hydrology Program--Proceedings of the technical meeting, Monterey, Calif., March 11-15, 1991: U.S. Geological Survey Water-Resources Investigations Report 91-4034, p. 689-697.

Ehlke, T.A., Imbrigiotta, T.E., Wilson, B.H., and Wilson, J.T., 1999, Natural attenuation of trichloroethylene and cis-1,2-dichloroethylene in an unconfined aquifer at Picatinny Arsenal, New Jersey: Bioremediation Journal, v. 3., in press.

Imbrigiotta, T.E., Ehlke, T.A., Wilson, B.H., and Wilson, J.T., 1996, Case study: Natural attenuation of a trichloroethylene plume at Picatinny Arsenal, New Jersey, *in* U.S. Environmental Protection Agency Symposium on Natural Attenuation of Chlorinated Organics in Ground Water, Dallas, Texas, September 11-13, 1996: EPA/540/R-96/509, p. 83-89.

Imbrigiotta, T.E., Ehlke, T.A., Martin, Mary, Koller, David, and Smith, J.A., 1995, Chemical and biological processes affecting the fate and transport of trichloroethylene in the subsurface at Picatinny Arsenal, New Jersey: Hydrological Science and Technology, v. 11, no. 1-4, p. 26-50.

Imbrigiotta, T.E., and Martin, Mary, 1991, Overview of research activities on the movement and fate of chlorinated solvents in ground water at Picatinny Arsenal, New Jersey, *in* Mallard, G.E., and Aronson, D.A., eds., U.S. Geological Survey Toxic Substances Hydrology Program--Proceedings of the technical meeting, Monterey, Calif., March 11-15, 1991: U.S. Geological Survey Water-Resources Investigations Report 91-4034, p. 673-680.

Imbrigiotta, T.E., and Martin, Mary, 1996, Overview of research activities on the transport and fate of chlorinated solvents in ground water at Picatinny Arsenal, New Jersey, 1991-93, *in* Morganwalp, D.W., and Aronson, D.A., eds., U.S. Geological Survey Toxic Substances Hydrology Program--Proceedings of the technical meeting, Colorado Springs, Colo., September 20-24, 1993: U.S. Geological Survey Water-Resources Investigations Report 94-4015, p. 297-305.

Koller, David, Imbrigiotta, T.E., Baehr, A.L. and Smith, J.A., 1996, Desorption of trichloroethylene from aquifer sediments at Picatinny Arsenal, New Jersey, *in* Morganwalp, D.W., and Aronson, D.A., eds., U.S. Geological Survey Toxic Substances Hydrology Program--Proceedings of the technical meeting, Colorado Springs, Colo., September 20-24, 1993: U.S. Geological Survey Water-Resources Investigations Report 94-4015, p. 329-337.

Martin, Mary, 1989, Preliminary results of a study to simulate trichloroethylene movement in ground water at Picatinny Arsenal, New Jersey, *in* Mallard, G.E., and Ragone, S.E., eds., U.S. Geological Survey Toxic Substances Hydrology Program--Proceedings of the technical meeting, Phoenix, Ariz., September 26-30, 1988: U.S. Geological Survey Water-Resources Investigations Report 88-4220, p. 377-383.

Martin, Mary, 1991, Simulation of reactive multispecies transport in two-dimensional groundwater-flow systems, *in* Mallard, G.E., and Aronson, D.A., eds., U.S. Geological Survey Toxic Substances Hydrology Program--Proceedings of the technical meeting, Monterey, Calif., March 11-15, 1991: U.S. Geological Survey Water-Resources Investigations Report 91-4034, p. 698-703.

Martin, Mary, 1996, Simulation of transport, desorption, volatilization, and microbial degradation of trichloroethylene in ground water at Picatinny Arsenal, New Jersey, *in* Morganwalp, D.W., and Aronson, D.A., eds., U.S. Geological Survey Toxic Substances Hydrology Program--Proceedings of the technical meeting, Colorado Springs, Colo., September 20-24, 1993: U.S. Geological Survey Water-Resources Investigations Report 94-4015, p. 307-313.

Martin, Mary, and Imbrigiotta, T.E., 1994, Contamination of ground water with trichloroethylene at the Building 24 site at Picatinny Arsenal, New Jersey, *in* U.S. Environmental Protection Agency Symposium on Intrinsic Bioremedia-

tion of Ground Water, Denver, Colo., August 30-September 1, 1994: EPA/540/R-94/515, p. 143-153.

Parsons, F.Z., Wood, P.R., and DeMarco, J., 1984, Transformations of tetrachloroethene and trichloroethene in microcosms and ground water: Journal of the American Water Works Association, v. 76, no. 2, p. 56-59.

Sargent, B.P., Fusillo, T.V., Storck, D.A., and Smith, J.A., 1990, Ground-water contamination in the area of Building 24, Picatinny Arsenal, New Jersey: U.S. Geological Survey Water-Resources Investigations Report 90-4057, 94 p.

Smith, J.A., Tisdale, A.K., and Cho, H.J., 1996, Quantification of natural vapor fluxes of trichloroethene in the unsaturated zone at Picatinny Arsenal, New Jersey: Environmental Science and Technology, v. 30, no. 7, p. 2243-2250.

Vogel, T.M., Criddle, C.S., and McCarty, P.L., 1987, Transformations of halogenated aliphatic compounds: Environmental Science and Technology, v. 21, no. 8, p. 722-736.

Voronin, L.M., 1991, Simulation of ground-water flow at Picatinny Arsenal, New Jersey, *in* Mallard, G.E., and Aronson, D.A., eds., U.S. Geological Survey Toxic Substances Hydrology Program--Proceedings of the technical meeting, Monterey, Calif., March 11-15, 1991: U.S. Geological Survey Water-Resources Investigations Report 91-4034, p. 713-720.

Voronin, L.M., and Rice, D.E., 1996, Hydrogeology and simulation of ground-water flow, Picatinny Arsenal and vicinity, Morris County, New Jersey: U.S. Geological Survey Water-Resources Investigations Report 96-4061, 64 p.

Wiedemeier, T.H., Swanson, M.A., Moutoux, D.E., Wilson, J.T., Kampbell, D.H., Hansen, J. E., and Haas, Patrick, 1996, Overview of the technical protocol for natural attenuation of chlorinated aliphatic hydrocarbons in ground water under development for the U.S. Air Force Center for Environmental Excellence, *in* U.S. Environmental Protection Agency Symposium on Natural Attenuation of Chlorinated Organics in Ground Water, Dallas, Texas, September 11-13, 1996: EPA/540/R-96/509, p. 35-59.

Wilson, B.H., Ehlke, T.A., Imbrigiotta, T.E., and Wilson, J.T., 1991, Reductive dechlorination of trichloroethylene in anoxic aquifer material from Picatinny Arsenal, New Jersey, *in* Mallard, G.E., and Aronson, D.A., eds., U.S. Geological Survey Toxic Substances Hydrology Program--Proceedings of the technical meeting, Monterey, Calif., March 11-15, 1991: U.S. Geological Survey Water-Resources Investigations Report 91-4034, p. 704-707.

Wilson, J.T., Weaver, J.W., and Kampbell, D.H., 1994, Intrinsic bioremediation of TCE in ground water at an NPL site in St. Joseph, Michigan, *in* U.S. Environmental Protection Agency Symposium on Intrinsic Bioremediation of Ground Water, Denver, Colo., August 30-September 1, 1994: EPA/540/R-94/515, p. 154-160.

Wilson, B.H., Wilson, J.T., and Luce, Darryl, 1996, Design and interpretation of microcosm studies for chlorinated compounds, *in* U.S. Environmental Protection Agency Symposium on Natural Attenuation of Chlorinated Organics in Ground Water, Dallas, Texas, September 11-13, 1996: EPA/540/R-96/509, p. 21-28.

AUTHOR INFORMATION

Thomas E. Imbrigiotta and Theodore A. Ehlke, U.S. Geological Survey, 810 Bear Tavern Road, Suite 206, West Trenton, New Jersey 08628.

Unsaturated-Zone Air Flow at Picatinny Arsenal, New Jersey: Implications for Natural Remediation of the Trichloroethylene-Contaminated Aquifer

By James A. Smith, Whitney Katchmark, Jee-Won Choi, and Fred D. Tillman, Jr.

ABSTRACT

The purpose of this study is to determine if natural atmospheric pressure variations contribute to unsaturated-zone air flow and the intrinsic remediation of trichloroethylene (TCE) in shallow ground water and the unsaturated zone at Picatinny Arsenal, New Jersey. Air pressure, temperature, and moisture content were measured as functions of depth and time at a location approximately above the center of the TCE ground-water plume during dry periods in August and October, 1996. Significant air-pressure gradients between the subsurface and the atmosphere were observed, but air pressures at depths between 0.5 to 1.7 m showed little variation at any given sampling time. Soil moisture content was relatively constant in time, with the highest moisture contents observed for the top 15-cm of soil. Attempts to simulate subsurface air pressures in response to changing atmospheric pressures were largely unsuccessful, even when two distinct subsurface air-permeability zones were used. Based on these results, the following conclusions were made: i) air flow is occurring in the unsaturated zone; ii) unsaturated zone air flow likely influences the transport of TCE vapors; iii) unsaturated-zone air flow cannot solely be explained by one-dimensional (vertical) air flow driven by atmospheric-pressure variations.

INTRODUCTION

Many processes contribute to the fate and transport of organic pollutants in ground water. These include physical transport processes such as advection and diffusion, biochemical processes such as biodegradation and hydrolysis, and interphase mass-transfer processes such as sorption and volatilization. The natural volatilization of pollutants from ground-water into the unsaturated-zone soil gas and eventual transport to the atmosphere has received relatively little attention in the scientific literature, probably because of the general belief that it is not a significant transport process relative to other processes. Unlike volatilization from surface waters, the concentration gradient which drives mass transfer from ground water to soil gas is comparatively small because of transport limitations in both the saturated and unsaturated zone. However, many common ground-water contaminants have relatively high Henry's Law constants and the upper surface area of many ground-water plumes may be significant relative to the total volume of contaminated ground-water. Consequently, volatilization may be a significant transport process given the large interfacial area available for phase transfer of the pollutant.

The primary hypothesis of this research is that advective fluxes of volatile organic contaminants (VOCs) can be significant relative to diffusion fluxes, and that failure to account for advective fluxes may significantly underestimate the total flux of VOCs from contaminated ground-water to the atmosphere. One likely cause of VOC advection in the unsaturated zone is changes in atmospheric pressure. As atmospheric pressure decreases, unsaturated-zone air flows upward to equalize pressure. As atmospheric pressure increases, unsaturated-zone air flows downward. Organic vapors in the soil gas are transported with the flowing air. At first thought, it might appear that the net effect of cyclic barometric pressure fluctuations would result in a net zero advective flux. However, organic-vapor transport is limited across the capillary fringe because the diffusion coefficient for most VOCs in water is approximately 4 orders of magnitude less than in air. By contrast, as organic vapors reach land surface, they are almost instantaneously diluted to nondetectable concentrations in the atmosphere. Therefore, the effect of this cyclic

pressure variation would be a net flux of the organic vapor to the atmosphere.

In this study, we present subsurface air-pressure data and simulations to investigate the effects of atmospheric pressure fluctuations on unsaturated-zone air flow. Our study site is the unsaturated zone above the TCE-contaminated aquifer at Picatinny Arsenal, New Jersey.

Description of Field Site

Picatinny Arsenal is located in Morris County, New Jersey. The study area (Figure 1) is located in a glaciated valley above 50-65 m of stratified and unstratified drift, which in turn lies above weathered bedrock. The unconsolidated sediments form three major hydrogeologic units: a 15-21-m-thick unconfined sand-and-gravel aquifer, an 8-21-m-thick confining layer of fine sand, silt, and clay, and an 8-35-m-thick confined sand-and-gravel aquifer. The water-table is 1-4 m below land surface (Imbrigiotta, Ehlke, and others, 1995; Imbrigiotta and Martin, 1996).

From 1960-83, TCE was used as a metal degreasing agent in Building 24. Wastewater from this process was discharged into two unlined waste ponds and an unlined overflow dry well. The TCE plume resulting from the wastewater discharge extends approximately 500 m downgradient from Building 24. Figure 1 identifies Building 24, the field sampling location for this study, and the region of ground water in the unconfined aquifer contaminated with TCE concentrations greater than 10 μg/L. TCE concentrations as high as 44 mg/L have been measured in ground water at the site, and TCE has been detected in the unsaturated-zone soil, soil gas, and water (Cho, Jaffé, and Smith, 1993; Imbrigiotta, Ehlke, and others, 1995; Imbrigiotta and Martin, 1996; Smith, Chiou, and others, 1990; Smith, Cho, and others, 1992; Smith, Tisdale, and Cho, 1996).

In 1992, a pump-and-treat ground-water remediation system was installed. The system consists of five extraction wells (shown in Figure 1) screened in the unconfined aquifer. Water extracted from the aquifer is treated to remove TCE by air stripping followed by activated carbon adsorption. In 1994, the pump-and-treat system removed approximately 70 kg of TCE from the subsurface (Imbrigiotta, Ehlke, and others, 1995).

In a recent study at the field site, mass fluxes of TCE vapor from the subsurface to the atmosphere were directly quantified using a vertical flux chamber (Smith, Tisdale, and Cho, 1996). This study showed that approximately 50 kg/yr of TCE is removed from the subsurface under natural conditions by vapor transport through the unsaturated zone, and that diffusion fluxes account for less than 1 percent of this total organic-vapor flux. They concluded that advective transport of organic vapors in response to atmospheric pressure variations was the primary cause of the relatively large organic vapor fluxes measured in the field (Smith, Tisdale, and Cho, 1996). However, no data on subsurface air pressure distributions were presented to support this hypothesis.

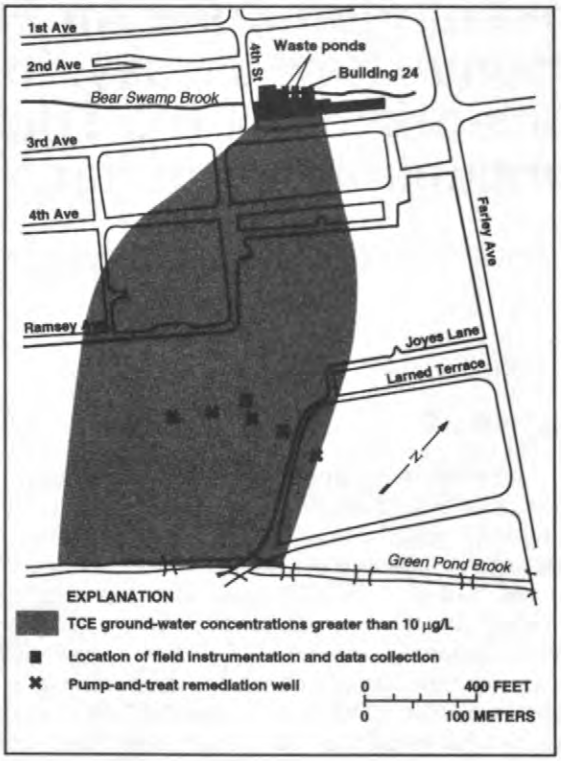

Figure 1. Map of study area, showing location of sampling site, pump-and-treat wells, and ground-water contamination.

EXPERIMENTAL MATERIALS AND METHODS

Data on unsaturated-zone moisture content, temperature, and air pressure (as functions of depth and time) and atmospheric pressure (as a function of time) were collected at the location indicated in Figure 1 during August and October, 1996. During these sampling events, the depth to the water table at this location ranged from 2.2 to 2.3 m.

Volumetric moisture content was quantified using time-domain reflectometry (TDR) (Smith, Tisdale, and Cho, 1996). Three-prong TDR probes were installed at depths of 0.30, 0.61, 1.07, and 1.52 m by hand-augering separate boreholes to the desired depth and pushing the prongs of each probe into undisturbed soil at the bottom of each borehole. The 7-cm-diameter boreholes were filled with native soil. For the October 1996 sampling, an additional TDR probe was installed in the upper 15 cm of the soil. The TDR probes were interfaced with a Tektronix 1502B metallic cable tester which quantified the apparent length of the probes. This value was used to calculate volumetric moisture content using the empirical relation given by Topp, Davis, and Annan (1980).

Air pressures and temperatures were quantified using four unvented Geokon vibrating-wire pressure transducers (model 4500LP, accurate to 70 N/m^2). Three of the transducers were attached to standard AW rods and installed at the bottom of separate 7-cm-diameter boreholes augered to depths of 0.49, 1.25, and 1.68 m (August, 1996 sampling event) or 0.33, 1.28, and 1.68 m (October, 1996 sampling event). The holes were filled with native soil around the transducer and a mixture of soil and bentonite from a distance 30 cm above the transducer to land surface. A fourth unvented Geokon transducer (model 4580, accurate to 35 N/m^2) was placed at land surface. The four transducers were interfaced with a Campbell CR10 datalogger with an AM416 Relay Multiplexer. The datalogger recorded temperature and pressure at each transducer every 5 min. All the Geokon transducers and TDR probes were installed within a 2-m radius.

For the August sampling event, data were collected from August 20-23, 1996. For the October sampling event, data were collected from October 6-9, 1996. During both sampling periods, there was no measureable precipitation.

AIR-FLOW SIMULATION MODEL

To simulate air pressures in the unsaturated zone, we have assumed a one-dimensional, transient system. For geologic systems with air permeabilities greater than 10^{-10} cm^2, the air velocity, v (m/s), can be estimated by Darcy's Law (Massman and Farrier, 1992):

$$v = -\frac{k}{\mu\theta_g}\frac{\partial P}{\partial z} \qquad (1)$$

where

k is the gas permeability (m^2)
μ is the gas viscosity (kg/m-s)
θ_g is the volumetric air content
P is pressure (N/m^2)
t is time *(s)*
z is distance *(m)*.

This formulation assumes that slip flow is negligible relative to viscous flow, which is a valid approximation for the pore sizes associated with the sandy porous media in the unsaturated zone at Picatinny Arsenal. Air pressures are obtained by solving the following linearized flow equation (Massman and Farrier, 1992; Massman and Madden, 1994):

$$\theta_g\frac{\partial P}{\partial t} = \frac{1}{\mu}\frac{\partial}{\partial z}\left(kP_0\frac{\partial P}{\partial z}\right) \qquad (2)$$

where P_0 is the mean atmospheric pressure.

Solution of equation (2) requires two boundary conditions and an initial condition. The upper boundary condition (at land surface) and the initial condition can be specified from pressures explicitly measured in the field. The lower boundary is located at the top of the capillary fringe, which we approximate as the location of the water table. For a constant-position water table, the velocity of the air at this boundary is necessarily zero. With consideration of equation (1), this gives rise to the following lower boundary condition:

$$\frac{\partial P}{\partial z} = 0 \qquad (3)$$

The above mathematical formulation ignores gravity effects (e.g. the equations are written in terms of pressure instead of potentiometric head) and assumes that fluid density is only a function of fluid pressure.

Equation (2) is solved numerically using finite differences (Sheets, 1997). The numerical solution was compared to an analytical solution of equation (2) for a sinusoidal variation in pressure at the upper boundary. The numerical and analytical solutions were found to be in excellent agreement (Sheets, 1997).

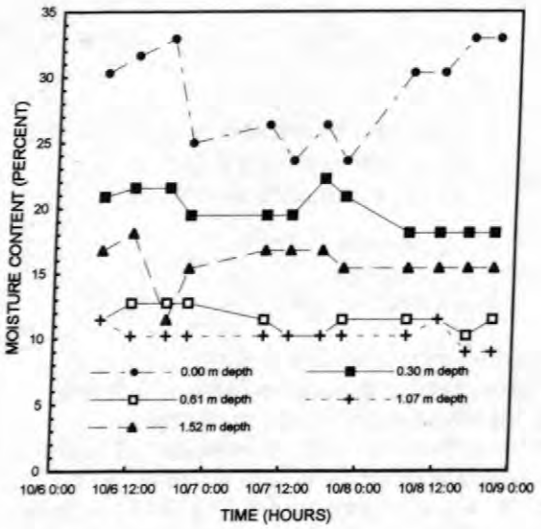

Figure 2. Moisture content as a function of time for the October 1996 sampling event.

RESULTS AND DISCUSSION

Figure 2 shows the volumetric moisture content in the unsaturated zone as a function of time for five depths for the October sampling event. Moisture contents remained relatively constant in time for any given depth, and this is consistent with the observation that there was no precipitation during the data collection period. The highest moisture contents were observed within the top 0.3 m of the unsaturated zone. This is probably a consequence of the finer-grained soil (and hence, a finer distribution of pore sizes) in this region compared to deeper soil. Smith, Chiou, and others (1990) have reported that surficial soil from the site (0.0 to 0.01-m depth) has a higher silt and clay content than deeper unsaturated-zone soil (1.5 to 2.0-m depth). Relatively high moisture contents were also observed in soil closest to the water table. Similar moisture content data were observed for the August sampling event. It is likely that the higher moisture contents in the surficial soil and soil just above the water table correlate with a reduced air permeability in these regions relative to soil at intermediate depths.

Figures 3 and 4 show land-surface and unsaturated-zone air pressures (at three depths) as a function of time for the August and October sampling events. Based on the land-surface pressure data, it is apparent that no sudden, large pressure changes occurred during the course of either sampling event. This is consistent with the observation that no major regional storms entered or left the area during either sampling event. Diurnal temperature changes account for locally high pressure values between 12:00 and 4:00 pm each day and locally low pressure values between 3:00 and 9:00 am each day. Superimposed on these diurnal pressure patterns, there appears to be a falling atmospheric pressure trend for the entire October sampling period and for the second half of the August sampling period. For reference purposes, atmospheric pressure changes caused by diurnal temperature changes usually range from 100 to 300 N/m^2, whereas pressure changes caused by regional storm systems can be as large as several thousand N/m^2 over a 24-hr period (Massman and Farrier, 1992). The atmospheric pressure data collected in this study agree well with data collected simultaneously by the National Oceanic Atmospheric Association at their weather station in Newark, New Jersey (Sheets, 1997).

The measured air pressures in the unsaturated zone are relatively constant with depth for any given time. The small differences measured between the subsurface pressure transducers are, for the most part, less than the accuracy of the transducer (70 N/m^2), suggesting that any real pressure differences between these sampling locations cannot be reliably quantified by the pressure transducers used in this study.

During most of the sampling periods, measureable pressure differences existed between the subsurface and the atmosphere. For the August and October sampling events, pressure differences greater than 200 N/m^2 were routinely observed. Both upward and downward pressure gradients were measured.

The subsurface pressures follow a trend similar to that of the atmospheric pressures for both the August and October sampling events on a time scale of several days. However, the subsurface pressures do not appear to be controlled solely by the atmospheric pressure changes when considering the data on a time scale of several hours. For example, at 9:00 pm on August 20th (Figure 3), atmospheric pressures and subsurface pressures are approximately equal. In the following 8-hr period, the atmospheric pressure decreases while the subsurface pressures generally increase. If atmospheric pressure changes control one-dimensional subsurface pressure changes, this behavior is contrary to expectations. The expected response would be for the subsurface pressures to also decrease, with the responses lagged in time. Several other examples of the above-described pressure-data inconsistencies can be found in the August and October data sets shown in Figures 3 and 4.

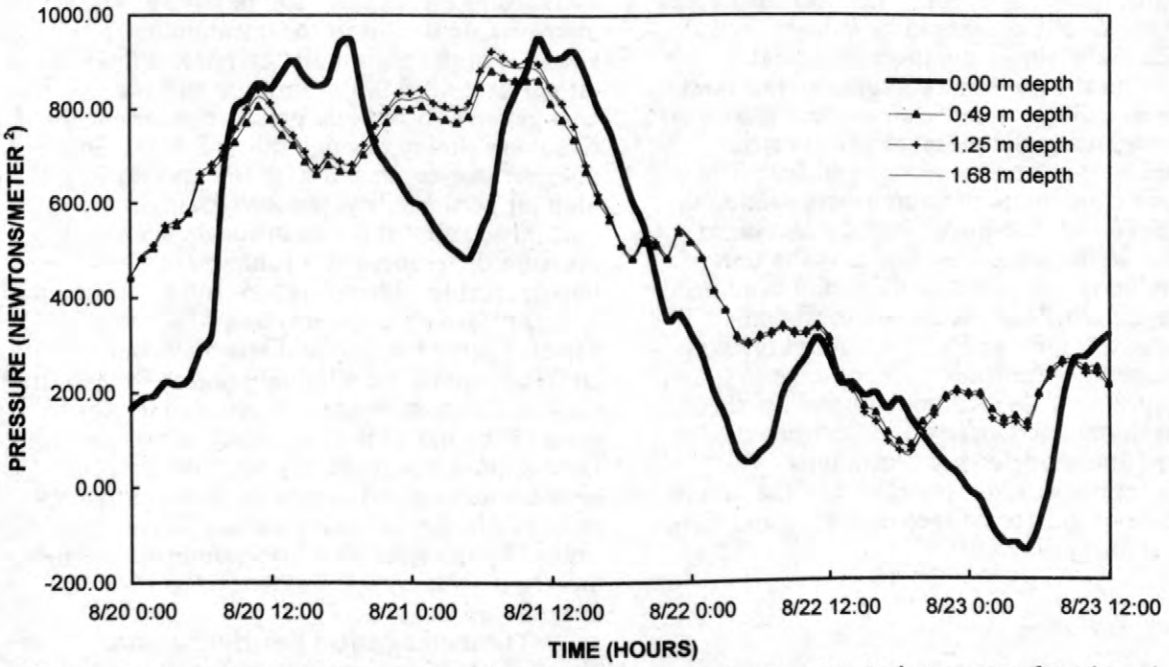

Figure 3. Air pressure at land surface and three depths in the unsaturated zone as a function of time for the August, 1996 sampling event. Symbols are only used to help distinguish between lines and do not necessarily represent actual data points. Actual data points were collected at 5-minute intervals for all depths.

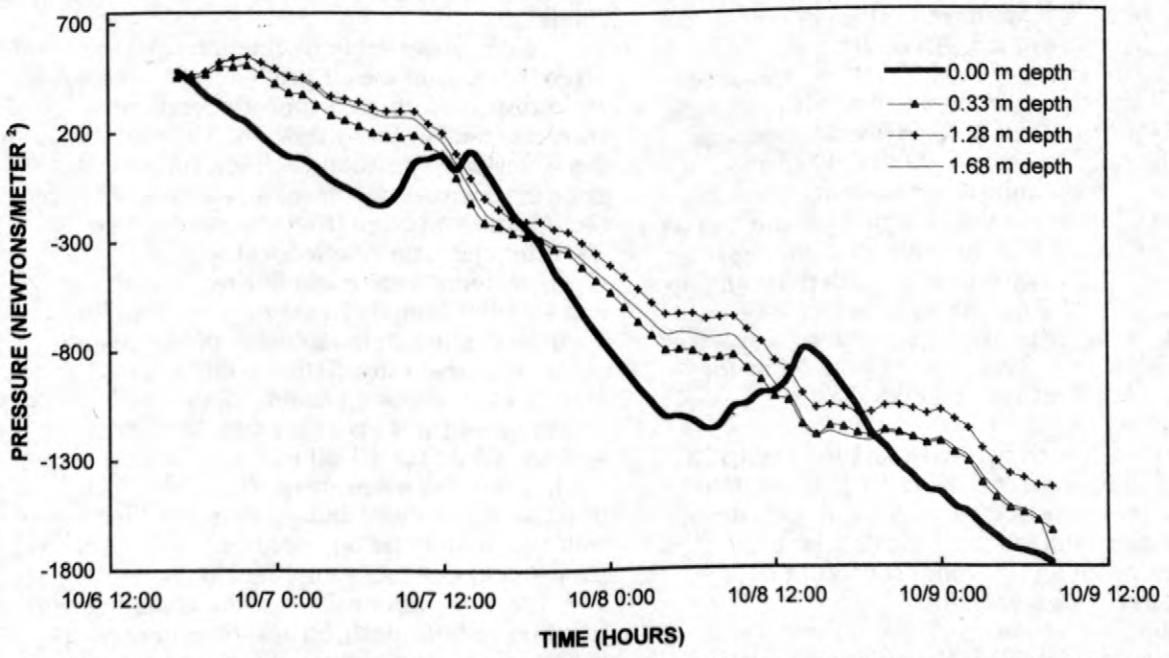

Figure 4. Air pressure at land surface and three depths in the unsaturated zone as a function of time for the October, 1996 sampling event. Symbols are only used to help distinguish between lines and do not necessarily represent actual data points. Actual data points were collected at 5-minute intervals for all depths.

Figures 5 and 6 present the results of attempts to simulate a subset of the data from the August sampling event. This data subset was chosen because it appears to be at least approximately free of the inconsistencies described in the previous paragraph. For both simulations, the volumetric air content used was determined using the measured volumetric moisture contents and a porosity of 0.3. The measured atmopheric pressures were used as the upper boundary condition, and the measured pressures in the unsaturated zone at the start of the simulation were used as the initial condition. Air permeability was used as a calibration parameter using Powell's direction set method for parameter optimization (Press, Flannery, and others, 1986). This technique minimizes the squared normalized differences between the observed and modeled concentrations. The merit function, or error, is defined as the sum of the square of the normalized deviation and is mathematically given as:

$$Merit\ \ function = \sum\left[(data - simulation\ \ result)/\ data\right]^2$$

This merit function ensures that the percentage error at each comparison point is given equal weight. For the simulations in Figure 5, the optimized air permeability is 2.43×10^{-14} m^2. For Figure 6, two optimized values of air permeability were used. An optimized permeability value of 8.09×10^{-15} m^2 was used in regions of the unsaturated zone with moisture contents greater than 25%. This corresponded to depths ranging from 0.00 to 0.30 m and 2.0 to 2.2 m. An optimized permeability value of 2.06×10^{-8} m^2 was used in regions of the unsaturated zone with moisture contents less than 25%. This corresponded to depths ranging from 0.30 to 2.00 m. At high moisture contents, a larger percentage of the pore space is filled with water. This reduces pore space for air flow and effectively reduces the air permeability.

As evidenced by the simulation results in Figure 5, the model was not able to accurately describe the measured subsurface air pressures. Simulation attempts for all the data in a sampling event and on other subsets of data were similarly unsuccessful.

The simulations in Figure 6 show some improvement, but still are unable to accurately described the measured pressures. One important element of the data was captured by this dual-permeability simulation, however. As shown in Figure 6, the simulated subsurface air pressures are indistinct from one another yet distinct from the atmospheric pressure. This results from the low air-permeability value assigned to the surficial soil relative to soil at intermediate depths in the unsaturated zone. Because of the high moisture content (and low air permeability) in the surficial soil zone, changes in atmospheric pressure are transmitted relatively slowly through this soil zone. In the intermediate-depth soil with low moisture and high air permeability, pressure changes are transmitted almost instantaneously such that pressure differences as a function of depth are imperceptable. Therefore, the small differences in subsurface air pressures as a function of depth observed at the field site may be a consequence of the relatively high-permeability (low moisture-content) soil between depths of 0.3 and 0.2 m in the unsaturated zone. Furthermore, the relatively large differences between atmospheric and subsurface pressures observed in the field may at least in part be caused by the relatively low-permeability (high moisture content) soil in the top 0.3 m of the unsaturated zone.

The mathematical description of the physical problem cannot describe the measured air-pressure distributions. Therefore, it is likely that the physical problem is more complex than the current simulation model (equations 1-3). We hypothesize that one or more of the following processes may be occurring at the field site that are not accounted for in the model.

First, water-table fluctuations may be affecting subsurface air pressures. As the water table rises, unsaturated zone air pressure increases and air flows upward. Conversely, as the water-table position declines, unsaturated-zone air pressure decreases and air is drawn into the unsaturated zone from the atmosphere. Unfortunately, no detailed water-table measurements were made during the August and October sampling events. The sampling location is close to the location of the central pump-and-treat remediation well (Figure 1). During each sampling event, the central pumping well was not operating. However, it was turned on for 15-30 min each day to back-wash filters at the treatment plant. Hence, it is possible that natural and pumping-induced water-table fluctuations occurred during the August and October sampling events.

Second, air density may be changing as a function of both position and time in response to changing temperature. Throughout both sampling events, temperatures measured at the subsurface probes were relatively constant in space and time. The maximum difference in temperature between the shallowest and deepest temperature probe was less than 4 °C. However,

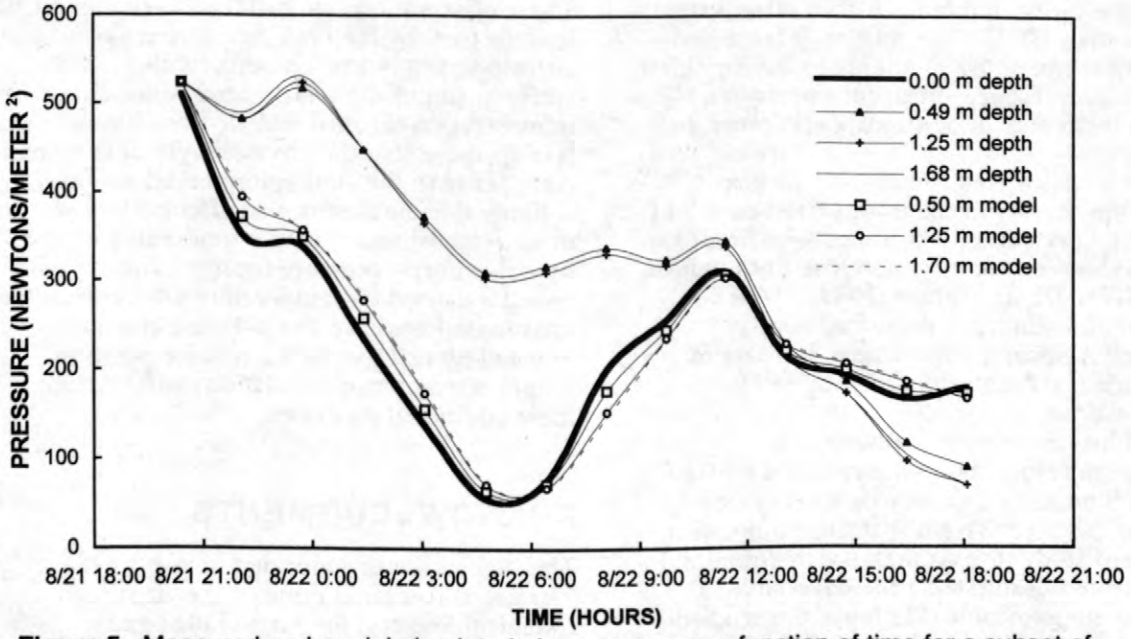

Figure 5. Measured and model-simulated air pressures as a function of time for a subset of the data from the August 1996 sampling event. A single air permeability was used for the simulation. Symbols are only used to help distinguish between lines and do not necessarily represent actual data points. Actual data points were collected at 5-minute intervals.

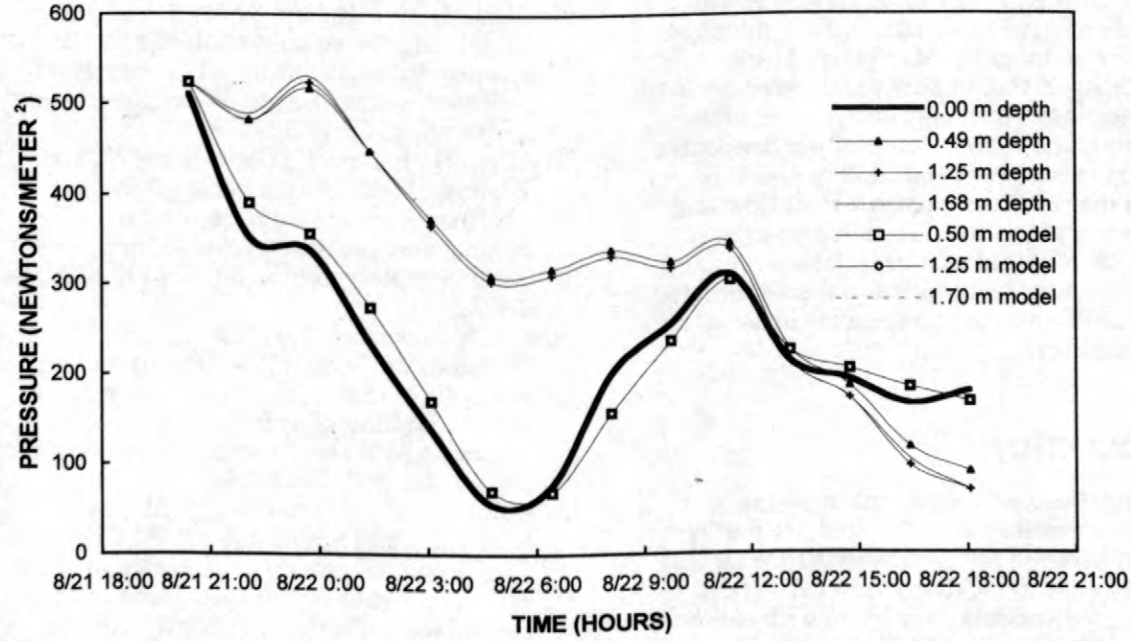

Figure 6. Measured and model-simulated air pressures as a function of time for a subset of the data from the August 1996 sampling event. Two air permeabilities were used for the simulation. Symbols are only used to help distinguish between lines and do not necessarily represent actual data points. Actual data points were collected at 5-minute intervals. The three model simulations are indistinguishable from one another.

temperature differences between the shallow subsurface probe and land surface often varied by more than 10 °C. The relatively large and changing temperature gradients in the top 0.3 m of soil may influence subsurface pressures and air flow independent of atmospheric pressure changes.

TCE vapor concentrations may also change the density of the unsaturated-zone soil gas, but this effect only becomes significant for organic vapor concentrations close to saturation (Falta, Javandel, and others, 1989). TCE concentrations in the unsaturated zone at Picatinny Arsenal are more than 3 orders of magnitude less than saturation-vapor concentrations.

Third, the current mathematical formulation assumes one-dimensional air flow. In other words, air can only flow up or down and flow cannot have a horizontal component. In a recent study, the air pressure distribution in a permeable unsaturated zone covered by a relatively impermeable clay layer was studied (Elberling, Larsen, and others, 1998). These researchers concluded that air flow was primarily in the horizontal direction. The permeable zone contacted the atmosphere at an outcrop of the geologic formation, and this outcrop acted as a "geologic window" for the flow of air into and out of the unsaturated zone. Air flow through the surficial clay layer was negligible relative to horizontal flow through the deeper, more permeable layer. If the permeability of the shallow unsaturated-zone soil at Picatinny Arsenal is low relative to the deeper soil, and if an outcrop of the permeable formation exists near the sampling site, it is possible that 2- or 3-dimensional air flow may be occurring at the site. To determine the importance of this mechanism, lateral pressure transducers must be installed in the unsaturated zone in addition to the transducers installed on a vertical transect.

CONCLUSIONS

Under natural conditions, pressure differences greater than 200 N/m^2 are routinely observed between the unsaturated zone air and the atmosphere at Picatinny Arsenal. These pressure-gradient data, combined with earlier direct measurements of TCE fluxes to the atmosphere that are at times significantly greater than diffusion fluxes (Smith, Tisdale, and Cho, 1996), strongly suggest that advection of TCE vapors is a significant transport process in the unsaturated zone at the field site. At a given sampling time, unsaturated-zone air pressures are relatively constant with depth, but not necessarily equal to atmospheric pressure. These observations are believed to be caused, at least in part, by the high moisture content (and correspondingly low air permeability) of the surficial soil of the unsaturated zone. Based on transient, one-dimensional air-flow simulations, it is apparent that the physical system is more complex than the simulation model assumes. It is likely that air flow is also affected by two- or three-dimensional pressure gradients induced by atmospheric pressure changes, fluid density changes caused by temperature gradients in the unsaturated zone, and/or pressure changes induced by changes in water-table position. Future research and simulations will address these additional processes.

ACKNOWLEDGMENTS

This research was supported in part by the Petroleum Research Fund of the American Chemical Society, the Toxic Substances Hydrology Program of the U.S. Geological Survey, and the U.S. Environmental Protection Agency.

REFERENCES

Cho, H.J., Jaffé, P.R., and Smith, J.A., 1993, Simulating the volatilization of solvents in unsaturated soils during laboratory and field infiltration experiments: Water Resources Research, v. 29, p. 3329-3342.

Elberling, B., Larsen, F., Christensen, S., and Postma, D., 1998, Gas transport in a confined unsaturated zone during atmospheric pressure cycles: Water Resources Research, v. 34, no. 11, p. 2855-2862.

Falta, R.W., Javandel, I., Pruess, K., and Witherspoon, P.A., 1989, Density-driven flow of gas in the unsaturated zone due to the evaporation of volatile organic compounds: Water Resources Research, v. 25, no. 10, p. 2159-2169.

Imbrigiotta, T.E., Ehlke, T.A., Martin, M., Koller, D., and Smith, J.A., 1995, Chemical and biological processes affecting the fate and transport of trichloroethylene in the subsurface at Picatinny Arsenal, New Jersey: Hydrological Science and Technology, v. 11, no. 1-4, p. 26-50.

Imbrigiotta, T.E., and Martin, M., 1996, Overview of research activities on the transport and fate of chlorinated solvents in ground water at Picatinny Arsenal, New Jersey, 1991-93, Morganwalp, D.W., and

Aronson, D.A., eds., U.S. Geological Survey Toxic Substances Hydrology Program--Proceedings of the technical meeting, Colorado Springs, Colo., September 20-24, 1993: U.S. Geological Survey Water Resources Investigation Report 94-4015, p. 297-306.

Massman, J., and Farrier, D.F., 1992, Effects of atmospheric pressures on gas transport in the vadose zone: Water Resources Research, v. 28, no. 3, p. 777-791.

Massman, J.W., and Madden, M., 1994, Estimating air conductivity and porosity from vadose-zone pumping tests: Journal of Environmental Engineering, v. 120, no. 2, p. 313-328.

Press, W.H., Flannery, B.P., Teukolsky, S.A., and Vetterling, W.T., 1986, Numerical Recipes: Cambridge, Cambridge University Press.

Sheets, W., 1997, Effect of atmospheric pressure variations on trichloroethylene vapor transport in the unsaturated zone: Charlottesville, University of Virginia, Department of Civil Engineering, unpublished M.S. thesis, 96 p.

Smith, J.A., Chiou, C.T., Kammer, J.A., and Kile, D.E., 1990, Effect of soil moisture on the sorption of trichloroethene vapor to vadose-zone soil at Picatinny Arsenal, New Jersey: Environmental Science and Technology, v. 24, no. 5, p. 676-683.

Smith, J.A., Cho, H.J., MacLeod, C.L., and Koehnlein, S.A., 1992, Sampling unsaturated-zone water for trichloroethene at Picatinny Arsenal, New Jersey: Journal of Environmental Quality, v. 21, no. 2, p. 264-271.

Smith, J.A., Tisdale, A.K., and Cho, H.J., 1996, Quantification of natural vapor fluxes of trichloroethene in the unsaturated zone at Picatinny Arsenal, New Jersey: Environmental Science and Technology, v. 30, no. 7, p. 2243-2250.

Topp, G.C., Davis, J.L., and Annan, A.P., 1980, Electromagnetic determination of soil water content: Measurements in coaxial transmission lines: Water Resources Research, v. 16, no. 3, p. 574-582.

AUTHOR INFORMATION

James A. Smith (jsmith@virginia.edu), Jee-Won Choi (jc5z@virginia.edu), Fred D. Tillman, Jr. (fdt2w@virginia.edu), University of Virginia, Charlottesville, VA. Whitney Katchmark (katchmarkws@efdlant.navfac.navy.mil), Naval Engineering Command, Norfolk, VA

Evaluation of RNA Hybridization to Assess Bacterial Population Dynamics at Natural Attenuation Sites

By Lisa A. Reynolds and Sheridan K. Haack

ABSTRACT

To improve site characterization and monitoring of natural attenuation sites, a better understanding of bacterial population dynamics is necessary. Bacterial populations found in contaminated aquifers can be quantified and identified using RNA (ribonucleic acid) hybridization. This technique allows for identification of specific bacterial populations that are active *in situ*. In addition, some biodegradation processes can be inferred using this method. RNA hybridization was used to analyze methane-producing bacterial populations at a natural attenuation site contaminated with jet fuel and chlorinated solvents. Preliminary results indicate spatial and temporal changes in methane-producing bacterial populations. Further work will characterize different groups of methanogens. These different groups of methane-producing bacteria will be used to predict the biodegradation processes that are likely to be occurring on specific dates and locations. Knowledge of the dynamics of these bacterial populations and processes will aid in modeling and evaluation of contaminated sites at which monitored natural attenuation has been chosen as a remediation strategy.

INTRODUCTION

It is widely recognized that biodegradation plays a significant role in the remediation of contaminated plumes. Because many organisms found *in situ* are capable of degrading groundwater contaminants (Edwards and Grbic'-Galic', 1992), monitored natural attenuation has been proposed as a possible remediation process for some contaminated aquifers (U.S. Environmental Protection Agency, 1997). This process relies on natural, physical, chemical and biological processes to remediate contaminated plumes, under monitored conditions. Natural attenuation may save some remediation costs, but often requires a detailed site characterization, extensive modeling, and long term monitoring. Understanding the spatial and temporal dynamics of bacterial populations and their relation to chemical and physical gradients found at the site, would prove to be very valuable in characterization and monitoring of natural attenuation sites.

Advances in molecular techniques have improved our ability to identify and quantify bacterial populations in environmental samples. Molecular techniques analyze genetic information that is unique to each bacterial population. Traditional methods identify bacterial populations by providing culturing media that are very different from *in situ* conditions for growth. These culturing methods enhance growth of some organisms but may inhibit growth of others, and do not necessarily represent the active population *in situ*. The application of molecular methods has shown that several organisms identified through culturing methods, and studied as representative of the environment, are not dominant *in situ* and do not play a significant role in degradation (Hugenholtz and Pace, 1996). RNA is genetic material, found in bacterial populations, and used to represent the biomass of active bacterial cells. RNA hybridization allows for the identification and quantification of

individual groups of bacteria or specific organisms that are active *in situ*. This is advantageous because there is no need to produce an artificial, laboratory growing, environment, and it is possible to quantify active bacteria. This method also allows for the detection of population changes in samples on a large scale.

The goals of the project described here are to identify, quantify, and assess the dynamics of selected bacterial populations, using hybridization techniques, and to relate these populations to geochemical gradients in the aquifer. We will focus our studies on methane-producing bacteria, their dynamics with respect to methane production at the site, and their function in natural attenuation. Relating the microbial populations to terminal electron accepting processes (TEAPs) or chemical gradients would be very useful in evaluating biodegradation rates and reactions.

TEAPs represent bacterial metabolic activities that use a succession of electron acceptors based on redox potential (Chapelle and others, 1995). In contaminated aquifers, zones of these processes are formed. One zone of interest is the methanogenic zone. Here one would expect to find methane-producing organisms, methanogens, carrying out the final step in anaerobic carbon degradation. Methane-producing bacteria have been known to degrade chlorinated compounds. A particular group of methane-producing bacteria that grows on acetate, known as acetoclastic methanogens has been found to degrade tetrachloroethylene (PCE) and trichloroethylene (TCE) by reductive dechlorination (Schocke and Schink, 1997; Jablonski and Ferry, 1992).

Little is known about the diversity of methanogenic bacteria in contaminated aquifers. There are genetic sequences, referred to as probes, available that can be used in molecular techniques to identify methanogenic bacteria and the two specific methanogenic pathways: H_2-CO_2 reduction and acetoclastic methanogenesis. The relation of methane-producing bacteria to TEAPs and other environmental gradients would provide a tool for modeling the biodegradation processes and changes that might occur. In addition, these relationships would provide information into the parameters that need to be monitored in evaluation of the ground-water contamination.

This paper describes how we are using RNA hybridization techniques to evaluate the bacterial populations present at a natural attenuation site. We will present how this knowledge enhances our ability to determine the biodegradation processes that are occurring, improving our ability to model and monitor the site.

SITE CHARACTERIZATION

The study site used for this work is at Wurtsmith Air Force Base in Oscoda, Michigan. Ground water at the site has been contaminated with jet-fuel- and chlorinated-solvents. A detailed site characterization can be found in Haack and Reynolds (1999, this Proceedings).

TEAP zones at this site were defined using hydrogen gas measurements (Chapelle and others, 1996). Sampling methods and ground-water analysis are described in Haack and Reynolds (1999, this Proceedings) and McGuire and others (1999, this Proceedings). For preliminary tests, aquifer sediments and ground-water chemistry were obtained near the location on two separate dates, October 1995 and June 1996. Additional samples were collected from the same location in October 1996. We also have aquifer sediment taken in 1998 at an upgradient site, an artificial substrate that was placed in selected wells in November 1998, and aquifer sediment received from a similar study site near Bemidji, Minnesota. These samples will be analyzed using the same molecular techniques to improve our understanding of population dynamics at natural attenuation sites.

APPROACH

RNA hybridization techniques will be used to identify microbial populations. Ribosomal RNA, (rRNA), is produced by all actively metabolizing cells and the RNA sequence is unique to each organism. RNA sequences are detected by extracting the rRNA from cells within the contaminated aquifer sediments, applying this extracted material to a filter, and detecting a desired sequence with a labelled

complementary sequence referred to as a probe (fig. 1). For this study, universal probes (Raskin, and others, 1994), were designed to detect all rRNA from these sediments. This allows us to quantify the total amount of rRNA found in the sediments and give an estimate of the total bacterial biomass for the sample. Following the identification of the total amount of RNA present, probes, will be used which are designed to detect the group of bacteria known as the archaebacteria, the group to which methane-producing organisms belong. The detection of archaebacteria allows us to see changes in likely methanogenic processes spatially and temporally. Then we can focus on methanogenic processes occurring *in situ*: H_2-CO_2 or acetoclastic methanogenesis. These different methanogenic processes are carried out by different groups of methane-producing bacteria. We can use probes that are specific for each individual group to determine the presence and biomass of these different methane producers (Raskin and others, 1994).

This method has some potential disadvantages. One disadvantage is that biases result from failure to extract all RNA present in the sample and the effective binding of labelled probes. A second disadvantage is that specific probes are limited to the gene sequences we can identify. We will evaluate these issues in our experiments.

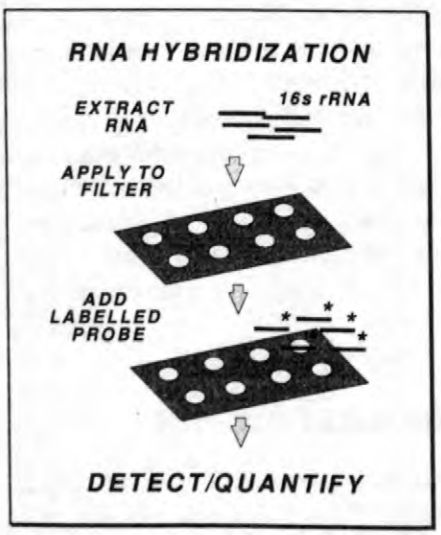

Figure 1. Schematic of the RNA hybridization method

RELATIONS BETWEEN TEAP ZONES AND BACTERIAL POPULATIONS

TEAP zones, hydrogen gas, methane and carbon dioxide measurements varied with sampling date and depth. Hydrogen gas, methane and carbon dioxide measurements can be found in table 1. The highest values for methane and carbon dioxide occurred near the water table (19 and 17.5 feet below land surface for October 1995 and June 1996, respectively). On the basis of hydrogen gas, methane, and carbon dioxide values, methane production by H_2-CO_2 methanogensis is not thermodynamically feasible at any date or depth. In other words, H_2-CO_2 methanogenesis would not support bacterial growth.

Table 1. Hydrogen gas, methane and carbon dioxide measurements at various depths. [ft, feet; nmol/L, nanomoles per liter; mg/L, milligrams per liter; nt, not tested]

Depth Below Land Surface	Date	H_2 nmol/L	CH_4 mg/L	CO_2 mg/L
17.81 ft	Oct 95	dry	dry	dry
18.31 ft	Oct 95	dry	dry	dry
22.00 ft	Oct 95	7.2	16.9	102
25.03 ft	Oct 95	6.0	6.5	29.7
27.99 ft	Oct 95	1.5	3.0	29.4
32.78 ft	Oct 95	1.2	2.2	19.6
37.59 ft	Oct 95	0.0	0.2	5.3
17.81 ft	June 96	1.3	nt	265
18.31 ft	June 96	7.9	9.43	304.7
22.00 ft	June 96	1.9	6.6	155.3
25.03 ft	June 96	2.4	nt	nt
27.99 ft	June 96	2.0	3.35	16.6
32.78 ft	June 96	2.2	nt	nt
37.59 ft	June 96	1.6	0.07	4.3

Preliminary RNA hybridization experiments were done on aquifer sediments taken in October 1995 and June 1996. Initial results show that samples taken at 17 and 19 feet below land surface have much higher total bacterial biomass for both dates sampled. These results were obtained using the universal probe signal. The highest percentage of archaebacteria (possible methane-producers) varied with depth and sampling date. These results are summarized in table 2.

Table 2. Bacterial population distribution based on RNA hybridization [ng/gdw, nanograms per gram dry weight; %, percent; ft, feet; nd, not detected; nt, not tested]

Sample Depth Below Land Surface	Total Bacterial RNA (ng/gdw)/ %Archaeal RNA	
	October 1995	June 1996
17 ft	[1]16/0.2%	[1]17/0.1%
19 ft	[1]127/0.2%	[2]222/10%
22 ft	[2]0.2/20%	[3]9/10%
30 ft	[3]0.1/nd	[3]0.6/10%
35 ft	0.2/nd	nt

[1]capillary fringe samples
[2]methanogenic zone based on H_2 measurements
[3]sulfate-reducing zone based on H_2 measurements

SUMMARY

Preliminary results of hybridization experiments show changes in bacterial populations over vertical intervals of less than five feet. They also show the presence and absence of archaebacteria (representative of methane producers) at various locations. Further investigation as to which methane-producing populations are present will allow for a comparison with calculated thermodynamic reactions. We will also be able to look for relation between changes in chemical parameters and the presence and absence of different methanogenic species. This would provide a better understanding of the dynamics of terminal carbon degradation, and both TEAP and dechlorination reactions in the plume of contaminated ground water.

Other work done on these samples has shown that methane-producing bacteria are present. The acetate-consuming methanogenic organism, *Methanosaeta concilii*, was identified along with *Syntophus gentianae* (Dojka and others, 1998). These organisms act together to degrade some aromatic hydrocarbons such as those in fossil fuels (Schocke and Schink, 1997). The presence of these organisms suggests specific pathways for aromatic hydrocarbon degradation at this site, and is consistent with site chemistry. Using such information along with hybridization results would provide knowledge of the location of the specific bacterial populations that are carrying out the degradation processes.

The location of microbial populations and processes provide us with information that will be useful for sampling and monitoring practices at natural attenuation sites. Knowing the populations that are present will provide evidence of the processes of degradation that might be occurring and the chemical factors affecting the system. Changes in microbial populations would provide insight into where monitoring would need to occur. Currently there are no criteria to make this determination. Consequently, critical samples might be missed or misinterpreted. Using hybridization techniques we are able to identify microbial populations at various depths and on separate sampling dates at a natural attenuation site. We are able to calculate biomass numbers for these microbial populations. Traditional culturing methods would not have provided such quantification results.

ACKNOWLEDGMENTS

In addition to funding by the U.S. Geological Survey Toxic Substances Hydrology Program, a portion of this work was also funded by the National Science Foundation (EAR-9708487 and BIR 9120006), and the National

Center for Integrated Bioremediation Research and Development, at Michigan University. We greatly appreciate the work done by Dyanne Christian on this project and contributions to the original experimental design by L. J. Forney.

REFERENCES

Edwards, E. A. and Grbic'-Galic', Dunja, 1992, Complete mineralization of benzene by aquifer microorganisms under strictly anaerobic conditions: Applied and Environmental Microbiology, vol. 58, no. 8, p. 2663- 2666.

Chapelle, F. H., McMahon, P. B., Dubrovsky, N. M., Fujii, R. F., Oaksford, E. T., Vroblesky, D. A., 1995, Deducing the distribution of terminal electron accepting processes in hydrologically diverse groundwater systems: Water Resources Research, vol. 31, no. 1, p. 359-371.

Chapelle, F. H., Haack S. K., Adriaens, Peter, Henry, M. A., and Bradley P. M., 1996, Comparison of Eh and H_2 measurements for delineating redox processes in a contaminated aquifer: Environmental Science and Technology, vol. 30, no. 12, p. 3565-3569.

Dojka, M. A, Hugenholtz, P. H, Haack, S. K., Pace, N. R., 1998, Microbial diversity in a hydrocarbon- and chlorinated-solvent-contaminated aquifer undergoing intrinsic bioremediation: Applied and Environmental Microbiology, vol. 64, no. 10, p. 3869-3877.

Haack , S. K. and Reynolds, L. A., 1999, Using molecular approaches to answer questions about microbial populations at contaminated sites: U.S. Geological Survey Toxics Substance Hydrology Program - - Proceedings of the technical meeting, Charleston, South Carolina, March 8-12, 1999.

Hugenholtz, Philip, and Pace, Norman, 1996, Identifying microbial diversity in the natural environment: a molecular phylogenetic approach. Trends in Biotechnology, vol. 14, no.1, p. 190-198.

Jablonski, P. E., Ferry, J. G., 1992, Reductive dechlorination by the CO-reduced CO dehydrogenease enzyme complex from *Methanosarcina thermophila*: FEMS Microbial Letters, vol. 96, no. 1, p. 55-60.

McGuire, J. T., Smith, E. W., Kolak, J. J., Long, D. T., Hyndman, D. W., Velbel, M. A., Klug, M. J., and Haack, S. K., 1999, Temporal variations in biogeochemical processes that influence ground-water redox zonation: U.S. Geological Survey Toxic Substances Hydrology program - -Proceedings of the technical meeting, Charleston, South Carolina, March 8-12, 1999.

Raskin, Lutgarde., Stromley J. M., Rittman B. E. and Stahl D. A., 1994, Group-specific 16S rRNA hybridization probes to describe natural communities of methanogens: Applied and Environmental Microbiology, vol. 60, no. 4, p. 1232-1240.

Schocke, L. and Schink, Bernard, 1997, Energetics of methanogenic benzoate degradation by *Syntrophus gentianae* in syntrophic coculture: Microbiology, vol. 143, p. 2345-2351.

U.S. Environmental Protection Agency, 1997, Use of monitored natural attenuation at superfund, RCRA corrective action, and underground storage tank sites. OSWER directive 9200.4-17, U. S. Environmental Protection Agency, Washington, D.C.

AUTHOR INFORMATION

Lisa A. Reynolds and Sheridan K. Haack, U.S. Geological Survey, Lansing, Michigan (lreynold@usgs.gov, skhaack@usgs.gov)

Temporal Variations in Biogeochemical Processes that Influence Ground-Water Redox Zonation

By Jennifer T. McGuire, Erik W. Smith, David T. Long, David W. Hyndman, Sheridan K. Haack, Jonathan J. Kolak, Michael J. Klug, Michael A. Velbel, and Larry J. Forney

ABSTRACT

Hydrogeological, microbiological and geochemical parameters are being measured in ground water to determine and model processes affecting redox zonation. The ultimate objective of this project is to construct a three-dimensional, transient, reactive flow and transport model for the evolution of redox zonation. The study site is a shallow sandy aquifer contaminated with petroleum hydrocarbons and chlorinated solvents. This paper explores temporal variations in the biogeochemistry of ground water collected from the study site over a period of three years. Selected indicators of biogeochemical processes include dissolved hydrogen (H_2) and dissolved methane (CH_4). Measurements of these indicators have documented changes in redox zonation over short time scales (months) superimposed on more gradual changes that occurred over a three-year period. The patterns of water-table fluctuations and biogeochemical changes in ground water indicate that monthly changes in redox zonation are influenced by solute transport (recharge). At longer time scales, changes in microbial processes unrelated to solute transport may also influence redox zonation. Temporal changes in dissolved potassium concentrations support the concept that a change in microbial processes has occurred over three years. Resolving the possible controls on redox zonation on these two, distinct time scales is the focus of on-going studies.

INTRODUCTION

A fundamental issue in aquifer biogeochemistry is the means by which solute transport and geochemical processes interact with microbiological activity to influence spatial and temporal variations in redox zonation. These processes control the availability of organic matter, nutrients, and electron donors and acceptors to the bacteria that carry out many redox reactions (Vroblesky and Chapelle, 1994). For example, with depth in marine and freshwater sediments, bacterial decay of organic matter lowers the redox of porewater (Berner, 1981) from aerobic respiration toward methanogenesis (Stumm and Morgan, 1981; Lovley and Goodwin, 1988). The specific redox condition present at a given sediment horizon varies as a function of availability of organic matter, nutrients, and electron donors and acceptors. Vertical solute transport, which is commonly diffusion dominated in aquatic environments, regulates the availability of these compounds. The entire sequence of redox processes, from aerobic respiration through methanogenic respiration, typically occurs in a narrow zone (less than 50 cm) of the upper sediment column (Baedecker and Back, 1979).

Along a flow path closed to the atmosphere, uncontaminated ground water evolves biogeochemically through a similar sequence of processes (Champ and others, 1979; Chapelle 1993). However, advection is the primary transport mechanism in saturated aquifers, thus the path length over which these sequences occur is much larger (approximately 10 km or more).

Characterizing the redox state of subsurface environments has been hindered by a lack of understanding of the hydrogeological, microbiological, and geochemical processes controlling redox. In addition, field measurement tools have lacked the capability to fully and accurately characterize redox conditions. For example, redox zonation is likely controlled by the electron-accepting (respiratory) activities of microorganisms. However, redox conditions are

commonly defined by electrode potential (Eh) or by the relative concentration of reduced and oxidized solute species, which depend on equilibrium thermodynamics. An alternative approach to define redox conditions is based on hydrogen (H_2) gas concentrations (Lovley and Goodwin, 1988), which reflects microbiological terminal electron accepting processes (TEAPs).

The need for an interdisciplinary effort to examine the development of and temporal changes in redox zonation in aquifers is particularly acute in the area of bioremediation of anthropogenic ground-water contaminants. Redox state affects the chemical form, mobility, and persistence of many ground-water contaminants (Stumm and Morgan, 1981; Christensen and others, 1994). It is generally understood that natural bioremediation of petroleum-derived aromatic hydrocarbons occurs under most redox conditions (Vogel, 1994; Chapelle, 1993). This has lead to remediation strategies that introduce nutrients, growth substrates, electron acceptors, and microorganisms into the subsurface. However, the efficiency and rate of hydrocarbon and chlorinated solvent degradation varies with redox environment (Norris and others, 1994).

A focus of the study reported here is to describe the temporal variability of H_2-defined redox zones by placing the governing microbiological reactions within the framework of hydrogeochemical models. This paper describes the objectives of our on-going research and outlines the methods used and the general nature of the study site. A brief summary of preliminary results that illustrate temporal variations in redox zonation is presented.

BACKGROUND

Redox Zonation

The development of redox zonation in aquatic systems is likely based on the activities of microorganisms, which first use O_2, and then a succession of alternate electron acceptors (in order of decreasing redox potential and free energy yield) to support their growth using a variety of carbon sources (Lovley 1991; Chapelle, 1993). In order of decreasing redox potential and free energy yield, the succession generally follows the order aerobic respiration, denitrification, Mn(IV) reduction, Fe(III) reduction, sulfate reduction, and methanogenesis, (Stumm and Morgan, 1981).

The redox state of aqueous systems has been defined by the variations in concentrations of methane, sulfide, Fe^{2+}, Mn^{2+} or NH_4^+ in water, which indicates microbes have utilized the respective oxidized forms of these compounds for growth processes. Another approach uses electron activity ($[e^-]$), measured on *pe* or Eh scales, to define redox state. However in ground-water studies, these approaches are limited because processes such as advection, dispersion, precipitation, and volatilization change concentrations of redox species, thereby affecting the accurate determination of zonation (Christensen and others, 1994).

Electrode measurements of redox potential or concentrations of redox couples have been the classic redox indicators, but have little practical value. Their value has been limited because (1) redox electrodes do not respond to many of the important oxidized or reduced species in aquatic environments, and (2) the assumption of redox equilibrium is not appropriate for most hydrogeologic systems (Lindberg and Runnells, 1984; Lovley and Goodwin, 1988; Barcelona and others, 1989; Chapelle, 1993; Chapelle and others, 1995).

The H_2 concentration in aquatic systems has recently been proposed as a more accurate indicator of *in-situ* terminal electron accepting processes (TEAPs) than the above approaches (Lovley and Goodwin, 1988). The H_2 concentrations associated with each TEAP, as measured in marine and freshwater sediments and in aquifers, are as follows: methanogenesis, greater than 5 nM; sulfate reduction, 1-4 nM; Fe(III) reduction, 0.2-0.6 nM; and Mn(IV) or nitrate reduction, less than 0.05-0.1 nM (Lovley and Goodwin, 1988; Chapelle and others, 1995).

Solute transport processes influence the spatial and temporal patterns of redox zonation in ground-water environments (Hess and others, 1992; LeBlanc and others, 1991). For example, Vroblesky and Chapelle (1994) demonstrated that variations in recharge and lateral transport result in temporal shifts in TEAPs. In addition, transport rates may gradually change because microbial activity can degrade these substrates as well as create biofilms that reduce the hydraulic conductivity of a region (Taylor and Jaffe, 1990). Solute transport and therefore the rate of supply of

electron acceptors, growth substrates, and nutrients, is controlled by both the hydraulic gradient and aquifer properties such as hydraulic conductivity, storage coefficient, dispersivity, effective porosity, and sorption coefficients. Spatial variations in hydraulic conductivity determine the predominant zones of solute transport since ground water follows the path of least resistance. Dispersivity accounts for lateral and transverse solute spreading due to small-scale ground-water velocity variability, which will be a critical factor in accurately describing the downgradient geometry of the redox zones. The lateral dispersive flux of electron acceptors is likely to be particularly important in the evolution of interfaces between different redox zones.

Aquifer mineralogy may also influence redox zonation, particularly the availability of Fe(III) (Lovley, 1991; 1994).

Redox Zonation in Contaminant Plumes

Complex redox zonation has been identified in contaminated ground water (Baedecker and Back, 1979; Vroblesky and Chapelle, 1994; Chapelle and others, 1995; Bennett and others, 1993). In most cases, the sequence of redox processes is similar to those in closed ground-water systems, albeit reversed (Baedecker and Back , 1979; Lovley, 1991; Chapelle, 1993). That is, the most reduced conditions (methanogenesis) occur near the contaminant source, while less reducing conditions (iron reduction) occur down the flow path from the contaminant source. The sequence of processes in contaminated aquifers also occurs over a much shorter flow path (approximately 1 km) compared to the sequence in natural ground-water systems (approximately 10 or more km). The sequence reversal and decreased spatial extent are likely the result of microbial activity in response to increased carbon input. Redox zones in contaminated aquifers may vary spatially and temporally (Christensen and others, 1994, Vroblesky and Chapelle, 1994), as influenced by heterogeneities in aquifer properties and temporal variation in recharge.

When alternate electron acceptors are available, anaerobic microbiological degradation processes may follow different metabolic pathways causing spatial and temporal variations in redox. Particular BTEX compounds can be directly used for growth by isolated iron- and sulfate-reducers (Lovley, 1994; Rabus and others, 1993), which may also use aromatic acids, aliphatic volatile fatty acids, or even H_2 and CO_2 for growth (Lovley, 1994). Therefore, in the appropriate environments, iron- and sulfate-reducers may be responsible for the direct mineralization of BTEX compounds or the extent of accumulation of intermediates, or both. Whether a particular iron- or sulfate-reducer uses a BTEX compound directly, or grows on an intermediate, is a function of (1) the relative abundance of carbon substrates or electron acceptors; (2) the thermodynamic constraints that govern the amount of reaction free energy (ΔG); and (3) aquifer hydrogeologic and geochemical properties that influence the rate of supply and relative abundance of electron acceptors. Thus, it is likely that spatial and temporal heterogeneity in aquifer redox zonation may be dramatically influenced by the relative activities of these groups of microorganisms.

DESCRIPTION OF STUDY

This on-going research is examining the interaction among hydrogeological, geochemical, and microbiological processes that influence redox zonation in a contaminated aquifer. Hypotheses are being tested regarding reactions that change redox zonation and factors controlling the spatial and temporal dimensions of redox zones. The objectives of this interdisciplinary study are to:

(1) quantitatively assess hydrogeologic, geochemical and microbiological processes that influence redox conditions within a zone;
(2) use these constraints to identify sets of reactions that describe the evolution of ground water from one zone to another; and
(3) integrate the reaction sets with a dynamic flow and transport model to simulate past observations regarding the dimensions of various redox zones at the site, as well as compare the predicted and observed outcome of ground-water hydrologic events such as prolonged periods of high or low water table.

These goals are being achieved by field sampling (seasonal and event), laboratory analysis and experimentation, *in-situ* hydrogeological, microbiological, and geochemical analyses, and

hydrogeochemical modeling. Unique aspects of the methods include:

(1) combining geophysical and hydrogeological data to estimate aquifer parameters,
(2) using 16S rRNA nucleic acid probe hybridization to determine microbial populations and 16S rDNA analysis to determine community structure (Haack and Reynolds, 1999, these Proceedings; Reynolds and Haack, 1999, these Proceedings),
(3) estimating redox state from H_2 gas concentrations,
(4) assessing mineral-microbial interactions using *in-situ* samplers, and
(5) combining geochemical and microbiological reaction sets in a reactive flow and transport model to quantitatively account for observed water chemistry and redox conditions at the study site.

Our study will be one of the first to apply a transport model to describe transient variations in redox zonation in response to recharge events. A significant aspect is that the model will be constrained by estimates of the hydrogeological, microbial, and geochemical processes obtained from field and laboratory tests.

FIELD SITE DESCRIPTION

The study site is a shallow sandy aquifer contaminated with petroleum hydrocarbons and chlorinated solvents (Wurtsmith Air Force Base, Michigan, U.S.A.) (fig. 1). Historically, this area, FTA-2, was used to train Air Force personnel in fire-fighting procedures and a variety of petroleum products and solvents were applied to the land surface to start fires. Over the 24-year operational life (1952-1986) of FTA-2, organic contaminants leached into the underlying aquifer, resulting in an extensive plume approximately 50 m wide and 400 m long (fig. 2). The aquifer at this site consists of alternating aeolian sands and glacial outwash material that is highly permeable with hydraulic conductivities on the order of 30 m/day. The water table is encountered at 4.5-5.5 m below land surface.

To document the vertical distribution of contaminants within the plume, the National Center for Integrated Bioremediation Research and Development (NCIBRD) installed a series of multi-level sampling wells at this site. The wells were constructed of 2.5 cm inner diameter PVC

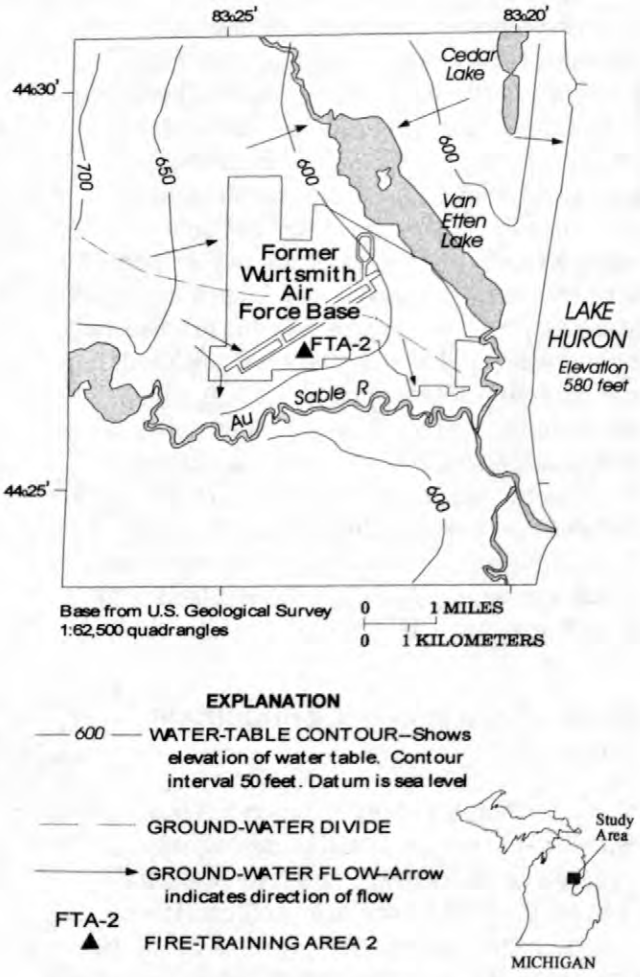

Figure 1. Map showing the location of the study site.

casing, with 0.33 m PVC screens at the bottom. The vertical spacing between the screens ranged from 0.5 to 2 m. The multi-level wells are oriented in a line perpendicular to ground-water flow located approximately 100 m downgradient from the suspected source. These wells are used to collect ground-water chemistry samples for this study.

METHODS

Seasonal measurements of hydrogeological, microbiological, and geochemical parameters are being collected at the site, adding to a dataset started in 1995 by Chapelle and others (1996). Each well is purged with a peristaltic pump at a rate of approximately 200 ml/min. A flow cell is used to continuously monitor temperature, pH, dissolved oxygen, Eh, and specific conductance until stable (usually 20-

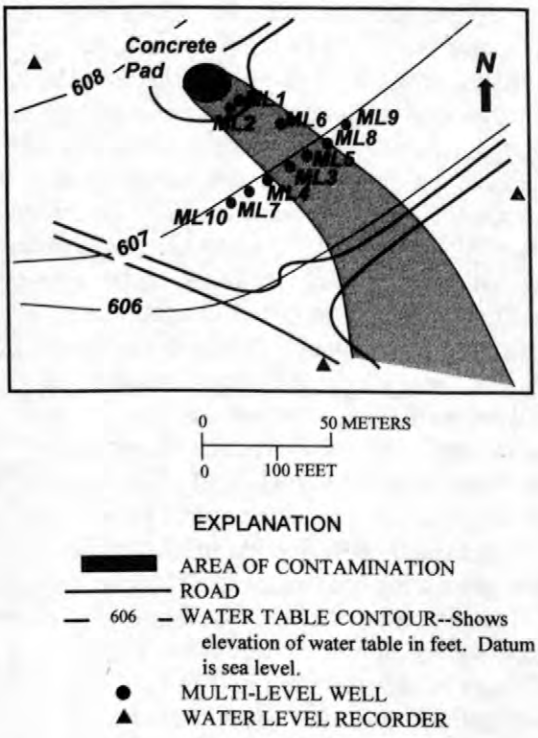

Figure 2. Plume map for the Fire-Training Area 2 (FTA-2) at the former Wurtsmith Air Force Base, Michigan. The concrete pad was the site of fire-training activities.

30 minutes). Once stable, H_2 samples are collected using the bubble-stripping method (Chapelle and McMahon, 1991). Water is continuously pumped through a standard 400 ml glass gas-sampling bulb. Previous experience has shown H_2 concentrations require 20 minutes to equilibrate (Chapelle and others, 1996). After 20 minutes, a gas sample (3 replicates of 7.5 ml each) is drawn from the bulb with a gas-tight glass syringe. Samples continue to be drawn at approximately 10-minute intervals until concentrations stabilize. The H_2 concentrations are analyzed in the field with a RGA3 reduction gas analyzer. Concentrations of H_2 in the aqueous phase are calculated using the Henry's Law coefficient. At 1 atm pressure and 10°C, 1.0µl/L of hydrogen in the gas phase coexists with 0.8 nmol/L (nM) of H_2 in the aqueous phase. The detection limit of this method is approximately 10 ppb.

In the field, concentrations of dissolved oxygen are analyzed colorimetrically to complement flow cell measurements. Nitrate, nitrite, and sulfide are measured by colorimetric analysis. Concentrations of dissolved Fe (II) are determined in the field using phenanthroline colorimetric analysis. Alkalinity is determined in the field by potentiometric titration. Ground-water samples are also collected and analyzed for major cations and anions, trace metals, dissolved inorganic carbon (DIC), dissolved organic carbon (DOC), methane, stable isotopes, sulfate (SO_4), ammonium ion (NH_4), volatile organic carbon (VOC), and volatile fatty acid (VFA).

When necessary, samples are filtered through 0.45 µm polyethersulfone membrane filters. Field blanks are collected daily. Samples for major cations and trace metals are preserved with optima nitric acid. Major cations are analyzed by atomic adsorption-flame technique. Trace metal concentrations are analyzed by induced coupled plasma mass spectrometry (ICP-MS). Anion samples are unpreserved and analyzed by specific ion electrode or capillary electrophoresis. Sulfate samples are preserved with formaldehyde and measured either by atomic adsorption-flame technique or by capillary electrophoresis. Silica is measured by molybdate blue colorimetric analysis. DIC and methane samples are preserved with mercuric chloride crystals and measured by headspace extraction on a DOC analyzer. $\delta^{18}O$, δD, and $\delta\ ^{13}C\ CH_4$ samples are analyzed by mass spectrometry. DOC and NH_4 samples are flash-frozen on dry ice until analysis by the DOC analyzer and capillary electrophoresis, respectively.

Hydrogeological data are collected from three hourly recording pressure transducers triangulated approximately 300 m apart about FTA-2 (fig. 2). Individual water level measurements were taken manually from all available wells at FTA-2 (about 20 wells) during seasonal sampling events.

SELECTED RESULTS

Chapelle and others, (1996) used H_2 concentrations in samples collected in October 1995 to interpret ground-water TEAP conditions at FTA-2. TEAPs considered included methanogenesis, sulfate reduction, and iron reduction (fig. 3a). Temporal measurements of H_2 (fig. 3a) in ground-water samples taken from the same vertical profile within the contaminant plume indicate that redox conditions changed over a 3 year period but that rates of change are on

time scales of less than a year. Our data indicate change may occur on the order of months or less (McGuire and others, 1998).

Hydrogen concentrations generally have decreased throughout the vertical profile over the three-year period. The inferred TEAP processes in this vertical profile indicate a change from a large area of methanogenesis in October 1995 to predominantly sulfate reduction in June 1996, to predominantly iron reduction in August 1998 (fig. 3a).

Changes in dissolved methane concentrations throughout the profile do not parallel those predicted by hydrogen concentrations (fig. 3b). Similar to hydrogen, dissolved methane concentrations decreased between October 1995 and June 1996, but concentrations increased in August 1998.

DISCUSSION

Two hypotheses being investigated to explain these types of changes are that:

(1) Ground-water recharge influences redox state by changing amounts of terminal electron acceptors (e.g., dissolved O_2), and
(2) Changes in dominant microbial process(es) cause shifts in biogeochemical reactions.

Fluctuations in water-table elevation (fig. 4), temperature, and water-quality concentrations (fig. 5) support both hypotheses. Samples from October 1995 were collected after a long period of a steadily declining water table (fig. 4). With no recharge, electron acceptors such as dissolved oxygen were highly depleted, resulting in extensive areas of methanogenesis. Samples from June 1996 were collected after a recharge event. Recharge water affected hydrogen and dissolved methane concentrations either through dilution or by limiting methanogenesis because the influx of more oxic water delivers more energetically favorable electron acceptors to the system.

Temporal changes in the temperature and concentrations of dissolved oxygen and dissolved methane in ground-water samples taken at the same depth from a multi-level well, provide evidence of the effect of recharge on biogeochemical changes and redox conditions in the plume (fig. 5). At multi-level well 3 (depth 18.31), hydrogen concentrations have been very low after October 1996 (fig. 5a). Changes in concentrations of dissolved methane are similar to those of hydrogen until October 1996. After this time, concentrations of dissolved methane fluctuate and the fluctuations are inversely related to fluctuations in concentrations of dissolved oxygen. When dissolved oxygen concentrations increased, dissolved methane concentrations decreased. Increased concentrations of dissolved oxygen for February 1998 and May 1998 ground-water samples are likely related to recharge events (fig. 3). Cooler ground-water temperatures (fig. 5a) also indicate recharge during these times.

Changes in TEAP conditions and dissolved methane concentrations from October 1995 to June 1996 can be related to changes in water-table elevations (recharge). The August 1998 samples were collected after a period of prolonged water-table decline similar to the conditions during the October 1996 sampling (fig. 4). Thus, it was anticipated that the August 1998 ground-water samples would reflect TEAP conditions as inferred from hydrogen concentrations, and have concentrations of dissolved methane similar to those of October 1995.

Although dissolved methane concentrations generally were higher in August 1998 than in June 1996, hydrogen concentrations are not. Because the hydrogen concentrations are low, the production of methane by reduction of carbon dioxide is not indicated, as it had been in October 1995 (Chapelle and others, 1996). Other processes, such as acetate-consuming methanogenesis or reductive dehalogenation (Suflita and others (1982), possibly involving complex pathways, may now be occurring and responsible for differences in the temporal changes of methane and hydrogen.

The decline in hydrogen concentrations over the three-year period and lack of similar decline in dissolved methane concentrations indicates recharge may only in part explain changes in H_2 concentrations in the plume. Changes in the biogeochemistry of the ground water may have occurred over a longer time period, driven by changes in microbial processes.

A. REDOX ZONATION BASED ON H_2 CONCENTRATIONS

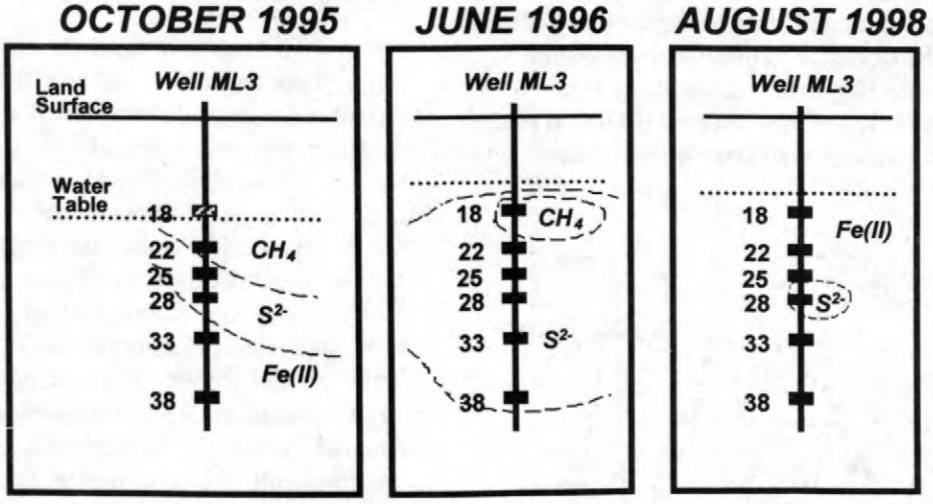

18 ■ WATER SAMPLING DEPTH IN FEET BELOW LAND SURFACE
18 ▨ DRY WATER SAMPLING DEPTH IN FEET BELOW LAND SURFACE

B. METHANE CONCENTRATIONS

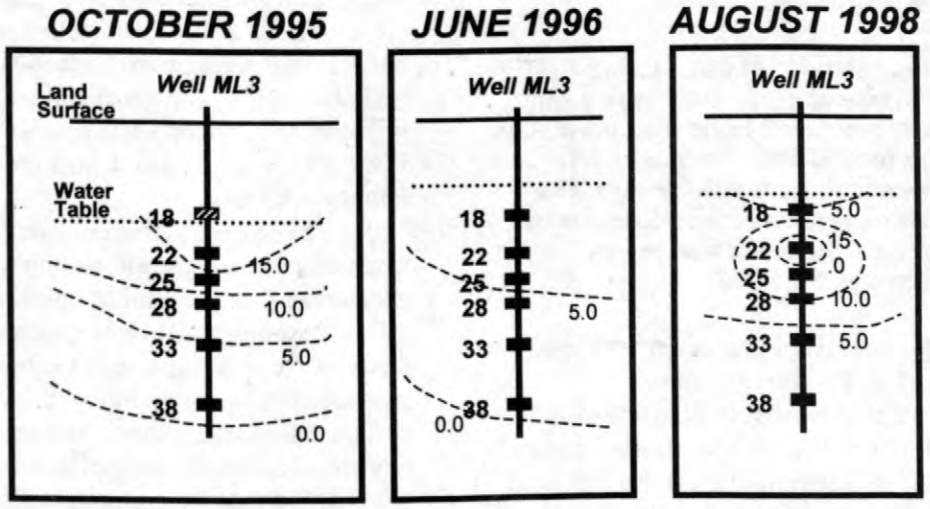

18 ■ WATER SAMPLING DEPTH IN FEET BELOW LAND SURFACE
18 ▨ DRY WATER SAMPLING DEPTH IN FEET BELOW LAND SURFACE

Figure 3. Vertical profiles of terminal electron accepting processes (TEAP) as implied from H_2 concentrations and dissolved methane concentrations at multi-level well site 3 (ML3). A: TEAP processes for sampling periods October 1995, June 1996, and August 1998. Methanogenic zones (CH_4), sulfate reducing zones (S^{2-}), and iron reducing zones (Fe(II)) are shown. B: Dissolved methane (CH_4) concentrations in milligrams per liter (dashed lines) for sampling periods October 1995, June 1996, and August 1998. Inferred TEAP processes for October 1995 and June 1996 are modified from Haack (1999, these proceedings). Dissolved methane concentrations are from Chapelle and others (1996) for October 1995 and from Haack (unpublished data) June 1996.

Further evidence for longer term changes in the biogeochemical state of the ground water at FTA-2 is the decrease in dissolved potassium concentrations (fig. 5b) over the three year monitoring period. This decrease is similar to the decrease in hydrogen concentrations. After

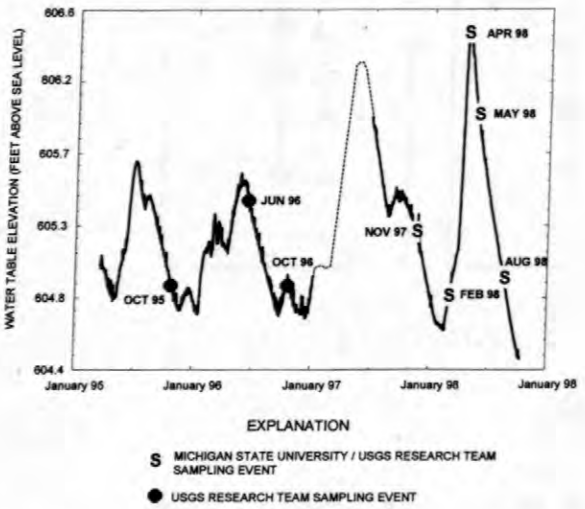

Figure 4. Graph showing of water-table elevation as a function of time at FT-2. Data were taken from water level recorder 2 (solid line) and manual measurements (dotted line). Periods when ground-water samples were collected are also shown. Circles represent samples collected by the U.S. Geological Survey. S's represent samples collected in this study.

October 1996, dissolved potassium in ground water from ML3-18.31 is similar to concentrations in ground water outside of the contaminant plume (fig. 5b). A similar change in dissolved sodium concentration is not observed and implies that processes such as dilution are not responsible for the changes in potassium concentrations.

Organic acids such as acetate are known to enhance mineral weathering and release cations to ground water (Drever, 1996). The decreased concentrations of dissolved potassium may be related to the decrease in the presence of organic acids due to the change in microbial activity from carbon dioxide reduction to acetate-consuming methanogenesis.

CONCLUDING REMARKS

The redox environment in a petroleum-derived plume influences the efficiency, rate, and extent of biodegradation (Vogel 1994, Chapelle, 1993; Norris and others, 1994). Biodegradation is most efficient under aerobic conditions, but has been demonstrated to occur under most redox conditions (Grbić-Galić and Vogel, 1987; Edwards and others,1992; Rabus and others, 1993; Lovley and others, 1995; Lovley and Lonergan, 1990; Baedecker and others, 1993; Hutchins and others, 1991). In aerobic environments, BTEX compounds are degraded completely to CO_2. In methanogenic environments, the complete transformation of organic compounds to CO_2 and CH_4, requires the combined activities of at least three different functional groups of microorganisms: fermenters, fatty-acid degraders, and methanogens. Thus, the effectiveness of ground-water remediation strategies will be influenced not only by our ability to accurately delineate redox zones in a contaminated aquifer (Chapelle and others, 1996), but also to determine the hydrogeological, microbiological, and geochemical factors influencing temporal variations in the zones. Results from this research will provide insights into these factors.

In summary, this on-going study is examining the interaction among hydrogeological, geochemical, and microbiological processes that influence redox zonation in ground water. One phase of the investigation is to characterize the spatial and temporal nature of the redox zonation in the contaminant plume. The results indicate that redox zonation changed on time scales of months, and that there also appears to have been changes that occurred over a three-year period.

Both ground-water recharge and changes in microbial processes appear to influence the temporal changes in redox zonation. As part of our study, the influence of these two possible controls on redox zonation will be further investigated. Plans for additional data collection include:

(1) Ground-water samples taken from new wells to provide a better three-dimensional geochemical characterization,
(2) *In-situ* and laboratory microcosm studies to identify microbial processes and rates,

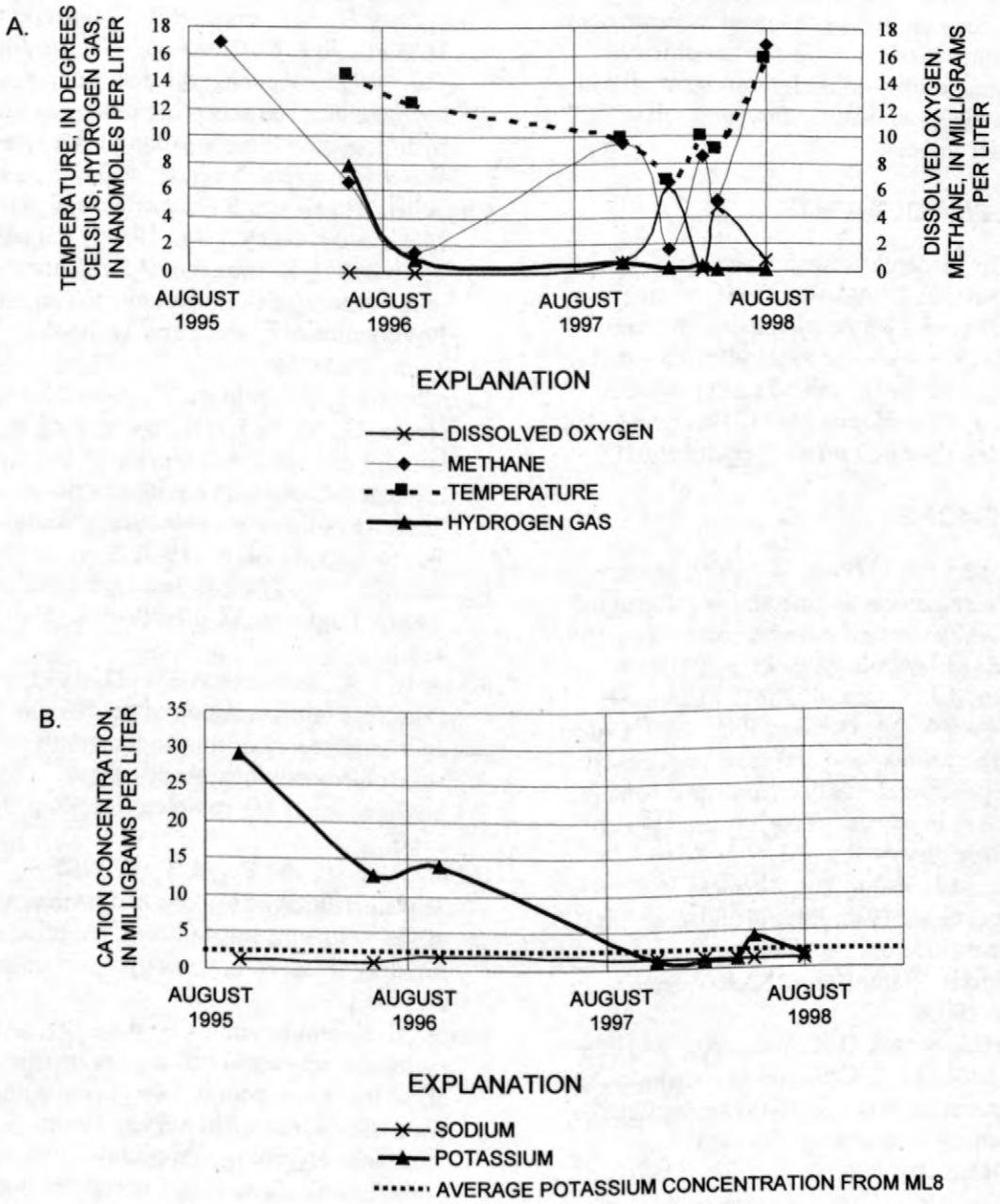

Figure 5. Graphs showing water temperature and concentrations of constituents in ground water from the contaminant plume at FT-2. Data collected from multi-level well site 3 at a depth of 18.31 feet in October 1995, June 1996, October 1996, November 1997, February 1998, April 1998, May 1998, and August 1998. A: Temperature, dissolved oxygen, hydrogen gas, dissolved methane. B: Dissolved sodium and dissolved potassium. Average dissolved K concentrations are shown for water samples taken from multi-level well 8 (ML8), located outside of the contaminant plume. Temperature, dissolved oxygen, hydrogen gas and dissolved methane data are from Chapelle and others (1996) for October 1995 and from Haack (unpublished data) June 1996.

(3) Geochemical measurements of the solid phase to determine reactive substrates, and
(4) More detailed hydrogeological measurements to characterize aquifer heterogeneities including cross-well radar tomography to help refine the ground-water flow and solute transport models.

ACKNOWLEDGMENTS

The research is funded by a grant from the National Science Foundation Environmental Geochemistry and Biogeochemistry Program, EAR-9708487. We would also like to thank the National Center for Integrated Bioremediation, Research, and Development (NCIBRD) and EFX Systems, Incorporated for their cooperation.

REFERENCES

Baedecker, M.J., and Back, W., 1979, Modern marine sediments as a natural ananlog to the chemically stressed environment of a landfill: Journal of Hydrology, v. 43, p. 393-414.

Baedecker, M.J., Cozzarelli, I.M., Eganhouse, R.P., Siegel, D.I., Bennett, P.C., 1993, Crude Oil in a shallow sand and gravel aquifer-III. Biogeochemical reactions and mass balance modeling in anoxic ground water: Applied Geochemistry, v. 8, no. 6, p. 569-586.

Barcelona, M.J., Holm, T.R., Schock, M.R., George, G.K., 1989, Spacial and temporal gradients in aquifer oxidation-reduction conditions: Water Resources Research, v. 25, p. 991-1003.

Bennett, P.C., Siegel, D.E., Baedecker, M.J., and Hult, M.F., 1993, Crude oil in a shallow sand and gravel aquifer – I. Hydrogeology and inorganic geochemistry: Applied Geochemistry, v. 8, no. 6, p. 529-549.

Berner, R.A., 1981, Early Diagenesis, A theoretical approach: Princeton, Princeton University Press, 241 p.

Champ, D.R., Gulens, J., Jackson, R.E., 1979, Oxidation-reduction sequences in ground water flowsystems: Canadian Journal of Earth Sciences, v. 16, p. 12-23.

Chapelle, F.H., 1993, Ground-water microbiology and geochemistry: New York, Wiley-Liss, 424 p.

Chapelle, F.H., and McMahon, P.B., 1991, Geochemistry of dissolved inorganic carbon in a Coastal Plain aquifer: Journal of Hydrology, v. 127, p. 85-108.

Chapelle, F.H., McMahon, P.B., Dubrovsky, N.M., Fujii, R.F., Oaksford, E.T., Vroblesky, D.A., 1995, Deducing the distribution of terminal electron accepting processes in hydrologically diverse groundwater systems: Water Resources Research, v. 31, p. 359-371.

Chapelle F.H., Haack, S.K., Adriaens, P., Henry, M.A., and Bradley, P.M., 1996, Comparison of Eh and H_2 measurements for delineating redox processes in a contaminated aquifer: Environmental Science and Technology, v. 30, p. 3565-3569.

Christensen, T.H., Kjeldsen, P., Albrechtsen, H.J., Heron, G., Nielsen, P.H., Bjerg, P.L., and Holm, P.E., 1994, Attenuation of landfill leachate pollutants in aquifers: Critical Reviews in Environmental Science and Technology, v. 24, p. 119-202.

Drever, J.I., 1996, The geochemistry of natural waters: Englewood Cliffs, Prentice Hall, Inc., 435 p.

Edwards, E.A., and Grbic-Galic, D., 1992, Complete mineralization of benzene by aquifer microorganisms under strictly anaerobic conditions: Applied and Environmental Microbiology, v. 58, p. 2663-2666.

Grbic-Galic, D., and Vogel, T.M., 1987, Transformation of toluene and benzene by mixed methanogenic cultures: Applied and Environmental Microbiology, v. 53, p. 254-260.

Haack , S. K. and Reynolds, L. A., 1999, Using molecular approaches to answer questions about microbial populations at contaminated sites: U.S. Geological Survey Toxics Substance Hydrology Program - - Proceedings of the technical meeting, Charleston, South Carolina, March 8-12, 1999.

Hess, K.M., Wolf, S.H., Celia, M.A., 1992, Large-scale natural gradient tracer test in sand and gravel, Cape Cod, Massachusetts 3. Hydraulic conductivity variability and calculated macrodispersivities: Water Resources Research, v. 28, no. 8, p. 2011-2027.

Hutchins, S.R., Downs, W.C., Wilson, J.T., Smith, G.B., Kovacs, D.A., Fine, D.D., Douglas, R.H., Hendrix, D.J., 1991, Effect of nitrate addition on biorestoration of fuel-

contaminated aquifer: field demonstration: Ground Water, v. 29, p.571-580.

LeBlanc, D.R., Garabedian, S.P., Hess, K.M., Gelhar, L.W., Quadri, R.D., Stollenwerk, K.G., Wood, W.W., 1991, Large-scale natural gradient tracer test in sand and gravel, Cape Cod, Massachusetts 1. Experimental design and observed tracer movement: Water Resources Research, v. 27, no. 5, p. 895-910.

Lindberg, R.D., Runnells, D.D., 1984, Ground water redox reactions: an analysis of equilibrium state applied to Eh measurements and geochemical modeling: Science, v. 255, p.925-927.

Lovely, D.R., 1991, Dissimilatory Fe (III) and Mn (IV) reduction: Microbiological Reviews, v. 55, p. 259-287.

Lovely, D.R., 1994, Microbial reduction of iron, manganese, and other metals: Advances in Agronomy, v. 54, p.175-227.

Lovely, D.R., Coates, J.D., Woodward, J.C., Phillips, E.J.P., 1995, Benzene oxidation coupled to sulfate reduction: Applied and Environmental Microbiology, v. 61, p. 953-958.

Lovely, D.R., and Goodwin, S., 1988, Hydrogen concentrations as an indicator of the predominant terminal electron accepting process in aquatic sediments: Geochimica Cosmochimica Acta, v. 52, p. 11-18.

Lovely, D.R., and Lonergan, D.J., 1990, Anaerobic oxidation of toluene, phenol, and p-cresol by the dissimilatory iron-reducing organisms, GS-15: Applied and Environmental Microbiology, v. 52, p. 1858-1864.

McGuire, J.T., Kolak, J.J., Long, D.T., Hyndman, D.W., Velbel, M.A., Klug, M.J., Haack, S.K., 1998, Biogeochemical observations of ground water redox dynamics, Geological Society of America Annual Meeting, Abstracts and Programs.

Norris, R.D., and others, 1994, Handbook of Bioremediation, U.S. EPA Robert S. Kerr Environmental Research Laboratory: Ann Arbor, Lewis Publishers.

Rabus, R.R., Nordhaus, N., Ludwig, W., and Widdel, F., 1993, Complete oxidation of toluene under strictly anoxic conditions by a new sulfate-reducing bacterium: Applied and Environmental Microbiology, v. 59, p. 1444-1451.

Reynolds, L. A., and Haack , S. K., 1999, Evaluation of RNA Hybridization to Assess Bacterial Population Dynamics at Natural Attenuation Sites: U.S. Geological Survey Toxics Substance Hydrology Program - - Proceedings of the technical meeting, Charleston, South Carolina, March 8-12, 1999.

Stumm, W. and Morgan, J.J., 1981, Aquatic Chemistry, 2nd Edition: New York, John Wiley and Sons, Inc., 780 p.

Sulfita, J.M., Horowitz, A., Shelton, D.R., Tiedje, J.M., 1982, Dehalogenation: A novel pathway for the anaerobic biodegradation of haloaromatic compounds: Science, v. 218, p. 1115-1117.

Taylor, S.W., and Jaffe, P.R., 1990, Biofilm growth and the related changes in the physical properties of a porous medium 1. Experimental investigation: Water Resources Research, v. 26, p. 2153-2159.

Vogel, T.M., 1994, Natural Bioremediation of chlorinated solvents, in Norris, R.D., and others, 1994. Handbook of Bioredmediation, U.S. EPA Robert S. Kerr Environmental Research Laboratory: Ann Arbor, Lewis Publishers.

Vroblesky, D.A., and Chapelle, F.H., 1994, Temporal and spacial changes of terminal electron accepting processes in a petroleum hydrocarbon-contaminated aquifer and the significance for contaminant biodegredation: Water Resources Research, v. 30, p. 1561-1570.

AUTHOR INFORMATION

Jennifer T. McGuire (mcguir20@pilot.msu.edu), Erik W. Smith, Jonathan J. Kolak, David T. Long, David W. Hyndman, and Michael A. Velbel, Dept. of Geological Sciences, Michigan State University, East Lansing, Michigan 48824
Sheridan K. Haack, U.S. Geological Survey, Lansing, Michigan 48911
Michael J. Klug, Kellogg Biological Station, Michigan State University, Hickory Corners, Michigan 49060
Larry J. Forney, Center for Ecological and Evolutionary Studies, University of Groningen, 30 Kerklaan, 9750 AA Haren, The Netherlands.

Natural Attenuation of Chlorinated Volatile Organic Compounds in a Freshwater Tidal Wetland, Aberdeen Proving Ground, Maryland

By Michelle M. Lorah and Lisa D. Olsen

Abstract

Field evidence collected along two ground-water flowpaths and laboratory evidence from microcosm experiments indicates that biodegradation naturally attenuates a plume of chlorinated volatile organic compounds as it discharges from an aerobic sand aquifer through anaerobic wetland sediments. A decrease in concentrations of two parent contaminants, trichloroethylene (TCE) and 1,1,2,2-tetrachloroethane (PCA), and a concomitant increase in concentrations of anaerobic daughter products occur along upward flowpaths through the wetland sediments. The daughter products *cis*-1,2-dichloroethylene (*cis*-12DCE), *trans*-1,2-dichloroethylene (*trans*-12DCE), vinyl chloride (VC), 1,1,2-trichloroethane, and 1,2-dichloroethane are produced from hydrogenolysis of TCE and from PCA degradation through hydrogenolysis and dichloroelimination pathways. Total concentrations of TCE, PCA, and their degradation products decrease to below detection levels within 0.15 to .30 m of land surface.

Microcosms constructed with wetland sediment and porewater from the site and incubated under methanogenic conditions confirmed field evidence of TCE and PCA degradation pathways and showed extremely rapid degradation rates. First-order anaerobic degradation rates for TCE and PCA ranged from 0.045 to 0.37 per day, corresponding to half-lives of 1.9 to 15 days. In aerobic microcosm experiments, biodegradation of *cis*-12DCE, *trans*-12DCE, and VC occurred only if methane consumption occurred, indicating that methanotrophs were involved. Aerobic biodegradation rates for *cis*-12DCE, *trans*-12DCE, and VC (0.05 to 0.21 per day) were within the same range as those measured for TCE and PCA under anaerobic conditions. Production of these anaerobic daughter products of TCE, therefore, could be balanced by their consumption where methanotrophs are active in the wetland sediment, such as near the land surface and near plant roots. This study indicates that natural attenuation can be a feasible ground-water remediation method where wetlands and similar organic-rich environments at ground-water/surface-water interfaces are discharge areas for plumes of chlorinated solvents.

Introduction and Background

Many hazardous-waste sites at military installations and at industrial facilities are located near surface-water bodies where wetlands are a dominant part of the landscape. U.S. Environmental Protection Agency (USEPA) data show that 75 percent of all Resource Conservation and Recovery Act (RCRA) and Comprehensive Environmental Response, Compensation, and Liability Act (CERCLA) hazardous-waste sites are within 0.5 miles of a surface-water body (Richard Willey, USEPA Region I, written commun., 1998). Ground-water contaminant plumes that are flowing toward or currently discharging to wetland areas present unique remediation problems because of the hydraulic connection between ground water and surface water, and the sensitive ecosystem in wetlands. Available engineered clean-up methods could seriously impact the viability of these ecosystems. Natural attenuation is a promising in situ remediation method that would keep the ecosystem largely undisturbed and be cost effective. The purpose of the present study was to determine whether chlorinated volatile organic compounds (VOCs) are naturally attenuated as a ground-water contaminant plume discharges through freshwater wetland sediments and whether biodegradation is a major attenuation process.

Although "natural attenuation" is a general term that includes all naturally occurring physical, chemical, and biological processes that can reduce contaminant concentrations or toxicity, biodegradation generally is considered the most important of these processes for ground-water remediation purposes because it can be a destructive process, unlike sorption, dilution, or volatilization (Wiedemeier and others, 1996). Compared to other subsurface environments, wetland sediments typically have a wide range of redox conditions and microbial populations that could lead to enhanced biodegradation of toxic organic compounds (Pardue and others, 1993). Anaerobic conditions typically are predominant in wetland sediments because oxygen diffusion is limited in waterlogged soils and because the abundance of natural organic substrates for microbial respiration causes rapid depletion of oxygen (Mitsch and Gosselink, 1986). Under anaerobic conditions, chlorinated VOCs can be biodegraded by reductive dehalogenation pathways, which entail the replacement of chlorine atoms by hydrogen to produce more reduced, less-chlorinated products (Bouwer, 1994). Biodegradation of highly chlorinated VOCs such as trichloroethylene (TCE) is known to occur under a range of anaerobic conditions, including nitrate-reducing, iron-reducing, sulfate-reducing, and methanogenic conditions; however, it is believed to be faster and more likely to result in complete dechlorination to the nontoxic end-products of ethene and ethane under methanogenic conditions than under less reducing conditions (McCarty and Semprini, 1994).

Methanotrophs, microorganisms that primarily oxidize methane for energy and growth, are one group of aerobic bacteria that have been shown through many laboratory studies to transform TCE and other chlorinated VOCs through cometabolic oxidation (see Wilson and Wilson, 1985; Little and others, 1988; Tsien and others, 1989). Although wetland sediments generally have bulk anaerobic conditions, aerobic conditions may be present in surficial sediments near the air-water interface and in subsurface sediments near plant roots. Many wetland plants transport oxygen from the atmosphere to their roots through an extensive system of internal gas spaces, creating suitable micro-environments for methanotrophs where oxygen is available from the roots and methane is available in the soil porewater (Burke and others, 1988; King, 1994). Aerobic oxidation is a desirable biodegradation pathway because no stable intermediate degradation products are formed, as in reductive dechlorination pathways (Little and others, 1988). In contrast to reductive dechlorination, where the degradation rate generally decreases as the degree of chlorination of the aliphatic hydrocarbon decreases, the less-chlorinated VOCs are more easily and rapidly degraded through aerobic oxidation reactions (Pfaender, 1990). Consequently, coupling of anaerobic and aerobic degradation processes has been suggested as the best possible bioremediation method for chlorinated VOCs such as TCE (Pfaender, 1990).

Purpose and Scope

This paper presents field and laboratory evidence of biodegradation of TCE and 1,1,2,2-tetrachloroethane (PCA), the two major parent contaminants at a wetland site along the West Branch Canal Creek at Aberdeen Proving Ground, a U.S. Army base in Maryland (fig. 1). Field evidence of the occurrence and pathways of anaerobic biodegradation is examined along two ground-water flowpaths through the wetland. Field evidence evaluated includes the distributions of redox-sensitive constituents, and of parent chlorinated VOCs and their potential daughter products. Laboratory microcosm experiments conducted using wetland sediment and ground water from the site were used to confirm field observations of anaerobic biodegradation and to provide evidence of the potential occurrence of aerobic biodegradation.

Background on Degradation Processes

Anaerobic degradation of TCE has been fairly well studied, but few studies of PCA degradation under environmental conditions have been conducted. TCE is biodegraded under anaerobic conditions through hydrogenolysis, a reductive dechlorination process that sequentially produces isomers of 1,2-dichloroethylene (12DCE), vinyl chloride (VC), and ethylene (fig. 2). Ethane also has been reported as a degradation product (Belay and Daniels, 1987; de Bruin and others, 1992). PCA also can be biodegraded by hydrogenolysis, sequentially producing 1,1,2-trichloroethane (112TCA), 1,2-dichloroethane (12DCA),

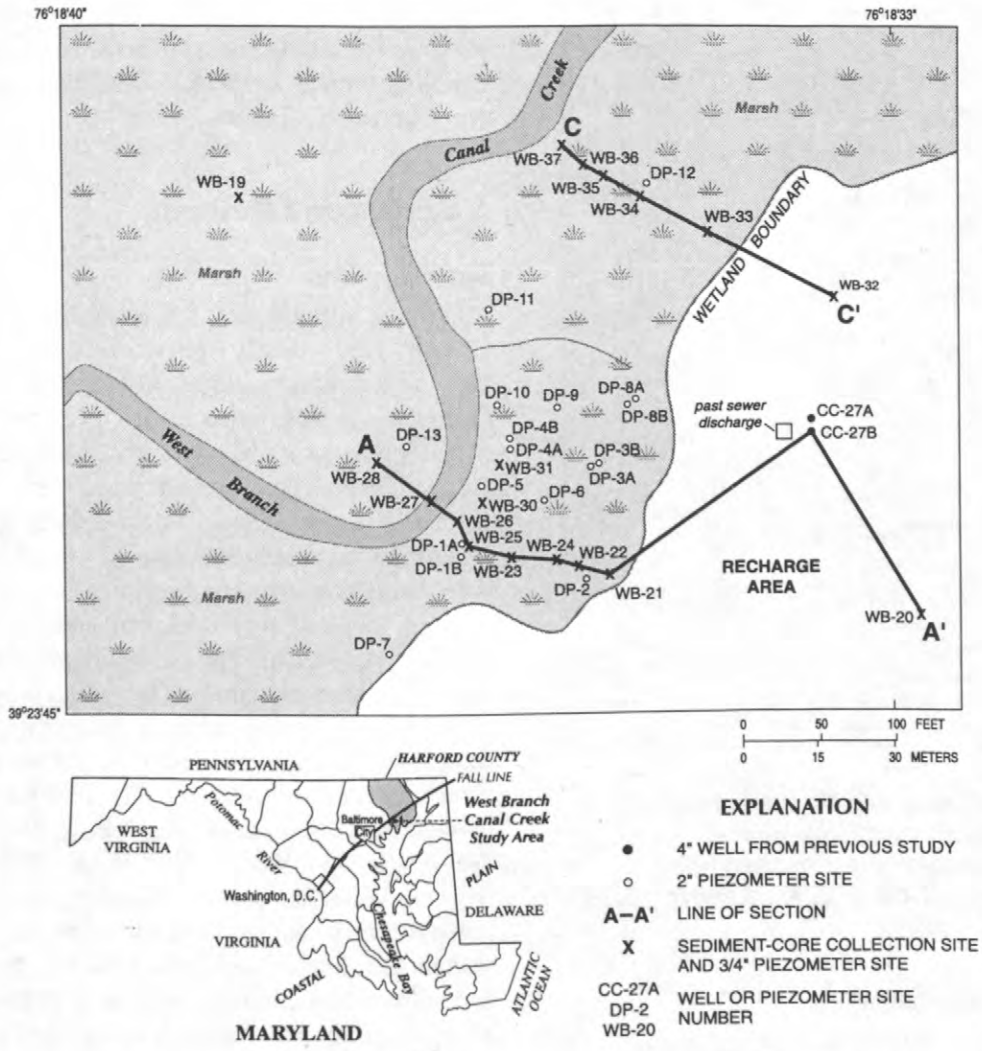

Figure 1. Sampling sites and locations of sections A-A' and C-C' in the wetland study area along the West Branch Canal Creek, Aberdeen Proving Ground, Maryland.

chloroethane, and ethane as daughter products (Vogel and others, 1987; Chen and others, 1996). Two other transformation processes are possible for PCA--dichloroelimination, which is the reductive elimination of two adjacent chlorine atoms to form an alkene, and dehydrochlorination, which is an abiotic elimination reaction (fig. 2). Dichloroelimination of PCA has been reported by transition-metal coenzymes (Schanke and Wackett, 1992) and by live cells in laboratory experiments with methanogenic municipal digester sludge (Chen and others, 1996). Dehydrochlorination of PCA to TCE was observed in cell-free extracts derived from municipal digester sludge (Chen and others, 1996).

Cometabolic aerobic biodegradation by methanotrophic bacteria occurs because methane monooxygenase, the enzyme used to catalyze the initial step of methane oxidation, has a broad substrate specificity and can fortuitously oxidize chlorinated aliphatic hydrocarbons such as TCE, VC, and 12DCE (Little and others, 1988; McCarty and Semprini, 1994). With these unsaturated chlorinated aliphatic hydrocarbons, the oxygenase adds oxygen across the double bond to form epoxides, which are chemically unstable and are transformed rapidly by abiotic hydrolysis to aldehydes and acids. Heterotrophic microorganisms can further metabolize these products to carbon dioxide, chlorine, and water (Little and others, 1988).

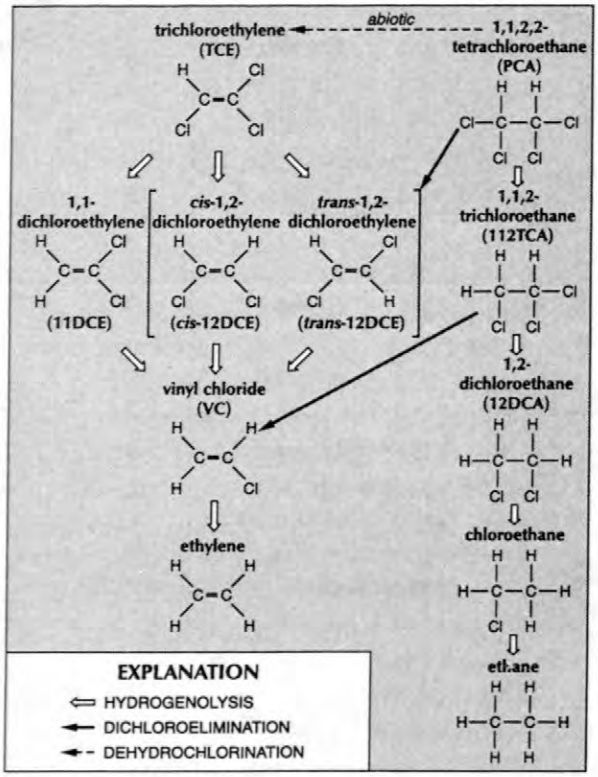

Figure 2. Possible anaerobic degradation pathways for trichloroethylene and 1,1,2,2-tetrachloroethane, (Modified from Chen and others, 1996, and Vogel and others, 1987.)

Field Site Description

Release of waste products by spills, landfilling, and discharge to sewers during past chemical manufacturing operations near the West Branch Canal Creek resulted in contamination of a shallow sand aquifer. A previous study indicated that the contaminated ground water was flowing toward the eastern side of the creek and discharging to it and the surrounding wetlands (Lorah and Clark, 1996). Nested drive-point piezometers were installed primarily along two, approximately parallel, transects about 68 m apart (fig. 1). The transects are aligned perpendicular to the creek, along the general ground-water-flow direction in the aquifer. Wetland sediments that overlie the aquifer consist of two distinct layers that have a combined thickness of about 1.8 to 3.6 m--a lower unit of silty to sandy clay or clayey sand and an upper unit of peat mixed with variable amounts of clay and silt (Lorah and others, 1997). The aquifer is recharged by rainfall infiltration upgradient of the wetland. Ground-water-flow directions within the wetland area are predominantly upward, with water from the aquifer discharging through the wetland sediments and the creek bottom sediments.

Materials and Methods

Ground-Water Sampling

Water samples were collected during June to October 1995, mainly from nested drive-point piezometers along sections A-A' and C-C' (fig. 1). Samples also were collected from selected piezometers during March-April, June, and August 1996. The piezometers are made of 0.75-in.-diameter stainless steel and contain an inner 0.50-in.-diameter Teflon-lined polyethylene tube that is connected to the top of the screened interval. Screens are 6.0 in. long and made of stainless-steel mesh with a 150-µm pore diameter. Porous-membrane sampling devices, commonly called "peepers," that collect ground water through diffusion were used to obtain water samples over 1.0-in.-depth intervals in the shallow wetland sediment at sites WB-24, WB-25, WB-26, WB-34, WB-35, WB-36, and WB-37 (fig. 1). Water samples were analyzed for VOCs, redox-sensitive constituents (dissolved oxygen, manganese, ferrous and ferric iron, sulfide, nitrate and ammonia, methane), major ions, pH, and alkalinity using procedures described in Lorah and others (1997).

Laboratory Microcosm Experiments

Ground-water and sediment samples were collected from the upper peat unit within 7 to 10 days prior to microcosm construction for the anaerobic and aerobic experiments, which occurred in May and October 1996, respectively. The microcosms prepared for the anaerobic experiments included incubations under methanogenic conditions with low and high initial (day 0) concentrations of TCE (about 3.0 and 7.5 µmol/L, respectively), incubations under sulfate-reducing conditions (10 mmol/L sulfate added) with high initial concentration of TCE (7.5 µmol/L), and incubations under methanogenic conditions with an initial PCA concentration of about 2.9 µmol/L. Sterile controls were prepared for all treatments using 1 percent formaldehyde by volume.

Anaerobic microcosms were constructed without headspace in 162-mL serum bottles using a 1.5:1 volumetric ratio of ground water to sediment. Sediment was sieved to remove particles greater than 4.75 mm. Sieving and microcosm construction were performed under a nitrogen atmosphere, and the bottles were then sealed with Teflon-lined rubber stoppers and aluminum crimp caps. Duplicate serum bottles were sacrificed at selected time intervals, and the water was analyzed for VOCs and methane (Lorah and others, 1997).

Aerobic microcosms were constructed with headspace in dark glass 130-mL bottles using 35 mL of ground water and 25 mL of wetland sediment. Some microcosms were constructed using sediment as it was collected, which included plant roots, whereas other microcosms were constructed using sediment that had been sieved to remove particles greater than 4.75 mm and all visible roots. Sieving and microcosm construction were performed under ambient air. The bottles were then sealed with caps that are designed to allow repeated withdrawals of headspace samples. Aqueous concentrations of *cis*-12DCE, *trans*-12DCE, and VC at day 0 were estimated to be 10, 10, and 9.6 µmol/L, respectively, from analysis of prepared stock solutions prior to microcosm amendment. To provide a substrate for methanotrophs, methane (99 percent pure, Scott Specialty Gases) was added to the headspace of the microcosms at initial concentrations of 1 or 3 percent by headspace volume, which is similar to the range measured in the wetland ground water (Lorah and others, 1997). In addition, dimethyl ether (DME), which is a specific inhibitor of methanotrophic activity (Oremland and Culbertson, 1992), was added to several sets of microcosms. Duplicate microcosm bottles were prepared for each experiment. Sterile controls were prepared by adding 1 percent formaldehyde by volume of water. Approximately every 3 days, oxygen gas (99.6 percent pure, Roberts Oxygen) was added to all microcosms at concentrations of 10 percent by volume in the headspace to maintain aerobic conditions. Methane was added as it was consumed. Headspace samples were withdrawn from each microcosm bottle at selected time intervals and analyzed for methane and VOCs (Lorah and others, 1997). The aqueous concentrations of VOCs were calculated using the following Henry's Law constants for *cis*-12DCE, *trans*-12DCE, and VC, respectively, at 25 °C: 0.179, 0.3814, 1.0836 (Mackay and others, 1993). Anaerobic and aerobic microcosms were stored upside down in the dark at 19 °C.

Field Evidence of Anaerobic Degradation

The parent contaminants TCE (fig. 3) and PCA (data not shown) had similar distributions along section A-A', with the highest concentrations upgradient from the eastern edge of the wetland at CC-27A and spreading downgradient predominantly in two fingers that remained shallow in the aquifer. Downward transport of the contaminants in the aquifer at site CC-27, which is near a suspected source from a past sewerline discharge point (Lorah and others, 1997), could have been partly impeded by the clayey silt layer below the screen in CC-27A. The fact that the contaminants then remain at shallow depths in the aquifer in the wetland area probably reflects the upward component of ground-water flow. Although concentrations of PCA (about 4,000 µg/L) were an order of magnitude higher than TCE (about 300 µg/L) close to the suspected source near site CC-27, their concentrations were similar downgradient in the aquifer along A-A'. Concentrations of TCE and PCA were each in the range of 100 to 300 µg/L in a thin zone that lies directly beneath the wetland sediments (fig. 3). The TCE and PCA plumes along section A-A' extend to the western side of the creek channel, which is consistent with measurements of hydraulic-head gradients that indicated a lateral component of ground-water flow in the aquifer beneath the creek and discharge to wetland sediments on the western side of the channel along this section (fig. 3).

Along section C-C', PCA was the major parent contaminant in the aquifer, occurring at a maximum concentration of about 2,000 µg/L at sites WB-32 and WB-33 at the eastern edge of the wetland (fig. 4). Unlike section A-A', where both PCA and TCE were major ground-water contaminants, TCE concentrations were much lower than PCA concentrations in the aquifer and wetland sediment along section C-C'. TCE concentrations were a maximum of 54 µg/L at site

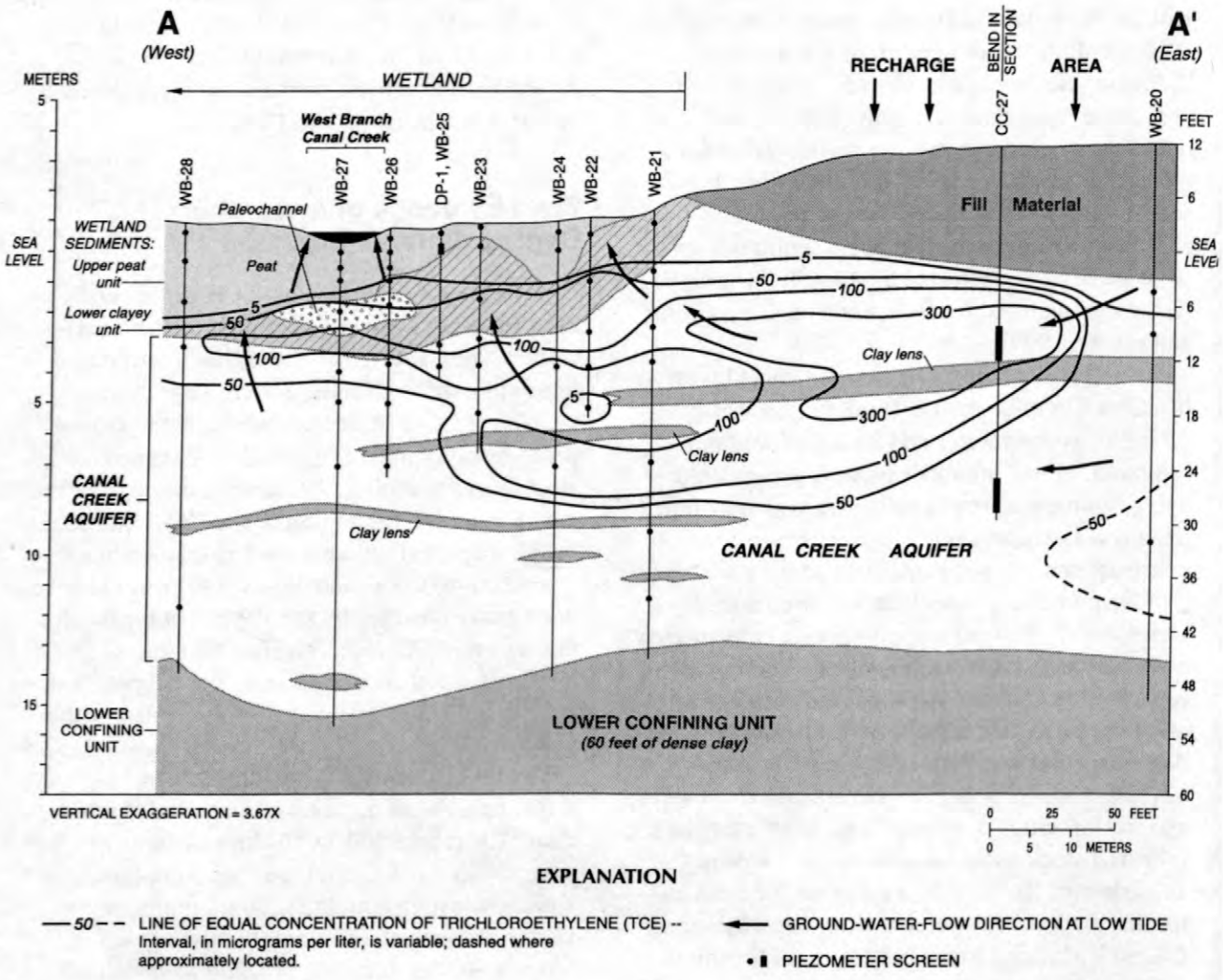

Figure 3. Concentrations of TCE in ground water along section A-A', June-October 1995. (From Lorah and others, 1997.)

WB-32 and decreased downgradient to less than about 20 µg/L at all piezometers within the wetland area (Lorah and others, 1997). As observed along section A-A', the PCA plume along section C-C' was primarily in the shallow region of the aquifer and had an upward trend into the wetland sediments (fig. 4). In contrast to section A-A', the contaminant plume along section C-C' does not appear to reach the creek channel or the western side of the creek. The PCA distribution was consistent with the head distributions, which indicated that the area around sites WB-35 and WB-36 is a focused discharge area at high tide (fig. 4) (Lorah and others, 1997).

Concentrations of TCE and PCA decreased substantially along the upward direction of flow through the overlying wetland sediments along both sections (figs. 3 and 4). Concentrations of TCE were in the range of 50 to 100 µg/L in the lower clayey unit of the wetland sediments and decreased to about 5 µg/L at the base of the upper peat unit along section A-A'. Along section C-C', the maximum PCA concentration in wetland porewater (300 µg/L) was measured in WB-35B, which is screened near the base of the upper peat unit. Even in this focused discharge area, PCA concentrations decreased greatly along the upward direction of flow in the wetland sediments. PCA concentrations were more than two orders of magnitude lower in water from piezometer WB-35A, which is screened about 0.3 m above WB-35B (fig. 4).

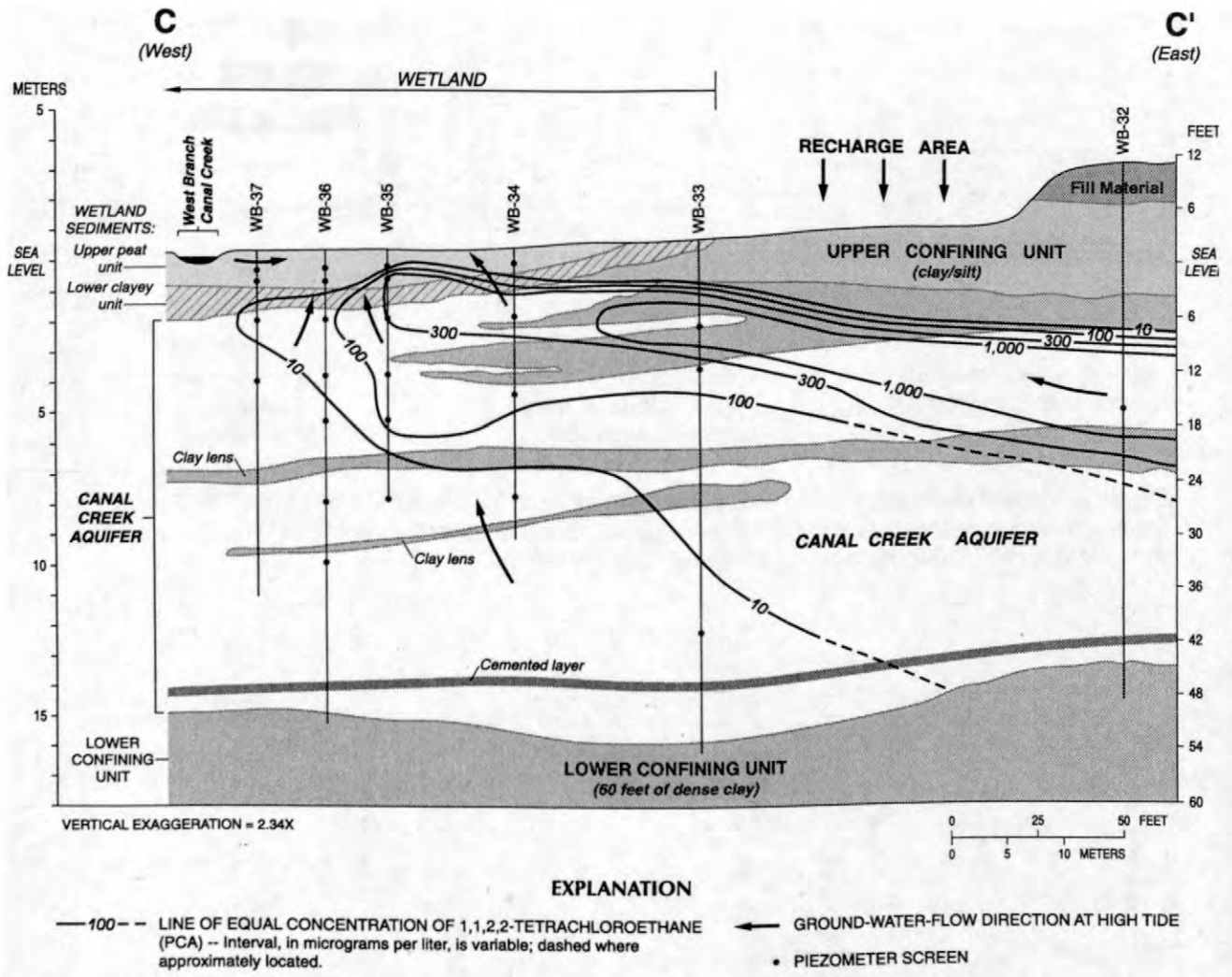

Figure 4. Concentrations of PCA in ground water along section C-C', June-October 1995. (From Lorah and others, 1997.)

Concentrations of potential anaerobic daughter products were low or undetectable in the aquifer along both sections, as would be expected under the predominantly aerobic conditions measured in the aquifer (Lorah and others, 1997). In contrast, possible anaerobic daughter products were present in relatively high concentrations in the wetland porewater, where concentrations of redox-sensitive consistuents indicated that conditions became increasingly reducing along the upward ground-water flowpath from the aquifer (figs. 5 and 6). Methanogenesis was predominant throughout the upper peat unit at site WB-26 (fig. 5) and in the top 50 cm of the upper peat unit at site WB-35 (fig. 6). The daughter products that were observed in the highest concentrations in the wetland porewater were 12DCE (total of *cis*- and *trans*-12DCE) and VC. These daughter products could be producec from TCE biodegradation by hydrogenolysis and from PCA degradation through hydrogenolysis and dichloroelimination pathways (fig. 2). The *trans* isomer always was lower than *cis*-12DCE along section A-A', commonly comprising less than 30 percent of the total 12DCE. In contrast, concentration of *trans*-12DCE were slightly higher than *cis*-12DCE over a large part of the profile obtained with the peepers at WB-35 (fig. 6) and commonly comprised 40 to 70 percent of the total 12DCE at other sites along section C-C'. Concentrations of 1,1-dichloroethylene were undetectable or low (less than 3 µg/L) along both sections. The daughter

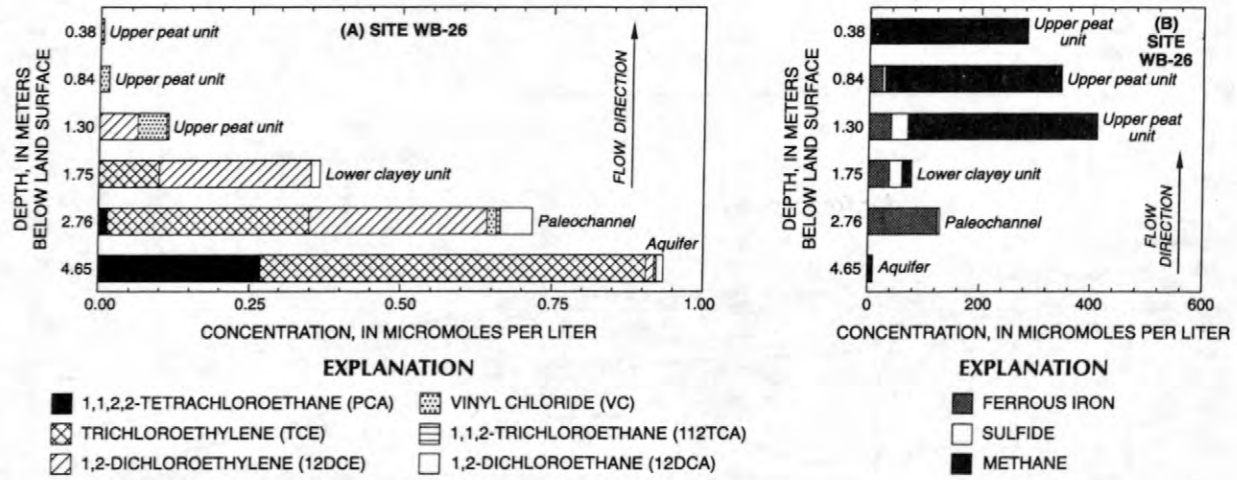

Figure 5. Vertical distribution of **(A)** the parent contaminants TCE and PCA and possible anaerobic daughter products and **(B)** selected redox-sensitive constituents at site WB-26, June-October 1995. (Modified from Lorah and others, 1997.)

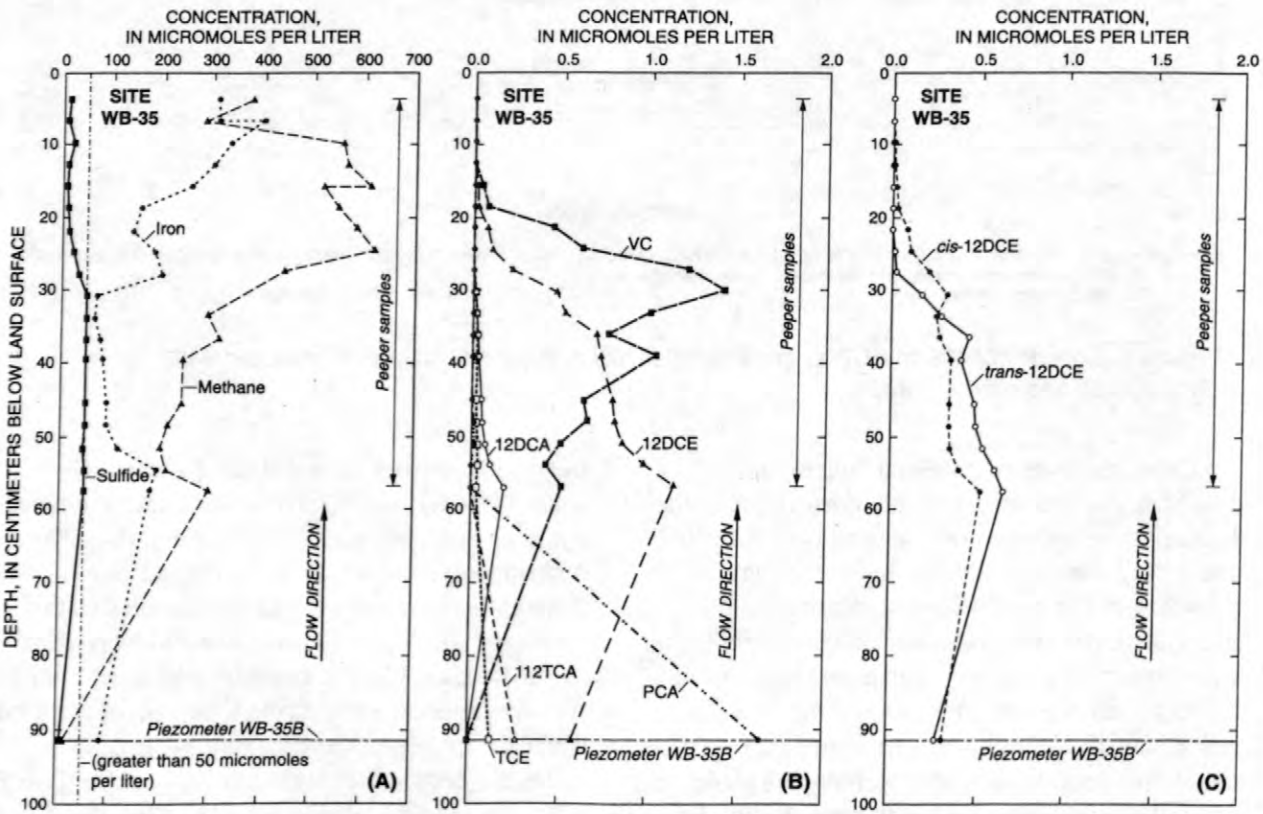

Figure 6. Vertical distributions of constituents in the upper peat unit at Site WB-35 (using data from peepers and piezometer WB-35B), June 1996. **(A)** Concentrations of selected redox-sensitive constituents (sulfide concentrations greater than 50 µmol/L were outside calibration reange); **(B)** concentrations of TCE and PCA and possible anaerobic daughter products; **(C)** concentrations of *cis*-12DCE and *trans*-12DCE.

products 112TCA and 12DCA, which can be produced by hydrogenolysis of PCA (fig. 2), also were commonly observed in the anaerobic wetland sediments but generally not in concentrations as high as those observed for 12DCE and VC. The non-chlorinated end-products of ethene and ethane were detected infrequently at trace concentrations in ground-water samples from the upper peat unit. Total concentrations of the parent and daughter compounds decreased along the upward flowpath until they were below detection within 0.15 to 0.30 m below land surface (figs. 5 and 6). Vertical profiles similar to those shown in figures 5 and 6 were observed at all contaminated sites for the two transects in the wetland.

Laboratory Evidence of Anaerobic Degradation

Rapid removal of TCE and PCA was observed in the microcosm experiments with wetland sediment and porewater under methanogenic conditions (fig. 7). TCE was below detection by day 24 in microcosms amended at day 0 with low (3.0 µmol/L) concentrations of TCE (fig. 7a) and high (7.5 µmol/L) concentrations of TCE (Lorah and others, 1997 (not shown). The live methanogenic microcosms amended with TCE at two concentration levels showed production of 12DCE and VC as the only daughter products. Production of 12DCE was observed before VC, consistent with the sequential degradation of TCE by hydrogenolysis. The *cis* isomer was the predominant form of the 12DCE, comprising more than 90 percent of the 12DCE in the

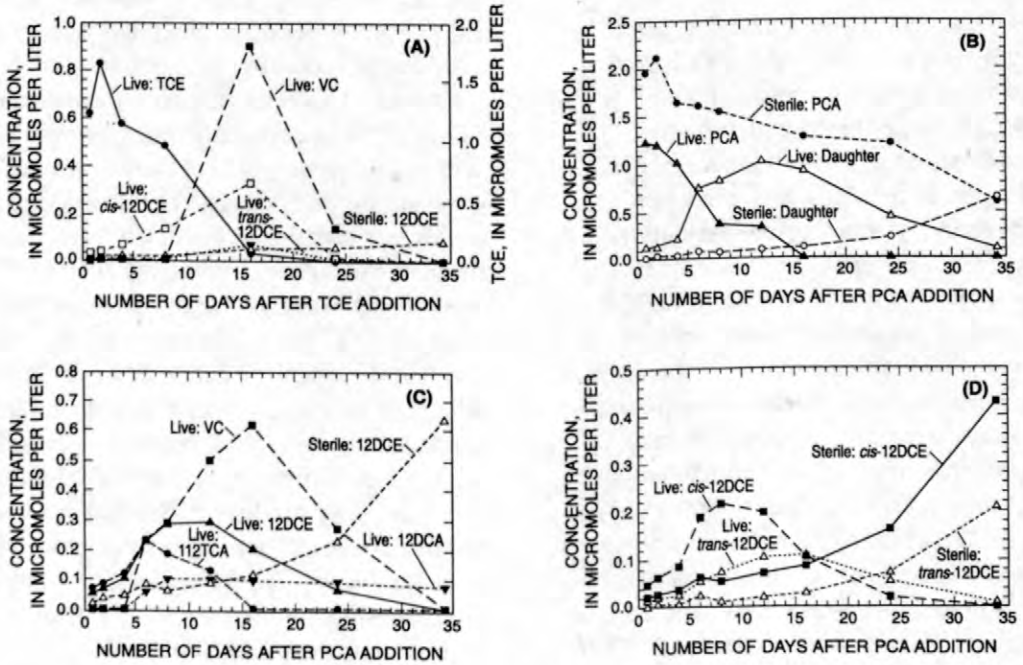

Figure 7. Degradation under methanogenic conditions in microcosms amended with 3.0 µmol/L of TCE or 2.9 µmol/L of PCA at day 0: **(A)** TCE and the daughter products *cis*-12DCE, *trans*-12DCE, and VC in the TCE-amended microcosms; **(B)** PCA and the sum of daughter products in the live and sterile PCA-amended microcosms; **(C)** daughter products 12DCE (total of the *cis* and *trans* isomers), VC, 112TCA, and 12DCA in the PCA-amended microcosms; **(D)** *cis*-12DCE and *trans*-12DCE in the PCA-amended microcosms. *(The concentrations shown are the average measured in duplicate microcosms sacrificed at each time step.)*

methanogenic microcosms. Hydrogenolysis of TCE has been shown to produce much higher proportions of the *cis* than the *trans* isomer of 12DCE in numerous field and laboratory studies (for example, Freedman and Gossett, 1989; de Bruin and others, 1992). Concentrations of the daughter products in TCE-amended microcosms decreased to below detection levels by day 34, indicating complete degradation of the VC to carbon dioxide and water (fig. 7a). Ethylene and ethane were not detected, indicating that these compounds were rapidly metabolized if they were produced. The sterile methanogenic microcosms amended with TCE had very low concentrations of 12DCE, and no detectable VC throughout the experiment (fig. 7a).

The predominant daughter products observed in the live PCA-amended microcosms under methanogenic conditions were the same as those in the TCE-amended microcosms--12DCE and VC (fig. 7b). The 12DCE is most likely produced through dichloroelimination of PCA. Although PCA potentially could abiotically degrade to TCE, which could then degrade to 12DCE by hydrogenolysis (fig. 2), TCE concentrations were insignificant (less than 0.05 µmol/L) throughout the experiment. Dichloroelimination of PCA to produce 12DCE may not have been a strictly biotic reaction because the 12DCE isomers were the only daughter products observed in the sterile microcosms (fig. 7c). The great increase in 12DCE concentrations in the sterile microcosms after day 16, however, could indicate that the formaldehyde used to prepare the sterile microcosms did not maintain effective controls. Although stable methane concentrations in the sterile microcosms throughout the experiment showed that methanogens remained inactive (Lorah and others, 1997), other microorganisms that favored the dichloroelimination pathway could have become active. Through day 16, concentrations of 12DCE in the sterile controls were less than about 50 percent of the 12DCE measured in the live microcosms.

Until day 12 in the live PCA-amended microcosms, *trans*-12DCE comprised up to 25 percent of the 12DCE (fig. 7c). In TCE-amended microcosms that were incubated under the same conditions as the PCA-amended microcosms, the *trans* isomer comprised less than 10 percent of the 12DCE (fig. 7a). Dichloroelimination of PCA, therefore, produced a greater proportion of the *trans* isomer than hydrogenolysis of TCE, indicating that the 12DCE isomer distribution could potentially assist in determining whether both TCE and PCA degradation are occurring at sites where both contaminants are present. The ratios of the 12DCE isomers changed after day 12 in the live PCA-amended microcosms as the concentrations of *cis*-12DCE began to decrease more rapidly than *trans*-12DCE (fig. 7c). This observation is consistent with another microcosm study that showed faster hydrogenolysis of *cis*-12DCE than *trans*-12DCE (Chen and others, 1996), and could account for the fact that concentrations of *trans*-12DCE were slightly higher than *cis*-12DCE over a large part of the profile obtained with the peepers (fig. 6c).

Production of 112TCA and 12DCA through hydrogenolysis of PCA also was observed in the PCA-amended microcosms (fig. 7b). Because VC, 112TCA, and 12DCA were not observed in the sterile microcosms amended with PCA, their production seems to be completely microbially mediated. The concentrations measured over time in the PCA-amended microcosms were consistent with the sequence of appearance and the relative concentrations of daughter products measured in porewater samples in the upward flow direction through the wetland sediments at site WB-35, where PCA was the primary parent contaminant (figs. 6b and 7b). Concentrations of 112TCA reached their peak and then decreased to below detection levels earlier than the other daughter products. The daughter product VC reached higher concentrations and peaked later than the other daughter products. This sequence and relative concentrations of the daughter products indicate that VC is produced by two mechanisms--dichloroelimination of the 112TCA and hydrogenolysis of the 12DCE.

First-order rate constants for degradation of TCE were 0.30 and 0.37 day^{-1} for the two TCE concentration levels incubated under methanogenic conditions, corresponding to half-lives of 1.9 to 2.3 days. The first-order rate constant for degradation of PCA was 0.25 day^{-1} under methanogenic conditions. A slower TCE degradation rate of 0.045 day^{-1} was measured under

sulfate-reducing conditions (Lorah and others, 1997). These anaerobic degradation rate constants for the wetland sediments are 2 to 3 orders of magnitude higher than those reported for anaerobic TCE biodegradation in microcosms constructed with sandy aquifer sediments (Rifai and others, 1995). For example, TCE degradation rates of 0.0001 to 0.003 day^{-1} were reported by Rifai and others (1995) for sand aquifers at Picatinny Arsenal, New Jersey, and at a Superfund site at St. Joseph, Michigan. The higher degradation rates in the wetland sediments probably result from higher organic-carbon content and microbial activity than typically found in sand aquifer sediments. The total organic carbon content of the peat unit averaged 18 percent in 15 sediment samples (Lorah and others, 1997).

Laboratory Evidence of Aerobic Degradation

Although initially it was difficult to establish aerobic conditions in the microcosms, rapid methane consumption was observed in the 12DCE- and VC-amended microcosms after 18 to 25 days (Lorah and others, 1997). The most rapid decrease in concentrations of *cis*-12DCE, *trans*-12DCE, and VC was observed after aerobic methane-oxidizing conditions were definitely established (fig. 8). Comparison to the sterile controls indicated significant microbially mediated removal of *cis*-12DCE, *trans*-12DCE, and VC in the aerobic microcosms (fig. 8a). First-order degradation rates in the live microcosms were highest for VC (0.19 to 0.21 day^{-1}) and lowest for *cis*-12DCE (0.05 to 0.07 day^{-1}). These results are consistent with another laboratory study that has shown faster degradation by mixed methane-utilizing cultures when the compounds are less halogenated (Fogel and others, 1986). A

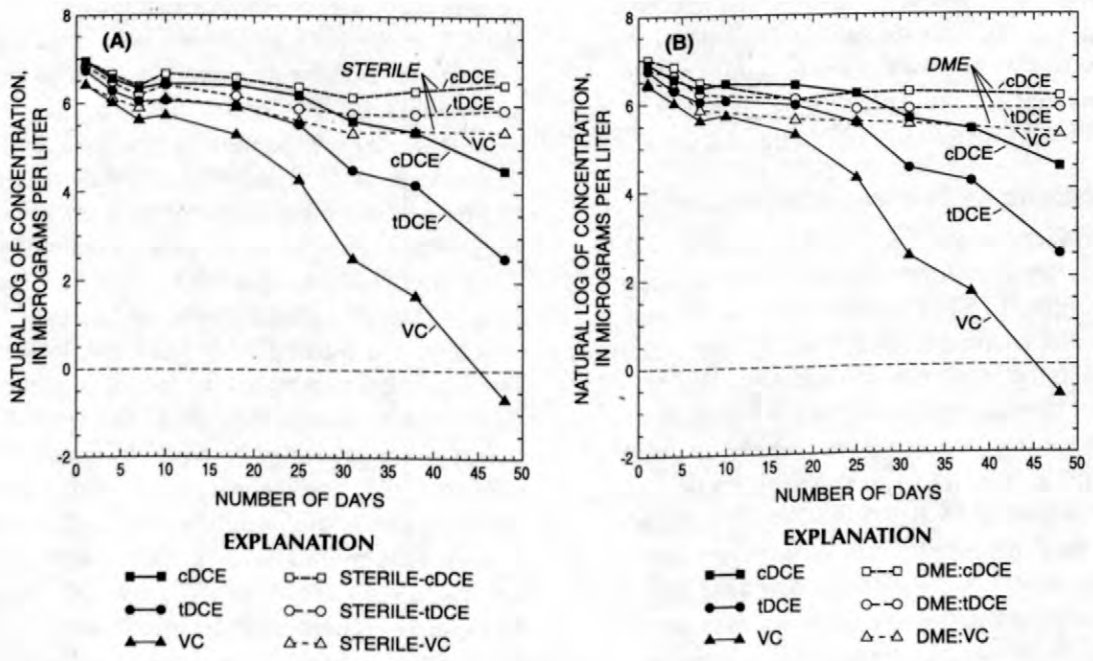

Figure 8. Aerobic microcosms amended with *cis*-12DCE, *trans*-12DCE, and VC and constructed using sieved sediment. **(A)** Concentrations of *cis*-12DCE, *trans*-12DCE, and VC in live and sterile microcosms. **(B)** Concentrations of *cis*-12DCE, *trans*-12DCE, and VC in live microcosms compared to those amended with inhibitor DME. *(Average data of duplicate microcosms are presented.)*

field experiment in which oxygen and methane were injected into an aquifer to stimulate aerobic biodegradation also indicated that degradation of VC is more rapid than degradation of 12DCE compounds, and that degradation of *trans*-12DCE is faster than degradation of *cis*-12DCE (Semprini and others, 1990). Other laboratory studies that have used pure cultures of methanotrophs, however, have not shown a direct relationship between cometabolic degradation and the degree of chlorination of a compound (Oldenhuis and others, 1989; Van Hylckama Vlieg and others, 1996).

Methane consumption was substantially lower in the DME-amended microcosms than in the live microcosms that did not contain this inhibitor, indicating that methanotrophic activity was inhibited by the DME. The removal rates of *cis*-12DCE, *trans*-12DCE, and VC in the DME-amended microcosms were the same as observed in sterile controls (figs. 3b and 4c). Aerobic degradation of these contaminants in the wetland sediment, therefore, was associated with active methane oxidation by methanotrophs. The degradation rate constants for the microcosms constructed with and without roots in the sediment were not significantly different. The extensive network of fine roots observed in sediment cores from the wetland could result in fairly uniform distribution of methanotrophs in the sediment.

Implications for Natural Attenuation

The decrease in concentrations of TCE, PCA, and their degradation products to below detection levels within 0.15 to 0.30 m below land surface in the wetland sediments (figs. 5 and 6) and within 34 days in the laboratory microcosms (fig. 7) indicates that natural attenuation is a feasible remediation method in the anaerobic wetland sediments at this site. The enhanced reductive dechlorination of TCE and PCA in the wetland compared to the aquifer sediments is associated with the natural increase in dissolved organic-carbon concentrations and decrease in redox state of the ground water in the wetland sediments (figs. 5 and 6) (Lorah and others, 1997). Because conditions in the wetland sediments are naturally conducive to biodegradation of the chlorinated VOCs in the discharging ground water, biodegradation could potentially be sustained indefinitely. In contrast, biodegradation of highly chlorinated VOCs in many aquifers is an electron-donor-limited process (Nyer and Duffin, 1997). Biodegradation commonly is localized where anaerobic conditions develop in the presence of co-contaminants, such as mono-aromatic compounds, that can act as electron donors for the microorganisms during reductive dechlorination (Major and others, 1991; Semprini and others, 1995).

The feasibility of natural attenuation as a remediation method ultimately is determined by the fate of 12DCE and VC, toxic compounds that are the predominant and most persistent of the daughter products. The laboratory microcosm experiments indicate that both anaerobic and aerobic degradation processes could be significant in degrading these daughter compounds in the wetland sediments (figs. 7 and 8). Although field evidence of aerobic degradation is difficult to obtain because of the unstable nature of the intermediate degradation products and the difficulty of obtaining mass balances, the aerobic microcosm experiments show that methanotrophs indigenous to the wetland sediments are able to degrade the 12DCE isomers and VC. The rate constants for aerobic biodegradation of *cis*-12DCE, *trans*-12DCE, and VC were within the same range as those measured for TCE and PCA under anaerobic conditions. Thus, production of these daughter compounds by anaerobic biodegradation of TCE and PCA could be balanced by their consumption where oxygen is available in the wetland sediment to support methanotrophs.

Although wetlands have been recognized for their potential to treat nutrient- and metal-contaminated water (Reddy and Gale, 1994), few studies have documented the fate of organic contaminants in wetlands. Field and laboratory observations presented here for chlorinated VOCs may be widely applicable to other wetlands where reducing conditions naturally exist and to similar organic-rich ground-water/surface-water interfaces such as bottom sediments of lakes. These environments may be important in intercepting ground water contaminated with chlorinated VOCs, and in naturally decreasing concentrations and toxicity before sensitive surface-water receptors are reached.

Acknowledgments

This project was funded by the U.S. Army Garrison Aberdeen Proving Ground (APG), Directorate of Safety, Health and the Environment, Environmental Conservation and Restoration Division (ECRD). Partial funding was obtained under SERDP (Strategic Environmental Research and Development Program). The authors thank John Wrobel of ECRD and Pete Pritchard of the Aberdeen Test Center at APG for logistical support. Henry Gardner, Thomas Shedd, and Alan Rosencrance of U.S. Army Center for Environmental Health Research, Fort Detrick, Maryland, are thanked for providing an on-site laboratory and logistical support for its operation.

References Cited

Belay, Negash, and Daniels, Lacy, 1987, Production of ethane, ethylene, and acetylene from halogenated hydrocarbons by methanogenic bacteria: Applied and Environmental Microbiology, v. 53, no. 7, p. 1604-1610.

Bouwer, E.J., 1994, Bioremediation of chlorinated solvents using alternate electron acceptors, ***in*** R.D. Norris and others, Handbook of Bioremediation: Ann Arbor, Michigan, Lewis Publishers, p. 149-175.

Burke, R. A., Jr., Barber, T.R., and Sackett, W. M., 1988, Methane flux and stable hydrogen and carbon isotope composition of sedimentary methane from the Florida Everglades: Global Biogeochemical Cycles, v. 2, no. 4, p. 329-340.

Chen, Chun, Puhakka, J.A., and Ferguson, J.F., 1996, Transformations of 1,1,2,2-tetrachloroethane under methanogenic conditions: Environmental Science and Technology, v. 30, no. 2, pp. 542-547.

de Bruin, W.P., Kotterman, M.J.J., Posthumus, M.A., Schraa, G., and Zehnder, A.J.B., 1992, Complete biological reductive transformation of tetrachloroethene to ethane: Applied and Environmental Microbiology, v. 58, no. 6, p. 1996-2000.

Fogel, M.M., Taddeo, A.R., and Fogel, Samuel, 1986, Biodegradation of chlorinated ethenes by a methane-utilizing mixed culture: Applied and Environmental Microbiology, v. 51, no. 4., p. 720-724.

Freedman, D.L., and Gossett, J.M., 1989, Biological reductive dechlorination of tetrachloroethylene and trichloroethylene to ethylene under methanogenic conditions: Applied and Environmental Microbiology, v. 55, no. 9, p. 2144-2151.

King, G. M., 1994, Associations of methanotrophs with the roots and rhizomes of aquatic vegetation: Applied and Environmental Microbiology, v. 60, no. 9, p. 3220-3227.

Little, C.D., Palumbo, A.V., Herbes, S.E., Lidstrom, M.E., Tyndall, R.L., and Gilmer, P.J., 1988, Trichloroethylene biodegradation by a methane-oxidizing bacterium: Applied and Environmental Microbiology, v. 54, no. 4, p. 951-956.

Lorah, M.M., and Clark, J.S., 1996, Contamination of ground water, surface water, and soil, and evaluation of selected ground-water pumping alternatives in the Canal Creek area of Aberdeen Proving Ground, Maryland: U.S. Geological Survey Open-File Report 95-282, 318 p.

Lorah, M.M., Olsen, L.D., Smith, B.L., Johnson, M.A., and Fleck, W.B., 1997, Natural attenuation of chlorinated volatile organic compounds in a freshwater tidal wetland, Aberdeen Proving Ground, Maryland: U.S. Geological Survey Water-Resources Investigations Report 97-4171, 95 p.

Mackay, Donald, Shiu, W.Y., and Ma, K.C., 1993, Illustrated handbook of physical-chemical properties and environmental fate for organic chemicals, volume III: Ann Arbor, Michigan, Lewis Publishers, 916 p.

Major, D.W., Hodgins, E.W., and Butler, B.J., 1991, Field and laboratory evidence of in situ biotransformation of tetrachlorethene to ethene and ethane at a chemical transfer facility in North Toronto, ***in*** On-Site Bioreclamation Processes for Xenobiotic and Hydrocarbon Treatment, R.E. Hinchee and R.D. Wolfenbuttel (eds.): Butterwort, Stonechat, Mass., p. 113-133.

McCarty, P.L., and Semprini, L., 1994, Ground-water treatment for chlorinated solvents, ***in*** R.D. Norris and others, Handbook of Bioremediation: Ann Arbor, Michigan, Lewis Publishers, p. 87-116.

Mitsch, W.J., and Gosselink, J.G., 1986, Wetlands: New York, Van Nostrand Reinhold, 537 p.

Nyer, E.K., and Duffin, M.E., 1997, The state of the art of bioremediation: Ground Water Monitoring and Remediation, v. 17, no. 2, p. 64-69.

Oldenhuis, Roelof, Vink, R.L.J.M., Janssen, D.B., and Witholt, Bernard, 1989, Degradation of chlorinated aliphatic hydrocarbons by Methylosinus trichosporium OB3b expressing soluble methane monooxygenase: Applied and Environmental Microbiology, v. 55, no. 11, p. 2819-2826.

Oremland, R.S., and Culbertson, C.W., 1992, Importance of methane-oxidizing bacteria in the methane budget as revealed by the use of a specific inhibitor: Nature, v. 356, p. 421-423.

Pardue, J.H., Masscheleyn, P.H., DeLaune, R.D., Patrick, W.H., Jr., and Adrian, D.D., 1993, Assimilation of hydrophobic chlorinated organics in freshwater wetlands: Sorption and sediment-water exchange: Environmental Science and Technology, v. 27, no. 5, p. 875-882.

Pfaender, F.K., 1990, Biological transformations of volatile organic compounds in groundwater, ***in*** N.M. Ram, R.F. Christman, and K.P. Cantor, (eds.), Significance and treatment of volatile organic compounds in water supplies: Chelsea, Michigan, Lewis Publishers, p. 205-226.

Reddy, K.R., and P.M. Gale, 1994, Wetland processes and water quality: A symposium overview: Journal of Environmental Quality, v. 23, p. 875-877.

Rifai, H.S., Borden, R.C., Wilson, J.T., and Ward, C.H., 1995, Intrinsic bioattenuation for subsurface restoration, ***in*** R.E. Hinchee and others (eds.), Intrinsic bioremediation: Columbus, Ohio, Battelle Press, p. 1-29.

Schanke, C.A., and Wackett, L.P., 1992, Environmental reductive elimination reactions of polychlorinated ethanes mimicked by transition-metal coenzymes: Environmental Science and Technology, v. 26, no. 4, p. 830-833.

Semprini, Lewis, Roberts, P.V., Hopkins, G.D., and McCarty, P.L., 1990, A field evaluation of in-situ biodegradation of chlorinated ethenes. *Part 2.* Results of biostimulation and biotransformation experiments: Ground Water, v. 28, no. 5, p. 715-727.

Semprini, L., Kitanidis, P.K., Kampbell, D.H., and Wilson, J.T., 1995, Anaerobic transformation of chlorinated aliphatic hydrocarbons in a sand aquifer based on spatial chemical distributions: Water Resources Research, v. 31, no. 4, p. 1051-1062.

Vogel, T.M., 1994, Natural bioremediation of chlorinated solvents, ***in*** R.D. Norris and others, Handbook of Bioremediation: Ann Arbor, Michigan, Lewis Publishers, p. 201-225.

Tsien, Hsien-Chyang, Brusseau, G.A., Hanson, R.S., and Wackett, L.P., 1989, Biodegradation of trichloroethylene by Methylosinus trichosporium OB3b: Applied and Environmental Microbiology, v. 55, no. 12, p. 3155-3161.

Van Hylckama Vlieg, J.E.T., de Koning, Wim, and Janssen, D.B., 1996, Transformation kinetics of chlorinated ethenes by Methylosinus trichosporium OB3b and detection of unstable epoxides by on-line gas chromatography: Applied and Environmental Microbiology, v. 62, no. 9, p. 3304-3312.

Vogel, T. M., Criddle, C.S., and McCarty, P.L., 1987, Transformations of halogenated aliphatic compounds: Environmental Science and Technology, v. 21, no. 8, p. 722-736.

Wiedemeier, T.H., Swanson, M.A., Moutoux, D.E., Gordon, E.K., Wilson, J.T., Wilson, B.H., Kampbell, D.H., Hansen, J.E., Haas, P., and Chapelle, F.H., 1996, Technical protocol for evaluating natural attenuation of chlorinated solvents in ground water: Draft prepared for U.S. Air Force Center for Environmental Excellence, Brooks Air Force Base, San Antonio, Texas. [variously paged].

Wilson, J.T., and Wilson, B.H., 1985, Biotransformation of trichloroethylene in soil: Applied and Environmental Microbiology, v. 49, no. 1, p. 242-243.

Research in Characterizing Fractured Rock Aquifers

Other than the multibillion-dollar investigations associated with high-level radioactive-waste isolation (which are not particularly relevant to issues of near-surface anthropogenic contamination), there has been a lack of detailed field investigations in fractured rock aquifers. Addressing issues of contamination in fractured rock also has been hindered by the fact that methods of site characterization applied in unconsolidated near-surface deposits are not necessarily applicable to highly heterogeneous bedrock environments. In fractured rock, geologic structure controls the occurrence of fractures, which are the predominant mechanism for fluid movement. No formation is uniformly fractured, and thus, assumptions of formation homogeneity and even anisotropy that are commonly applied in unconsolidated porous media may not be appropriate for the description of fluid movement in fractured rock. Hydraulic conductivity of fractures can vary over many orders of magnitude in contrast to the range associated with unconsolidated geologic media. Furthermore, because of complex geologic structures and fracture connectivity, hydraulic properties of fractured rock do not vary smoothly in space. It is not uncommon to observe abrupt spatial changes in the hydraulic properties in fractured rock with both depth and areal extent.

In 1990, the Toxic Substances Hydrology Program initiated research activities in the bedrock of the Mirror Lake watershed and its vicinity in central New Hampshire (figure 1). The Mirror Lake watershed falls nearly entirely within the Hubbard Brook Experimental Forest, which is a site for long-term ecosystem studies administered by the Forest Service (U.S. Department of Agriculture). The site is characterized by fractured metamorphic and igneous rocks overlain by a thin veneer of glacial drift. Although the site is uncontaminated, research has focused on developing and testing field techniques and interpretive methods of characterizing the properties of bedrock that affect ground-water flow and chemical migration. The intention is to transfer these techniques to other bedrock terrain and sites of contamination. The basic premise of the investigations at the Mirror Lake site has been that a knowledge of fluid movement and nonreactive transport must be a precursor to the characterization of the more vexing issues associated with the fate of toxic substances in heterogeneous subsurface environments.

Because of the extreme heterogeneity in fractured rock, there is no single method that can map explicitly and unambiguously the spatial distribution of hydraulic properties that control fluid movement and chemical migration. Investigations at the Mirror Lake site have focused on integrating interpretations from geologic and fracture mapping, surface and borehole geophysics, hydrologic testing and geochemical and isotopic methods. Although the individual characterization methods developed and tested at the Mirror Lake site can stand alone, the synthesis of information from multiple characterization methods is the only means of developing a defensible conceptual understanding of heterogeneity in bedrock terrain.

In addition, an infrastructure has been developed at the Mirror Lake site to investigate ground-water flow and chemical migration over distances from meters to kilometers. Two well clusters referred to as the FSE and CO well fields have been constructed for detailed investigations in bedrock over distances up to 100 meters (figure 1). In addition, bedrock wells and overburden piezometers have been installed over a 4 square kilometer area for investigating regional ground-water flow and chemical migration. Characterization over distances of kilometers is also important in many problems of environmental assessment, because fractures usually have low porosity, and thus have the potential to transport fluid and constituents over large distances in a short time. Because of the detailed multidisciplinary investigations

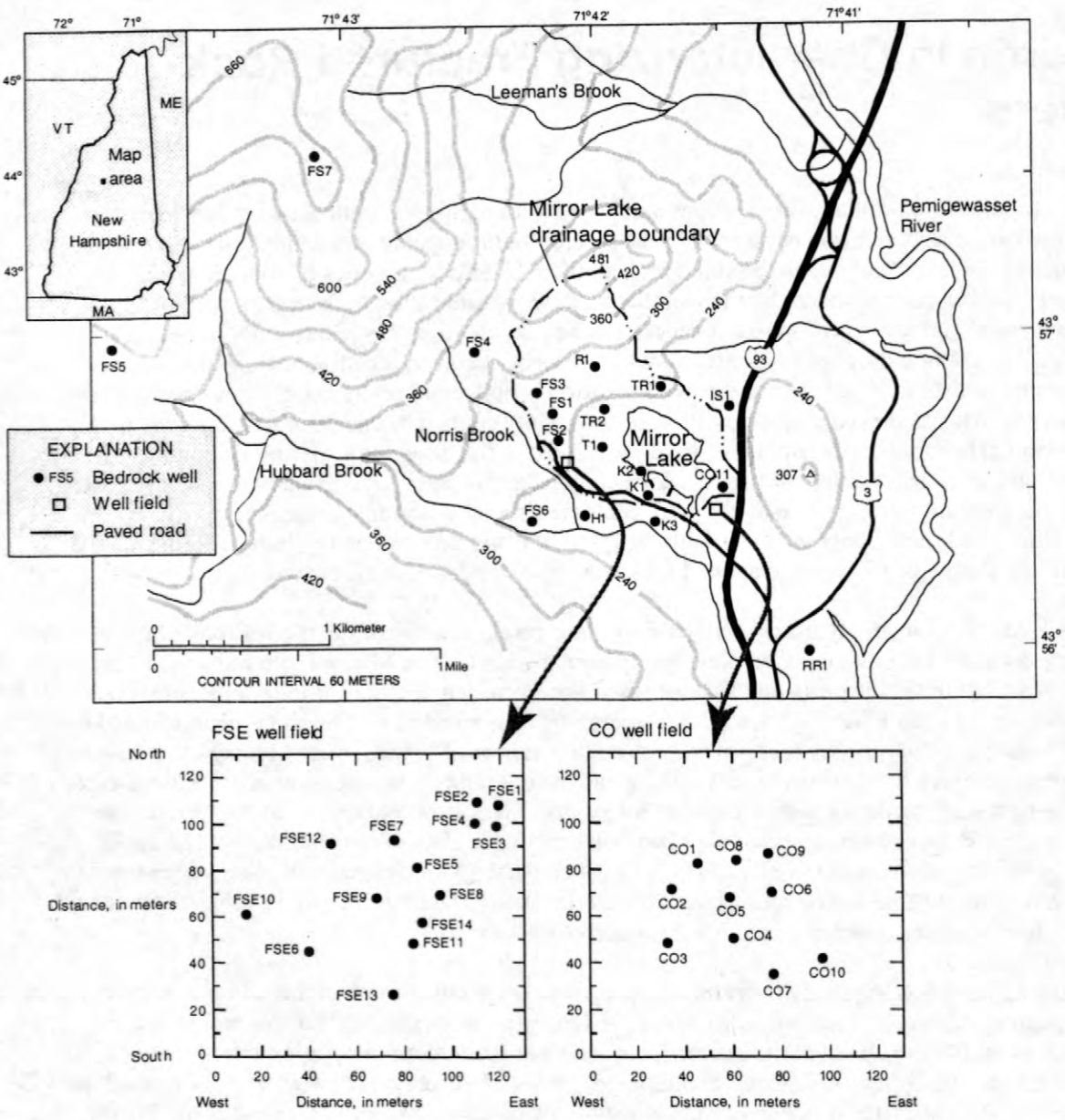

Figure 1. Location of Mirror Lake, New Hampshire research site and well network.

conducted to identify geologic features, fractures and hydraulic and transport properties of the bedrock over distances from meters to kilometers, the data and infrastructure of the Mirror Lake site make it a field-research laboratory that can be used to test new site-characterization tools, field techniques, and interpretive approaches to conceptualizing heterogeneity in fractured rock.

For additional information contact:

Allen M. Shapiro, USGS, Reston, Virginia (email: ashapiro@usgs.gov)

Integrating Multidisciplinary Investigations in the Characterization of Fractured Rock

By Allen M. Shapiro, Paul A. Hsieh, F. Peter Haeni

ABSTRACT

Because site conditions and project objectives vary from site to site, there is no single approach to the characterization of fractured rock for problems of environmental assessment. There is, however, a unifying theme that is consistent in problems of site characterization; that is, most problems depend to a great extent on advective ground-water movement. Once the spatially heterogeneous hydraulic properties of the bedrock are conceptualized to define advective ground-water flow in the detail consistent with project objectives, other physical, chemical, and biological processes of interest can then be the focal point of characterization. Without first characterizing advective ground-water movement, it is likely that ambiguous and perhaps erroneous interpretations of complex physical, chemical, and biological processes will result. Because of the extreme heterogeneity that is anticipated in fractured rock, no single method of characterization can explicitly and unambiguously map the spatial distribution of hydraulic properties that control advective fluid movement. The integration of geologic, geophysical, hydrologic and geochemical information is a necessity in developing a defensible model of heterogeneity in fractured rock. A multiple-method hierarchical approach to characterization in fractured rock is presented, where in regional geologic and hydrologic information is first synthesized to act as a background to more detailed site-specific reconnaissance using fracture network mapping and surface geophysics. These noninvasive reconnaissance techniques can be used to observe or infer the location and orientation of fractures and fracture zones and fracture properties that are critical in siting bedrock boreholes in which to conduct *in situ* investigations using single- and multiple-borehole techniques. Single-hole techniques that can be used to characterize heterogeneity in the bedrock include conventional geophysical logging, borehole scanning, borehole flow, borehole radar, hydraulic testing, and chemical sampling. Multiple-borehole methods, such as seismic and radar tomography, borehole flow, hydraulic and tracer testing, are conducted to infer the connectivity and spatial extent of transmissive fractures. Although the characterization methods summarized in this article can be conducted independently, the synthesis of information from multiple characterization methods is the only means of developing an accurate understanding of heterogeneity in bedrock.

INTRODUCTION

The degree of hydrogeologic characterization that is warranted for a given investigation depends to a large extent on the project objectives, the physical dimensions of the problem, time and monetary constraints, and the level of risk that can be tolerated. Thus, it is impossible to postulate a single approach to hydrogeologic characterization that can be applied in all situations. Nevertheless, a common theme is fundamental to the demands of hydrogeologic characterization for a wide range of problems related to the quantity and quality of ground-water resources; that is, most problems depend to a great extent on the advective movement of ground water. In some instances, it may be sufficient to identify only the gross quantity of ground water moving through a large volume of a formation, while in other instances it may be necessary to identify explicitly the spatial distribution of the fluid velocity as dictated by zones of high- and low-hydraulic conductivity. Once advective ground-water movement has been characterized in

the detail consistent with project objectives, other physical, chemical, and biological processes of interest can then be the focal point of characterization.

This article describes field characterization methods used to conceptualize heterogeneity in fractured rock terrain. Characterizing heterogeneity in fractured rock is particularly challenging. In most instances, geologic structure controls the occurrence of fractures, which are the predominant pathways for fluid movement. No formation is uniformly fractured, and thus, assumptions of formation homogeneity and even anisotropy may not be appropriate to meet project objectives in characterizing fluid movement. Furthermore, the transmissivity of fractures usually ranges over many orders of magnitude (Shapiro and Hsieh, 1998) and, because of the complexity of geologic structure and fracture connectivity, hydraulic properties of fractured rock do not vary smoothly in space. It is not uncommon to observe abrupt spatial changes in the hydraulic properties of fractures with both depth and areal extent (Hsieh and Shapiro, 1996; Shapiro and Hsieh, 1998).

Because of the extreme heterogeneity that is anticipated in fractured rock, no single characterization method can explicitly and unambiguously map the spatial distribution of hydraulic properties that control advective fluid movement. Although the characterization methods summarized in this article can stand alone, the synthesis of information from multiple characterization methods is the only means of developing a defensible conceptual understanding of heterogeneity in bedrock. The characterization methods discussed in this article are presented in a hierarchical fashion, working from large-scale, noninvasive reconnaissance techniques to methods that require access to multiple bedrock boreholes. In general, not all of the methods need to be applied at a given site. The choice of methods will depend on site conditions, as well as project objectives, the dimensions of the physical problem, time and monetary constraints, and the level of risk that can be tolerated. To narrow the scope of this article, the methods presented here focus on the characterization of fractured rock over areas of up to several hectares. Characterization of fluid movement over distances of kilometers is also important in many engineering problems; however, it is beyond the scope of this article.

The characterization methods summarized in this article are not intended as an exhaustive survey, nor is the discussion of the various methods intended to be detailed. The purpose of this article is to highlight the informational gains from the various characterization techniques, and the uncertainty that arises in characterizing formations having extreme variations in hydraulic properties without the integration of interdisciplinary investigations. Most of the information presented in this article is derived from investigations of fluid movement and chemical migration conducted under the U.S. Geological Survey (USGS) Toxic Substances Hydrology and National Research Programs at the fractured-rock field-research site in the Mirror Lake watershed and its vicinity in central New Hampshire. The investigations at the Mirror Lake site, conducted since 1990, are intended to test and develop field and interpretive methods of characterizing ground-water flow and chemical migration in fractured rock over distances from meters to kilometers, with the intention of transferring results to other geologic terrain, including contaminated fractured rock sites (Shapiro and Hsieh, 1991, 1996; Shapiro and others, 1995). Investigations at the Mirror Lake site have emphasized the integration of geologic, hydrologic, geophysical, and geochemical methods to characterize and simulate ground-water flow and chemical transport.

REGIONAL RECONNAISSANCE METHODS

Although the focus of this article is hydrogeologic characterization of bedrock over areas of up to several hectares, it is always necessary to place the local-scale hydrology and geology into the larger framework of the regional hydrologic stresses and geologic controls. Characterizing the regional geology and geologic structures through field mapping and the use of

remotely sensed data in photolineament analyses is intended to provide information on geologic features that may either be zones of enhanced ground-water movement or barriers to flow (Lattman and Parizek, 1964; Siddiqui and Parizek, 1971; Clark and others, 1996). In general, supporting information, in the form of hydraulic tests or ground-water elevations, is needed to confirm whether geologic structures and fracture traces are actually conduits or barriers. In addition, it is necessary to understand the regional hydrology as it is affected by physiography and natural and anthropogenic sources and sinks of ground water. Such information provides insight into the quantity and direction of ground water moving through the area of interest. In geologically complex areas where there are several distinct bedrock aquifers or overlying unconsolidated geologic deposits, ground-water modeling may be needed to assess the quantity and direction of ground-water flow (see, for example, Tiedeman and others, 1997, 1998).

LOCAL-SCALE RECONNAISSANCE METHODS

Local reconnaissance methods are conducted over distances ranging from tens to hundreds of meters, which is consistent with the dimensions of a problem area covering several hectares. Fracture network mapping on bedrock exposures and surface geophysics provide details of bedrock lithology, rock properties, and fracture location and orientation that are not provided from regional reconnaissance. Hydrologic data collection, in the form of ground-water elevations and sources and sinks of ground water, may also be available in the problem area. This information can be used to substantiate hypotheses formulated from regional reconnaissance. Although it is advantageous to conduct the local reconnaissance at the site under investigation, site conditions may not be suitable for local reconnaissance methods, which are generally noninvasive and may be hampered by surficial material overlying the bedrock. Areas of similar geology and fracture properties may need to be used and the information extrapolated to the site under consideration. If the local-scale reconnaissance can be conducted at the site under consideration, information pertinent to the siting of bedrock boreholes for invasive investigations may be obtained.

Fracture Mapping

Mapping fractures on bedrock exposures such as outcrops and highway roadcuts can quantify interconnectedness, trace-length distribution, and spatial distribution of fractures, as well as fracture characteristics such as orientation, roughness, mineralization, and aperture (Barton and Hsieh, 1989; Barton, 1996). In complex geologic terrain containing multiple rock types, the mapping of rock types in conjunction with mapping fracture networks provides insight into the potential role that lithology may play in ground-water flow. Such hypotheses, however, need to be verified with *in situ* observations of rock type, fracturing, and hydraulic properties. Furthermore, fracture mapping is only a two-dimensional sample of a three-dimensional fracture network, and fractures mapped on surface exposures may not be consistent with fractures mapped at depth. Conseqently, it is necessary confirm results of fracture mapping with *in situ* observations of fractures characteristics and oreintation from bedrock boreholes.

Surface Geophysics

Surface geophysical methods are used to infer the location and orientation of individual fractures zones or bulk rock properties affected by the presence of multiple fractures (Lewis and Haeni, 1987). Besides identifying fracture zones, surface geophysical methods can also be used to detect buried objects, contaminated ground water, the depth to the water table, and the depth to bedrock surface, all of which may be important in hydrogeologic characterization. Surface geophysics also provides a means of extrapolating fractures and fracture zones from locations where they are physically observed, such as bedrock exposures, to areas overlain by surficial material.

Multiple surface geophysical methods are available for inferring rock properties, anisotropy

in rock properties and the location and orientation of fracture zones by measuring the formation response to applied acoustic, electric, or electromagnetic (EM) perturbations (Lewis and Haeni, 1987). Spatial changes in the bedrock lithology and cultural interferences may yield responses for a particular geophysical method that may be falsely interpreted as fracture zones. Also, specific geophysical methods may fail to detect fracture zones having given properties or orientations. Consequently, it is recommended that the interpretation of a suite of surface geophysical methods be used to infer fracture location and orientation and rock properties (Haeni and others, 1996). In addition, correlation with other reconnaissance techniques, as well as borehole information, should be used to further strengthen the interpretation of fracture zones and bedrock properties (Haeni and others, 1996). Also, fracture zones inferred from surface geophysical methods are not necessarily transmissive. Correlation with ambient water-table elevations and with techniques that infer hydraulic properties of fractures through borehole methods are needed to provide evidence of transmissive zones.

SINGLE-BOREHOLE METHODS

Bedrock boreholes provide locations for observing or inferring bedrock lithology, fractures, and hydraulic properties of fractures. But, boreholes act as unnatural high-permeability pathways that disturb the ambient hydrochemical conditions in the bedrock. If maintaining the ambient hydrochemical conditions is crucial, as in cases of subsurface contamination, borehole packers should be installed to eliminate hydraulic communication of fractures connected by the borehole during periods when testing is not being conducted.

Collecting core in bedrock is expensive, but bedrock core is valuable in situations where properties of the rock matrix are of interest. If the core is oriented, it also can provide information on fracture orientation. In general, however, core samples provide an extremely small sample of the fractures, and core recovery may be poor in the vicinity of highly weathered fractures. Hence, fractures properties are usually poorly determined from core samples. *In situ* single-borehole methods can be used to infer rock properties, fractures, and hydraulic properties of fractures at a substantial cost savings over using core alone, and a variety of borehole scanning methods provide images from which a virtual core can be constructed along with identifying fracture orientation, borehole conditions, and lithology. Thus, core can be collected judiciously to address specific project objectives rather than as a technique of characterization.

Conventional geophysical logging, borehole scanning, and borehole radar are used to observe or infer rock properties and fractures in the vicinity of a borehole. The fractures that are detected or inferred with these methods, however, may not be transmissive and should be confirmed using hydraulic methods that test the capacity of individual fractures or fracture zones to transmit water. Also, the appearance of fractures at the borehole may not be indicative of their overall orientation in the rock or their hydraulic properties, and fractures intersecting the borehole may not be hydraulically connected to a network of fractures that transmit water. Therefore, it is necessary to correlate such information with other single- and multiple-borehole methods that identify transmissive fractures.

Conventional Geophysical Logging

Conventional geophysical logging with electrical, electromagnetic, nuclear, and acoustic sensors are used to infer changes in rock properties and may also indicate the presence of fractures; variability in rock properties, however, may yield similar anomalies (Keys, 1990; Paillet, 1993; Williams and Lane, 1998). Conventional geophysical logging also routinely includes surveys to characterize physical properties of boreholes, such as borehole diameter and borehole deviation, as well as sensors to monitor fluid temperature and resistivity. These logs also can be used to infer fracture locations, but they are not direct observations and would need to be verified using other borehole characterization methods.

Borehole Scanning

The acoustic televiewer and borehole cameras visualize the interior of boreholes and identify the location and orientation of fractures (Zemanek and others, 1970; Paillet and Kapucu, 1989; Johnson, 1998; Johnson and Dunstan, 1998). Analog and digital borehole cameras can also identify rock type, changes in borehole diameter, chemical precipitation, suspended particulate material, bacterial growth, and certain types of contamination (Johnson, 1998). The information from digital borehole camera can also be used to construct a virtual borehole core which can be viewed from any orientation. Optical tools can not be applied, however, in boreholes with turbid water, and the acoustic televiewer can be used only in fluid-filled boreholes.

Borehole Radar

Single-hole borehole radar uses the reflections from high-frequency EM waves to infer the location and orientation of dipping fractures in the vicinity of bedrock boreholes, including fractures that may not intersect the borehole (Olsson and others, 1992; Lane and others, 1994; Haeni and Lane, 1996). Large aperture water-filled fractures yield enhanced reflections in comparison to tight fractures. Thus, borehole radar may indicate fractures that are significant in transmitting water. The distance at which fractures can be detected from the borehole depends on the electrical conductivity of the rock. In shale, the penetration of EM waves may be approximately a meter, while in electrically resistive rocks, such as granite, the penetration may be tens of meters. Spatial variations in the electrical properties of the rock may also yield reflections of geologic structures that are not necessarily transmissive fractures and would need to be verified through other characterization approaches.

Borehole Flow

Sensitive borehole flowmeters can detect vertical flow in the borehole under ambient and hydraulically stressed conditions (Hess, 1986; Molz and Young, 1993). Under ambient conditions, vertical flow indicates borehole locations of inflow and outflow that arise due to differences in the hydraulic head of fractures intersecting the borehole. Under hydraulically stressed conditions, borehole flow measurements show step increases associated with the contributions of specific fractures (Paillet, 1998). Using borehole scanning methods, individual fractures responsible for borehole flow can be identified. From measurements of borehole flow under stressed conditions, the transmissivity of the contributing fractures can be estimated if simplified models of flow geometry are assumed (Paillet, 1998).The resolution of the flowmeter, however, usually constrains estimates of fracture transmissivity to only the upper one or two orders of magnitude of fracture transmissivity in the borehole.

Hydraulic Testing

Single-hole hydraulic tests are conducted by inducing a perturbation and measuring the hydraulic response in the same borehole. Fractures with the highest transmissivity can usually be tested by pumping; however, the lower permeability fractures require fluid injection. This approach can identify hydraulic properties over many orders of magnitude (Hsieh and others, 1993; Shapiro and Hsieh, 1998). Single-hole hydraulic tests conducted in an open borehole are used to infer the hydraulic properties of the formation intersected by the open hole. The hydraulic properties of individual fractures intersecting the borehole, or groups of fractures, can be inferred from single-hole hydraulic tests that are conducted over discrete intervals of the borehole isolated by borehole packers (Hsieh and others, 1993; Shapiro and Hsieh, 1998).

Inferring hydraulic properties requires identifying an appropriate model of fluid flow and then estimating the parameters of that model to reproduce the measured data (National Research Council, 1996). Fluid pressure responses, however, are relatively insensitive to heterogeneity at larger distances from the well being tested. Consequently, the assumption of homogeneous hydraulic properties usually accompanies the interpretation of single-hole

tests. Although it is recognized that fractured rock is heterogeneous, the homogeneous hydraulic property estimated from a single-hole test should be viewed as a bulk hydraulic property and not as indicative of the intricate flow paths within an individual fracture or rock volume.

Chemical Sampling

In many problems of characterization it is crucial to understand the spatial distribution of contaminants in ground water to address project objectives. Also, understanding the distribution of naturally occurring constituents may provide insight regarding the origin and residence time of the ground water. At sites that are only several hectares in area, the chemical composition of ground water due to interactions with the rock may not show significant variability over the areal dimensions of the site; however, the variability of water chemistry with depth may provide insight into ground-water flow (Harte and Winter, 1996). Also, testing ground water for constituents in precipitation may indicate the residence time of the ground water (Busenberg and Plummer, 1996; Drenkard and others, 1996).

Collecting water samples for geochemical analyses by pumping open boreholes will draw water preferentially from the highest permeability fractures and will result in a composite sample from multiple fractures. Composite water samples do not provide insight into chemical stratification along the length of the borehole. For problems in which the details of water chemistry as a function of depth in the borehole are needed, ground-water samples must be collected by isolating intervals using borehole packers, or other specially designed equipment that can guarantee water samples that are indicative of formation fluids from a given fracture or fracture zone.

MULTIPLE-BOREHOLE METHODS

The single-hole methods discussed above do not address the issue of the connectivity of fractures within a rock volume. Being able to map the connectivity of transmissive fractures to the degree warranted for a given problem is the primary component of hydrogeologic characterization. With single-hole methods conducted in multiple boreholes, extrapolation from borehole to borehole can be attempted with the aid of geologic and fracture mapping. Extrapolating single-hole information, however, is fraught with uncertainty in complex geologic terrain. Even in geologically simple bedrock terrain, such as horizontally bedded sedimentary formations, fractures that appear to be areally extensive have hydraulic properties that vary as a function of space (Shapiro and Nicholas, 1989).

Seismic and Radar Tomography

Both seismic and EM waves have been used to image the bedrock between boreholes (Wright and others, 1996a, 1996b; Ellefsen and others, 1998). The formation properties between the transmitter in one bedrock well and receivers in an adjacent borehole affects the travel time and attenuation of the transmitted signal. By moving the location of the transmitter and receiver, raypaths are generated over the cross section of the rock and the spatial distribution of the physical property associated with transmission and attenuation of the signal are estimated so as to reproduce the measured responses. For example, from the arrival of the pressure wave used in seismic tomography, the spatial distribution of seismic velocity between the two wells is inferred. Zones of low seismic velocities may indicate the presence of fractures, whereas zones of high seismic velocity may indicate more intact rock. In general, the frequency of the signals used in tomographic imaging is not sufficient to identify individual fractures. Nevertheless, tomography provides a means of inferring spatial changes in rock properties in a cross-section of the formation, from which one can potentially infer location, oreintation and spatial extent of fracture zones.

As with other geophysical techniques, zones of fracturing inferred from tomographic imaging would need to be verified by hydraulic tests. EM waves, however, are affected by both fluid and rock properties. Injecting a highly conductive fluid to displace the ambient fluid in fractures will change the spatial distribution of the radar attenuation (Lane and others, 1996a, 1998; Wright

and Lane, 1998). Subtracting the radar attenuation tomograms conducted under ambient and chemically stressed conditions highlights those fractures or zones that transmit fluid and chemical constituents. This approach provides a direct observation of zones between bedrock boreholes that transmit fluid and constituents.

Borehole Flow

The measurement of vertical borehole flow using sensitive borehole flowmeters can also be used to identify the connectivity of fractures between boreholes. This technique is conducted by pumping water from one borehole and monitoring the vertical flow in nearby boreholes. The fluid pressure response from the pumped borehole propagates most rapidly through the most permeable fractures. Because the open borehole acts as a high-permeability pathway, the first fluid pressure response at a fracture in the unpumped borehole will result in vertical flow from other water bearing fractures in the unpumped borehole (Paillet, 1998). The connectivity of fractures between boreholes as inferred from this approach provides valuable qualitative evidence of the lateral extent of highly transmissive fractures. If simplified conceptual models of fracture connectivity are assumed, type curves can be developed to estimate the hydraulic properties of fractures (Lapcevic and others, 1993; Paillet, 1998). Because of the complexity of fracture connections, such analyses may not be unique; however, the use of information from other single-borehole and cross borehole characterization methods may act to constrain the conceptual model of heterogeneity.

Hydraulic Testing

Hydraulic tests using multiple boreholes to observe fluid pressure responses from pumping or injecting fluid may indicate the location of highly transmissive fractures and fracture connectivity (Hsieh and Shapiro, 1996). Multiple-hole hydraulic tests can be conducted using open boreholes or using borehole packers to isolate discrete intervals in bedrock boreholes. A test design using open holes or borehole packers depends on project objectives. Tests conducted with borehole packers, however, provide the best means of identifying the intricate spatial heterogeneity of a bedrock environment over an area of several hectares. Also, isolating borehole intervals with packers prevents the borehole from acting as a highly transmissive pathway that connects other permeable fractures in the rock. Borehole geophysics, borehole scanning methods, and results from single- and cross-hole borehole flow are crucial in designing a hydraulic test in bedrock environments (Paillet, 1996).

The estimation of fracture or formation properties from the fluid pressure responses first requires a conceptual model of heterogeneity. In general, interpreting hydraulic tests conducted in complexly fractured bedrock environments requires numerical simulation of ground-water flow, where the spatial variable hydraulic properties can be incorporated into the numerical simulator (Long and Billaux, 1987; Hsieh and Shapiro, 1996). The structure of the heterogeneity proposed for the simulation should be consistent with the interpretations of single- and cross-hole geophysical tests and single-hole hydraulic tests. Methods of quantitatively incorporating geophysical information with hydraulic testing in the estimation of hydraulic properties is an area of current research (Day-Lewis and others, 1997).

Tracer Testing

To estimate ground-water residence time, it is necessary to identify the effective porosity. Estimates of fracture porosity from cores are unreliable, as are estimates of fracture porosity based on measured mechanical apertures or hydraulic apertures inferred from single-hole hydraulic tests. The only means of obtaining reliable estimates of fracture porosity is through *in situ* tracer tests, where a known mass of a traced fluid is injected into the formation and its concentration is measured at one or more down-gradient locations. Usually such tests are conducted in fractured rock under hydraulically stressed conditions by injecting the tracer into a fractures in one borehole and pumping from an adjacent borehole (Shapiro, 1996). Interpretation of the time-varying concentration of the tracer at the pumped well first requires a mathematical

model of fluid movement. The breakthrough curve can then be interpreted to estimate the effective porosity, as well as processes such as dispersion and matrix diffusion.

INTEGRATING MULTIDISCIPLINARY INVESTIGATIONS

The methods discussed in this article can be applied separately in an attempt to characterize fractured rock. In highly heterogeneous subsurface environments like fractured rock, however, it is unlikely that a single characterization method will yield an unambiguous interpretation of spatially heterogeneous hydraulic properties that define advective fluid movement. Concequently, it is necessary to use a multiple-method approach to conduct the hydrogeologic characterization. For example, regional reconnaissance of bedrock geology may identify geologic structures such as faults that may be hypothesized as transmissive zones in the bedrock. Without detailed measurements of ambient hydraulic head, or hydraulic testing, however, such zones could conceivably be barriers to ground-water flow rather than conduits. Nevertheless, regional and local reconnaissance techniques provide information that guide further characterization, for example, the siting of boreholes and *in situ* testing. Similarly, *in situ* characterization methods such as geophysical logging and borehole scanning may by used to infer the location and orientation of fractures. These techniques, however, cannot ascertain the hydraulic properties of those fractures; only hydraulic testing and borehole flow measurements provides such information.

Although hydraulic testing using both single- and multiple-hole methods, is used to infer the hydraulic properties that govern advective fluid movement, the characterization approach should not forsake other methods and proceed directly to hydraulic testing. The successful design of hydraulic tests in heterogeneous bedrock terrain first requires substantial investment in characterizing borehole conditions, fracture locations, and preliminary estimates of conductive fractures using methods such as borehole flow and borehole radar. In addition, the interpretation of hydraulic tests is greatly aided by information from single-hole borehole radar and cross-hole tomography to hypothesize the geometry of potential connections between bedrock boreholes.

Not all techniques of characterization need to be applied at a given site. The choice of characterization tools will depend on the site conditions, as well as project objectives, monetary and time constraints, and the degree of uncertainty that can be tolerated (Lane and others, 1996b). In this article, it is impossible to speculate on the latter issues; however, the effect of site conditions on the successful application of certain characterization methods is well known and can act as a guide in choosing a subset of characterization approaches. For example, ground-penetrating radar or borehole radar may not be appropriate if rock properties are not conducive to the propagation of EM waves. Also, in situations where borehole fluid is turbid, borehole scanning with optical methods would not be fruitful.

It is advantageous to proceed in the hierarchical multiple-method approach discussed in this article by first considering regional reconnaissance, then focusing on site-specific reconnaissance, and finally on single- and multiple-borehole investigations. Such an approach may not be feasible, however, because of the need to simultaneously conduct various aspects of site characterization or summarize historical data records. Nevertheless, it is advantageous to use a systematic approach of synthesizing available information from the regional scale before dwelling on detailed site information and *in situ* observations. The process of site characterization, however, should be viewed as an iterative procedure where the synthesis of information directs the choice of characterization methods and may include revisiting reconnaissance activities.

REFERENCES

Barton, C. C., 1996, Characterizing bedrock fractures in outcrop for studies of ground-water hydrology: An example from Mirror Lake, Grafton County, New Hamsphire, *in* Morganwalp, D. W. and Aronson, D. A., eds., U.S. Geological Survey Toxic Substances Hydrology Program--Proceedings of the Technical Meeting, Colorado Springs, CO, September 20-24, 1993: U.S. Geological Survey Water-Resources Investigations Report 94-4015, p. 81-87.

Barton, C. C., and Hsieh, P. A., 1989, Physical and hydrologic-flow properties of fractures, Field Trip Guidebook T385, American Geophysical Union, Washington, DC, 36 p.

Busenberg, E., and Plummer, L. N., 1996, Concentrations of chlorofluorocarbons and other gases in ground water at Mirror Lake, New Hampshire, *in* Morganwalp, D. W. and Aronson, D. A., eds., U.S. Geological Survey Toxic Substances Hydrology Program--Proceedings of the Technical Meeting, Colorado Springs, CO, September 20-24, 1993: U.S. Geological Survey Water-Resources Investigations Report 94-4015, p. 151-158.

Clark, S. F. , Jr., Moore, R. B., Ferguson, E. W., and Picard, M. A., 1996, Criteria and methods for fracture-trace analysis of the New Hampshire bedrock aquifer: U.S. Geological Survey Open-File Report 96-479, 12 p.

Day-Lewis, F. D., Lane Jr., J. W., Haeni, F. P., and Gorelick, S. M., 1997, One approach to identifying flow paths in fractured rock: combining borehole radar, saline tracer tests, and numerical modeling [abs.]: Eos, Transactions, American Geophysical Union, v. 78, no. 46, p.F322.

Drenkard, S., Torgersen, T., Weppernig, R., Farley, K., Schlosser, P., Michel, R. L., Shapiro, A. M., and Wood, W. W., 1996, Helium isotope analysis and tritium-helium age dating in the Mirror Lake Basin, Grafton County, New Hampshire, *in* Morganwalp, D. W. and Aronson, D. A., eds., U.S. Geological Survey Toxic Substances Hydrology Program--Proceedings of the Technical Meeting, Colorado Springs, CO, September 20-24, 1993: U.S. Geological Survey Water-Resources Investigations Report 94-4015, p. 81-87.

Ellefsen, K. J., Kibler, J. E., Hsieh, P. A., and Shapiro, A. M., 1998, Crosswell seismic tomography at the USGS fractured rock research site: Data collection, data processing and tomograms: U.S. Geological Survey Open-File Report 98-510.

Haeni, F. P., and Lane, J. W., Jr., 1996, Use of borehole-radar methods to detect fractures in crystalline rocks, Mirror Lake area, Grafton County, Hew Hampshire, *in* Stevens, P. R., and Nicholson, T. J., eds., Joint U.S. Geological survey, U.S. Nuclear Regulatory Commission Workshop on research related to low-level radioactive-waste disposal, May 4-6, 1993, National Center, Reston, VA: U.S. Geological Survey Water-Resources Investigations Report 95-4015, p. 175-182.

Haeni, F. P., Lane, J. W., Jr., Barton, C. C., and Lieblich, D. A., 1996, Fracture detection in crystalline rocks, Mirror Lake area, Grafton County, New Hampshire, *in* Morganwalp, D. W. and Aronson, D. A., eds., U.S. Geological Survey Toxic Substances Hydrology Program--Proceedings of the Technical Meeting, Colorado Springs, CO, September 20-24, 1993: U.S. Geological Survey Water-Resources Investigations Report 94-4015, p. 95-102.

Harte, P. T., and Winter, T. C., 1996, Factors affecting recharge to crystalline rock in the Mirror Lake area, Grafton County, New Hampshire, *in* Morganwalp, D. W. and Aronson, D. A., eds., U.S. Geological Survey Toxic Substances Hydrology Program--Proceedings of the Technical Meeting, Colorado Springs, CO, September 20-24, 1993: U.S. Geological Survey Water-

Resources Investigations Report 94-4015, p. 141-150.

Hess, A. E., 1986, Identifying hydraulically conductivity fractures with a slow-velocity borehole flowmeter: Canadian Geotechnical Journal, v. 23, no. 1, p. 69-78.

Hsieh, P. A., and Shapiro, A. M., 1996, Hydraulic characteristics of fractured bedrock underlying the FSE well field at the Mirror Lake site, Grafton County, New Hampshire, *in* Morganwalp, D. W. and Aronson, D. A., eds., U.S. Geological Survey Toxic Substances Hydrology Program--Proceedings of the Technical Meeting, Colorado Springs, CO, September 20-24, 1993: U.S. Geological Survey Water-Resources Investigations Report 94-4015, p. 127-130.

Hsieh, P. A., Shapiro, A. M., Barton, C. C., Haeni, F. P., Johnson, C. D., Martin, C. W., Paillet, F. L., Winter, T. C., Wright, D. L., 1993, Methods of characterizing fluid movement and chemical transport in fractured rock, *in* Cheney, J. T., and Hepburn, J. C., eds., Field Trip Guidebook for Northeastern United States, v. 2: Geological Society of America, Boulder, CO, p. R1-R30.

Johnson, C.D., 1998, Subsurface lithology and fracture occurrence and their effects on hydraulic conductivity: Mirror Lake Research Site, Grafton County, New Hampshire: University of New Hampshire, Durham, New Hampshire, unpublished Masters Thesis, 159 p.

Johnson, C.D. and Dunstan, A.M., 1998, Lithology and fracture characterization from drilling investigations in the Mirror Lake area from 1979 through 1995 in Grafton County New Hampshire: U.S. Geological Survey Water-Resources Investigations Report 98-4183, 210 p.

Keys, W. S., 1990, Borehole geophysics applied to ground-water investigations: U.S. Geological Survey Techniques of Water-Resources Investigation, Book 2, Chap. E2, 150 p.

Lane, J. W., Jr., Haeni, F. P., and Day-Lewis, F. D., 1998, Use of time-lapse attenuation-difference radar tomography methods to monitor saline tracer transport in fractured crystalline bedrock, *in* GPR '94, Proceedings of the Seventh International Conference on Ground-Penetrating Radar, University of Kansas, May 27-30, 1998, Lawrence, Kansas, p.533-538.

Lane, J. W., Jr., Haeni, F. P., and Williams, J. H., 1994, Detection of bedrock fractures and lithologic changes using borehole radar at selected sites, *in* GPR '94, Proceedings of the Fifth International Conference on Ground-Penetrating Radar, v. 3,Waterloo Centre for Groundwater Research and Canadian Geotechnical Society, June 12-16, 1994, Kitchener, Ontario, Canada, p. 577-592.

Lane, J. W., Jr., Haeni, F. P., Placzek, G., and Wright, D. L., 1996a, Use of borehole-radar methods to detect a saline tracer in fractured crystalline bedrock, Mirror lake Grafton County, New Hampshire, USA, *in* GPR '96, Proceedings of the Sixth International Conference on Ground-Penetrating Radar, Tohoku University Department of Geoscience and Technology, September 30-October 3, 1996, Sendai, Japan, p. 185-190.

Lane, J. W., Jr., Haeni, F. P., Soloyanis, S., Placzek, G., Williams, J. H., Johnson, C. D., Buursink, M. L., Joesten, P. K., and Knutson, K. D., 1996b, Geophysical Characterization of a fractured-bedrock aquifer and blast-fractured contaminant-recovery trench, *in* Procceedins of the Symposium on the Application of Geophysics to Engineering and Environmental Problems, April 28 – May 2, 1996, Keystone, CO, Environmental and Engineering Geophysical Society, Wheat Ridge, CO, p. 429-441.

Lapcevic, P. A., Novakowski, K. S., and Paillet, F. L., 1993, Analysis of transient flow in an

observation well intersecting a single fracture: Journal of Hydrology, v. 151, p. 229-239.

Lattman, L. H., and Parizek, R. R., 1964, Relationship between fracture traces and the occurrence of ground water in carbonate rocks: Journal of Hydrology, v. 2, p. 73-91.

Lewis, M. R., and Haeni, F. P., 1987, The use of surface geophysical techniques to detect fractures in bedrock—annotated bibliography: U.S. Geological Survey Circular 987, 14 p.

Long, J. C. S., and Billaux, D. M., 1987, From field data to fracture network modeling: An example incorporating spatial structure: Water Resources Research, v. 23, no. 7, p. 1201-1216.

Molz, F. J., and Young, S. C., 1993, Development and application of borehole flowmeters for environmental assessment: Log Analyst, v. 34, no. 1, p. 13-23.

National Research Council, 1996, Rock Fractures and Fluid Flow: Contemporary Understanding and Application, National Academy Press, Washington, DC, 551 p.

Olsson, O., Falk, L., Forslund, O., Lundmark, L., and Sandberg, E., 1992, Borehole radar applied to the characterization of hydraulically conductive fracture zones in crystalline rock: Geophysical Prospecting, v. 40, p. 109-142.

Paillet, F. L., 1993, Application of borehole geophysics in characterization of flow in fractured rocks: U.S. Geological Survey Water-Resources Investigations Report 93-4214, 36 p.

Paillet, F. L., 1998, Flow modeling and permeability estimation using borehole flow logs in heterogeneous fractured formations: Water Resources Research, v. 34, no. 5, p. 997-1010.

Paillet, F. L., 1996, Use of well logs to prepare the way for packer strings and tracer tests: Lessons from the Mirror Lake study, *in* Morganwalp, D. W. and Aronson, D. A., eds., U.S. Geological Survey Toxic Substances Hydrology Program--Proceedings of the Technical Meeting, Colorado Springs, CO, September 20-24, 1993: U.S. Geological Survey Water-Resources Investigations Report 94-4015, p. 103-109.

Paillet, F. L., and Kapucu, K., 1989, Fracture characterization and fracture-permeability estimates from geophysical logs in the Mirror Lake watershed, New Hampshire: U.S. Geological Survey Water-Resources Investigation Report 89-4058, 49 p.

Shapiro, A. M., 1996, Estimation of effective porosity in fractured crystalline rock by controlled-tracer tests, *in* Stevens, P. R., and Nicholson, T. J., eds., Joint U.S. Geological survey, U.S. Nuclear Regulatory Commission Workshop on research related to low-level radioactive-waste disposal, May 4-6, 1993, National Center, Reston, VA: U.S. Geological Survey Water-Resources Investigations Report 95-4015, p. 185-190.

Shapiro, A. M., and Hsieh, P. A., 1991, Research in fractured-rock hydrogeology: Characterizing fluid movement and chemical transport in fractured rock at the Mirror Lake drainage basin, New Hampshire, *in* Mallard, G. E., and Aronson, D. A., eds., U.S. Geological Survey Toxic Substances Hydrology Program--Proceedings of the Technical Meeting, Monterey, CA, March 11-15, 1991: U.S. Geological Survey Water-Resources Investigations Report 91-4034, p. 155-161.

Shapiro, A. M., and Hsieh, P. A., 1996, Overview of research on use of hydrologic, geophysical and chemical methods to characterize flow and chemical transport in fractured rock at the Mirror Lake site, NH, *in* Morganwalp, D. W. and Aronson, D. A., eds., U.S. Geological Survey Toxic Substances Hydrology Program--Proceedings of the Technical Meeting, Colorado Springs, CO, September 20-24, 1993: U.S. Geological Survey Water-

Resources Investigations Report 94-4015, p. 71-80.

Shapiro, A. M., and Hsieh, P. A., 1998, How good are estimates of transmissivity from slug tests in fractured rock?: Ground Water, v. 36, no. 1, p. 37-48.

Shapiro, A. M., Hsieh, P. A., and Winter, T. C., 1995, The Mirror Lake Fractured Rock Research Site--A Multidisciplinary Research Effort in Characterizing Ground-Water Flow and Chemical Transport in Fractured Rock: U.S. Geological Survey Fact Sheet FS-138-95, 2 p.

Shapiro, A. M., and Nicholas, J. R., 1989, Assessing the validity of the channel model of fracture aperture under field conditions: Water Resources Research, v. 25, no. 5, p. 817-828.

Siddiqui, S. H., and Parizek, R. R., 1971, Hydrogeologic factors influencing well yields in folded and faulted carbonate rocks in central Pennsylvania: Water Resources Research, v. 7, no. 5, p. 1295-1312.

Tiedeman, C. R., Goode, D. J., and Hsieh, P. A., 1997, Numerical simulation of ground-water flow through glacial deposits and crystalline bedrock in the Mirror Lake area, Grafton County, New Hampshire: U.S. Geological Survey Professional Paper 1572, 50 p.

Tiedeman, C. R., Goode, D. J., and Hsieh, P. A., 1998, Characterizing a ground-water basin in a New England mountain and valley terrain: Ground Water, v. 36, no. 4, p. 611-620.

Williams, J. H., and Lane, J. W., Jr., 1998, Advances in borehole geophysics for ground-water investigations: U.S. Geological Survey Fact Sheet FS-002, 4 p.

Wright, D. L., and Lane J. W., Jr., 1998, Mapping hydraulically permeable fractures using directional borehole radar and hole-to-hole tomography with a saline tracer, *in* Proceedings of the Symposium on the Application of Geophysics to Engineering and Environmental Problems, March 22-26, 1998, Chicago, Illinois, Environmental and Engineering Geophysical Society, Wheat Ridge, CO, p. 379-388.

Wright, D. L., Olhoeft, G. R., and Grover, T. P., 1996a, Velocity, attenuation and dispersion elecromagnetic tomography in fractured rock, *in* Morganwalp, D. W. and Aronson, D. A., eds., U.S. Geological Survey Toxic Substances Hydrology Program--Proceedings of the Technical Meeting, Colorado Springs, CO, September 20-24, 1993: U.S. Geological Survey Water-Resources Investigations Report 94-4015, p. 111-118

Wright, D. L., Olhoeft, G. R., Hsieh, P. A., Majer, E. L., Paillet, F. L., and Lane, J. W., Jr., 1996b, Electromagnetic and seismic tomography compared to borehole acoustic televiewer and flowmeter logs for subsurface fracture mapping at the Mirror Lake site, New Hampshire, *in* Morganwalp, D. W. and Aronson, D. A., eds., U.S. Geological Survey Toxic Substances Hydrology Program--Proceedings of the Technical Meeting, Colorado Springs, CO, September 20-24, 1993: U.S. Geological Survey Water-Resources Investigations Report 94-4015, p. 119-126.

Zemanek, J., Glenn, E. E., Norton, L. J., and Caldwell, R. L., 1970, Formation evaluation by inspection with the borehole televiewer: Geophysics, v. 35, no. 2, p. 254-269.

AUTHOR INFORMATION

Allen M. Shapiro, U.S. Geological Survey, Reston, VA

Paul A. Hsieh, U.S. Geological Survey, Menlo Park, CA

F. Peter Haeni, U.S. Geological Survey, Storrs, CT

Exchangeable Ions, Fracture Volume, and Specific Surface Area in Fractured Crystalline Rocks

By Warren W. Wood, Thomas F. Kraemer, and Allen Shapiro

ABSTRACT

A new approach is described in which a combination of a brine injection field test and radiometric laboratory examination of rock samples can provide critical parameters of exchangeable cations, fracture volume, and specific surface area required for solute transport simulation in fractured rocks.

INTRODUCTION

A new approach (Solute Stress Testing - SST) is proposed to evaluate several geochemical parameters required for successful simulation of solute transport in fractured rocks. In this approach, a large, known chemical stress is applied to the aquifer, and the response of the system to that stress is measured. This procedure allows recovery of information not available by analysis of traditional self-potential methods, stresses typically associated with reactive tracer tests with dilute concentrations, or poorly-defined temporal and spatial variation in concentration associated with contamination or naturally-occurring environmental tracers.

The dipole-SST approach, combined with laboratory tests, can provide information on fracture volume, fracture surface area, exchangeable cations, cation exchange capacity, mobilization of iron, manganese and other sorbed metals, and other parameters of interest. A dipole design with multiple injection of increasing concentrations of the "stress" solute permits acquisition of high quality data. The SST approach integrates a much larger rock volume than does laboratory analysis of core, providing an acceptable *in situ* estimate of the critical parameters necessary to simulate solute transport in transmissive fractured rocks.

FIELD TEST

A preliminary field-scale evaluation to test the SST concept was made using archived samples from a geophysical test in the Concord Granite at Hubbard Brook Experimental Forest, Grafton County, New Hampshire, U. S. A. (42° 56'N, 71° 43' W). The experimental design for the test consisted of injecting a NaCl (sodium chloride) brine in one well (FSE-1) and withdrawing it along with exchangeable ions at an extraction well (FSE-4). The distance between the injection and withdrawal well was 14.1 m (meters). The test was conducted in a highly transmissive zone in the bedrock with fractures that were intersected by both the injection and withdrawal wells. Because there is less than 1 m elevation difference between the land surface at the injection and pumping wells, it is assumed that the highly transmissive zone is nearly horizontal. An injection apparatus installed in FSE-1 consisted of two packers separated by a pipe with holes drilled along its length to act as a diffuser for the injected tracer. The highly transmissive zone was isolated for injection in FSE-1 by inflating the packers between 39.7 and 46.9 m below land surface. A pump was installed between two packers set at 41.5 and 44.0 m below land surface in FSE-4. This highly transmissive zone had been previously identified by dilute NaBr (sodium bromide) pulse tracer test. An ion-exchange solution was prepared using approximately 2,100 L of water previously pumped from FSE-4, and mixed with 60 kilograms of NaCl,

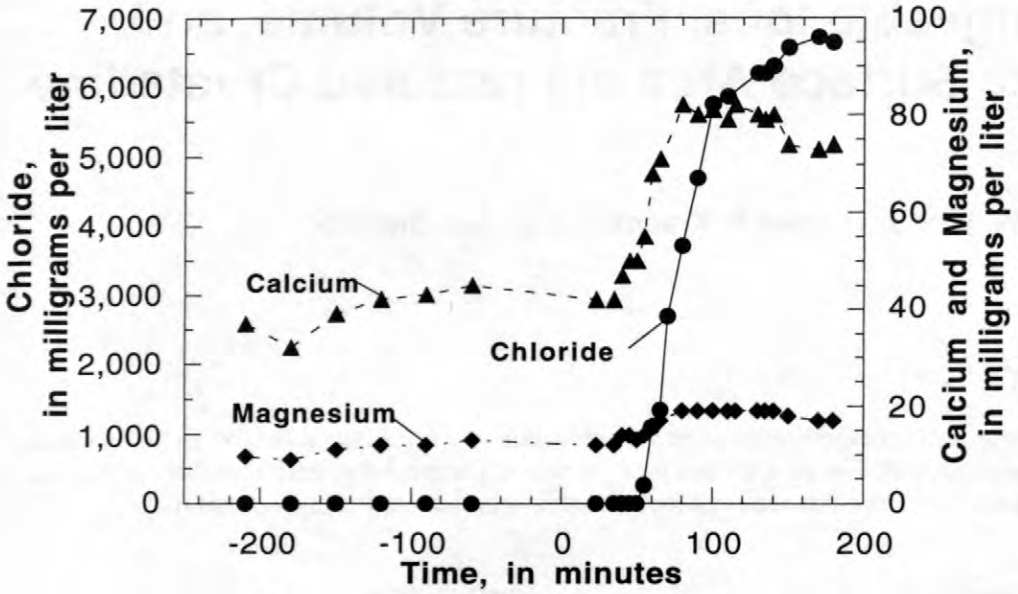

Figure 1. Rate of change of calcium, magnesium, and chloride concentration with respect to pumping time in a fractured granite gneiss at Mirror Lake, New Hampshire. Time of zero indicates when the brine solution was injected.

yielding a solution of 16,170 mg/L (milligrams per liter) Cl. Pumping from well FSE-4 commenced at 1115 hours September 11, 1995 to establish a steady-state flow field surrounding the well and to provide water for making the brine solution. At 1500 hours, the brine solution was injected continuously at 10L/min (liters per minute) while pumping continued from well FSE-4 at the same 10L/min rate. Pumping and injection were terminated 180 minutes after start of injection when steady-state chloride concentration was observed at the withdrawal well (FSE-4).

This test yielded interesting information on both the character of the fractures and the matrix-controlled geochemical parameters of the aquifer (fig.1). Water samples were analyzed for dissolved solutes using standard analytical methods (table 1). Figure 1 illustrates the change in concentration of calcium, magnesium, and chloride as a function of pumping time since brine injection. We interpret the increase of calcium and magnesium in the output to be the result of ion exchange with the sodium in the input solution. Potassium, strontium, barium, and radium (table 1) were identified in elevated concentrations at approximately the same time as the calcium and magnesium shown in Figure 1. The exchanger is assumed to be a combination of the ubiquitous iron hydroxide coating the fractures and weathered feldspar from the fracture faces of the granite.

While this test provides an estimate of exchangeable ions, sampling for this test was terminated before removal of the brine; thus, no declining limb of the concentration curve is available, and the mass of ion removed cannot be calculated. Also, the efficiency of the exchanging ion could not be determined from this experiment. Multiple injection of increasing concentration of sodium would be necessary to ascertain the efficiency of the sodium as an exchanging ion, and continued sampling during removal of the brine would be necessary to determine the mass of exchangeable ions. This experiment does, however, permit calculation of the water filled volume V_f of the transmissive fractures sensed by the brine solution using the following expression

$$V_f = \frac{(t)(P)}{\frac{Cl_{in}}{Cl_{ss}}} \qquad (1)$$

where t is time to achieve steady-state chloride concentration (170 min), P is the pumping rate (10 L/min), Cl_{in} is the input chloride concentration, (16,175 mg/L), and Cl_{ss} is the steady state chloride concentration in the withdrawal well (6,700 mg/L). The volume of the void space of the fractures "seen" by this brine solution under the test conditions is approximately 0.70 m^3. This calculated volume includes volume of diffusion that in the short time of this test is assumed to be negligible.

LABORATORY TEST

A radiometric approach that uses natural radon in the system can be utilized to estimate the surface area of the fracture volume calculated by the SST method. Area can be obtained by measuring the radon flux from a known area on the face of the fracture and comparing this flux to the mass of radon in the volume of water in the fracture. This area is calculated from the equation

$$A = \frac{^{222}Rn_w}{^{222}Rn_x}(V) \tag{2}$$

where A is the area of the fracture, $^{222}Rn_x$ is the radon flux from the face of the rock matrix (0.3 dpm/cm^2 -- disintegrations per minute per square centimeter from a core area of 4.9 cm^2) based on preliminary measurements of core, $^{222}Rn_w$ is the radon activity in water (900 dpm/L), and V is volume of the fracture determined from Equation 1 above (0.70 m^3). Solving for area (A) yields a value of approximately 210 m^2. It should be noted that the core used to determine radon flux (0.3 dpm/cm^2) in this experiment was obtained from a borehole 30 m away from the injection and withdrawal wells and is located at the same depth as the highly transmissive zone. Also, the radon in the water (900 dpm/L) was an average from fractures above and below the sampled interval and not from the pumped interval.

An important parameter in transport modeling is specific surface area (surface area per unit rock volume, with units of 1/L). The radiometric determination of surface area described above allows comparison with physically-based methods of computing specific surface area. Specific surface area is generally estimated by measuring the number of fractures observed in a borehole and assuming that parallel plate fractures extend out from the borehole. Carole Johnson (USGS, written commun., 1998) estimated the average fracture spacing to be 3.2 m or 0.31 fractures/m in the FSE well field. Using this value and the fact that a fracture has two faces, the specific surface area of the fractures in a cubic meter of rock would be approximately 0.62 m^2/m^3.

Combining the radiometrically-determined area and the volume determined by the SST test, the data can be used to calculate an improved estimate of specific surface area. It is known from *in situ* tracer tests that fracture porosity averages approximately 0.01 for the high transmissivity zone. Thus, the total rock volume V_t associated with this test interval is

$$\frac{V_f}{V_t} = 0.01 \tag{3}$$

where V_f is the volume of the fractures (0.7 m^3) as estimated above from the concentration history of the injection test. Thus, V_t in this case has a value of 70 m^3.

Specific surface area (S_a) is defined as

$$S_a = \frac{A}{V_t} \tag{4}$$

where A and V_t are defined above. From the area calculation using V_t, the specific surface area of fractures can be calculated to be approximately 3 m^2/m^3. This value is five times greater than the value 0.6-m^2/m^3 value determined by enumerating the physical fracture.

It is not unreasonable nor unexpected that the radiometrically-specific surface area is larger than the idealized physical method because of the roughness of the fracture face surfaces, fracture undulation, and other factors. The radiometric value does, however, provide an independent method of calculating specific surface area and a constraint on any value used in transport simulation.

SUMMARY AND CONCLUSION

While the available archived samples were inadequate to define the ion exchange capacity of this system, it does illustrate the potential of the SST method to determine a number of useful properties necessary for simulation of solutes in fractured rocks. The use of radon to calculate

surface area is an independent estimate of the surface area. While this test utilized sodium as a simple ion exchanger, the SST concept can be applied to any chemical test that is presently performed in the laboratory, such as calculating the mass of iron and trace metals mobilized under varying Eh/pH conditions. Philosophically, SST extends the concept of chemical-reactive testing by moving to a larger, *in situ* sample of the system, and higher concentrations of reactive tracer than used in a typical "tracer" test. This is analogous to the move from determining hydraulic conductivity of a core in the laboratory to a field-scale aquifer test.

Table 1. Chemical analyses of water in milligrams per liter (mg/L), micrograms per liter (µg/L), and disintegrations per minute per liter (dpm/L).

Minutes since start	Cl mg/L	Ca mg/L	Mg mg/L	Na mg/L	K mg/L	Sr mg/L	Fe mg/L	Ba µg/L	226-Ra dpm/L	U µg/L
-210	4.7	37	9.6	14	4.3	0.3	31	26		0.3
-180	4.7	32	9.0	14	4.4	0.3	30	27	7.7±0.9	0.4
-150	4.7	39	11	15	4.3	0.3	28	26		0.5
-120	4.6	42	12	17	4.5	0.4	31	27	7.1±0.2	0.6
-90	4.7	43	12	17	4.5	0.4	28	27		0.6
-60	4.7	45	13	18	4.7	0.4	30	27	7.6±1.1	0.7
0										
23	4.7	42	12	20	4.6	0.4	29	26	7.6±0.8	0.7
35	4.7	42	12	17	4.7	0.4	28	28	7.9±0.1	0.7
40	4.8	47	14	19	4.7	0.4	26	27		0.9
45	4.8	50	14	19	4.9	0.5	29	29	8.7±0.6	1.0
50	4.8	50	13	18	4.6	0.4	25	27		0.9
55	265	55	14	175	4.8	0.5	21	37		0.8
60	1100	68	16	711	5.0	0.6	35	70	23.7±1.1	1.0
65	1340	71	17	1200	6.6	0.6	38	88		0.9
70	2700							108	46.1±2.7	
80	3725	82	19	2500	5.9	0.7	40	134		0.9
90	4700	80	19	3000	6.4	0.7	43	145	76.5±1.2	0.9
100	5750	81	19	3500	7.6	0.7	41	131		0.8
110	5870	79	19	3850	6.9	0.6	41	139		0.8
115	6900	82	19	4000	7.0	0.7	42	134		0.8
125								157	73.1±2.8	
130	6200	80	19	4250	8.4	0.6	41	139		0.7
135	6200	79	19	4450	10	0.7	41	140		0.7
140	6300	80	19	4150	10	0.6	41	147		0.7
150	6575	74	18	4350	11	0.6	46	170	64±5.4	0.8
170	6725	73	17	4350	11	0.6	44	155	61.5±7	0.7
180	6650	74	17	4450	12	0.6	42	142		0.6
Input Brine	16350	55	13	9700	6.7	0.4	32	48		0.2
Input Brine	16000	55	13	9700	7.8	0.4	35	56	7.6±0.3	0.2

AUTHOR INFORMATION

Warren W. Wood and Thomas F. Kraemer, U.S. Geological Survey, 430 National Center, Reston, Virginia 20192

Allen M. Shapiro, U.S. Geological Survey, 431 National Center, Reston, Virginia 20192

Geostatistical Simulation of High-Transmissivity Zones at the Mirror Lake Site in New Hampshire: Conditioning to Hydraulic Information

By Frederick D. Day-Lewis, Paul A. Hsieh, Allen M. Shapiro, and Steven M. Gorelick

ABSTRACT

A new approach is presented to include hydraulic information as conditioning data in geostatistical simulation of high-transmissivity zones. A simulated-annealing algorithm is used to generate three-dimensional geostatistical realizations conditioned to borehole data and inferred hydraulic connections between packer-isolated borehole intervals. High-transmissivity zones were identified by Hsieh and Shapiro (1996) in the bedrock underlying the FSE well field at the U.S. Geological Survey Fractured Rock Research Site near Mirror Lake, Grafton County, New Hampshire. These zones are conceptualized to consist of connected, highly transmissive fractures that are embedded within a surrounding network of less transmissive fractures. During multiple-well hydraulic tests, well intervals connected by a high-transmissivity zone exhibit similar drawdown responses, whereas well intervals not connected by a high-transmissivity zone exhibit different responses. To analyze the test data, Hsieh and others (1999) constructed and calibrated a deterministic ground-water flow model. In this study, alternative spatial patterns of hydraulic properties are based on geostatistical realizations. The simulated-annealing algorithm is used to generate conditional realizations of high-transmissivity zones in the bedrock underlying the FSE well field, using an indicator-variogram model of spatial variability. Statistical analysis of the generated zones yields three-dimensional images of the probability that a high-transmissivity zone occurs and the likely spatial extents of specific zones. For selected realizations, ground-water flow is simulated with a finite-element model. Hydraulic conductivity and specific storage values of high-transmissivity zones and background rock are calibrated. Simulation results for realizations conditioned to borehole and hydraulic connection data compare favorably to the test data, and realizations exhibit more complex spatial variability than previous deterministic modeling by Hsieh and others (1999).

INTRODUCTION

Based on results of single- and multiple-well hydraulic tests, Hsieh and Shapiro (1996) identified four high-transmissivity zones in the bedrock underlying the FSE well field, a 120 by 80 meter (m) area consisting of 14 boreholes at the U.S. Geological Survey (USGS) Fractured-Rock Research Site near Mirror Lake, Grafton County, New Hampshire (fig. 1). Packer-isolated borehole intervals that are connected by a high-transmissivity zone show similar drawdown responses during pumping, whereas other intervals show significantly different drawdown response. Hsieh and Shapiro (1996) hypothesized that these high-transmissivity zones contain connected, highly transmissive fractures which are embedded within a surrounding network of less transmissive fractures (fig. 2). To analyze the test data (fig. 3), Hsieh and others (1999) constructed and calibrated a deterministic ground-water flow model. In this study, a geostatistical framework is adopted to examine the spatial occurrence and extents of the high-transmissivity zones, and to consider alternative ground-water flow models that could explain the field data.

Hydraulic conductivity in fractured rock can range over many orders of magnitude,

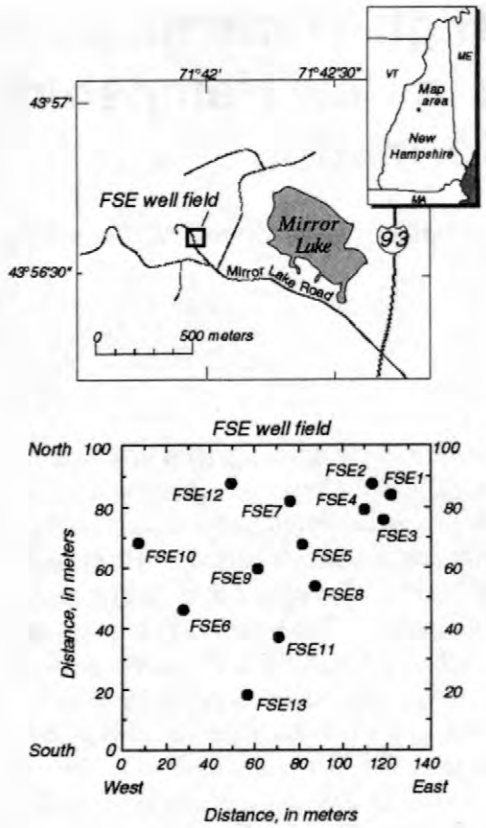

Figure 1. Map of the Fractured-Rock Research Site near Mirror Lake, in Grafton County, New Hampshire.

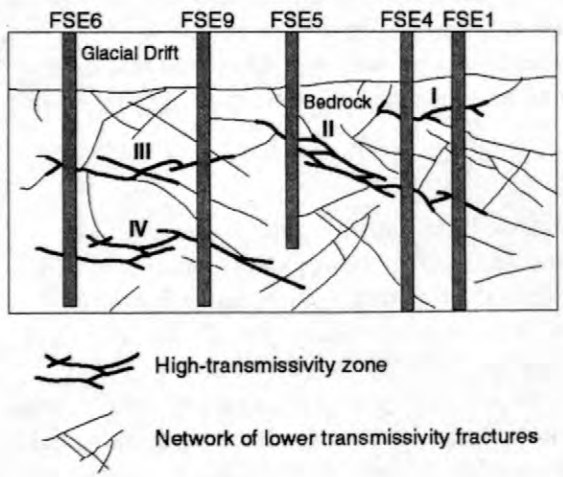

Figure 2. Conceptualized fracture distribution in a cross-section between wells FSE6 and FSE1 (after Hsieh and Shapiro, 1996).

rendering characterization extremely difficult and prediction of ground-water flow highly uncertain. Geostatistics provides tools to assess this uncertainty through Monte Carlo analysis (Deutsch and Journel, 1998). Realizations of hydraulic conductivity are generated, based on available field data and assumptions about spatial variability. The uncertainty of model-computed heads can be studied by simulating ground-water flow for many realizations.

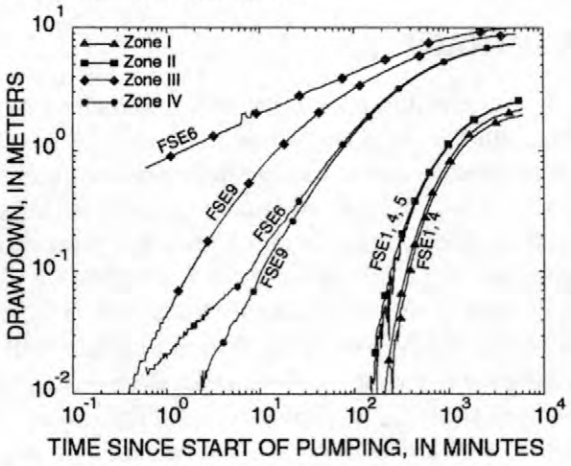

Figure 3. Drawdowns due to pumping from FSE6 during a multiple-well hydraulic test conducted in July 1993.

Conditioning data for geostatistical simulation are typically limited to local measurements of the quantity to be simulated, or estimates of that quantity from geophysical measurements. For example, in geostatistical simulation of hydraulic conductivity (K), conditioning data are typically K estimates from local hydraulic tests. However, conditioning to data related to hydraulic properties through the physical governing equations can provide significant additional information. Conditioning geostatistical simulation of hydraulic conductivity to head data might significantly reduce uncertainty and provide the correct hydraulic response to match field observations.

A major drawback in using hydraulic head data to condition the geostatistical simulation is that a ground-water flow model must be repeatedly run in the simulation algorithm. The computation time could be prohibitively long. Here, we avoid prohibitive computational expense by conditioning to borehole data and

inferred hydraulic connections between borehole intervals via high-transmissivity zones. Borehole data—classification of a borehole interval as high-transmissivity or background-transmissivity rock—are derived form single-hole hydraulic test results. Hydraulic-connection data are inferred from multiple-well hydraulic tests, in which connected borehole intervals show similar hydraulic response. A simulated-annealing algorithm is used to generate conditional realizations of high-transmissivity zones, using an indicator variogram to model spatial variability. Statistical analysis of the realizations yields three-dimensional images of the probability that a high-transmissivity zone occurs, and the likely spatial extents of specific zones. Flow modeling is then used to demonstrate the value of using connectivity information in addition to borehole data.

METHOD

Geostatistical Simulation

Deutsch and Journel (1998) and Goovaerts (1997) discuss indicator and simulated-annealing simulation algorithms in detail. We present only a brief summary of the methods here.

Simulated annealing is a stochastic optimization method based on an analogy to the physical process of cooling and consequent solidification of metals. As in other optimization methods, an objective function is defined, and the goal is to find a set of parameter values that minimizes the objective function. Each optimization starts from a different initial model in which data are relocated to grid cells and all other cell values are drawn from the histogram of the data. Parameter values are perturbed in a random fashion, so that the final results from each simulated-annealing optimization are equiprobable. Early in the optimization, more perturbations that increase the objective function are accepted to avoid convergence to local minima. Parameters corresponding to hard data at measurement locations are not perturbed. Thus realizations are constrained to local borehole data. The simulated-annealing code **sasim** (Deutsch and Journel, 1998) was adopted as the starting point in this work. The code was modified to include inferred hydraulic connections as conditioning data and to simulate a categorical variable, e.g. high-transmissivity zone versus background-transmissivity bedrock.

The original code can generate realizations based on many different types of information, including secondary geophysical data, histograms, local constraint intervals, variograms, and vertical averages. Each type of information is represented as a component term in the objective function. The simulated-annealing optimization minimizes the discrepancy between the realization and the desired spatial features.

We consider an objective function (eq. 1) with three component terms, corresponding to (1) an indicator variogram, (2) the probability density function (pdf)—percent of rock volume occupied by high-transmissivity zones, and (3) inferred hydraulic connections.

$$O = w_{pdf} O_{pdf} + w_{iv} O_{iv} + w_{conn} O_{conn} \qquad (1)$$

where

O is the global objective function,
O_{iv} is the indicator-variogram term,
w_{iv} is the weight on the indicator-variogram term,
O_{pdf} is the pdf term,
w_{pdf} is the weight on the pdf term,
O_{conn} is the hydraulic-connections term, and
w_{iv} is the weight on the connections term.

Component terms are weighted so that they contribute equally to changes in the objective function. Deutsch and Journel (1998) provide a complete description of the original code and the procedure to determine weights for component terms.

The pdf term of the objective function, O_{pdf} (eq. 2), is the squared difference between the proportion of the rock volume occupied by high-transmissivity zones in the realization and in the data. We treat the bedrock underlying the FSE well field as a categorical indicator variable, equal to 1 where high-transmissivity zones occur, and 0 in the surrounding background-transmissivity bedrock. Grid cells along boreholes are classified as high-transmissivity cells if they fall within a single-hole test interval with transmissivity greater than 10^{-7} m^2/s and

include fractures as determined from televiewer data.

$$O_{pdf} = \left(F^{*} - F \right)^2 \qquad (2)$$

where

O_{pdf} is the pdf term of the objective function,

F^{*} is the fraction of grid cells in the realization occupied by high-transmissivity zone, and

F is the estimated fraction of the rock volume occupied by high-transmissivity zone.

From the FSE well field borehole data, the fraction of the rock volume occupied by high-transmissivity zone, F, is estimated to be 0.11 for the discretization used.

The indicator-variogram term of the objective function, O_{iv} (eq. 3), is a measure of the discrepancy between the variogram of the indicator variable in the realization and in our conceptual model.

$$O_{iv} = \sum_{m=1}^{nlags} \frac{\left[\gamma_I^{*}(\mathbf{h}_m) - \gamma_I(\mathbf{h}_m) \right]^2}{\gamma_I(\mathbf{h}_m)^2} \qquad (3)$$

where

O_{iv} is the indicator-variogram term of the objective function,

$\gamma^{*}_I(\mathbf{h}_m)$ is the indicator variogram of the realization for all cell pairs separated by lag vector $\mathbf{h}_m$,

$\gamma_I(\mathbf{h}_m)$ is the model indicator variogram for all point pairs separated by lag vector $\mathbf{h}_m$,

$\mathbf{h}_m$ is lag vector for lag m, and

$nlags$ is the number of variogram lags.

Based on the experimental variogram of the FSE well field borehole data and a conceptual model of high-transmissivity zone size, the model indicator variogram has a horizontal range of 15 meters, a vertical range of 0 meters (pure nugget effect), and a nugget effect of 0 in the horizontal direction. The sill, or variance, is .0979, as determined from the pdf. Investigation of alternative variogram models is ongoing.

For the hydraulic connections term of the objective function, O_{conn} (eq. 4), we define two grid cells as being connected if (1) both are high-transmissivity, and (2) some path exists between them through vertical or lateral faces of other high-transmissivity cells. The addition of O_{conn} to the simulated-annealing objective function in **sasim** required development of subroutines to efficiently trace and update high-transmissivity connections.

$$O_{conn} = \sum_{i=1}^{n-1} \left[\sum_{j=i+1}^{n} \left(\left| C^{*}(i,j) - C(i,j) \right| \right) \right] \qquad (4)$$

where

O_{conn} is a measure of the difference between the conceptual model of hydraulic connections and the connections existing in the realization,

n is the number of high-transmissivity zone cells to check for connections,

$C^{*}(i,j)$ is 1 if cells i and j are connected in the realization, and 0 if not, and

$C(i,j)$ is 1 if cells i and j are connected in the conceptual model of connections, and 0 of not.

The three-dimensional geostatistical simulation grid is 60 cells in the x-direction (south to north), 50 cells in the y-direction (west to east), and 60 cells in the z-direction [elevation above the National Geodetic Vertical Datum of 1929 (NGVD)]. The cell dimensions are 5 meters in the horizontal directions and 2.5 meters in the vertical direction. To generate a single realization requires approximately 60 minutes of CPU time on a system equipped with a single 195MHz SGI Origin 2000 R10000 processor.

Flow Modeling

The finite element method is used to simulate multiple-well aquifer tests for several geostatistical realizations. Flow modeling is used to determine which realizations can be calibrated to exhibit the general features in hydraulic response found in the field data. Values for horizontal and vertical hydraulic conductivity (K_h and K_v), and specific storage (S_s) of the high-transmissivity zones, surrounding bedrock, and bedrock-overburden interface were calibrated manually, by repeated simulations (Table 1).

Table 1. Parameter values used for ground-water flow simulation.

	K_h m/s	K_v m/s	S_s m^{-1}
High-transmissivity zone	5×10^{-5}	5×10^{-5}	2.3×10^{-6}
Surrounding bedrock	5×10^{-9}	2.5×10^{-8}	1×10^{-7}
Bedrock-overburden interface	5×10^{-9}	5×10^{-9}	2.3×10^{-6}

We use a constant-head (zero-drawdown) boundary condition at the top of the finite-element mesh (the contact with the overburden) and no-flow boundary conditions on the other sides. The finite element mesh is comprised of 41 elements in the x-direction, 31 in the y-direction, and 62 in the z-direction, and corresponds to an interior subgrid of that used for geostatistical simulation, plus a top layer to represent a lower hydraulic-conductivity interface between the bedrock and overburden. A finer discretization is used in the vicinity of the pumped interval of FSE6, where a specified discharge of 10 L/min is imposed. To assess the value of connectivity information, flow also was simulated on a realization conditioned only to borehole data.

RESULTS

Geostatistical Simulation Results

Figure 4 displays two realizations of high-transmissivity zones. Only those zones that intersect boreholes are shown; other zones in the simulations, for which there are no borehole data, are not shown. Each realization is consistent with the inferred hydraulic connections, the borehole data, and our statistical model of spatial variability. Away from the boreholes, where there are no conditioning data, the spatial distribution of high-transmissivity zones is governed purely by the indicator variogram.

The ensemble of 50 realizations is used to compute the probability of high-transmissivity zone occurrence for each grid cell. This information is summarized by images of the probability of exceedence for various thresholds. Figure 5 shows those cells with a 30% or greater probability of falling within a high-transmissivity zone. Such an image is useful to increase the probability of finding a high-transmissivity zone. For example, given the borehole data alone, there is an 11% probability of any given cell being in a high-transmissivity zone. However, selecting the white cells in figure 5 improves the probability of finding a high-transmissivity zone by a factor of at least 2.7 (at least a 30% chance). Note that the above does not apply to the apparent artifacts in figure 5, appearing as stray cells far from boreholes. These artifacts are due to the limited number of realizations used.

The ensemble is also used to determine the probability of cells falling within specific zones. Figure 6 shows the region composed of cells that fall within Zone IV in 5 or more realizations. Thus, cells outside this region have less than 10% probability of inclusion in Zone IV.

Flow Modeling Results

Simulated drawdowns at observation wells (fig. 7) based on a realization conditioned to only borehole data do not exhibit the hydraulic behavior characteristic of this flow system (fig. 3). Simulated drawdowns (fig. 8) for a realization conditioned to hydraulic connections and borehole data (fig. 4a) compare more favorably with the field data—borehole intervals connected by a high-transmissivity zone display similar drawdown responses. However, there are still significant differences between the simulated and observed drawdowns—the Zone IV response is late compared with the field data. Presumably such differences are due to either (1) discrepancies between the geometry of high-transmissivity zones in the realization and the true geometry, or (2) variability of hydraulic properties within or between high-transmissivity zones.

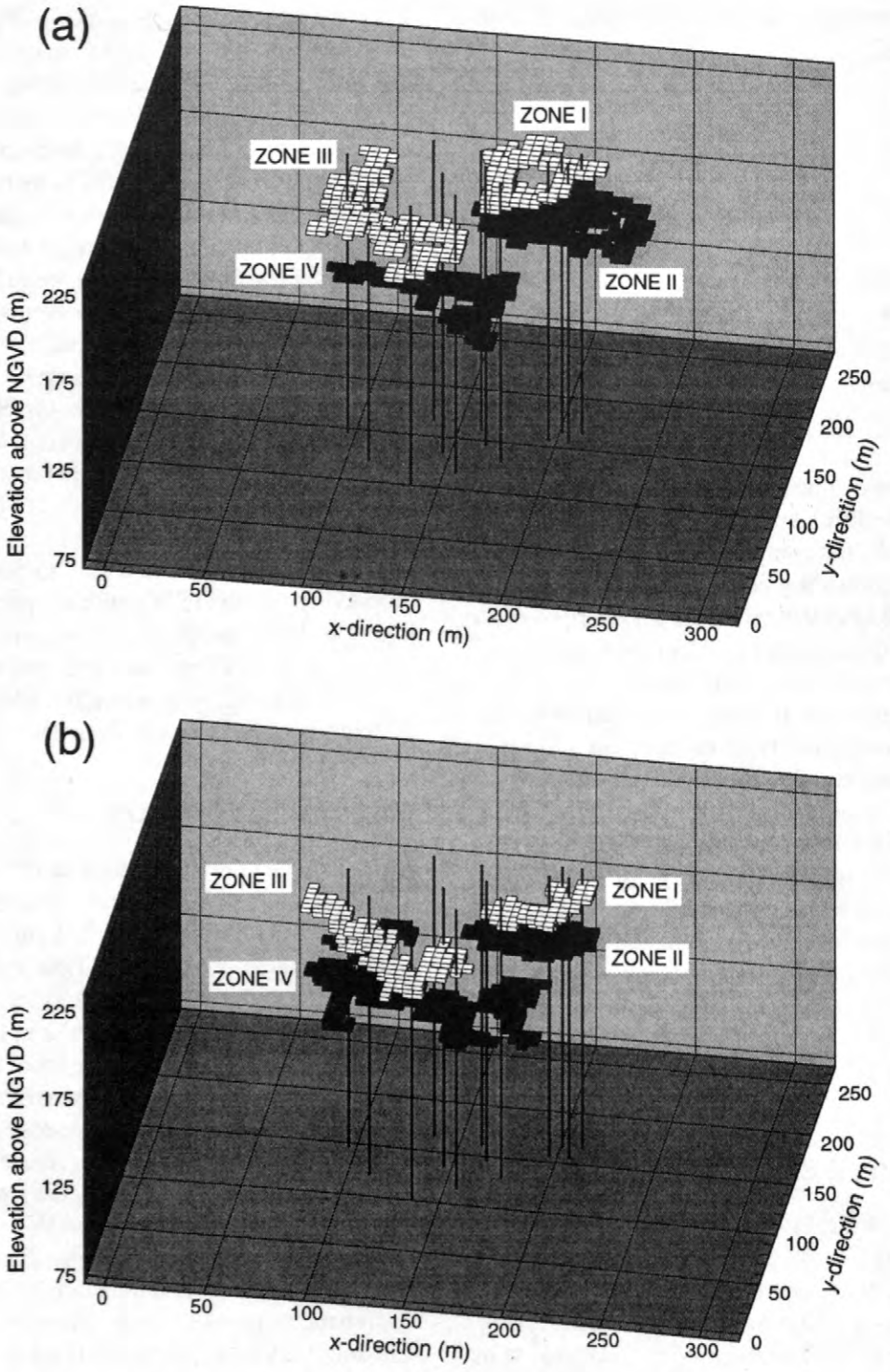

Figure 4. (a) and (b) Two geostatistical realizations of high-transmissivity zones that intersect wells in the FSE well field.

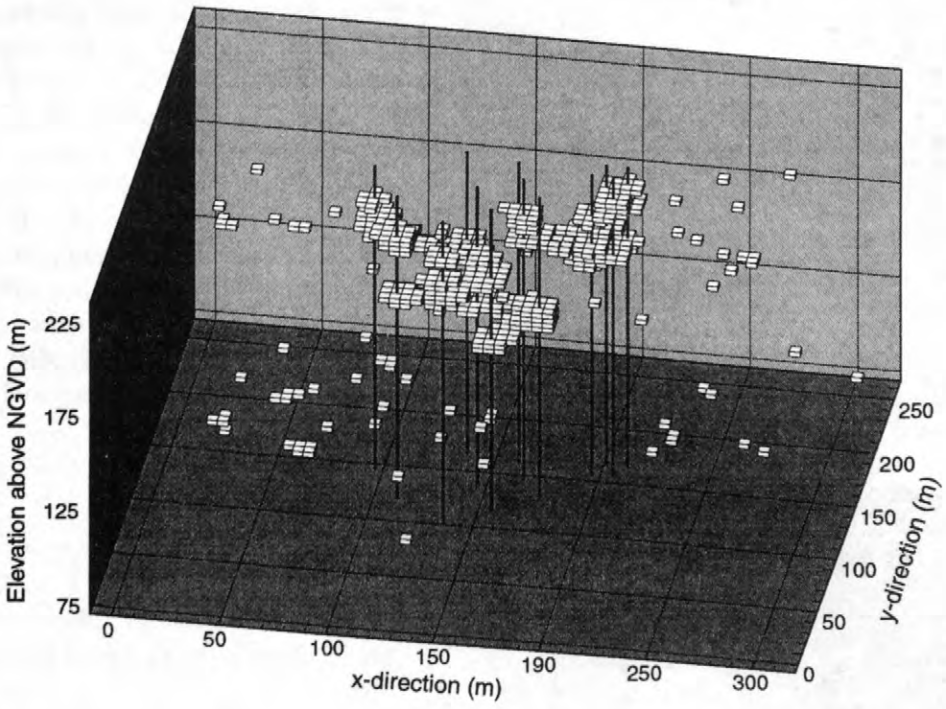

Figure 5. Grid cells with 30% or greater probability of having high transmissivity.

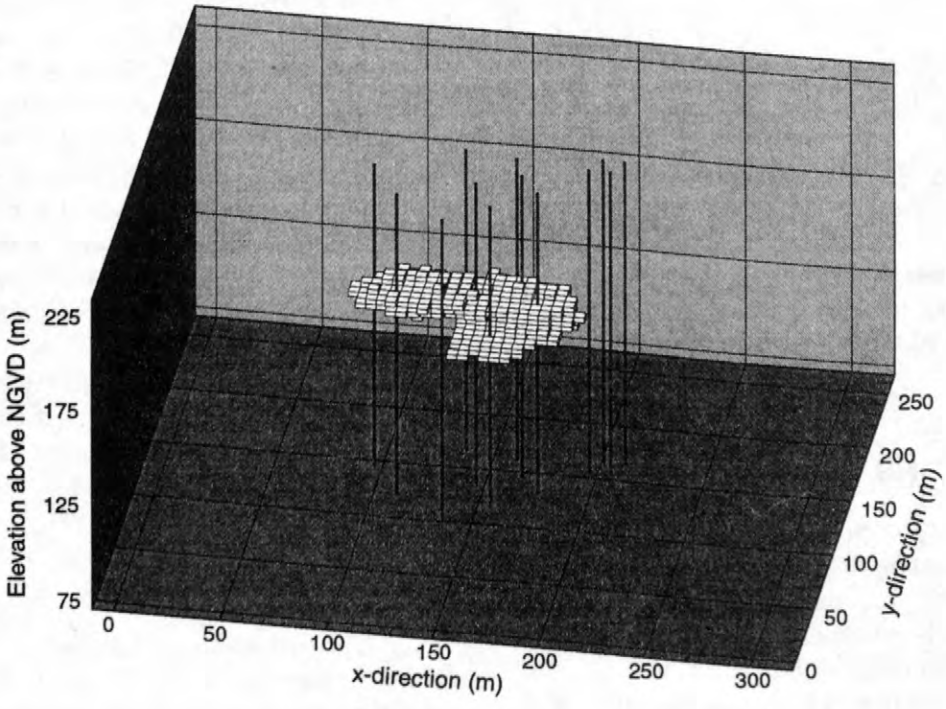

Figure 6. Grid cells with 10% or greater probability of inclusion in Zone IV.

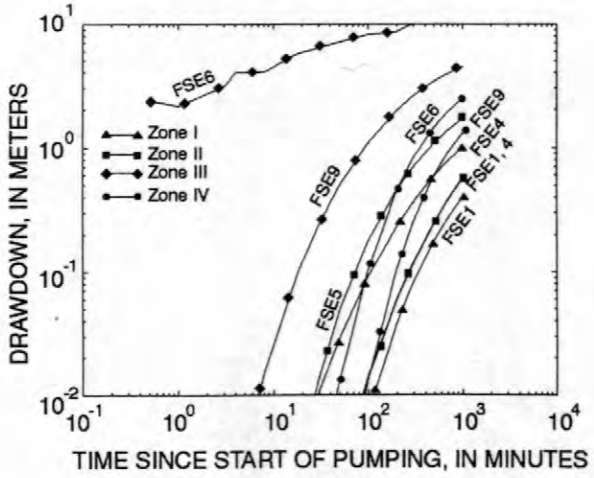

Figure 7. Simulated drawdowns at observation wells for a realization conditioned to borehole data and neglecting hydraulic connections.

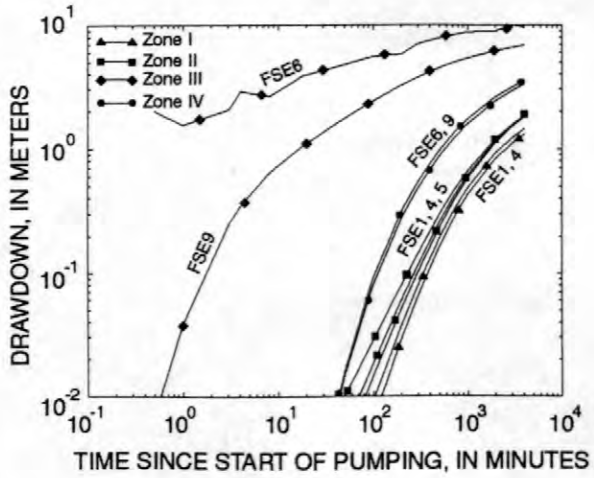

Figure 8. Simulated drawdowns at observation wells for a realization conditioned to borehole data and inferred hydraulic connections.

CONCLUSIONS

A new approach uses a simulated-annealing algorithm to generate geostatistical realizations of high-transmissivity zones conditioned to borehole data and hydraulic connections that intersect boreholes. The method was used to study alternative models of high-transmissivity zones in the bedrock underlying the FSE well field. In general, flow simulations based on realizations conditioned to borehole and connection data compare favorably with the field data. Simulations based on realizations conditioned to borehole data and neglecting inferred connections compare less favorably with the field data. The approach is a fast, efficient use of hydraulic information. Realizations honoring hydraulic connections represent improved starting points for defining high-transmissivity zones and hydraulic properties for further conditioning to hydraulic, tracer or geophysical data. The results of this study will be used in ongoing work involving inverse modeling and the integration of other types of information, including geophysical and tracer data.

REFERENCES

Deutsch, C.V., and Journel, A.J., 1998, GSLIB Geostatistical Software Library and User's Guide: New York, Oxford University Press, 369p.

Goovaerts, P.A., 1997, Geostatistics for Natural Resources Evaluation: New York, Oxford University Press, 483p.

Hsieh, P.A., and Shapiro, A.M., 1996, Hydraulic Characteristics of Fractured Bedrock Underlying the FSE Well Field at the Mirror Lake Site, Grafton County, New Hampshire, Morganwalp, D.W., and Aronson, D.A. eds., U.S. Geological Survey Toxic Substances Hydrology Program—Proceedings of the technical meeting, Colorado Springs, Colorado, September 20-24, 1993: U.S. Geological Survey Water-Resources Investigations Report 94-4015, p. 127-130.

Hsieh, P.A., Shapiro, A.M., and Tiedeman, C.R., 1999, Computer Simulation of Fluid Flow in Fractured Rocks at the Mirror Lake FSE Well Field: this volume.

ACKNOWLEDGMENTS

The first author was supported by EPA STAR Fellowship U-915155-01-0. The first and last authors gratefully acknowledge NSF support through grants numbered EAR-9705812 and EAR-9707031.

AUTHOR INFORMATION

Frederick D. Day-Lewis, Stanford University, Stanford, California (daylewis@geo.stanford.edu)

Paul A. Hsieh, U.S. Geological Survey, Menlo Park, California (pahsieh@usgs.gov)

Allen M. Shapiro, U.S. Geological Survey, Reston, Virginia (ashapiro@usgs.gov)

Steven M. Gorelick, Stanford University, Stanford, California (gorelick@geo.stanford.edu)

Microbial Processes and Down-Hole Mesocosms in Two Anaerobic Fractured-Rock Aquifers

By Don A. Vroblesky, Paul M. Bradley, Jon W. Lane, Jr., and John F. Robertson

ABSTRACT

Aqueous chemistry, hydrogen-gas measurements, and downhole mesocosms were used to characterize the microbial terminal electron-accepting processes in anaerobic fractured-rock aquifers at Montville, Connecticut, and at the Mirror Lake research site, New Hampshire, and to examine the potential for the microbial community to degrade a target contaminant, toluene. At the most contaminated horizon in the petroleum-hydrocarbon-contaminated aquifer at Montville, the terminal electron-accepting process was methanogenesis. At shallower horizons, sulfate- or iron-reduction prevailed. The presence of organic carbon allowed similar depletion of oxygen in ground water at wells CO-11 and RR-1 (Mirror Lake site). At well CO-11, the advective transport of sulfate apparently was rapid enough or sufficient amounts of oxidized iron were available to prevent methanogenic conditions from developing. At well RR-1, however, the lack of more efficient electron acceptors and the increased availability of organic carbon resulted in methanogenic conditions. Downhole mesocosms placed next to fractures in the aquifer were colonized by native bacteria. The mesocosms provided a sampling approach to recover native bacteria and to use the recovered bacteria to examine the potential for contaminant biodegradation.

INTRODUCTION

The redox conditions, or terminal electron-accepting processes (TEAPs), that dominate in a ground-water system can have significant impact on biodegradation rates of many contaminants. For example, Hutchins (1991) showed that biodegradation rates of toluene, o-xylene, and m-xylene were faster under nitrate-reducing conditions than under sulfate-reducing conditions, and Mihelcic and Luthy (1988) showed that degradation of naphthalene and acenaphthalene was faster under denitrifying conditions than under anaerobic conditions in the absence of nitrate. Similarly, Smolenski and Suflita (1987) showed that the rate of biodegradation of several cresol isomers was faster under sulfate-reducing conditions than under methanogenic conditions. These observations indicate that differing anaerobic TEAPs directly affect microbial degradation rates of a variety of organic contaminants in ground water. Therefore, it is important to characterize the microbially mediated TEAPs in contaminated ground-water systems.

Characterization of microbial processes in fractured-rock aquifers (Vroblesky and others, 1997; Yager and others, 1997) has received less attention than in clastic-rock aquifers. This difference is largely a reflection of the extreme difficulty involved in obtaining undisturbed samples of fractured-rock-aquifer material suitable for microbiological investigations. Previous work has involved examining the microbial content of ground water pumped from bedrock wells (Pedersen and Ekendahl, 1990; Stevens and others, 1993); however, the free-living (unattached) bacteria sampled by such methodology constitute an extremely small percentage of the microbial population because most are attached to aquifer material (Hazen and others, 1991; Harvey and Barber, 1992).

To characterize the microbial community more adequately, samples of the aquifer material are needed. In the case of fractured rock, the samples obtained during drilling typically are inadequate because of the disturbances incurred during drilling and because of the small surface area available for colonization in the radius of core.

As part of the ongoing research to investigate microbial activity in fractured-rock aquifers, downhole mesocosms were placed adjacent to fracture zones in anaerobic aquifers for colonization by native bacteria. The mesocosms consisted of autoclaved, sieved (grain size 0.08 to 0.16 in.) crushed granite. The purpose of the mesocosms was to provide recoverable media, similar to the aquifer material, with increased surface area. Upon recovery of the mesocosms, the material was placed in serum vials and amended with a target contaminant for the determination of biodegradation potential.

Downhole mesocosms previously have been used in unconsolidated sediment to examine aquifer microbiology. Introduction of a sediment mesocosm into a well bore has been successfully used to characterize subsurface microbiology in a Coastal Plain aquifer (Hirsch and Rades-Rohkohl, 1990). Similarly, Hiebert and Bennett (1992) lowered rock fragments down a shallow well in an organic-rich sedimentary aquifer and noted microbially related silicate dissolution. To our knowledge, the present investigation represents the first use of a downhole mesocosm to obtain a sample of the native microbial population in a fractured-rock aquifer.

Two anaerobic fractured-rock aquifers were examined during this investigation. One was at a domestic well in Montville, Connecticut. The other was at the U.S. Geological Survey fractured-rock-aquifer research site in Mirror Lake, New Hampshire. An anaerobic aquifer is defined in this report as containing less than 0.5 mg/L of dissolved oxygen (DO).

Ground water in the granitic fractured-rock aquifer in Montville, Connecticut, was contaminated at a depth of about 190 ft with petroleum hydrocarbons from a nearby gasoline station. Shallower horizons in the aquifer appear to be substantially less contaminated (Aaron Green, Connecticut Department of Environmental Protection, written commun., 1997). Ground water in the wells tested for this investigation (CO-11 and RR-1) at the Mirror Lake site contained total organic carbon (TOC) from an unknown source. The bedrock at the Mirror Lake site consists of schist, granite, pegmatite, and lamprophyre (Tiedeman and others, 1997).

METHODS

Laboratory and field methods (Chapelle and others, 1996) can be used to determine the rate at which native subsurface microbes can degrade target contaminants and, therefore, to estimate the potential for natural attenuation. These methods are difficult, however, in fractured-rock systems. Field methods involve examining changes in water chemistry along ground-water flow paths, and flow paths are not easily defined in fractured-rock systems. Laboratory methods involve recovering a sample of aquifer material; however, the samples obtained during drilling in fractured-rock typically are inadequate for microbial investigations.

Downhole mesocosms were placed adjacent to fracture zones for colonization by native bacteria. Upon recovery of the mesocosms, the material was placed in serum vials and amended with a target contaminant, toluene. The biodegradation potential was determined by observing the rate of contaminant depletion or end-product accumulation.

At the Montville site, the mesocosm used in this investigation was attached to pump tubing. The mesocosm was placed adjacent to fracture zones in an open borehole at a depth of 190 ft in March 1998. The mesocosm was recovered in July 1998. Previous packer tests implied that there was an upward component of flow in the open borehole (Aaron Green, Connecticut Department of Environmental Protection, written commun., 1997). Because the deepest major fracture zone in the borehole was at a depth of about 190 ft, the ground water in contact with the mesocosm at 190 ft was representative of the ground water in the adjacent fracture system.

The mesocosm was recovered prior to collecting water samples. To collect water samples, a positive-displacement pump, fixed between two polyvinyl chloride (PVC) straddle packers, was lowered into the well to bracket the target horizons. The packed interval was 6.6 ft. Water samples were collected from horizons centered at 61-, 106-, 133-, and 190-ft depths as in

March (prior to mesocosm installation) and July 1998.

Mesocosm recovery at the Montville site consisted of detaching the mesocosm from the pump tubing, wrapping it in flame-sterilized aluminum foil, and transferring it to a helium-filled glove bag. Mesocosm substrate then was transferred into flame-sterilized mason jars, purged with helium, and capped.

Part of the recovered water that was collected was added to the mesocosm samples. Water for this purpose was first collected in flame-sterilized mason jars, and helium was bubbled through the water sample to remove volatile organic compounds (VOCs) and sulfide. Under aerobic conditions, the jar then was capped and shaken to aerate the sample; then it was allowed to set for several hours to facilitate iron-oxide precipitation. The water then was filtered through sterile 0.45 micrometer porous-membrane syringe filters to remove particulate iron. To remove dissolved oxygen introduced during the agitation phase, the sample was bubbled with helium. Finally, the water was added to the mesocosm substrate, collected earlier, in a glove bag under helium headspace. The jars were capped and chilled until analysis.

Mesocosms were collected at the Mirror Lake site by withdrawing the packer assemblies and attached mesocosms. Mesocosms were transferred to mason jars and were purged with nitrogen prior to sealing. The samples were chilled until analyzed.

At the Mirror Lake site, a downhole mesocosm was installed adjacent to transmissive fractures in well CO-11, at the Mirror Lake site, in August 1996. The mesocosms were isolated in intervals separated by straddle packers. The packed intervals were at depths of 40.5 to 233.4 ft, 235.7 to 259.4 ft, and 261.7 to 603 ft. The uppermost packed interval at well CO-11 contained a highly transmissive fracture at a depth of 104 ft and moderately transmissive fractures at a depth of 135 to 150 ft and at 212 ft. The middle packed interval contained a highly transmissive fracture zone at a depth of 240 to 256 ft. The lowermost packed interval contained a moderately transmissive fracture zone at a depth of 340 to 360 ft, and the mesocosm used in this investigation was placed at a depth of 350 ft in August 1996 (P.A. Hsieh, U.S. Geological Survey, written commun., 1997).

One packed interval (430.7 to 602 ft depth) was tested in well RR-1, at the Mirror Lake site. The interval contained a highly transmissive fracture at about 575 ft (P.A. Hsieh, written commun., 1997). A mesocosm was placed in the well at a depth of 570 ft.

At the Mirror Lake site, the packed intervals were sampled, and the mesocosms were recovered in July 1997. Water samples also were collected during an earlier sampling event in August 1995. Sampling consisted of lowering the intake of a positive-displacement sampling pump to the target fracture through the packers. The interval was pumped until drawdown stabilized in the packed interval (as measured with an electric water-level indicator), and then pumped to remove an additional 5 to 10 gal. The pumping rate then was reduced, and water samples were collected. Mesocosms were collected following water sampling.

At all sites, ferrous iron [Fe(II)] concentration was measured in the field using the Hach colorimeter/FerroZine method (Stookey, 1970). Ground-water temperature and pH were measured in the field. Suflide was measuerd by colorimetric method. The DO concentration in ground water was determined in the field by the CHEMets colorimetric method at the Montville well and by a Winkler titration at well RR-1 (Mirror Lake site). The DO measurement from well CO-11 was determined in the laboratory (A.M. Shapiro, U.S. Geological Survey, written commun., 1998).

Water samples for analysis of VOCs were collected following established U.S. Environmental Protection Agency (USEPA) protocols. All sample bottles were sealed with Teflon-lined bottle caps. The water samples for VOCs were analyzed using USEPA method 8240 (U.S. Environmental Protection Agency, 1986). Water samples for TOC were analyzed by USEPA method 415.1 (U.S. Environmental Protection Agency, 1983).

To determine methane and dissolved inorganic carbon (DIC) concentrations, a 5-mL water sample was collected by using a clean syringe and injected into septated vials through a 0.45- μm porous-membrane filter. The vials were rinsed with filtered sample water prior to sample collection. The samples were stored on ice until analyzed. Methane was quantified by thermal-conductivity-detection gas chromatography.

Dissolved methane concentrations were calculated using Henry's Law coefficients (Stumm and Morgan, 1996). The DIC samples were acidified in the laboratory with a 42.5 percent phosphoric acid solution, and concentrations were quantified by thermal-conductivity-detection gas chromatography. Sample DIC concentrations were corrected for atmospheric carbon dioxide (CO_2) present in sample-free blanks collected in the field.

Water samples for analysis of inorganic ions were collected in sample-rinsed polyethylene bottles after passing through a 0.45-μm porous-membrane filter. The inorganic ion samples were packed in ice immediately following collection. The samples were analyzed for calcium (method 215.1), magnesium (method 242.1), sulfate (method 375.4), and nitrate (method 352.1) (U.S. Environmental Protection Agency, 1983). Anions were analyzed using ion-exchange chromatography with chemical suppression [method 300.0 (U.S. Environmental Protection Agency, 1983)].

A ground-water hydrogen-gas (H_2) sample was collected from selected intervals using the bubble-strip method of Chapelle and McMahon (1991). Dissolved hydrogen gas was measured using a gas chromatograph (GC) equipped with a reduction gas detector. The detection limit of this method ranged from 0.1 to 0.5 nanomole per liter (nM). All dissolved H_2 samples were collected in duplicate.

Hydrogen-gas analysis has been used to document the zonation of TEAPs in various systems by Chapelle and Lovley (1990; 1992), Chapelle and McMahon (1991), and Vroblesky and Chapelle (1994). These studies concluded that characteristic dissolved H_2 concentrations were 5 to 25 nM for methanogenesis, 1 to 4 nM for sulfate reduction, and 0.1 to 0.8 nM for ferric iron [Fe(III)] reduction.

The ability of microorganisms to mineralize acetate and toluene under various TEAPs was evaluated using radiolabelled [1-^{14}C] acetate and uniformly-labeled [UL]-^{14}C toluene (Sigma Chemical Co., St. Louis). The reported radiochemical purities of the [1-^{14}C] acetate and [UL]-^{14}C toluene were 98.5 percent. The chemical purity of both test substrates was independently confirmed by gas chromatography/flame ionization detection and mass spectrometry to be 99 percent.

Laboratory microcosms consisted of 20-mL serum vials, which were amended with 15 g of saturated granite substrate from the mesocosms (water content = 20 percent weight/weight) and sealed with Teflon-lined butyl rubber stopper/base trap assemblies (Bradley and Chapelle, 1996). Anaerobic microcosms were created with a head space of 100 percent helium and amended with 1.0 mL of anoxic, sterile distilled water (unamended treatment) or 1.0 mL of an anoxic, sterile Fe-EDTA (iron-reducing treatments), or magnesium sulfate ($MgSO_4$)(sulfate-reducing treatment). The final dissolved concentration of sulfate and Fe-EDTA in the sulfate- and iron-reducing microcosms was 1 millimole per liter. Killed controls were prepared in the same manner and autoclaved twice for 1 hour at 15 lb/in^2 and 121°C. The absence of oxygen was confirmed in all anaerobic microcosms initially and at the end of the study by headspace analysis using thermal-conductivity-detection gas chromatography. Production of dissolved iron and sulfide was confirmed in iron-reducing and sulfate-reducing treatments, respectively, by spectrophotometric analyses using colorimetric test kits (Hach Company, Loveland, Colorado).

Triplicate experimental microcosms and duplicate killed controls were prepared for each granite substrate and each terminal electron-accepting treatment. The microcosms were pre-incubated 5 days to acclimate the indigenous microorganisms to the various electron-acceptor amendments. To begin the experiments, approximately 200,000 disintegrations per minute (DPM) of [1-^{14}C] acetate or [UL]-^{14}C toluene was injected below the surface of the saturated sediments. To sample, the base traps of individual microcosms were rinsed with 0.5 mL of sterile distilled water and filled with 0.3 mL of 3 molar potassium hydroxide (KOH). After a 24-hour collection period, the KOH was removed and the amount of trapped radiolabelled carbon dioxide ($^{14}CO_2$) was quantified by scintillation counting.

Granite-substrate microcosms were incubated in the dark at room temperature for up to 8 days. Production of $^{14}CO_2$ was confirmed in select vials by addition of barium chloride as described previously (Davis and Carpenter, 1990; Bradley and Chapelle, 1996). The fact that no radioactivity was detected in the base traps of sterile serum vials, which contained radiolabeled substrate but no granite substrate, indicates that

trapping of radiolabeled acetate and toluene was not significant (less than 1 percent) in experimental microcosms. The amount of radioactivity initially present in the experimental microcosms as $^{14}CO_2$ was estimated based on the percentage recovery observed in killed and sediment-free control microcosms to be less than 1 percent of the total radioactivity added as acetate or toluene. The $^{14}CO_2$ production data were corrected for the recovery efficiency of $H^{14}CO_3^-$ and the amount of radioactivity present initially in sediment microcosms (less than 1 percent). The recovery efficiency was consistent (62±3 percent) but relatively low due to the circum-neutral pH of the interstitial water and the non-sacrificial (no acidification) recovery method employed in this study.

RESULTS AND DISCUSSION

At the Montville well, borehole flowmeter data (fig. 1A) show that water enters the borehole through fractures at depths of about 70 ft, 130 ft, and 195 ft in response to pumping from near the water-table surface. Thus, these probably are the most permeable fracture zones. Although most of the fractures appear to dip at high angles, some fractures at about 190 ft are approximately horizontal (fig. 1B). The 190-ft horizon is also the zone contributing the most contaminants to the well (figs. 1C and 1D). Thus, the horizontal fractures may facilitate lateral transport of contaminants in this system.

All intervals tested at the Montville well were anaerobic. The concentration of H_2 (19 nM) from 190 ft was in the range characteristic of methanogenesis (fig. 2A). This interpretation (fig. 2B) is consistent with the presence of high methane and low sulfate concentrations from that zone (fig. 2A).

The H_2 concentrations from the 106-ft (3.0 nM) and 133-ft horizons (0.6 nM) imply that the predominant TEAPs were sulfate reduction and iron reduction, respectively (figs. 2A and 2C). Although a H_2 measurement was not taken from the 70-ft horizon, the high sulfide concentration implies that sulfate reduction was the predominant TEAP (figs. 2B and 2C). Lower sulfide concentrations elsewhere probably are the result of iron sulfide precipitation.

These data imply that the TEAP zones in this contaminated fractured-rock well vary substantially with depth (fig. 2C). The controlling factor driving methanogenesis in the deeper part of the aquifer is the presence of oxidizable petroleum-hydrocarbon contamination. At shallower horizons, the presence of greater than 10 mg/L of sulfate maintains sulfate-reducing conditions in this anaerobic system, except where oxidized iron apparently is present in sufficient amounts to maintain iron reduction.

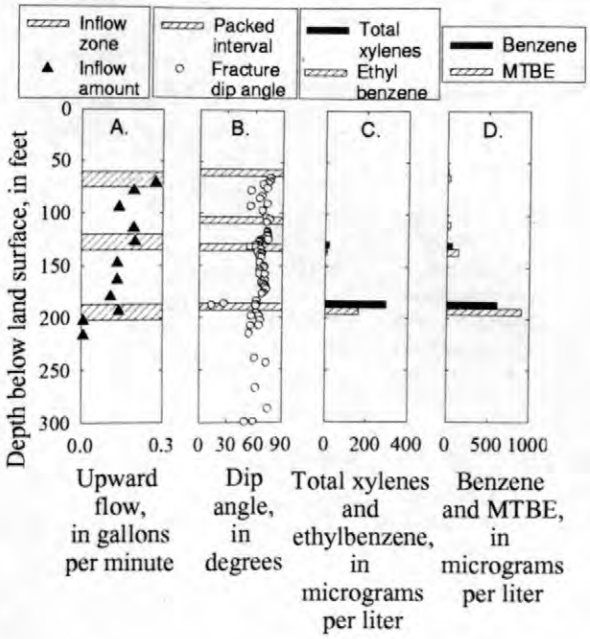

Figure 1. Bore-hole flowmeter response to shallow pumping (A), packed intervals and fracture dip angles interpreted from borehole televiewer data (J.W. Lane, U.S. Geological Survey, written commun., 1997) (B), concentrations of total xylenes and ethylbenzene (C), and benzene and methyl *tert*-butyl ether (MTBE) (D) in ground water, Montville well, March 1998.

Ground water at wells CO-11 and RR-1, at the Mirror Lake research site in New Hampshire, also was anaerobic. The ground water at those sites contained TOC from an unknown source. Well CO-11 contained 2.3 mg/L of TOC at both the middle and deeper horizons in August 1995. Ground water from well RR-1 contained 18.8 mg/L of TOC in August 1995 (sampling interval

was 582 to 596 ft depth) and 45.3 mg/L of TOC in July 1996 (sampling interval was 430.7 to 602 ft depth).

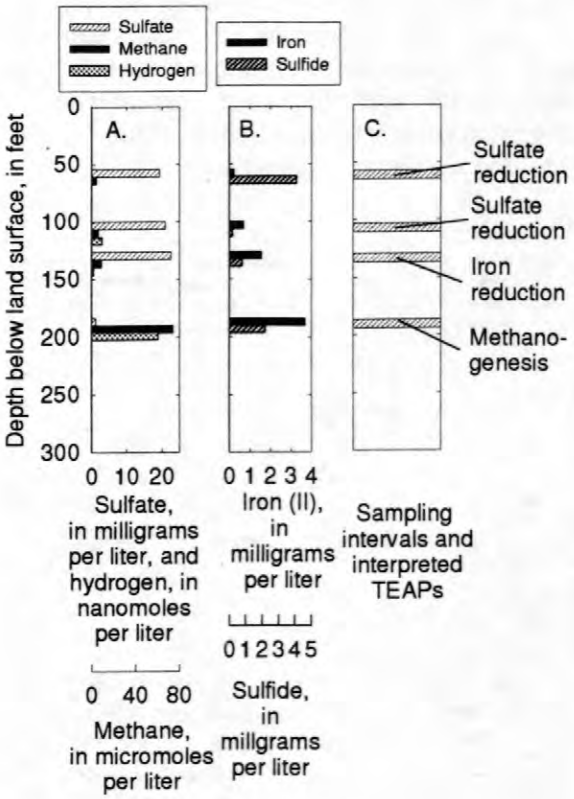

Figure 2. Concentrations of sulfate, hydrogen gas, methane (A), ferrous iron, and sulfide (B) in ground water and the interpreted terminal electron-accepting process (C), Montville well, March 1998.

At the deepest interval in well CO-11, the ground-water H_2 concentration (1.9 nM) was in the range of characteristic of sulfate reduction, and 18 mg/L of sulfate was present (fig. 3A), implying that the predominant TEAP was sulfate reduction (fig. 3B). No H_2 data were collected from the shallowest horizon; however, the presence of 15 mg/L of sulfate (fig. 3A) and 6.6 mg/L of sulfide (the highest concentration measured in well CO-11) imply that sulfate reduction was also the predominant TEAP in that horizon. The H_2 concentration in the middle horizon (0.8 nM) was in the range characteristic of iron reduction (fig. 3A), although low concentrations of sulfide (2.7 mg/L) also were present. Thus, the probable predominant TEAP in the middle horizon was iron reduction, although there may be some sulfate-reducing activity within the sampled horizon (fig. 3B).

If sufficient amounts of oxidizable organic compounds were added to this system, such as in the event of a petroleum spill, then the potential exists for consumption of the electron donor (organic compounds) to outpace the advective delivery of an electron acceptor (sulfate). In such a case, the microbial processes probably would shift from sulfate reduction to methanogenesis, a less efficient petroleum-hydrocarbon degradation process.

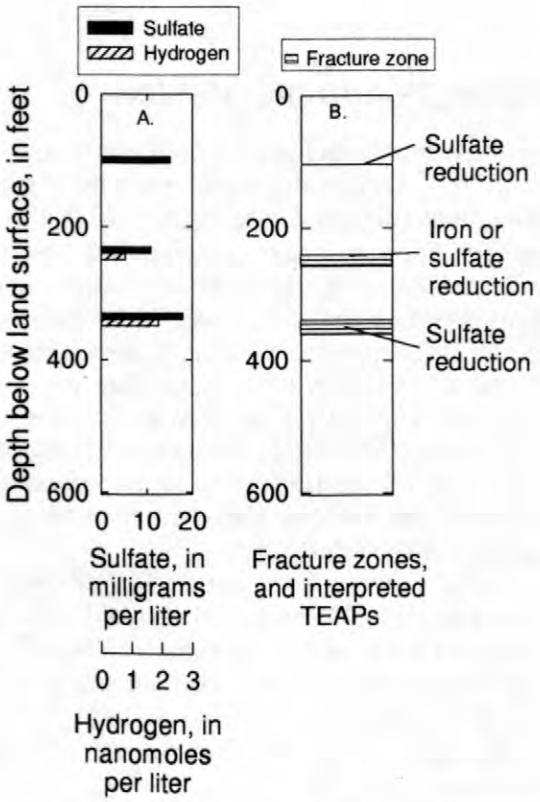

Figure 3. Concentrations of (A) sulfate and hydrogen in ground water and (A) locations of dominant fracture zones and interpreted terminal electron-accepting processes, well CO-11, Mirror Lake research site, NH, July 1997.

The second well (RR-1) tested at the Mirror Lake research site provides an example of the aquifer under conditions of higher organic-carbon

concentration than at well CO-11. Substantially TOC was available in the aquifer at well RR-1 (19-50 mg/L) than at well CO-11 (2-3 mg/L). In addition, the aquifer at well RR-1 contained very little sulfate (less than 0.5 mg/L). The comparitive lack of sulfate probably is caused by increased amounts of sulfate reduction driven by the increased availability of an electron donor (TOC). The lack of sulfate and oxygen, and the presence of 6,730 μM of methane imply that the predominant TEAP in the fracture zone at well RR-1 was methanogenesis. The electron-accepting conditions at well RR-1 probably represent the fate of the aquifer at well CO- 11 if more organic compounds, such as petroleum hydrocarbons, were present at well CO-11.

The data from this investigation show that microbial processes were active anaerobic fractured-rock systems with available organic carbon. In the Montville well, the predominant electron-accepting process varied significantly over distances of less than 100 ft. In Montville, the presence of petroleum hydrocarbons drove the microbial processes to methanogenesis by depleting all of the more efficient electron acceptors. At the Mirror Lake site, the presence of organic carbon allowed microbial processes to deplete the DO. At well CO-11, the advective transport of sulfate apparently was rapid enough or sufficient amounts of oxidized iron were available to prevent methanogenic conditions from developing. At well RR-1, however, the apparent lack of more efficient electron acceptors and the increased availability of organic carbon resulted in methanogenic conditions. The vertical variation in microbial processes at the Montville well indicates the need to use packer systems to isolate individual fracture zones of interest when investigating microbial processes in contaminated fractured-rock aquifers.

Analysis of the downhole mesocosms provided evidence of colonization by microbes characteristic of the in-situ microbial community. The ability of mesocosm microbes from well CO-11 (350-ft depth) to degrade toluene was nearly identical under unamended and sulfate-reducing treatments, but was significantly different than the rate under iron-reducing treatments (fig. 4). Because the field-derived predominant TEAP for that horizon was sulfate-reduction, the data show that the mesocosm microbes reflect the predominant TEAP for in-situ conditions.

In the methanogenic contaminated horizon at the Montville well, the unamended treatment (methanogenesis) produced significantly higher initial toluene degradation rates than the sulfate-reducing treatment (fig. 5). These data suggest that, despite the more efficient ability of sulfate reducers to oxidize organic compounds, the relative abundance of methanogenic bacteria in the contaminated horizon makes toluene degradation more rapid under methanogenic conditions than sulfate-reducing conditions.

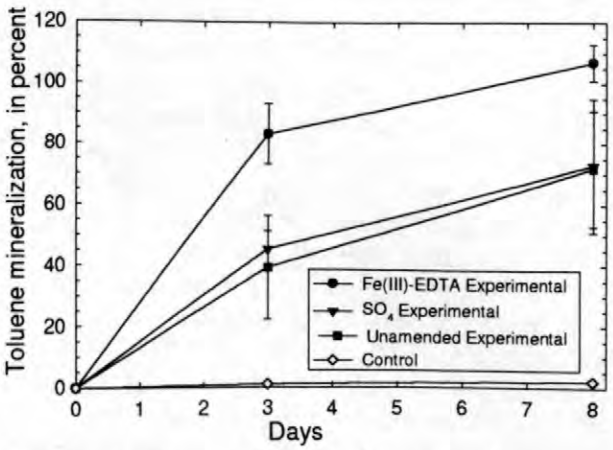

Figure 4. Toluene mineralization rates of mesocosm microbes collected from a depth of 350 ft adjacent to a fracture zone, well CO-11, Mirror Lake research site, NH, July 1997.

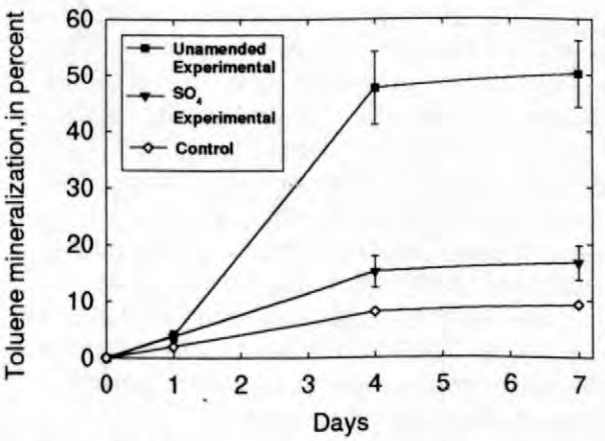

Figure 5. Toluene mineralization rates of mesocosm microbes collected from a depth of 190 ft adjacent to a petroleum-hydrocarbon-contaminated fracture zone, Montville well, July 1998.

SUMMARY AND CONCLUSIONS

A variety of approaches were used to characterize the microbial TEAPs in fractured-rock aquifers and to examine the potential for the microbial community to degrade a target contaminant, toluene. The predominant electron-accepting process varied significantly over vertical distances of less than 100 feet in a petroleum-hydrocarbon contaminated well (Montville). At the most contaminated horizon in the fractured-rock well, the presence of petroleum hydrocarbons drove the microbial processes to methanogenesis by depleting all of the more efficient electron acceptors. At shallower horizons, sulfate- or iron-reduction prevailed. The high degree of vertical variation in microbial processes indicates the need to use packer systems to isolate individual fracture zones of interest when investigating microbial processes in contaminated fractured-rock aquifers.

Similar depletion of oxygen was observed in the aquifer at wells CO-11 and RR-1 at the Mirror Lake site. The presence of TOC apparently allowed microbial depletion of DO. At well CO-11, the advective transport of sulfate apparently was rapid enough or sufficient amounts of oxidized iron were available to prevent methanogenic conditions from developing. At well RR-1, however, the apparent lack of more efficient electron acceptors and the increased availability of organic carbon resulted in methanogenic conditions.

Laboratory analysis of the mesocosm from well CO-11 showed that the toluene biodegradation rate by mesocosm microbes was nearly identical under unamended and sulfate-reducing conditions, but was significantly different than the rate under iron-reducing treatments. Because the field-derived predominant TEAP for that horizon was sulfate-reduction, the data show that the mesocosm microbes reflect the predominant TEAP for in-situ conditions. These data support the hypothesis that the mesocoms had been colonized by bacteria native to the fractured-rock aquifer.

In the methanogenic contaminated horizon at the Montville well, the unamended treatment (methanogenesis) produced significantly higher initial toluene degradation rates than the sulfate-reducing treatment. These data suggest that despite the more thermodynamically efficient ability of sulfate reducers to oxidize organic compounds, the relative abundance of methanogenic bacteria in the contaminated horizon makes toluene degradation more rapid under methanogenic conditions than sulfate-reducing conditions.

REFERENCES

Bradley, P.M., and Chapelle, F.H., 1996, Anaerobic mineralization of vinyl chloride in Fe(III)- reducing, aquifer sediments: Environmental Science and Technology, v. 30, p. 2084-2086.

Chapelle, F.H., and Lovley, D.R., 1990, Hydrogen concentrations in ground water as an indicator of bacterial processes in deep aquifer systems: Proceedings of the First International Symposium on the Microbiology of the Deep Subsurface, U.S. Environmental Protection Agency, Orlando, Florida, p. 23.

_____ 1992, Competitive exclusion of sulfate reduction by Fe(III)-reducing bacteria: A mechanism for producing discrete zones of high-iron ground water: Ground Water, v, 30, p. 29-36.

Chapelle, F.H., Bradley, P.M., Lovley, D.R., and Vroblesky, D.A., 1996, Measuring rates of biodegradation in a contaminated aquifer using field and laboratory methods: Ground Water, v. 34, no. 4, p. 691-698.

Chapelle, F.H., and McMahon, P.B., 1991, Geochemistry of dissolved inorganic carbon in a coastal plain aquifer: Sulfate from confining beds as an oxidant in microbial CO2 production, Journal of Hydrology, v. 127, p. 85-108.

Davis, J.W., and Carpenter, C.L., 1990, Aerobic biodegradation of vinyl chloride in groundwater samples: Applied and Environmental Microbiology, v. 56, p. 3870-3880.

Harvey, R.W., and Barber, L.B. II, 1992, Associations of free-living bacteria and dissolved organic compounds in a plume of contaminated ground water: Journal of Contaminant Hydrology, v. 9, p. 91-103.

Hazen, T.C., Jimeniz, Luis, Lopez de Victoria, Geralyne, and Fliermans, C.B., 1991, Comparison of bacteria from deep subsurface

sediment and adjacent ground water: Microbial Ecology, v. 22, p. 293-304.
Hiebert, F.K., and Bennett, P.C., 1992, Microbial control of silicate weathering in organic-rich ground water: Science, v. 258, p. 278-281.
Hirsch, Peter, and Rades-Rohkohl, Ellen, 1990, Microbial colonization of aquifer sediment exposed in a ground water well in northern Germany: Applied and Environmental Microbiology, v. 56, p. 2963-2966.
Hutchins, S.R., 1991, Biodegradation of monoaromatic hydrocarbons by aquifer microorganisms using oxygen, nitrate, or nitrous oxide as the terminal electron acceptor: Applied and Environmental Microbiology, v. 57, p. 2403-2407.
Mihelcic, James, and Luthy, R.G., 1988, Degradation of polycyclic aromatic hydrocarbon compounds under various redox conditions in soil-water systems: Applied and Environmental Microbiology, v. 54, p. 1182-1187.
Pedersen, Karsten, and Ekendahl, Susanne, 1990, Distribution and activity of bacteria in deep granitic ground waters of southeastern Sweden: Microbial Ecology, v. 20, p. 37-52.
Smolenski, W.J., and Suflita, J.M., 1987, Biodegradation of cresol isomers in anoxic aquifers: Applied and Environmental Microbiology, v. 53, p. 710-716.
Stevens, T.O., McKinley, J.P., and Fredrickson, J.K., 1993, Bacteria associated with deep, alkaline, anaerobic ground waters in southeast Washington: Microbial Ecology, v. 25, p. 35-50.
Stookey, L.L., 1970, FerroZine, a new spectrophotometric reagent for iron: Analytical Chemistry, v. 42, p. 779-781.
Stumm, Werner, and Morgan, J.J., 1996, Aquatic chemistry (3rd ed.): John Wiley and Sons, New York, 1022 p.
Tiedeman, C.R., Goode, D.J., and Hsieh, P.A., 1997, Numerical simulation of ground-water flow through glacial deposits and crystalline bedrock in the Mirror Lake area, Grafton County, New Hampshire: U.S. Geological Survey Professional Paper 1572, 50 p.
U.S. Environmental Protection Agency, 1983, Methods for chemical analysis of water and waste, EPA-600/4-79-020: U.S. Environmental Protection Agency, Washington, D.C.
_____ 1986, Test methods for evaluating solid waste, Physical/chemical methods, SW-846 (3rd ed.): U.S. Environmental Protection Agency, Washington, D.C., 1919 p.
Vroblesky, D.A., and Chapelle, F.H., 1994, Temporal and spatial changes of terminal electron-accepting processes in a petroleum-hydrocarbon-contaminated aquifer and the significance for contaminant biodegradation: Water Resources Research, v. 30, no. 5, p. 1561-1570.
Vroblesky, D.A., Bradley, P.M., Lane, J.W. Jr., and Robertson, J.F., 1997, Transport and transformations of chlorinated-solvent contamination in a saprolite and fractured-rock aquifer near a former wastewater-treatment plant, Greenville, South Carolina: U.S. Geological Survey Water-Resources Investigations Report 97-4003, 76 p.
Yager, R.M., Bilotta, S.E., Mann, C.L., and Madsen, E.L., 1997, Metabolic adaption and in situ attenuation of chlorinated ethenes by naturally occurring microorganisms in a fractured dolomite aquifer near Niagara Falls, New York: Environmental Science and Technology, v. 31, no. 11, p. 3188-3147.

AUTHOR INFORMATION

Don A. Vroblesky is a geochemist with a Ph.D. from George Washington University. Paul M. Bradley is a microbial ecologist with a Ph.D. from the University of South Carolina. John F. Robertson, is a hydrologist with bachelor's degree from the University of North Carolina. All authors are currently employed at the U.S. Geological Survey in Columbia, South Carolina.

Bedrock Geologic Framework of the Mirror Lake Research Site, New Hampshire

By William C. Burton, Thomas R. Armstrong, and Gregory J. Walsh

ABSTRACT

The geology of the Hubbard Brook watershed in the vicinity of Mirror Lake, New Hampshire consists of metasedimentary rocks of the Silurian Rangeley and Perry Mountain Formations that have been intruded by Devonian granite and Cretaceous-Jurassic lamprophyre dikes. The metasedimentary rocks were affected by at least three episodes of deformation in the Devonian Acadian orogeny. The dominant regional foliation is second-generation (S2) and formed during metamorphic conditions that produced sillimanite-muscovite and sillimanite-kspar mineral assemblages. Both lithologic contacts and the S2 foliation trend east-west to northeast and dip steeply northward in the vicinity of the CO and FSE well fields. Dikes of Devonian granite cut contacts and S2 and appear to be syn-D3. The well fields and the nearby I-93 roadcut appear to be in a zone of more abundant granitic rocks than areas farther west up the watershed, where granite dikes and migmatite are rare. Steeply-dipping fractures in outcrops near the eastern boundary of the Hubbard Brook watershed show a northeast preferred orientation, in agreement with subsurface fracture orientations in the CO well field, whereas the area to the northwest of the well fields has fractures with a northwest preferred orientation. Both lithologic and fracture-orientation data suggest that the geology of the Mirror Lake research site is not representative of areas elsewhere in the watershed.

INTRODUCTION

Since 1990, Mirror Lake, New Hampshire has been the site of hydrologic research by the USGS on the flow of ground water in fractured bedrock; yet until recently little has been published on the regional bedrock geology. In 1997, Barton published the first detailed bedrock geologic map of the area, using as a base the 1:12,000-scale topographic map prepared in 1956 by the U.S. Forest Service for the Hubbard Brook Experimental Forest, which encompasses most of the Hubbard Brook watershed. The map of Barton (1997) shows the eastern part of the watershed to be underlain mostly by metasedimentary rocks of the Silurian Rangeley Formation, which he subdivided into an upper and lower member in accord with the regional geologic mapping of Lyons and others (1997). Three other Silurian metasedimentary units stratigraphically above the Rangeley, the Perry Mountain, Smalls Falls, and Madrid Formations, are also shown on his map, as well as bodies of two generations of Devonian granite and mafic Cretaceous-Jurassic dikes.

Our study was undertaken for the following reasons: 1) to ascertain whether the area might have a greater number of mappable lithologic units than shown on Barton's (1997) map, and to verify the stratigraphically higher formations shown on the map; 2) to have sufficient data to draw a geologic cross-section through the Mirror Lake research site that shows the regional structure; 3) to gather more data on brittle fracture distribution and orientation; and 4) to assess the degree to which the subsurface lithologies, ductile structures, and fractures observed at the two Mirror Lake well fields correlate with the geology of the surrounding

region. One of the main goals of the fractured-rock research at Mirror Lake is that it be transferable to other areas, and our work is aimed towards that goal.

This paper summarizes the results of our first season of mapping (summer, 1998), which was concentrated around Mirror Lake and the east end of the Hubbard Brook watershed using the same 1:12,000-scale base map as Barton (1997). Measurements were made of the penetrative ductile structures such as foliation and fold axes, and of conspicuous fractures, which are mostly joint faces. Detailed fracture analysis of the kind conducted on the I-93 roadcut (Barton, 1997; Hsieh and others, 1993) was not attempted in our regional-scale investigation.

BEDROCK LITHOLOGY

Mirror Lake and the eastern portion of the Hubbard Brook watershed are underlain by high-grade metasedimentary rocks of the Rangeley and Perry Mountain Formations, which have been intruded by small elongate bodies of Devonian granite and Cretaceous-Jurassic mafic dikes (Fig. 1). Much of the Rangeley Formation exposed in the area consists of medium-grained, weakly layered schists which are subdivided into lithologic map units on the basis of subtle differences in modal mineralogy, texture, and layering characteristics (Units Srq, Srg, Srs, Srr, Srbs, Fig. 1). The uppermost Rangeley (Units Srlg, Srgm, Srgs, Srgg, Fig. 1) and Perry Mountain (Units Spqr, Spbg, and Sprg, Fig. 1) rocks consist of well-layered schists, quartzites, and granofels that locally exhibit graded bedding.

Despite the extensive deformation and metamorphic recrystallization of the region, the rocks exposed in the eastern Hubbard Brook watershed appear to correlate with the Rangeley-Perry Mountain type section exposed in western Maine for the following reasons: 1) the more pelitic composition of the Rangeley compared to the Perry Mountain; 2) the transitional increase of quartz-rich layers at the Rangeley-Perry Mountain contact; and 3) the presence of "slow" graded beds in the Rangeley versus "quick" graded beds in the Perry Mountain (Moench and Boudette, 1987; R. Moench, oral comm., 1998). Graded beds in the rocks of the Perry Mountain Formation indicate that the stratigraphy youngs from north to south across the field area.

The metasedimentary rocks are intruded by small (outcrop-scale) elongate bodies or dikes of medium- to coarse-grained, two-mica granite and pegmatite of probable Devonian age (Dg, Fig. 1) that were mapped by Barton (1997) as 370-365 Ma Devonian Concord Granite. The dikes are only weakly foliated and intrude across lithologic contacts (Fig. 1), and in some places cut at high angles the regional penetrative S2 foliation (Fig. 2). They generally trend northeast, locally subparallel to regional S3 foliation or the axial traces of F3 folds (Fig. 2), suggesting that they are roughly contemporaneous with the weaker regional D3 deformation. The granitic bodies increase in abundance from west to east across the field area (Fig. 1A), so that the area that includes the FSE and CO well fields has a greater abundance of granitic dikes and migmatite than the area farther west up Hubbard Brook.

Intruding the Devonian and Silurian rocks are scattered mafic dikes of Cretaceous-Jurassic age (KJd, Fig. 1), as shown on the map of Barton (1997), which are generally less than one meter wide and perhaps only meters to tens of meters long. They trend northeast with the exception of a few northwest-trending dikes to the west of the area shown on Fig. 1A. The dikes are lamprophyric in composition and thought to be associated with the White Mountain Plutonic-Volcanic Suite (McHone, 1984; Lyons and others, 1997), and their orientation may be a reflection of the regional stress field in Cretaceous or Jurassic time.

DUCTILE DEFORMATION AND METAMORPHISM

The oldest rocks in the region, the metasedimentary rocks of the Silurian Rangeley and Perry Mountain Formations, were subjected to extensive deformation and metamorphic recrystallization prior to intrusion of the granite bodies. The metamorphic grade ranges from sillimanite-muscovite to sillimanite-kspar. Most primary sedimentary structures were obliterated, with the exception of fine layering preserved in calc-silicate and granofelsic pods in the Rangeley

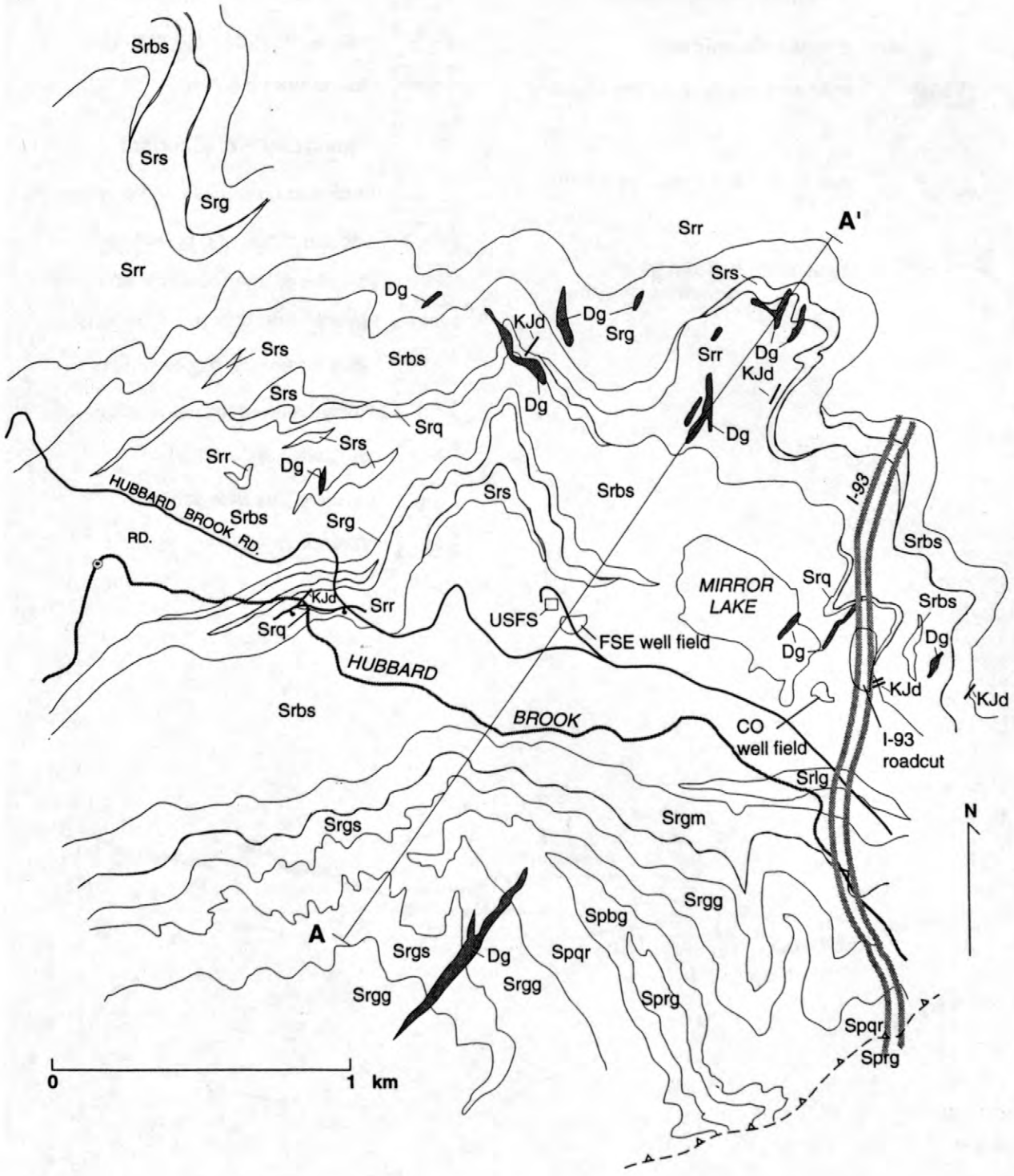

Figure 1A. Bedrock geologic map of Mirror Lake area. Description of map units and symbols on Figure 1B.

Intrusive rocks (Cretaceous-Jurassic)

KJd — Mafic (lamprophyre) dikes

Intrusive rocks (Devonian)

Dg — Granite and pegmatite dikes and sills

Thrust fault - teeth on upper plate

Normal fault - bar and ball on downthrown block

Perry Mountain Fm. (Silurian)

Sprg — Rusty sulfidic schist and gneiss

Spbg — Bedded quartzite and granofels

Spqr — Quartz-ribbed schist

Rangeley Fm. (Silurian)

Srgg — Laminated granofels and quartzite

Srgs — Bedded schist and granofels

Srgm — Massive sillimanite schist and gneiss

Srlg — Layered quartz-biotite granofels

Srbs — Gray muscovite-biotite schist

Srr — Rusty biotite-muscovite schist

Srs — Gray sillimanite schist

Srg — Massive granulite schist

Srq — Vitreous quartzite

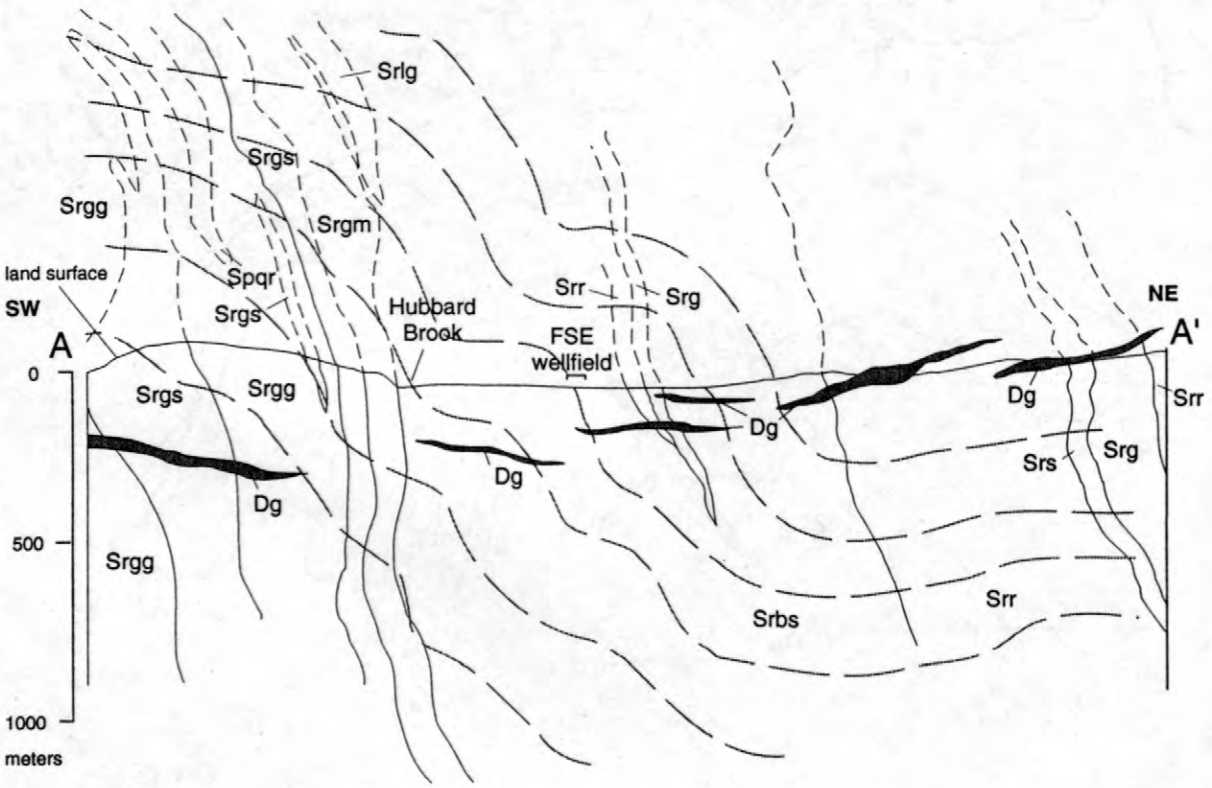

Figure 1B. Cross section A-A' and description of map units for Figures 1A and 1B. Dashed lines indicate intersection of S2 foliation with plane of cross section.

Formation and graded beds in the uppermost Rangeley and Perry Mountain Formations. The paucity of primary structures and high degree of deformation contrasts with the type locality for these rocks, where relatively mild deformation has preserved sedimentary structures and stratigraphy despite staurolite to sillimanite-grade metamorphism (Moench and Boudette, 1987; R. Moench, personal comm., 1998). The age of peak metamorphism can be bracketed between the Silurian age of the Rangeley and Perry Mountain Formations and the late Devonian age of the granite and is part of the Acadian orogenic event (Armstrong and others, 1992).

The dominant foliation in the area is a penetrative schistosity that is second generation (S2) and corresponds to a second deformation event D2, based on local cross-cutting of D1 structures by S2. Formlines illustrating the general trend of S2 schistosity (Fig. 2), assembled from individual outcrop measurements, show that S2 generally trends northeast with steep north or south dips. S2 trends are both parallel and at high angles to lithologic contacts, and transect map-scale, first-generation (F1) isoclinal folds in the uppermost Rangeley and Perry Mountain Formations in the southern part of the map area (Fig. 2). There a first-generation schistosity (S1), subparallel to primary layering, is also locally preserved. Sillimanite-grade peak metamorphic conditions were attained during the D2 event.

Lithologic contacts and S2 are both deformed by outcrop- to map-scale, open to tight folds that are considered to be third-generation (F3), corresponding to a D3 deformational event, which also locally produced an S3 schistosity axial-planar to the folds. Metamorphic conditions were at sillimanite-muscovite grade during the D3 event. The F3 folds have steeply-dipping to vertical axial planes that trend northeast in the southeastern part of the map area and north elsewhere (Fig. 2). F3 fold hinges are mostly north- to northeast-plunging. Roughly contemporaneous with F3 deformation was the intrusion of granite bodies that cut S2 schistosity, are themselves weakly foliated, and are locally subparallel to F3 structural trends.

In the southeast corner of the map is a northeast-trending, northwest-dipping thrust fault (Fig. 1A), exposed in a roadcut on I-93, that juxtaposes two units (Spqr and Sprg) and is believed to be D3 in age because it truncates S2 structures in outcrop. Also suggestive of a D3 age for the fault is the increasing parallelism of F3 structures and S3 schistosity as one approaches the fault (Fig. 2). Elsewhere in the field area a few widely-scattered zones of weakly-developed ductile shear fabric have been found that are no more than a few tens of cm thick. These truncate S2 schistosity at low angles and are perhaps D3 in age, but do not appear to have had a high amount of displacement.

A geologic cross section (Fig. 1B; A-A', Fig. 1A), constructed to pass through the FSE well field, shows steep north-dipping lithologic contacts in the metasedimentary rocks, which contrast sharply with gentle apparent dips of the tabular granite bodies. The dominant schistosity, S2, also dips northward over the southern part of the cross section but has a shallow apparent dip in the northern part, where the line of section is nearly parallel to S2. The cross section shows that both contacts and schistosity in the FSE well field should dip steeply.

BRITTLE DEFORMATION AND FRACTURES

Brittle faulting does not appear to have played a significant role in the tectonic history of the Mirror Lake area, at least in terms of the distribution of lithologies. No major through-going fault zones were identified, although it is possible that some topographic lows contain faults that are buried in glacial deposits.

There is evidence for brittle faulting at one location along Hubbard Brook (Fig. 1A), where an east-west-trending, south-dipping contact separates massive vitreous quartzite from a highly-weathered zone of sheared micaceous rock that appears to be fault gouge. Slickenlines at the contact plunge downdip, and the fault is interpreted to be a normal fault. Lack of control, however, does not permit an accurate assessment of the extent or sense of displacement of the fault.

The northeast-trending brittle fault identified in the I-93 roadcut by Barton (1997) was found by the authors to be a highly weathered zone of concentrated jointing with no significant

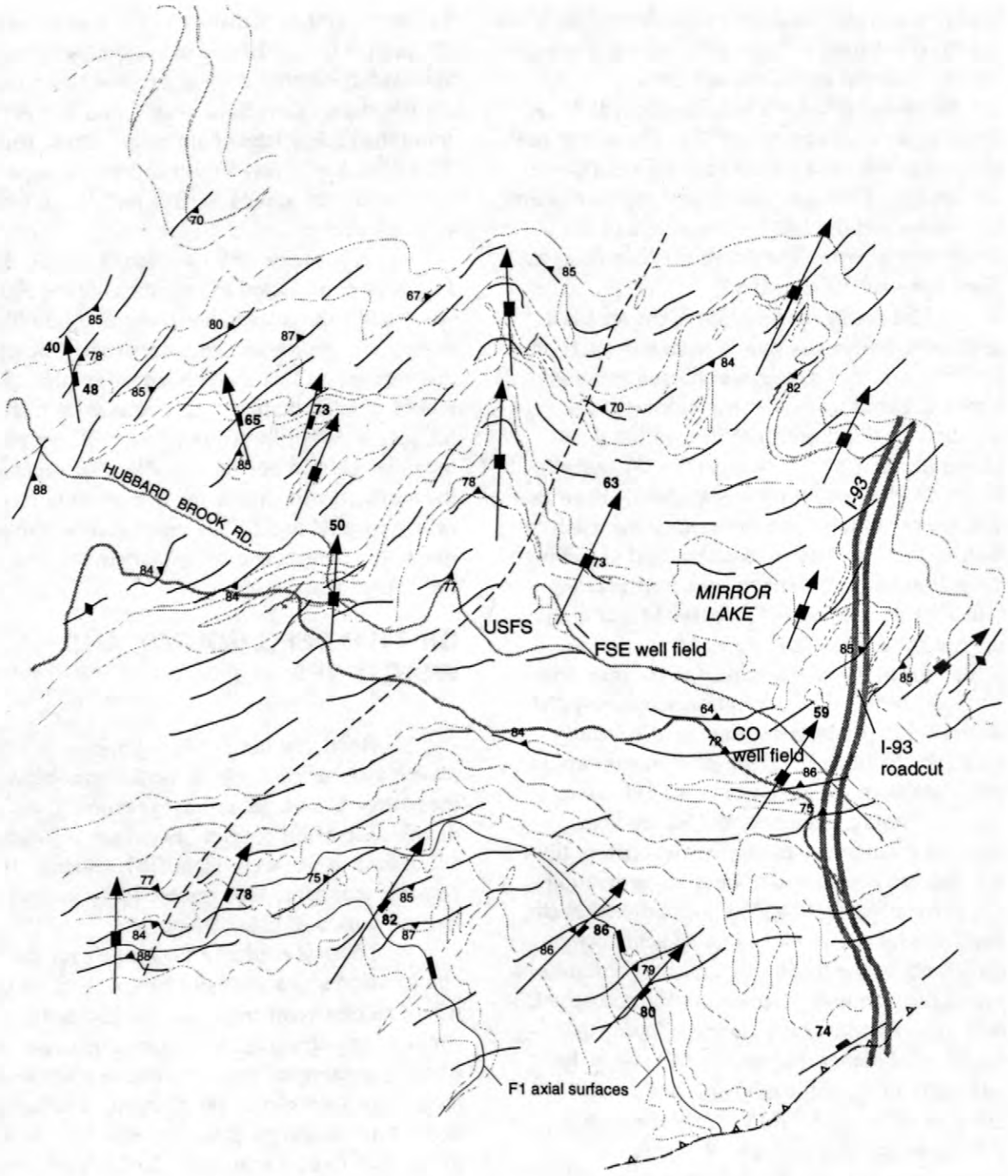

Figure 2. Formline map of F1 axial traces (thin unbroken lines), S2 schistosity (dashed lines), and F3 folds (arrows). Small triangles with numbers refer to measured dips of S2 schistosity; rectangles with numbers refer to measured dips of F3 axial planes; arrow heads with numbers refer to measured F3 fold plunges. Dashed line separates areas of north- and northeast-trending F3 structures.

offset. At one locality in the roadcut a pegmatite body is traceable across the fracture zone.

Orientations of fractures measured in the field area, consisting mostly of well-exposed joint faces, are summarized in contoured lower-hemisphere equal-area projections of poles to fractures (stereonets) and rose diagrams in Fig. 3. Bullseye contour patterns near the centers of the stereonets (Fig. 3) indicate subhorizontal sheeting fractures, which were observed throughout the field area. The steeper-dipping fractures, however, have regional differences in preferred orientation. Fractures in the northwest part of the map area have preferred trends in WNW-ESE and NW-SE directions. In contrast, fractures in the northeastern and the southern part of the map area have preferred orientations in a NE-SW direction. An area along Hubbard Brook appears to be transitional between these two trends, with a scattering of orientations in both NE and NW directions. The fracture orientation data suggest that the fracture setting of the Mirror Lake well fields may not be exactly representative of areas elsewhere in the Hubbard Brook watershed.

COMPARISON WITH OTHER GEOLOGIC STUDIES AT MIRROR LAKE

Our geologic mapping in the Mirror Lake area places in a regional context the downhole geologic investigations conducted at the two well fields as well as the intensive study of the I-93 roadcut by Barton (1997), providing some measure of the representativeness of the previous in situ studies. Our study also points out discrepancies that can arise from comparison of borehole and roadcut data with those from natural outcrops within a larger area.

For instance, our mapping shows bodies of granite occupying no more than a few percent by volume of the bedrock exposures in the eastern Hubbard Brook watershed; yet the borehole logs compiled by Johnson and Dunstan (1998) show that granite and pegmatite make up about 70% of the section drilled at the FSE well field, with the remainder schist. At the CO well field and the I-93 roadcut the proportions are reversed, with schist making up 70% of the total rock and granite the rest (Barton, 1997; Johnson and Dunstan, 1998). Our reconnaissance of the I-93 roadcut generally confirmed the proportions of schist and granite as mapped by Barton, with a significant proportion of the granitic material being migmatite derived from intrusion or partial melting of metasediment. Migmatite was rarely observed in outcrop in the Hubbard Brook watershed, however.

The increase of mapped bodies of granite from west to east towards the research site, and the relatively high abundance of granite and/or migmatite at the two well fields and the roadcut compared to outcrops elsewhere, suggests that the Mirror Lake research site is in a zone that experienced a higher degree of granitic intrusion and partial melting than areas elsewhere in the watershed; hence its geology may not be representative of a larger area.

The fairly strong northeast preferred orientation of the steeply-dipping fractures that we observed for the eastern Hubbard Brook watershed (Fig. 3) agrees fairly well with the fracture data of Barton (1997) for the I-93 roadcut, which also show a preferred dip in a southeast direction. In both sets of measurements there is also a weaker northwest-trending fracture set and gently-dipping to subhorizontal sheeting fractures. Measured orientations of fractures in boreholes in the CO well field also show a strong northeast preferred orientation for steeply-dipping fractures, after correction for vertical sampling bias, as well as a subhorizontal set probably related to sheeting (C. Johnson, written comm., 1999). The CO fracture data have a preferred northwest dip direction, opposite that of the roadcut, whereas our data show no preferred dip direction for steeply-dipping fractures.

SUMMARY

Detailed bedrock geologic mapping has shown the Hubbard Brook watershed and the area of the Mirror Lake research site to be underlain by highly deformed, sillimanite-grade metasedimentary rocks of the Silurian Rangeley and Perry Mountain Formations, which have been subdivided into twelve lithologic units. Contacts and first-generation schistosity (S1) in these units are locally parallel to but also crosscut by the

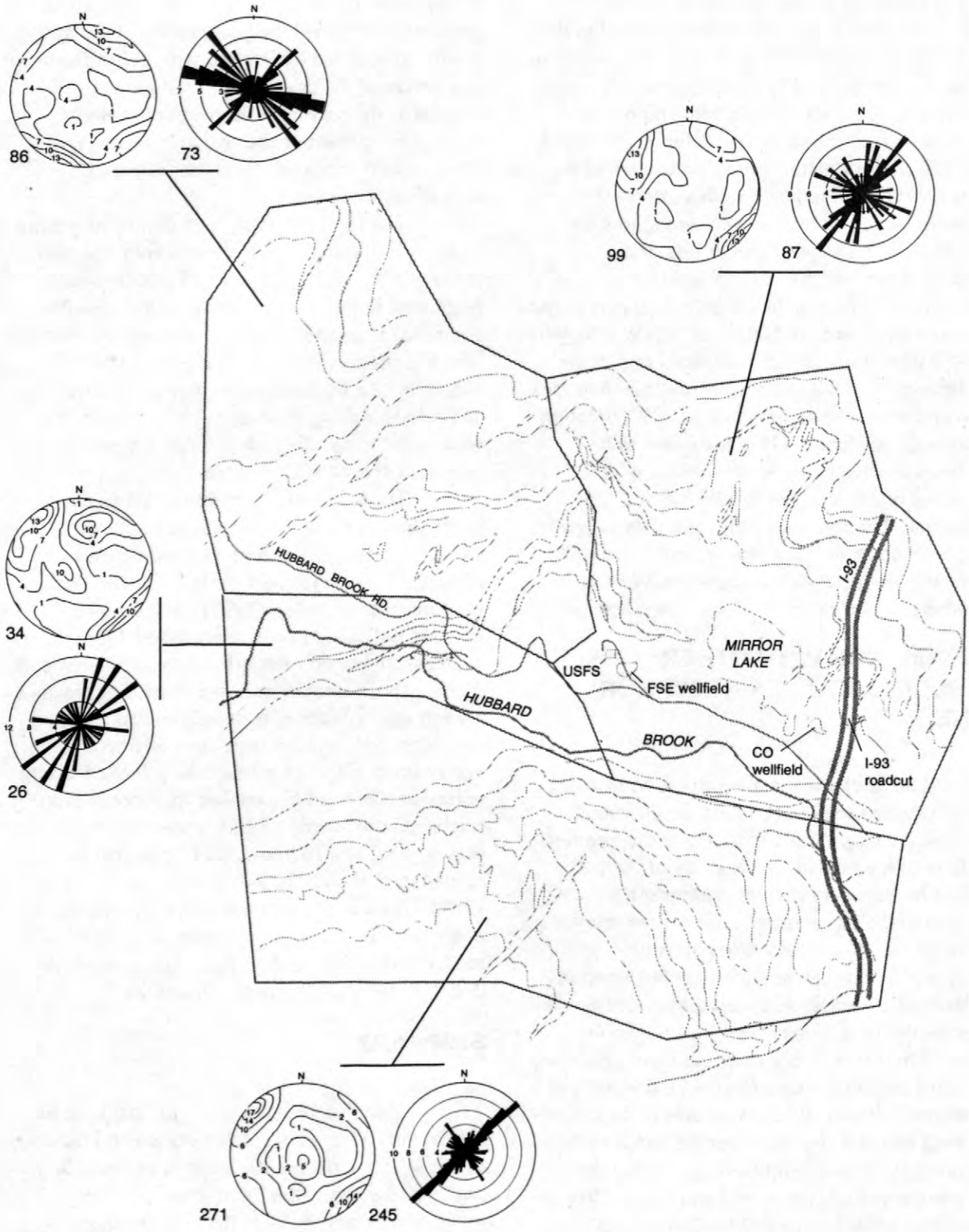

Figure 3. Contoured lower-hemisphere equal-area projections of poles to fractures, and frequency-azimuth plots (rose diagrams) of fractures steeper than 45 degrees, for selected domains. Number of measurements shown to lower left of plots.

regionally dominant second-generation schistosity (S2), which in turn is broadly folded by north- to northeast-trending F3 folds. Small bodies of Devonian granite appear to have intruded contemporaneously with the development of F3 structures. In the vicinity of the FSE and CO well fields, lithologies and S2 schistosity generally trend east-west, are steeply-dipping, and are plicated by upright F3 folds with north-plunging axes. The well fields and the I-93 roadcut appear to be situated in a zone of more intense granitic intrusion and partial melting than areas farther up the Hubbard Brook watershed.

Orientations of fractures in outcrop indicate that steeply-dipping fractures in the easternmost Hubbard Brook watershed have a strong preferred northeast orientation, in general agreement with fracture orientations determined from the I-93 roadcut and the well fields. Cretaceous-Jurassic lamprophyre dikes have similar orientations, suggesting either that the stress regime producing this dominant fracture set was operative during dike intrusion or that the dikes utilized preexisting fractures. Farther up the watershed, however, a west-northwest-trending set is dominant, suggesting a different stress regime or history.

REFERENCES

Armstrong, T.R., Tracy, R.J., and Hames, W.E., 1992, Contrasting styles of Taconian, eastern Acadian, and western Acadian metamorphisms, central and western New England: Journal of Metamorphic Geology, v. 10, p. 415-426.

Barton, C.B., 1997, Bedrock geology map of Hubbard Brook Experimental Forest and maps of fractures and geology in roadcuts along Interstate 93, Grafton County, N.H.: U.S. Geological Survey Miscellaneous Investigations Series Map 1-2562, 1 sheet, scale 1:12,000.

Hsieh, P.A., Shapiro, A.M., Barton, C.C., Haeni, F.P., Johnson, C.D., Martin, C.W., Paillet, F.L., Winter, T.C., and Wright, D.L., 1993, Methods of characterizing fluid movement and chemical transport in fractured rock, in Cheney, J.T., and Hepburn, J.C., eds., 1993, Field Trip Guidebook for Northeastern United States: Geological Society of America, Annual Meeting, October 25-28, Boston, Mass., p. R1-29.

Johnson, C.D. and Dunstan, A.M., 1998, Lithology and fracture characterization from drilling investigations in the Mirror Lake Area: from 1979 through 1995 in Grafton County, New Hampshire, U.S. Geological Survey Water-Resources Investigations Report 98-4183, 210 p.

Lyons, J.B., Bothner, W.A., Moench, R.H., and Thompson, J.B., Jr., 1997, Bedrock geologic map of New Hampshire: U.S. Geological Survey State Geologic Map, 2 sheets, scales 1:250,000 and 1:500,000.

McHone, J.G., 1984, Mesozoic igneous rocks of northern New England and adjacent Quebec-Summary, description map, and bibliography of data sources: Geological Society of America, Map and Chart Series, MC-49.

Moench, R.H., and Boudette, E.L., 1987, Stratigraphy of the Rangeley area, western Maine: Geological Society of America Centennial Field Guide--Northeast Section, p. 273-278.

AUTHOR INFORMATION

William C. Burton and Thomas R. Armstrong, U.S. Geological Survey, Reston, Virginia (bburton@usgs.gov and tarmstrong@usgs.gov)

Gregory J. Walsh, U.S. Geological Survey, Montpelier, Vermont (gwalsh@usgs.gov)

Integrating Surface and Borehole Geophysics--Examples Based on Electromagnetic Sounding

By Frederick L. Paillet and John W. Lane, Jr.

ABSTRACT

Integration of surface and borehole geophysical data is important in site characterization because there are rarely enough boreholes to effectively characterize complex aquifers, while surface soundings alone are usually too ambiguous, or lack enough spatial resolution, to provide completely noninvasive characterization. Three specific applications of logs are useful in such data integration: (1) calibration of geophysical variables, (2) definition of model layer or cell structure in the implementation of data inversion schemes, and (3) multivariate analysis of geophysical response. We demonstrate how the collective application of these three lines of approach has resulted in the successful characterization of a heterogeneous, secondary-permeability aquifer at a study site in southwestern Florida. A similar integration of surface and borehole data will be needed to effectively characterize the large-scale transport properties of bedrock aquifers buried under a thick cover of overburden such as the fractured bedrock aquifer at the Mirror Lake, New Hampshire, fractured rock field-study site.

INTRODUCTION

Relatively homogeneous and stratigraphically continuous sedimentary aquifers are readily characterized with data from a few boreholes. Heterogeneous secondary permeability aquifers are much more difficult to characterize because data from a few boreholes cannot be simply extrapolated across the study site. Surface geophysical soundings provide a useful, noninvasive technique for characterization of the subsurface in complex hydrogeologic terrain. However, these soundings rarely provide enough spatial resolution to unambiguously identify the individual flow paths for ground water flow and contaminant transport in heterogeneous aquifers. Geophysical and hydraulic measurements made in boreholes can provide such spatial resolution, but there is unlikely to be enough borehole data to effectively characterize heterogeneous aquifers on the basis of borehole logs alone. Truly effective characterization of complex aquifers will be based on a combination of borehole and surface geophysical methods. In this approach, a limited representative sample of the subsurface geophysical response given by well logs is used to develop interpretation models that can be effectively extrapolated across the study site using much more spatially extensive surface geophysical soundings. In this paper we first discuss the general theoretical considerations related to the integration of surface and borehole geophysical data. We then illustrate the successful integration of surface and subsurface data for a project in southwestern Florida. We conclude by suggesting ways in which this general technique might be applied to the characterization of fracture flow hydrogeology at the Mirror Lake, New Hampshire, study site.

GEOPHYSICAL SOUNDINGS AND THEIR INTERPRETATION

Geophysical field data consist of measurements made on the surface of the earth (surface geophysical soundings) or at a point adjacent to the borehole wall (geophysical well logs) at some depth below the surface. The major difference between these two classes of measurement is the scale of investigation. Surface soundings are conducted so that measurements are made over large sample vol-

umes extending into the subsurface. The scale of the sample volume usually increases significantly with depth of investigation. In contrast, well logs sample a volume only slightly larger than the borehole diameter and have the same sample volume at each data point. Thus, both soundings and logs represent profiles of subsurface properties (fig. 1). The well logs contain much greater spatial detail but measurements can only be made in boreholes. The surface soundings contain much less vertical resolution but can be made virtually anywhere at the study site.

Geophysical soundings are analyzed by expressing the subsurface distribution of properties as a series of contributions from layers or cells within the sample volume. The predicted model response from the integrated sounding sample volume is systematically adjusted until there is a close match between model and data. The rate at which the model computations converge on a match with the data set is often taken as a qualitative measure of the reliability of the model. However, the interpretation is always qualified by the lack of a uniqueness theorem for such inversion: there is no way to prove that an alternate model might not produce an even better fit to the data set (Parker, 1994). In the following section of this paper we explore the specific ways in which the inclusion of geophysical well log data can both improve the resolution of the interpretation model and address the uniqueness of interpretation issue.

INTEGRATING SURFACE AND BOREHOLE GEOPHYSICS

Careful consideration of the geophysical inversion problem indicates that geophysical logs can improve the interpretation of surface geophysics in three different ways:

1. RESPONSE CALIBRATION Surface soundings map the subsurface distribution of such physical properties as electrical resistivity or seismic attenuation, rather than such hydraulic quantities as permeability or water quality. Geophysical logs can give the same measurement over a much smaller sample volume within a borehole. Therefore, the interval averaged geophysical quantity can be correlated with hydraulic measurements made over precisely the same interval in the borehole. This regression generates a calibration of the surface sounding in the hydraulic parameter of interest.
2. INVERSION MODEL FORMULATION AND UNIQUENESS Geophysical logs can be used to define and corroborate models used for sounding inversion. For example, logs can indicate when the layered models typically assumed by inversion software are appropriate. Alternatively, the logs may indicate that continuously varying subsurface properties are best modeled by series expansions that are truncated at a finite number of terms. In either case, the character of the geophysical logs provides independent support that the proper inversion model has been selected for use in data interpretation.
3. MULTIVARIATE GEOPHYSICAL MODELS Almost all geophysical interpretation models involve dependence on more than one physical parameter. Thus, a single surface sounding may not be uniquely inverted to give the subsurface distribution of a hydraulic parameter of interest. Geophysical logs are usually run in suites consisting of several physically independent measurements, such as acoustic, electric, and nuclear logs. These different geophysical logs generate distinctly different interpretation equations, which can be solved for several independent variables (Paillet and Crowder, 1996). These multivariate solutions can be used to identify the variables that influence the surface soundings. One simple approach might be to break the study site into sub-regions where the sounding inversion can be effectively based on a single variable.

SURFACE TIME DOMAIN SOUNDINGS IN SOUTHWESTERN FLORIDA

An aquifer exploration project where surface and borehole geophysics have been effectively combined to generate a useful subsurface hydraulic model is described by Weedman and others (1997) and Paillet and others (1998). This study was undertaken to generate a subsurface model for the relatively unexplored ground-water region of the Big Cypress National Preserve area in southwestern Florida. The subsurface was sampled with a series of boreholes drilled approximately 10 km apart. Although core recovery was not always complete,

the geologic description was extrapolated to the entire depth of each borehole using the geophysical logs as a guide (fig. 2). In general, the sediments encountered by the boreholes were variable, exhibited no obvious lateral continuity, and were characterized by a heterogeneous distribution of secondary permeability related to dissolution of carbonate sediments.

A series of surface induction surveys (time domain electromagnetic soundings, TDEM; Fitterman and Stewart, 1986) were made along profiles connecting boreholes to define large-scale subsurface stratigraphy across the study area. The relationship between formation electrical conductivity at each borehole site and nearby TDEM soundings verified that the TDEM soundings reproduced the structure of the induction conductivity logs (fig. 3). Furthermore, comparison of neutron porosity logs (assumed to reflect variations in sediment permeability) with induction logs (assumed to indicate both permeability and pore water salinity) indicated that the subsurface was divided into compartments characterized by constant salinity and separated by thin confining units. As boreholes were extended further east in the study area, electrically conductive clay confining units were also identified, further complicating the relationship between formation conductivity and pore water salinity. Borehole flow logs were used to identify inflow zones where fluid column resistivity could be related to formation conductivity under ambient or pumping conditions. These data were used to regress formation conductivity versus water sample salinity, generating a direct relationship between formation resistivity from induction soundings and water quality (fig. 4). The regression assumes that the fluid column logs are used to give a "true" value for pore-water electrical conductivity, whereas the formation electrical conductivity is taken as a "predictor" of these values. Also note that the one outlying data point in figure 4 strongly influences the correlation coefficient. Repeating the regression without this one point introduces a negligible change in the slope and intercept, and only a modest reduction in correlation coefficient.

The combination of borehole logs and surface TDEM soundings was used to construct a useful model of aquifer properties (fig. 5). The analysis indicates that the TDEM data can be used to define a two-layer model in which the upper layer represents a surficial aquifer continuously recharged by and discharging to surface flow, and a deeper layer representing all formations below the uppermost confining unit. Geophysical logs contributed to this interpretation by:

1. Providing estimates of pore water salinity based on formation resistivity, showing that the uppermost layer is characterized by water quality identical to that of surface water bodies;
2. Demonstrating that the aquifer is divided into compartments of relatively uniform water quality and thus supporting the use of the layered inversion model applied in the TDEM data interpretation; and
3. Indicating which regions of the aquifer could be used in the interpretation and restricting the analysis to clay-free regions where the interpretation model can be applied.

As a final check on the interpretation, several locations along the TDEM profiles were selected for verification. Rotary drilled boreholes were logged at these locations, confirming the presence of the layers, the depth of the interface, and the variation in pore water salinity predicted by the TDEM interpretation.

A PROPOSED STUDY AT THE MIRROR LAKE FRACTURED ROCK STUDY SITE

Characterization of the heterogeneous distribution of permeability in fractured bedrock aquifers under a variable thickness of overburden provides one of the greatest challenges in hydrogeology. Comparison of inversion results to known site conditions at such a site would establish the relative merit of the coupled application of surface and borehole geophysics. The CO-wellfield within the Mirror Lake fractured rock field-research site is a good example of a site where the coupled approach could be tested using two-dimensional surface direct-current resistivity and borehole geophysical methods. Depth to rock at the site is generally less than 10 meters (m) and numerous boreholes are located along several possible surface resistivity-profiling directions. The hydrogeology of the site has been studied extensively, providing an excellent data-base of borehole geophysical logs, lithologic logs, and results of geochemical and hydraulic testing. The site is located within 100 m of extensive road cuts along Interstate Highway 93 that have been mapped in detail. Finally, seasonal changes in

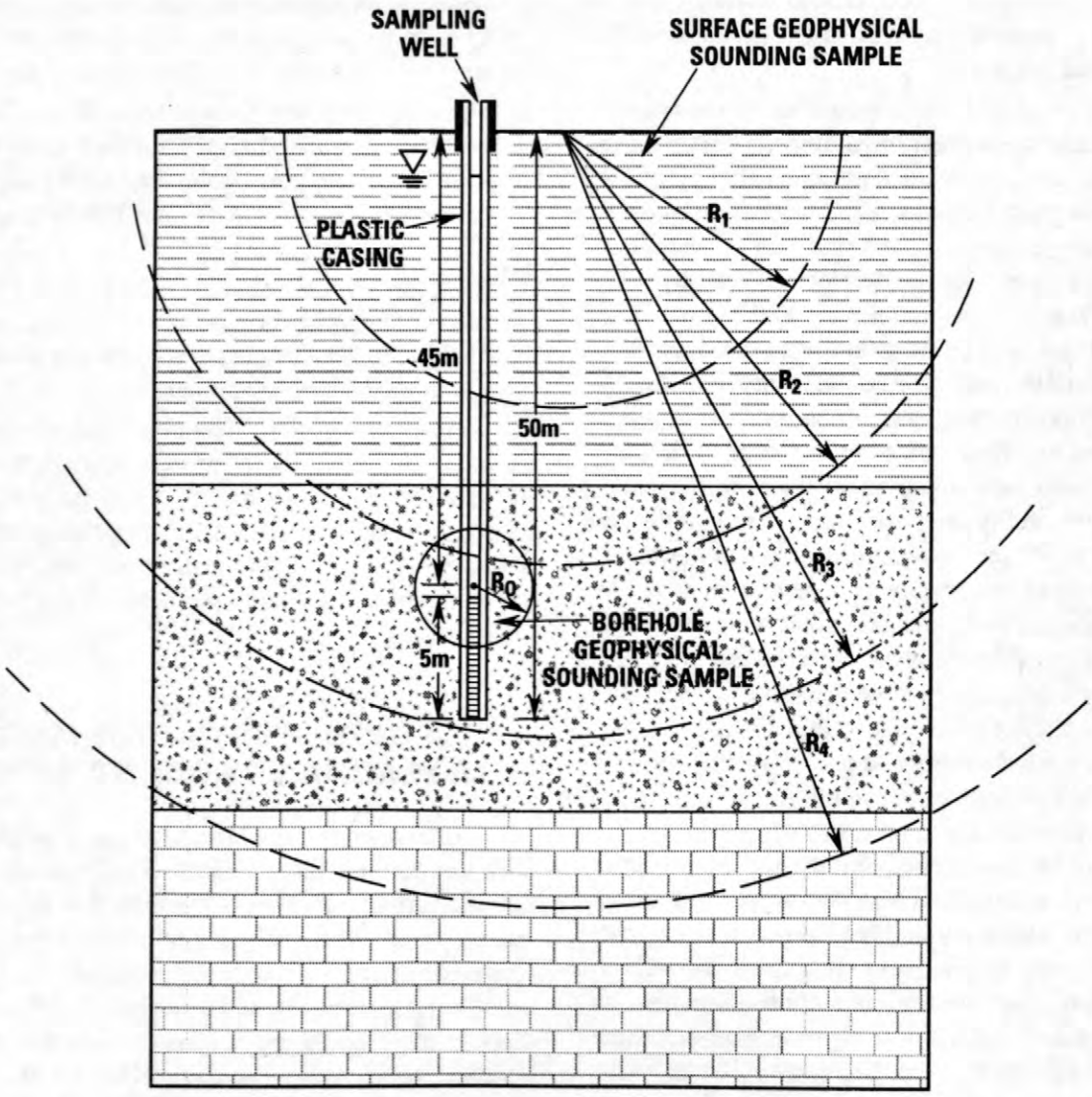

Figure 1. Schematic comparison of surface soundings and borehole geophysics, illustrating how borehole logs can be averaged over screened intervals for comparison with hydraulic test results or water sample data.

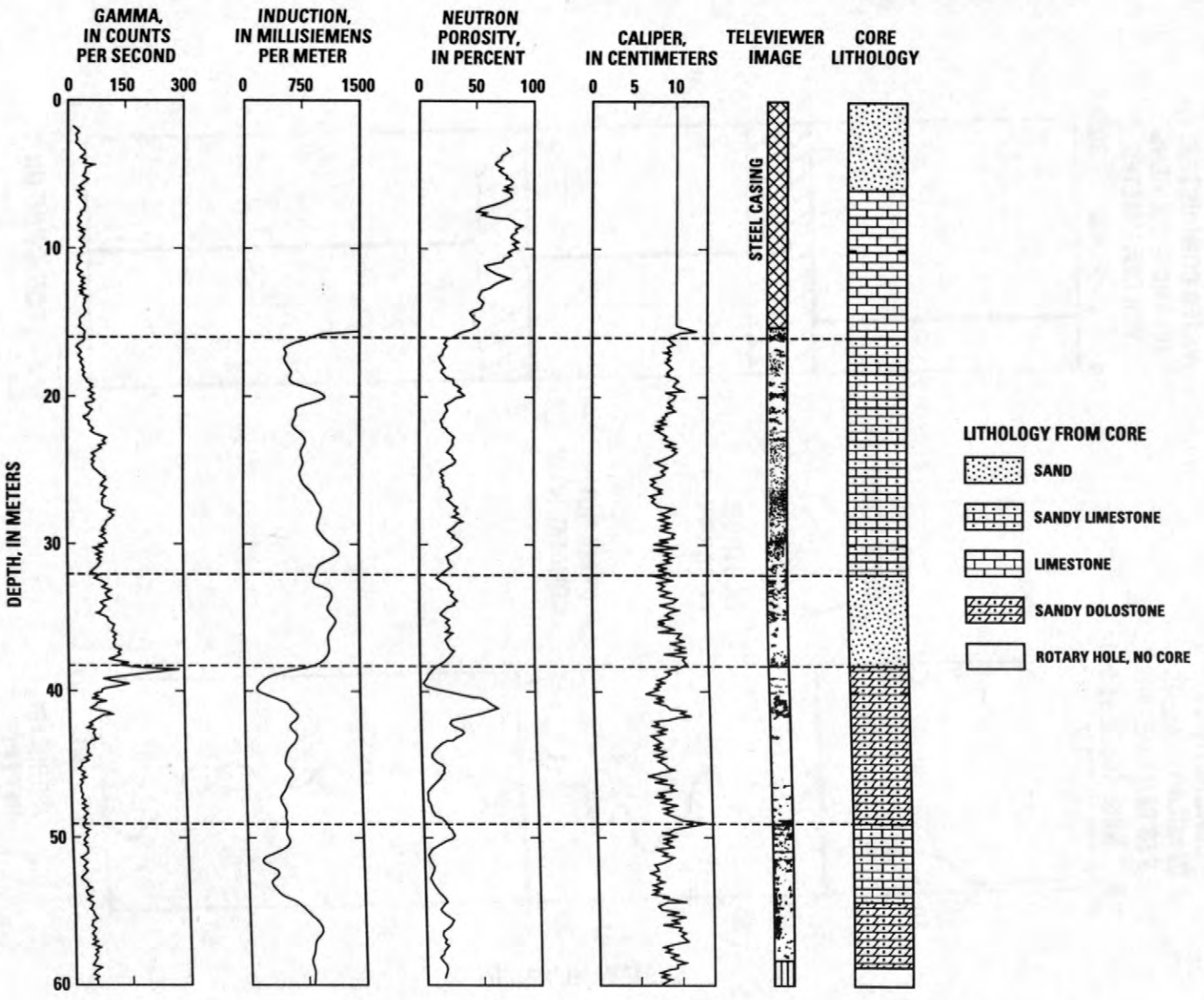

Figure 2. Log composite from southwestern Florida, where logs have been used to complete the lithologic description for missing intervals by correlating lithologic contacts in the core with the indications of such contacts on the logs as shown in the figure.

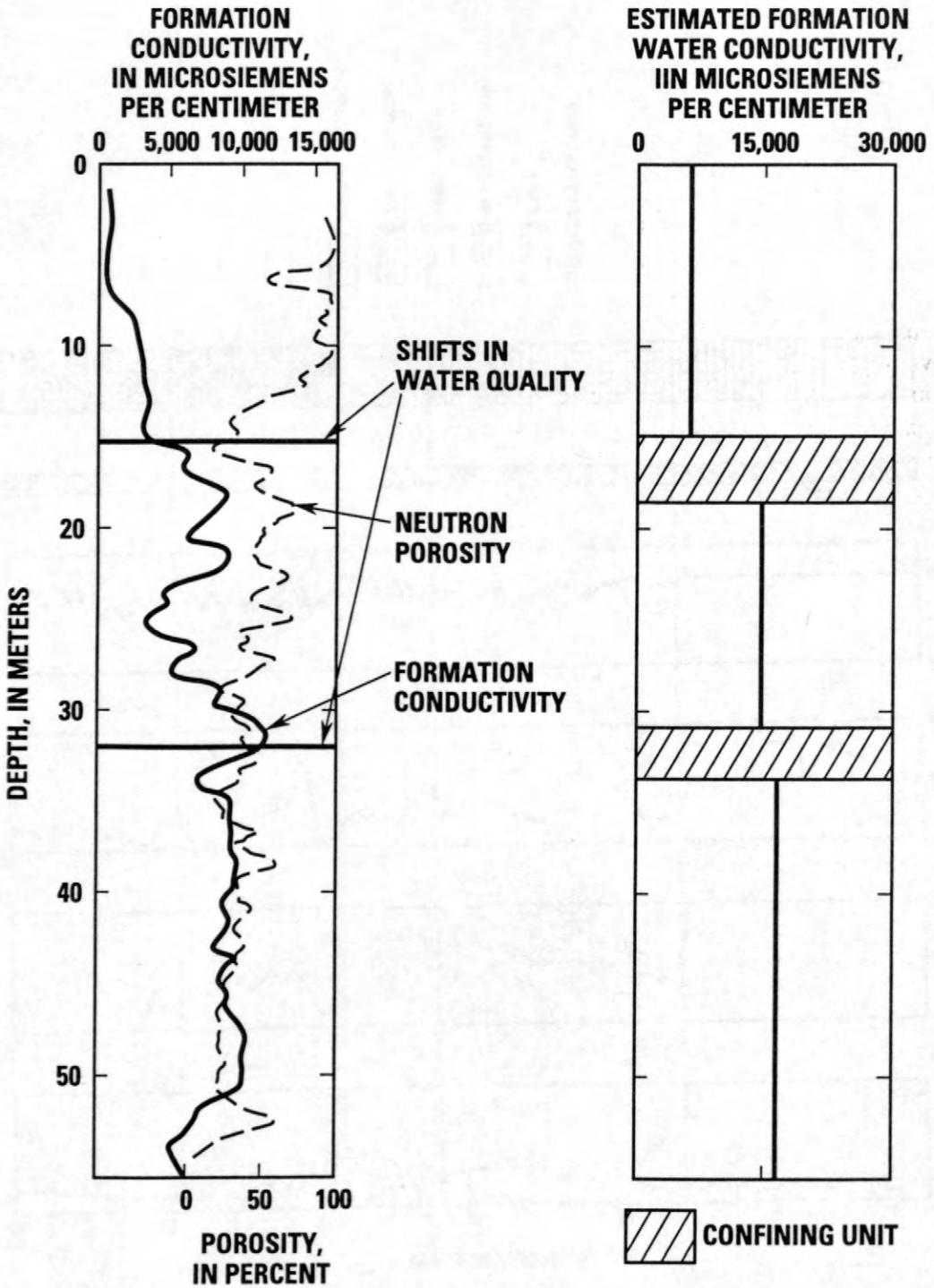

Figure 3. Neutron and induction log overlay from southwestern Florida, illustrating probable existence of aquifers and confining units, and compared to layers inferred from TDEM electromagnetic soundings.

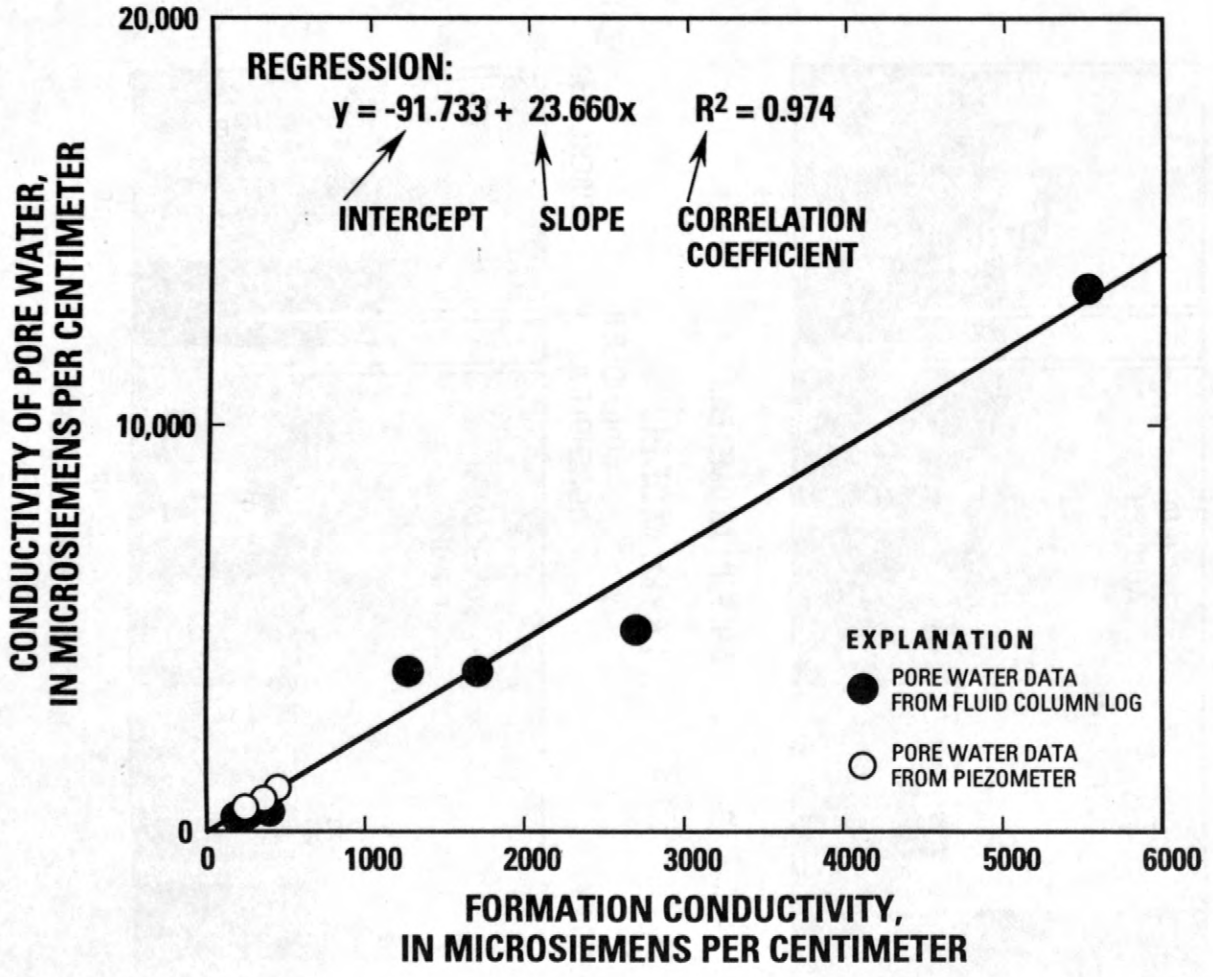

Figure 4. Regression of water sample conductivity against formation conductivity from induction logs used to generate a relationship between formation conductivity and pore water conductivity.

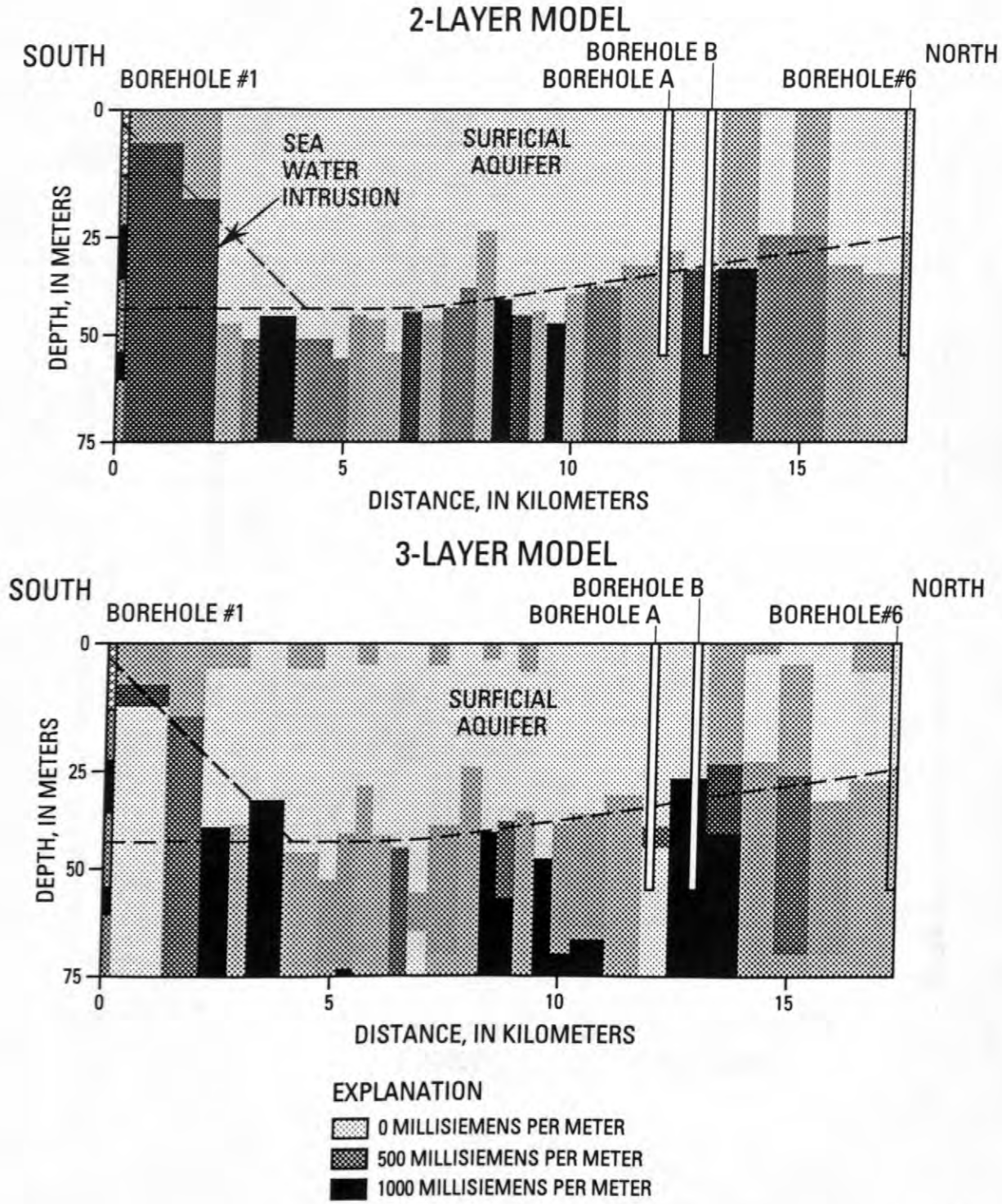

Figure 5. Interpretation of a north-south series of TDEM soundings along a transect connecting boreholes in the southwestern Florida study; results of two and three layer model interpretations show that there is no significant improvement in the model resolution when more than two layers are included.

water quality resulting from infiltration of road-salt runoff can be expected to perturb the fluid resistivity in fractures, providing a natural tracer indicating fluid flow in transmissive fracture zones. We propose conducting two-dimensional surface resistivity profiling at several locations and orientations through the CO well field at Mirror Lake. Inversion of the resistivity data would be accomplished "blindly" and by systematic inclusion of borehole geophysical logs to (1) identify appropriate inversion approaches (for example, layered earth versus other methods); and (2) constrain inversion parameters near borehole locations. The "quality" of the inversion would be tested by comparing resistivity-with-depth models along the profile to geophysical logs from nearby boreholes. Periodic repetition of surface and borehole geophysical surveys provide geophysical data appropriate for difference-analysis to identify water quality changes within transmissive zones. These results would be used to test the veracity of interpretations of resistivity inversions to predict locations of increased transmissivity.

CONCLUSIONS

Although there is usually considerable ambiguity in the interpretation of surface geophysical soundings in the characterization of heterogeneous aquifers, the integration of surface and borehole geophysics can significantly improve the quality of interpretations. Such data integration is important in site characterization because one can never have enough boreholes to effectively characterize complex aquifers, while surface soundings alone are usually too ambiguous, or lack enough spatial resolution, to provide completely noninvasive characterization. These considerations highlight the importance of developing effective techniques for the combined interpretation of surface and subsurface data sets. We identify three specific points of attack in such data integration: (1) calibration of geophysical variables, (2) conditioning of inversion problem formulation, and (3) multivariate analysis of geophysical response. We demonstrate how the collective application of these three lines of approach has resulted in the successful characterization of a heterogeneous, secondary-permeability aquifer at a study site in southwestern Florida. We suggest that a similar integration of surface and borehole data will be needed to effectively characterize the large-scale transport properties of bedrock aquifers buried under a thick cover of overburden such as the fractured bedrock aquifer at the Mirror Lake study site.

REFERENCES

Fitterman, D.V., and Stewart, M.T., 1986, Transient electromagnetic sounding for groundwater: Geophysics, v. 51, no. 4, p. 995-1005.

Paillet, F.L., and Crowder, R.E., 1996, A generalized approach for the interpretation of geophysical well logs in ground water studies--Theory and application: Ground Water, v. 34, no. 5, p. 883-898.

Paillet, F.L., Hite, Laura, and Carlson, Matt, 1998, Integrating surface and borehole geophysics in ground water studies - an example using electromagnetic soundings in south Florida: Symposium on the Application of Geophysics to Engineering and Environmental Problems, Chicago, Ill., 1998, [Proceedings], p. 349-358.

Parker, R.L., 1994, Geophysical inverse theory: Princeton, New Jersey, University Press, 386 p.

Weedman, S.D., Paillet, F.L., Means, G.H., and Scott, T.M., 1997, Lithology and geophysics of the surficial aquifer system in western Collier County, Florida: U.S. Geological Survey Open-File Report 97-436, 167 p.

AUTHOR INFORMATION

Frederick L. Paillet, U.S. Geological Survey, Denver, Colorado.

John W. Lane, Jr., U.S. Geological Survey, Storrs, Connecticut.

Geophysical Reconnaissance in Bedrock Boreholes--Finding and Characterizing the Hydraulically Active Fractures

By Frederick L. Paillet

ABSTRACT

Geophysical well logs are used to identify the depth where permeable fractures intersect boreholes in fractured bedrock aquifers. This information is used to sample fracture populations and to develop models for fracture flow networks at field sites. Conventional geophysical logs do not indicate the hydraulic properties of fractures and only characterize fractures in the immediate vicinity of the borehole. Direct hydraulic characterization is possible using high-resolution flow profile logging. A well-posed inversion problem can be formulated to solve for estimates of fracture-zone transmissivity and hydraulic head if two different steady or quasi-steady flow profiles are obtained, along with drawdown information. At the Mirror Lake, New Hampshire, study site, these profiles are obtained under ambient and steady pumping at about 4 liters per minute, but steady injection may be more convenient at other sites. When cross-borehole flow experiments are conducted, the technique can be expanded to generate estimates of fracture-zone storage coefficient and to infer patterns of fracture connections in the region between pumped and observation boreholes. The effectiveness of these techniques is demonstrated by the agreement between flow profile analysis and straddle-packer hydraulic tests conducted at the Mirror Lake site.

INTRODUCTION

Site monitoring in bedrock aquifers is made difficult by the heterogeneous distribution of fracture permeability and the inability to identify possible flow paths without extensive subsurface investigation. Borehole geophysics or "well logging" serves an important role in the study of bedrock aquifers by providing an array of reconnaissance techniques that can be used to identify and characterize the "hydraulically active" zones in bedrock boreholes. This paper presents an overview of geophysical logging techniques developed over more than a decade of research at the U.S. Geological Survey's Mirror Lake, New Hampshire, fractured rock field-research site. Special emphasis is placed on flow logging as direct measurement of borehole hydraulics, in contrast to most geophysical techniques which provide measurements that are indirectly related to fracture hydraulics.

GEOPHYSICAL LOGS

Geophysical logs are used to give a profile of the physical properties of rocks adjacent to a borehole, with measurements made over a sample volume that varies from a few millimeters for borehole wall image logs up to several tens of centimeters for induction and nuclear logs (fig. 1). This example illustrates almost all of the geophysical logs that are routinely available for bedrock applications, including gamma, induction resistivity, single-point resistance, neutron, and caliper logs. These logs are typically presented on highly compressed vertical scales. Although some of the logs indicate spikes and other features that appear to represent fractures, the vertical scale indicates that these spikes repre-

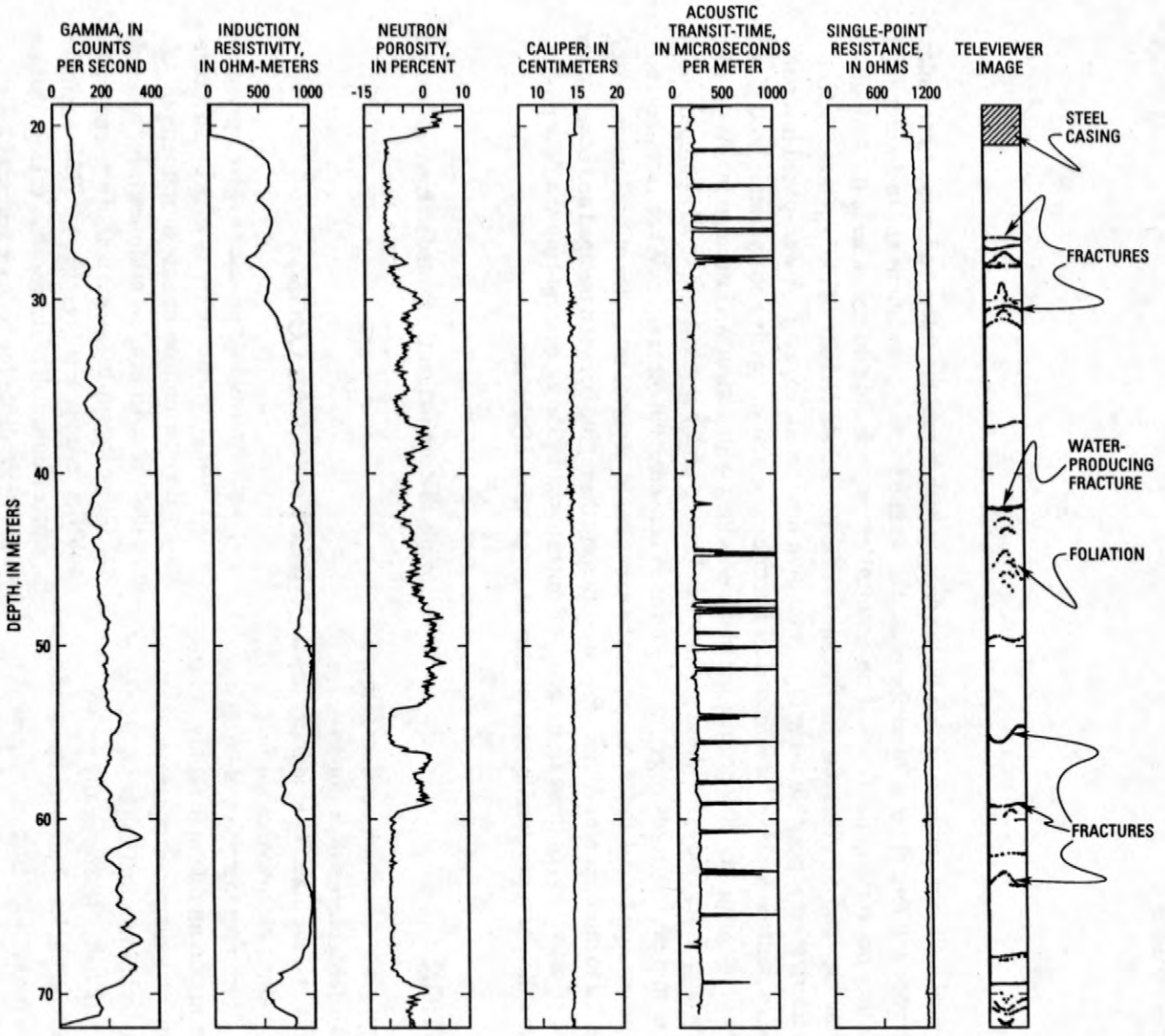

Figure 1. Geophysical logs for borehole FSE-9 at the Mirror Lake, New Hampshire, study site.

sent intervals that are several to tens of centimeters in thickness. Therefore, the depth scale of these features is unlikely to be directly related to fracture aperture, and many small-aperture fractures are probably not indicated by the logs.

The only geophysical log in figure 1 that provides direct and unambiguous information about the location, size, and orientation of fractures is the televiewer log. The televiewer log is one of several different borehole wall image techniques that are based on either optical, acoustic, or electrical measurements (Barton and others, 1997). The shape of the fracture trace on such images can be used to estimate fracture strike and dip, whereas the thickness of the fracture image can be related to local aperture as influenced by drilling damage and erosion of infilling minerals (Paillet, 1998). The combination of highly localized but geometrically precise information given by image logs and volume-averaged geophysical response given by the other logs can be useful in fracture analysis. The image log can be used to identify where fractures intersect boreholes, and then other logs can be used to investigate the effects of these fractures on the bulk properties of more extended sample volumes in which those fractures are embedded. For example, the televiewer log in figure 1 indicates that anomalies or "kicks" on resistivity, neutron, acoustic, and caliper logs are associated with major fractures near 28, 42, and 59 meters (m) in depth. Such anomalies indicate that these fractures may be hydraulically conductive and are probably surrounded by alteration halos where they extend into the surrounding rock mass (Paillet, 1993). At the same time, a number of acoustic log anomalies that might be mistaken for fractures correlate with foliation indicated by the televiewer log and lithologic contacts indicated on gamma and neutron logs. All of this information can be used to generate fracture population models where the size, orientation, density, and extent of alteration associated with each fracture can be included in the fracture data set.

HIGH-RESOLUTION FLOW LOGGING

Although geophysical logs can be used to characterize fractures where they intersect boreholes, numerous studies indicate that fracture flow is mostly controlled by the pattern of fracture connections (Paillet and others, 1987; Long and others, 1991). For example, we find no significant correlation between fracture density or apparent fracture aperture and the measured transmissivity of packer-isolated zones in hydraulic testing (figs. 2A and 2B). These results indicate that geophysical logging techniques in bedrock boreholes should include logging methods capable of directly measuring the amount of water produced by fractures identified using borehole image logs. High-resolution flow logging equipment such as the heat-pulse (Hess, 1986) and electromagnetic (Molz and others, 1994) flowmeters provide such information in the form of estimated inflow under normalized drawdown conditions (Paillet and Allen, 1996). For example, flowmeter logs indicate that more than 95% of all inflow to borehole FSE-9 (fig. 1) enters at a single fracture located near 42 m in depth, while no measurable flow enters at other fractures that appear permeable on the basis of apparent fracture aperture or extent of alteration. This general result applies to all of the bedrock boreholes at the Mirror Lake site: water production in bedrock boreholes is attributed to a small fraction of fractures that otherwise appear indistinguishable from the full population of identified fractures (Johnson and Dunstan, 1998; Paillet and others, 1987). Comparison of normalized inflow estimates and interval hydraulic test results confirm a significant correlation between normalized inflow from flowmeter logs and interval transmissivity from hydraulic tests (fig. 2C).

FLOW LOG INTERPRETATION MODEL

The interpretation of flowmeter profiles in bedrock boreholes is based on a numerical flow model where an arbitrary number, N, of producing fractures are in communication with the open borehole and are connected to M far-field aquifers (fig. 1; Paillet, 1998). In general, each fracture is modeled as a confined aquifer characterized by transmissivity, T, storage coefficient, S, and far-field hydraulic head, H. The model computes the borehole flow from the mass balance equation for inflow from each fracture (q), using the difference between hydraulic head (H), hydraulic head loss (h), and water level in the borehole (w), and accounts for pumping (Q) (fig. 3B). In steady or quasi-steady flow analysis, the flow field is assumed to be independent of S. In that situation, each water-producing zone is characterized by two variables, T and H.

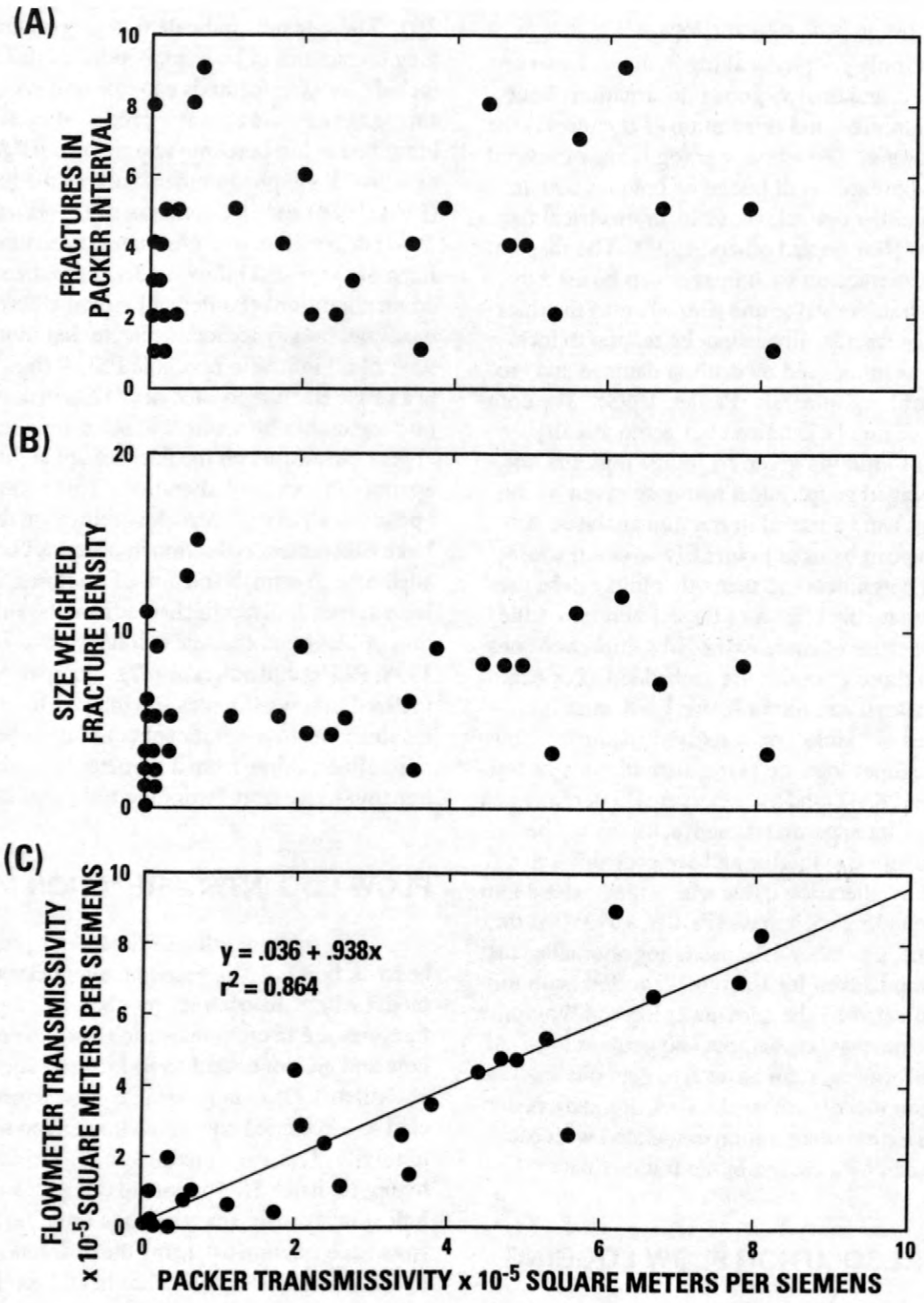

Figure 2. Comparison of (A) Number of fractures in the test interval, (B) Size-weighted fracture density in the test interval; and (C) Normalized inflow from all fractures in the test interval with packer test estimates of interval transmissivity (Paillet and Allen, 1996).

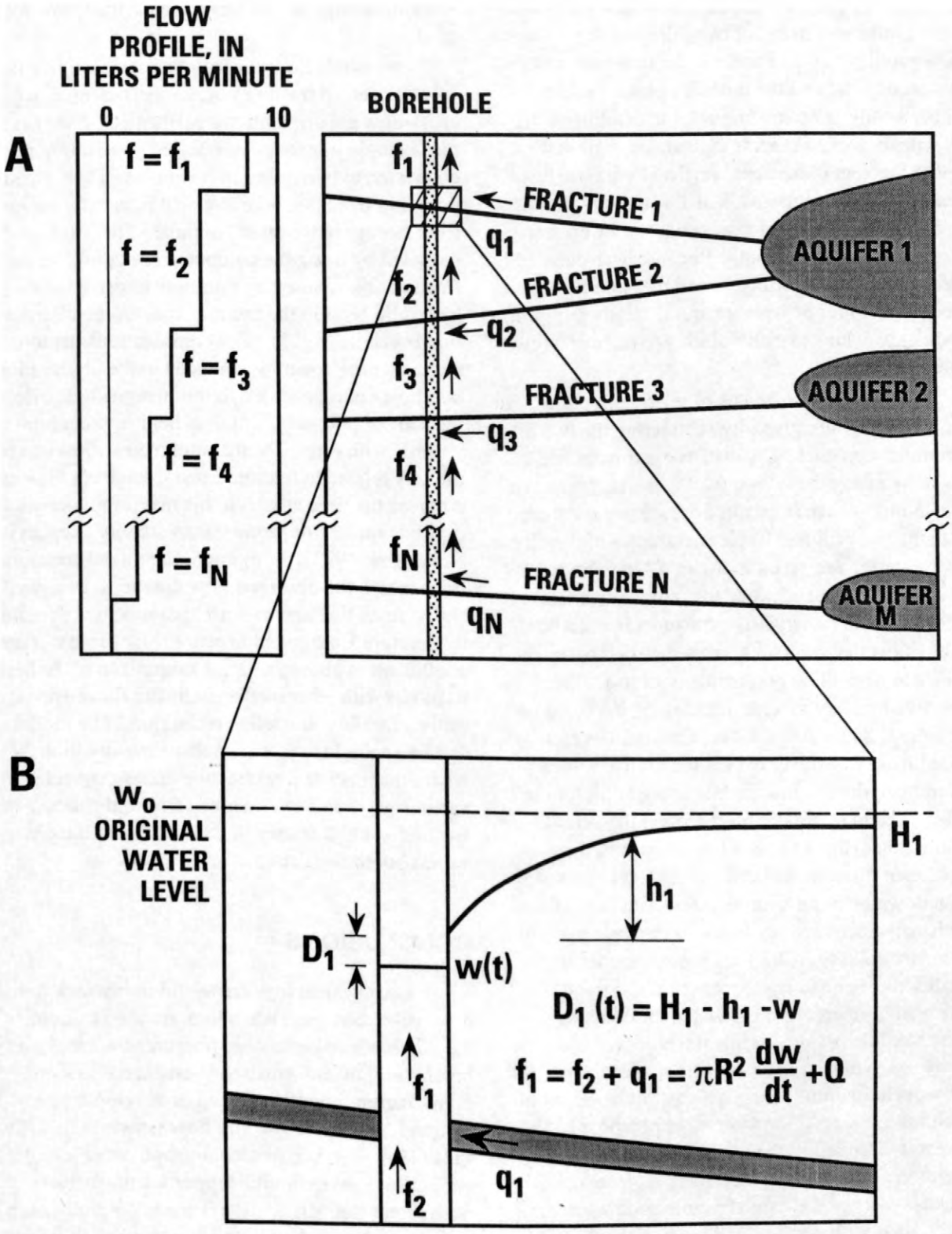

Figure 3. Schematic illustration of borehole flow profile interpretation model (Paillet, 1998).

Therefore, a properly posed steady flow interpretation inversion consists of two different steady-state flow profiles. One of these is the flow under ambient conditions, and the other is obtained under either steady injection or pumping conditions. Whenever measurements indicate negligible flow under ambient conditions, vertical hydraulic-head gradients can be ignored, and T is directly proportional to the amount of flow produced by each fracture under steady pumping. Because heat-pulse and electromagnetic flowmeters can measure flow as small as 0.1 liter per minute, quasi-steady pumping is quickly achieved using discharge rates of a few liters per minute.

Qualitative estimates of relative fracture transmissivity are given by subtracting the two different flow profiles. Quantitative estimates are given by fitting the flow model to the two flow profiles, along with the measured drawdown associated with the two profiles. Typical examples of flow log interpretation are given in figure 4. In these examples, pumping was adjusted to optimize estimates of T for the most transmissive fractures in each borehole. Flow measurement errors then determine the ability to detect less permeable fractures. The effective limit of fracture detection is indicated on the figure. In most situations, the T values estimated from flowmeter data agree with T values given by hydraulic tests, while accounting for the differences in hydraulic head among the various inflow zones (fig. 4A). In a few situations, there are significant differences between T values estimated from flowmeter and hydraulic test data (fig. 4B). Such differences are attributed to the difference in boundary conditions for the specific aquifer test conditions. For example, subsets of the fractures indicated in figure 4B were tested individually using straddle packers, while the borehole was always open during the flowmeter experiments. Subsequent hydraulic tests indicated that the set of fractures in the 65-73 m interval in borehole FSE-8 are short-circuited in the vicinity of the borehole. Therefore, the secondary fractures indicate the transmissivity of the entire fracture zone when they are isolated with packers, but most of the flow is conducted into the borehole by the one large fracture near 72 m in depth whenever the borehole is open. In general, straddle-packer hydraulic tests provide more accurate estimates of fracture transmissivity, but these measurements involve much more time, equipment, and expense than flow logging.

Borehole flow experiments can also give useful estimates of fracture storage coefficient, S, when cross-flow experiments are performed. For example, a single transmissive fracture zone might be connected to two different boreholes. Then, steady pumping from one borehole will induce downflow from storage in the other borehole. This situation is modeled by using the computed drawdown in the fracture zone caused by pumping to drive the hydraulic head in the fracture zone in the observation borehole (fig. 5). The computations demonstrate that the downflow induced in the observation borehole approaches a maximum some time after the start of pumping, and then begins to decline steadily with time. The maximum downflow can be directly related to fracture-zone storage coefficient, whereas the time at which this maximum occurs depends on fracture zone transmissivity (Lapcevic and others, 1993). In figure 5, the model computations match the observed flow data for a transmissivity value that agrees with hydraulic test data for the fracture zone and indicates a reasonable storage coefficient of about 2×10^{-5}. Comparison of the best fit model with other models indicates the sensitivity of the crossflow modeling technique. The model can be applied to more complex flow situations where there are several fracture zones connected in various ways and can be used to infer the nature of fracture zone geometry in the vicinity of the observation borehole (Paillet, 1996).

CONCLUSIONS

Geophysical logs are useful in bedrock borehole reconnaissance, when logs are used to identify the depth where permeable fractures intersect the borehole. This information is employed in sampling fracture populations and in developing geometrical models for fracture flow networks at field sites. However, conventional geophysical logs do not indicate the hydraulic properties of fractures. Such direct characterization is made possible using high-resolution flow profile logging. A well-posed inversion problem can be formulated to solve for estimates of fracture-zone transmissivity and hydraulic head if two different steady or quasi-steady flow profiles are obtained. At Mirror Lake, these profiles are obtained under ambient and

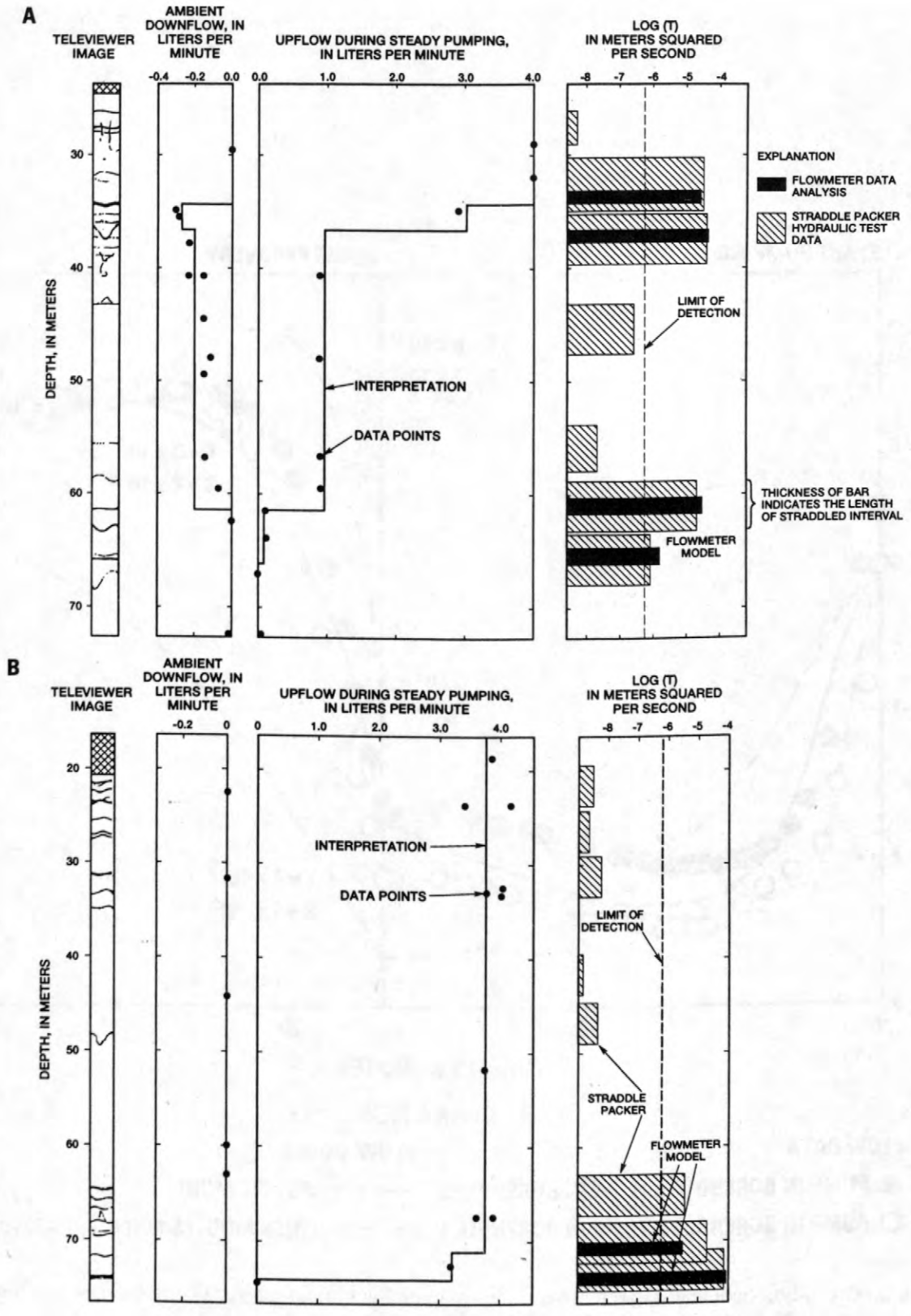

Figure 4. Flow profiles under pumped and ambient conditions and estimates of fracture transmissivity given by flowmeter analysis and hydraulic tests for boreholes (A) FSE-6 and (B) FSE-8 at the Mirror Lake study site (Paillet and Allen, 1996).

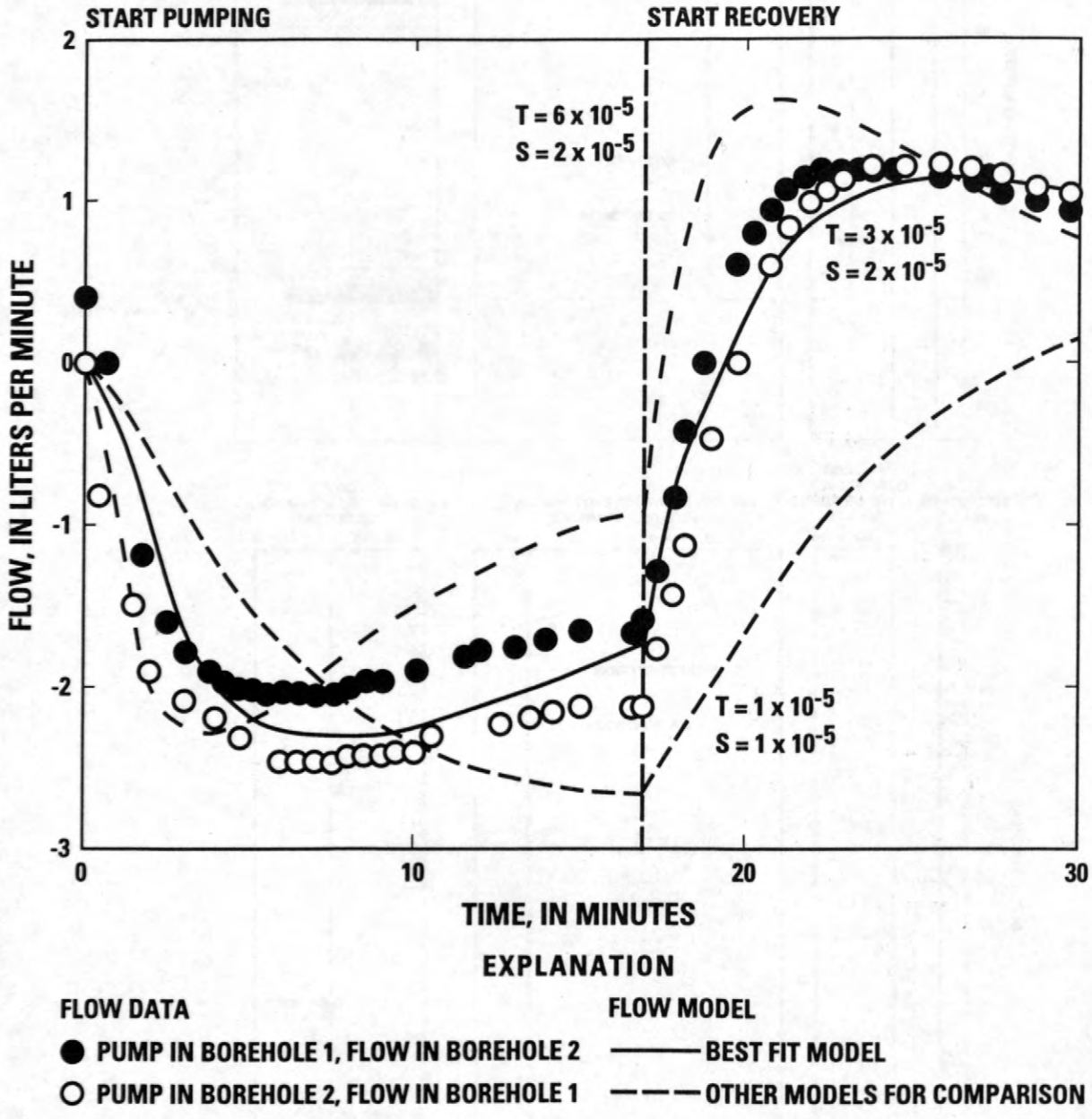

Figure 5. Cross-borehole flow experiment used to estimate the transmissivity (T) and storage coefficient (s) of a water-producing fracture zone (Paillet, 1998).

steady pumping at about 4 liters per minute, but steady injection may be more convenient at other sites. When cross-borehole flow experiments are conducted, the technique can be expanded to generate estimates of fracture-zone storage coefficient and to infer patterns of fracture connections in the region between pumped and observation boreholes.

REFERENCES

Barton, Colleen, Moos, Daniel, Peska, Pavel, and Zoback, Mark, 1997, Using wellbore image data to determine the complete stress tensor - application to permeability anisotropy and wellbore stability: Log Analyst, v. 38, no. 6, p. 21-33.

Hess, A.E., 1986, Identifying hydraulically conductive fractures with a slow-velocity borehole flowmeter: Canadian Geotechnical Journal, v. 23, no. 1, p. 69-78.

Johnson, C.D., and Dunstan, A.M., 1998, Lithology and fracture characterization from drilling investigations in the Mirror Lake area - from 1979 through 1995 in Grafton County, New Hampshire: U.S. Geological Survey Water-Resources Investigations Report 98-4183, 210 p.

Lapcevic, P.A., Novakowski, K.S., and Paillet, F.L., 1993, Analysis of transient flow in an observation well intersecting a single fracture: Journal of Hydrology, v. 151, p. 229-239.

Long, J.C.S., Karasaki, K., Dave, A., Peterson, J., Landsfeld, M., Kemeny, J., and Martel, S., 1991, An inverse approach to the construction of fracture hydrology models conditioned by geophysical data; an example from the validation exercises at the Stripa Mine: International Journal of Rock Mechanics and Mining Science & Geomechanics, v. 28, no. 213, p. 121-142.

Molz, F.J., Bowman, G.K., Young, S.C., and Waldrop, W.R., 1994, Borehole flowmeters--field application and data analysis: Journal of Hydrology, v. 163, p. 347-371.

Paillet, F.L., 1993, Application of borehole geophysics in the characterization of flow in fractured rocks: U.S. Geological Survey Water-Resources Investigations Report 93-4214, 36 p.

———1998, Flow modeling and permeability estimation using borehole flow logs in heterogeneous fractured formations: Water Resources Research, v. 34, no. 5, p. 997-1010.

Paillet, F.L., and Allen, B.S., 1996, Comparison of flowmeter estimates of fracture zone permeability with the results of conventional straddle packer injection tests: International Symposium of the Minerals and Geotechnical Logging Society, 6th, Santa Fe, N. Mex., 1995 [Proceedings], p. Y1-Y23.

Paillet, F.L., Hess, A.E., Cheng, C.H., and Hardin, E.L., 1987, Characterization of fracture permeability with high-resolution vertical flow measurements during borehole pumping: Ground Water, v. 25, no. 1, p. 28-40.

AUTHOR INFORMATION

Frederick L. Paillet, U.S. Geological Survey, Denver, Colorado.

Relation between Seismic Velocity and Hydraulic Conductivity at the USGS Fractured Rock Research Site

By Karl J. Ellefsen, Paul A. Hsieh, and Allen M. Shapiro

ABSTRACT

An analysis of velocities, derived from crosswell seismic data collected at the USGS Fractured Rock Research Site, shows that the velocities are related to the hydraulic conductivities of the fractured bedrock. The conductivities are calculated from measurements made with a straddle packer. A histogram of conductivities associated with low velocities (less than 5100 m/s) shows that low velocities are indicative of a wide range of conductivies. In contrast, a histogram of conductivities associated with high velocities (greater than or equal to 5100 m/s) shows that high velocities are indicative of low conductivities. Using these histograms, a frequency distribution of conductivity could be assigned to every point in a seismic velocity tomogram.

INTRODUCTION

In hydrologic studies of fractured bedrock, a significant problem is finding the hydraulically conductive zones that are between wells. Because finding these zones is difficult, geophysical methods, especially those using elastic waves, are often used first to locate fracture zones, which may or may not be conductive. Laboratory studies show that fractures diminish both the speed and the amplitude of elastic waves (see, for example, Birch, 1961; Hadley, 1976; Pyrak-Nolte and others, 1990). This effect is often exploited in field studies involving crosswell seismic, vertical seismic profiling, acoustic logging, and seismic reflection (see, for example, Paillet, 1980; Carswell and Moon, 1989; Gelbke and others, 1989; Hornby, 1989; Kim and others, 1994; Majer and others, 1997).

In a few studies, the properties of a single, conductive fracture are estimated using either acoustic logging data or vertical seismic profiling data (Beydoun and others, 1985; Hornby and others, 1989; Cicerone, 1991). However, determining properties of a single fracture from its effects on elastic waves is difficult: The permeability of a fracture can be estimated with acoustic logging data only if its porosity and its thickness are independently known (Tang and others, 1991). In another study, estimates of fracture transmissivities, made with acoustic logging data and vertical seismic profiling data, differ significantly from estimates based on data from pump tests (Hardin and others, 1987).

In this study, velocities derived from crosswell seismic data, collected at the USGS Fractured Rock Research Site, are analyzed. Unlike the previous studies, for which the focus is finding fracture zones or estimating properties of single fractures, this study uses histograms to relate velocities and hydraulic conductivities. These histograms are developed from comparisons of the tomographic velocities at the wells to the conductivities calculated from straddle packer measurements in those wells.

FIELD SITE

The USGS Fractured Rock Research Site is located in central New Hampshire, within the watershed of Mirror Lake (Figure 1). Overlying the bedrock is glacial drift, whose the thickness varies roughly between 15 and 20 m near the well field in which the crosswell seismic data were collected. The water table is within the glacial

drift. The bedrock consists of schist that was extensively intruded by granite, then by pegmatite, and finally by lamprophyre. In the bedrock, ground water flows along fractures. The fracture orientation is highly variable, although the dominant strike is N 30° E. Most fractures end in the rock matrix without connecting to other fractures, indicating that the fracture network is poorly connected. For additional information about the geology and the hydrology see Winter (1984), Barton (1994), Tiedeman and others (1997), and the references therein.

The crosswell seismic data were collected in a group of wells called the FSE well field (Figure 1). The depths of the wells range from 61 to 230 m below ground surface; in the glacial drift and the very top of the bedrock, the wells are cased with steel pipe to prevent collapse of the boreholes.

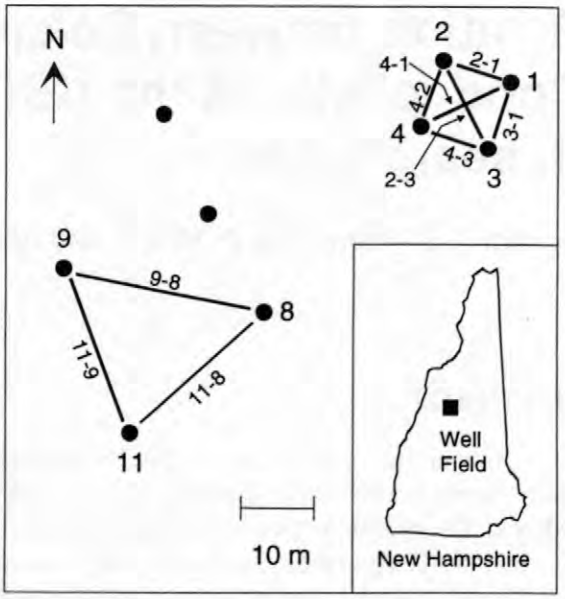

Figure 1. Map of the FSE well field and inset showing its approximate location in New Hampshire. Each dot represents a well; adjacent to each dot is the well number. Each line between two wells represents a tomogram; adjacent to each line is the tomogram number.

METHODS

Crosswell seismic tomography

To collect crosswell seismic data, a seismic source was placed in one well, below the water table (Figure 2a). The source generated a pressure wave (*P*-wave) that propagated through the bedrock where its speed and amplitude were affected by the fractures (as well as other rock properties). (In geophysics, "speed" is called "velocity," although a direction is not associated with it. For the rest of this article, the term "velocity" will be used.) As the *P*-wave propagated past the other well, it was detected by receivers (transducers), which were also below the water table. Each receiver generated a time-varying electrical voltage, a seismogram, that was digitally recorded by a computer located on the ground surface. This procedure was repeated for many different depths of both the source and the receivers so that the bedrock was thoroughly probed in many different directions by the *P*-waves. Additional information about the data acquisition is in Ellefsen and others (1998).

Some typical seismograms from the FSE well field are in Figure 2b. The horizontal axis is time; zero on this axis corresponds to the firing of the source. A voltage scale for the seismograms is not shown because it depends upon the source strength, which is unknown. The time at which the first part of the *P*-wave passed the receiver is used for tomography. This time is indicated by the arrows in Figure 2b and is called the "initial traveltime."

To process the crosswell seismic data, the initial traveltimes of all seismograms were measured, a procedure called "picking." The picking was done manually (that is, by eye) from a display on a computer screen; although this method was slow, its advantage was that unreliable traveltimes, which were usually caused by low amplitude *P*-waves, were readily detected and deleted. Additional information about the picking and about the procedure for checking of the traveltimes is in Ellefsen and others (1998).

Using a parameter estimation (inversion) algorithm, the *P*-wave velocities between the source and the receiver wells were estimated from the traveltimes. The mathematical model for the inversion represented the rock as perfectly elastic, heterogeneous, isotropic, and three-dimensional. A three-dimensional model was needed because most wells were highly deviated, making the source and the receiver locations outside any common plane. The coordinate system for this model was chosen with the origin just above the

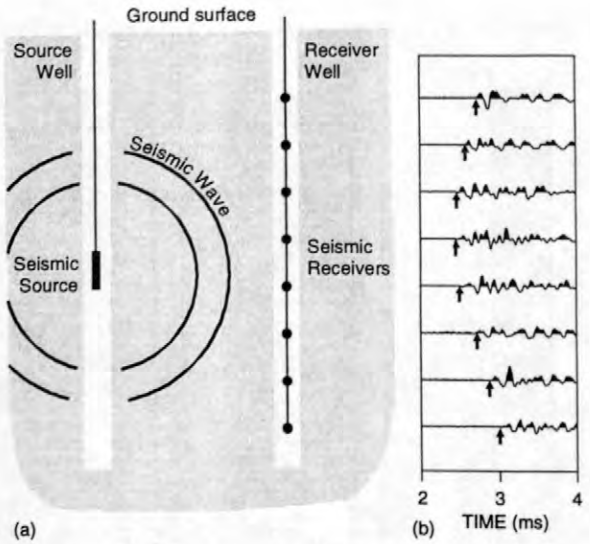

Figure 2. (a) Cross section between two wells showing how the crosswell seismic data were collected. (b) Seismograms showing the seismic waves that propagated past the receiver well. The arrows point to the initial traveltimes of the *P*-wave, which were used for tomography.

source well and at the elevation of the coordinate system for the well field. The x axis was horizontal and pointed from the source well to the receiver well; the z axis was vertical and pointed downward; the y axis was perpendicular to the x-z plane. With this orientation of the coordinate system, the sources and the receivers were somewhat close to the x-z plane at $y = 0$. The velocities were allowed to vary in the x and z directions but not in the y direction because velocity changes in the y direction cannot be well resolved. That is, the velocity changes were constrained to two dimensions, although the model is three-dimensional. The inversion algorithm changed the velocities until the calculated traveltimes matched the field traveltimes. Additional details regarding the inversion algorithm are in Ellefsen and others (1998).

The velocities estimated with the inversion algorithm are displayed as a map, which is called a "tomogram." All tomograms that are analyzed in this article are shown in Figure 3. Examine, for example, Figure 3a. The estimated velocities are shown by contours; the spatial resolution in the velocities — the shortest distance over which a significant change can be detected — is roughly 2 m. The top and the bottom edges of the tomogram are the boundaries beyond which the *P*-waves did not sample the bedrock enough to estimate satisfactorily the velocity. The left and right edges are at wells 4 and 2 respectively. This tomogram is designated "4-2" — the first number indicates the source well, the second the receiver well. The coordinate system for tomogram 4-2 is that used for the inversion. Although the coordinate systems for every tomogram in Figure 3 are different, their vertical axes (depth) are all referenced to the same elevation.

Straddle-packer tests

Single-well straddle-packer tests were conducted at the FSE well field. Two packers, separated by a distance of 3 to 4 m, were lowered into a well and then inflated with compressed air. The expansion of the packer gland against the rock formed a water-tight seal, thus isolating a 3 to 4 m interval for testing. After fluid pressure in the test interval returned to equilibrium from the initial disturbance, water was injected into the test interval at a constant pressure of about 1.0 atm (15 psi) above pretest pressure. Both the injection pressure and the injection flow rate were recorded. When the injection flow rate reached a steady value, the injection pressure was increased to about 2.0 atm (30 psi) above pretest pressure. Again, the injection pressure and flow rate were monitored until a steady state was reached. This procedure was repeated at successive intervals in every well.

The hydraulic conductivity K of the test interval was calculated with the Theim equation (see, for example, Bear, 1979, p. 306):

$$K = \frac{Q\rho g}{2\pi b\,\delta p} \ln\left(\frac{r_e}{r_w}\right) \qquad (1)$$

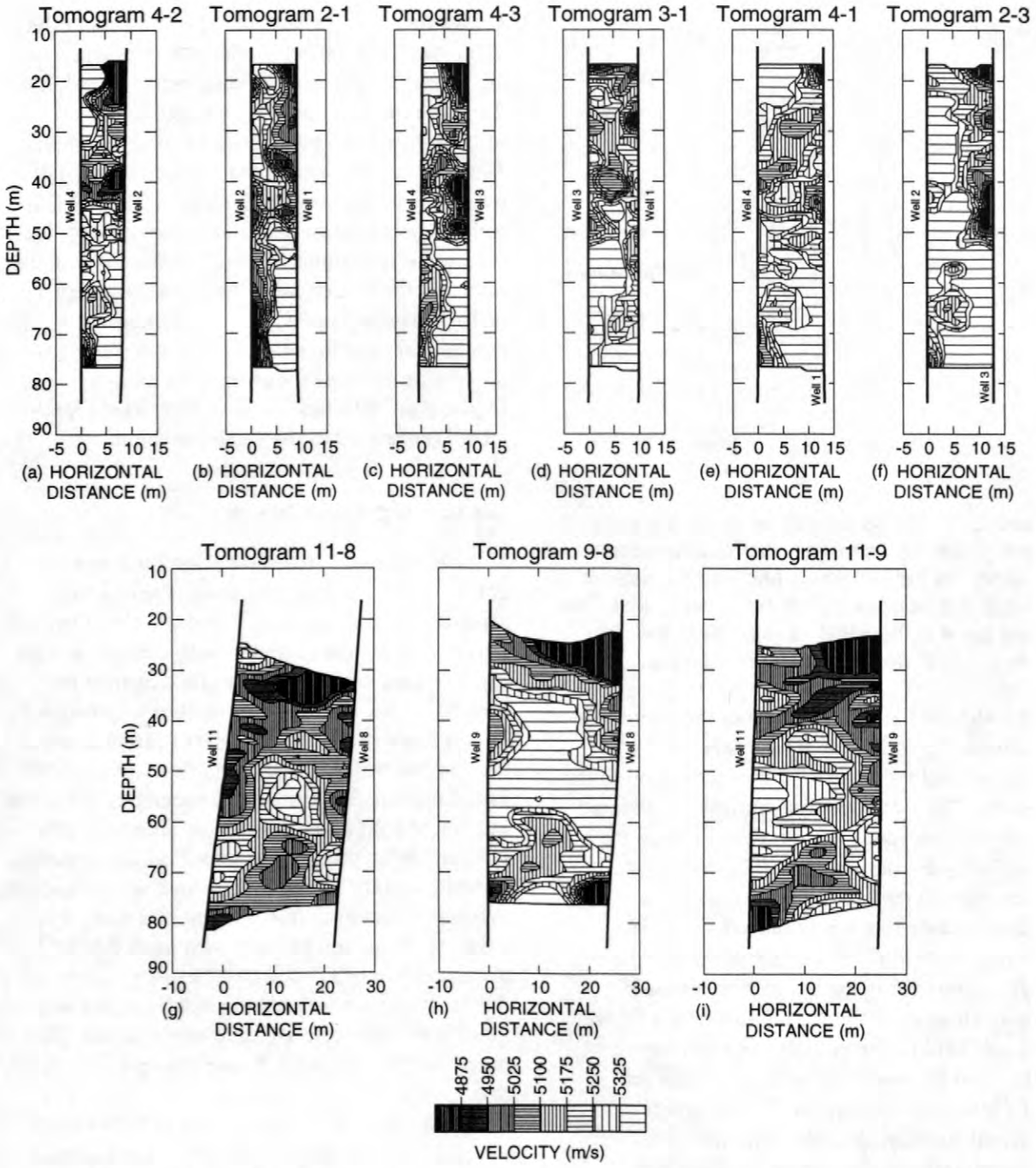

Figure 3. (a) (b) (c) (d) (e) (f) (g) (h) and (i) Velocity tomograms. All tomograms are plotted with the source well on the left and the receiver well on the right. The location of each tomogram within the well field is shown in Figure 1.

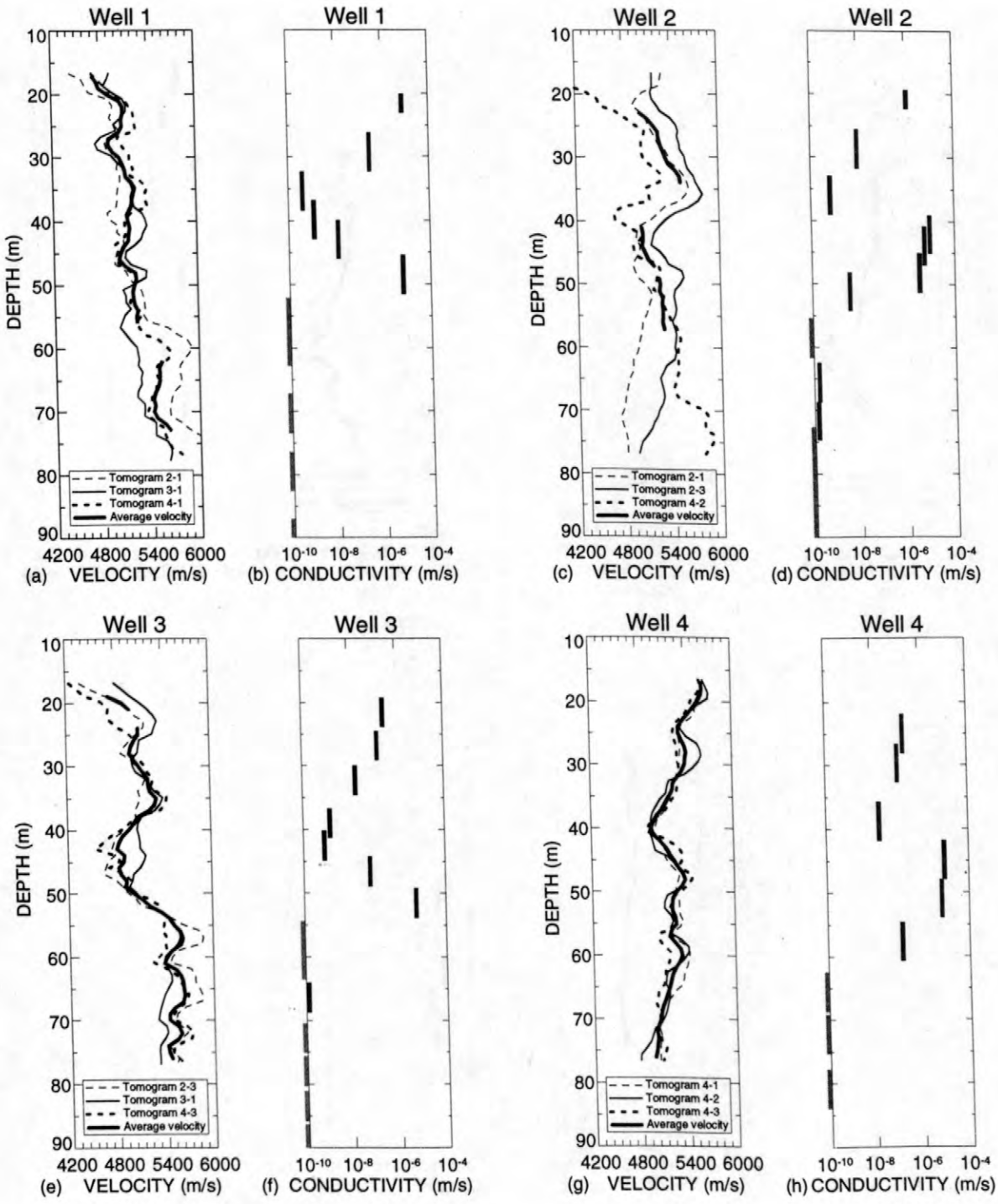

Figure 4. (a) (b) (c) (d) (e) (f) (g) and (h) Data at wells 1, 2, 3, and 4. The velocities for well 1, for example, are from those tomograms adjoining well 1 (Figure 3b, d, and e). The average velocities are computed from the tomographic velocities using the procedure described in the text. For the plots of conductivity, the gray bars on the left side indicate those intervals for which the injection flow rates were below the detection limit of the straddle packer equipment; for these intervals the hydraulic conductivity is less than 10^{-10} m/s. The top and the bottom of a gray or a black bar correspond to the top and the bottom, respectively, of the straddle packer equipment; the conductivity value applies to this entire interval.

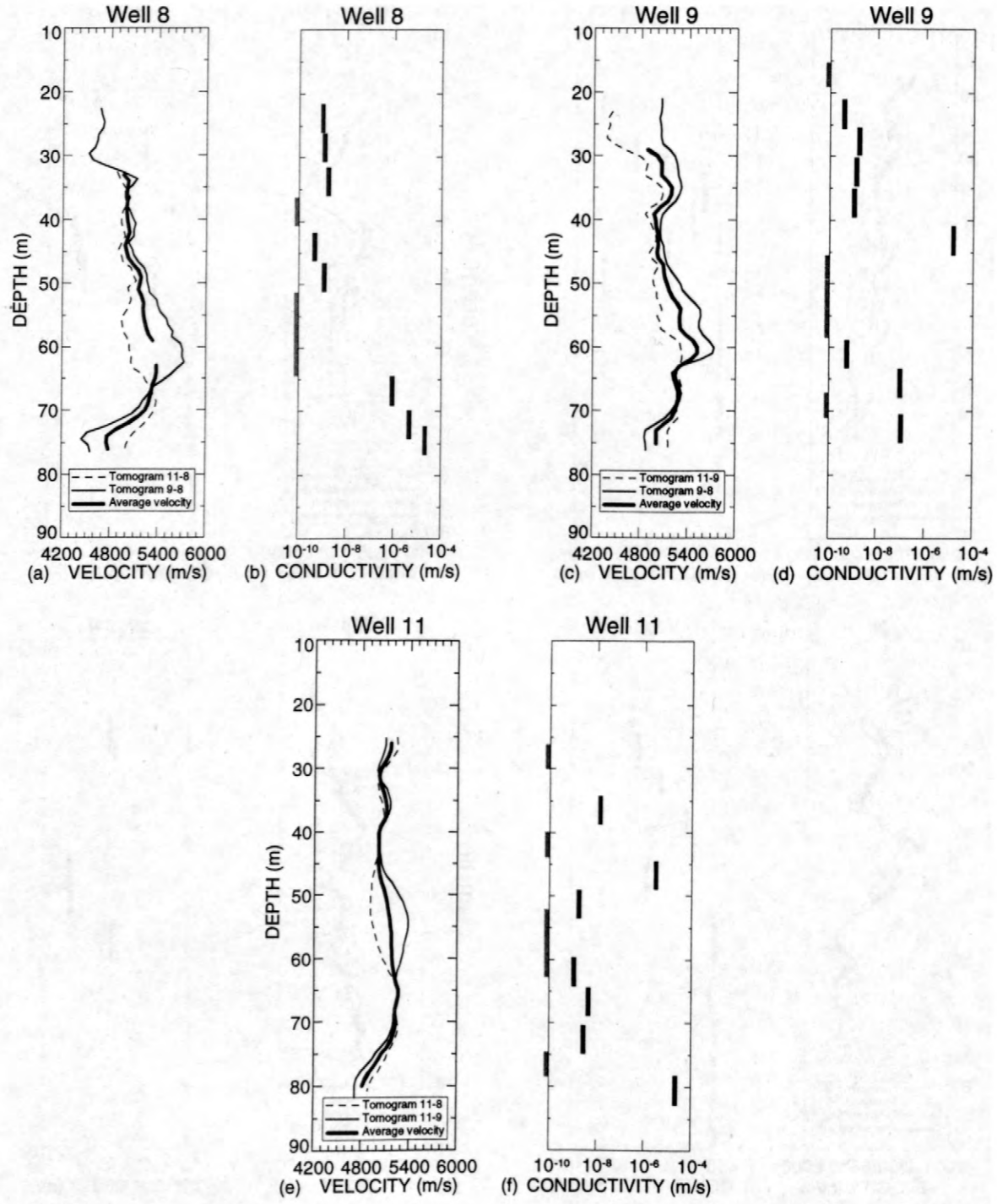

Figure 5. (a) (b) (c) (d) (e) and (f). Data at wells 8, 9, and 11. See the caption of Figure 4 for an explanation.

where

Q is the injection flow rate,

ρ is the density of water,

g is acceleration of due to gravity,

b is the length of the test interval,

δp is the injection pressure above pretest pressure,

r_w is the well radius, and

r_e is the effective radius beyond which the pressure increase due to injection is negligible.

The effective radius r_e which was unknown, was estimated to be 10 m. Because r_e is inside the natural log function of equation (1), the uncertainty in its value had only a small effect on the calculated value of K.

The use of two injection pressures yielded two values of hydraulic conductivity for each test interval, thus providing a reproducibility test. In all cases, the two values differed by no more than a few percent. In some intervals with very low conductivities, the injection flow rates were below the detection limit of the straddle packer equipment. Here the conductivities were unknown, but their upper bound was 10^{-10} m/s. The conductivities are shown in Figure 4 for wells 1, 2, 3, and 4 and in Figure 5 for wells 8, 9, and 11.

ANALYSIS

The velocities along the wells are extracted from the tomograms (Figure 3) and are plotted in Figure 4 for wells 1, 2, 3, and 4 and in Figure 5 for wells 8, 9, and 11. At each depth in each well, there are 1, 2, or 3 velocities. At any given depth, the differences between the smallest and the largest velocities from different tomograms should be somewhat small. For well 4 (Figure 4g), the differences are always less than 300 m/s. In contrast, for well 2 (Figure 4c), the differences are much larger. Between 69 and 76 m (depth), for example, the differences range from 860 to 1100 m/s. In other crosswell seismic surveys, similar velocity differences at wells have been observed (see, for example, Pratt and others, 1993).

There are several reasons for the velocity differences. There could be errors in the source locations, the receiver locations, or the traveltimes; these errors would cause errors in the tomographic velocities. Another reason is related to the spatial resolution in the velocities. Near a well, the angular coverage of the rays is limited, causing the spatial resolution in the horizontal direction to diminish (Bregman and others, 1989). Another reason is related to the velocity changes in the model, which are constrained to two dimensions. The heterogeneity (for example, fractures, granite intrusions, pegmatite intrusions), however, is three-dimensional, and sometimes it may affect the tomographic velocities.

At any given depth where there are two or more tomographic velocities, they are averaged (Figures 4 and 5). At some depths, a velocity could be spurious (for the reasons just given), and so the average could be spurious. These are identified according to this criterion: At a given depth, an average that differs from any tomographic velocity by more than 300 m/s is deemed spurious. Spurious averages are not plotted in Figures 4 and 5. Also, where there is only one tomographic velocity, the average cannot be tested, and so it too is not plotted. Despite this rigorous criterion, there are suitable average velocities at most depths in all wells, except well 2. These average velocities probably have smaller errors than the tomographic velocities have.

In each depth interval for which there is a calculated hydraulic conductivity, there are typically 4 to 6 average velocities (Figures 4 and 5). For conductivities less than 10^{-10} m/s, the ranges of these velocities are plotted in Figure 6a; for conductivities greater than 10^{-10} m/s, the ranges are plotted against conductivity in Figure 6b. The focus of the analysis is on the minimum velocity from each range. The reason is that the fracture properties, and hence the conductivity and the velocity, vary over the depth interval spanned by the straddle packer equipment. The sub-interval having the highest conductivity determines the conductivity for the entire interval; this sub-interval probably has the lowest velocity.

In Figure 6a and b, there is no curvilinear (linear, quadratic, etc.) relation between the conductivity and the minimum velocity, and so a different approach is used to search for a relation. Each conductivity in Figures 6a and b is placed into one of two groups, according to whether the

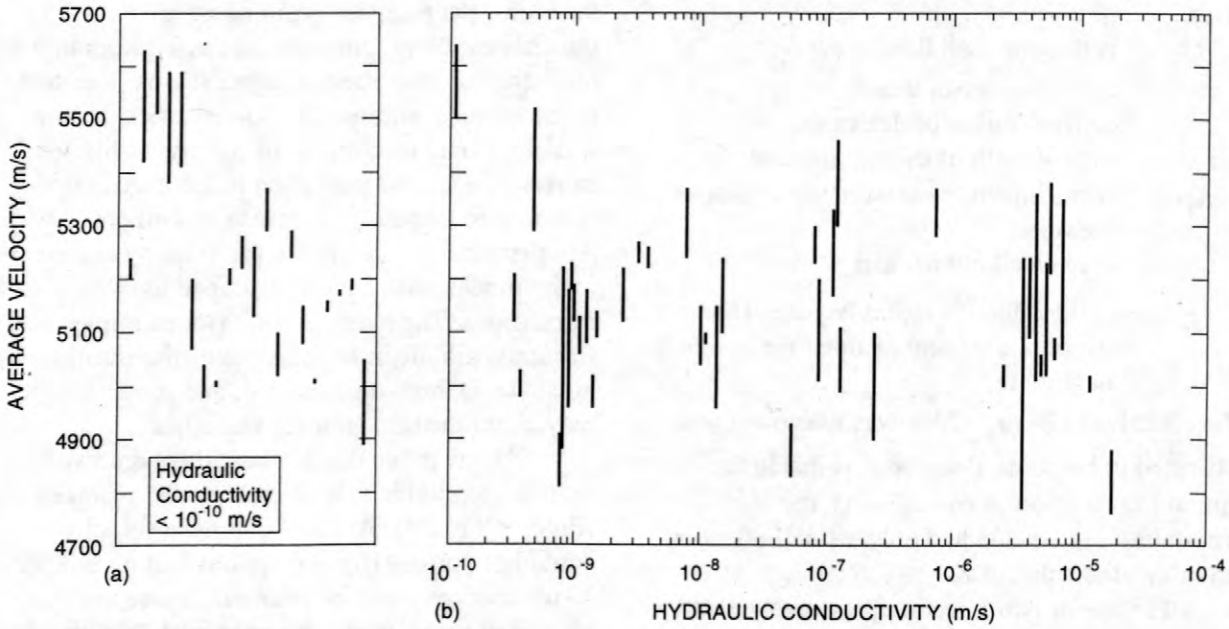

Figure 6. Ranges of (average) velocities for hydraulic conductivities (a) less than 10^{-10} m/s and (b) greater than 10^{-10} m/s. Each bar represents the data from one straddle packer test. The abscissa in plot (a) has no physical meaning — it is only used to separate the bars. The data are from Figures 4 and 5.

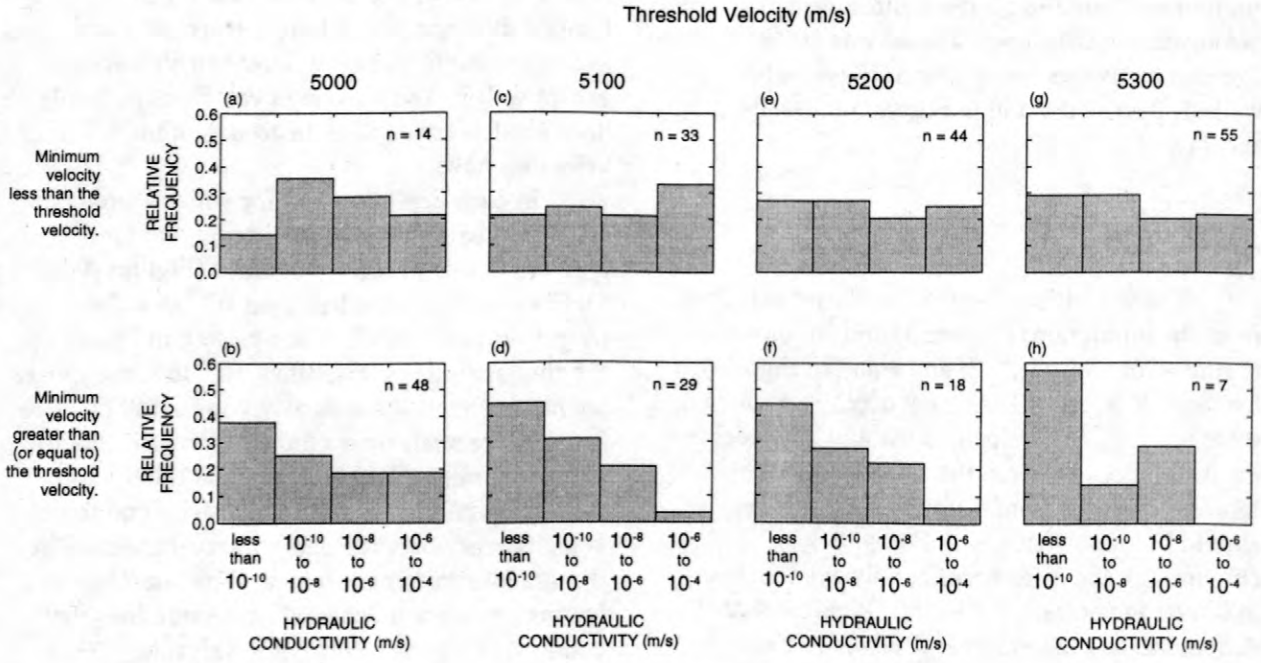

Figure 7. (a), (b), (c), (d), (e), (f), (g), and (h) Histograms of the hydraulic conductivity for four threshold velocities. The data are from Figure 6. The number of conductivity values used to construct a histogram is "*n*."

associated minimum velocity is less than some threshold, or greater than (or equal to) that threshold. For both groups, histograms of the conductivities are constructed. Since the most suitable threshold velocity is unknown, pairs of histograms are also made for 4 different threshold velocities — 5000, 5100, 5200, and 5300 m/s (Figure 7). The amount of confidence given to a histogram is related to the number of conductivity values from which it is constructed, n. Little confidence should be given to the histogram with $n=7$ (Figure 7h), somewhat more to the histogram with $n=14$ (Figure 7a), etc., and a lot of confidence to the histogram with $n=55$ (Figure 7g).

Examine those histograms for which the minimum velocity is less than the threshold velocity (Figure 7a, c, e, and g). The relative frequencies for all conductivities are roughly the same; in Figures 7g, for example, the relative frequencies are 0.29, 0.29, 0.20, and 0.22. These histograms indicate that low velocities are associated with a wide range of conductivities. The likely reason is that fractures cause the velocity to be low. The nature of the fractures, however, determines the conductivity: If the fractures are conductive and they from an interconnected network, then the conductivity will be high. On the other hand, if either condition (or both conditions) are not satisfied, then the conductivity will be low. In this particular well field, a common assumption — low velocities are always associated with high conductivities — is not correct.

Examine the histograms for which the minimum velocity is greater than or equal to the threshold velocity (Figure 7b, d, f, and h). For the histogram in Figure 7b, the relative frequency for conductivities between 10^{-6} and 10^{-4} m/s is moderately high (0.19) and is much higher than the corresponding relative frequencies for the other histograms (Figure 7d, f, and h). For this case, the threshold velocity is so low that intervals with both low velocities and high conductivities are included in the histogram. For the histograms in Figure 7d, f, and h, the relative frequencies are large only for low conductivities. This result indicates that low conductivities are associated with high velocities; the likely reason is that the rock contains few fractures.

The pair of histograms with the threshold velocity of 5300 m/s should not be used to interpret tomograms because little confidence can be given to the histogram constructed with 7 values (Figure 7h). In addition, the pair of histograms with the threshold velocity of 5000 m/s should not be used because their frequency distributions (Figure 7a and b) are similar. Of the two remaining pairs, the pair with the threshold velocity of 5100 m/s (Figure 7c and d) seems most suitable because a lot of confidence can be given to both histograms — both are constructed from a large number of conductivity values.

CONCLUSIONS

In this study, velocities derived from crosswell seismic data collected at the USGS Fractured Rock Research Site are compared to hydraulic conductivities. At each depth in each well, velocities from different tomograms are averaged, and the mimimum of the average velocities along the straddle packer is used for the comparison.

In the histogram of conductivities associated with low velocities (less than 5100 m/s), the relative frequencies are roughly equal; this result shows that low velocities are indicative of a wide range of conductivities. The likely reason is that fractures cause the velocity to be low. The nature of the fractures, however, determines the conductivity: If the fractures are conductive and they form an interconnected network, then the conductivity will be high. On the other hand, if either condition (or both conditions) are not satisfied, then the conductivity will be low. In the histogram of conductivities associated with high velocities (greater than or equal to 5100 m/s), the relative frequencies are large only for low conductivities; this result shows that high velocities are indicative of low conductivities. The likely reason is that the rock contains few fractures.

Either of the two histograms could be assigned to every point in a tomogram according to its velocity; thus, there would be a frequency distribution of conductivity for every point. Such information would be used to constrain a hydrologic model of the fractured bedrock. It is

expected that, for studies of fractured bedrock in other areas, similar statistical relations between velocity and conductivity could be developed.

ACKNOWLEDGEMENTS

This work is supported by the Toxics Substances Hydrology Program of the U. S. Geological Survey.

REFERENCES

Barton, C. C., 1996, Characterizing bedrock fractures in outcrop for studies of ground-water hydrology: An example from Mirror Lake, Grafton County, New Hampshire *in* Morganwalp, D. W., and Aronson, D. A., eds., U. S. Geological Survey Toxic Substances Hydrology Program – Proceedings of the technical meeting, Colorado Springs, Colorado, September 20–24, 1993; U. S. Geological Survey Water-Resources Investigations Report 94-4015, p. 81–87.

Bear, Jacob, 1979, Hydraulics of Ground Water: McGraw Hill, New York, 569 p.

Beydoun, W. B., Cheng, C. H., and Toksöz, M. N., 1985, Detection of open fractures with vertical seismic profiling: Journal of Geophysical Research, v. 90, no. B6, p. 4557–4566.

Birch, F., 1961, The velocity of compressional waves in rocks to 10 kilobars, Part 2: Journal of Geophysical Research, v. 66, no. 7, p. 2199–2224.

Bregman, N. D., Bailey, R. C., and Chapman, C. H., 1989, Ghosts in tomography: The effects of poor angular coverage in 2-D seismic traveltime inversion: Canadian Journal of Exploration Geophysics, v. 25, p. 7–27.

Carswell, A., and Moon, W. M., 1989, Application of multioffset vertical seismic profiling in fracture mapping: Geophysics: vol. 54, no. 6, p. 737–746.

Cicerone, R. D., 1991, Detection and characterization of in-situ fractures in the Earth from vertical seismic profiling data: Massachusetts Institute of Technology, Ph. D. dissertation, 208 p.

Ellefsen, K. J., Kibler, J. E., Hsieh, P. A., and Shapiro, A. M., 1998, Crosswell seismic tomography at the USGS Fractured Rock Research Site: Data collection, data processing and tomograms: U. S. Geological Survey Open-File Report 98–510.

Gelbke, C., Miranda, F., and Sattel, G., 1989, Results of a seismic transmission tomography survey at the Grimsel Rock Laboratory: The Log Analyst, v. 30, no. 4, p. 243–260.

Hadley, K., 1976, Comparison of calculated and observed crack densities and seismic velocities in Westerly granite: Journal of Geophysical Research, v. 81, no. 20, p. 3484–3494.

Hardin, E. L., Cheng, C. H., Palliet, F. L., and Mendelson, J. D., 1987, Fracture characterization by means of attenuation and generation of tube waves in fractured crystalline rock at Mirror Lake, New Hampshire: Journal of Geophysical Research, v. 92, no. B8, p. 7989–8006.

Hornby, B. E., 1989, Imaging of near-borehole structure using full-waveform sonic data: Geophysics, vol. 54, no. 6, p. 747–757.

Hornby, B. E., Johnson, D. L., Winkler, K. W., and Plumb, R. A., 1989, Fracture evaluation using reflected Stoneley-wave arrivals: Geophysics, vol. 54, no. 10, p. 1274–1288.

Kim, J. S., Moon, W. M., Lodha, G., Mulu, S., and Soonawala, N., 1994, Imaging of reflection seismic energy for mapping shallow fracture zones in crystalline rocks: Geophysics, vol. 59, no. 5, p. 753–765.

Majer, E. L., Peterson, J. E., Daley, T., Kaelin, B., Myer, L. Queen, J., D'Onfro, P., and Rizer, W., 1997, Fracture detection using crosswell and single well surveys: Geophysics: vol. 62, no. 2, p. 495–504.

Paillet, F. L., 1980, Acoustic propagation in the vicinity of fractures which intersect a fluid-filled borehole, *in* Transactions of the 21st Annual Logging Symposium, Society of Professional Well Log Analysts, paper DD.

Pratt, R. G., McGaughey, W. J., and Chapman, C. H., 1993, Anisotropic velocity tomography: A case study in a near-surface rock mass: Geophysics, v. 58, no. 12, p. 1748–1763.

Pyrak-Nolte, L. J., Meyer, L. R., Cook, N. G. W., 1990, Transmission of seismic waves across single natural fractures: Journal of Geophysical Research, v. 95, no. B6, p. 8617–8638.

Tang, X. M., Cheng, C. H., and Paillet, F. L., 1991, Modeling borehole Stoneley wave propagation across permeable in-situ fractures *in* Transactions of the 32nd Annual Logging Symposium, Society of Professional Well Log Analysts, paper GG.

Tiedeman, C. R., Goode, D. J., Hsieh, P. A., 1997, Numerical simulation of ground-water flow through glacial deposits and crystalline bedrock in the Mirror Lake area, Grafton County, New Hampshire: U. S. Geological Survey Professional Paper 1572, 50 p.

Winter, T. C., 1984, Geohydrologic setting of Mirror Lake, West Thorton, New Hampshire: U. S. Geological Survey Water-Resources Investigations Report 84–4266, 61 p.

Borehole Radar Tomography using Saline Tracer Injections to Image Fluid Flow in Fractured Rock

By John W. Lane, Jr., David L. Wright, and F. Peter Haeni

ABSTRACT

Cross-hole radar tomography surveys using saline tracer injections have been developed and tested at the U.S. Geological Survey Mirror Lake fractured-rock field-research site in Grafton County, New Hampshire to delineate transmissive fracture zones and image fluid flow at a scale of a meter to about 100 meters (m). High concentration (20-50 gram per liter) sodium chloride tracers injected into transmissive fractures increase the electromagnetic (EM) attenuation observed in cross-hole radar scans as compared to the observed background attenuation. The observed differences in EM attenuation are inverted to produce attenuation-difference tomograms.

Attenuation-difference tomograms acquired under 'steady-state' injection and pumping conditions were used to delineate the locations and orientations of transmissive fracture zones between boreholes. Time-lapse radar-tomography methods can monitor slug-injection saline tracer tests and image fluid flow paths in fractured-rock. Time-lapse cross-hole radar data sets were acquired at Mirror Lake by using controlled injections of fixed volumes of a high-concentration saline tracer, while scanning small sections of the tomographic image. Equivalent time data from each scanned section are sorted, analyzed to determine attenuation differences, and inverted. Time-lapse attenuation-difference tomograms delineate transmissive zones, identify variability within transmissive zones, and provide kinematic information that images ground-water flow and transport at a scale of a meter to 100 m.

The location of transmissive zones within the tomographic image plane and tracer travel times to the image plane are provided by steady-state and time-lapse attenuation-difference tomograms. Results of steady-state and time-lapse tomography surveys were used to help construct and calibrate ground-water flow and transport models in the FSE well field.

Time-lapse tomography would be more useful if time-dependent attenuation changes could be used to estimate tracer specific conductance and concentration at the image plane. A simple effective medium method of analyzing time-dependent attenuation changes to estimate tracer specific conductance was tested on radar data acquired over a meter-scale fractured granite block. Preliminary results illustrate the importance of estimating secondary porosity accurately, and suggest that robust analysis may require (1) accounting for effects of EM scattering on attenuation, and (2) modifying field methods to include several steady-state injection tests using different tracer concentrations.

INTRODUCTION

In fractured-rock aquifers, direct observation of fractures and measurement of hydraulic properties is limited by the location, number, and orientation of boreholes. Geophysical methods can supplement direct observations by measuring physical-property changes induced by fractures at borehole to field scales. Cross-hole radar tomography is one of the geophysical methods that has been used at the U.S. Geological Survey (USGS) Mirror Lake fractured-rock field-research site in the Hubbard Brook Experimental Forest, Grafton County, New Hampshire (fig. 1), to image fracture zones and lithologic changes at field scales useful for flow and transport modeling.

The interpretation of radar anomalies to identify transmissive fractures has been improved at Mirror Lake by combining borehole-radar surveys in cross-hole tomography and single-hole reflection modes with the injection of high-salinity sodium chloride (NaCl) (20-50 grams per liter (g/l) NaCl) tracers (Lane and others, 1996;

Wright and others 1996; Day-Lewis and others, 1997; Lane, Haeni, and Versteeg, 1998; Lane, Haeni, and Day-Lewis, 1998; Liu and others, 1998; Wright and Lane, 1998).

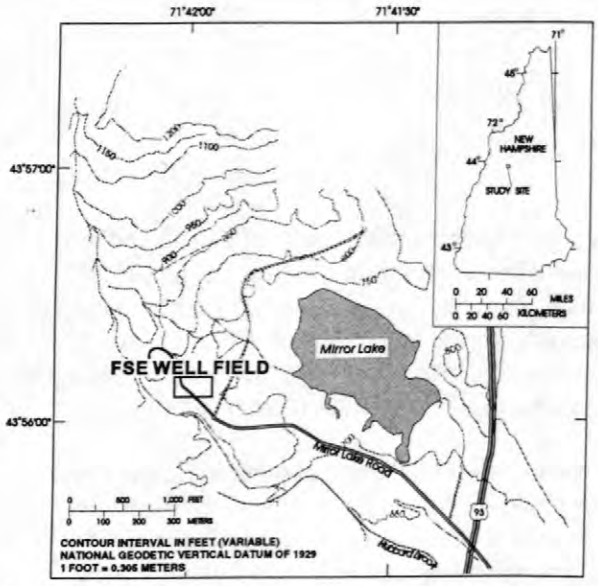

Figure 1. Location of study area and the FSE well field at the U.S. Geological Survey Fractured-Rock Field Research site, Mirror Lake, Grafton County, New Hampshire.

Saline tracers are electrically conductive. The attenuation of an electromagnetic (EM) wave that propagates across a fracture increases if the electrical conductivity of the water within that fracture is increased. By conducting cross-hole radar surveys before, during, and after saline tracer tests, it is possible to identify differences in EM attenuation induced by transport of the tracer through transmissive fractures. Differences in attenuation can be analyzed tomographically to image transmissive zones between boreholes (Ramirez and Lytle, 1986; Niva and others, 1988; Olsson and others, 1992).

This paper summarizes methods developed at Mirror Lake that combine cross-hole radar tomography with saline tracer injections to delineate transmissive fractures and image fluid flow.

FIELD EXPERIMENTS

A series of field experiments was begun in 1995 to test and develop cross-hole radar attenuation-difference tomography methods in fractured rock. The experiments were conducted at the USGS Mirror Lake fractured-rock field-research site in the Hubbard Brook Experimental Forest, Grafton County, New Hampshire. A description of the hydrogeology of the Mirror Lake site is given in Shapiro and Hseih (1991, 1996) and Shapiro and others (1995). Additional experimental details and results are given in Lane and others (1996), Lane, Haeni, and Day-Lewis (1998), Lane, Haeni, and Versteeg (1998), and Wright and Lane (1998).

Cross-hole radar tomography surveys were conducted with instruments designed and built by the USGS and with commercially available systems, using borehole antennas with center frequencies ranging from 30 to 100 megahertz (MHz). The experiments have been conducted at the FSE 1-4 cluster within the FSE well field, an arrangement of four boreholes that approximate a 9-meter (m) square (fig. 2).

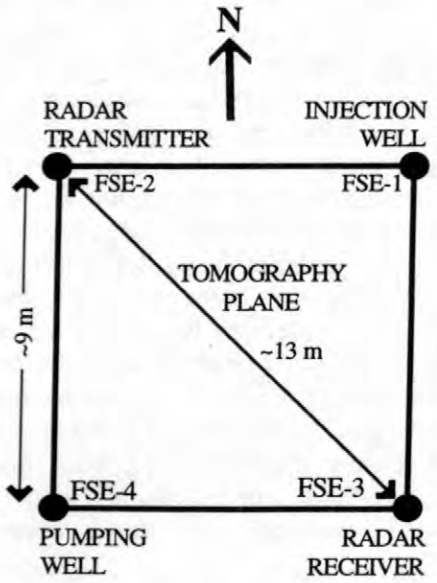

Figure 2. Plan view of FSE 1 to 4 borehole cluster, FSE well field, Mirror Lake, Grafton County, New Hampshire.

The experiments focused on tomographic imaging of a transmissive zone connecting the boreholes at a depth of about 40 m. Straddle-packers were used to isolate the transmissive zone in the injection and pumped boreholes (FSE-1 and FSE-4; fig. 3). NaCl solutions in concentrations ranging from 20-50 g/L were used as tracers. Different tracer injection procedures and pumping

rates were used, depending on the objectives of the experiment. In 1995 and 1996, the transmissive zone in the observation boreholes (FSE-2 and FSE-3; fig. 2) was left open to permit radar logging. In 1997, specially constructed, reusable PVC packers were used. These packers allow radar and other borehole logs to be collected through the PVC core pipe that suspends the packers (fig. 4). The PVC packers were used to isolate the transmissive zone in the injection and observation boreholes (FSE 1-3) to minimize movement of tracer into the radar-logging boreholes.

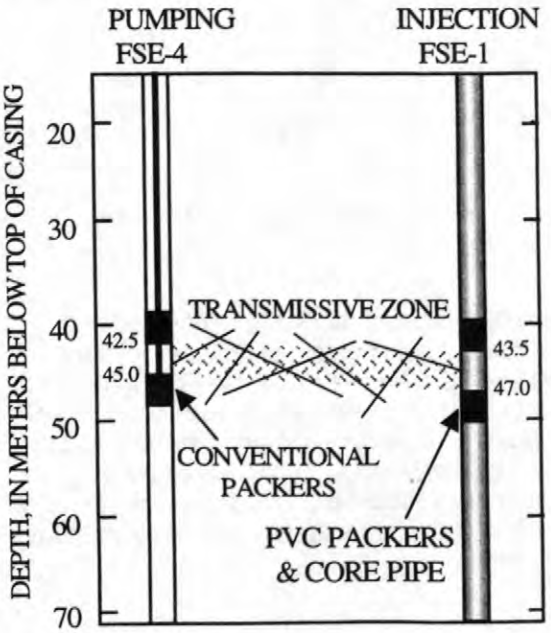

Figure 3. Arrangement of PVC and conventional straddle packers used to isolate a transmissive zone in FSE-1 and FSE-4.

Robust tomographic inversion of attenuation-difference data requires that any change in the distribution and concentration of the tracer that occurs during radar-data acquisition be small. One way this 'steady-state' requirement has been satisfied at Mirror Lake is through near-continuous injection and pumping of the tracer during radar-data acquisition.

'Steady-state' attenuation-difference tomograms delineate transmissive zones within the tomographic image plane. For example, figure 5 shows an attenuation difference tomogram between FSE-2 and FSE-3. The attenuation difference anomalies in figure 5 are consistent with a subhorizontal fracture zone and a steeply dipping fracture zone. This interpretation is qualitatively consistent with the pattern of fractures observed intersecting FSE-2 and FSE-3 on acoustic televiewer logs (F.L. Paillet, U.S. Geological Survey, written commun., 1994), borehole video logs (Johnson and Dustan, 1998), and results of single-hole directional radar surveys in the FSE 1-4 cluster (Lane and others, 1996). Steady-state attenuation tomograms provide insights about the location and geometry of transmissive zones in fractured rocks, but do not provide time-dependent information useful for understanding flow and transport.

Cross-hole radar methods *can* record transient hydraulic processes. For example, in Wright and Lane (1998), repeated cross-hole radar scanning during the start of an injection test identified the 'break-through' of the tracer as it passed across the image plane (fig. 6). The use of conventional cross-hole radar tomography methods to image time-dependent processes is difficult at Mirror Lake and other fractured-rock sites because significant changes in tracer location and concentration can occur in minutes, whereas a complete cross-hole radar tomography survey can require hours.

Figure 4. Photograph of log-through PVC packer assembly developed at Mirror Lake.

In order to monitor field-scale slug-injection saline-tracer tests, a time-lapse attenuation-difference tomography method was developed using sequential tracer injection and incremental cross-hole radar scanning (Day-Lewis and others,

1997; Lane, Haeni, and Day-Lewis, 1998). The method requires carefully repeating a dipole saline-tracer injection test using a small fixed volume of saline tracer. During tracer injection and recovery, a portion of the tomographic image plane is repeatedly scanned (fig. 7). The start of each scan is timed relative to the start of the injection cycle to permit *equivalent* time sorting of the data. The amount of time required to complete one scan is minimized to meet the 'steady-state' assumption, while maximizing temporal resolution. The cross-hole data from each section collected during equivalent time intervals are merged to form a time-lapse series of tomography data sets suitable for attenuation-difference analysis and for tomographic inversion.

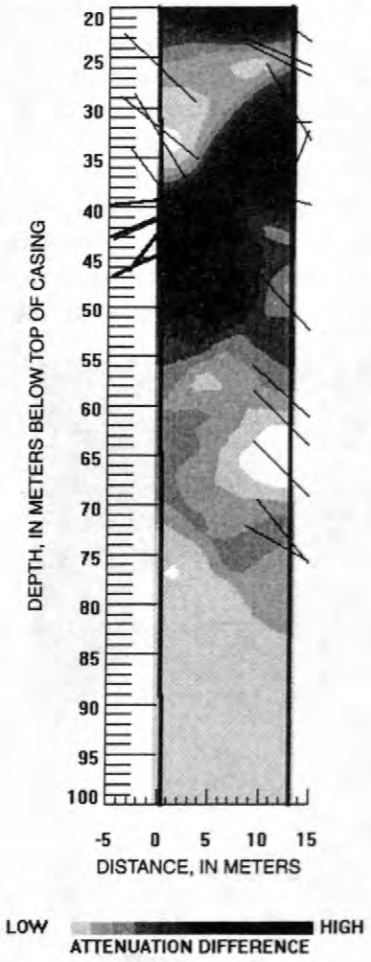

Figure 5. 30 MHz attenuation-difference tomogram between FSE-2 and FSE-3 in the FSE well field at Mirror Lake, New Hampshire. Interpreted reflectors from single-hole directional borehole radar surveys in the FSE 1-4 cluster are superimposed on the tomogram. Dark lines represent known transmissive zones.

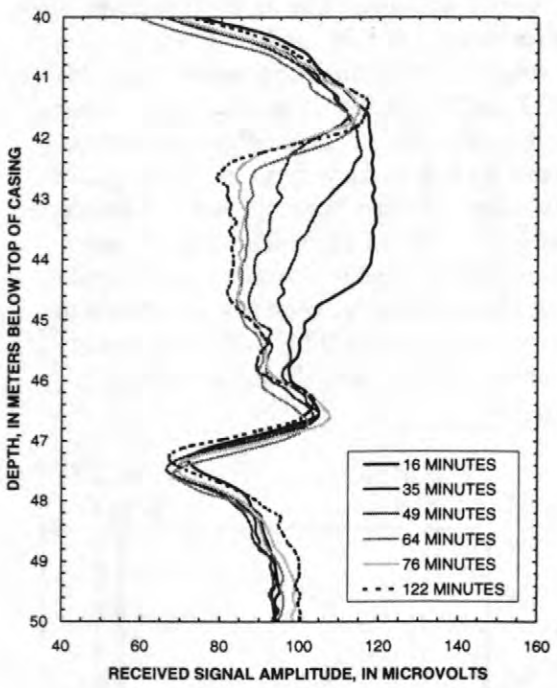

Figure 6. Common-depth cross-hole radar amplitudes plotted against measurement depth between FSE-2 and FSE-3 in the FSE well field at Mirror Lake N.H. for six logging runs conducted over a 2-hour time period starting at the onset of tracer injection. Amplitude decreases between 42 and 46 meters record the arrival and breakthrough of tracer across the image plane (after Wright and Lane, 1998).

Figure 8 shows the effects of tracer on EM wave attenuation. Wave attenuation behavior with time resembles 'break-through' curves. These waves record the passage of the tracer across the image plane. The attenuation of waves traversing non-transmissive regions remains unchanged with time.

Tomographic inversion of equivalent time data produces a series of attenuation-difference 'snapshots' that delineate the location and orientation of attenuation-difference anomalies *and* identify kinematic changes in attenuation associated with the transport of the saline tracer. For example, figure 9 contains a subset of 31 tomograms produced from time-lapse cross-hole radar monitoring of a slug-injection saline tracer test conducted at the FSE well field in 1997. The tomograms show the general location, geometry,

and kinematic characteristics of attenuation anomalies in the FSE-2 to FSE-3 plane.

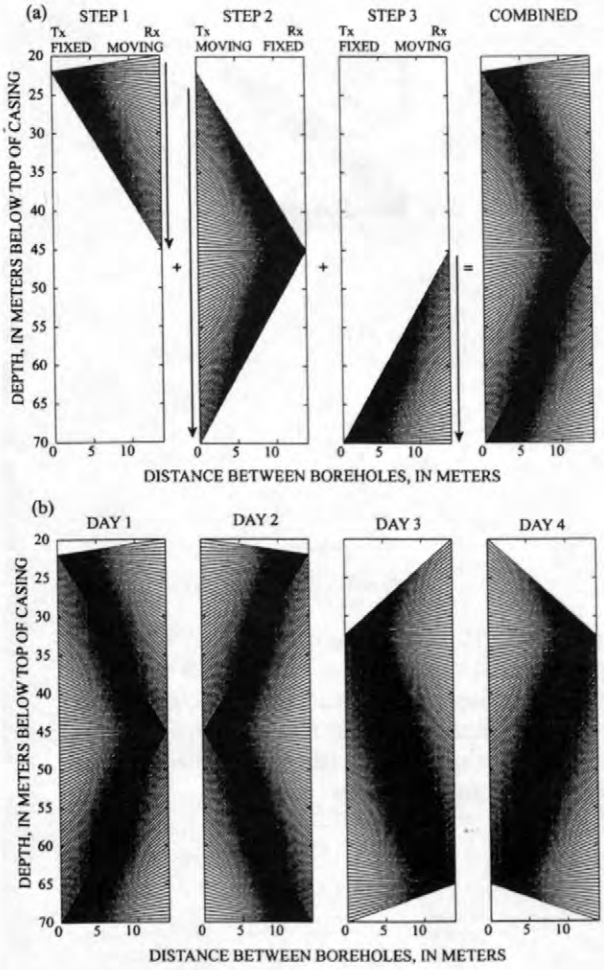

Figure 7. Radar-data acquisition method used for time-lapse radar monitoring of a slug-injection saline tracer test conducted at the FSE well field, Mirror Lake, New Hampshire, in 1997. Transmitter (Tx) - receiver (Rx) geometry used for consecutive saline-tracer injections; (a) fixed and moving antenna locations for day 1, (b) complete transmitter-receiver pattern for each day.

The time-lapse tomography results are consistent with hydraulic tests (Hsieh and Shapiro, 1996), 'steady-state' attenuation-difference tomograms (Lane and others, 1996; Wright and Lane, 1998), and results of single-hole directional radar surveys in the FSE 1-4 cluster (Lane and others, 1996) (fig. 10). In addition, the time-lapse tomography results indicate that within the transmissive zone connecting FSE 1-4, a high-permeability pathway exists, connecting FSE-1 to FSE-4 through fractures that pass through or near FSE-2.

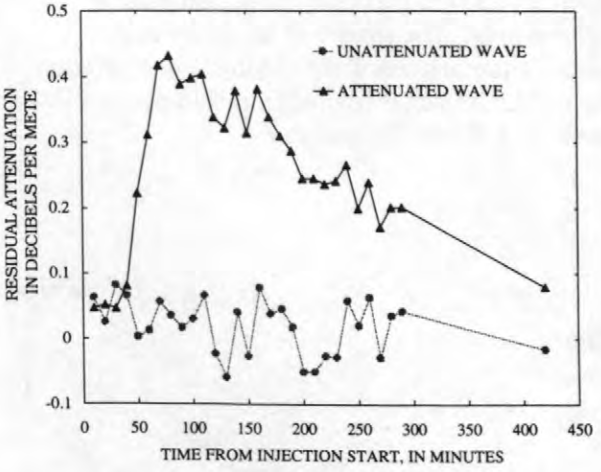

Figure 8. Examples of time-varying effects of saline tracer on wave attenuation history.

Time-lapse radar attenuation-difference tomography results can be used in flow and transport modeling. For example, the location and orientation of attenuation-difference anomalies and travel times interpreted from tracer 'break-through' across the image plane along with results of previous USGS work in the FSE well field (Hseih and Shapiro, 1996) were used by Day-Lewis (Day-Lewis and others,1997; Lane, Haeni, and Day-Lewis, 1998) and Shapiro (Shapiro and others, 1998) to help construct and calibrate simplified ground-water flow and transport models of the FSE 1-4 cluster using MODFLOW (McDonald and Harbaugh, 1988) and MT3D (Zheng, 1990).

ANALYSIS OF ATTENUATION DIFFERENCES TO ESTIMATE IMAGE-PLANE TRACER CONCENTRATION

Time-lapse cross-hole radar tomography methods would be more useful for flow and transport modeling in fractured rock if observed time-dependent radar attenuation differences could be interpreted to estimate tracer concentrations. The relationship between time-dependent attenuation differences and outlet

concentration is shown in figure 11. Outlet chloride concentration and integrated tomogram attenuation changes (sum of pixel attenuation) from the 1997 experiment are shown plotted against time. The shapes of the integrated attenuation-difference and chloride concentration curves are remarkably similar, including double-peaks at 100 and 200 minutes.

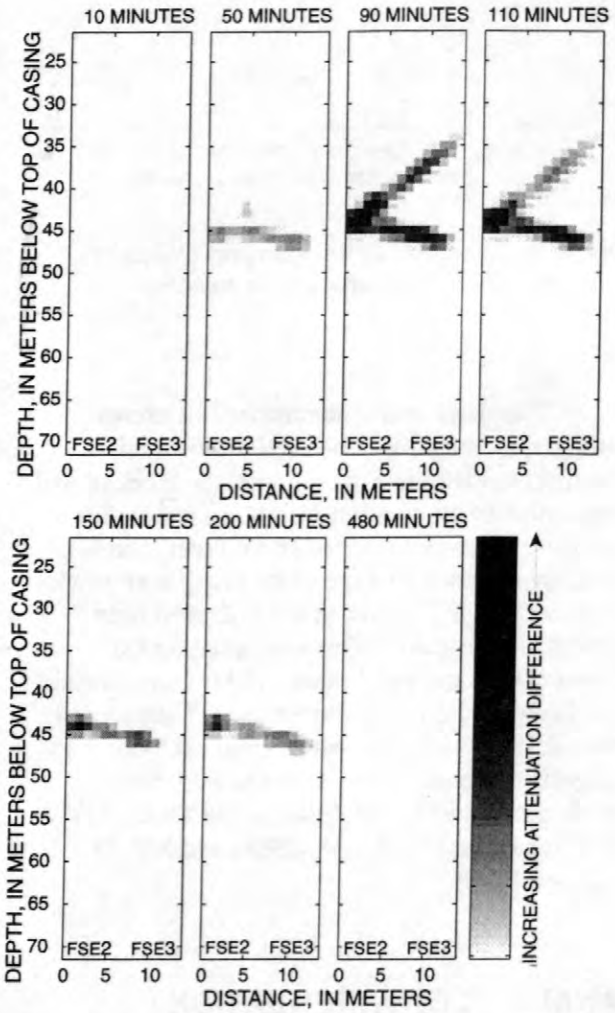

Figure 9. 100 MHz Time-lapse attenuation-difference tomograms between FSE-2 and FSE-3 at the FSE well field, Mirror Lake N.H., produced using a sequential injection and incremental scanning method.

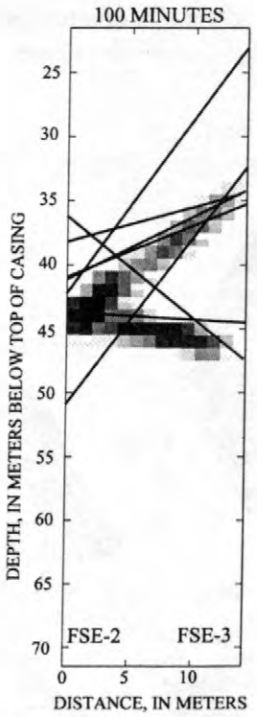

Figure 10. 100 MHz attenuation-difference tomogram between FSE-2 and FSE-3 extracted from a time-lapse radar survey. Selected single-borehole directional-radar reflectors from the FSE 1 to 4 cluster are projected onto the FSE-2 to FSE-3 tomography plane.

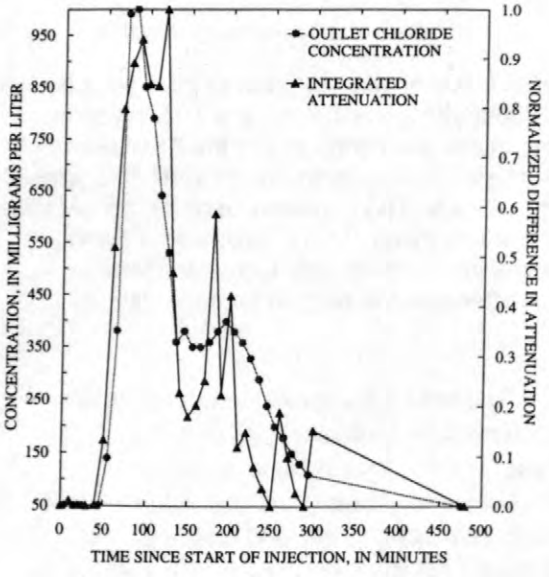

Figure 11. Chloride concentration in milligrams per liter and integrated radar attenuation-difference normalized to maximum and minimum values plotted against time.

In Lane, Joesten, and others (1998), a simple effective medium approach was used to interpret attenuation differences observed during a saline tracer injection experiment in carbonate rocks to estimate changes in total dissolved solids. Effective medium analysis uses 'mixing' laws and known or measured physical properties of individual constituents to interpret a measured physical property (such as EM attenuation).

It is unclear if the same effective medium approach can be applied to radar attenuation-difference data from saline tracer tests in fractured rock. Effective medium analysis is based on the assumption that the medium is homogeneous on the measurement scale. This assumption may be invalid in fractured rocks because fractures can have random or arbitrary distribution, spatial density, orientation, and scale-length. Another complication is reflection and scattering of EM waves by fractures. EM attenuation in fractured rock is a measure of scattering losses as well as conductive losses. The effective medium approach used by Lane, Joesten, and others (1998) does not explicitly account for the effects of EM scatter. Another problem with the effective medium approach in fractured rocks is the linkage between EM attenuation, porosity, and fluid specific conductance. Equivalent EM-attenuation changes can be expected from different combinations of porosity and specific conductance.

Despite these problems, the effective medium approach may have merit where secondary porosity can be estimated. For example, the effective medium approach was applied to radar transmission data obtained over a meter-scale block of fractured granite. The sub-horizontal fracture penetrating the block has an aperture of about 2 millimeters, which corresponds to an average secondary porosity of about 1.5×10^{-3}. The edges of the fracture are sealed to prevent leakage; plastic valves installed in the edges of the block permit the injection and withdrawal of fluids. The radar transmission data shown in figure 12 were acquired through the center of the block by using broadband electric-dipole impulse-antennas with a center frequency of about 870 MHz. Saturating the fracture and increasing the NaCl concentration of the water in the fracture decreases the transmitted pulse amplitude (fig. 13). EM-attenuation change is given by:

$$-20 \log (A_b/A_\sigma) = \Delta\alpha \quad , \qquad (1)$$

where:

$\Delta\alpha$ is the EM attenuation change,
A_b is the background transmitted pulse amplitude, and
A_σ is the transmitted pulse amplitude for specific conductance, σ.

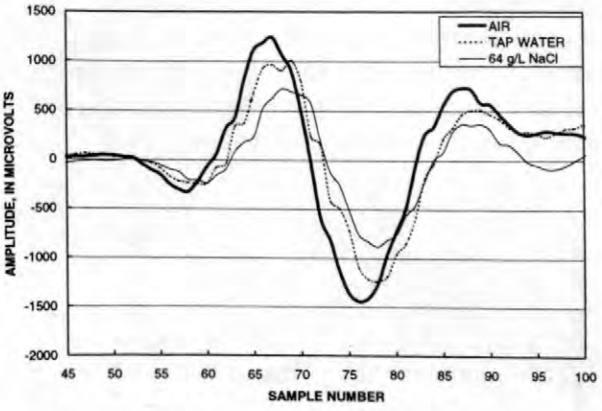

Figure 12. 870 MHz cross-block radar-pulse waveforms recorded after passing through the center of a meter-scale fractured granite block. Data shown are for an unsaturated fracture (largest amplitude), fracture saturated with tap-water (specific conductance about 150 microsiemens per centimeter) and fracture saturated with a 64 g/L NaCl solution (smallest amplitude).

The dotted line in figure 13 shows observed EM attenuation changes calculated from the physical model data plotted against fluid specific conductance. As specific conductance increases, EM attenuation increases. The effective media method used here is based on the assumption that attenuation changes are related to the fluid specific conductance (σ_{fluid}) and secondary porosity ($\phi_{fracture}$):

$$f(\sigma_{fluid}, \phi_{fracture}) = \Delta\alpha \qquad (2)$$

Predicted attenuation changes for several values of secondary porosity plotted against tracer specific conductance using the EM analysis method given in Lane, Joesten, and others (1998)

are also shown in figure 13. Note the effect of secondary porosity on the magnitude and rate of change of attenuation with respect to specific conductance. The attenuation-difference data from the physical model correspond with predicted values assuming a secondary porosity of $1.8x10^{-3}$. The secondary porosity at the center of the granite block inferred by effective media analysis is significantly different from the estimated average value of $1.5x10^{-3}$. The results could indicate: (1) secondary porosity (i.e. fracture aperture) is larger over the measured interval than the mean value for the block and/or (2) scattering losses and/or other loss factors are significantly increasing attenuation.

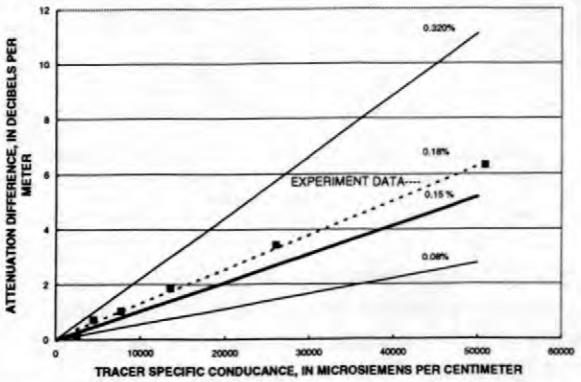

Figure 13 Predicted attenuation-difference plotted against specific conductance for selected values of secondary porosity and measured attenuation-differences from the center of a meter-scale fractured granite block for a range of tracer specific conductance (black squares). Measured attenuation differences plot along the 0.0018 secondary porosity line. Estimated block secondary porosity is 0.0015.

These results suggest the analysis of attenuation-difference data from saline tracer tests using an effective media approach could have merit if accurate estimates of secondary porosity can be made, but might require modification to account for scattering losses or other loss mechanisms. One possible approach is suggested by the effect of secondary porosity on attenuation-difference shown in figure 13. Secondary porosity is inversely proportional to the rate of change of attenuation with specific conductance. Conducting several 'steady-state' experiments using different tracer concentrations could provide data to estimate secondary porosity within the tomographic image plane. These estimates could then be used to interpret time-lapse attenuation differences from slug-injection saline tracer tests in terms of specific conductance or tracer concentration.

CONCLUSION

Methods of coupling cross-hole radar tomography surveys using saline tracer injections have been developed and tested at the USGS Mirror Lake fractured-rock field-research site in Grafton County, New Hampshire to delineate transmissive fracture zones and image fluid flow at field-scales. High concentration (20-50 g/L) NaCl tracers injected into transmissive fractures increase EM attenuation observed in cross-hole radar scans compared to background measurements. Changes in EM attenuation are inverted to produce attenuation-difference tomograms

Attenuation-difference tomograms acquired under 'steady-state' injection and pumping conditions were used to delineate the location and orientation of transmissive fracture zones between boreholes. Time-lapse radar tomography methods can monitor slug-injection saline tracer tests and image fluid flow in fractured rock. Time-lapse cross-hole radar sets acquired at Mirror Lake have coupled the controlled injection of fixed volumes of high-concentration saline tracer with the scanning of small sections of the tomographic image. Equivalent time data from each scanned section are sorted, analyzed to determine attenuation-differences, and inverted. Time-lapse attenuation-difference tomograms delineate transmissive zones, identify variability within transmissive zones, and provide kinematic information that images field-scale ground water flow and transport.

The locations of transmissive zones within the tomographic image plane are shown by steady-state attenuation difference tomograms. Travel times across the image plane are provided by time-lapse attenuation-difference tomograms. Results of steady-state and time-lapse tomography surveys were used to help construct and calibrate ground water flow and transport models in the FSE well field.

Time-lapse tomography would be more useful if time-dependent attenuation changes

could be used to estimate tracer specific conductance and concentration at the image plane. A simple effective media method of analyzing time-dependent attenuation changes to estimate tracer specific conductance was tested on radar data acquired over a meter-scale fractured granite block. Preliminary results illustrate the importance of accurately estimating secondary porosity, and suggest robust analysis may require (1) accounting for effects of EM scattering on attenuation, and (2) modifying field methods to include several steady-state injection tests using different tracer concentrations.

ACKNOWLEDGMENTS

The Hubbard Brook Experimental Forest is operated and maintained by the Northeastern Forest Experiment Station, USDA Forest Service, Radnor, Pennsylvania.

REFERENCES

Day-Lewis, F.D., Lane, J.W. Jr., Haeni, F.P., and Gorelick, S.M., 1997, One approach to identifying flow paths in fractured rock--combining borehole radar, saline tracer tests, and numerical modeling [abs.]: EOS, Transactions, American Geophysical Union, v. 78, no. 46, p. F322.

Hsieh, P.A., and Shapiro, A.M., 1996, Hydraulic characteristics of fractured bedrock underlying the FSE well field at the Mirror Lake site, Grafton County, New Hampshire, *in* Morganwalp, D.W., and Aronson, D.A., eds., U.S. Geological Survey Toxic Substances Hydrology Program-Proceedings of the Technical Meeting, Colorado Springs, Colorado, September 20-24, 1993: U.S. Geological Survey Water-Resources Investigation Report 94-4015, p.127-130.

Johnson, C.D., and Dunstan, A.M., 1998, Lithology and fracture characterization from drilling investigations in the Mirror Lake area--from 1979 through 1995 in Grafton County, New Hampshire: U.S. Geological Survey Water-Resources Investigations Report 98-4183, 210 p.

Lane, J.W., Jr., Haeni, F.P., and Day-Lewis, F.D., 1998, Use of time-lapse attenuation difference radar tomography methods to monitor saline tracer transport in fractured crystalline bedrock, in Seventh International Conference of Ground Penetrating Radar (GPR'98), Lawrence, Kansas, May 27-30, 1998., Proceedings: Lawrence, Kans., University of Kansas, Radar Systems and Remote Sensing Laboratory, p. 533-538.

Lane, J.W., Jr., Haeni, F.P., Placzek, Gary, and Wright, D.L., 1996, Use of borehole radar methods to detect a saline tracer in fractured crystalline bedrock at Mirror Lake, Grafton County, New Hampshire, *in* Sixth International conference of Ground Penetrating Radar (GPR'96), Sendai, Japan, September 30-October 3, 1996, Proceedings: Sendai, Japan, Tohoku University, Department of Geoscience and Technology, p. 185-190.

Lane, J.W., Jr., Haeni, F.P., and Versteeg, Roelof, 1998, Use of a multi-offset borehole-radar reflection method in fractured crystalline bedrock at Mirror Lake, Grafton County, New Hampshire, *in* Symposium on the Application of Geophysics to Engineering and Environmental Problems (SAGEEP), Chicago, Illinois, March 22-26, 1998, Proceedings: Wheat Ridge, Colo., Environmental and Engineering Geophysical Society, p. 359-368.

Lane, J.W., Jr., Joesten, P.K., Haeni, F.P., Vendl, Mark, and Yeskis, Doug, 1998, Use of borehole radar methods to monitor the movement of a saline tracer in carbonate rock at Belvidere, Illinois, *in* Symposium on the Application of Geophysics to Engineering and Environmental Problems (SAGEEP), Chicago, Illinois, March 22-26, 1998, Proceedings: Wheat Ridge, Colo., Environmental and Engineering Geophysical Society, p. 323-332.

Liu, Lanbo, Lane, J.W., Jr., and Quan, Youli, 1998, Radar attenuation tomography using the frequency downshift method: Journal of Applied Geophysics, v. 40, p. 105-116.

McDonald, M.G., and Harbaugh, A.W., 1988, Modular three-dimensional finite-difference ground-water flow model: U.S. Geological Survey Techniques of Water-Resources Investigations, book 6, chap. A1, 586 p.

Niva, B., Olsson, O., and Blumping, P., 1988, Radar cross-hole tomography at the Grimsel

Rock Laboratory with application to migration of saline tracer through fracture zones: Nationale Genossenschaft fur die lagerung radioaktiver Abfalle, NTB 88-31.

Olsson, O., Andersson, P., Carlsten, S., Falk, L., Niva, B., and Sandberg, E., 1992, Fracture characterization in crystalline rocks by borehole radar, *in* Pilon, J., ed., Ground Penetrating Radar: Geological Survey of Canada Paper 90-4, p. 139-150.

Ramirez, A.L., and Lytle, R.J., 1986, Investigation of fracture flow paths using alterant geophysical tomography: Journal of Rock Mechanics and Mining Sciences and Geomechanics, v. 23, no. 2, p.165-169.

Shapiro, A.M., and Hsieh, P.A., 1991, Research in fractured-rock hydrogeology--characterizing fluid movement and chemical transport in fractured rock at the Mirror Lake drainage basin, New Hampshire, *in* Mallard, G.E., and Aronson, D.A., eds., U.S. Geological Survey Toxic Substances Hydrology Program-Proceeedings of the Technical Meeting, Monterey, California, March 11-15, 1991: U.S. Geological Survey Water-Resources Report 91-4034, p. 155-161.

Shapiro, A.M., and Hsieh, P.A., 1996, Overview of research on use of hydrologic, geophysical, and chemical methods to characterize flow and chemical transport in fractured rock at the Mirror Lake site, New Hampshire, *in* Morganwalp, D.W., and Aronson, D.A., eds., U.S. Geological Survey Toxic Substances Hydrology Program-Proceedings of the Technical Meeting, Colorado Springs, Colorado, September 20-24, 1993: U.S. Geological Survey Water Resources Investigations Report 94-4015, p. 71-80.

Shapiro, A.M., Hsieh, P.A., and Winter, T.C., 1995, The Mirror Lake fractured rock research site-a multidisciplinary research effort in characterizing ground-water flow and chemical transport in fractured rock: U.S. Geological Survey Fact Sheet FS-138-95, 2 p.

Shapiro, A.M., Lane, J.W., Jr., and Day-Lewis, F.D., 1998, Characterizing heterogeneity in fractured rock through a combination of tracer testing and radar tomography: EOS, Transactions of the American Geophysical Union, v. 79, no. 17, p. S134.

Wright, D.L., Grover, T.P., Ellefsen, K.J., Lane, J.W., Jr., and Kase, P.G., 1996, Radar tomograms at Mirror Lake, New Hampshire--3-D visualization and a brine tracer experiment *in* Symposium on the Application of Geophysics to Engineering and Environmental Problems (SAGEEP), Keystone, Colorado, April 28-May 2, 1996, Proceedings: Wheat Ridge, Colorado, Environmental and Engineering Geophysical Society, p. 565-575.

Wright, D.L., and Lane, J.W., Jr., 1998, Mapping hydraulically permeable fractures using directional borehole radar and hole-to-hole tomography with a saline tracer, *in* Symposium on the Application of Geophysics to Engineering and Environmental Problems (SAGEEP), Chicago, Illinois, March 22-26, 1998, Proceedings: Wheat Ridge, Colo., Environmental and Engineering Geophysical Society, p. 565-575.

Zheng, C., 1990, MT3D--A modular three-dimensional transport model for simulation of advection, dispersion and chemical reactions of contaminants in ground-water systems: S.S. Papadopulos & Associates, Inc.

AUTHOR INFORMATION

John W. Lane, Jr. U.S. Geological Survey, Storrs Mansfield, Connecticut (jwlane@usgs.gov)

David L. Wright, U.S. Geological Survey, Denver, Colorado (dwright@usgs.gov)

F. Peter Haeni, U.S. Geological Survey, Storrs Mansfield, Connecticut (phaeni@usgs.gov)

Integration of Surface Geophysical Methods for Fracture Detection in Bedrock at Mirror Lake, New Hampshire

By C.J. Powers, Kamini Singha, and F. Peter Haeni

ABSTRACT

Five surface geophysical methods were used to determine the locations of fracture zones in crystalline bedrock for predicting fluid flow and chemical migration at the U.S. Geological Survey Fractured Rock Research Site at Mirror Lake, Grafton County, New Hampshire. Two methods of direct-current (dc) resistivity (two-dimensional (2D) and crossed square-array profiling), two methods of inductive terrain conductivity, and very-low-frequency electromagnetics (VLF) were used over survey lines extending about 200 meters. The results of the five methods were correlated to locate fracture zones; anomalies that were detected in one or two of the results were eliminated, increasing the confidence in the interpretation of anomalies detected in all of the results.

Two low resistivity anomalies were detected with all the geophysical methods in the southeast part of the study area. Based on the geophysical, outcrop, and photolinear data, the anomalous areas were interpreted as steeply dipping fracture zones approximately 10-meters wide. One interpreted fracture zone strikes approximately north 45 degrees east and the other strikes approximately north 17 degrees east.

Results of dc-resistivity surveys were analyzed to estimate the secondary porosity of the two interpreted fracture zones. Crossed square-array dc-resistivity profiling data indicates the secondary porosity is between 0.65 to 0.75 percent, whereas the 2D dc-resistivity profiling results indicate the secondary porosity to be 1.6 to 1.9 percent. Estimates from the 2D dc-resistivity profiling could indicate the effects of alteration and/or iron precipitate observed in outcrops near the survey lines.

INTRODUCTION

The location and orientation of fracture zones is important for modeling fluid flow and contaminant transport in fractured rocks. Surface geophysical methods are a rapid, inexpensive addition to drilling for determining the locations and orientation of fractured zones in bedrock. Surface geophysics can be used in conjunction with geologic, hydrologic, and borehole-geophysical investigations to optimize well siting (Jansen and Jurcek, 1997), or as a stand-alone method of fracture detection (Lewis and Haeni, 1987; Lieblich and others, 1991; Haeni and others, 1993).

Five different surface geophysical methods were used during the summer of 1997 at Mirror Lake, Grafton County, New Hampshire to determine the location of saturated fracture zones in crystalline bedrock. 2D dc-resistivity profiling, crossed square-array dc-resistivity profiling, two inductive terrain conductivity methods (EM-34[1] and Slingram) and very-low-frequency electromagnetics (VLF) were used to detect low resistivity zones that indicate the location of fracture zones. By comparing the results from all of the methods, anomalies induced by noise were identified and eliminated, increasing the

[1] Use of tradenames is for descriptive purposes only and does not constitute endorsement by the U.S. Geological Survey.

confidence with which fracture zones were interpreted from the remaining low resistivity anomalies. The study site was selected to profile across several photo-lineaments identified by Clark and others (1999).

SITE CHARACTERIZATION

The USGS Fractured Rock Field Research Site is located at Mirror Lake, in the Hubbard Brook Valley, Grafton County, New Hampshire. The data presented in this paper were collected approximately 1 kilometer (km) west of Mirror Lake (fig. 1). At this location, results of 2D dc-resistivity surveys indicate that a layer of glacially deposited sediment 3- to 6- meters (m) thick covers the bedrock. Overlying the till is a layer of organic material, approximately 0.2-m thick, consisting mainly of organic-rich soil and leaf matter. Small cavities in the organic layer were observed in several locations within the study site.

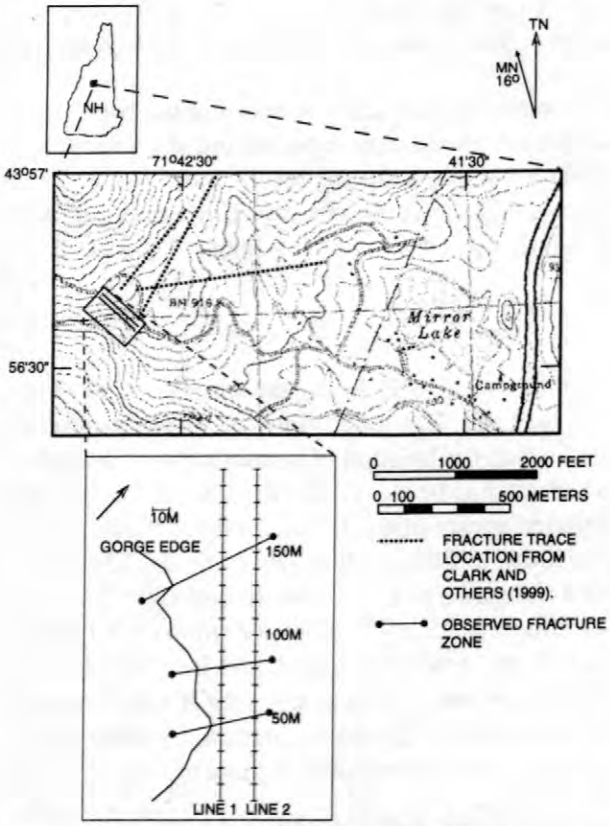

Figure 1. Site map of the study site, Mirror Lake, Grafton County, New Hampshire.

Geophysical data were collected along two parallel lines oriented north 43 degrees west, about 200-m long and 20-m apart. The average slope of the land surface along the lines dips 8 degrees to the southeast. The survey lines were located and oriented to intersect the maximum possible number of geologic features and lineaments observed in air-photos. Lineaments observed in low altitude aerial photos served to focus the initial study site selection, but due to the lineament map scale, the intersection of the lineaments with the survey lines could not be accurately determined. The first 140 m of Line 1 were 10 to 40 m from the northeast of the edge of the Hubbard Brook gorge. Preferential erosion, rockslides, and weathered zones along the walls and edge of the gorge likely mark the location of several large fracture zones.

PRINCIPLES OF SURFACE GEOPHYSICAL TECHNIQUES

Dc resistivity

Dc resistivity methods measure the electrical resistivity distribution of the subsurface using current transmitted into the ground from dc- or low-frequency sources, by two electrodes (C1 and C2), and measuring the potential difference between a second pair of electrodes (P1 and P2) (fig. 2). The apparent resistivity of the subsurface can be calculated by applying a geometric correction (K) to Ohm's law ($R = \Delta V/I$, where R is the resistance, ΔV is the measured potential difference, and I is the injected current), based on the specific electrode spacing and geometry. These geometrically corrected measurements are defined as apparent resistivities rather than true resistivities because a resistively homogeneous subsurface is assumed. Measured resistivity values are controlled by material resistivity, and the presence, quality, and quantity of ground water (Haeni and others, 1993). The resistivity of a fracture zone is controlled by the secondary porosity, and the presence of altered secondary minerals and/or precipitate. The maximum penetration depth is directly proportional to the electrode spacing and inversely proportional to the subsurface conductivity (Edwards, 1977).

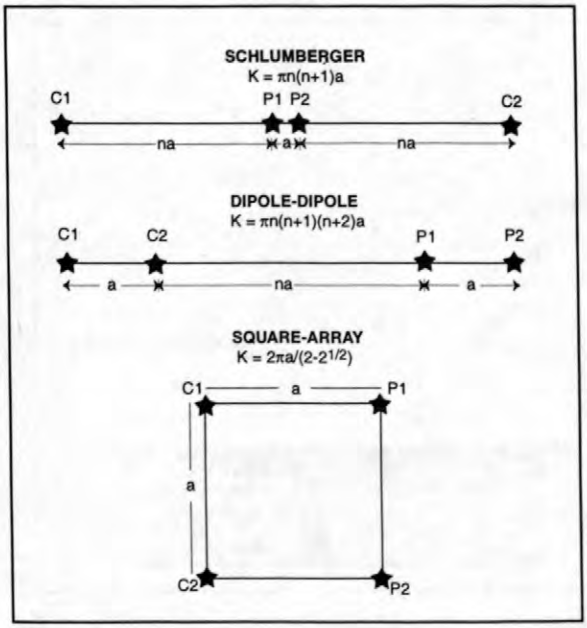

Figure 2. Schematic of Schlumberger, dipole-dipole, and square-array dc-resistivity electrode configuration.

Two dc-resistivity methods were used at Mirror Lake: 2D dc-resistivity profiling and crossed square-array dc-resistivity profiling. 2D dc-resistivity profiling is conducted by making many measurements at different locations along the profile and at different offsets. The 2D dc-resistivity profiling data are inverted to create a tomogram-like model of resistivity along a section of the subsurface that can be used to detect and define individual fracture zones. The crossed square-array profiling method measures changes in apparent resistivity with measurement direction along a profile.

The 2D dc-resistivity profiling system manufactured by Advanced Geosciences, Inc. consists of a linear array of 28 electrodes that are connected to a measurement control unit by a specially designed cable. The control unit uses an automated data-collection program to control the location of current and potential electrodes. Two types of arrays were used for profiling: a dipole-dipole array and a Schlumberger array (fig. 2). The dipole-dipole array has better horizontal resolution, but poorer depth of penetration compared to the Schlumberger array (Loke, 1997). By using an iterative smoothness-constrained least-squares inversion method (deGroot-Hedlin and Constable, 1990; Sasaki, 1992), apparent resistivity data collected by the 2D dc-resistivity system are inverted to create a model of subsurface resistivity that approximates the true subsurface resistivity distribution (Loke, 1997). Linear zones of low resistivity that are continuous with depth are interpreted as fracture zones.

The crossed square-array profiling method uses two squares of electrodes of equal side length "a" rotated by 45 degrees around a center point, defined as the measurement location (fig. 2). Apparent resistivity is measured along the lengths of the arrays (the ρ_α and ρ_β measurements) and also across the diagonals (ρ_γ) for each square. A series of crossed squares are collected along the length of a line as shown in figure 3. In a layered medium

$$\rho_\gamma = \rho_\alpha - \rho_\beta \,, \qquad (1)$$

where

ρ_γ is the resistivity between C1 and P2,
ρ_α is the resistivity between C1 and P1, and
ρ_β is the resistivity between C1 and C2.

The crossed square-array data provide information about the resistivity as a function of direction (every 45 degrees) at each station along the profile. From this data, the mean apparent

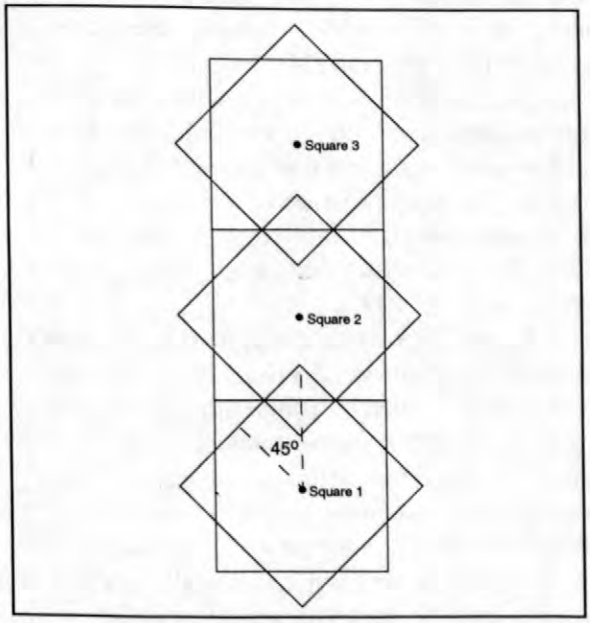

Figure 3. Crossed square-array dc-resistivity profiling.

resistivity, and the magnitude of apparent anisotropy in the resistivity are determined for each crossed square. The magnitude of the anisotropy can be used to calculate a secondary porosity in saturated bedrock. A decreased mean resistivity and an increased secondary porosity can indicate the location of a fracture zone.

Inductive terrain conductivity

Inductive terrain conductivity is an electromagnetic method that measures subsurface electrical conductivity. Two inductive terrain-conductivity instruments were employed: the EM-34 from Geonics and the Slingram from ABEM Instrument AB. Terrain-conductivity instruments consist of a transmitting coil, a receiving coil, a control unit for each, and intercoil cables. The coils are held coplanar at a constant offset, and data are collected at discrete intervals along a survey line.

For this study, the EM-34 was used in the vertical dipole configuration, where the coils are held horizontally. The vertical dipole configuration of the equipment is most sensitive to material at a depth of 0.45 times the coil spacing, and can penetrate depths about 1.5 times the transmitter-receiver spacing. This configuration of the EM-34 is fairly insensitive to near-surface material (McNeill, 1980a).

The Slingram is used in a similar manner, with the transmitter and receiver coils kept at a constant separation, and held parallel to the ground. The depth of penetration of the Slingram is about 0.75 times the coil spacing (Borje Niva, Swedish Geological Company, written commun.,1997).

A qualitative method was used to interpret the inductive terrain-conductivity data. Fracture zones were identified by comparing measured data to instrument response calculated for models of conductors with similar shapes. The vertical dipole response over a thin, vertical conductor is shown in figure 4. Vertical dike-like conductive bodies, such as water-bearing fractures, produce negative anomalies in the conductivity response curve; the true conductivity is not measured (McNeill, 1980b). Based on the modeling results, anomalies were selected that had negative or low measured conductivity values over several data points.

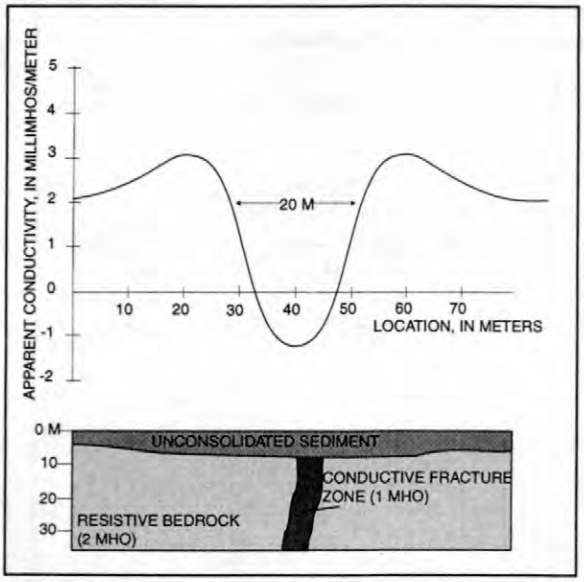

Figure 4. Vertical-dipole response of an inductive terrain-conductivity instrument to a thin vertical conductor.

Very-low-frequency electromagnetics (VLF)

The VLF method is a passive electromagnetic (EM) method that utilizes powerful military transmitters operating between 15-30 kilohertz (kHz) as the primary EM wave source. VLF methods can be used to determine the locations of saturated, sub-vertical conductive zones in which the primary EM wave induces current flow. The field radiated from a VLF transmitter over a uniform or horizontally layered earth consists of a vertical electric field component and a horizontal magnetic field component, each perpendicular to the direction of propagation (McNeill, 1990). Because the source of the electromagnetic field is usually greater than 50 miles away, the long wavelength EM wave approximates a plane wave. In this study, the VLF was used in two modes: tilt angle and resistivity.

Although the primary magnetic field is oriented horizontally and perpendicularly to its source, induced current flowing in fracture zones produces a secondary magnetic field that is out-of-phase with the primary magnetic field and is

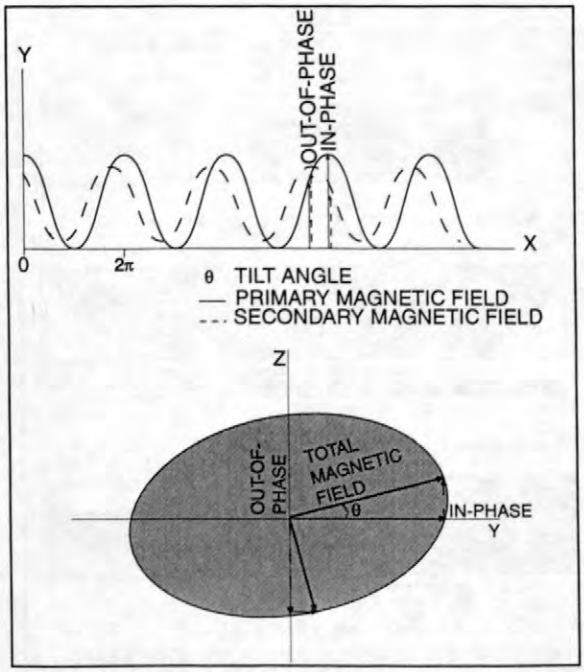

Figure 5. Tilt angle and ellipticity of a VLF field.

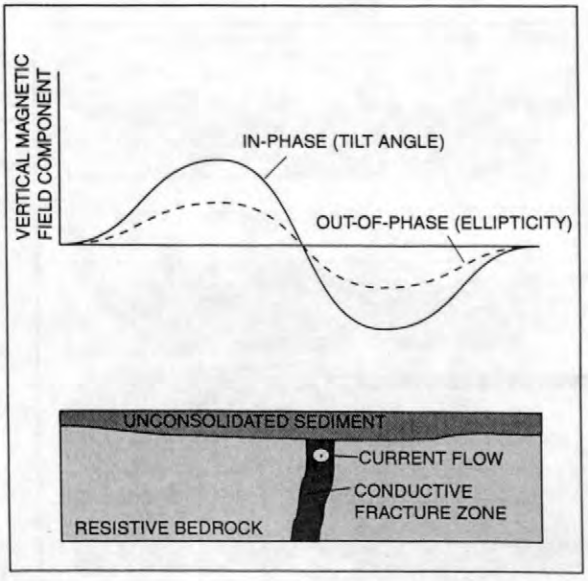

Figure 6. VLF response to a thin vertical conductor.

oriented in any direction (McNeill and Labson, 1990). The vector sum of the two fields traces out an ellipse over time, the tilt of which is measured in the VLF tilt angle mode (fig. 5). The tilt angle is approximately equal to the in-phase part of the vertical component of the magnetic field ellipse. (Iris Instruments, 1993).

For tilt angle measurements, magnetic field coupling with the fracture zone is important. Therefore, the VLF-transmitter should be located along the strike of the target. The depth of investigation is dependent on the frequency used and the resistivity of the host medium. At the study site, the local resistivity minimum is 400 ohm-m (based on the 2D dc-resistivity data), therefore, the VLF depth of investigation is more than 65 m (Iris Instruments, 1993).

Measuring resistivity with the VLF requires measuring the electric field with two electrodes connected to the control unit by a wire. In the resistivity-mode, the VLF is similar to the high frequency magnetotelluric method (Kaikkonen and Sharma, 1997) and measures apparent resistivity and phase angle (time-delay) between the electric and magnetic fields. For resistivity measurements, the electrical field coupling with the fracture zone is important, therefore, the transmitter should be located in a direction perpendicular to the target (Iris Instruments, 1993).

A qualitative method was used to interpret the VLF tilt-angle data to identify fracture zones by comparing measured data to instrument response calculated for models of conductors with similar shapes.

A conductive fracture zone produces a tilt-angle anomaly that looks like a distorted sinusoid (fig. 6). The top of the fracture zone is centered at the inflection point of the anomaly. In the VLF resistivity data, low resistivity zones were interpreted as possible fracture zones.

DATA ACQUISITION AND PROCESSING

2D dc-resistivity profiling

Two 275-m 2D dc-resistivity profiles were collected. The 2D dc-resistivity profiles extend beyond the ends of each survey line to provide 200 m of complete data coverage because of a limited imaging depth for about 35 m on each end of the profile. For each line, a dipole-dipole array and a Schlumberger array were used. The apparent resistivity data were inverted to create a model of the resistivity of the subsurface using

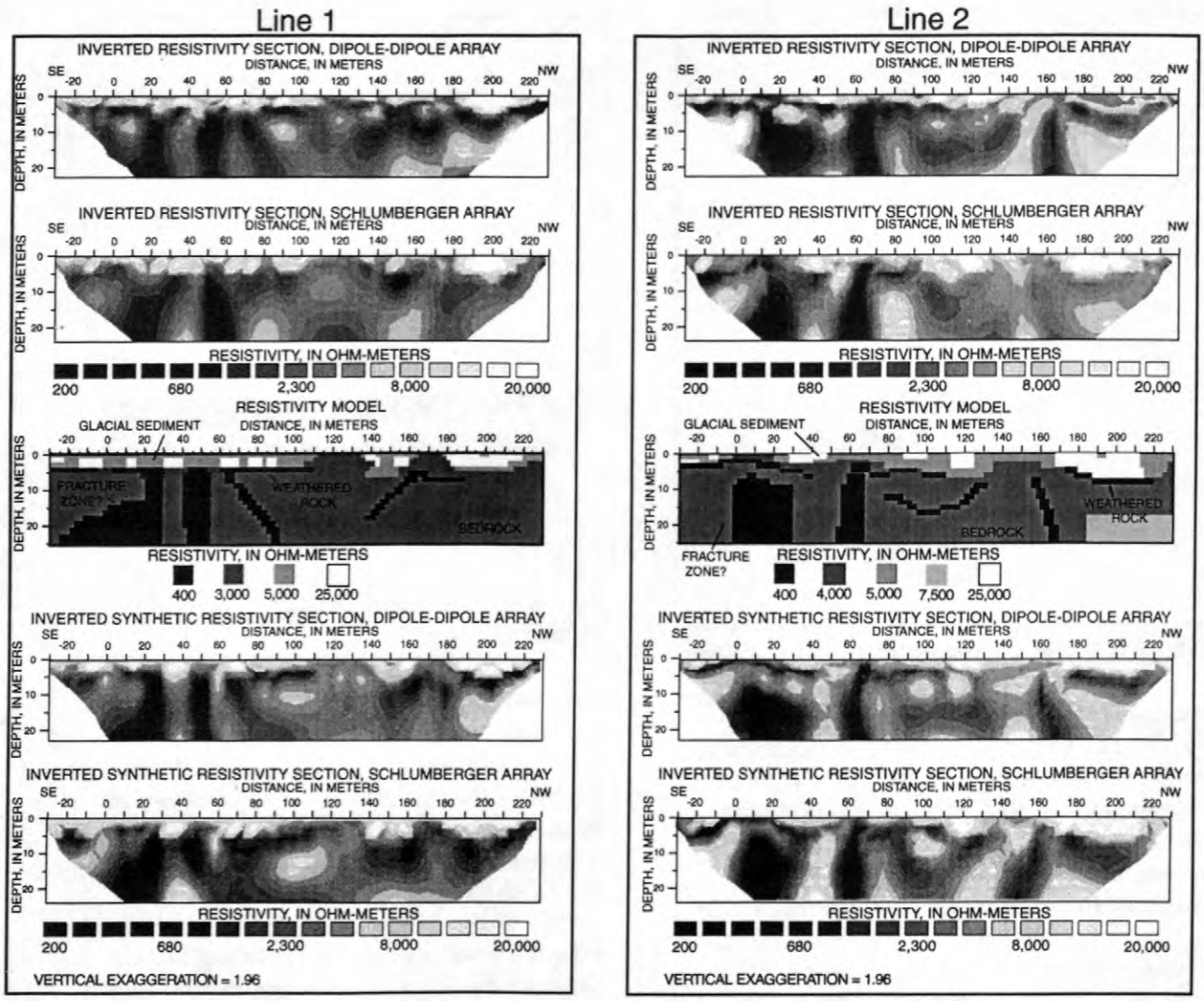

Figure 7. Results of 2D dc-resistivity data and modeling from Mirror Lake, New Hampshire.

Res2dinv. Res2dinv uses an iterative smoothness-constrained least-squares method (deGroot-Hedlin and Constable, 1990, Sasaki, 1992).

To test interpretation, resistivity models were created based on the inversion results. The resisitivity models were used to generate synthetic apparent resistivity data. The synthetic apparent resistivity data were inverted using Res2dinv and the resulting inversions were compared with the original inverted resistivity section. The resistivity models were adjusted and simplified to qualitatively match the field-data inversions. Generating resistivity models helped constrain interpretation of the field-data inversions to identify locations and orientations of anomalies.

The 2D dc-resistivity field-data inversions, resistivity models and synthetic-data inversions are shown in figure 7. Bedrock is calculated to have an average resistivity of 3,000 and 4,000 ohm-m along Line 1 and Line 2, respectively. Within the bedrock there are several linear features of low resistivity (400 ohm-m) that are interpreted as fracture zones. Line 1 has a blocky anomaly, dipping to the southeast from 40 to 30 m, a vertical linear anomaly from 40 to 55 m, a dipping linear anomaly from 60 to 100 m and another dipping anomaly from 140 to 190 m. Line 2 has vertical linear anomalies from 0 to 30 m and 55 to 70 m, a sub-horizontal linear anomaly from 80 to 135 m and a sub-vertical linear anomaly from 155 to 175 m.

Crossed square-array dc-resistivity profiling

A dc-resistivity system manufactured by ABEM Instruments AB was used to collect crossed-square data at 10-m intervals along Line 1, with the first square centered on 5 m. A 10-m a-spacing and a current of 5 mA were used. Data were collected four times and averaged at each station.

The mean apparent resistivity for each crossed square was calculated to determine an azimuthally independent value for each square (Habberjam, 1972):

$$\rho_m = \sqrt[4]{\rho_{a1} \cdot \rho_{a2} \cdot \rho_{a3} \cdot \rho_{a4}}, \quad (2)$$

where

ρ_m is the geometric mean resistivity,

ρ_{a1} is the apparent resistivity parallel to Line 1,

ρ_{a2} is the apparent resistivity at 45 degrees to Line 1,

ρ_{a3} is the apparent resistivity perpendicular to Line 1, and

ρ_{a4} is the apparent resistivity at 135 degrees to Line 1.

The secondary porosity was calculated following Habberjam (1975) from apparent anisotropy in the resistivity, which is a measure of the magnitude of resistivity variation as a function of direction. The calculation of secondary porosity assumes that apparent anisotropy is due to fractures and does not account for anisotropy due to schistosity or heterogeneity.

The crossed square-array dc-resistivity profiling data are shown in figure 8. A decreased mean resistivity, and an increased secondary porosity are interpreted as fracture zones. Areas of decreased mean apparent resistivity are located at 5, between 45 and 55 m, and possibly at 155 m. Areas of increased anisotropy and, therefore, increased calculated secondary porosity are located at 5, 45, and 175 m.

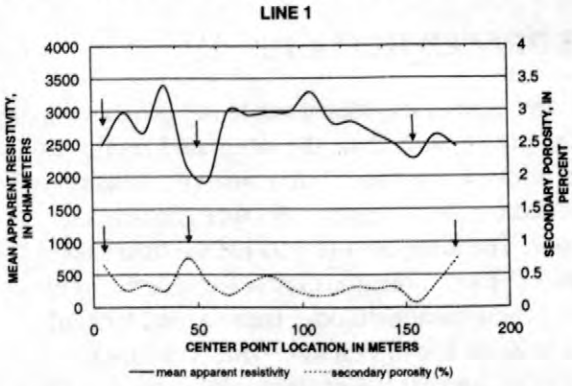

Figure 8. Results of square-array profiling at the Mirror Lake, N.H.

Inductive terrain conductivity

The EM-34 was used in the vertical dipole configuration, with a 20-m coil separation. Data were collected every 2.5 m. The 20-m EM-34 data is shown in figure 9. To minimize the effects of random noise, an eight-point moving average

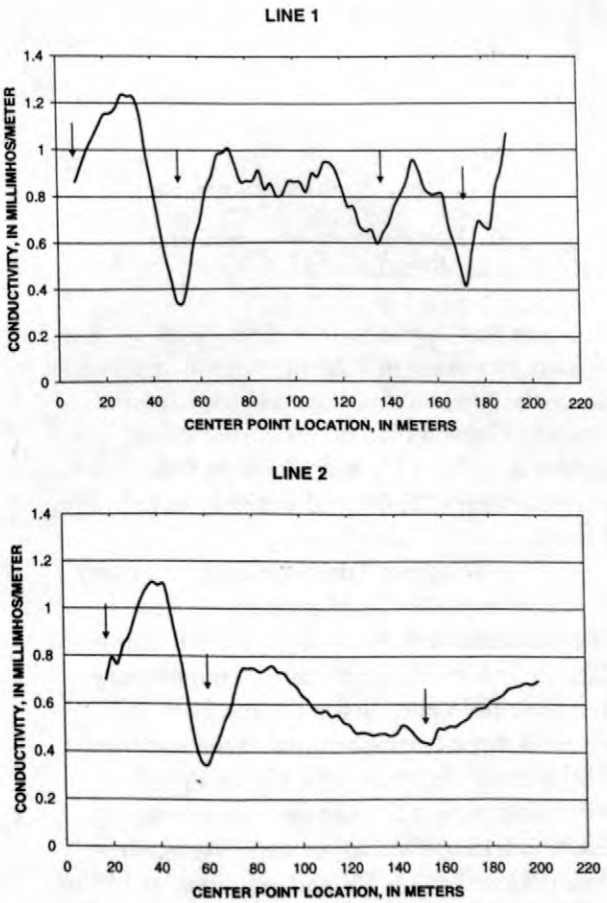

Figure 9. Results from EM-34 data collection at Mirror Lake, N.H.

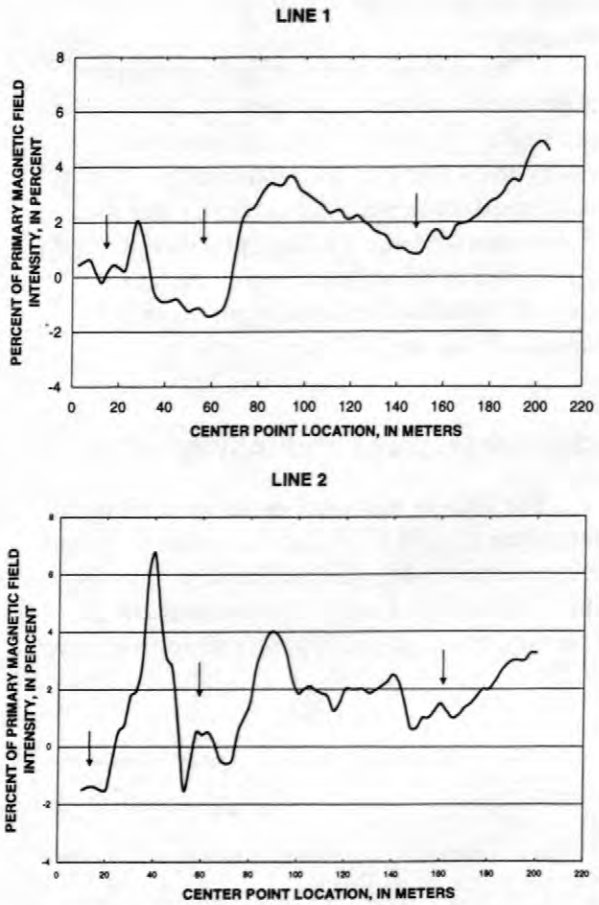

Figure 10. Results from Slingram data collection at Mirror Lake, N.H.

function was applied to the data. With a 2.5-m station increment and 20-m intercoil spacing, an anomaly due to a dipping conductor should extend at least 8 data points. Anomalies appear at 5, 55, 135, and 170 m on Line 1 and approximately 15, 60, and possibly at 155 m on Line 2.

The Slingram data were collected every 2.5 m, using a 40-m coil separation. The Slingram data are shown in figure 10. Slingram data are recorded as a percent of the primary magnetic field intensity at the receiver coil, which is directly proportional to the apparent conductivity. Because of a higher signal-to-noise ratio, only a 2 point moving-average function was applied to the data. Anomalies were detected at 15, 55, and, possibly, at 145 m on Line 1. On Line 2, anomalies were detected at 10, 60, and, possibly, at 160 m.

Very-low-frequency electromagnetics (VLF)

A VLF transmitting station in Cutler, Maine (24 kHz) was the only VLF station with a strong enough signal for VLF data acquisition. At the Hubbard Brook Site, the direction to the Cutler, Maine transmitter approximately east 10 degrees north. The direction to the transmitter intersects the survey line at an angle of less than 60 degrees to the strike of the suspected fracture zone; suitable for the resistivity survey, but less suitable for the tilt angle survey. However, precise tilt-angle measurements were obtained using the Cutler, Maine station.

Tilt angle and resistivity data were collected along the survey lines every 2.5 m. For the resistivity survey, the electrodes were separated by 10 m. A minimum of three measurements were collected and averaged at each station to reduce the effects of random noise. The VLF data is shown in figure 11. A two point moving average function was applied to the tilt angle data. Resistivity data collected with the VLF were first converted to conductivity values in order to more clearly show the anomalies. A four point moving–average function was applied to the resistivity data. Tilt angle anomalies were detected at 50, and, possibly, at 20 m on Line 1 and approximately 60 m, and, possibly, at 20 m on Line 2. VLF resistivity anomalies were detected at 80 m, and, possibly, at 135 m on Line 1 and 15, 60, and 100 m on Line 2. An area of higher conductivity is measured from 140 to 190 m on Line 2.

INTEGRATED RESULTS

Because of the robust modeling program and the high quality data, the integrated results are based primarily on the 2D dc-resistivity inversions supported by the results of the other geophysical methods. The integrated results are summarized in Figure 12. Two anomalous areas were detected by all the geophysical methods. These areas, labeled Fracture Zone 1, and Fracture Zone 2, indicate the presence of fracture zones from 0 to 20 m, and 45 to 55 m on Line 1, and from 0 to 25 m, and 55 to

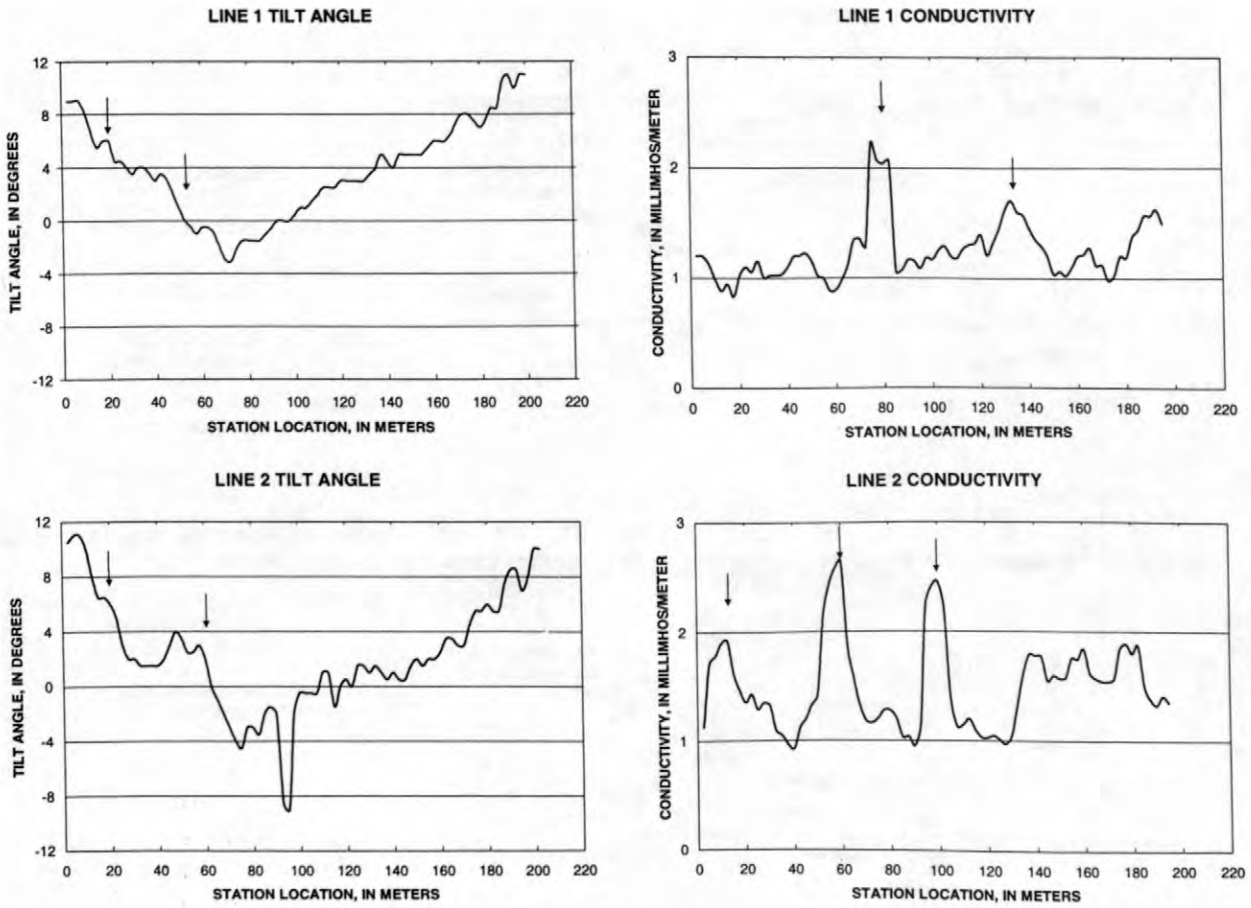

Figure 11. Results of VLF data from Mirror Lake, N.H.

65 m on Line 2. Several other anomalies interpreted with one or two methods in other locations along the survey lines were eliminated because no clear correlation between methods or from one line to the other was found.

Fracture Zone 1, located from 0 to 20 m on Line 1 and from 0 to 25 m on Line 2, was detected by all geophysical methods (fig. 12). The strike of this zone across Line 1 and Line 2, is approximately north 45 degrees east. 2D dc-resistivity modeling suggests the fracture zone is irregular, indicating that more than one fracture zone may be producing the anomaly. The blockiness of Fracture Zone 1 on Line 1 may actually be two fracture zones, one dipping 21 degrees to the southwest and the other sub-vertical. On Line 2, the anomaly that characterizes Fracture Zone 1 is more vertical, suggesting that the sub-vertical fracture zone extends between the two lines, while the shallowly dipping feature does not.

Fracture Zone 2 is located from 45 to 55 m on Line 1 and from 55 to 65 m on Line 2. Fracture Zone 2 is the most prominent anomaly in most of the geophysical surveys and was detected by all geophysical methods. The strike of this zone across Line 1 and Line 2 is approximately north 17 degrees east. Results of 2D dc-resistivity modeling indicate that the anomaly is sub-vertical. Observations on the face of the Hubbard Brook Gorge show a sub-vertical fracture zone 5 to 6 m wide, striking north 34 degrees east (+/- 10 degrees). The zone consists of heavily fractured, incompetent schist thinly coated with iron precipitate. The fracture zone projects between 45 to 50 m on Line 1 and 46 to 56 m on Line 2, consistent with the location of Fracture Zone 2. A lineament observed in low altitude aerial photos also projects through this approximate area.

A group of anomalies, interpreted as a probable fracture zone, is located on Line 1 from 135 to 170 m and on Line 2 from 160 to 170 m.

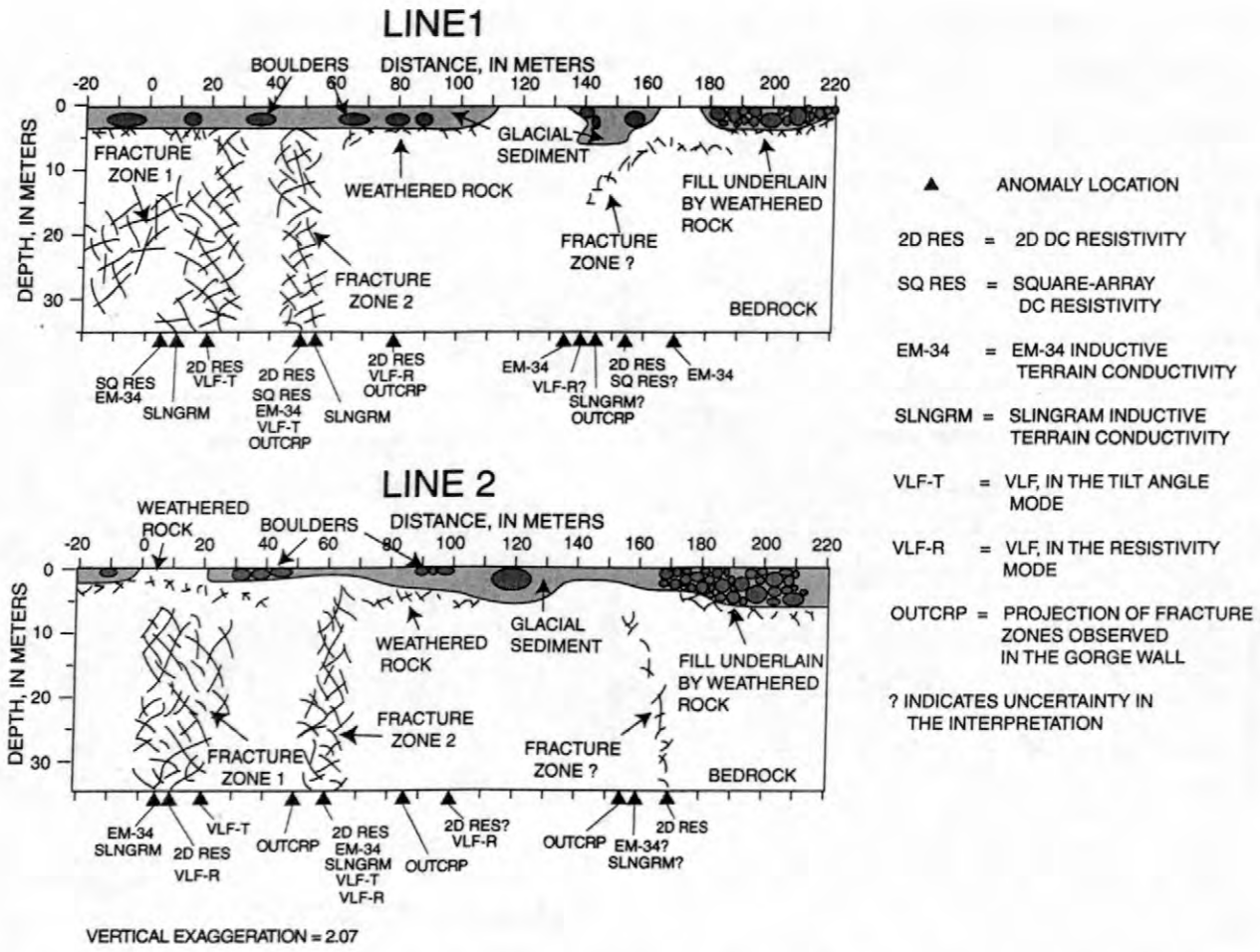

Figure 12. Interpreted cross-section of Lines 1 and 2, Mirror Lake, New Hampshire.

Within this group, all the geophysical methods detected an anomaly on Line 1 and most methods detect an anomaly on Line 2, but the interpreted location on Line 1 is inconsistent (the anomalies were detected from 135 to 170 m), and all of the anomalies are low magnitude. Factors that may cause the anomalies to be poorly formed include multiple interfering anomalies, a greater overburden thickness, or a decreased fracture thickness. Projection of a possible fracture zone observed in the Hubbard Brook gorge intersect Line 1 at 145 to 150 m, and Line 2 at 150 to 160 m, which is consistent with the anomaly grouping. A second lineament observed in low altitude aerial photos also projects through the northwestern part of the survey lines and may correlate with this zone.

Modeling of the 2D dc-resistivity data indicate that the resistivity of the fracture zones is approximately 400 ohm-m, whereas the resistivity of the surrounding rock is approximately 3,000 to 4,000 ohm-m. Assuming pore fluid resistivity is 3.3 ohm-m, a secondary porosity of both fracture zones of 1.6 to 1.9 percent was calculated using values based on 2D dc-resistivity and square array dc-resistivity data and Archie's Law (Archie, 1942):

$$\frac{\rho_r}{\rho_f} = a\phi^{-m} \qquad (3)$$

where

ρ_r is the rock resistivity in the fracture zones, ohm-meters,
ρ_f is the resistivity of the pore fluid,
a is the coefficient of saturation (1 for complete saturation),
ϕ is the porosity, and
m is the cementation factor.

The value of m was calculated using Archie's law, by setting ρ_r to 3,000 to 4,000 ohm-m (average bedrock based on 2D resistivity modeling) and ρ_f to 3.3 ohm-m. A secondary porosity of 0.29 percent was assumed based on the average value of the secondary porosity calculated from the square-array dc-resistivity data collected over non-anomalous areas. The coefficient of saturation was assumed to be equal to 1.

Using the calculated cementation factor of 1.17 to 1.22, the secondary porosity of 1.6 percent to 1.9 percent for the fracture zone was calculated from the 2D dc-resistivity modeling. Crossed square-array dc-resistivity profiling data indicates the secondary porosity is between 0.65 to 0.75 percent in the same location.

The secondary porosity calculated from the 2D dc-resistivity data is higher than that calculated from the square-array dc-resistivity data in the same area. One reason is that the value of the secondary porosity determined from the square-array dc-resistivity is an average of the entire volume under the array, whereas the secondary porosity value determined from the 2D dc-resistivity inversion only includes the volume from the fracture zone.

The high secondary porosity calculated from the 2D dc-resistivity modeling may indicate that the fracture zones contains rubble, or iron precipitate. On the face of the gorge, both rubble and iron precipitate were observed in Fracture Zone 2.

CONCLUSIONS

Five surface geophysical methods were used to determine the locations of fracture zones in crystalline bedrock for predicting fluid flow and chemical migration at the U.S. Geological Survey Fractured Rock Research Site at Mirror Lake, Grafton County, New Hampshire. Two methods of direct-current (dc) resistivity (two-dimensional (2D) and crossed square-array profiling), two methods of inductive terrain conductivity(EM-34 and Slingram), and very-low-frequency electromagnetics (VLF) were used over survey lines extending about 200 meters. The results of the five methods were correlated to locate fracture zones; anomalies that were detected in one or two of the results were eliminated, increasing the confidence in the interpretation of anomalies detected in all of the results.

Two low resistivity anomalies were detected with all the geophysical methods in the southeast part of the study area. Based on the geophysical, outcrop, and photolinear data, the anomalous areas were interpreted as steeply dipping fracture zones approximately 10-meters wide. One interpreted fracture zone strikes approximately north 45 degrees east and the other strikes approximately north 17 degrees east.

Results of dc-resistivity surveys were analyzed to estimate the secondary porosity of the two interpreted fracture zones. Crossed square-array dc-resistivity profiling data indicates the secondary porosity is between 0.65 to 0.75 percent, whereas the 2D dc-resistivity profiling results indicate the secondary porosity to be 1.6 to 1.9 percent. Estimates from the 2D dc-resistivity profiling could indicate the effects of alteration and/or iron precipitate observed in outcrops near the survey lines.

ACKNOWLEDGEMENTS

The U.S. Geological Survey Fractured Rock Research Site is located within the Hubbard Brook Experimental Forest. The Hubbard Brook Experimental Forest is operated and maintained by the Northeastern Forest Experiment Station, USDA Forest Service, Radnor, Pennsylvania.

REFERENCES

Archie, G.E., 1942, The electrical resistivity log as an aid in determining some reservoir characteristics: Trans. Am. Inst. Min., Metal. and Petr. Eng., v. 146, p. 54-62

Clark, S.F., Jr., Ferguson, E.W., Short, H.A., Marcoux, G.J., and Moore, R.B., 1999, Lineament map area 9 of New Hampshire bedrock aquifer assessment, north-central New Hampshire: U.S. Geological Survey Open-File Report 99-63, scale: 1:48000.

deGroot-Hedlin, C. and Constable, S., 1990, Occam's inversion to generate smooth, two-dimensional models from magnetotelluric

data: Geophysics, v. 55, p.1613-1624.
Edwards, L.S., 1977, A modified pseudosection for resistivity and IP: Geophysics, v. 42, no. 5, p. 1020-1036.
Habberjam, G.M., 1972, The effects of anisotropy on square array resistivity measurements: Geophysical Prospecting, v. 20, p. 249-266.
Habberjam, G.M., 1975, Apparent resistivity, anisotropy, and strike measurements, Geophysical Prospecting, v. 23, p. 211-247.
Haeni, F.P., Lane, J.W., Jr., and Lieblich, D.A., 1993, Use of surface-geophysical and borehole-radar methods to detect fractures in crystalline rocks, Mirror Lake area, Grafton County, New Hampshire *in* Banks, D. and Banks, S., eds., Hydrogeology of Hard Rocks, Memoires of the XXIVth Congress, Oslo, Norway: International Association of Hydrologists, p. 577-587.
Iris Instruments, 1993, T-VLF Operating manual (Release 1.0), Orleans, France.
Jansen, J., and Jurcek, P., 1997, The application of surficial geophysics to well site exploration and wellhead protection in fracture controlled aquifers *in* The Symposium on the Application of Geophysics to Environmental and Engineering Problems '97 Volume II: Wheat Ridge, Colorado, Environmental and Engineering Geophysical Society, p. 635-644.
Kaikkonen, P., and Sharma, S.P., 1997, Delineation of near-surface structures using VLF and VLF-R data—an insight from the joint inversion results: The Leading Edge, v. 16, no. 11, p. 1683-1686.
Lewis, M.R., and Haeni, F.P., 1987, The use of surface geophysical techniques to detect fractures in bedrock—an annotated bibliography: U.S. Geological Survey Circular 987, 14p.
Lieblich, D.A., Lane, J.W., Jr., and Haeni, F.P., 1991, Results of integrated surface-geophysical studies for shallow subsurface fracture detection at three New Hampshire Sites *in* Expanded Abstracts with Biographies, SEG 61st Annual International Meeting Volume I: Society of Exploration Geophysicists, p. 553-556.
Loke, M.H., 1997, Electrical imaging surveys for environmental and engineering studies: a practical guide to 2D and 3D surveys: Unpublished short training course lecture notes, Universiti Sains Malaysia, Penang, Malaysia.
McNeill, J.D., 1980a, Electromagnetic terrain conductivity measurements at low induction numbers: Geonics Ltd. Technical Note TN-6, Mississauga, Ontario, Canada.
McNeill, J.D., 1980b, EM 34-3 survey interpretation techniques: Geonics Ltd. Technical Note TN-8, Mississauga, Ontario, Canada.
McNeill, J.D., 1990, Use of electromagnetic methods for groundwater studies, *in* Ward, Stanley H. ed., Geotechnical and Environmental Geophysics, Volume 1: Tulsa, Oklahoma, Society of Exploration Geophysicists, p. 191-218.
McNeill, J.D., and Labson, V.F., 1990, Geological mapping using VLF radio fields, in Nabighian, M. ed., Electromagnetic Methods in Applied Geophysics, Volume 2, Part B: Tulsa, Oklahoma, Society of Exploration Geophysicists, p. 521-640.
Sasaki, Y., 1992, Resolution of resistivity tomography inferred from numerical simulation: Geophysical Prospecting, v. 40, p. 453-464.

AUTHOR INFORMATION

C.J. Powers, U.S. Geological Survey, Storrs, CT (cjpowers@usgs.gov)

Kamini Singha, U.S. Geological Survey, Storrs, CT (ksingha@usgs.gov)

F. Peter Haeni, U.S. Geological Survey, Storrs, CT (phaeni@usgs.gov)

Characterizing Fractures in a Bedrock Outcrop Using Ground-Penetrating Radar at Mirror Lake, Grafton County, New Hampshire

By Marc L. Buursink and John W. Lane, Jr.

ABSTRACT

A study incorporating numerical modeling, physical modeling, and field surveys at the U.S. Geological Survey Fractured Rock Research Site at Mirror Lake, Grafton County, New Hampshire, was conducted to test the use of ground-penetrating radar (GPR) surface reflection methods to delineate fractures in heterogeneous bedrock. Results of one- and 2.5-dimensional numerical modeling correlate with results of laboratory-scale physical modeling and establish different GPR reflection characteristics for saturated and unsaturated (dry) fractures. Saturated fractures generate higher amplitude reflections than unsaturated fractures and have an opposite phase. GPR reflection data collected over a highway bedrock outcrop near Mirror Lake were processed to reduce noise and clutter, to correct geometric and topographic distortions, and to enhance weak reflections from structures more than 15 meters (m) deep.

Guided by the results of numerical modeling, 18 reflectors with lengths ranging from 4 to 32 m and dips ranging from 5 to 40 degrees were interpreted as fractures in the processed GPR field records. All of the interpreted fractures that project above land surface correlated with fractures recorded by detailed outcrop mapping. Interpretation of the processed field data was limited to reflectors dipping less than 45 degrees, although more steeply dipping fractures exist at the field site. Spatial aliasing effects and other limitations constrain the range of dip-angles that GPR reflection methods can usefully image from the surface. The results of the field study together with the results of the numerical and physical modeling indicate that surface GPR reflection methods can be used to help characterize fractures in heterogeneous bedrock.

INTRODUCTION

This paper presents the results of a ground-penetrating radar (GPR) field study conducted at the U.S. Geological Survey (USGS) Fractured Rock Research Site at Mirror Lake, Grafton County, New Hampshire, to test the use of this surface reflection method to delineate fractures in heterogeneous bedrock. The study also used numerical and physical modeling to establish GPR reflection characteristics in fractured bedrock and to identify reflection characteristics useful for understanding and interpreting the processed GPR field data.

GPR has been used in many studies to identify and characterize fractures and faults in rock (Ulriksen, 1982; Holloway, 1992; Benson, 1995; Stevens and others, 1995; Toshioka and others, 1995; Grasmueck, 1996; Serzu and others, 1996). In general, these studies have been conducted at field sites where interpretation of GPR data to delineate fractures or faults is constrained by relatively simple geologic conditions.

In contrast, the geology at the Mirror Lake research site is extremely heterogeneous. Bedrock at the site consists of gneiss and schist intruded by granite and pegmatite dikes (Hsieh and others, 1993; Barton, 1996). Bedrock fractures at the Mirror Lake site have highly variable orientations, are poorly connected, and occur at length scales from centimeters to tens of meters.

NUMERICAL AND PHYSICAL MODELING

Numerical and physical modeling of the GPR signal response to fractures in bedrock was conducted to predict radar reflection characteristics in fractured rock. A one-dimensional (1-D) forward modeling program (Powers and Olhoeft, 1995) and a 2.5-dimensional (2.5-D) forward modeling program (Powers, 1995) were used to simulate saturated and unsaturated (dry) fractures in bedrock.

Results from 1-D GPR models containing a single fracture show the response of a 100-megahertz (MHz) radar signal to fractures with a range of apertures. The 1-D full waveform modeling results for 1-, 4-, and 16-millimeter (mm) aperture saturated and unsaturated fractures are shown in figure 1. The modeled radar reflections from the fractures are shown adjacent to the reflection from the overburden-bedrock interface to provide a relative scale for assessing the differences in normalized reflection amplitude and phase. The modeled radar reflections from saturated fractures have the largest normalized peak-to-peak amplitudes and are out of phase with the transmitted pulse and the overburden-bedrock reflection. The reflection amplitude increases and the waveform changes as the modeled fracture aperture increases from 1 to 16 mm. Modeled radar reflections from unsaturated fractures have amplitudes that are slightly larger than the overburden-bedrock reflection and are in-phase with it and the transmitted pulse.

Radar reflection characteristics were also simulated using a 2.5-D modeling program. The 2.5-D modeling program generates data that resemble field GPR data. For example, individual fracture or fracture-zone reflections with horizontal or sub-horizontal dips simulated in 2.5-D provide a visual image of what may be observed in the field data.

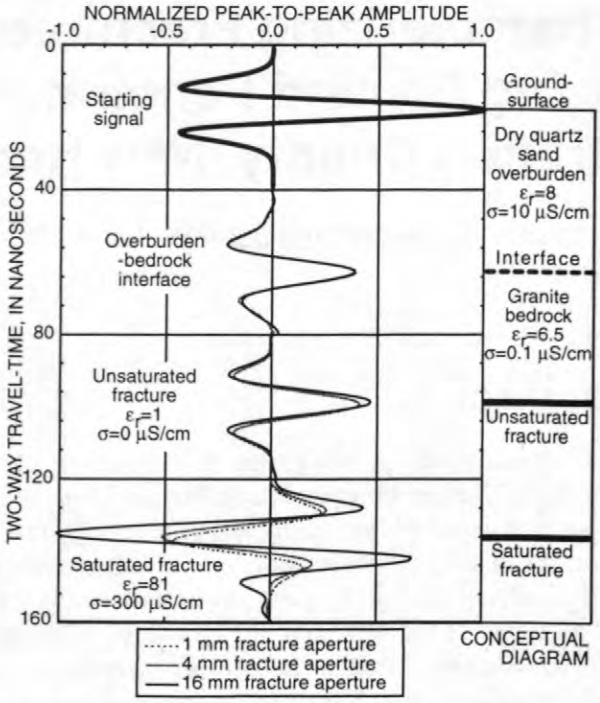

Figure 1. Results of 1-D radar modeling using a 100 MHz starting wavelet, showing the overburden-bedrock interface reflection and showing changes in the reflection amplitude and waveform for 1-, 4-, and 16-mm aperture saturated and unsaturated fractures. Model values for the dielectric permittivity (ε_r) and electrical conductivity (σ) are indicated.

Figure 2. The fractured granite block used for the laboratory-scale physical modeling of GPR reflection characteristics. A GPR reflection survey in progress is shown.

The results from the 1- and 2.5-D numerical modeling were compared to GPR data acquired over a laboratory-scale physical model. The physical model comprised a relatively homogeneous, feldspathic granite block about 1.9 meters (m) long, 1.1 m wide and 1.4 m high (fig. 2). A sub-horizontal fracture was induced through the center of the block about 0.8 m from the top. The edges of the fracture were sealed to prevent leakage, and plastic valves were installed in the upper and lower edges of the block permit water injection and withdrawal.

Radar data were acquired with a commercial radar field-instrument (manufactured by Geophysical Survey Systems Inc.[1]) using a 500 MHz center-frequency antenna. Thirty traces of radar reflection data were acquired at discrete 5-centimeter (cm) intervals by stepping the antenna across the length the block. Figure 3 shows the radar reflection data for the saturated (fig. 3a) and unsaturated (fig. 3b) fracture experiments. The reflection from the fracture appears at about 14 nanoseconds (ns) in the GPR records. The amplitude of the radar reflection from the saturated fracture is greater than the amplitude from the unsaturated fracture. The phase of the radar reflection from the saturated fracture is opposite the phase of the reflection from the unsaturated fracture. The amplitude of the reflections varies across the face of the block, increasing in amplitude from the left (higher end of the block) to the right side (lower end of the block). The differences in the reflection amplitude and waveform are caused by the increase in the fracture aperture at the lower end of the block.

Comparing the results of both the 1-D and 2.5-D numerical modeling to the results of the physical modeling indicates that the numerical models accurately predict radar reflection amplitude and phase characteristics for simple geologic models. Both modeling methods indicate that saturated fractures generate high-amplitude reflections with a phase opposite that of the transmitted pulse. Based on the correlation between the numerical and the physical model data, 2.5-D modeling results were used to interpret field GPR data to identify bedrock fractures.

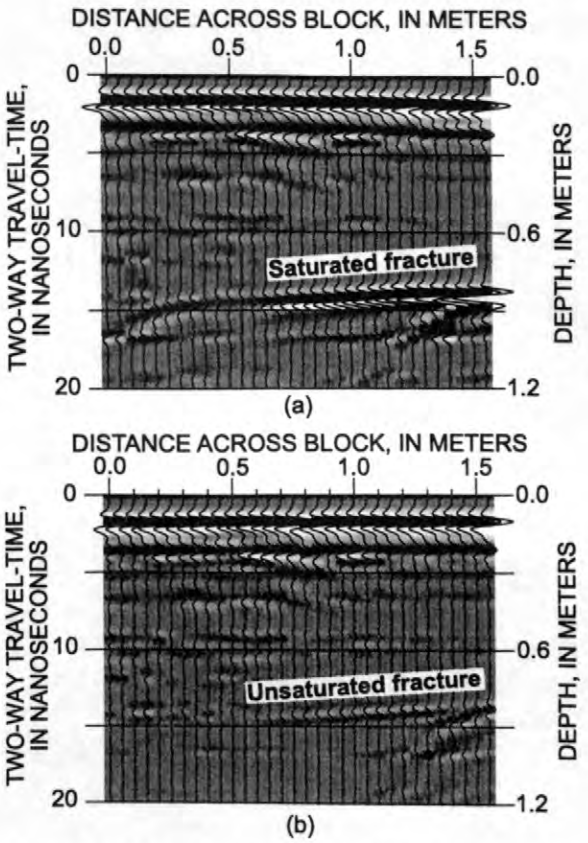

Figure 3. 500 MHz GPR reflection record from the physical model: (a) saturated fracture, (b) unsaturated fracture. The reflection from the fracture at 14 ns is labeled. The depth scale was calculated assuming a radar propagation velocity of 117 m/μs.

FIELD EXPERIMENT

GPR reflection surveys were conducted at the I-93 highway outcrop near Mirror Lake (fig. 4). The outcrop, along the center median of the highway, is more than 200 m long and 20 m wide. The average height of the outcrop is about 6 m above land surface, with the lowest point at land surface, and the highest at 12 m. Fractured bedrock exposed by the outcrop is representative of that underlying most of the study area (Barton, 1996). The outcrop is particularly suitable to GPR reflection surveys because (1) the bedrock is

[1] The use of trade, product, or firm names in this report is for identification purposes only and does not constitute endorsement by the U.S. Geological Survey.

electrically resistive, a physical property favorable for penetration of the radar; (2) the large area of exposed bedrock is not covered with overburden, therefore minimizing sources of near surface noise and clutter; and (3) the fractures exposed in the bedrock outcrop walls have been extensively mapped (Barton, 1997), providing excellent ground-truth.

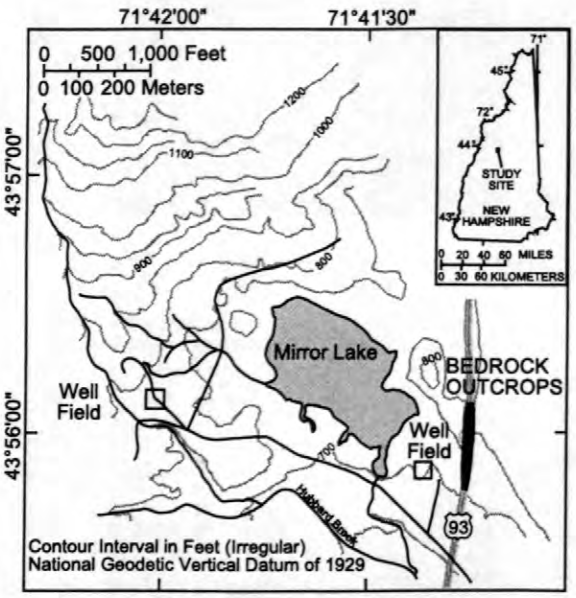

Figure 4. Site diagram showing the Mirror Lake Fractured Rock Research Site, Grafton County, New Hampshire. The bedrock outcrop that was used as the location for the GPR surveys is located at the eastern end of the study area.

The GPR surveys were conducted along the centerline of the median outcrop, about 10 m from the outcrop wall. GPR data were collected with a portable battery-operated, commercial radar field-instrument (manufactured by Malå GeoScience, A.B.) using 200 MHz center-frequency antennas. For this study, two types of GPR surveys were conducted on the bedrock outcrop: (1) continuous profiling common-offset (CO) reflection surveys (fig. 5a), and (2) common mid-point (CMP) reflection surveys (fig. 5b). The continuous profiling surveys were conducted to image the subsurface; the CMP surveys were conducted to establish the radar propagation velocity in bedrock, a value required for data processing.

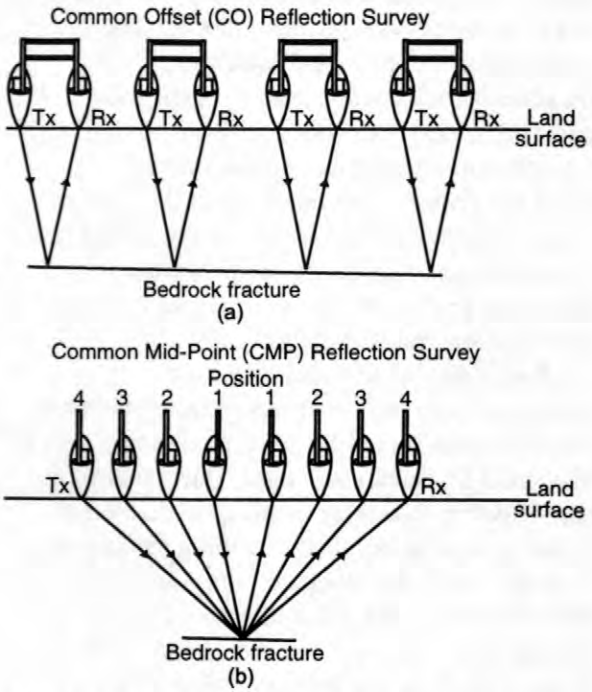

Figure 5. Diagram showing (a) the antenna geometry for a common-offset (CO) ground-penetrating radar reflection survey and (b) the antenna geometry for a common mid-point (CMP) survey used to derive the average subsurface radar propagation velocity. In both, Tx and Rx indicate the locations of the transmitting and receiving antennas, respectively.

For the CO profiling surveys, the receiver and transmitter antennas were separated by 40 cm in a fiberglass sled, which was pulled across the outcrop surface. A GPR trace was collected every 10 cm along the profile, with a recording window of 350 ns. The use of these acquisition parameters ensured that reflections from structures dipping less than 45 degrees were accurately imaged. For dips exceeding 45 degrees, however, geometric distortion from spatial aliasing hinders the interpretation of steeply dipping fractures when using CO reflection methods. The CMP survey was collected by placing the antennas on the rock surface and increasing the transmitter-receiver antenna offset from 0.5 to 25 m, in 0.5-m increments.

DATA PROCESSING

Data processing methods can reduce the presence of noise and can correct the geometric and topographic effects that severely limit the usefulness of the unprocessed field data. The GPR reflection data from the outcrop were processed and displayed in a manner that facilitated the interpretation and identification of continuous reflectors (fig. 6). Details of the methods used to process the field data can be found in Yilmaz (1987) and Telford and others (1990). The data processing methods used in this study included (1) filtering to reduce random noise, instrument noise, and clutter, (2) application of a time-range gain to enhance deep reflections, (3) depth conversion and topographic correction to compensate for changes in surface elevation, and (4) migration to focus reflection energy and to correct for geometric distortion.

De-wow, frequency, and horizontal filtering methods were applied to the field data to remove noise and to preserve true GPR reflections. Instrument noise (DC-shift) was removed with a very low frequency low-cut or de-wow filter. High frequency clutter and noise, and the remaining low frequency noise, both outside the useful 200 MHz antenna frequency range, were removed with a band-pass filter. Horizontal filtering reduced background noise that was consistent from trace to trace thereby accentuating dipping reflectors.

A time-range gain was applied to the data after filtering. Time-range gain compensates for geometric spreading losses and material absorption losses of the radar signal.

Converting radar arrival-times to depth (depth-conversion) requires the radar propagation velocity. The CMP data were analyzed using a common velocity analysis method to determine radar propagation velocity (Telford and others, 1990). Analysis of CMP data from the outcrop yielded a radar propagation velocity in the bedrock outcrop of 117 meters per microsecond (m/μs). This is comparable to the propagation velocity calculated from borehole-radar experiments at Mirror Lake (118 m/μs) and to the propagation velocity for granite (100 m/μs) reported by Annan (1992). The calculated radar propagation velocity (117 m/μs) was used to establish the vertical scale of the GPR records. Following depth conversion, the elevation of each GPR trace was shifted to account for topography along the survey line.

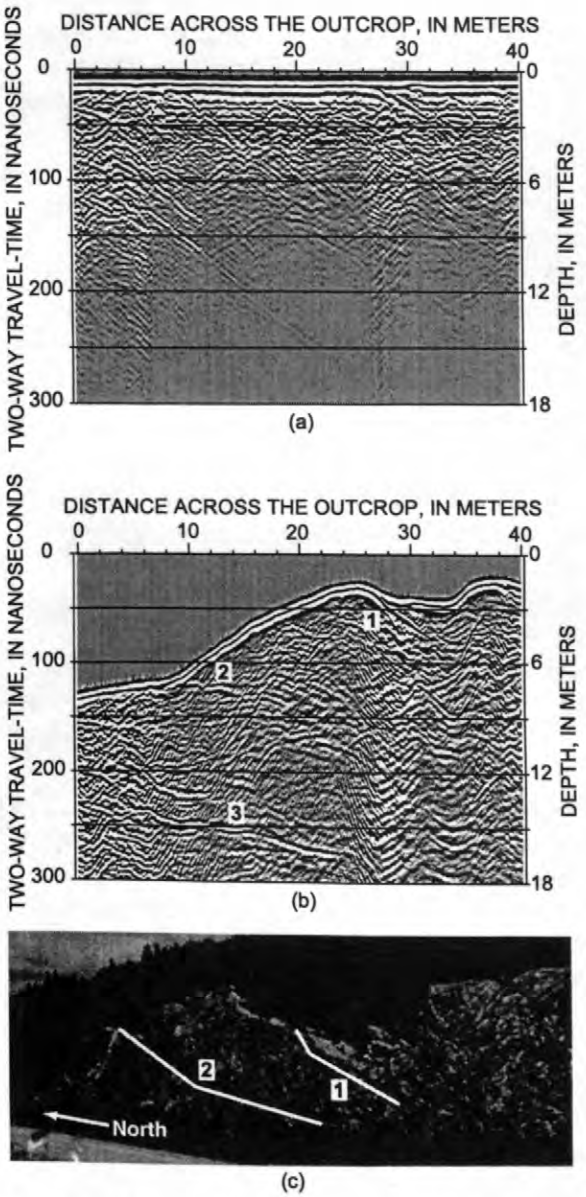

Figure 6. (a) 200 MHz unprocessed GPR field record from the bedrock outcrop. (b) Data shown in (a) after processing and topographic correction. Interpreted reflections are labeled 1 through 3. (c) Photograph of the section of outcrop surveyed with GPR. Fractures 1 and 2 are annotated in the photograph. The depth scale was calculated assuming a radar propagation velocity of 117 m/μs. The vertical exaggeration is 1.7 times.

After the topographic correction was applied to the data, the data were migrated. The migration processing method uses the radar

propagation velocity and the antenna geometry in relation to the target, and correctly locates reflectors in the subsurface.

Figure 6 shows a 40 m section of the field data from the outcrop before (fig. 6a) and after (fig. 6b) data processing. Processing improved the field data in several ways. First, true dipping reflectors were differentiated from background clutter caused by small-scale bedrock heterogeneities. Second, deep reflectors were enhanced, increasing the apparent depth of penetration of the GPR survey to at least 17 m below the top of the outcrop. Third, reflectors were correctly positioned and oriented.

DATA INTERPRETATION

Interpretation of the processed field data was based on the results of the numerical and physical modeling. Reflectors interpreted as fractures (1) displayed the reflection amplitude and phase characteristics identified in the numerical and physical modeling and (2) were linear and were continuous from trace to trace for at least 40 traces. In figure 6b, for example, three continuous reflectors (labeled 1 to 3) are interpreted as fractures. The depth and orientation of reflectors labeled 1 and 2 in the figure correlate with fractures observed on the walls of the outcrop (fig. 6c). The reflector labeled 3 cannot be confirmed by ground-truth because it projects below the land surface.

Although steeply dipping fractures are present in the outcrop, only reflectors dipping less than 45 degrees were considered in the interpretation process. This constraint, based on calculations using trace spacing, radar signal frequency and propagation velocity (Yilmaz, 1987), was imposed to prevent interpretation of reflectors whose orientation could be affected by spatial aliasing distortions. In the processed data, 18 reflectors with lengths ranging from 4 to 32 m and dips ranging from 5 to 40 degrees were interpreted as fractures. All of the fractures interpreted from the processed GPR records and projecting above land surface correlated with the ground-truth fractures provided by detailed mapping.

Radar data from 2.5-D modeling simulating unsaturated and saturated fractures were used to guide the interpretations of reflections in the GPR field data. For example, figure 7 shows a reflector interpreted as a fracture in the field data next to the results of a 2.5-D model of a fracture pair. Two fractures dipping approximately 5 degrees with apertures of 1 mm are shown; one is unsaturated, the other is saturated (fig. 7a). The amplitude, continuity, and phase of the reflector in the field data (fig. 7b) and in the modeled data for the saturated fracture are similar. The reflector in the field data is, therefore, interpreted as a saturated fracture. Most reflectors interpreted as fractures were consistent with numerical models of saturated fractures.

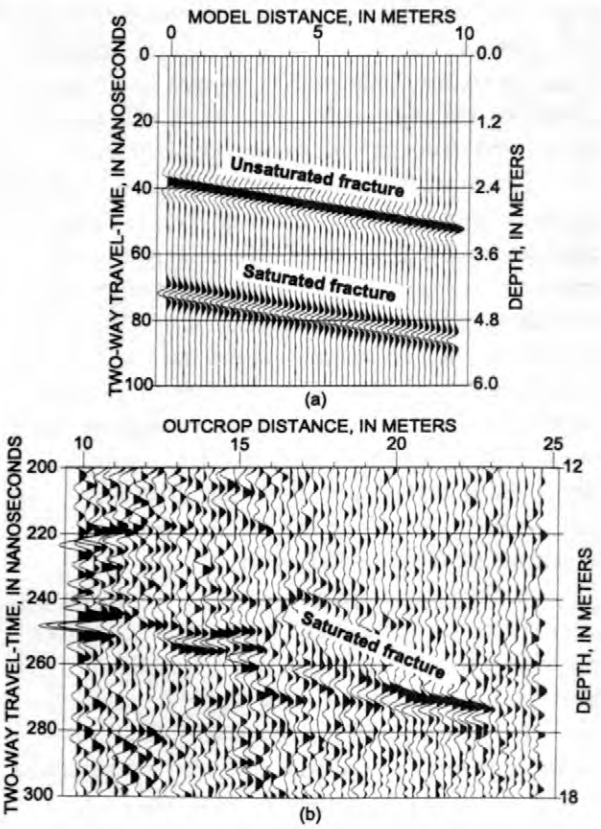

Figure 7. (a) Radar data modeled in 2.5-D using a 200 MHz starting wavelet. The reflectors are modeled as fractures with an aperture of 1 mm dipping 5 degrees. The results show the difference in the reflection amplitude and phase for an unsaturated (upper) and saturate (lower) fracture. (b) A reflector extracted from the GPR field record of 200 MHz data. The depth scale was calculated assuming a radar propagation velocity of 117 m/μs. The vertical exaggeration is 2 times.

CONCLUSIONS

A study incorporating numerical modeling, physical modeling, and field surveys at the USGS Fractured Rock Research Site at Mirror Lake, Grafton County, New Hampshire, was conducted to test the use of GPR surface reflection methods to delineate fractures in heterogeneous bedrock. Results of 1-D and 2.5-D numerical modeling correlate with results of laboratory-scale physical modeling and establish different GPR reflection characteristics for saturated and unsaturated fractures. Saturated fractures generate higher amplitude reflections than unsaturated fractures and have an opposite phase.

GPR data collected over a highway outcrop near Mirror Lake were processed to reduce noise and clutter, correct geometric and topographic distortions, and enhance weak reflections from structures more than 15 m deep. Guided by the results of numerical modeling, 18 reflectors with lengths ranging from 4 to 32 m and dips ranging from 5 to 40 degrees were interpreted as fractures in the processed field data. All of the interpreted fractures that project above land surface correlated with fractures recorded by detailed mapping. Interpretation of processed field data was limited to reflectors dipping less than 45 degrees, although more steeply dipping fractures exist at the field site. Spatial aliasing effects and other limitations constrain the range of dip-angles that GPR reflection methods can usefully image from the surface.

The results of the field study and the results of the numerical and physical modeling indicate that surface GPR methods can be used, within limits, to characterize fracture location and orientation in heterogeneous bedrock.

ACKNOWLEDGMENTS

The authors thank Prof. Lanbo Liu at the Department of Geology and Geophysics, University of Connecticut, for his input into the data processing of the GPR field data. We especially thank Wayne Martin of the U.S. Forest Service for permitting the experiment to be conducted at the Hubbard Brook Experimental Forest, Grafton County, New Hampshire. The Hubbard Brook Experimental Forest is operated and maintained by the Northeastern Forest Experiment Station, USDA Forest Service, Radnor, Pennsylvania.

REFERENCES

Annan, A.P., 1992, Ground penetrating radar workshop notes: Mississauga, Ontario, Sensors & Software, Inc., 128 p.

Barton, C.C., 1997, Bedrock geologic map of Hubbard Brook Experimental Forest and maps of fractures and geology in roadcuts along Interstate 93, Grafton County, New Hampshire: U.S. Geological Survey Miscellaneous Investigations Series Map I-2562, scale 1:12,000, 2 sheets.

——— 1996, Characterizing bedrock fractures in outcrop for studies of ground-water hydrology – an example from Mirror Lake, Grafton County, New Hampshire, *in* Morganwalp, D.W., and Aronson, D.A., eds., U.S. Geological Survey Toxics Substances Hydrology Program--Proceedings of the Technical Meeting, Colorado Springs, Colorado, September 20-24, 1993: U.S. Geological Survey Water-Resources Investigations Report 94-4015, v. 1, p. 81-87.

Benson, A.K., 1995, Applications of ground-penetrating radar in assessing some geologic hazards--examples of groundwater contamination, faults, and cavities: Journal of Applied Geophysics, v. 33, p. 177-193.

Grasmueck, M., 1996, 3-D ground-penetrating radar applied to fracture imaging in gneiss: Geophysics, v. 61, no. 4, p. 1050-1064.

Holloway, A.L., 1992, Fracture mapping in granite rock using ground probing radar *in* Pilon, J., ed., Ground Penetrating Radar: Geological Survey of Canada Paper 90-4, p. 85-100.

Hsieh, P.A., Shapiro, A.M., Barton, C.C., Haeni, F.P., Johnson, C.D., Martin, C.W., Paillet, F.L., Winter, T.C., and Wright, D.L., 1993, Methods of characterizing fluid movement

and chemical transport in fractured rock *in* Field Trip Guidebook for the Northeastern United States: Geological Society of America, Field Trip Guidebook for the Northeastern United States, v. 2, chap. R, 30 p.

Powers, M.H., 1995, Dispersive ground penetrating radar modeling in 2D: Golden, Colorado, Colorado School of Mines, Ph.D. Thesis T-4820.

Powers, M.H., and Olhoeft, G.R., 1995, GPRMODV2--One dimensional full waveform forward modeling of dispersive ground penetrating radar data, Version 2.0: U.S. Geological Survey Open File Report 95-58, 41 p. and floppy diskette.

Serzu, M.H., Street, P.J., Lodha, G.S., and Stevens, K.M., 1996, Characterization of a moderately fractured granitic rock using single-hole radar reflection, crosshole radar tomography, and ground penetrating radar at AECL's underground research laboratory, Pinawa, Manitoba, Canada *in* Sixth International Conference on Ground Penetrating Radar (GPR'96), Sendai, Japan, September 30-October 3, 1996, Proceedings: Sendai, Japan, Tohoku University, Department of Geoscience and Technology, p. 173-177.

Stevens, K.M., Lodha, G.S., Holloway, A.L., and Soonawala, N.M., 1995, The application of ground penetrating radar for mapping fractures in plutonic rocks within the Whiteshell Research Area, Pinawa, Manitoba, Canada: Journal of Applied Geophysics, v. 33, p. 125-141.

Telford, W.M., Geldart, L.P., and Sheriff, R.E., 1990, Applied Geophysics (2d ed.): New York, N. Y., Cambridge University Press, 770 p.

Toshioka, T., Tsuchida, T., and Sasahara, K., 1995, Application of GPR to detecting and mapping cracks in rock slopes: Journal of Applied Geophysics, v. 33, p. 119-124.

Ulriksen, C.P.F., 1982, Application of impulse radar to civil engineering: Lund, Sweden, Lund University of Technology, Ph.D. dissertation, 179 p., *published by* Geophysical Survey Systems, Inc., North Salem, N.H.

Yilmaz, O., 1987, Seismic Data Processing, *ed. by* Doherty, S.M., *of the series* Neitzel, E.B., ed., Investigations in Geophysics Series, Vol. 2: Tulsa, Okla., Society of Exploration Geophysicists, 526 p.

AUTHOR INFORMATION

Marc L. Buursink, U.S. Geological Survey, Storrs Mansfield, CT (buursink@usgs.gov).

John W. Lane, Jr., U.S. Geological Survey, Storrs Mansfield, CT (jwlane@usgs.gov).

Computer Simulation of Fluid Flow in Fractured Rocks at the Mirror Lake FSE Well Field

By Paul A. Hsieh, Allen M. Shapiro, and Claire R. Tiedeman

ABSTRACT

A numerical finite-difference model is developed to simulate fluid flow in the fractured rock underlying the FSE well field at the U.S. Geological Survey Fractured Rock Research Site near Mirror Lake, New Hampshire. Highly transmissive fracture clusters in the bedrock are represented by model cells of comparatively higher hydraulic conductivity. The surrounding bedrock containing less transmissive fractures is represented by model cells of comparatively lower hydraulic conductivity. The model is calibrated to drawdown data from a multiple-well hydraulic test. Calibration results suggest that the highly transmissive fracture clusters are three to four orders of magnitude more conductive than the surrounding bedrock with less transmissive fractures. Relatively good matches between simulated and observed drawdowns suggest that a heterogeneous continuum model can be applied to simulate fluid flow in the fractured rock underlying the FSE well field.

INTRODUCTION

Results of hydraulic tests and borehole geophysical logging at the U.S. Geological Survey Fractured Rock Research Site near Mirror Lake, Grafton County, New Hampshire suggest the presence of highly transmissive fracture clusters in the topmost 50 meters (m) of crystalline bedrock underlying the FSE well field, which occupies a 120-m by 80-m area (fig 1). Hsieh and Shapiro (1996) identified four fracture clusters embedded within a network of less transmissive fractures. The hypothesized distribution of fractures in the vertical section between wells FSE1 and FSE6 is shown in figure 2. The four fracture clusters are denoted by I to IV. Each cluster occupies a near horizontal, tabular-shaped volume that extends tens of meters in the horizontal direction and several meters in the vertical.

During multiple-well hydraulic tests, packer-isolated well intervals that are hydraulically connected by highly transmissive fractures exhibit nearly identical drawdown responses. By contrast, well intervals that are not hydraulically connected by highly transmissivity fractures exhibit significantly different responses.

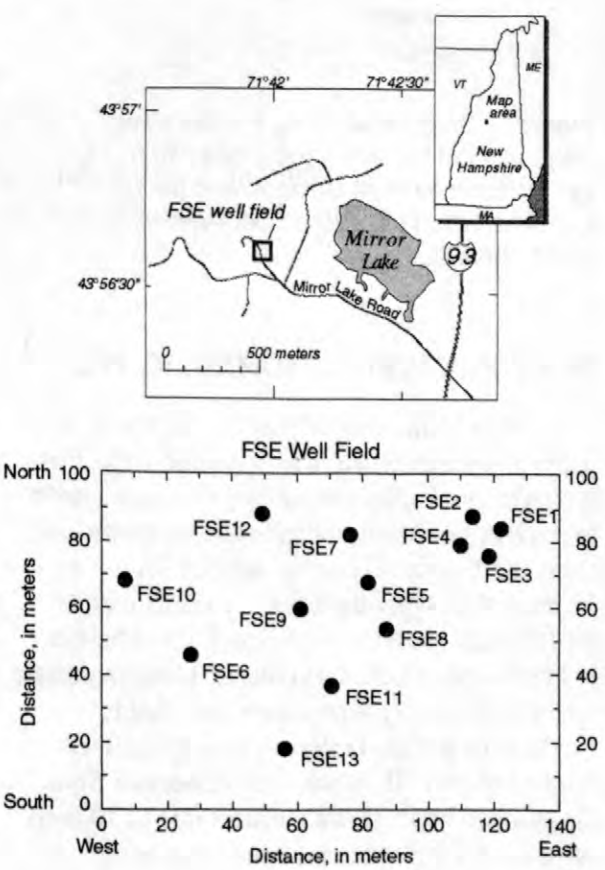

Figure 1. Map showing arrangement of wells in the FSE well field.

Such behavior cannot be analyzed by classical aquifer-testing methods that assume a homogeneous aquifer. Instead, a method of analysis is needed to explicitly represent the heterogeneity in the bedrock. This paper presents the development of a numerical model to simulate fluid flow during the multiple-well hydraulic test at the FSE well field.

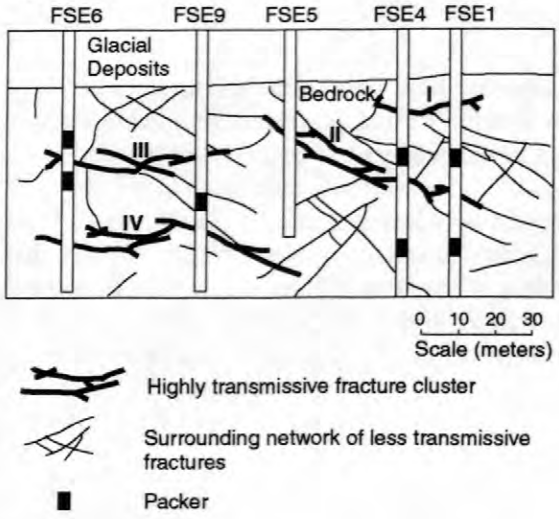

Figure 2. Diagram showing hypothesized distribution of fractures, the extents of highly transmissive fracture clusters, and packer locations in vertical section between wells FSE1 and FSE6.

MULTIPLE-WELL HYDRAULIC TEST

Prior to the start of the hydraulic test, packers were installed in observation wells that intersect two highly transmissive fracture clusters to prevent fluid flow and pressure transmission from one fracture cluster to another via the well. To ensure pressure-tight seals, packers were placed at an interval of solid rock about halfway between fracture clusters (fig. 2). In the pumped well (FSE6), two packers were installed to straddle the pumped interval, which intersects fracture cluster III. Water was withdrawn from the pumped interval at a constant rate of 10 liters per minute for 80 hours. Drawdowns in the bedrock were monitored by pressure transducers connected to each well interval, and were occasionally checked by manual measurement with an electric water-level probe.

Observed drawdowns in the well intervals show the effect of highly transmissive fracture clusters, which tend to equalize the hydraulic head within the fractures. Figure 3 shows drawdowns in well intervals which are labels according to the well name and the fracture cluster intersected by the interval. Note that well intervals intersecting fracture cluster II (FSE1-II, FSE4-II and FSE5-II) exhibit nearly identical drawdowns, even though well FSE5 is 58 m from the pumped well (FSE6) while well FSE1 is 101 m from the pumped well. Similar responses are observed in well intervals intersecting fracture cluster I (FSE1-I and FSE4-I), and fracture cluster IV (FSE6-IV and FSE9-IV).

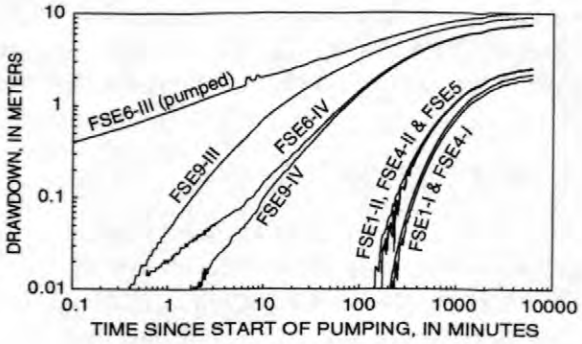

Figure 3. Observed drawdown in well intervals during multiple-well hydraulic test. A well interval is identified by the well name followed by the fracture cluster intersected by the interval.

NUMERICAL MODEL

The U.S. Geological Survey modular finite-difference ground-water flow model (Harbaugh and McDonald, 1996), commonly known as MODFLOW-96, was used to simulate ground-water flow during the hydraulic test. The application of MODFLOW-96, a continuum model, assumes that flow in the fractured rock underlying the FSE well field can be represented by flow in a heterogeneous continuum. The model grid is composed of two types of cells. The highly transmissive fracture clusters are represented by cells of comparatively higher hydraulic conductivity. The surrounding bedrock with less

transmissive fractures is represented by cells of comparatively lower hydraulic conductivity. The model grid covers an area of 340 m by 270 m that is centered about the well field. This area is discretized into 42 rows and 34 columns of nonuniform spacings. The grid is finest around the pumped well, FSE6, and coarsens with distance from the pumped well. In the vertical direction, the grid consists of 10 layers. The topmost layer (Layer 1) represents the glacial deposits. The remaining 9 layers represent the topmost 50 m of bedrock. The four fracture clusters are represented by cells in Layers 3, 6, and 10, which are each 1.5 m thick. The 7 remaining bedrock layers are each 7.5 m thick. Figure 4 shows the spatial extents of fracture clusters II and III in Layer 6. Figure 5 shows a vertical section (A-A') of the model.

The four sides and the bottom surface of the model grid are specified as no-flow boundaries. Cells in the top model layer (representing glacial deposits) are specified as constant-head cells (zero drawdown). Because the water table lies in the glacial deposits, and storage in the glacial deposits is significantly larger than storage in the fractured bedrock, the glacial deposits is the primary source of pumped water. Although a small drawdown was observed in piezometers installed in the glacial deposits, this drawdown is negligible when compared to the much larger drawdown in the bedrock.

Because the highly transmissive fracture clusters are represented as relatively thin cells (1.5 m thick), their vertical hydraulic conductivity and specific storage have little effect on model simulation results. Thus, cells representing highly transmissive fracture clusters are assumed to be isotropic, and their specific storage is set equal to the specific storage of cells representing the surrounding bedrock with less transmissive fractures. The model parameters are:

- K_{high}, isotropic hydraulic conductivity of cells representing highly transmissive fracture clusters,
- $K_{h,low}$, horizontal hydraulic conductivity of cells representing the surrounding bedrock with less transmissive fractures,
- $K_{v,low}$, vertical hydraulic conductivity of cells representing the surrounding network of less transmissive fractures,
- C_v, vertical conductance of the interface between Layers 1 and 2, defined as the vertical hydraulic conductivity divided by the effective thickness of the interface between Layers 1 and 2, and
- S_s, specific storage of all cells in the model.

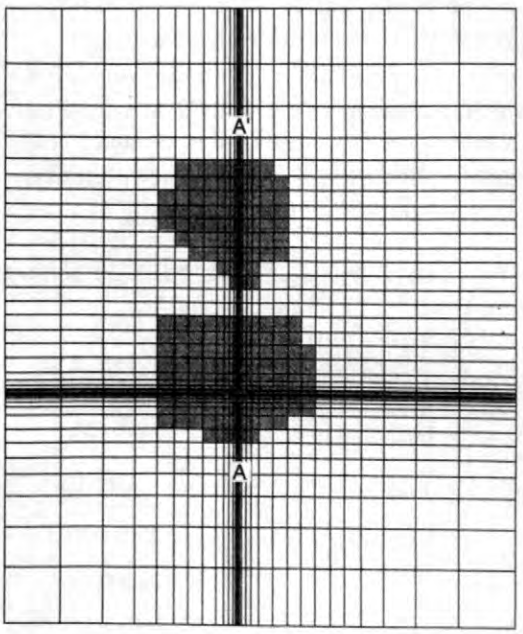

Figure 4. Areal view of Layer 6 of model grid. Gray cells represent highly transmissive fracture clusters. White cells represent surrounding bedrock with less transmissive fractures.

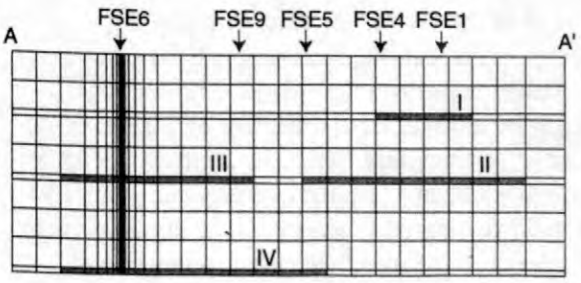

Figure 5. Vertical section A-A' of model grid. Gray cells represent highly transmissive fracture clusters. White cells represent surrounding bedrock with less transmissive fractures. Vertical exaggeration is 4x.

The parameter C_v is equivalent to the parameter *VCONT* in MODFLOW-96. It is used in the present model to characterize a thin, interface layer that controls the movement of water between the glacial deposits and the bedrock. This interface is not explicitly represented as a model layer.

The model was calibrated by finding parameter values that minimize the sum of squared differences between model simulated drawdowns and observed drawdowns. The calibration procedure uses the nonlinear least-squares method of Hill (1992). The calibrated parameter values are given in Table 1.

Table 1. Table showing calibrated value of model parameters.

Model parameter	Calibrated value
K_{high}	2×10^{-4} m/s
$K_{h,low}$	1.8×10^{-8} m/s
$K_{v,low}$	3.7×10^{-7} m/s
C_v	1.8×10^{-9} s^{-1}
S_s	2×10^{-6} m^{-1}

Cells representing highly transmissive fracture clusters are three to four orders of magnitude more conductive than cells representing the surrounding bedrock with less transmissive fractures. The hydraulic conductivity of the surrounding bedrock is about 20 times higher in the vertical direction than in the horizontal direction. This suggests that near-vertical fractures in the surrounding bedrock might be denser, more transmissive, or better connected than near-horizontal fractures. The parameter C_v is a lumped quantity and cannot be directly compared to the hydraulic conductivities. However, if the interface between the glacial deposits and the bedrock is assumed to be 1 m thick, then the vertical hydraulic conductivity of this interface layer is 1.8×10^{-9} m/s. This relatively low hydraulic conductivity value suggests that fractures at bedrock surface might be partially clogged by fine-grained glacial deposits resulting in a lowering of hydraulic conductivity. Relatively good matches were achieved between the model simulated drawdowns and the observed drawdowns. Although the matches are not perfect, the simulated and observed responses exhibit similar behaviors and magnitudes. Representative examples are shown in figures 6 and 7.

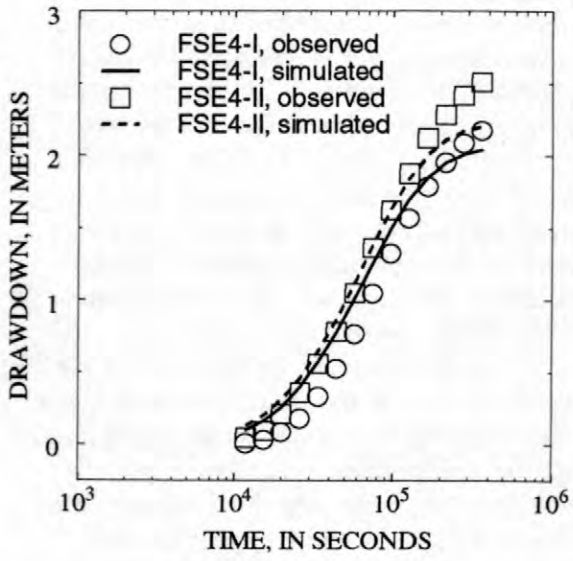

Figure 6. Comparison between observed and model simulated drawdown in the two well intervals of FSE4.

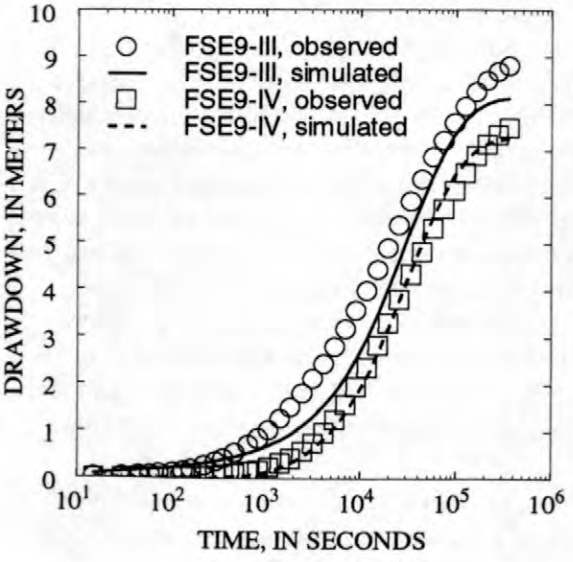

Figure 7. Comparison between observed and model simulated drawdown in the two well intervals of FSE9.

CONCLUSION

From a fluid flow perspective, the controlling features in the bedrock are the four highly transmissive fracture clusters. Representing these fracture clusters in the model requires information about their spatial extents, which requires multiple-well hydraulic tests and borehole geophysical logging. Calibration results suggest that the highly transmissive fracture clusters are three to four orders of magnitude more conductive than the surrounding bedrock with less transmissive fractures. The good matches between observed and simulated drawdowns suggest that a heterogeneous continuum model can be used to simulate fluid flow in the fractured bedrock underlying the FSE well field.

REFERENCES

Harbaugh, A.W., and McDonald, M.G., 1996, User's documentation for MODFLOW-96, an update to the U.S. Geological Survey modular finite-difference ground-water flow model: U.S. Geological Survey Open-File Report 96-485, 56 p.

Hill, M.C., 1992, A computer program (MODFLOWP) for estimating parameters of a transient, three- dimensional, ground-water flow model using nonlinear regression: U.S. Geological Survey Open-File Report 91-484, 358 p.

Hsieh, P.A., and Shapiro, A.M, 1996, Hydraulic characteristics of fractured bedrock underlying the FSE well field at the Mirror Lake Site, Grafton County, New Hampshire, in Morganwalp, D.W., and Aronson, D.A., eds., U.S. Geological Survey Toxic Substances Hydrology Program—Proceedings of the technical meeting, Colorado Springs, Colorado, September 20-24, 1993: U.S. Geological Survey Water-Resources Investigations Report 94-4015, p. 127-130.

AUTHOR INFORMATION

Paul A. Hsieh, U.S. Geological Survey, Menlo Park, California (pahsieh@usgs.gov)

Allen M. Shapiro, U.S. Geological Survey, Reston, Virginia (ashapiro@usgs.gov)

Claire R. Tiedeman, U.S. Geological Survey, Menlo Park California (tiedeman@usgs.gov)

Analysis of an Open-Hole Aquifer Test in Fractured Crystalline Rock

by Claire R. Tiedeman and Paul A. Hsieh

ABSTRACT

A multiple-well open-hole aquifer test was conducted in fractured crystalline rock underlying the FSE well field at the Mirror Lake, New Hampshire fractured-rock hydrology research site. The relation of measured drawdown to distance from the pumped well is markedly different from that theoretically observed during radial flow in a homogeneous aquifer. The open-hole aquifer test is analyzed using a numerical ground-water flow model with the rock represented as vertically uniform and heterogeneity simulated by two irregularly-shaped high-transmissivity zones. Model calibration results in a very good match of simulated and measured drawdowns. In addition, the transmissivity estimates for both the highly-permeable and less-permeable parts of the rock are very similar to those estimated by analysis of an aquifer test conducted with high-permeability fracture clusters isolated by packers in all wells. This suggests that the open-hole test does provide useful information about the hydraulic properties of the rock. However, the heterogeneity structure of the rock inferred from analysis of the open-hole test is overly simplified, because it ignores vertical variation in rock properties. Application of leaky-aquifer and double-porosity analytical models indicates that while a fair match to some subsets of the FSE wells can be produced, neither model can simultaneously reproduce drawdowns at all wells, because each assumes that the hydraulic properties of the pumped aquifer are homogeneous. In the FSE well field, highly-transmissive fracture clusters equalize drawdowns in wells that intersect the same clusters, while the less-transmissive part of the rock has a predominant effect on the magnitude of drawdowns because the fracture clusters are finite in extent. Attempts to simultaneously reproduce drawdowns at all wells with analytical models fail because the hydraulic parameters of these models cannot be manipulated so that they mimic the distinct effects that the high- and low-transmissivity parts of the rock have on drawdown in the FSE well field.

INTRODUCTION

When performing a multiple-well aquifer test to estimate the hydraulic properties of highly-heterogeneous fractured crystalline rock at the well-field scale, it is preferable to vertically isolate highly permeable fractures intersected by the boreholes. This can be accomplished by installing inflatable packers in boreholes that are open to permeable fractures located at different depths, or by constructing boreholes so that they are open to only one permeable fracture or group of closely-spaced permeable fractures. When the fractures are vertically isolated by one of these methods, the boreholes are prevented from acting as short-circuits between the permeable fractures, and the pumping-induced flow system within the fractured rock more closely resembles the flow system that would arise in the absence of the boreholes. Analysis of drawdown in the isolated fractures can then reveal the hydraulic connection between permeable fractures encountered in the boreholes. However, because of time or financial constraints, isolating the permeable fractures might not be feasible, and an open-hole aquifer test might be performed using boreholes that are intersected by many permeable fractures.

In the FSE well field at the Mirror Lake, New Hampshire, fractured-rock hydrology research site, multiple-well aquifer tests have been performed both with and without inflatable packers installed in boreholes that are intersected by permeable fractures at different depths. Hsieh and others (1999) analyzed the multiple-well aquifer test in which borehole intervals were isolated by packers (hereaf-

ter referred to as the 'packed-off aquifer test') using a three-dimensional numerical ground-water flow model to estimate locations of highly transmissive fracture clusters and hydraulic properties of the rock. In this paper, we analyze the multiple-well aquifer test in which inflatable packers were not installed in any of the wells (hereafter referred to as the 'open-hole aquifer test'). The goals of this work are to (1) demonstrate the necessity of explicitly representing heterogeneities in the hydraulic properties of the rock when analyzing the open-hole aquifer test, (2) compare hydraulic properties estimated by analysis of the open-hole test with those estimated by analysis of the packed-off aquifer test, and (3) show why analytical models cannot simultaneously match open-hole drawdown data from all FSE wells.

DESCRIPTION OF FSE WELL FIELD AND OPEN-HOLE AQUIFER TEST

The U.S. Geological Survey has been investigating ground-water flow at the Mirror Lake, New Hampshire, research site since the late 1970's (Winter, 1984; Hsieh and others, 1993; Shapiro and Hsieh, 1996). At the FSE well field, glacial till and sand deposits that are approximately 15 to 20 m (meters) thick overlie fractured crystalline rock consisting of schist that is extensively intruded by granite and pegmatite. Exposed rocks on roadcuts and analysis of drill cuttings and video images from boreholes indicate that rock type at the Mirror Lake site is highly variable over distances of a few meters. The 120 m by 80 m FSE well field contains 13 wells drilled to depths of 61 to 229 m (fig. 1). Eight of these wells, including FSE6, are 75 to 85 m deep. During well construction, steel casing was installed to a depth of 3 m below the bedrock surface, to isolate the overlying glacial deposits from the rock borehole.

In August 1996, an open-hole aquifer test was conducted in the FSE well field. Ground water was withdrawn from well FSE6 (fig. 1) at a steady pumping rate of 10.8 liters per minute for seven days. Water levels in the 13 open bedrock wells were recorded by pressure transducers at time intervals ranging from 5 seconds at early time to 5 minutes at late time. Water levels in the wells and in piezometers completed in the glacial deposits near FSE6 also were measured periodically with an

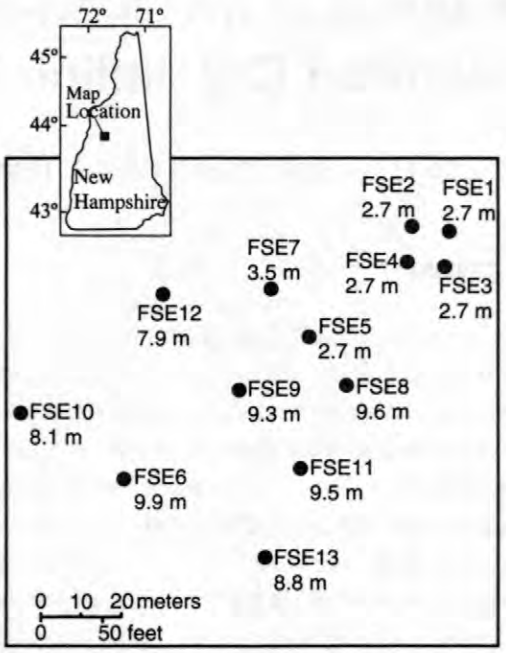

Figure 1. Location of wells in the FSE well field, showing well identifier and late-time drawdown measured during the open-hole aquifer test.

electric tape. The responses in the 13 bedrock wells (fig. 2) clearly show that drawdowns in the FSE well field are markedly different from those theoretically observed during radial flow in a homogeneous aquifer. For example, drawdowns are identical in wells FSE1, 2, 3, 4, and 5, although these wells lie at distances of 58 to 101 m from FSE6. Drawdowns are distinctly different in FSE5, 7, and 8, although these wells each lie about 60 m from FSE6. The data also suggest that drawdown is not strongly controlled by the direction of an observation well from the pumped well. For example, drawdown is similar in FSE8, 9, 11, and 13 but these wells lie at widely varying directions from FSE6 (fig. 1).

ANALYSIS OF OPEN-HOLE TEST DATA BY A NUMERICAL FLOW MODEL

Because open-hole drawdown in the FSE well field differs substantially from that expected in a homogeneous aquifer, analytical models that assume the hydraulic properties of the pumped aquifer are homogeneous cannot simultaneously reproduce drawdown measured at all wells during the open-hole aquifer test. Application of such analytical models is explored in more detail in the latter

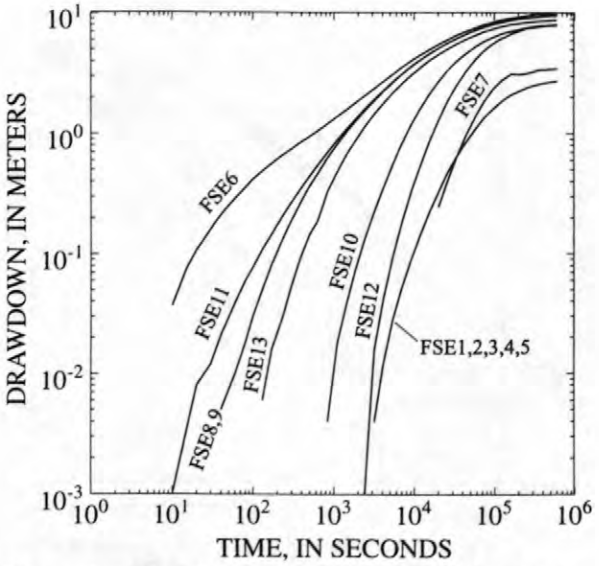

Figure 2. Drawdown measured during the open-hole aquifer test conducted in the FSE well field in August 1996.

part of this paper. Simultaneously matching the drawdowns measured at all wells during the open-hole aquifer test requires the use of a numerical model in which heterogeneity in subsurface properties is explicitly represented. A numerical ground-water flow model of the FSE well field is constructed using the U.S. Geological Survey finite-difference code MODFLOW (Harbaugh and McDonald, 1996).

The MODFLOW model contains two layers and the 340 m by 270 m domain is discretized into 42 rows and 34 columns (fig. 3). The FSE well field lies in the central part of the model domain, and no-flow boundaries on all model sides are placed far enough from the well field that they do not affect drawdown in the well field. To realistically simulate drawdown in the pumped well, the area of the square cell representing FSE6 is equal to that of the 0.15-m-diameter well. Cell size increases with distance from FSE6. The maximum cell size within the FSE well field is 7.6 m by 7.6 m. The top model layer represents the glacial deposits. A zero-drawdown boundary condition is specified throughout this layer because less than 0.1 m drawdown was measured at the water table near FSE6 during the open-hole aquifer test. With this boundary condition, the glacial deposits are simulated solely as a source of water for the underlying pumped aquifer, and ground-water flow through these deposits is not explicitly simulated. The 50-m-thick bottom layer

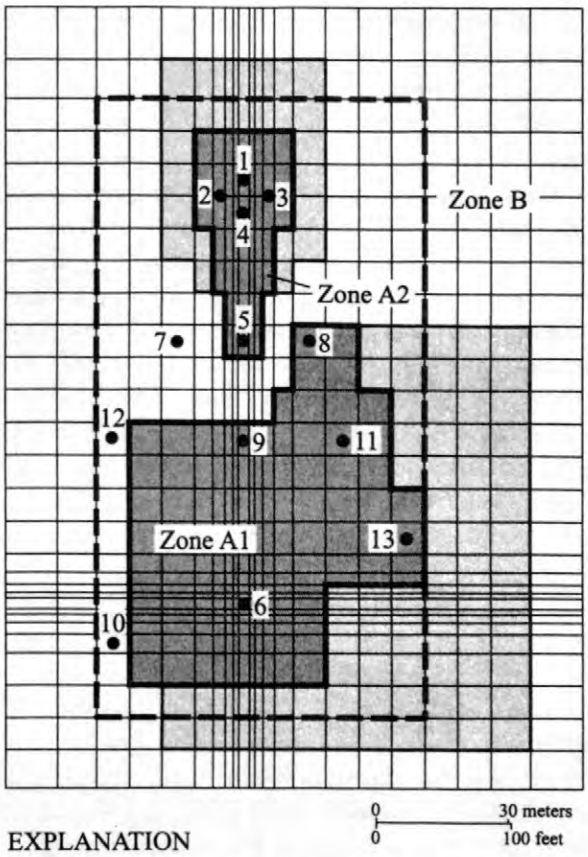

Figure 3. Subregion of the finite-difference model grid (rows 4-38 and columns 4-31) showing representation of heterogeneity in the bottom layer. Model boundaries are approximately 70 m from all sides of the subregion shown here. Rows 24-30 and columns 13-19 are not explicitly shown.

represents the fractured crystalline rock. A single model layer is used to represent the rock because the nature of the open-hole test did not permit measurement of vertical variation in hydraulic head or inference of vertical variation in rock properties. A no-flow boundary is specified at the bottom of the model. Drawdown is computed at 80 time steps. The time step length increases geometrically during the simulation so that there are approximately the same number of time steps in each logarithmic cycle of time.

Heterogeneity in rock hydraulic properties is simulated in a fairly simple manner by two irregularly-shaped high-transmissivity zones (zones A1 and A2) that represent clusters of highly permeable fractures that are well connected, hydraulically (fig. 3). The transmissivity and storativity within each of these zones are uniform, and the values of these hydraulic properties are the same for each of the two zones. The remainder of the rock (zone B) has uniform transmissivity and represents the less-permeable part of the rock that surrounds the high-transmissivity zones. The geometry of each of the high-transmissivity zones is delineated on the basis of drawdowns measured during the open-hole test (figs. 1, 2). Zone A1 (fig. 3) includes wells FSE6, 8, 9, 11, and 13. Drawdown is similar in the four observation wells in this group. Drawdown in FSE6 is somewhat greater because there is a hydraulic gradient toward the pumped well. Zone A1 extends towards FSE10 and 12, but does not include these wells because early-time drawdown occurs significantly later and late-time drawdown is smaller, compared to drawdown at FSE8, 9, 11, and 13. Zone A2 (fig. 3) includes wells FSE1, 2, 3, 4, and 5. The responses at these wells are identical throughout the open-hole test but are significantly smaller than drawdown at wells in zone A1 (figs. 1, 2).

Numerical model parameters include the vertical conductance that controls flow between the glacial deposits and bedrock (C_V), defined as the vertical hydraulic conductivity of the interface between the glacial deposits and bedrock divided by the effective thickness of the interface, the transmissivity (T_A) and storativity (S_A) of Zones A1 and A2, and the transmissivity (T_B) and storativity (S_B) of the surrounding rock (fig. 3). These five hydraulic parameters are estimated by a nonlinear least-squares regression procedure (Hill, 1992). Approximately nine measured drawdowns per log cycle of time at each of the 13 FSE wells are used as observations, resulting in a total of 354 drawdown measurements used in the regression procedure.

The fit to the drawdown data with the calibrated numerical model is very good at all wells except FSE12 (fig. 4). At early time, the match at FSE12 is poor. With the representation of heterogeneity restricted to two zones with uniform hydraulic properties, then either the early-time or late-time match at FSE12 is poor. For example, if the configuration of zones shown in figure 3 is changed so that zone A1 does not lie as close to FSE12, then the

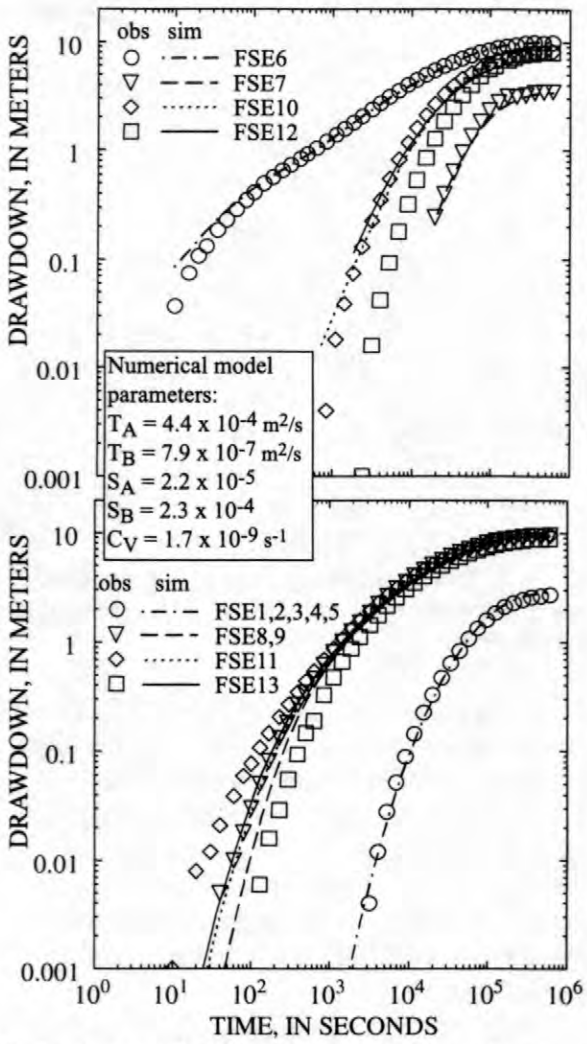

Figure 4. Comparison of measured drawdown with drawdown simulated by the numerical groundwater flow model of the FSE well field. (Abbreviations: obs, observed; sim, simulated)

fit to the early-time data will improve, but simulated late-time drawdown will be too small. Increasing the storativity within zone A1 near FSE12 delays the simulated early-time response, and improves the overall fit. However, one goal of this work is to show that a numerical model with hydraulic properties of the rock characterized by a simple configuration of two zones that represent the highly transmissive fracture clusters can produce a significantly better fit to the data compared to that produced by analytical models that assume the hydraulic properties of the pumped aquifer are homogeneous. Adjusting the numerical-model hydraulic properties in the vicinity of each well can result in an improved fit of simulated and observed drawdowns, but the drawdown data provide much

less information about such small-scale heterogeneity than about the large-scale heterogeneities that are represented by zones A1 and A2 in the numerical model. Furthermore, addition of small-scale heterogeneity increases the number of hydraulic parameters, which generally decreases the confidence in the identified parameters.

Although drawdown computed by the numerical model with heterogeneity represented by high-transmissivity zones A1 and A2 results in a good fit to the data, the model is not unique. The nonuniqueness is evident when the model is re-calibrated with either the size of zone A1 or A2 approximately doubled (fig. 3). These new calibrations produce simulated drawdowns that are very similar to those shown in figure 4. There is no significant change in the sum of squared differences between simulated and observed drawdowns, compared to that of the original calibration. The drawdown data do provide some constraints on the configuration of the zones, however. The fit to the data at wells FSE1, 2, 3, 4, and 5 would significantly worsen if zones A1 and A2 were joined in the small area of the model in between these two zones. The fit at FSE7 would likely worsen if either zone A1 or zone A2 were enlarged to include this well, and the fit at FSE10 and 12 would deteriorate if zone A1 were enlarged to include these wells.

The numerical model is modified for the purpose of calculating the effective hydraulic conductivity of the rock underlying the FSE well field. Several rows and columns of the original model domain are removed so that the modified 137 m by 76 m model domain is just large enough to enclose the 13 FSE wells (fig. 3). Parameter values and the configuration of zones A1 and A2 are the same as in the original model, but there are no pumping wells. Constant hydraulic heads of 0 and 137 m are imposed in the rock at, respectively, the first and the last rows of the model. The constant-head boundaries are located in this manner so that simulated ground-water flow paths sample the maximum amount of heterogeneity. The effective hydraulic conductivity is calculated from Darcy's law as

$$K_{eff} = \frac{Q}{A(dh/dl)} \qquad (1)$$

where

Q is the simulated steady-state discharge through the entire model (L^3/T),

A is the cross-sectional area of the model (L^2), and

dh/dl is the horizontal hydraulic gradient across the model domain (L/L).

The computed value of K_{eff} is $2x10^{-7}$ m/s (meters per second). This value is dependent on the particular size chosen for the modified model domain, and should be viewed as an order-of-magnitude estimate.

Comparison with results from analysis of packed-off aquifer test

An important issue motivating our implementation of the open-hole aquifer test in the FSE well field is whether such a test in sparsely fractured crystalline rock can provide useful information about the hydraulic properties of the flow system. This question can best be answered by comparing the hydraulic properties and heterogeneity structure estimated for the numerical model used to analyze the open-hole test (hereafter called the 2-D numerical model) with those estimated for the numerical model used to analyze the packed-off aquifer test in the FSE well field (hereafter called the 3-D numerical model) as reported by Hsieh and others (1999). This comparison indicates that the transmissivities estimated from analyses of the two different tests are very similar, especially when viewed in the context of the several-order-of-magnitude variation in transmissivity measured during single-well injection tests at the Mirror Lake site.

The transmissivity of the less-permeable part of the rock estimated from the open-hole test (T_B= $7.9x10^{-7}$ m^2/s [meters squared per second]) is about 12 percent smaller than that estimated from the packed-off test ($9.0x10^{-7}$ m^2/s). The transmissivity of the highly permeable part of the rock estimated from the open-hole test (T_A=$4.4x10^{-4}$ m^2/s) is about 27 percent smaller than that inferred from analysis of the packed-off test, which showed that simulated drawdowns are insensitive to the transmissivity value as long as it is equal to or larger than about $6x10^{-4}$ m^2/s. However, the part of the rock containing more permeable, well-connected fractures is represented as 50 m thick in the 2-D numerical model because information about the vertical variation in hydraulic properties was not obtained during

the open-hole test. Thus, the estimated hydraulic conductivity of this part of the rock ($8.8x10^{-6}$ m/s) is more than an order of magnitude smaller than that obtained by analysis of the packed-off tests (about $2x10^{-4}$ m/s or larger) (Hsieh and others, 1999) because in the 3-D numerical model, the total thickness of the highly permeable fracture clusters in the FSE well field is estimated to be only 3 m. The effective hydraulic conductivity of the rock calculated from analysis of the open-hole test ($2x10^{-7}$ m/s) is about one-half of that calculated from analysis of the packed-off test ($5x10^{-7}$ m/s), which is a small difference considering the large range of rock transmissivities measured in single-well hydraulic tests. The estimate of the vertical conductance controlling flow between the glacial deposits and bedrock is $1.7x10^{-9}$ s^{-1}, which is essentially the same as the $1.8x10^{-9}$ s^{-1} estimate from analysis of the packed-off test.

A major conclusion that can be drawn from comparison of analyses of the open-hole and packed-off aquifer tests is that the open-hole test does provide useful information about the hydraulic properties of the rock. It is promising that similar transmissivity estimates are obtained among the two analyses for both the highly permeable and less permeable parts of the rock. The highly permeable part of the rock is assumed to be 50 m thick in the 2-D numerical model, whereas analysis of the packed-off aquifer test together with other hydraulic and geophysical data from the FSE well field suggests that in the horizontal position of both zones A1 and A2 (fig. 3), there are two discrete 1.5-m-thick highly transmissive fracture clusters at different depths (Hsieh and others, 1999). If hydraulic properties estimated from the open-hole test are used in predictions of chemical transport in the well field, then representing the permeable part of the rock as 50 m thick would result in considerable errors in predicted transport times and paths. However, if borehole flow were logged during an open-hole aquifer test, information obtained about the direction and relative quantity of flow within different parts of the FSE wells might enable inferences about which fractures or clusters of fractures are the major conduits for flow between boreholes. These observations could then be used to constrain the locations and thicknesses of highly transmissive fracture clusters in three-dimensional models that test hypotheses about the heterogeneity structure of the rock, and the total transmissivity of the highly permeable parts of the rock could be set equal to the transmissivity estimate from analysis of the open-hole test. The heterogeneity structure of the rock in such three-dimensional models would not be as accurate as if a packed-off aquifer test were performed to delineate the highly transmissive, hydraulically-connected fracture clusters, but would be a great improvement over models in which the rock is assumed to have vertically uniform hydraulic properties.

Because the effective hydraulic conductivity of the rock that is estimated from analysis of the open-hole test is similar to that from analysis of the packed-off test, this hydraulic property estimate from the open-hole test also is useful. An estimate of this effective hydraulic conductivity can be used primarily in simulations of flow at length scales larger than the size of the well field, provided that the heterogeneity structure of the rock at these larger scales is similar to that in the well field. In numerical model simulations of ground-water flow over a 4 km (kilometer) by 4 km region at the Mirror Lake site, Tiedeman and others (1997, 1998) estimated the effective hydraulic conductivity of the part of this region that includes the FSE well field to be $3x10^{-7}$ m/s. The similarity of this estimate to that from both the open-hole and packed-off tests supports the usefulness of this hydraulic property estimate from well-field aquifer tests.

The similarity of the regional-scale and well-field-scale estimates of effective hydraulic conductivity suggests that the heterogeneity structure of the rock in other parts of the Mirror Lake site might be similar to that identified in the FSE well field. This inference is supported by preliminary analysis of drawdowns measured during a packed-off aquifer test at the CO well field, located about 1 km from the FSE well field. This analysis suggests that the first-order heterogeneity structure in the CO well field also is characterized by highly transmissive fracture clusters separated by less transmissive rock. Thus, there is some indication that analysis of an open-hole aquifer test in fractured rock elsewhere at the Mirror Lake site might yield useful transmissivity estimates of the rock. It is difficult to further generalize the results presented here to application of open-hole tests at other fractured-rock settings. However, for fractured crystalline rock settings with a heterogeneity structure similar to that at Mirror Lake, results presented here suggest that a multiple-well open-hole aquifer test

might be a useful means of obtaining limited information about rock hydraulic properties, if it is infeasible to perform a test in which transmissive fractures or fracture clusters are vertically isolated from one another.

ANALYSIS OF OPEN-HOLE TEST DATA BY ANALYTICAL MODELS

Because the discrete highly-transmissive fracture clusters that are intersected by the FSE boreholes strongly influence the drawdown distribution in the well field, analytical models that simulate radial flow to a well in a homogeneous pumped aquifer cannot match the measured drawdowns at all the FSE wells simultaneously. Application of such analytical models helps demonstrate the necessity of explicitly representing heterogeneities in hydraulic properties when analyzing the open-hole test. We consider models of two simple conceptual subsurface settings, each of which might be considered a reasonable potential representation of conditions in the FSE well field. These analytical models simulate drawdown in response to constant discharge from a well in (1) a homogeneous isotropic leaky aquifer overlain by a storative semiconfining layer (Hantush, 1960; Moench, 1985), and (2) an isotropic confined double-porosity aquifer (Boulton and Streltsova, 1977; Moench, 1984).

Leaky-Aquifer Analytical Model

The fractured crystalline rock underlying the FSE well field behaves like a leaky aquifer in that it is overlain by glacial deposits containing the water table. Toward the end of the test, drawdowns were nearly constant in all wells (fig. 2), which is characteristic of the late-time response in leaky aquifers. In the leaky-aquifer analytical model, the hydraulic conductivity of the pumped aquifer is assumed to be homogeneous and isotropic, and flow to the fully penetrating well is assumed to be strictly horizontal. The pumped aquifer is bounded above by a storative semiconfining layer through which ground water flows vertically from an overlying aquifer to the pumped aquifer, and is underlain by an impermeable boundary. Hydraulic parameters include the transmissivity (T) and storativity (S) of the pumped aquifer and the vertical conductance (C_v') and storativity (S′) of the overlying semiconfining layer. The vertical conductance is defined in the same manner as for the numerical model. Hantush (1960) derived a solution for early- and late-time drawdown in the pumped aquifer. Moench (1985) included the effect of well-bore storage in the pumped well and derived a solution valid for all times.

Application of the Moench (1985) solution indicates that the leaky-aquifer model cannot simultaneously reproduce drawdowns at all FSE wells. Model parameters can be adjusted to obtain an excellent match to drawdowns at individual wells, but a different set of model parameters must generally be used for each match. Thus, this approach is inconsistent with the underlying model assumption that the pumped aquifer is homogeneous. A fair match can be achieved to drawdown at some subsets of the FSE wells, but the resulting fit at other wells is poor. For example, trial-and-error adjustment of model parameters yields a fair match to observed drawdowns throughout the test at FSE 1, 2, 3, and 4 and for late-time at FSE6, but the model parameter values that produce this fit yield a very poor match to observed drawdown at wells FSE8 through 13 (fig. 5).

Inferences from the numerical model analyses presented above and by Hsieh and others (1999) about the positions of highly-transmissive fracture clusters in the FSE well field can help explain the limitations of using the analytical model to analyze the open-hole aquifer test. Drawdown in the well field is more strongly a function of which highly-transmissive fracture clusters a well intersects and of the configuration of these clusters, than it is a function of the distance from the pumped well. Measured drawdowns at FSE6, 8, 9, 11, and 13 are similar (fig. 2) because each of these wells intersects at least one of two highly-transmissive, hydraulically-connected, sub-horizontal fracture clusters (Hsieh and others, 1999). During the open-hole test, these two clusters (represented by zone A1 in the 2-D numerical model) are hydraulically connected by the open boreholes. Observed drawdowns at FSE1, 2, 3, 4, and 5 are identical for similar reasons. However, because the transmissive fracture clusters are finite in extent, the magnitude of drawdown in wells that intersect fracture clusters also is strongly influenced by the hydraulic conductivity of the less transmissive part of the rock.

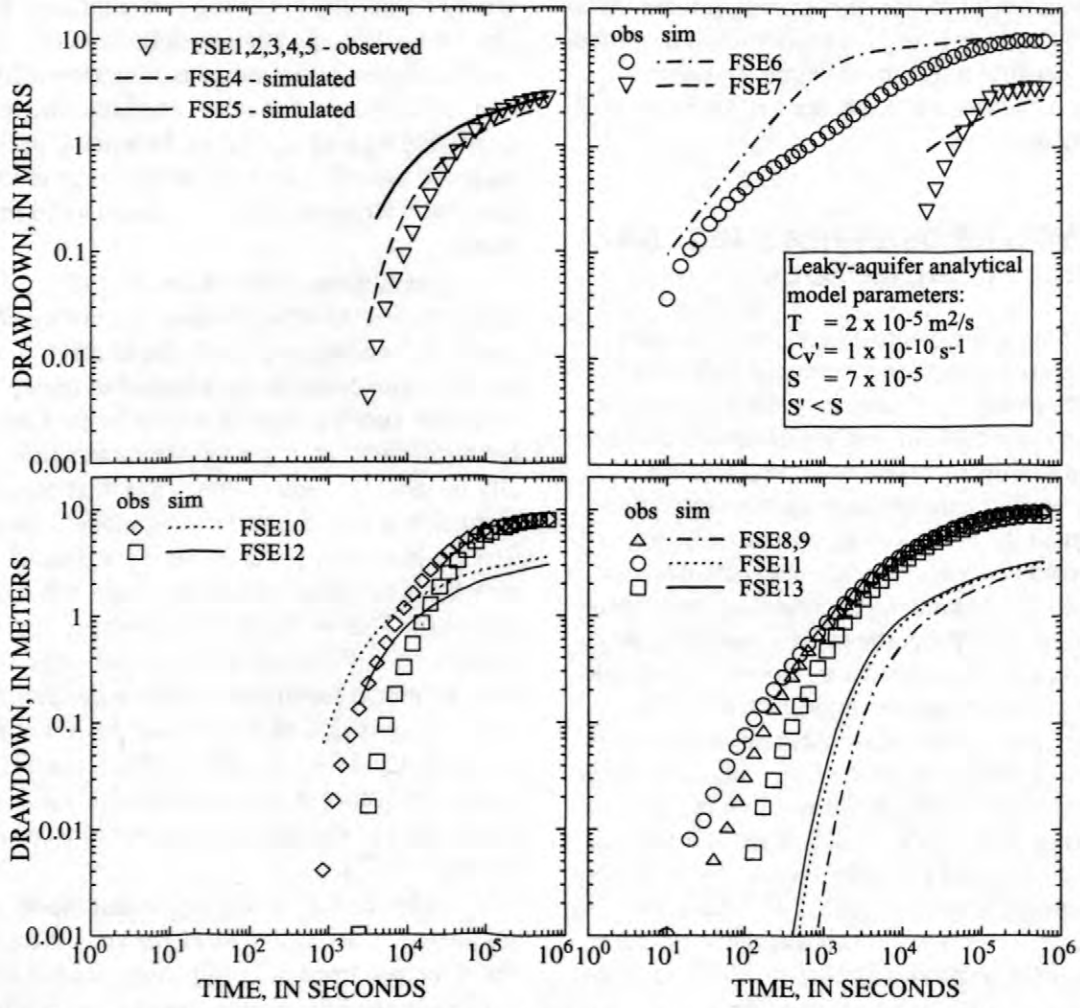

Figure 5. Comparison of measured drawdown with drawdown simulated by the leaky-aquifer analytical model, with model parameters adjusted by trial and error to achieve a match at wells FSE1, 2, 3, 4, and 6. Simulated drawdowns at FSE1, 2, and 3 are very similar to that shown for FSE4.

The hydraulic conductivity of the pumped aquifer in the leaky-aquifer model simulation that produces a fair match to drawdowns at FSE1, 2, 3, 4, and 6 (fig. 5) is equal to about 5 x 10^{-7} m/s (T divided by the assumed 50-m thickness of the pumped aquifer). This hydraulic conductivity value is similar to K_{eff}, primarily because there is a region of the less transmissive part of the rock as well as regions of highly transmissive fracture clusters between the group of wells FSE1 through 4 and the pumped well (fig. 3). Observed drawdown can be simultaneously matched at FSE1 through 4 because each of these wells lies at a comparable distance (90 to 100 m) from FSE6 and thus simulated drawdown is similar at these locations. In contrast, the fit is somewhat worse at FSE5 because although observed drawdown is identical to that in FSE1 through 4, simulated drawdown is greater in FSE5 (fig. 5) because it is 30 m closer to FSE6. At FSE8, 9, 11, and 13, which are 36 to 60 m from the pumped well, observed drawdowns are greatly underpredicted (fig. 5) because the presence of the transmissive fracture clusters causes drawdown at these wells to be nearly equal to that at FSE6. In fact, there is no unique set of parameter values that can simultaneously produce a good match to FSE6, 8, 9, 11, and 13. As the value of T in the leaky-aquifer model increases, simulated drawdowns in FSE8, 9, 11, and 13 become more similar to those in FSE6, but simulated drawdowns also become much smaller than the observed drawdowns, even if leakance from the overlying aquifer is reduced by

specifying a small value of C_v'. Although observed drawdowns in FSE8, 9, 11, and 13 are similar to that in FSE6 because of the presence of the highly transmissive fracture clusters, the magnitude of the drawdowns is controlled by the hydraulic conductivity of the less transmissive part of the rock. No combination of hydraulic parameters in the leaky aquifer model can mimic the effect that both these parts of the rock have on drawdowns at observation wells that intersect the same transmissive fracture cluster as the pumped well.

The fit of the leaky-aquifer model shown in figure 5 is obtained by specifying an unrealistically small value of C_v' ($1x10^{-10}$ s^{-1}), compared to the estimate of C_v ($2x10^{-9}$ s^{-1}) in both the 2-D and 3-D numerical model analyses. In the leaky-aquifer model, decreasing C_v' reduces leakance and results in larger simulated drawdowns at late time. An unrealistically small value of C_v' is needed to simultaneously obtain a match to FSE1, 2, 3, 4, and 6 because the true distance between FSE1, 2, 3, and 4 and the pumped well is in effect shortened by the presence of the highly transmissive fracture clusters (fig. 3). With the same value of T shown in figure 5 and a value of C_v' equal to that estimated by numerical model analysis of the aquifer test, simulated late-time drawdowns 90 to 100 m from the pumped well would be much too large.

Double-Porosity Analytical Model

In the double-porosity analytical model, the pumped aquifer is confined and assumed to be composed of a system of fractures with high hydraulic conductivity and low specific storage that overlaps and interacts with a system of matrix blocks characterized by low hydraulic conductivity and high specific storage. Transient flow occurs from the matrix blocks to the fractures and within the fracture system, but water does not flow from one matrix block to another. The hydraulic conductivity of the aquifer as a whole can be considered homogeneous and isotropic because of the overlapping, continuous nature of the fracture-matrix system. Boulton and Streltsova (1977) derived the first analytical solution for drawdown in response to constant discharge from a well in a double-porosity aquifer with transient block-to-fracture flow. Moench (1985) modified the solution to include the effects of well bore storage and well bore skin in the pumped well and the effects of a fracture skin at the fracture-block interface.

Because of the fractured nature of the crystalline rock in the FSE well field, the double-porosity analytical model is a logical conceptual model of the flow system. However, attempts to reproduce observed drawdown in the FSE well field with the double-porosity analytical model produces results that are similar to those obtained by application of the leaky-aquifer analytical model. As in the leaky-aquifer analytical model, simulated drawdown in the double-porosity model decreases with increasing radial distance from the pumped well because the hydraulic properties of the fracture-matrix system are homogeneous and isotropic. Consequently, the double-porosity analytical model with a unique set of hydraulic parameters cannot simultaneously reproduce drawdowns throughout the FSE well field, and has limited success at matching subsets of the wells. The match to the subset of wells FSE1, 2, 3, 4, and 6 looks much the same as that for the leaky-aquifer model (fig. 5), except that in the double-porosity model, late-time drawdown continues to increase with time. As in the application of the leaky-aquifer model, it is largely the effect of the discrete highly transmissive fracture clusters that limits the ability of the double-porosity model to reproduce observed drawdowns in the FSE well field.

The leaky-aquifer and double-porosity analytical models differ from the Theis solution for flow to a well in a homogeneous isotropic confined aquifer, in which drawdown at a given time and distance is a function only of the transmissivity and storativity of the pumped aquifer, in that there is an additional flow-system compartment that is characterized by separate hydraulic parameters. However, although these two analytical models might appear to be more reasonable conceptual models than the Theis model for simulating flow to a well in the FSE well field, the features of these models that set them apart from the simpler Theis solution do not significantly improve their ability to simultaneously match the open-hole aquifer test drawdown data from all wells, with the exception of the mechanism of late-time leakance from an overlying aquifer. The fundamental problem with applying these analytical models to reproduce the observed drawdowns at all FSE wells is that they assume that the pumped aquifer has homogeneous and isotropic hydraulic properties. With this assumption, these

models fail to simultaneously match even the major features of the drawdown curves for all FSE wells, such as the position of the early-time drawdown data with respect to the horizontal axis and the position of the late-time data with respect to the vertical axis.

SUMMARY

A multiple-well open-hole aquifer test was conducted in fractured crystalline rock underlying the FSE well field at Mirror Lake, New Hampshire. Goals of analyzing the test included demonstrating the necessity of explicitly representing rock heterogeneities in the analysis, comparing estimated hydraulic properties with those estimated by analysis of a packed-off aquifer test, and illustrating the limitations of the use of analytical models for analyzing the test. During the open-hole aquifer test, ground water was withdrawn from FSE6 for seven days, and drawdown was measured in the 13 open FSE wells. The drawdown response clearly shows that in the FSE well field, the relation of drawdown to distance from the pumped well is markedly different from that theoretically observed during radial flow in a homogeneous aquifer.

The open-hole aquifer test is analyzed using a numerical ground-water flow model in which the rock is represented as vertically uniform. Heterogeneity in hydraulic properties is simulated by two irregularly-shaped high-transmissivity zones that are delineated on the basis of the measured drawdowns. Model calibration results in a very good match to measured drawdowns but indicates that the configuration of high-transmissivity zones that produces this fit is not unique. Model hydraulic-property estimates compare favorably to those estimated by analysis of a packed-off aquifer test in the FSE well field (Hsieh and others, 1999), suggesting that the open-hole test does provide useful information about the hydraulic properties of the rock. The transmissivity estimates for both the highly-permeable and less-permeable parts of the rock are very similar to those estimated by analysis of the packed-off test, as are the estimates of the effective hydraulic conductivity of the block of rock containing the FSE well field. However, the heterogeneity structure of the rock inferred from analysis of the open-hole test is overly simplified, because information about the vertical variation in rock properties was not obtained during the test.

Results of the numerical-model analyses of the open-hole and packed-off aquifer tests help explain the limitations of using analytical models for analyzing the open-hole test. Application of the leaky-aquifer and double-porosity analytical models indicates that, while a fair match to some subsets of the FSE well can be produced, neither model can simultaneously reproduce drawdowns at all FSE wells because each assumes that the hydraulic properties of the pumped aquifer are homogeneous. In the FSE well field, highly-transmissive fracture clusters equalize drawdowns in wells that intersect the same clusters, while the less-transmissive part of the rock has a strong control on the magnitude of drawdown in all wells because the fracture clusters are finite in extent. Attempts to simultaneously match drawdowns at all wells fail because the hydraulic parameters of the analytical models cannot be manipulated so that the models mimic the distinct effects that the high- and low-transmissivity parts of the rock have on drawdowns in the FSE well field.

REFERENCES

Boulton, N.S., and Streltsova, T.D., 1977, Unsteady flow to a pumped well in a fissured water-bearing formation: Journal of Hydrology, v. 35, p. 257-270.

Hantush, M.S., 1960, Modification of the theory of leaky aquifers: Journal of Geophysical Research, v. 65, no. 11, p. 3713-3725.

Harbaugh, A.W., and McDonald, M.G., 1996, User's documentation for MODFLOW-96, an update to the U.S. Geological Survey modular finite-difference ground-water flow model: U.S. Geological Survey Open-File Report 96-485, 56 p.

Hill, M.C., 1992, A computer program (MODFLOWP) for estimating parameters of a transient, three-dimensional, ground-water flow model using nonlinear regression: U.S. Geological Survey Open-File Report 91-484, 358 p.

Hsieh, P.A., Shapiro, A.M, and Tiedeman, C.R., 1999, Computer simulation of fluid flow in fractured rocks at the Mirror Lake FSE well field: this volume.

Hsieh, P. A., Shapiro, A. M., Barton, C. C., Haeni, F. P., Johnson, C. D., Martin, C. W., Paillet, F. L., Winter, T. C., and Wright, D. L., 1993, Methods of characterizing fluid movement and chemical transport in fractured rock: in Chaney, J. T., and Hepburn, C., (eds.) Field Trip Guidebook for Northeastern United States, Geological Society of America, Annual Meeting, October 25-28, 1993, Boston, Massachusetts, v. 2, chap. R, p. R1-R23.

Moench, A.F., 1984, Double-porosity models for a fissured groundwater reservoir with fracture skin: Water Resources Research, v. 20, no. 7, p. 831-846.

Moench, A.F., 1985, Transient flow to a large-diameter well in an aquifer with storative semi-confining layers: Water Resources Research, v. 21, no. 8, p. 1121-1131.

Shapiro, A. M., and Hsieh, P.A., 1996, Overview of research on use of hydrologic, geophysical, and geochemical methods to characterize flow and chemical transport in fractured rock at the Mirror Lake site, New Hampshire: p. 71-80 in Morganwalp, D.W. and Aronson, D.A., (eds.), U.S. Geological Survey Toxic Substances Hydrology Program--Proceedings of the Technical Meeting, Colorado Springs, Colorado, September 20-24, 1993: U.S. Geological Survey Water-Resources Investigations Report 94-4015.

Tiedeman, C.R., Goode, D.J., and Hsieh, P.A., 1997, Numerical simulation of ground-water flow through glacial deposits and crystalline bedrock in the Mirror Lake area, Grafton County, New Hampshire: U.S.Geological Survey Professional Paper 1572, 50 p.

Tiedeman, C.R., Goode, D.J., and Hsieh, P.A., 1998, Characterizing a ground water basin in a New England mountain and valley terrain: Ground Water, v. 36, no. 4, p. 611-620.

Winter, T. C., 1984, Geohydrologic setting of Mirror Lake, West Thornton, New Hampshire: U.S. Geological Survey Water-Resources Investigations Report 84-4266, 61 p.

AUTHOR INFORMATION

Claire R. Tiedeman (tiedeman@usgs.gov) and Paul A. Hsieh (pahsieh@usgs.gov), U.S. Geological Survey, Menlo Park, California.

Effects of Lithology and Fracture Characteristics on Hydraulic Properties in Crystalline Rock: Mirror Lake Research Site, Grafton County, New Hampshire

By Carole D. Johnson

ABSTRACT

A combination of subsurface borehole imaging data and drilling logs were used to characterize the fractures and lithology in 40 bedrock wells at the fractured-rock research site in the Mirror Lake area in Grafton County, New Hampshire. The purpose of the research was to determine whether subsurface lithology and fractures have an effect on the hydraulic conductivity of the crystalline-rock aquifer in the Mirror Lake area. The distribution of fractures and lithology was quantified with respect to depth, altitude, topographic setting, and spatial distribution. The density of fracturing was described and comparisons were made between lithology, fracture characteristics, and hydraulic-conductivity measurements. Fracturing was found to be related to lithology, depth, and topographic setting. No clear correlation was established between hydraulic conductivity and fracture properties including alteration, oxidation, aperture, orientation, and density.

INTRODUCTION

The problem of investigation and remediation of contamination in fractured crystalline rock has been compounded by a lack of understanding of how to conceptualize and simulate fluid flow and chemical transport in these aquifers. In order to remediate these aquifers, however, the extent and location of contamination and the potential pathways for flow and transport must be understood. In fractured-rock systems, this requires determining the dominant features and processes that control flow. In order to better understand these aquifers, the U.S. Geological Survey established a fractured-rock research site in a pristine area in the White Mountains near Mirror Lake in Grafton County, New Hampshire. The site serves as a field-scale laboratory for developing and testing tools and methods used to characterize flow and transport in crystalline rock. An overview of the research project is provided by Shapiro and Hsieh (1991).

This paper describes the results of research to determine whether subsurface lithology and fractures have an effect on hydraulic conductivity at the Mirror Lake site. The objectives of the research were (1) to characterize the subsurface lithology and fractures and the relation between them; and (2) to use this detailed information to analyze the effects of subsurface lithology and fractures on hydraulic conductivity. Results are described in more detail by Johnson and Dunstan (1998) and by Johnson (1998).

DESCRIPTION OF STUDY AREA

The bedrock at Mirror Lake is predominantly high-grade pelitic schist and gneiss that has been intruded by igneous rocks. Approximately 97 percent of the bedrock is covered with discontinuous layers of glacial deposits that vary in thickness from less than 10 m (meter) to as much as 50 m. Bedrock exposures are generally limited to the streambeds,

ridges, and to outcrops exposed by highway excavations. Detailed characterization of the lithology and fractures relies on the limited surface exposures, subsurface exploratory drilling, and geophysical techniques. Forty bedrock wells, ranging in depth from 60 to 305 m were drilled to characterize the subsurface. The investigations at Mirror Lake were designed to observe hydrogeology over multiple scales of interest, including measurements in a single well, measurements between closely spaced wells (over tens of meters) in a well field, and measurements between wells separated by hundreds of meters. This investigation focused on a set of 15 "index" wells, which included 13 deep areally-distributed wells and the deepest well in each of two well fields. Shallow and spatially clustered wells (in the two well fields) were not included in this set of index wells to avoid potential sampling bias.

GEOLOGIC SETTING

The predominant lithology of the Mirror Lake area is the Silurian Rangeley Formation (Lyons and others, 1997). The lower part of this formation is a metapelite, and the upper part is a pelitic schist of sillimanite-grade metamorphism (Lyons and others, 1997). The strike of foliation ranges from N25°E to 45°E, and it dips predominantly 60° to 67°NW and 40° to 80°SE (Barton, 1996). Folding, faulting, metamorphism, and igneous intrusions associated with the Acadian orogeny (and possibly the Alleghanian orogeny) have resulted in a complex distribution of lithology and fractures. The "pavement method" was used by Barton (1996; 1997) on a glaciated surface and four highway road cuts near Mirror Lake. Exposures on highway road cuts exhibit a high degree of lithologic and structural variability.

STUDY METHODS

Analog video images were used to describe the subsurface lithology in terms of color, mineralogy, texture, and size and shape of rock features. The fractures observed in borehole images were characterized by location, host rock, relative size, presence of mineralization, alteration, and (or) oxidation, all of which can be compared to hydraulic properties of the fractures. Techniques and equipment for borehole video imaging were described by Johnson (1996) and Johnson and Dunstan (1998). In addition, an oriented digital borehole camera was used at selected wells to determine the orientation of fractures for comparison to surficial-fracture mapping and to hydraulic conductivity estimated from fluid-injection tests conducted over discrete intervals in the wells. Borehole images consist of a magnetically oriented, digitized, 360-degree, color image of the borehole wall. Because the image is oriented, the strike and dip of the planar features can be determined directly from the image. Methods of data collection and interpretation for the digital borehole camera are provided in Johnson (1998).

CHARACTERIZATION OF LITHOLOGY IN WELLS

The lithologies were described in terms of spatial distribution in the Mirror Lake area, with respect to depth, and in terms of persistence or average length within wells. Analysis of data from the 15 index wells indicates the proportions of the lithologies vary, but collectively, the group of index wells consists of approximately equal amounts of granitoids and schist, with pegmatite and basalt comprising less than 5 percent of the rock. The lithologies change frequently (approximately every 5 to 9 m) over the length of the wells. The length of each rock unit exposed in each well was determined for all index wells. The average length of schist was 5.3 m, and the average length of granitoid units was 4.6 m. The average lengths of pegmatite and basalt units encountered in the index wells were each less than 1 m. There was no apparent correlation between rock type and depth, altitude, or topographic setting.

FRACTURE CHARACTERIZATION AND DISTRIBUTION IN WELLS

Fractures were characterized by density or intensity of fracturing, which was compared to rock type, physical parameters (depth, altitude,

and topographic setting), and hydraulic-conductivity measurements. The intensity of fracturing was computed as the distance between all fractures that were observed in the index wells – regardless of the fracture orientation, mode of fracturing, or rock type. This estimate of fracture intensity is referred to as the "interfracture spacing." The arithmetic average of the interfracture spacings was 2.1 m, which corresponds to an average fracture density of 0.47 m^{-1}. The frequency plot of the 1,244 interfracture spacings observed in the index wells was compared to theoretical frequency distributions, including exponential, power, poisson, and logarithmic functions. The best fit was obtained for the power-law function by the method of least squares, with a coefficient of determination of 0.80 (fig. 1). The fitting parameters for the power function, $y = ax^b$, were a = 20.6, b = -0.85, and x varied as the length (m) of interfracture spacing. The lower cut-off value for this function was 0.06 m. This distribution of fractures, at least in the vertical direction, suggests the fracture network comprises highly fractured zones surrounded by zones that are less fractured.

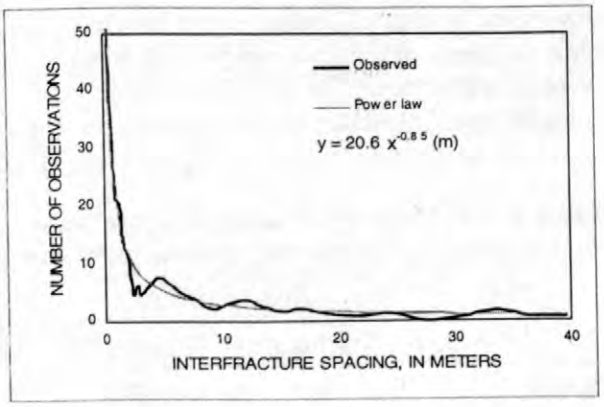

Figure 1. Comparison of observed frequency of interfracture spacing fitted to a power-law distribution.

The distribution of all fractures in the index wells with respect to depth does not follow a linear distribution. Highly fractured intervals typically occur in the top 100 m of the wells. Although less numerous, some highly fractured zones exist at depths greater than 100 m. A scatterplot of fracture density (frequency of fractures divided by the interval length for each 3-m interval) plotted as a function of depth are shown in figure 2a. In general, the plot shows there is a higher density of fractures at shallow depths than at deeper depths. Unfractured zones or minimally fractured zones, which plot on or near the x-axis, were observed at all depths. The linear-correlation coefficient between depth and fracture frequency is, therefore, low (only -0.05). To reduce the scatter in the fracture density data, the mean-fracture density was computed and plotted for each 3-m interval of depth in each well (fig.2b). The mean fracture density versus depth has a linear-correlation coefficient of -0.67. Although fractured zones can occur at depth, the probability of encountering them is lower; however, a linear correlation does not lend itself to extrapolation beyond 300 m. Alternatively, an exponential distribution, with a coefficient of determination of 0.51, could be fit to the mean-fracture density plotted as a function of depth. Although the exponential distribution had a poorer fit to the data than the linear distribution, it may be more reasonable to extrapolate the exponential distribution beyond 300 m, because the expected fracture density approaches zero, but does not equal zero or negative values.

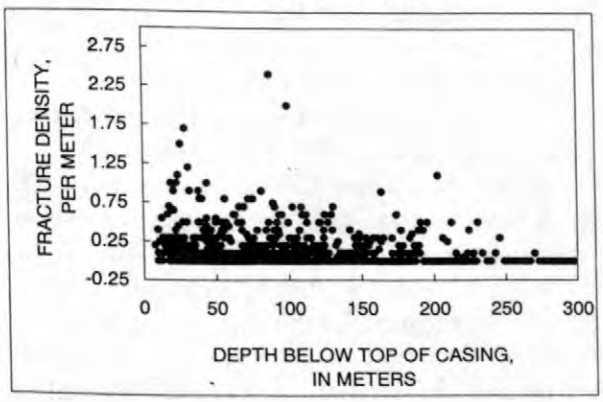

Figure 2a. Fracture density as a function of depth below top of casing in selected wells near Mirror Lake in Grafton County, New Hampshire. Fracture density is shown for each 3-m interval.

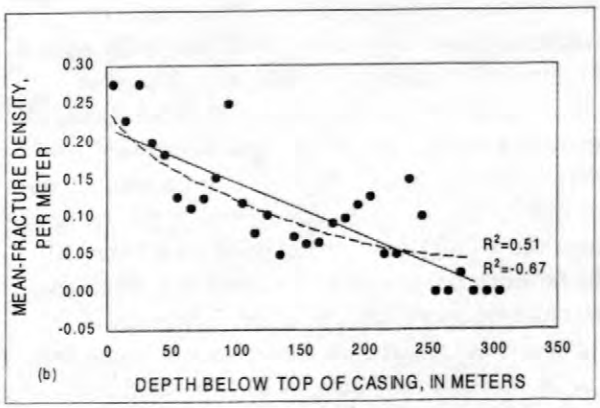

Figure 2b. Mean fracture density plotted as a function of depth and fitted with linear and exponential distributions.

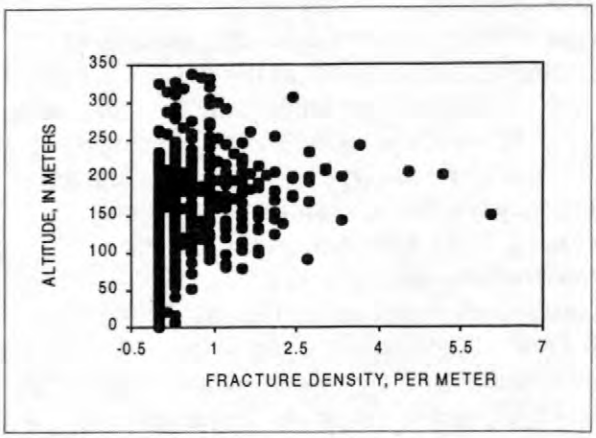

Figure 3. Fracture density plotted as a function of altitude.

Fracture Distribution with Altitude

The fracture density for each 3-m interval in the well was referenced to altitude. A scatterplot (fig. 3) of the fracture density plotted as a function of altitude shows a low intensity of fracturing below 100 m. Because the linear-correlation coefficient for density as a function of altitude was only 0.2, the data cannot be described by a linear distribution. There appear to be more fractures at the high elevations beneath the hill slopes than beneath the valleys. Harte (1997) made a similar observation for bedrock core collected from the top 3 to 5 m of the bedrock surface at six locations.

To test this observation, all fracture-density data from the index wells were separated into 2 categories –data below 100 m and data above 100 m. A rank-sum test, or WMW (Wilcoxon-Mann-Whitney) test, had a p-value of 0.0001, indicating the two groups are statistically different. One possible explanation for this distribution of fractures with respect to altitude is that during the two periods of glaciation, the glaciers followed major valleys that were preferentially fractured prior to glaciation. The high density of fractures in the valleys is assumed to be more easily eroded than the less fractured hillslopes, causing the valleys to be preferentially deepened, thereby removing the upper zones of fractured rock. This corresponds to the general finding that wells sited in valley settings are characterized by a lower average-fracture density than the wells sited on hillslopes and terraces.

Fracture Distribution with Respect to Rock Type

A comparison of rock type with respect to fracturing indicates that fractures are geologically controlled. In general in the study area, the granitoids are more intensely fractured than the schist and gneissic rocks, and pegmatite, basalt, and quartzite are relatively unfractured. In the index wells, the count of fractures with respect to the lithology indicates that approximately 72 percent of the total number of fractures were in granitoids, whereas 23 percent were in schist. Only 5 percent of the total number of fractures were in pegmatite and basalt. The average fracture spacing (m) and fracture density (m^{-1}) is summarized for the various lithologies (table 1).

Table 1. Average fracture spacing and average fracture density per meter for individual rock types

Rock Type	Average fracture	
	Spacing (m)	Density (m^{-1})
Schist	3.86	0.26
Gneiss and migmatite	16.06	.06
Granitoid	1.54	.65
Pegmatite	5.35	.19
Basalt	1.26	.79

Fracture orientation

Fracture orientation was determined from inages produced with a digital camera in seven wells in the Camp Osceola (CO) well field. The fractures strike predominantly N40°E and dip predominantly 10°NW and 68°NW and appear to be parallel to subparallel to the foliation of the metamorphic rock. The fractures from the wells in the CO well field were also compared to the fractures mapped in the nearby highway outcrops that are approximately 150 to 275 m east of the well field. The fracture orientations appear to have the same strike but dip in different directions. The outcrop data (Barton, 1997, fig. 2A) shows a mixture of shallow and steeply dipping fracture sets, which have a preferred strike of N30°E, with dips of 7°NW, 50°SE and 82°SE. Although similar fracture orientations were determined in wells CO1-CO7 in acoustic televiewer measurements (McDonald and others, 1997), no geologic structures have been mapped in this area that would explain the difference in fracture dip between the two sites (William Burton, U.S. Geological Survey, oral commun., 1998). Regardless of the physical basis for differences in the dip direction of fractures, these natural variations of dip found over distances of 150 to 275 m indicate the importance of measuring subsurface fractures and emphasize the need for caution in extrapolating outcrop data to the subsurface.

DISTRIBUTION OF HYDRAULIC CONDUCTIVITY

Hydraulic conductivity was estimated by pumping or injection tests conducted within discrete packed-off intervals that were on average 4.6 m long (Shapiro and Hsieh, 1997). The hydraulic-conductivity data were compared to physical parameters of the fracture system, such as the depth, altitude, topographic setting, rock type, fracture density, and presence of altered or oxidized fractures. The comparisons were made using 176 hydraulic-conductivity measurements from 11 of the areally distributed wells for which hydraulic conductivity data were available (Paul Hsieh, U.S Geological Survey, written commun., 1997). The hydraulic-conductivity measurements ranged over 6 orders of magnitude, from the lower detection limit of the equipment at $1x10^{-10}$m/s to $5.0x10^{-5}$m/s. Hydraulic conductivity could not be correlated with altitude or with depth of the measurement intervals.

COMPARISON OF FRACTURING AND LITHOLOGY TO HYDRAULIC CONDUCTIVITY

Theoretically, the fracture density of the bedrock relates to high connectivity and possibly high hydraulic conductivity. To test this widely held concept, the fracture density and hydraulic conductivity were compared. The scatterplot in figure 4 indicates there is no correlation between the magnitude of hydraulic conductivity and fracture density for the individual measurement zones. Because alteration and oxidation can be indicators of past or present hydraulically active fractures, the density was weighted by codes that include the presence of oxidation or alteration in the rocks. No correlation was found between the presence of alteration and (or) oxidation with fracture density that could be used as a predictor of hydraulically conductive zones.

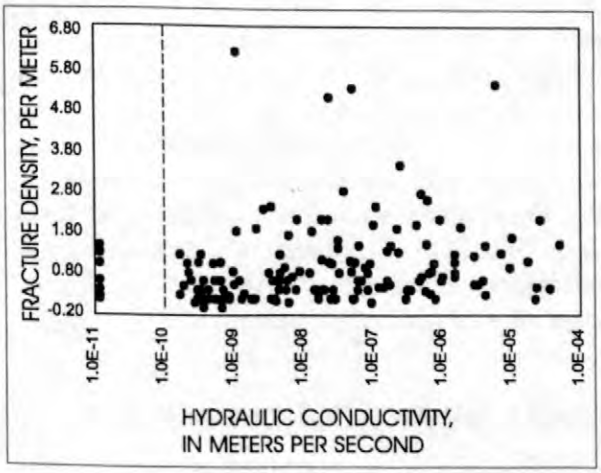

Figure 4. Hydraulic conductivity plotted against fracture density of the measurement zone. (Dashed line indicates lower detection limit of the field equipment.)

A WMW test was used to test whether the hydraulic conductivity values for the two major lithologies in the Mirror Lake area (igneous and metamorphic) are statistically different. The null hypothesis for this test, which states the values come from the same population, could not be rejected, thus indicating the distributions of hydraulic conductivity for the lithologies are not statistically different. The distribution of measured hydraulic conductivity in igneous and metamorphic rocks is shown in figure 5a and 5b, respectively. The frequency in each histogram has been normalized to 144, which is the total number of tests conducted in the igneous and metamorphic rocks combined. The results indicate hydraulic conductivity is not distinctly different for the different lithologies; however, there is a higher probability of fracturing and higher probability of measurable hydraulic conductivity in the igneous rocks than in the metamorphic rocks.

To determine if there is a preferred orientation to the hydraulically conductive fractures, a comparison between hydraulic conductivity and strike and dip was made for the limited set of wells with oriented fracture data (for wells CO1-CO7). The hydraulically active fractures strike approximately N30°E and dip predominantly towards the NW, with a few fractures dipping SE. Another weak fracture set strikes NW and has a shallow dip to the SW. The orientation of fractures in the zones with measurable hydraulic conductivity was similar to the entire population of fracture orientations for wells CO1-CO7. There was no distinct preferred orientation of fracturing that relates to the magnitude of hydraulic conductivity.

SUMMARY AND CONCLUSIONS

Detailed fracture and lithology data collected from 40 wells at the Mirror Lake research site in Grafton County, New Hampshire were used to compare the occurrence of lithologies, fractures, physical parameters, and hydraulic measurements. A set of 15 index wells was used to summarize the fracture characterizations and to test for statistical correlations. There does not appear to be a correlation between rock type and depth, altitude, or topographic setting. There may be a relation, however, between topographic setting and fracturing; that is, there is a low probability of encountering highly fractured wells in valley settings. In addition, there is a low probability of encountering fractured zones at depth. Although the metamorphic and igneous rocks comprise equal proportions of the rock

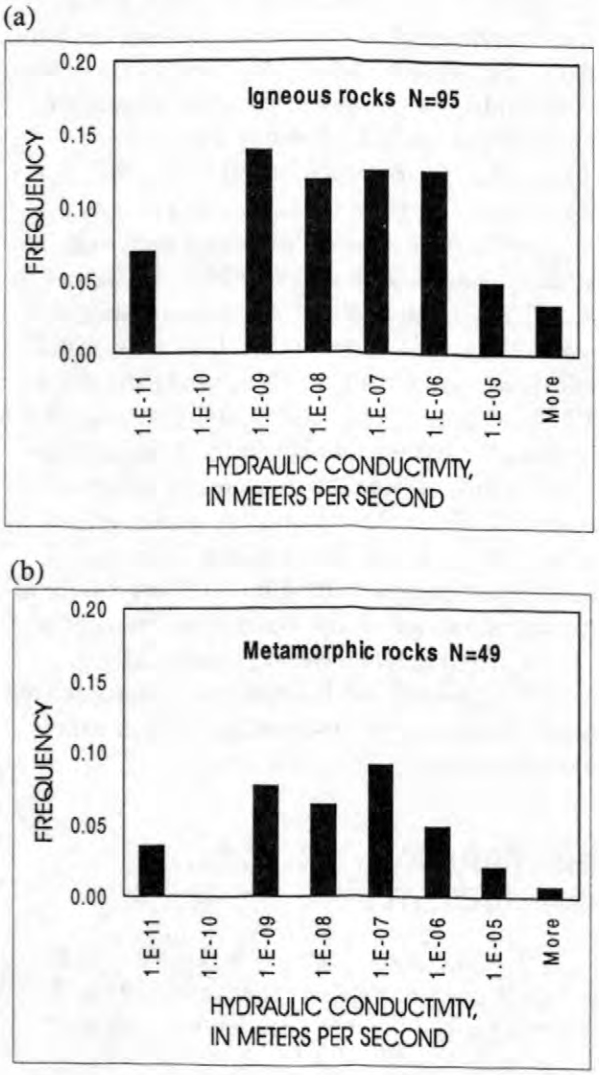

Figure 5. Histogram of hydraulic conductivity for igneous (a) and metamorphic (b) rocks. (N indicates the number of zones in each histogram. The histograms show only the zones measured for hydraulic conductivity and do not show the unfractured zones that were not tested. The lower detection limit for measuring hydraulic conductivity was E^{-10} meters per second.)

types in the index wells, most of the fractures observed in boreholes were in igneous rocks (granitoids), indicating the fracturing is lithologically controlled.

The data from all 15 index wells were combined and statistics were compiled on the distribution of spacing between fractures. The interfracture spacing (computed for the well data) was best defined by a power-law function. This distribution of fractures, at least in the vertical direction, suggests the fracture network comprises tightly-spaced fractures surrounded by zones that are less fractured. Over the scale of a well field, this distribution of fractures would likely cause a spatially variable distribution of hydraulic conductivity.

Digital images were collected in a small subset of wells to describe the lithologies and fracture location and orientation. Analysis of the images indicates a generally good agreement in the strike of fractures measured in the CO well field and on the nearby highway outcrop. Most of the fractures in the subsurface of the CO well field, however, dip in the opposite direction from those on the outcrop. The differences in fracture orientations could indicate fracture variability and a potential weakness in the extrapolation of outcrop data to subsurface fracturing.

Hydraulic-conductivity values available from 11 of the index wells were compared to rock type, fracture density, fracture aperture, fracture density weighted for presence of alteration and oxidation, fracture orientation, and physical parameters such as depth, altitude, and topographic setting. No correlations were established for these comparisons. Fracture intensity alone cannot predict hydraulic properties of fractured rock, because fracture density is not correlated to hydraulic conductivity. This finding indicates that theoretical equations that rely on fracture density are unable to describe hydraulic properties of the aquifer.

A Wilcoxon-Mann-Whitney test was performed on the hydraulic conductivity measurements for the two major lithologies – igneous and metamorphic. Although there are more zones of measurable hydraulic conductivity in the igneous rock, the ranges, means, and variances were similar between the igneous and metamorphic rocks. The test indicated that evidence is not sufficient to conclude that the hydraulic-conductivity data for the two different lithologies come from different populations. Because of the high probability of fractures occurring in granitic rocks, there is a higher probability of finding hydraulically conductive fractures in granitic rocks than in metamorphic rocks.

Fractured-crystalline aquifer systems are extremely heterogeneous and complex. The data and interpretations presented in this paper indicate there is no simple relation or predictor that describes fracture occurrence and probability of hydraulic conductivity. Although some properties of the fracture system have been described, and relations have been defined between fracture occurrence and physical parameters of the aquifer system, the results can be viewed only in a probabilistic sense.

REFERENCES

Barton, C.B., 1996, Characterizing bedrock fractures in outcrop for studies of ground-water hydrology—An example from Mirror Lake, Grafton County, New Hampshire, *in* Morganwalp, D.W. and Aronson, D.A., eds., U.S. Geological Survey Toxic Substances Hydrology Program—Proceedings of the Technical Meeting, Colorado Springs, Colo., September 20-24, 1993: U.S. Geological Survey Water-Resources Investigations Report 94-4015, v. 1, p. 81 - 88.

——— 1997, Bedrock geology map of Hubbard Brook Experimental Forest and maps of fractures and geology in roadcuts along Interstate 93, Grafton County, New Hampshire: U.S. Geological Survey Miscellaneous Investigations Series MAP 1-2562, 1 sheet, 1:12,000 scale.

Harte, P.T., 1997, Preliminary assessment of the lithologic and hydraulic properties of the glacial drift and shallow bedrock in the Mirror Lake area, Grafton County, New Hampshire: U.S. Geological Survey Open-File Report 96-654A, 56 p.

Lyons, J.B., Bothner, W.A., Moench, R.A., and Thompson, J.B., Jr., 1997, Bedrock geologic map of New Hampshire: U.S. Geological

Survey State Geologic Map, 2 sheets, scales 1:250,000 and 1:500,000.

Johnson, C.D., 1996, Use of a borehole color video camera to identify lithologies, fractures, and borehole conditions in bedrock wells in the Mirror Lake Area, Grafton County, New Hampshire, *in* Morganwalp, D.W. and Aronson, D.A., eds., U.S. Geological Survey Toxic Substance Hydrology Program—Proceedings of the Technical Meeting, Colorado Springs, Colo., September 20-24, 1993: U.S. Geological Survey Water-Resources Investigations Report 94-4015, v. 1, p. 89-94.

——— 1998, Subsurface lithology and fracture occurrence and their effects on hydraulic conductivity: Mirror Lake Research Site, Grafton County, New Hampshire: Durham, N.H., University of New Hampshire, unpublished master's thesis, 159 p.

Johnson, C.D., and Dunstan, A.M., 1998, Lithology and fracture characterization from drilling investigations in the Mirror Lake Area: from 1979 through 1995 in Grafton County, New Hampshire: U.S. Geological Survey Water-Resources Investigations Report 98-4183, 210 p.

McDonald, G., Paillet, F.L., Barton, C.B., Johnson, C.D., 1997, Borehole sampling of fracture populations - identifying flow paths and correcting borehole bias in bedrock aquifers: ISRM International Symposium, U.S. Rock Mechanics Symposium (36th) N.Y., June 29-July 2, 1997, Columbia University, 6 p.

Shapiro, A.M., and Hsieh, P.A., 1991, Research in fractured rock hydrogeology: Characterizing fluid movement and chemical transport in fractured rock at the Mirror Lake drainage basin, New Hampshire, *in* Mallard, G.E., and Aronson, D.A., eds., U.S. Geological Survey Toxic Substances Hydrology Program Proceedings of Technical Meeting, Monterey, Calif., March 11-15, 1991: U.S. Geological Survey Water-Resources Investigations Report 91-4034, p. 155-161.

——— 1997, How good are estimates of transmissivity from slug tests in fractured rock?: Ground Water, v. 36, no. 1, p. 37-46.

AUTHOR INFORMATION

Carole D. Johnson, U.S. Geological Survey, Pembroke, New Hampshire (cjohnson@usgs.gov)

Characterizing Recharge to Wells in Carbonate Aquifers Using Environmental and Artificially Recharged Tracers

By Earl A. Greene

ABSTRACT

Stable environmental isotopes were used as tracers to identify the sources of recharge from sinking streams to wells and springs several kilometers downgradient in the karst Madison aquifer near Rapid City, South Dakota. Temporal sampling of steamflow above the swallets identified a distinct isotopic signature that was used to define the spatial dimensions of recharge to the aquifer. An artifical dye tracer (Rhodamine WT) was directly injected into a swallet at one of the sinking streams (Boxelder Creek) and traced to the city municipal well system to determine the flow paths and the volume of water that is contributed to the wells from this recharge source. Analysis of the breakthrough curves showed that first arrival of dye to the municipal well field is very rapid--between 26 and 49 days--and it takes up to 200 days after injection for the concentration of dye to reach background levels.

From these analyses it was possible to link sinking stream recharge to individual wells and springs in the Rapid City area and to illustrate the lateral movement of ground water across surface drainage divides. These results emphasize that when estimating areas of contributing recharge to wells in carbonate aquifers, water managers need to consider the lateral movement of ground-water flow from adjacent surface-drainage basins.

INTRODUCTION

With the present concern and interest regarding the transport of solutes (contaminantes) in the subsurface, there is a continuing need to evalute and understand the mechanisms and properties that control the movement of these solutes, especially in fractured and dissolution-enhanced carbonate aquifers. Characterization and prediction of fluid-flow and solute transport in these rocks are complex because of the difficulty in physically and mathematically identifying the spatial variability in hydraulic and transport properties.

Carbonate (karst) aquifers characterized by resurgent springs, sinkholes that capture streams, collapse breccias, fractures, and dissolution-enhanced openings (vugs and caves) are highly heterogeneous and thus, more difficult to study than porous-media aquifers. Furthermore, carbonate rocks containing extensive networks of solutional features (conduits) and fractures have the ability to transport contaminantes from non-point and point-source pollution over large distances and at large velocities. In extreme cases waters recharged in one basin may end up as recharge to wells or spring flow in another basin. The basic question then becomes, "How can recharge to wells be determined in highly heterogeneous aquifers when the flow in the aquifer cannot be modelled analytically or numerically using porous media techniques?"

The Madison aquifer is a major source of domestic water supply for Rapid City, South Dakota; thus, there have been several investigations of gound water flow and transport processes in this dissolution-enhanced and fractured aquifer (Greene, 1993, 1997; Greene and Rahn, 1995; Rahn, 1971, 1989, 1992). This paper describes ongoing research using tracers in the Madison aquifer to identify and characterize the source of ground-water recharge and identify corresponding flow paths to the municipal well field (Figure 1).

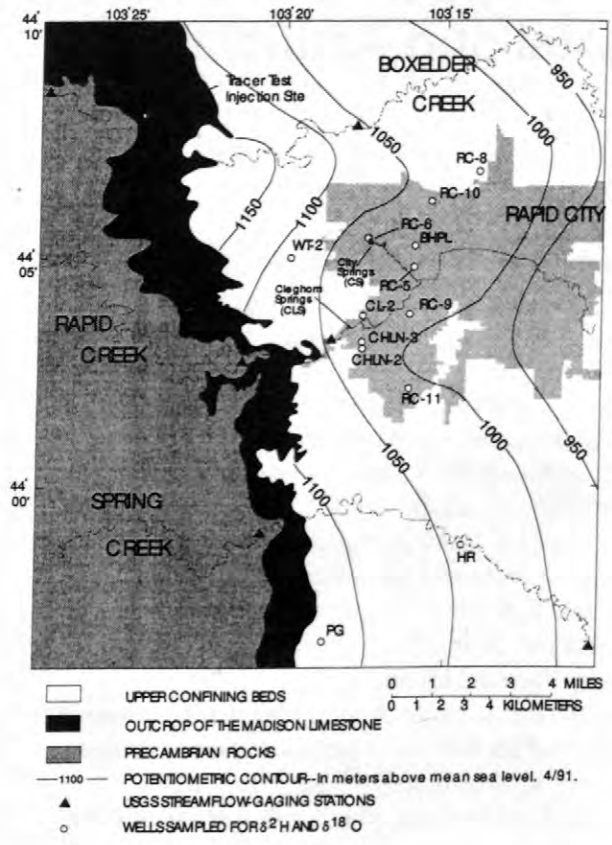

Figure 1. Location of sampled streams, wells, and springs near Rapid City, South Dakota.

STREAM RECHARGE

One of the unique geomorphic features of a karst aquifer is the relation of stream recharge from swallets (sinkholes) to water derived from wells and springs. In many karst regions, localized recharge to the conduit flow system occurs where the surface streams are captured by swallets or closed depressions that collect overland flow. This process has been the subject of much research and study in karst hydrology because of the potential for contamination of the aquifer from surface-water recharge. Swallet recharge and corresponding well or spring discharge is commonly studied by use of artificial tracers (dye-tracing methods) to determine the direction of ground-water flow and delineate recharge and corresponding flow paths (Rahn, 1971; Thrailkill, 1985; and Smart, 1988). Dye-tracing methods in karst terrain, are usually not able to quantify the percentage or contribution of recharge water to wells and springs over spatial dimensions of kilometers. Environmental tracers, especially naturally occuring stable isotopes, have been applied succesfully as a natural tracer to study karst systems (Dincer and Payne, 1971; Ellins, 1992; and Greene, 1997) .

Boxelder Creek, Rapid Creek, and Spring Creek lose some or all of their flow as they cross the outcrop of the Madison Limestone west of Rapid City (Figure 1). All three streams are monitored by the US Geological Survey as part of its South Dakota surface-water basic data program.

Environmental Tracers

The sources and proportions of stream recharge from swallets to wells and springs were identified in the karst Madison aquifer near the Black Hills of South Dakota using δ^2H and $\delta^{18}O$. The isotopic composition of stream recharge at the swallets were determined from a time series of 18 monthly samples and traced to individual wells and springs over spatial dimensions of several kilometers. In addition, when the isotopic content of the water from the sampled wells or springs indicated more than one sinking stream-recharge source, the relative porportions from each source were estimated.

The δ^2H and $\delta^{18}O$ composition of surface-water samples indicates a distinct spatial variation in the isotopic content of stream recharge to the Madison aquifer in the study area (Figure 2 and 3). Generally, Boxelder Creek is depleted in δ^2H and $\delta^{18}O$ as compared to Rapid Creek and Spring Creek. Spring Creek is isotopically enriched as compared to Boxelder Creek.

The average isotopic composition of Boxelder Creek, Rapid Creek and Spring Creek (Figure 3) was weighted on the basis of net recharge to the aquifer as measured at the gaging stations upstream of the swallets to determine a recharge-weighted isotopic composition of recharge. The recharge-weighted isotopic composition of recharge waters is mixed using equation (1) to form the isotopic content of waters sampled at the wells or springs.

$$\delta^{18}O_{well} = ax\delta^{18}O_{stream\ 1} + bx\delta^{18}O_{stream\ 2} \quad (1)$$

where

a,b	is fraction of stream 1 or stream 2, a + b =1;
$x\delta^{18}O_{stream\ 1}$	is recharge-weighted average $\delta^{18}O$ content of stream 1;
$x\delta^{18}O_{stream\ 2}$	is recharge-weighted average $\delta^{18}O$ content of stream 2;
$\delta^{18}O_{well}$	$\delta^{18}O$ content in a well or spring.

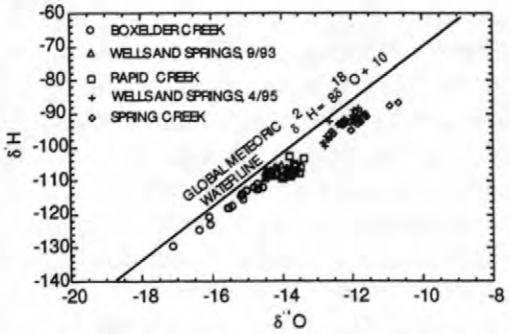

Figure 2. Relation of δ^2H and $\delta^{18}O$ in sampled streams, wells, and springs to the Global Meteoric Water Line (Craig, 1961).

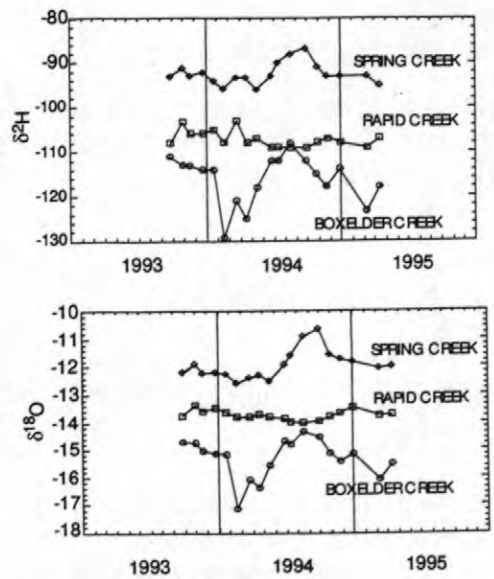

Figure 3. Temporal variation of δ^2H and $\delta^{18}O$ in Boxelder Creek, Rapid Creek, and Spring Creek from September 1993 to April 1995.

The results of using $\delta^{18}O$ to determine the relative proportions of Boxelder Creek, Rapid Creek, and Spring Creek recharge to wells and springs are presented in Table 1. Several assumptions in the use of equation (1) were made to mix recharge waters from the stream recharge. These are: (a) recharge from direct precipitation on the outcrop is minor; (b) no recharge from other aquifers enter through confining beds; and (c) temporal variation in stable isotopes does not vary significantly. Generally, the use of either δ^2H or $\delta^{18}O$ gave similar results except for CHLN-3 and RC-5 in which the mixing ratio is significantly different depending on which isotope is used. The results of this mixing model to determine the spatial distribution of stream recharge to water derived from wells and springs near Rapid City are summarized in Figure 4.

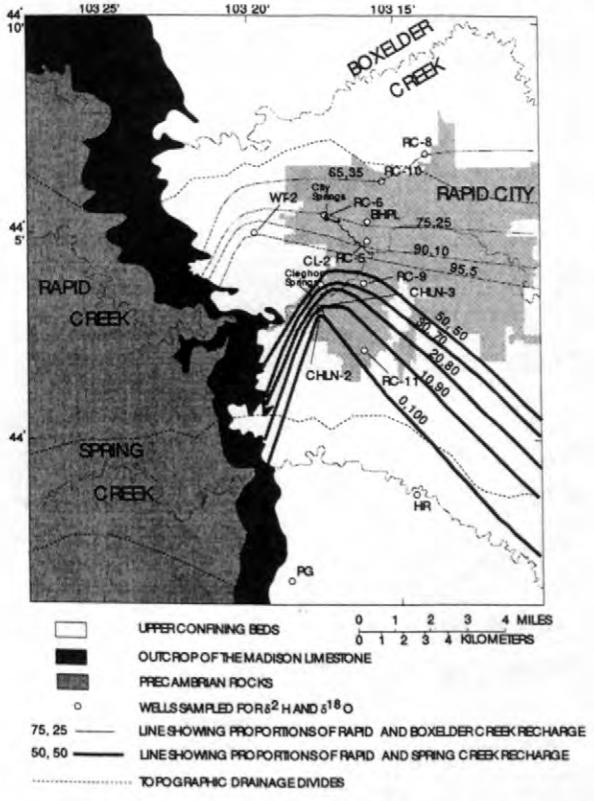

Figure 4. Map showing the spatial distribution of recharge from sinking streams near Rapid City, South Dakota.

Recharge to well WT-2 is primarily from Rapid Creek, and the wells in the northwest part of the Rapid City (RC-6, RC-10, BHPL, RC-8 and RC-5) including City Springs, obtain approximately 75 percent of their water from Rapid Creek and about 25 percent from Boxelder Creek. Water pumped from wells in the central part of the city (RC-9, CL-2) is composed of

approximately 40 percent water from Rapid Creek and 60 percent water from Spring Creek. The largest resurgent spring in Rapid City, Cleghorn Springs, discharges at about 0.3 m^3/s (Rahn and Gries, 1973) and is a mixture of about 55 percent Rapid Creek water and 45 percent Spring Creek water.

Table 1. Relative Proportions (percent) of Boxelder Creek, Rapid Creek, and Spring Creek recharge waters to wells in the Madison Aquifer.

Well ID (Figure 1)	Boxelder Creek		Rapid Creek		Spring Creek	
	δ^2H	$\delta^{18}O$	δ^2H	$\delta^{18}O$	δ^2H	$\delta^{18}O$
WT-2	0	6	100	94	--	--
RC-6	18	29	82	71	--	--
RC-10	27	41	73	59	--	--
BHPL	27	30	73	70	--	--
RC-8	27	41	73	59	--	--
RC-5	0	23	100	77	--	--
RC-9	--	--	35	42	65	58
CL-2	--	--	35	42	65	58
CHLN-2	--	--	0	0	100	100
CHLN-3	--	--	7	31	93	69
RC-11	--	--	0	11	100	89
PG	--	--	0	0	100	100
HR	--	--	0	0	100	100
City Springs (CS)	28	41	72	59	--	--
Cleghorn Springs (CLS)	--	--	57	53	43	47

Recharge to wells (RC-11 and CHLN-3) in the southern part of Rapid City is primarily from Spring Creek with a small amount of Rapid Creek water. RC-11 is recharged with about 90 percent Rapid Creek water. CHLN-3 is recharged with about 80 percent Spring Creek and 20 percent Rapid Creek water. Wells south of Rapid City, CHLN-2, HR, and PG obtain most of their recharge water from Spring Creek (Figure 4).

Artificially Recharged Tracer

A large-scale dye tracer test (Boxelder Tracer Test) was initiated in August 1993 when 14 kilograms of Rhodamine WT was injected into the swallet at the loss zone of Boxelder Creek (Figure 1). The concentration of Rhodamine WT was monitored daily in samples collected up to one year after injection in seven discharging wells (WT-2, RC-6, RC-10, BHPL, RC-5, RC-8, RC-9), two observation wells (CQ-1, CQ-2), and two resurgent springs (CS, CLS) downgradient from the injection point. Rhodamine WT was detected in four of the discharging wells (Table 2), one observation well (CQ-2), and one of the resurgent springs (CS). The temporal distribution (breakthrough curves) of Rhodamine WT concentration at the monitoring points is shown in Figure 5. First arrival at the nearest monitoring point, WT-2, 9.3 kilometers away from the injection site, was 26 days. First arrival at the farthest monitoring point, BHPL, 12.4 kilometers away from the injection site, was 49 days.

Table 2. Transport parameters for the Boxelder Tracer Test.

	Breakthrough Curve Data					
Well	Initial Days (days)	Peak Days (days)	End Days (days)	Mass Recovered (grams)	Percent Recovered	Mean Mass (days)
WT2	26	32	73	112.5	0.8	40
CS	30	48	261	1604.9	11.5	90
RC6	30	45	186	1442.1	10.3	74
RC10	41	53	198	1882.3	13.4	79
BHPL	49	57	159	41.7	0.3	90
Total Mass Recovered				5083.46		
Percent Recovered					36.3	

All six of the breakthrough curves had an abrupt rise to a peak followed by a gradual decrease to background levels. The breakthrough curves were analyzed for mass recovery and transport parameters.

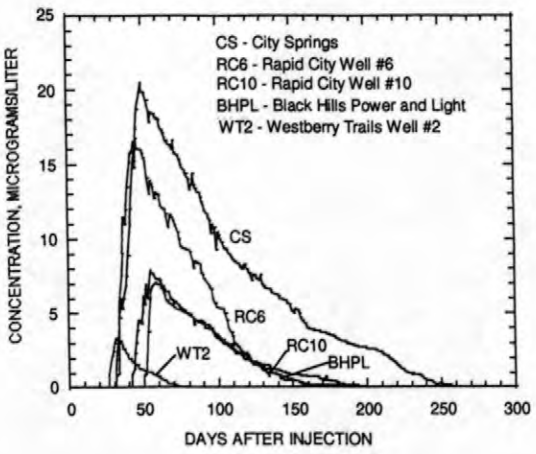

Figure 5. Breakthrough curves of Rhodamine WT sampled from wells and springs near Rapid City, South Dakota.

SUMMARY

One of the unique geomorphic features of a karst aquifer is the complex relation of stream recharge from swallets (sinkholes) to water derived from wells and springs. This process has been the subject of much research in the Madison Limestone near Rapid City, because the aquifer is a major source of municipal water supply for the city and there is a large potential for contamination from surface-water recharge. Stable isotope composition (δ^2H and $\delta^{18}O$) in stream recharge above the swallets was characterized by temporal sampling and traced to individual wells and springs in the aquifer. The sources and proportions of stream recharge to wells and springs were determined from the isotopic analysis. The results show that there is a significant laterial movement of ground water between basins in the Rapid City area.

Rhodamine WT dye was injected into the recharge zone at Boxelder Creek (swallet) and traced to the city municipal well system to determine flow paths and the volume of water that is contributed to the well from this recharge source. Analysis of the breakthrough curves showed that first arrival of dye is rapid, from 26 and 49 days at the wells, and that it takes up to 200 days after injection for the concentration to reach background levels.

REFERENCES

Craig, H., 1961, Isotopic variations in meteoric waters: Science, v. 133, p.1702-1703.

Dincer, T. and Payne, B.R., 1971, An environmental isotope study of the southwestern karst region of Turkey: Journal of Hydrology, v. 14, p. 307-321.

Ellins, K.K., 1992, Stable isotope study of the ground water of the Martha Brae River Basin, Jamaica: Water Resources Research, v. 28, no. 6, p. 1597-1604.

Greene, E.A., 1993, Hydraulic properties of the Madison aquifer system in the western Rapid City Area, South Dakota: U.S. Geological Survey Water-Resources Investigations Report 93-4008, 56 p.

——— 1997, Tracing recharge from sinking streams over spatial dimensions of kilometers in a karst aquifer: Ground Water, v. 35, no. 5, p. 898-904.

Greene, E.A. and Rahn, P.A., 1995, Localized anisotropic transmissivity in a karst aquifer: Ground Water, v. 33, no. 5, p. 806-816.

Rahn, P.A., 1971, The hydrologic significance of the November, 1968 dye test on Boxelder Creek, Black Hills, South Dakota, *in* Proceedings of the South Dakota Academy of Sciences, v. 50, p. 52-56.

Rahn, P.A., 1989, Recharge to the Pahasapa Limestone, *in* Proceedings of the South Dakota Academy of Sciences, v. 69, p. 59-66.

Rahn, P.A., 1992, Permeability of the Madison aquifer in the Black Hills area: Final report to the Department of Environment and Natural Resources, Ground Water Research and Public Education Program. 131 p.

Rahn, P.A. and Gries, J.P., 1973, Large springs in the Black Hills, South Dakota and Wyoming: South Dakota Geological Survey Report of Investigations, No. 7, 46 p.

Smart, C.C., 1988, Artifical tracer techniques for determination of the structure of conduit aquifers: Ground Water, v. 26, p. 445-453.

Thrailkill, J., 1985, Flow in a limestone aquifer as determined from water tracing and water levels in wells: Journal of Hydrology, v. 78, p. 123-136.

AUTHOR INFORMATION

Earl A. Greene, U.S. Geological Survey, Baltimore, MD (eagreene@usgs.gov)

CFC's in the Unsaturated Zone and in Shallow Ground Water at Mirror Lake, New Hampshire

By Daniel J. Goode, Eurybiades Busenberg, L. Niel Plummer, Allen M. Shapiro, and Don A. Vroblesky

ABSTRACT

At the U.S. Geological Survey's fractured-rock hydrology research site at Mirror Lake, N.H., concentrations of chlorofluorocarbons (CFC's) and other chemical constituents in ground water were measured to help identify large-scale flow and transport properties of the crystalline bedrock. The use of CFC's as environmental tracers in ground water is based on the assumption that CFC concentrations in recharge are in equilibrium with atmospheric levels. Results of a 3-year field study to identify the input source function for CFC's in ground-water recharge indicate that use of CFC's as an environmental tracer at this site, and presumably at other forested, humid sites underlain by glacial deposits, may be significantly complicated by anaerobic degradation reactions in shallow ground water. CFC concentrations near the water table are depleted where dissolved oxygen levels are low. CFC-11 and CFC-113 are absent under anaerobic conditions; CFC-12 is as low as one-third of modern concentrations. Methanogenic and sulfate-reduction conditions have been identified by use of hydrogen-gas measurements, and methane has been detected in several anaerobic samples. One area of active degradation appears to be associated with streamflow loss to ground water. Soil-gas concentrations are generally close to atmospheric levels, although limited spatial correlation is observed between depleted concentrations of CFC-11 and CFC-113 in soil gas and water-table samples.

CFC'S AS ENVIRONMENTAL TRACERS

Chlorofluorocarbons (CFC's; also called Freon, chlorofluoromethane) have emerged as useful age-dating tracers for young ground water (Plummer and others, 1993). The atmospheric source for CFC's is relatively well known and is almost linear in time, and the CFC concentration of fresh water in equilibrium with the atmosphere is well described as a function of temperature alone. CFC-12, CFC-11, and CFC-113 are man-made volatile organic compounds that are widely used as refrigerants and components of many manufactured goods. The atmospheric concentration of CFC's has been increasing since their creation in the 1940's, although concentrations have very recently begun to level off, and slightly decrease for CFC-11, due to production reductions and losses from the atmosphere.

Assuming that recharging ground water is in CFC equilibrium with the atmosphere, a measured CFC concentration in water can be converted to a corresponding atmospheric concentration, which in turn can be used to compute a corresponding date of recharge. The difference between the date of recharge and the date of sampling is the apparent age of the ground water.

The dating of ground water with the use of CFC's depends, in part, on the assumption that CFC's are inert; once isolated from the atmosphere, the CFC concentration in moving water is constant in time. However, several processes may change CFC concentrations during flow. These processes include mixing and dispersion, exchange with solids, gases, or immobile waters, and degradation by biotic or abiotic reactions (Busenberg and Plummer, 1992). It is known that CFC's, particularly CFC-11 and CFC-113, are degraded under anaerobic conditions in ground water (Semprini and others, 1990; Terauds and others, 1993; Oster and others, 1996; Plummer and others, 1998). In oxygenated waters, however, CFC's appear to be virtually inert. Furthermore, the gradual increase in atmospheric concentrations over time means that CFC concentrations are less affected by mixing and dispersion than are tracers with highly variable sources, such as tritium (Plummer and others, 1993). Exchange processes may be important for CFC's, especially in highly heterogeneous formations such as fractured rock (Shapiro, 1996; Wood and others, 1996). Sorption of CFC's to most natural aquifer materials is believed to be

insignificant. Despite these beneficial factors, CFC concentrations in ground water are not always easy to interpret. The U.S. Geological Survey (USGS) Mirror Lake, N.H., research site is one location where CFC's have not been as useful as hoped in characterizing large-scale transport properties (Busenberg and Plummer, 1996; Shapiro and others, 1996).

MIRROR LAKE FIELD SITE

The USGS is investigating multi-scale flow and transport in a glaciated fractured-rock setting at the Mirror Lake, N.H., site (Winter, 1984; Shapiro and Hsieh, 1996; Hsieh and others, 1993; several other papers in these proceedings). This site is part of the Hubbard Brook Experimental Forest, administered by the U.S. Forest Service (USFS). Ground water from the fractured bedrock and from the overlying glacially deposited formations has been analyzed for numerous environmental tracers (Busenberg and Plummer, 1996; Drenkard and others, 1996).

Hydrogeologic Setting

Glacial drift overlyies crystalline bedrock the Mirror Lake site (Winter, 1984). The glacial drift has a highly variable composition ranging from uniform sandy terraces to fine-grained till filled with large boulders (Winter, 1984; Harte, 1992; Harte and Winter, 1995, 1996). The permeability of the glacial drift is generally low (Wilson, 1991; Harte, 1997). Regional-scale flow modeling indicates the transmissivities of the glacial drift and the underlying fractured bedrock are low and of the same order of magnitude (Tiedeman and others, 1997, 1998). Base flow to streams in the Mirror Lake drainage basin is significantly higher than in other parts of the Hubbard Brook drainage basin because of the increased thickness of glacial drift (Winter and others, 1989; Mau and Winter, 1997). Sandy terrace deposits located throughout the watershed may have strong local control on ground-water flow and ground-water/surface-water interaction (Shattuck, 1991; Harte and Winter, 1995, 1996). The climate is humid and long-term average recharge to ground water is on the order of 30 cm/yr (centimeters per year) (Mau and Winter, 1997).

Ground-Water Ages from CFC Data at Mirror Lake

Ground-water ages derived from CFC concentrations in samples from bedrock wells at Mirror Lake do not follow a readily apparent spatial (vertical and horizontal) distribution (Busenberg and Plummer, 1996; Shapiro and others, 1996). In homogeneous formations, ground-water age is expected to increase gradually along flow paths from recharge to discharge locations. In the highly heterogeneous fractured rock at Mirror Lake, however, in which the small-scale hydraulic conductivity varies over at least seven orders of magnitude (Hsieh and Shapiro, 1996), complex patterns may be expected. No general spatial pattern is observed in apparent ages; indeed, some of the youngest apparent ages measured are close to Mirror Lake, which is the primary discharge area for the basin.

Possible geochemical processes that contribute to the complex age spatial pattern at Mirror Lake, and the corresponding CFC concentration pattern, are in situ processes that modify CFC concentrations. These include, but may not be limited to, sorption, exchange, and degradation. Furthermore, seasonal temperature cycles may cause corresponding cycles in CFC concentrations in recharging waters. These cycles may lead to variability in CFC concentrations along a flow path that may be misinterpreted as variable ages.

SCOPE AND OBJECTIVES

The goals of the field study described here are to characterize the concentrations of CFC's in water recharging the saturated zone at Mirror Lake, to identify the processes that control those concentrations, and to describe the source function for CFC's in infiltrating waters that recharge the saturated zone. The field program (1995-97) investigated the following properties and processes: CFC concentrations at or near the water table, and in the unsaturated zone; temperature cycles where CFC air/water equilibrium is occurring; biogeochemical factors that may be related to CFC concentrations; and hydraulic properties of the unsaturated zone. This paper focuses on CFC concentration results. Details of the methods used and other results are discussed in Goode (1998).

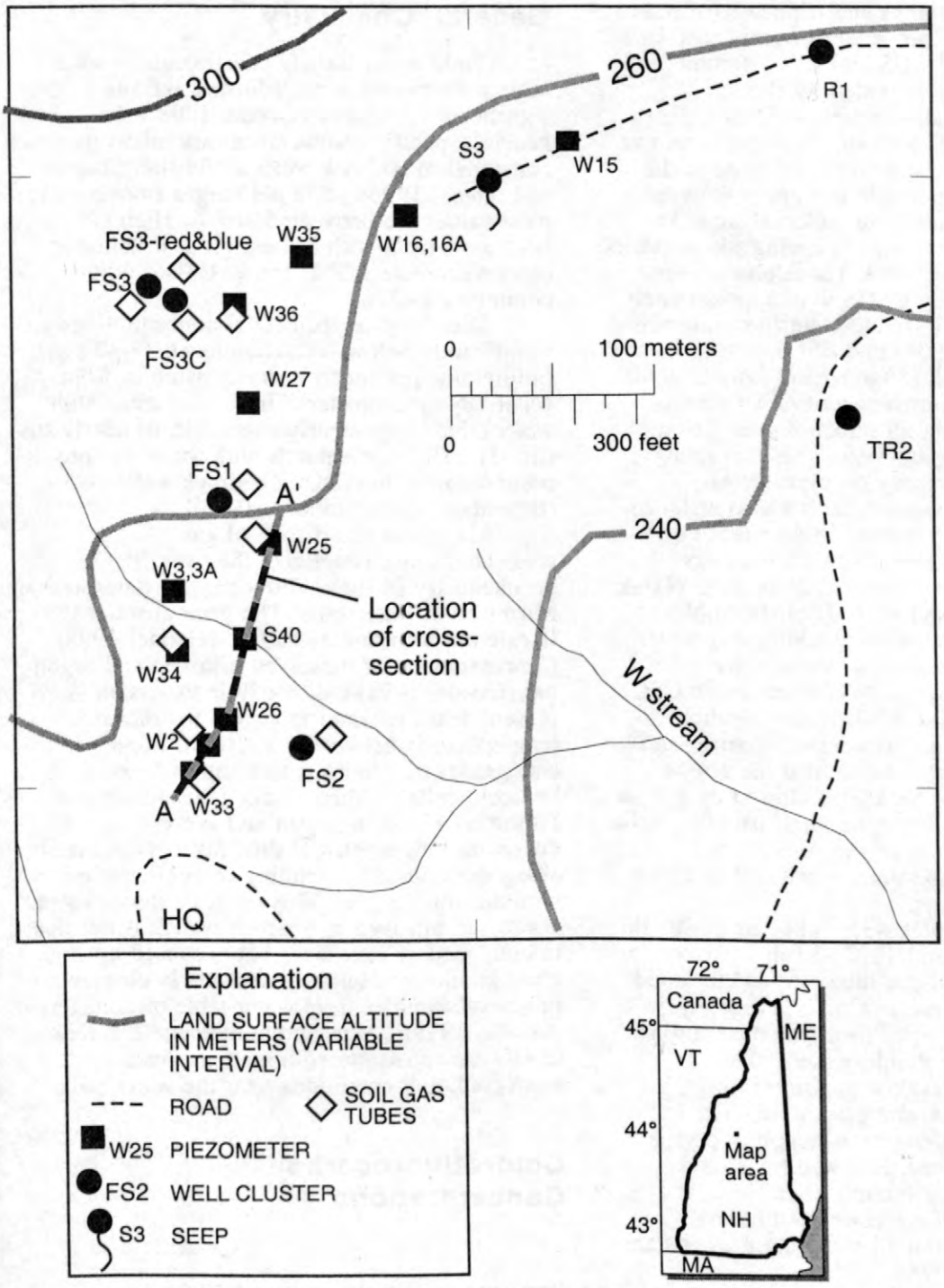

Figure 1. Locations of individual piezometers, well clusters (1-4 piezometers and 1 bedrock well), seep, and soil gas tubes at the Mirror Lake, New Hampshire, research site.

SUMMARY OF METHODS

Some data used in this study were obtained from previous and ongoing research conducted by USFS, Institute of Ecosystems Studies (IES), USGS, and numerous universities at Mirror Lake and at Hubbard Brook Experiment Forest. Geochemical data, including CFC results from bedrock wells and piezometers, were provided by the USGS national lab and research laboratories. Quality-assurance methods included the collection and

analysis of field blanks and triplicate (or more) water samples. Water-level measurements were also provided by USGS and IES. Barometric pressure data were provided by IES. Precipitation and air-temperature data were provided by USFS, Radnor, Pa. Hydrogen-gas concentrations in water were measured in the field by use of a portable gas chromatograph.

Water samples were collected from 31 shallow piezometers (fig. 1) during the summers of 1995, 1996, and 1997. These piezometers were constructed by USGS over approximately 20 years as part of ground-water/lake interaction studies (Winter, 1984) and of fractured-rock hydrology research (Shapiro and Hsieh, 1996). Piezometers are constructed of either steel or PVC and are almost all screened over 0.6- to 0.9-m (meter) long intervals. This sampling effort focused primarily on piezometers screened near the water table but also included some piezometers screened in the glacial drift beneath the water table. New piezometers constructed for the present study include W16A, W33, W34, W35, and W36. These boreholes were power augered without adding any water during drilling, and the piezometers were constructed of threaded PVC to minimize CFC contamination. Except where the borehole caved in during auger withdrawal, coarse sand was placed in the annulus around the screen, followed by natural backfill, followed by a layer of ground silica flour, and natural backfill to the surface. The purpose of the fine-grained ground silica is to minimize vertical flow within the borehole annulus.

Soil-gas samples were collected during the summers of 1996 and 1997 and in January 1997 from steel soil-gas tubes (fig. 1) installed by hand or power auger or, in one case, by manual drive point. Each soil-gas tube consists of 0.6-cm diameter stainless steel tubing, stainless steel or brass compression fittings, a stainless steel screen, and glass wool. The borehole annulus around the sampling port is filled with coarse sand, followed by natural backfill, followed by ground silica flour, and natural backfill to the surface. Additional details on soil-gas and air sampling methods are given in Goode (1998).

RESULTS

The results of analyses of water samples, including CFC concentrations, and soil-gas CFC concentrations, are summarized below. Other results of this field study, including soil moisture content and temperature monitoring, are described in Goode (1998).

General Chemistry

Field water-quality constituents in water-table piezometers at the Mirror Lake site exhibit significant variability (Goode, 1998). In general, specific conductances are relatively low compared to bedrock wells at the site (Shapiro and others, 1996). The pH ranges from 5 to 11; most values are between 5 and 7. High pH has been associated with cement grout installed at older piezometers (P.T. Harte, USGS, written commun., 1991).

Dissolved oxygen (DO) concentrations are significantly below saturation levels (7-12 mg/L (milligrams per liter)) in many samples from water-table piezometers. In several areas, the water table is apparently anaerobic, or nearly so (fig. 2). This corresponds with the wide-spread observation of low-DO in bedrock wells (Busenberg and Plummer, 1996).

Major ion and dissolved gas concentrations characterize the overall geochemistry of the shallow ground water in the Mirror Lake watershed. The general water type is calcium-bicarbonate-sulfate (Goode, 1998). Concentrations of dissolved nitrogen and argon gas (Goode, 1998) indicate little excess air is present near the water table and the recharge temperature is between 5 and 10°C (degrees centigrade). In contrast to samples from bedrock wells at Mirror Lake (Busenberg and Plummer, 1996), nitrogen and argon concentrations in glacial drift fall approximately along the line corresponding to equilibration with the atmosphere. This suggests the elevated argon and nitrogen in bedrock waters is not due to entrapped or excess air but is caused by some other in situ production. Methane is observed in several samples from water-table piezometers (Goode, 1998). Measurable methane and lack of DO are consistent with methanogenic biodegradation conditions near the water table.

Chlorofluorocarbon Concentrations

Concentrations in Ground Water

About half of the uncontaminated water samples from shallow piezometers contain CFC concentrations near modern (1995-97) atmospheric-equilibrium levels, which are about 950, 450, and 150 pg/kg (picograms per kilogram) for CFC-11, CFC-12, and CFC-113, respectively (at 7 °C). This observation supports use of CFC concentrations to date saturated-zone ground water.

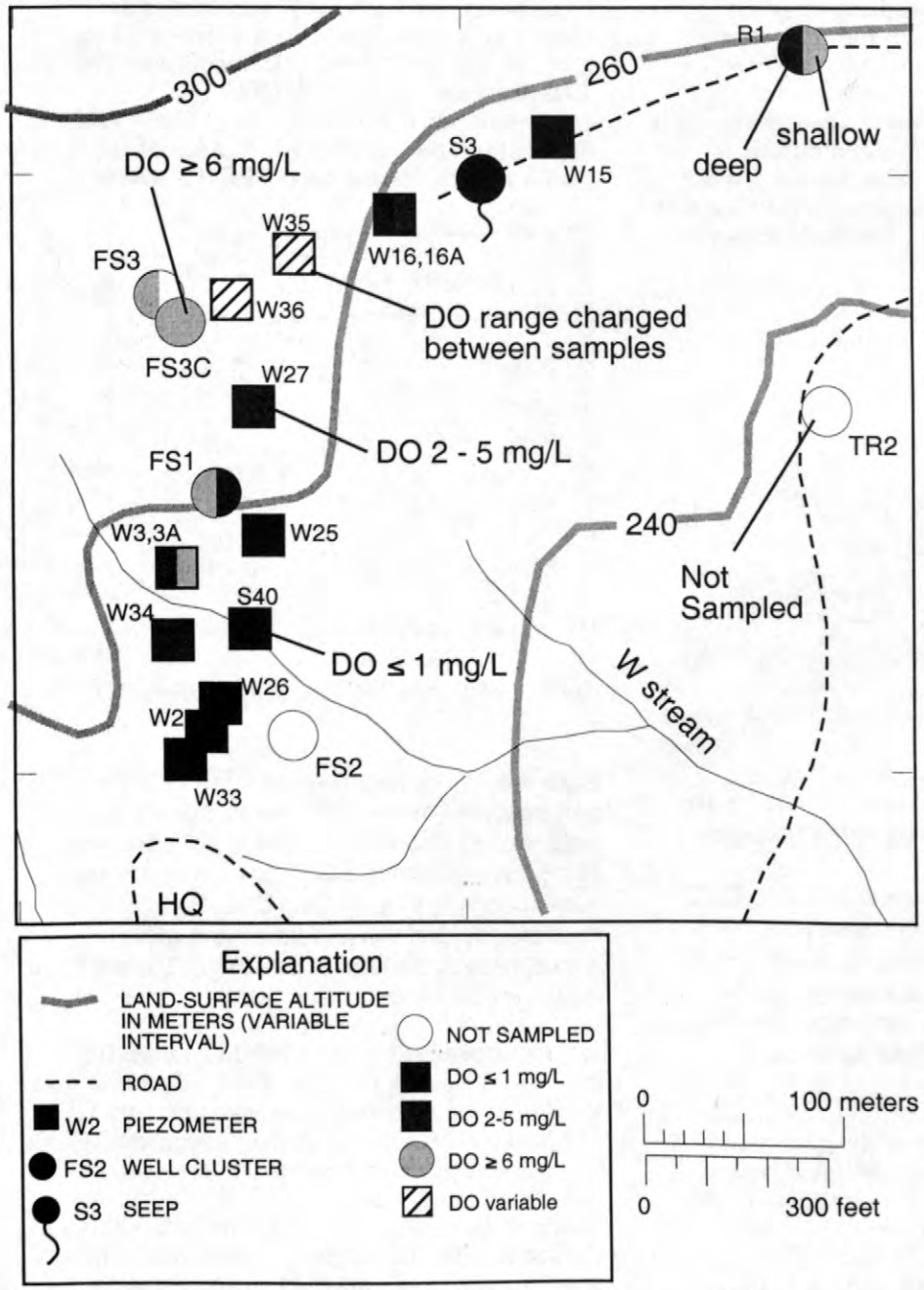

Figure 2. Spatial distribution of dissolved oxygen concentrations in water samples from shallow piezometers at the Mirror Lake, New Hampshire, research site. (Abbreviation: mg/L, milligrams per liter.)

Samples from about one-quarter of the piezometers at Mirror Lake contain CFC concentrations higher than those in equilibrium with the atmosphere. Following Busenberg and Plummer (1992), these samples are designated "contaminated." In some cases, contamination of samples was so high that the analytical procedures used to concentrate the normal low levels resulted in analytical responses beyond the instrumentation limits. Possible sources of this contamination include sampling equipment (Busenberg and Plummer, 1996) and well-construction materials, including the sand installed at well screens, grout used to seal the borehole annulus, and PVC adhesives.

About half of the uncontaminated samples collected from water-table piezometers for this study contain CFC concentrations significantly less than those in equilibrium with the modern atmosphere. The observed CFC-12 and CFC-11 concentrations indicate some process is, or several processes are, modifying the

concentrations from atmospheric equilibrium (fig. 3). Water isolated from the atmosphere during the last 50 years should have CFC-12 and CFC-11 concentrations that lie on the atmospheric equilibrium line (shown in fig. 3) if the only process affecting concentrations is advection with moving saturated-zone ground water. The fact that most samples fall below this line indicates more CFC-11 has been removed relative to CFC-12.

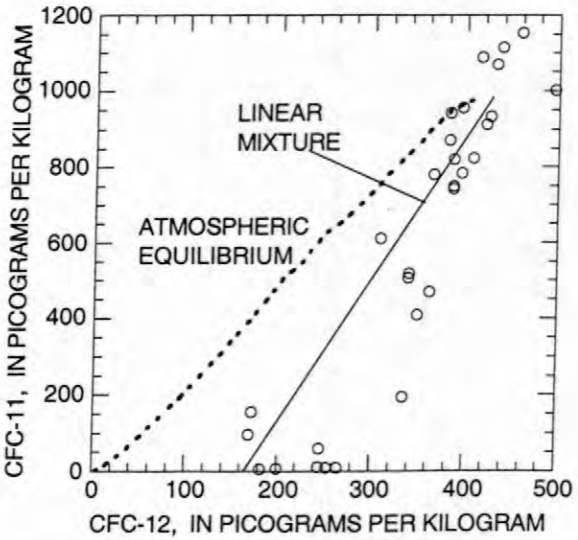

Figure 3. Concentrations of CFC-11 and CFC-12 in water samples from water-table piezometers at the Mirror Lake, New Hampshire, research site. The dashed line shows the concentrations in water in equilibrium with the atmosphere during the last 50 years (at 7 °C). The solid line is a suggested linear mixing line.

A preliminary review of the data indicates that CFC concentrations are correlated with DO. CFC-12 concentrations range from about 160 pg/kg to about 2,300 pg/kg. For uncontaminated samples, CFC-12 concentrations are correlated with DO (fig. 4). Samples containing zero or very small amounts of oxygen have CFC-12 concentrations about 1/3 of the concentration of water in equilibrium with modern air. High oxygen concentrations correspond to CFC-12 concentrations near modern levels.

Concentrations of CFC-11 range from zero to 88,000 pg/kg. Some samples were so highly contaminated with CFC-11 that quantification of the concentrations was not analytically possible. For uncontaminated samples, CFC-11 concentrations are strongly correlated with DO (fig. 4). Samples containing zero or very small amounts of oxygen also contain zero or very small amounts of CFC-11. High oxygen concentrations correspond to CFC-11 concentrations near modern levels. Taken at face value, these CFC-11 concentrations correspond to ages of 0 years, for the high concentrations, to ages of more than 45 years, for the zero-CFC-11 waters.

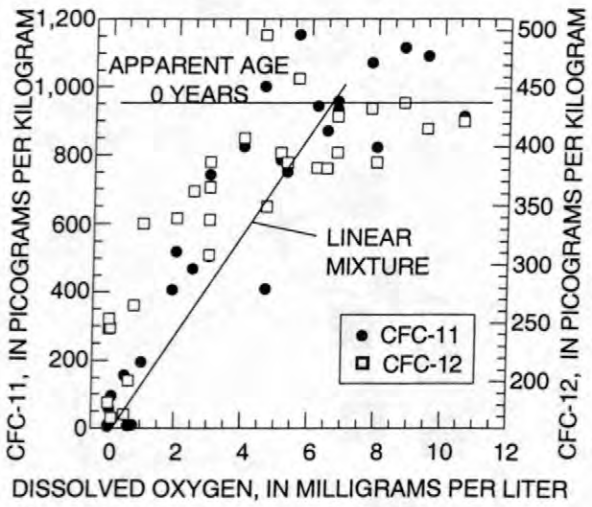

Figure 4. Concentrations of CFC-11, CFC-12, and dissolved oxygen in water samples from water-table piezometers at the Mirror Lake, New Hampshire, research site. The horizontal line corresponds to CFC-11 and CFC-12 concentrations in water equilibrated with the atmosphere at the time of sampling. The solid line is a suggested linear mixing line.

Concentrations of CFC-113 range from zero to 240 pg/kg (Goode, 1998). Some samples were so highly contaminated with CFC-113 that quantification of the concentrations was not analytically possible. For uncontaminated samples, CFC-113 concentrations are strongly correlated with DO, similar to CFC-11 results. Samples containing zero or very small amounts of oxygen also contain zero or very small amounts of CFC-113. High oxygen concentrations correspond to CFC-113 concentrations near modern levels. The scatter in CFC-113 concentrations in high-DO samples is larger than the scatter for either CFC-12 or CFC-11 (Goode, 1998).

The similarity between the correlations of CFC-11 and CFC-12 to DO is shown in fig. 4. The only major difference is that the lowest CFC-12 concentrations correspond to about one-third of modern levels, whereas the lowest CFC-11 concentrations are zero. The correlation between CFC-113 and DO is virtually the same as the CFC-11 pattern but

with more scatter at the upper concentration levels.

The hypothetical mixing line of figs. 3 and 4 corresponds to concentrations of CFC-11 and CFC-12, and dissolved oxygen, in a volumetric mixture of two end-member waters: (a) anaerobic water containing no CFC-11 and 160 pg/kg CFC-12, and (b) water containing 7 mg/L DO, 950 pg/kg CFC-11, and 430 pg/kg CFC-12. Without this mixing, the apparent degradation of CFC's in the presence of 1 to 4 mg/L of dissolved oxygen is difficult to explain because it is assumed that degradation occurs only under anaerobic conditions. Generally, anaerobic conditions are considered to be prevalent when DO is much less than 1 mg/L.

The relation between CFC-11 and tritium in samples from water-table piezometers is shown in fig. 5. Tritium concentrations generally indicate modern recharge (Plummer and others, 1993) but CFC-11 concentrations suggest ages from zero to over 45 years. Almost all measured tritium concentrations are about 10-15 TU (tritium units). All of these tritium concentrations are significantly below bomb-peak levels dating from the late 50's and early 60's. The concentration of tritium in waters recharged in 1963, accounting for subsequent radioactive decay until 1995, would be more than 150 TU (Busenberg and Plummer, 1996), about an order of magnitude higher than measured concentrations. On the basis of the age-dating assumptions, a sample containing zero CFC-11 was recharged prior to 1945. The concentration of tritium in recharge in 1945, decayed to 1995, would amount to less than 5 TU, and older waters would contain even less tritium. The observed tritium and CFC concentrations suggest these water samples represent modern recharge, but CFC concentrations have been reduced by degradation.

Concentrations in Soil Gas

Concentrations of CFC's in soil gas exhibit much less variability than concentrations in water (Goode, 1998). All CFC-12 soil-gas concentrations are close to 100 percent of modern atmospheric levels (fig. 6). The average CFC-12 soil gas concentration at each sampling location ranges from 0.97 to 1.06 times modern air concentrations. CFC-12 concentrations in local air are close to the global average; individual measurements range from 0.93 to 1.07 times the global average.

CFC-11 concentrations in soil gas vary somewhat more than CFC-12 concentrations and are reduced compared to modern air. The average CFC-11 soil-gas concentration at each sampling location ranges from 0.81 to 1.13 times modern air concentrations. CFC-11 soil-gas concentrations are low near piezometer W33 (fig. 7), where zero CFC-11 is measured in shallow water-table piezometers, and where the water table is anaerobic (fig. 2).

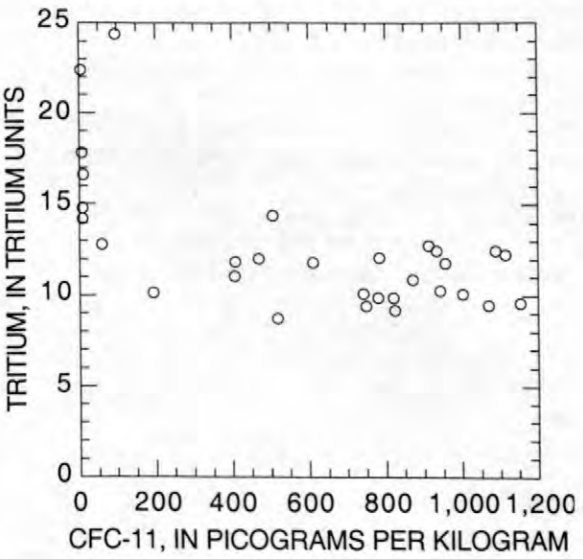

Figure 5. Concentrations of CFC-11 and tritium in water samples from piezometers at the Mirror Lake, New Hampshire, research site.

CFC-113 concentrations in soil gas vary somewhat more than either CFC-12 or CFC-11 concentrations, and several locations exhibit reduced concentrations compared to modern air. The average CFC-113 soil-gas concentration at each sampling location ranged from 0.78 to 1.22 times modern air concentrations. CFC-113 soil-gas concentrations are low near piezometer W33, where zero CFC-113 is measured in shallow water-table piezometers, and where the water table is anaerobic (fig. 2).

CFC concentrations in soil gas show virtually no correlation with depth. In a few cases, however, a systematic pattern in time is present. In these cases, the winter concentrations of soil gas CFC-11 and CFC-113 are a lower fraction of modern air than the summer concentrations. This may be caused by increasing partitioning into the liquid phase as unsaturated zone temperatures decrease. CFC-12 concentrations show no temporal pattern.

DISCUSSION

One of the goals of this field study was to characterize the concentrations of CFC's in

water recharging the saturated zone. Where DO concentrations are relatively high (greater than 5 mg/L), CFC concentrations at the water table appear to be approximately in equilibrium with the modern atmosphere. Even in these well-oxygenated samples, however, CFC concentrations vary widely. The observed range of concentrations in aerobic water-table samples corresponds to uncertainty in ground-water ages determined from CFC-12, CFC-11, and CFC-113 concentrations on the order of ± 4, 7, and 8 years, respectively. This variability in concentrations at the water table presumably affects the uncertainty in ages associated with water samples from deeper in the saturated zone at the Mirror Lake site. This uncertainty is significantly larger than the analytical uncertainty in the laboratory (± 1 yr).

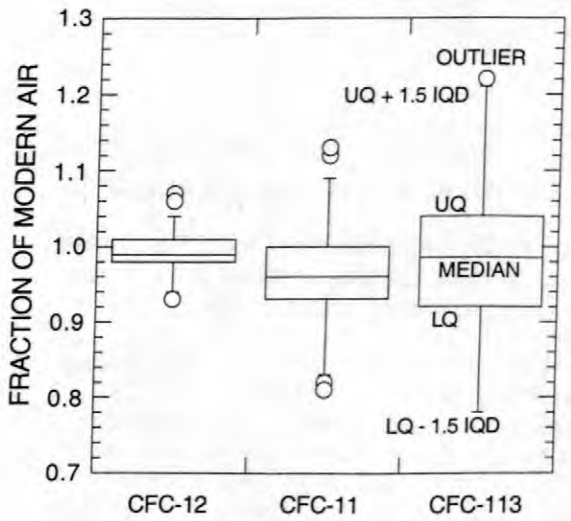

Figure 6. CFC concentrations in soil gas, as a fraction of modern air concentrations, at the Mirror Lake, New Hampshire, research site. (Abbreviations: UQ, upper quartile; LQ, lower quartile; IQD, inner quartile distance = UQ - LQ.)

Samples from piezometers screened near the water table that contain low DO (< 1 mg/L) also contain low CFC's relative to atmospheric equilibrium. In the case of CFC-11 and CFC-113, these compounds are absent from some anaerobic samples. CFC-12 is not reduced as much; concentrations in anaerobic samples are as low as one-third of modern levels. Ground water in the saturated zone that was anaerobic shortly after it was recharged near the water table is likely to have low CFC concentrations. These low CFC concentrations would yield apparent ages for deeper saturated-zone samples that are much larger than the actual time since recharge.

CFC concentrations are also significantly reduced in samples that have DO concentrations ranging from 1 to 4 mg/L. This pattern is not consistent with degradation of CFC's only under anaerobic conditions because these DO levels are not low enough to be considered anaerobic. This pattern of intermediate CFC concentrations in samples having intermediate DO, however, is consistent with a linear mixing model.

The general pattern of the correlation between CFC's and DO suggests a linear mixing model, although there is scatter in the measurements. This mixing model assumes that samples are linear mixtures of two end-members: (a) aerobic water having about 7 mg/L DO and CFC concentrations in equilibrium with the modern atmosphere; and (b) anaerobic water having no oxygen, no CFC-11 or CFC-113, and CFC-12 concentrations about one-third of modern atmospheric-equilibrium levels. That a water sample pumped from a piezometer with a 0.6- to 0.9-m long screen represents a mixture of water is not surprising. Numerous investigators have reported small-scale variations in ground-water quality. Such small-scale variability is supported by limited diffusion in saturated ground water and by large variations in permeability. Other evidence of mixing of waters is the presence of iron (II) and methane in oxygenated samples. With this mixing model, the lower concentrations in low-DO waters are explained not as degradation under low-DO conditions but as degradation under anaerobic conditions, occurring in only a fraction of the total sample volume.

Although anaerobic degradation of CFC-11 and CFC-113 has been observed in the laboratory (Lovely and Woodward, 1992) and the field (Plummer and others, 1998), CFC-12 degradation has only recently been reported for ground waters (Oster and others, 1996). These field results are consistent with the observations reported herein in that CFC-12 is less degraded, but concentrations of CFC-12 are apparently reduced to as little as one-third of modern levels. This amount of CFC-12 loss would cause tens of years differences between apparent and actual ages of modern ground water.

Independent evidence of anaerobic biodegradation is presented by hydrogen gas, methane, and carbon dioxide concentrations measured in several piezometers (Goode, 1998). Hydrogen-gas concentrations can identify the controlling redox processes in anaerobic systems (Lovely and Goodwin, 1988). Results

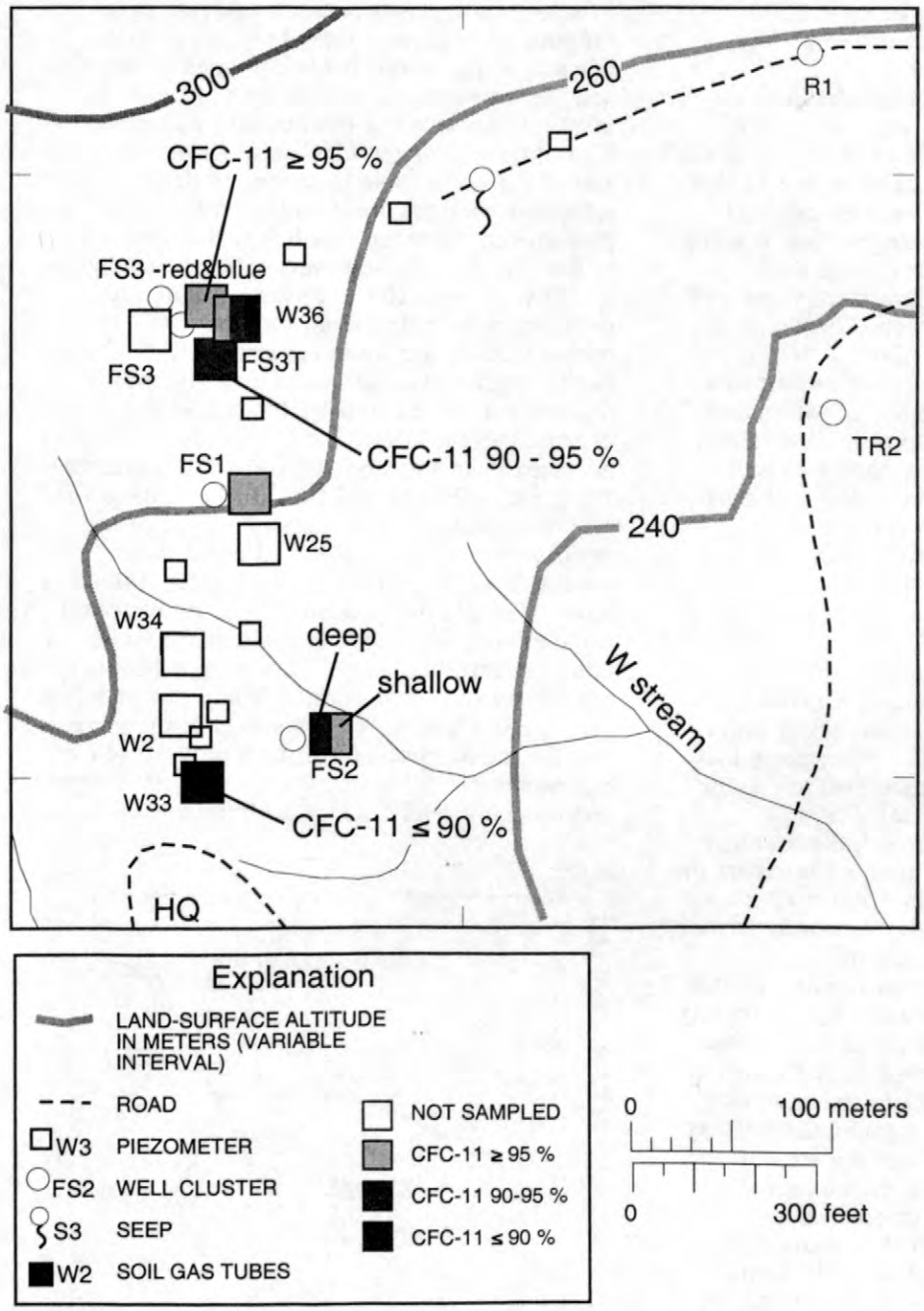

Figure 7. Spatial distribution of CFC-11 concentrations in soil gas, as percentages of modern air concentrations, from sampling tubes at the Mirror Lake, New Hampshire, research site in January 1997.

at anaerobic piezometers indicate methanogenesis is the controlling terminal-electron-accepting-process (TEAP) in piezometer W2, sulfate reduction is the TEAP in W26 and W33, and conditions are intermediate between sulfate reduction and methanogenesis in W25. CFC-11 degradation has been observed in the laboratory for sulfate-reduction and methanogenesis redox conditions (Lovely and Woodward, 1992). Sulfate and iron (II) are present in shallow ground water at Mirror Lake to support sulfate-reduction and iron-reduction reactions (Goode, 1998). Limited laboratory evidence shows that iron (II) may play a role in abiotic degradation of CFC-11 under anaerobic conditions (Lovely and Woodward, 1992).

Overall, CFC-12 concentrations appear to be least affected by anaerobic degradation or contamination. The use of CFC-12 for age-dating ground water is likely to be more robust in the field, particularly for systems in which anaerobic degradation conditions may exist.

However, even CFC-12 may be degraded to levels that cause tens of years differences in ages.

Given the variability in geochemical conditions observed in different water-table piezometers, it is not possible to characterize the distribution of CFC's in recharge in the Mirror Lake drainage basin on the basis of these 31 piezometers. These results suggest that in areas where the shallow water table is anaerobic, CFC's in recharge will be significantly reduced from modern equilibrium levels. Furthermore, concentrations also may be reduced due to anaerobic degradation in micro-environments, even though the apparent redox conditions in pumped samples are not anaerobic. It is likely, however, that these micro-environments will have relatively low permeability and thus may play a less important role in controlling recharge chemistry, which will be weighted toward conditions in higher-permeability zones.

Although the processes causing anaerobic ground water at the Mirror Lake site have not been fully identified, there appears to be a connection between anaerobic conditions and areas of ground-water/surface-water exchange. A local flow system associated with stream loss and flow across a sandy terrace exhibits strong anaerobic conditions. Shattuck (1991) identified an area in the Mirror Lake drainage basin where the water-table gradient is across the W stream. In this area, stream water may enter the subsurface and flow across the sandy terrace to another branch of the W stream. Concentrations of DO and total organic carbon (TOC) in water-table piezometers located nearly parallel to the apparent flow direction suggest the provision of organic carbon to the aquifer by the stream may contribute to the anaerobic redox conditions (fig. 8). Organic carbon may be carried into the aquifer from the stream bottom. DO is consumed by the biologic activity and is only slowly replenished by diffusion downward through the unsaturated zone. This stream loss is not the only factor contributing to anaerobic conditions, because such low-DO environments also are present upgradient of streams (for example, W25 in fig. 8).

SUMMARY

The use of chlorofluorocarbons (CFC's) as age-dating tracers for ground water at the Mirror Lake fractured-rock research site may be limited because concentrations of CFC's in at least some areas are significantly reduced by anaerobic degradation. CFC concentrations in water samples from high-conductivity fractures in schist and granite bedrock indicate ages ranging from greater than 45 years to about 7 years, but the spatial pattern of ages is complex and the youngest measured ages are near the lake at the bottom of the forested watershed. Equilibrium between CFC in the atmosphere and at the water table is needed to date saturated-zone waters. Samples from piezometers screened just below the water table in the glacial drift, however, indicate that CFC-11, CFC-12, and CFC-113 are substantially degraded where dissolved oxygen (DO) concentrations are low. Anaerobic (DO < 0.1 mg/L) conditions existing in a sandy terrace deposit may be caused by biodegradation of organic carbon in infiltrating stream water. Samples from this and other shallow anaerobic zones lack CFC-11 and CFC-113 and have CFC-12 concentrations as low as one-third of modern equilibrium concentrations. Furthermore, several low-DO (0.1 < DO < 4 mg/L) samples have substantially reduced CFC's. As expected, samples with high DO collected at the water table generally contain CFC's near atmospheric-equilibrium concentrations. Many samples plot on a mixing line for CFC's and DO, suggesting that the water sampled can be a mixture of two end members: (1) waters saturated with oxygen and containing CFC's in equilibrium with the

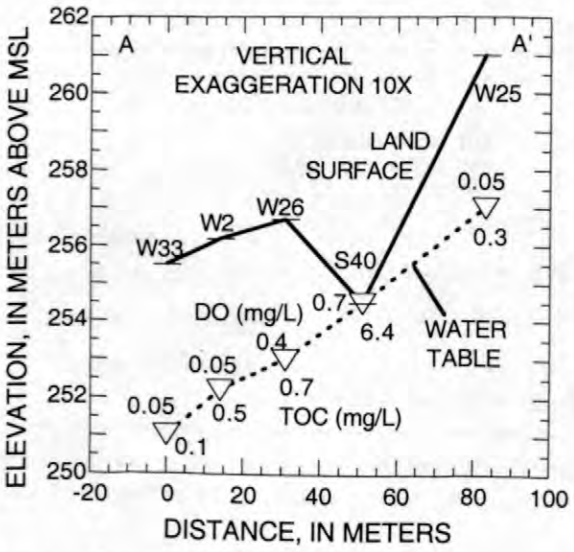

Figure 8. Cross-section A-A' in the lower part of the W stream drainage basin at the Mirror Lake, New Hampshire, research site showing the land surface elevation, water table elevation, and concentrations of dissolved oxygen (DO) and total organic carbon (TOC) in samples from water-table piezometers (indicated by W#). Cross-section location shown in fig. 1. (Abbreviation: MSL, mean sea level)

modern atmosphere, and (2) zero-DO waters containing no CFC-11 or CFC-113 and containing about 1/3 of modern CFC-12. Several samples contain CFC-11 and CFC-113 concentrations higher than those from equilibration with peak atmospheric levels, suggesting a non-atmospheric source. Evidence of active anaerobic biodegradation, which can degrade CFC's, includes high methane, ample iron (Fe-II) and sulfate, and generally low DO. Hydrogen-gas concentrations in anaerobic samples from water-table piezometers are consistent with methanogenesis or sulfate-reduction as the terminal electron-accepting process.

REFERENCES

Busenberg, E., and Plummer, L.N., 1992, Use of chlorofluorocarbons (CCl_3F and CCl_2F_2) as hydrologic tracers and age-dating tools: The alluvium and terrace system of central Oklahoma: Water Resources Research, v. 28, p. 2257-2283.

——— 1996, Concentrations of chlorofluorocarbons and other gases in ground water at Mirror Lake, New Hampshire, *in* Morganwalp, D.W. and Aronson, D.A., eds., U.S. Geological Survey Toxic Substances Hydrology Program—Proceedings of the technical meeting, Colorado Springs, Colo., September 20-24, 1993: U.S. Geological Survey Water-Resources Investigations Rep. 94-4015, p. 151-158.

Drenkard, S., Torgersen, T., Weppernig, R., Stute, M., Farley, K., and Schlosser, P., 1996, Helium isotopes and tritium-helium age dating in the Mirror Lake basin, Grafton County, New Hampshire, *in* Morganwalp, D.W. and Aronson, D.A., eds., U.S. Geological Survey Toxic Substances Hydrology Program—Proceedings of the technical meeting, Colorado Springs, Colo., September 20-24, 1993: U.S. Geological Survey Water-Resources Investigations Rep. 94-4015, p. 159-165

Goode, D.J., 1998, Ground-water age and atmospheric tracers: Simulation studies and analysis of field data from the Mirror Lake site, New Hampshire: Princeton, N.J., Princeton University, Ph.D. thesis, 194 p. <http://pa.water.usgs.gov/projects/frhr/thesis.html>

Harte, P.T., 1992, Regional ground-water flow in crystalline bedrock and interaction with glacial drift in the New England uplands: Durham, University of New Hampshire, M.S. thesis, 147 p.

——— 1997, Preliminary assessment of the lithologic and hydraulic properties of the glacial drift and shallow bedrock in the Mirror Lake area, Grafton County, New Hampshire: U.S. Geological Survey Open-File Report 96-654A, 56 p.

Harte, P.T., and Winter, T.C., 1995, Simulations of flow in fractured crystalline rock in a hypothetical New England setting: Ground Water, v. 33, no. 3, p. 953-964.

——— 1996, Factors affecting recharge to crystalline rock in the Mirror Lake area, Grafton County, New Hampshire, *in* Morganwalp, D.W. and Aronson, D.A., eds., U.S. Geological Survey Toxic Substances Hydrology Program—Proceedings of the technical meeting, Colorado Springs, Colo., September 20-24, 1993: U.S. Geological Survey Water-Resources Investigations Rep. 94-4015, p. 141-150

Hsieh, P.A., Shapiro, A.M., Barton, C.C., Haeni, F.P., Johnson, C.D., Martin, C.W., Paillet, F.L., Winter, T.C., and Wright, D.L., 1993, Methods of characterizing fluid movement and chemical transport in fractured rock, *in* Chaney, J.T., and Hepburn, C., eds., Field Trip Guidebook for northeastern United States, Annual Meeting, October 25-28, 1993, Boston, Mass.: Geological Society of America, v. 2, chap. R, p. R1-R23.

Hsieh, P.A., and Shapiro, A.M., 1996, Hydraulic characteristics of fractured bedrock underlying the FSE well field at the Mirror Lake site, Grafton County, New Hampshire, *in* Morganwalp, D.W. and Aronson, D.A., eds., U.S. Geological Survey Toxic Substances Hydrology Program—Proceedings of the technical meeting, Colorado Springs, Colo., September 20-24, 1993: U.S. Geological Survey Water-Resources Investigations Rep. 94-4015, p. 127-130.

Lovely, D.R., and Goodwin, S., 1988, Hydrogen concentrations as an indicator of the predominant terminal electron-accepting reactions in aquatic sediments: Geochmica et Cosmochimica Acta, v. 52, p. 2993-3003.

Lovely, D.R., and Woodward, J.C., 1992, Consumption of Freon CFC-11 and CFC-12 by anaerobic sediments and soils: Environmental Science and Technology, v. 26, p. 925-929.

Mau, D.P., and Winter, T.C., 1997, Estimating ground-water recharge from streamflow hydrographs for a small mountain watershed in a temperate humid climate, New Hampshire, USA: Ground Water, v. 35, no. 2, p. 291-304.

Oster, H., Sonntag, C., and Munnich, K.O., 1996, Groundwater age dating with

chlorofluorocarbons: Water Resources Research, v. 32, no. 10, p. 2989-3001.
Plummer, L.N., Michel, R.L., Thurman, E.M. and Glynn, P.D., 1993, Environmental tracers for age dating young ground water, in *Regional Ground-Water Quality*, Alley, W.M., ed., New York, Van Nostrand Reinhold, p. 255-294.
Plummer, L.N., Busenberg, E., Drenkard, S., Schlosser, P., Ekwurzel, B., Weppernig, R., McConnell, J.B., and Michel, R.L., 1998, Flow of river water into a karstic limestone aquifer--2. Dating the young fraction in groundwater mixtures in the upper Floridan Aquifer near Valdosta, Georgia,: Applied Geochemistry, v. 13, no. 8, p. 1017-1043.
Semprini, L., Hopkins, G.D., Roberts, P.V., and McCarty, P.L., 1990, In-situ biotransformation of carbon tetrachloride, 1,1,1-trichloroethane, Freon-11, and Freon-113 under anoxic conditions [abs.], Eos, Trans. AGU, San Francisco, American Geophysical Union, p. 1324.
Shapiro, A.M., 1996, Using environmental tracers to estimate matrix diffusion in fractured rock over distances of kilometers: Results from the Mirror Lake site, New Hampshire: Eos, Trans. AGU, v. 77, no. 17, p. S107.
Shapiro, A.M., and Hsieh, P.A., 1996, Overview of research on use of hydrologic, geophysical, and geochemical methods to characterize flow and chemical transport in fractured rock at the Mirror Lake site, New Hampshire, *in* Morganwalp, D.W. and Aronson, D.A., eds., U.S. Geological Survey Toxic Substances Hydrology Program—Proceedings of the technical meeting, Colorado Springs, Colo., September 20-24, 1993: U.S. Geological Survey Water-Resources Investigations Rep. 94-4015, p. 71-80.
Shapiro, A.M., Wood, W.W., Busenberg, E., Drenkard, S., Plummer, L.N., Torgersen, T., and Schlosser, P., 1996, A conceptual model for estimating regional ground-water velocity in bedrock of the Mirror Lake area, Grafton County, New Hampshire, *in* Morganwalp, D.W. and Aronson, D.A., eds., U.S. Geological Survey Toxic Substances Hydrology Program—Proceedings of the technical meeting, Colorado Springs, Colo., September 20-24, 1993: U.S. Geological Survey Water-Resources Investigations Rep. 94-4015, p. 171-177.
Shattuck, P.C., 1991, Shallow water-table response to precipitation and evapotranspiration in an ephemeral stream valley, Woodstock, New Hampshire: Durham, University of New Hampshire, M.S. thesis, 113 p.
Terauds, V.I., Contaldo, G., McCarthy, C.M., and Smith, G.B., 1993, Field and laboratory evidence for *in situ* biotransformation of isopropanol and Freon-11 [abs.]: Ground Water, v. 31, no. 5, p. 850-851.
Tiedeman, C.R., Goode, D.J., and Hsieh, P.A., 1997, Numerical simulation of ground-water flow through glacial deposits and crystalline bedrock in the Mirror Lake area, Grafton County, New Hampshire: U.S. Geological Survey Professional Paper 1572, 50 p.
——— 1998, Characterizing a ground water basin in a New England mountain and valley terrain: Ground Water, v. 36, no. 4, p. 611-620.
Wilson, Alicia, 1991, Distribution of hydraulic conductivity in the glacial drift at Hubbard Brook Experimental Forest, West Thornton, New Hampshire: Hanover, N.H., Dartmouth College, Senior honors thesis, 56 p.
Winter, T. C., 1984, Geohydrologic setting of Mirror Lake, West Thornton, New Hampshire: U.S. Geological Survey Water-Resources Investigations Report 84-4266, 61 p.
Winter, T.C., Eaton, J. S., and Likens, G. E., 1989, Evaluation of inflow to Mirror Lake, New Hampshire: Water Resources Bulletin, v. 25, no. 5, p. 991-1008.
Wood, W.W., Shapiro, A.M., Hsieh, P.A., and Councell, T.B., 1996, Observational experimental and inferred evidence for solute diffusion in fractured granite aquifers: Examples from Mirror Lake Watershed, Grafton County, New Hampshire, *in* Morganwalp, D.W. and Aronson, D.A., eds., U.S. Geological Survey Toxic Substances Hydrology Program—Proceedings of the technical meeting, Colorado Springs, Colo., September 20-24, 1993: U.S. Geological Survey Water-Resources Investigations Rep. 94-4015, p. 167-170.

AUTHOR INFORMATION

Daniel J. Goode, U.S. Geological Survey, Malvern, Pennsylvania (djgoode@usgs.gov)

Eurybiades Busenberg, L. Niel Plummer, Allen M. Shapiro, U.S. Geological Survey, Reston, Virginia

Don A. Vroblesky, U.S. Geological Survey, Columbia, South Carolina

Modifications to the Solute-Transport Model MOC3D for Simple Reactions, Double Porosity, and Age, with Application at Mirror Lake, New Hampshire, and Other Sites

By Daniel J. Goode

ABSTRACT

The U.S. Geological Survey (USGS) three-dimensional solute-transport model MOC3D has been extended to increase the flexibility of first- and zero-order reaction terms to approximate geochemical reactions and to simulate double-porosity exchange and ground-water age. The flexibility of first- and zero-order reaction modeling is increased by allowing the rate coefficients to vary from cell to cell in space and to change in time in a step-wise manner. This flexibility improves the ability of this single-solute model to approximate the effects of multi-species solute interactions during reactive transport. Double-porosity exchange accounts for diffusive exchange of solute mass between water flowing in the aquifer and immobile water. This first-order formulation can approximate the effects of dead-end pores or matrix diffusion. Ground-water age is simulated by a zero-order source term of unit strength that accounts for the aging of water during transport. Using this option, the output from the model is the spatial distribution of age and the volume-weighted age of mixtures such as water in discharging wells. These new capabilities are illustrated by applications at Mirror Lake, N.H., and at other sites where research on transport in ground water has been carried out through the USGS Toxic Substances Hydrology Program.

CAPABILITIES OF MOC3D

This paper summarizes the existing and new capabilities of the U.S. Geological Survey (USGS) three-dimensional solute-transport model MOC3D (Konikow and others, 1996). Full documentation of the modifications described here (in review), are expected to be made available in 1999 on the web at <http://water.usgs.gov/software/moc3d.html>.

Solute-Transport Simulation

MOC3D is a general-purpose computer model developed by the USGS for simulation of three-dimensional solute transport in ground water (Konikow and others, 1996). The model is an update to the widely used USGS two-dimensional solute-transport model (MOC) and is implemented as an optional 'package' for the ground-water flow model MODFLOW (Harbaugh and McDonald, 1996). The model simulates transport processes affecting a single solute in saturated ground water that include:

- Advection - Transport of a dissolved solute at the same rate as the average ground-water flow velocity.
- Diffusion - Spreading of solute from areas of high concentration to areas of low concentration, caused by 'random' molecular motion.
- Dispersion - Diffusion-like spreading of solute that is caused primarily by spatial variability in aquifer properties, which in turn causes spatial variability in transport velocity.
- Retardation^{+} - Reduction in the apparent solute velocity, compared to the ground-water velocity, caused by linear equilibrium sorption on aquifer materials.
- Decay^{+} - Disappearance of solute caused by reactions such as radioactive decay or biodegradation that are proportional to concentration.
- Growth* - Creation (or disppearance) of solute mass caused by reactions that proceed independent of the solute concentration, such as some biodegradation processes.
- Double-porosity exchange* - rate-limited exchange of solute mass between mobile

and immobile phases, for example between fractures and rock matrix.

The symbol * indicates new model capabilities. The symbol + indicates model capabilities that have increased flexibility with the modifications discussed here. MOC3D also accounts for solute sources and sinks associated with a wide range of water sources and sinks.

Growth is a zero-order internal source of solute specified as a mass rate per unit volume of water. This reaction is independent of solute concentration. If the growth rate is specified as negative, this is the rate of loss of solute mass. In this case, the reaction rate changes to zero when the concentration decreases to zero. The growth rate is allowed to vary spatially from cell to cell in the model and to change in time. Sorbed solute may have a separate growth rate.

Double-porosity exchange is a simple model of the diffusive exchange of solute mass between flowing water in the aquifer and immobile or nearly immobile water. Applications include simulation of dead-end pores or porosity within solid grains in granular porous media and matrix diffusion in fractured rock. The mass exchange rate is given by the product of a linear exchange coefficient and the concentration difference between the flowing water and water in the immobile phase. Within the immobile phase, zero-order growth and first-order decay can be simulated.

The retardation factor, which originally could be changed layer by layer, is now allowed to vary spatially from cell to cell in the model. Likewise, the decay rate coefficient, which originally was uniform throughout the model, is now allowed to vary spatially from cell to cell in the model. Furthermore, sorbed solute can decay at a different rate than dissolved solute, and the decay rate can change in time.

Simulation of Ground-Water Age

The volume-weighted average age of ground water in an aquifer may be simulated by use of a standard solute-transport equation with an additional zero-order source term of unit strength (Goode, 1996, 1998). The output from the model is the age, or time since the water entered the aquifer, at all locations. Furthermore, the volumetric average age of a mixed discharge, such as that at a pumping well, is computed. Boundary and initial conditions for the transport equation are similar to the solute transport case. Generally, incoming water is assumed to have age zero, by definition. External sources of ground water, however, such as an adjacent aquifer, can be simulated as water sources with specified age. Most model applications will probably be for steady-state age, in which case the initial condition is not needed, mathematically. Transient age simulations require that the initial age throughout the aquifer be specified.

The primary advantage of this method over particle tracking for modeling ground-water age is that the effects of diffusion, dispersion, and other mixing processes are directly handled through the solute-transport equation. In cases where dispersion is low, results of this method should generally agree with particle tracking. The effect of longitudinal dispersion is limited because age gradients along a streamline are by definition gradual, hence the 'age flux' due to these gradients is also small. Steep age gradients can exist in the direction perpendicular to flow, however, and the resulting transverse diffusion or dispersion can have significant effects on ground-water age (Goode, 1996).

EXAMPLES OF MOC3D CAPABILITIES

The following examples illustrate some of the capabilities of MOC3D for simulation of spatially variable reactions and ground-water age. Comparison of simulation results to analytical solutions for simple test cases, which are not presented here, demonstrate that the numerical methods used can accurately solve the governing equations under restrictive test conditions. The examples here serve to illustrate the use of MOC3D as a general-purpose hydrogeologic tool.

Approximation of Biodegradation Using Spatially Variable Decay Rates

An illustrative simulation uses time- and space-varying decay coefficients to approximate biodegradation of benzene at the Laurel Bay, S.C., research site (Landmeyer and others, 1998). Benzene attenuation depends on decay rates that are generally higher in aerobic (oxygen rich) zones and lower in anaerobic (zero oxygen) zones (fig. 1). In fact, anaerobic biodegradation rates are dependent on the specific terminal-electron-accepting-process (TEAP) controlling the redox state.

The estimated first-order biodegradation decay rates for benzene at Laurel Bay vary from 0.0005 to 0.1 /day (per day), depending on the redox conditions. Fast aerobic degradation takes place outside the anaerobic zones, except at early time when the microbes are assumed to be in low concentrations. As oxygen is consumed, the area of anaerobic redox conditions spreads. Degradation rates are lower in the iron and sulfate reduction zones than in the aerobic zone and are lowest in the methanogenic (carbon dioxide) TEAP zone in the center of the plume.

MOC3D simulation with temporally and spatially varying decay coefficients realistically approximates the extent of benzene migration observed at the site, which can not be modeled successfully by use of a single decay coefficient. A transect through the center of the simulated plume, transverse to the general direction of flow is shown in figure 1. The shaded area indicates the area of iron and sulfate reduction that is modeled using a decay rate of 0.001 /day. In the center of the plume, methanogenesis is occurring, which is modeled using a decay rate of 0.0005 /day. At the time of the illustration, aerobic degradation rates are very high, 0.1 /day. The flexibility to vary the decay rate from cell to cell allows the simulation to capture the rapid degradation of benzene on the outskirts of the plume as well as the elevated concentrations in the center of the plume, where degradation is slow. The simulation with a uniform decay rate of 0.001 /day overestimates benzene concentrations in the aerobic zone and underestimates concentrations in the plume center.

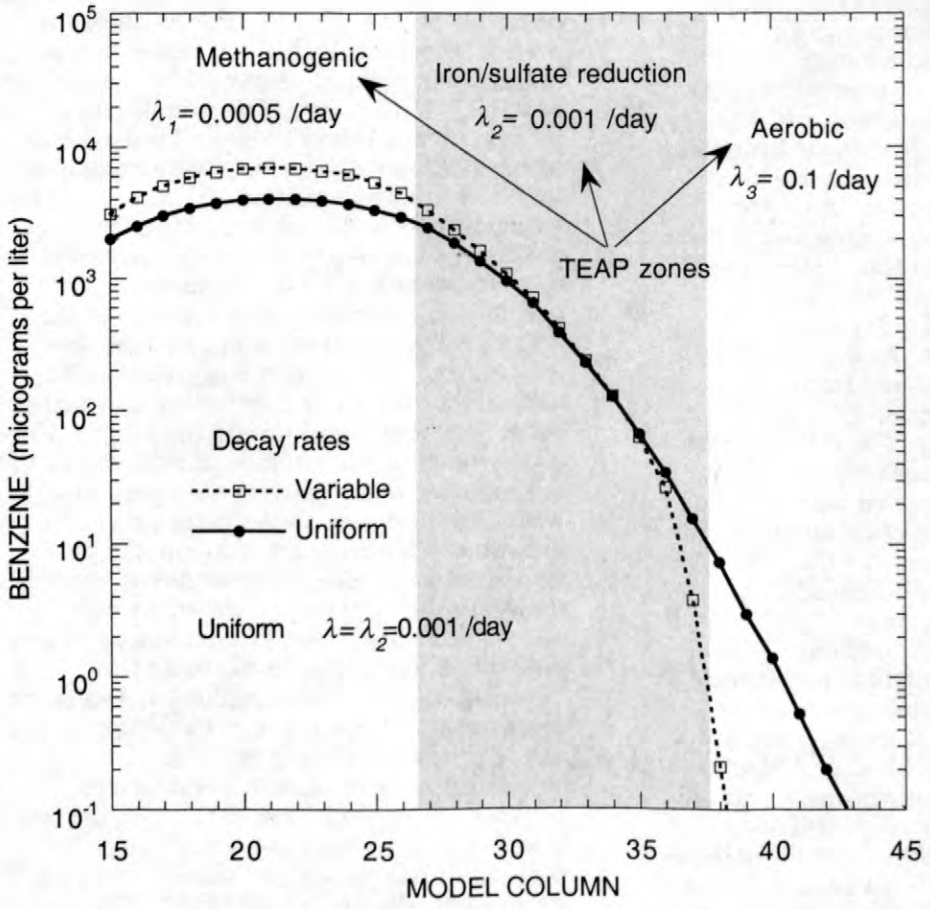

Figure 1. Comparison of benzene concentrations along a transverse transect spanning three terminal-electron-accepting-process (TEAP) zones simulated by use of MOC3D with spatially variable decay rates (λ_1, λ_2, λ_3) to concentrations simulated with a uniform decay rate (λ).

Two-Dimensional Age Distribution in a Mildly Heterogeneous Aquifer

Simulation of the age distribution in a hypothetical aquifer illustrates features of ground-water age in mildly heterogeneous porous media. Intensive field tracer experiments have been conducted at a military reservation on Cape Cod, Mass. LeBlanc and others (1991) describe a natural gradient tracer test conducted over 2 years using nonreactive and reactive tracers in a mildly heterogeneous sand and gravel aquifer. Garabedian and others (1991) analyze the spreading of a nonreactive tracer and estimate asymptotic dispersivities from the temporal growth in the spatial moments of the tracer distribution. Hess and others (1992) compare field and laboratory measurements of hydraulic conductivity and estimate macrodispersivities from theoretical relations.

A hypothetical two-dimensional aquifer is generated that has heterogeneous hydraulic conductivity with spatial statistics similar to those from the Cape Cod tracer test. The turning bands method (Mantoglou and Wilson, 1982; Zimmerman and Wilson, 1989) is used to generate a spatially correlated field of hydraulic conductivity *(K)*. Hydraulic conductivity is assumed to be lognormally distributed with mean 110 m/d (meters per day) (Garabedian and others, 1991) and variance of the natural log of K = 0.24 (Hess and others, 1992). An exponential spatial covariance function is assumed with zero nugget and isotropic correlation length of 2.6 m (meters) (Hess and others, 1992). The grid is 100 m by 20 m and is discretized by 500 x 100 square blocks having $\Delta x = \Delta y$ = 0.2 m. The single realization of K used (fig. 2) reflects the underlying statistical properties: most of the K values are clustered near and below the mean, the size of the high and low zones are larger than individual grid blocks and smaller than the grid dimensions, and only a few isolated zones exhibit $K > 300$ m/d.

The boundary conditions for the steady-state flow model are fixed hydraulic head $h(x = 0) = 0.148$ m; $h(x = 100$ m$) = 0$ m; and no-flow at $y = 0$ and $y = 20$ m. These boundary conditions, along with an assumed porosity of 0.39 (LeBlanc and others, 1991), yield an average velocity of about 0.4 m/d.

The steady-state age distribution (fig. 2b) is more variable than the head distribution and indicates significant persistence of thin 'fingers' of contrasting age. Youngest ages are along a somewhat continuous zone of elevated K in the upper half ($y < 10$ m) of the aquifer. An adjacent zone with older water, however, reflects the effect of a large zone of low K located at about (x,y) = (20 m, 5 m). The resulting large difference in age between closely spaced streamlines persists downstream to the end of the aquifer. The variable traveltimes of different streamlines would be modeled as longitudinal dispersion if the small-scale K variability were not explicitly simulated.

The spatial variability of the steady-state age distribution can also be illustrated by plots of age as a function of distance. In the longitudinal direction, the age generally increases more or less smoothly in the average direction of flow (fig. 3). For much of the domain, the variability in the x-direction is relatively smooth, as illustrated by the transects at y = 7.3 and 13.3 m. The overall rate of increase in age versus x shown for these two transects essentially brackets all longitudinal transects in this simulation. Significantly more variability along x is illustrated near the position of the large low-K zone, as shown by the transect at y = 5.3 m. At this position, the age does not monotonically increase in the mean direction of flow. For example, the water at (x, y) = (45 m, 5.3 m) is about 30 days older than water 5 m further down (the mean) gradient at (x,y) = (50 m, 5.3 m). Close examination of other transects indicates that in this simulation all transects have portions where age decreases in the mean flow direction. This decrease in age in the mean flow direction is due to the difference between the actual streamlines and the mean path.

Variability in age is pronounced in the y-direction, transverse to the mean flow direction (fig. 4). The variability is less at the upstream boundary because by definition the age is uniform at 0 days at $x = 0$. A significant peak of older water develops between x = 10 and 30 m because of the large low-K zone discussed above. Although the y position of this peak shifts due to shifting streamlines, the magnitude of the difference between the age on this peak and on adjacent streamlines persists through the simulated domain.

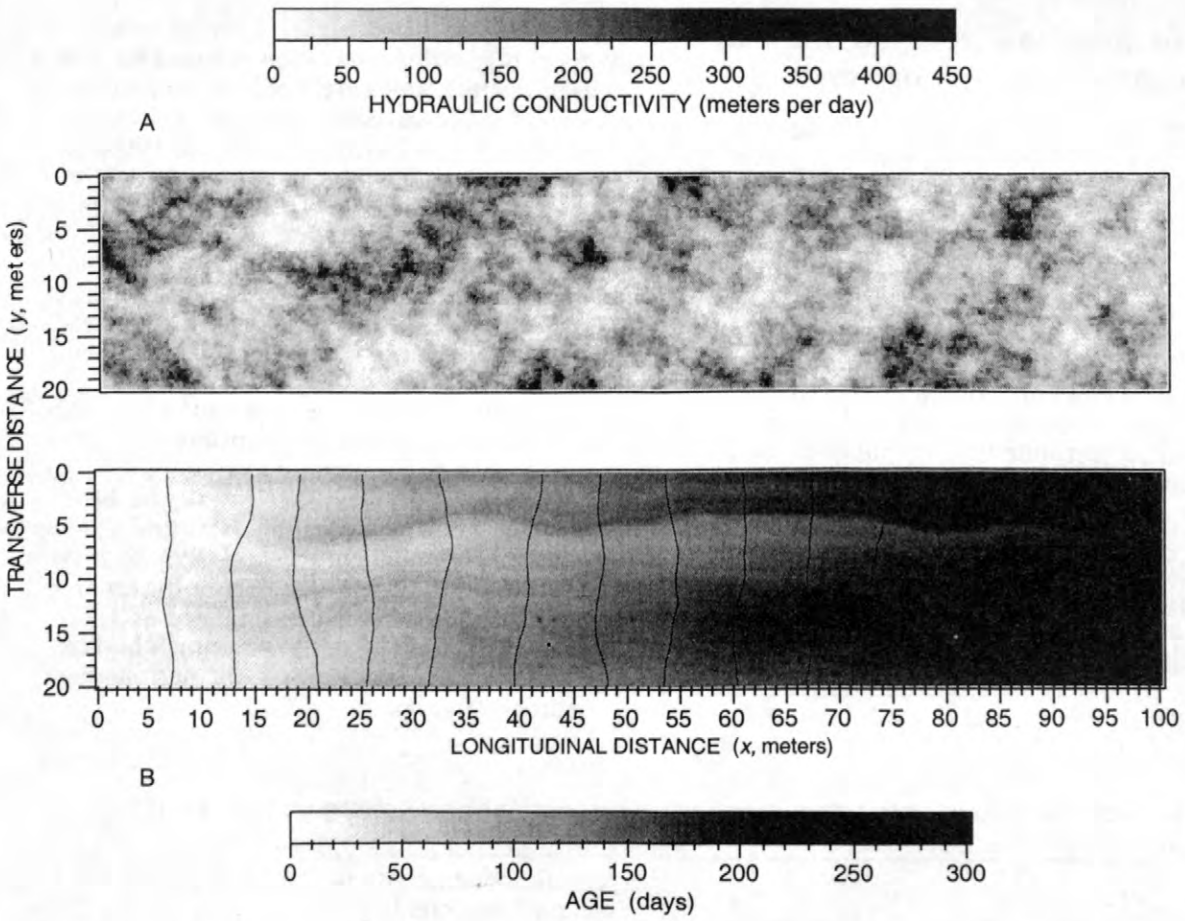

Figure 2. Age simulation in a mildly heterogeneous two-dimensional aquifer: (a) Hydraulic conductivity distribution; (b) Hydraulic head contours (0.01 m interval) and age distribution for advection-only.

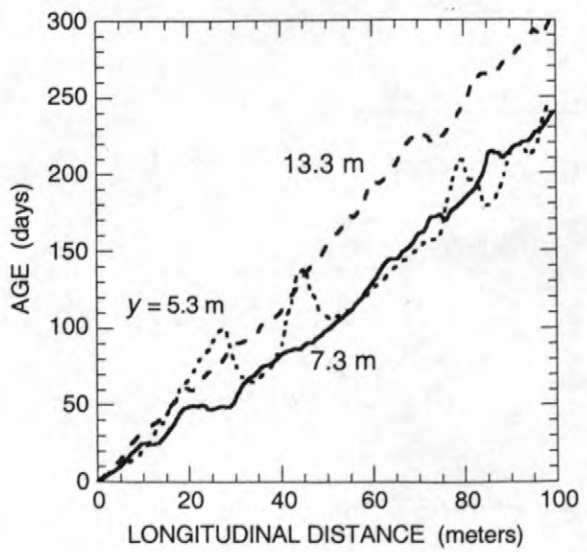

Figure 3. Age variation along transects oriented longitudinal to the average flow direction for a mildly heterogeneous two-dimensional aquifer. The transverse location of each transect is given by *y*.

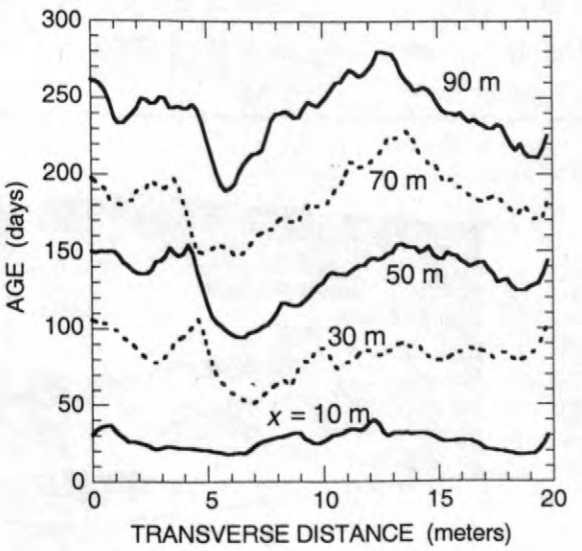

Figure 4. Age variation along transects oriented transverse to the average flow direction for a mildly heterogeneous two-dimensional aquifer. The longitudinal location of each transect is given by *x*.

Age of Samples Pumped from a Heterogeneous Formation

The age of the water in a ground-water system can be estimated from concentrations of environmental tracers in samples pumped from wells. For example, the time since water has been isolated from the atmosphere can be estimated from concentrations of chlorofluorocarbons (CFC's) because atmospheric concentrations have been increasing for about the last 50 years (Plummer and others, 1993). When drawing water from a well, particularly one with a long screened or open interval, the pumped water is a mixture of water from different parts of the aquifer. This mixing can significantly complicate or add uncertainty to estimation of ground-water age. Furthermore, the age of discharging water after a pump is turned on would change in time as water from a larger and larger capture volume enters the well.

A hypothetical simulation illustrates use of the direct age method to model the time-evolution of age in water discharging from a pumping well in a highly heterogeneous formation. This simulation is based on a well-field scale model developed by Paul Hsieh (U.S. Geological Survey, written commun., 1994; see also Hsieh and Shapiro, 1996) of ground-water flow during an aquifer test in fractured rock at Mirror Lake, N.H. Shapiro and Hsieh (1996) provide an overview of research at the site on flow and transport in fractured rock. Aquifer hydraulic properties (table 1) were estimated by calibrating steady-state and transient models of three-dimensional flow during the test. These properties are used here in a model of steady-state age distribution and transient age transport during pumping tests.

The model grid is 22 rows *(y)* x 14 columns *(x)* x 38 layers *(z)*. The grid spacing is uniform throughout the grid with $\Delta x = \Delta y =$ 7.62 m, $\Delta z = 1.5$ m. The highly fractured zones of the bedrock are simulated as 1.5 m thick porous media units with much higher hydraulic conductivity than the surrounding bedrock (fig. 5).

Table 1. Hydraulic properties of a three-dimensional model of a highly heterogeneous formation (Paul A. Hsieh, U.S. Geological Survey, written commun., 1994).

		Hydraulic conductivity (meters per second)	
Hydrogeologic unit	Model layers	Horizontal	Vertical
Glacial drift	1-5	1.8×10^{-6}	1.8×10^{-6}
Bedrock surface	between 5 & 6	--	1.9×10^{-8}
Highly fractured	parts of 11, 22 & 38	5.6×10^{-5}	--
Less fractured	6-38	3.3×10^{-8}	1.9×10^{-7}

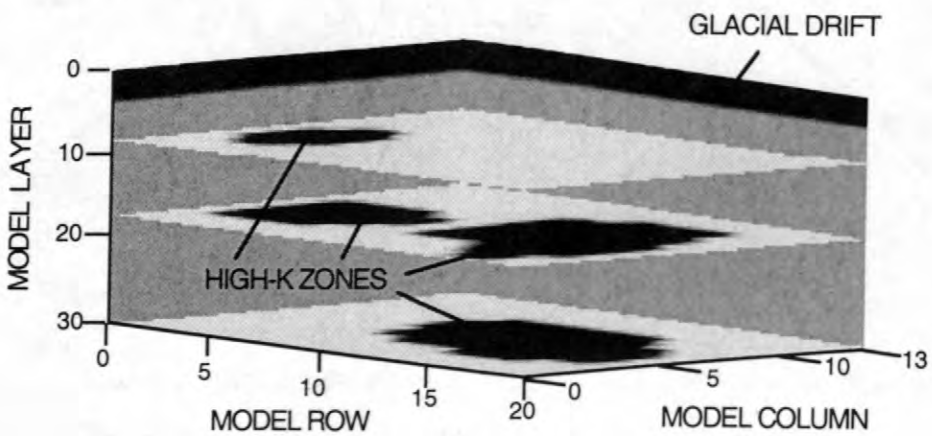

Figure 5. Horizontal hydraulic conductivity (*K*)distribution for three-dimensional highly-heterogeneous case. Glacial drift at top (dark gray) has $K = 1.8 \times 10^{-6}$ m/s (meters per second); four horizontal highly fractured zones (black) occur at three different depths and have $K = 5.6 \times 10^{-5}$ m/s; the remainder of the less-fractured bedrock has $K = 3.3 \times 10^{-8}$ m/s.

The initial steady-state distribution of ground-water age is assumed to represent conditions prior to pumping. The average annual recharge of 368 mm/yr (millimeters per year) is distributed over the top of the model. All other boundaries are no-flow, except the outflow face at y = 168 m, where the head in all model layers is fixed at 0.0. Age is simulated only in the bedrock part of the aquifer and it is assumed that all water inflowing from the glacial drift has age zero. For advection alone, the age distribution is efficiently computed by use of particle tracking. For the age simulation, the bedrock porosity is assumed to be 0.001, which corresponds to the fracture volume per unit volume of rock.

Maximum ages are at the bottom of the system, where less-fractured bedrock underlies the highly-fractured zones (figs. 6-8). Flow is generally downward from the glacial drift into the horizontal fracture zones and then laterally out along the outflow face (front face in fig. 6; right end of cross-section in fig 7). The fracture zone at the bottom of the model is shown as the area of light-gray near well 3 in fig. 6. The maximum ages are diluted downgradient from the dark-gray area beneath well 2 by much younger waters in the fracture flow system. Resulting outflow face ages are high only at the very bottom of the aquifer (fig. 8).

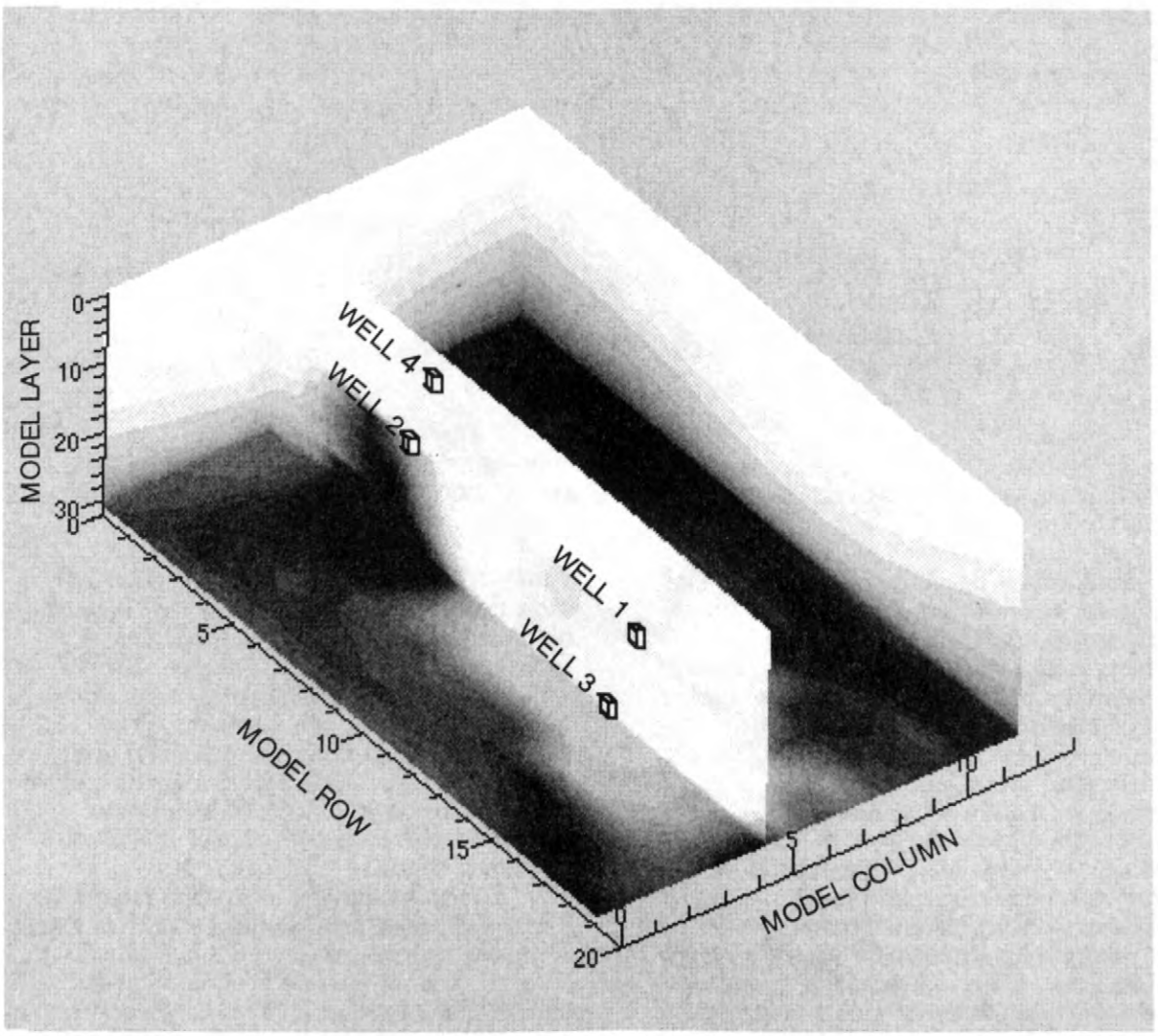

Figure 6. Results of direct simulation of steady-state ground-water age in a highly heterogeneous fractured bedrock. Hydraulic properties are shown in fig. 5 and summarized in table 1. Also shown are locations of wells that are not pumping in this simulation. The grayscale corresponds to age, ranging from less than 3 years (white) to greater than 700 years (black).

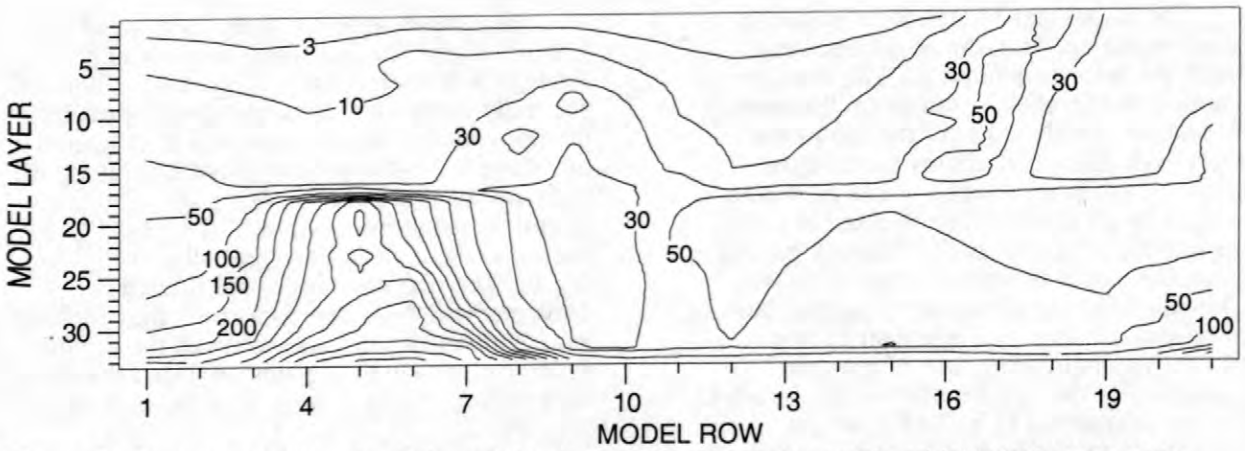

Figure 7. Results of direct simulation of steady-state ground-water age in a highly heterogeneous fractured bedrock in a *y-z* cross-section along the middle of the model at column 7 ($x = 53$ m), variable contour intervals in years.

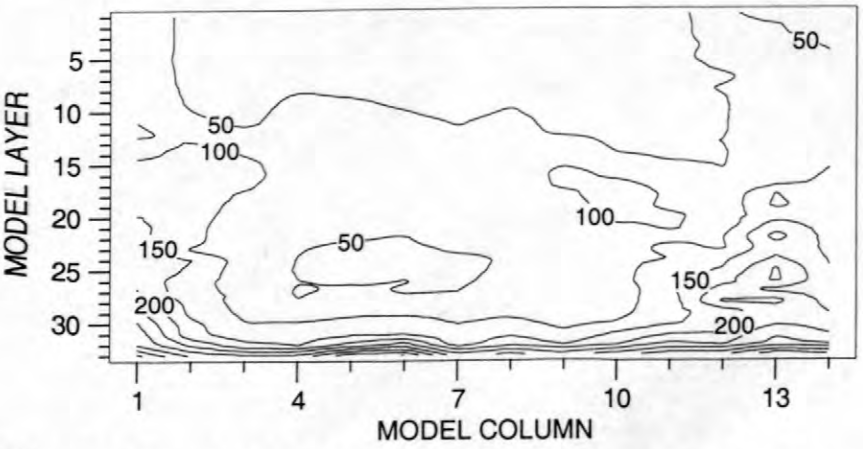

Figure 8. Results of direct simulation of steady-state ground-water age in a highly heterogeneous fractured bedrock in a *x-z* cross-section at the outflow end of the model along row 21 ($y = 160$ m), contour intervals are 50 years.

Ground-water age in pumped samples is evaluated for four fracture-zone well locations. In each case, the initial age distribution is that from the previous steady-state age simulation. A steady-state flow field is generated for each pumping scenario by imposing no-flow boundaries on the model bottom and all four sides. The top layer of the overburden is modeled as a fixed-head boundary from which all of the flow to the well is ultimately derived. Each well is pumped separately at a rate of 10.6 L/min (liters per minute).

The evolution of ground-water age of pumped samples is different for each well (fig. 9). Wells 1 and 2 are in upgradient fracture zones near mid-depth in the model. The age of water in well 1, which is closer to the outflow, increases sharply at early time from about 37 years to more than 40 years, levels off near 43 years, and appears to be gradually increasing after 10 hours of pumping. Well 2 pumps from a separate fracture zone at the same depth, and water from this well is initially older than that at well 1, even though it is farther from the outflow. The age of water in well 2 drops, but not as sharply in time, from 54 years to less than 46 years and then increases to about 56 years at the end of the simulation. The small-scale fluctuations in the age are numerical artifacts of the discrete method-of-characteristics model (Konikow and other, 1996).

Ground-water age in samples from wells 3 and 4 decrease logarithmically in time from the initial ages (fig. 9). Well 3 is located (fig. 5) in the bottom fracture zone and has the oldest initial age, over 200 years. However, the age decreases sharply to less than 120 years after 2 hours of pumping and is less than 100 years after 10 hours. Well 4 shows a similar pattern, but at much younger ages. This well is located in the top fracture zone, much closer

to the recharge source in the overburden. Ages in samples from well 4 decrease from more than 12.5 years initially to less than 8.5 years after 10 hours.

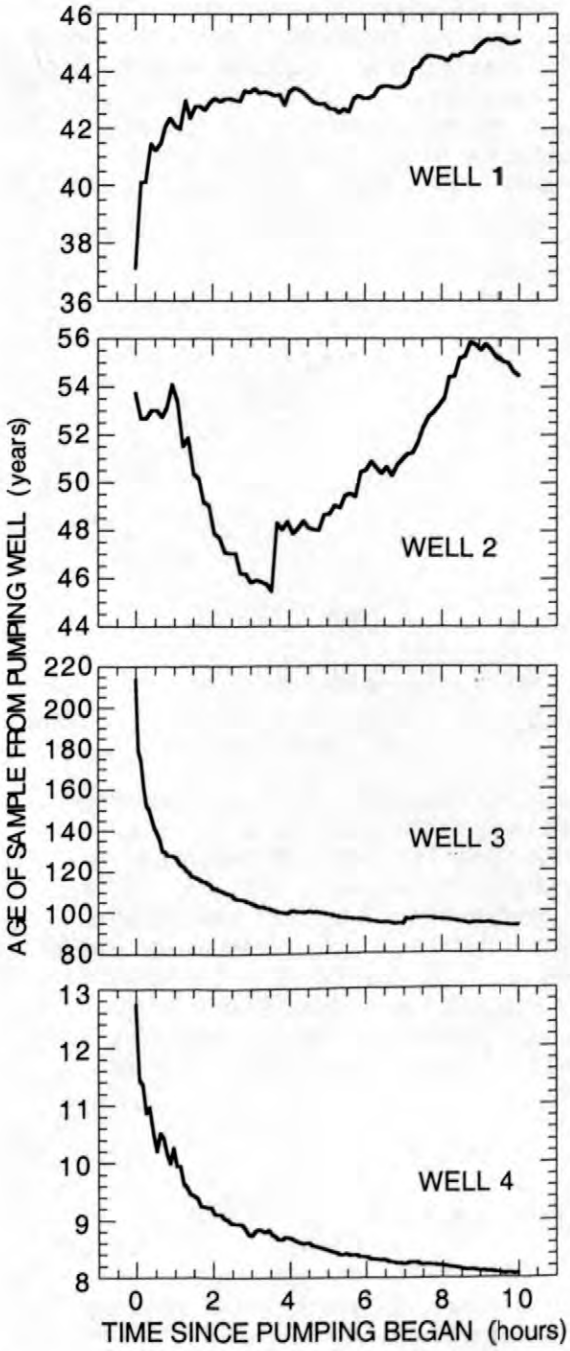

Figure 9. Sample age as a function of pumping time in a highly heterogeneous aquifer. Age transport to the pumping well is simulated with four different steady-state flow models having only the well of interest pumping. Locations for each well are shown in fig. 6.

Matrix Diffusion of Age in a Single Fracture

Matrix diffusion can be an important aspect of transport of solutes in ground water, particularly in fractured-rock settings (Shapiro, 1996). Matrix diffusion generally refers to diffusive exchange between high-permeability fractures or fracture zones and low-permeability rock matrix, whether much less fractured or unfractured. Water flow is primarily in the fractures, and the rock matrix is usually assumed to be impermeable. However, diffusive exchange of solutes between the flowing water in the fractures and the immobile water in the rock matrix can have significant effects on solute migration (Wood and others, 1996).

The age transport concept can be used to evaluate the effect of matrix diffusion on steady-state age distribution. Consider age transport in a fractured-rock system, which is modeled as advection and dispersion in a continuum of connected fractures, coupled with diffusion to and from the rock matrix. Normally, diffusion of water itself is ignored because the properties of individual water molecules are identical. In the case of age, however, diffusion of water changes the distribution of water ages. Under steady-state conditions, an integrated age conservation equation for the rock matrix has only three components: (1) accumulation of age (zero for steady state), (2) boundary flux, and (3) production of age by aging. Because (1) is zero in steady state, (2) and (3) must balance. Hence, the net boundary flux of age out of the rock matrix into the fracture is equal to the total age production rate in the matrix, which is the rock porosity. The rate of aging in the fracture and the added age flux from the rock matrix is equivalent to the aging rate of a single-porosity system in which the porosity is the sum of the fracture and rock matrix porosity.

Thus, the age distribution is identical to that of a single continuum system in which the porosity is the sum of the fracture and rock matrix porosities (Goode, 1998). The apparent velocity is 'retarded' compared to the velocity of water in the fractures alone, and the rate of dispersive spreading is likewise reduced by the total porosity. Of course, this analysis assumes that the age distribution is in steady state. Because of the slow rate of diffusion in rock, disequilibrium between the age production in the rock and diffusion out into the fracture may exist for millions of years.

The effect of matrix diffusion on transient age transport is examined here for a one-dimensional flow system using the double-porosity exchange process in MOC3D. A 1-m long column is discretized with 10 cells (Δx = 0.1 m). Imposed fixed-head boundary conditions yield a specific discharge of 1 m/d, and the porosity of 0.01 results in a uniform velocity of 100 m/d. This porosity represents the high-permeability fractures in the rock column. Ignoring dispersion and matrix diffusion, the steady-state age at x = 9.5 m is simply the advective traveltime, 0.095 day.

At steady state, the effect of matrix diffusion is an apparent increase in porosity, from that of the fractures alone to the sum of fracture and matrix porosity. In this case, the apparent traveltime to x = 9.5 m, and the steady-state age, is 0.95 day or an increase by an order-of-magnitude. This increase corresponds directly to the increase in porosity from 0.01 to 0.10. However, the rate at which this steady state is approached depends on the double-porosity exchange rate.

The linear exchange coefficient (β) is generally proportional to the diffusion coefficient (D_m) divided by a characteristic diffusion length (b) squared (Bibby, 1981):

$$\beta \propto \frac{D_m}{b^2} \quad . \qquad (1)$$

For example, for the case of planar fractures, the linear exchange coefficient corresponding to a one-node finite-difference approximation is given by:

$$\beta = \frac{1}{2}\frac{D_m}{b^2} \quad , \qquad (2)$$

where b is the block half-thickness. This simple linear model of matrix diffusion is strictly accurate only for relatively small diffusion distances. However, this kinetic exchange model can be considered a first-order approximation of the effect of exchange between high-permeability and much-lower-permeability portions of a flow system, whether limited strictly to diffusion or not.

The initial age is assumed to be zero throughout the aquifer. At early time, water at all locations ages as simulation time progresses (fig. 10). If the linear exchange coefficient is $\beta = 10^{-4}$ /day, the age temporarily stabilizes at a level corresponding to the traveltime in the fractures alone, 0.095 day (fig. 10). Eventually, however, the age in the matrix builds up to such high levels that the diffusive age flux into the fracture is sufficient to increase the age in the fractures and ultimately reach the steady-state value corresponding to the traveltime computed from the total porosity, 0.95 day. The magnitude of the linear exchange coefficient controls the time at which matrix diffusion has a significant effect on simulated ages in the fracture. For very high β, the initial plateau is not present because the fracture and matrix ages are virtually in equilibrium at all times (fig. 10).

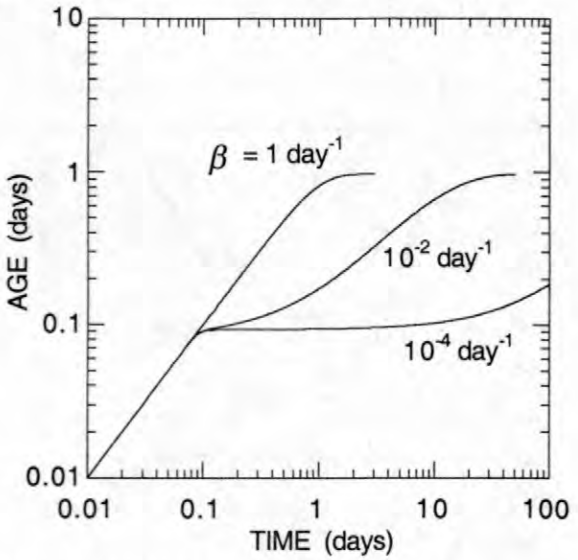

Figure 10. Age at x = 9.5 m from the inflow boundary of a one-dimensional rock column having fracture porosity 0.01, rock matrix porosity 0.09, and specific discharge 1 m/day. The initial condition is age = 0 at all locations. Age is shown as a function of simulation time for three values of linear exchange coefficient (β) characterizing the rate of mass transfer by diffusion between the flowing water in the fractures and the immobile water in the rock matrix.

SUMMARY

MOC3D can simulate transport of a single solute in saturated ground water under a wide range of conditions. New capabilities of the model include a zero-order internal source term that can vary in space and time; double-porosity exchange, which can approximate matrix diffusion and other rate-limited exchange processes; and simulation of ground-water age. Improved flexibility allows the retardation and first-order decay model components to more accurately approximate

biodegradation and other reactions that change in space and time due to changing geochemical conditions.

Example simulations demonstrate uses of MOC3D for transport simulation. These examples are drawn from research conducted at Laurel Bay, S.C., Cape Cod, Mass., and Mirror Lake, N.H., research sites under the U.S. Geological Survey Toxic Substances Hydrology Program. The spatially variable decay rate coefficients can be used to approximate biodegradation of organic contaminants in plumes having spatially variable biogeochemistry. The age transport model can account for mixing of waters of different ages caused by diffusion and dispersion, or by mixing in pumping wells. These new and extended capabilities improve the usefulness of MOC3D for simulation of solute transport in aquifers having variable hydraulic and geochemical conditions.

REFERENCES

Bibby, Robert, 1981, Mass transport of solutes in dual-porosity media: Water Resources Research, v. 17, no. 4, p. 1075-1081.

Garabedian, S.P., LeBlanc, D.R., Gelhar, L.W., and Celia, M.A., 1991, Large-scale natural gradient tracer test in sand and gravel, Cape Cod, Massachusetts 2. Analysis of spatial moments for a nonreactive tracer: Water Resources Research, v. 27, no. 5, p. 911-924.

Goode, D.J., 1996, Direct simulation of groundwater age: Water Resources Research, v. 32, no. 2, p. 289-296.

——— 1998, Ground-water age and atmospheric tracers: Simulation studies and analysis of field data from the Mirror Lake site, New Hampshire: Princeton, N.J., Princeton University, Dept. Civil Engineering and Operations Research, unpublished Ph.D. thesis, 194 p. <http://pa.water.usgs.gov/projects/frhr/thesis.html>

Harbaugh, A.W., and McDonald, M.G., 1996, User's documentation for MODFLOW-96, an update to the U.S. Geological Survey modular finite-difference ground-water flow model: U.S. Geological Survey Open-File Report 96-485, 56 p.

Hess, K.M., Wolf, S.H., and Celia, M.A., 1992, Large-scale natural gradient tracer test in sand and gravel, Cape Cod, Massachusetts 3. Hydraulic conductivity variability and calculated macrodispersivities: Water Resources Research, v. 28, no. 8, p. 2011-2027.

Hsieh, P.A., and Shapiro, A.M., 1996, Hydraulic characteristics of fractured bedrock underlying the FSE well field at the Mirror Lake site, Grafton County, New Hampshire, *in* Morganwalp, D.W. and Aronson, D.A., eds., U.S. Geological Survey Toxic Substances Hydrology Program—Proceedings of the technical meeting, Colorado Springs, Colo., September 20-24, 1993: U.S. Geological Survey Water-Resources Investigations Rep. 94-4015, p. 127-130.

Konikow, L.F., Goode, D.J., and Hornberger, G.Z., 1996, A three-dimensional method-of-characteristics solute-transport model (MOC3D): U.S. Geological Survey Water-Resources Investigations Report 96-4267, 87 p.

Landmeyer, J.E., Chapelle, F.H., Bradley, P.M., Pankow, J.F., Church, C.D., and Tratnyek, P.G., 1998, Fate of MTBE relative to benzene in a gasoline-contaminated aquifer (1993-98): Ground Water Monitoring and Remediation, v. 18, no. 4, p. 93-102.

LeBlanc, D.R., Garabedian, S.P., Hess, K.M., Gelhar, L.W., Quadri, R.D., Stollenwerk, K.G., and Wood, W.W., 1991, Large-scale natural gradient tracer test in sand and gravel, Cape Cod, Massachusetts 1. Experimental design and observed tracer movement: Water Resources Research, v. 27, no. 5, p. 895-910.

Mantoglou, A., and Wilson, J.L., 1982, The turning bands method for simulation of random fields using line generation by a spectral method: Water Resources Research, v. 18, no. 5, p. 1379-1394.

Plummer, L. N., Michel, R.L., Thurman, E.M. and Glynn, P.D., 1993,. Environmental tracers for age dating young ground water, *in* Alley, W.M., ed., *Regional Ground-Water Quality* , New York, Van Nostrand Reinhold, p. 255-294.

Shapiro, A.M., 1996, Using environmental tracers to estimate matrix diffusion in fractured rock over distances of kilometers: Results from the Mirror Lake site, New Hampshire [abs.]: Eos, Transactions American Geophysical Union, v. 77, no. 17, p. S107.

Shapiro, A. M., and Hsieh, P.A., 1996, Overview of research on use of hydrologic, geophysical, and geochemical methods to characterize flow and chemical transport in fractured rock at the Mirror Lake site, New Hampshire, *in* Morganwalp, D.W. and Aronson, D.A., eds., U.S. Geological Survey Toxic Substances Hydrology Program—Proceedings of the technical

meeting, Colorado Springs, Colo., September 20-24, 1993: U.S. Geological Survey Water-Resources Investigations Rep. 94-4015, p. 71-80.

Wood, W.W., Shapiro, A.M., Hsieh, P.A., and Councell, T.B., 1996, Observational experimental and inferred evidence for solute diffusion in fractured granite aquifers: Examples from Mirror Lake Watershed, Grafton County, New Hampshire, *in* Morganwalp, D.W. and Aronson, D.A., eds., U.S. Geological Survey Toxic Substances Hydrology Program—Proceedings of the technical meeting, Colorado Springs, Colo., September 20-24, 1993: U.S. Geological Survey Water-Resources Investigations Rep. 94-4015, p. 167-170.

Zimmerman, D.A., and Wilson, J.L., 1989, Description and user's manual for TUBA—A computer code for generating two-dimensional random fields via the turning bands method: Socorro, New Mexico Institute of Mining and Technology, unpublished report, Geosciences Department.

AUTHOR INFORMATION

Daniel J. Goode, U.S. Geological Survey, Malvern, Pennsylvania (djgoode@usgs.gov)

Simulation of Mass Transport Using the FracTran98 Module of FracSys2000

By David M. Diodato

ABSTRACT

FracTran98 is the transport module of FracSys2000, a new suite of simulation tools for modeling flow and transport in multiphase or single phase, fractured or unfractured porous media. FracTran98 simulates transport by advection alone or by coupled advection-dispersion in a one- or two-phase flow field. An optional immobile "free" phase may be present. Linear kinetic partitioning between the mobile phases and the immobile free and solid phases is supported. An example of toluene contamination in the unsaturated zone shows that sluggish kinetics can substantially extend the time required for remediation in porous media. FracSys2000 also includes a flow module (FracFlow96), and a visualization module (FracVis98).

INTRODUCTION

FracSys2000 (FS2K) is a four-dimensional numerical modeling package for simulation of multiphase fluid flow and single component transport in fractured geologic media. It consists of three modules: FracFlow96, a multiphase flow simulator; FracTran98, a single component multiphase transport simulator; and FracVis98, a scientific visualization and animation utility.

The principle of parsimony is a guiding philosophy for the methods used in FS2K, using the fewest possible parameters sufficient to describe the physical and chemical processes at spatial and temporal scales commonly encountered in field problems.

FracFlow96 is written in Fortran90 and has been executed under DOS, Windows95, WindowsNT, and Cray UNICOS. Capabilities, limitations, model tests, and an example application of FracFlow96 to a Yucca Mountain test problem are described in Diodato (1997).

FracVis98 is a Windows95/WindowsNT utility for visualization and animation of three- and four-dimensional data. It is designed to be used for visualization of discrete volumetric data gridded into arbitrary hexahedra. Data requirements include grid specification (three-dimensional nodal positions and lists of nodes defining each hexahedral element), and a list of values of the variable to be displayed for each element for each time step. In the input files to FS2K, a flag can be set to either 0, 1, 2, or 3. 0 indicates that no visualization file should be produced. 1, 2, or 3 indicate that visualization files of gas pressure, gas phase concentrations, or liquid phase concentrations, respectively, should be generated. FracVis98 is based on the OpenGL applications programming interface. It is written in C and C++ and makes use of the Microsoft foundation classes (MFC). It has been executed on Windows95 and WindowsNT platforms.

The purpose of this document is to describe the conceptual and mathematical models comprising FracTran98. In addition, the numerical methods used are briefly outlined. FracTran98 is written in Fortran90 using Fortran95 extensions. FracTran98 transports a single component in either a single phase or multiphase hydrogeologic regime. Phase partitioning between liquid, gas, free, and solid phases is accommodated through linear kinetic partitioning functions.

FracTran98 CONCEPTUAL MODEL AND SIMULATED PROCESSES

FracTran98 is based on a conceptual model of a preferentially water wet (hydrophyllic) geologic environment. The wetting order on the solid rock is liquid, free phase, gas. This conceptual model is applicable to a broad class of compounds

commonly encountered in contaminant hydrogeology.

The geologic environment is taken to be static in space and time. Any extant free phase is assumed to be at residual saturation without phase continuity. As such, potential flow, and advective and dispersive fluxes of the free phase, are not simulated. Advection, mechanical dispersion, and molecular diffusion are simulated in the liquid and gas phases.

FracTran98 simulates interphase partitioning through linear kinetic rate laws. Figure 1 illustrates

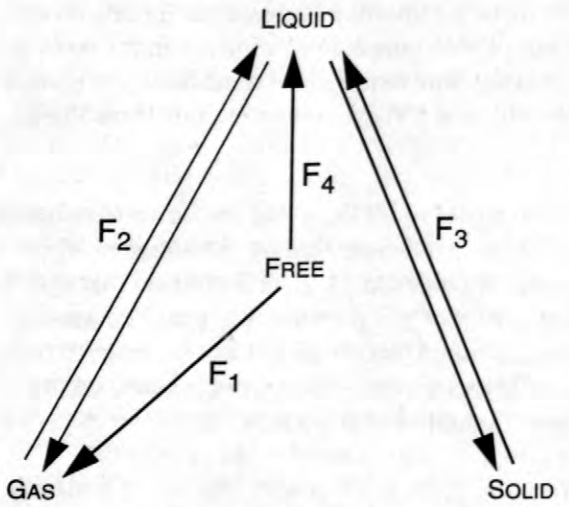

Figure 1. Phase partitioning phenomena simulated by FracTran98.

the phase partitioning functionality of FracTran98. GAS, LIQUID, SOLID, and FREE represent chemical species mass in each of the phases. Interphase partitioning functions are identified by F_1, F_2, F_3, and F_4. In summary, FracTran98 simulates:

1. Advection, mechanical dispersion, and molecular diffusion in the liquid and gas phases;
2. Linear kinetic interphase partitioning by the following processes:
   - Volatilization from the free phase to the gas phase (F_1),
   - Condensation/volatilization between the liquid phase and the gas phase (F_2),
   - Adsorption/desorption between the liquid phase and the solid phase (F_3), and
   - Dissolution from the free phase into the liquid phase (F_4).

MASS CONSERVATION EQUATIONS

After de Marsily (1986), the equations for conservation of mass for the liquid and gas phases with transport due to advection, dispersion, and diffusion, are written as

$$\nabla\bullet(\phi S_g D\nabla C_g - q_g C_g) = \phi S_g \frac{\partial C_g}{\partial t} \text{ and}$$
$$\nabla\bullet(\phi S_l D\nabla C_l - q_l C_l) = \phi S_l \frac{\partial C_l}{\partial t}, \quad (1)$$

where

ϕ	is porosity,
S	is phase saturation,
D	is phase-specific hydrodynamic dispersion, and includes diffusion on the main diagonal,
C	is phase concentration,
q	is Darcy flux, and
g,l	indicate gas and liquid phases.

Equations of Interphase Mass Transfer

In general, mass transfer functions are written as source-sink terms Q in the transport equations, where Q has units of $ML^{-3}t^{-1}$. Thus, for phase p, a system with a single source-sink would be written as

$$\nabla\bullet(\phi S_p D\nabla C_p - q_p C_p) = \phi S_p \frac{\partial C_p}{\partial t} + Q_p. \quad (2)$$

After de Marsily(1986), a generic linear reversible kinetic rate law for Q may be written as

$$Q_p = K(C_p^o - C_p), \quad (3)$$

where

K is a nonnegative linear kinetic rate constant, taken to range from 0 to 1, and

C_p^o is equilibrium concentration in the phase.

Q_p describes the deviation from equilibrium due to K. For K=0, no phase exchange takes place. For K=1, the system behaves as an equilibrium system

(if C_p is zero). As C_p rises from zero, the mass transfer rate declines, reaching zero when C_p equals the equilibrium concentration. The user must determine the appropriate values of the linear kinetic rate constant for each partitioning process. The remaining task is to define the equilibrium concentrations C_p^o for each interphase transfer process. The derivation of the partitioning functions for the chemical partitioning processes will not be considered in detail here. For further discussion, the reader is referred to Baehr (1984), Corapciouglu and Baehr (1987), and Looney (1985). FracTran98 allows for four interphase mass transfer processes, F_1 through F_4. Here we will consider each one in turn.

Volatilization from the free phase to the gas phase

The processes of volatilization between the free phase to the gas phase is described by F_1. The rate law for concentration in the gas phase due to free phase volatilization is

$$\frac{\partial F_1}{\partial t} = K_1(C_{g1}^{\circ} - C_g). \tag{4}$$

Equilibrium gas phase concentration can be determined by application of Raoult's Law (after Corapciouglu and Baehr, 1987). Raoult's Law states

$$p_{g_i} = \chi_i p^o, \tag{5}$$

where

p_{g_i} is partial pressure of component i in the gas phase,

χ_i is mole fraction of component i, and

p^o is vapor pressure of the pure compound

(Domenico and Schwartz, 1990). For a single component system, $\chi_i \equiv 1$ and $p_{g_i} = p^o$. Using the ideal gas law,

$$p_{g_i} = \frac{nRT}{V} = \frac{C_g RT}{\omega^{\circ}}, \tag{6}$$

where n is number of moles. Equating (5) and (6) and rearranging gives

$$C_{g1}^{\circ} = \frac{\omega^{\circ} p^o}{RT}, \tag{7}$$

where

C_{g1}° is the equilibrium vapor concentration,

ω° is the molecular weight of the species in solution,

R is the universal gas constant, and

T is temperature.

The term on the right side of (7) will be referred to as K_{RA}. At this point it is worthwhile to discuss units. The fundamental units in FS2K are mass, length, and time. FS2K adheres to the Systemè International (SI) meter-kilogram-second (MKS) convention for all basic units. Thus, concentrations in each phase are expressed in units of kg m^{-3}. The user is responsible for the specification of K_{RA} in units of kg m^{-3}. For toluene in air at 25 °C, K_{RA} is 0.133 kg m^{-3} (Corapciouglu and Baehr, 1987).

Condensation-volatilization between the liquid phase and the gas phase

The processes of condensation and volatilization can occur between the liquid phase and the gas phase. These phenomena are accommodated through process F_2. For concentration in the gas phase due to volatilization or condensation from the liquid phase, the rate law is written as

$$\frac{\partial F_2}{\partial t} = K_2(C_{g2}^o - C_g). \tag{8}$$

Equilibrium vapor partial pressures above a liquid containing a volatile solute can be described by Henry's Law. For a vapor phase behaving as an ideal gas, Henry's Law has a high degree of accuracy for low solubility, nonelectrolytic constituents (Noggle, 1985 in Corapciouglu and Baehr, 1987). The Henry's Law coefficient reflects the difference in source strength relative to the pure substance resulting from aqueous phase solubility. It is written here as

$$K_H = K_{RA}/S_{sol}, \tag{9}$$

where S_{sol} is the equilibrium solubility of the compound in water. (The solubility of toluene in water at 25 °C is 0.515 kg m^{-3} [EPA RREL Treatability Database, revision 5.0].) Thus, the equilibrium expression for gas phase concentration due to volatilization can be written as

$$C^o_{g2} = K_H C_l. \tag{10}$$

Adsorption-Desorption

Adsorption-desorption between the liquid phase and the solid phase is accommodated through process F_3. For concentration on the soil phase due to adsorption or desorption, the rate law is written as

$$\frac{\partial F_3}{\partial t} = K_3(C^o_s - C_s). \tag{11}$$

A linear isotherm relating liquid phase concentrations to mass adsorbed on a solid phase can be written as (Domenico and Schwartz, 1990)

$$C'_s = K_d C_l, \tag{12}$$

where

C'_s is mass adsorbed on the solid phase per unit mass of solid phase, and

K_d is the distribution coefficient ($m^3\ kg^{-1}$).

Because K_d is highly dependent on solid surface properties, redox state, pH, and availability of alternative solution phases such as ligands or colloids (Looney, 1985), it is important to evaluate the applicability of any reported K_d value in the context of the particular problem to be simulated.

Because (12) yields the mass of the transported species per unit mass of the solid phase, it is desirable to modify the expression to give mass on the solid phase per solid volume as

$$C^o_s = \rho_b C'_s = \rho_b K_d C_l\ . \tag{13}$$

For homogeneous mineralogy, the dry mass basis bulk density of the volume can be specified as $\rho_b = (1-\phi)\rho_s$, where ρ_s is the mineral density.

Dissolution between the free phase and the liquid phase

The process of dissolution from the free phase to the liquid phase is described by F_4. The rate law for liquid phase concentration due to free phase dissolution is

$$\frac{\partial F_4}{\partial t} = K_4(C^o_l - C_l)\ . \tag{14}$$

Equilibrium liquid concentrations are described by the equilibrium solubility limit, S_{sol}, of the free phase at the thermodynamic state of interest. Thus, the equilibrium liquid concentration can be specified by

$$C^o_l = S_{sol}. \tag{15}$$

Summary of mass fluxes due to source-sink terms

The change in mass for each of the gas, liquid, solid, and free phases due to interphase exchange can now be summarized as

$$\begin{aligned} Q_g &= \frac{\partial F_1}{\partial t} + \frac{\partial F_2}{\partial t} \\ Q_l &= -\frac{\partial F_2}{\partial t} - \frac{\partial F_3}{\partial t} + \frac{\partial F_4}{\partial t} \\ Q_s &= \frac{\partial F_3}{\partial t} \\ Q_f &= -\frac{\partial F_1}{\partial t} - \frac{\partial F_4}{\partial t}\ , \end{aligned} \tag{16}$$

which is in conformance with the additional constraint $Q_g + Q_l + Q_s + Q_f = 0$. Where phase saturation coefficients in (4), (8), (11), and (14) are less than unity, it is necessary to modify the terms in (16) accordingly.

NUMERICAL METHODS

The user has the option of solving either the advection or the advection-dispersion equations. If the user chooses to solve the advection-dispersion equations, he or she should set the upstream weighting parameter to zero. In either case, these equations are solved using the integral finite-difference method (IFDM). Recalling Green's First Identity, for a volume-normalized extensive quantity α (de Marsily, 1986; Pruess, 1987),

$$\iiint_{\Omega_i} \nabla \bullet \alpha dx dy dz = \int_{\Gamma_j} (\alpha, n) ds, \qquad (17)$$

where

Ω_i is the domain of interest,

Γ_j are the bounding surfaces of the domain, and

n is the outward normal to Γ_j.

The surface integral in (17) is evaluated as a sum of all fluxes over all interfaces as

$$\int_{\Gamma_j} (\alpha, n) ds = \sum_j (\alpha_{xj} A_{xj} + \alpha_{yj} A_{yj} + \alpha_{zj} A_{zj}), \quad (18)$$

where the A_i terms are cross-sectional areas normal to the component of flux. For example, taking the volume integral as in (17), and writing it as the summation of (18), the IFDM approximation of the equation describing advection of phase *p* can be written as

$$-\sum_j \{(q_p C_p)_{xj} A_{xj} + (q_p C_p)_{yj} A_{yj} + (q_p C_p)_{zj} A_{zj}\}$$
$$= \iiint \phi_i S_p \frac{\partial C_p}{\partial t} dx dy dz \qquad (19)$$
$$= \phi_i S_p V_i \frac{\partial C_{pi}}{\partial t}.$$

Rearranging (19),

$$-\sum_j \left\{ (q_p A|_{xj} + q_p A|_{yj} + q_p A|_{zj}) C_p \right\} = \phi_i S_p V_i \frac{\partial C_{pi}}{\partial t} \qquad (20)$$

where all fluxes are evaluated at the interfaces and the concentrations on the left hand side of (20) are either C_j or C_i depending on the sign of the flux term.

Because solution of the equations depends on the values of the dependent variables, an iterative method is required. For each Picard iteration, the equations are re-evaluated until the residual between the calculated advective or advective-dispersive fluxes and the temporal derivative of phase concentration satisfies a convergence criterion. The maximum value of the residual for the simulations reported here was 10^{-15}.

After the flux calculation is completed, the interphase mass transfer is calculated for each element according to (16), and the concentrations are updated accordingly.

MODEL TESTS

FracTran98 has not been tested extensively. Two simple example tests are reported here. Both of these tests are one-dimensional. The test problem consists of an aquifer 10 m long in the x-direction, discretized into 100 grid elements. The y and z dimensions are specified as unity. Porosity is 0.2. Permeability is 1×10^{-14} m^2. In grid block 1, gas-phase pressure is specified as 104,500 Pa. In grid block 100, it is specified as 94,600 Pa. Air and water properties are both set to those of water, ρ is 1.0×10^3, μ is 1.12×10^{-3}, and compressibility is 4.4×10^{-10}. Both gas and liquid are initially at 50 percent saturation. Liquid flow occurs according to capillary pressure gradients, which are specified through the van Genuchten parameters. The gas phase is used for the model tests reported here.

Figure 2 shows the effect of upstream weighting on the calculation of the advective transport solution using a generic compound. The concentration specification is for the gas phase, where for t<0, C(x,t)=0, and for t>0, C(0.05,t)=1, C(0.95,t)=0.

Figure 3 shows the solution of the advection-dispersion equation for the same system. The analytical solution shown for this system is (Domenico

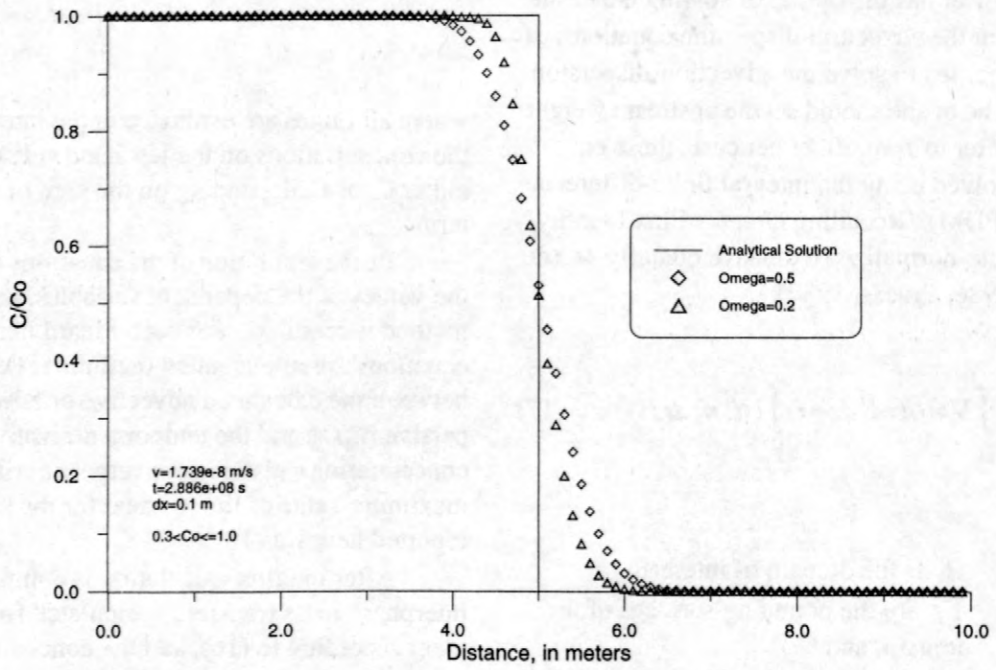

Figure 2. Effect of upstream weighting parameter (omega) on calculation of gas-phase advection.

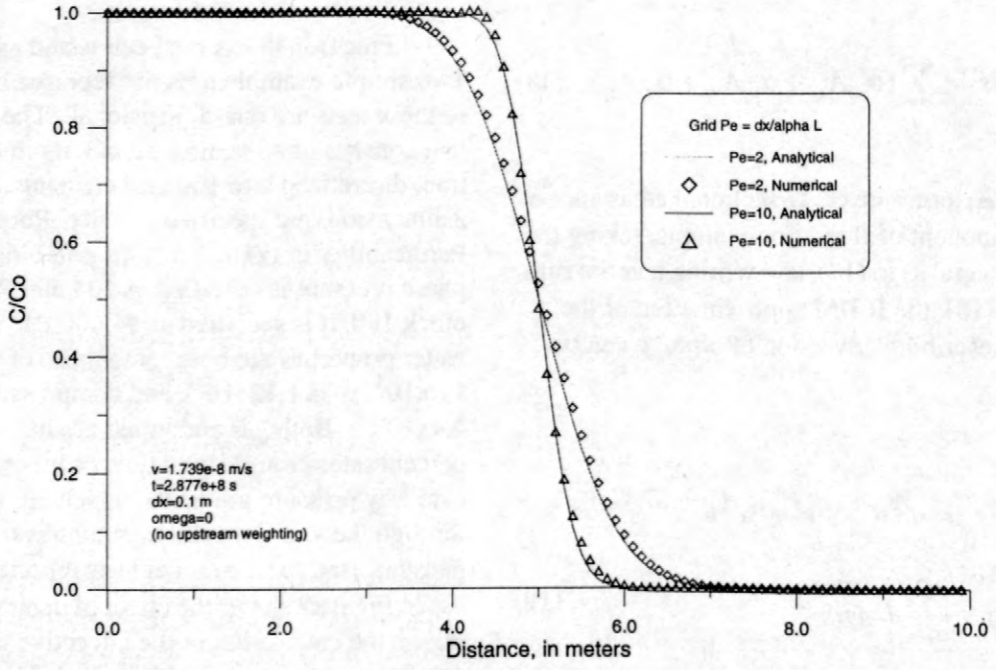

Figure 3. Solution of the advection-dispersion equation for two different values of the Peclet number.

and Schwartz, 1990)

$$\frac{C}{C_o} = \frac{1}{2}\left[erfc\left\{\frac{x - vt}{\sqrt{4\alpha_L vt}}\right\}\right]. \qquad (21)$$

EXAMPLE APPLICATION

An example of the effect of kinetic partitioning control on remediation time is provided. The problem specification uses the same geometry as in the previous section. In this case, the system is simulating the environmental remediation process known variously as soil vapor extraction or *in situ* volatilization. A free phase saturation of one percent of toluene (0.1734 kg) is specified for the initial condition in grid element 1. No toluene is initially present anywhere else in the system. The advection-dispersion equation is solved for 1000 time steps, once with equilibrium partitioning for all processes and once with kinetic partitioning set to 0.01 for the free phase-liquid phase mass transfer. The results are shown in Figure 4.

The sluggish kinetics can be seen to increase the time required for dissolution of free phase into the liquid phase, and the times required for the related interphase partitioning between the liquid, gas, and solid phases. About 10 years of additional pumping is required for the mass removal in this small system.

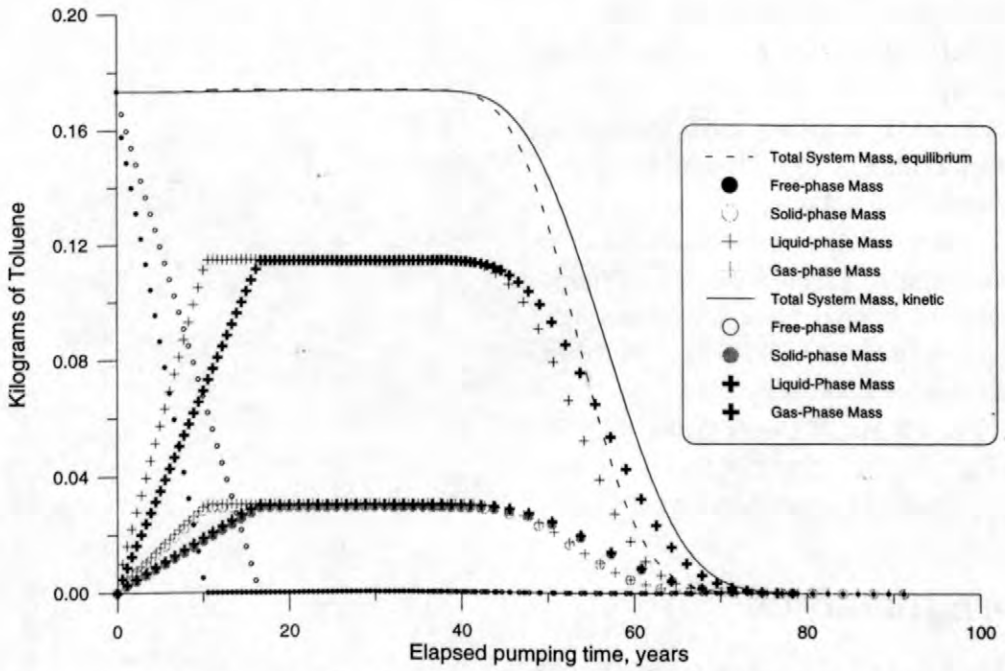

Figure 4. Equilibrium and kinetic partitioning of toluene with advective-dispersive transport.

CONCLUSIONS

FracSys2000 is a versatile modeling package designed to support investigations of physical and chemical hydrogeologic phenomena in fractured unsaturated rocks. With FracFlow96, investigators can simulate single-phase or two-phase flow in fractured or unfractured porous media. The transport capabilities of the FracTran98 module allow for the simulation of either advective or advective-dispersive fluxes, and linear kinetic interphase partitioning between gas, liquid, solid, and an optional free phase. The FracVis98 module allows the user to visualize and animate three-dimensional data, substantially aiding interpretation of simulation results. FracSys2000 is designed to be used for field-scale investigations of flow and transport processes in the unsaturated zone, but it also can be used for laboratory and theoretical investigations.

REFERENCES

Baehr, A., 1984, Immiscible contaminant transport in soils with an emphasis on gasoline hydrocarbons: Newark, University of Delaware, unpublished Ph.D. thesis.

Corapcioglu, M., and A. Baehr, 1987, A compositional multiphase model for groundwater contamination by petroleum products, 1. Theoretical considerations, Water Resources Research, v. 23, no. 1, p. 191-200.

de Marsily, G., 1986, Quantitative Hydrogeology: San Diego, Academic Press, 440 p.

Diodato, D.M., 1997, FracFlow96: A numerical model for simulating multiphase fluid flow in fractured porous media with an application at Yucca Mountain, Nevada: University Park, The Pennsylvania State University, unpublished Ph.D. dissertation, 87 p, 1 computer disk, 1 video tape.

Domenico, P., and F. Schwartz, 1990, Physical and Chemical Hydrogeology: New York, John Wiley and Sons, 824 p.

Looney, B., 1985, Estimation of Geochemical Parameters for Assessing Subsurface Transport at the Savannah River Plant, Environmental Information Document DPST-85-904: Aiken, Savannah River Laboratory, 50 p.

Pruess, K., 1987, TOUGH User's Guide, SAND86-7104, LBL-20700, NUREG/CR-4645: Albuquerque, Sandia National Laboratories, 73 p.

AUTHOR INFORMATION

David M. Diodato, U.S. Geological Survey, Reston, Virginia (*ddiodato@usgs.gov*)

ACKNOWLEDGMENTS

This work is an outgrowth of work begun at Argonne National Laboratory with T.H. Filley, pursued at Penn State University with R.R. Parizek, and continued at the U.S. Geological Survey with L.F. Konikow. Without their steady support, and helpful guidance, it would not have been possible. I am grateful to have had the opportunities that they afforded me.

Borehole Packers for *In Situ* Geophysical and Microbial Investigations in Fractured Rock

By Allen M. Shapiro, John W. Lane, Jr., and Joseph R. Olimpio

ABSTRACT

Bedrock boreholes act as unnatural, high-permeability pathways that can disturb ambient hydraulic and geochemical conditions in the bedrock. To avoid the distrubances caused by open boreholes, many investigations require the use of packers to isolate discrete intervals of bedrock boreholes; packers are either pneumatic or mechanical devices that seal against the borehole wall and hydraulically isolate a section of the borehole. Usually, packers are constructed with a metal core pipe and metal pressure-tight fittings; in some *in situ* investigations, however, a metal-free environment is required. Pneumatic borehole packers were designed and constructed using a polyvinyl-chloride (PVC) core pipe and teflon pressure-tight fittings. These PVC packers were used to conduct borehole radar surveys during hydraulic and tracer testing, as metal in the borehole attenuates the radar signal. The PVC packers also were used to collect water samples for analysis of dissolved hydrogen to characterize redox conditions at a hydrocarbon-contaminated fractured rock site, as metal-water interactions are known to produce dissolved hydrogen.

INTRODUCTION

Bedrock boreholes are frequently used to collect hydrogeologic data to characterize fractured rock. For example, measurements of hydraulic head, collection of water samples for geochemical and isotopic analyses, and geophysical logging to identify fractures and rock properties, all require the use of boreholes. Boreholes, however, act as high permeability pathways in the rock, which may hydraulically connect different hydrogeologic horizons and disturb the ambient hydrologic and geochemical setting.

To reduce or eliminate the effect that open boreholes have on the collection of hydrologic data, borehole packers are used (Shuter and Pemberton, 1978). Borehole packers are pneumatic or mechanical devices that hydraulically isolate sections of a borehole. For example, pneumatic borehole packers are constructed using a flexible bladder that can be inflated (with pressurized gas or fluid) once they are placed at the desired location in the borehole. Assigning locations for borehole packers, however, requires a knowledge of borehole conditions and the location of fractures and hydraulic properties of fractures, which can be obtained only from a combination of geophysical logging and *in situ* hydrologic testing.

Usually borehole packers are constructed using a metal core pipe to support the down-hole equipment. In some applications, however, metal may interfere with the collection of data, yet *in situ* equipment to isolate discrete intervals of bedrock boreholes is still needed. This article describes borehole packers constructed using a polyvinyl-chloride (PVC) core pipe and nonmetallic pressure-tight fittings. The PVC-borehole packers were designed for water sampling during investigations of microbial activity at a hydrocarbon-contaminated fractured rock site and for borehole-radar surveys in bedrock. In both applications, metal used in down-hole equipment would have interfered with data collection.

PVC-BOREHOLE PACKERS

A pneumatic borehole packer was designed with the intention of minimizing the use of metal in down-hole equipment used in investigations of fractured rock. The equipment is designed for bedrock boreholes approximately 15 centimeters (cm) in diameter. A schematic of the PVC-borehole packer is shown in Figure 1 and photo of the packer is shown in Figure 2. A 7.6-cm-diameter schedule-80 PVC core pipe was used in the construction of the packer. The core pipe is threaded into 12.1-cm-diameter PVC packer heads at the top and bottom of the packer. A flexible rubber bladder is attached to the packer heads at the top and bottom using 1.9-cm-wide stainless-steel bands; the bands are the only metal used in the assembly of the packer. The metal bands are used to maintain a pressure-tight fitting between the rubber bladder and the top and bottom packer heads. The presence of the thin metal bands did not affect the borehole radar surveys or the water sampling for microbial investigations for which the packers were designed.

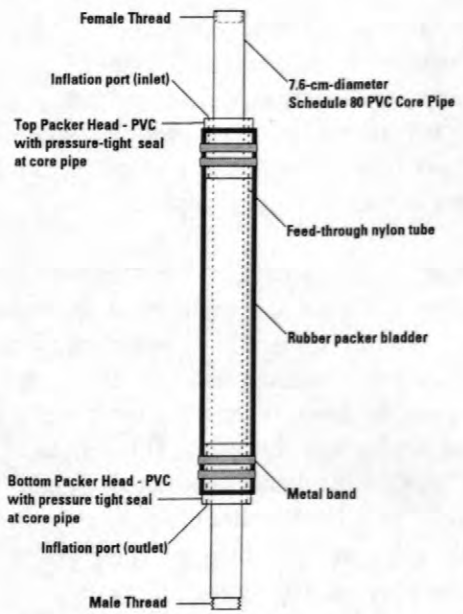

Figure 1. Schematic of PVC-borehole packer.

The flexible bladder is inflated through a threaded pressure-tight fitting in the packer head. Also, feed-through tubes constructed of nylon extend between the top and bottom packer heads and are fixed to the packer heads using pressure-tight fittings. All pressure tight fittings were constructed of teflon. The feed-through tubes are used to access hydraulically isolated intervals below the packer.

Figure 2. Installation of PVC-borehole packer.

For the applications described in this article, two PVC packers were used to straddle a short interval of the bedrock borehole. The PVC-borehole packers were connected with 7.6-cm-diameter schedule-80 PVC pipe or PVC well screen. The straddle-packer apparatus was lowered down the borehole using 7.6-cm-diameter schedule-80 PVC pipe. The packers were lowered to depths of up to 60 meters (m) below land surface in the applications discussed in this article.

APPLICATION FOR BOREHOLE RADAR

Hydrologic tests were designed to couple hydraulic and tracer testing with cross-hole borehole radar surveys to identify and visualize paths of chemical movement in fractured rock. The tests were conducted in the FSE well field at the U.S. Geological Survey fractured-rock field-research site in the Mirror Lake watershed in central New Hampshire. A brief overview of the hydrogeology and investigations conducted at the Mirror Lake site is given in Shapiro and others (1995) and Shapiro and Hsieh (1991, 1996).

The hydraulic and tracer tests were conducted in a highly permeable fractured interval detected in the bedrock of the FSE well field (Hsieh and Shapiro, 1996). The highly permeable interval was intersected by four bedrock boreholes, FSE1, FSE2, FSE3 and FSE4 at approximately 45 meters below land surface. In the FSE well field, these boreholes form a square array, which is approximately 9 meters on a side. The hydraulic and tracer tests were conducted by pumping continuously from the highly permeable interval using a submersible pump in FSE4, while injecting a tracer solution into the highly permeable interval in FSE1; the line between FSE2 and FSE3 is perpendicular to the line between the pumped borehole (FSE4) and the injection borehole (FSE1). A highly conductive saline solution was used as the tracer because of its ability to attenuate the radar signal when compared with the ambient ground water. Borehole packers were used to isolate the highly permeable interval in all boreholes to avoid the effects of open boreholes on the test results. Lane and others (1998a, 1998b) and Wright and Lane (1998) provide additional details of the tests and data acquisition.

Bedrock boreholes FSE1, FSE2 and FSE3 were used to conduct cross-hole borehole radar surveys to identify the transient movement of the tracer in the rock. These wells were instrumented with a straddle-packer assembly that was composed of two PVC-borehole packers and PVC pipe that was used to lower the equipment down-hole. The inside diameter of the core pipe of the PVC-borehole packers and the PVC pipe was designed to allow the borehole radar equipment access to the entire length of the borehole. A straddle-packer assembly with a metal core pipe was used in the pumped borehole to support the submersible pump. Consequently, FSE4 could not be accessed by the borehole radar equipment.

The interpretation of the tracer tests and the borehole radar surveys demonstrated the transient movement of the tracer between the injection and pumped boreholes and the heterogeneous flow regime through the highly permeable fractured interval in the rock. A detailed description of the results is given in Lane and others (1998a, 1998b), Shapiro and others (1998), and Wright and Lane (1998).

APPLICATION FOR *IN SITU* MICROBIAL INVESTIGATIONS

If water samples are collected from open boreholes in fractured rock, water will be drawn preferentially from those fractures with the highest permeability, regardless of the location of the pump intake. The result will be a water sample and ground-water chemistry that is not representative of any individual fracture or fracture zone. Instead, the water chemistry will be a flux-weighted average of the water chemistry from the fractures intersecting the borehole. To identify the chemical properties of ground-water in specific fractures or fracture zones, a straddle-packer apparatus is needed to isolate discrete intervals.

In investigations of microbial activity in ground water, the presence of dissolved hydrogen is a significant parameter when attempting to characterize naturally occurring redox processes (Chapelle and others, 1995). Metal-water reactions, however, also generate dissolved hydrogen (Bjerg and others, 1997). Therefore, to accurately characterize microbial activity, it is advantageous to collect ground-water samples from a metal-free environment.

The need for collecting water samples in discrete intervals of bedrock boreholes and maintaining a metal-free environment during the sample collection prompted the use of the PVC-borehole packers. A straddle-packer apparatus with a 1.5-m-long slotted screen between the PVC-borehole packers was used to isolate discrete intervals of a bedrock borehole in a hydrocarbon-contaminated fractured rock site near Montville, CT (A. Green, CT Department of Environmental Protection, written commun., 1998). Above the top packer, PVC pipe was used to lower the straddle-packer apparatus to specified intervals in the borehole. The packers were inflated and a submersible pump was lowered down the core pipe to a depth adjacent to the slotted well screen between the two packers. With the packers inflated, the pump withdrew water from only the packed-off interval in the borehole.

The PVC-borehole packers were successful in maintaining a metal-free environment for ground-water sampling. The results of the analyses of the samples showed a highly stratified geochemical environment for identifying terminal electron-accepting processes in the ground water, which was attributed to the stratified nature of the hydrocarbon contamination (D. Vroblesky, U.S. Geological Survey, written commun., 1998). If water samples had been collected from the open borehole without use of the PVC-borehole packers to isolate the desired sampling interval, the details of the chemical stratification would have been lost.

SUMMARY

A pneumatic PVC-borehole packer was designed and constructed to minimize the metal in down-hole equipment used in field techniques of characterizing fractured rock. The packer was constructed using PVC core pipe and teflon pressure-tight fittings. Thin metal bands were used to maintain a pressure-tight fitting between the packer bladder and the packer heads. The use of these packers served two purposes: (1) they eliminate the effect that open boreholes have on hydrologic and geochemical investigations in formations intersected by long open boreholes, and (2) they reduce or eliminate interferences that arise due to the presence of metal in the down-hole equipment. Applications of the PVC-borehole packers include borehole radar surveys conducted in conjunction with hydrologic testing, and the collection of water samples from bedrock boreholes to analyze for dissolved hydrogen in investigations of microbial activity at a hydrocarbon-contaminated fractured rock site. In both examples, hydraulically isolated intervals and a metal-free environment were needed to conduct the investigations.

ACKNOWLEDGMENTS

The authors gratefully acknowledge the logistical support provided by Mr. C. Wayne Martin of the U.S. Forest Service, who is stationed at the Hubbard Brook Experimental Forest in Grafton County, New Hampshire. The Hubbard Brook Experimental Forest is operated and maintained by the Northeastern Forest Experiment Station, USDA Forest Service, Radnor, Pennsylvania.

REFERENCES

Bjerg, P.L., Jakobsen, R., Bay, H., Rasmussen, M., Albrechtsen, H.-J., and Christensen, T.H., 1997, Effects of sampling well construction on H_2 measurements made for characterization of redox conditions in a contaminated aquifer: Environmental Science and Technology, v. 31, no. 10, p. 3029-3031.

Chapelle, F.H., McMahon, P.B., Dubrovsky, N.M., Fujii, R.F., Oaksford, E.T., and Vroblesky, D.A., 1995, Deducing the distribution of terminal electron-accepting processes in hydrologically diverse ground-water systems: Water Resources Research, v. 31, no. 2, p. 359-371.

Hsieh, P.A., and Shapiro, A.M., 1996, Hydraulic characteristics of fractured bedrock underlying the FSE well field at the Mirror Lake site, Grafton County, NH, in Morganwalp, D. W. and Aronson, D. A., eds., U.S. Geological Survey Toxic Substances

Hydrology Program--Proceedings of the Technical Meeting, Colorado Springs, CO, September 20-24, 1993: U.S. Geological Survey Water-Resources Investigations Report 94-4015, p. 127-130.

Lane, J.W. Jr., Haeni, F.P., and Day-Lewis, F.D.. 1998a. Use Of Time-Lapse Attenuation-Difference Radar Tomography Methods To Monitor Saline Tracer Transport In Fractured Crystalline Bedrock: Proceedings of the Seventh International Conference on Ground-Penetrating Radar (GPR '98), May 27-30, 1998, Lawrence, Kansas. Published by Radar Systems and Remote Sensing Laboratory, Lawrence, Kansas. pp. 533-538.

Lane, J.W. Jr., Haeni, F.P., and Versteeg, R.. 1998b. Use of a Multi-Offset Borehole-Radar Reflection Method in Fractured Crystalline Bedrock at Mirror Lake, Grafton County, New Hampshire: Proceedings of the Symposium on the Application of Geophysics to Environmental and Engineering Problems (SAGEEP), March 22-26, 1998, Chicago, Illinois. Published by Environmental and Engineering Geophysical Society, Wheat Ridge, Colorado. pp.359-368.

Shapiro, A. M., and Hsieh, P. A., 1991, Research in fractured-rock hydrogeology: Characterizing fluid movement and chemical transport in fractured rock at the Mirror Lake drainage basin, New Hampshire, *in* Mallard, G. E., and Aronson, D. A., eds., U.S. Geological Survey Toxic Substances Hydrology Program--Proceedings of the Technical Meeting, Monterey, CA, March 11-15, 1991: U.S. Geological Survey Water-Resources Investigations Report 91-4034, p. 155-161.

Shapiro, A. M., and Hsieh, P. A., 1996, Overview of research on use of hydrologic, geophysical and chemical methods to characterize flow and chemical transport in fractured rock at the Mirror Lake site, NH, *in* Morganwalp, D. W. and Aronson, D. A., eds., U.S. Geological Survey Toxic Substances Hydrology Program--Proceedings of the Technical Meeting, Colorado Springs, CO, September 20-24, 1993: U.S. Geological Survey Water-Resources Investigations Report 94-4015, p. 71-80.

Shapiro, A. M., Hsieh, P. A., and Winter, T. C., 1995, The Mirror Lake Fractured Rock Research Site--A Multidisciplinary Research Effort in Characterizing Ground-Water Flow and Chemical Transport in Fractured Rock: U.S. Geological Survey Fact Sheet FS-138-95, 2 p.

Shapiro, A. M., Lane, J. W., Jr., and Day-Lewis, F. D., 1998, Characterizing heterogeneity in fractured rock through a combination of tracer testing and radar tomography: EOS, Transactions of the American Geophysical Union, v. 79, no. 17, p. S134.

Shuter, E., and Pemberton, R. R., 1978, Inflatable straddle packers and associated equipment for hydraulic fracturing and hydrologic testing: U.S. Geological Survey Water-Resources Investigations Report 78-55, 16 p.

Wright, D.W., and Lane, J.W. Jr.. 1998. Mapping Hydraulically Permeable Fractures Using Directional Borehole Radar and Hole-To-Hole Tomography With a Saline Tracer: Proceedings of the Symposium on the Application of Geophysics to Environmental and Engineering Problems (SAGEEP), March 22-26, 1998, Chicago, Illinois. Published by Environmental and Engineering Geophysical Society, Wheat Ridge, Colorado. pp.379-388.

AUTHOR INFORMATION

Allen M. Shapiro, U.S. Geological Survey, Reston, Virginia (ashapiro@usgs.gov)

John W. Lane, Jr., U.S. Geological Survey, Storrs, CT (jwlane@usgs.gov)

Joseph R. Olimpio, U.S. Geological Survey, Pembroke, NH (jolimpio@usgs.gov)